The Development and Application of Transition Metal–Hydrides in Catalysis for Alkene Hydrosilylation and Isomerization Reactions

by

Alison Sy-min Chang

A dissertation accepted and approved in partial fulfillment of the

requirements for the degree of

Doctor of Philosophy

in Chemistry

Dissertation Committee:

Darren W. Johnson, Chair

Amanda K. Cook, Advisor

Mike Pluth, Core Member

Stephanie Majewski, Institutional Representative

University of Oregon

Winter 2024

© 2024 Alison Sy-min Chang

DISSERTATION ABSTRACT

Alison Sy-min Chang

Doctor of Philosophy in Chemistry

Title: The Development and Application of Transition Metal –Hydrides in Catalysis for Alkene Hydrosilylation and Isomerization Reactions

Metal-mediated alkene transformations is a rapidly developing field to obtain various organic precursors for pharmaceutical compounds, industrial chemicals, and consumer products. The pursuit of developing Earth-abundant catalysts is of great interest due to catalyst affordability in comparison to precious metal catalysts. Specifically, Ni catalysts serve as viable alternatives to previous metal catalysts due to the versatile reactivity of Ni. In addition to catalyst development, the catalyst mechanism is also just as important to inform future catalyst design. This often results in guided catalyst optimization and byproduct inhibition. The focal point of this thesis surrounds the development and investigation of Ni-catalyzed alkene hydrosilylation and alkene isomerization. Particularly, the formation of Ni–H intermediates to mediate these organic transformations. Reaction and catalyst optimization, substrate scope, and mechanism determination are reported for both alkene hydrosilylation and isomerization systems. Chapter I highlights the utility of Ni–H in these organic reactions, motivating our work described in Chapters II-VI.

Chapter II reports on the reaction development and substrate scope of the homogeneous hydrosilylation (NHC)Ni (NHC = *N*-heterocyclic carbene) catalyst.

Chapter III outlines the mechanistic investigation of the (NHC)Ni-catalyzed alkene hydrosilylation system described in Chapters II.

Chapter IV is a continuation of the catalytic system developed in Chapter II and III and delves more deeply to explore the electronic structure of (NHC)Ni(alkene) catalysts. Modification of the NHC ligand gives rise to trends in catalytic ability. To obtain a deeper understanding of this system, ligand steric and electronic variation are tested to observe its influence on catalyst behavior.

Chapter V illustrates the incorporation of the in situ hydrosilylation system developed in Chapter II into the remote hydrosilylation of a long chain alkene. This work also includes preliminary data on an in situ generated Ni-catalyzed alkene isomerization system in combination with a hydrosilylation system to install a silicon group distal to the initial reaction site.

Chapter VI outlines the development, characterization, and investigation of a heterogeneous Ni alkene isomerization system. This chapter includes catalyst substrate scope, preliminary mechanistic data, and comparison to other Ni-catalyzed alkene isomerization systems.

This dissertation includes previously published and unpublished coauthored material.

CURRICULUM VITAE

NAME OF AUTHOR: Alison Sy-min Chang

GRADUATE AND UNDERGRADUATE SCHOOLS ATTENDED:

University of Oregon, Eugene
Rhodes College, Memphis

DEGREES AWARDED:

Doctor of Philosophy, Chemistry, 2024, University of Oregon
Master of Science, Chemistry, 2020, University of Oregon
Bachelor of Science, Chemistry, 2018, Rhodes College

AREAS OF SPECIAL INTEREST:

Organometallic chemistry
Earth-abundant transition metal catalysis
Homogeneous and Heterogeneous catalyst development
Reaction mechanism elucidation

PROFESSIONAL EXPERIENCE:

Science Communication Seminar Chair, Alliance for Diversity in Science and Engineering, 2020-2022

Summer Academy to Inspire Learning Chemistry Summer Camp Head Organizer and Module Leader, 2022

Co-Founder, Co-President, Treasurer, Social Media Chair, Co-Workshop Chair, Alliance for Diversity in Science and Engineering, 2020-2021

Treasurer, A Community for Minorities in STEM, 2019-2022

GRANTS, AWARDS, AND HONORS:

American Association for University Women Dissertation Fellowship, American Association for University Women, 2023-2024

CAS Future Leaders Award, American Chemical Society, 2023

Diversity, Equity, and Inclusion Chemistry Department Community Builder Award, University of Oregon, 2022

University of Oregon Women in Graduate Sciences Graduate Leadership Award, University of Oregon, 2022

NSF Graduate Research Fellow, National Science Foundation, 2020-2023

University of Oregon General University Scholarship, University of Oregon, 2020, 2021

PUBLICATIONS:

Chang, A. S.; Kascoutas, M. A.; Valentine, Q. P.; How, K. I.; Thomas, R. M. Cook, A. K. Alkene Hydrosilylation using a Heterogeneous Nickel-Hydride Catalyst. *Submitted* **2023**.

Chang, A. S.; Kawamura, K. E.; Henness, H. S.; Salpino, V. M.; Greene, J. C.; Zakharov, L. N.; Cook, A. K. (NHC)Ni(0)-Catalyzed Branched-Selective Alkene Hydrosilylation with Secondary and Tertiary Silanes. *ACS Catal*. **2022**, *12*, 1102–11014.

Kawamura, K. E.; Chang, A. S.; Martin, D. J.; Smith, H. M.; Morris, P. T.; Cook, A. K. Modular Ni(0)/Silane Catalytic System for the Isomerization of Alkenes. *Organometallics* **2022**, *41*, 486–496.

ACKNOWLEDGMENTS

First off, thank you Prof. Amanda Cook for trusting me with independence from the start, for always being available to answer my myriad of questions whenever I randomly showed up to your office, for teaching me the art of organization, for supporting my outreach activities, and for always being an open ear to talk to. You have helped me grow so much as a chemist and a leader since I joined your lab in 2019. Thank you, Dr. Michael Hurst, for showing me that it's possible to be incredibly hard-working through trying times and for your key lime pies–I will also never forget that it's possible for a human being to completely function off 100% black coffee. Thank you, Dr. Kiana Kawamura, for being my research and outreach mentor, for always being open to having heart-felt conversations in the office, for guiding and teaching me how to traverse throughout graduate school, and for being a good friend. I appreciate all your baked goods from Sally's baking blog and miss you and them a lot ever since you defended. Thank you, Melanie Kascoutas, for being so supportive of my every step in graduate school, for teaching me so much about passion in science and your own life journey, for providing me with so much wisdom, and for being the most considerate coworker to ever exist. Thank you to the youngest member of our lab, Allison La Salvia, for teaching me how to be calm and collected and for cracking me up in the office. Thank you to my first undergraduate, Hayden Henness, for always being a ray of sunshine whenever you stepped into lab. I appreciate everything you have contributed towards my well-being, and for being a good companion. Thank you, Victor Salpino, for showing me your drive to understand literally every single detail in reaction set up and work up and never letting go of ≤100% yield reactions. Thank you to my other undergraduate students, Lucas Thigpen, Kiera How, and Lilly Granados, for all keeping me humble and teaching me how to be a better mentor. Thank you, Cailey Carpenter, my superstar REU student in the summer of 2022. You are by far

one of the most hard-working undergraduate students I have had the luck to work with. You inspire me every day with each accomplishment you make in this world. Thank you to all my first-year graduate student mentees for helping me grow as a mentor and to think critically about my own research and beyond, specifically Li HaoKun, Arman Garcia, Jack Greene, and Gaby Bailey for having the greatest impact on me. Especially Gaby Bailey, who is one of my best friends in graduate school. Thank you, Gaby, for always being there for me. I am so lucky that we met during the time that we did, and that Otis was a big part of our lives then too. Thank you Khoa Le for being one of my best friends in graduate school. I have our serendipitous encounters at the UO gym during our first year to thank since we never overlapped in classes. I appreciate our Zoom lunch dates during the pandemic, our lunch dates outside the pandemic, our outings in Eugene, and your ability to be so kind and generous to everyone. Thank you to my recreational volleyball teams for keeping me grounded and active. I want to thank all my other friends who have contributed to my success and survival throughout my graduate career.

I want to thank my family for always understanding my circumstances while in graduate school even if y'all may not know what I'm doing here. Thank you, mom, for taking care of me in Eugene, OR both times that I broke myself, you are amazing. Thank you Valerie for going on adventures abroad with me. Thank you, Fischer Harvel, for being my rock throughout graduate school. You are sincerely the most considerate, generous, kind, patient, and beautiful soul that I get to always laugh with and cry to. Thank you, Gene Lamanilao and Prof. William Eckenhoff, for teaching me that anything is possible to achieve and accomplish. Thank you, Andrew and Ashley at Pisces Aquaria, the owners of the local aquascaping and fish store in Eugene for opening my life to a new hobby and passion. Lastly, thank you to all the dogs in my life, especially my Appa, (Otis, Amelia, Pye, and Wesley) for showing me that happiness can be achieved >99% of the time.

DEDICATION

To my mom.

TABLE OF CONTENTS

Chapter Page

I. CHAPTER I: The Development and Application of Transition Metal–Hyrdides in Catalysis for Alkene Hydrosilylation and Isomerization Reactions 17

1.1 Introduction 17

1.2 Pt–H and Ni–H in Alkene Hydrosilylation 20

1.3 Heterogeneous Ni Alkene Isomerization Cataylsts 24

1.4 Conclusions and Outlook 26

II. CHAPTER II: Development of a (NHC)Ni(0)-Catalyzed Alkene Hydrosilylation System using 2° and 3° Silanes 27

2.1 Introduction 27

2.2 Results and Discussion 30

2.3 Conclusions 33

III. CHAPTER III: Mechanistic Investigation of a Homogeneous (NHC)Ni(0)-Catalyzed Alkene Hydrosilylation System 36

3.1 Introduction 36

3.2 Results and Discussion 37

3.3 Conclusions 46

IV. CHAPTER IV: Investigations of (NHC)Ni(styrene)$_2$ Electronic Structures and Their Relation to Alkene Hydrosilylation 47

4.1 Introduction 47

4.2 Results and Discussion 48

4.3 Conclusions 58

Chapter Page

V. CHAPTER V: Development of a Homogeneous (NHC)Ni(0)-Catalyzed Remote Hydrosilylation System 60

5.1 Introduction 60

5.2 Results and Discussion 62

5.3 Conclusions 67

VI. CHAPTER VI: Development of a Heterogeneous Nickel–Hydride Catalyst for Alkene Isomerization 68

6.1 Introduction 68

6.2 Results and Discussion 71

6.3 Conclusions 86

APPENDICES 87

A. SUPPLEMENTARY CONTENT FOR CHAPTER II 87

B. SUPPLEMENTARY CONTENT FOR CHAPTER III 251

C. SUPPLEMENTARY CONTENT FOR CHAPTER IV 312

D. SUPPLEMENTARY CONTENT FOR CHAPTER V 374

E. SUPPLEMENTARY CONTENT FOR CHAPTER VI 389

REFERENCES CITED 529

LIST OF FIGURES

Figure Page

1. **Figure 1.1.** Examples of M–H in industry for the following reactions: (a) Shell Higher Olefin Process, (b) polymerization of α-olefins, and (c) hydroformylation. Ph, phenyl 18

2. **Figure 1.2.** Catalyst tuning of: (a) ligand modulation for an alkene isomerization catalyst, and (b) metal modulation for an allene hydrosilylation catalyst. Ph, phenyl; Ar, aryl; Me, methyl; Et, ethyl..... 18

3. **Figure 1.3.** Dupont adiponitrile process catalyzed by a homogeneous Ni–H species. Ar, aryl. 20

4. **Figure 1.4.** (a) Alkene hydrosilylation, and (b) Pt catalysts for alkene hydrosilylation. Cy, cyclohexyl 22

5. **Figure 1.5.** Ni alkene hydrosilylation precatalysts with corresponding product selectivity and silane compatibility 23

6. **Figure 1.6.** Development of a branched-selective (NHC)Ni-catalyzed alkene hydrosilylation system to activate 2° and 3° silanes. 24

7. **Figure 1.7.** Exploration of the electronic structures of (NHC)Ni(alkene)$_2$ complexes 25

8. **Figure 1.8.** Proposed heterogeneous Ni–H catalyst capable of undergoing alkene isomerization and hydrofunctionalization reactions 26

9. **Figure 2.1.** (a) General scheme of transition metal-catalyzed hydrosilylation. (b) Base metal-catalyzed hydrosilylation catalysts. (c) Our proposed strategy to investigate the mechanism of (NHC)Ni(0) complexes to yield branched organosilicon products using 2° and 3° silanes 28

10. **Figure 2.2.** Hydrosilylation screen of **2a** and **3a** at 70 °C in toluene with a series of (NHC)Ni(dvtms) complexes to yield **4aa** (dvtms = 1,3-divinyltetramethyldisiloxane). Conditions: styrene (**2a**, 0.088 mmol, 1.0 equiv), H_2SiPh_2 (**3a**, 0.088 mmol, 1.0 equiv), (NHC)Ni(dvtms) (0.0044 mmol, 5.0 mol %), and toluene (0.40 mL). Selectivity and yields are determined by GC-MS analysis using mesitylene or durene as an internal standard..... 31

11. **Figure 2.3.** Scope of alkene hydrosilylation 34

12. **Figure 3.1.** Hammett plots for **1e**-catalyzed hydrosilylation of (a) electronically modified diarylsilanes (**3a**,**b**,**d**,**e**) with **2a** and of (b) electronically modified vinylarenes (**2a**,**c**,**e**-**f**) with **3a**. 39

13. **Figure 3.2.** Deuterium labeling studies. a) Expected outcomes of deuterium incorporation via Chalk-Harrod pathway for hydrosilylation, b) deuterium labeling studies with **2a** and **3a-d$_2$**, and c) crossover study with **2a**, **3a-d$_2$**, and **3b** 41

14. **Figure 3.3.** ^{2}H NMR monitoring of the hydrosilylation of **2a** and **3a-*d$_2$*** by **1e** over time at 75 °C. ^{1}H NMR spectrum shown on the top is used as a reference for starting materials, catalyst, and product 43

15. **Figure 3.4.** Proposed catalytic cycle for the hydrosilylation of **2a** and **3a** by **1e**.. 45

16. **Figure 4.1.** Hammet plots for **1e**-catalyzed hydrosilylation and corresponding 4-X-styrene derivative (X = OMe, F, or CF_3) to form a mixture of complexes **A** and **B**..... 49

17. **Figure 4.2.** ^{1}H NMR monitoring of the hydrosilylation of **2c** and **3a** by **1e** over time at 75 °C 51

18. **Figure 4.3.** ^{1}H NMR monitoring of the hydrosilylation of **2a** and **3a** by **1e** over time at 75 °C 52

19. **Figure 4.4.** Visual Kinetic Analysis experiments: (a) reaction scheme, (b) time adjusted kinetic profile overlap of experiments A and B, (c) time adjusted kinetic profile overlap of experiments A and C..... 53

20. **Figure 4.5.** VT NMR spectra of **1k** recorded in C_6D_6 at various temperatures (25-95 °C) 54

21. **Figure 4.6.** (a) Library of (NHC)Ni(styrene)$_2$ complexes tested with the corresponding steric (%V_{Bur}) and electronic (TEP) parameters for each NHC. TEP, Tolman electronic parameter are measured in cm^{-1}. (b) (NHC)Ni(styrene)$_2$-catalyzed hydrosilylation monitored by GC using mesitylene or durene as an internal standard. Error bars are omitted for clarity 56

22. **Figure 4.7.** Left: CV data for complexes **1e**, **1k**, **1m**, **1n**, and **1o**. Right: Ni complex of interest, the voltage corresponding to the first oxidation (Ni^0/Ni^I) followed by the second oxidation (Ni^I/Ni^{II}) 58

23. **Figure 5.1.** (a) Remote hydrosilylation of a terminal alkene and a 3° silane catalyzed by a transition metal complex. (b) Example of a branched-selective remote hydrosilyation catalyst in the literature. (c) This work on remote hydrosilylation utilizing (NHC)Ni cataylsts.. 61

24. **Figure 6.1.** a) Alkene isomerization. (b) Types of heterogeneous catalysts for alkene isomerization. (c) Ni/H_2SO_4 generation and decomposition. (d) This work: development of Ni/SZO_{300} for alkene isomerization 69

25. **Figure 6.2.** (a) Comparison of the acid sources (H^+) in isomerization of **1c** to **2c**. Conditions: allylbenzene (**1c**, 0.13 mmol, 1.0 equiv), Ni[P(OEt)$_3$]$_4$ (0.0036 mmol, 3.0 mol %), H^+ (0.0062 mmol, 5.0 mol %), and Et_2O (2.0 mL). (b) Hot-filtration experiment..... 74

26. **Figure 6.3.** (a) Catalyst aging study of Ni/H_2SO_4 (blue squares) and Ni/SZO_{300} (green diamonds). Conditions: **1c** (0.12 mmol, 1.0 equiv), $Ni[P(OEt)_3]_4$ (0.0036 mmol, 3.0 mol %), H_2SO_4 or SZO_{300} (0.0060 mmol H^+, 5.0 mol %), and Et_2O (2.0 mL). (b) Catalyst recyclability study for the isomerization of **1c**. 76

27. **Figure 6.4.** (a) Substrate scope for isomerization using Ni/SZO_{300}. Isolated yields and selectivity (*E*/*Z*) of the isolated products are reported. The selectivity was determined by relative integrations in the ^1H NMR. Conditions: **1** (1.0 mmol, 1.0 equiv), $Ni[P(OEt)_3]_4$ (0.030 mmol, 3.0 mol %), SZO_{300} (0.050 mmol H^+, 5.0 mol %), Et_2O (17 mL), 30 °C, 1-24 h. (b) Substrate scope with Ni/H_2SO_4. Conversion is reported as % conversion to product. Conversion and selectivity were determined by GC or GC-MS 79

28. **Figure 6.5.** Kinetic analysis of Ni and Pd isomerization catalysts. 82

29. **Figure 6.6.** $[Ni–H]^+$-catalyzed reactions under unoptimized conditions. (a) Hydroalkenylation of styrene to afford **3a**. (b) hydroboration of **2u** and B_2Pin_2 to afford **3b**. (c) Hydrosilylation of styrene and H_2SiPh_2 to afford **3c**.. 85

LIST OF TABLES

Table Page

1. **Table 5.1.** Solvent screen for the hydrosilylation of **B-2b** and **3a** by ITMe/Ni(COD)(DQ) 65

2. **Table 6.1.** Evaluation of acid sources for the isomerization of **1a** to **2a**..... 72

LIST OF SCHEMES

Scheme Page

1. **Scheme 1.1.** Catalytic cycle of the Chalk-Harrod mechanism 22

2. **Scheme 1.2.** Hydride insertion/elimination reaction mechanism of (NHC)Ni-catalyzed alkene hydrosilylation of styrene and H_2SiPh_2 25

3. **Scheme 1.3.** Remote hydrosilylation of a terminal long-chain alkene to install a silicon group at the most internal position 25

4. **Scheme 3.1.** Possible transition metal-catalyzed hydrosilylation mechanisms: (a) Chalk-Harrod mechanism, (b) modified Chalk-Harrod mechanism, and (c) a radical mechanism. 37

5. **Scheme 3.2. 1e**-catalyzed hydrosilylation of a 1,6-diene **2s** and **3a.** Conditions: **2s** (0.87 mmol, 1.0 equiv), **3a** (0.96 mmol, 1.1 equiv), **1e** (0.044 mmol, 5.0 mol %), toluene (4.0 mL), 100 °C, 4 h, under N_2 38

6. **Scheme 5.1.** NHC screen for the isomerization of **1a** to **2a** by $Ni(COD)_2$/NHC/$HSiPh_3$ 63

7. **Scheme 5.2.** Evaluation of Ni(0) precatalysts for the isomerization of **2a** to **A-2a** and **B-2a** 64

8. **Scheme 6.1.** Mechanistic experiments. (a) Reactivity with vinylcyclopropane (**1ac**). (b) Reactivity with a 1,6-diene (**1ad**). (c) Crossover experiment between **1a** and **1c-d_n**.. 85

CHAPTER I

THE DEVELOPMENT AND APPLICATION OF TRANSITION METAL–HYDRIDES IN CATALYSIS FOR ALKENE HYDROSILYLATION AND ISOMERIZATOIN REACTIONS

This chapter was written by Alison Sy-min Chang and presents an unpublished perspective on work developed and presented in Chapters II-VI.

1.1 Introduction

Transition metal-catalyzed organic reactions are effective routes to access precursors for various types of materials and pharmaceutical compounds. Specifically, the importance of metal-hydride (M–H) motifs within these reactions cannot be understated. Some valuable examples of M–H utilized in industry are (1) the Shell Higher Olefin Process[1], a Ni–H mediated reaction that oligomerizes ethylene into α-olefins on a one million tonne scale annually (**Figure 1.1.a.**), (2) the polymerization of 1-alkenes into various thermoplastics for consumer goods (*e.g.*, polyethylene, polypropylene, and others) mediated by a Zr–H complex known as a Zeigler-Natta catalyst[2], (**Figure 1.1.b.**), and (3) the hydroformylation of syngas and ethylene promoted by a Rh–H catalyst[3–5], known as the oxo process (**Figure 1.1.c.**).

In addition to such valued catalytic processes, the mechanism by which these catalysts operate is also of great significance. Unveiling these catalytic pathways is an effective way to inform future catalyst design to inhibit byproduct formation, increase reaction efficiency, and obtain high product selectivity. This often results in metal and ligand sphere tuning to induce specific reactivity. An elegant study that establishes a structure-activity relationship through ligand modification from our group is a (NHC)Ni/$HSiAr_3$-catalyzed (NHC = *N*-heterocyclic carbene, Ar = aryl) alkene isomerization system.[6] The silane is required to generate an active Ni–H species through the oxidative addition of the H–Si bond to the Ni(0) center. The systematic alteration in sterics of the NHC led to the realization that a bulky NHC is more compatible with smaller alkenes. On the contrary, a smaller NHC is well-suited for sterically hindered trisubstituted alkenes because the substantial coordination site can not only promote substrate binding, but also faster migratory

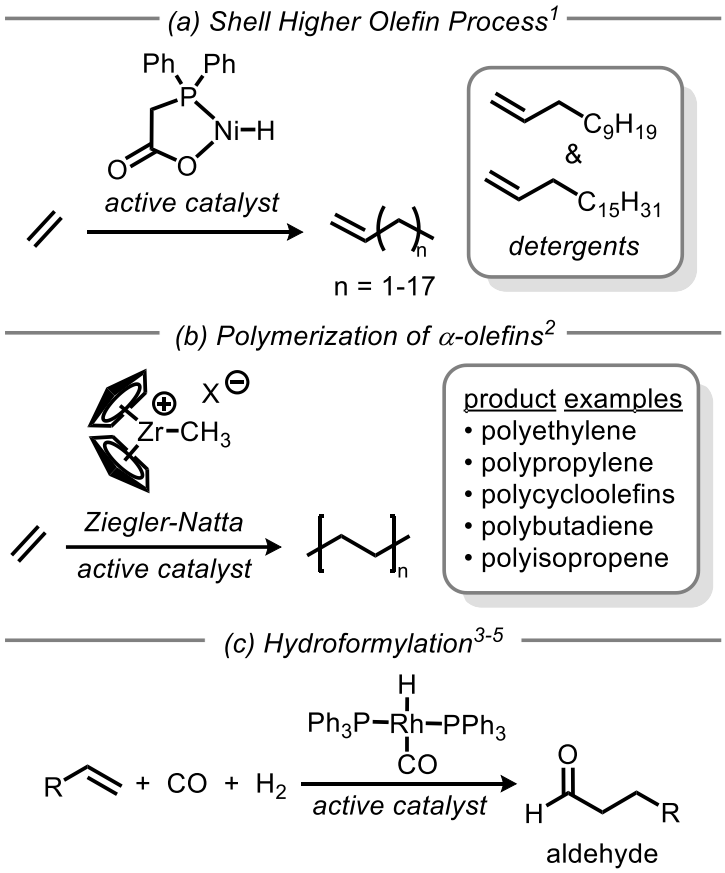

Figure 1.1. Examples of M–H in industry for the following reactions: (a) Shell Higher Olefin Process, (b) polymerization of α-olefins, and (c) hydroformylation. Ph, phenyl.

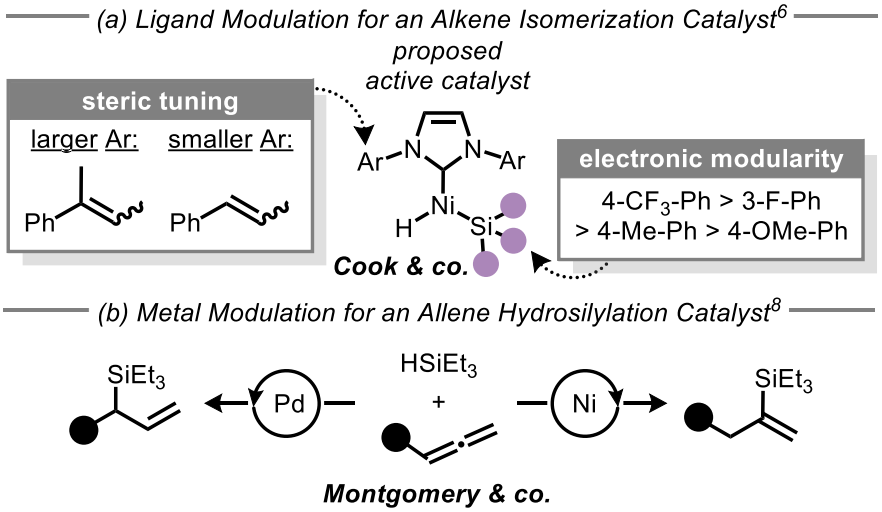

Figure 1.2. Catalyst tuning of: (a) ligand modulation for an alkene isomerization catalyst, and (b) metal modulation for an allene hydrosilylation catalyst. Ph, phenyl; Ar, aryl; Me, methyl; Et, ethyl.

insertion (**Figure 1.2.a.**).[7] Additionally, further electronic adjustment of the $HSiAr_3$ resulted in faster reaction kinetics with more electronic withdrawing groups appended to the silane aryl substituents (**Figure 1.2.a.**). Work by Montgomery and co.[8] showcases reversed catalyst regioselectivity for allene hydrosilylation simply by changing the metal identity from Pd to Ni (**Figure 1.2.b.**). These results highlight how critical catalyst tuning and mechanistic determination is in aiding reaction development. Furthermore, the prevalent use of M–H in various catalytic processes give rise to their potential for various hydrofunctionalization applications.

Our group is particularly interested in developing Ni catalysts that can readily form a Ni–H. We specifically target the investigation of Ni due to its Earth abundance and versatile reactivity, as Ni catalysts have been documented to undergo both one- and two-electron pathways, which is heavily influenced by both the ligand coordination sphere and reaction conditions. Due to these factors, Ni can be a sustainable alternative to Pd and Pt catalysts. The widespread use of Ni in both homogeneous and heterogeneous transformations provides us with strong motivation to investigate organic transformations mediated by Ni catalysis such as alkene isomerization and hydrosilylation. When the two reactions are paired together, the isomerization of alkenes followed by the hydrosilylation of the newly synthesized alkene is an attractive method to obtain value-added products from a reaction known as remote hydrosilylation. This type of reactivity can also be applied to other types of hydrofunctionalization reactions if the catalyst(s) are compatible. Remote functionalization can be mediated by a single catalyst that performs both transformations or by two separate catalysts having their unique function, either in a single pot or in tandem with one another. One example of an applied remote functionalization reaction is an intermediate step in the preparation of Nylon 6,6, known as the DuPont adiponitrile synthesis (**Figure 1.3.**).[9] This $Ni[P(OAr)_3]_4$-catalyzed reaction forms an active Ni–H species from the oxidative addition of HCN to Ni. After the hydrocyanation of one equivalent of HCN to butadiene (*step i*), the internal alkene that is formed is then isomerized to the terminal alkene (*step ii*) prior to a second equivalent of hydrocyanation (*step iii*). The product of this reaction is then further reduced and polymerized to form the desired product, Nylon 6,6. Remote functionalization is a powerful method to install a functional group distal to the initial reaction site using accessible precursors (*e.g.*, terminal vs. internal alkenes) to generate valuable products that cannot otherwise be achieved.

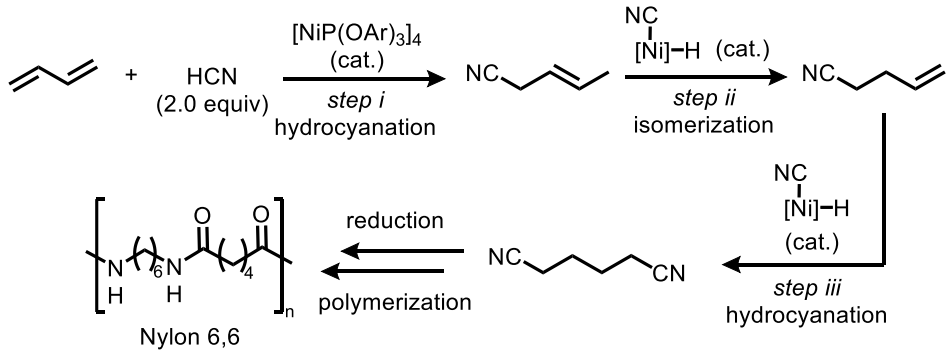

Figure 1.3. Dupont adiponitrile process catalyzed by a homogeneous Ni–H species. Ar, aryl.

Having versatile activity, Ni is a promising candidate to develop catalytic systems with. This thesis will convey the utility of Ni catalysis in separate homogeneous and heterogeneous systems for various organic transformations.

1.2 Pt–H and Ni–H in Alkene Hydrosilylation

Alkene hydrosilylation, the addition of a H–Si bond across a π-bond, is a widespread reaction owing to its prevalence in the silicone industry (**Figure 1.4.a.**).[10] This metal-mediated reaction has led to the development of various catalyst designs, including the initial discovery of Speier's catalyst, H_2PtCl_6/*i*-PrOH (**Figure 1.4.b.**).[11] This linear-selective Pt catalyst spurred the initial development of the silicone industry; however, due to long induction periods prior to catalyst activation, a dangerously exothermic process on a large scale, this catalyst has mostly been replaced by Karstedt's catalyst, $Pt_2(DVTMS)_3$ (DVTMS = 1,3-divinyl-1,1,3,3-tetramethyldisiloxane, **Figure 1.4.b.**). Karstedt's catalyst has truly advanced the hydrosilylation reaction to its current state in industry and is the most widespread hydrosilylation catalyst to date. The use of Karstedt's catalyst has expanded silane compatibility and catalyst activation is less harsh compared to Speier's catalyst. Although only a small amount of Karstedt's catalyst is required for hydrosilylation reactions (ppm-ppb amounts depending on the reagent)[10], the incredibly fast reaction kinetics of the catalyst often leads to undesirable side reactions (*e.g.*, isomerization, hydrogenation, and dehydrogenative silylation).[12] Due to the extremely high activity of Karstedt's catalyst, extensive work has been dedicated to reveal the reaction mechanism. Karstedt's catalyst was found to proceed through the Chalk-Harrod mechanism, by which a Pt–H intermediate is the active catalyst and is formed by the oxidative addition of H–Si

to the Pt(0) precatalyst (**Scheme 1.1.**).[13] Catalyst stability was found to be dependent on excess alkene in solution to inhibit colloidal Pt formation, which are postulated to be responsible for side reactivity. The findings from these mechanistic experiments give rise to further optimization of reaction conditions to inhibit catalyst decomposition, demonstrating the importance of understanding how a catalyst facilitates a reaction.

Despite the high activity of Karstedt's catalyst, further work to prepare improved hydrosilylation catalysts to inhibit catalyst decomposition led to the discovery of Markó's catalyst, (NHC)Pt(VTMS) (NHC = *N*-heterocyclic carbene, VTMS = vinyltetramethyldisiloxane, **Figure 1.4.b.**).[12] Indeed, the presence of the strongly σ-donating ligand, an NHC, alleviates catalyst decomposition routes and thereby hinders byproduct formation. The tunable sterics of the NHC substituents trend with regioselectivity, and the functional group compatibility of Markó's catalyst can be expanded from that of Karstedt's catalyst to include expoxy groups. Despite the progress in Pt hydrosilylation development, much work has been devoted to developing hydrosilylation catalysts with Earth-abundant metals such as Ni, as an alternative.

With the affordable cost associated with Ni in comparison to Pt and its versatile reactivity, there are several reports on the utility of Ni–H in alkene hydrosilylation. For example, Chirik and co. developed a linear-selective (α-diimine)Ni–H dimer that is proposed to undergo a one-electron process due to the redox active nature of the ligand (**Figure 1.5.**).[14] To our knowledge, this notable finding is the only linear-selective Ni catalyst that exhibits 3° silane activation. Alternatively, several examples of branched-selective Ni–H catalysts have been reported, albeit with limitation to 1° and 2° silane activation. For example, Schmidt and co. document the synthesis of a series of (P,N-ligand)Ni complexes that mediate alkene hydrosilylation activating 1° and 2° silanes with preliminary mechanistic studies alluding to the formation of a Ni–H active species (**Figure 1.5.**).[15] Additional systems by Zargarian and co.[16,17] and Valerga and co.[18] tentatively show that an (indenyl)Ni and a (picolyl-NHC)Ni complex, respectively, generate a Ni–H active species for alkene hydrosilylation with H_3SiPh, a 1° silane (**Figure 1.5.**). Motived by the lack of branched-selective Ni hydrosilylation catalysts able to activate 3° silanes, Chapter II of this dissertation describes the reaction development of a branched-selective (NHC)Ni(0)-catalyzed alkene hydrosilylation system that is compatible with 2° and 3° silanes (**Figure 1.6.**). Modulating ligand steric influences catalyst reactivity, and we show the applicability of this reactivity handle in the substrate scope. Within our substrate scope, we show an expansion in silane compatibility

compared to previous reports with particular use of industrially relevant 3° alkoxy- and chlorosilanes. The work on Chapter II was published in *ACS Catalysis* in 2022. This chapter was written by Alison Sy-min Chang with editorial assistance from Dr. Kiana E. Kawamura and Victor M. Salpino contributed synthetically through the preparation of starting materials. Hayden S. Henness contributed through rate laws experiments. Jack C. Greene contributed intellectually.

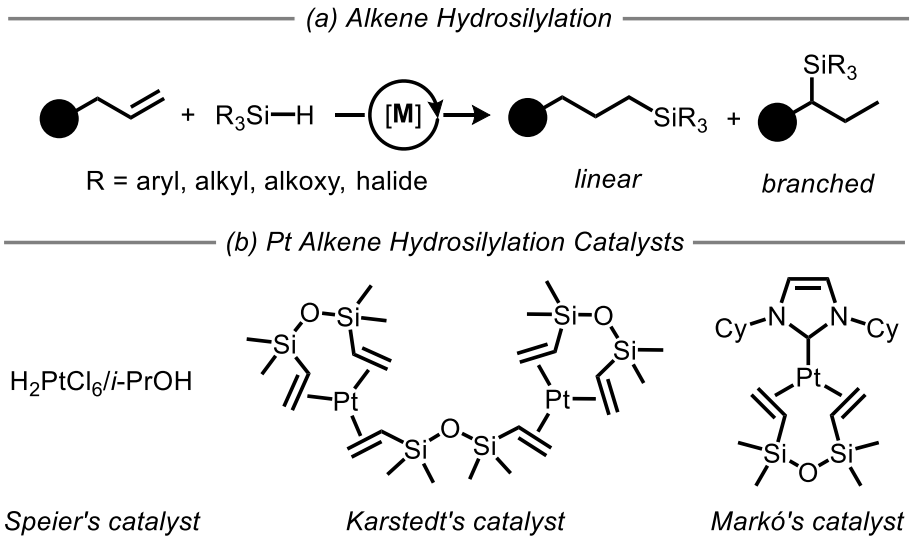

Figure 1.4. (a) Alkene hydrosilylation, and (b) Pt catalysts for alkene hydrosilylation. Cy, cyclohexyl.

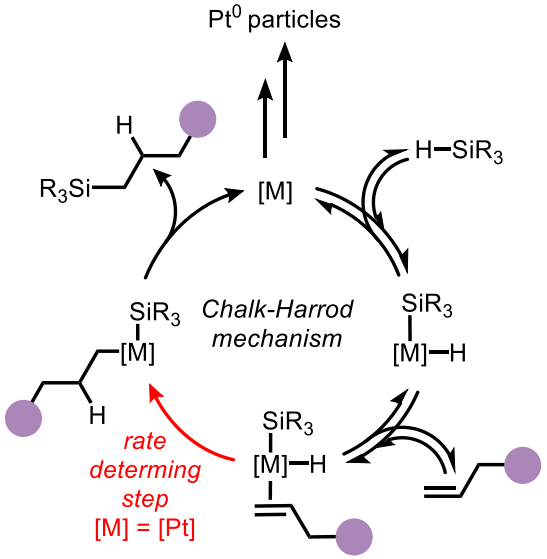

Scheme 1.1. Catalytic cycle of the Chalk-Harrod mechanism.

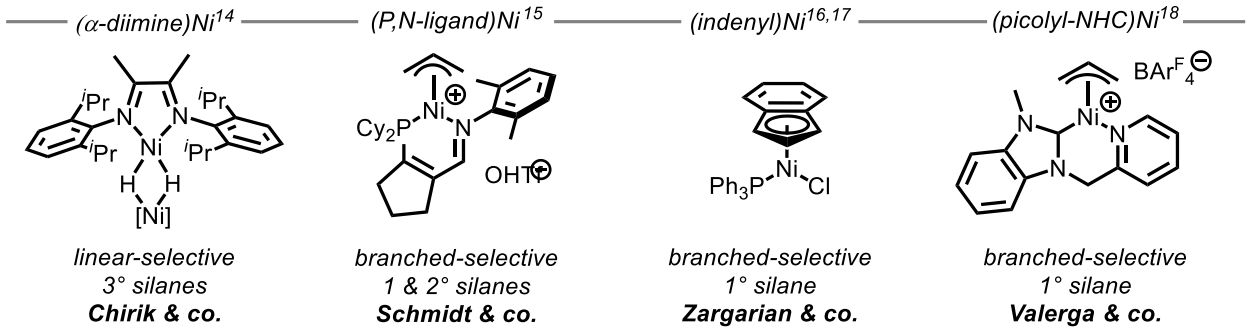

Figure 1.5. Ni alkene hydrosilylation precatalysts with corresponding product selectivity and silane compatibility.

Building upon Chapter II, Chapter III describes the mechanistic elucidation of alkene hydrosilylation using a (NHC)Ni(styrene)$_2$ catalysts, pointing towards a metal-hydride insertion/elimination pathway (**Scheme 1.2.**). This chapter was written by Alison Sy-min Chang, with editorial assistance from Dr. Kiana E. Kawamura and Professor Amanda K. Cook. Dr. Kiana E. Kawamura and Victor M. Salpino contributed synthetically through the preparation of starting materials. Hayden S. Henness carried out rate law experiments.

As a continuation of Chapter II and III, Chapter IV further explores the electronic structures of various (NHC)Ni(alkene)$_2$ complexes and their relation to alkene hydrosilylation (**Figure 1.7.**). This is achieved by utilizing both NMR spectroscopy and cyclic voltammetry methods. Part of the work presented in Chapter III was published in *ACS Catalysis* in 2022 and written by Alison Sy-min Chang, with editorial assistance from Dr. Kiana E. Kawamura and Professor Amanda K. Cook. Dr. Kiana E. Kawamura and Victor M. Salpino contributed synthetically through the preparation of starting materials. The remaining unpublished work in Chapter III was developed and experimentally carried out by Alison Sy-min Chang.

As previously mentioned, remote hydrosilylation is a commanding tool to obtain internally functionalized alkenes. Therefore, we took advantage of our newly established (NHC)Ni-catalyzed alkene hydrosilylation system described in Chapters II-IV and coupled it with alkene isomerization to induce remote hydrosilylation described in Chapter V (**Scheme 1.3.**). Remote hydrosilylation is a process that installs a silicon group at a position distal to the initial reaction site. The work in Chapter V was developed by Alison Sy-min Chang and Professor Amanda K. Cook and the synthetic and catalytic system development was carried out by Cailey Carpenter, Gaby Bailey, and

Alison Sy-min Chang. This chapter was written by Alison Sy-min Chang, with editorial assistance from Cailey Carpenter and Professor Amanda Cook.

1.3 Heterogeneous Ni Alkene Isomerization Catalysts

Several homogeneous Ni isomerization catalysts have been developed, in conjunction with extensive mechanistic studies to elucidate the reaction pathway.[19,20,14,21,6] Although, the field is dominated by precious metal catalysts due to their significantly higher activity. Furthermore, limited progress has been made in the field of heterogeneous alkene isomerization catalysts despite the practical use of recyclability. This lack of progress is largely influenced by the uncontrolled nature by which these complexes are prepared, making their active sites indiscernible. Select examples by Kegnæs and co. show alkene isomerization facilitated by Ni/Co nanoparticles encapsulated in nitrogen-doped carbon shells.[22] However, stoichiometric amounts of $HSiEt_3$, elevated temperatures (140 °C), and high catalyst loading (8 mol % Co/Ni) are all required for full conversion to product. Other examples of solid Nicatalysts active for alkene isomerization are $Ni_2P/SiO_2–Al_2O_3$ activated by $LiAlH_4$[23], Ni/MCM-41 or Ni/AlMCM-41[24], H_2-reduced NiO/Cr_2O_3[25], and NiNaY modified by picolinic acid or NaOH[26]. Notably, these solid catalysts are prepared in a crude fashion, making the catalytic sites indiscernible and often leading to low selectivity, yield, and undesirable byproduct formation. To alleviate these factors, we have prepared a modular heterogeneous Ni–H catalyst using a surface organometallic chemistry (SOMC) method described in Chapter VI of this thesis. SOMC applies molecular organometallic

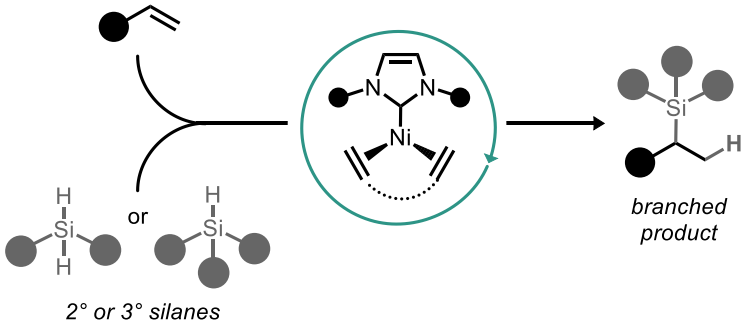

Figure 1.6. Development of a branched-selective (NHC)Ni-catalyzed alkene hydrosilylation system to activate 2° and 3° silanes.

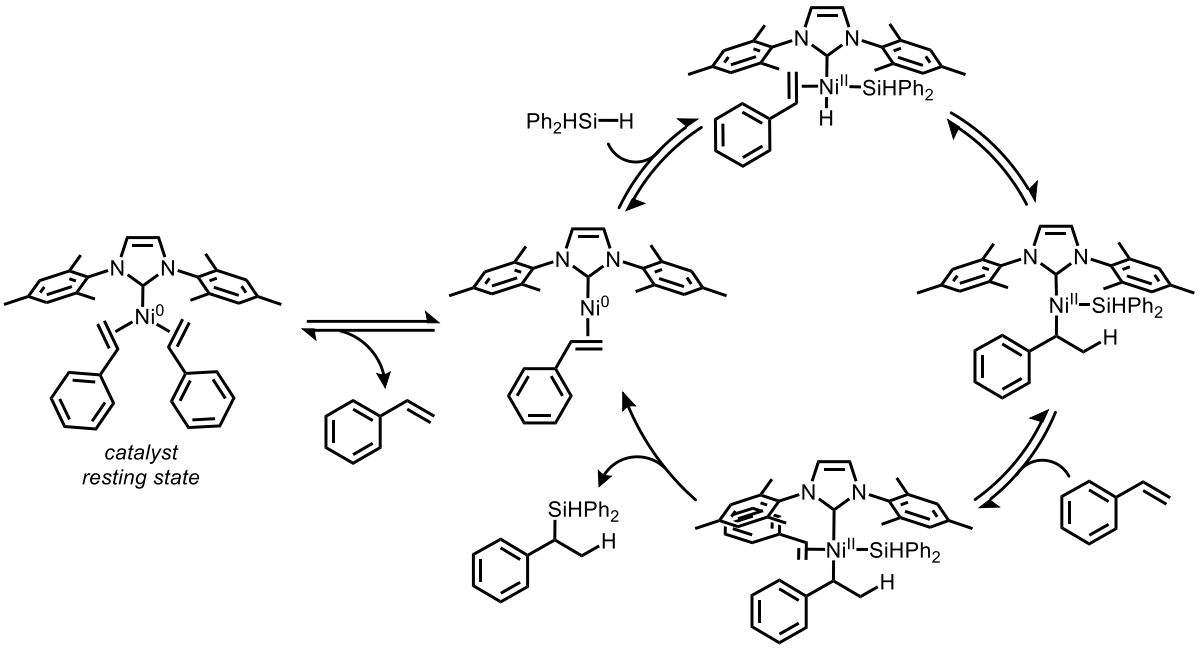

Scheme 1.2. Hydride insertion/elimination reaction mechanism of (NHC)Ni-catalyzed alkene hydrosilylation of styrene and H_2SiPh_2.

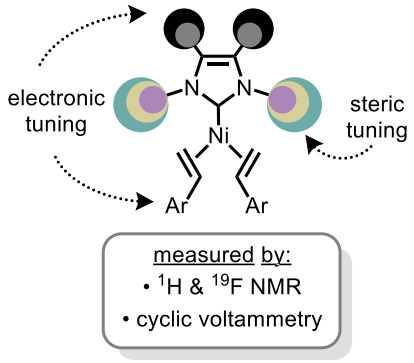

Figure 1.7. Exploration of the electronic structures of (NHC)Ni(alkene)$_2$ complexes.

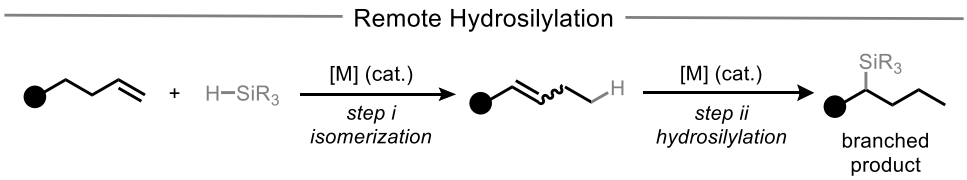

Scheme 1.3. Remote hydrosilylation of a terminal long-chain alkene to install a silicon group at the most internal position.

principles onto a heterogeneous system. Using these principles with the intention to translate a previously developed molecular [Ni–H]$^+$-mediated alkene isomerization system developed by

Cramer and Lindsay[19], we can obtain the desired $[Ni–H]^+$ scaffold via protonation of the Ni(0) precursor with a solid acid, namely sulfated zirconia. This newly generated species was found to be active for alkene isomerization. We show that this solid catalyst can tolerate a wide range of functional groups, is highly recyclable, and can also be applied to various hydrofunctionalization reactions (**Figure 1.8.**). Chapter VI includes unpublished work done by Alison Sy-min Chang as well as submitted and co-authored material from Chang, A. S.; Kascoutas, M. A.; Valentine, Q. P.; How, K. I.; Thomas, R. M.; Cook, A. K. *Alkene Isomerization using a Heterogeneous Nickel–Hydride Catalyst*. *Submitted*. This article was written by Alison Sy-min Chang, with editorial assistance from Melanie A. Kascoutas and Professor Amanda K. Cook. Melanie A. Kascoutas and Kiera I. How contributed synthetically through the preparation of starting materials. Quinn P. Valentine and Rachel M. Thomas performed preliminary work to establish the project.

1.4 Conclusions and Outlook

M–H motifs are often highlighted throughout catalysis through the application in various organic transformations ranging from alkene isomerization to hydrofunctionalization reactions. These critical catalytic intermediates are utilized in industrial reactions, as determined through experimental mechanistic realizations. The frequent use of M–H motifs within catalysis highlights the importance of such scaffolds, deeming them as noteworthy intermediates to investigate.

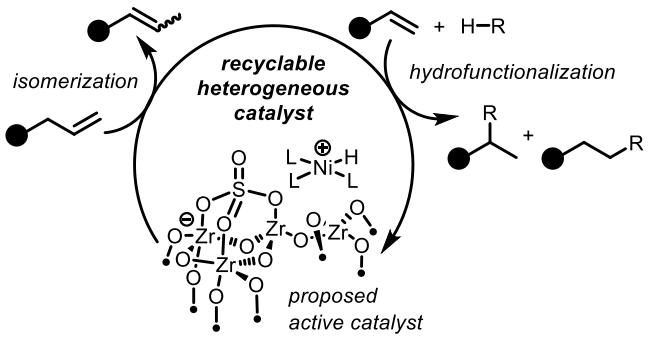

Figure 1.8. Proposed heterogeneous Ni–H catalyst capable of undergoing alkene isomerization and hydrofunctionalization reactions.

CHAPTER II

DEVELOPMENT OF A (NHC)Ni(0)-CATALYZED ALKENE HYDROSILYLATION SYSTEM USING 2° AND 3° SILANES

This chapter includes previously published and co-authored material from Chang, A. S.; Kawamura, K. E.; Henness, H. S.; Salpino, V. M.; Greene, J. C.; Zakharov, L. N.; Cook, A. K. (NHC)Ni(0)-Catalyzed Branched-Selective Alkene Hydrosilylation with Secondary and Tertiary Silanes. *ACS Catal*. **2022**, *12*, 1102–11014. https://doi.org/10.1021/acscatal.2c03580. This article was written by Alison Sy-min Chang, with editorial assistance from Dr. Kiana E. Kawamura and Professor Amanda K. Cook. Dr. Kiana E. Kawamura and Victor M. Salpino contributed synthetically through the preparation of starting materials. Hayden S. Henness carried out rate law experiments. Jack C. Green contributed intellectually.

2.1 Introduction

As one of the most industrially valuable transition metal-catalyzed reactions, the hydrosilylation of π-bonds supplies the feedstock to produce silicon-based materials (**Figure 2.1.a.**).[27–31] These products have widespread applications in both organic and materials chemistry[32] and are utilized to yield high-value durable organosilicon materials,[27–31] silicon-based cross-coupling agents,[33–35] alcohol precursors,[36–38] and pharmaceuticals.[39–41] The tremendous advancement of the silicone industry is owed to the discovery of the highly active, linear-selective, platinum catalysts, particularly Karstedt's catalyst [$Pt_2(dvtms)_3$] (dvtms, 1,3-divinyltetramethylsiloxane).[42,30] Because Pt is one of the most expensive metals and much of the Pt used in silicone production is unrecoverable,[31] there is a strong desire to shift the reliance on Pt to more Earth-abundant metal catalysts.

Catalysts composed of base metals[31,43–45] like Ni,[46–52,14,53–57] Mn,[58–64] Co,[65–85] and Fe[86–96,68,97–106] have been developed for linear-selective alkene hydrosilylation. As a congener of Pt, Ni is especially promising as a base metal candidate for alkene hydrosilylation. Ni(II) complexes possessing pincer,[49,51,55] salicylaldiminato,[48] allyl,[50] amido,[47] and acetylacetonato[52,54] ancillary ligands and no added ligand[56] exhibit high linear selectivity for the hydrosilylation of alkenes with

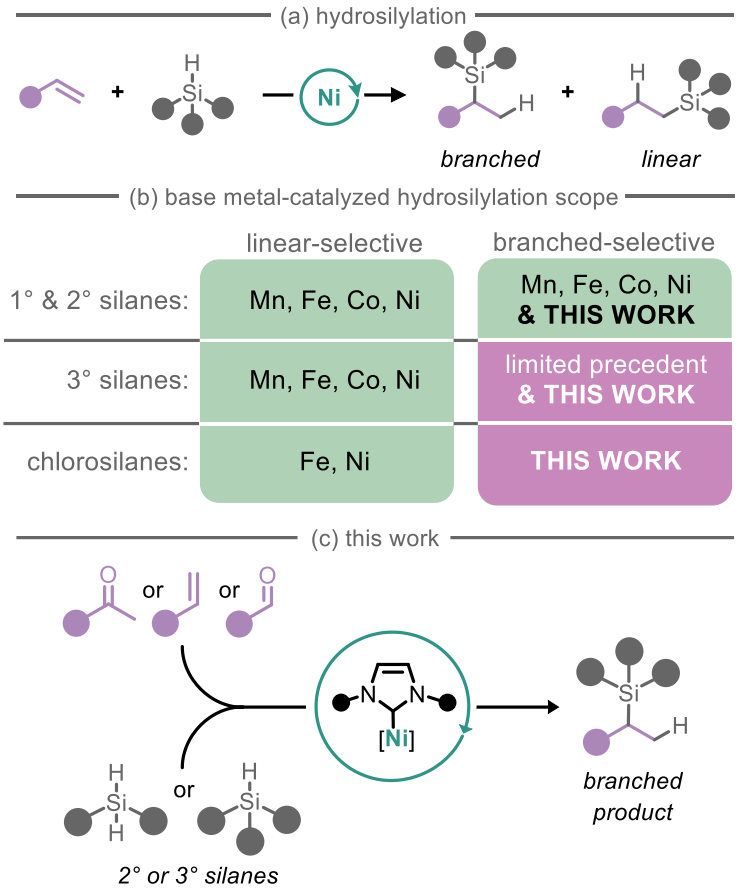

Figure 2.1. (a) General scheme of transition metal-catalyzed hydrosilylation. (b) Base metal-catalyzed hydrosilylation catalysts. (c) Our proposed strategy to investigate the mechanism of (NHC)Ni(0) complexes to yield branched organosilicon products using 2° and 3° silanes.

primary (1°) or secondary (2°) silanes. Expansion to tertiary (3°) silanes has been a recent focus due to the relevance in industrial hydrosilylation,[44] and particularly important advances have been made using alkoxy-substituted silanes to form the linear hydrosilylation products with exceptional regioselectivity. [27,30,35,43,45,46,48,56,64,66,67,73] Despite these advances, most reports focus on 1° and 2° aryl silanes, *emphasizing the need to develop catalysts that enable the hydrosilylation of 3° silanes, especially chloro- and alkoxy-substituted silanes* (**Figure 2.1.b.**). Notably, only a handful of base metal catalysts have been developed to react with chlorosilanes, and all of them either give poor selectivity or have limited scopes.[107,86,108,109,55] Indeed, investigation and expansion of the silane scope is often neglected in hydrosilylation reactions, despite the fact that both changes in the

silane's electronic[110–112] and steric[113,111,114,115] characteristics impact reactivity and properties of hydrosilylation products.

Another challenge in hydrosilylation lies in accessing branched organosilicon products, which has been substantially less developed than that of linear-selective systems.[116,117] Branched organosilicon products are valuable and are highly sought out for the production of adhesion promotors, RTV silicone additives, and silicone coatings,[27] as well as in the enantioselective synthesis of therapeutic agents.[28] In the emergent field of base metal-catalyzed branched-selective alkene hydrosilylation, noteworthy work achieving high regioselective control employ Mn,[61] Co,[98,72,118,103,84] Fe,[102,119] Ni,[16–18,15] and Cu[120] complexes that readily react with 1° silanes. Even fewer examples enabling activation of 2° silanes have been reported.[120,77,15,82,83,57,85] To our knowledge, examples with 3° silanes are limited to the (pincer)Co-catalyzed hydrosilylation of 1-octene using $(EtO)_3SiH$[98] and the ([P~C]-chelate)Co-catalyzed hydrosilylation of styrene with Ph_3SiH and $Me(EtO)_2SiH$.[83] *A significant challenge remaining in base metal-catalyzed alkene hydrosilylation is the synthesis of branched hydrosilylation products using 3° silanes with alkyl-, aryl-, alkoxy-, or chloro-substituents* (**Figure 2.1.b.**).

An additional deficit in the literature is a fundamental understanding of the silane's steric and electronic properties on hydrosilylation.[44] Previous work on Pt catalysts exploit electronically diverse silanes to illuminate the impact on hydrosilylation reactivity, giving rise to key mechanistic insights.[121,110,111,122] Our group has recently investigated the effect of silane electronics[112] and sterics[115] on oxidative addition of Si–H bonds to Pd(0). While these reports offer foundational information on hydrosilylation using precious metal catalysts, analogous studies have not been carried out using catalysts with base metals.

Herein we report a Ni-catalyzed, branched-selective hydrosilylation system employing alkenes and 2° or 3° silanes. Taking inspiration from Montgomery's seminal work on (NHC)Ni-catalyzed allene[8,123] and alkyne[124] hydrosilylation systems, we demonstrate that structurally defined (NHC)Ni(0)[125,126] complexes are active for the branched-selective hydrosilylation of alkenes with both 2° and 3° silanes with broad electronic and steric scopes including the use of alkoxy- and chlorosilanes (**Figure 2.1.c.**). We additionally report mechanistic findings that establish a two-electron pathway proceeding via an insertion/elimination pathway. Data that

support our proposed mechanism were obtained using isotopic labeling studies, rate law determination, Hammett analyses, and ligand exchange experiments.

2.2 Results and Discussion

Catalyst Ligand Design

Our investigations commenced with evaluation of the effect of the NHC substituents on the hydrosilylation of styrene (**2a**) and H_2SiPh_2 (**3a**). Using (NHC)Ni(dvtms) derivatives **1a-1c** (**Figure 2.2.**) enabled steric variation of the NHC while keeping the supporting alkenyl ligands unchanged.[127,128] We hypothesized that smaller ancillary ligands would lead to more branched product, so we chose three readily synthesizable complexes: (ITMe)Ni(dvtms) (**1a**), (IMes)Ni(dvtms) (**1b**), and (IPr)Ni(dvtms) (**1c**). The $\%V_{bur}$ values of the corresponding ligands are a reflection of the steric imposition of the ligands and are in the ascending order of: ITMe (26.1) < IMes (36.5) < IPr (44.5) (values taken from ref. 129 at an M–C bond length of 2.00 Å).[129] As hypothesized, the catalyst with the smallest NHC, **1a**, gave the highest selectivity for the branched product (*l*/*b* = 1:2.0, 56% yield **4aa**), and the catalyst with the largest NHC, **1c** gave the lowest selectivity (*l*/*b* = 1:1.2, 12% yield **4aa**) (**Figure 2.2.**), with the medium-sized NHC complex (IMes)Ni(dvtms) giving intermediate selectivity and yield (*l*/*b* = 1:1.5, 21% yield **4aa**).

We next assessed the impact that the supporting alkene ligand has on reactivity and selectivity. We chose (IMes)Ni complexes as the platform from which to study the effect of alkenes because a library of (IMes)Ni(alkene)$_2$ complexes are known and readily synthesized.[130,125,126] Of the (IMes)Ni(alkene)$_2$ complexes we tested, (IMes)Ni(styrene)$_2$ (**1e**) gave the highest yield (*l*/*b* = 1:3.3, 49% yield **4aa**) and (IMes)Ni(1,5-hexadiene) (**1d**) gave the best selectivity (*l*/*b* = 1:8.1, 29% yield **4aa**). Attempts to combine the best NHC (ITMe) and the best supporting alkene (1,5-hexadiene or styrene) to form a discrete Ni complex, (ITMe)Ni(1,5-hexadiene) or (ITMe)Ni(styrene)$_2$, were unsuccessful; therefore, we proceeded to optimize the reaction conditions using **1e**, since it is easily synthesized and gave good yield and selectivity under unoptimized conditions. The reaction conditions were optimized to be 100 °C in toluene and using catalyst **1e**, product **4aa** was formed in 95% yield with exceptional branched selectivity of 1:>99 (*l*/*b*) (see Appendix A for full optimization).

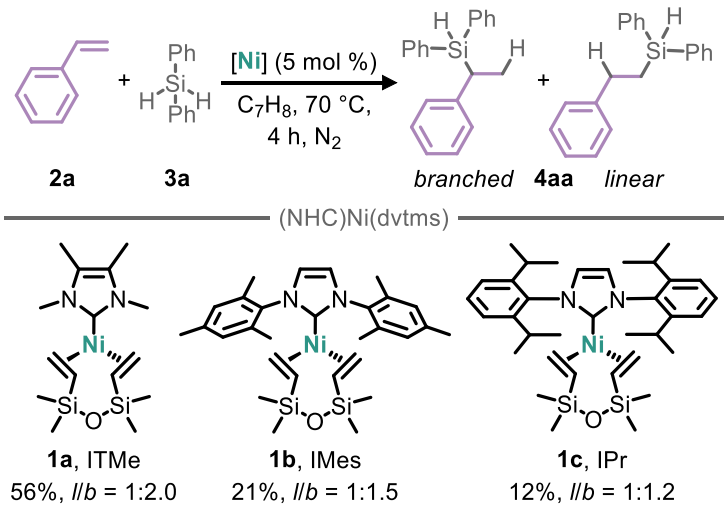

Figure 2.2. Hydrosilylation screen of **2a** and **3a** at 70 °C in toluene with a series of (NHC)Ni(dvtms) complexes to yield **4aa** (dvtms = 1,3-divinyltetramethyldisiloxane). Conditions: styrene (**2a**, 0.088 mmol, 1.0 equiv), H_2SiPh_2 (**3a**, 0.088 mmol, 1.0 equiv), (NHC)Ni(dvtms) (0.0044 mmol, 5.0 mol %), and toluene (0.40 mL). Selectivity and yields are determined by GC-MS analysis using mesitylene or durene as an internal standard.

Substrate Scope

With optimal conditions decided, we investigated the compatibility of complex **1e** with different alkene and silane substrates. Preliminary results reveal that pre-coordinated styrene on **1e** underwent hydrosilylation during what we hypothesize is catalyst activation, motivating us to use a slight excess of silane (1.1 equiv relative to added alkene). A series of 4-substituted styrene derivatives spanning across electron-donating (**2a**-**e**) and electron-withdrawing (**2f**,**g**) groups were well-tolerated in relatively high isolated yields (**4aa**-**4ga**, 68-92%) while maintaining excellent branched selectivity (*l*/*b* = 1:≥33, **Figure 2.3.**). Increasing the steric bulk of the alkene (**2h**-**j**) did not hinder reactivity (isolated yields of **4ha**-**4ja** were 71-88%) nor selectivity (*l*/*b* = 1:≥26). Substrate **2j** demonstrates the catalyst's ability to react with internal alkenes, giving product **4ja** (71%, *l*/*b* = 1:>99). This catalytic system also tolerates sensitive functional groups and heteroaromatics. The acetoxy-containing substrate **2k** was tolerated with moderate yield (59%) and excellent selectivity (*l*/*b* = 1:51) for **4ka**. 2-Vinyl-thiophene (**2l**) was tolerated well and furnished **4la** in a good yield of 74%, albeit with diminished yet good selectivity (*l*/*b* = 1:13) and a longer reaction time was required (24 h). We hypothesize the suppressed reaction rate results from competing coordination modes between Ni and the vinyl group versus the sulfur atom. Due

to the difficulty in purifying **4la** away from **4aa** (a byproduct of catalyst activation), catalyst (IMes)Ni(1,5-hexadiene) (**1d**) was used instead to avoid introducing styrene to the reaction. Formation of sulfur-containing product **4la** is especially remarkable since sulfur is known to poison Pt-based hydrosilylation catalysts.[31] Amino groups are also tolerated well, with 4-dimethylaminostyrene (**2b**) undergoing hydrosilylation in good yield (77%) with remarkable selectivity (*l*/*b* = 1:>99) to obtain product **4ba**. Terminal aliphatic alkenes are also well tolerated, although the selectivity was reversed to favor the linear product (**4ma-4oa**). These data demonstrate the necessity of an aryl ring to obtain the branched product, alluding to the intermediacy of a Ni-benzallyl intermediate. Without the presence of an aromatic moiety to stabilize a Ni-intermediate, the regiodivergent behavior may arise from steric hinderance provided by the alkyl substituent. This substrate-dependent reversal in selectivity is precedented in base metal hydrosilylation systems.[16,18,67,61,102,15,83,57,85]

Illustrating the breadth of catalyst **1e** to functionalize vinylarene derivatives, we further diversified the substrate scope by synthesizing a collection of electronically (**3b**-**3e**) and sterically modified diarylsilanes (**3f-i**) and examined their hydrosilylation reactivity with **2a**. The reactivity of **1e** with modified silanes maintained outstanding selectivity for the branched product (*l*/*b* = 1:>99) and achieved moderate to high isolated yields (51%-99%) to obtain products **4ab**-**4ae** (electronic modification) and **4af**-**4ai** (steric modification). Using H_2SiEt_2 (**3j**) in place of a diarylsilane proved to be quite successful, yielding 94% of **4aj** while preserving excellent selectivity (*l*/*b* = 1:20).

Having shown a wide range of 2° silanes to be effective in the hydrosilylation of alkenes, we next applied this catalytic system to 3° chlorosilanes, which are particularly relevant for industrial applications. We were pleased to find that **1e** is catalytically active for the hydrosilylation of **2a** and chlorosilanes (**3r**-**s**) to give **4ar**-**4as** in excellent yields (77-84%) and high branched selectivity (*l*/*b* = 1:>99). Hexanes was used in place of toluene as the reaction solvent for ease of product purification. Chlorosilanes are often not tolerated (or not investigated) in hydrosilylation reactions, and it has been demonstrated that early Ni-based catalysts enable the exchange of Si–Cl bonds for Si–H bonds, with the reduced products often being the major product.[107,108] *The inclusion of chlorosilanes in the substrate scope is a significant advance*, particularly in light of their relevance to polysiloxane chemistry.

In pursuit of expanding the identity of 3° silanes, we tested the hydrosilylation of triarylsilanes (**3k**-**m**) with **2a** using catalyst **1e**. **1e** indeed proved to be catalytically active for the hydrosilylation of $HSiPh_3$ (**3l**) and $HSi(4\text{-}CF_3\text{-}C_6H_4)_3$ (**3m**) with **2a** (74% yield, *l*/*b* = 1:>99 and 79% yield, *l*/*b* =1:>99, respectively), however not with $HSi(4\text{-}OMe\text{-}C_6H_4)_3$ (**3k**). Additionally, employing 3° silanes with one or more alkyl or alkoxy substituents ($HSiPh_2Me$ (**3n**), $HSiPhMe_2$ (**3o**), $HSi(OEt)_3$ (**3p**), and $HSi(Me)(OSiMe_3)_2$ (**3q**)) also proved to be unproductive using catalyst **1e**. These results encouraged us to revisit our catalyst's structure-activity relationship by modifying the steric bulk of the NHC ligand. We postulated that a less sterically bulky ligand (ITMe vs. IMes) would permit the hydrosilylation of challenging alkyl- and alkoxy-substituted silanes with **2a**. Due to the difficulty in elucidating the structure of the product formed in the attempted synthesis of $(ITMe)Ni(styrene)_2$, we hypothesized that the active catalyst could be formed in situ through the introduction of $Ni(cod)_2$ and ITMe (**Figure 2.3.**). This approach offers a practical alternative to isolation of an $(NHC)Ni(alkene)_2$ complex, and excitingly, enabled the formation of products **4ak**-**ao** formed from the hydrosilylation of **2a** with the challenging 3° silanes in good to excellent yields (74-94%) with branched selectivity (*l*/*b* = 1:>99). Like chlorosilanes, 3° alkoxy-substituted silanes are particularly relevant for industrial applications. Notably, alkoxy-substituted silanes (**3p**, **3q**) are also tolerated well under our conditions, forming products **4ap** and **4aq** in good yield (both 62%) and excellent branched selectivity (both *l*/*b* = 1:>99). Beyond vinylarene substrates, an aldehyde (**2p**) and ketones (**2q**, **2r**) readily reacted with $HSiPh_3$ (**3l**) to form **4pl**, **4ql**, and **4rl**, respectively, in high yields (94-99%) with only the O–silyl product formed.

Overall, the scope of silanes and alkenes that undergo hydrosilylation demonstrate the broad utility of this (NHC)Ni(0) catalyst system. We further show that the steric bulk of the NHC can be tuned to enhance yields with particularly unreactive silanes.

2.3 Conclusion and Outlook

Low-valent (NHC)Ni complexes are active pre-catalysts for the branched-selective hydrosilylation of olefins. Notably, the catalytic system developed is compatible with 3° silanes, including industrially relevant alkoxy- and chloro-containing silanes. The ability to use 3° silanes was accomplished through construction of a ligand structure-activity relationship: more sterically demanding silanes required a sterically smaller ancillary ligand, ITMe. A practical approach to

Figure 2.3. Scope of alkene hydrosilylation

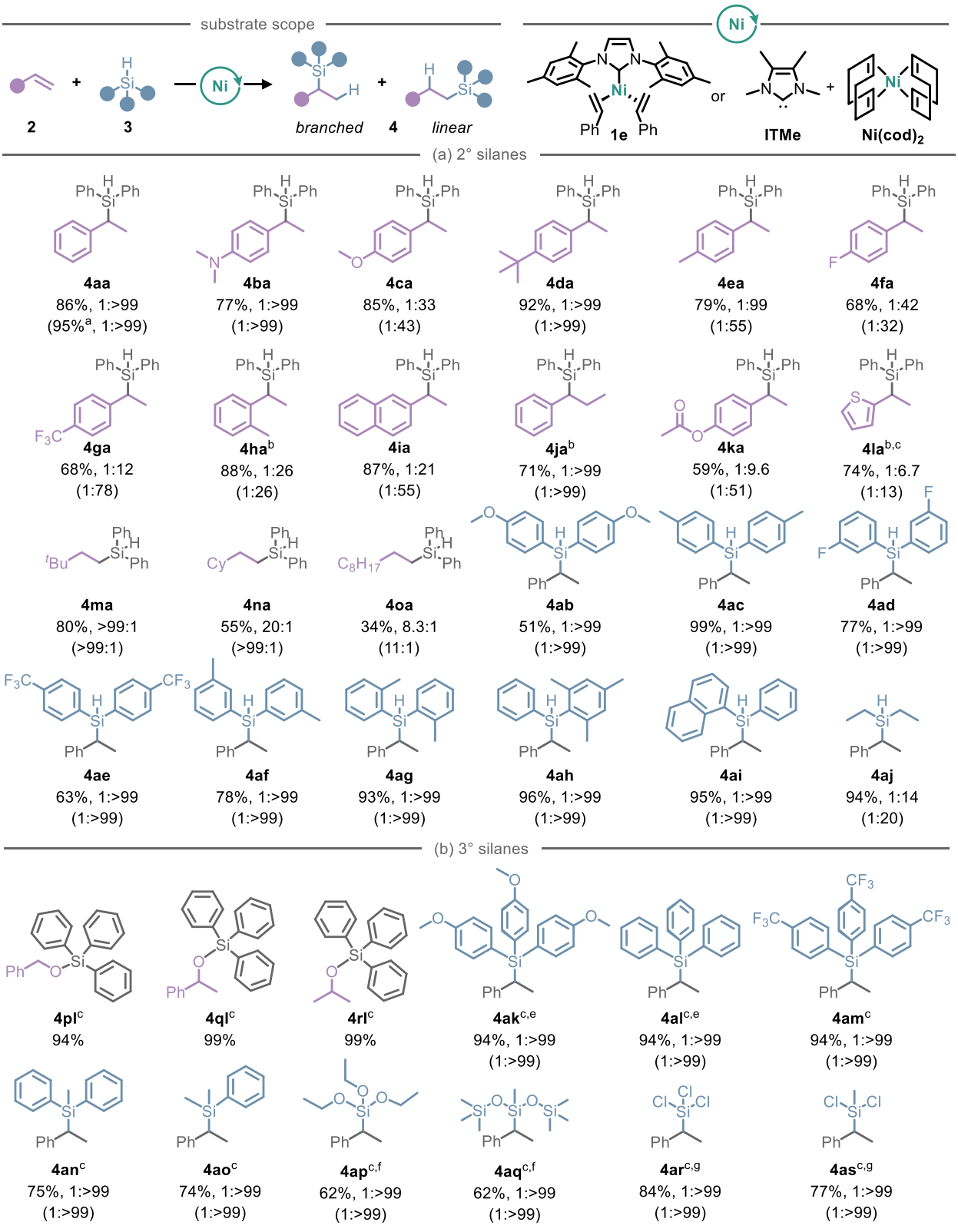

Isolated yields and selectivity (*l*/*b*) determined by relative integrations in the ^{1}H NMR are reported. Selectivity values in parentheses are determined by GC or GC-MS from the crude reaction mixture before purification and represent inherent catalyst selectivity. Conditions: **1e** (0.05 mmol, 5 mol %) or $Ni(cod)_2$ (0.05 mmol, 5 mol %) and ITMe (0.05 mmol, 5 mol %), alkene (**2a-2r**, 1.0 mmol, 1.0 equiv), silane (**3a-3s**, 1.1 mmol, 1.1 equiv), toluene (4.6 mL or 0.42 mL), 100 °C, 4 h, under N_2. [a]Reaction yield determined by GC using durene as an internal standard. [b]**1d** was used in place of **1e**. [c]24 h. [d]3 equiv **2a**. [e]2 equiv silane. [f]1.25 equiv silane, hexanes.

generating the (ITMe)Ni(0) pre-catalyst in situ was developed to expand reactivity. A larger NHC ligand, IMes, was found to be optimal for 2° silanes. Both sterically and electronically diverse silanes and styrenes are tolerated well, giving high selectivity for the branched product (often 1:>99, *l*/*b*) in good-to-excellent yields. Even functional groups like aryl esters and methoxy groups, which often react with low-valent Ni, are well-tolerated.

CHAPTER III

MECHANSITIC INVESTIGATION OF A HOMOGENEOUS (NHC)Ni(0)-CATALYZED ALKENE HYDROSILYLATION SYSTEM

This chapter includes previously published and co-authored material from Chang, A. S.; Kawamura, K. E.; Henness, H. S.; Salpino, V. M.; Greene, J. C.; Zakharov, L. N.; Cook, A. K. (NHC)Ni(0)-Catalyzed Branched-Selective Alkene Hydrosilylation with Secondary and Tertiary Silanes. *ACS Catal*. **2022**, *12*, 1102–11014. https://doi.org/10.1021/acscatal.2c03580. This article was written by Alison Sy-min Chang, with editorial assistance from Dr. Kiana E. Kawamura and Professor Amanda K. Cook. Dr. Kiana E. Kawamura and Victor M. Salpino contributed synthetically through the preparation of starting materials. Hayden S. Henness carried out rate law experiments. Jack C. Greene contributed intellectually.

3.1 Introduction

The Chalk-Harrod mechanism is the widely accepted reaction pathway for the hydrosilylation of alkenes by Pt catalysts (**Scheme 3.1.a.**).[131,29,13] The mechanism is comprised of four steps: *i*) oxidative addition of the H–Si bond to the Pt center, *ii*) olefin coordination, *iii*) olefin insertion into the Pt–H bond (which is both the regioselectivity- and rate-determining step[13]), and *iv*) reductive elimination of the organosilicon product. Alternatively, the modified Chalk-Harrod mechanism is often invoked to explain how the branched isomer forms; in this mechanism, the olefin inserts into the Pt–Si bond (**Scheme 3.1.b.**, step *iii*) instead of the Pt–H bond.[132,67] Xie and Fan,[133] who carried out mechanistic studies using a computational approach on Montgomery's (NHC)Ni-catalyzed (NHC = IPr or IPr*^{OMe}) hydrosilylation of allenes,[8,134] determined that the hydrosilylation of allenes proceeds via the modified Chalk-Harrod method with a ligand-to-ligand silyl transfer into the double-bond of the allene as the rate-determining step (RDS).[133] As is common with base metal catalysts, radical pathways must also be considered. Typically, the linear products of hydrosilylation are formed when a radical mechanism is operating;[29,54,63] this selectivity is due to the formation of a silyl radical, which then reacts with the alkene to give the more stable secondary alkyl radical; after H-atom abstraction from the metal-hydride, the linear

product is formed (Error! Reference source not found..**c.**).[29] Because fewer reports of branched-selective hydrosilylation exist than linear-

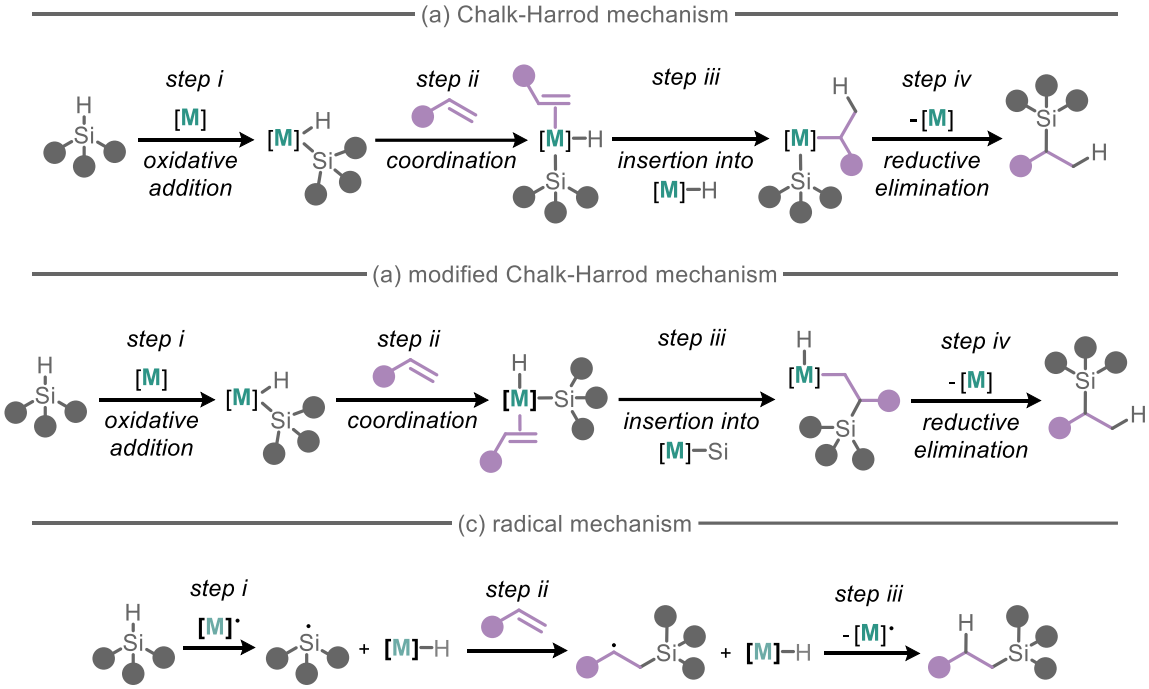

Scheme 3.1. Possible transition metal-catalyzed hydrosilylation mechanisms: (a) Chalk-Harrod mechanism, (b) modified Chalk-Harrod mechanism, and (c) a radical mechanism.

selective hydrosilylation, there is little insight into the mechanism of branched-selective hydrosilylation of alkenes. We therefore sought to answer the following mechanistic questions: 1) does the reaction proceed through a one- or two-electron pathway? 2) what is the impact of the silane substituents on reactivity? 3) how do alkene electronics affect (NHC)Ni stability and reactivity? and 4) what are the rate-determining steps (RDSs)?

3.2 Results and Discussion

One-Electron versus Two-Electron Pathway

Initial experiments were designed to identify whether **1e** is participating in a one- or two-electron pathway. We first monitored the formation of **4aa** using catalyst **1e** over time, both in the presence and absence of a radical trap: 1.1 equiv 1,1-diphenylethylene (DPE). If the hydrosilylation proceeds through an uncaged radical pathway (e.g., if either the silyl radical and/or

the alkyl radical depicted in **Scheme 3.1.c.** are uncaged), we hypothesized that the radical would diffuse and be trapped by DPE; this hypothesis assumes that the rate of diffusion of the radicals is

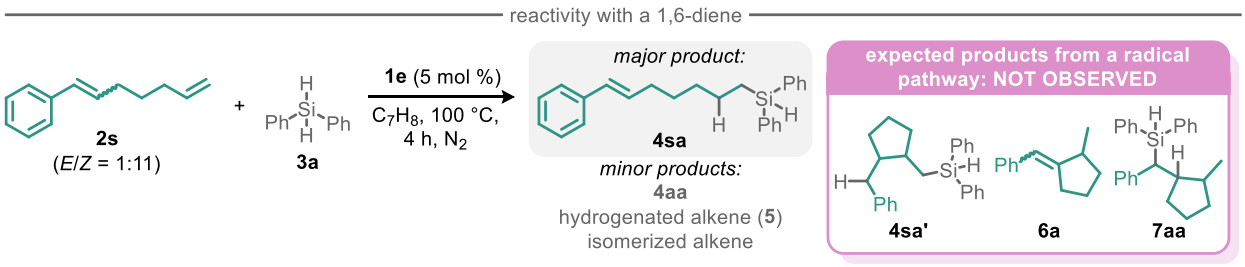

Scheme 3.2. 1e-catalyzed hydrosilylation of a 1,6-diene **2s** and **3a.** Conditions: **2s** (0.87 mmol, 1.0 equiv), **3a** (0.96 mmol, 1.1 equiv), **1e** (0.044 mmol, 5.0 mol %), toluene (4.0 mL), 100 °C, 4 h, under N_2.

faster than that of recombination. Addition of DPE did not affect the rate of formation or yield of **4aa** (Appendix C, section C.1.7.a.), nor was DPE active as a substrate in hydrosilylation with **3a**, likely due to the increased steric hinderance of DPE preventing alkene coordination to Ni. This result suggests that the mechanism is not proceeding through an uncaged radical mechanism.

Additional experimentation to assess if hydrosilylation is proceeding through a radical pathway led us to react **3a** with the 1,6-diene **2s**. If a radical pathway is operative, the 2° alkyl radical which is expected to form upon addition of the silyl radical to the terminal alkene (**Scheme 3.1.c.**, *step ii*) would undergo rapid intramolecular cyclization followed by H-atom transfer (HAT) from the Ni–H. Shown in **Scheme 3.2.**, the reaction of **2s** with **3a** and catalyst **1e** gave a mixture of isomerized (geometric and positional alkene isomerization), hydrogenated, and hydrosilylation products, with the major product being the terminally functionalized linear hydrosilylation product **4sa** (the internal alkene remained unreacted). This reaction selectivity is consistent with the linear-selective reactivity of **1e** with aliphatic substrates (e.g., see products **4ma**-**4oa** in **Figure 2.3.**). No cyclized product **6a** was observed by ^{1}H NMR or GC-MS. We also do not observe cyclization that would occur from other radical pathways (e.g., HAT prior to silyl addition leading to products **6a** and/or **7aa**). To validate this conclusion, we independently synthesized the cyclized alkene **6a** and subjected it to hydrosilylation with **3a** by **1e** under identical reaction conditions. **6a** did not undergo hydrosilylation, nor was it observed in the hydrosilylation of **2s**. The results from these two radical trap experiments are inconsistent with a radical mechanism. We continued with mechanistic studies to gain further understanding of the reaction mechanism.

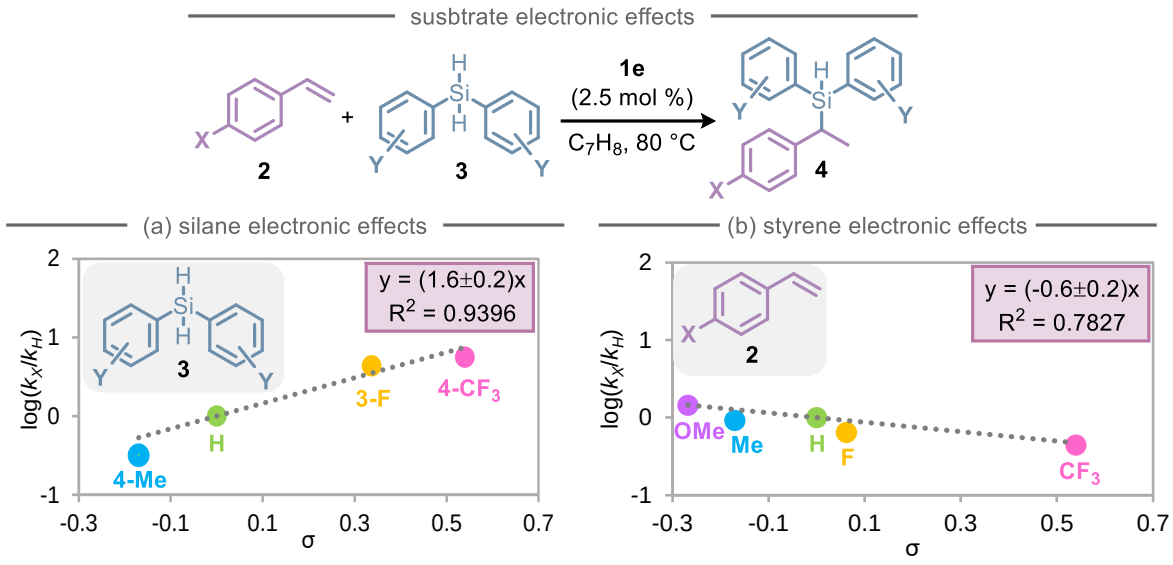

Figure 3.1. Hammett plots for **1e**-catalyzed hydrosilylation of (a) electronically modified diarylsilanes (**3a**,**b**,**d**,**e**) with **2a** and of (b) electronically modified vinylarenes (**2a**,**c**,**e-f**) with **3a**. Conditions: vinylarene (0.13 mmol, 1.0 equiv), diarylsilane (0.14 mmol, 1.1 equiv), **1e** (0.0030 mmol, 2.5 mol %), and toluene (2.4 mL, 0.060 M), 80 °C, under N_2. Yields are determined by calibrated GC analysis using mesitylene as an internal standard.

Linear-Free Energy Relationships

As electronic variation of both the silane and styrene derivatives were tolerated (**Figure 3.3.**), we next sought to quantify the electronic influence of each component on the rate of hydrosilylation. Using the method of initial rates, we first varied the electron-richness of the silane by incorporating electron-withdrawing and electron-donating groups at the 3- or 4-position of diarylsilanes (**3a**, **c-e**; **Figure 3.1.a.**). Using our optimized conditions, the rates of reaction were too fast to measure accurately, especially for electron-poor silanes (e.g., **3e**). To decrease the rate of the reaction, we modified the reaction conditions (temperature lowered to 80 °C, catalyst loading decreased to 2.5 mol %, and decreased reaction concentration to 0.060 M), which allowed for reliable measurements of reaction rates. Hammett analysis (**Figure 3.1.a.**) shows that the reaction is faster with electron-poor silanes with a sensitivity coefficient of $\rho = +1.6 \pm 0.2$. Our group has shown that oxidative addition of Si–H bonds to Pd(0) is faster and more favorable with electron-poor silanes,[112] suggesting that oxidative addition is one of the RDSs in hydrosilylation.

Analogous analysis with styrene derivatives (**2a**, **c**, **e-g**) shows a trend opposite to that of the silane: rates are faster with electron-rich alkenes, and the magnitude of the sensitivity factor is

smaller (ρ = -0.6 ± 0.2) than that of the silane (**Figure 3.1.b.**). Notably, our data are consistent with migratory insertion of vinylarenes into Rh–H[135] and Nb–H[136] bonds but is inconsistent with insertion into Pd–N[137] and Pd–C[138] bonds. These data point toward migratory insertion of the alkene into the Ni–H bond ([2,1]-insertion) operating during the catalytic cycle (Chalk-Harrod mechanism, **Scheme 3.1.a.**) and not insertion into the Ni–Si bond (modified Chalk-Harrod mechanism, **Scheme 3.1.b.**). The effect that electronic modulation of both substrates has on the observed rate of reaction provides evidence that both substrates are involved in the steps between the catalyst resting state and the RDS.

Deuterium Labelling Studies

Having obtained evidence supporting the Chalk-Harrod mechanism being operative (see Hammett analyses above), we next sought to support this conclusion further and to obtain a better understanding on factors influencing the regioselectivity and the reversibility of migratory insertion steps. To do so, we embarked on deuterium-labeling experiments with D_2SiPh_2 (**3a-*d*$_2$**) (**Figure 3.2.**). Starting from the [(styrene)Ni(D)(silyl)] complex **C** (**Figure 3.2.a.**), the first step is insertion of the alkene into the Ni–D bond to form **D**. This intermediate can either proceed via *path a* or *path b*. *Path a* is direct reductive elimination to form **4aa-*d*$_2$'**, which leads to 100% deuterium incorporation at Si and 33% deuterium incorporation at the methyl group (the other 66% are protium originating from **2a**). *Path b* consists of intermediate **D** undergoing β-hydride elimination to give **E**, Ni–H/Si–D scrambling via reductive elimination of Si–D and oxidative addition of Si–H to form **F**, migratory insertion of the alkene into the Ni–D bond to form **G**, followed by reductive elimination to give isotopomer **4aa-*d*$_2$''**, in which 0% deuterium incorporation is expected at Si and 66% is expected at the methyl position. Notably, both pathways *a* and *b* do not predict incorporation of deuterium at the benzylic position of **4aa**. If the modified Chalk-Harrod mechanism (**Scheme 3.1.b.**) were operative, significant D-incorporation at the benzylic position would be expected (from reversible migratory insertion/β-hydride elimination analogous to that depicted in **Figure 3.2.a.**), as would the formation of dehydrogenative silylation byproducts, which are not observed under our reaction conditions.

The reaction between 5 mol % **1e**, 1.0 equiv **2a**, and 1.1 equiv **3a-*d*$_2$** at 100 °C produced **4aa-*d*$_2$**, which was characterized and analyzed by ^{1}H and ^{2}H NMR spectroscopy. At the end of the

reaction, approximately 56% deuterium erosion was observed at the Si–D bond, 3% deuterium incorporation was detected at the benzylic position, and 45% deuterium incorporation was detected

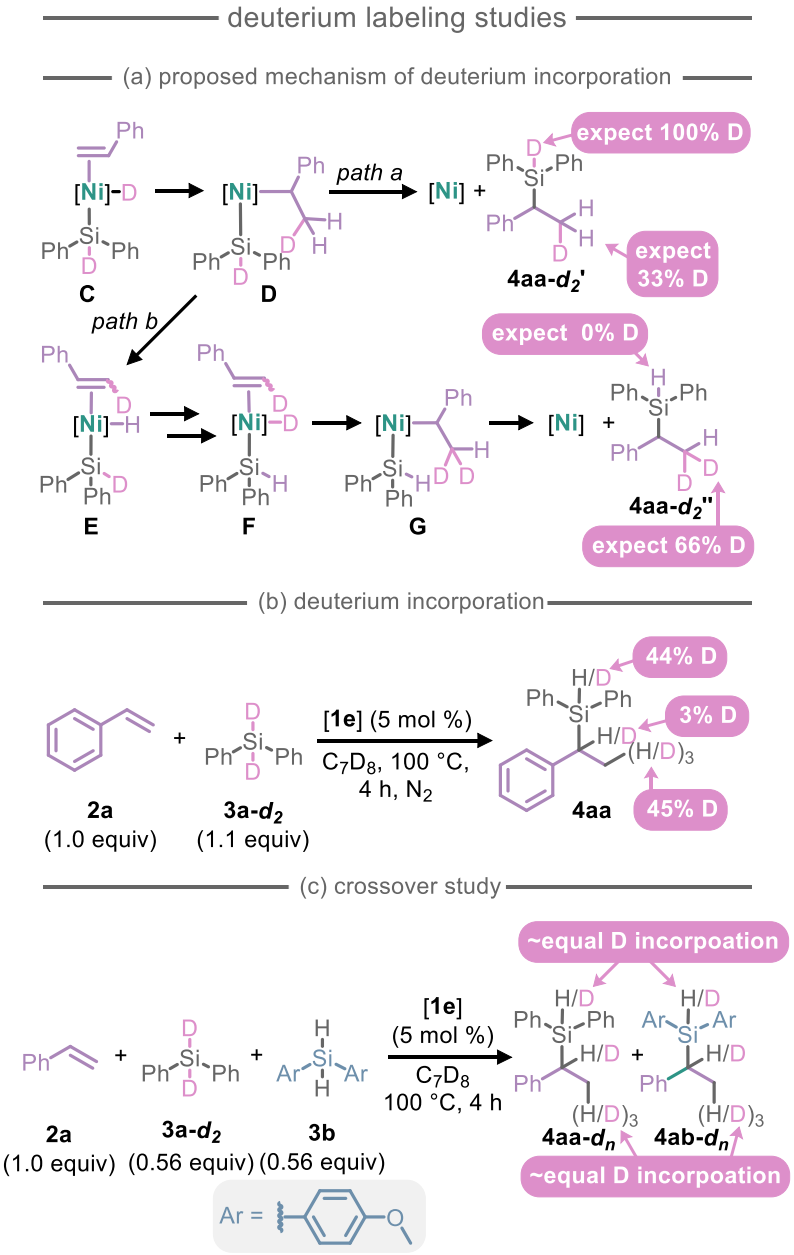

Figure 3.2. Deuterium labeling studies. a) Expected outcomes of deuterium incorporation via Chalk-Harrod pathway for hydrosilylation, b) deuterium labeling studies with **2a** and **3a-d₂**, and c) crossover study with **2a**, **3a-d₂**, and **3b**.

at the methyl position (**Figure 3.2.b.**). The lack of significant deuterium incorporation at the benzylic position supports our conclusion that the modified Chalk-Harrod mechanism is not

operative (i.e., the alkene inserts into the Ni–H and not into the Ni–Si bond). The measured deuterium distribution in **4aa-*d*$_2$** alludes to both *path a* and *path b* being operative and the Chalk-Harrod mechanism as the major mechanistic pathway.

To further support an insertion/elimination pathway involving alkenes formed after deuterium incorporation (**E** and **F** in **Figure 3.2.a.**), a crossover experiment was designed using 0.56 equiv **3a-*d*$_2$** and 0.56 equiv $H_2Si(4\text{-}OMe\text{-}C_6H_4)_2$ (**3b**) reacting with 1.0 equiv **2a** (**Figure 3.2.c.**). Deuterium crossover was indeed obtained, as determined by ^{1}H and ^{2}H NMR. Integration of the Si–H/D peaks gives an approximate ratio of 1.1:1 (**4aa-*d*$_n$**/**4ab-*d*$_n$**), as does the integration of the methyl peaks (**Figure 3.2.c.**, **Figure B.5.**, **B.6.**). This result points towards an insertion/elimination pathway. A supplementary experiment was performed to probe the reversibility of this insertion/elimination step by monitoring the hydrosilylation of **2a** and **3a-*d*$_2$** by **1e** by *in operando* ^{2}H NMR (**Figure 3.3.**). Heating the reaction to 75 °C for 20 min, a prominent peak at 5.60 ppm corresponding to a deuterium on the alkene in **2a** appears. The growth of this peak indicates that **1e** readily exchanges hydrogen and deuterium from **2a** to **3a-*d*$_2$** prior to **4aa** formation. In addition to the peak at 5.60 ppm, the appearance of a smaller peak at 2.60 ppm at 20 min corresponds to coordinated **2a-*d*$_n$** on **1e**. Throughout the reaction, the peaks at 2.60 and 5.60 ppm gradually disappear as they become incorporated into **4aa-*d*$_n$**. These result support our conclusion that migratory insertion and β-hydride elimination are reversible, and suggest that reductive elimination is the final step of the set of rate-limiting steps.[138]

To gather additional insight on the RDS, a kinetic isotope effect (KIE) was measured by comparing the rates of hydrosilylation of **2a** with **3a** or **3a-*d*$_2$** at 80 °C. Using the method of initial rates, we obtained an inverse KIE of 0.64 ± 0.06. Inverse KIE values have been reported for systems with a reversible pre-equilibrium step that involves a hydride-insertion/elimination step prior to the RDS.[139–141] Inverse KIEs found in C–H activation reactions result from a multistep reaction that reflects a composite of an equilibrium isotope effect (EIE) and a KIE.[136,142,143] Applying this concept to our system, the observed isotope effect is a combination of EIEs and KIEs, since we showed that migratory insertion/β-H elimination and Si–H oxidative addition/reductive elimination steps are reversible.

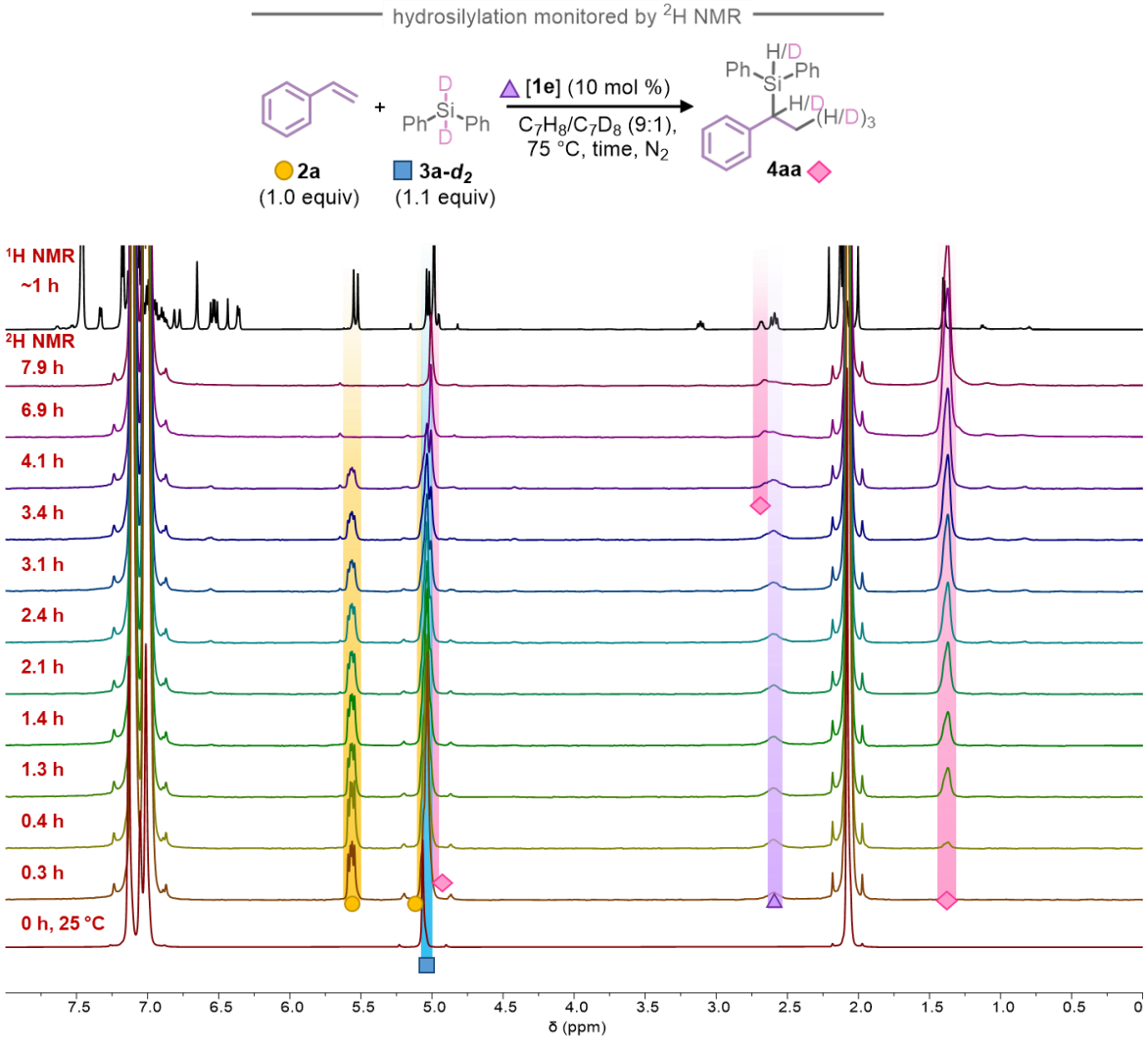

Figure 3.3. ^{2}H NMR monitoring of the hydrosilylation of **2a** and **3a-*d*$_2$** by **1e** over time at 75 °C. ^{1}H NMR spectrum shown on the top is used as a reference for starting materials, catalyst, and product. Conditions: **2a** (0.14 mmol, 1.0 equiv), **3a** (0.15 mmol, 1.1 equiv), **1e** (0.013 mmol, 10 mol %), C_7H_8/C_7D_8 (9:1, 0.6 mL, 0.22 M), under N_2.

Rate Law Determination

To further understand the reaction mechanism, we next sought to determine the reaction's rate law (Appendix B, **Section B.1.6.c.**). The order of each of the reagents **2a** and **3a** and catalyst **1e** was obtained by measuring the initial rates of reaction at varying concentrations of the reagent or catalyst. First, we measured the rate of product **4aa** formation as a function of **1e** concentration (2.19–21.9 mM). Under standard reaction conditions, the rates are too quick to obtain initial rates of reaction; therefore, the reaction temperature was decreased to 80 °C. The **1e**-catalyzed

hydrosilylation of **2a** and **3a** displayed half order dependence on [Ni] (0.6 ± 0.1). This value is in line with previously reported, monomeric catalysts that are activated by a pre-equilibrium ligand dissociation.[144–146] Next, we determined that there is an inverse order in **2a** (-0.4 ± 0.1), indicating that dissociation of **2a** from Ni is an important step between the catalyst resting state and the RDS.[144] The influence of olefin coordination to Ni is supported by our data from the Hammett study (**Figure 3.1.b.**) as well as the ligand exchange equilibrium study (**Figure 3.2.**). Lastly, we determined that the reaction is first order (1.0 ± 0.1) in **3a**, which correlates well with the reaction rate's dependence on silane electronics (**Figure 3.1.a.**).

Eyring Analysis

To shed light on the overall kinetic barrier of the reaction, the rates of reaction were measured at temperatures between 60 and 100 °C and an Eyring plot was constructed. The following values were obtained: $\Delta H^{\ddagger}$ = 20.4 ± 0.2 kcal·mol^{-1}, $\Delta S^{\ddagger}$ = -0.28 ± 0.2 cal·mol^{-1}·K^{-1}, and $\Delta G^{\ddagger}_{373K}$ = 20.5 ± 0.2 kcal·mol^{-1} (Appendix B, **Section B.1.6.b.**). A $\Delta S^{\ddagger}$ value that is close to zero suggests that the transition state of the RDS is not very ordered or disordered, which supports our conclusion that oxidative addition (*step ii*) and alkene coordination (*step iv*) are not the RDS, as both would give large, positive values of $\Delta S^{\ddagger}$. The data from the Eyring plot is consistent with either migratory insertion (*step iii*) or reductive elimination (*step v*) being the RDS (**Figure 3.4.**).

Compilation of Mechanistic Data

Figure 3.4. shows the proposed mechanism that is most consistent with the data we collected. **1e** enters the catalytic cycle by alkene dissociation (*step i*), and then oxidatively adds the silane to form an (IMes)Ni(styrene)(silyl)(H) complex (*step ii*). *Step iii* is migratory insertion of the coordinated styrene into the Ni–H bond, resulting in the (IMes)Ni(alkyl)(silyl) complex with an open coordination site, which is then filled by coordination of styrene in *step iv* to form the 16-electron complex, (IMes)Ni(alkyl)(silyl)(styrene). Reductive elimination (*step v*) of the alkyl and silyl ligands forms the C–Si bond, releases the product, and regenerates the active catalyst, (IMes)Ni(styrene)$_2$.

The radical trap experiments support our hypothesis that the reaction is not proceeding via a one-electron pathway. Monitoring the reaction by ^{1}H NMR shows that complex **1e** is the resting state when using styrene **2a** as the substrate. Analysis of mixtures of **1e** and electronically varied styrene derivatives shows that the alkene dissociation and coordination to Ni is rapid and

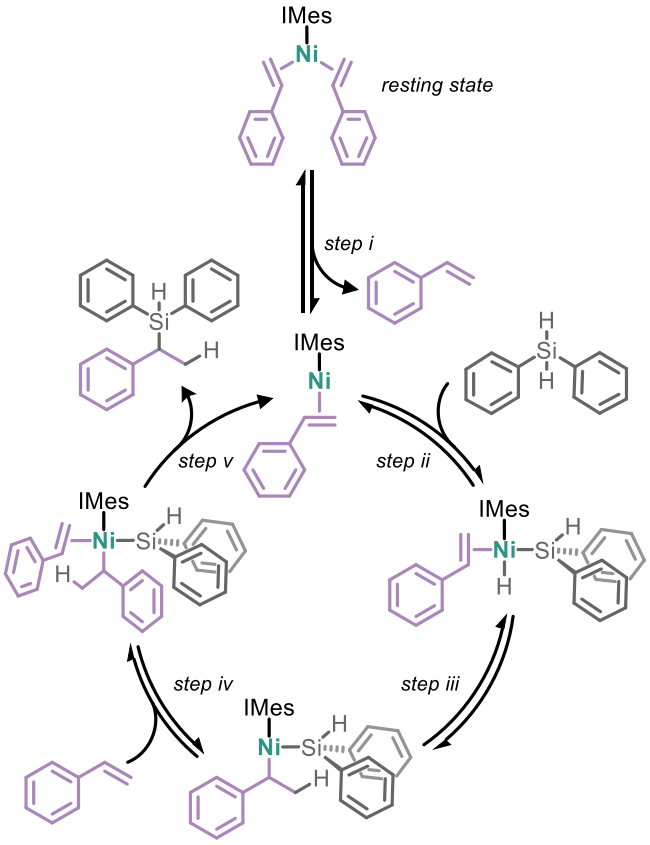

Figure 3.4. Proposed catalytic cycle for the hydrosilylation of **2a** and **3a** by **1e**.

reversible; additionally, the order in **2a** was found to be inverse. These data support dissociation of the alkene (**Figure 3.4.**, *step i*) occurring between the resting state and the RDS. (NHC)Ni complexes are known to oxidatively add Si–H bonds,[147,148] supporting the viability of *step ii*. First-order dependence on the silane and the fact that the rate of the reaction is dependent on the electronics of the silane show that *step ii* is either the RDS or lies between the catalyst resting state and the RDS. The erosion of deuterium at Si in the deuterium-incorporation experiment (**Figure 3.2.b.**) suggests *that step ii* is reversible and therefore likely not the final RDS.

Because of the strong σ-donation of the silyl group, making it a very strong trans influence ligand, the alkene, which is the weakest trans influence ligand, is trans to the silyl group and cis to the hydride ligand. The easiest pathway is then migratory insertion into the Ni–H. Styrene derivatives undergo [2,1]-insertion, the product of which is likely stabilized by the benzallyl

bonding mode. With aliphatic substrates, there is no additional electronic stabilization to favor [2,1]-insertion; therefore, sterics dominate and [1,2]-insertion occurs, leading to the linear product. Likewise, the deuterium scrambling seen in the reaction between **2a** and **3a-*d*$_2$** support that *step iii* is partially reversible. The lack of deuterium incorporation at the benzylic position in the deuterium-incorporation experiment supports our conclusion that migratory insertion of the alkene occurs with the Ni–H bond (*step iii*) and not the Ni–Si bond.

The inverse KIE observed with **3a** and **3a-*d*$_2$** results from a combination of a KIE of the RDS and the EIEs of *steps ii* and *iii*. An inverse secondary KIE observed with **2a** and **3a-*d*$_2$** is consistent with the migratory insertion in *step iii* being the RDS or before the RDS due to the change in hybridization from C(sp^2) in the alkene to C(sp^3). The reaction's rate law and the activation parameters determined from the Eyring analysis support the viability of migratory insertion (*step iii*) and/or reductive elimination (*step v*) being the RDS. Further confirmation from the in operando ^{2}H NMR studies indicate that migratory insertion is highly reversible and therefore reductive elimination is indeed the RDS. Altogether, our data supports that this branched-selective hydrosilylation follows a Chalk-Harrod mechanism with migratory insertion of the alkene occurring into the Ni–H bond.

3.3 Conclusion

In-depth mechanistic studies using catalyst **1e** allude to a Chalk-Harrod-type mechanism in which the alkene inserts into the Ni–H bond of the (silyl)Ni–H species that forms after oxidative addition of Ni(0) to the Si–H bond of the silane. Mechanistic experiments suggest against a radical pathway being operative. The catalyst resting state is the pre-catalyst **1e**, which is described in Chapter IV. The observed electronic influence of both the alkene and the silane suggests the involvement of both substrates in the RDS. This conclusion is further supported by both the ligand exchange reactions (see Chapter IV details) with **1e** and electronically varied styrenes as well as the reaction's rate law. The compilation of our mechanistic data points towards reductive elimination being the RDS.

CHAPTER IV

INVESTIGATIONS OF (NHC)Ni(STYRENE)$_2$ ELECTRONIC STRUCTURES AND THEIR RELATION TO ALKENE HYDROSILYLATION

This chapter includes previously published and co-authored material from Chang, A. S.; Kawamura, K. E.; Henness, H. S.; Salpino, V. M.; Greene, J. C.; Zakharov, L. N.; Cook, A. K. (NHC)Ni(0)-Catalyzed Branched-Selective Alkene Hydrosilylation with Secondary and Tertiary Silanes. *ACS Catal*. **2022**, *12*, 1102–11014. https://doi.org/10.1021/acscatal.2c03580. This article was written by Alison Sy-min Chang, with editorial assistance from Dr. Kiana E. Kawamura and Professor Amanda K. Cook. Dr. Kiana E. Kawamura and Victor M. Salpino contributed synthetically through the preparation of starting materials. The unpublished work in Chapter IV was developed and experimentally carried out by Alison Sy-min Chang.

4.1 Introduction

The discovery of N-heterocyclic carbenes (NHC) only three decades ago benchmarked the rapid development of various NHC-ligated complexes.[149–151,126] NHCs have been combined with transition metals from group 10 (*i.e.*, Ni, Pd, and Pt) to develop rather active homogeneous catalysts for cross-coupling[152], hydrosilylation[8,124], cycloaddition[153], and amination reactions[154], to list a few. NHCs are a well-developed class of ancillary ligands in transition metal catalysts largely due to their modifiable steric and electronic properties that can tune the reactivity of the metal center. This modularity is achieved through the synthetically accessible substitution of the NHC backbone and of the *N*-moieties, making them great ligands to screen and construct catalyst structure-activity relationships. As both the steric and electronic components of NHCs can readily influence catalyst behavior, the evaluation of such parameters has been deeply studied. Specifically, the steric parameter of NHCs measures the total volume that the NHC occupies in the first coordination sphere of the metal is known as percent buried volume (%V_{Bur}).[155,126] One method to quantify the electronics of NHCs is through the Tolman electronic parameter (TEP).[156] TEP was originally developed to assess phosphine electronics through simple substitutions on the phosphorous atom and has now been an adopted method to apply to NHC electron donating ability.

TEP values are achieved by measuring the CO stretch of the CO ligand trans to the NHC in $(NHC)M(CO)_x(X)_y$ complexes by IR to relate the electron density in wavenumbers.[127] Both $\%V_{Bur}$ and TEP are powerful methods commonly applied to optimizing catalytic systems, and the information extracted from these systems can benefit future catalyst design.

Within group 10 metals, (NHC)Ni catalysis has been of great interest largely due to the Earth-abundance and versatile reactivity of Ni. Outlined in Chapter II, our group has developed an (NHC)Ni(0)-catalyzed alkene hydrosilylation system for vinyl arenes and 2° and 3° silanes. The establishment of a homogeneous hydrosilylation catalyst inspired us to extract more information on the electronic structure of the $(NHC)Ni(styrene)_2$ complexes and relate these findings to catalytic activity. In constructing a comprehensive understanding of the factors that influence stability, we also sought to understand the mechanism of the (NHC)Ni-catalyzed alkene hydrosilylation system. A few questions to address in this chapter are the following, 1) what affects catalyst stability? 2) what is the resting state of the catalyst? 3) how does NHC modification affect catalytic activity? This chapter describes the examination of electronic alteration of the pre-coordinated styrene through ligand exchange experiments and how it affects Ni catalyst stability and hydrosilylation reactivity. Additionally, initial mechanistic explorations of the $(IMes)Ni(styrene)_2$ catalyst are presented here using ^1H NMR resting state analysis. Lastly, a series of electronically and sterically altered NHC ligands were tested to understand what ligand properties assist in catalyst behavior, and the oxidation potential of these $(NHC)Ni(styrene)_2$ complexes were probed using cyclic voltammetry (CV).

4.2 Results and Discussion

Investigation of Electronic Influence on (IMes)Ni(0) Complexes

After establishing the alkene substrate scope and observing the influence that electronically modified styrenes affect (IMes)Ni kinetics, we sought to investigate whether the resulting active catalyst formed was dependent on styrene identity. Therefore, to deconvolute the initial rates of reaction with possible ligand exchanges at Ni between the pre-coordinated styrene and free 4-substituted styrene substrate, we devised an experiment to further probe the styrene electronic contributions using styrenes **2c** (OMe), **2f** (F), and **2g** (CF_3). We measured the equilibrium

constants (K_{eq}) of the ligand exchange reaction between **1e** and styrene derivatives via ^{1}H and ^{19}F NMR spectroscopy (**Figure 4.1.**).

Reacting complex **1e** with 2.0 equiv of electronically varied styrenes (**2c**, **2f**, **2g**) in C_7D_8 at 75 °C for 4 h, a distribution of products consisting of the starting complex **1e**, a monosubstituted 4-X-styrene complex (**A**), a disubstituted 4-X-styrene complex (**B**), uncoordinated styrene, and

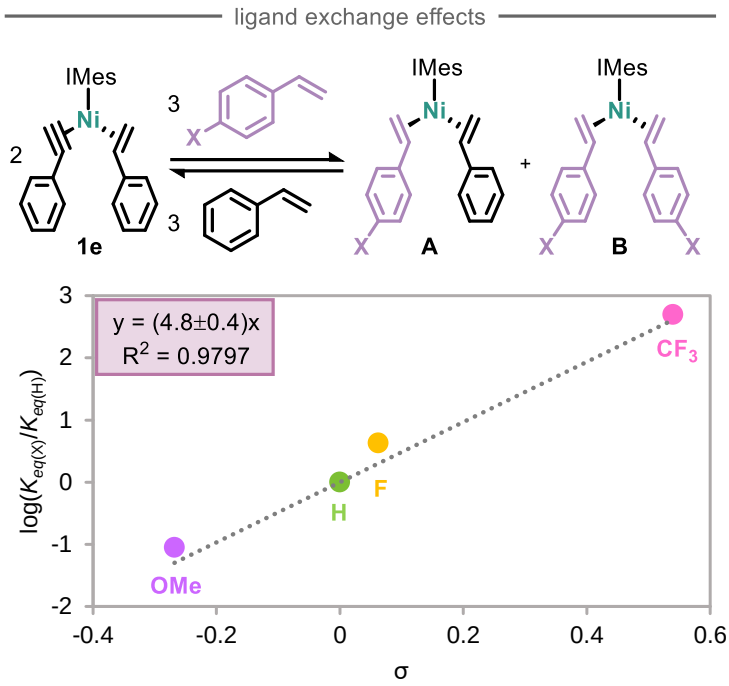

Figure 4.1. Hammett plot for the ligand exchange between **1e** and corresponding 4-X-styrene derivative (X = OMe, F, or CF_3) to form a mixture of complexes **A** and **B**. Conditions: **1e** (0.013 mmol, 1.0 equiv), **2c**, **2f** or **2g** (2.0-2.1 equiv, 0.026-0.027 mmol), C_7D_8 (0.60 mL, 0.22 M), under N_2. Concentrations of each species in solution was determined by integrations found in the ^{1}H NMR spectra.

uncoordinated styrene derivative was observed (**Figure 4.1.**). A Hammett plot was constructed employing the following derived equilibrium expression (See Appendix C, section C.1.5.a. for derivation):

$$K_{eq} = \frac{[\mathbf{A}][\mathbf{B}][\text{styrene}]^3}{[4\text{–X–styrene}]^3[\mathbf{1e}]^2} \qquad (1)$$

A significant ρ value of +4.8 ± 0.4 was obtained, which reveals that ligand exchange from the bis-styrene complex **1e** is more favorable with more electron-deficient vinylarene derivatives.[135,136]

Notably, this trend for alkene coordination, which is a thermodynamic measurement, is opposite to the trend for the rate of hydrosilylation, a kinetic effect. Taken together, the kinetic trend observed in hydrosilylation is influenced by the ground-state effect: rates with electron-rich alkenes are faster because the alkene-Ni complex is higher in energy. Mechanistically, these data imply that *a ligand exchange process is occurring between precatalyst **1e** and/or the resting state of the catalyst and the RDS.*

Catalyst Resting State and Decomposition Products

To identify the resting state of the catalyst, we performed in operando studies using ^{1}H NMR spectroscopy. We began with our simplest conditions: **2a**, **3a**, and **1e** as the catalyst (10 mol % of **1e** was used to facilitate observation of the Ni species present) reacting in C_7D_8 at 75 °C (**Figure 4.2.**). Conversion of **2a** and **3a** to product **4aa** in 92% yield was observed. Notably, the selectivity of this reaction is moderate (*l*/*b* = 1:10), which is consistent with reactions at lowered temperatures (see **Table A.2.**). The only Ni species detected during the course of the reaction was complex **1e**, demonstrating that ***1e** is the resting state of the catalyst when **2a** and **3a** are used.*

To observe the influence that styrene derivatives have on the resting state of the catalyst, analogous studies were carried out using 4-OMe-styrene (**2c**), **3a**, and **1e** as the catalyst. We questioned whether the resting state would be complex **1e** or (IMes)Ni(4-OMe-styrene)$_2$ (**1h**) because **1e** is more stable than **1h** (as demonstrated by the Hammett plot in **Figure 4.1.**), but there is a large excess of **2c** relative to **1e**, which would favor formation of **1h**. The major Ni species observed during catalysis is indeed **1h**, which reveals that the excess of **2c** is sufficient to overcome the increased stability of **1e** compared to **1h** (**Figure 4.2.**). Because **1h** is less stable than **1e** and **1h** is the major species formed and is therefore the resting state during catalysis, we can conclude that *the ground-state stability of the catalyst resting state contributes to the increased rate of hydrosilylation with electron-rich alkenes.*

After reaction completion using **2a**, **3a**, and **1e** as the catalyst, an emergent peak at -2.30 ppm assignable to a novel Ni dimer complex **1g** was detected (**Figure 4.3.**). This complex was isolated and fully characterized by NMR spectroscopy as well as by single-crystal X-ray crystallography (see Appendix C, section C.1.3.). To test the competency of **1g** as a catalyst, we subjected this Ni dimer to the hydrosilylation of **2a** and **3a** under standard reaction conditions. The hydrosilylation product **4aa** was indeed obtained in 74% yield, albeit with regioselectivity favoring

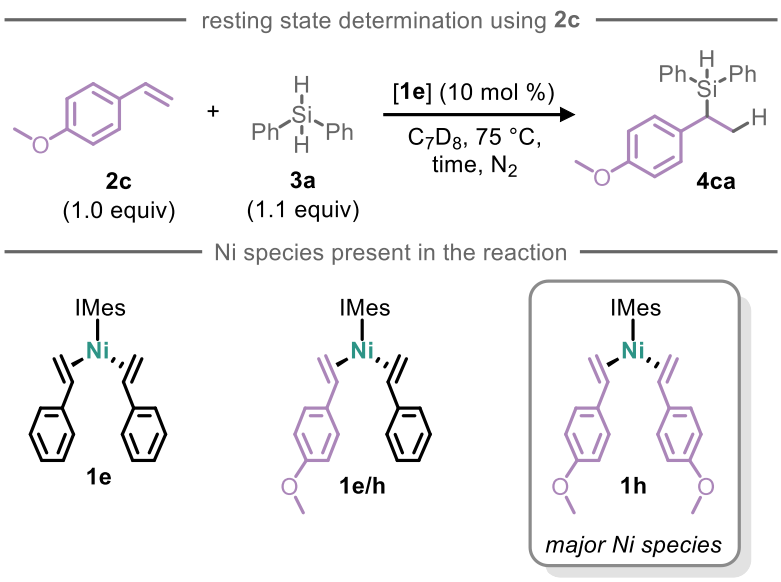

Figure 4.2. ^{1}H NMR monitoring of the hydrosilylation of **2c** and **3a** by **1e** over time at 75 °C. Conditions: **2c** (0.13 mmol, 1.0 equiv), **3a** (0.14 mmol, 1.1 equiv), **1e** (0.013 mmol, 10 mol %), C_7D_8 (0.6 mL, 0.22 M), under N_2. Yield calculated using mesitylene as an internal standard. Bottom: spectroscopically observed Ni species in solution with the major species being **1h**.

the linear isomer (*l*/*b* = 1:0.9), which contrasts with that obtained when **1e** is used as the catalyst (Table S1). Due to the divergent selectivity of **1g** compared to **1e** under identical reaction conditions in conjunction with observing the formation of **1g** only at the end of the reaction, we attributed the formation of **1g** to catalyst decomposition rather than catalyst activation. Stoichiometric studies between **1e** and **3a** were done to further understand the inclination of **1e** to convert to **1g**. Treating **1e** with 2.0 equiv **3a** in C_7D_8 yielded a mixture of **1g**, **1e**, and **4aa** (1.0:1.4:2.0, respectively) within 5 minutes (see Appendix C). Therefore, we conclude that **1e** is susceptible to degradation into **1g** in the absence of excess alkene.

To further confirm that **1e** is not degrading during the reaction, "same excess" experiments from the Visual Kinetic Analysis approach to mechanistic studies was used (**Figure 4.4.**).[157] Two reactions were performed side-by-side: reaction A used the standard conditions (0.22 M **2a**, 0.24 M **3a**, 0.011 M **1e**), and reaction B used altered reaction conditions with decreased initial concentrations of reactants **2a** and **3a** (0.13 M **2a**, 0.14 M **3a**, 0.011 M **1e**). After time adjustment, the reaction profiles ([**4aa**] versus time) overlay, indicating that the catalyst is not decomposing

(**Figure 4.4.a.**). Additionally, a third experiment, reaction C, used the same conditions as reaction B but with the

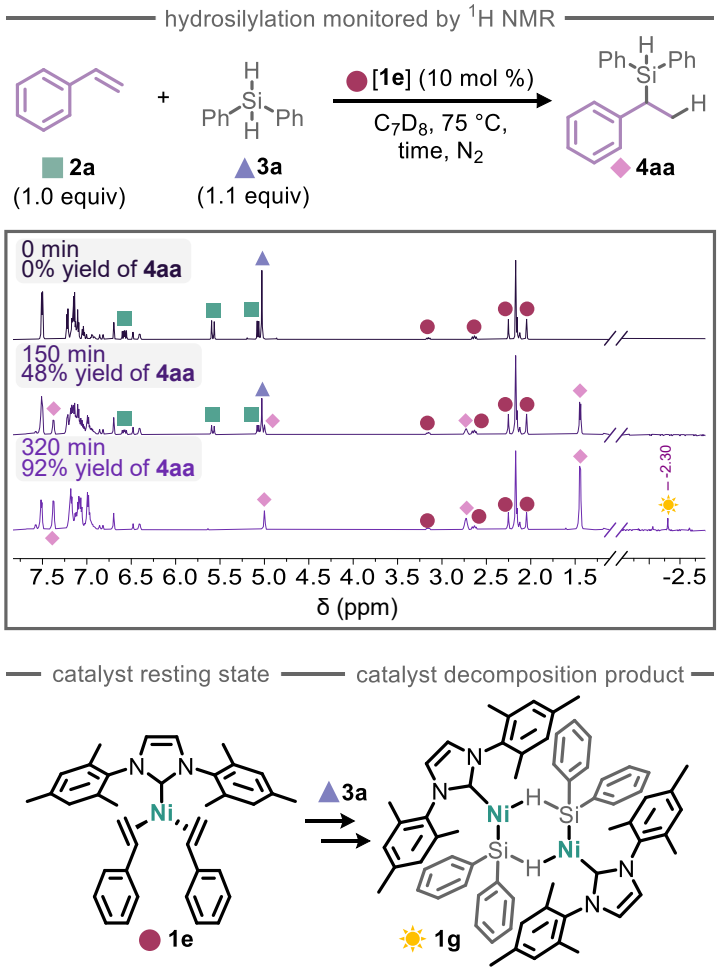

Figure 4.3. ^{1}H NMR monitoring of the hydrosilylation of **2a** and **3a** by **1e** over time at 75 °C. Conditions: **2a** (0.13 mmol, 1.0 equiv), **3a** (0.14 mmol, 1.1 equiv), **1e** (0.013 mmol, 10 mol %), C_7D_8 (0.6 mL, 0.22 M), under N_2. Yield calculated using mesitylene as an internal standard. Bottom: proposed catalyst resting state (**1e**) and catalyst decomposition product (**1g**).

addition of **4aa** (0.087 mM) from the outset of the reaction. After time and [**4aa**] adjustment, the reaction profiles also overlay, suggesting that product **4aa** does not inhibit catalysis (**Figure 4.4.b.**).

Synthesis and Characterization of (ITMe)Ni(styrene)$_2$ (1k)

Once establishing the electronic influence that the pre-coordinated alkenes on (IMes)Ni(0)(alkene)$_2$ complexes have on catalyst stability, we sought to construct a more in depth

understanding of how ancillary ligands affect catalytic behavior. Revisiting our ligand optimization results from Chapter II, ITMe was found to be the most promising ligand to yield the

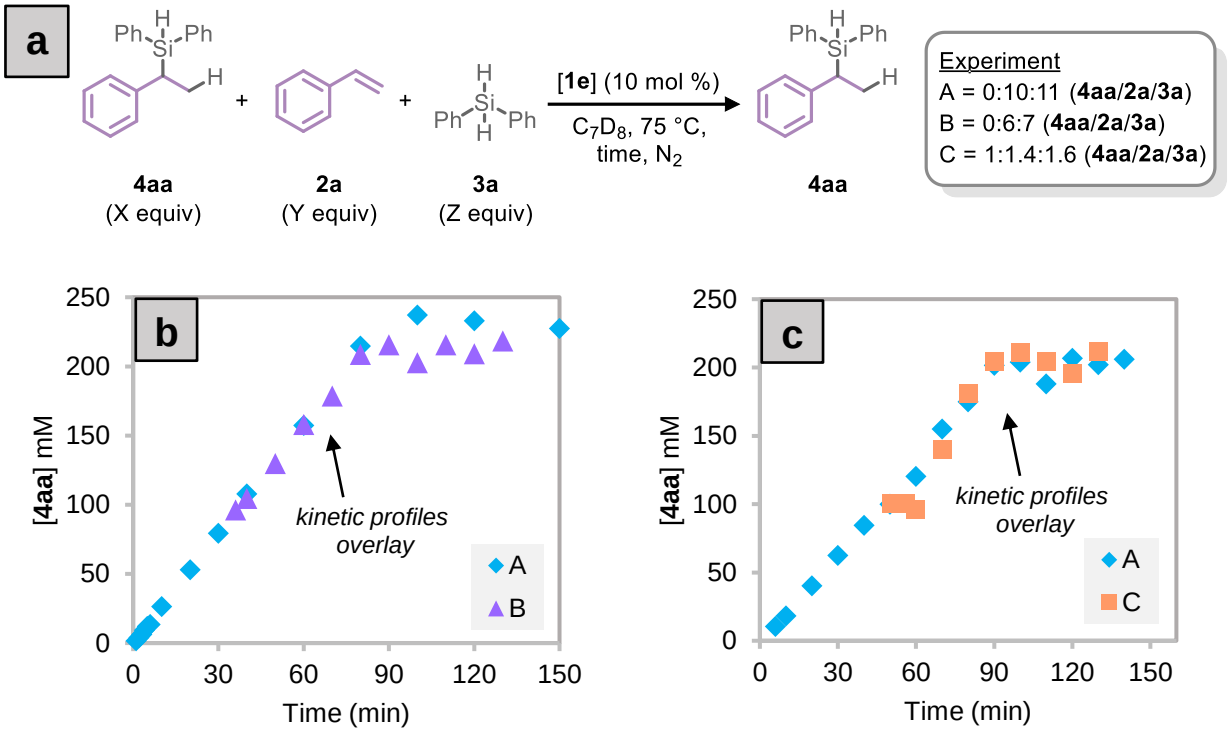

Figure 4.4. Visual Kinetic Analysis experiments: (a) reaction scheme, (b) time adjusted kinetic profile overlap of experiments A and B, (c) time adjusted kinetic profile overlap of experiments A and C.

greatest amount of **4aa** and best branched selectivity under unoptimized conditions performed at 70 °C (56% yield, *l*/*b* = 1:2) compared to IMes (21% yield, *l*/*b* = 1:1.5) and IPr (12% yield, *l*/*b* = 1:1.2) as the NHC (**Figure 2.2.** in Chapter II). Although, the characterization of a discreet (ITMe)Ni(styrene)$_2$ species (**1k**) following similar synthetic protocols to obtain **1e** proved confusing. A single crystal of **1k** was isolated through slow THF/hexanes vapor diffusion but was unable to be fully characterized by single crystal XRD due to twinning effects. However, one out of two potential structures correspond to the bis-ligated styrene complex with both arenes on the styrene ligands facing downwards (**Figure 4.5.**, left). Similarly, a previous report on the synthesis and structural analysis of a PtCl$_2$(styrene)$_2$ complex revealed the presence of multiple rotamers having varied styrene binding modes as determined by ^{1}H and ^{195}Pt NMR.[158] ^{1}H NMR analysis of **1k** displays a mixture of two distinct species, which are hypothesized to be rotamers shown in

Figure 4.5. (possible rotamers are shown on the left). To probe this, DOSY NMR was performed to unveil the number of species with different diffusion constants present in solution. DOSY NMR revealed that both species in solution have identical diffusion rates and are therefore likely identical in mass, supporting our hypothesis that **1k** was isolated as a mixture of rotamers. Drawn in **Figure 4.5.**, rotamer **A** is labelled as pink circles and these peaks correspond to **1k** having symmetry down the z-axis. Rotamer **B** is labelled as a purple triangle and does not have symmetry along the same axis, as characterized by the four distinct peaks that correspond to each methyl group on ITMe (1.35, 1.45, 1.91, and 2.97 ppm). In further deconvoluting the mixture of rotamers, we performed variable temperature ^{1}H NMR (VT NMR) on **1k** was performed to see if **1k** would coalesce into a single species at elevated temperatures. Monitoring changes in **1k** by VT NMR over a temperature range (25 to 100 °C), the coordinated alkene peak at 2.73 ppm shifts upfield to about 2.61 ppm (hidden under methyl group in rotamer **A**). Additionally, in rotamer **B**, two methyl groups on ITMe (1.91 and 2.97 ppm) significantly shift downfield to 1.99 and 3.08 ppm relative to the other peaks in rotamer **B**. Whereas, peaks for rotamer **A** all shift downfield an equivalent amount. After heating **1k** at 95 °C for 10 minutes, rotamer **A** and **B** did not coalesce, and remained as separate species in

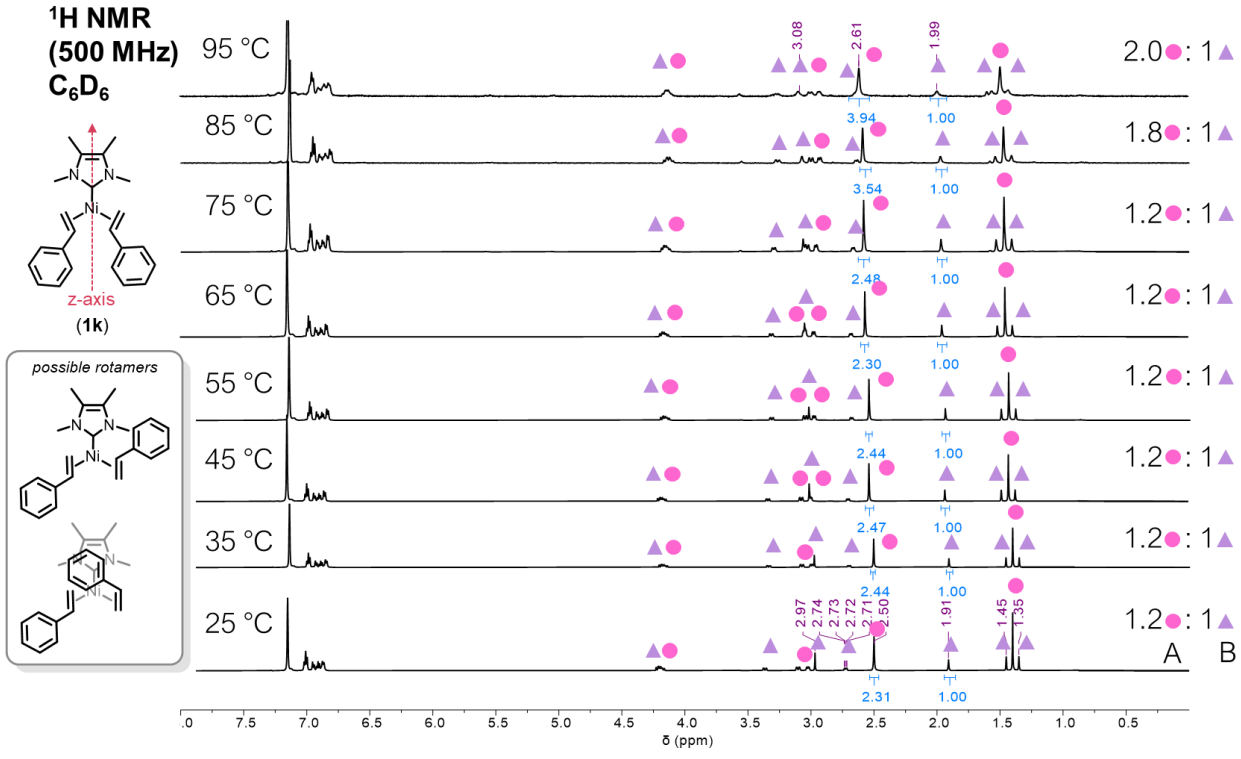

Figure 4.5. VT NMR spectra of **1k** recorded in C_6D_6 at various temperatures (25-95 °C).

solution. The ratios of **A** and **B** slightly increased to favor **A** (from 1.2:1 to 2:1, **A**/**B**) throughout the heating process, however, the two remained relatively constant; therefore, we concluded that rotamers **A** and **B** are not in equilibrium with each other.

Influence of (NHC)Ni(styrene)$_2$ Catalyst Structure on Hydrosilylation

Catalyst **1e** was previously found to be the best performing hydrosilylation catalyst to react **2a** with **3a** to afford **4aa** at 100 °C in toluene. Despite efforts to optimize the NHC ligand for alkene hydrosilylation, further exploration of the steric and electronics influence of the NHC on the Ni center is essential to enable advancements in (NHC)Ni-catalysis on a broader scale. Louie and coworkers have synthesized and characterized a library of electronically and sterically modifiable (NHC)Ni(styrene)$_2$ complexes through simple alteration of the NHC backbone and/or *N*-moieties.[126] Taking advantage of these complexes, we synthesized and prepared a series of sterically and electronically different (NHC)Ni(styrene)$_2$ complexes (**1e**, **1k**-**1o**) to test for alkene hydrosilylation (**Figure 4.6.a.**). Shown in **Figure 4.6.a.**, the NHC ligands are ordered in ascending size from left to right as represented by the steric parameter, %V_{Bur} values, which were calculated using an (NHC)–M bond distance of 2.0 Å.[129,126] The TEP values of each NHC evaluated are shown below the %V_{Bur} value for each NHC in **Figure 4.6.a.** and were determined by measuring the CO stretches of the CO ligand trans to the NHC ligand of interest on an [Ir] complex measured by IR[127], apart from ITMe which was computationally derived[128]; a smaller wavenumber is equivalent to greater electron donation ability.

To compare the reactivity of these complexes, we subjected 5 mol % of [Ni] for the hydrosilylation of 1.0 equiv **2a** and 1.1 equiv **3a** to yield **4aa** at 80 °C in toluene (**Figure 4.6.b.**). In order to apply the method of initial rates, lower reaction temperatures (from 100 °C) were used to slow down the reaction enough to be able to accurately measure initial rates (**Figure C.28., Table C.14.**). **1k** (ITMe) proved to be the fastest catalyst exhibiting 3.8x the rate compared to the parent complex **1e** (IMes), followed by **1m** (SIMes, 3.2x faster) and MeIMes (**1n**, 1.4x faster). The remaining two NHCs, **1l** (ClIMes) and **1o** (IPr), were 1.5x and 12x slower than **1e** (IMes), respectively. At first glance, it appears that sterics may have the greatest influence on catalyst behavior with the fastest catalyst **1k** bearing the smallest ligand (ITMe) and the slowest catalyst **1o** having the largest ligand (IPr). However, the relationship between ligand sterics and catalyst kinetics fails to trend with the class of IMes-derivative NHCs (**1e**, **1l**-**1n**), which may be due to the

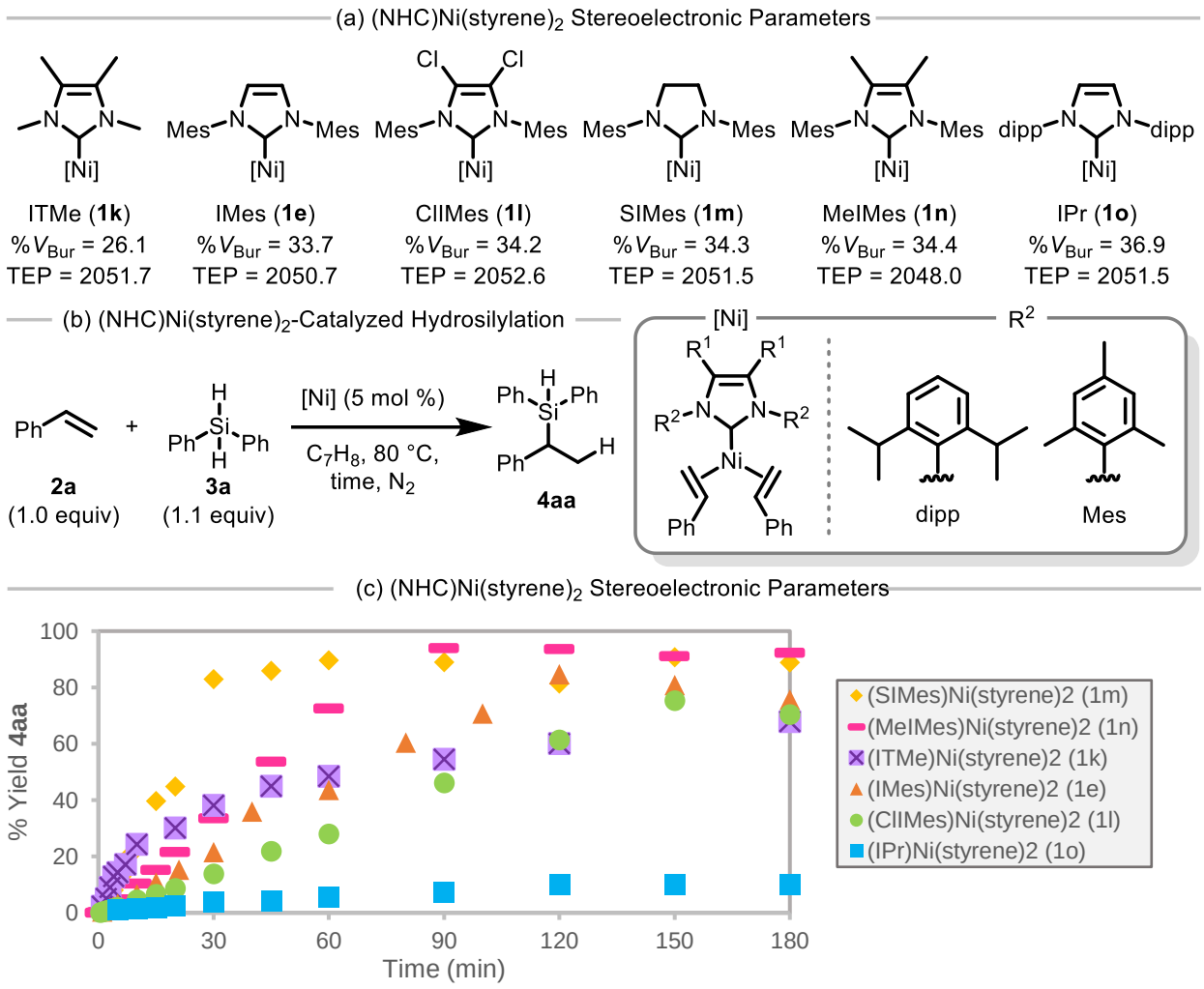

Figure 4.6. (a) Library of (NHC)Ni(styrene)$_2$ complexes tested with the corresponding steric (%V_{Bur}) and electronic (TEP) parameters for each NHC. TEP, Tolman electronic parameter are measured in cm^{-1}. (b) (NHC)Ni(styrene)$_2$-catalyzed hydrosilylation monitored by GC using mesitylene or durene as an internal standard. Error bars are omitted for clarity.

minimal change in sterics amongst these Mes ligands with only a $\Delta\%V_{Bur} = 0.5$. Taking a closer look at the TEP values of **1e** and **1l-1n**, no clear electronic trend is responsible for catalyst reactivity. This data suggests that neither the %V_{Bur} nor TEP forms of analysis to construct a catalyst structure-activity relationship are valid methods to parse out the factors responsible for (NHC)-catalyzed hydrosilylation activity.

Beyond initial rates, we can analyze the full kinetic profile shown in **Figure 4.6.b.**. Despite **1k** (ITMe) initially exhibiting the most rapid kinetics, it gradually levels out at 60% yield of **4aa**

after 90 min and never reaches completion after 180 min, suggesting catalyst decomposition mid-reaction. Similarly, **1l** (ClIMes) also decomposes by 150 min. The worst performing catalyst, **1o** (IPr), is not a suitable catalyst for this transformation likely due to the excessive steric bulk of the IPr NHC ligand around the Ni center as previously discussed in Chapter II. Overall, **1m** (SIMes) is significantly more reactive than the parent catalyst **1e** (IMes), completing the reaction within 30 min while maintaining excellent branched selectivity of over 1:70 (*l*/*b*). This is a significant improvement in catalyst behavior to what is currently known for (NHC)-catalyzed alkene hydrosilylation. Following the best catalyst was found to be **1n** (MeIMes), yielding 94% **4aa** by 90 min and maintaining excellent selectivity (~1:50; *l*/*b*). These two ligands have similar steric parameters, but SIMes (**1m**) is slightly less electron donating than MeIMes (**1n**).[159] These data infer the delicate interplay between sterics, electronics, and catalyst stability that contributes towards the structure-activity relationship of (NHC)Ni catalysts for alkene hydrosilylation. More ligand analysis and experimentation are required to conclude what major factors contribute to catalyst behavior.

Electronic Characterization of (NHC)Ni(styrene)$_2$ Complexes

As previously shown, NHC ligand sterics and electronics are not adequate parameters to explain the reactivity of (NHC)Ni(styrene)$_2$ complexes in alkene hydrosilylation. Therefore, we sought to explore the fundamentals of (NHC)Ni(styrene)$_2$ complexes by relating the NHC identity in these complexes to the oxidation potential of (NHC)Ni(styrene)$_2$ complexes. To investigate this, cyclic voltammetry (CV) studies of (NHC)Ni(styrene)$_2$ complexes (**1e**, **1k**, **1m**-**1o**) bearing varied NHC structures were collected in an electrolyte solution of 0.01 M [NBu_4][ClO_4] in DMF at 100 mV•s^{-1}. Scanning oxidatively, **1e**, **1k**, **1m**-**1o** all display two oxidative peaks corresponding to Ni^0/Ni^I and Ni^I/Ni^{II}, while no reversible redox features were observed (**Figure 4.7.**, left). Attempts to scan reductively to observe reversible redox features were unsuccessful. The complexes that most readily oxidized (Ni^0/Ni^I) were found to be **1n** (MeIMes) and **1k** (ITMe) with oxidative features appearing at -0.73 V (all potentials are calibrated vs Fc^+/Fc) and -0.72 V, respectively, followed by **1m** (SIMes) at -0.64 V, **1e** (IMes) at -0.62 V, and lastly **1o** (IPr) at -0.47 V (**Figure 4.7.**, right). Complexes that were more readily oxidized trended well with the rates of hydrosilylation with the exception of **1m** (SIMes). Namely, **1k** (ITMe) and **1n** (MeIMes) have the highest oxidation potential and exhibit faster kinetics while **1o** (IPr) had the lowest oxidation

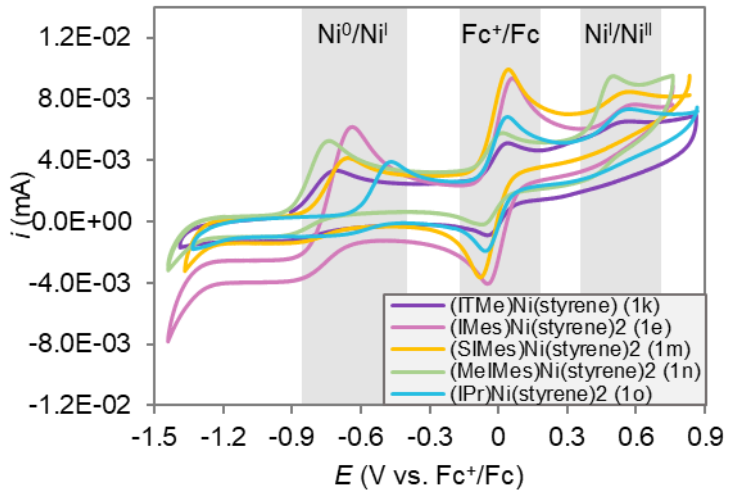

complex	Ni^0/Ni^I (V)	Ni^I/Ni^{II} (V)
1n (MeIMes)	-0.73	0.51
1k (ITMe)	-0.72	0.56
1m (SIMes)	-0.64	0.57
1e (IMes)	-0.62	0.51
1o (IPr)	-0.47	0.55

Figure 4.7. Left: CV data for complexes **1e**, **1k**, **1m**, **1n**, and **1o**. Right: Ni complex of interest, the voltage corresponding to the first oxidation (Ni^0/Ni^I) followed by the second oxidation (Ni^I/Ni^{II}).

potential of -0.47 V and was also the slowest to catalyze hydrosilylation. All complexes displayed an oxidation peak that corresponds to Ni^I/Ni^{II} with similar oxidation potentials ranging from 0.51-0.57 V. Although the CVs of these complexes are unable to fully elucidate the trends observed for hydrosilylation of (NHC)Ni complexes, it does provide insight into how the NHC influences the Ni complex oxidation potential. This method has the potential to be used as a metric for NHC–Ni bond strength or even Ni stability for both current and future studies for these types of complexes.

3.3 Conclusion

In summary, the work in Chapter IV describes the assessment of the electronic structure of the (NHC)Ni(alkene)$_2$ complexes using both NMR and CV techniques and its mechanistic implications in alkene hydrosilylation. Building upon Chapter II and III, a deeper understanding on the influence of the styrene and NHC ligands in (NHC)Ni(styrene)$_2$-catalyzed alkene hydrosilylation has been developed. In short, styrene ligands that possess stronger electron withdrawing ability are more stable than their electron donating counterparts. Thus, more efficient catalyst activation is achieved with more electron rich styrenes while simultaneously destabilizing the Ni center. To provide insight on catalyst behavior, an in operando ^{1}H NMR catalyst resting state experiment was performed. Mechanistically, we can attribute the starting (IMes)Ni(styrene)$_2$

(**1e**) complex as the resting state, indicating that the pre-catalyst reformation is highly reversible. Next, the synthesis and analysis of (ITMe)Ni(styrene)$_2$ (**1k**) was achieved using multiple NMR spectroscopy methods to discern the mixture of species, which are predicted to be two distinct rotamers. After identifying the speciation of **1k** (ITMe), this complex along with other (NHC)Ni(styrene)$_2$ derivatives (**1e**, **1l-1o**) were tested as catalysts for alkene hydrosilylation to evaluate NHC impact on catalytic behavior. SIMes was found to be the best NHC for this transformation, which did not trend with either NHC electronics or sterics when applying the %V_{Bur} and TEP parameters, respectively. This result led us to explore a new avenue to probe the electronic structures of **1e**, **1k**, **1m-1o** by CV. Both **1n** (MeIMes) and **1k** (ITMe) exhibited the highest oxidation potential of -0.73 V and -0.72 V (vs. Fc^+/Fc), respectively, while the bulkiest complex, **1o** (IPr), displayed the lowest oxidation potential of -0.47 V.

Overall, new methods have been presented in Chapter IV to assess the electronic structure and stability of (NHC)Ni(alkene)$_2$ complexes have been developed using ^{1}H NMR ligand exchange and CV experiments. However, attempts to rationalize **1m** (SIMes) exhibiting the best catalytic reactivity remains unsuccessful. Future work can be done to further explore this phenomenon such as performing more in depth CV analysis using varied (IMes)Ni(alkene) complexes with chelating alkene ligands to increase Ni(0) stability. Additionally, density functional theory can be applied to predict the mechanism of (NHC)Ni-catalyzed hydrosilylation as well as the relative stability that each NHC provides.

The assessment of using different NHC ligands described in Chapter IV can potentially be applied to remote hydrosilylation systems. Knowing the relative rates that each NHC induces on the (NHC)Ni(styrene)$_2$ complexes, we can control the desired rate of reaction relative to isomerization to install a silicon group distal to the original reactive site. More details on this chemistry are further discussed in chapter V.

CHAPTER V

DEVELOPMENT OF A HOMOGENEOUS (NHC)Ni(0)-CATALYZED REMOTE HYDROSILYLATION SYSTEM

The work in Chapter V was developed by Alison Sy-min Chang and Professor Amanda K. Cook and the synthetic and catalytic system development was carried out by Cailey Carpenter, Gaby Bailey, and Alison Sy-min Chang.

5.1 Introduction

Alkene hydrosilylation is an industrially relevant reaction that adds a H–Si bond across a double bond, yielding precursors for silicone materials that are utilized in our daily lives.[29] Unsustainable Pt catalysts are currently used for this transformation, and are typically limited to the formation of just one product, the linear isomer.[13,30,42] Formation of the branched isomer has been substantially less developed.[116,117] The branched isomers are highly valuable, since they are used in specialty applications like silicone coatings and adhesion promoters.[27,28] Furthermore, selective conversion of a long chain alkene to afford a branched organosilicon product remains elusive. This transition metal-catalyzed reaction, known as remote hydrosilylation (RHS), is an efficient method to obtain organosilicon products that originate from an alkene distal to the initial reaction site (**Figure 5.1.a.**). This reactivity is achieved through alkene isomerization along a long alkyl chain followed by functionalization to yield high-value organosilicon products. As with standard hydrosilylation, known precious[160–165] and base metal[166,88,49,66,167,68,168,169] catalysts perform RHS to form the linear product, thus highlighting the significant unmet challenge in obtaining branched products through this method. To our knowledge, only one example by Zhu and coworkers displays this reactivity using a (phenanthroline)Fe catalyst, but there are limitations to this work, including a lack of substrate scope and only moderate selectivity for the branched product (*b*/*l* = 9.0:1, **Figure 5.1.b.**).[102] The potential to contribute to the field motivated us to develop a modular, branched-selective RHS system.

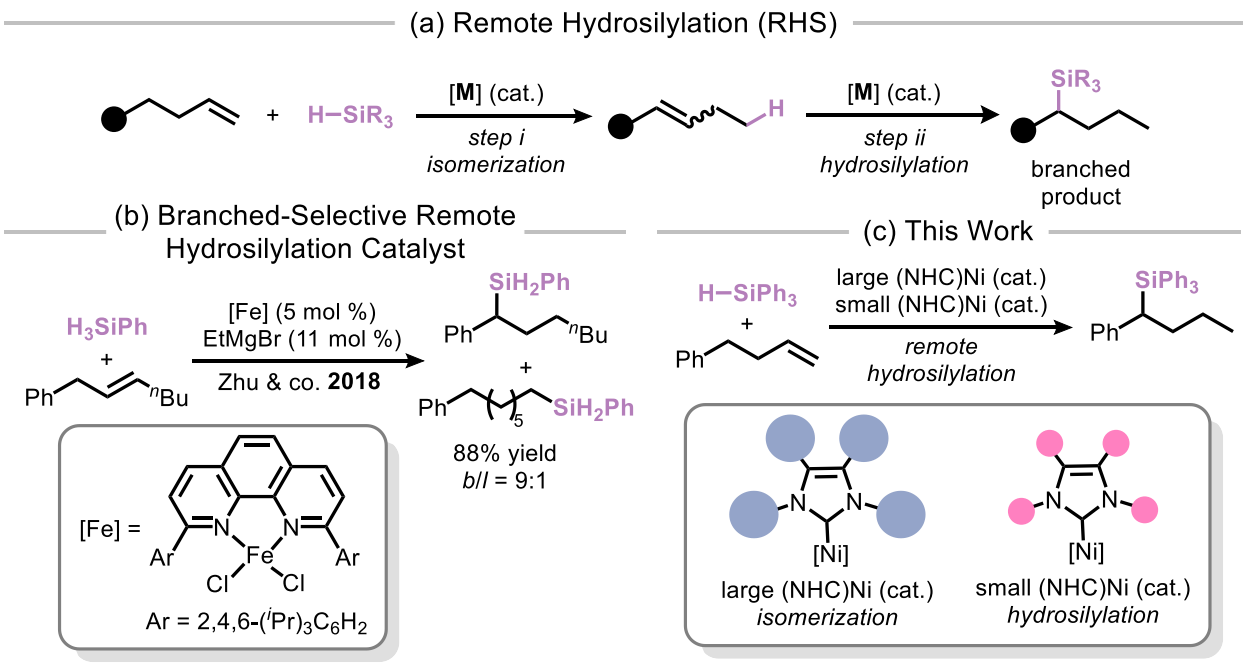

Figure 5.1. (a) Remote hydrosilylation of a terminal alkene and a 3° silane catalyzed by a transition metal complex. (b) Example of a branched-selective remote hydrosilyation catalyst in the literature. (c) This work on remote hydrosilylation utilizing (NHC)Ni cataylsts.

As described in Chapters II-IV, we have developed a (NHC)Ni (NHC = *N*-heterocyclic carbene) catalytic system that readily activates 2° and 3° silanes for alkene hydrosilylation to from the branched product.[170] Other work in our group has led to the development of a tunable homogeneous (NHC)Ni/$HSiPh_3$ alkene isomerization system.[6] Thorough mechanistic investigations of each (NHC)Ni-catalyzed hydrosilylation and isomerization systems were performed, separately, to reveal that each reaction is likely facilitated by a Ni–H species. Furthermore, NHC ligand screening was found to impact catalyst activity. Taking advantage of our previously gained mechanistic understanding of these catalytic processes, we sought to develop a dual catalyst system based on (NHC)Ni complexes composed of Earth-abundant elements for RHS of long-chain alkenes to install a silicon group at the benzylic position.[6,170] This is achieved by using a large (NHC)Ni catalyst for alkene isomerization, and a small (NHC)Ni catalyst for hydrosilylation (**Figure 5.1.c.**). In developing an accessible dual catalytic system, we have strategized to generate the active Ni catalysts *in situ* using a Ni(0) precursor and corresponding ligands. This approach removes many synthetic steps required to synthesize the catalyst and it allows for rapid evaluation of ligand combinations, facilitating reaction optimization.

5.2 Results and Discussion

Alkene Isomerization

The first step in RHS is alkene isomerization followed by the second step, alkene hydrosilylation. Therefore, the rate of isomerization from a terminal alkene to an internal alkene must be greater than the rate of hydrosilylation. Kawamura et al. showed an NHC ligand size dependence on catalyst activity such that a larger NHC (IPr) yielded more isomerized product. Following this trend, we hypothesized that a larger IPr NHC would facilitate alkene isomerization more efficiently. We initiated our optimization by screening three sterically diverse IPr (IPr = 1,3-bis(2,6-diisopropylphenyl)imidazol-2-ylidene) derivatives for the isomerization of allylbenzene (**1a**, Figure 5.2.). The steric bulk of the three IPr NHCs evaluated for this reaction are determined by $\%V_{Bur}$ and are listed in ascending steric bulk[126]: IPr (38.5), ClIPr (39.1), and MeIPr (39.6). The isomerization of **1a** to **2a** was facilitated by 5 mol % $Ni(COD)_2$ (COD = 1,5-cyclooctadiene), IPr NHC, and $HSiPh_3$ at 60 °C in toluene and monitored by GC (**Scheme 5.1.**). As expected, the largest NHC, MeIPr, exhibited the fastest kinetics and completed isomerization within 44 min. Following MeIPr is IPr, converting 46% **1a** to **2a** within 5 h and the slowest NHC was ClIPr, only reaching 6% conversion to **2a**. These results indicate that sterics are not the main contributing factor to catalyst activity, encouraging us to evaluate the NHCs as a function of σ-donating strength measured in Tolman electronic parameter (TEP); smaller TEP values correlate to stronger σ-donating strength. Indeed, the stronger NHC σ-donation correlated to faster isomerization rates: MeIPr is the most electron donating followed by IPr and then ClIPr.

With MeIPr as the best ligand for alkene isomerization, we continued optimization using a longer chain alkene, 4-Ph-1-butene (**1b**), as our model substrate. We next evaluated the Ni(0) source and envisioned that an air-tolerant Ni(0) precatalyst would increase catalyst stability throughout the reaction. Therefore, we tested $Ni(COD)_2$ and Ni(COD)(DQ) (DQ = duroquinone), an air-tolerant Ni(0) source. DQ has been reported to stabilize Ni by adopting various binding modes to Ni in Ni(COD)(DQ)-catalyzed reactions.[171] Using MeIPr as the NHC source, the isomerization of **1b** to **A-2b** and **B-2b** was tested using $Ni(COD)_2$ and Ni(COD)(DQ) at 40 °C in toluene (**Scheme 5.2.**). As the goal of this RHS system is to install a silicon group on the most

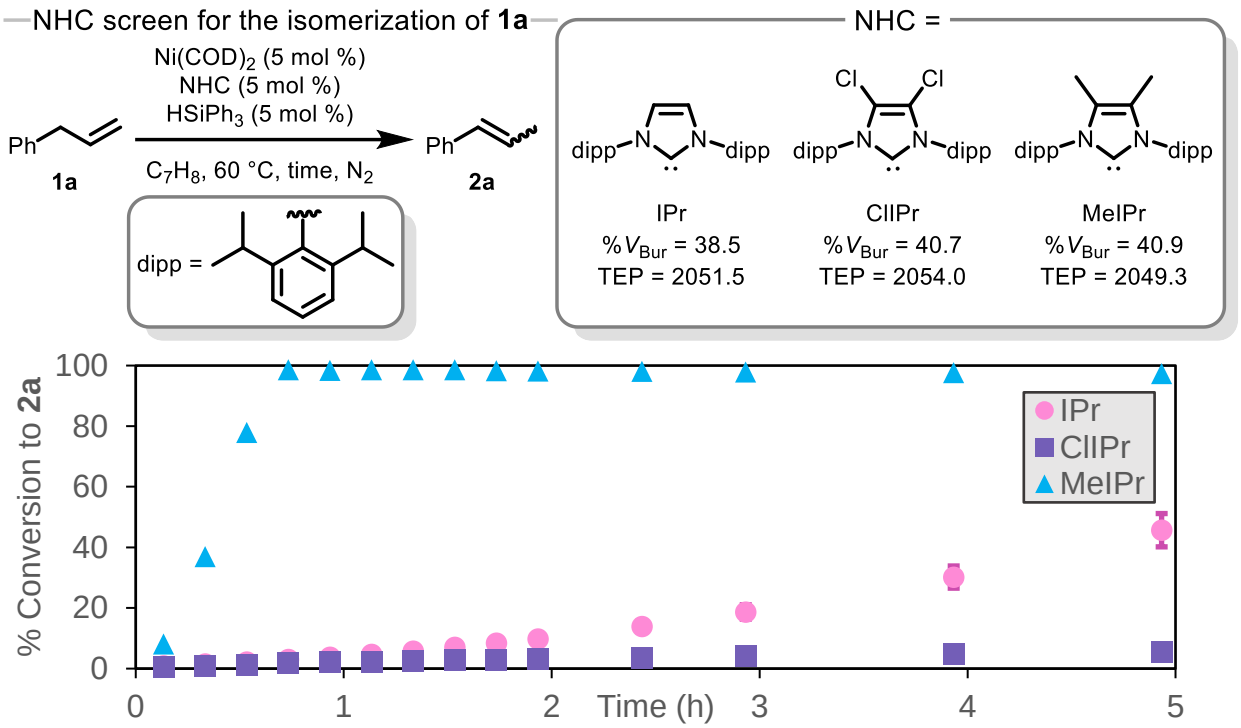

Scheme 5.1. NHC screen for the isomerization of **1a** to **2a** by $Ni(COD)_2$/NHC/$HSiPh_3$. NHC, *N*-heterocyclic carbene; COD, 1,5-cyclooctadiene; dipp, diisopropylphenyl; $\%V_{Bur}$, % buried volume; TEP, Tolman electronic parameter. Conditions: $Ni(COD)_2$ (0.0091 mmol, 5 mol %), NHC (0.0091 mmol, 5 mol %), $HSiPh_3$ (0.0091 mmol, 5 mol %), **1a** (0.18 mmol, 1.0 equiv), toluene (1.1 mL, 0.16 M), 60 °C. Yields are determined by calibrated GC analysis using durene as an internal standard.

internal position of the alkyl chain, we are targeting the formation of **B-2b** due to benzylic functionalization accessibility. In order to achieve this site selectivity, the Ni catalyst must chain-walk, the sequential movement of a double bond along an alkyl chain, across two carbons to obtain the desired product, **B-2b** (**Scheme 5.2.**, top). To accurately observe this reactivity, a decreased reaction temperature was used to assess the rate of **B-2b** formation over time. An induction period of 1 h was observed with $Ni(COD)_2$, and the formation of **B-2b** (gray triangles) did not initiate until 71% **A-2b** (orange squares) was formed (**Scheme 5.2.**, bottom left). Approximately 77% **B-2b** formed by 6 h. No induction period was observed using Ni(COD)(DQ), and 98% of **1b** was fully converted to form 46% **A-2b** and 52% **B-2b** (**Scheme 5.2.**, bottom right). The gradual formation of **B-2b** led to a similar total conversion of 75% in comparison to using $Ni(COD)_2$ (77% **B**-2b) within 6 h. Due to the presence of the induction period using $Ni(COD)_2$ as the precatalyst, we chose to use Ni(COD)(DQ) as the Ni(0) source moving forward.

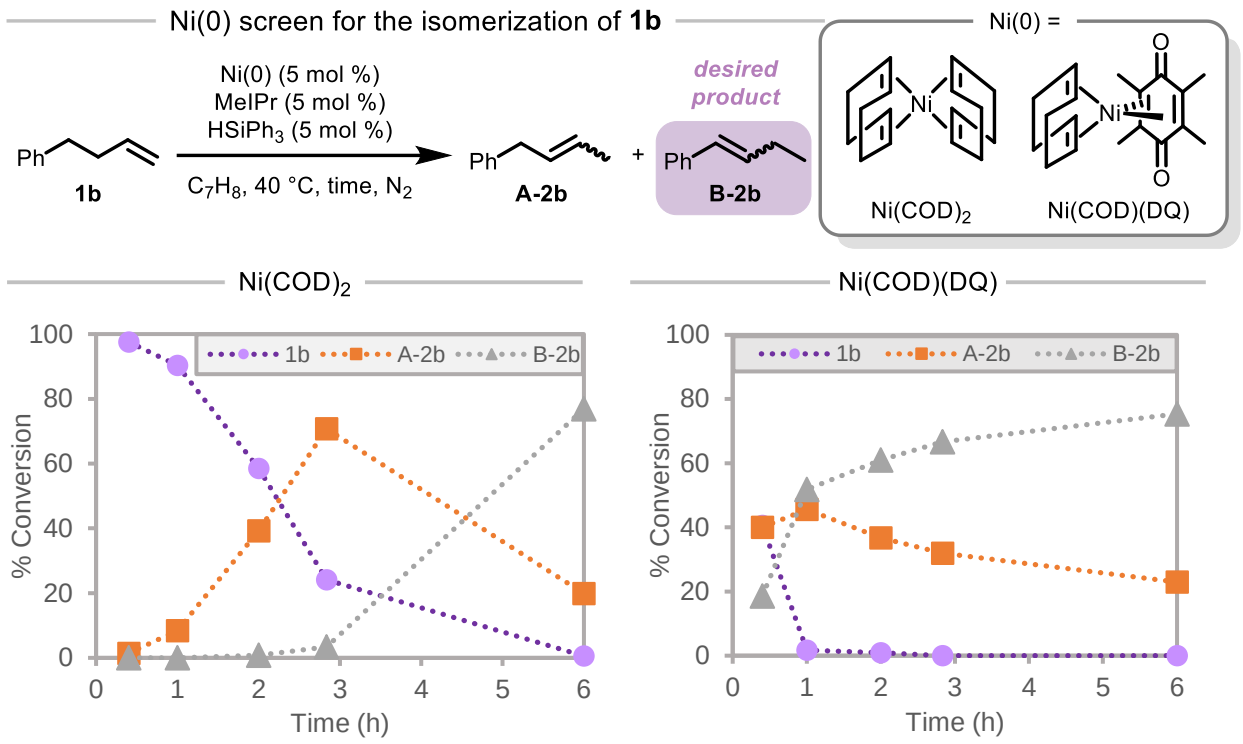

Scheme 5.2. Evaluation of Ni(0) precatalysts for the isomerization of **2a** to **A-2a** and **B-2a**. Conditions: [Ni] (0.0060 mmol, 5 mol %), MeIPr (0.0060 mmol, 5 mol %), $HSiPh_3$ (0.0060 mmol, 5 mol %), **1a** (0.12 mmol, 1.0 equiv), toluene (0.5 mL, 0.24 M), 40 °C. Yields are determined by calibrated GC-MS analysis using mesitylene as an internal standard.

Alkene Hydrosilylation

Described in Chapter IV, NHC optimization for (NHC)Ni-catalyzed alkene hydrosilylation of styrene and diphenylsilane led to SIMes as the best performing ligand, completing the reaction within 30 min at 80 °C (see **Figure 3.4.** for details). Considering the desired relative rates of reaction for RHS, faster isomerization in comparison to hydrosilylation is desired. Therefore, we moved forward using the second-best ligand for hydrosilylation, MeIMes, to optimize for the RHS and **1b** and **3a** using the optimal Ni(0) source found for alkene isomerization, Ni(COD)(DQ). Reacting **1b** and **3a** by 5 mol % MeIPr, 5 mol % MeIMes, and 10 mol % Ni(COD)(DQ) at 80 °C in toluene for 24 h, 75% conversion of alkene to RHS product was achieved with a 0.9:1 (**4a**/**4b**-**4d**) selectivity of the desired hydrosilylation product (entry 1, **Table D.7.**). The product selectivity was rather low, suggesting that alkene hydrosilylation was too fast relative to isomerization. To slow down the rate of hydrosilylation, we proceeded in testing the RHS of **1b** and **3a** using IMes

instead of MeIMes. Indeed, product selectivity increased to 1.9:1 (**4a**/**4b**-**4d**) with only 53% of the alkene converted to RHS product (entry 2, **Table D.7.**).

With variations in RHS product selectivity, we revisited our previously established optimal conditions for (NHC)Ni-catalyzed alkene hydrosilylation of styrene and a 3° silane discussed in Chapter II. ITMe was found to be the most compatible ligand at 100 °C due to smaller steric bulk. Therefore, we continued our optimizations using ITMe as the hydrosilylation ligand. To achieve good **4a** selectivity, we redirected the optimization to solely focus on the hydrosilylation of **B-2b** and **3a** by modifying the reaction solvent. As (NHC)Ni-catalyzed alkene hydrosilylation was more efficient in less polar solvents, we tested four non-polar solvents at 100 °C (**Table 5.1.**). Toluene was the worst performing solvent in terms of both yield (32%) and selectivity of **4a** (10:1, **4a**/**4b**-**4c**; entry 1) followed by *n*-octane (entry 3, 43% yield; 13:1, **4a**/**4b**-**4c**; **Table 5.2.**). Both cyclohexane (entry 2) and hexanes (entry 4) were both selective for **4a** (20:1 and 32:1, respectively; **Table 5.1.**), we proceeded optimization using cyclohexane because it was consistently higher yielding of 41%.

Remote Hydrosilylation

After establishing the optimal NHC ligands for both alkene isomerization and alkene hydrosilylation, separately, we tested RHS at various temperature regimes. Shown in **Figures 5.2.** and **5.3.**, alkene isomerization readily proceeds at lower temperatures (40 and 60 °C), however, hydrosilylation requires an elevated reaction temperature (100 °C) as described in Chapter II. Therefore, we envision that the formation of **4a** from **1b** and **3a** can be kinetically obtained by

Table 5.1. Solvent screen for the hydrosilylation of **B-2b** and **3a** by ITMe/Ni(COD)(DQ).

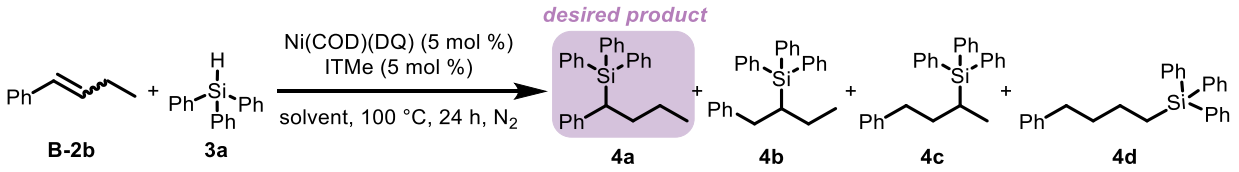

Entry	Solvent	Dielectric Constant	% Yield 4a	Selectivity (4a/4b-4d)
1	Toluene	2.38	32	10:1
2	Cyclohexane	2.02	41	20:1
3	*n*-octane	1.95	43	13:1
4	Hexanes	1.89	29	32:1

% Yield determined by ^{1}H NMR using trimethoxybenzene as an internal standard. Selectivity determined by GC-MS.

promoting alkene isomerization to afford **B-2b** while inhibiting hydrosilylation at a lower reaction temperature followed by increasing the reaction temperature to 100 °C for alkene hydrosilylation. The RHS of 1.0 equiv **1b** and 1.0 equiv **3a** by 1:1 ITMe/MeIPr and 10 mol % $Ni(COD)_2$ was conducted in toluene at 50 °C while monitoring isomerization by GC. $Ni(COD)_2$ and toluene were chosen for solubility at lower temperatures. After 8.5 h at 50 °C, 86% of **1b** was converted to 25% **A-2b** and 75% **B-2b** and increasing the reaction temperature to 100 °C for 24 h converted 64% alkene to yield 3.1:1 **4a**/**4b**-**4d** (entry 1, **Table D.8.**). We hypothesized that the low **4a**-selectivity was a result of incomplete isomerization, therefore by increasing the isomerization temperature to 60 °C for 7 h, 16% **A-2b** and 84% **B-2b** was obtained followed by 68% of alkene converted to product and resulted in a higher ratio of 4.2:1 **4a**/**4b**-**4d** after stirring the reaction at 100 °C for an additional 24 h (entry 2, **Table D.8.**).

As isomerization ran for ~8 h prior to activating the hydrosilylation catalyst, we wondered if the hydrosilylation catalyst was decomposing while stirring in solution. Therefore, we tested the RHS of 1.0 equiv **1b** and 1.0 equiv **3a** by 1:1 MeIPr/ITMe (5 mol % of each NHC was used) and 10 mol % Ni(COD)(DQ) in cyclohexane at 100 °C for 21 h. 78% of **1b** was consumed to form **4a** and **4b** with a selectivity of 5.0:1 (**4a/4b**, entry 3, **Table D.9.**). Within the same reaction, 0% of **3a** and 20% of unreacted **B-2b** remained, respectively, along with 5% hydrogenated **1b**, an undesirable byproduct of this reaction. The presence of unreacted **B-2b** implies that isomerization was faster than hydrosilylation before the hydrosilylation catalyst decomposed. To encourage hydrosilylation, we increased the MeIPr/ITMe ratio to 1:3 while maintaining 10 mol % Ni(COD)(DQ), however no improvement in reactivity was observed (entry 4, **Table D.9.**). With minimal amounts of **3a** remaining coupled with the formation of hydrogenated **1b**, this competing side reaction between **3a** and **1b** complicates desired catalytic activity. We hypothesized that a method to inhibit this side reactivity could be achieved by lowering the reaction temperature to 90 °C. Using standard conditions at 90 °C for 24 h, 93% alkene was consumed and a selectivity of 10:1 **4a**/**4b**-**4d** was achieved with only 3% **B-2b** remaining; albeit with a greater amount of hydrogenated **1b** forming (13%). Overall, these preliminary results showcase the potential in further optimizing the RHS of **2a** and **3a** to obtain **4a** in high yield and selectivity >10:1 (**4a**/**4b**-**4d**).

5.3 Conclusion

RHS, the isomerization of an alkene to a position distal to the initial reaction site followed by hydrosilylation of the newly formed alkene, is a powerful method to obtain high value branched organosilicon products. Chapter V describes our motivation to devise a dual catalytic system by combining and simplifying our previously established (NHC)Ni-catalyzed alkene isomerization and hydrosilylation systems to increase reaction efficiency and decrease chemical waste from sequential work ups. Building upon work done by Dr. Kawamura et al[6], we show that a thorough investigation in modifying the stereoelectronics of the IPr ligand for isomerization was successful– MeIPr, the strongest NHC σ-donor, proved to be the best candidate. Once identifying MeIPr as the ligand of choice for alkene isomerization, we next evaluated optimal conditions for hydrosilylation and found that ITMe paired with Ni(COD)(DQ) was the best performing system, which is consistent with results discussed in Chapter II. Cyclohexane was also found to be the best solvent environment to mediate hydrosilylation. Lastly, the combination of these two systems led to further optimization through temperature variations to acquire kinetic control over the desired product selectivity.

We show that optimization via hypothesis-driven rationale such as modifying the ligand, solvent environment, and reaction temperature has the potential to yield the branched product (**4a**) in high yield and selectivity. The foundational establishment of this RHS system has contributed to further understanding the relative rates of each reaction. Additionally, the work described in Chapter V can inform future (NHC)Ni catalytic systems, of which a detailed understanding of ligand electronics on isomerization and ligand sterics on hydrosilylation is presented and shows that Ni reactivity is indeed deeply affected.

CHAPTER VI

DEVELOPMENT OF A HETEROGENEOUS NICKEL–HYDRIDE CATALYST FOR ALKENE ISOMERIZATION

This chapter includes unpublished work done by Alison Sy-min Chang as well as submitted and co-authored material from Chang, A. S.; Kascoutas, M. A.; Valentine, Q. P.; How, K. I.; Thomas, R. M.; Cook, A. K. Alkene Isomerization using a Heterogeneous Nickel–Hydride Catalyst. *Submitted*. 10.26434/chemrxiv-2023-rt2gt. This article was written by Alison Sy-min Chang, with editorial assistance from Melanie A. Kascoutas and Professor Amanda K. Cook. Melanie A. Kascoutas and Kiera I. How contributed synthetically through the preparation of starting materials. Quinn P. Valentine and Rachel M. Thomas performed preliminary work to establish the project.

6.1 Introduction

Transition metal-catalyzed alkene isomerization is an appealing approach to reposition an alkene within a molecule (**Figure 6.1.a.**).[172,173] Significant advancements in the field of homogeneously catalyzed isomerization have been made,[174–176] but efficient and selective heterogeneous catalysts for isomerization remain sparse, despite the potential to apply the advantages of heterogeneous catalysis (recyclability, added stability, complementary selectivity).[177,178] Currently, this area of catalysis is severely underdeveloped and dominated by the use of precious metals, specialty organic polymers as supports, and ill-defined active sites in nanoparticles. Notable examples of single-site catalysts include works by Ley,[179] Grotjahn,[180] and Jia[181] which immobilize Ir, Ru, or Rh complexes, respectively, onto ligand-modified organic polymers (**Figure 6.1.b.**). These systems display good catalyst recyclability, but at the expense of reduced catalytic activity and/or *E*/*Z*-selectivity in comparison to their homogeneous analogues. Many nanoparticle-based catalysts for alkene isomerization are known, but because of their crude synthesis methods (*e.g.*, treatment under hydrogen at elevated temperatures), the active sites are unknown, making structure-activity relationships challenging to elucidate (**Figure 6.1.b.**, top right).[182,183] Likely because of this lack of control in the synthesis, the activity and selectivity of the catalysts tend to be low. Because the structure of single-site catalysts can be designed and

systematically modified, they have the potential to control, understand, and improve reactivity.[178,184]

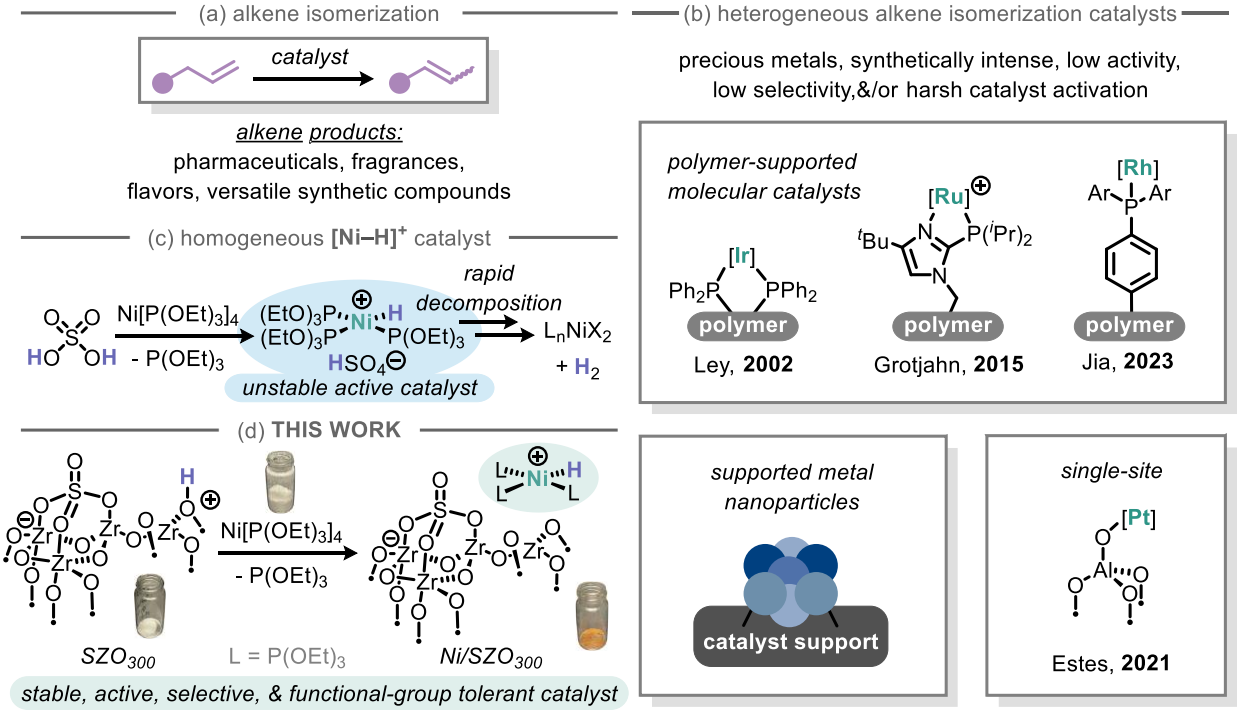

Figure 6.1. (a) Alkene isomerization. (b) Types of heterogeneous catalysts for alkene isomerization. (c) Ni/H_2SO_4 generation and decomposition. (d) This work: development of Ni/SZO_{300} for alkene isomerization.

A pivot towards more precise methods to prepare heterogeneous catalysts bearing well-defined active sites grants the ability to develop structure–activity relationships and encourages further catalyst development. Strategies to synthesize single-site catalysts include the surface organometallic chemistry (SOMC) approach[185] and the use of metal-organic and covalent organic frameworks (MOFs and COFs, respectively), and both have had limited success with alkene isomerization. Estes demonstrated that an alumina-supported platinum-hydride is effective at 1-hexene isomerization (**Figure 6.1.c.**, bottom right),[186] and a handful of examples of MOFs show activity for 1-butene isomerization and *E*/*Z* isomerization.[187–189] While these advancements demonstrate the potential of single-site catalysts in alkene isomerization, their substrate scopes are highly limited and often utilize precious metals as the active site.

SOMC is an evolving method that reaps the benefits of both homogeneous and heterogeneous catalysts. Typically, catalysts prepared using a SOMC approach deliver reactive

species with molecular precision and enhanced stability compared to their homogeneous analogs. Select examples show marked catalytic improvement over their homogeneous analogs (*e.g.*, [W]/SiO_2–catalyzed alkene metathesis,[190] [Ir]/SiO_2–catalyzed methane borylation,[191] and [Hf]/sulfated zirconia-catalyzed ethylene/1-octene copolymerization),[192] demonstrating the potential of this approach.

Cramer and Lindsey found that Ni(0) in combination with sulfuric acid generates a highly active catalyst for alkene isomerization,[193] and Tolman studied the reaction's mechanism and the structure of the active catalyst.[194,195] A cationic Ni–H is proposed as the active catalyst, which forms from protonation of the Ni(0) center with the strong acid. This catalyst, while highly active, decomposes rapidly by a second equivalent of H^+, irreversibly forming an inactive Ni(II) species and H_2 (**Figure 6.1.c.**). We hypothesized that immobilization of the $[Ni–H]^+$ catalyst would prevent this decomposition, thereby improving catalyst stability and broadening its use in organic synthesis. Efforts to improve this catalyst's stability by means of heterogenization were performed using sulfated polymers;[196,197] this strategy improved the catalyst stability and recyclability, but at the expense of catalytic activity and alkene selectivity compared to the homogeneous catalyst (*vide infra*).

Using acidic metal oxides offers significant advantages over polymer-based supports, including ease and precision of synthesis and cost of materials.[198,199] Because of these advantages, the SOMC approach using acidic metal oxides has been taken to generate active catalysts for a wide variety of applications, such as hydrogenation,[200,201] ethylene (co)polymerization,[202,203,192] H/D exchange,[204,205] hydrogenolysis,[206] and alkane metathesis.[206] These active sites are generated by protonolysis or abstraction of an X-type ligand at the metal center. We hypothesized that the novel strategy of protonating metal centers with these strongly acidic metal oxides would be effective in generating immobilized $[M–H]^+$ species, which are broadly invoked as active sites in catalysis. Due to its straightforward nature, this SOMC approach also has the potential to inform future catalyst design and rationale for analogous systems. This strategy would be particularly useful in addressing the challenge of the decomposing $[Ni–H]^+$ catalyst for alkene isomerization.

In this report, we demonstrate that our novel approach is successful: the acidic metal oxide, sulfated zirconia (SZO_{300}) is an excellent proton source and support for generating a putative $[Ni–H]^+$ active site, which is highly active and selective catalysts for alkene isomerization (**Figure 6.1.d.**). We demonstrate that the catalyst, Ni/SZO_{300}, is compatible with a broad scope of alkenes

including those containing functional groups with heteroatoms, halides, acid-labile groups, and electronically and sterically diverse groups. Recyclability and catalyst aging studies reveal enhanced catalyst stability. Notably, this heterogeneous catalyst shows marked improvements in stability, selectivity, and functional group tolerance in comparison to the homogeneous analog. Lastly, we show the versatility of this heterogeneous $[Ni–H]^+$ catalyst and have successfully applied it to various alkene hydrofunctionalization reactions.

6.2. Results and Discussion

Optimization

We initiated our investigations using metal oxides as potential acid sources to generate $[Ni–H]^+$ species from protonation of $Ni[P(OEt)_3]_4$. We speculated that $[Ni–H]^+$ active sites could be formed by reacting this Ni^0 complex with isolated surface hydroxyls. A series of metal-oxide supports commonly used in SOMC, silica dehydroxylated at 700 °C ($SiO_{2\text{-}700}$), alumina dehydroxylated at 700 °C ($Al_2O_{3\text{-}700}$), and zirconia dehydroxylated at 700 °C ($ZrO_{2\text{-}700}$),[185,198] were screened for the isomerization of 4-allylanisole (**1a**) to anethole (**2a**), but all failed to demonstrate any desired reactivity (**Table 6.1.**, entries 1-3). We postulated that the surface hydroxyls were not acidic enough to favorably generate the $[Ni–H]^+$ active species, so we tested a more acidic metal oxide, sulfated zirconia (SZO_{300}).[199,207] Isomerization of **1a** proceeded to a good yield and selectivity of **2a** with SZO_{300} (78% yield **2a**, *E*/*Z* = 17:1; **Table 6.1.**, entry 4). The major isomer is the *E*-isomer, which is more thermodynamically stable than the *Z*-isomer. The reaction proceeds easily at room temperature, but we chose to run most reactions at 30 °C to ensure consistent temperature control. We proceeded with SZO_{300} as the acid source for **1a** isomerization. No yield of **2a** or conversion of **1a** was observed under these conditions when nickel or SZO_{300} was excluded from the reaction (**Table E.2.**).

As a direct comparison to the homogeneous catalyst, the isomerization of **1a** to **2a** using H_2SO_4 as the acid source provided **2a** in higher yield (86%; Table 1, entry 5) than when SZO_{300} was used (78%; Table 1, entry 4), but the *E*/*Z* selectivity was comparable (*E*/*Z* = 17:1 for both H_2SO_4 and SZO_{300}). Additional Ni^0 sources were also evaluated, and all gave low yields of product (<5%; Table S2). The catalyst loadings of $Ni[P(OEt)_3]_4$ and SZO_{300} were optimized to 3 and 5 mol %, respectively, and Et_2O remained the optimal solvent (**Table E.2.**). Under these conditions, **1a**

is isomerized to **2a** in 1 h in high yield (83%) and high selectivity (*E*/*Z* = 22:1; **Table 6.1.**, entry 6), exhibiting a similar yield to that of using 3 mol % of H_2SO_4 (86%), but with better *E*-selectivity

Table 6.1. Evaluation of acid sources for the isomerization of **1a** to **2a**.

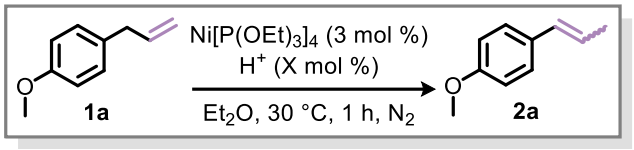

Entry	Acid Source	(mol %)	Yield	Selectivity (*E*/*Z*)
1	$SiO_{2\text{-}700}$	(3)	0%	n.d.[a]
2	$Al_2O_{3\text{-}700}$	(3)	0%	n.d.
3	$ZrO_{2\text{-}700}$	(3)	0%	n.d.
4	SZO_{300}	(3)	78%	17:1
5	H_2SO_4	(3)	86%	17:1
6	SZO_{300}	(5)	83%	22:1
7[b]	H_2SO_4	(5)	63%	11:1
8	Nafion™	(5)	10%	15:1
9	Amberlyst®-15	(5)	20%	11:1

Conditions: **1a** (0.060 mmol, 1.0 equiv), $Ni[P(OEt)_3]_4$ (0.0018 mmol, 3.0 mol %), Et_2O (1.0 mL). Yields and selectivities determined by gas chromatography (GC) analysis using cyclooctane as an internal standard. [a]n.d., not determined. [b]**1a** (0.12 mmol, 1.0 equiv), $Ni[P(OEt)_3]_4$ (0.0060 mmol, 5.0 mol %), Et_2O (2.0 mL).

(*E*/*Z* =17:1 for H_2SO_4). Increasing H_2SO_4 loading to 5 mol % gave a lower yield of **2a** (63%) with poor selectivity (*E*/*Z* = 11:1; **Table 6.1.**, entry 7), suggesting that the active Ni catalyst may be decomposing in the presence of this slight excess H_2SO_4, as previously reported.[194,195]

Nafion™ and Amberlyst®-15 are both acidic organic polymers and have been used as supports in heterogeneous catalysis.[196,197,208] Evaluating these materials in place of SZO_{300} under our conditions revealed that they are not as effective as SZO_{300}. Nafion™ was the worst-performing acid, yielding 10% **2a** (*E*/*Z* = 15:1; **Table 6.1.**, entry 8), and Amberlyst®-15 gave slightly higher yield (20% yield; *E*/*Z* = 11:1; **Table 6.1.**, entry 9). The reactions using three acidic supports (SZO_{300}, Nafion™, and Amberlyst®-15) and H_2SO_4 were studied more deeply by analyzing the reaction progress over time. The plot of the yield of **2c** over time using the three solid acids shows linear formation of the product from 0-45 min (**Figure 6.2.a.**). The slopes of these linear portions were calculated, and comparing these slopes shows that the Ni/SZO_{300} catalyst is 4 and 10 times faster than the Ni/Amberlyst®-15 and Ni/Nafion™ catalysts, respectively (**Figure E.12.**).

Catalyst Characterization

To unveil the amount of Ni that grafts onto SZO_{300}, a reaction between 3:5 [Ni]/SZO was performed. This organometallic complex was prepared by gently stirring a reaction of 0.0187 mmol $Ni[P(OEt)_3]_4$ and 0.0300 H^+ mmol SZO_{300} in Et_2O for 1.5 h at 23 °C. A stark color change from white (SZO_{300}) to bright orange (grafted material, [Ni]-SZO) was immediately observed upon introducing the colorless solution of $Ni[P(OEt)_3]_4$ to SZO_{300}, visually indicating that a reaction on the surface had occurred (**Figure 6.1.d.**, bottom right). The reaction filtrate was analyzed by $^{31}P\{^1H\}$ NMR in C_6D_6 against tetraethyl ethylenediphosphonate as an internal standard. Approximately 73% of $Ni[P(OEt)_3]_4$ successfully grafted onto SZO_{300} using 3:5 [Ni]-SZO (see Appendix E for details).

Upon isolation, the surface organometallic complex, [Ni]-SZO (6.08 wt % Ni by ICP-MS), was characterized by solid state NMR spectroscopy. As expected, the ^1H MAS NMR spectrum showcases signals corresponding to coordinated $P(OEt)_3$ at 4.09 and 1.28 ppm. Two additional signals further upfield show characteristic hydride resonances at -12.10 and -14.21 ppm, indicating that $Ni[P(OEt)_3]_4$ is indeed protonated by SZO_{300}. The appearance of two hydride signals could correspond to the corresponding $[Ni–H]^+$ species: $HNi[P(OEt)_3]_4$ and $HNi[P(OEt)_3]_3$, which were previously observed in the homogeneous analog using H_2SO_4 as the acid source.[194] Additionally, other late transition metal-hydride complexes prepared via SOMC are commonly found within this region.[209,173] The IR spectrum of [Ni]-SZO further corroborates the presence of a Ni–H in the grafted material as indicated by a weak band at 1935 cm^{-1}.[210,211] This data is consistent with previously reported $[Ni–H]^+$ complexes. The ^{13}C MAS NMR spectrum of [Ni]-SZO exhibits two peaks at 61.8 and 15.5 ppm that also corresponds to the coordinated $P(OEt)_3$ ligands. Lastly, a single resonance at 134.28 ppm was observed in the ^{31}P MAS NMR spectrum, which is significantly upfield compared to $Ni[P(OEt)_3]_4$ taken in C_6D_6 (159.23 ppm). This change in chemical shift is expected to correspond to a loss in electron density at the Ni center after protonation to form cationic $[Ni–H]^+$ complexes, as similar homogeneous cationic Ni^{II} species are found within this region.[212] Overall, these data point towards the likelihood of $Ni[P(OEt)_3]_4$ protonation by SZO_{300} to form $[Ni–H]^+$ species on the surface.

Catalyst Heterogeneity, Stability, Robustness, and Practicality

To investigate the heterogeneity of Ni/SZO_{300}, a hot-filtration test was conducted using grafted [Ni]-SZO that was previously prepared. Using standard reaction conditions, two experiments with **1a** were run in parallel and the reaction progress was monitored over time (**Figure 6.2.b.**). The standard conditions and procedure were used for one reaction (**Figure 6.2.b.**, green diamonds); the other reaction was filtered while at 23 °C after 20 minutes and the reaction progress of the filtrate was continued to be monitored (**Figure 6.2.b.**, yellow triangles). Heterogeneously catalyzed isomerization will cease after filtration, and if the active catalyst is leaching from the surface to form a homogeneous catalyst in situ, the concentration of product will keep increasing. ICP-MS analysis of the filtered reaction filtrate resulted in 5% of Ni leaching from the solid catalyst, which is likely due to the solid catalyst breaking down by the stir bar, thereby releasing Ni into solution. However, as anticipated, the filtered reaction stagnated, with no additional conversion of **1a**, formation of **2a**, or change in the *E*/*Z* ratio. This key finding supports the notion that this catalyst is heterogeneous in nature.

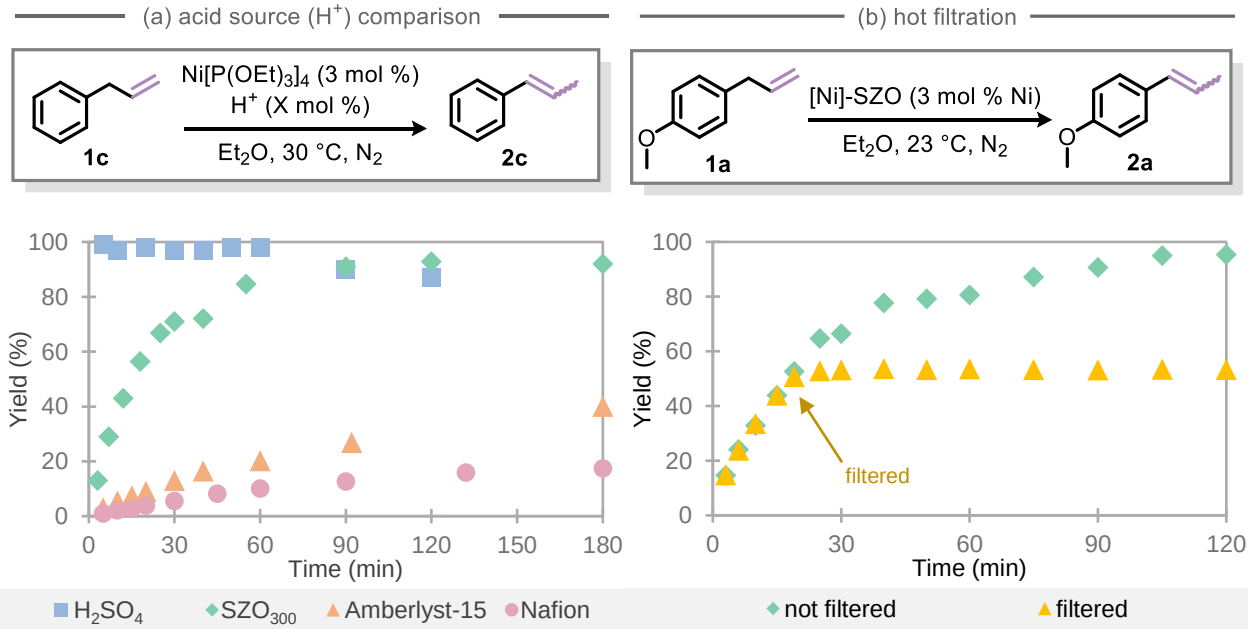

Figure 6.2. (a) Comparison of the acid sources (H^+) in isomerization of **1c** to **2c**. Conditions: allylbenzene (**1c**, 0.13 mmol, 1.0 equiv), $Ni[P(OEt)_3]_4$ (0.0036 mmol, 3.0 mol %), H^+ (0.0062 mmol, 5.0 mol %), and Et_2O (2.0 mL). (b) Hot-filtration experiment. Conditions: **1a** (0.12 mmol, 1.0 equiv), [Ni]-SZO (0.0036 mmol, 3.0 mol %), and Et_2O (2.0 mL). Typical reaction conditions without filtration (green diamonds); filtered reaction (yellow triangles). Yield and selectivity determined by GC analysis using cyclooctane as an internal standard for all experiments.

After validating the heterogeneity of the catalyst, we investigated catalyst stability. Tolman found that the active catalyst generated from $Ni[P(OEt)_3]_4$ and H_2SO_4 is highly unstable, converting just 22% of 1-butene after aging the catalyst for 85 minutes, whereas 95% of 1-butene was converted when using freshly prepared catalyst.[22,195] He showed that this catalyst deactivation is due to the reaction between an acid (either excess H_2SO_4 or the counterion HSO_4^-, which forms after protonation of Ni^0) and the proposed active catalyst $[Ni–H]^+$, generating H_2 and an inactive Ni^{II} complex.[194] We hypothesized that the low surface densities of acidic sites on SZO_{300} and the coulombic attraction of the $[Ni–H]^+$ site to the surface anions are effectively immobilizing and localizing the active site, thereby preventing the $[Ni–H]^+$ species from reacting with other acid sites and undergoing this detrimental deactivation pathway.

To test this hypothesis and compare the stabilities of both the Ni/SZO_{300} and Ni/H_2SO_4 catalysts, both catalysts were generated and aged in Et_2O for 24 hours and then their isomerization activity was compared to the activity of freshly prepared catalyst. **Figure 6.3.a.** shows the reaction progress over time for both catalysts and both freshly generated and aged catalysts using allylbenzene (**1c**) as the substrate. The freshly prepared homogeneous catalyst is highly active, reaching quantitative yield before the first aliquot was removed from the reaction for analysis (5 minutes; filled blue squares); aging this catalyst for 24 hours completely deactivates it, and no formation of **2c** is measured after 2 hours (hollow blue squares). The freshly prepared heterogeneous catalyst is slower than fresh Ni/H_2SO_4 (as discussed above for **1a**), reaching 92% yield after 2 hours (filled green diamonds); in contrast to Ni/H_2SO_4, aging Ni/SZO_{300} for 24 hours had essentially no impact on the catalyst activity (hollow green diamonds). This stability is also visually observable: both freshly prepared catalysts are bright orange (see **Figure 6.1.d.** for a picture of Ni/SZO_{300}), but the homogeneous catalyst gradually becomes colorless over the first hour, and the heterogeneous catalyst retains its orange color throughout the 24-hour aging period. These data support our hypothesis that catalyst deactivation is prevented by isolating the active site. However, upon exposing [Ni]-SZO to ambient atmosphere for 1 h, the resulting catalyst was inactive for isomerization.

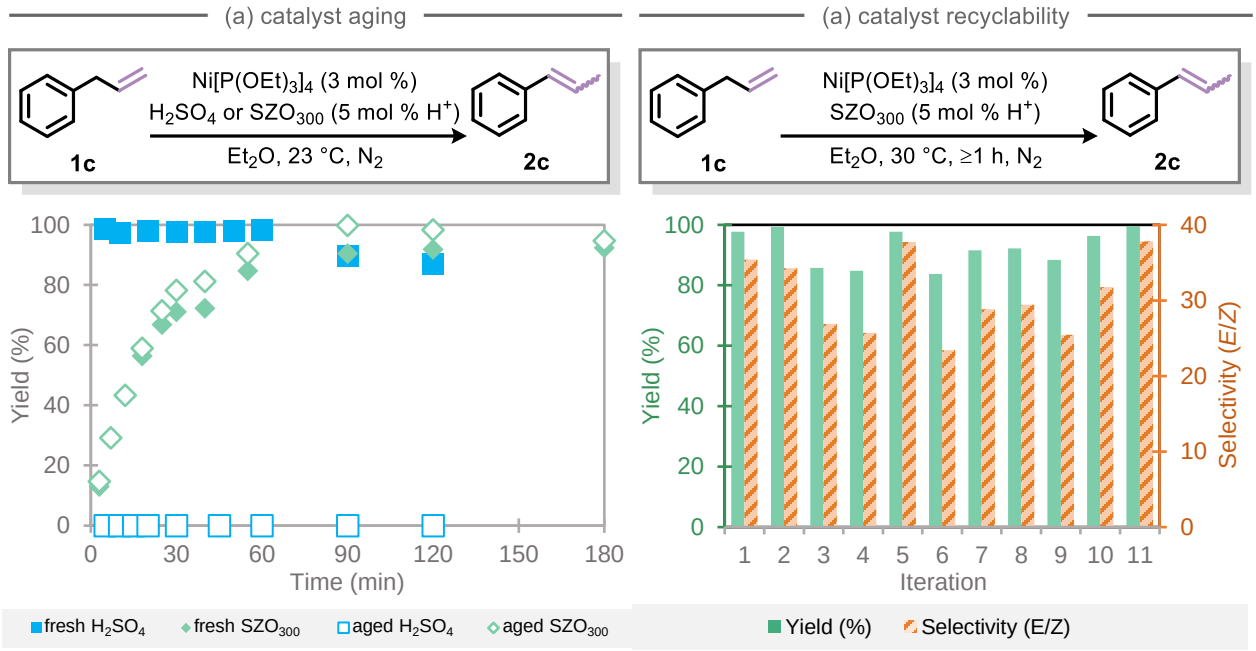

Figure 6.3. (a) Catalyst aging study of Ni/H_2SO_4 (blue squares) and Ni/SZO_{300} (green diamonds). Conditions: **1c** (0.12 mmol, 1.0 equiv), $Ni[P(OEt)_3]_4$ (0.0036 mmol, 3.0 mol %), H_2SO_4 or SZO_{300} (0.0060 mmol H^+, 5.0 mol %), and Et_2O (2.0 mL). (b) Catalyst recyclability study for the isomerization of **1c**. Conditions: (**1c**, 0.060 mmol), $Ni[P(OEt)_3]_4$ (0.0018 mmol, 3.0 mol %), SZO_{300} (0.0030 mmol H^+, 5.0 mol %), and Et_2O (1.0 mL). Yield and selectivity determined by GC analysis using cyclooctane as an internal standard.

The remarkable stability of the heterogeneous catalyst demonstrated in the catalyst aging study inspired us to investigate the recyclability of the catalyst. After generating the catalyst in Et_2O, allylbenzene (**1c**) was added to the reaction at 23 °C. The reaction was allowed to stir for at least 1 h between each cycle to ensure reaction completion. After the reaction, the solution was decanted from the solid and analyzed by GC; then fresh solution of **1c** was introduced to the catalyst. This process was repeated for a total of 10 cycles, giving good-to-excellent yields of **2c** (**Figure 6.3.b.**, left axis) and excellent *E*/*Z* selectivity (**Figure 6.3.b.**, right axis) with little to no catalyst decomposition observed between each cycle (**Figure 6.3.b.**).

Substrate Scope

Having good evidence demonstrating the heterogeneity and high activity of Ni/SZO_{300} and using our optimized reaction conditions, we tested a library of alkenes to demonstrate the broadness of the substrate scope (**Figure 6.4.**). All reactions were performed using 3 mol % $Ni[P(OEt)_3]_4$, 5 mol % H^+ sites in SZO_{300}, Et_2O as the solvent, and 30 °C reaction temperature,

unless stated otherwise. We initially evaluated a variety of functional groups using the additive screening protocol (**Table E.3.**)[213] and used those results as a guide in substrate choice. A wide range of electronically (**1a**-**1g**) varied akenes were well-tolerated, resulting in good-to-excellent yield (77-94%) and selectivity (*E*/*Z* ≥ 25:1). Adding steric bulk, as seen in substrate **1h**, does not diminish the yield (97%), but the selectivity does decrease to 13:1 (*E*/*Z*). The formation of trisubstituted alkenes in high *E*/*Z* selectivity is a significant challenge in base metal-catalyzed alkene isomerization, with notable advancements using Co and Fe homogeneous catalysts recently disclosed.[214–221] Isomerization of **1i**, a 1,1-disubstituted alkene, to **2i**, a trisubstituted alkene, gave 97% yield and modest selectivity (*E*/*Z* = 7.7:1).

We hypothesized that having a slight molar excess of acidic sites relative to Ni (5 mol % and 3 mol %, respectively) under our optimized conditions might lead to intolerance of acid-sensitive functional groups. However, they are compatible, suggesting that the remaining acidic sites are inaccessible. Substrates with a methoxy methyl ether (**2j**) and trimethylsilyl ether (**2k**) were well-tolerated, giving 68% and 93% yield and 19:1 and 18:1 *E*/*Z* ratios, respectively. Substrates with functional groups that would typically deactivate late transition metal catalysts like phenol (**1l**; 98% yield; *E*/*Z* = >99:1), nitrile (**1m**; 98% yield; *E*/*Z* = 25:1), and carboxylic acid (**1n;** 74% yield; *E*/*Z* = >99:1) are tolerated very well, giving excellent yield and *E*/*Z* selectivity.

Heterocyclic substrates are also tolerated: the indole derivative **1o** yields 70% of **2o** and thiophenes **1p** and **1q** yield 88% of **2p** and 98% of **2q**, respectively. However, the presence of a sulfone in **1r** was not as well-tolerated, with only 37% of **1r** converting to **2r**. The reaction of allylthiophene **1p** did not complete at 30 °C (~60% conversion was measured) but increasing the catalyst loading to 4:7 mol % $Ni[P(OEt)_3]_4/SZO_{300}$, the reaction temperature to 50 °C, and the reaction time to 24 h gave full conversion, and **2p** was isolated in 88% yield. The *E*/*Z* selectivity of products **2o** and **2p** is good, although lower than allylbenzene derivatives (9.5:1 and 7.4:1, respectively). The selectivity of the reaction forming product **2q** reverses, favoring the *Z*-isomer (*E*/*Z* = 1:1.7). The switch in selectivity to favor formation of the *Z* isomer is also seen in phenyl allyl ether **2s** (73% yield; *E*/*Z* = 1:2.8). The *E*- and Z-isomers of enol ethers are known to have similar thermodynamic stabilities, which informs us that the selectivity of the Ni/SZO_{300} catalyst is likely dictated by thermodynamics.[222–224] This conclusion is supported by the data in Tables S5 and S6; at early reaction times, low *E*/*Z* ratios are measured, and the selectivity increases over time, even after conversion of the substrate completes (*i.e.*, more of the *Z*-isomer is formed at the

beginning of the reaction, and then the *Z*-isomer is converted to the *E*-isomer as the reaction proceeds).

Other challenging functional groups with heteroatoms are excellently tolerated. In addition to the amino functional group in **1o**, the tosyl-protected allyl amine **1t** and the amide **1u** both proceed to high yield (97% and 91%, respectively) and *E*/*Z* selectivity (24:1 and >99:1, respectively). The allyl boronic ester **1v** isomerized to the vinyl boronic ester **2v** in 61% yield and 8.8:1 *E*/*Z* selectivity. Protected phenol derivatives **1w** and **1x** gave excellent yields and *E*/*Z* selectivity (97% and >99% yield; *E*/*Z* = 16:1 and 29:1, respectively). The presence of (pseudo)halides and halides in **1x** and **1y**, respectively, were well tolerated to yield >99% and 92%, respectively, and high selectivity (*E*/*Z* = 29:1 and >99:1, respectively). **1q**, **1x**, and **1y** exemplify the compatibility of halides and (pseudo)halides with these catalytic conditions, holding potential for future derivatization. Likewise, the aldehyde in **1g** was compatible with these reaction conditions, affording the alkene isomerization product **2g** in 94% yield and >99:1 *E*/*Z* selectivity.

1-decene **1z** is readily isomerized to 2-decene **2z** in 88% yield with good selectivity (*E*/*Z* = 8.9:1) and a 6.7:1 ratio of the 2-decene to the 3-, 4-, and 5-decene isomers, demonstrating good positional selectivity. To rationalize the favorability of 2-decene formation over other internal isomers, the relative rates of isomerization of **1aa** to **2aa** and **2aa** to **2ab** were monitored by GC. Taking the linear portion of the first 10 min of each reaction, the isomerization of **1aa** to **2aa** is 55x faster than that of the isomerization of **2aa** to **2ab** (**Figure E.4.**, see Appendix E for details). This is likely due to accessible binding mode of the terminal alkene (**1aa**) than the internal alkene (**2aa**) for isomerization to proceed.[225] These data inspired us to evaluate the potential of controlling the positional selectivity of Ni/SZO_{300}. Using a lower reaction temperature of 0 °C, migration of the alkene in homoallylbenzene **1aa** was controlled to one bond, and **2aa** was formed in 88% yield, 5.0:1 *E*/*Z* selectivity, and 14:1 positional selectivity (**2aa**/**2ab**). Using an elevated temperature (70 °C), alkene migration proceeded to the most thermodynamically favorable site, forming β-ethylstyrene **2ab** in 87% yield, >99:1 *E*/*Z* selectivity, and 1:16 positional selectivity (**2aa**/**2ab**).

To show the practicality of this Ni/SZO_{300} catalyst, we performed the isomerization of **1a** on a 1.26 g scale (8.53 mmol) under optimized reaction conditions. **1a** proceeded to complete conversion to **2a** after 2 h. The product was purified by a simple filtration to remove the solid

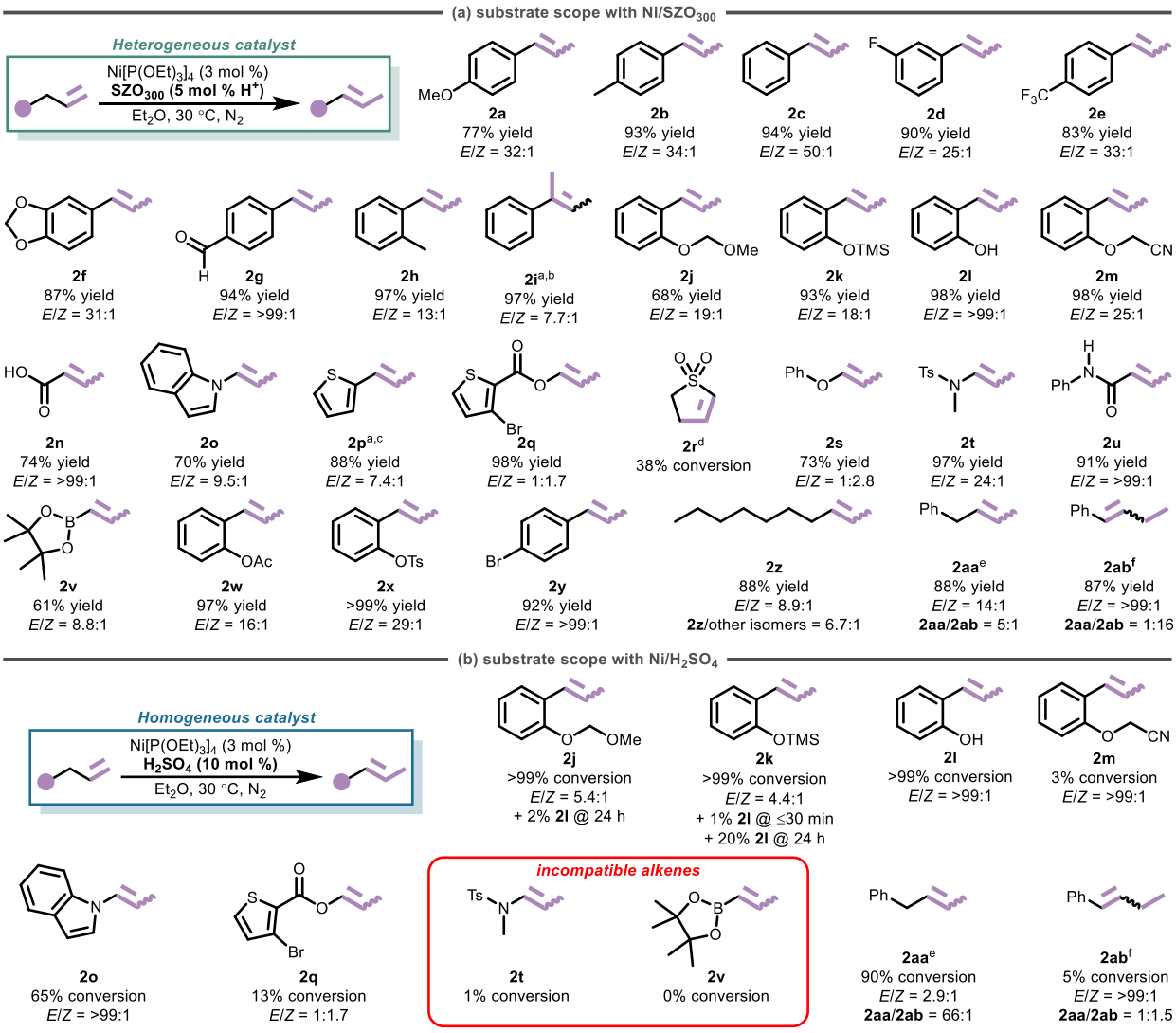

Figure 6.4. (a) Substrate scope for isomerization using Ni/SZO_{300}. Isolated yields and selectivity (*E*/*Z*) of the isolated products are reported. The selectivity was determined by relative integrations in the ^{1}H NMR. Conditions: **1** (1.0 mmol, 1.0 equiv), Ni[$P(OEt)_3$]$_4$ (0.030 mmol, 3.0 mol %), SZO_{300} (0.050 mmol H^+, 5.0 mol %), Et_2O (17 mL), 30 °C, 1-24 h. (b) Substrate scope with Ni/H_2SO_4. Conversion is reported as % conversion to product. Conversion and selectivity were determined by GC or GC-MS. Conditions: **1** (0.060 mmol), Ni[$P(OEt)_3$]$_4$ (0.0018 mmol, 3.0 mol %), H_2SO_4 (0.0030 mmol H^+, 5 mol %), Et_2O (1.0 mL). Ts, tosyl; TMS, trimethylsilane, Ac, acyl. [a]50 °C. [b]0.87 mmol **1i**, 3.4 mol % Ni[$P(OEt)_3$]$_4$, 5.6 mol % SZO_{300}. [c]0.68 mmol **1p**, 4.4 mol % Ni[$P(OEt)_3$]$_4$, 7.4 mol % SZO_{300}. [d]Isolated as a mixture of **1r** and **2r**. [e]0 °C. [f]70 °C.

catalyst and concentration to give product **2a**. This straightforward process gave an excellent isolated yield of 98% (1.24 g, 8.37 mmol) while retaining high *E*/*Z* selectivity of 33:1 (*E*/*Z*). These results paired with the diverse functional group tolerance showcase the potential usefulness of this heterogeneous $[Ni–H]^+$ isomerization catalyst.

As an effort to simply the system, we wondered if the pre-heat treated SZO_{300} precursor, $Zr(OH)_4•H_2SO_4$, was a viable acid source for alkene isomerization. Under standard reaction conditions, $Zr(OH)_4•H_2SO_4$ was used in place of SZO_{300} for the isomerization of **1c** to **2c**. Analysis by GC shows that at 80 minutes, the reaction reaches 88% yield with good *E*-selectivity of 20:1, which is comparable to that of using SZO_{300} (81% yield and *E*/*Z* = 26:1). At 120 minutes, the yield remains the same (90%) while *E*-selectivity continues to rise (*E*/*Z* = 27:1) similarly to that of the Ni/SZO system (90% yield, *E*/*Z* = 30:1). As a test to confirm that the $Ni/Zr(OH)_4•H_2SO_4$ system behaved the same as the Ni/SZO, we tested the isomerization of **1t**, an alkene that was incompatible with Ni/H_2SO_4, on a 1 mmol scale under standard conditions. After 24 h, ^{1}H NMR analysis of the crude reaction indicates 9% of unreacted **1t**, 65% of **2t** with low *E*-selectivity of 6.2:1 (*E*/*Z*), as well as deallylated **1t** to form the 2° amine, **S1** (see Appendix E for details). Both Ni and Pd have been previously reported to undergo deallylation of amines.[226,227] Although the isomerization of **1t** to **2t** was observed by $Ni/Zr(OH)_4•H_2SO_4$, the low *E*/*Z* selectivity and competing side reaction deems this catalytic system less effective than the Ni/SZO system. This highlights the crucial role that SZO has in alkene isomerization efficiency and activity.

Comparison of Ni/SZO$_{300}$ to Homogeneous Catalysts

A subset of the substrates included in **Figure 6.4.a.** were also evaluated for isomerization using Ni/H_2SO_4, the homogeneous analog of Ni/SZO_{300}, using standard conditions (**Figure 6.4.b.**). With a few exceptions, we found that the heterogeneous catalyst is generally more compatible with more functional groups and is more selective. Substrates **1t** and **1v** are incompatible with Ni/H_2SO_4 (≤1% conversion), and substrates **1m** and **1q** give very low conversions to the isomerized product (3% and 13%, respectively), but all of these substrates give excellent yields with Ni/SZO_{300} (97%, 61%, 98%, and 98%, respectively). Notably, we have not found a substrate that is compatible with Ni/H_2SO_4 and incompatible with the heterogeneous Ni/SZO_{300} catalyst, highlighting the unique advantages offered by this heterogeneous catalyst. Ni/H_2SO_4 outcompeted Ni/SZO_{300} with only one identified substrate, **1l**: >99% conversion and >99:1 *E*/*Z* selectivity in <30 min with Ni/H_2SO_4, 98% yield and >99:1 *E*/*Z* selectivity in 4 h with Ni/SZO_{300}. Ni/H_2SO_4 took 24 hours to catalyze **1o** to **2o** in 65% conversion with an *E*/*Z* ratio of >99:1, but this substrate reached complete conversion and higher *E*/*Z* ratio of 9.5:1 (*E*/*Z*) in just 8 hours with Ni/SZO_{300}. Conversion of **1f, 1j,** and **1k** using Ni/H_2SO_4 was high (>99% for all) after less than 30 minutes, while the Ni/SZO_{300} catalyst

required 5 hours, 8 hours, and 5 hours, respectively, to reach similar conversion. However, for all alkenes **1j,** and **1k** the *E*/*Z* selectivity with Ni/SZO_{300} (19:1, and 18:1, respectively) was significantly better than with Ni/H_2SO_4 (5.4:1 and 4.4:1, respectively). Further demonstrating the advantage of using Ni/SZO_{300} over its homogeneous analog, approximately 1% of the deprotected phenol (**2l**) was observed after just 30 minutes of reaction time with substrate **1k**. A longer reaction time of 24 h to form **2j** and **2k** with Ni/H_2SO_4 revealed further deprotection of **2j** and **2k** to form 2% and 20% **2l**, respectively, while no evidence of deprotection was present with Ni/SZO_{300}. We wondered if positional selectivity could also be achieved using the Ni/H_2SO_4 system. At 0 °C, 90% **1aa** was converted to **2aa** with improved positional (**2aa**/**2ab** = 66:1) but with diminished *E*-selectivity (*E*/*Z* = 2.9:1) as the Ni/SZO_{300} system (**2aa**/**2ab** = 14:1, *E*/*Z* = 5.0:1). On the contrary, the Ni/H_2SO_4 catalyst was rather unstable at 70 °C revealed by the low conversion of **1aa** to **2ab** (5%) and poor positional selectivity (**2aa**/**2ab** = 1:1.5). These results further show the advantages of having enhanced catalyst stability, seen in the Ni/SZO_{300} system, compared to the much less stable homogeneous analog.

To further demonstrate the exceptional performance of Ni/SZO_{300}, we sought to compare its activity and selectivity to those from other state-of-the-art homogeneous Ni and Pd catalysts (**Figure 6.5.**). Schoenebeck,[228] Engle,[229] our lab,[230] and others[4,47–52] have recently developed Ni-catalyzed isomerization catalysts that are *E*-selective. Additionally, Skrydstrup reported a Pd-catalyzed isomerization system that is highly compatible with a diverse set of alkene-containing substrates.[237] Despite the rich display of reactivity exhibited by these homogeneous catalysts, minimal work has been done to unveil relative isomerization rates.

We initiated our studies by monitoring the formation of **2a** from **1a** over time for the following systems: Ni[$P(OEt)_3$]$_4$/SZO_{300} (**A**; this work); $(IPr)_2Ni_2Cl_2$ (**B**; Schoenebeck;[228] IPr = 1,3-bis(2,6-diisopropylphenyl)imidazol-2-ylidene), Ni$(cod)_2$/PCy_3•HBF_4, (**C**; Engle;[229] cod = cyclooctadiene; Cy = cyclohexyl), (IPr)Ni(hex)/$HSiPh_3$, (**D**; Cook;[230] hex = 1,5-hexadiene), and $Pd(dba)_2$/P(*t*-Bu)$_3$/*i*-PrC(O)Cl (**E**; Skrydstrup;[237] dba = dibenzoylacetone). Each isomerization reaction was performed under its respective optimized conditions and the product formation over time was measured by GC (**Figure 6.5.**).

Monitoring the reactions over time, we see that all but system **D** (**Figure 6.5.**, yellow triangles) reach completion by 180 min. Due to the induction periods observed for systems **C** and

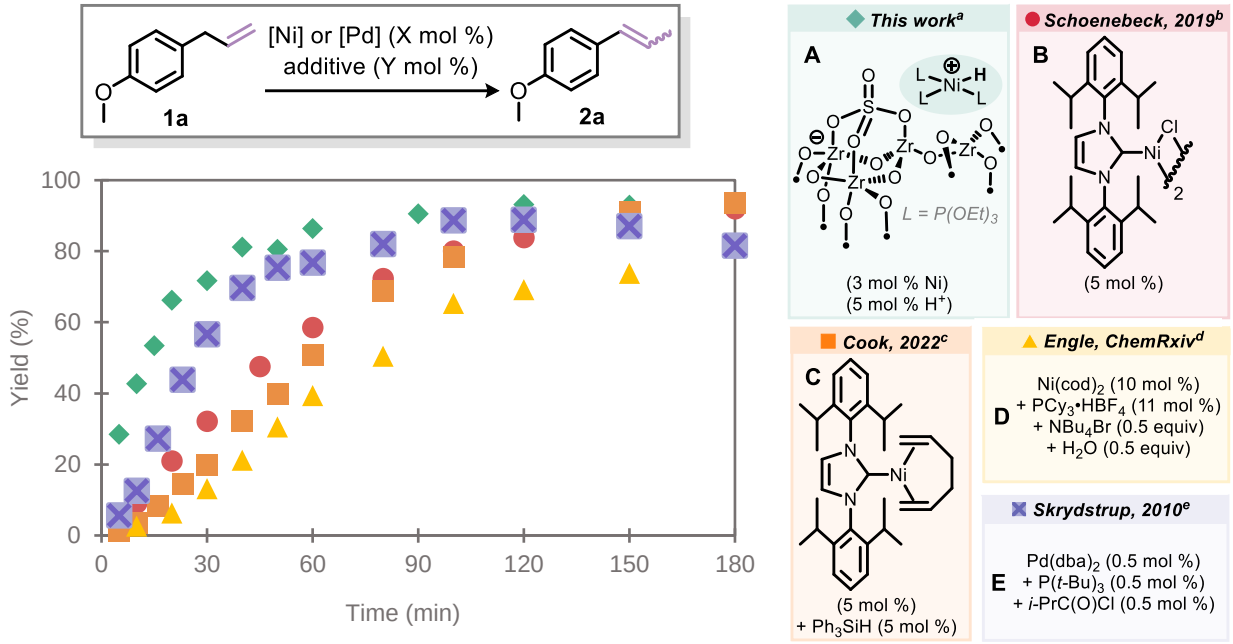

Figure 6.5. Kinetic analysis of Ni and Pd isomerization catalysts. **1a** (0.12 mmol unless otherwise stated). [a]$Ni[P(OEt)_3]_4$ (0.0036 mmol, 3.0 mol %), SZO_{300} (0.0060 mmol H^+, 5.0 mol %), Et_2O (2.0 mL), 30 °C. [b]$(IPr)_2Ni_2Cl_2$ (0.0060 mmol, 5.0 mol %), ClC_6H_5 (0.3 mL), 30 °C. [c](IPr)Ni(hex) (0.0060 mmol, 5.0 mol %), $HSiPh_3$ (0.0061 mmol, 5.0 mol %), hexanes (0.38 mL), 80 °C. [d]**1a** (0.25 mmol), $Ni(cod)_2$ (0.025 mmol, 10 mol %), PCy_3•HBF_4 (0.027 mmol, 11 mol %), NBu_4Br (0.12 mmol), H_2O (0.12 mmol), DMF (5.0 mL), 30 °C. [e]$Pd(dba)_2$ (0.00061 mmol, 0.50 mol %), P(*t*-Bu)$_3$ (0.00061 mmol, 0.50 mol %), *i*-PrC(O)Cl (0.00061 mmol, 0.50 mol %), toluene (2.9 mL), 80 °C. IPr, (IPr = 1,3-bis(2,6-diisopropylphenyl)imidazol-2-ylidene); cod, 1,5-cyclooctadiene; hex, 1,5-hexadiene; dba, dibenzylideneacetone.

D, linear rates were not calculated to compare relative isomerization rates between each system. Visual analysis of the reaction progress over time reveal that systems **B**, **C**, and **D** all exhibit slower reaction kinetics than **A** and **E**. It is notable that system **A** (Ni/SZO_{300}) is performed at 30 °C using 3 mol % Ni, while system **E** requires an elevated reaction temperature of 80 °C, but performs well using just 0.5 mol % Pd. The corresponding selectivity profile for systems **C**, **D**, and **E** equilibrates to ~15:1 (*E*/*Z*) at 3 h, whereas systems **A** and **B** gradually increase over time to ~30:1 *E*/*Z* by 3 h (Figure S30). These catalyst systems were also all compared at equal catalyst loadings (3 mol % Ni or Pd and 3 mol % additive/ligand) and reaction temperature (30 °C), but with each respective system's optimal reaction solvent and concentration (**Figures E.41.-E.42.**). Ni/SZO_{300} reaches completion in ~90 min (91% yield), systems **B**, **D**, and **E** reach ~20% conversion after 150 min, and system **C** does not produce any product. Both Ni/SZO_{300} and **B** reach the highest selectivity

after 2 h compared to the other catalysts. These data further demonstrate the excellent performance of Ni/SZO_{300}, even in comparison to the state-of-the-art Ni and Pd catalysts.

Mechanistic Studies

Having successfully developed a heterogeneous isomerization catalyst with a large substrate scope, we embarked on preliminary mechanistic investigations. We hypothesized that the heterogeneous catalyst has similar reaction and catalyst activation mechanisms as the Ni/H_2SO_4 catalyst. Alkene isomerization most often occurs via 1) a radical mechanism, 2) $C_{allylic}$–H activation to form a metal-allyl intermediate, and 3) M–H (M = metal) insertion/elimination pathways.[172–176] Tolman demonstrated that the homogeneous Ni/H_2SO_4 catalyst proceeds though a M–H insertion/elimination pathway,[195] so we hypothesized that Ni/SZO_{300} would operate under the same mechanism. To probe whether a radical pathway is occurring, we tested the reaction of Ni[$P(OEt)_3$]$_4$ with **1ac** (**Scheme 6.1.a.**). If isomerization proceeds through a radical pathway, a few rearrangement products are possible.[214,238,239] However, none were observed at 30 °C, 50 °C, and 70 °C, implying that a radical pathway is not proceeding. This result also suggests that there is no or very little Ni(0) present, since Ni(0) complexes are known to oxidatively add to cyclopropane rings and rearrange the carbon skeleton.[230,240] As an additional radical probe, the 1,6-diene **1ad**, which is expected to cyclize to form a methylenecyclopentane under radical conditions, shows only alkene isomerization with Ni/SZO_{300} (**Scheme 6.1.b.**). After reacting **1ad** for 5 h at 30 °C, 97% of **1ad** was converted to the 1,5-diene (**2ad**), and no trace of cyclized product was identified by GC or ^{1}H NMR, further confirming that this reaction is likely not going through a radical pathway.[230,240]

We next wanted to distinguish between an allyl (intramolecular) or Ni–H insertion-elimination (intermolecular) mechanism. A crossover experiment was performed with 0.5 equiv **1a** and 0.5 equiv **1c-*d*$_n$** (**Scheme 6.1.c.**). If an allyl pathway is occurring, no protium/deuterium scrambling between the two substrates is expected.[173] Deuterium incorporation into **2a** and protium incorporation into **2c-*d*$_n$** is predicted if the mechanism proceeds via a Ni–H insertion/elimination mechanism, since the Ni–H/D formed during the reaction could exchange one alkene ligand for another. Analysis of the products by ^{1}H and ^{2}H NMR revealed significant protium/deuterium scrambling in both **2a** and **2c-*d*$_n$**, supporting the viability of an intermolecular, Ni–H insertion-elimination pathway (**Figures E.28.-E.30.**).

Potential of Ni/SZO$_{300}$ in Additional Catalytic Reactions

As metal–hydrides are often invoked in catalysis, our final goal is to demonstrate the broad utility of this heterogeneous catalyst by evaluating its activity in other catalytic reactions. Metal-catalyzed alkene hydrofunctionalization reactions offer access to value-added chemicals by installing structural diversity.[241–245] Specifically, hydroalkenylation is utilized in the Shell higher olefin process to produce 1x10^6 tons of olefins annually.[246] Additionally, hydroboration[247,248] products are excellent Suzuki-Miyaura cross-coupling partners to construct C–C bonds in organic synthesis.[249–251] Hydrosilylation reactions produce valuable organosilicon compounds used in reactions like Hiyama couplings for C–C bond formation,[252,252] Tamao-Fleming oxidations to form alcohols,[253–256] and polymerizations to form silicone materials[257–259]

Ni/SZO$_{300}$ is a viable catalyst for hydroalkenylation, hydroboration, and hydrosilylation of alkenes (**Figure 6.6.**). Notably, the results of these Ni/SZO$_{300}$-catalyzed reactions are unoptimized. Ni/SZO$_{300}$ is an excellent styrene hydroalkenylation catalyst, affording 94% yield (determined ^{1}H NMR spectroscopy using an internal standard) of product **3a**, with no evidence of formation of the other hydrovinylation isomers. Hydroboration[260,261] of the vinyl amide **2u** using B_2pin_2, LiO*t*-Bu, and MeOH resulted in 55% yield of product **3b** (determined by GCMS using an internal standard); like hydrovinylation, this reaction is highly selective, and product **3b** is the only isomer observed by both GC-MS and ^{1}H NMR spectroscopy. Lastly, styrene is hydrosilylated[262] by Ph_2SiH_2 using catalyst Ni/SZO$_{300}$, giving 21% yield of **3c** in 7:1 selectivity (branched/linear), as determined by GC-FID using an internal standard. These results demonstrate the potential for broad utility that this novel heterogeneous catalyst, Ni/SZO$_{300}$, holds.

Scheme 6.1. Mechanistic experiments. (a) Reactivity with vinylcyclopropane (**1ac**). (b) Reactivity with a 1,6-diene (**1ad**). (c) Crossover experiment between **1a** and **1c-*d*$_n$**.

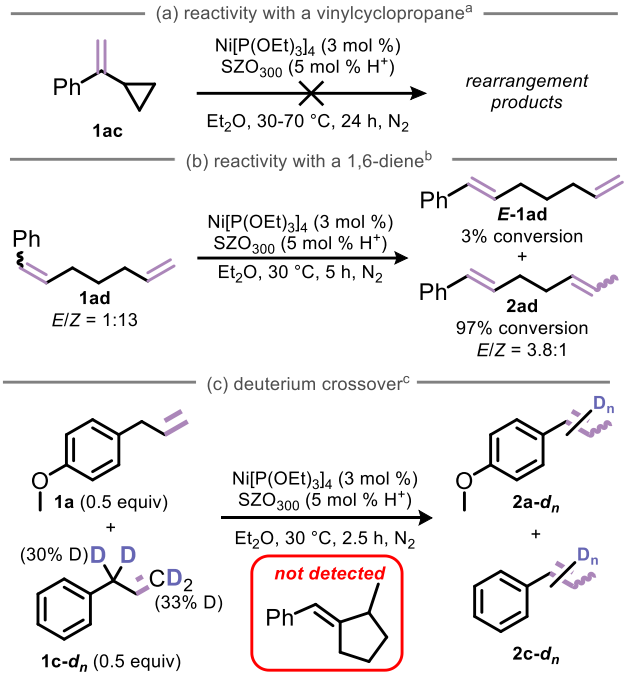

[a]Conditions: **1ac** (0.060 mmol), Ni[P(OEt)$_3$]$_4$ (0.0018 mmol, 3.0 mol %), SZO$_{300}$ (0.0030 mmol H$^+$, 5.0 mol %), Et$_2$O (1.0 mL). [b]Conditions: **1ad** (1.0 mmol), Ni[P(OEt)$_3$]$_4$ (0.030 mmol, 3.0 mol %), SZO$_{300}$ (0.050 mmol H$^+$, 5.0 mol %), Et$_2$O (17 mL). [c]**1a** (0.28 mmol, 0.50 equiv), **1c-*d*$_n$** (0.28 mmol, 0.50 equiv), Ni[P(OEt)$_3$]$_4$ (0.017 mmol, 3.0 mol %), SZO$_{300}$ (0.028 mmol H$^+$, 5.0 mol %), Et$_2$O (9.6 mL).

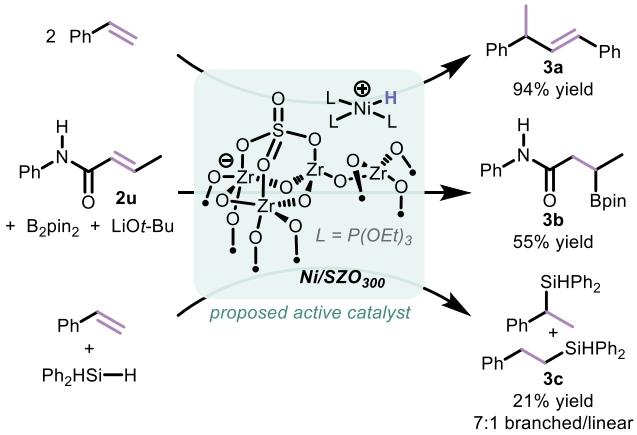

Figure 6.6. [Ni–H]$^+$-catalyzed reactions under unoptimized conditions. (a) Hydroalkenylation of styrene to afford **3a**. (b) hydroboration of **2u** and B$_2$Pin$_2$ to afford **3b**. (c) Hydrosilylation of styrene and H$_2$SiPh$_2$ to afford **3c**.

6.3 Conclusion

The combination of $Ni[P(OEt)_3]_4$ and SZO_{300} generates a potent alkene isomerization catalyst, with marked improvement over previous work that used sulfated polymers to heterogenize the $Ni[P(OEt)_3]_4/H^+$ isomerization system. Ni/SZO_{300} is heterogeneous in nature, as demonstrated by a hot-filtration test, and is highly recyclable and robust, as demonstrated with catalyst aging studies. Remarkably, the substrate scope is very broad and includes various heteroatoms, acid-labile groups, halides, carboxylic acids, and amides. The catalyst can also be kinetically controlled to achieve specific positional isomers when using a long chain alkene. Preliminary mechanistic results suggest against radical and allyl pathways but do allude to a M–H insertion/elimination mechanism for alkene isomerization. Ni/SZO_{300} also outcompetes state-of-the-art homogeneous Ni and Pd catalysts in head-to-head comparisons, in terms of both reaction rates and selectivity. The rational approach to designing this active site led to a heterogeneous catalyst with significantly increased catalyst versatility over its homogeneous counterpart.

APPENDIX A

SUPPLEMENTARY CONTENT FOR CHAPTER II

Experimental details

A.1.1. Materials and Methods

All syntheses and manipulations were carried out under nitrogen using standard Schlenk (vacuum 10^{-2} mbar) techniques or in a nitrogen-filled glovebox unless otherwise indicated. All reagents and solvents were used after drying and stored under nitrogen, unless otherwise indicated. Tetrahydrofuran (THF; Fisher Chemical; HPLC grade, unstabilized), hexanes (Fisher Chemical; HPLC grade), diethyl ether (B&J Brand; HPLC grade, unstabilized) and acetonitrile (Fisher Chemical; HPLC grade) were dispensed under nitrogen from an LC Technology SP-1 solvent system. Benzene (ACS grade) and pentane (HPLC grade) were refluxed overnight with CaH_2 and distilled under nitrogen before use. The dried solvents were thereafter stored on activated 4Å molecular sieves under nitrogen. CD_3CN, C_6D_6 and $CDCl_3$ were purchased from Cambridge Isotope Laboratories, degassed by freeze-pump-thaw, and thereafter stored on activated 4Å molecular sieves under nitrogen. All stock solutions were prepared by mass and were dispensed into the reaction vessel by difference from syringe, as detailed in the procedure for each experiment.

The following reagents were used from commercial sources without further purification: *N*,*N*'-dimethylthiourea (TCI), acetoin (TCI), potassium (Acros), 2,6-diisopropylaniline (TCI), 2,4,6-trimethylaniline (TCI), glyoxal (40 wt%, Sigma Aldrich), paraformaldehyde powdered (Oakwood Chemical), glacial acetic acid (Fisher Chemical, ACS grade), formic acid (Fisher Scientific), HCl (4M in dioxanes; Oakwood), trimethylsilylchloride (TCI), tetrafluoroboric acid (50 wt%; Beantown Chemical), potassium *tert*-butoxide (Strem, Oakwood Chemical), sodium hydride (60% dispersion in mineral oil; Aldrich), bis(1,5-cyclooctadiene)nickel(0) ($Ni(cod)_2$; Strem), allyl ether (TCI), 1,3-divinyltetramethyldisiloxane (dvtms, TCI), 1,5-hexadiene (TCI), allyl bromide (Aldrich Chemical), methyltriphenylphosphonium bromide (TCI), 4-(dimethylamino)benzaldehyde (Aldrich), 4-(trifluoromethyl)benzaldehyde (Alfa Aesar), 2-thiophenecarboxaldehyde (Aldrich), diisopropylamine (DIPA; Acros), 4-dimethylaminopyridine (DMAP; Aldrich), triethylamine (TEA; EM Science), 4-hydroxybenzaldehyde (Sigma), *p*-

toluenesulfonyl chloride (TCI), chloromethylmethylether (Sigma Aldrich), potassium carbonate (Fisher Chemical, ACS grade), lithium aluminum hydride (Aldrich), magnesium (Acros), iodine (Mallinckrodt), 4-bromoanisole (TCI), 4-bromotoluene (Aldrich), 1-bromo-3-fluorobenzene (Aldrich), 4-bromobenzotrifluoride (Matrix Scientific), 3-bromotoluene (Fluka), 2-bromotoluene (Aldrich), 2-bromomesitylene (Acros), 1-bromo-4-chlorobenzene (TCI), styrene (**2a**; TCI), 4-methoxystyrene (**2c**; Alfa Aesar), 4-*tert*-butylstyrene (**2d**; TCI), 4-methylstyrene (**2e**; TCI), 4-fluorostyrene (**2f**; Matrix), 2-methylstyrene (**2h**; TCI), 2-vinylnaphthalene (**2i**; Alfa Aesar), *trans*-β-methylstyrene (**2j**; TCI), 3,3-dimethyl-1-butene (**2m**; Acros), vinylcyclohexane (**2n**; TCI), 1-decene (**2o**; TCI), benzaldehyde (**2p**; Sigma Aldrich), acetophenone (**2q**; Sigma Aldrich), acetone (**2r**; Fisher Chemical, ACS grade), phenylacetylene (Aldrich), (+/-)-limonene (TCI), cyclooctene (Acros), diphenylsilane (**3a**; Oakwood), diethylsilane (**3j**; Alfa Aesar), 1-naphthylphenylsilane (**3i**; Sigma Aldrich), methyldiphenylsilane (**3n**; Alfa Aesar), dimethylphenylsilane (**3o**; TCI), triphenylsilane (**3l**; Thermo Scientific), triethoxysilane (**3p**; Acros), 1,1,1,3,5,5,5-heptamethyltrisiloxane (**3q**; TCI), trichlorosilane (**3r**; Alfa Aesar), dichloromethylsilane (**3s**; Alfa Aesar), dichlorodiphenylsilane (TCI), trichlorophenylsilane (TCI), and durene (Eastman Chemical Company).

1c was synthesized via reported procedure.[6,125]

A.1.2. General Experimental

Nuclear magnetic resonance (NMR) spectra were collected at room temperature (298 K) unless otherwise stated on a Bruker AV-III HD 600 NMR (600.13 MHz for ^{1}H; 150.90 MHz for 13C; 564.69 MHz for ^{19}F; 119.23 MHz for ^{29}Si; 92.12 MHz for ^{2}H), Bruker Avance-III HD 500 NMR (499.90 MHz for ^{1}H; 126 MHz for ^{13}C; 471 MHz for ^{19}F; 99 MHz for ^{29}Si), or Varian Inova 500 NMR (499.90 MHz for ^{1}H; 126 MHz for ^{13}C; 471 MHz for ^{19}F; 99 MHz for ^{29}Si). ^{1}H and ^{13}C spectra were referenced to the residual solvent peak ($CDCl_3$: ^{1}H δ = 7.26 ppm, ^{13}C δ = 77.16 ppm; C_6D_6: ^{1}H δ = 7.16 ppm, ^{13}C δ = 128.06 ppm, CD_3CN: ^{1}H δ = 1.94 ppm, ^{13}C δ = 1.32 ppm (NC*C*D_3)). Chemical shifts for ^{1}H, ^{13}C, and ^{29}Si NMR spectra are reported in parts per million (ppm, δ) relative to tetramethylsilane at 0.00 ppm. Peaks are characterized as follows: s (singlet), d (doublet), t (triplet), q (quartet), pent (pentet), hept (heptet), m (multiplet), qd (quartet of doublets), br (broad), app (apparent), and/or ms (multiple signals). Coupling constants, *J*, are reported in Hz. $^{1}J_{H–Si}$

coupling constants were determined, when possible, using the ^{29}Si satellites in the ^{1}H NMR spectrum.

Infrared (IR) spectroscopy for air-stable organic compounds was performed on an Agilent Nicolet 6700 FT-IR using the ATR sampling technique. IR spectra for air-sensitive nickel complexes were recorded as self-supported pellets diluted with KBr using a Bruker Alpha II FT-IR spectrometer that is housed in a nitrogen-filled glovebox. All bands are reported in wavenumbers (cm^{-1}) and are described as broad (br), strong (s), medium (m), and weak (w).

For catalytic reactions, yields were determined using Gas Chromatography-Mass Spectrometry (GC-MS) or Gas Chromatography-Flame Ionization Detector (GC) against an internal standard. GC-MS was carried out on a Shimadzu GC-2010 Plus/GCMS-QP2010 SE using a Restek Rtx®- 5 (Crossbond 5% diphenyl – 95% dimethyl polysiloxane; 15 m, 0.25 mm ID, 0.25 μm df) column. GC was carried out on a Thermo Fisher Trace 1300 Gas Chromatograph using a Restek Rtx®-5 (Crossbond 5% diphenyl – 95% dimethyl polysiloxane; 15 m, 0.25 mm ID, 0.25 μm df) column. High-resolution mass spectrometry (HRMS) was carried out on a Waters XEVO G2-XS TOF mass spectrometer.

A.1.3. Synthesis of Reagents

a. Synthesis of Ligands and Nickel Complexes

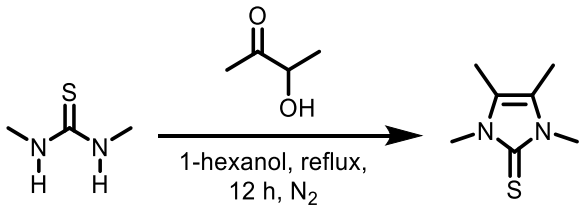

(L1)

1,3,4,5-Tetramethylimidazole-2(3*H*)-thione (**L1**) was synthesized in accordance with a literature procedure:[263] To a 250-mL Schlenk flask equipped with a stir bar was added *N*,*N*'-dimethylthiourea (4.2 g, 40 mmol, 1.0 equiv), acetoin (3.5 g, 40 mmol, 1.0 equiv) and 1-hexanol (100 mL). The reaction was refluxed for 12 h while stirring. The reaction was cooled to room temperature and the solvent was distilled off under reduced pressure. The flask was opened to atmosphere, washed with water (50 mL), followed by Et_2O (50 mL) and then filtered over a fine frit to yield **L1** as an off-white powder. (3.9 g, 25 mmol, 62% yield). NMR spectra match values previously reported.[263]

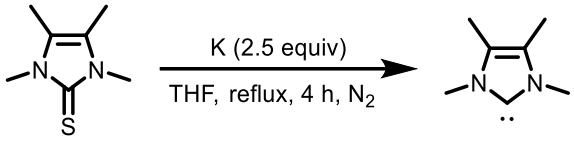

(L1) (ITMe)

1,3,4,5-Tetramethylimidazol-2-ylidene (ITMe) was synthesized in accordance with literature a procedure:[263] To a 100-mL Schlenk Flask equipped with a stir bar was added **L1** (1.2 g, 7.7 mmol, 1.0 equiv) and THF (45 mL) and the reaction was cooled to 0 °C in an ice/water bath while stirring. To this, potassium chunks (0.73 g, 19 mmol, 2.5 equiv) were added. The reaction was warmed to room temperature and then refluxed for 4 h. The reaction was cooled to room temperature, the solid was separated by filtration using a medium-porosity frit under N_2, and the filtrate was concentrated to yield **ITMe** as a white powder. (0.81 g, 6.5 mmol, 85% yield). NMR spectra match values previously reported.[263]

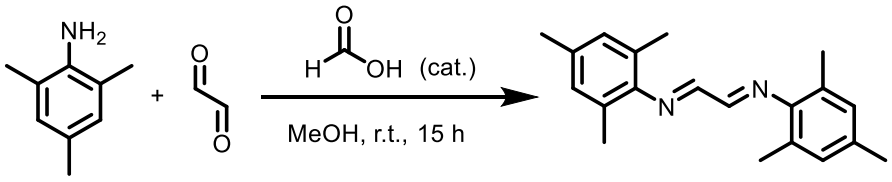

(2.0 equiv) (L2)

***N,N'*-Bis(2,4,6-trimethylphenyl)ethane-1,2-diimine (L2)** was synthesized in accordance with literature procedure:[264] Without exclusion of air and moisture, in a 25-mL round-bottom flask equipped with a stir bar was added 2,4,6-trimethylaniline (3.0 g, 22 mmol, 2.0 equiv) in methanol (10 mL). To this stirring solution, glyoxal (40 wt%, 1.3 mL, 11 mmol, 1.0 equiv) and formic acid (2 drops) were added. The reaction was capped and stirred for 15 h at room temperature. The product was collected via vacuum filtration, washed with methanol (3 x 10 mL) and dried under vacuum to obtain **L2** as a bright yellow powder (2.5 g, 8.5 mmol, 77% yield). NMR spectra match values previously reported.[264]

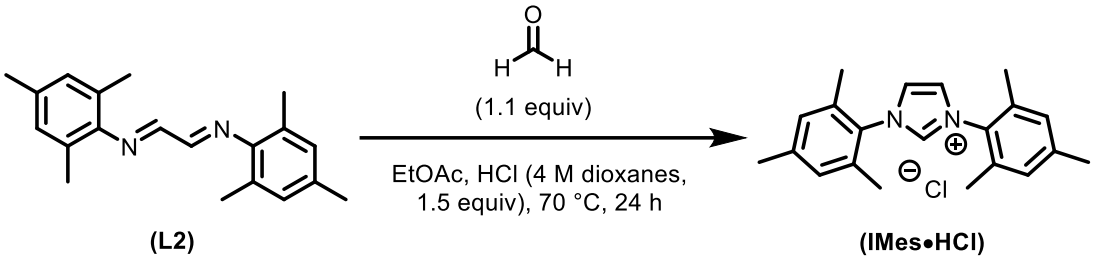

(L2) **(IMes•HCl)**

1,3-Bis(2,4,6-trimethylphenyl)imidazolium chloride (IMes·HCl) was synthesized in accordance with literature procedure:[264] Without exclusion of air or moisture, in a 50-mL round bottom flask equipped with a stir bar, **L2** (2.5 g, 8.5 mmol, 1.0 equiv) was dissolved in ethyl acetate (17 mL) and heated to 70 °C while stirring. In a separate 10-mL round bottom flask equipped with a stir bar was added paraformaldehyde (0.28 g, 9.3 mmol, 1.1 equiv) and HCl (4 M in dioxanes, 3.2 mL, 13 mmol, 1.5 equiv) and was stirred at 70 °C until all solids dissolved. The paraformaldehyde solution was added dropwise to the stirring solution of **L2**. The reaction was stirred at 70 °C for an hour, removed from the heat, allowed to cool to room temperature, and stirred overnight. The product was collected via vacuum filtration, washed with ethyl acetate (3 x 10 mL) and dried under reduced pressure to yield **IMes·HCl** as a fluffy yellow powder (2.9 g, 8.5 mmol, 99% yield). NMR spectra match values previously reported.[264]

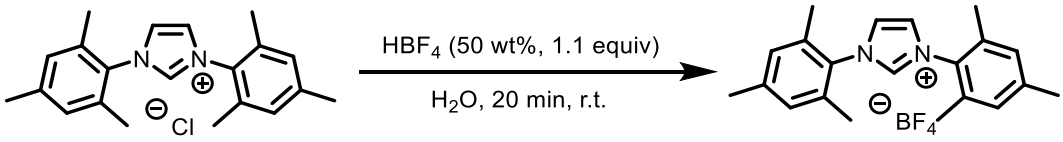

(IMes•HCl) **(IMes•HBF$_4$)**

1,3-Bis(2,4,6-trimethylphenyl)imidazolium tetrafluoroborate (IMes·HBF$_4$) was synthesized in accordance with literature procedure:[264] Without exclusion of air or moisture, in a 50-mL round bottom flask equipped with a stir bar was added **IMes·HCl** (2.3 g, 6.7 mmol, 1.0 equiv) and a minimal amount of water (10 mL). The mixture was stirred until **IMes·HCl** was dissolved. HBF_4 (50 wt%, 0.91 mL, 7.3 mmol, 1.1 equiv) was added to the stirring solution and a white precipitate immediately formed. This mixture was stirred for 20 min at room temperature. The product was extracted with dichloromethane (3 x 100 mL) and the organic layers were combined, and dried with $MgSO_4$, filtered, and concentrated under reduced pressure. The product was purified by solvating the crude product in minimal amounts of dichloromethane (3.0 mL) and then precipitated by the addition of diethyl ether (50 mL). The product was collected via vacuum filtration, washed

with diethyl ether (50 mL), and dried under reduced pressure to yield **IMes·HBF₄** as a white powder (2.0 g, 5.1 mmol, 76% yield). NMR spectra match values previously reported.[264]

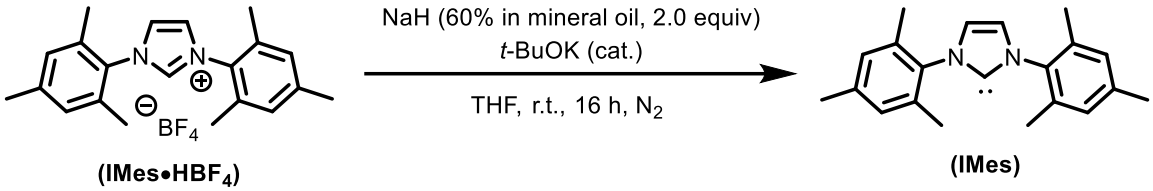

1,3-Bis(2,4,6-trimethylphenyl)-1,3-dihydro-2*H*-imidazol-2-ylidene (IMes) was synthesized in accordance with literature procedure:[264] In a 100-mL round bottom flask equipped with a stir bar was added **IMes·HBF₄** (2.0 g, 5.1 mmol, 1.0 equiv) in THF (20 mL). The mixture was stirred upon the slow addition of NaH (60% dispersion in mineral oil, 0.40 g, 10 mmol, 2.0 equiv) and *t*-BuOK (a spatula tip-ful). The reaction was vented for the first 15 min to release the initial formation of H_2 (g), capped, and stirred overnight at room temperature. After stirring for 16 h, the reaction mixture was filtered through a pad of Celite, and the filtrate was concentrated. The crude product was solvated in minimal amounts of THF (5.0 mL), hexanes was added (50 mL), and the vessel was capped and placed in the freezer (-30 °C). The product was collected via vacuum filtration, washed with cold hexanes, and dried under reduced pressure to obtain **IMes** as off-white crystals (0.93 g, 3.1 mmol, 60% yield). NMR spectra match values previously reported.[264]

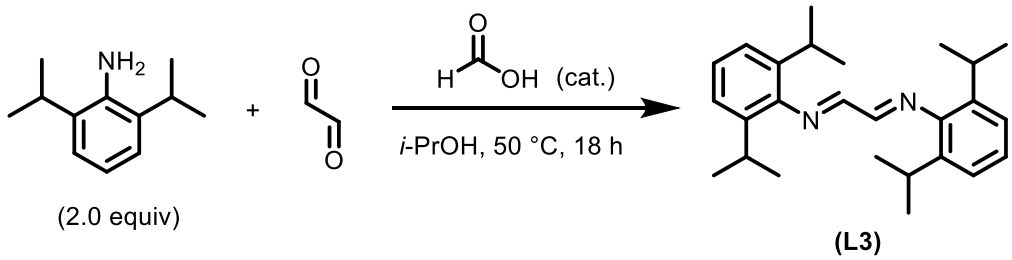

(1*E*,2*E*)-1,2-Bis(2,6-Diisopropylphenylimino)ethane (L3) was synthesized in accordance with literature procedure:[264] Without exclusion of air or moisture, to a 50-mL round bottom flask equipped with a stir bar was added 2,6-diisopropylaniline (3.0 g, 17 mmol, 2.0 equiv), glacial acetic acid (a few drops), and *i*-PrOH (10 mL) and stirred at 50 °C. To this solution, a mixture of glyoxal (40 wt%, 0.97 mL, 8.5 mmol, 1.0 equiv) and *i*-PrOH (5.0 mL) was added dropwise. After the addition of reagents, the reaction was lifted from the heat and slowly cooled to room temperature and stirred for 16 h. The crude mixture was placed in the freezer (- 25 °C) for 5 hours.

The product was collected via vacuum filtration, washed with *i*-PrOH (20 mL), and dried under reduced pressure to afford **L3** as a yellow powder (2.4 g, 6.4 mmol, 75% yield). NMR spectra match values previously reported.[264]

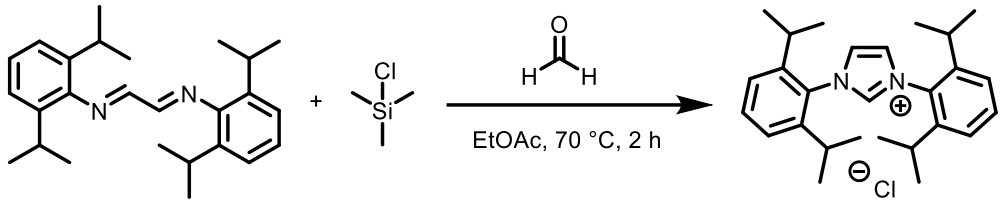

(L3) **(IPr•HCl)**

1,3-Bis(2,6-diisopropylphenyl)imidazolium chloride (IPr·HCl) was synthesized in accordance with literature procedure:[265] Without exclusion of air or moisture, to a 50-mL round bottom flask equipped with a stir bar was added **L3** (2.2 g, 5.8 mmol, 1.0 equiv), paraformaldehyde (0.17 g, 5.8 mmol, 1.0 equiv), and EtOAc (12 mL). The mixture was heated to 70 °C and stirred for 30 min. A solution of trimethylsilylchloride (0.75 mL, 5.9 mmol, 1.0 equiv) in EtOAc (5.0 mL) was added dropwise to the solution and the reaction was left to stir at 70 °C for 2 h. The reaction was taken off the heat to cool to room temperature and then placed in the freezer (-25 °C) overnight. The product was collected via vacuum filtration, washed first with EtOAc (10 mL) followed by *tert*-butyl methyl ether (10 mL), and dried in an oven at 100 °C for 4 h to yield **IPr·HCl** as a white powder (1.7 g, 4.0 mmol, 69% yield). NMR spectra match values previously reported.[264]

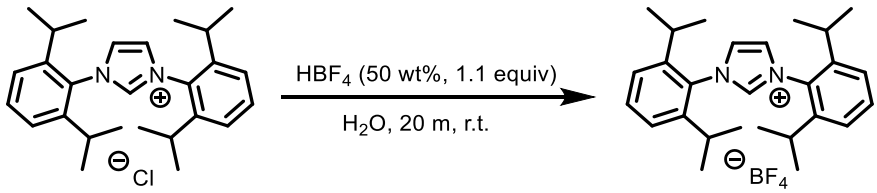

(IPr•HCl) **(IPr•HBF$_4$)**

1,3-Bis(2,6-diisopropylphenyl)-1*H*-imidazol-3-ium tetrafluoroborate (IPr·HBF$_4$) was synthesized in accordance with literature procedure:[264] Without exclusion of air or moisture, to a 50-mL round bottom flask equipped with a stir bar was added **IPr·HCl** (1.5 g, 3.5 mmol, 1.0 equiv) and a minimal amount of water (7.0 mL) until all solids dissolved. HBF_4 (50 wt%, 0.48 mL, 3.9 mmol, 1.1 equiv) was added and immediately a white precipitate formed. This mixture was stirred for 20 min at room temperature. The product was extracted with dichloromethane (3 x 100 mL)

and the organic layers were combined and dried with $MgSO_4$, filtered, and concentrated under reduced pressure. The product was purified by dissolving the crude product in minimal amounts of dichloromethane (3.0 mL) and then precipitating out with the addition of diethyl ether (50 mL). The product was collected via vacuum filtration, washed with diethyl ether (50 mL), and dried under reduced pressure to yield **IPr·HBF$_4$** as a white powder (1.5 g, 3.2 mmol, 90% yield). NMR spectra match values previously reported.[264]

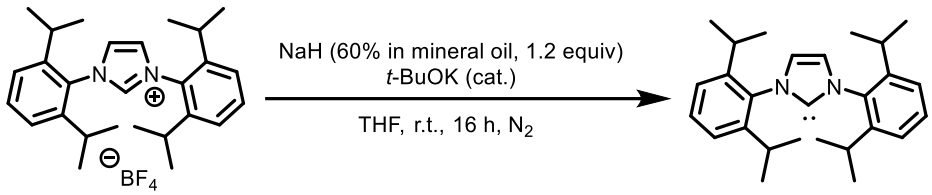

1,3-Bis(2,6-diisopropylphenyl)-1,3-dihydro-2*H*-imidazol-2-ylidene (IPr) was synthesized in accordance with literature procedure:[264] To a 50-mL round bottom flask equipped with a stir bar was added **IPr·HBF$_4$** (1.5 g, 3.2 mmol, 1.0 equiv) and THF (15 mL). To this solution, NaH (60% dispersion in mineral oil, 0.15 g, 3.8 mmol, 1.2 equiv) and *t*-BuOK (spatula tip-ful) were added slowly. The reaction vessel was vented for 15 min while stirring to allow the initial H_2 (g) production to be released, capped, and stirred for 16 h at room temperature. The reaction was filtered through a pad of Celite, and the filtrate was concentrated under reduced pressure. The crude product was dissolved in minimal amounts of THF (4 mL) and then hexanes (50 mL) was added to crystallize the product to obtain **IPr** as a white powder (0.41 g, 1.0 mmol, 33% yield). NMR spectra match values previously reported.[264]

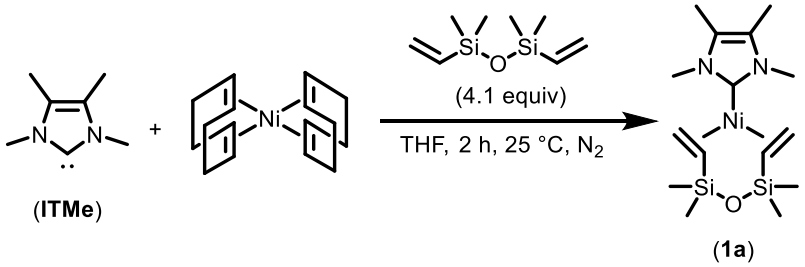

(dvtms)Ni(ITMe) (1a): To a 4-dram scintillation vial equipped with a magnetic stir bar was added $Ni(cod)_2$ (0.10 g, 0.36 mmol, 1.0 equiv) in THF (5.0 mL). To the stirring solution was added dvtms (0.34 mL, 1.5 mmol, 4.1 equiv). After 1 min of stirring, **ITMe** (0.046 g, 0.37 mmol, 1.0 equiv)

solvated in THF (5.0 mL) was added and the reaction turned into a bright orange solution. The reaction was left to stir overnight and then concentrated under reduced pressure. The crude product was solvated in minimal hexanes (5.0 mL) and filtered through Celite. The solution was concentrated to a third of its volume and crystallized in the freezer at -30 °C overnight. The filtrate was decanted, and the solid was dried under reduced pressure to yield **1a** as shiny, white crystals (76 mg, 0.21 mmol, 57% yield).

^{1}H NMR (500 MHz, C_6D_6, 298 K): δ 2.97 (s, 3H, NCH_3), 2.91 (d, J = 12.1 Hz, 2H, HC=CH_{cis}), 2.79 (s, 3H, NCH_3), 2.67 (d, J = 15.5 Hz, 2H, HC=CH_{trans}), 2.58 (dd, J = 15.5, 12.1 Hz, 2H H_2C=CH), 1.44 (d, J = 0.9 Hz, 3H, CCH_3), 1.41 (d, J = 0.9 Hz, 3H, CCH_3), 0.72 (s, 6H, SiCH_3), 0.18 (s, 6H, SiCH_3).

^{13}C{^{1}H} NMR (126 MHz, C_6D_6, 298 K): δ 199.2 (NiC), 124.4 (N-C=C), 124.3 (N-C=C), 52.7 (SiC=CH$_2$), 50.5 (SiC=CH$_2$), 33.7 (NCH$_3$), 33.4 (NCH$_3$), 8.48 (C=C-CH$_3$), 8.46 (C=C-CH$_3$), 2.6 (SiCH$_3$), -0.2 (SiCH$_3$).

^{29}Si NMR (99 MHz, C_6D_6, 298 K): δ 3.00 (s).

IR (FT, KBr pellet) ν: 3002-2782 (s), 1660 (w), 1380 (s), 983 (s), 775 (s).

ASAP/HRMS (m/z): [M^+] calculated for $C_{15}H_{30}N_2NiOSi_2$ 368.1250, found 368.1241.

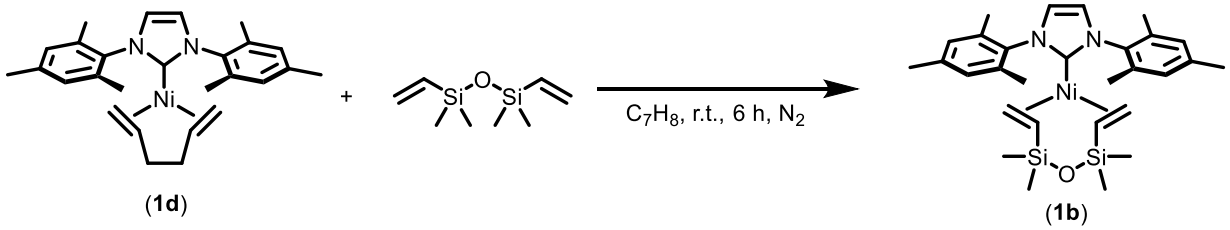

(**1d**) (**1b**)

(dvtms)Ni(IMes) (1b) was synthesized via a modified route:[130] To a round bottom flask equipped with a magnetic stir bar was added **1d** (0.050 g, 0.10 mmol, 1.0 equiv) and toluene (0.50 mL). To this stirring solution, dvtms (0.24 µL, 0.10 mmol, 1.0 equiv) was added, resulting in the solution turning dark red. The reaction turned orange after stirring for 6 h. The solution was concentrated under reduced pressure and the crude solid was redissolved in minimal hexanes (3.0 mL) and filtered through Celite into a scintillation vial. Half of the solvent was removed under reduced pressure and the remaining solution was placed in the freezer (-30 °C) for 2 h. The product precipitated and was isolated by filtration through a glass frit, yielding **1b** as pale orange crystals (0.037 g, 0.068 mmol, 68% yield).

^{1}H NMR (500 MHz, C_6D_6, 298 K): δ 6.69 (s, 4H, $H_{mesityl}$), 6.32 (s, 2H, NC*H*), 2.75 (d, *J* = 12.7 Hz, 2H, HC=CH_{cis}), 2.45 (d, *J* = 16.0 Hz, 2H, HC=CH_{trans}), 2.11 (s, 12H, $C_{mesityl}$-CH_3), 2.09 (obscured dd, H_2C=C*H*), 2.06 (s, 6H, $C_{mesityl}$-CH_3), 0.46 (s, 6H, SiCH_3), -0.33 (s, 6H, SiCH_3).
^{13}C{^{1}H} NMR (151 MHz, C_6D_6, 298 K): δ 202.9 (Ni*C*), 138.4 ($C_{mesityl}$), 137.6 ($C_{mesityl}$), 135.4 ($C_{mesityl}CH_3$), 129.3 ($C_{mesityl}$H), 122.8 (N-*C*=C), 53.9 (SiC=*C*H_2), 53.4 (Si*C*=CH_2), 20.9 ($C_{mesityl}CH_3$), 18.4 ($C_{mesityl}CH_3$), 2.4 (Si*C*H_3), -0.9 (Si*C*H_3).
IR (FT, KBr pellet) ν: 3153-2861 (s), 1481 (s), 1308 (s), 971 (s), 784 (s).
ASAP/HRMS (m/z): [M^+] calculated for $C_{29}H_{42}N_2NiOSi_2$ 548.2189, found 548.2193.

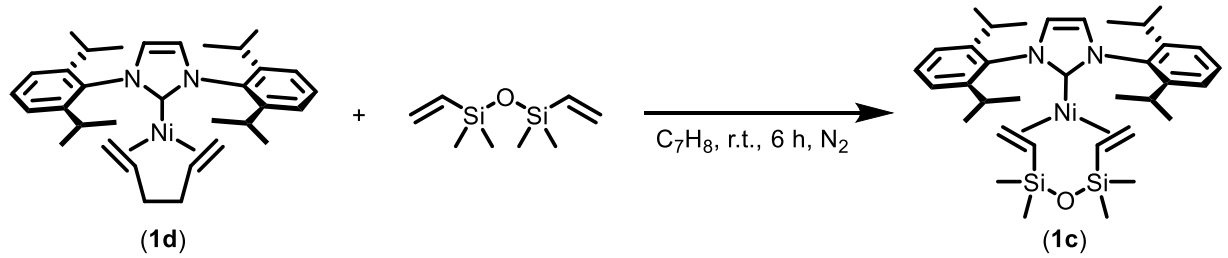

(dvtms)Ni(IPr) (1c) was synthesized via a reported procedure.[125] NMR spectra match values previously reported.[125]

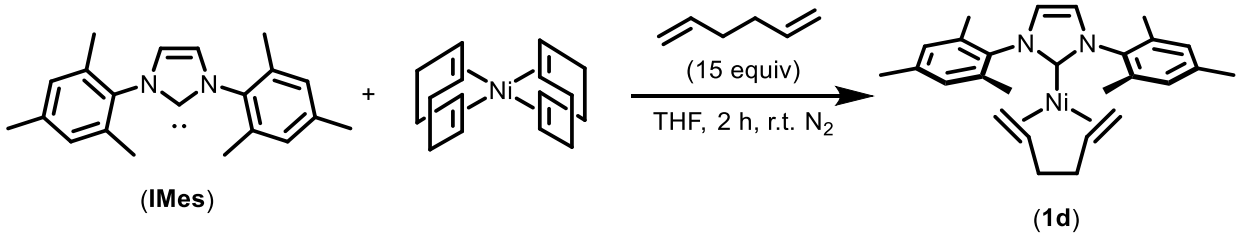

(1,5-hexadiene)Ni(IMes) (1d) was synthesized via a modified route:[125] To a 20-mL scintillation vial equipped with a stir bar was added Ni(cod)$_2$ (0.5 g, 1.8 mmol, 1.0 equiv) and THF (5.0 mL). To this stirring solution was added 1,5-hexadiene (3.2 mL, 27 mmol, 15 equiv) and the reaction was allowed to stir for 10 min to afford a red/orange solution. In a separate vial was added **IMes** (0.55 g, 1.8 mmol, 1.0 equiv) and THF (5.0 mL). This solution was added to the Ni(cod)$_2$/1,5-hexadiene mixture, and the reaction was capped and stirred overnight to obtain an orange solution. The reaction vessel was opened, the reaction was filtered through Celite, and the filtrate was concentrated under reduced pressure. The crude product was dissolved in minimal amounts of hexanes and placed in the freezer (-30 °C) for 24 h. After the product precipitated, the remaining

solution was decanted, and the product was washed with cold hexanes. The product was dried under reduced pressure to yield **1d** as bright, orange crystals. (0.38 g, 0.86 mmol, 48% yield). NMR spectra match values previously reported.[125]

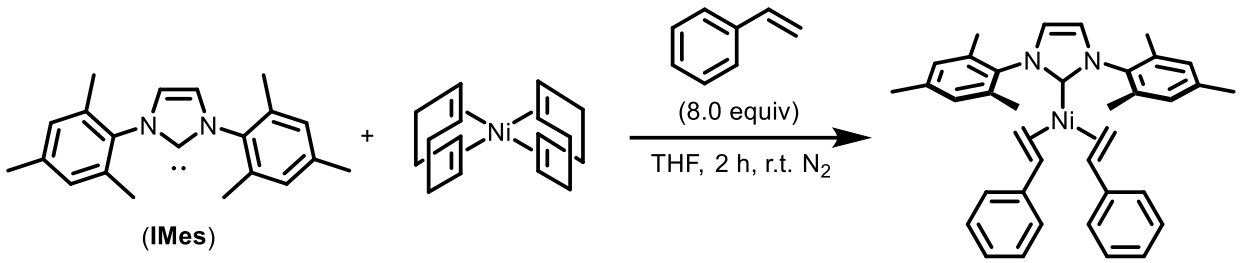

(styrene)$_2$Ni(IMes) (1e) was synthesized via a modified literature procedure:[126] To a 100-mL round bottom flask equipped with a magnetic stir bar was added Ni(cod)$_2$ (1.0 g, 3.6 mmol, 1.0 equiv), styrene (3.3 mL, 29 mmol, 8.0 equiv), and THF (32 mL). This red solution was stirred for 15 min at room temperature. In a separate 50-mL round bottom flask equipped with a stir bar was added **IMes** (1.1 g, 3.6 mmol, 1.0 equiv), and THF (32 mL). This solution was added dropwise to the Ni(cod)$_2$ and styrene solution to afford an orange solution. This reaction was stirred for 2 h and then concentrated under reduced pressure to give an orange solid. The crude product was dissolved in a minimal amount of THF (5.0 mL) and filtered through Celite. The filtrate was concentrated under reduced pressure, solvated in minimal THF (3.0 mL) and hexanes (50 mL) was added to crash **1e** out of solution. The product was collected via vacuum filtration and dried under reduced pressure to yield **1e** as a bright orange powder (1.8 g, 3.2 mmol, 88% yield). NMR spectra match values previously reported.[126]

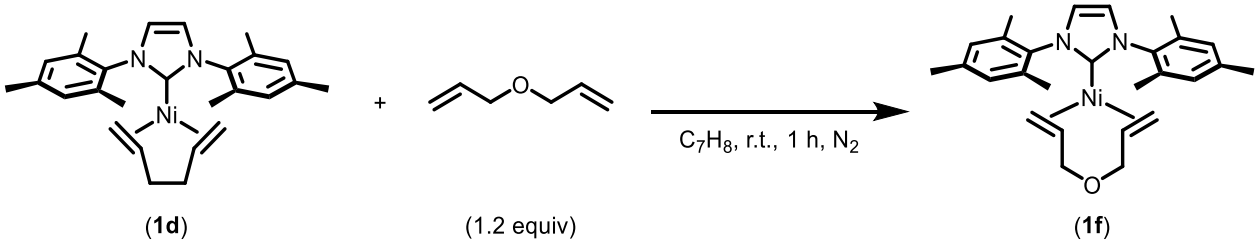

(allylether)Ni(IMes) (1f) To a round bottom flask equipped with a magnetic stir bar was added **1d** (0.050 g, 0.11 mmol, 1.0 equiv) and toluene (0.5 mL). To this stirring solution, allyl ether (16 μL, 0.13 mmol, 1.2 equiv) was added. The reaction was stirred at room temperature for 12 h,

concentrated to leave ¼ of the solvent volume, and crystallized via slow vapor diffusion (toluene/hexanes). After pale yellow crystals formed, the solution was decanted away from the crystals, which were then washed with cold hexanes (0.032 g, 0.069 mmol, 63% yield).

^{1}H NMR (500 MHz, C_6D_6, 298 K): δ 6.65 (s, 4H), 6.34 (s, 2H), 4.71 (dd, *J* = 12.0, 3.5 Hz, 2H), 3.08 (m, 2H), 2.16 (dd, *J* = 8.8, 1.2 Hz, 2H), 2.13 (d, 11.6 Hz, 2H), 2.10 (s, 12H), 2.02 (s, 6H), 1.82 (d, *J* = 12.5 Hz, 2H).

^{13}C{^{1}H} NMR (126 MHz, C_6D_6, 298 K): δ 203.6, 138.1, 137.8, 135.4, 129.1, 122.3, 70.9, 65.5, 41.1, 20.9, 18.3.

IR (FT, KBr pellet) ν: 3155-2829 (w), 1488 (s), 1310 (s), 928 (s), 695 (m).

ASAP/HRMS (m/z): [M^+] calculated for $C_{27}H_{34}N_2NiO$ 460.2025, found 460.2041.

b. Synthesis of Alkenes

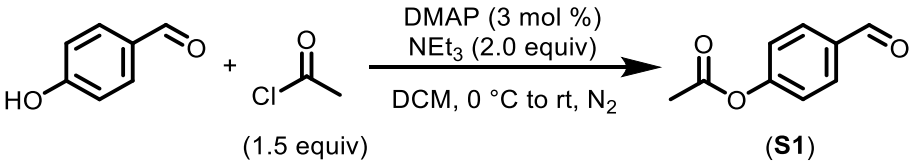

4-(acetoxy)-benzaldehyde (S1) To an oven-dried Schlenk flask equipped with a magnetic stir bar was added 4-hydroxybenzaldehyde (1.23 g, 10.1 mmol, 1.0 equiv) and DCM (30 mL). The reaction was cooled with an ice/water bath before triethylamine (2.8 mL, 20 mmol, 2.0 equiv) was added slowly. DMAP (37 mg, 0.30 mmol, 0.030 equiv) was added portion-wise followed by dropwise addition of acetyl chloride (1.1 mL, 15 mmol, 1.5 equiv). The reaction was monitored by TLC (70/30 hexanes/EtOAc) and upon complete consumption of 4-hydroxybenzaldehyde, the reaction was opened to air and quenched with $NaHCO_3$ (saturated aqueous, 50 mL). The aqueous layer was separated and extracted with Et_2O (3 x 60 mL). The combined organic layers were washed with H_2O (2 x 50 mL) and brine (2 x 50 mL). The organic layer was dried over Na_2SO_4, filtered, and concentrated under reduced pressure. The crude material was partially purified by column chromatography (silica, gradient 0-30% EtOAc/hexanes) to yield crude product as a white oil which was carried forward without further purification. NMR spectra match values previously reported.[266]

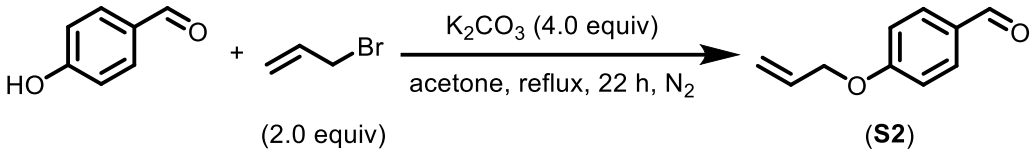

4-(2-propen-1-yloxy)benzaldehyde (S2) was synthesized following a literature procedure:[267] To a two-neck round-bottom flask equipped with a magnetic stir bar was added 4-hydroxybenzaldehyde (1.53 g, 12.5 mmol, 1.0 equiv), acetone (65 mL), K_2CO_3 (6.91 g, 50.0 mmol, 4.0 equiv), and allyl bromide (2.2 mL, 25.4 mmol, 2.0 equiv). The reaction was equipped with a condenser and placed in a pre-heated oil bath at 70 °C to reflux. After 22 h, the reaction was cooled to room temperature and EtOAc (50 mL) and H_2O (50 mL) were added to the reaction. This mixture was then transferred to a separatory funnel. The aqueous phase was separated and extracted with EtOAc (3 x 60 mL). The combined organic layers were dried over $MgSO_4$, filtered and concentrated under reduced pressure to give the crude product. The crude material was purified by column chromatography (silica, gradient 0-5% EtOAc/hexanes) to give the product as a clear, colorless oil (1.00 g, 6.2 mmol, 50% yield). NMR spectra match values previously reported.[268]

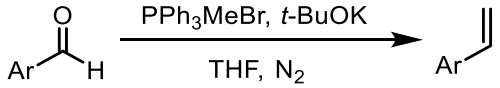

Styrene derivatives were synthesized from the corresponding aldehydes via a modified literature procedure:[269] To an oven-dried Schlenk flask equipped with a stir bar was added methyltriphenylphosphonium bromide and THF, which were stirred for 15 min at 0 °C (ice/water bath). To this mixture was added *t*-BuOK and stirred for 1 h at 0 °C. The corresponding aldehyde was added either neat or as a solution in THF to the reaction mixture dropwise. The reaction was taken out of the bath and allowed to warm to room temperature to stir for 24 h. After reaction completion determined by TLC, the reaction was quenched with NH_4Cl (saturated aq.) and extracted with Et_2O. The organic layer was separated, dried over $MgSO_4$, filtered, and the resulting filtrate was concentrated under reduced pressure to obtain the crude product. Purification details are included below.

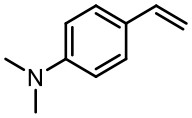

4-ethenyl-*N*,*N*-dimethylbenzenamine (**2b**)

Synthesis details: methyltriphenylphosphonium bromide (2.8 g, 7.8 mmol, 1.6 equiv), *t*-BuOK (0.50 g, 4.5 mmol, 1.7 equiv), THF (50 mL), 4-(dimethylamino)benzaldehyde (0.73 g, 4.9 mmol, 1.0 equiv), THF (10 mL).

Purification details: Column chromatography: silica, ethyl acetate/hexanes/TEA (3:96:1). Product is a pale-yellow oil (0.388 g, 2.64 mmol, 54% yield).

NMR spectra match values previously reported.[270]

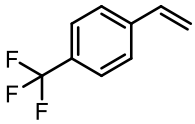

1-ethenyl-4-(trifluoromethyl)benzene (**2g**)

Synthesis details: methyltriphenylphosphonium bromide (9.1 g, 25 mmol, 1.8 equiv), *t*-BuOK (1.6 g, 14 mmol, 1.0 equiv), THF (50 mL), 4-(trifluoromethyl)benzaldehyde (2.0 mL, 15 mmol, 1.0 equiv), THF (10 mL), quenched with NH_4Cl (60 mL), extracted with Et_2O (3 x 50 mL).

Purification details: Column chromatography: silica, hexanes. Product is a colorless oil (0.640 g, 3.72 mmol, 25% yield).

NMR spectra match values previously reported.[271]

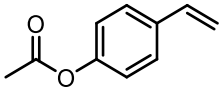

4-acetoxystyrene (**2k**)

Synthesis details: methyltriphenylphosphonium bromide (1.6 g, 4.6 mmol, 1.6 equiv), *t*-BuOK (0.52 g, 4.6 mmol, 1.6 equiv), THF (20 mL), 4-(acetoxy)-benzaldehyde (0.50 g, 3.0 mmol, 1.0 equiv).

Purification details: Column chromatography: silica, gradient eluent (0-15% EtOAc/hexanes). Product is a clear liquid (0.20 g, 1.2 mmol, 41% yield).

NMR spectra match values previously reported.[272]

IR (ATR, neat) v: 1757 (s), 1504 (m), 1188 (s), 908 (m), 850 (m).

2-vinylthiophene (**2l**)

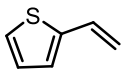

Synthesis details: methyltriphenylphosphonium bromide (4.59 g, 12.8 mmol, 1.2 equiv), *t*-BuOK (1.44 g, 12.8 mmol, 1.2 equiv), Et_2O (75 mL), 2-thiophenecarboxaldehyde (1.03 mL, 11.0 mmol, 1.0 equiv).

Purification details: Column chromatography: silica, hexanes. Product is a clear liquid (0.49 g, 4.4 mmol, 40% yield).

NMR spectra match values previously reported.[273,274]

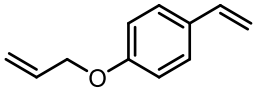

1-ethenyl-4-(2-propen-1-yloxy)benzene (**2t**)

Synthesis details: methyltriphenylphosphonium bromide (1.65 g, 4.62 mmol, 1.5 equiv), *t*-BuOK (0.51 g, 4.5 mmol, 1.5 equiv), THF (20 mL), 4-(2-propen-1-yloxy)benzaldehyde (0.49 g, 3.0 mmol, 1.0 equiv).

Purification details: Column chromatography: silica, gradient eluent (0-5% EtOAc/hexanes). Product is a clear liquid (0.27 g, 1.7 mmol, 57% yield).

NMR spectra match values previously reported.[275]

---

c. Synthesis of Silanes

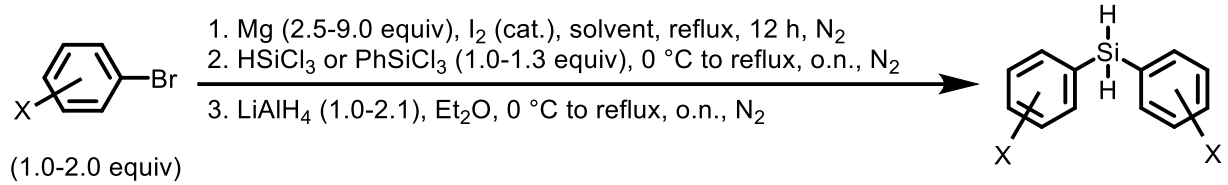

Diaryl silanes were synthesized via modified literature procedure:[276] To an oven-dried Schlenk flask equipped with a stir bar was added magnesium (2.5-9.0 equiv), iodine (cat.), and solvent. This mixture was cooled to 0 °C in an ice/water bath. A one-fourth portion of the aryl bromide was added slowly and this mixture was stirred for 10 min after a color change was observed. The remaining aryl bromide was added dropwise, and the reaction was equipped with a condenser and heated to reflux for 12 h. The reaction was removed from heat and allowed to cool to room temperature. In a separate oven-dried Schlenk flask, $HSiCl_3$ or $PhSiCl_3$ (1.0-1.3 equiv) and the reaction solvent were cooled to 0 °C in an ice/water bath. The Grignard solution was added dropwise to the chlorosilane solution via cannula. Upon complete addition, the flask was equipped with a condenser and heated to reflux and reacted overnight. The reaction was lifted from heat to

slowly cool to room temperature. The magnesium salts were filtered off with a swivel frit and the filtrate was transferred to another oven-dried Schlenk flask. The filtrate was added dropwise to an oven-dried Schlenk flask equipped with a stir bar containing $LiAlH_4$ (1.0-2.1 equiv) and Et_2O which was cooled to 0 °C in an ice/water bath. Upon complete addition, the reaction was allowed to warm to room temperature and stirred overnight. The reaction was slowly quenched with ice, acidified with 3 M HCl, and the crude product was extracted with Et_2O. The combined organic layers were dried over $MgSO_4$, the solids were filtered off, and the filtrate was concentrated to obtain crude product. Further purification details are included below.

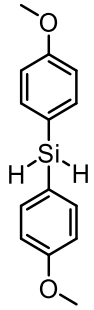

Di(4-methoxyphenyl)silane (**3b**)

Synthesis details: 4-Bromoanisole (5.0 mL, 40 mmol, 2.0 equiv), THF (50 mL), magnesium (4.30 g, 177 mmol, 8.9 equiv), iodine (a chip), $HSiCl_3$ (2.01 mL, 19.9 mmol, 1.0 equiv), THF (50 mL), $LiAlH_4$ (0.907 g, 23.9 mmol, 1.2 equiv), Et_2O (30 mL), quenched with ice (10 g), acidified with 3 M HCl (5 mL), extracted with Et_2O (3 x 50 mL).

Purification details: The compound was isolated by recrystallization in cyclohexane to yield a crystalline, white solid (0.66 g, 2.7 mmol, 14% yield).

^{1}H NMR (600 MHz, $CDCl_3$, 298 K): δ 7.52 (d, J = 8.5 Hz, 4H), 6.93 (d, J = 8.5 Hz, 4H), 4.89 (s, $^1J_{H–Si}$ = 197.5 Hz, 2H), 3.82 (s, 6H).

$^{13}C\{^1H\}$ NMR (151 MHz, $CDCl_3$, 298 K): δ 161.2, 137.3, 122.7, 114.1, 55.2.

$^{29}Si\{^1H\}$ NMR (119 MHz, $CDCl_3$, 298 K): δ -34.47 (s).

IR (ATR, neat) ν: 2962 (m), 2141 (s, Si–H), 2117 (s, Si–H), 1593 (m), 1278 (s), 814 (s).

ASAP/HRMS (m/z): [M^+] calculated for $C_{14}H_{16}O_2Si$ 244.0920, found 244.0950.

Di(4-methylphenyl)silane (**3c**)

Synthesis details: 4-bromotoluene (4.0 mL, 33 mmol, 2.0 equiv), THF (60 mL), magnesium (3.52 g, 145 mmol, 9.0 equiv), iodine (a chip), $HSiCl_3$ (1.64 mL, 16.2 mmol, 1.0 equiv), THF (35 mL), $LiAlH_4$ (1.23 g, 32.4 mmol, 2.0 equiv), Et_2O (30 mL),

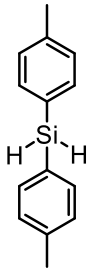

quenched with ice (10 g), acidified with 3 M HCl (5 mL), extracted with Et_2O (3 x 50 mL).

Purification details: Column chromatography: silica gel, pentane to yield a colorless oil (0.862 g, 4.06 mmol, 25% yield).

NMR spectra match values previously reported.[276]

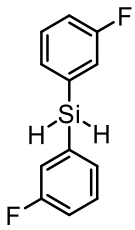

Di(3-fluorophenyl)silane (**3d**)

Synthesis details: 1-bromo-3-fluorobenzene (4.0 mL, 36 mmol, 2.0 equiv), THF (80 mL), magnesium (3.87 g, 159 mmol, 8.9 equiv), iodine (a chip), $HSiCl_3$ (1.81 mL, 17.9 mmol, 1.0 equiv), THF (40 mL), $LiAlH_4$ (0.81 g, 21 mmol, 1.2 equiv), Et_2O (20 mL), quenched with ice (10 g), acidified with 3 M HCl (5 mL), extracted with Et_2O (3 x 50 mL).

Purification details: Column chromatography: silica gel, pentanes to a colorless oil (1.36 g, 6.18 mmol, 34% yield).

^{1}H NMR (600 MHz, C_6D_6, 298 K): δ 7.14 (dd, J = 8.4, 2.0 Hz, 2H), 7.04 (d, J = 7.1 Hz, 2H), 6.87 (m, 2H), 6.79 (td, J = 8.7, 2.5 Hz, 2H), 4.80 (s, $^1J_{H–Si}$ = 203.8 Hz, 2H).

^{13}C{^{1}H} NMR (151 MHz, C_6D_6, 298 K): δ 163.6 (d, J = 248.8 Hz), 133.9 (d, J = 4.5 Hz), 131.5 (d, J = 3.2 Hz), 130.4 (d, J = 7.0 Hz), 122.2 (d, J = 19.1 Hz), 117.4 (d, J = 21.0 Hz).

^{19}F NMR (471 Hz, C_6D_6, 298 K): δ -112.37 (td, J = 8.8, 5.2 Hz).

^{29}Si{^{1}H} NMR (199 MHz, C_6D_6, 298 K): δ -33.81 (s).

IR (ATR, neat) ν: 3064-2879 (m), 2143 (s, Si–H), 1574 (s), 1217 (s), 825 (s).

ASAP/HRMS (m/z): [M^+] calculated for $C_{12}H_{10}F_2Si$ 220.0520, found 220.0526.

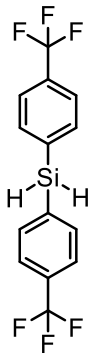

Di[4-(trifluoromethyl)phenyl]silane (**3e**)

Synthesis details: 4-bromobenzotrifluoride (5.0 mL, 36 mmol, 1.9 equiv), Et_2O (40 mL), magnesium (3.50 g, 146 mmol, 7.5 equiv), iodine (a chip), $HSiCl_3$ (2.45 mL, 24.3 mmol, 1.3 equiv), Et_2O (20 mL), $LiAlH_4$ (0.74 g, 19.5 mmol, 1.0 equiv), Et_2O (15 mL), quenched with ice (10 g), acidified with 3 M HCl (5 mL), extracted with Et_2O (3 x 50 mL).

Purification details: Column chromatography: silica gel, pentanes/Et_2O (95:5), concentrated, and then distilled to yield a colorless oil (1.06 g, 3.31 mmol, 17% yield).

^{1}H NMR (500 MHz, C_6D_6, 298 K): δ 7.31 (d, J = 7.8 Hz, 4H), 7.19 (d, J = 7.8 Hz, 4H), 4.76 (s, $^1J_{H–Si}$ = 204.8 Hz, 2H).

^{13}C{^{1}H} NMR (126 MHz, C_6D_6, 298 K): δ 136.2, 135.5, 132.4 (q, J = 32.2 Hz), 125.0 (q, J = 3.8 Hz), 124.7 (q, J = 272.5 Hz)*.

*Note that the most upfield peak of this quartet (assigned to CF_3) is obscured by the C_6D_6 peak.

^{19}F NMR (471 Hz, C_6D_6, 298 K): δ -62.88 (s).

^{29}Si{^{1}H} NMR (99 MHz, C_6D_6, 298 K): δ -34.00 (s).

IR (ATR, neat) ν: 2154 (m, Si–H), 1394 (m), 1321 (s), 1059 (s), 820 (s).

ASAP/HRMS (m/z): [M^+] calculated for $C_{14}H_{10}F_6Si$ 320.0456, found 320.0455.

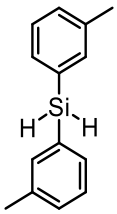

Di(3-methylphenyl)silane (**3f**)

Synthesis details: 3-bromotoluene (4.5 mL, 37 mmol, 1.9 equiv), THF (60 mL), magnesium (4.0 g, 160 mmol, 9.0 equiv), iodine (a chip), $HSiCl_3$ (1.9 mL, 19 mmol, 1.0 equiv), THF (40 mL), $LiAlH_4$ (0.85 g, 22.4 mmol, 1.2 equiv), Et_2O (40 mL), quenched with ice (10 g), acidified with 3 M HCl (5 mL), extracted with Et_2O (3 x 50 mL).

Purification details: Column chromatography: silica gel, pentane to yield a colorless oil (1.36 g, 6.40 mmol, 34% yield).

NMR spectra match values previously reported.[277]

IR (ATR, neat) ν: 3064-2877 (w), 2127 (s, Si–H), 1396 (w), 1120 (s), 823 (s).

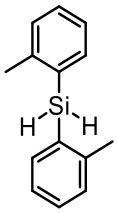

Di(2-methylphenyl)silane (**3g**)

Synthesis details: 2-bromotoluene (4.0 mL, 33 mmol, 2.0 equiv), THF (45 mL), magnesium (3.59 g, 148 mmol, 8.9 equiv), iodine (a chip), $HSiCl_3$ (1.68 mL, 16.6 mmol, 1.0 equiv), THF (30 mL), $LiAlH_4$ (0.631 g, 16.6 mmol, 1.0 equiv), Et_2O (20 mL), quenched with ice (10 g), acidified with 3 M HCl (5 mL), extracted with Et_2O (3 x 50 mL).

Purification details: Column chromatography: silica gel, cyclohexane to yield a colorless oil (1.13 g, 5.32 mmol, 32% yield).

^{1}H NMR (600 MHz, $CDCl_3$, 298 K): δ 7.51 (d, J = 7.3 Hz, 2H), 7.36 (t, J = 7.5 Hz, 2H), 7.23 (d, J = 7.5 Hz, 2H), 7.19 (t, J = 7.3 Hz, 2H), 5.00 (s, $^1J_{H–Si}$ = 198.2 Hz, 2H), 2.43 (s, 6H).

$^{13}C\{^1H\}$ NMR (126 MHz, $CDCl_3$, 298 K): δ 144.7, 137.1, 130.9, 130.5, 129.6, 125.4, 22.7.

$^{29}Si\{^1H\}$ NMR (99 MHz, $CDCl_3$, 298 K): δ -39.76 (s).

IR (ATR, neat) ν: 3051-2858 (w), 2131 (s, Si–H), 1446 (m), 1132 (m), 847 (s).

ASAP/HRMS (m/z): [M^+] calculated for $C_{14}H_{16}Si$ 212.1021, found 212.1011.

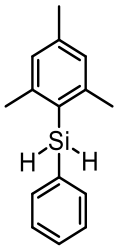

Mesitylphenylsilane (**3h**)

Synthesis details: 2-bromomesitylene (2.14 mL, 14.0 mmol, 1.0 equiv), THF (100 mL), magnesium (0.85 g, 35 mmol, 2.5 equiv), iodine (a chip), $SiPhCl_3$ (2.24 mL, 14.0 mmol, 1.0 equiv), $LiAlH_4$ (1.13 g, 29.8 mmol, 2.1 equiv), quenched with ice (10 g), acidified with 3 M HCl (5 mL), extracted with Et_2O (3 x 100 mL).

Purification details: Column chromatography: silica gel, hexanes to yield a colorless oil (1.36 g, 6.01 mmol, 43% yield).

NMR matches previously reported values.[278]

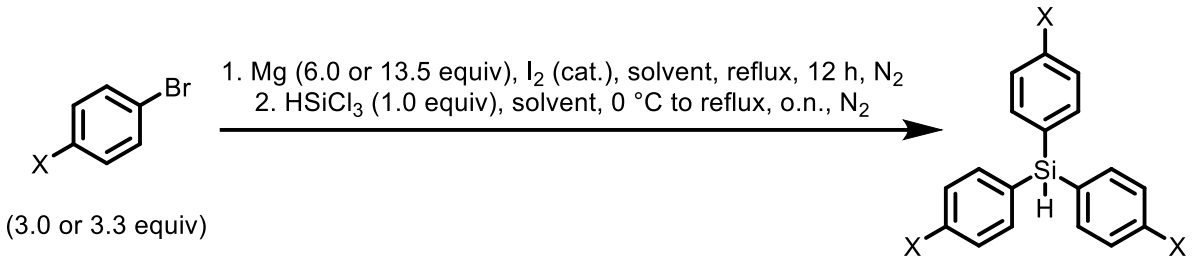

Triaryl silanes were synthesized in accordance with a literature procedure.[112] Purification details are included below.

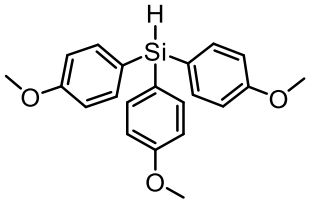

Tri[4-(methoxy)phenyl]silane (**3k**)

Synthesis details: 4-bromoanisole (2.7 mL, 21 mmol, 3.0 equiv), Et_2O (26 mL), magnesium (1.0 g, 42 mmol, 6.0 equiv), iodine (a chip), $HSiCl_3$ (0.71 mL, 7.0 mmol, 1.0 equiv), quenched with 3M HCl (5 mL), extracted with Et_2O (5 x 50 mL).

Purification details: Column chromatography: silica gel, hexanes/Et_2O (95:5) to give the product as a white solid (2.16 g, 6.15 mmol, 89% yield).

NMR matches previously reported values.[112]

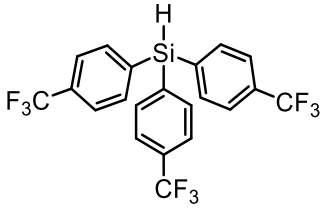

Tri[4-(trifluoromethyl)phenyl]silane (**3m**)

Synthesis details: 4-bromobenzotrifluoride (4.0 mL, 29 mmol, 3.3 equiv), Et_2O (40 mL), magnesium (2.79 g, 115 mmol, 13 equiv), iodine (a chip), $HSiCl_3$ (0.88 mL, 8.7 mmol, 1.0 equiv), quenched with water (20 mL), extracted with Et_2O (3 x 50 mL).

Purification details: Column chromatography: silica gel, hexanes/Et_2O (95:5) to give the product as a white solid (1.36 g, 2.93 mmol, 34% yield).

NMR matches previously reported values.[112]

A.1.4. Evaluation of Nickel Complexes for Hydrosilylation

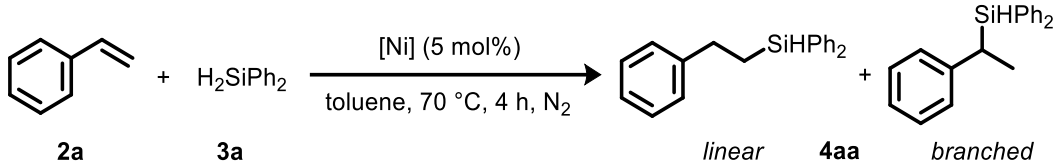

In a nitrogen-filled glovebox, Ni complexes were added to a 1-dram vial equipped with a stir bar via stock solutions prepared by weighing out the complex, dissolving it in the appropriate volume of toluene using volumetric glassware, and distributing the stock solutions using a 250-µL syringe. **2a** (10 µL, 0.088 mmol, 1.0 equiv) and **3a** (16 µL, 0.088, 1.0 equiv) were added to each vial using a 25-µL syringe, separately. The vials were sealed with a Teflon-lined thermoset cap, removed from the glovebox, and placed on a pre-heated aluminum vial block at the appropriate temperature. After 4 h, the vial was quenched by cooling in a liquid N_2 bath, opening to air, and durene or trimethoxybenzene was added to the reaction as a stock solution via a 250-µL syringe; the stock solution had been prepared by weighing out durene or trimethoxybenzene and dissolving in hexanes using volumetric glassware. After mixing, an aliquot (5 µL) of the reaction was removed using a 25-µL syringe and filtered with hexanes through Celite directly into a GC vial. The filtrate was analyzed by GC and/or GC-MS to assess reaction progress and selectivity (linear, *l*; branched, *b*). The product yield was determined by relative integration (by GC or GC-MS) of the product peaks and standard against a calibration curve. Yields reported are the average of at least two trials and the errors in yield are the standard deviation.

Table A.1. Evaluation of the reactivity of nickel complexes.

Entry	Ni source	Yield (%)	Selectivity (*l*:*b*)
1	(dvtms)Ni(ITMe) (**1a**)	56 ± 8	1:2.0
2	(dvtms)Ni(IMes) (**1b**)	21 ± 6	1:1.5
3	(dvtms)Ni(IPr) (**1c**)	11.6 ± 0.2	1:1.2
4	(1,5-hexadiene)Ni(IMes) (**1d**)	29 ± 1	1:8.1
5	$(styrene)_2$Ni(IMes) (**1e**)	49 ± 0	1:3.3
6	(allylether)Ni(IMes) (**1f**)	39[a]	1:0.8
7	(IMes)Ni(µ-H–$SiPh_2$)$_2$Ni(IMes) (**1g**)	31 ± 1	1:0.8
8	(IMes)Ni(µ-H–$SiPh_2$)$_2$Ni(IMes) (**1g**)	74 ± 2 [b]	1:0.9

[a]Only one trial was carried out. [b]Reaction carried out at 100 °C.

A.1.4. Evaluation of Reaction Conditions for Hydrosilylation

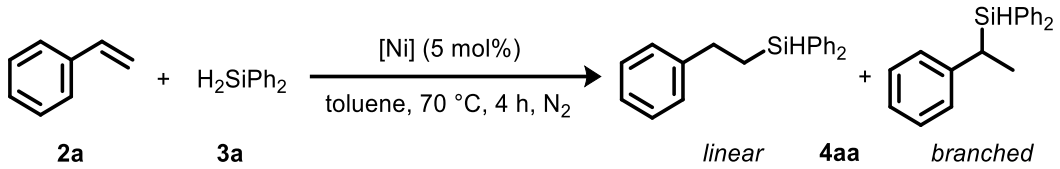

In a nitrogen-filled glovebox, Ni complexes were added to a 1-dram vial equipped with a stir bar via stock solutions prepared by weighing out the complex, dissolving it in the appropriate volume of solvent using volumetric glassware, and distributing the stock solutions using a 250-µL syringe. For the reaction in Table S2, entry 2, **IMes•HCl** (0.0088 mmol, 0.050 equiv) and KO*t*-Bu (0.0089 mmol, 0.050 equiv) were weighed out directly into the appropriate vial before the addition of the Ni stock solution. Additional solvent was added using a disposable plastic syringe to bring the total reaction volume to the appropriate volume. **2a** (10 µL, 0.088 mmol, 1.0 equiv) and **3a** (16 µL, 0.088, 1.0 equiv) were added to each vial using a 25-µL syringe, separately. The vials were sealed with a Teflon-lined thermoset cap, removed from the glovebox and placed on a pre-heated aluminum vial block at the appropriate temperature. After 4 h, the vial was quenched by cooling in a liquid N_2 bath, opening to air, and durene or trimethoxybenzene was added to the reaction as a stock solution via a 250-µL syringe; the stock solution had been prepared by weighing out durene or trimethoxybenzene and dissolving in hexanes using volumetric glassware. After mixing, an aliquot (5 µL) of the reaction was removed using a 25-µL syringe and filtered with hexanes through Celite directly into a GC vial. The filtrate was analyzed by GC and/or GC-MS to assess reaction progress and selectivity. The product yield was determined by relative integration (by GC or GC-MS) of the product peaks and standard against a calibration curve. Yields reported are the average of at least two trials and the errors in yield are the standard deviation.

Table A.2. Evaluation of the reaction conditions.

Entry	[Ni]	Deviation from standard conditions	Yield (%)	Selectivity (*l*:*b*)
1	$Ni(cod)_2$ (5 mol %)	None	77 ± 8	1:0.7
2	$Ni(cod)_2$ (5 mol %)	Addition of **IMes•HCl** (5 mol %) and KO*t*-Bu (5 mol %)	67 ± 2	1:7.4
3	No catalyst	None	n.d.[a]	--
4	**1e** (2.5 mol %)	None	60 ± 10	1:3.0
5	**1e** (5 mol %)	None	72 ± 5	1:4.0
6	**1e** (10 mol %)	None	79 ± 4	1:6.8
7	**1e** (20 mol %)	None	81 ± 7	1:6.8

8	**1e** (5 mol %)	Hexanes used instead of toluene	70 ± 7	1:5.2
9	**1e** (5 mol %)	1,4-dioxane used instead of toluene	65 ± 5	1:4.9
10	**1e** (5 mol %)	THF used instead of toluene	43.8 ± 0.9	1:2.3
11	**1e** (5 mol %)	DMF used instead of toluene	31 ± 9	1:1.6
12	**1e** (5 mol %)	ACN used instead of toluene	31 ± 2	1:0.4
13	**1e** (5 mol %)	DCM used instead of toluene	48.9 ± 3	1:0.6
14	**1e** (5 mol %)	25 °C instead of 70 °C	2.3 ± 0.3	1:2.3
15	**1e** (5 mol %)	60 °C instead of 70 °C	38 ± 5	1:1.4
16	**1e** (5 mol %)	80 °C instead of 70 °C	76 ± 5	1:8.6
17	**1e** (5 mol %)	90 °C instead of 70 °C	85.0 ± 0.5	1:11
18[b]	**1e** (5 mol %)	100 °C instead of 70 °C	95	1:>99
19	**1d** (5 mol %)	100 °C instead of 70 °C	93 ± 1	1:55

[a]n.d., not detected. [b]Only one trial was carried out.

A.1.5. Evaluation of the Substrate Scope for Hydrosilylation

a. General Procedures

General procedure A (GP-A): In a nitrogen-filled glovebox, a 4-dram scintillation vial was charged with **1e** (28.6 mg, 0.0500 mmol, 0.050 equiv) and toluene (4.6 mL). The alkene substrate (1.0 mmol, 1.0 equiv) was added to this mixture followed by the silane substrate (1.1 mmol, 1.1 equiv) using a 250-µL syringe. The vial was sealed with a Teflon-lined thermoset cap, brought out of the glovebox, and heated at 100 °C on a pre-heated vial block for 4 h. The reaction was quenched by cooling it in a liquid N_2 bath and then it was allowed to warm to room temperature. An aliquot (~5 µL) was removed for analysis by GC-MS, and the reaction was then concentrated under reduced pressure to yield the crude product. The product was purified as described below for each substrate.

General procedure B (GP-B): Followed **GP-A** except catalyst **1d** (23 mg, 0.050 mmol, 0.050 equiv) was used instead of **1e**.

General procedure C (GP-C): In a nitrogen-filled glovebox, a 2-dram scintillation vial equipped with a stir bar was charged with **1e** (28.6 mg, 0.0500 mmol, 0.050 equiv), **2a** (120 µL, 1.0 mmol, 1.0 equiv), and hexanes (4.6 mL). The vial was sealed with a septum cap and brought out of the glovebox, injected with the silane substrate (1.25 mmol, 1.25 equiv) using a disposable 1-mL syringe, and heated at 100 °C in a pre-heated oil bath for 24 h. The reaction was quenched by

cooling it in a liquid N_2 bath and then it was allowed to warm to room temperature. An aliquot (~5 µL) was removed for analysis by GC-MS. The product was purified as described below for each substrate.

General procedure D (GP-D): In a nitrogen-filled glovebox, a 1-dram scintillation vial equipped with a stir bar was charged with $Ni(cod)_2$ (14 mg, 0.050 mmol, 0.050 equiv), **ITMe** (6.2 mg, 0.050 mmol, 0.050 equiv), and toluene (0.42 mL). The reaction was stirred for 5 min and then **2a** (120 µL, 1.0 mmol, 1.0 equiv, unless stated otherwise in the table below) was added via a 250-µL syringe, and the reaction was stirred for an additional 5 min. Finally, the silane substrate (see amount in table below) was added directly as a solid or using a 250-µL syringe or a disposable 1-mL syringe. The vial was sealed with a Teflon-lined thermoset cap, brought out of the glovebox, and heated at 100 °C on a pre-heated aluminum vial block for 24 h. The reaction was quenched by cooling it in a liquid N_2 bath and then it was allowed to warm to room temperature. An aliquot (~5 µL) was removed for analysis by GC, and the reaction was then concentrated under reduced pressure to yield the crude product. The product was purified as described below for each substrate.

General procedure E (GP-E): In a nitrogen-filled glovebox, a 1-dram scintillation vial equipped with a stir bar was charged with $Ni(cod)_2$ (14 mg, 0.050 mmol, 0.050 equiv), **ITMe** (6.2 mg, 0.050 mmol, 0.050 equiv), and toluene (0.42 mL). The reaction was stirred for 5 min and then **2a** (115 µL, 1.0 mmol, 1.0 equiv) was added via 250-µL syringe, and the reaction was stirred for an additional 5 min. The vial was sealed with a septum cap, brought out of the glovebox, and injected with triethoxysilane **3p** (0.37 mL, 2.0 mmol, 2.0 equiv) using a disposable 1-mL syringe, and heated at 100 °C in a pre-heated oil bath for 24 h. The reaction was quenched by cooling it in a liquid N_2 bath and then it was allowed to warm to room temperature. An aliquot (~5 µL) was removed for analysis by GC, and the reaction was then concentrated under reduced pressure to yield the crude product. The product was purified as described below for each substrate.

b. Successful Substrates

(1-Phenylethyl)diphenylsilane (**4aa**)

Synthesis details: **GP-A**, styrene (**2a**), H_2SiPh_2 (**3a**).

Selectivity before purification: 1:>99 (*l*/*b*) measured by GC-MS.

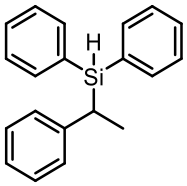

Purification details: Column chromatography: silica, benzene/hexanes (2:98) to give the product as a clear oil (0.248 mg, 0.860 mmol, 86% yield, *l*/*b* = 1:>99). NMR spectra match values previously reported.[279]

^{1}H NMR (500 MHz, CD_3CN, 298 K): δ 7.59 (d, *J* = 7.3 Hz, 2H), 7.44-7.34 (ms, 6H), 7.29 (t, *J* = 7.2 Hz, 2H), 7.17 (t, *J* = 7.6 Hz, 2H), 7.09-7.06 (ms, 3H), 4.79 (d, *J* = 4.2 Hz, $^{1}J_{H–Si}$ = 196.1 Hz, 1H), 2.94 (qd, *J* = 7.4, 4.2 Hz, 1H), 1.43 (d, J = 7.4 Hz, 3H).

^{13}C{^{1}H} NMR (126 MHz, CD_3CN, 298 K): δ 145.6, 136.4, 136.3, 134.3, 134.2, 130.9, 130.7, 129.2, 129.1, 128.9, 128.7, 125.9, 27.2, 17.2.

^{29}Si{^{1}H} NMR (99 MHz, CD_3CN, 298 K): δ -7.42 (s).

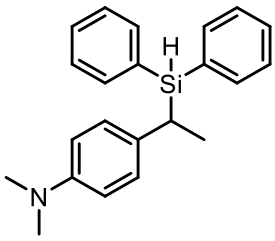

[1-(4-Dimethylaminophenyl)ethyl]diphenylsilane (**4ba**)

Synthesis details: **GP-A**, 4-dimethylaminostyrene (**2b**), H_2SiPh_2 (**3a**).

Selectivity before purification: 1:>99 (*l*/*b*) measured by GC-MS.

Purification details: Column chromatography: silica, Et_2O/hexanes (5:95) to give the product as an amber oil. (0.26 g, 0.77 mmol, 77% yield, *l*/*b* = 1:>99).[280]

^{1}H NMR (500 MHz, $CDCl_3$, 298 K): δ 7.52 (d, *J* = 7.9 Hz, 2H), 7.41-7.32 (m, 6H), 7.26 (m, 2H), 6.90 (d, *J* = 8.4 Hz, 2H), 6.62 (d, *J* = 8.4 Hz, 2H), 4.83 (d, *J* = 3.2 Hz, $^{1}J_{H–Si}$ = 196.2 Hz, 1H), 2.88 (s, 6H), 2.73 (qd, *J* = 7.5, 3.3 Hz, 1H), 1.42 (d, *J* = 7.5 Hz, 3H).

^{13}C{^{1}H} NMR (126 MHz, $CDCl_3$, 298 K): δ 148.6, 135.9, 135.8, 133.73, 133.67, 132.6, 129.7, 129.5, 128.4, 128.0, 127.8, 113.2, 41.1, 25.6, 17.1.

^{29}Si{^{1}H} NMR (99 MHz, $CDCl_3$, 298 K): δ -9.24 (s).

IR (ATR, neat) ν: 3066-2804 (w), 2102 (s, Si–H), 1518 (s), 1105 (m), 696 (s).

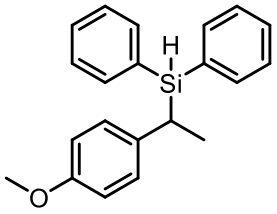

[1-(4-Methoxyphenyl)ethyl]diphenylsilane (**4ca**)

Synthesis details: **GP-A**, 4-methoxystyrene (**2c**), H_2SiPh_2 (**3a**).

Selectivity before purification: 1:43 (*l*/*b*) measured by GC-MS.

Purification details: Column chromatography: silica, methyl-*t*-butyl ether/cyclohexane (5:95) to give the product as a white solid (0.270 g, 0.85 mmol, 85% yield, *l*/*b* = 1:33). NMR spectra match values previously reported.[92,279]

The major product isolated is the branched isomer, and the linear isomer is seen in the NMR spectra as well. The ratio of these isomers was determined by relative integrations of the benzylic C–H positions and was found to be 1:33 (*l*/*b*). The branched product is fully characterized below, and the peaks visible and clearly assignable to the linear isomer are given directly following the NMR characterization of the branched product.

Branched product:

^{1}H NMR (500 MHz, CD_3CN, 298 K): δ 7.58 (d, *J* = 7.5 Hz, 2H), 7.45-7.35 (ms, 6H), 7.29 (t, *J* = 7.4 Hz, 2H), 7.01 (d, *J* = 8.5 Hz, 2H), 6.75 (d, *J* = 8.5 Hz, 2H), 4.79 (d, *J* = 4.1 Hz, $^{1}J_{H–Si}$ = 195.1 Hz, 1H), 3.71 (s, 3H), 2.87 (qd, *J* = 7.5, 4.2 Hz, 1H), 1.39 (d, *J* = 7.5 Hz, 3H).

^{13}C{^{1}H} NMR (126 MHz, CD_3CN, 298 K): δ 158.3, 137.4, 136.4, 136.3, 134.6, 134.4, 130.8, 130.7, 129.6, 129.1, 128.9, 114.6, 55.8, 26.1, 17.5.

^{29}Si{^{1}H} NMR (99 MHz, CD_3CN, 298 K): δ -7.65 (s).

Linear product:

^{1}H NMR (500 MHz, CD_3CN, 298 K): δ 7.11 (d, *J* = 8.4 Hz, 0.07H), 6.81 (d, *J* = 8.4 Hz, 0.08H), 4.82 (t, *J* = 3.9 Hz, 0.03 H), 3.74 (s, 0.09H), 2.68 (m, 0.06 H).

^{29}Si{^{1}H} NMR (99 MHz, CD_3CN, 298 K): δ -7.42 (s).

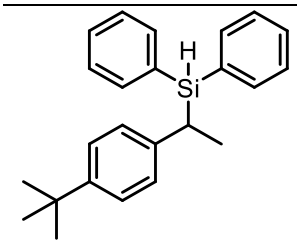

[1-(4-*tert*-Butylphenyl)ethyl]diphenylsilane (**4da**)

Synthesis details: **GP-A**, 4-*tert*-butylstyrene (**2d**), H_2SiPh_2 (**3a**). Selectivity before purification: 1:>99 (*l*/*b*) measured by GC-MS. Purification details: Column chromatography: silica, benzene/hexanes (gradient 0:100 to 5:95) to give the product as a clear oil (0.318 g, 0.923 mmol, 92% yield, *l*/*b* = 1:>99). NMR spectra match values previously reported.[77]

^{1}H NMR (500 MHz, CD_3CN, 298 K): δ 7.58 (d, *J* = 7.9 Hz, 2H), 7.45-7.35 (ms, 6H), 7.29 (t, *J* = 7.3 Hz, 2H), 7.23 (d, *J* = 8.2 Hz,

2H), 7.04 (d, *J* = 8.2 Hz, 2H), 4.80 (d, *J* = 4.1 Hz, $^{1}J_{H–Si}$ = 195.5 Hz, 1H), 2.91 (qd, *J* = 7.5, 4.2 Hz, 1H), 1.41 (d, J = 7.5 Hz, 3H), 1.26 (s, 9H).

$^{13}C\{^{1}H\}$ NMR (126 MHz, CD_3CN, 298 K): δ 148.8, 142.5, 136.4, 136.3, 134.5, 134.4, 130.8, 130.7, 129.1, 128.9, 128.4, 126.1, 34.9, 31.6, 26.5, 17.4.

$^{29}Si\{^{1}H\}$ NMR (99 MHz, CD_3CN, 298 K): δ -7.88 (s).

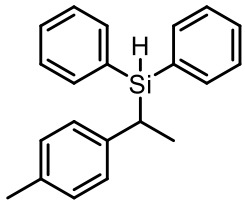

[1-(4-Methylphenyl)ethyl]diphenylsilane (**4ea**)

Synthesis details: **GP-A**, 4-methylstyrene (**2e**), H_2SiPh_2 (**3a**).

Selectivity before purification: 1:55 (*l*/*b*) measured by GC-MS.

Purification details: Column chromatography: silica, benzene/hexanes (gradient 0:100 to 5:95) to give the product as a clear oil (0.238 g, 0.787 mmol, 79% yield, *l*/*b* = 1:>99). NMR spectra match values previously reported.[279]

^{1}H NMR (500 MHz, CD_3CN, 298 K): δ 7.61 (d, *J* = 7.5 Hz, 2H), 7.47 (m, 1H), 7.41 (t, *J* = 7.5 Hz, 2H), 7.36-7.32 (ms, 3H), 7.25 (t, *J* = 7.4 Hz, 2H), 7.10 (m, 2H), 7.04 (d, *J* = 7.3 Hz, 1H), 6.99 (t, *J* = 7.3 Hz, 1H), 4.79 (d, *J* = 4.1 Hz, $^{1}J_{H–Si}$ = 195.6 Hz, 1H), 3.09 (qd, *J* = 7.3, 4.1 Hz, 1H), 2.11 (s, 3H), 1.40 (d, *J* = 7.4 Hz, 3H).

$^{13}C\{^{1}H\}$ NMR (126 MHz, CD_3CN, 298 K): δ 142.5, 136.3, 136.2, 135.3, 134.6, 134.4, 130.8, 130.7, 129.8, 129.1, 128.9, 128.6, 26.6, 20.9, 17.4.

$^{29}Si\{^{1}H\}$ NMR (99 MHz, CD_3CN, 298 K): δ -8.54 (s).

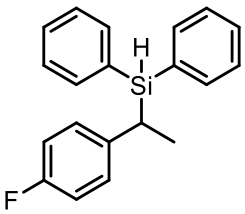

[1-(4-Fluorophenyl)ethyl]diphenylsilane (**4fa**)

Synthesis details: **GP-A**, 4-fluorostyrene (**2f**), H_2SiPh_2 (**3a**).

Selectivity before purification: 1:33 (*l*/*b*) measured by GC-MS.

Purification details: Column chromatography: silica, benzene/hexanes (5:95) to give the product as a clear oil (0.209 g,

0.690 mmol, 69% yield, *l*/*b* = 1:42). NMR spectra match values previously reported.[120,77]

The major product isolated is the branched isomer, and the linear isomer is seen in the NMR spectra as well. The ratio of these isomers was determined by relative integrations of the benzylic C–H positions and was found to be 1:42 (*l*/*b*). The branched product is fully characterized below, and the peaks visible and clearly assignable to the linear isomer are given directly following the NMR characterization of the branched product.

Branched product:

^{1}H NMR (500 MHz, CD_3CN, 298 K): δ 7.59 (d, *J* = 7.5 Hz, 2H), 7.45 (m, 1H), 7.41 (d, *J* = 7.3 Hz, 4H), 7.37 (m, 1H), 7.30 (t, *J* = 7.3 Hz, 2H), 7.06 (dd, *J* = 8.4, 5.8 Hz, 2H), 6.91 (t, *J* = 8.8 Hz, 2H), 4.79 (d, *J* = 4.1 Hz, $^{1}J_{H–Si}$ = 196.2 Hz, 1H), 2.95 (qd, *J* = 7.5, 4.1 Hz, 1H), 1.41 (d, *J* = 7.6 Hz, 3H).

^{13}C{^{1}H} NMR (126 MHz, CD_3CN, 298 K): *δ* 161.5 (d, *J* = 240.8 Hz), 141.6 (d, *J* = 3.2 Hz), 136.4, 136.3, 134.1, 134.0, 130.9, 130.8, 130.1 (d, *J* = 7.7 Hz), 129.1, 128.9, 115.7 (d, *J* = 21.2 Hz), 26.5, 17.3.

^{19}F NMR (471 MHz, CD_3CN, 298 K): δ -120.36 (m).

^{29}Si{^{1}H} NMR (99 MHz, CD_3CN, 298 K): δ -7.36 (s).

Linear product:

^{1}H NMR (500 MHz, CD_3CN, 298 K): δ 7.17 (m, 0.24H), 7.10 (m, 0.28H), 4.80 2.72 (m, 0.06H).

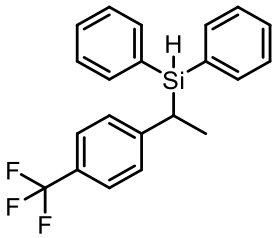

[1-(4-(Trifluoromethyl)phenyl)ethyl]diphenylsilane (**4ga**)

Synthesis details: **GP-A**, 4-(trifluoromethyl)styrene (**2g**), H_2SiPh_2 (**3a**).

Selectivity before purification: 1:78 (*l*/*b*) measured by GC-MS.

Purification details: Column chromatography: silica, hexanes to give the product as a clear oil (0.242 g, 0.679 mmol, 68% yield, *l*/*b* = 1:12). NMR spectra match values previously reported.[280]

The major product isolated is the branched isomer, and the linear isomer is seen in the NMR spectra as well. The ratio of these isomers was determined by relative integrations of the benzylic C–H positions and was found to be 1:12 (*l*/*b*). The branched product is fully characterized below, and the peaks visible and clearly assignable to the linear isomer are given directly following the NMR characterization of the branched product.

IR (ATR, neat) ν: 3069-2843 (w), 2120 (s, Si–H), 1428 (m), 1322 (s), 695 (s).

Branched product:

^{1}H NMR (500 MHz, CD_3CN, 298 K): δ 7.59 (d, *J* = 7.6 Hz, 2H), 7.46 (t, *J* = 7.2 Hz, 3H), 7.42-7.37 (ms, 5H), 7.30 (t, *J* = 7.5 Hz, 2H), 7.22 (d, *J* = 8.0 Hz, 2H), 4.79 (d, *J* = 4.0 Hz, $^{1}J_{H–Si}$ = 197.5 Hz, 1H), 3.07 (qd, *J* = 7.5, 4.0 Hz, 1H), 1.45 (d, *J* = 7.5 Hz, 3H)

^{13}C{^{1}H} NMR (126 MHz, CD_3CN, 298 K): δ 150.8, 136.4, 136.2, 133.6, 133.5, 131.1, 130.9, 129.2, 129.1, 129.0, 127.3 (q, *J* = 32.0 Hz), 125.9 (q, *J* = 3.8 Hz), 125.6 (q, *J* = 270.9 Hz)*, 27.6, 16.6.

*Note that the most downfield peak of this quartet (assigned to a *C*F_3) is obscured by the product peak at 128.8 ppm.

^{19}F NMR (471 MHz, CD_3CN, 298 K): δ -62.61 (s).

^{29}Si{^{1}H} NMR (99 MHz, CD_3CN, 298 K): δ -6.99 (s).

Linear product:

^{1}H NMR (500 MHz, CD_3CN, 298 K): δ 7.56 (m), 4.83 (t, *J* = 3.8 Hz, 0.09H), 2.81 (m, 0.18)

^{19}F NMR (471 MHz, CD_3CN, 298 K): δ -62.71 (s).

[1-(2-Methylphenyl)ethyl]diphenylsilane (**4ha**)

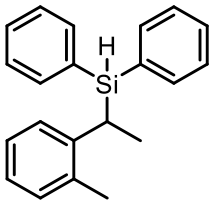

Synthesis details: **GP-B**, 2-methylstyrene (**2h**), H_2SiPh_2 (**3a**).

Selectivity before purification: 1:26 (*l*/*b*) measured by GC.

Purification details: Column chromatography: silica, benzene/hexanes (gradient 0:100 to 5:95) to give the product as a clear oil (0.266 g, 0.880 mmol, 88% yield, *l*/*b* = 1:26). NMR spectra match values previously reported.[280]

^{1}H NMR (600 MHz, $CDCl_3$, 298 K): δ 7.61 (d, *J* = 7.9 Hz, 2H), 7.49 (t, *J* = 7.5 Hz, 1H), 7.44 (t, *J* = 7.6 Hz, 2H), 7.40-7.36 (ms, 3H), 7.30 (t, *J* = 7.4 Hz, 2H), 7.19 (t, *J* = 7.3 Hz, 1H), 7.13-7.08 (m, 3H), 4.88 (d, *J* = 3.3 Hz, $^1J_{H–Si}$ = 197.7 Hz, 1H), 3.08 (qd, *J* = 7.4, 3.3 Hz, 1H), 2.14 (s, 3H), 1.51 (d, *J* = 7.4 Hz, 3H).

$^{13}C\{^1H\}$ NMR (126 MHz, $CDCl_3$, 298 K): δ 143.0, 136.0, 135.4, 135.3, 133.5, 133.0, 130.2, 129.9, 129.7, 128.1, 127.8, 126.9, 126.2, 124.9, 22.1, 20.2, 16.7.

$^{29}Si\{^1H\}$ NMR (99 MHz, $CDCl_3$, 298 K): δ -9.70 (s).

IR (ATR, neat) ν: 3068-2061 (w), 2123 (s, Si–H), 1427 (s), 1106 (s), 796 (s).

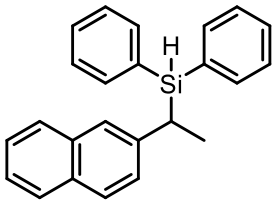

[1-(2-Naphthyl)ethyl]diphenylsilane (**4ia**)

Synthesis details: **GP-A**, 2-vinylnapthylene (**2i**), H_2SiPh_2 (**3a**).

Selectivity before purification: 1:55 (*l*/*b*) measured by GC.

Purification details: Column chromatography: silica, benzene/pentane (2:98) to give the product as a clear oil (0.296 mg, 0.873 mmol, 87% yield, *l*/*b* = 1:21). NMR spectra match values previously reported for the branched product.[279]

The major product isolated is the branched isomer, and the linear isomer is seen in the NMR spectra as well. The ratio of these isomers was determined by relative integrations of the benzylic C–H positions and was found to be 1:21 (*l*/*b*). The branched product is fully

characterized below, and the peaks visible and clearly assignable to the linear isomer are given directly following the NMR characterization of the branched product.

Branched product:

^{1}H NMR (500 MHz, CD_3CN, 298 K): δ 7.78 (d, *J* = 7.8 Hz, 1H), 7.68 (d, *J* = 8.5 Hz, 2H), 7.61 (d, *J* = 7.5 Hz, 2H), 7.53 (s, 1H), 7.46-7.37 (ms, 7H), 7.33 (m, 1H), 7.27-7.24 (ms, 3H), 4.87 (d, *J* = 4.1 Hz, $^{1}J_{H–Si}$ = 196.2 Hz, 1H), 3.12 (qd, *J* = 7.5, 4.1 Hz, 1H), 1.53 (d, *J* = 7.5 Hz, 3H).

^{13}C{^{1}H} NMR (126 MHz, CD_3CN, 298 K): δ 143.4, 136.4, 136.3, 134.7, 134.2, 134.1, 132.5, 130.9, 130.7, 129.1, 128.9, 128.4 (2 signals), 128.1, 128.1, 126.9, 126.1, 125.9, 27.5, 17.1.

^{29}Si{^{1}H} NMR (99 MHz, CD_3CN, 298 K): δ -7.51 (s).

Linear product:

^{1}H NMR (500 MHz, CD_3CN, 298 K): δ 2.91 (m, 0.10H).

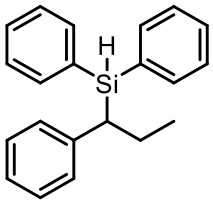

[1-Phenylpropyl]diphenylsilane (**4ja**)

Synthesis details: **GP-B**, Trans-β-methylstyrene (**2j**), H_2SiPh_2 (**3a**).

Selectivity before purification: 1:>99 (*l*/*b*) measured by GC.

Purification details: Column chromatography: silica, benzene/hexanes (gradient 0:100 to 5:95) to give the product as a clear oil (0.215 g, 0.711 mmol, 71% yield, *l*/*b* = 1:>99). NMR spectra match values previously reported.[15,77]

^{1}H NMR (500 MHz, CD_3CN, 298 K): δ 7.60 (d, *J* = 7.6 Hz, 2H), 7.46-7.38 (ms, 5H), 7.34 (t, *J* = 7.3 Hz, 1H), 7.26 (t, *J* = 7.4 Hz, 2H), 7.18 (t, *J* = 7.5 Hz, 2H), 7.08 (m, 3H), 4.83 (d, *J* = 4.4 Hz, $^{1}J_{H–Si}$ = 195.4 Hz, 1H), 2.71 (dt, *J* = 10.6, 4.6 Hz, 1H), 1.87 (m, 2H), 0.81 (t, *J* = 7.2 Hz, 3H).

$^{13}C\{^{1}H\}$ NMR (126 MHz, CD_3CN, 298 K): δ 143.4, 136.4, 136.2, 134.6, 134.3, 130.8, 130.6, 129.5, 129.2, 129.1, 128.8, 126.0, 36.1, 25.3, 14.2.

$^{29}Si\{^{1}H\}$ NMR (99 MHz, CD_3CN, 298 K): δ -9.35 (s).

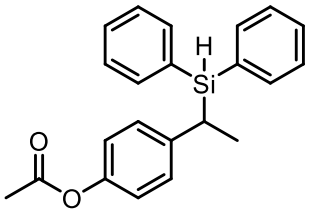

[1-(4-Acetoxyphenyl)ethyl]diphenylsilane (**4ka**)

Synthesis details: **GP-A**, 4-acetoxystyrene (**2k**), H_2SiPh_2 (**3a**).

Selectivity before purification: 1:51 (*l*/*b*) measured by GC.

Purification details: Column chromatography: silica, EtOAc/hexanes (5:95) to give the product as a colorless oil. (0.204 g, 0.589 mmol, 59% yield, *l*/*b* = 1:9.6). NMR spectra for the branched isomer match values previously reported.[120]

The major product isolated is the branched isomer, and the linear isomer is seen in the NMR spectra as well. The ratio of these isomers was determined by relative integrations of the benzylic C–H positions and was found to be 1:9.6 (*l*/*b*). The branched product is fully characterized below, and the peaks visible and clearly assignable to the linear isomer are given directly following the NMR characterization of the branched product.

Branched product:

^{1}H NMR (500 MHz, CD_3CN, 298 K): δ 7.59 (m, 2H), 7.46-7.36 (ms, 6H), 7.30 (t, *J* = 7.3 Hz, 2H), 7.09 (d, *J* = 8.6 Hz, 2H), 6.89 (d, *J* = 8.6 Hz, 2H), 4.78 (d, *J* = 4.1 Hz, $^{1}J_{H-Si}$ = 196.2 Hz, 1H), 2.97 (qd, *J* = 7.5, 4.1 Hz, 1H), 2.20 (s, 3H) 1.42 (d, *J* = 7.5 Hz, 3H).

$^{13}C\{^{1}H\}$ NMR (126 MHz, CD_3CN, 298 K): δ 170.48, 149.3, 143.1, 136.4, 136.3, 134.1, 134.0 130.9, 130.8, 129.4, 129.1, 128.9, 122.4, 26.7, 21.3, 17.3.

$^{29}Si\{^{1}H\}$ NMR (99 MHz, CD_3CN, 298 K): *δ* -7.45 (s).

Linear product:

---

^{1}H NMR (500 MHz, CD_3CN, 298 K): δ 7.22 (d, *J* = 8.4 Hz, 0.25H), 6.97 (d, *J* = 8.4 Hz, 0.23H), 4.83 (t, *J* = 3.7 Hz, 0.12H), 2.74 (m, 0.24H) 2.22 (s, 0.28H).

^{13}C{^{1}H} NMR (126 MHz, CD_3CN, 298 K): 170.55, 150.0, 142.9, 136.0, 135.1, 129.8, 129.2, 122.6, 30.6, 26.3, 14.8.

^{29}Si{^{1}H} NMR (99 MHz, CD_3CN, 298 K): *δ* -13.86 (s).

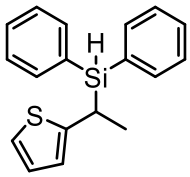

[1-(2-Thiophenyl)ethyl]diphenylsilane (**4la**)

Synthesis details: **GP-B**, 2-vinylthiophene (**2l**), H_2SiPh_2 (**3a**), reaction time of 24 h.

Selectivity before purification: 1:13 (*l*/*b*) measured by GC.

Purification details: Column chromatography: silica, hexanes to give the product as colorless oil. (0.219 g, 0.744 mmol, 74% yield, *l*/*b* = 1:6.7). NMR spectra for the branched isomer match values previously reported.[77]

The major product isolated is the branched isomer, and the linear isomer is seen in the NMR spectra as well. The ratio of these isomers determined by relative integrations of the benzylic C–H positions and was found to be 1:6.7 (*l*/*b*). The branched product is fully characterized below, and the peaks visible and clearly assignable to the linear isomer are given directly following the NMR characterization of the branched product.

IR (ATR, neat) ν: 3069-2865 (w), 2117 (s, Si–H), 1427 (s), 1110 (s), 686 (s).

ASAP/HRMS (m/z): [M^+] calculated for $C_{18}H_{18}SSi$ 294.0898, found 294.0885.

Branched product:

^{1}H NMR (500 MHz, $CDCl_3$, 298 K): δ 7.58-7.56 (ms, 2H), 7.46-7.43 (ms, 3H), 7.42-7.37 (ms, 3H), 7.33 (m, 2H), 7.03 (dd, *J* = 5.1 Hz, 1.0

Hz, 1H), 6.88 (dd, *J* = 5.1, 3.5 Hz, 1H), 6.61 (d, *J* = 3.5 Hz, 1H), 4.94 (d, *J* = 3.3 Hz, $^{1}J_{H–Si}$ = 199.1 Hz, 1H) 3.15 (qd, *J* = 7.5, 3.3 Hz, 1H) 1.53 (d, *J* = 7.5 Hz, 3H).

$^{13}C\{^{1}H\}$ NMR (126 MHz, $CDCl_3$, 298 K): δ 148.3, 135.8, 135.7, 132.9, 132.7, 130.0, 129.92, 128.1, 128.0, 126.9, 122.9, 121.9, 22.4, 18.2

$^{29}Si\{^{1}H\}$ NMR (99 MHz, $CDCl_3$, 298 K): δ -9.12 (s).

Linear product:

^{1}H NMR (500 MHz, $CDCl_3$, 298 K): δ 7.60 (m, 0.88H), 7.12 (dd, *J* = 5.1, 1.1 Hz, 0.15H), 6.91 (dd, *J* = 5.1, 3.4 Hz, 0.16H), 6.80 (m, 0.15H), 4.93 (m), 3.00 (m, 0.31H), 1.63 (m, 0.31H).

$^{13}C\{^{1}H\}$ NMR (126 MHz, $CDCl_3$, 298 K): δ 147.9, 135.3, 133.9, 129.88, 128.2, 126.80, 123.6, 123.0, 25.0, 15.0.

$^{29}Si\{^{1}H\}$ NMR (99 MHz, $CDCl_3$, 298 K): δ -14.44 (s).

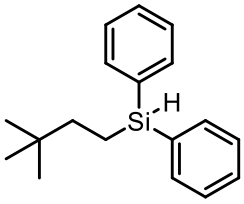

(3,3-Dimethyl-1-butyl)diphenylsilane (**4ma**)

Synthesis details: **GP-A**, 3,3-dimethyl-1-butene (**2m**), H_2SiPh_2 (**3a**).

Selectivity before purification: >99:1 (*l*/*b*) measured by GC.

Purification details: Column chromatography: silica, benzene/hexanes (5:95) to give the product as a clear oil (0.215 g, 0.800 mmol, 80% yield, *l*/*b* = >99:1). NMR spectra match values previously reported.[281]

^{1}H NMR (500 MHz, CD_3CN, 298 K): δ 7.58 (d, *J* = 7.7 Hz, 4H), 7.43-7.37 (ms, 6H), 4.78 (t, *J* = 3.8 Hz, $^{1}J_{H–Si}$ = 191.2 Hz, 1H), 1.30 (m, 2H), 1.14 (m, 2H), 0.87 (s, 9H).

$^{13}C\{^{1}H\}$ NMR (126 MHz, CD_3CN, 298 K): δ 135.9, 135.6, 130.6, 129.1, 39.2, 31.8, 29.0, 6.9.

$^{29}Si\{^{1}H\}$ NMR (99 MHz, CD_3CN, 298 K): δ -11.77 (s).

IR (ATR, neat) ν: 3068-2840 (w), 2114 (s, Si–H), 1427 (s), 1115 (s), 694 (s).

ASAP/HRMS (m/z): [M^+] calculated for $C_{18}H_{24}Si$ 268.1647, found 268.1624.

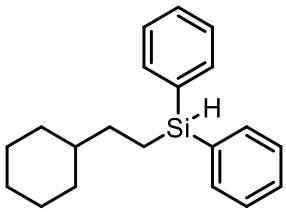

(2-cyclohexylethyl)diphenylsilane (**4na**)

Synthesis details: **GP-A**, vinylcyclohexane (**2n**), H_2SiPh_2 (**3a**).

Selectivity before purification: >99:1 (*l*/*b*) measured by GC.

Purification details: Column chromatography: silica, benzene/hexanes (5:95) to give the product as a clear oil (0.162 g, 0.550 mmol, 55% yield, *l*/*b* = 20:1). NMR spectra match values previously reported.[75]

The major product isolated is the linear isomer, and the branched isomer is seen in the NMR spectra as well. The ratio of these isomers determined by relative integrations of Si–*H* and was found to be 20:1 (*l*/*b*). The linear product is fully characterized below, and the peaks visible and clearly assignable to the branched isomer are given directly following the NMR characterization of the linear product.

IR (ATR, neat) ν: 3067-2848 (w), 2110 (s, Si–H), 1427 (s), 1116 (s), 695 (s).

Linear product:

^{1}H NMR (500 MHz, $CDCl_3$, 298 K): δ 7.58 (d, *J* = 7.2 Hz, 4H), 7.43-7.37 (ms, 6H), 4.86 (t, *J* = 3.7 Hz, $^1J_{H–Si}$ = 192.3 Hz, 1H), 1.77-1.65 (ms, 5H), 1.37 (m, 2H), 1.23-1.13 (ms, 6H), 0.87 (q, *J* = 12.0 Hz, 2H).

^{13}C{^{1}H} NMR (126 MHz, CD_3CN, 298 K): δ 135.3, 134.9, 129.6, 128.1, 40.6, 33.1, 32.0, 26.9, 26.5, 9.3.

^{29}Si{^{1}H} NMR (99 MHz, $CDCl_3$, 298 K): δ -13.08 (s).

Branched product:

---

^{1}H NMR (500 MHz, $CDCl_3$, 298 K): δ 7.62 (d, *J* = 7.3 Hz, 0.08H), 4.90 (d, *J* = 3.5 Hz, 0.05H).

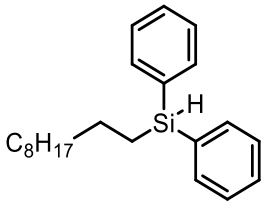

(1-decyl)diphenylsilane (**4oa**)

Synthesis details: **GP-A**, 1-decene (**2o**), H_2SiPh_2 (**3a**).

Selectivity before purification: 11:1 (*l*/*b*) measured by GC.

Purification details: Column chromatography: silica, benzene/hexanes (5:95) to give the product as a clear oil (0.11 g, 0.34 mmol, 34% yield, *l*/*b* = 8.3:1). NMR spectra match values previously reported.[75]

The major product isolated is the linear isomer, and the branched isomer is seen in the NMR spectra as well. The ratio of these isomers determined by relative integrations of the Si–H positions and was found to be 8.3:1 (*l*/*b*). The linear product is fully characterized below, and the peaks visible and clearly assignable to the branched isomer are given directly following the NMR characterization of the linear product.

IR (ATR, neat) v: 3067-2851 (w), 2113 (s, Si–H), 1428 (s), 1115 (s), 695 (s).

Linear product:

^{1}H NMR (500 MHz, $CDCl_3$, 298 K): δ 7.56 (d, *J* = 7.2 Hz, 4H), 7.40-7.34 (ms, 6H), 4.85 (t, *J* = 3.7 Hz, $^{1}J_{H–Si}$ = 192.3 Hz, 1H), 1.46 (m, 2H), 1.35 (m, 2H), 1.30-1.23 (ms, 12H), 1.14 (m, 2H), 0.88 (t, *J* = 7.1 Hz, 3H).

$^{13}C\{^{1}H\}$ NMR (126 MHz, $CDCl_3$, 298 K): δ 135.3, 134.9, 129.6, 128.1, 33.3, 32.1, 29.8, 29.7, 29.5, 29.4, 24.6, 22.9, 14.3, 12.3.

$^{29}Si\{^{1}H\}$ NMR (99 MHz, $CDCl_3$, 298 K): δ -13.74 (s).

Branched product:

---

^{1}H NMR (500 MHz, $CDCl_3$, 298 K): δ 7.59, 7.40, 4.74 (d, *J* = 3.0 Hz, 0.12H), 1.08 (0.5H), 0.97 (0.5H), 0.90 (0.22H).

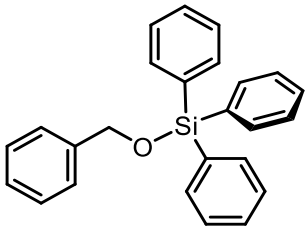

Benzyloxytriphenylsilane (**4pl**)

Synthesis details: **GP-D**, benzaldehyde (**2p**), $HSiPh_3$ (**3l**).

Purification details: Hexanes (5.0 mL) was added to the crude reaction mixture and this mixture was filtered through celite to remove all solids. The filtrate was concentrated, dissolved in minimal hexanes (1.0 mL) and allowed to crystallize overnight in the freezer (-20 °C). The resulting solution was decanted away from the solids, which were then dried under vacuum to give the product as a white solid (0.343 g, 0.937 mmol, 94% yield). NMR spectra match values previously reported.[282]

^{1}H NMR (500 MHz, $CDCl_3$, 298 K): *δ* 7.82-7.80 (ms, 6H), 7.57-7.54 (m, 3H), 7.52-7.47 (ms, 8H), 7.43 (t, *J* = 7.5 Hz, 2H), 7.36 (t, *J* = 7.3 Hz, 1H), 5.04 (s, 2H).

^{13}C{^{1}H} NMR (126 MHz, $CDCl_3$, 298 K): δ 140.7, 135.6, 134.1, 130.2, 128.4, 128.1, 127.2, 126.5, 65.7.

^{29}Si{^{1}H} NMR (99 MHz, $CDCl_3$, 298 K): δ -11.88 (s).

IR (ATR, neat) v: 3064-2825 (w), 1586 (w), 1426 (s), 1114 (s), 695 (s).

ASAP/HRMS (m/z): [M^+] calculated for $C_{25}H_{22}OSi$ 366.1440, found 366.1420.

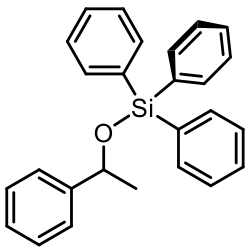

(1-Phenylethoxy)triphenylsilane (**4ql**)

Synthesis details: **GP-A**, acetophenone (**2q**), $HSiPh_3$ (**3l**), reaction time of 24 h.

Purification details: Column chromatography: silica, Et_2O/hexanes (5:95) to give the product as a white solid (0.379 g, 0.996 mmol, 99.6% yield). NMR spectra match values previously reported.[283]

^{1}H NMR (500 MHz, CD_3CN, 298 K): δ 7.57 (d, *J* = 7.4 Hz, 6H), 7.49-7.42 (ms, 3H), 7.37 (t, *J* = 7.4 Hz, 6H), 7.33 (m, 2H), 7.28 (t, *J* = 7.5 Hz, 2H), 7.22 (t, *J* = 7.3 Hz, 1H), 5.07 (q, *J* = 6.4 Hz, 1H), 1.40 (d, *J* = 6.3 Hz, 3H).

^{13}C{^{1}H} NMR (126 MHz, CD_3CN, 298 K): δ 146.8, 136.2, 135.4, 131.1, 129.1, 128.9, 128.0, 126.3, 72.9, 27.4.

^{29}Si{^{1}H} NMR (99 MHz, CD_3CN, 298 K): δ -13.92 (s).

IR (ATR, neat) v: 3066-2864 (w), 1589 (w), 1427 (s), 1115 (s), 694 (s).

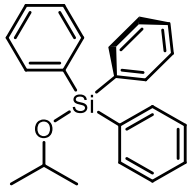

Isopropoxytriphenylsilane (**4rl**)

Synthesis details: **GP-A**, acetone (**2r**), $HSiPh_3$ (**3l**), reaction time of 24 h.

Purification details: Column chromatography: silica, Et_2O/hexanes (5:95) to give the product as a white solid (0.314 g, 0.986 mmol, 99% yield). NMR spectra match values previously reported.[284]

^{1}H NMR (500 MHz, CD_3CN, 298 K): δ 7.62 (d, *J* = 7.3 Hz 6H), 7.45 (t, *J* = 7.1 Hz, 3H), 7.41 (t, *J* = 7.2 Hz, 6H), 4.18 (sept, *J* = 6.0 Hz, 1H), 1.16 (d, *J* = 6.0 Hz, 6H).

^{13}C{^{1}H} NMR (126 MHz, CD_3CN, 298 K): δ 136.2, 135.9, 131.1, 128.9, 67.3, 25.9.

^{29}Si{^{1}H} NMR (99 MHz, CD_3CN, 298 K): δ -15.96 (s).

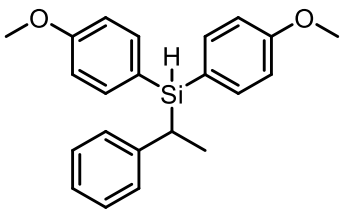

(1-Phenylethyl)di(4-methoxyphenyl)silane (**4ab**)

Synthesis details: **GP-A**, styrene (**2a**), $H_2Si(4\text{-}OCH_3\text{-}C_6H_4)_2$ (**3b**)

Selectivity before purification: 1:>99 (*l*/*b*) measured by GC.

Purification details: Column chromatography: silica, Et_2O/cyclohexanes (gradient 0:100 to 5:95) to give the product as a clear oil (0.179 g, 0.514 mmol, 51% yield, *l*/*b* = 1:>99).

^{1}H NMR (500 MHz, CD_3CN, 298 K): δ 7.48 (d, *J* = 8.6 Hz, 2H), 7.31 (d, *J* = 8.6 Hz, 2H), 7.17 (t, *J* = 7.6 Hz, 2H), 7.08-7.06 (ms, 3H), 6.95 (d, *J* = 8.6 Hz, 2H), 6.85 (d, *J* = 8.6 Hz, 2H), 4.76 (d, *J* = 3.9 Hz, $^{1}J_{H–Si}$ = 193.8 Hz, 1H), 3.79 (s, 3H), 3.74 (s, 3H), 2.85 (qd, *J* = 7.5, 3.9 Hz, 1H), 1.40 (d, *J* = 7.5 Hz, 3H).

^{13}C{^{1}H} NMR (126 MHz, CD_3CN, 298 K): δ 162.1, 162.0, 146.0, 137.9, 137.8, 129.1, 128.6, 125.8, 125.2, 125.1, 114.8, 114.6, 55.7, 55.7, 27.7, 17.2.

^{29}Si{^{1}H} NMR (99 MHz, CD_3CN, 298 K): δ -8.35 (s).

IR (ATR, neat) v: 3058-2834 (w), 2107 (s, Si–H), 1591 (s), 1028 (s), 798 (s).

ASAP/HRMS (m/z): [M^+] calculated for $C_{22}H_{24}O_2Si$ 348.1546, found 348.1534.

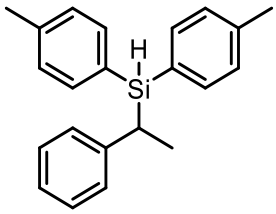

(1-Phenylethyl)di(4-methylphenyl)silane (**4ac**)

Synthesis details: **GP-A**, styrene (**2a**), $H_2Si(4\text{-}Me\text{-}C_6H_4)_2$ (**3c**)

Selectivity before purification: 1:>99 (*l*/*b*) measured by GC.

Purification details: Column chromatography: silica, benzene/hexanes (gradient 0:100 to 5:95) to give the product as a clear oil (0.314 mg, 0.992 mmol, 99% yield, *l*/*b* = 1:>99).

^{1}H NMR (500 MHz, CD_3CN, 298 K): δ 7.46 (d, *J* = 7.6 Hz, 2H), 7.29 (d, *J* = 7.4 Hz, 2H), 7.21 (d, *J* = 7.4 Hz, 2H), 7.17 (t, *J* = 7.5 Hz, 2H), 7.12-7.05 (ms, 5H), 4.76 (d, *J* = 4.0 Hz, $^{1}J_{H–Si}$ = 194.3 Hz, 1H), 2.89 (qd, *J* = 7.5, 4.0 Hz, 1H), 2.34 (s, 3H), 2.28 (s, 3H), 1.41 (d, *J* = 7.5 Hz, 3H).

^{13}C{^{1}H} NMR (126 MHz, CD_3CN, 298 K): δ 145.9, 140.9, 140.7, 136.4, 136.3, 130.8, 130.7, 129.8, 129.6, 129.1, 128.7, 125.8, 27.4, 21.6, 21.5, 17.3.

^{29}Si{^{1}H} NMR (99 MHz, CD_3CN, 298 K): δ -7.76 (s).

IR (ATR, neat) ν: 3059-2866 (s), 2110 (s, Si–H), 1599 (s), 1109 (s), 777 (s).

ASAP/HRMS (m/z): [M^+] calculated for $C_{22}H_{24}Si$ 316.1647, found 316.1645.

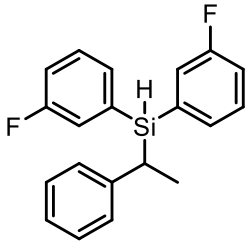

(1-Phenylethyl)di(3-fluorophenyl)silane (**4ad**)

Synthesis details: **GP-A**, styrene (**2a**), $H_2Si(3\text{-}F\text{-}C_6H_4)_2$ (**3d**).

Selectivity before purification: 1:>99 (*l*/*b*) measured by GC.

Purification details: Column chromatography: silica, benzene/hexanes (gradient 0:100 to 5:95) to give the product as a clear oil (0.249 g, 0.767 mmol, 77% yield, *l*/*b* = 1:>99).

^{1}H NMR (500 MHz, CD_3CN, 298 K): δ 7.47-7.40 (ms, 2H) 7.34-7.29 (ms, 2H), 7.21-7.18 (ms, 4H), 7.12-7.06 (ms, 5H), 4.80 (d, *J* = 4.4 Hz, $^1J_{H–Si}$ = 200.6 Hz, 1H), 2.96 (qd, *J* = 7.5, 4.4 Hz, 1H), 1.43 (t, *J* = 7.5 Hz, 3H).

^{13}C{^{1}H} NMR (126 MHz, CD_3CN, 298 K): δ 164.5 (d, *J* = 246.8 Hz), 162.5 (d, *J* = 246.5 Hz), 145.0, 136.9 (d, *J* = 4.3 Hz), 136.8 (d, *J* = 4.4 Hz), 132.3 (d, *J* = 3.0 Hz), 132.2 (d, *J* = 2.8 Hz), 131.4 (d, *J* = 7.0 Hz), 131.1 (d, *J* = 7.2 Hz), 129.3, 128.7, 126.2, 122.4 (d, *J* = 19.5 Hz), 122.3 (d, *J* = 19.1 Hz), 118.0 (d, *J* = 21.8 Hz), 117.8 (d, *J* = 21.1 Hz), 26.9, 17.0.

^{19}F NMR (471 MHz, CD_3CN, 298 K): δ -117.68 (td, *J* = 8.8, 7.0 Hz, 1F), -117.96 (td, *J* = 8.5, 6.4 Hz, 1F).

^{29}Si{^{1}H} NMR (99 MHz, CD_3CN, 298 K): δ -8.00 (s).

IR (ATR, neat) ν: 3061-2870 (w), 2125 (s, Si–H), 1574 (s), 1215 (s), 775 (s).

ASAP/HRMS (m/z): [M^+] calculated for $C_{20}H_{18}F_2Si$ 324.1146, found 324.1171.

(1-Phenylethyl)di[4-(trifluoromethyl)phenyl]silane (**4ae**)

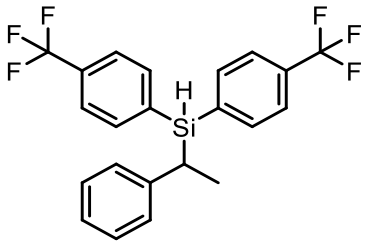

Synthesis details: **GP-A**, styrene (**2a**), $H_2Si(4\text{-}CF_3\text{-}C_6H_4)_2$ (**3e**).

Selectivity before purification: 1:>99 (*l*/*b*) measured by GC.

Purification details: Column chromatography: silica, benzene/hexanes (5:95) to give the product as a clear oil (0.266 g, 0.627 mmol, 63% yield, *l*/*b* = 1:>99).

^{1}H NMR (500 MHz, C_6D_6, 298 K): δ 7.37 (d, *J* = 7.7 Hz, 2H), 7.28 (d, *J* = 7.8 Hz, 2H), 7.26 (d, *J* = 7.7 Hz, 2H), 7.12 (d, *J* = 7.7 Hz, 2H), 7.06 (t, *J* = 7.5 Hz, 2H), 6.98 (t, *J* = 7.4 Hz, 1H), 6.86 (d, *J* = 7.6 Hz, 2H), 4.83 (d, *J* = 3.6 Hz, $^1J_{H–Si}$ = 201.7 Hz, 1H), 2.54 (qd, *J* = 7.5, 3.6 Hz, 1H), 1.27 (d, *J* = 7.5 Hz, 3H).

^{13}C{^{1}H} NMR (126 MHz, C_6D_6, 298 K): δ 143.3, 137.5, 137.4, 136.2, 136.1, 132.2 (q, *J* = 32.2 Hz), 132.1 (q, *J* = 32.2 Hz), 128.8, 127.9, 125.9, 124.9 (q, *J* = 3.7 Hz), 124.7 (q, *J* = 3.8 Hz), 124.80 (q, *J* = 272.4 Hz)*, 124.78 (q, *J* = 272.4 Hz)**, 26.5, 16.4.

*Note that the two most downfield peaks of this quartet (assigned to a *C*F_3) are obscured by the C_6D_6 peak at 128.1 ppm and the product peak at 125.9 ppm.

**Note that the most downfield peak of this quartet (assigned to a *C*F_3) is obscured by the C_6D_6 peak at 128.1 ppm.

^{19}F NMR (471 MHz, C_6D_6, 298 K): δ -62.81 (s, 3F), -62.87 (s, 3F).

^{29}Si{^{1}H} NMR (99 MHz, C_6D_6, 298 K): δ -9.10 (s).

IR (ATR, neat) v: 3035-2881 (w), 2125 (m, Si–H), 1317 (s), 1057 (s), 800 (s).

ASAP/HRMS (m/z): [M^+] calculated for $C_{22}H_{18}F_6Si$ 424.1082, found 424.1079.

(1-Phenylethyl)di(3-methylphenyl)silane (**4af**)

Synthesis details: **GP-A**, styrene (**2a**), $H_2Si(3\text{-}Me\text{-}C_6H_4)_2$ (**3f**).

Selectivity before purification: 1:>99 (*l*/*b*) measured by GC.

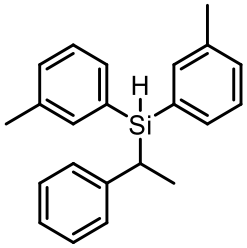

Purification details: Column chromatography: silica, benzene/hexanes (5:95) to give the product as a clear oil (0.248 mg, 0.784 mmol, 78% yield, *l*/*b* = 1:>99).

^{1}H NMR (500 MHz, CD_3CN, 298 K): δ 7.41-7.37 (ms, 2H), 7.30-7.25 (ms, 2H), 7.22-7.17 (ms, 6H), 7.10-7.06 (ms, 3H), 4.76 (d, *J* = 4.1 Hz, $^{1}J_{H–Si}$ = 195.0 Hz, 1H), 2.92 (qd, *J* = 7.4, 4.2 Hz, 1H), 2.32 (s, 3H), 2.24 (s, 3H), 1.42 (d, J = 7.4 Hz, 3H).

^{13}C{^{1}H} NMR (126 MHz, CD_3CN, 298 K): δ 145.8, 138.6, 138.3, 136.9, 136.9, 134.4, 134.2, 133.3, 133.2, 131.5, 131.3, 129.1, 129.0, 128.8, 128.7, 125.9, 27.3, 21.5, 21.4, 17.3.

^{29}Si{^{1}H} NMR (99 MHz, CD_3CN, 298 K): δ -7.25 (s).

IR (ATR, neat) ν: 3059-2866 (w), 2112 (s, Si–H), 1448 (s), 1117 (s), 694 (s).

ASAP/HRMS (m/z): [M^+] calculated for $C_{22}H_{24}Si$ 316.1647, found 316.1630.

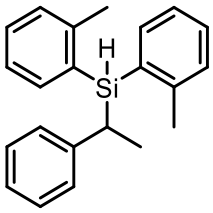

(1-Phenylethyl)di(2-methylphenyl)silane (**4ag**)

Synthesis details: **GP-A**, styrene (**2a**), $H_2Si(2\text{-Me-}C_6H_4)_2$ (**3g**).

Selectivity before purification: 1:>99 (*l*/*b*) measured by GC.

Purification details: Column chromatography: silica, cyclohexane to give the product as a clear oil (0.294 g, 0.929 mmol, 93% yield, *l*/*b* = 1:>99).

^{1}H NMR (500 MHz, CD_3CN, 298 K): δ 7.66 (d, *J* = 7.3 Hz, 1H), 7.48 (d, *J* = 7.4 Hz, 1H), 7.34 (t, *J* = 7.5 Hz, 1H), 7.25-7.14 (ms, 7H), 7.09-7.03 (ms, 3H), 5.05 (d, *J* = 5.3 Hz, $^{1}J_{H–Si}$ = 195.1 Hz, 1H), 3.09 (qd, *J* = 7.5, 5.3 Hz, 1H), 2.25 (s, 3H), 2.06 (s, 3H), 1.46 (d, *J* = 7.5 Hz, 3H).

$^{13}C\{^{1}H\}$ NMR (126 MHz, CD_3CN, 298 K): δ 146.1, 145.3, 145.2, 136.9, 136.9, 133.7, 133.5, 131.0, 130.83, 130.79, 130.5, 129.2, 128.7, 126.1, 125.9, 125.8, 26.2, 22.9, 22.7, 17.9.

$^{29}Si\{^{1}H\}$ NMR (99 MHz, CD_3CN, 298 K): δ -14.98 (s).

IR (ATR, neat) v: 3055-2868 (w), 2127 (m, Si–H), 1448 (m), 1126 (m), 742 (s).

ASAP/HRMS (m/z): [M^+] calculated for $C_{22}H_{24}Si$ 316.1647, found 316.1650.

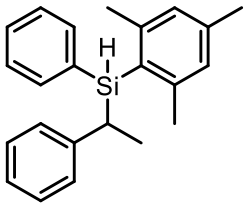

(1-Phenylethyl)phenylmesitylsilane (**4ah**)

Synthesis details: **GP-A**, styrene (**2a**), $H_2SiMesPh$ (**3h**).

Selectivity before purification: 1:>99 (*l*/*b*) measured by GC.

Purification details: Column chromatography: silica, benzene/hexanes (gradient 0:100 to 5:95) to give the product as a viscous, clear oil (0.317 g, 0.959 mmol, 96% yield, *l*/*b* = 1:>99).

The major products isolated are two diastereomers denoted diastereomer **A** and diastereomer **B**. The ratio of these isomers determined by integration of the Si–H was found to be 1.1:1 (**A**/**B**) (Figure S262, S272).

A second, slow, gradient column with benzene/hexanes (0:100-5:95) as the eluent was carried out, with careful analysis of the fractions to obtain better separation of the two diastereomers for easier characterization. The first set of fractions contained primarily diastereomer **A** (**A**:**B** = 7.1:1, Figures S263-266), and the second set of fractions contained primarily diastereomer **B** (**A**:**B** = 1:3.8, Figures S267-S271). Using these two sets of NMR spectra, we were able to assign all peaks to either diastereomer **A** or **B**.

Diastereomer **A**:

^{1}H NMR (500 MHz, $CDCl_3$, 298 K): δ 7.28 (m, 3H, overlapping with $CHCl_3$ peak), 7.23 (d, *J* = 7.6 Hz, 2H), 7.17-7.13 (ms, 3H), 7.10 (d, *J* = 7.2 Hz, 2H), 6.88 (s, 2H), 5.13 (d, *J* = 5.8 Hz, $^{1}J_{H–Si}$ = 196.0 Hz, 1H), 2.94 (m, 1H), 2.38 (s, 6H), 2.30 (s, 3H), 1.43 (d, *J* = 7.5 Hz, 3H).

^{29}Si{^{1}H} NMR (119 MHz, $CDCl_3$, 298 K): δ -17.92

^{13}C{^{1}H} NMR (126 MHz, $CDCl_3$, 298 K): δ 145.7, 145.3, 139.8, 135.4, 134.2, 129.2, 128.9, 128.5, 128.2, 127.7, 125.3, 27.7, 24.7, 21.3, 17.8.

Diastereomer **B**:

^{1}H NMR (500 MHz, $CDCl_3$, 298 K): δ 7.60 (d, *J* = 7.3 Hz, 2H), 7.35-7.30 (ms, 3H), 7.09 (d, *J* = 7.2 Hz, 2H), 7.04 (d, *J* = 7.5 Hz, 2H), 7.00 (t, *J* = 7.1 Hz, 1H), 6.67 (s, 2H), 5.11 (d, *J* = 5.39 Hz, $^{1}J_{H–Si}$ = 195.8 Hz, 1H), 3.00 (app pentet, *J* = 6.9 Hz, 1H), 2.18 (s, 3H), 2.16 (s, 6H), 1.65 (d, *J* = 7.5 Hz, 3H).

^{13}C{^{1}H} NMR (126 MHz, $CDCl_3$, 298 K): δ 145.3, 144.9, 139.4, 135.5, 135.2, 129.2, 128.5, 128.2, 128.0, 127.8, 127.4, 124.9, 26.5, 24.5, 21.2, 18.3.

^{29}Si{^{1}H} NMR (119 MHz, $CDCl_3$, 298 K): δ -17.45

Mixture of diastereomers **A** and **B** (**A**/**B** = 1.1:1):

IR (ATR, neat) ν: 3030-2867 (w), 2140 (m, Si–H), 1603 (m), 1103 (w), 695 (s).

ASAP/HRMS (m/z): [M^+] calculated for $C_{23}H_{26}Si$ 330.1804, found 330.1850.

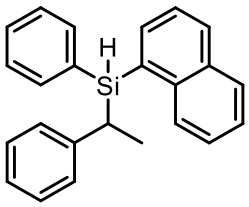

(1-Phenylethyl)(1-naphthyl)phenylsilane (**4ai**)

Synthesis details: **GP-A**, styrene (**2a**), H_2SiPh(1-naphthyl) (**3i**).

Selectivity before purification: 1:>99 (*l*/*b*) measured by GC.

Purification details: Column chromatography: silica, benzene/hexanes (5:95) to give the product as a viscous, clear oil (0.320 g, 0.945 mmol, 95% yield, *l*/*b* = 1:>99).

The major products isolated are two diastereomers denoted diastereomer **A** and diastereomer **B**. The ratio of these isomers determined by integration of the Si–H was found to be 1:1.04 (**A**/**B**, Figures S273, S284).

A slow, gradient column with benzene/hexanes (0:100-5:95) as the eluent was carried out, with careful analysis of the fractions to obtain better separation of the two diastereomers for easier characterization. The first set of fractions contained primarily diastereomer **A** (**A**:**B** = 8.3:1, Figures S274-278), and the second set of fractions contained primarily diastereomer **B** (**A**:**B** = 1:4.5, Figures S279-S283). Using these two sets of NMR spectra, we were able to assign all peaks to either diastereomer **A** or **B**.

Diastereomer **A**:

^{1}H NMR (500 MHz, $CDCl_3$, 298 K): δ 8.02 (d, *J* = 8.4 Hz, 1H), 7.93 (d, *J* = 8.1 Hz, 1H), 7.87 (d, *J* = 8.0 Hz, 1H), 7.80 (dd, *J* = 6.7 Hz, 1.0 Hz, 1H), 7.47 (dd, *J* = 8.0, 6.8 Hz, 2H), 7.41 (m, 1H), 7.29 (t, *J* = 7.4 Hz, 1H), 7.24 (d, *J* = 6.4 Hz, 2H), 7.20-7.17 (ms, 4H), 7.12 (d, *J* = 7.4 Hz, 1H), 7.08 (m, 2H), 5.25 (d, *J* = 4.4 Hz, $^{1}J_{H–Si}$ = 197.5 Hz, 1H), 3.04 (qd, *J* = 7.6 Hz, 4.4 Hz 1H), 1.46 (d, *J* = 7.6 Hz, 3H).

^{13}C{^{1}H} NMR (126 MHz, $CDCl_3$, 298 K): δ 144.7, 137.5, 136.3, 135.7, 133.5, 133.3, 131.7, 130.7, 129.6, 129.0, 128.4, 128.3, 128.0, 127.8, 126.2, 125.8, 125.3, 125.2, 27.2, 17.3.

^{29}Si{^{1}H} NMR (99 MHz, $CDCl_3$, 298 K): δ -10.41 (s).

Diastereomer **B**:

^{1}H NMR (500 MHz, $CDCl_3$, 298 K): δ 7.88 (d, *J* = 8.5 Hz, 1H), 7.85 (d, *J* = 8.3 Hz, 1H) 7.80 (d, *J* = 8.0 Hz, 1H), 7.70 (d, *J* = 6.9 Hz, 1H), 7.60 (d, *J* = 7.2 Hz, 2H), 7.42-7.37 (ms, 3H), 7.36-7.30 (ms, 3H), 7.08 (m, 2H), 7.03-6.98 (ms, 3H), 5.28 (d, *J* = 3.7 Hz, $^{1}J_{H–Si}$ = 197.2 Hz, 1H), 3.06 (qd, *J* = 7.5 Hz, 3.7 Hz, 1H), 1.55 (d, *J* = 7.5 Hz, 3H).

$^{13}C\{^{1}H\}$ NMR (126 MHz, $CDCl_3$, 298 K): δ 144.9, 137.4, 136.0, 135.9, 133.7, 133.3, 131.6, 130.6, 129.8, 128.8, 128.3, 128.2, 128.1, 127.7, 125.9, 125.6, 125.1, 125.0, 26.9, 17.2.

$^{29}Si\{^{1}H\}$ NMR (99 MHz, $CDCl_3$, 298 K): δ -9.94 (s).

Mixture of diastereomers **A** and **B** (**A**/**B** = 1.04:1):

IR (ATR, neat) ν: 3053-2867 (w), 2116 (m, Si –H), 1427 (m), 1033 (m), 695 (s).

ASAP/HRMS (m/z): [M^+] calculated for $C_{24}H_{22}Si$ 338.1491, found 338.1478.

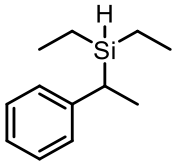

(1-Phenylethyl)diethylsilane (**4aj**)

Synthesis details: **GP-A**, styrene (**2a**), H_2SiEt_2 (**3j**).

Selectivity before purification: 1:20 (*l*/*b*) measured by GC.

Purification details: Column chromatography: silica, benzene/hexanes (5:95) to give the product as a clear oil (0.180 g, 0.936 mmol, 94% yield, *l*/*b* = 1:14). NMR spectra match values previously reported.[48,93]

The major product isolated is the branched isomer, and the linear isomer is seen in the NMR spectra as well. The ratio of these isomers was determined by relative integrations of the benzylic C–H positions and was found to be 1:14 (*l*/*b*). The branched product is fully characterized below, and the peaks visible and clearly assignable to the linear isomer are given directly following the NMR characterization of the branched product.

IR (ATR, neat) ν: 3070-2875 (m), 2094 (m, Si–H), 1452 (m), 1014 (m), 800 (s).

Branched product:

^{1}H NMR (500 MHz, CD_3CN, 298 K): δ 7.25 (t, *J* = 7.6 Hz, 2H), 7.14 (d, *J* = 7.6 Hz, 2H), 7.10 (t, *J* = 7.5 Hz, 1H), 3.63 (m, $^{1}J_{H–Si}$ = 180.5

Hz, 1H), 2.41 (qd, *J* = 7.5, 3.2 Hz, 1H), 1.41 (d, *J* = 7.5 Hz, 3H), 0.96 (t, *J* = 7.9 Hz, 3H), 0.89 (t, *J* = 8.0 Hz, 3H), 0.63 (dq, *J* = 7.9, 3.0 Hz, 2H), 0.52 (m, 2H).

$^{13}C\{^{1}H\}$ NMR (126 MHz, CD_3CN, 298 K): δ 147.0, 129.2, 128.0, 125.5, 26.5, 16.4, 8.55, 8.51, 2.3, 2.2.

$^{29}Si\{^{1}H\}$ NMR (99 MHz, CD_3CN, 298 K): δ 5.32 (s).

Linear product:

^{1}H NMR (500 MHz, CD_3CN, 298 K): δ 3.69 (s, 0.08H), 2.69 (m, 0.15H), 1.00 (m).

$^{13}C\{^{1}H\}$ NMR (126 MHz, CD_3CN, 298 K): 146.0, 129.3, 128.8, 126.5, 31.4, 13.6, 3.3.

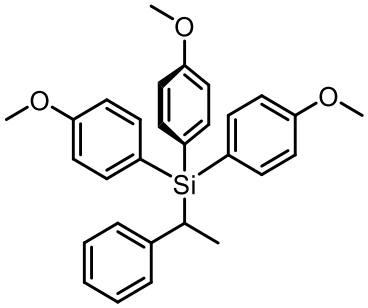

(1-Phenylethyl)tri(4-methoxyphenyl)silane (**4ak**)

Synthesis details: **GP-D**, styrene (**2a**, 3 equiv), $HSi(4\text{-}OCH_3\text{-}C_6H_4)_3$ (**3k**, 1 equiv).

Selectivity before purification: 1:>99 (*l*/*b*) measured by GC.

Purification details: Column chromatography: silica, Et_2O/hexanes (gradient 0:100 to 5:95) to give the product as a white solid (0.427 g, 0.939 mmol, 94% yield, *l*/*b* = 1:>99).

^{1}H NMR (500 MHz, CD_3CN, 298 K): *δ* 7.30 (d, *J* = 8.6 Hz, 6H), 7.12-7.05 (ms, 3H), 6.91-6.87 (ms, 8H), 3.78 (s, 9H), 3.11 (q, *J* = 7.5 Hz, 1H), 1.45 (d, *J* = 7.5 Hz, 3H).

$^{13}C\{^{1}H\}$ NMR (126 MHz, CD_3CN, 298 K): δ 161.8, 146.1, 138.6, 129.5, 128.8, 126.1, 125.8, 114.5, 55.7, 28.6, 18.3.

$^{29}Si\{^{1}H\}$ NMR (99 MHz, CD_3CN, 298 K): δ -11.60 (s).

IR (ATR, neat) v: 3028-2837 (w), 1509 (s), 1178 (s), 1028 (s), 797 (s).

ASAP/HRMS (m/z): $[M^+]$ calculated for $C_{29}H_{30}O_3Si$ 454.1964, found 454.1984.

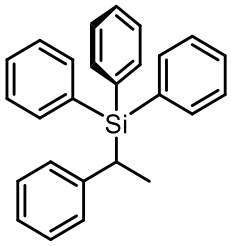

(1-Phenylethyl)triphenylsilane (**4al**)

Synthesis details: **GP-D**, styrene (**2a**, 3.3 mmol, 3.0 equiv), $HSiPh_3$ (**3l**, 1.1 mmol, 1.0 equiv).

Selectivity before purification: 1:>99 (*l*/*b*) measured by GC.

Purification details: Column chromatography: silica, benzene/hexanes (5:95) to give the product as a white solid (0.374 g, 1.03 mmol, 93% yield, *l*/*b* = 1:>99).

^{1}H NMR (500 MHz, $CDCl_3$, 298 K): δ 7.44-7.42 (ms, 9H), 7.36-7.33 (ms, 6H), 7.17-7.11 (ms, 3H), 6.91 (dd, *J* = 7.8, 1.8 Hz, 2H), 3.12 (q, *J* = 7.6 Hz, 1H), 1.60 (d, *J* = 7.6 Hz, 3H).

$^{13}C\{^{1}H\}$ NMR (151 MHz, $CDCl_3$, 298 K): δ 144.5, 136.6, 133.9, 129.6, 128.8, 128.1, 127.8, 125.2, 28.2, 17.9.

$^{29}Si\{^{1}H\}$ NMR (119 MHz, $CDCl_3$, 298 K): δ -11.08 (s).

IR (ATR, neat) v: 3064-2860 (w), 1423 (m), 1107 (m), 997 (w), 696 (s).

ASAP/HRMS (m/z): [M^+] calculated for $C_{26}H_{24}Si$ 364.1647, found 364.1649.

Using **GP-A**: 0.269 g, 0.738 mmol, 74% yield, *l*/*b* = 1:>99

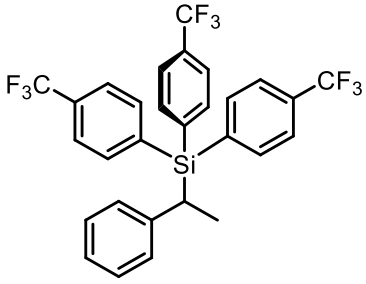

(1-Phenylethyl)tri[4-(trifluoromethyl)phenyl]silane (**4am**)

Synthesis details: **GP-D**, styrene (**2a**, 1 equiv), $HSi(4\text{-}CF_3\text{-}C_6H_4)_3$ (**3m**, 1.1 equiv).

Selectivity before purification: 1:>99 (*l*/*b*) measured by GC.

Purification details: Column chromatography: silica, benzene/hexanes (5:95) to give the product as a white solid (0.537 g, 0.944 mmol, 94% yield, *l*/*b* = 1:>99).

^{1}H NMR (500 MHz, $CDCl_3$, 298 K): δ 7.60 (d, J = 7.7 Hz, 6H), 7.45 (d, J = 7.7 Hz, 6H), 7.16-7.15 (ms, 3H), 6.84 (m, 2H), 3.14 (q, J = 7.5 Hz, 1H), 1.58 (d, J = 7.5 Hz, 3H).

^{13}C{^{1}H} NMR (126 MHz, $CDCl_3$, 298 K): δ 142.8, 137.4, 136.7, 132.2 (q, J = 32.5 Hz), 128.6, 126.0, 124.2 (q, J = 272.5 Hz), 124.7 (q, J = 3.7 Hz), 27.7, 17.6.

^{19}F NMR (471 MHz, $CDCl_3$, 298 K): δ -63.10 (s).

^{29}Si{^{1}H} NMR (99 MHz, $CDCl_3$, 298 K): δ -11.09 (s).

IR (ATR, neat) v: 3026-2845 (w), 1392 (m), 1319 (s), 1057 (s), 700 (s).

ASAP/HRMS (m/z): [M^+] calculated for $C_{29}H_{21}F_9Si$ 568.1269, found 568.1272.

Using **GP-A**: 0.449 g, 0.786 mmol, 79% yield, *l*/*b* = 1:>99.

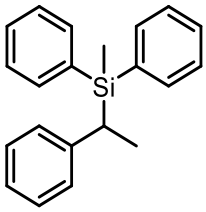

(1-Phenylethyl)diphenylmethylsilane (**4an**)

Synthesis details: **GP-D**, styrene (**2a**), $HSiMePh_2$ (**3n**).

Selectivity before purification: 1:>99 (*l*/*b*) measured by GC.

Purification details: Column chromatography: silica, hexanes, to give the product as a white solid (0.227 g, 0.750 mmol, 75% yield, *l*/*b* = 1:>99). NMR spectra match values previously reported.[285]

^{1}H NMR (500 MHz, CD_3CN, 298 K): δ 7.61 (m, 2H), 7.45-7.35 (ms, 6H), 7.30 (m, 2H), 7.15 (m, 2H), 7.07 (t, J = 7.3, 1H), 7.00 (d, J = 7.4 Hz, 2H), 2.94 (q, J = 7.6 Hz, 1H), 1.42 (d, J = 7.6 Hz, 3H), 0.52 (s, 3H).

^{13}C{^{1}H} NMR (126 MHz, CD_3CN, 298 K): δ 145.7, 136.9, 136.5, 135.9, 135.7, 130.3, 130.2, 128.81, 128.80, 128.7, 128.6, 125.6, 28.4, 16.5, -6.1.

^{29}Si{^{1}H} NMR (99 MHz, CD_3CN, 298 K): δ -6.30 (s).

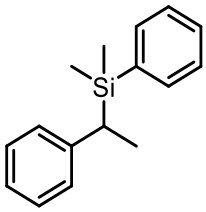

(1-Phenylethyl)phenyldimethylsilane (**4ao**)

Synthesis details: **GP-D**, styrene (**2a**), $HSiMe_2Ph$ (**3o**).

Selectivity before purification: 1:>99 (*l*/*b*) measured by GC.

Purification details: Column chromatography: silica, hexanes, to give the product as a white solid (0.177 g, 0.736 mmol, 74% yield, *l*/*b* = 1:>99). NMR spectra match values previously reported.[285]

^{1}H NMR (500 MHz, CD_3CN, 298 K): δ 7.44 (d, *J* = 7.6 Hz, 2H), 7.38-7.31 (ms, 3H), 7.18 (t, *J* = 7.7 Hz, 2H), 7.07 (t, *J* = 7.1 Hz, 1H), 6.99 (d, *J* = 7.5 Hz, 2H), 2.45 (q, *J* = 7.5 Hz, 1H), 1.32 (d, *J* = 7.5 Hz, 3H), 0.23 (s, 3H), 0.18 (s, 3H).

^{13}C{^{1}H} NMR (126 MHz, CD_3CN, 298 K): δ 146.4, 138.6, 135.1, 130.0, 128.9, 128.6, 128.3, 125.4, 29.9, 15.6, -4.2, -5.2

^{29}Si{^{1}H} NMR (99 MHz, CD_3CN, 298 K): δ -1.05 (s).

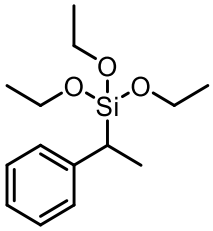

(1-Phenylethyl)triethoxysilane (**4ap**)

Synthesis details: **GP-E**, styrene, $HSi(OEt)_3$ (**3p**, 2 equiv).

Selectivity before purification: 1:>99 (*l*/*b*) measured by GC.

Purification details: Column chromatography Et_2O:hexanes (gradient 0:100 to 1:99) to give the product as a clear oil (0.167 g, 0.622 mmol, 62% yield, *l*/*b* = 1:>99). NMR spectra match values previously reported.[286]

Tetraethoxysilane, formed from silane redistribution, was inseparable from the product and is seen in the NMR spectra. Integration of the methylene protons gives a 1:12 (tetraethoxysilane:product) ratio. The branched product is fully characterized below.

^{1}H NMR (500 MHz, $CDCl_3$, 298 K): δ 7.29-7.25 (ms, 4H), 7.13 (m, 1H), 3.75 (q, *J* = 7.0 Hz, 6H), 2.35 (q, *J* = 7.6 Hz, 1H), 1.46 (d, *J* = 7.6 Hz, 3H), 1.18 (t, *J* = 7.0 Hz, 9H).

$^{13}C\{^{1}H\}$ NMR (126 MHz, $CDCl_3$, 298 K): δ 144.2, 128.2, 128.0, 125.0, 58.9, 26.3, 18.4, 15.7.

$^{29}Si\{^{1}H\}$ NMR (119 MHz, $CDCl_3$, 298 K): δ -52.45 (s).

IR (ATR, neat) v: 3081-2874 (w), 1601 (w), 1389 (w), 1704 (s), 776 (s).

ASAP/HRMS (m/z): [M^+] calculated for $C_{14}H_{24}O_3Si$ 268.1495, found 268.1469.

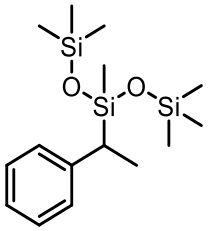

1,1,1,3,5,5,5-Heptamethyl-3-(1-phenylethyl)trisiloxane (**4aq**)

Synthesis details: **GP-D**, styrene (1.0 equiv), $HSiCH_3(OSiMe_3)_2$ (**3q**, 2.0 equiv).

Selectivity before purification: 1:>99 (*l*/*b*) measured by GC-MS.

Purification details: Column chromatography hexanes to give the product as a clear oil (0.201 g, 0.615 mmol, 62% yield, *l*/*b* = 1:>99).

^{1}H NMR (500 MHz, $CDCl_3$, 298 K): δ 7.23 (m, 2H), 7.11-7.07 (ms, 3H), 2.10 (q, *J* =7.5 Hz, 1H), 1.35 (d, *J* = 7.5 Hz, 3H), 0.03 (s, 9H), 0.03 (s, 9H), -0.04 (s, 3H).

$^{13}C\{^{1}H\}$ NMR (126 MHz, $CDCl_3$, 298 K): δ 145.0, 128.1, 127.8, 124.6, 30.9, 14.7, 1.88, 1.86, -2.3.

$^{29}Si\{^{1}H\}$ NMR (99 MHz, $CDCl_3$, 298 K): δ 7.67 (s), 7.52 (s), -26.55 (s).

IR (ATR, neat) v: 3061-2872 (m), 1492 (w), 1251 (s), 1041 (s), 834 (s).

ASAP/HRMS (m/z): [M^+] calculated for $C_{15}H_{30}O_2Si_3$ 326.1554, found 326.1559.

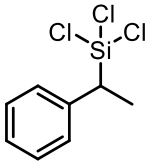

(1-Phenylethyl)trichlorosilane (**4ar**)

Synthesis details: **GP-C**, styrene (**2a**), $HSiCl_3$ (**3r**, 1.25 equiv).

Selectivity before purification: 1:>99 (*l*/*b*) measured by GC.

Purification details: Distillation (approximately 0.05 Torr, 60 °C) to give the product as a clear oil (0.200 g, 0.835 mmol, 84% yield, *l*/*b* = 1:>99).

^{1}H NMR (500 MHz, $CDCl_3$, 298 K): δ 7.34 (m, 2H), 7.27-7.24 (ms, 3H), 2.90 (q, *J* = 7.5 Hz, 1H), 1.63 (d, *J* = 7.5 Hz, 3H).

^{13}C{^{1}H} NMR (126 MHz, $CDCl_3$, 298 K): δ 138.1, 128.8, 128.5, 127.0, 36.3, 14.5.

^{29}Si{^{1}H} NMR (99 MHz, $CDCl_3$, 298 K): δ 9.82 (s).

IR (ATR, neat) v: 3062-2875 (w), 1602 (w), 1492 (m), 760 (s), 694 (s).

ASAP/HRMS (m/z): [M^+] calculated for $C_8H_9Cl_3Si$ 237.9539, found 237.9515.

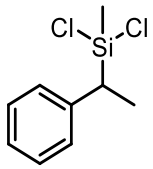

(1-Phenylethyl)dichloromethylsilane (**4as**)

Synthesis details: **GP-C**, styrene (**2a**), $HSiCl_2Me$ (**3s**, 1.25 equiv).

Selectivity before purification: 1:>99 (*l*/*b*) measured by GC.

Purification details: Distillation (approximately 0.05 Torr, 60 °C) to give the product as a clear oil (0.169 g, 0.771 mmol, 77% yield, *l*/*b* = 1:>99).

^{1}H NMR (500 MHz, $CDCl_3$, 298 K): δ 7.31 (t, *J* = 7.70 Hz, 2H), 7.23-7.19 (ms, 3H), 2.66 (q, *J* = 7.5 Hz, 1H), 1.56 (d, *J* = 7.5 Hz, 3H), 0.64 (s, 3H).

^{13}C{^{1}H} NMR (126 MHz, $CDCl_3$, 298 K): δ 140.3, 128.7, 128.1, 126.3, 34.0, 14.4, 3.4.

^{29}Si{^{1}H} NMR (99 MHz, $CDCl_3$, 298 K): δ 29.76 (s).

IR (ATR, neat) v: 3083-2874 (w), 1600 (w), 1259 (s), 1076-995 (m), 696 (s).

ASAP/HRMS (m/z): [M^+] calculated for $C_9H_{12}Cl_2Si$ 218.0085, found 218.0040.

---

c. Incompatible Substrates

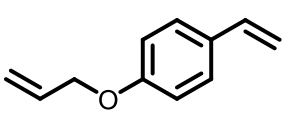

(**2t**)

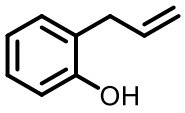

2-allylphenol

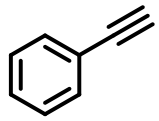

phenylacetylene

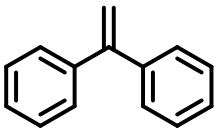

DPE

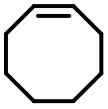

cyclooctene

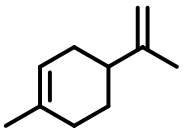

(+/-)-limonene

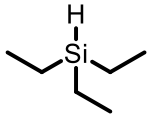

triethylsilane

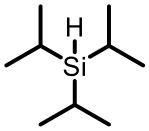

triisopropylsilane

A.1.6. NMR and IR Spectra

a. Nickel Complexes

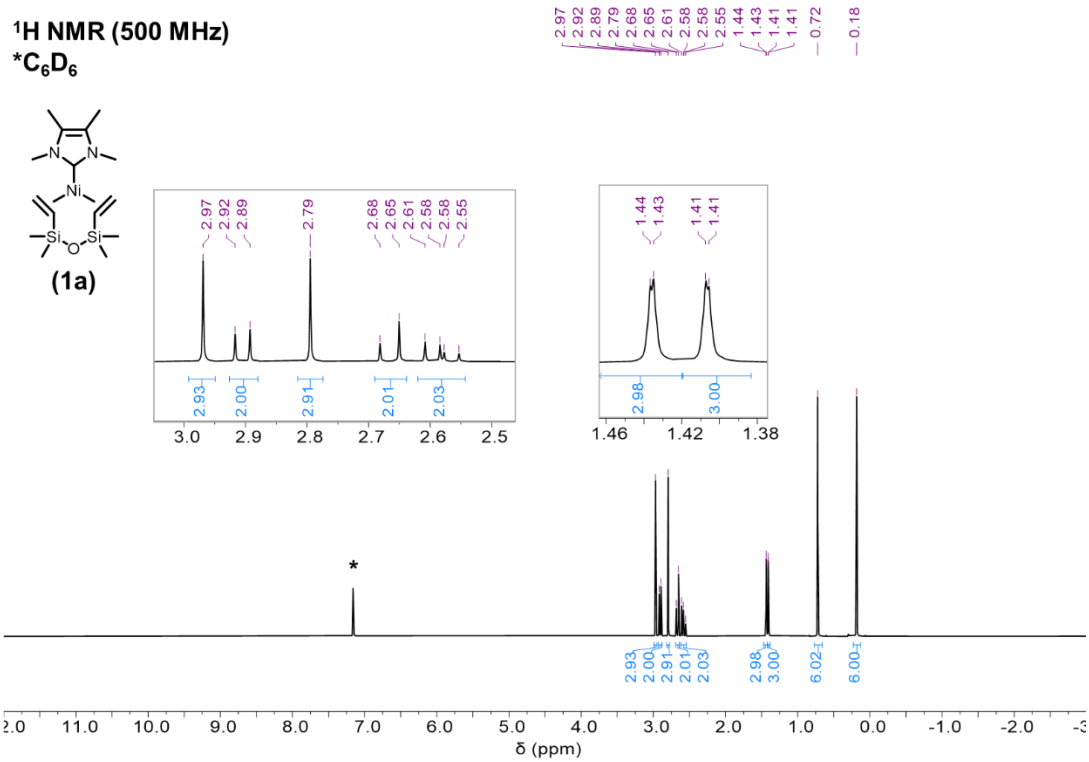

Figure A.1. ^{1}H NMR spectrum of (dvtms)Ni(ITMe) (**1a**) recorded in C_6D_6 at 298 K.

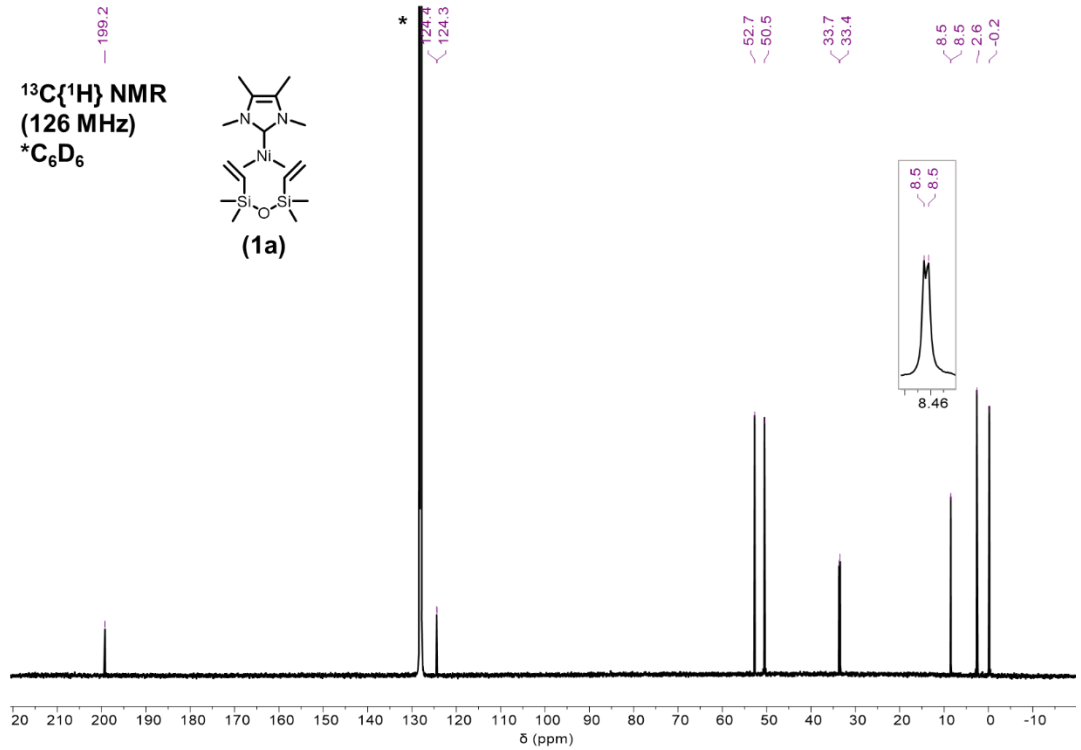

Figure A.2. ^{13}C{^{1}H} NMR spectrum of (dvtms)Ni(ITMe) (**1a**) recorded in C_6D_6 at 298 K.

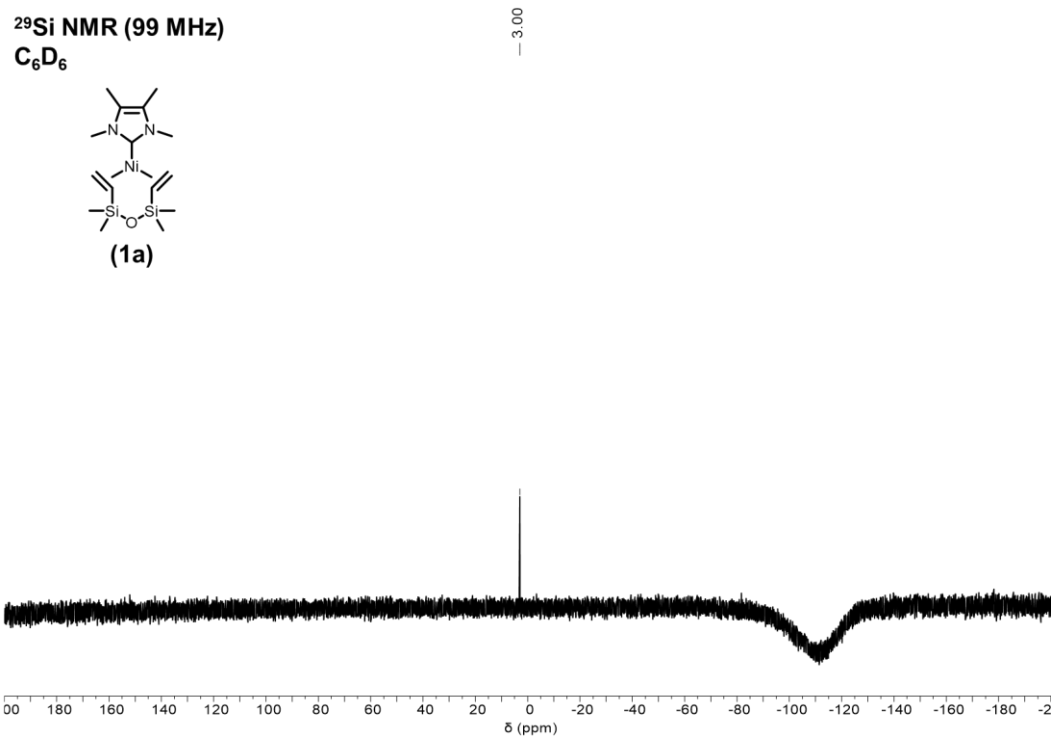

Figure A.3. ^{29}Si NMR spectrum of (ITMe)Ni(dvtms) (**1a**) recorded in in C_6D_6 at 298 K.

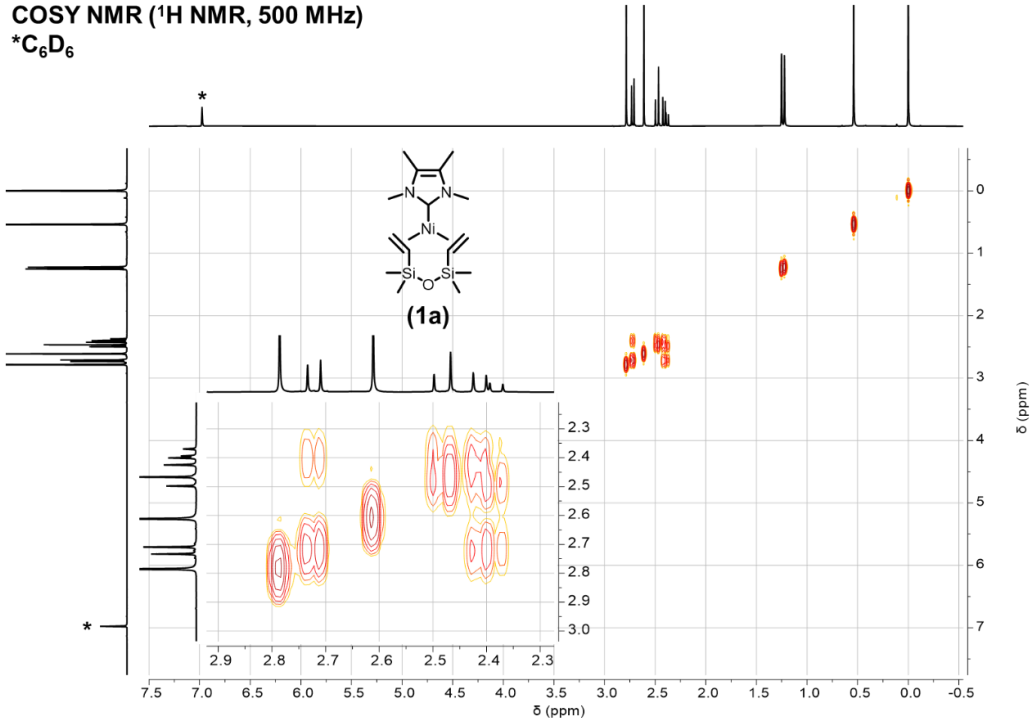

Figure A.4. COSY NMR spectrum of (dvtms)Ni(ITMe) (**1a**) recorded in C_6D_6 at 298 K.

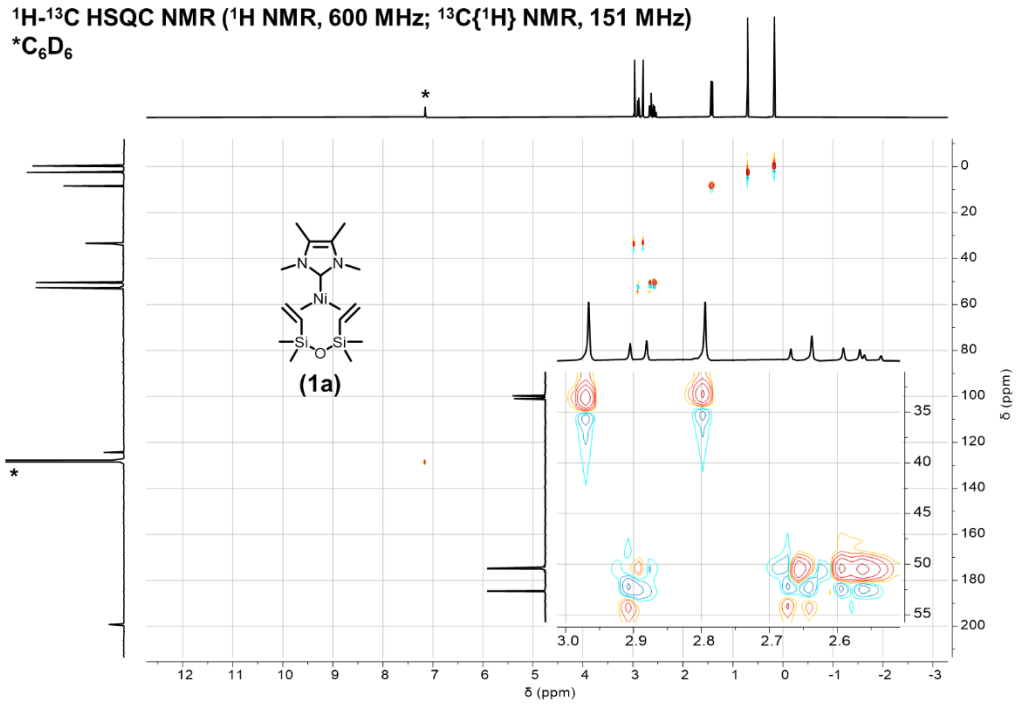

Figure A.5. HSQC NMR spectrum of (dvtms)Ni(ITMe) (**1a**) recorded in C_6D_6 at 298 K.

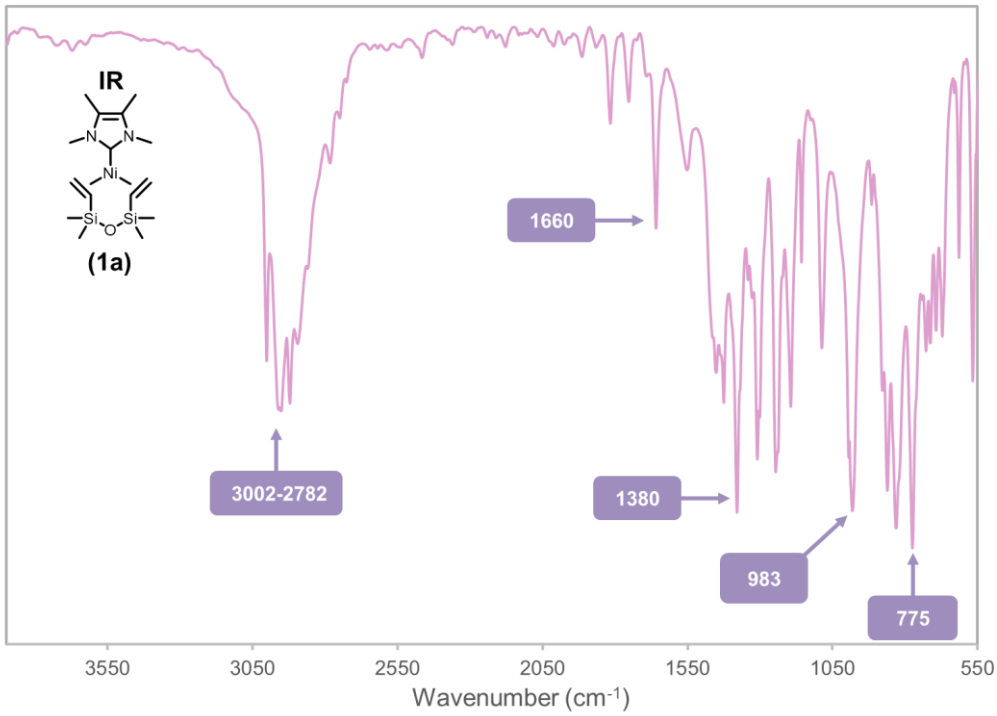

Figure A.6. IR spectrum of (dvtms)Ni(ITMe) (**1a**) recorded as a KBr pellet at 298 K.

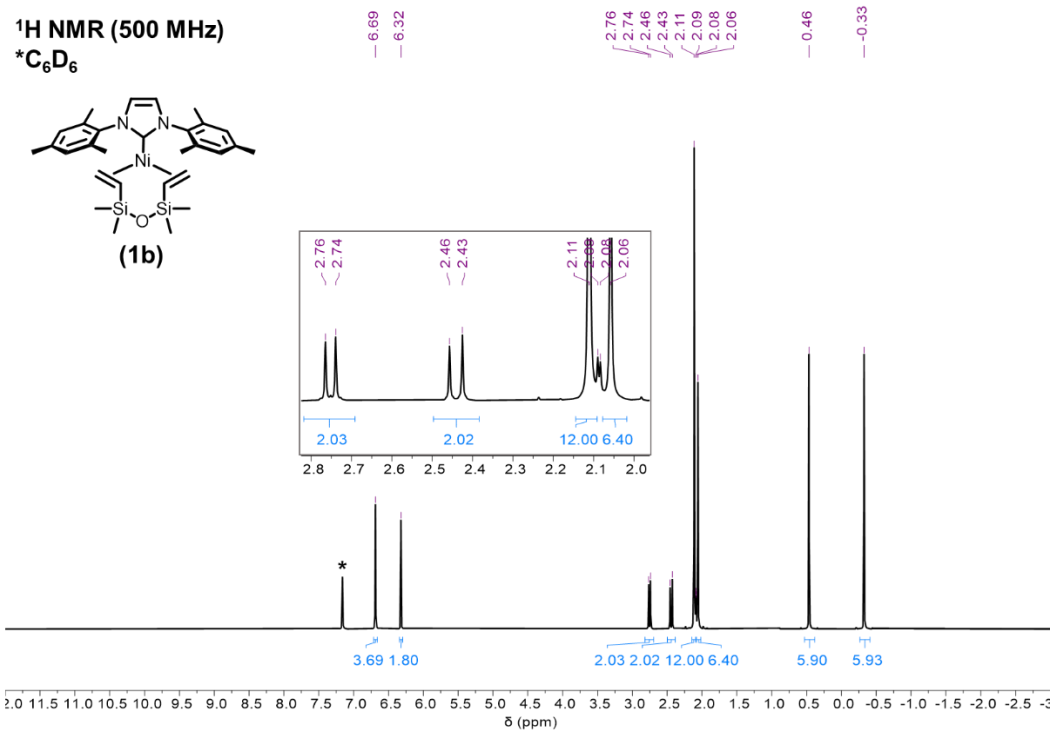

Figure A.7. ^{1}H NMR spectrum of (dvtms)Ni(IMes) (**1b**) recorded in C_6D_6 at 298 K.

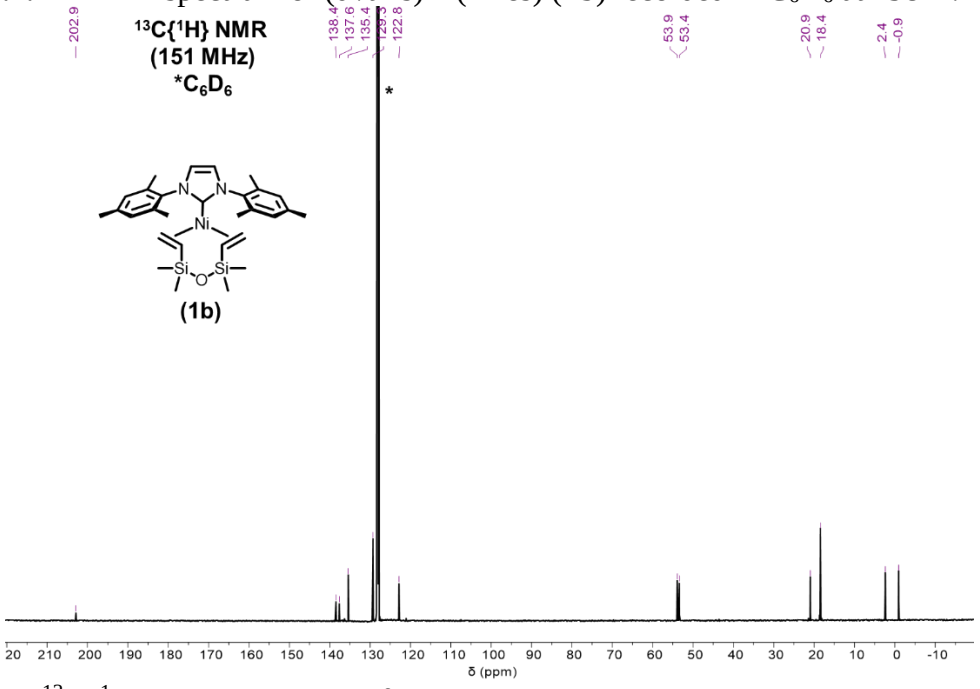

Figure A.8. ^{13}C{^{1}H} NMR spectrum of (dvtms)Ni(IMes) (**1b**) recorded in C_6D_6 at 298 K.

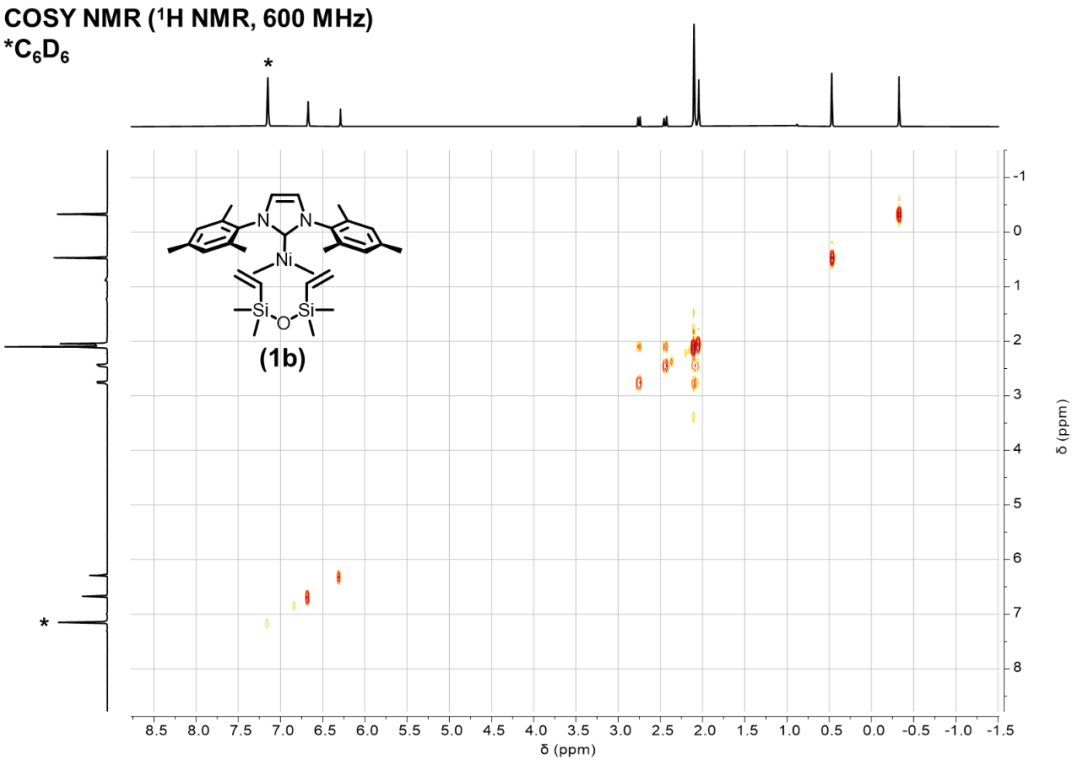

Figure A.9. COSY NMR spectrum of (dvtms)Ni(IMes) (**1b**) recorded in C_6D_6 at 298 K.

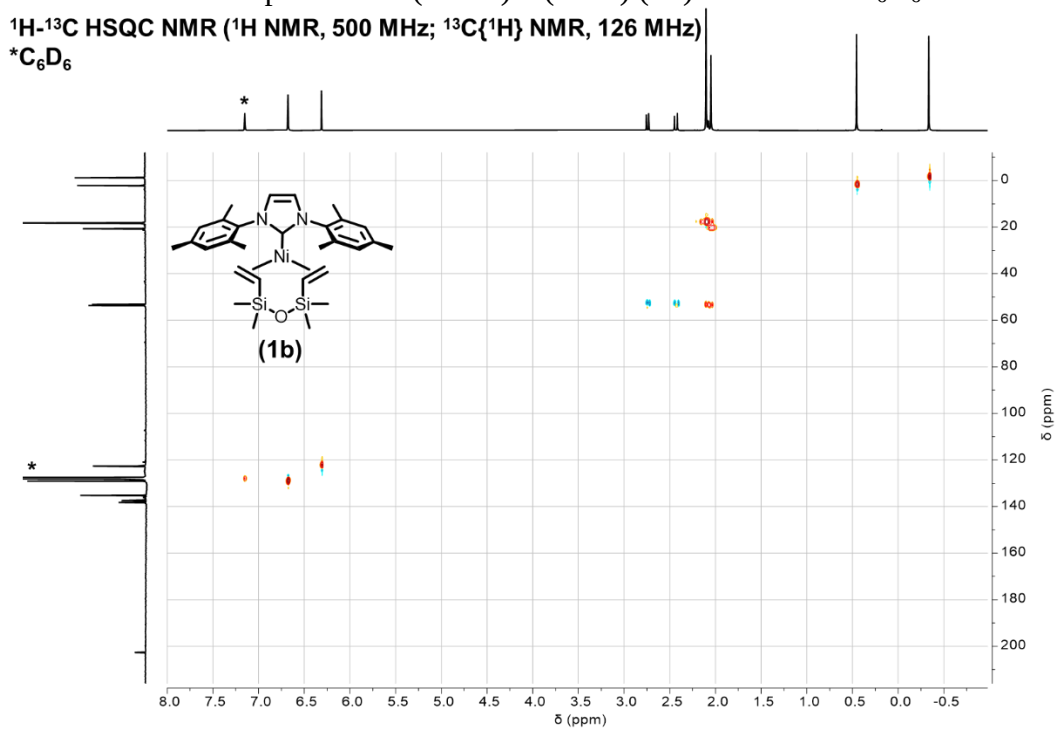

Figure A.10. HSQC NMR spectrum of (dvtms)Ni(IMes) (**1b**) recorded in C_6D_6 at 298 K.

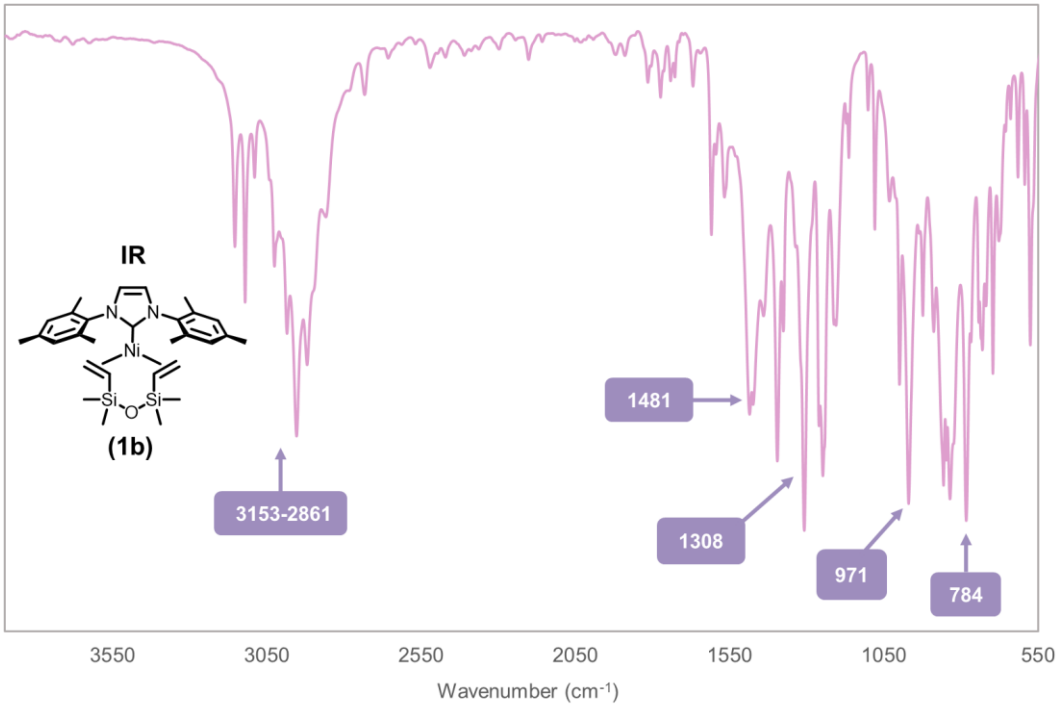

Figure A.11. IR spectrum of (dvtms)Ni(IMes) (**1b**) recorded as a KBr pellet at 298 K.

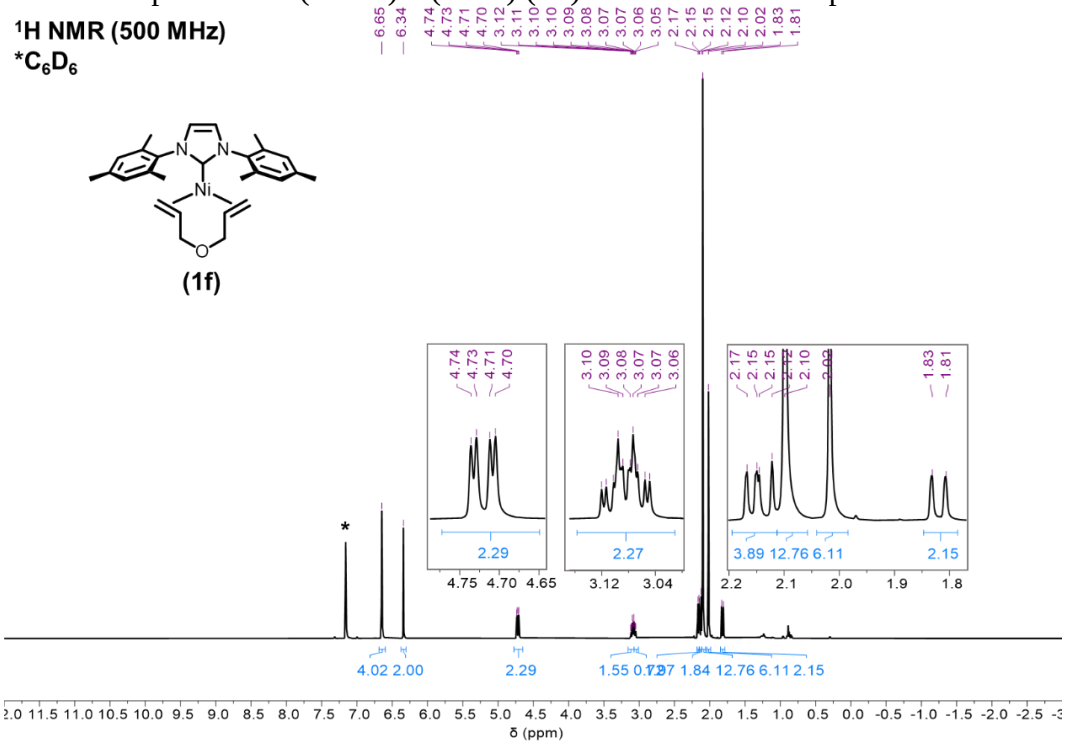

Figure A.12. ^{1}H NMR spectrum of (diallylether)Ni(IMes) (**1f**) recorded in C_6D_6 at 298 K.

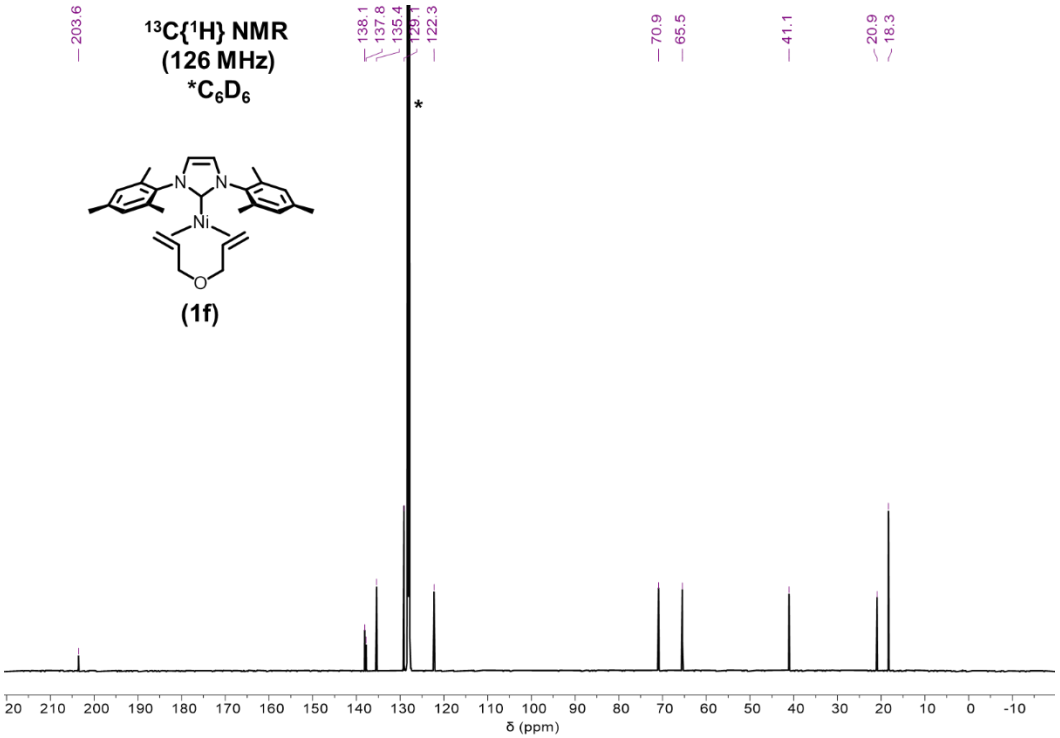

Figure A.13. $^{13}C\{^1H\}$ NMR spectrum of (diallylether)Ni(IMes) (**1f**) recorded in C_6D_6 at 298 K.

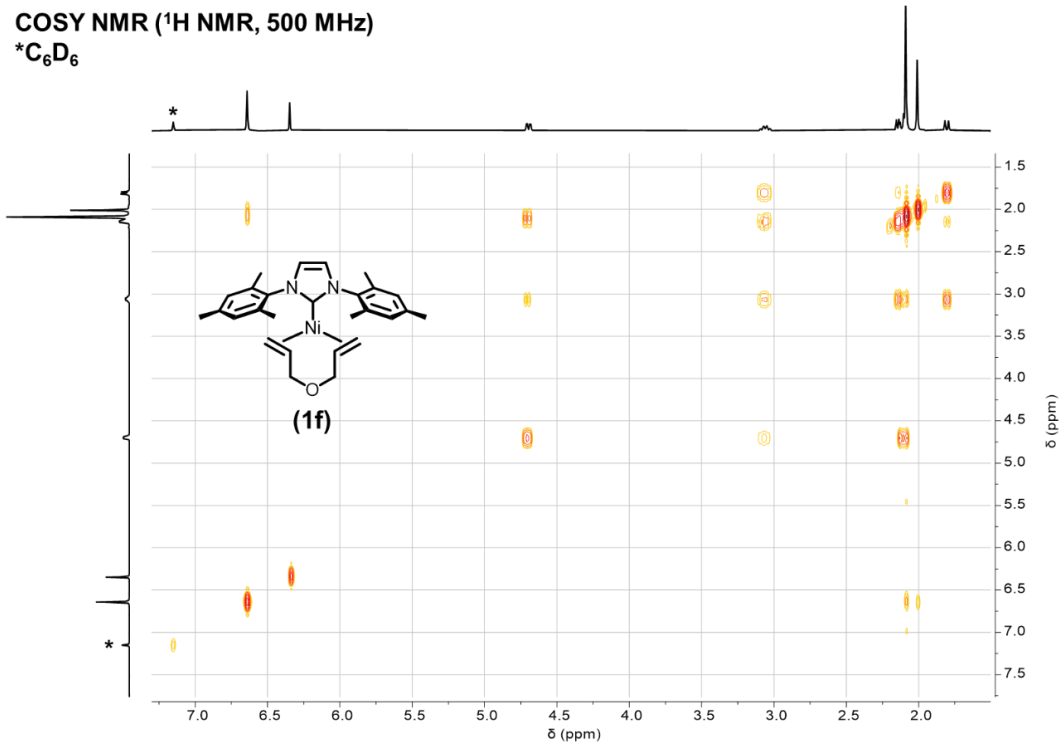

Figure A.14. COSY NMR spectrum of (diallylether)Ni(IMes) (**1f**) recorded in C_6D_6 at 298 K.

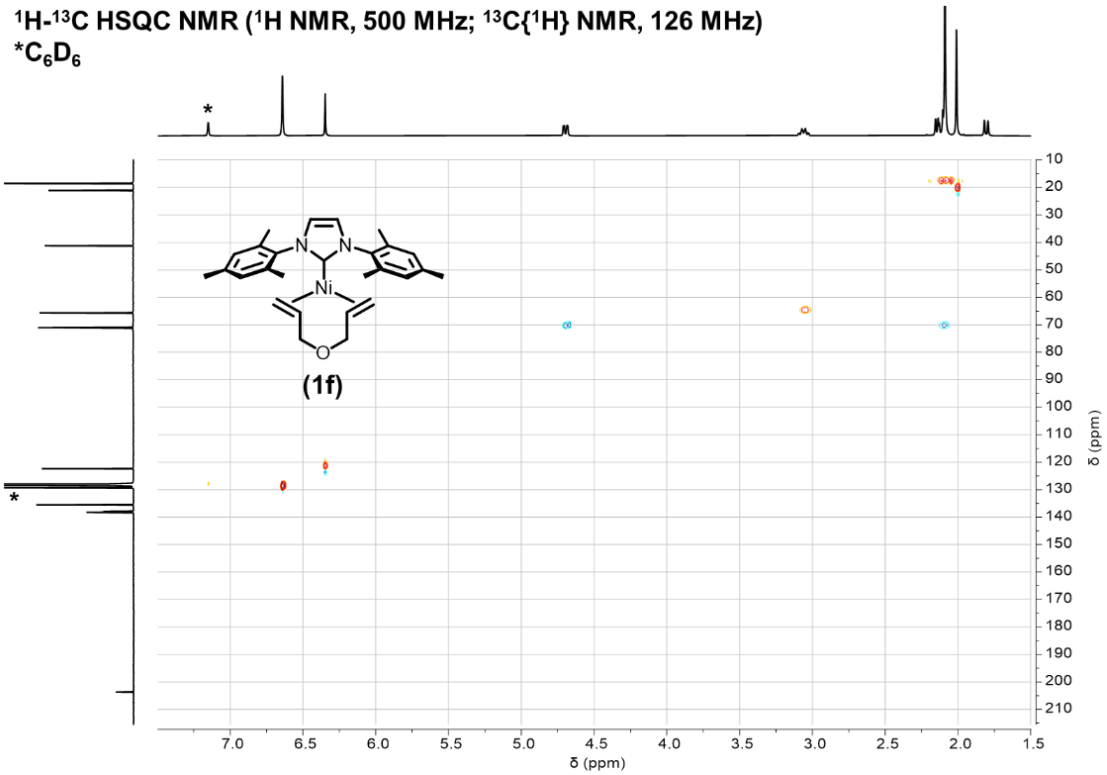

Figure A.15. HSQC NMR spectrum of (diallylether)Ni(IMes) (**1f**) recorded in C_6D_6 at 298 K.

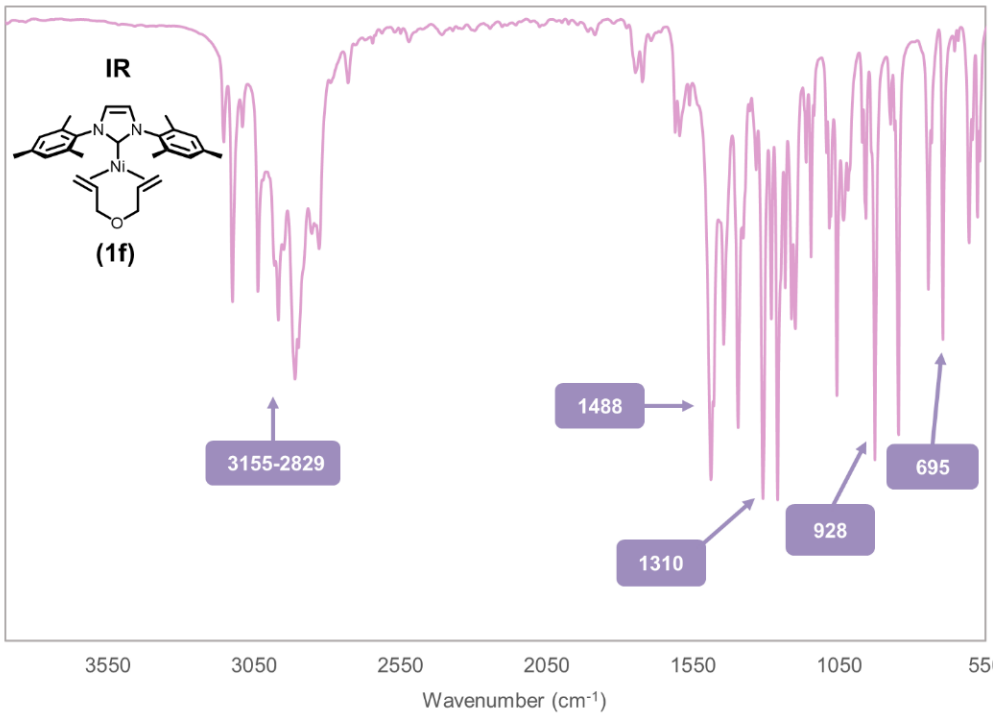

Figure A.16. IR spectrum of (diallylether)Ni(IMes) (**1f**) recorded as a KBr pellet at 298 K.

b. Styrene Derivative

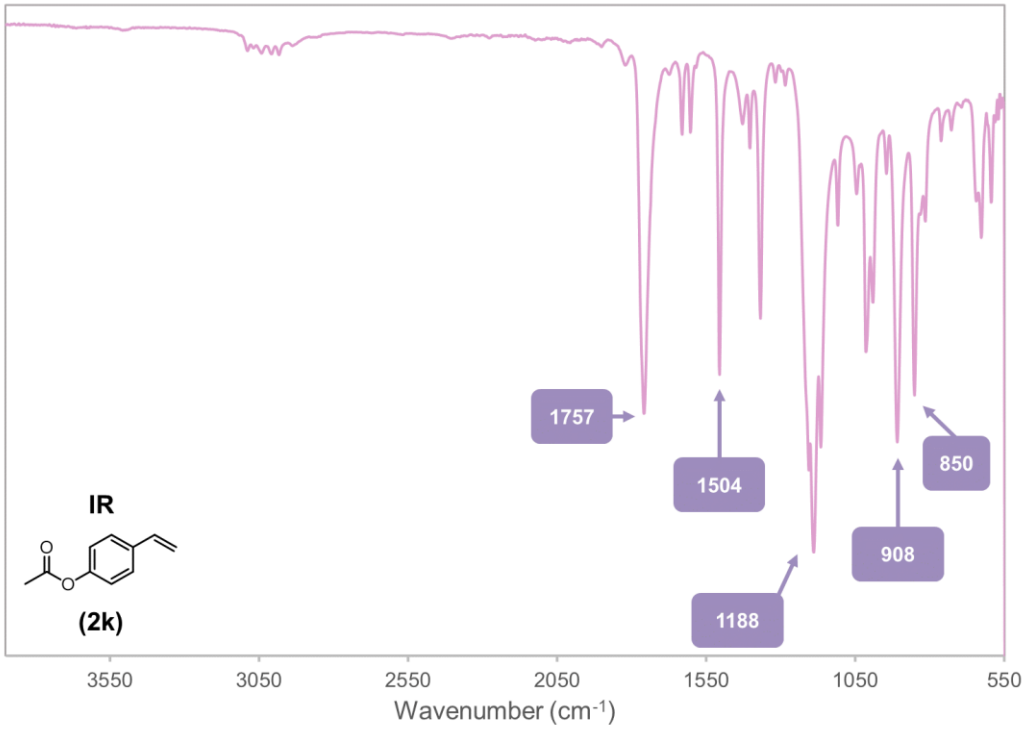

Figure A.17. IR spectrum of 4-acetoxystyrene (**2k**) recorded neat at 298 K.

c. Silanes

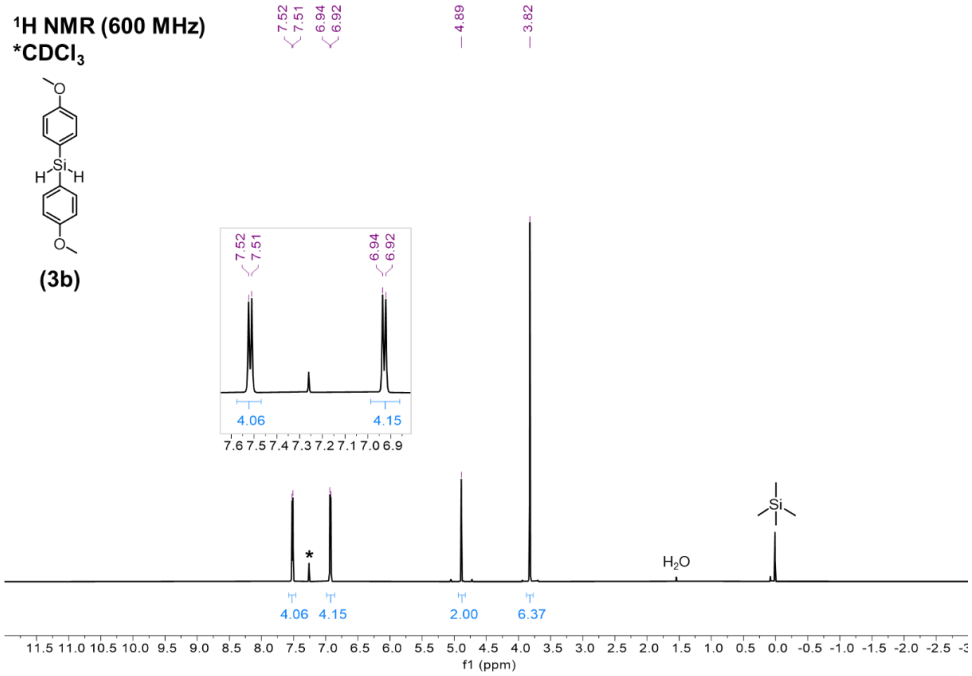

Figure A.18. ^{1}H NMR spectrum of di(4-methoxyphenyl)silane (**3b**) recorded in $CDCl_3$ at 298 K.

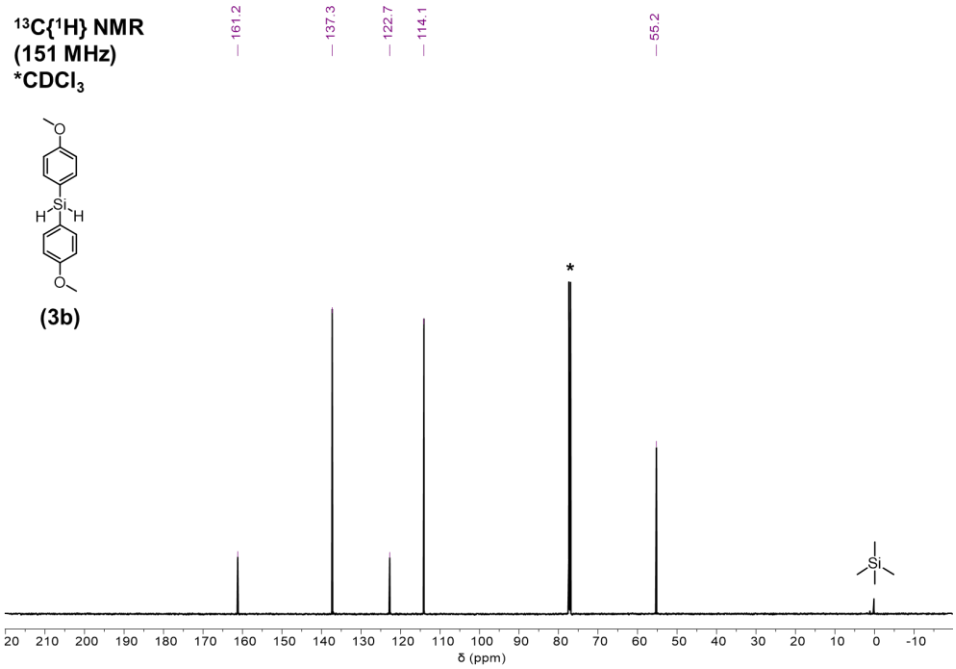

Figure A.19. $^{13}C\{^{1}H\}$ NMR spectrum of di(4-methoxyphenyl)silane (**3b**) recorded in $CDCl_3$ at 298 K.

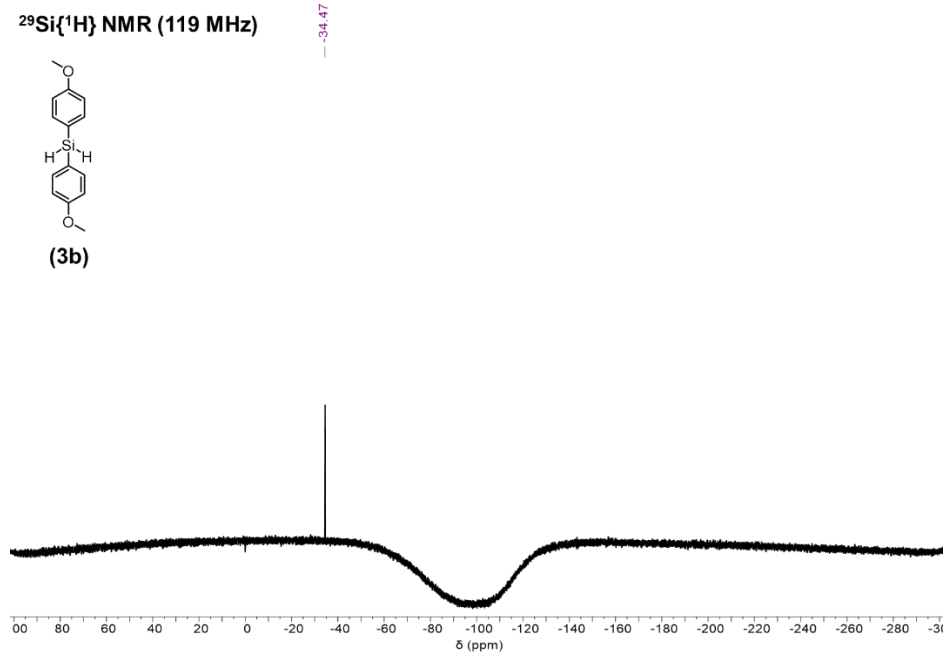

Figure A.20. ^{29}Si NMR spectrum of di(4-methoxyphenyl)silane (**3b**) recorded in $CDCl_3$ at 298 K.

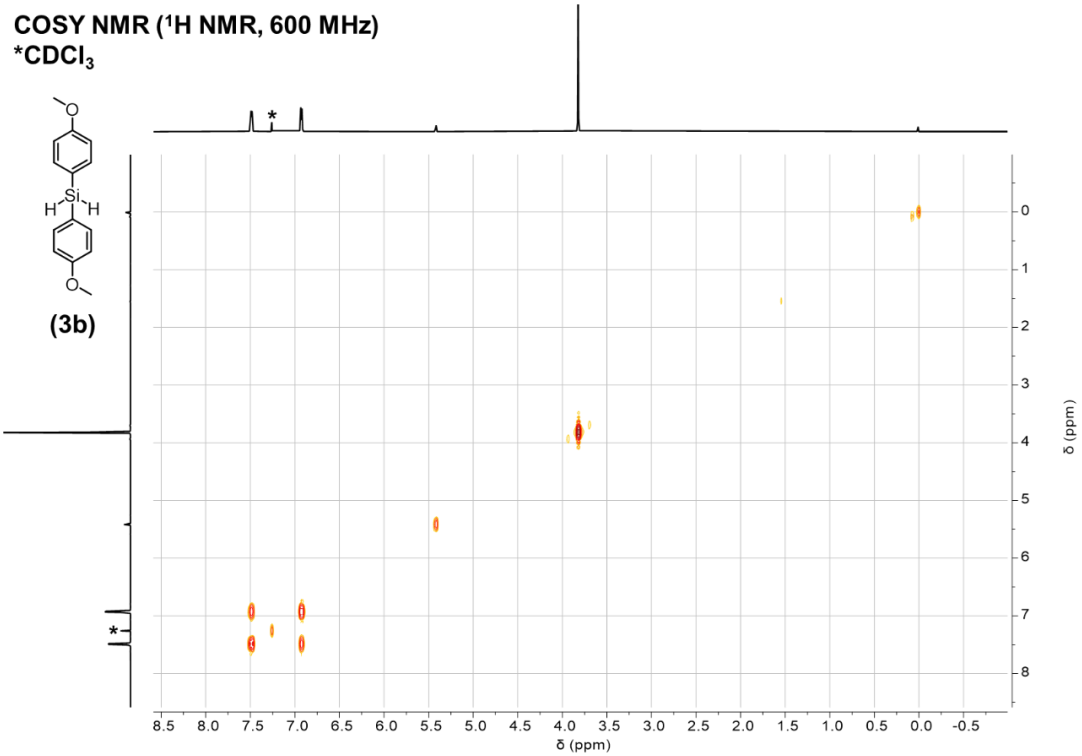

Figure A.21. COSY NMR spectrum of di(4-methoxyphenyl)silane (**3b**) recorded in $CDCl_3$ at 298 K.

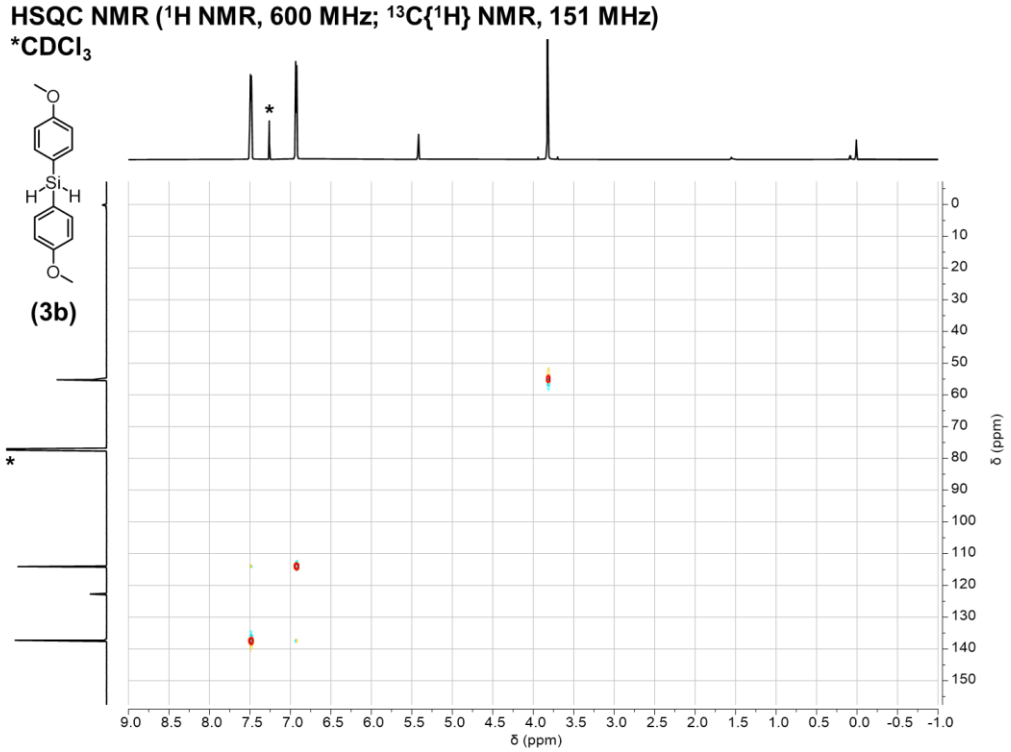

Figure A.22. HSQC NMR spectrum of di(4-methoxyphenyl)silane (**3b**) recorded in $CDCl_3$ at 298 K.

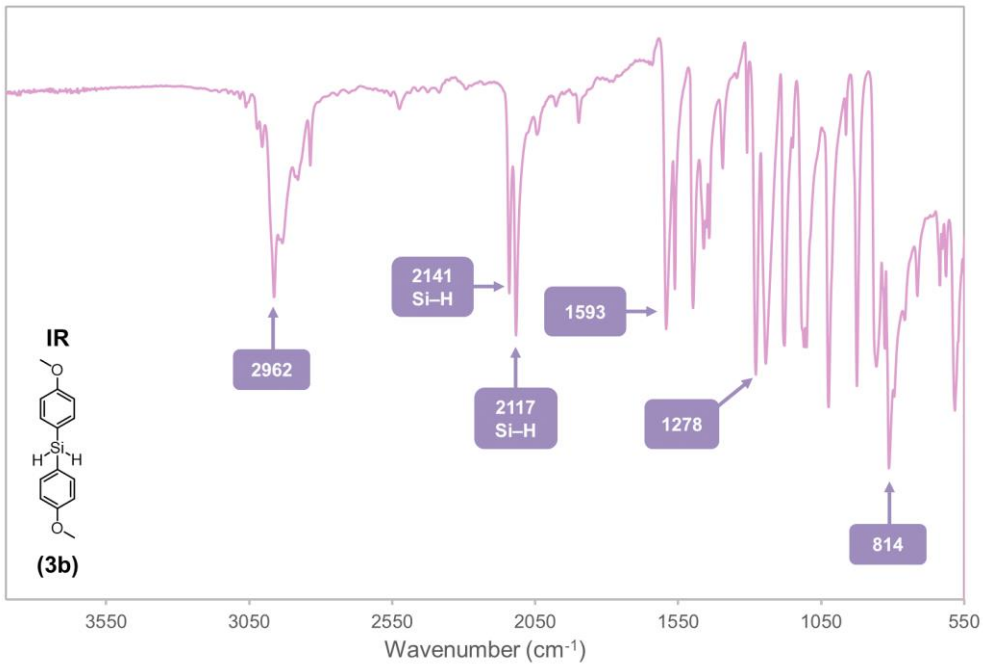

Figure A.23. IR spectrum of di(4-methoxyphenyl)silane (**3b**) recorded neat at 298 K.

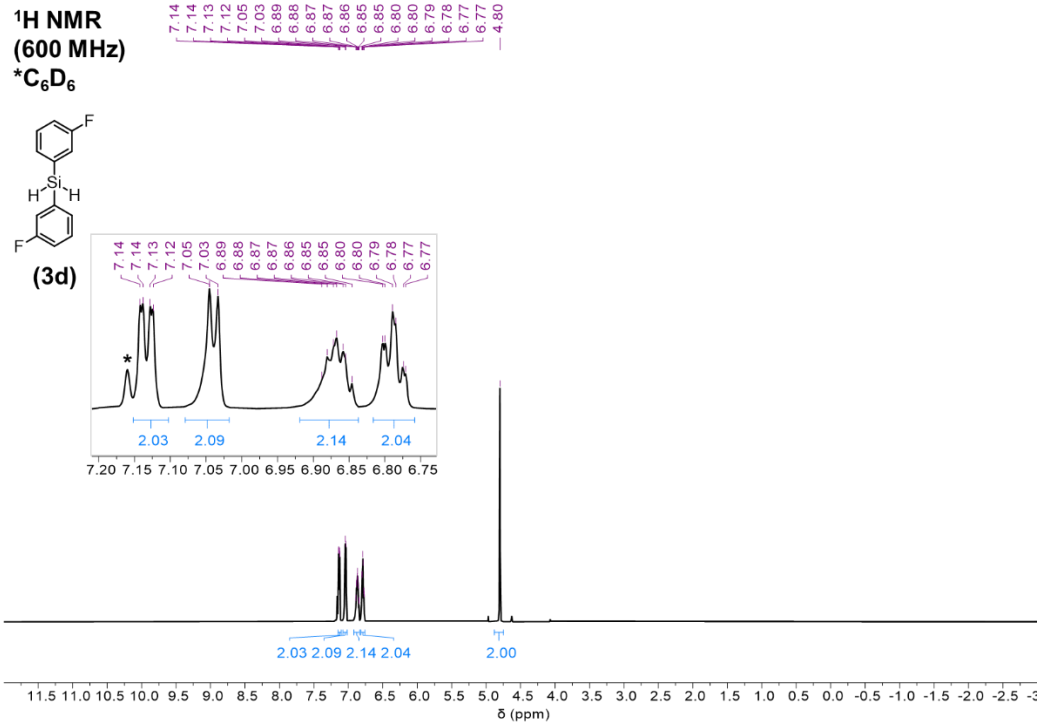

Figure A.24. ^{1}H NMR spectrum of di(3-fluorophenyl)silane (**3d**) recorded in C_6D_6 at 298 K.

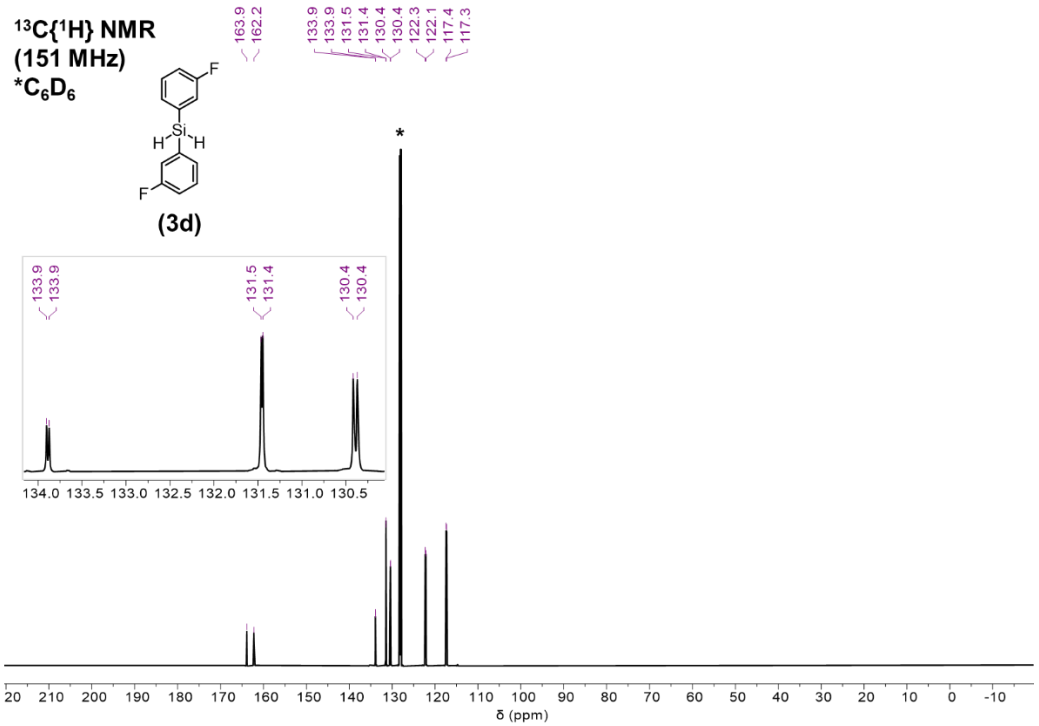

Figure A.25. $^{13}C\{^{1}H\}$ NMR spectrum of di(3-fluorophenyl)silane (**3d**) recorded in C_6D_6 at 298 K.

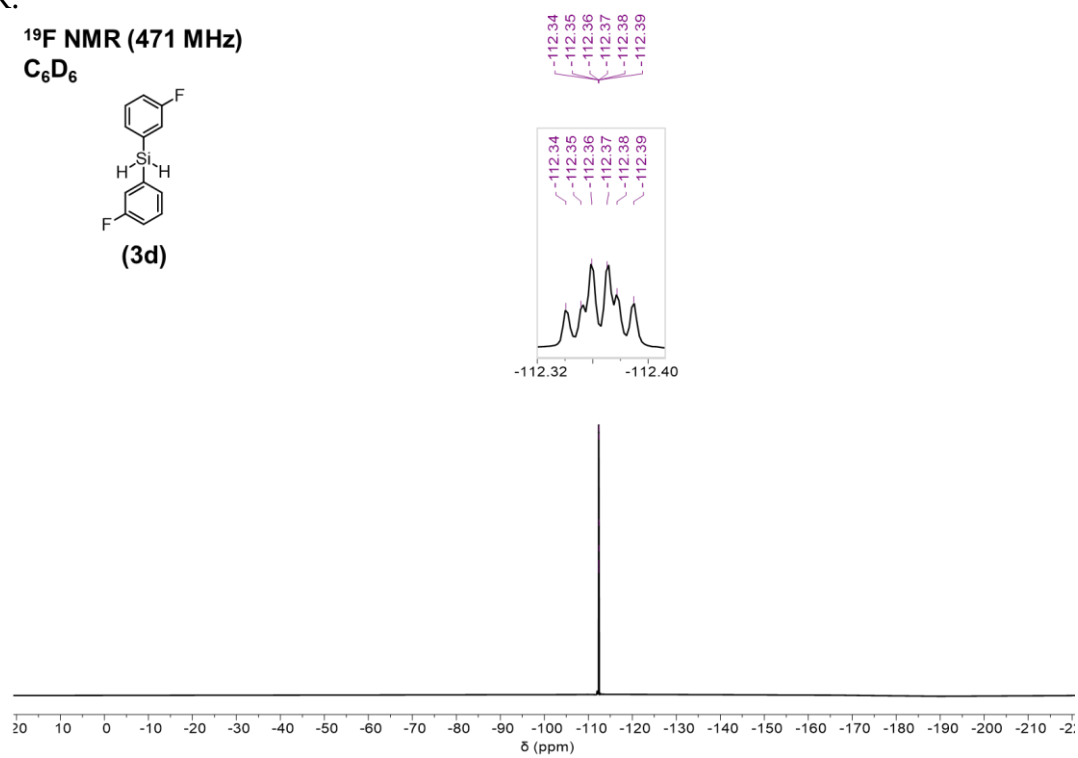

Figure A.26. ^{19}F NMR spectrum of di(3-fluorophenyl)silane (**3d**) recorded in C_6D_6 at 298 K.

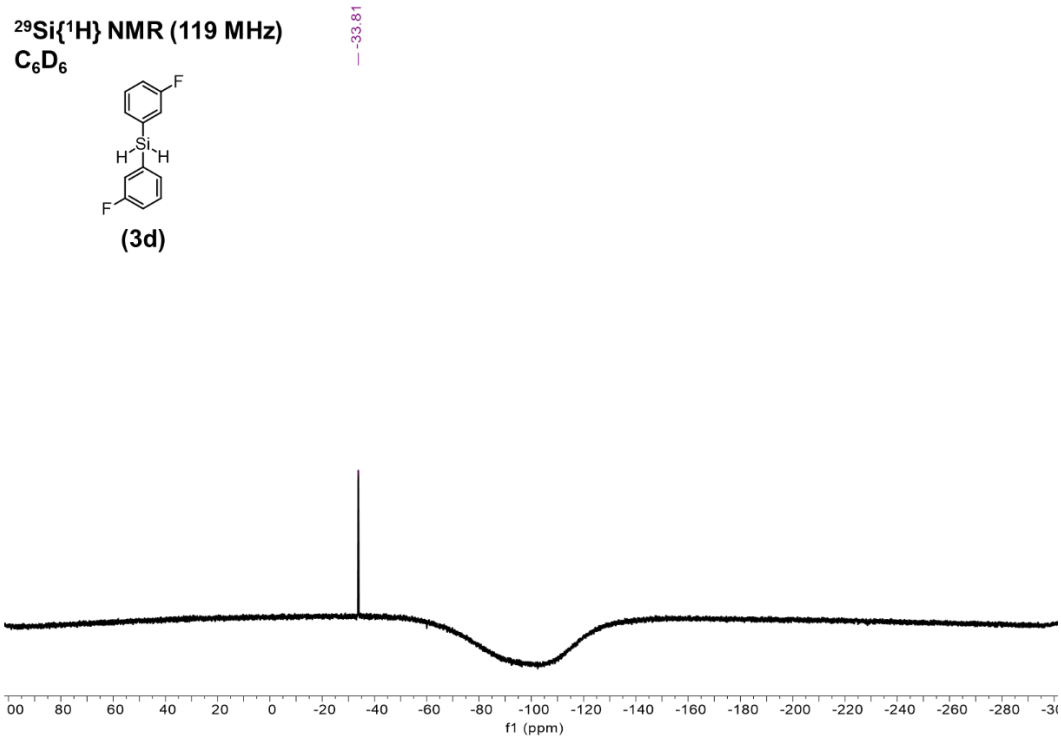

Figure A.27. ^{29}Si NMR spectrum of di(3-fluorophenyl)silane (**3d**) recorded in C_6D_6 at 298 K.

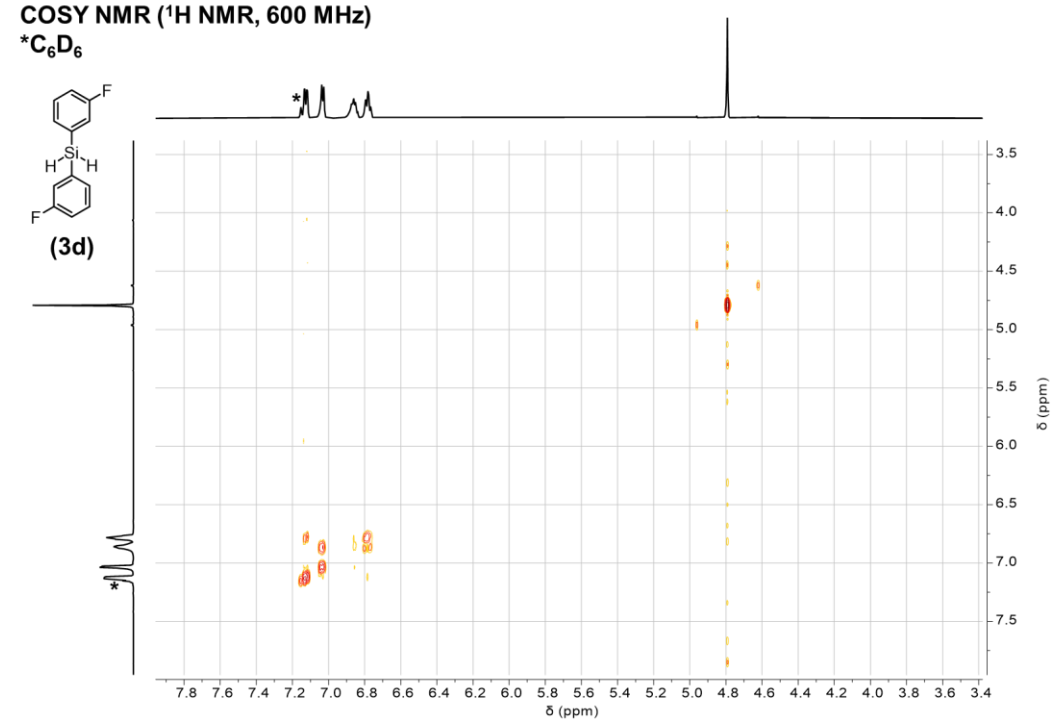

Figure A.28. COSY NMR spectrum of di(3-fluorophenyl)silane (**3d**) recorded in C_6D_6 at 298 K.

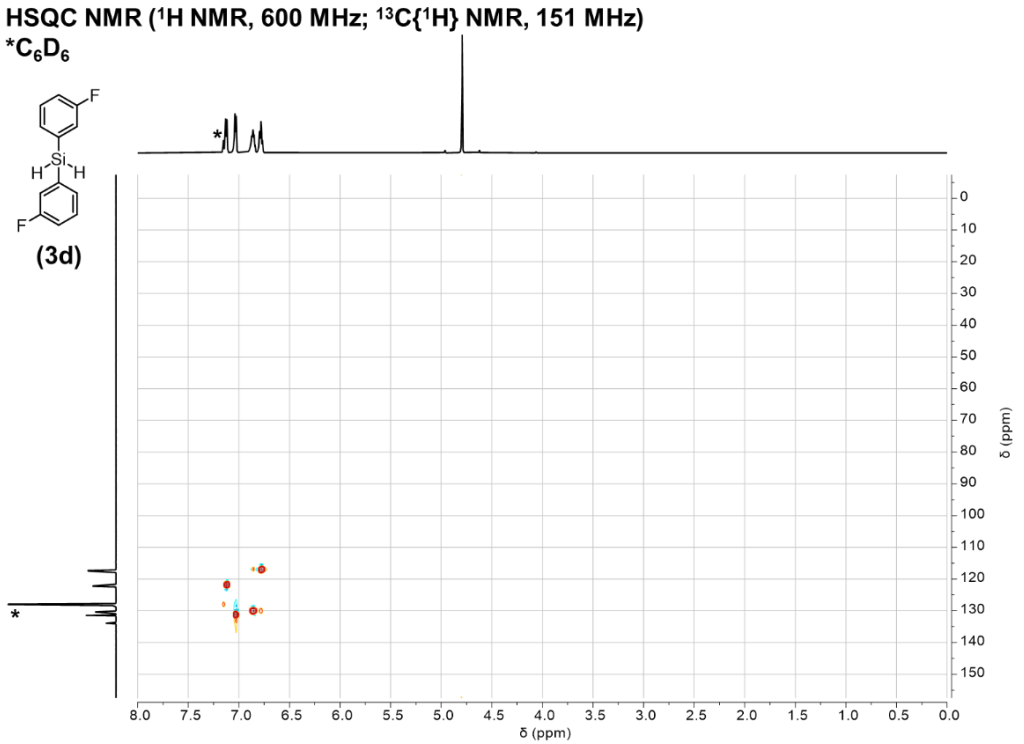

Figure A.29. HSQC NMR spectrum of di(3-fluorophenyl)silane (**3d**) recorded in C_6D_6 at 298 K.

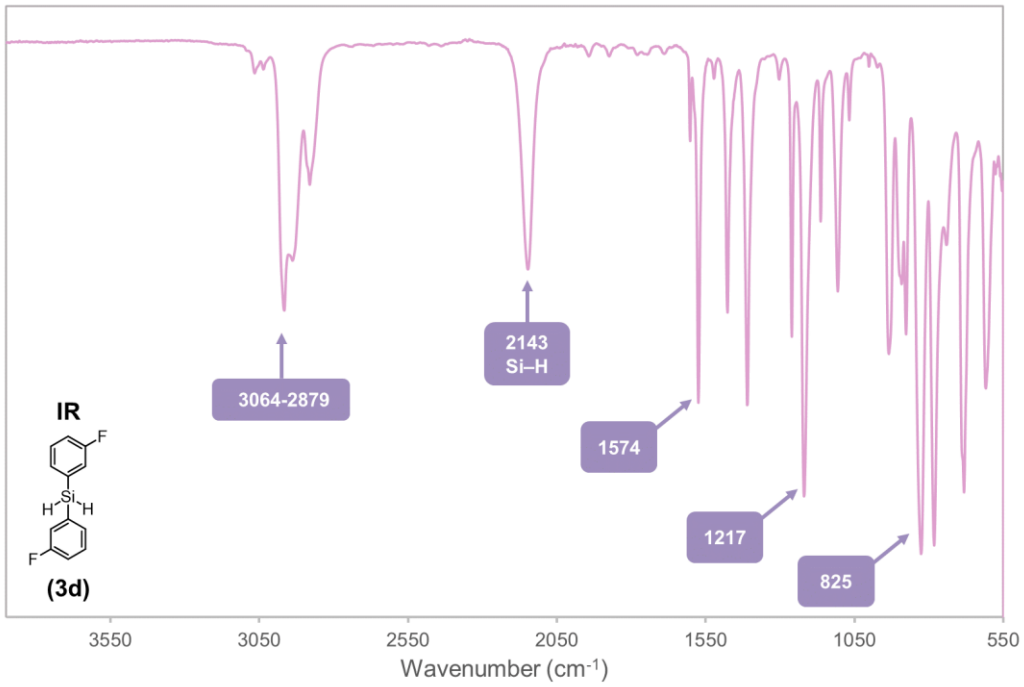

Figure A.30. IR spectrum of di(3-fluorophenyl)silane (**3d**) recorded neat at 298 K.

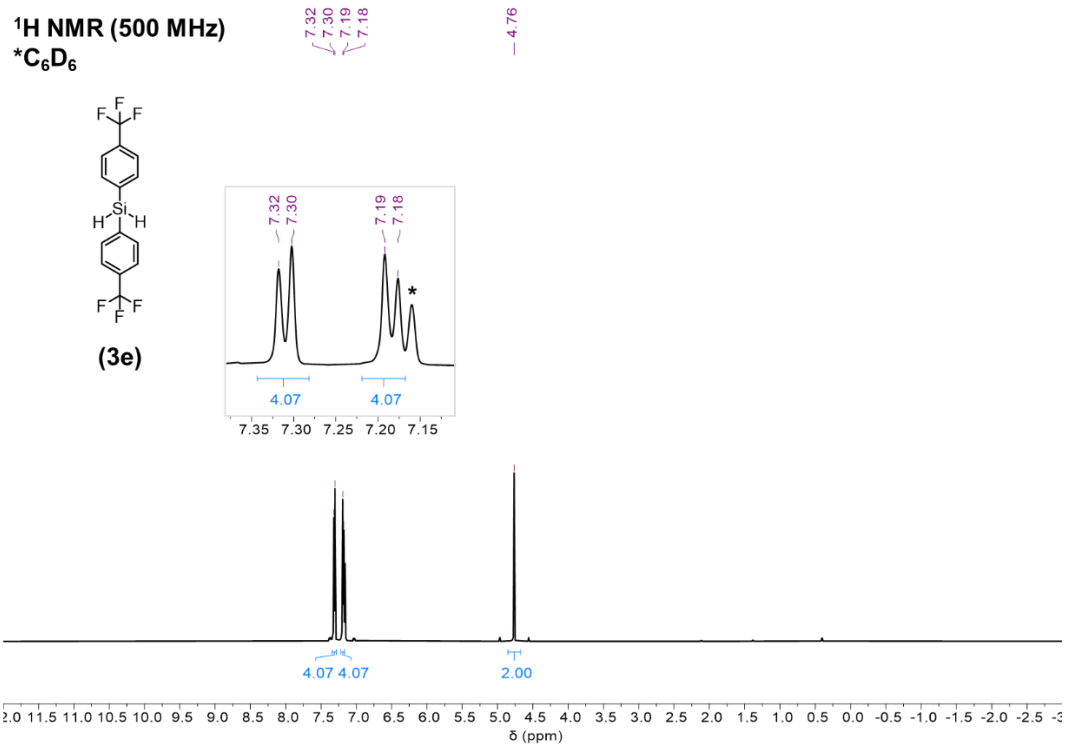

Figure A.31. ^{1}H NMR spectrum of di(4-trifluoromethylphenyl)silane (**3e**) recorded in C_6D_6 at 298 K.

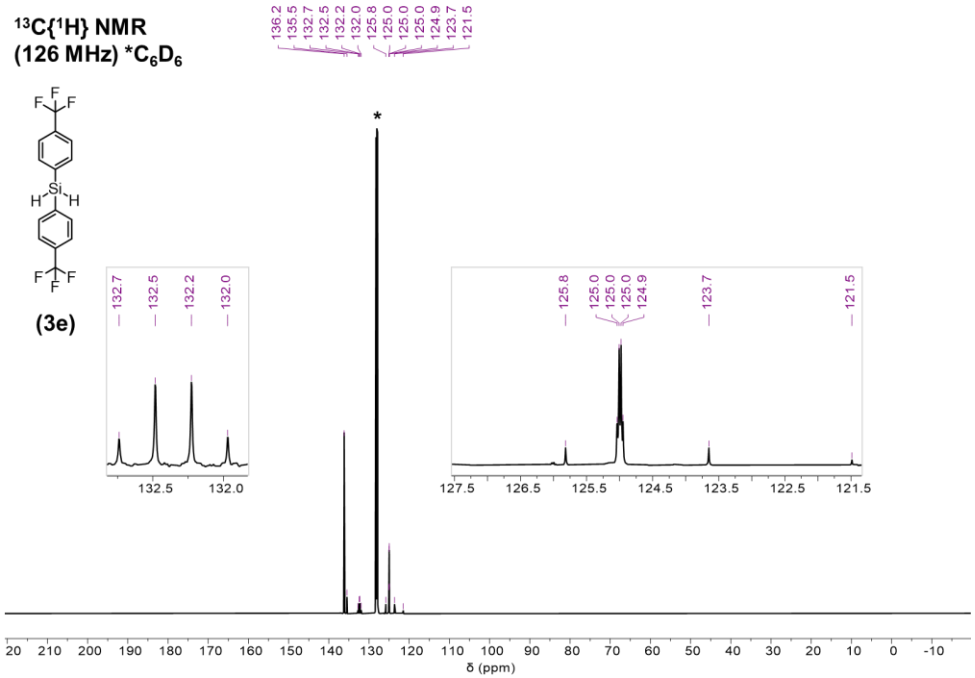

Figure A.32. ^{13}C{^{1}H} NMR spectrum of di(4-trifluoromethylphenyl)silane (**3e**) recorded in C_6D_6 at 298 K.

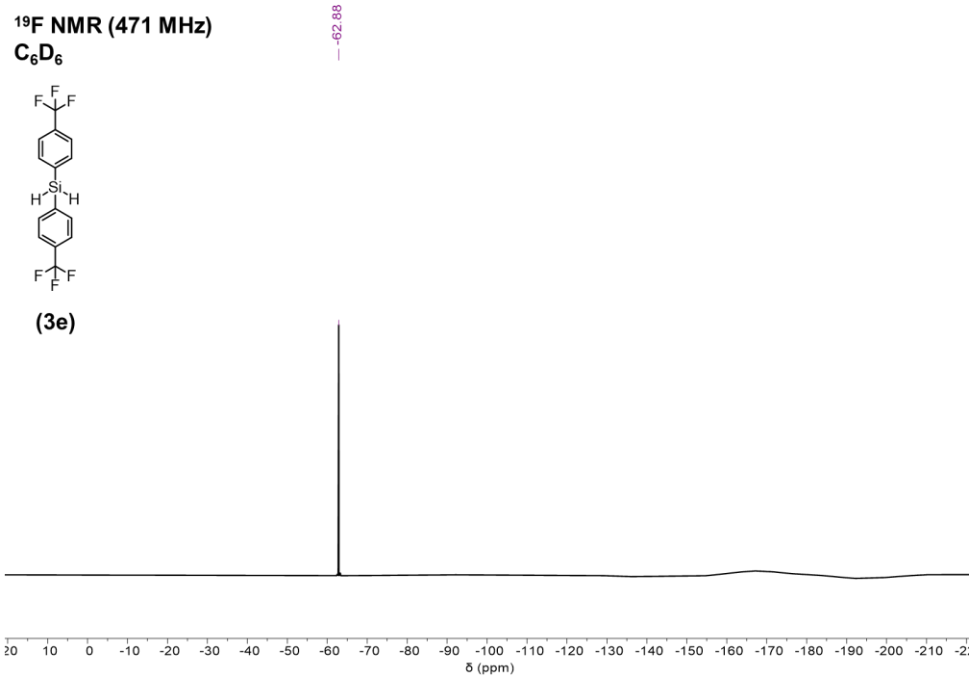

Figure A.33. ^{19}F NMR spectrum of di(4-trifluoromethylphenyl)silane (**3e**) recorded in C_6D_6 at 298 K.

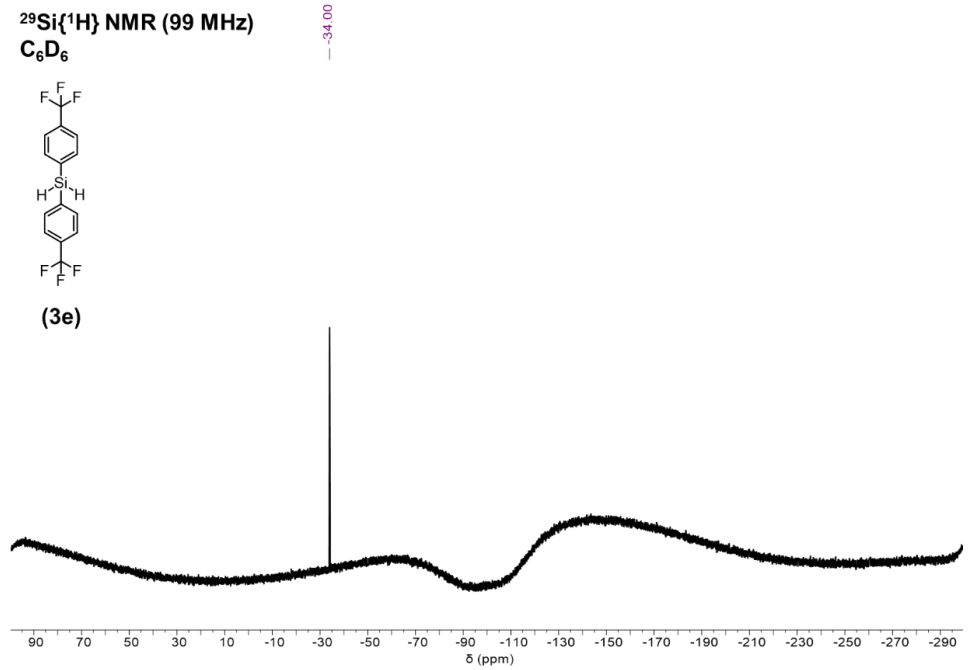

Figure A.34. ^{29}Si NMR spectrum of di(4-trifluoromethylphenyl)silane (**3e**) recorded in C_6D_6 at 298 K.

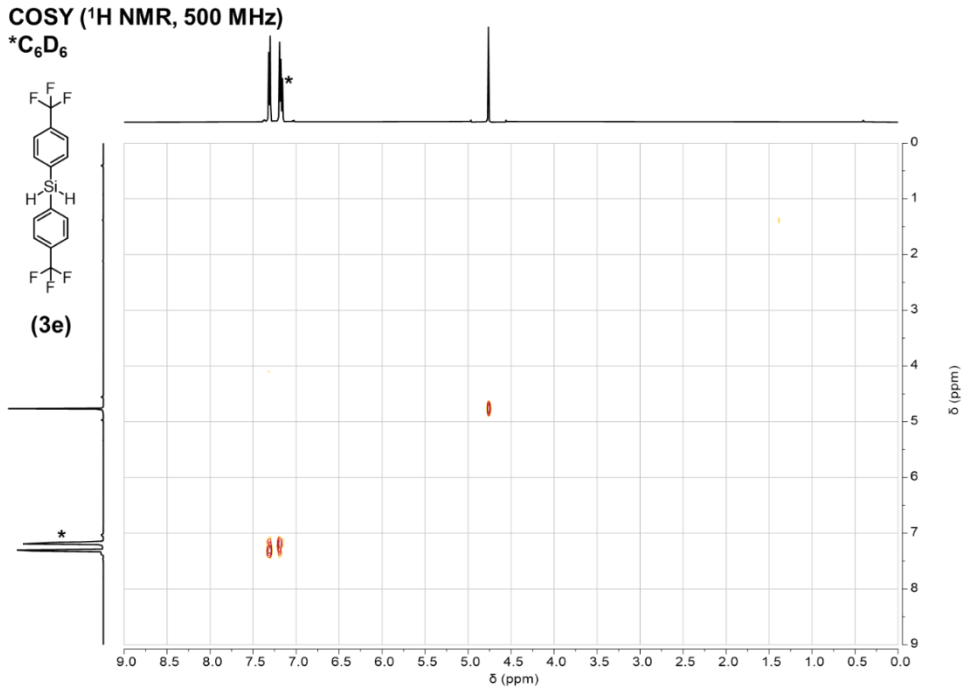

Figure A.35. COSY NMR spectrum of di(4-trifluoromethylphenyl)silane (**3e**) recorded in C_6D_6 at 298 K.

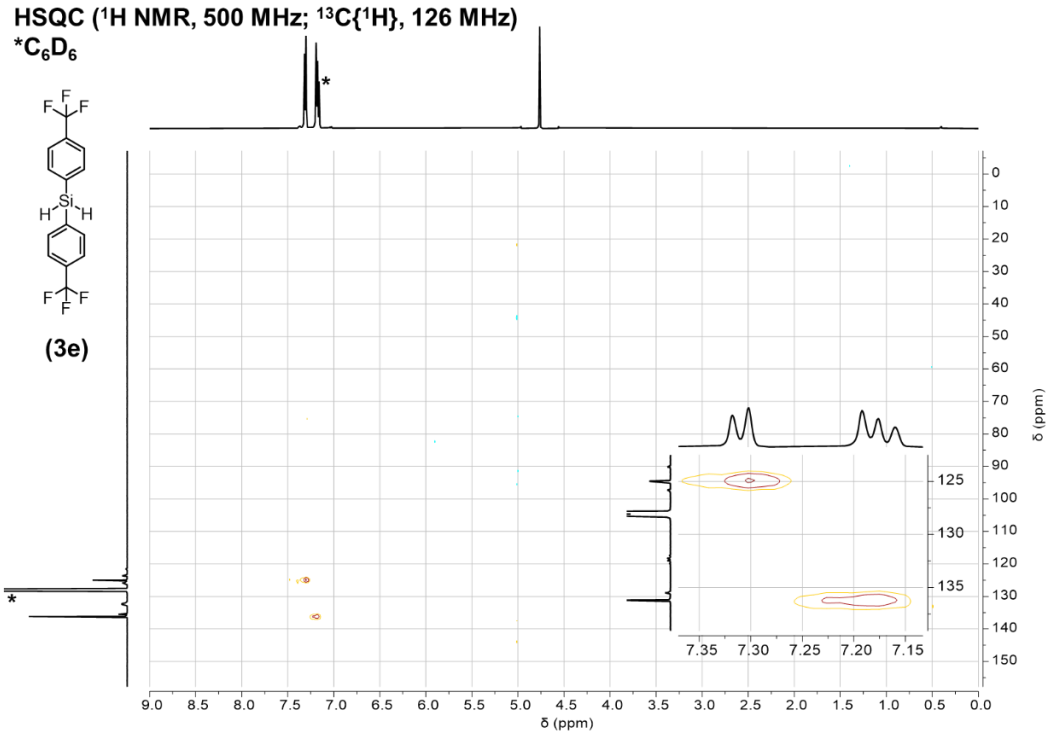

Figure A.36. HSQC NMR spectrum of di(4-trifluoromethylphenyl)silane (**3e**) recorded in C_6D_6 at 298 K.

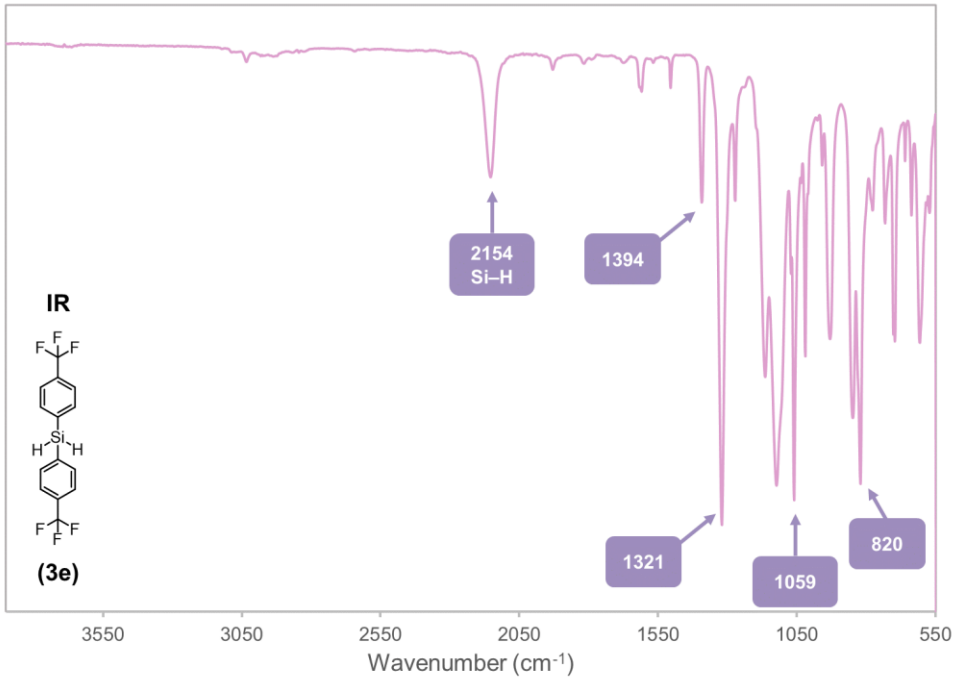

Figure A.37. IR spectrum of di(4-trifluoromethylphenyl)silane (**3e**) recorded neat at 298 K.

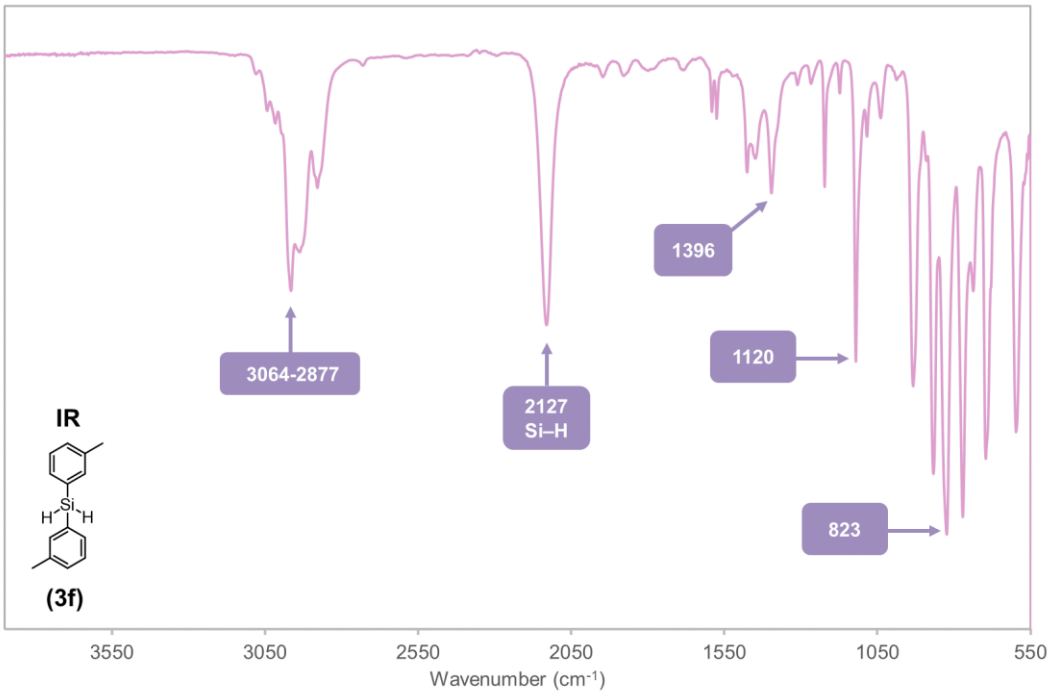

Figure A.37. IR spectrum of di(3-methylphenyl)silane (**3f**) recorded neat at 298 K.

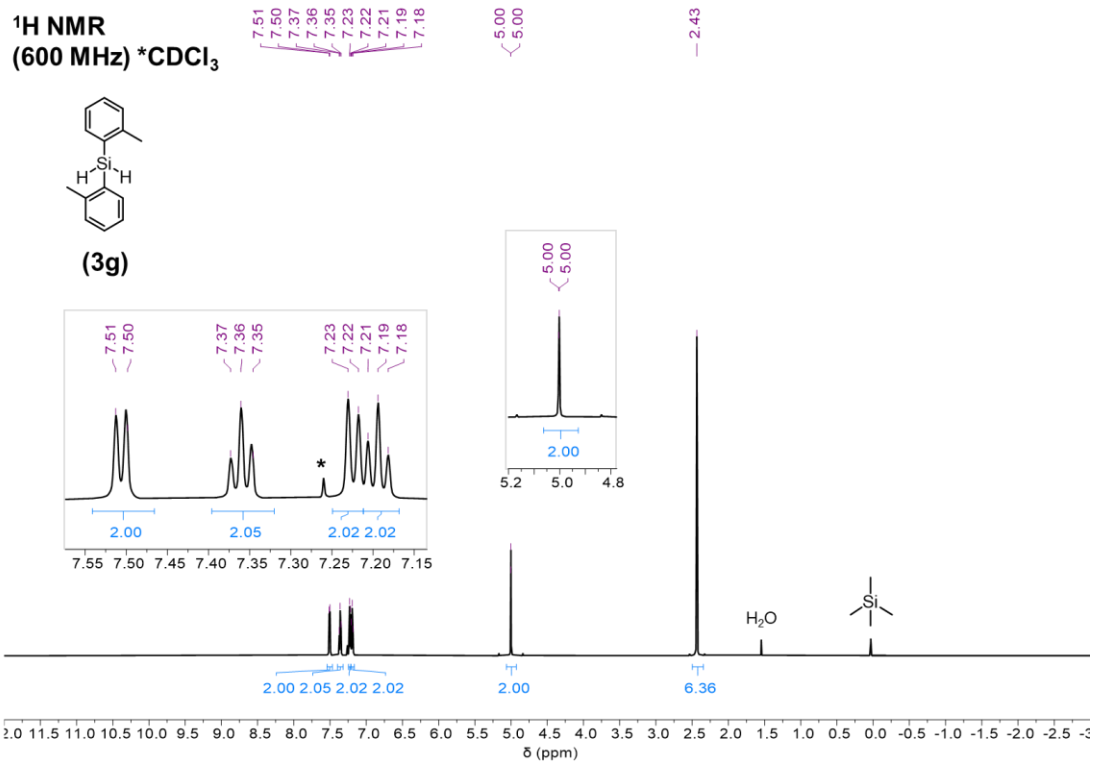

Figure A.38. ^{1}H NMR spectrum of di(2-methylphenyl)silane (**3g**) recorded in $CDCl_3$ at 298 K.

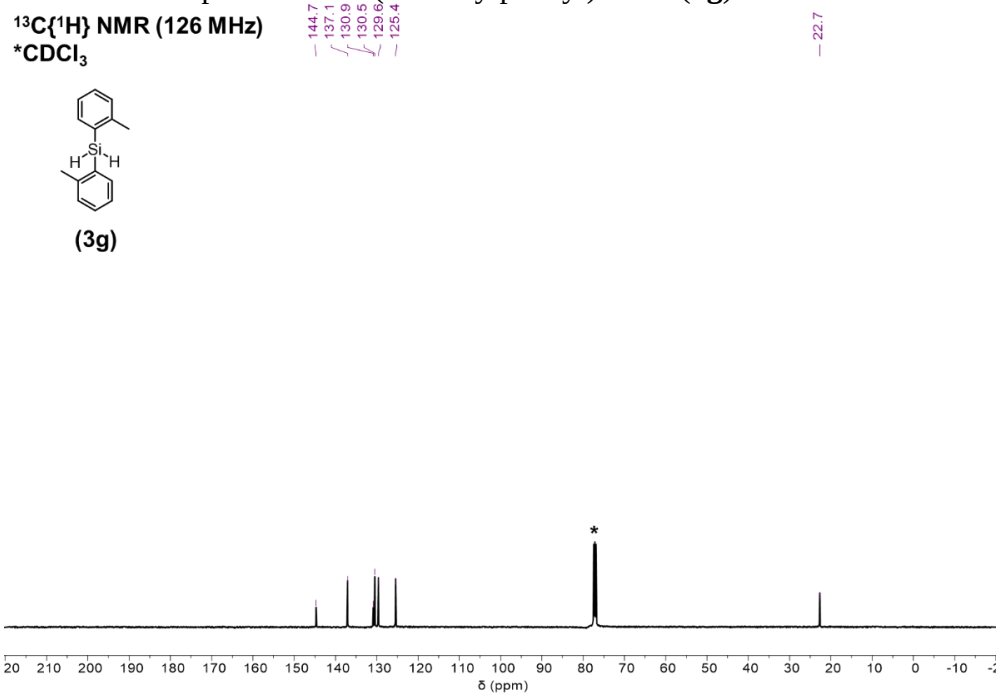

Figure A.39. $^{13}C\{^{1}H\}$ NMR spectrum of di(2-methylphenyl)silane (**3g**) recorded in $CDCl_3$ at 298 K.

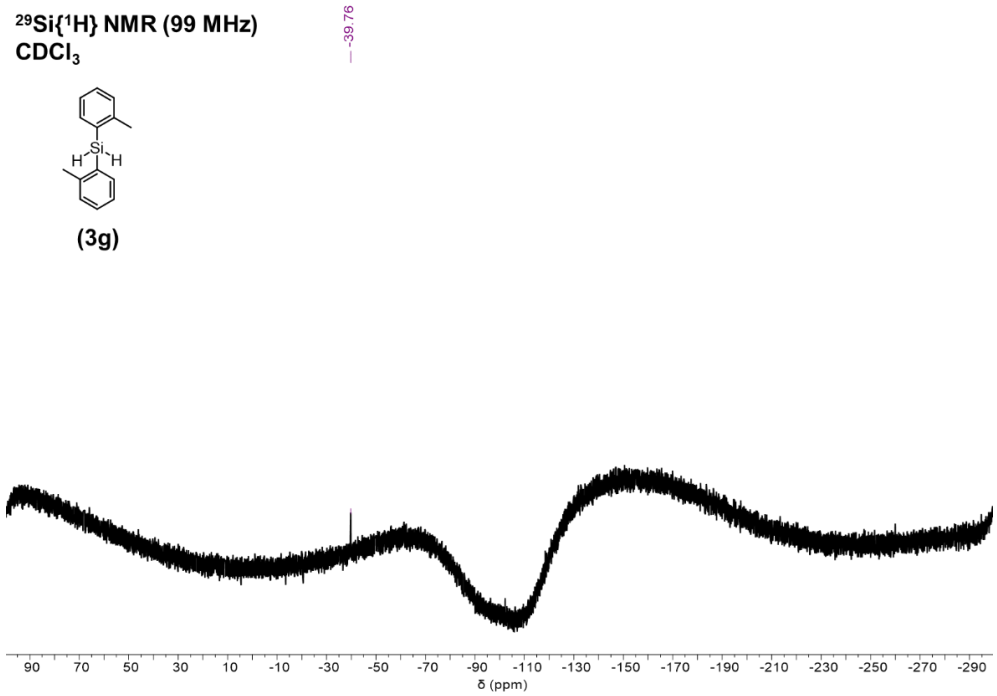

Figure A.40. ^{29}Si NMR spectrum of di(2-methylphenyl)silane (**3g**) recorded in $CDCl_3$ at 298 K.

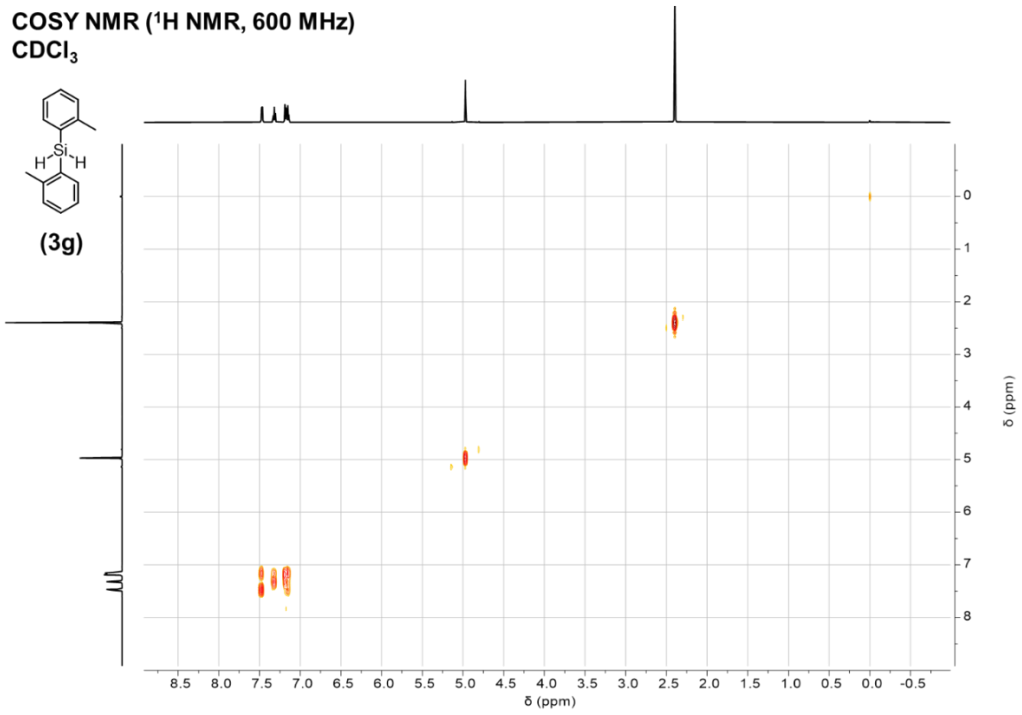

Figure A.41. COSY NMR spectrum of di(2-methylphenyl)silane (**3g**) recorded in $CDCl_3$ at 298 K.

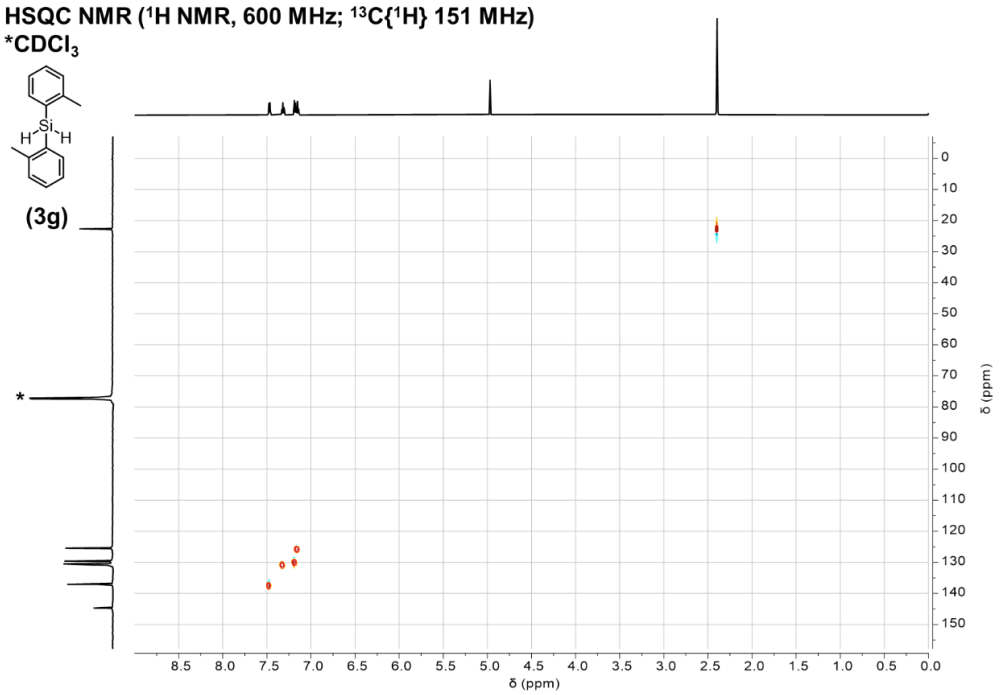

Figure A.42. HSQC NMR spectrum of di(2-methylphenyl)silane (**3g**) recorded in $CDCl_3$ at 298 K.

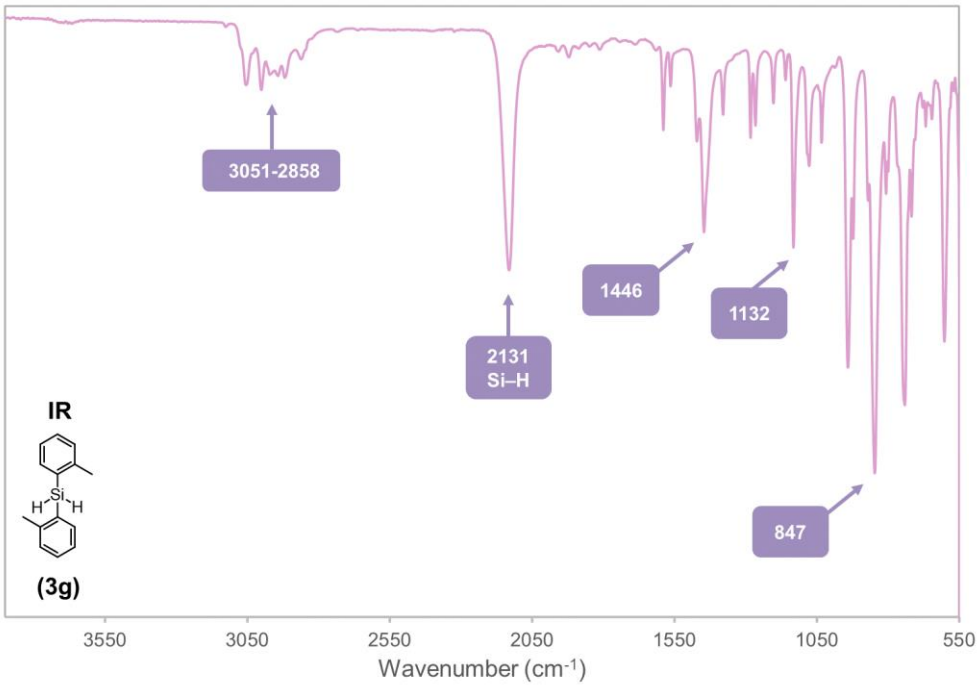

Figure A.43. IR spectrum of di(2-methylphenyl)silane (**3g**) recorded neat at 298 K.

d. Hydrosilylation Products

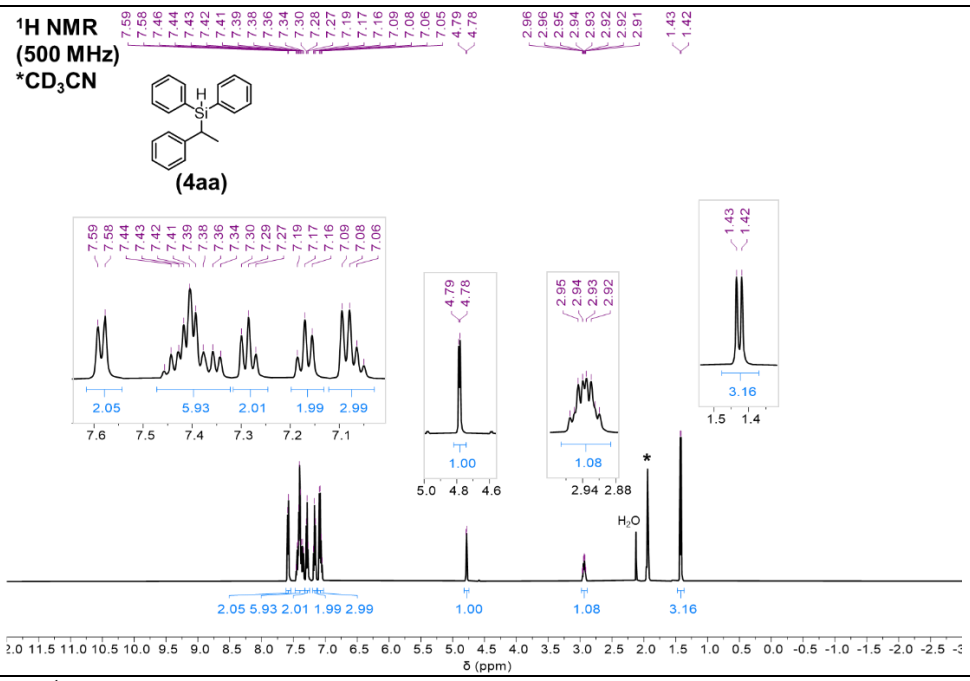

Figure A.43. ^{1}H NMR spectrum of (1-phenylethyl)diphenylsilane (**4aa**) recorded in CD_3CN at 298 K.

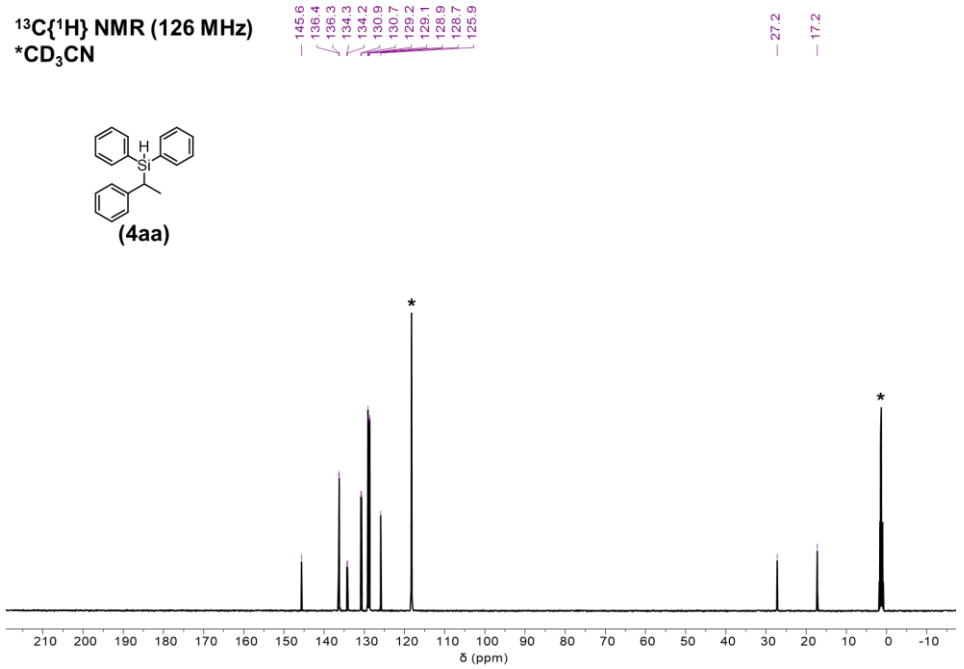

Figure A.44. $^{13}C\{^{1}H\}$ NMR spectrum of (1-phenylethyl)diphenylsilane (**4aa**) recorded in CD_3CN at 298 K.

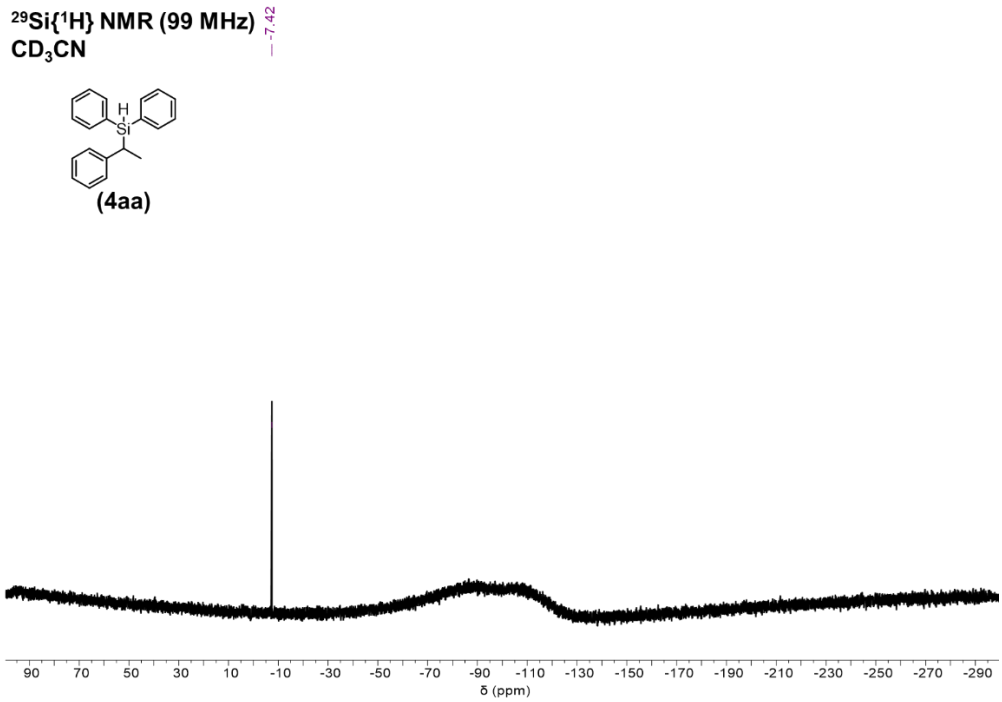

Figure A.45. ^{29}Si{^{1}H} NMR spectrum of (1-phenylethyl)diphenylsilane (**4aa**) recorded in CD_3CN at 298 K.

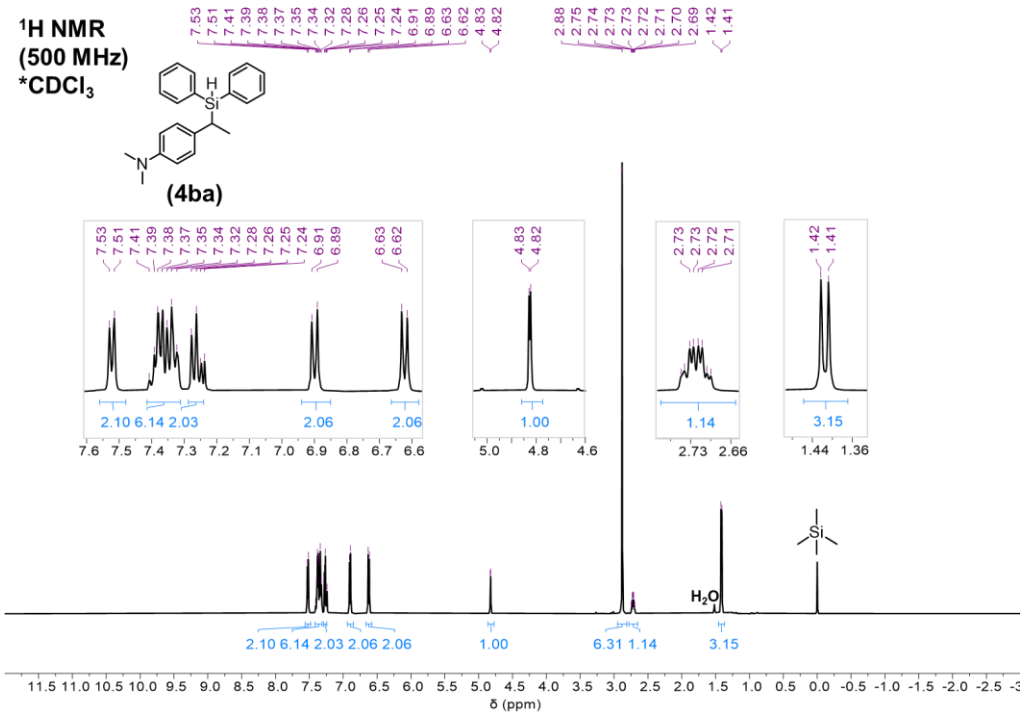

Figure A.46. ^{1}H NMR spectrum of [1-(4-dimethylaminophenyl)ethyl]diphenylsilane (**4ba**) recorded in $CDCl_3$ at 298 K.

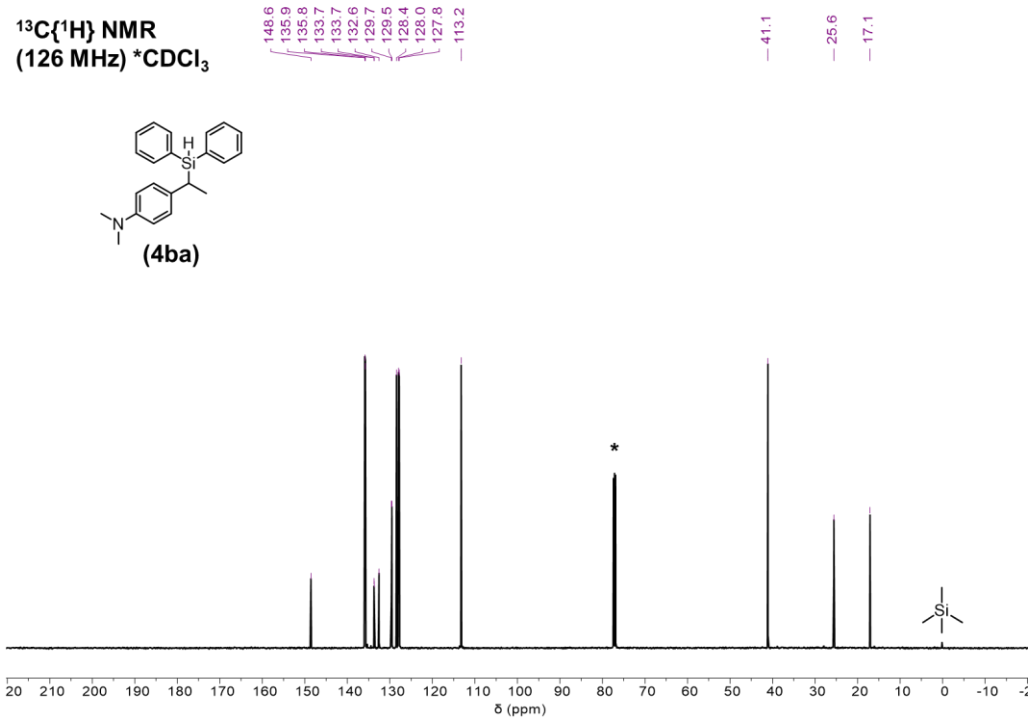

Figure A.47. $^{13}C\{^{1}H\}$ NMR spectrum of [1-(4-dimethylaminophenyl)ethyl]diphenylsilane (**4ba**) recorded in $CDCl_3$ at 298 K.

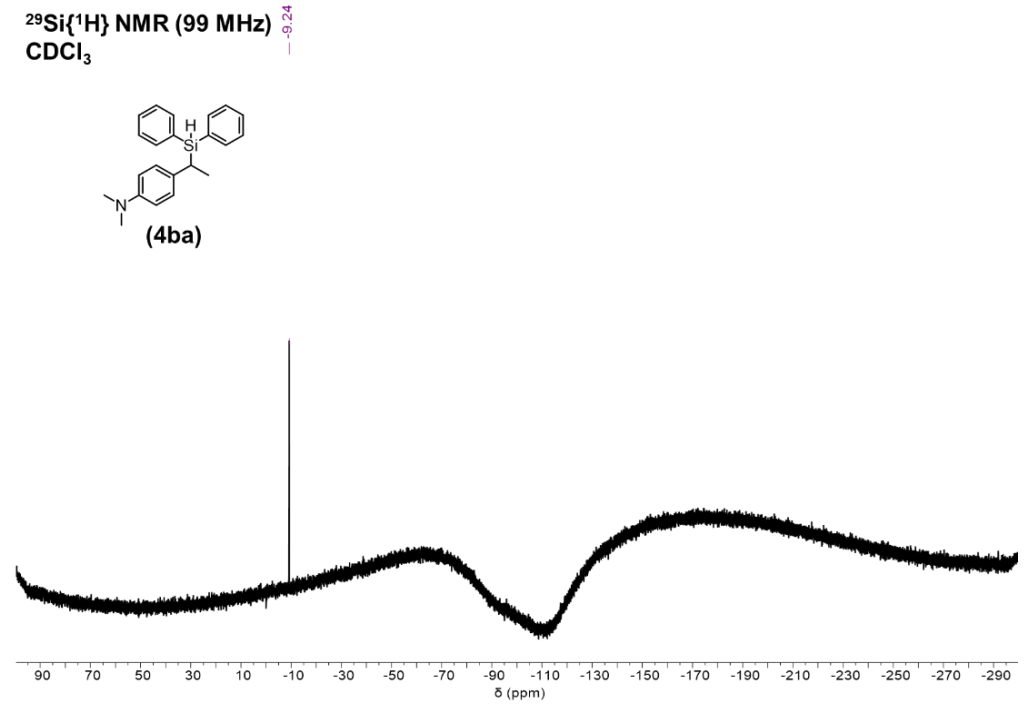

Figure A.48. $^{29}Si\{^{1}H\}$ NMR spectrum of [1-(4-dimethylaminophenyl)ethyl]diphenylsilane (**4ba**) recorded in $CDCl_3$ at 298 K.

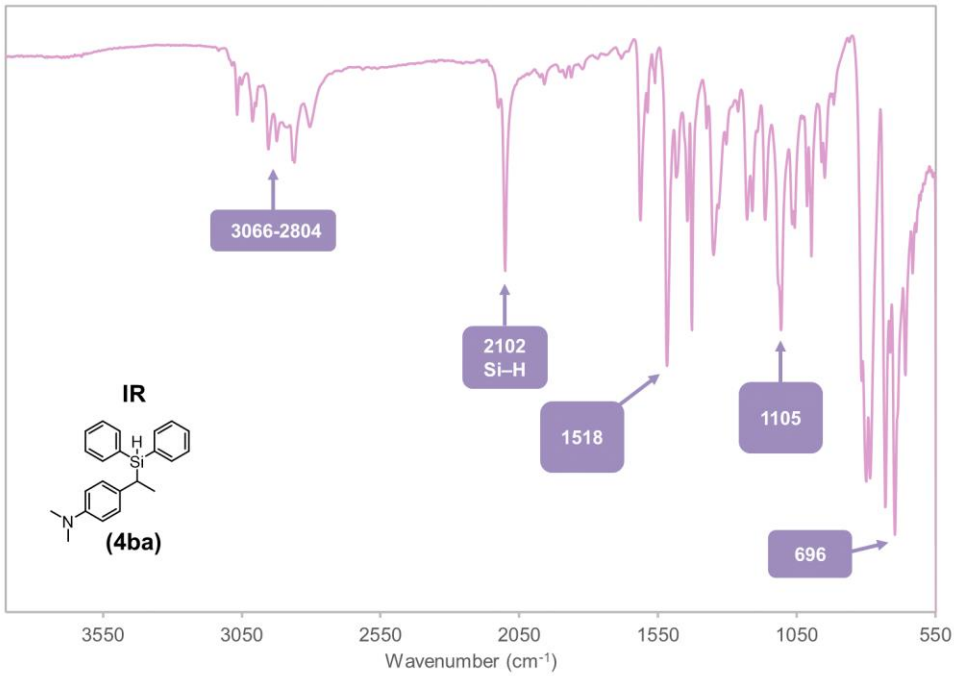

Figure A.49. IR spectrum of [1-(4-dimethylaminophenyl)ethyl]diphenylsilane (**4ba**) recorded neat at 298 K.

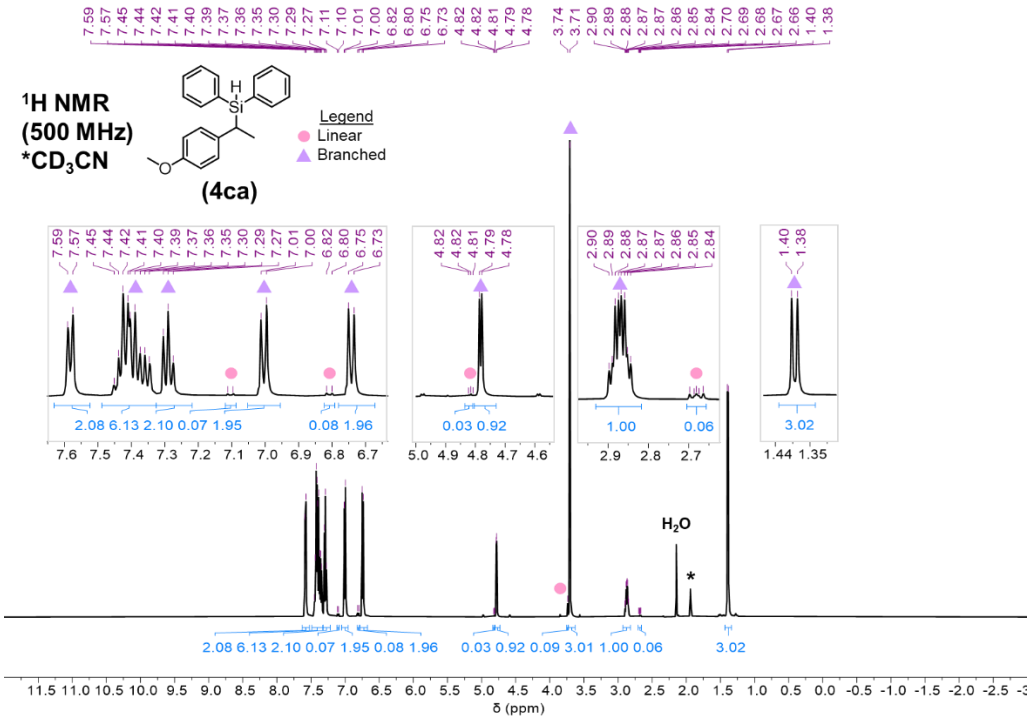

Figure A.50. ^{1}H NMR spectrum of [1-(4-methoxyphenyl)ethyl]diphenylsilane (**4ca**) recorded in CD_3CN at 298 K.

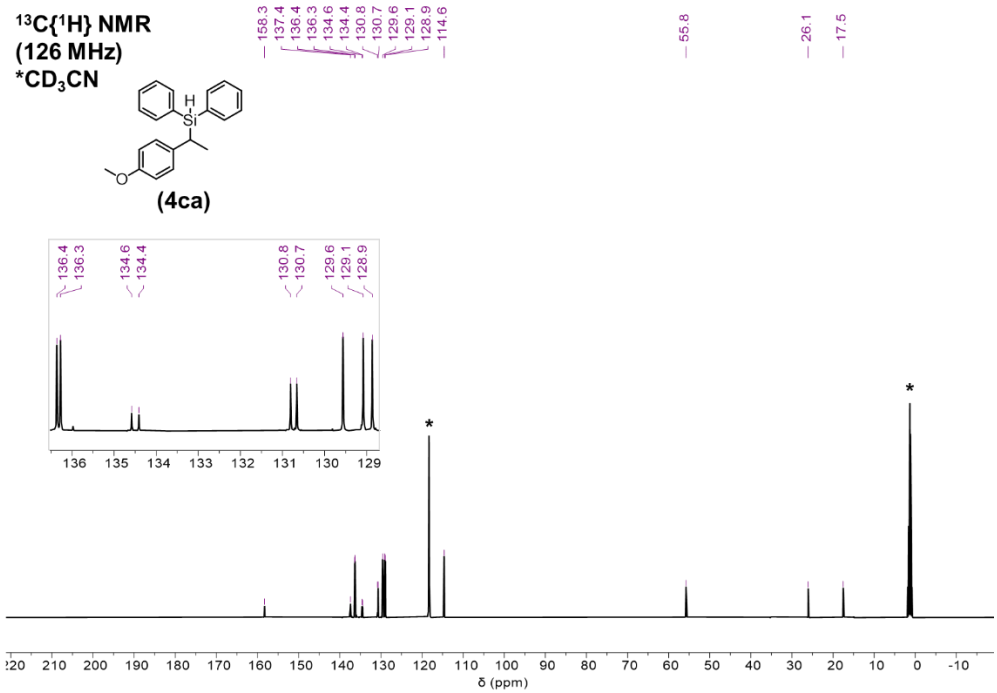

Figure A.51. $^{13}C\{^{1}H\}$ NMR spectrum of [1-(4-methoxyphenyl)ethyl]diphenylsilane (**4ca**) recorded in CD_3CN at 298 K.

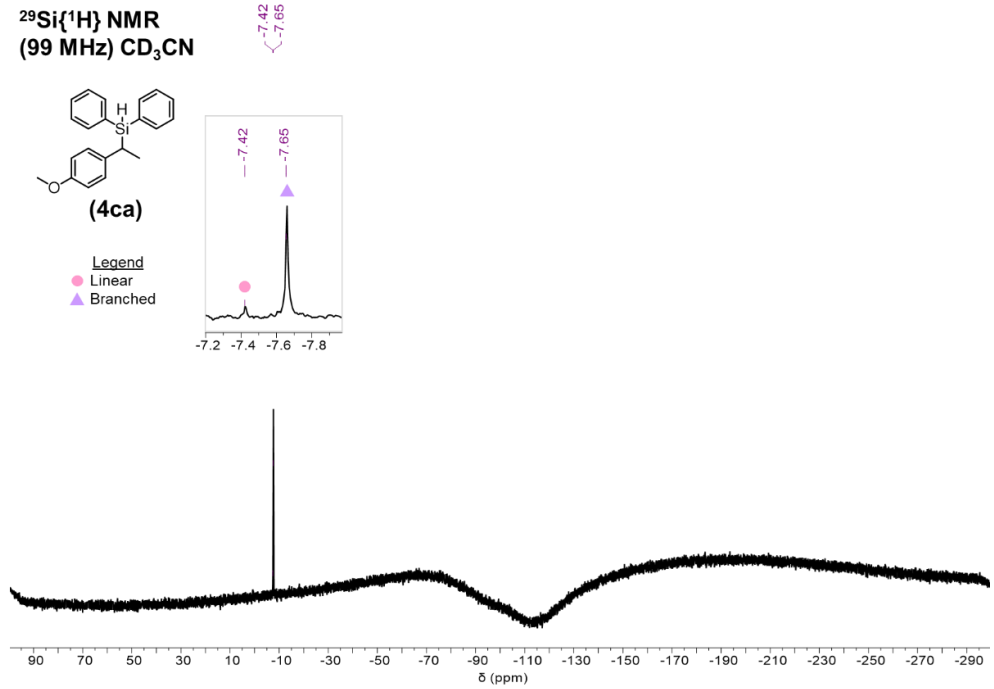

Figure A.52. $^{29}Si\{^{1}H\}$ NMR spectrum of [1-(4-methoxyphenyl)ethyl]diphenylsilane (**4ca**) recorded in CD_3CN at 298 K.

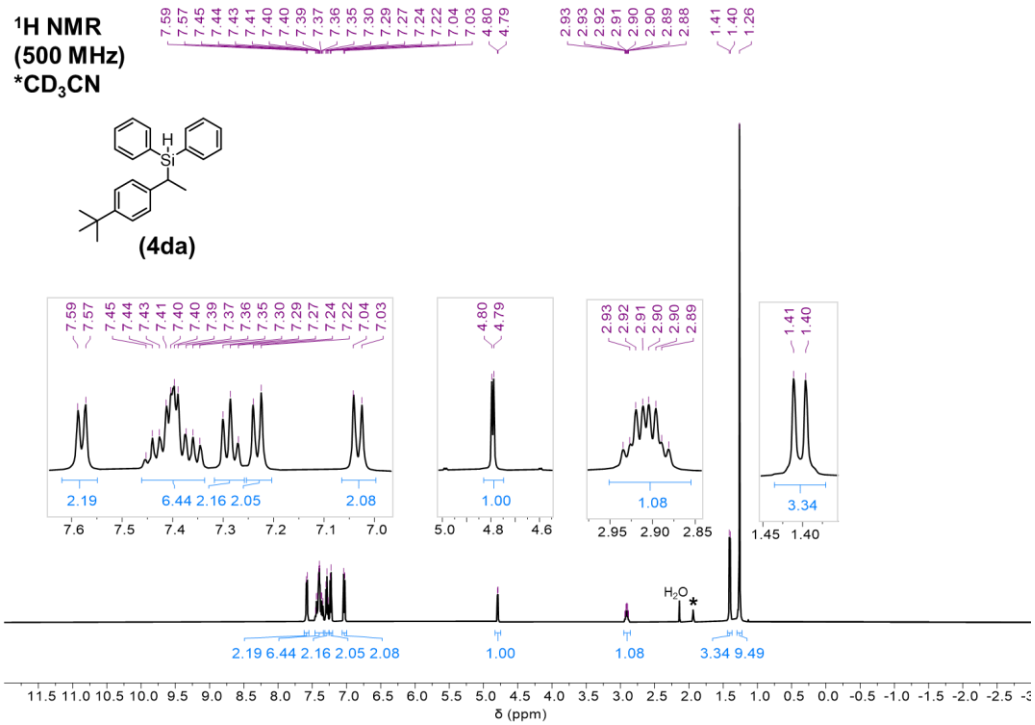

Figure A.53. ^{1}H NMR spectrum of [1-(4-*tert*-butylphenyl)ethyl]diphenylsilane (**4da**) recorded in CD_3CN at 298 K.

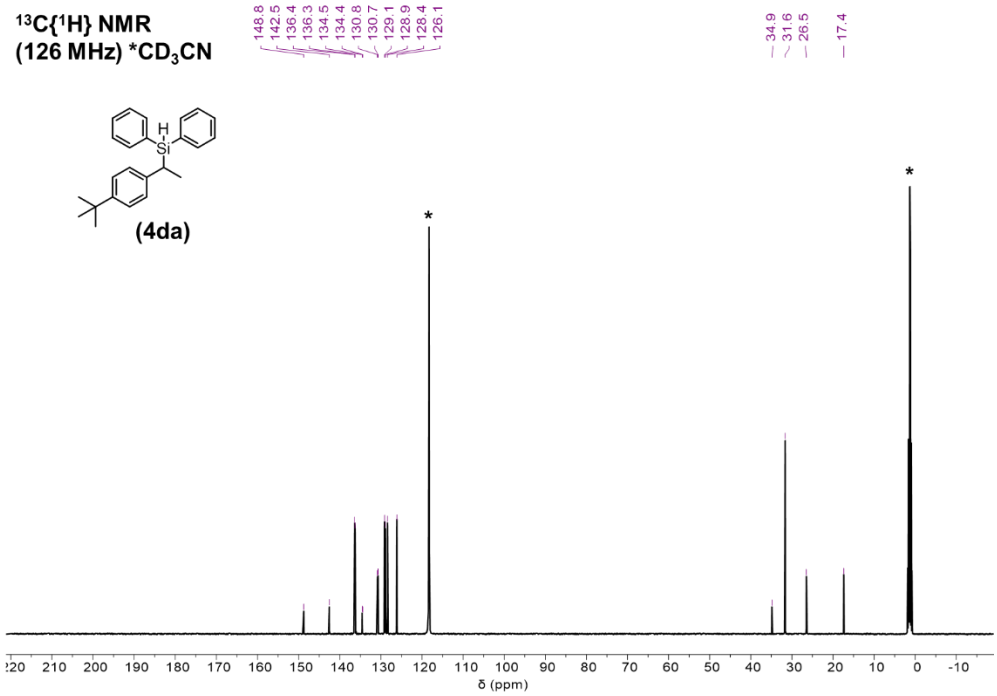

Figure A.54. ^{13}C{^{1}H} NMR spectrum of [1-(4-*tert*-butylphenyl)ethyl]diphenylsilane (**4da**) recorded in CD_3CN at 298 K.

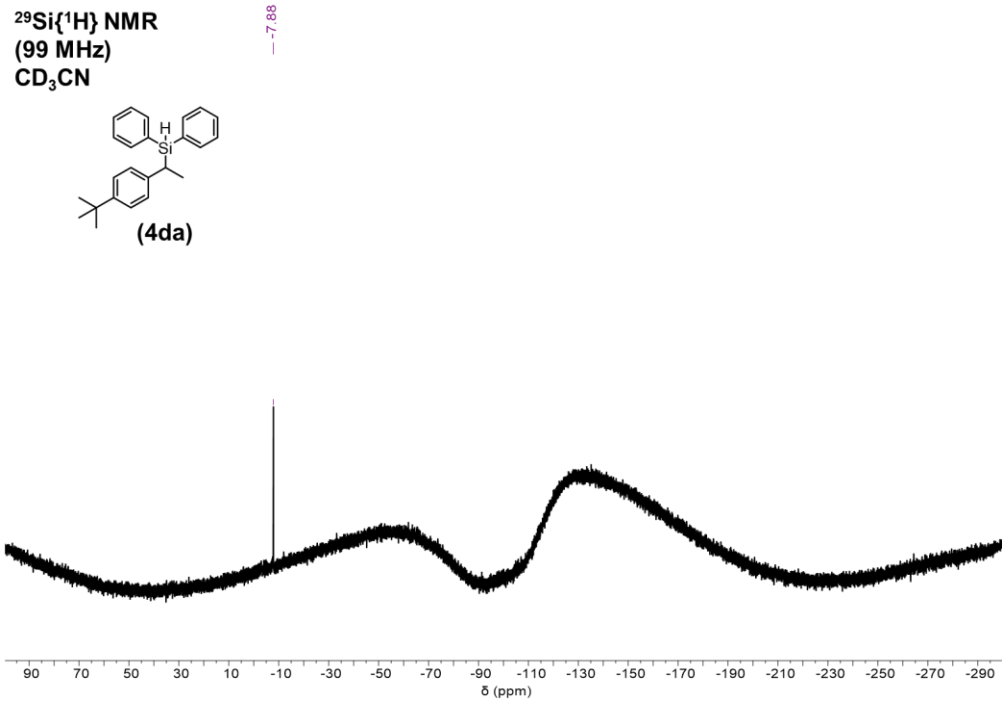

Figure A.55. $^{29}Si\{^{1}H\}$ NMR spectrum of [1-(4-*tert*-butylphenyl)ethyl]diphenylsilane (**4da**) recorded in CD_3CN at 298 K.

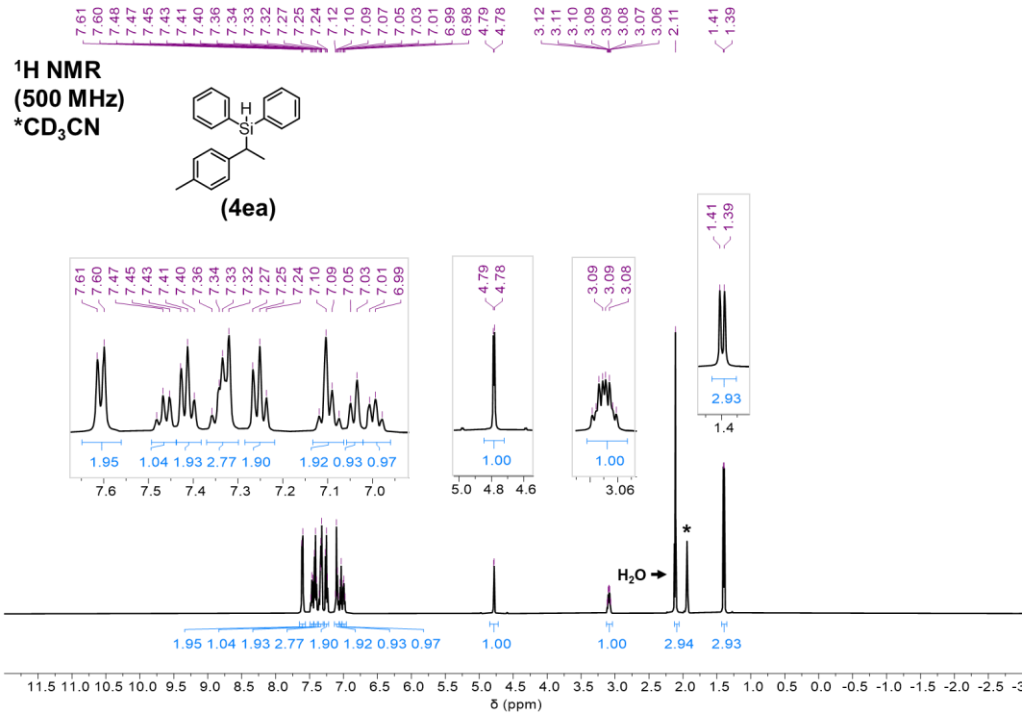

Figure A.56. ^{1}H NMR spectrum of [1-(4-methylphenyl)ethyl]diphenylsilane (**4ea**) recorded in CD_3CN at 298 K.

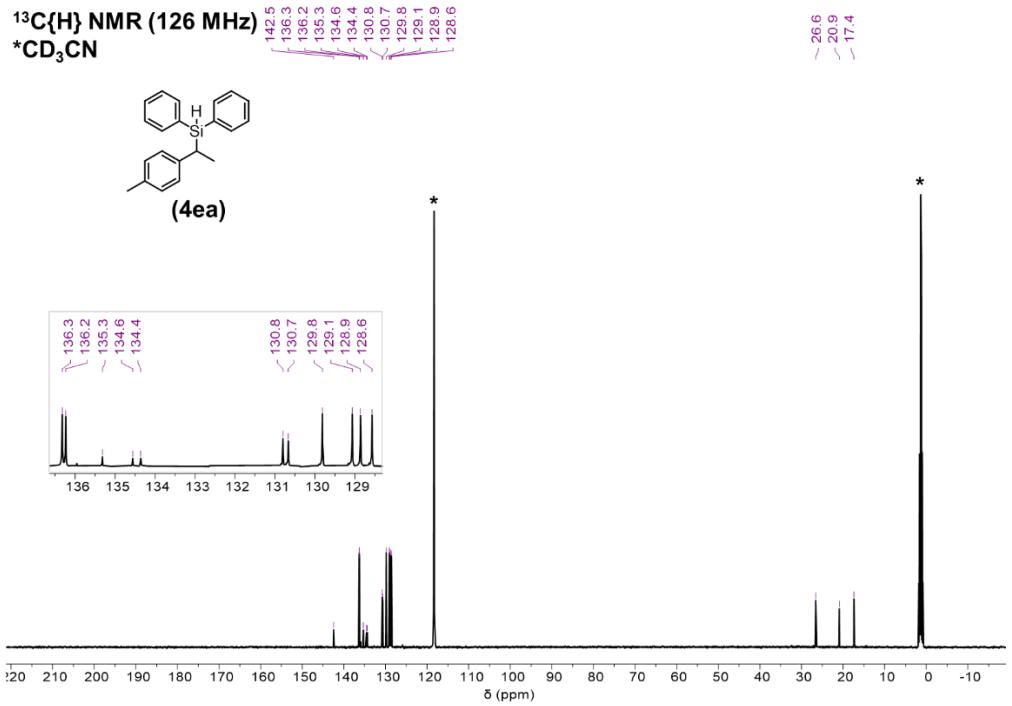

Figure A.57. $^{13}C\{^{1}H\}$ NMR spectrum of [1-(4-methylphenyl)ethyl]diphenylsilane (**4ea**) recorded in CD_3CN at 298 K.

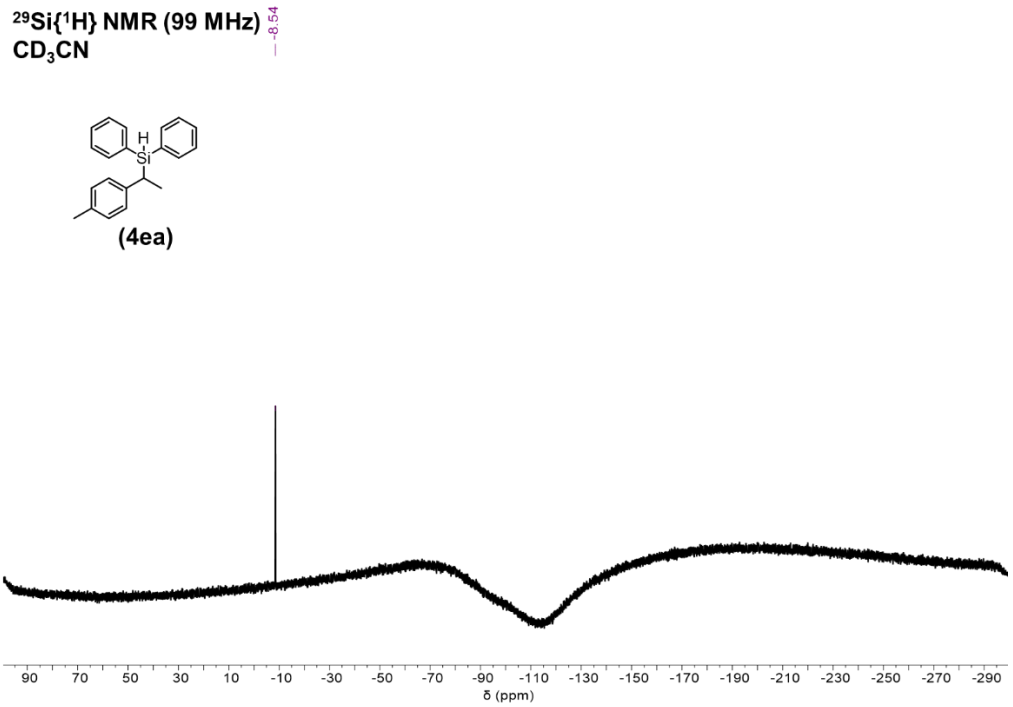

Figure A.58. $^{29}Si\{^{1}H\}$ NMR spectrum of [1-(4-methylphenyl)ethyl]diphenylsilane (**4ea**) recorded in CD_3CN at 298 K.

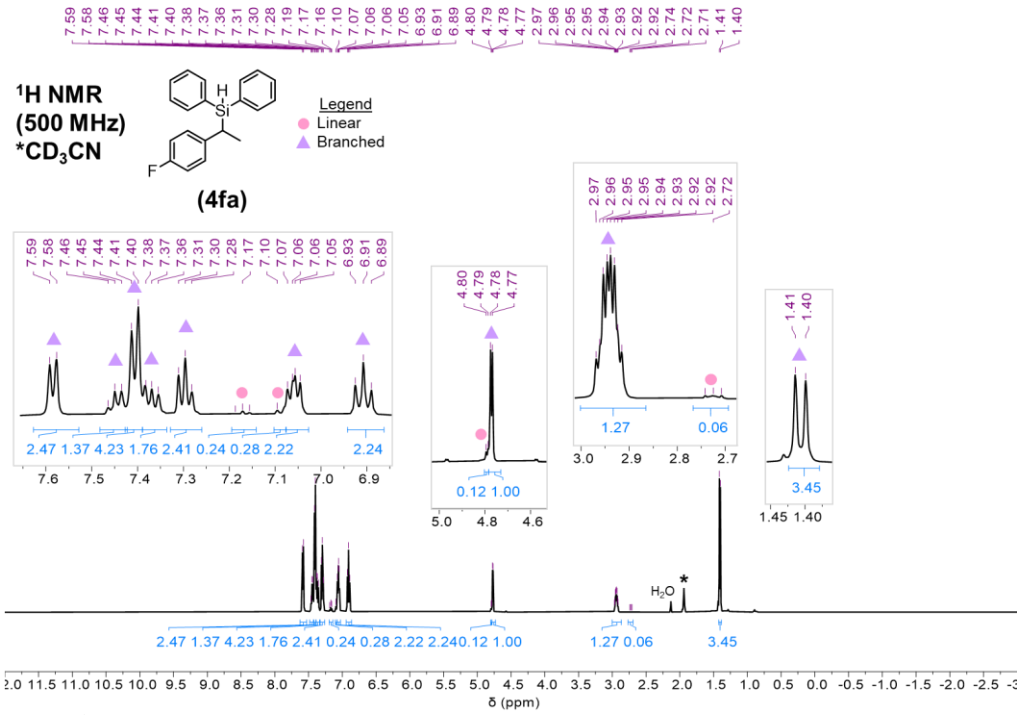

Figure A.59. ^{1}H NMR spectrum of [1-(4-fluorophenyl)ethyl]diphenylsilane (**4fa**) recorded in CD_3CN at 298 K.

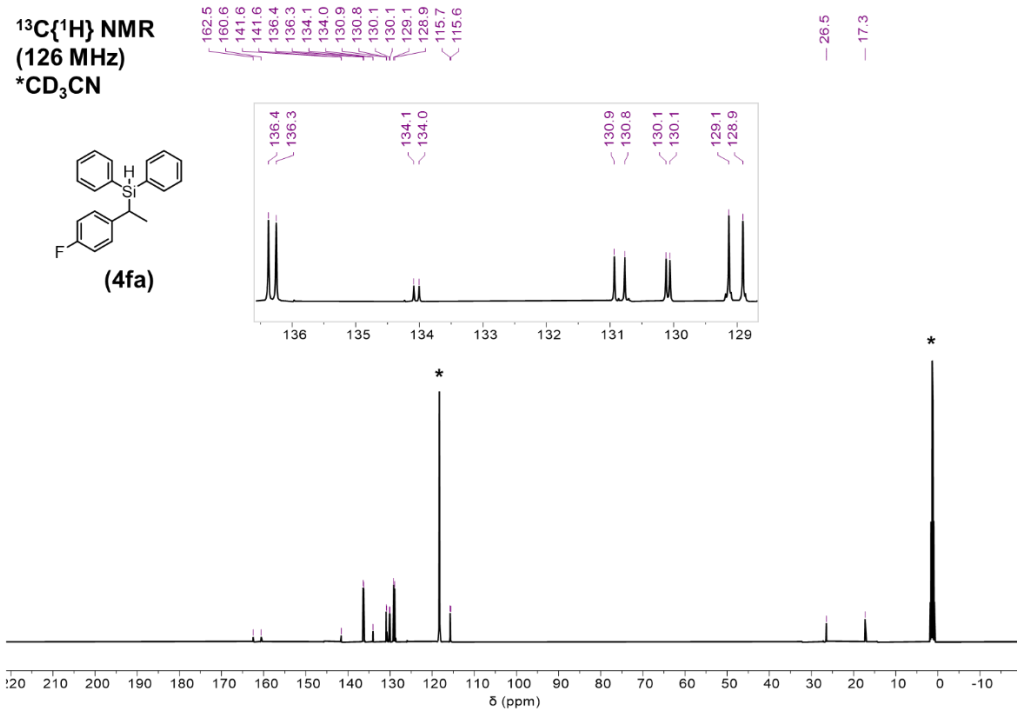

Figure A.60. ^{13}C{^{1}H} NMR spectrum of [1-(4-fluorophenyl)ethyl]diphenylsilane (**4fa**) recorded in CD_3CN at 298 K.

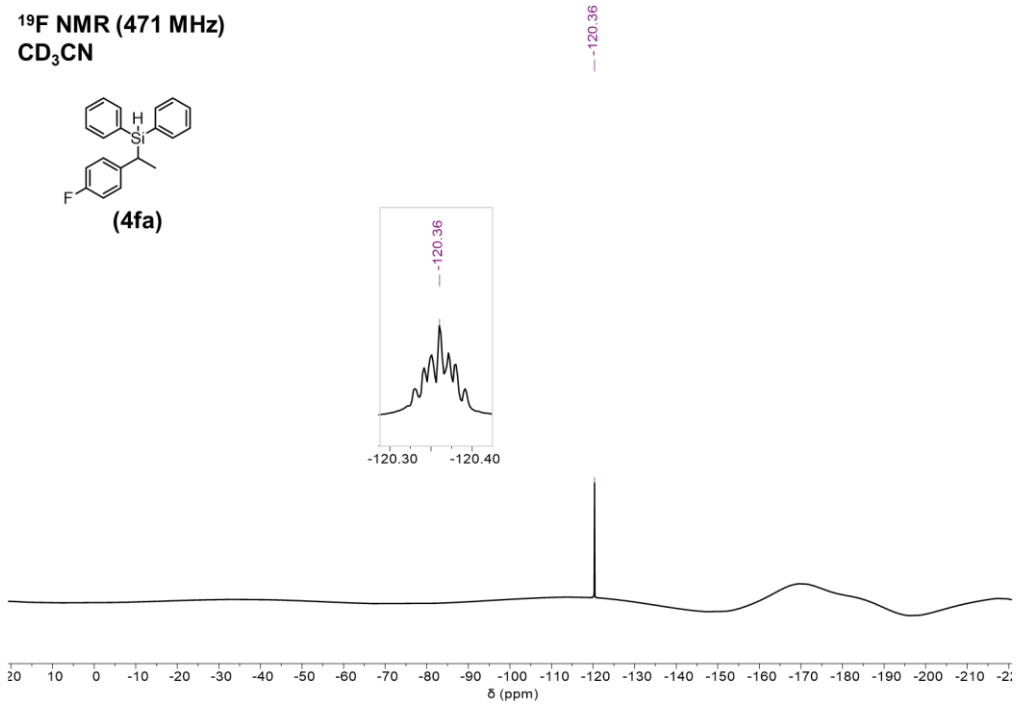

Figure A.61. ^{19}F NMR spectrum of [1-(4-fluorophenyl)ethyl]diphenylsilane (**4fa**) recorded in CD_3CN at 298 K.

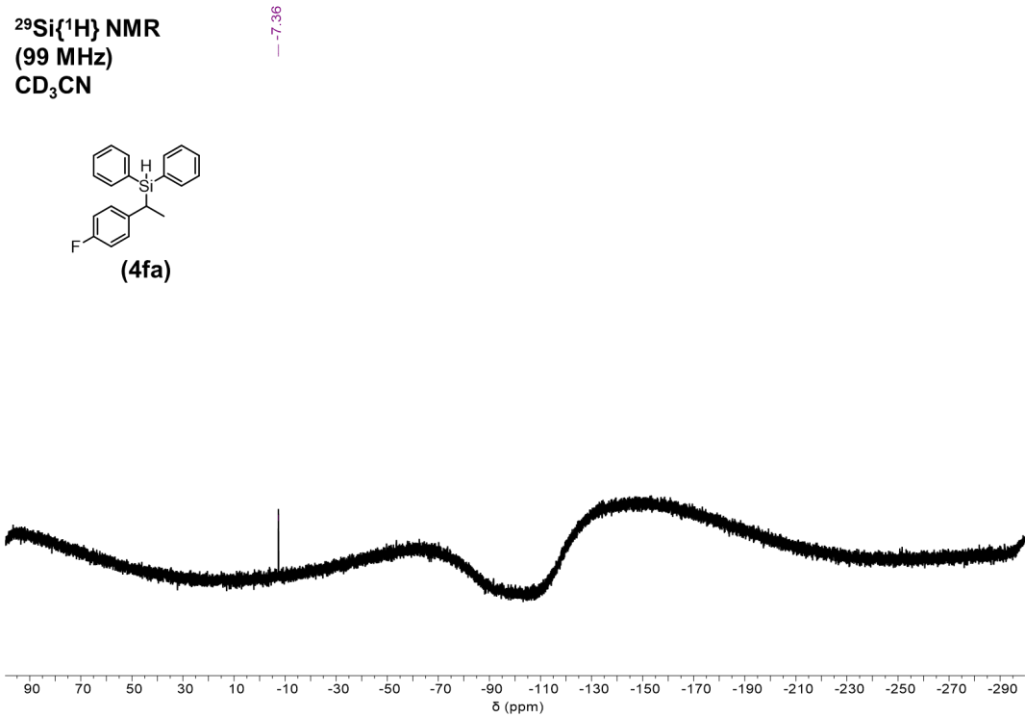

Figure A.62. $^{29}Si\{^1H\}$ NMR spectrum of [1-(4-fluorophenyl)ethyl]diphenylsilane (**4fa**) recorded in CD_3CN at 298 K.

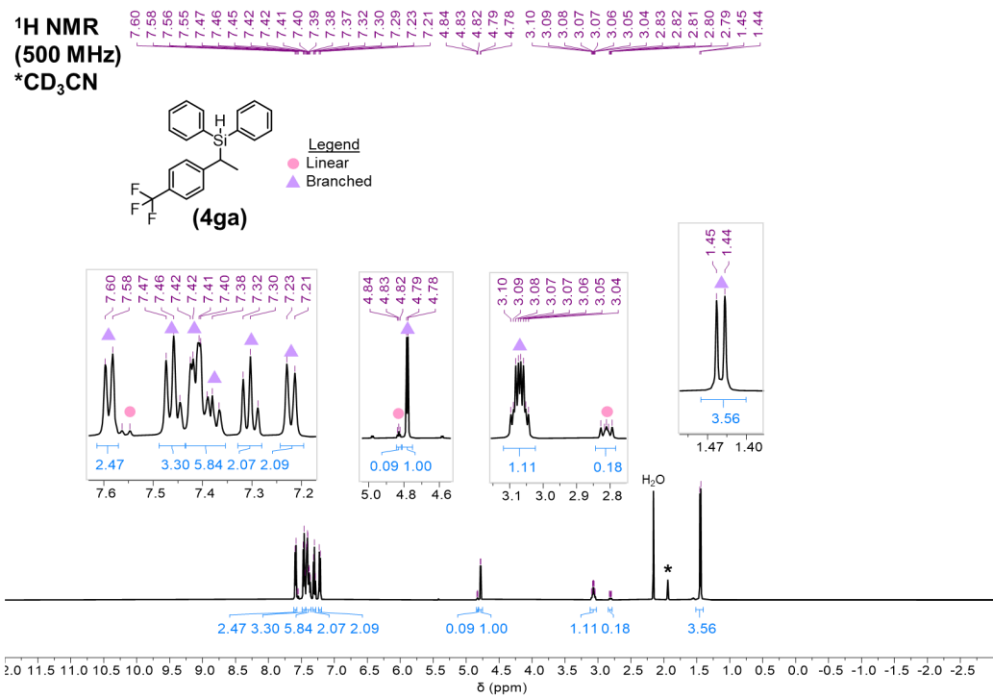

Figure A.63. ^{1}H NMR spectrum of [1-(4-(trifluoromethyl)phenyl)ethyl]diphenylsilane (**4ga**) recorded in CD_3CN at 298 K.

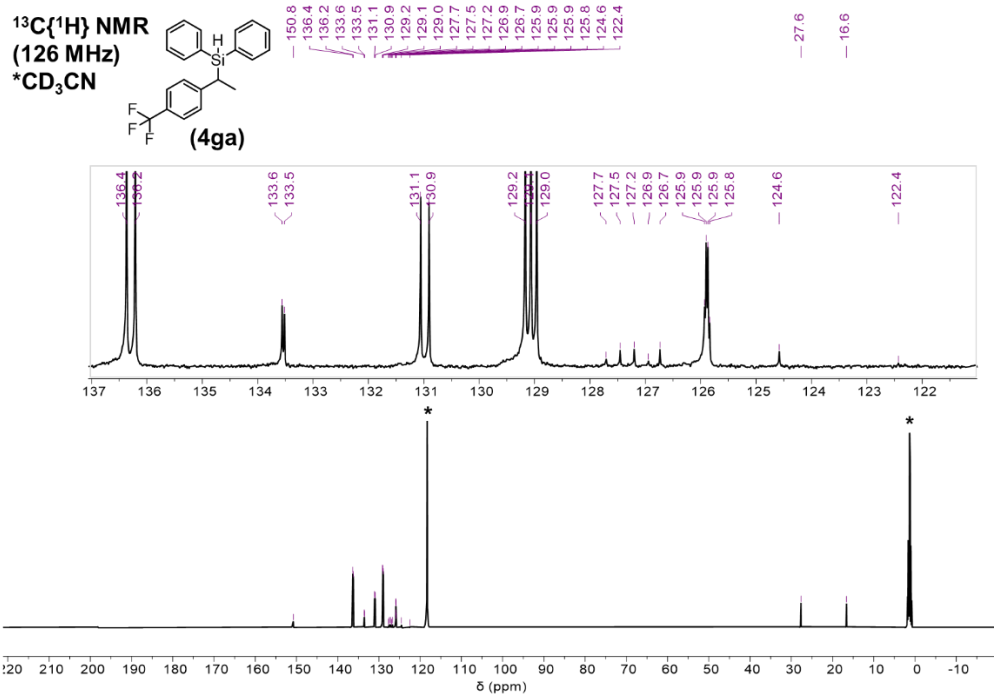

Figure A.64. $^{13}C\{^{1}H\}$ NMR spectrum of [1-(4-(trifluoromethyl)phenyl)ethyl]diphenylsilane (**4ga**) recorded in CD_3CN at 298 K.

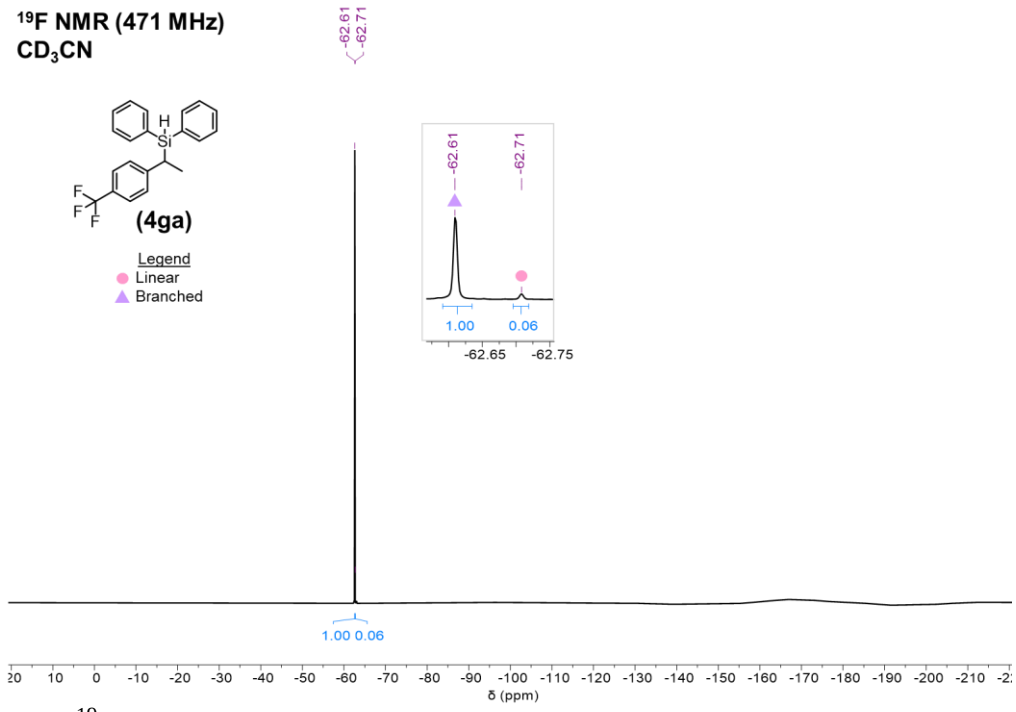

Figure A.65. ^{19}F NMR spectrum of [1-(4-(trifluoromethyl)phenyl)ethyl]diphenylsilane (**4ga**) recorded in CD_3CN at 298 K.

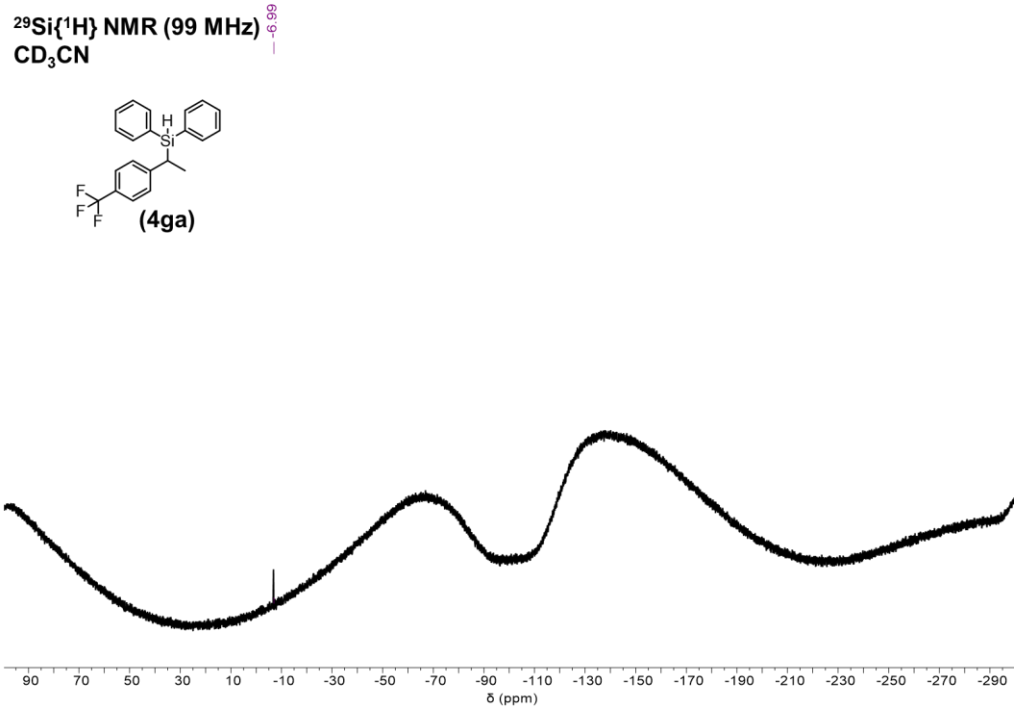

Figure A.66. $^{29}Si\{^1H\}$ NMR spectrum of [1-(4-(trifluoromethyl)phenyl)ethyl]diphenylsilane (**4ga**) recorded in CD_3CN at 298 K.

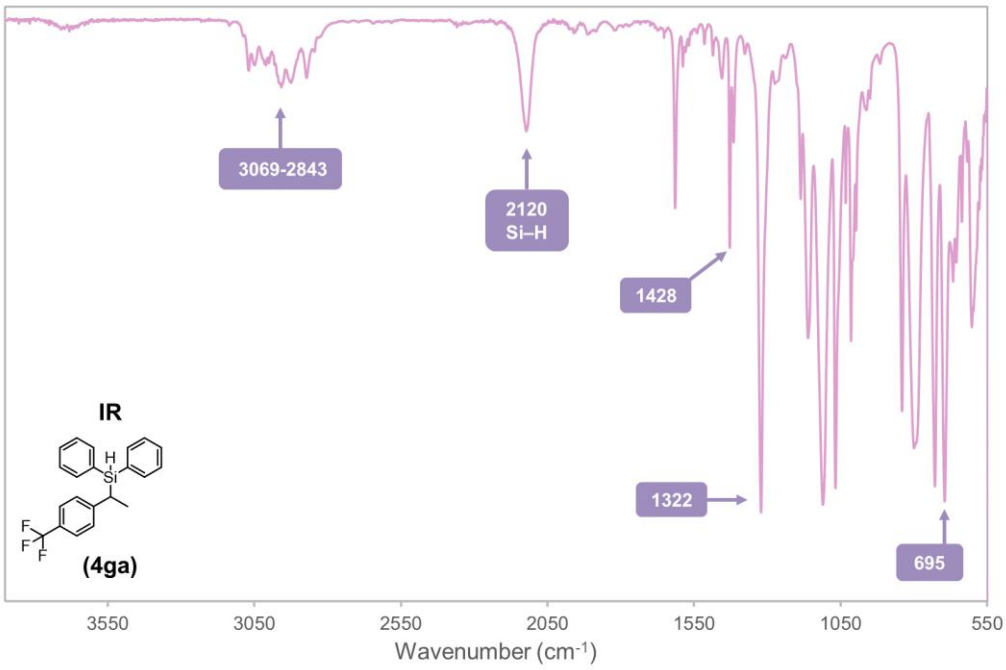

Figure A.67. IR spectrum of [1-(4-(trifluoromethyl)phenyl)ethyl]diphenylsilane (**4ga**) recorded neat at 298 K.

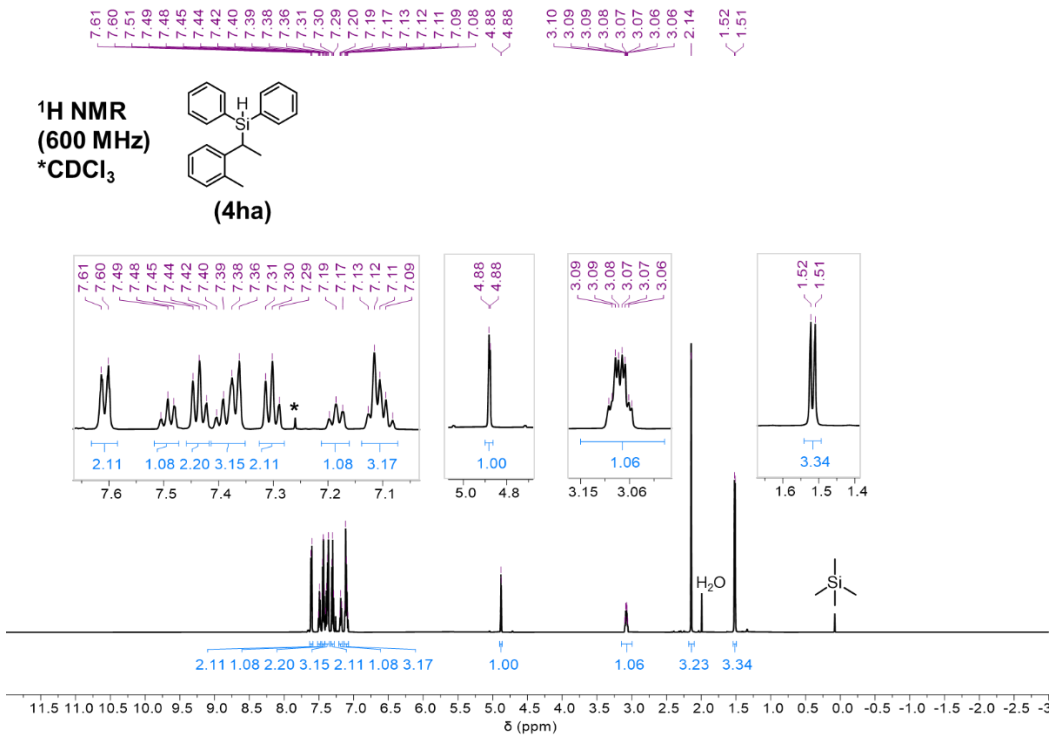

Figure A.68. ^{1}H NMR spectrum of [1-(2-methylphenyl)ethyl]diphenylsilane (**4ha**) recorded in $CDCl_3$ at 298 K.

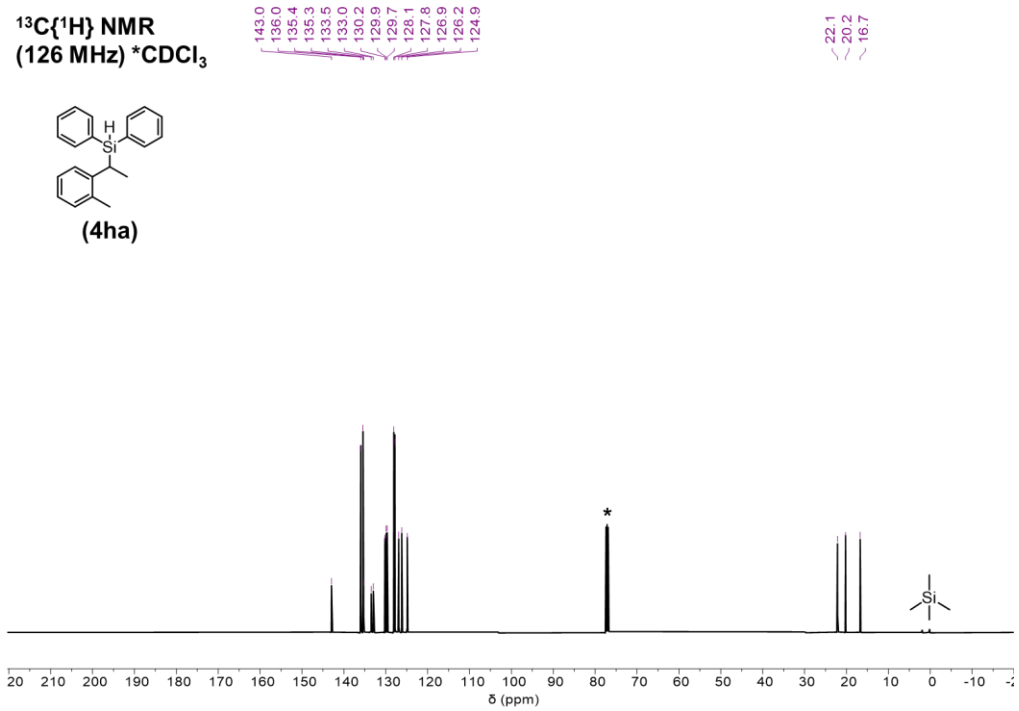

Figure A.69. $^{13}C\{^{1}H\}$ NMR spectrum of [1-(2-methylphenyl)ethyl]diphenylsilane (**4ha**) recorded in $CDCl_3$ at 298 K.

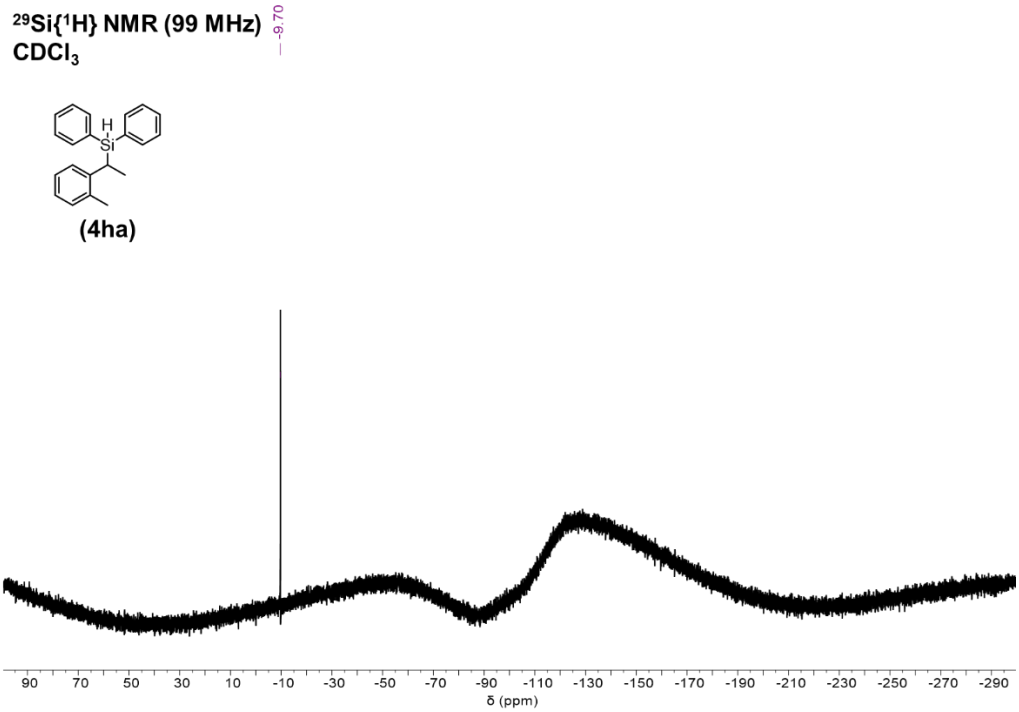

Figure A.70. $^{29}Si\{^{1}H\}$ NMR spectrum [1-(2-methylphenyl)ethyl]diphenylsilane (**4ha**) recorded in $CDCl_3$ at 298 K.

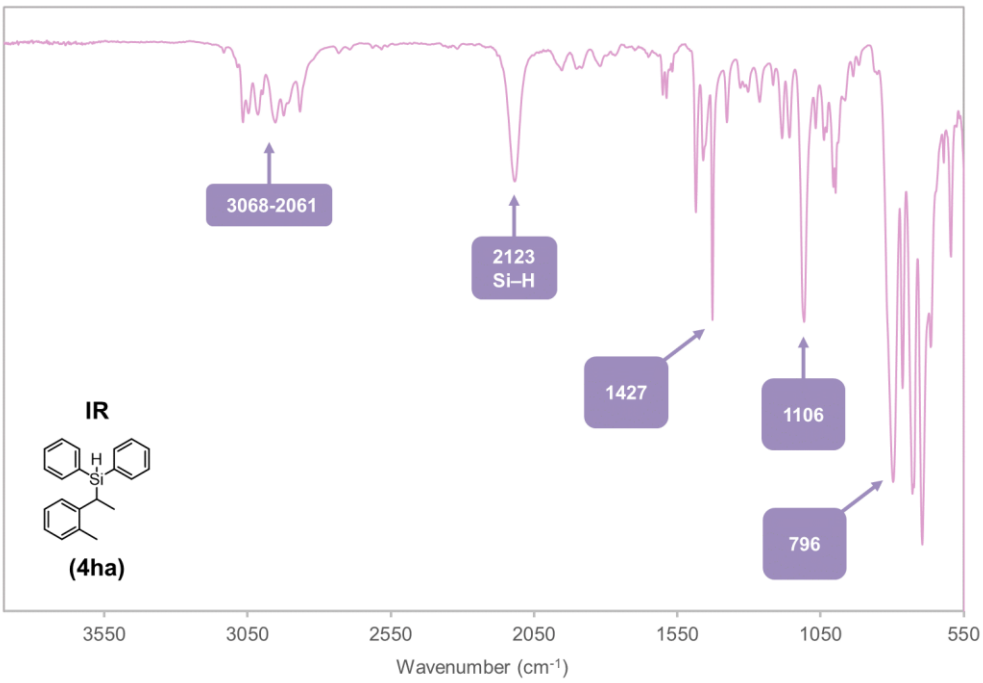

Figure A.71. IR spectrum of [1-(2-methylphenyl)ethyl]diphenylsilane (**4ha**) recorded neat at 298 K.

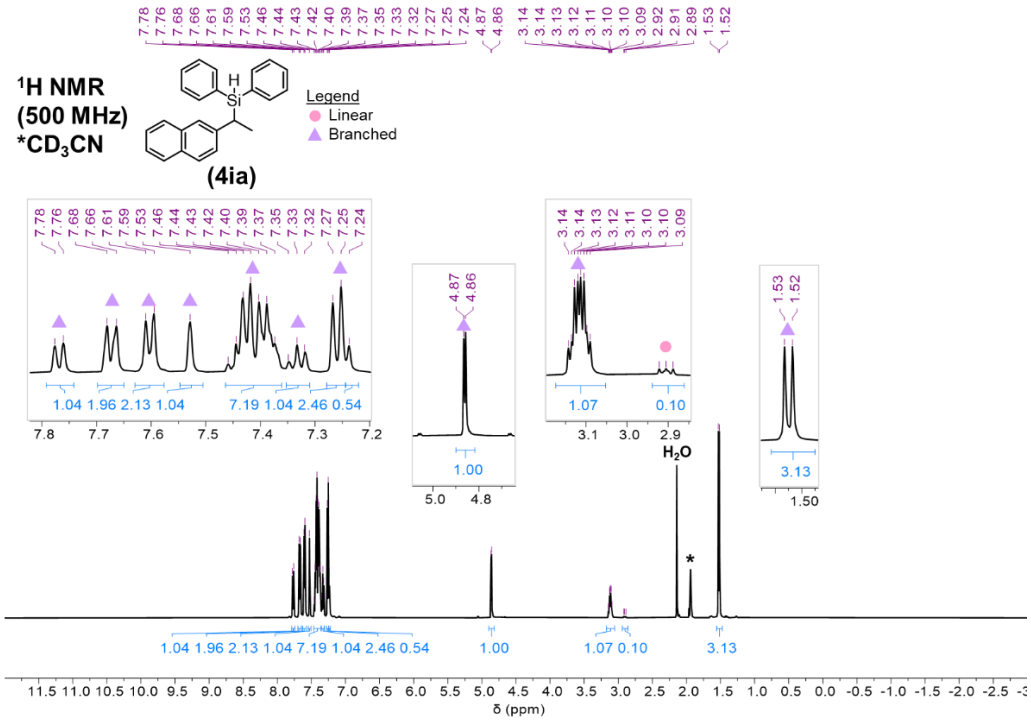

Figure A.72. ^{1}H NMR spectrum of [1-(2-naphthyl)ethyl]diphenylsilane (**4ia**) recorded in CD_3CN at 298 K.

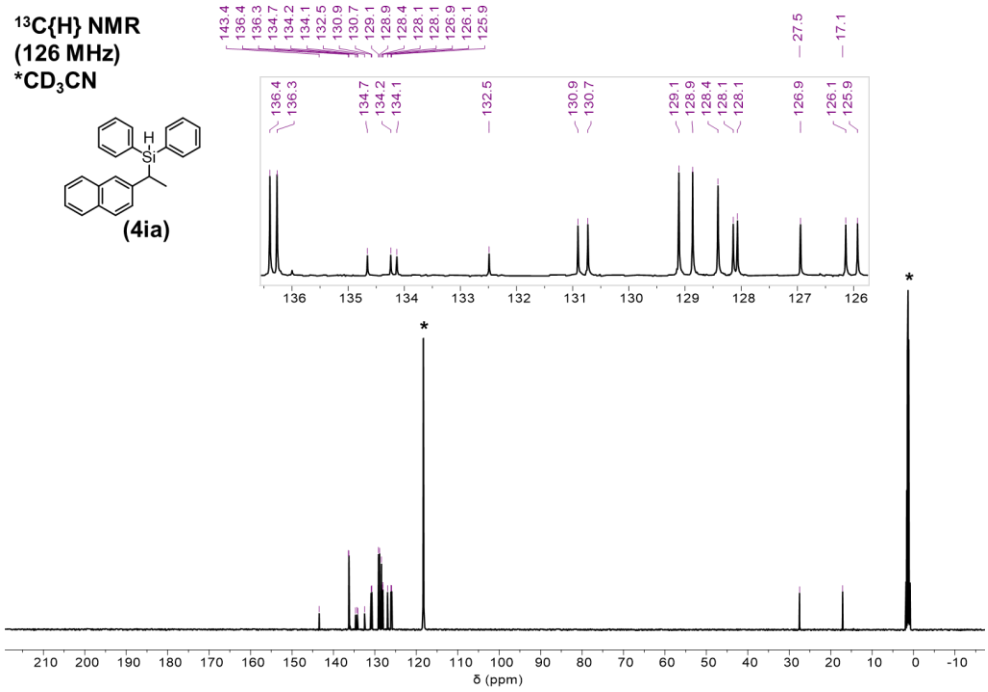

Figure A.73. $^{13}C\{^{1}H\}$ NMR spectrum of [1-(2-naphthyl)ethyl]diphenylsilane (**4ia**) recorded in CD_3CN at 298 K.

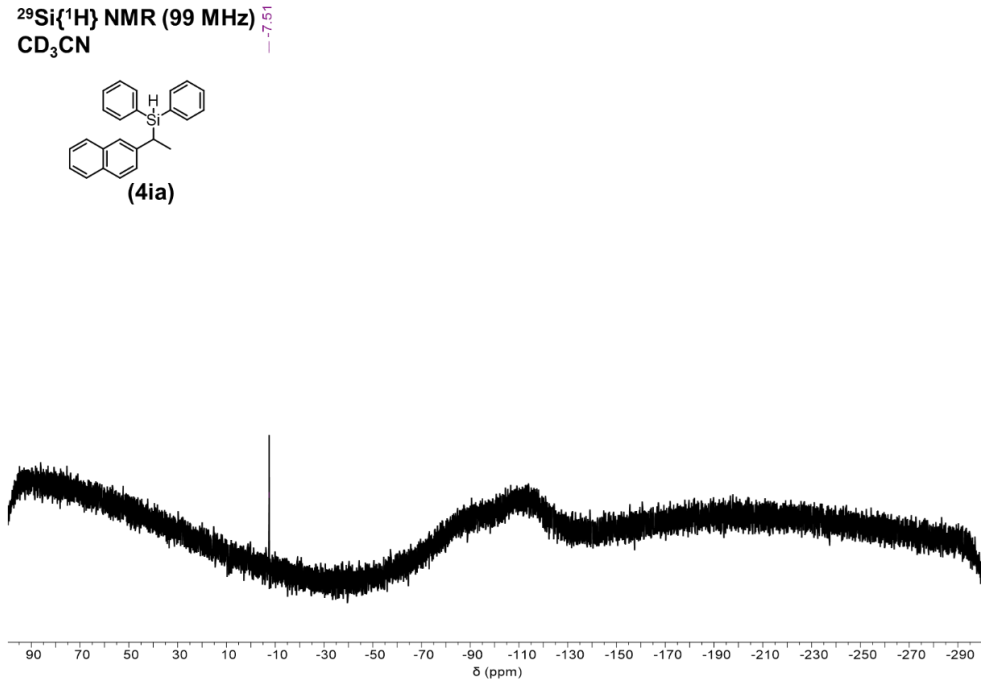

Figure A.74. $^{29}Si\{^{1}H\}$ NMR spectrum of [1-(2-naphthyl)ethyl]diphenylsilane (**4ia**) recorded in CD_3CN at 298 K.

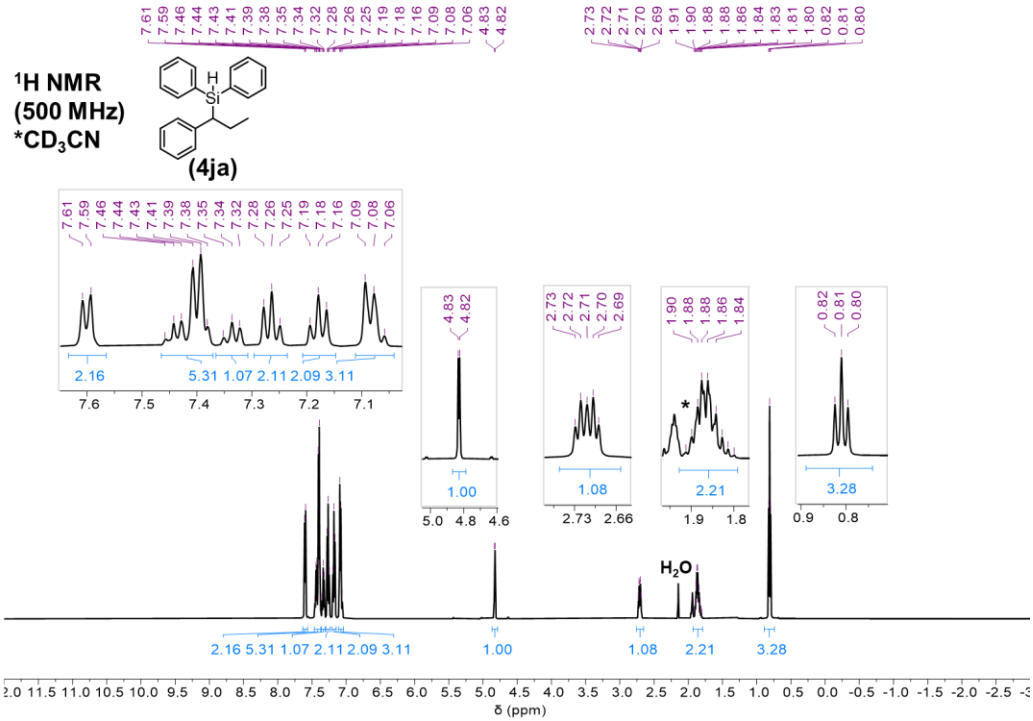

Figure A.75. ^{1}H NMR spectrum of [1-phenylpropyl]diphenylsilane (**4ja**) recorded in CD_3CN at 298 K.

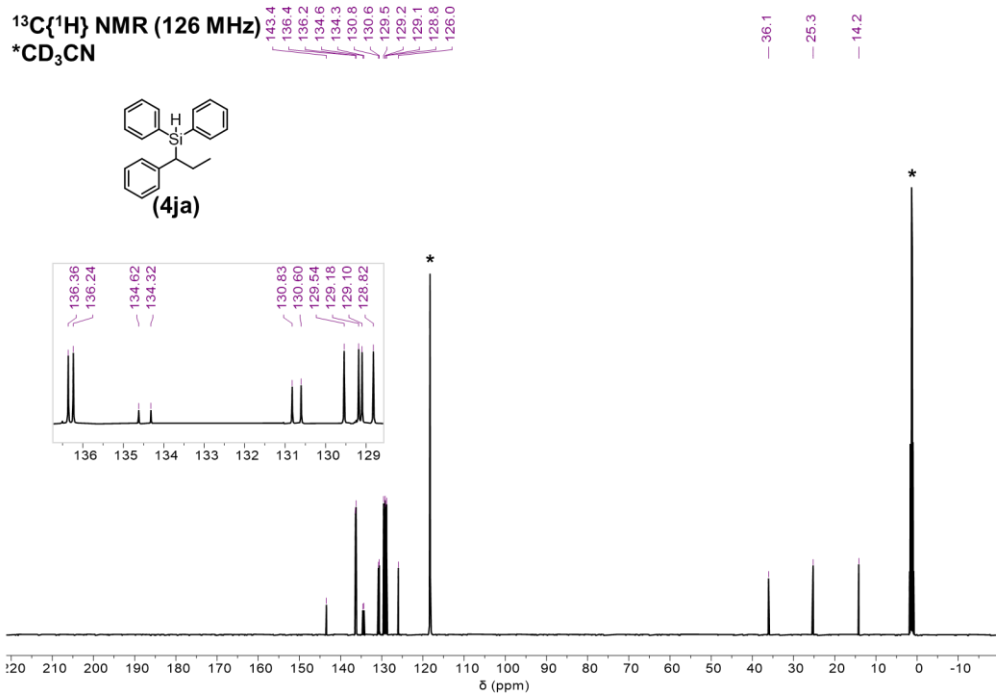

Figure A.76. $^{13}C\{^{1}H\}$ NMR spectrum of [1-phenylpropyl]diphenylsilane (**4ja**) recorded in CD_3CN at 298 K.

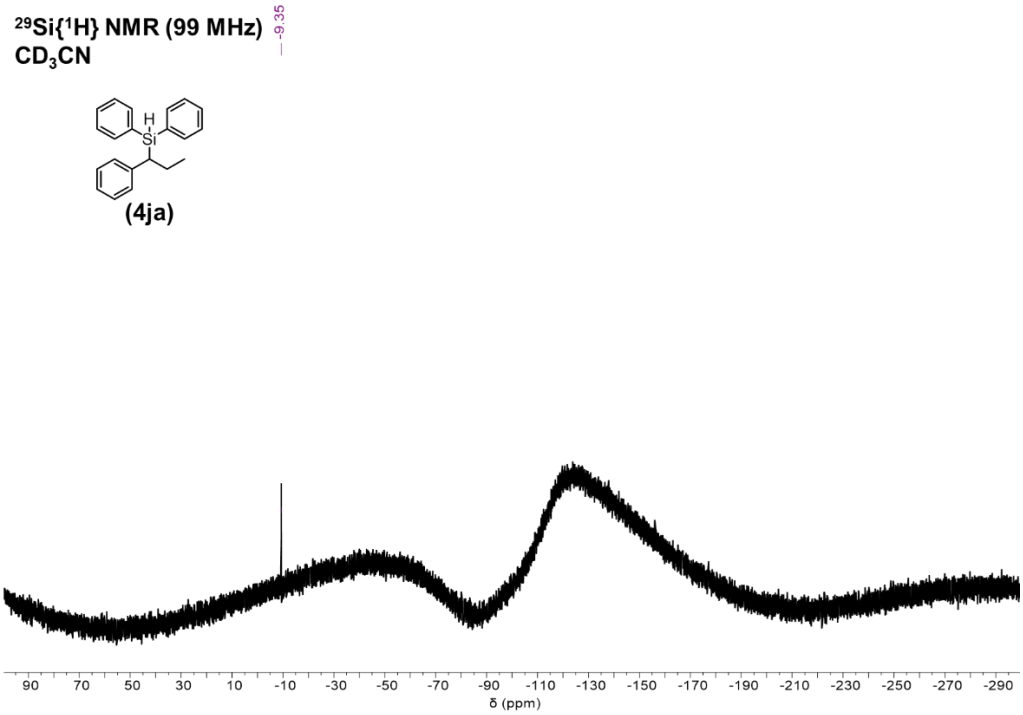

Figure A.77. $^{29}Si\{^{1}H\}$ NMR spectrum of [1-phenylpropyl]diphenylsilane (**4ja**) recorded in CD_3CN at 298 K.

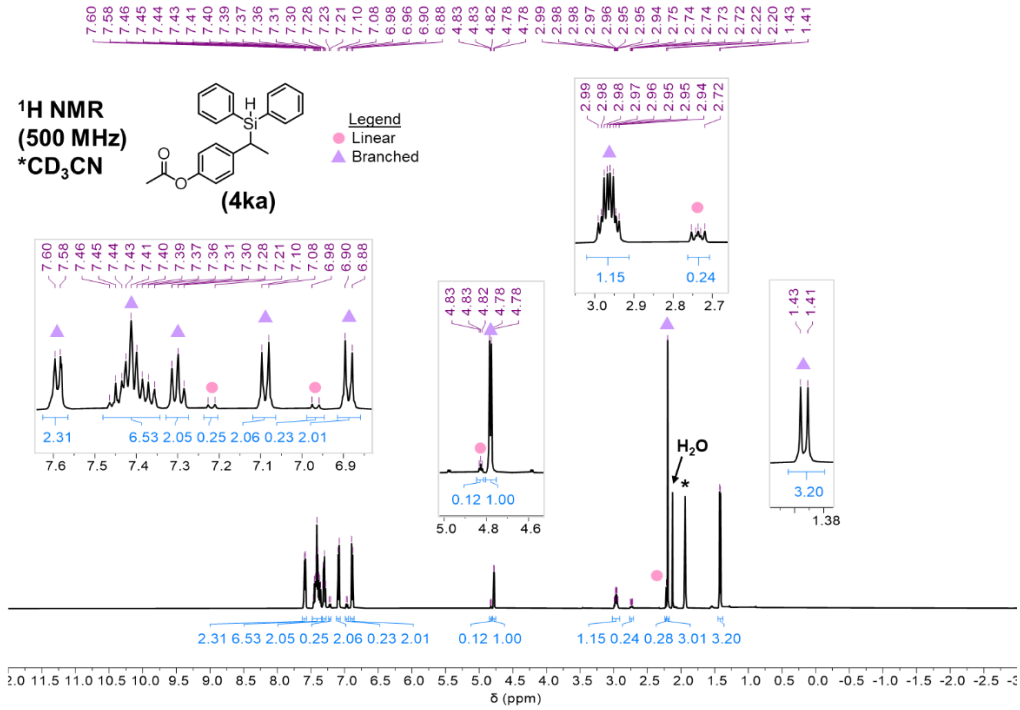

Figure A.78. ^{1}H NMR spectrum of [1-(4-acetoxyphenyl)ethyl]diphenylsilane (**4ka**) recorded in CD_3CN at 298 K.

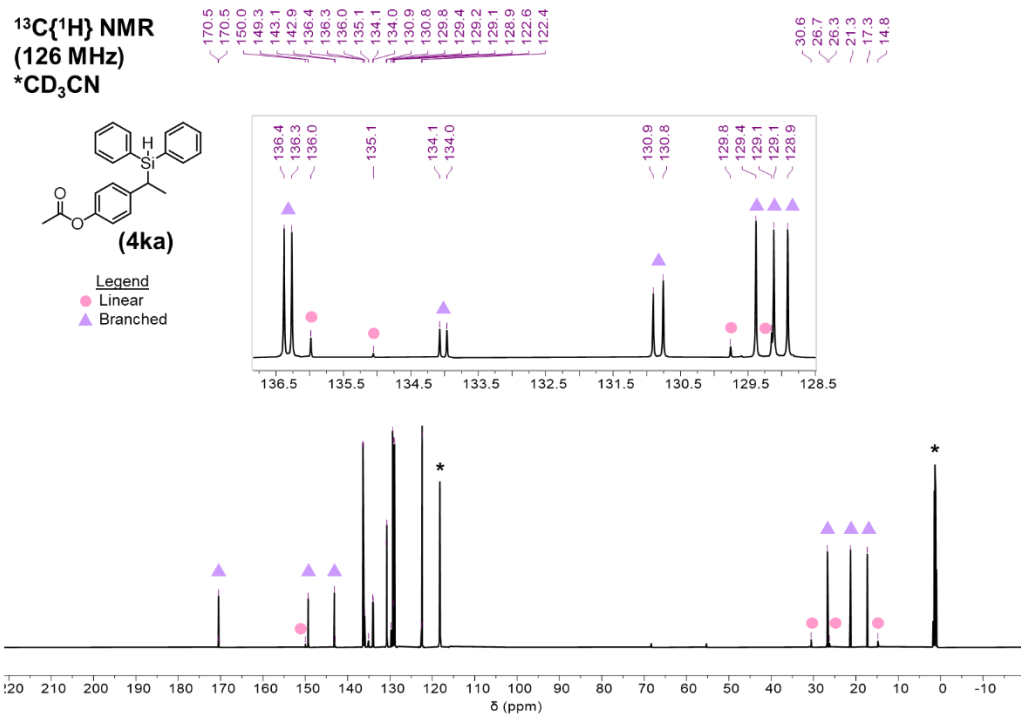

Figure A.79. $^{13}C\{^{1}H\}$ NMR spectrum of [1-(4-acetoxyphenyl)ethyl]diphenylsilane (**4ka**) recorded in CD_3CN at 298 K.

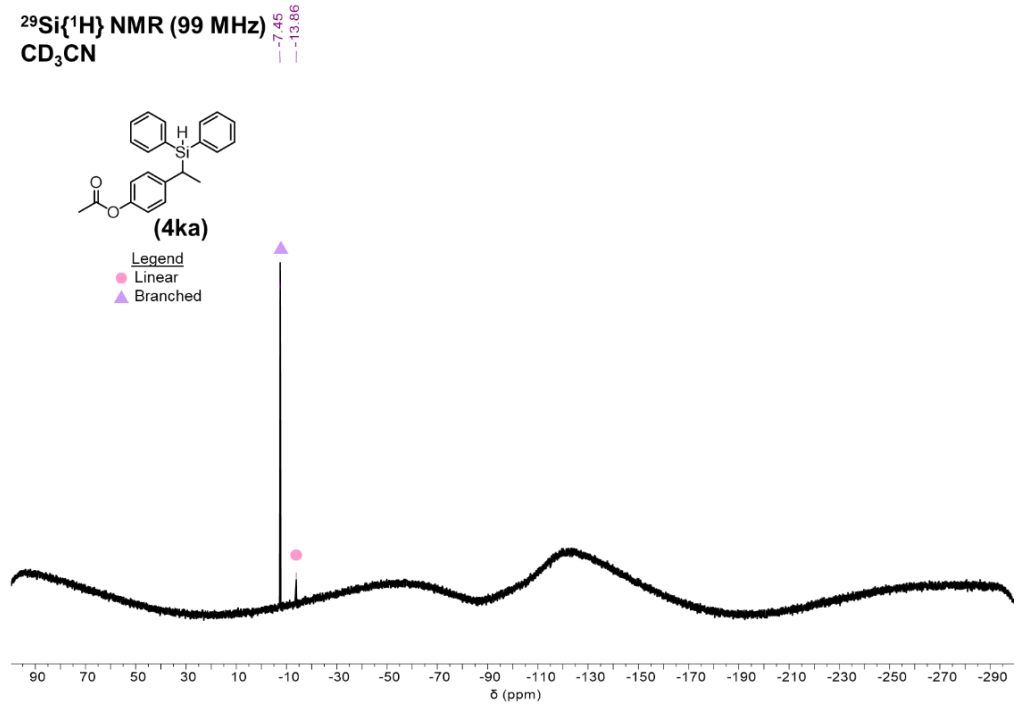

Figure A.80. $^{29}Si\{^{1}H\}$ NMR spectrum [1-(4-acetoxyphenyl)ethyl]diphenylsilane (**4ka**) recorded in CD_3CN at 298 K.

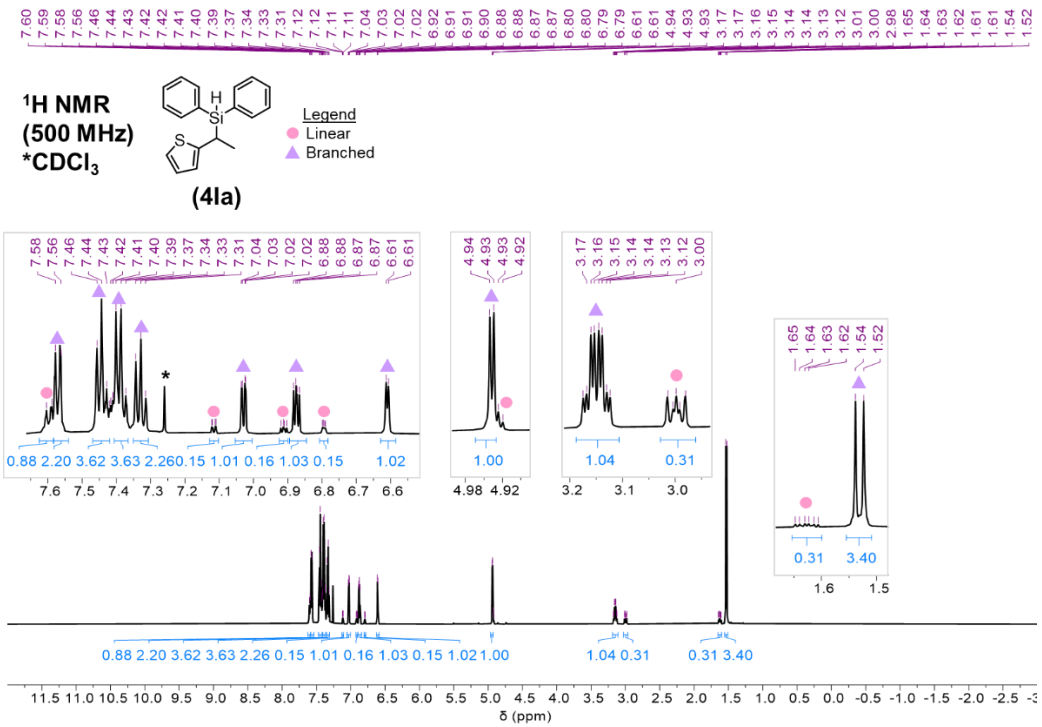

Figure A.81. ^{1}H NMR spectrum of [1-(2-thiophenyl)ethyl]diphenylsilane (**4la**) recorded in $CDCl_3$ at 298 K.

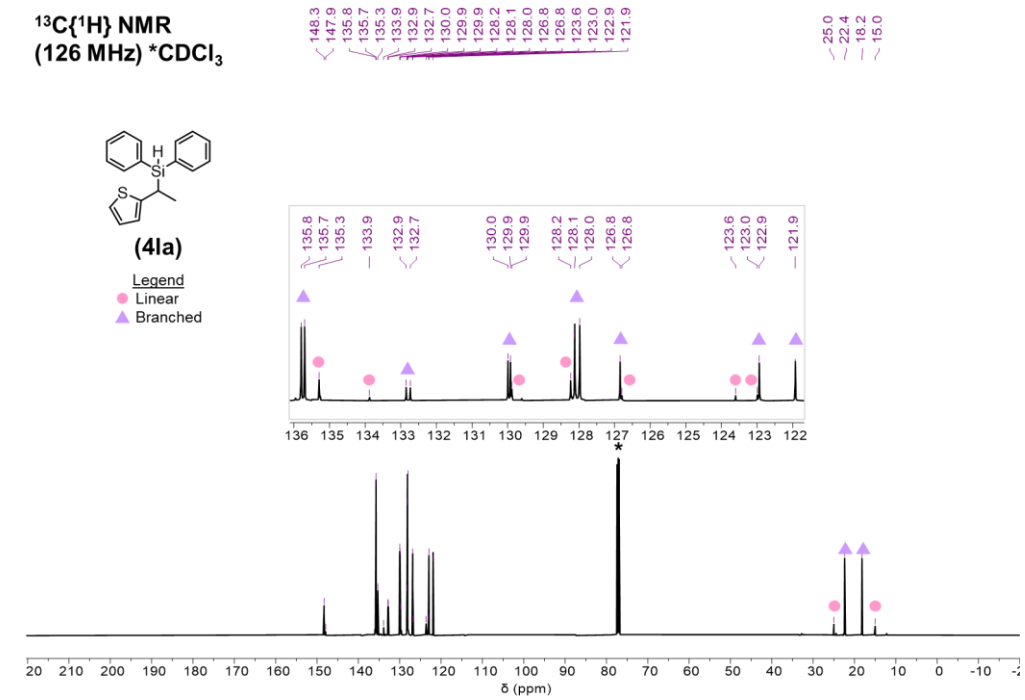

Figure A.82. ^{13}C{^{1}H} NMR spectrum of [1-(2-thiophenyl)ethyl]diphenylsilane (**4la**) recorded in $CDCl_3$ at 298 K.

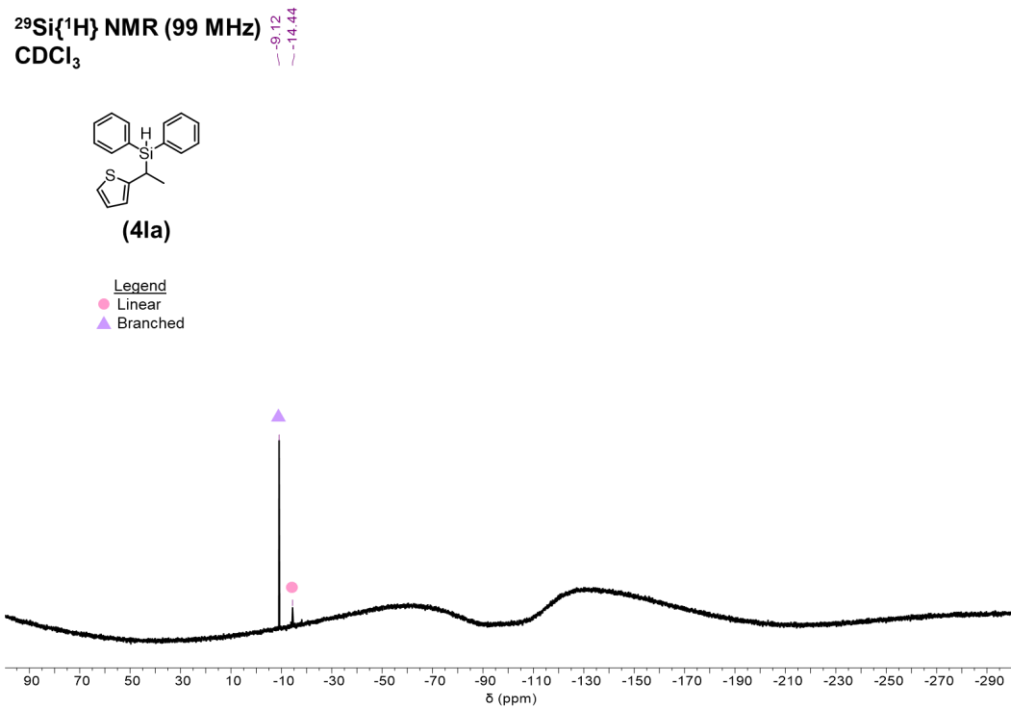

Figure A.83. $^{29}Si\{^{1}H\}$ NMR spectrum [1-(2-thiophenyl)ethyl]diphenylsilane (**4la**) recorded in $CDCl_3$ recorded in CD_3CN at 298 K.

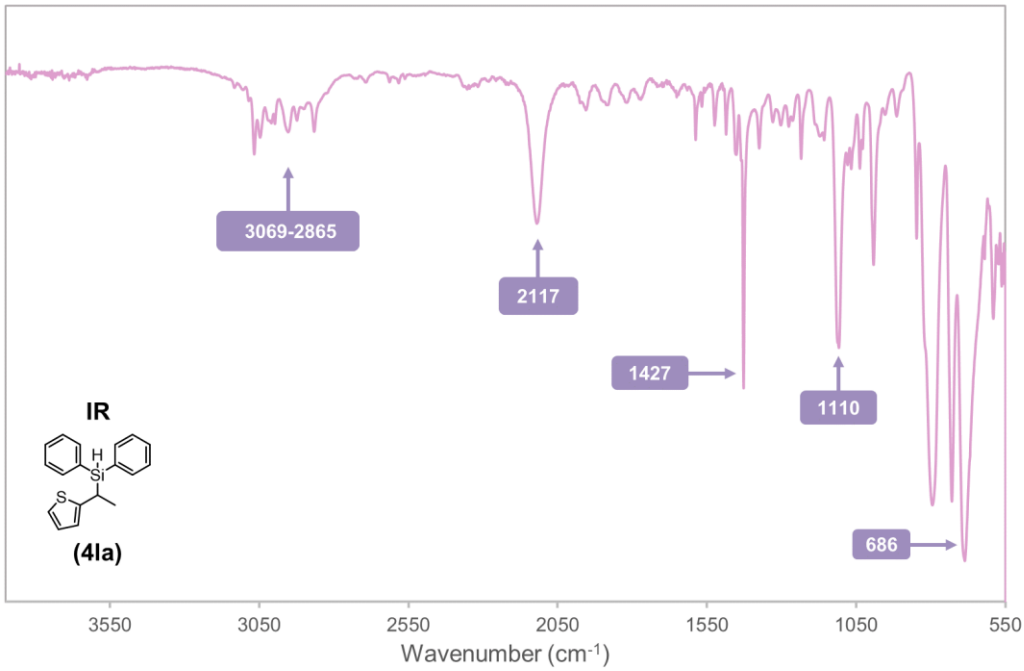

Figure A.84. IR spectrum of [1-(2-thiophenyl)ethyl]diphenylsilane (**4la**) recorded neat at 298 K.

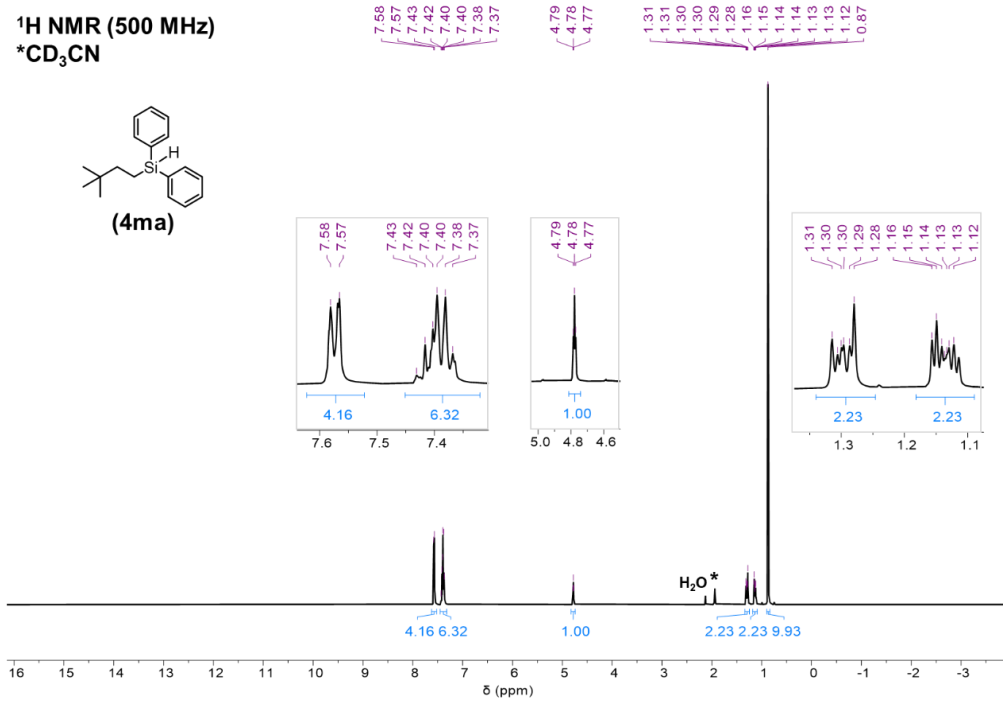

Figure A.85. ^{1}H NMR spectrum of (3,3-dimethyl-1-butyl)diphenylsilane (**4ma**) recorded in CD_3CN at 298 K.

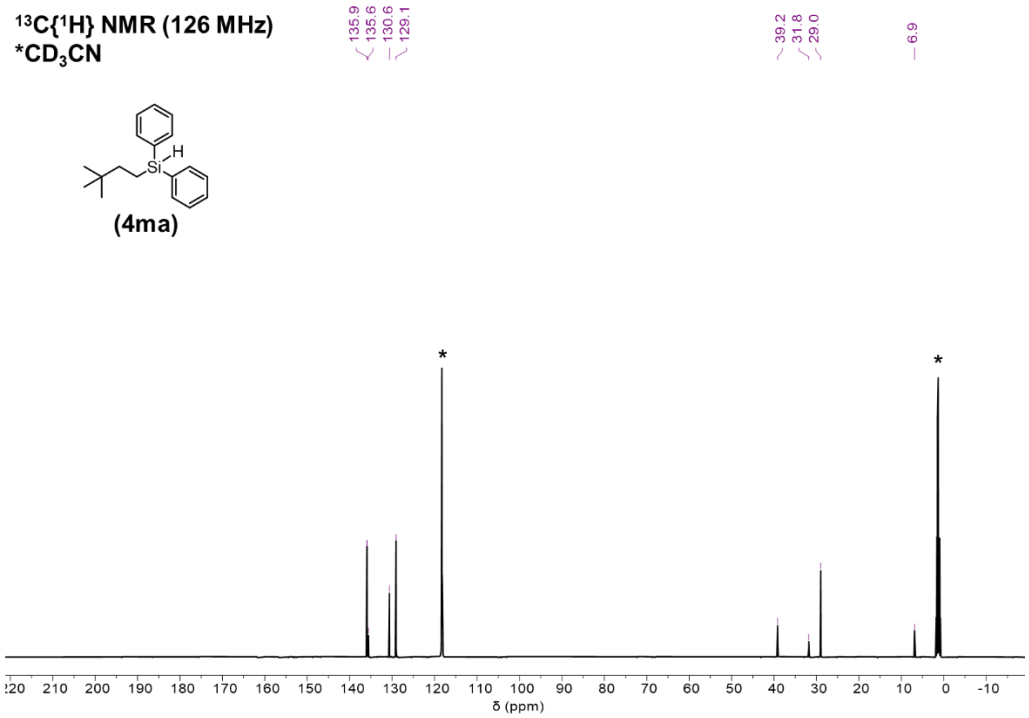

Figure A.86. $^{13}C\{^{1}H\}$ NMR spectrum of (3,3-dimethyl-1-butyl)diphenylsilane (**4ma**) recorded in CD_3CN at 298 K.

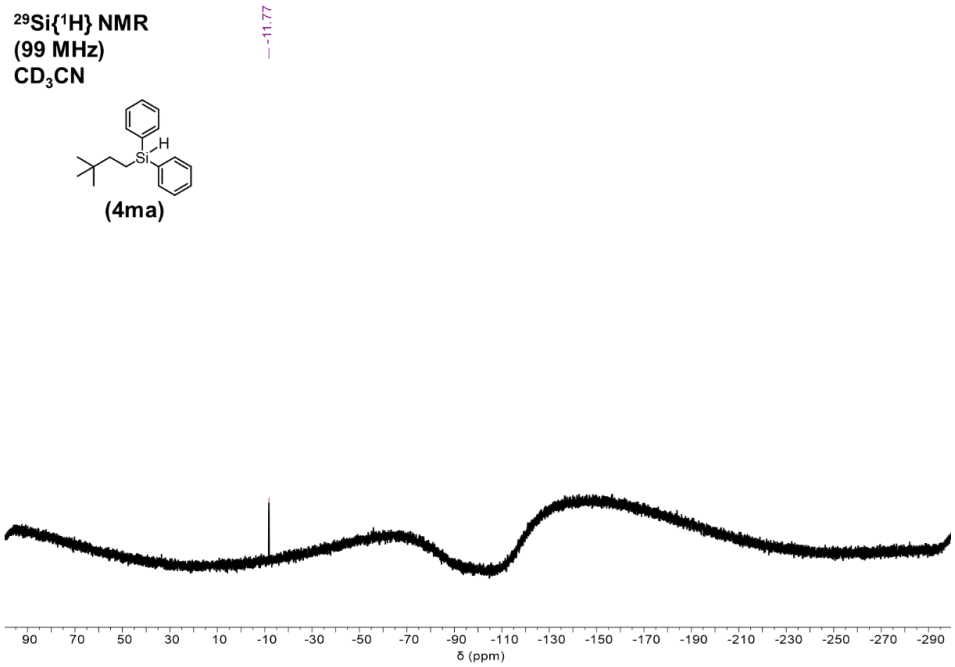

Figure A.87. ^{29}Si{^{1}H} NMR spectrum (3,3-dimethyl-1-butyl)diphenylsilane (**4ma**) recorded in CD_3CN at 298 K.

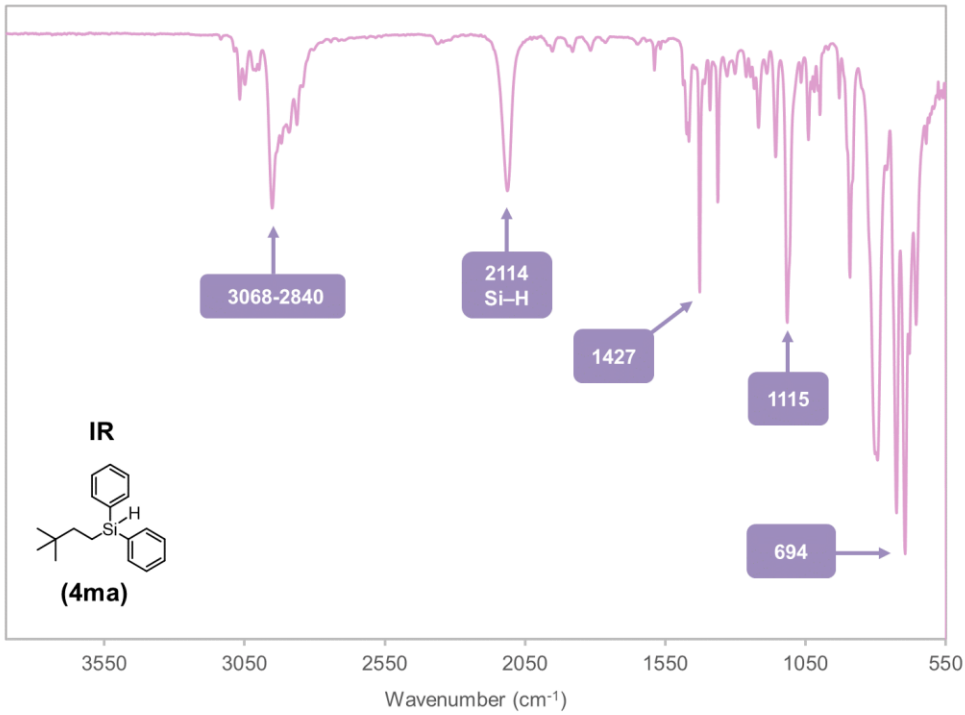

Figure A.88. IR spectrum of (3,3-dimethyl-1-butyl)diphenylsilane (**4ma**) recorded neat at 298 K.

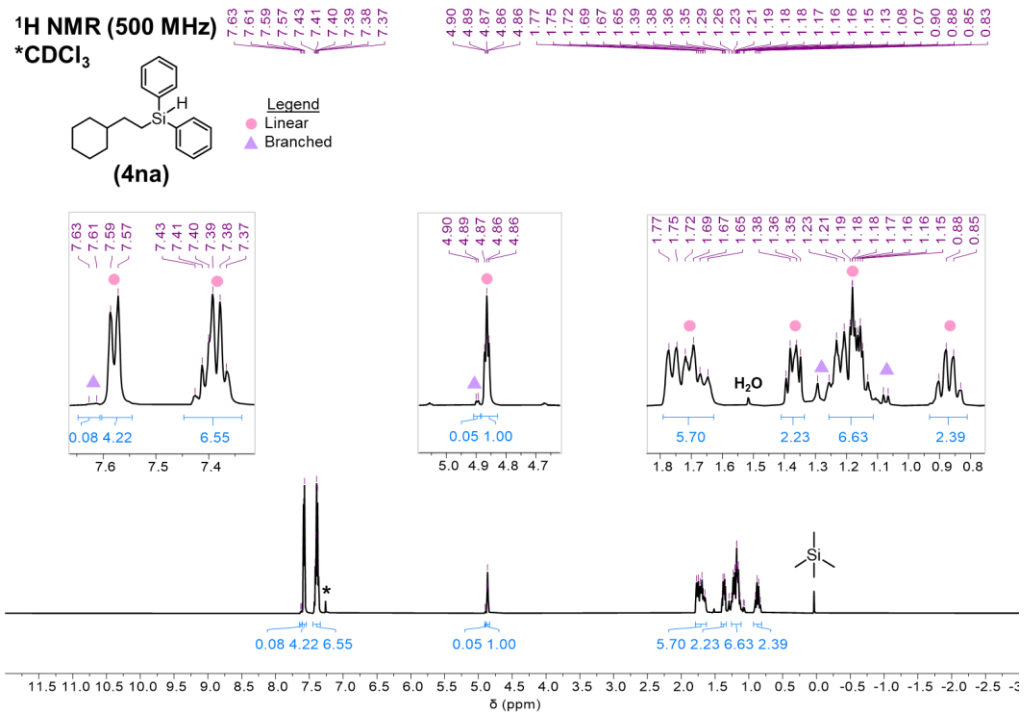

Figure A.89. ^{1}H NMR spectrum of (2-cyclohexylethyl)diphenylsilane (**4na**) recorded in CD_3CN at 298 K.

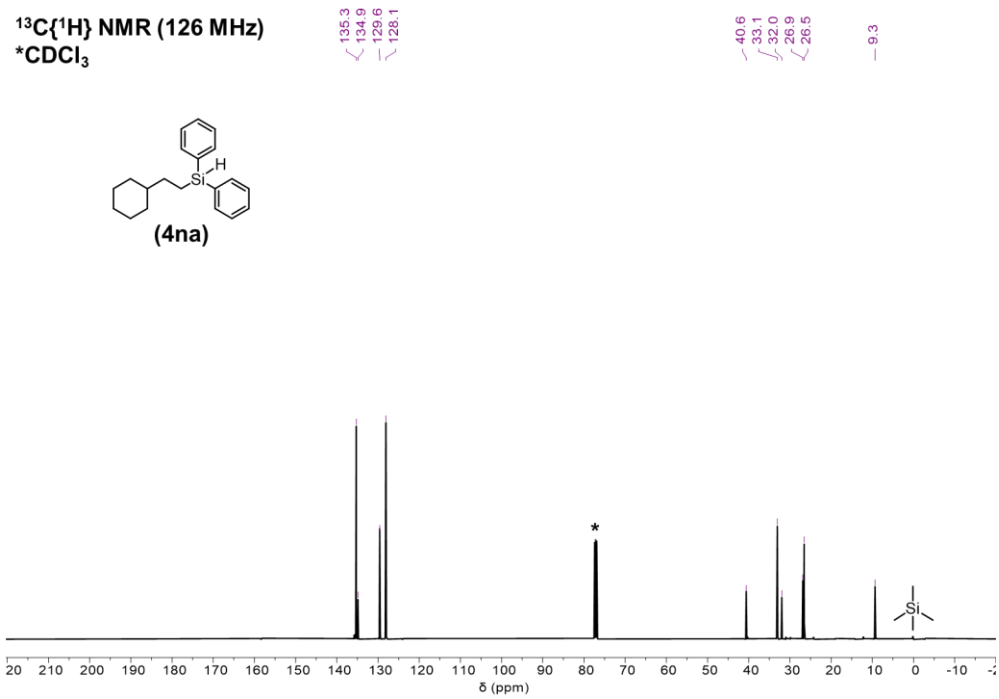

Figure A.90. ^{13}C{^{1}H} NMR spectrum of (2-cyclohexylethyl)diphenylsilane (**4na**) recorded in CD_3CN at 298 K.

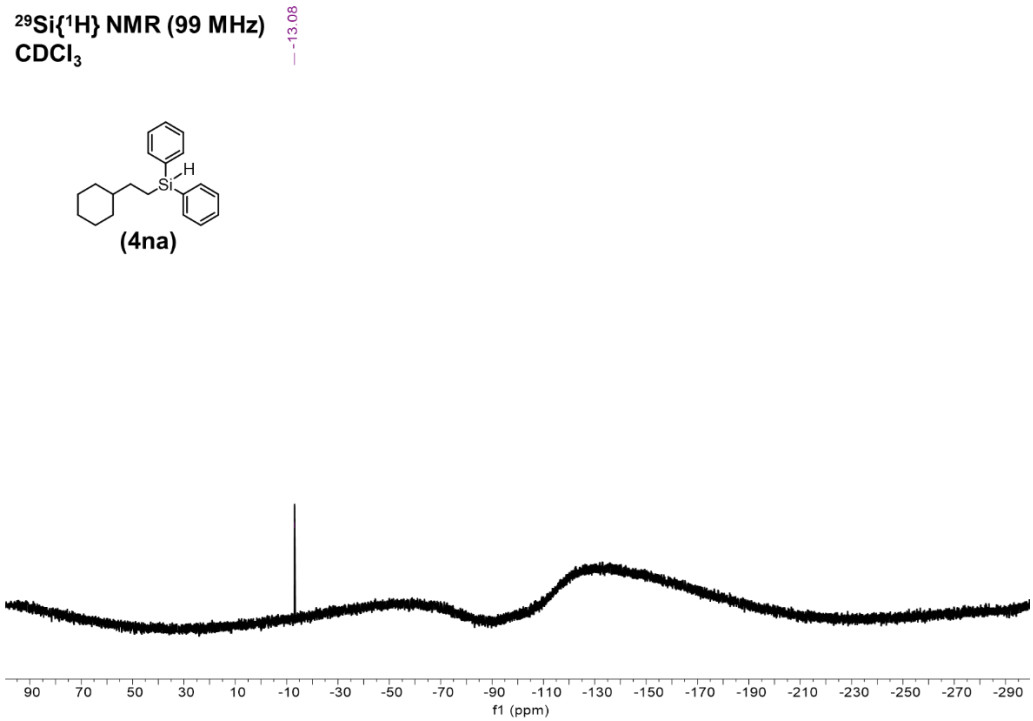

Figure A.91. $^{29}Si\{^{1}H\}$ NMR spectrum (2-cyclohexylethyl)diphenylsilane (**4na**) recorded in CD_3CN at 298 K.

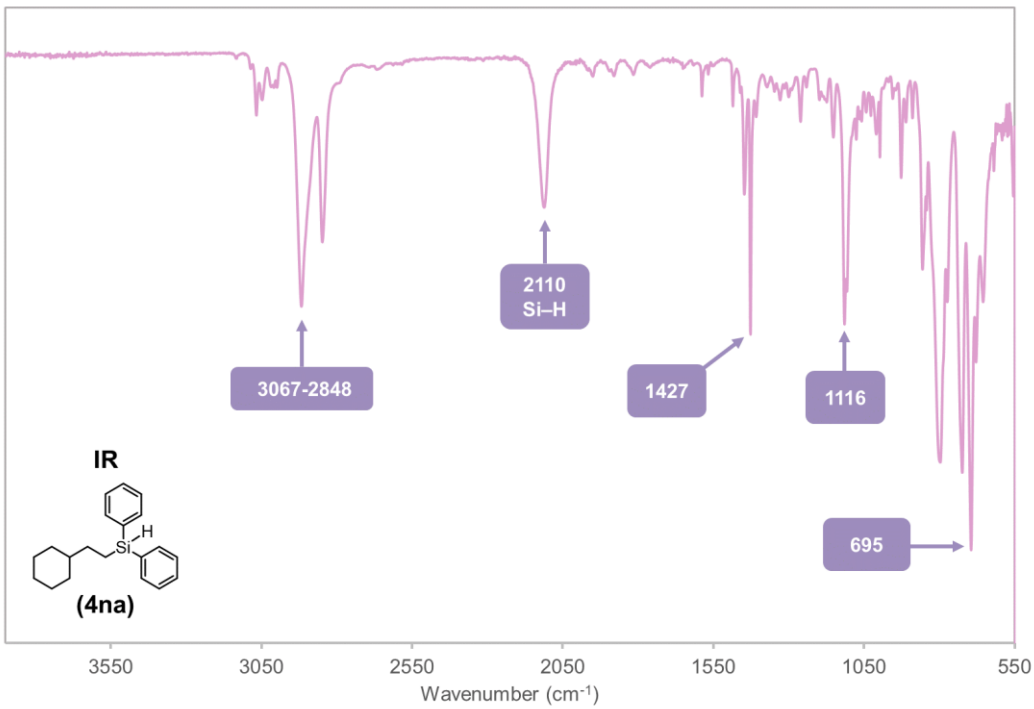

Figure A.92. IR spectrum of (2-cyclohexylethyl)diphenylsilane (**4na**) recorded neat at 298 K.

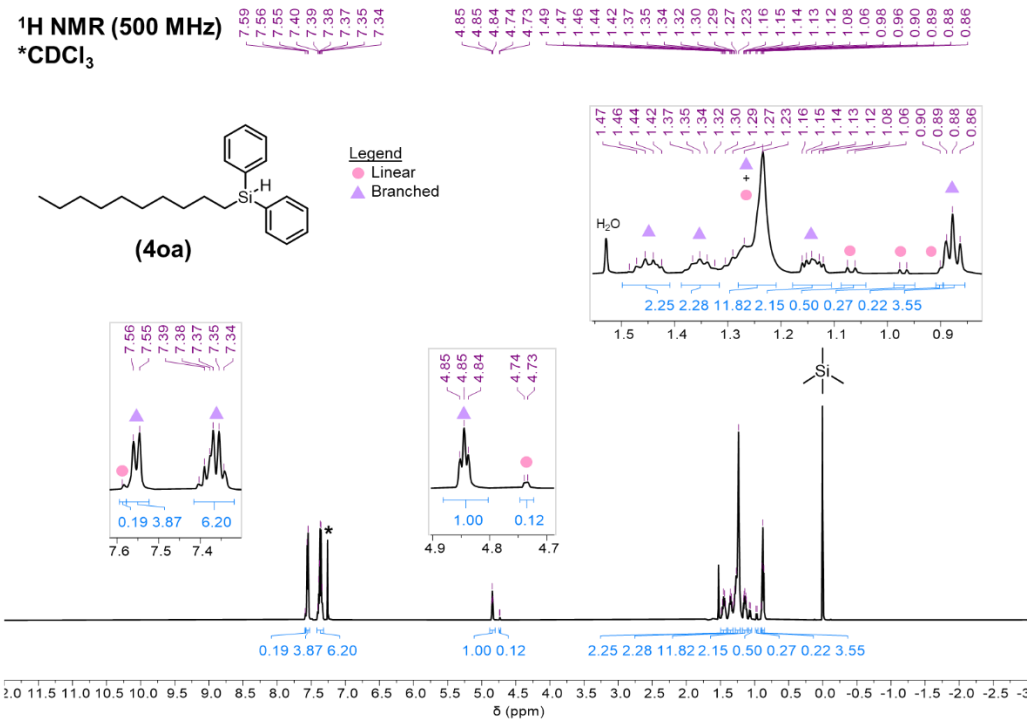

Figure A.92. ^{1}H NMR spectrum of (1-decyl)diphenylsilane (**4oa**) recorded in $CDCl_3$ at 298 K.

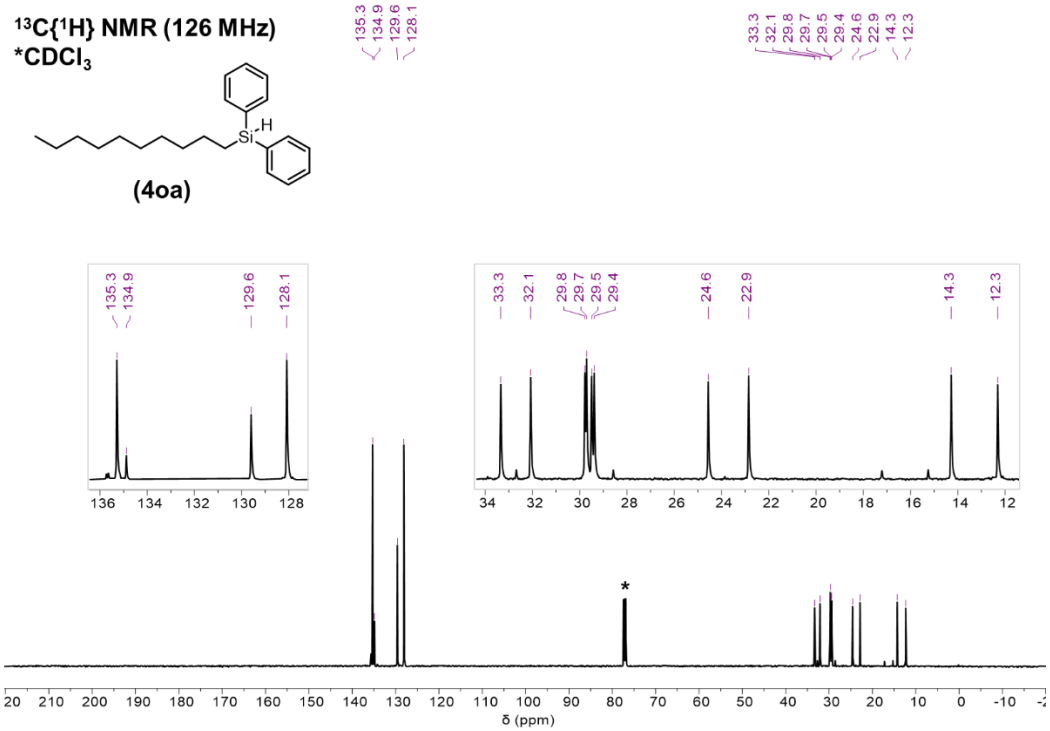

Figure A.93. ^{13}C{^{1}H} NMR spectrum of (1-decyl)diphenylsilane (**4oa**) recorded in $CDCl_3$ at 298 K.

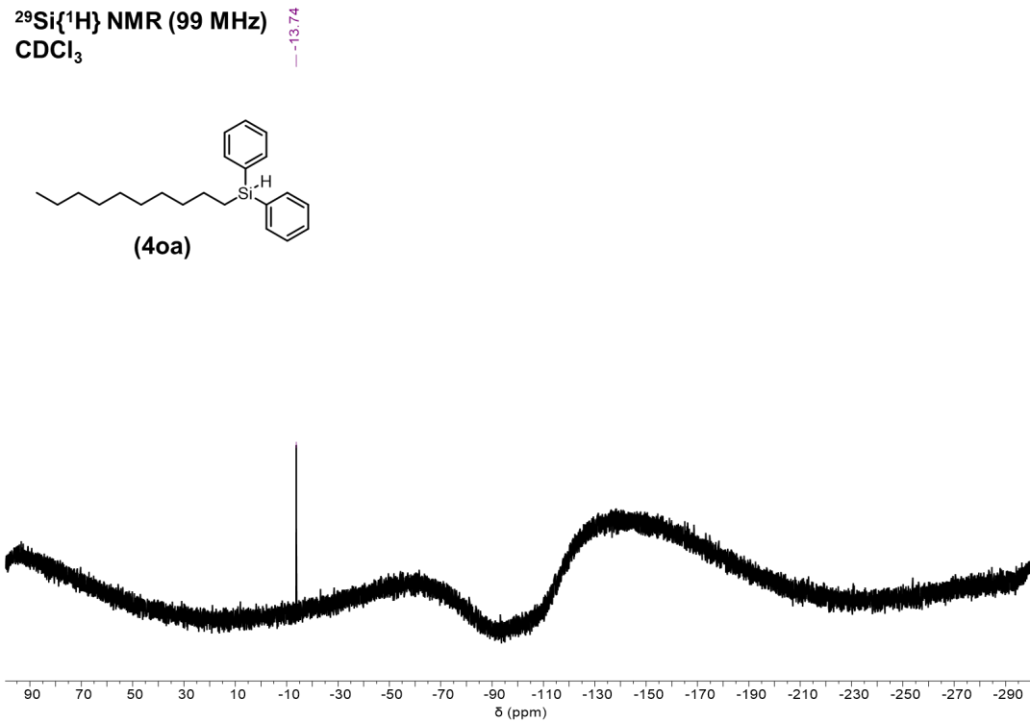

Figure A.94. $^{29}Si\{^{1}H\}$ NMR spectrum (1-decyl)diphenylsilane (**4oa**) recorded in $CDCl_3$ at 298 K.

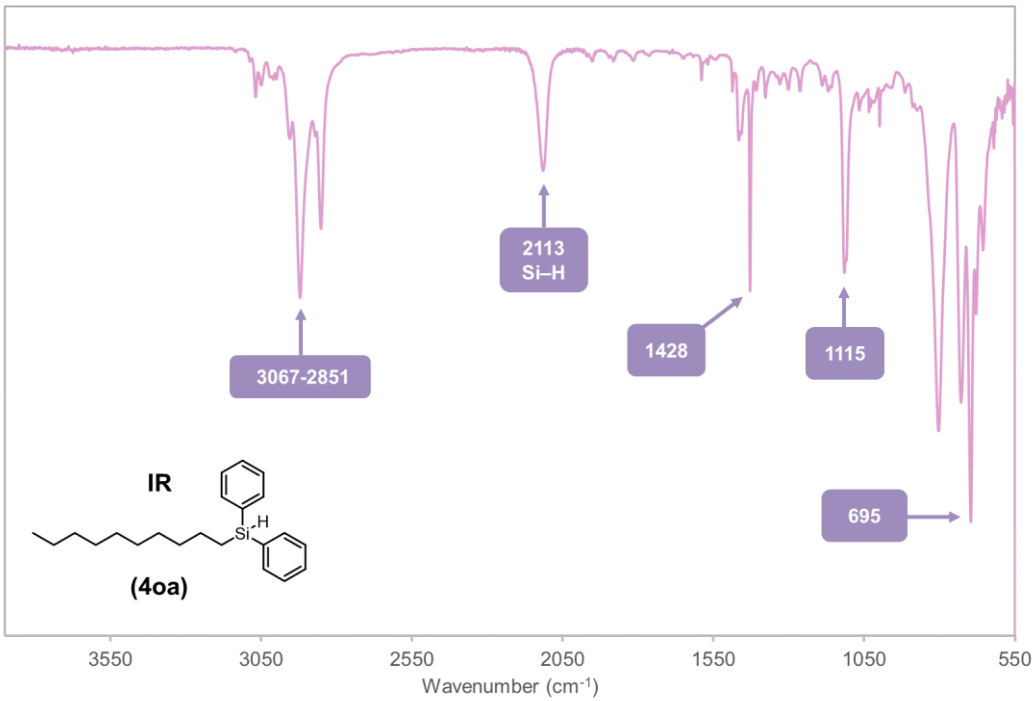

Figure A.95. IR spectrum of (1-decyl)diphenylsilane (**4oa**) recorded neat at 298 K.

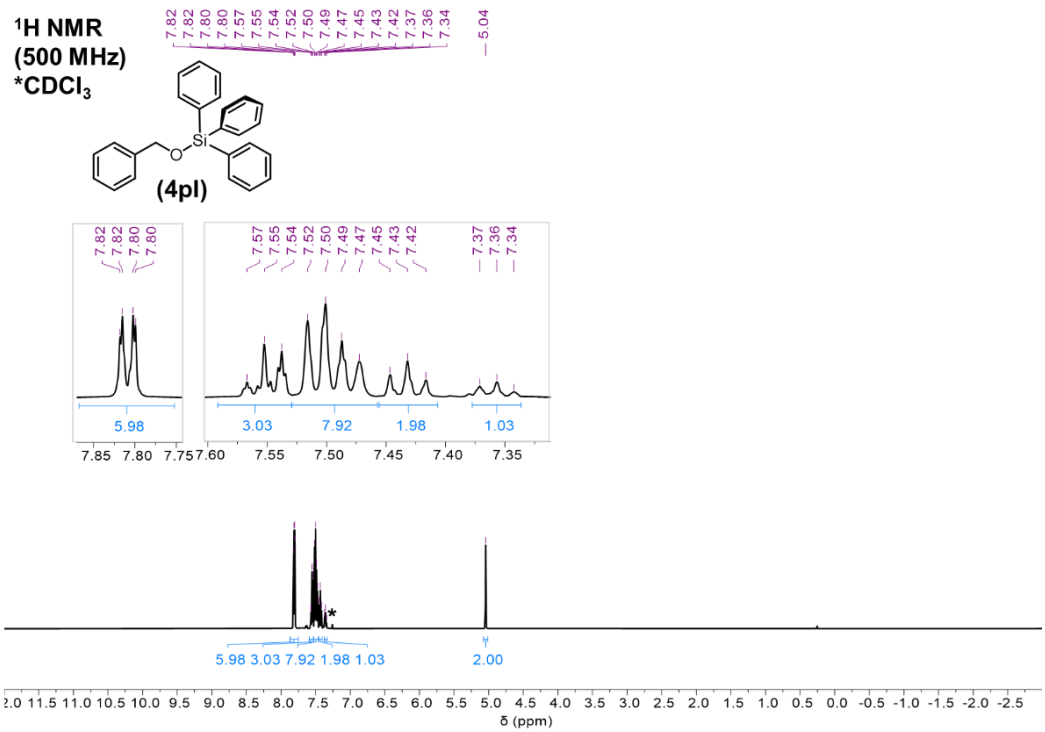

Figure A.96. ^{1}H NMR spectrum of benzyloxytriphenylsilane (**4pl**) recorded in $CDCl_3$ at 298 K.

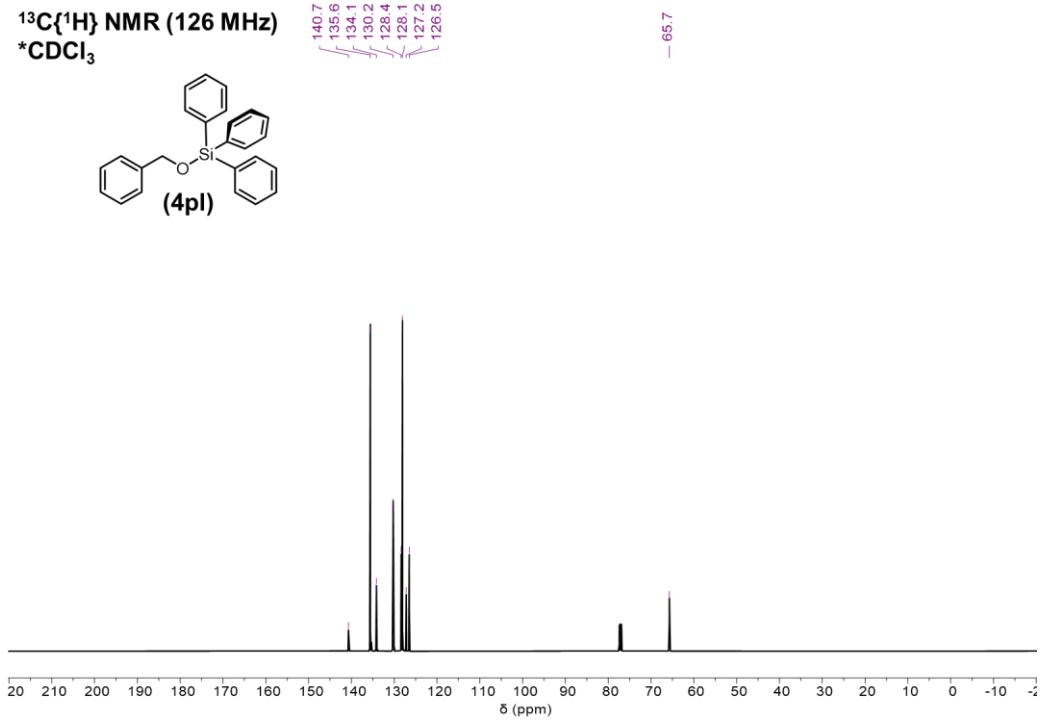

Figure A.97. $^{13}C\{^{1}H\}$ NMR spectrum of benzyloxytriphenylsilane (**4pl**) recorded in CD_3CN at 298 K.

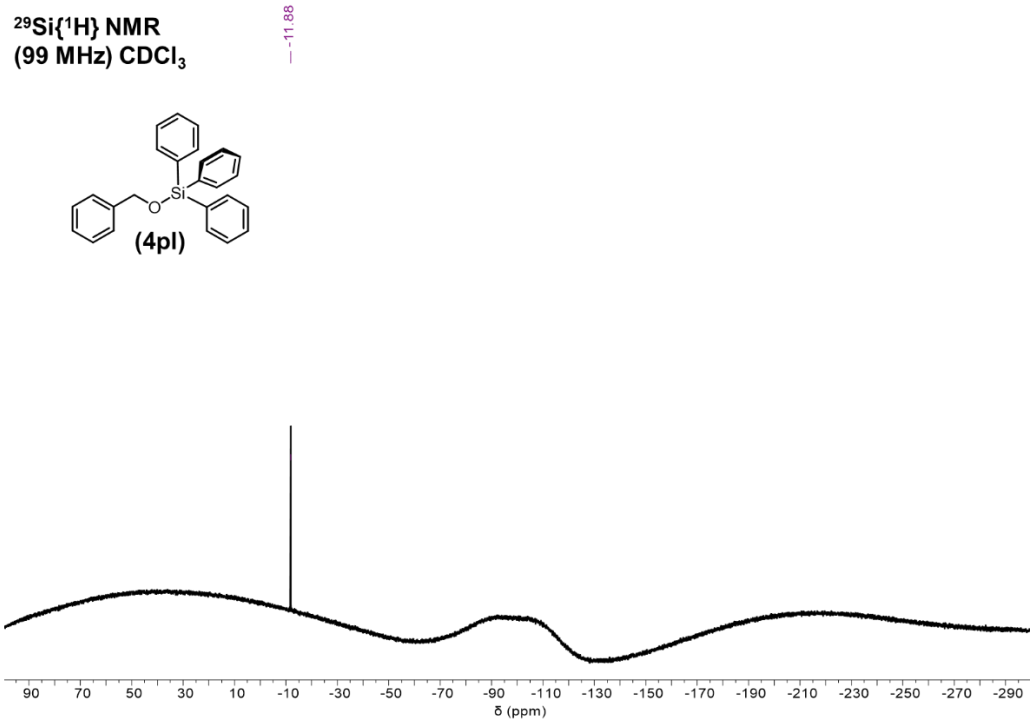

Figure A.98. $^{29}Si\{^{1}H\}$ NMR spectrum benzyloxytriphenylsilane (**4pl**) recorded in CD_3CN at 298 K.

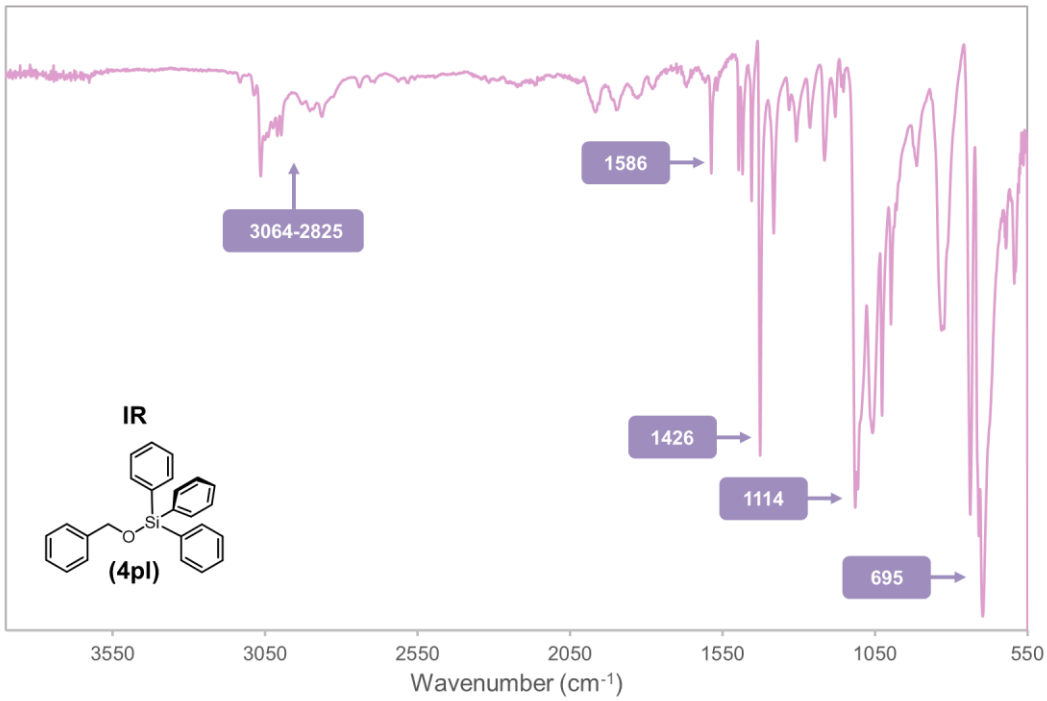

Figure A.99. IR spectrum of benzyloxytriphenylsilane (**4pl**) recorded neat at 298 K.

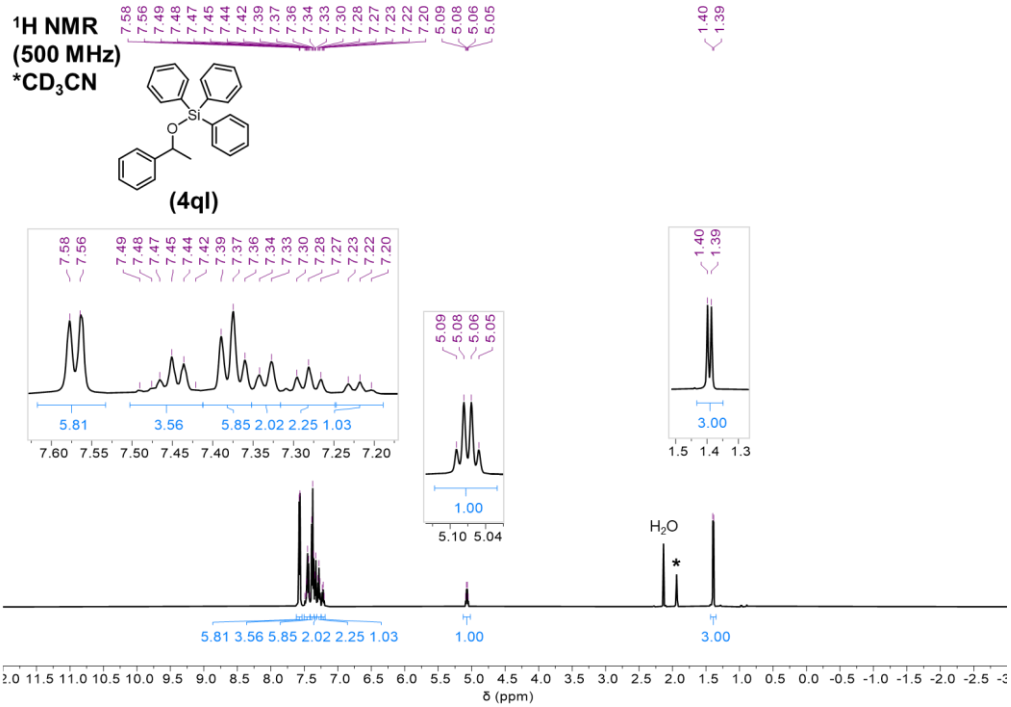

Figure A.100. ^{1}H NMR spectrum of (1-phenylethoxy)triphenylsilane (**4ql**) recorded in CD_3CN at 298 K.

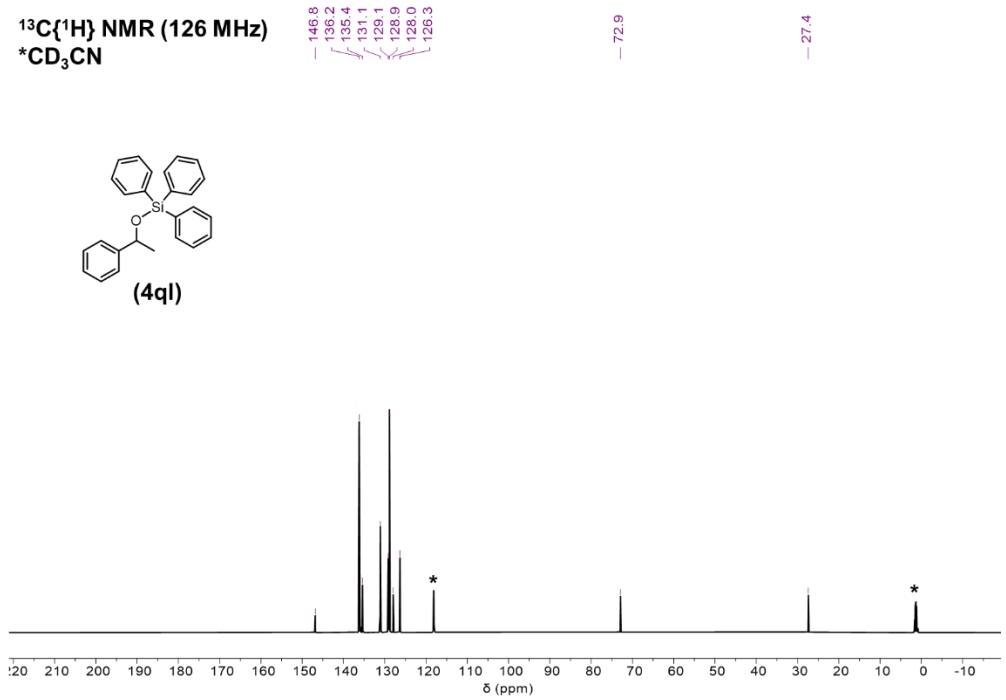

Figure A.101. $^{13}C\{^{1}H\}$ NMR spectrum of (1-phenylethoxy)triphenylsilane (**4ql**) recorded in CD_3CN at 298 K.

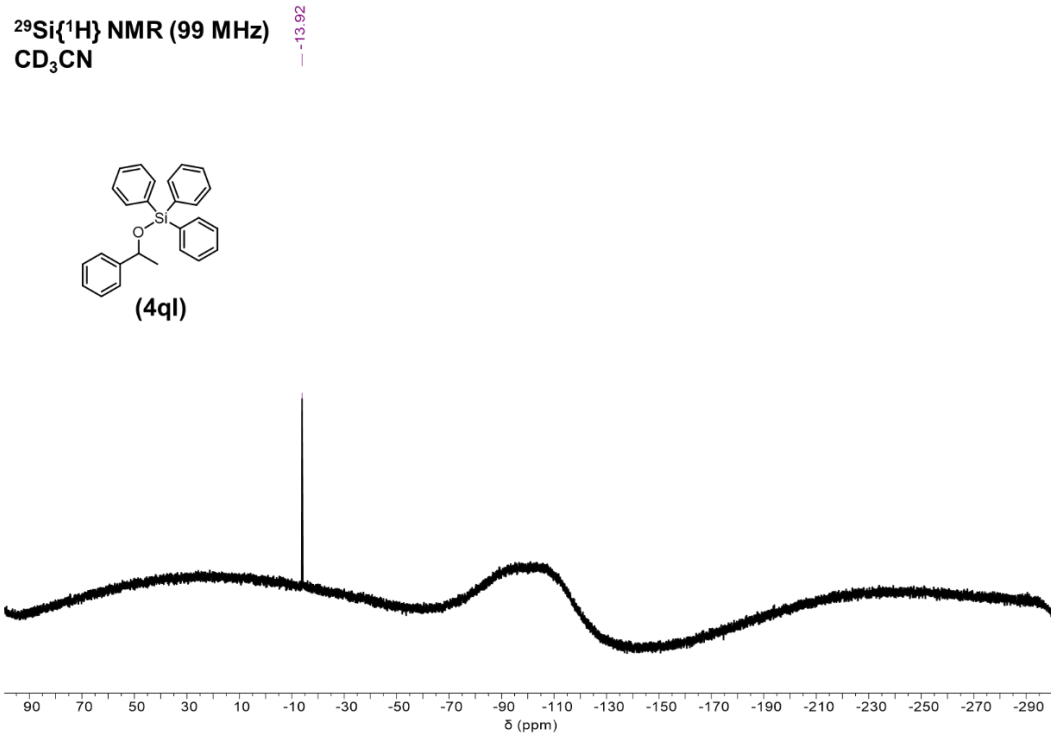

Figure A.102. $^{29}Si\{^{1}H\}$ NMR spectrum (1-phenylethoxy)triphenylsilane (**4ql**) recorded in CD_3CN at 298 K.

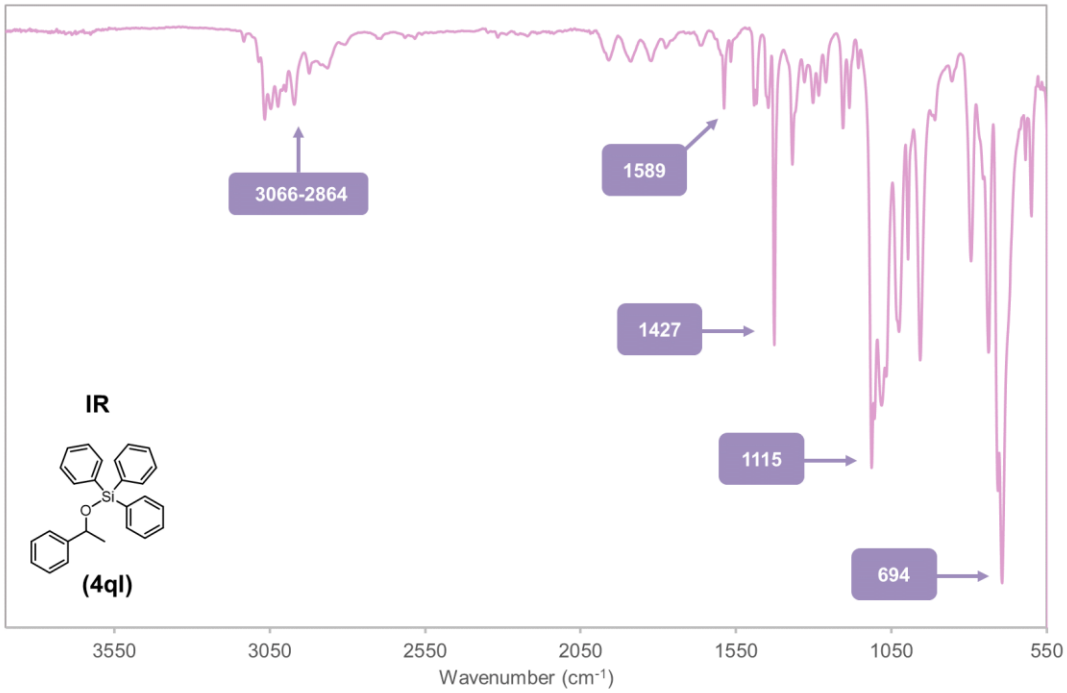

Figure A.103. IR spectrum of (1-phenylethoxy)triphenylsilane (**4ql**) recorded neat at 298 K.

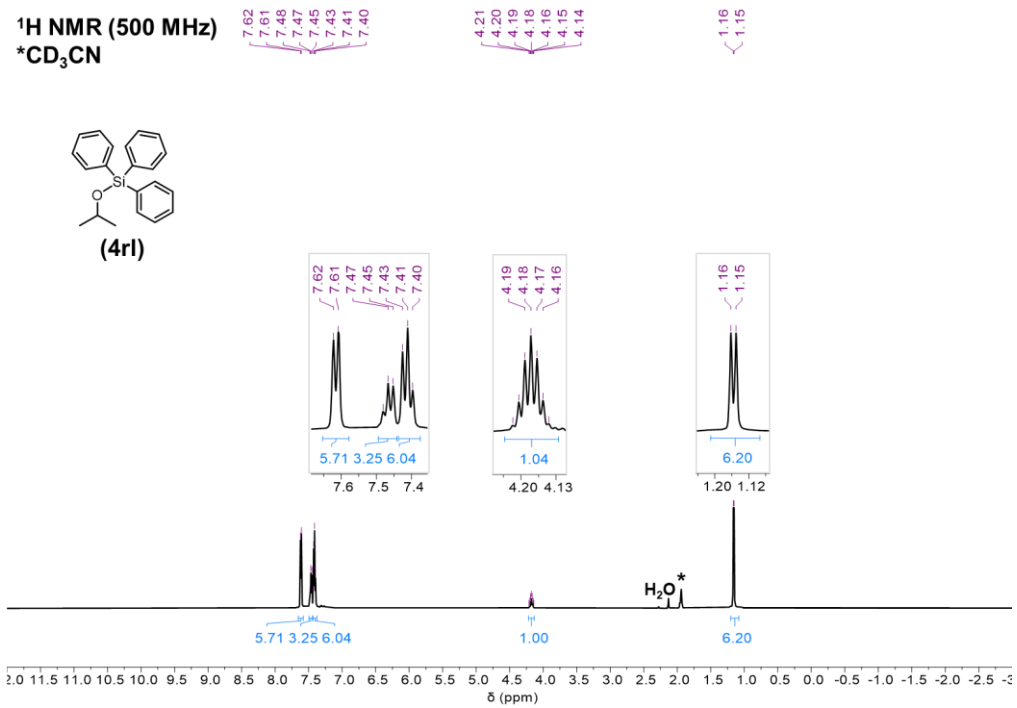

Figure A.104. ^{1}H NMR spectrum of isopropoxytriphenylsilane (**4rl**) recorded in CD_3CN at 298 K.

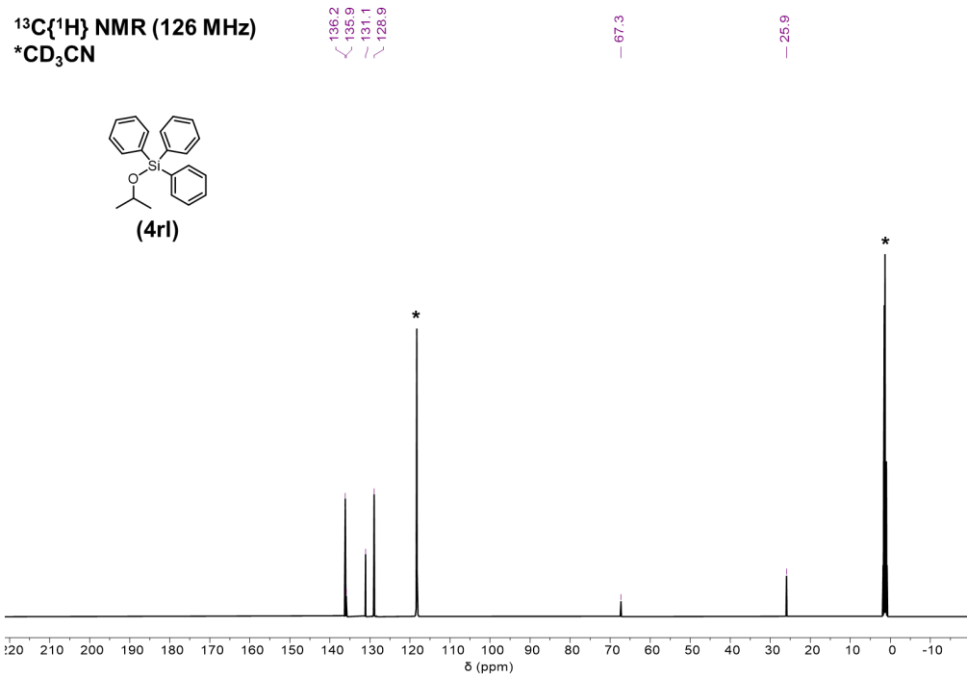

Figure A.105. $^{13}C\{^{1}H\}$ NMR spectrum of isopropoxytriphenylsilane (**4rl**) recorded in CD_3CN at 298 K.

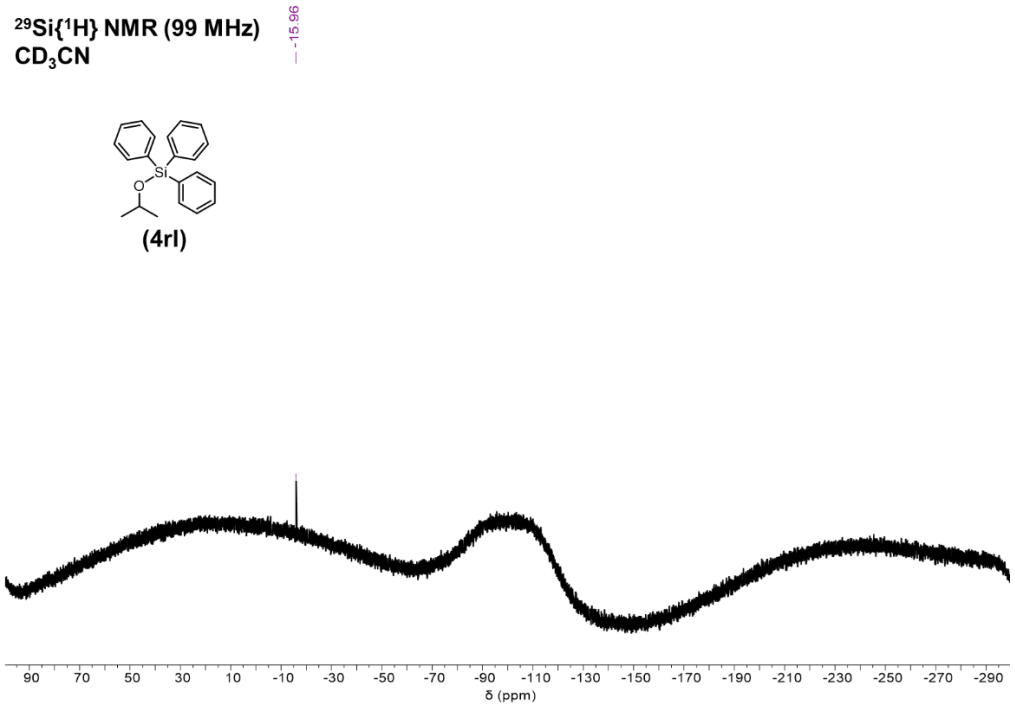

Figure A.106. $^{29}Si\{^{1}H\}$ NMR spectrum isopropoxytriphenylsilane (**4rl**) recorded in CD_3CN at 298 K.

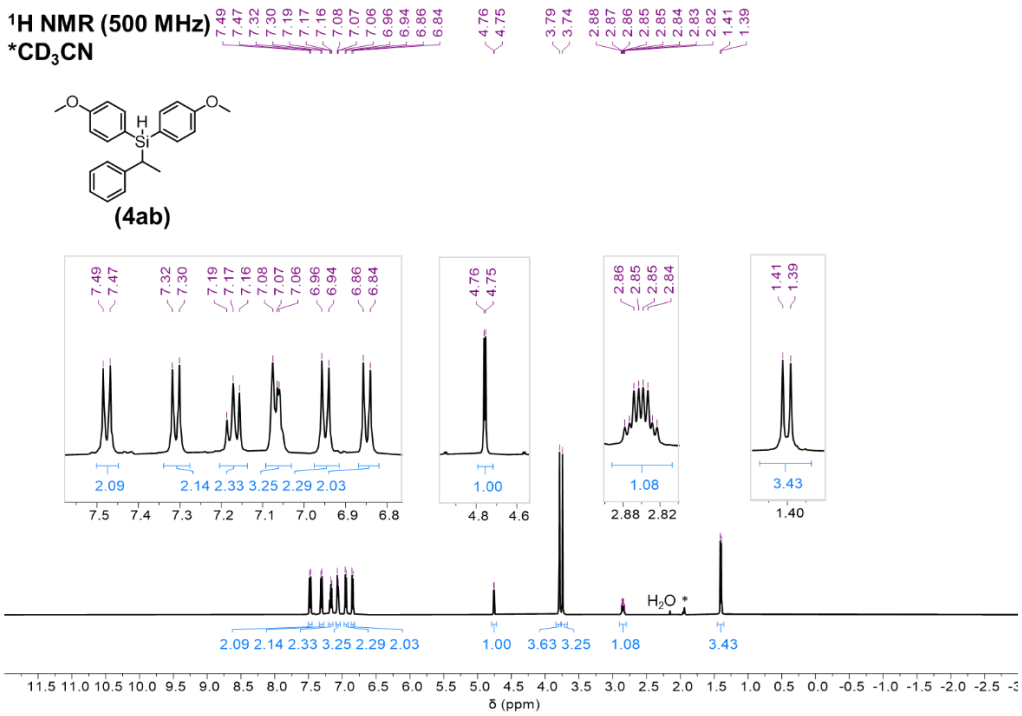

Figure A.107. ^{1}H NMR spectrum of (1-phenylethyl)di(4-methoxyphenyl)silane (**4ab**) recorded in CD_3CN at 298 K.

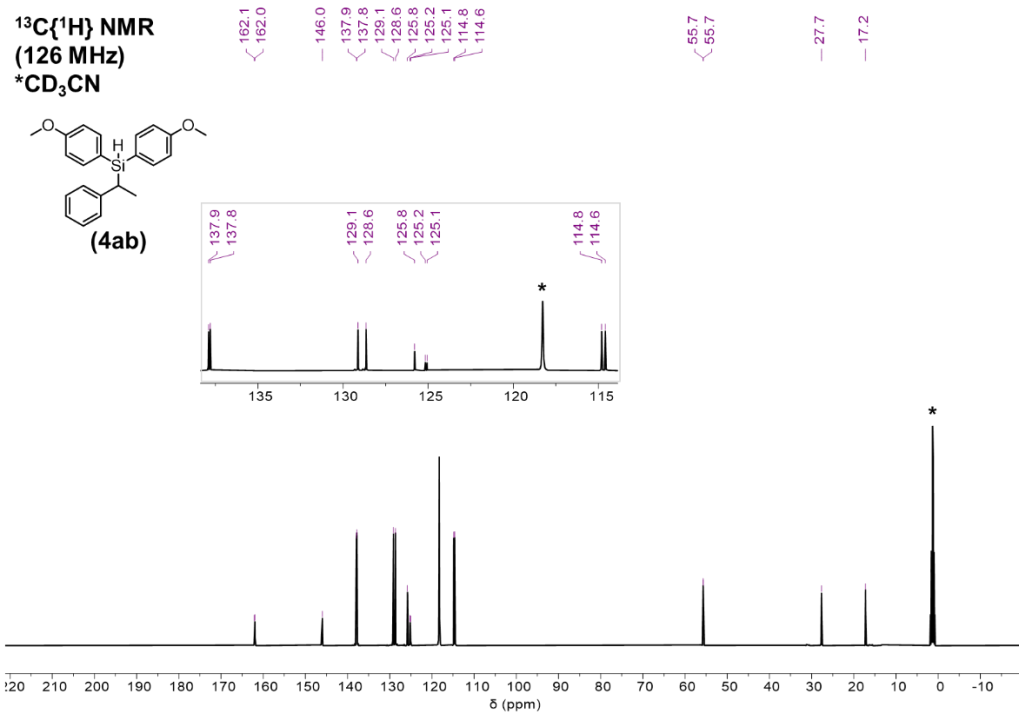

Figure A.108. $^{13}C\{^{1}H\}$ NMR spectrum of (1-phenylethyl)di(4-methoxyphenyl)silane (**4ab**) recorded in CD_3CN at 298 K.

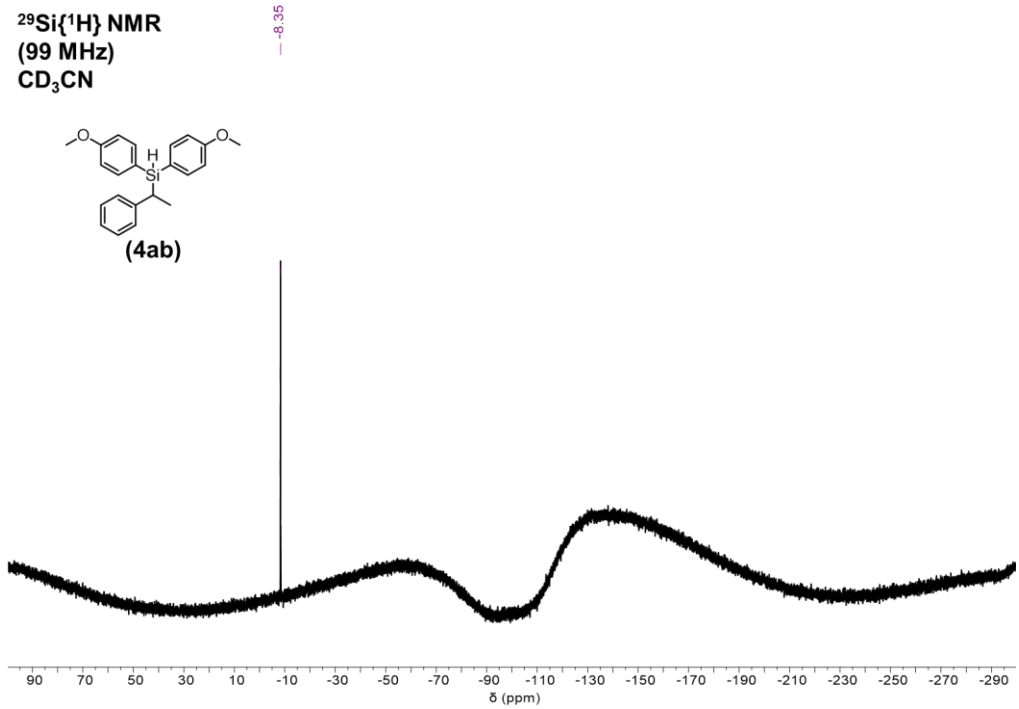

Figure A.109. $^{29}Si\{^{1}H\}$ NMR spectrum (1-phenylethyl)di(4-methoxyphenyl)silane (**4ab**) recorded in CD_3CN at 298 K.

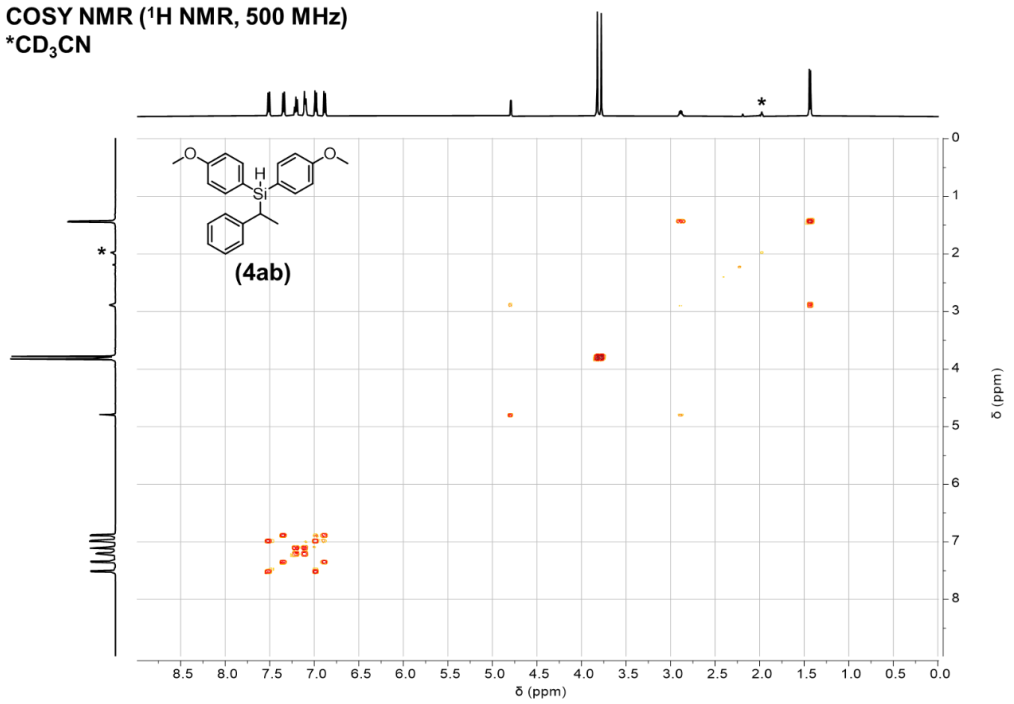

Figure A.110. COSY NMR spectrum of (1-phenylethyl)di(4-methoxyphenyl)silane (**4ab**) recorded in CD_3CN at 298 K.

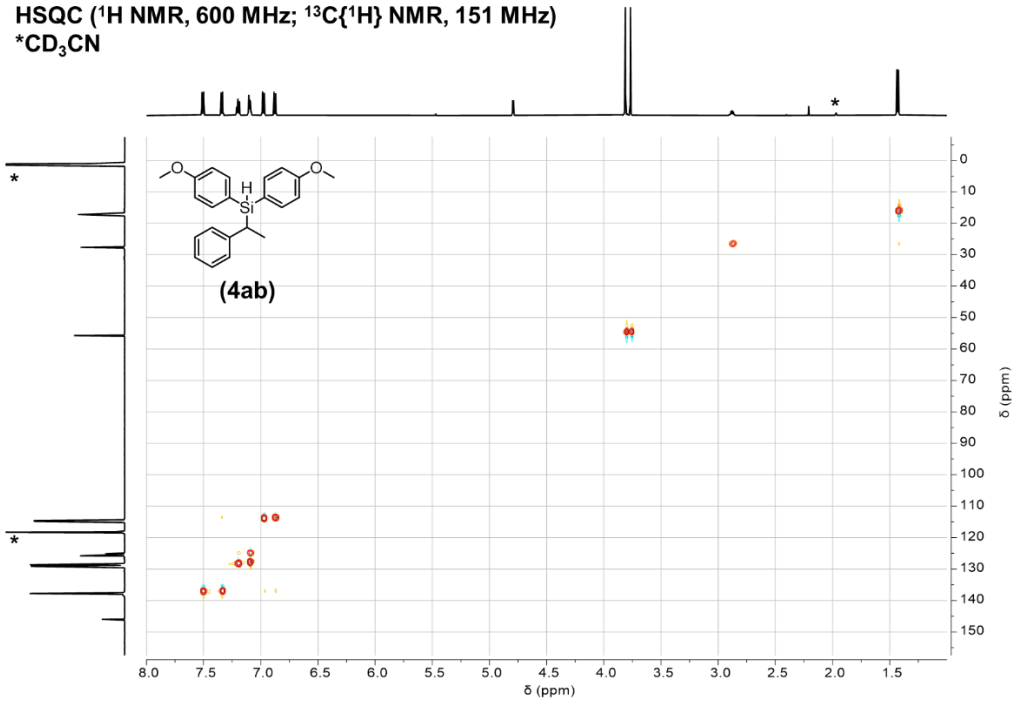

Figure A.111. HSQC NMR spectrum of (1-phenylethyl)di(4-methoxyphenyl)silane (**4ab**) recorded in CD_3CN at 298 K.

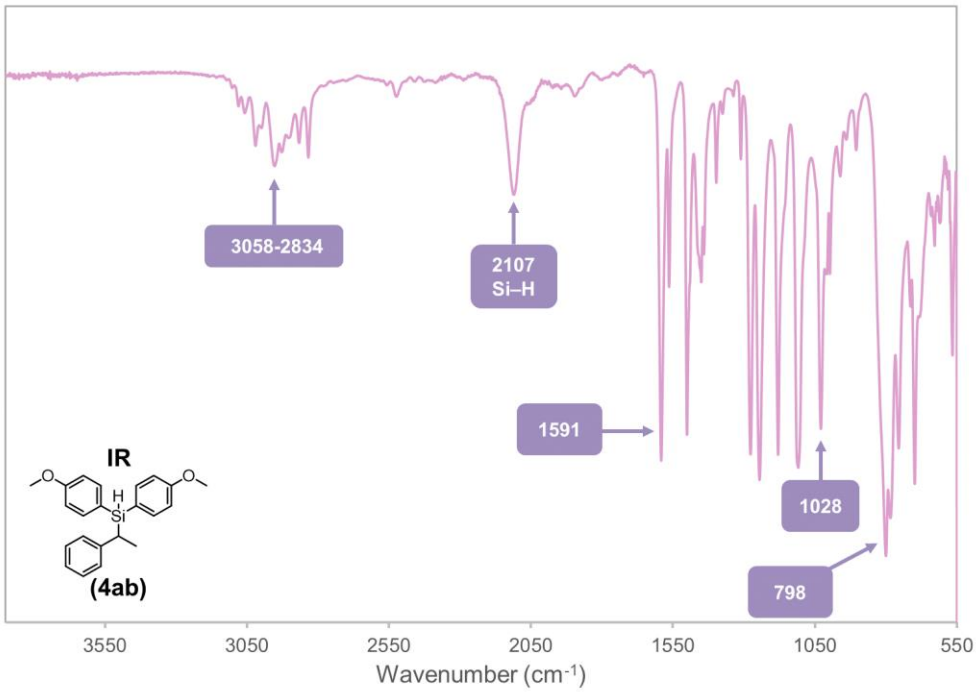

Figure A.112. IR spectrum of (1-phenylethyl)di(4-methoxyphenyl)silane (**4ab**) recorded neat at 298 K.

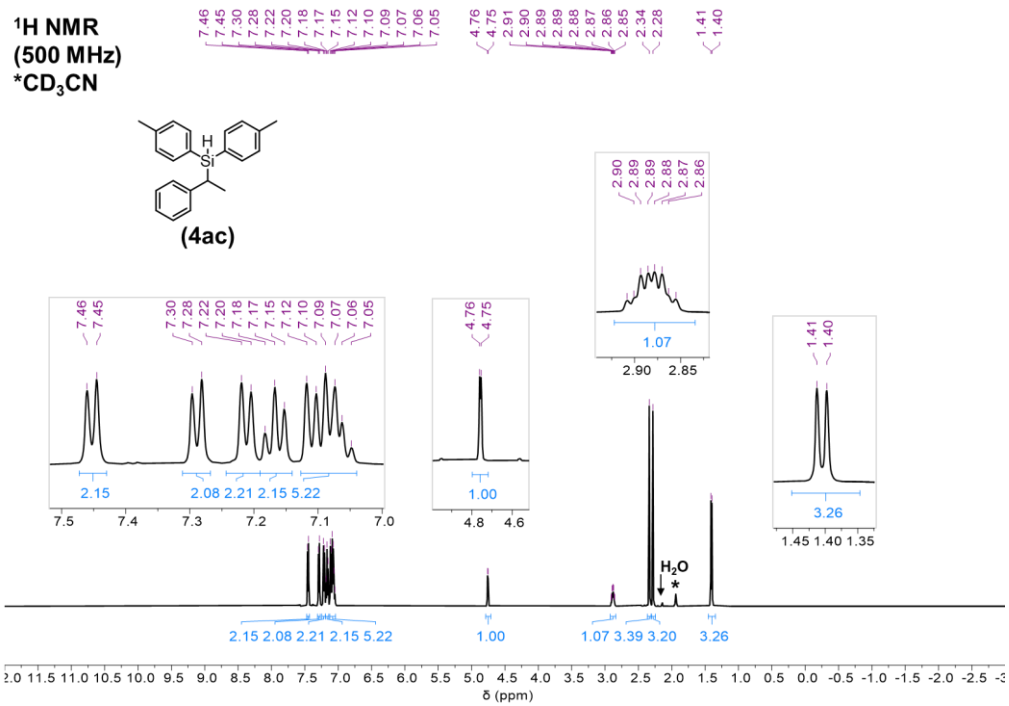

Figure A.113. ^{1}H NMR spectrum of (1-phenylethyl)di(4-methylphenyl)silane (**4ac**) recorded in CD_3CN at 298 K.

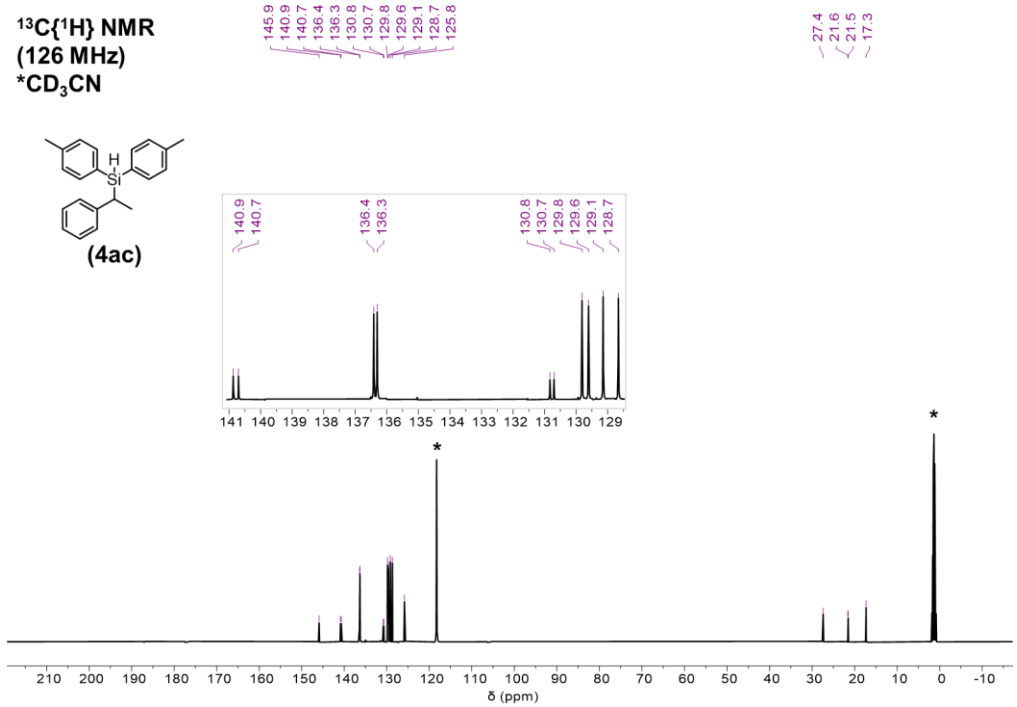

Figure A.114. $^{13}C\{^{1}H\}$ NMR spectrum of (1-phenylethyl)di(4-methylphenyl)silane (**4ac**) recorded in CD_3CN at 298 K.

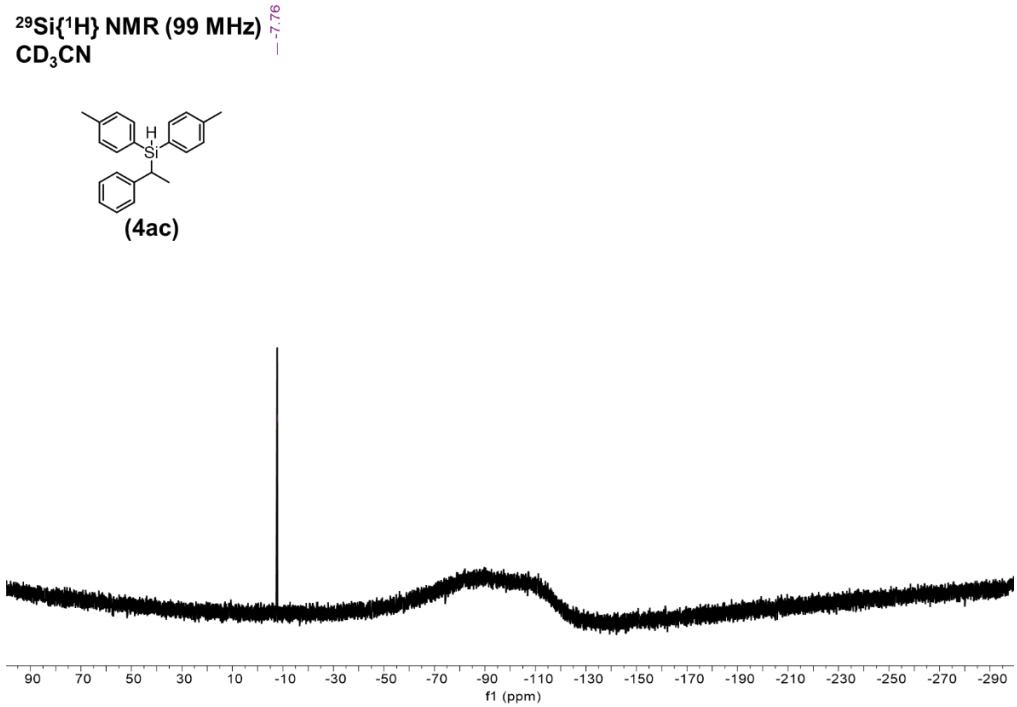

Figure A.115. $^{29}Si\{^{1}H\}$ NMR spectrum (1-phenylethyl)di(4-methylphenyl)silane (**4ac**) recorded in CD_3CN at 298 K.

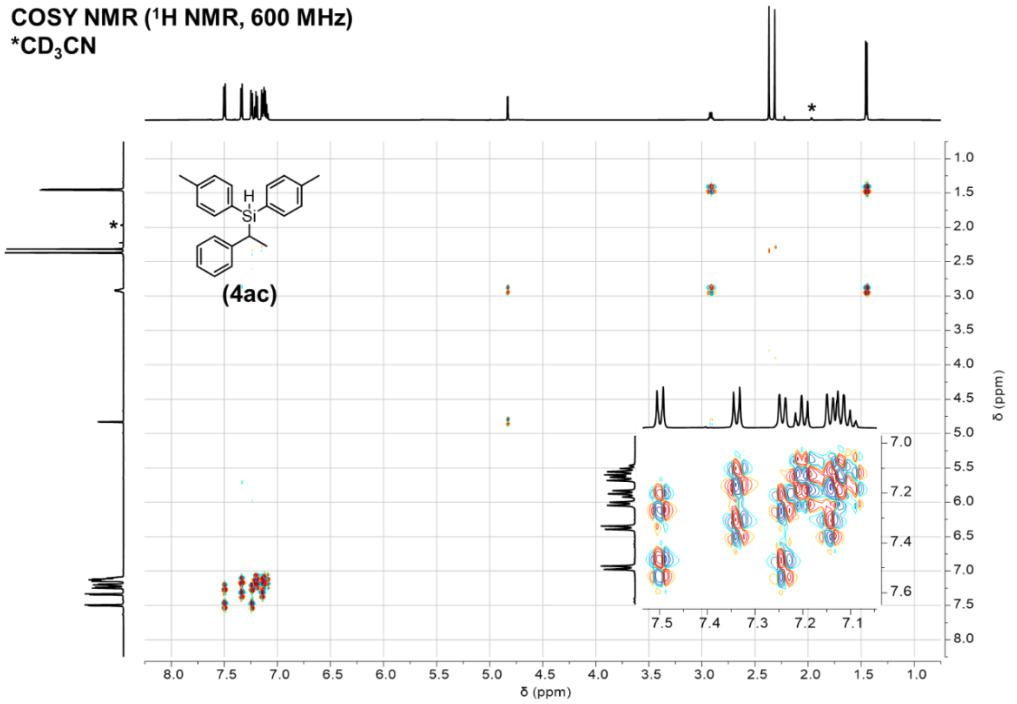

Figure A.116. COSY NMR spectrum of (1-phenylethyl)di(4-methylphenyl)silane (**4ac**) recorded in CD_3CN at 298 K.

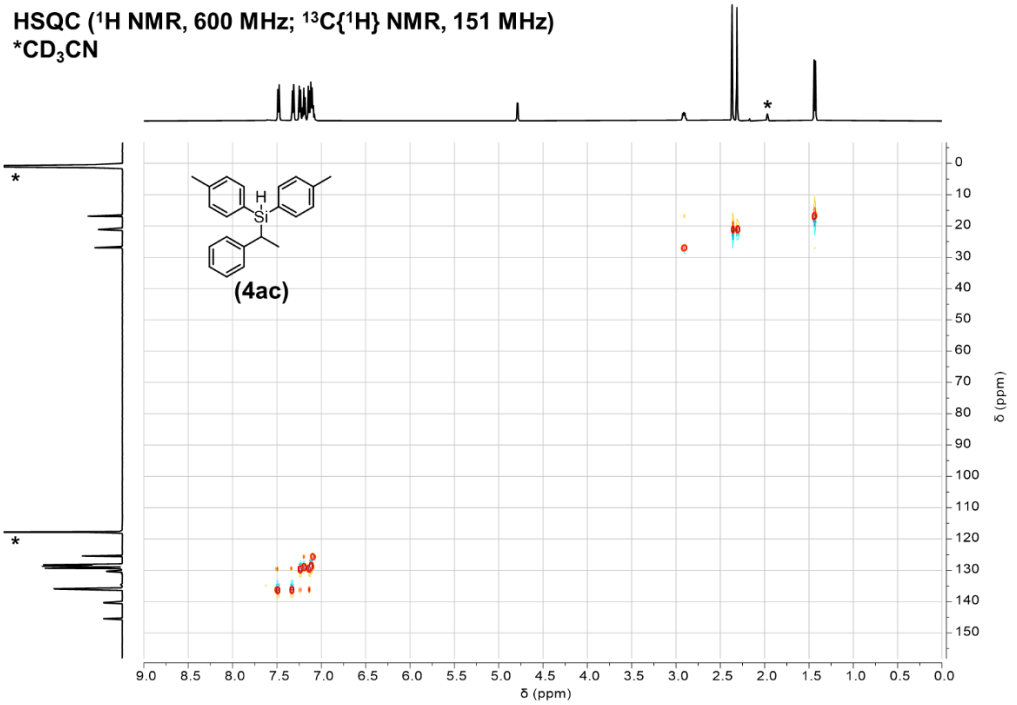

Figure A.117. HSQC NMR spectrum of (1-phenylethyl)di(4-methylphenyl)silane (**4ac**) recorded in CD_3CN at 298 K.

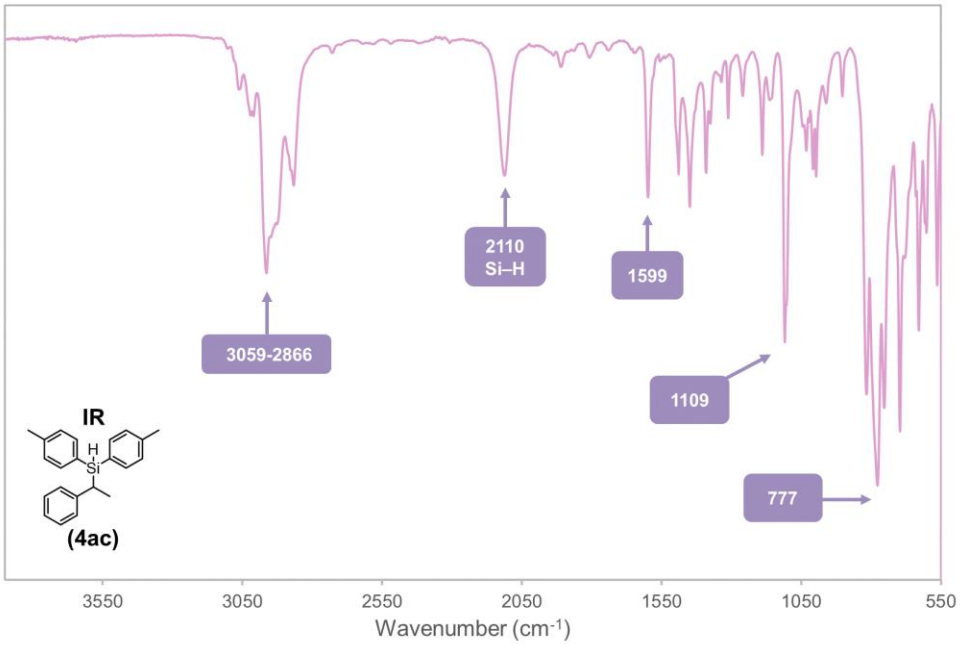

Figure A.118. IR spectrum of (1-phenylethyl)di(4-methylphenyl)silane (**4ac**) recorded neat at 298 K.

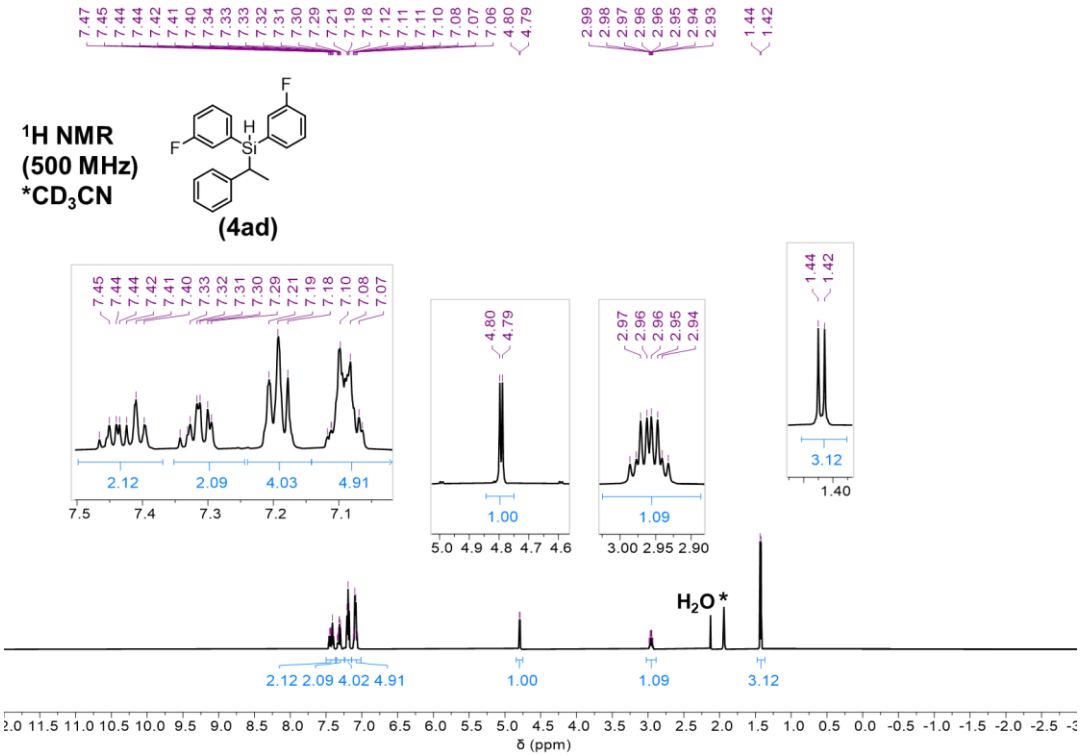

Figure A.119. ^{1}H NMR spectrum of (1-phenylethyl)di(3-fluorophenyl)silane (**4ad**) recorded in CD_3CN at 298 K.

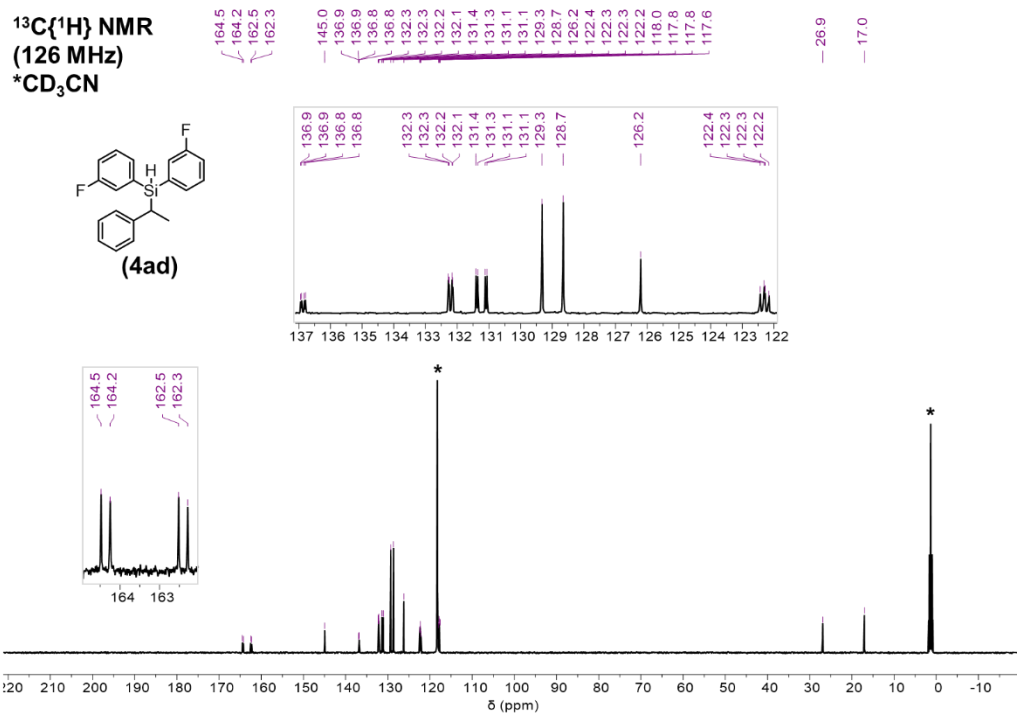

Figure A.120. $^{13}C\{^{1}H\}$ NMR spectrum of (1-phenylethyl)di(3-fluorophenyl)silane (**4ad**) recorded in CD_3CN at 298 K.

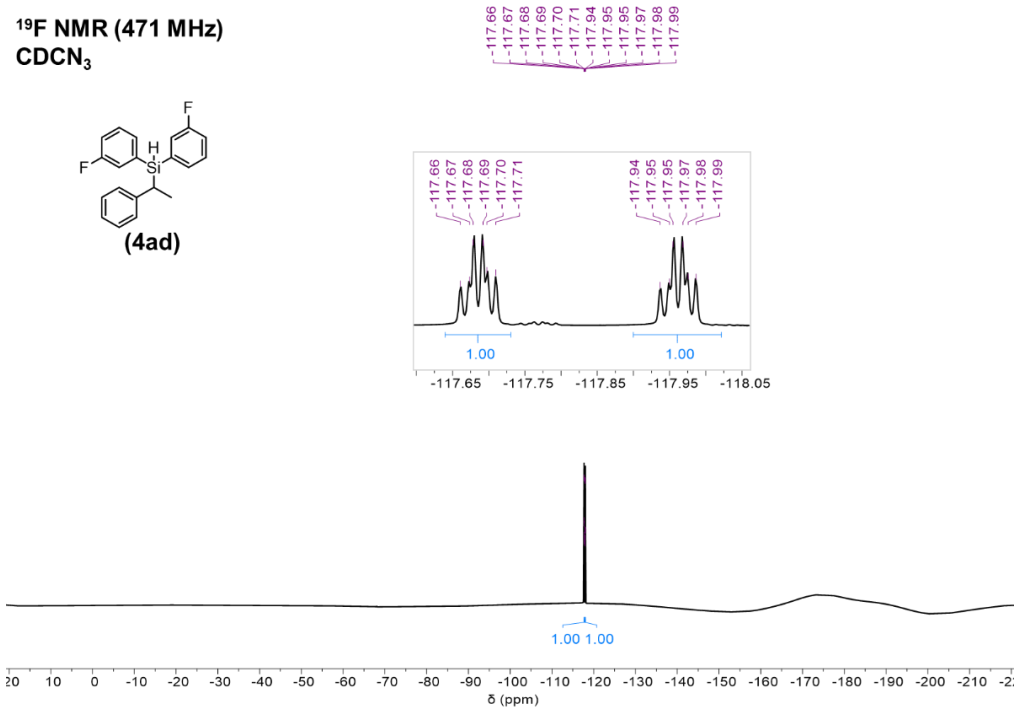

Figure A.121. ^{19}F NMR spectrum of (1-phenylethyl)di(3-fluorophenyl)silane (**4ad**) recorded in CD_3CN at 298 K.

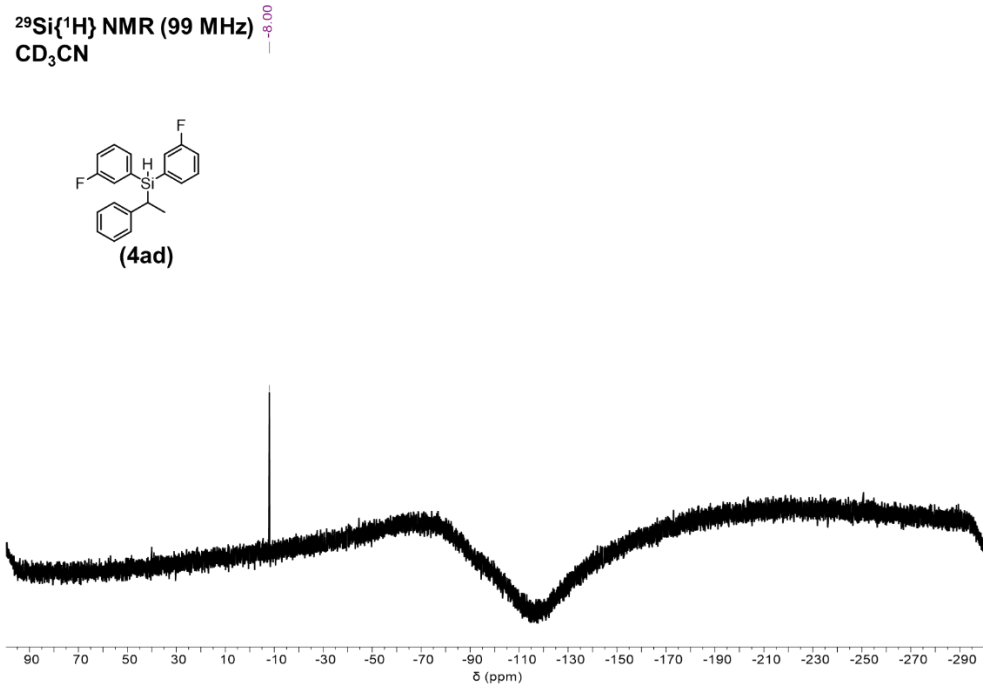

Figure A.122. $^{29}Si\{^{1}H\}$ NMR spectrum of (1-phenylethyl)di(3-fluorophenyl)silane (**4ad**) recorded in CD_3CN at 298 K.

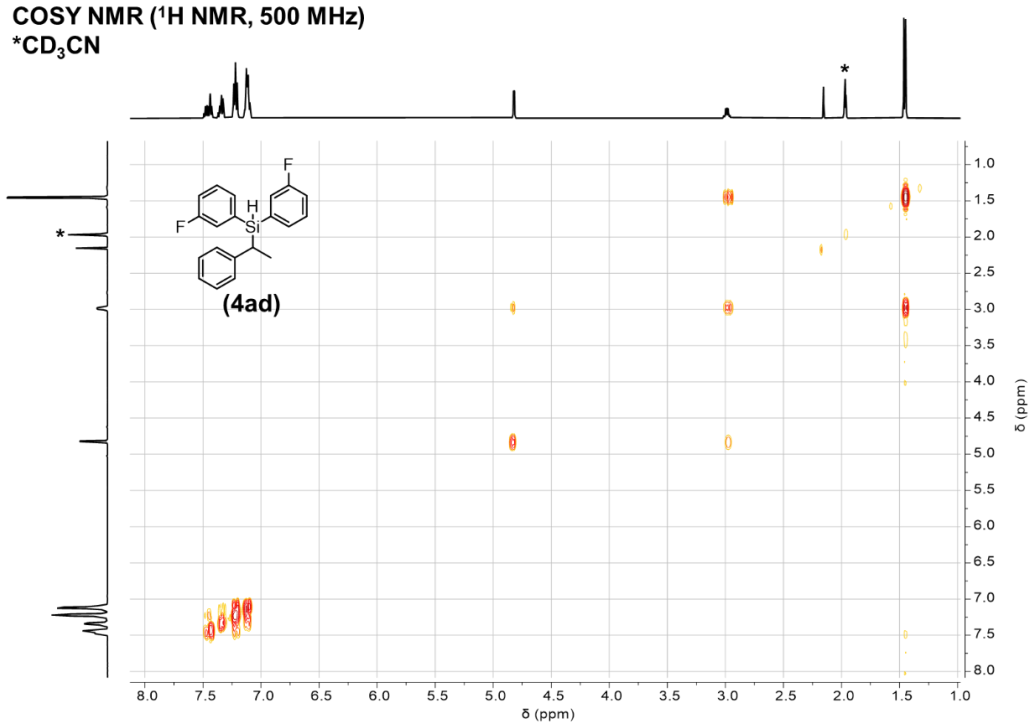

Figure A.123. COSY NMR spectrum of (1-phenylethyl)di(3-fluorophenyl)silane (**4ad**) recorded in CD_3CN at 298 K.

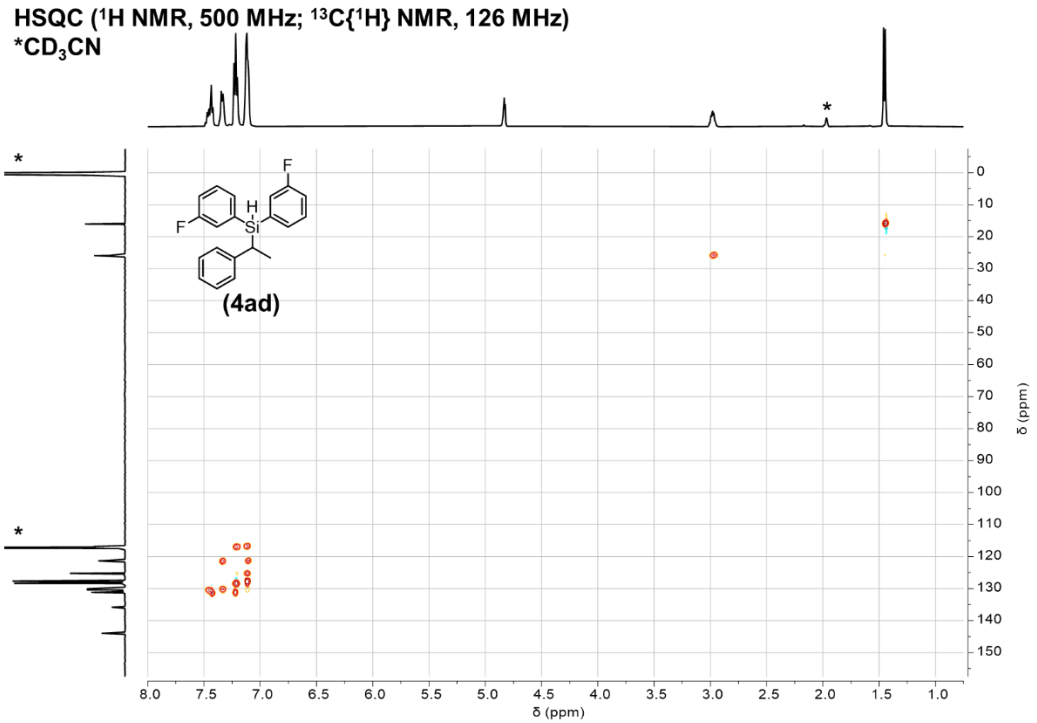

Figure A.124. HSQC NMR spectrum of (1-phenylethyl)di(3-fluorophenyl)silane (**4ad**) recorded in CD_3CN at 298 K.

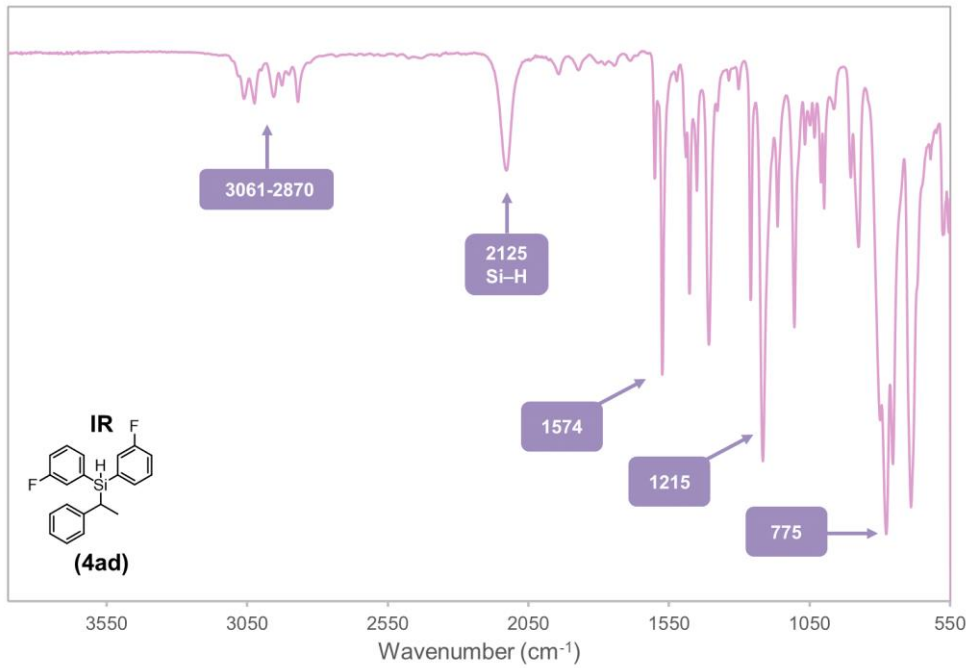

Figure A.125. IR spectrum of (1-phenylethyl)di(3-fluorophenyl)silane (**4ad**) recorded neat at 298 K.

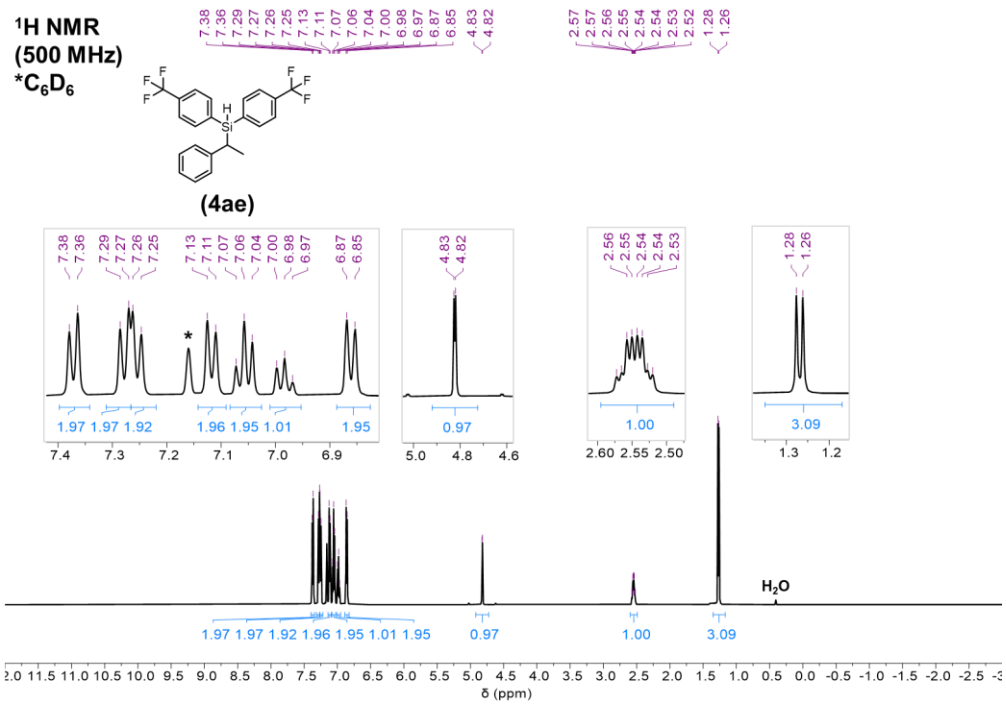

Figure A.126. ^{1}H NMR spectrum of (1-phenylethyl)di[4-(trifluoromethyl)phenyl]silane (**4ae**) recorded in CD_3CN at 298 K.

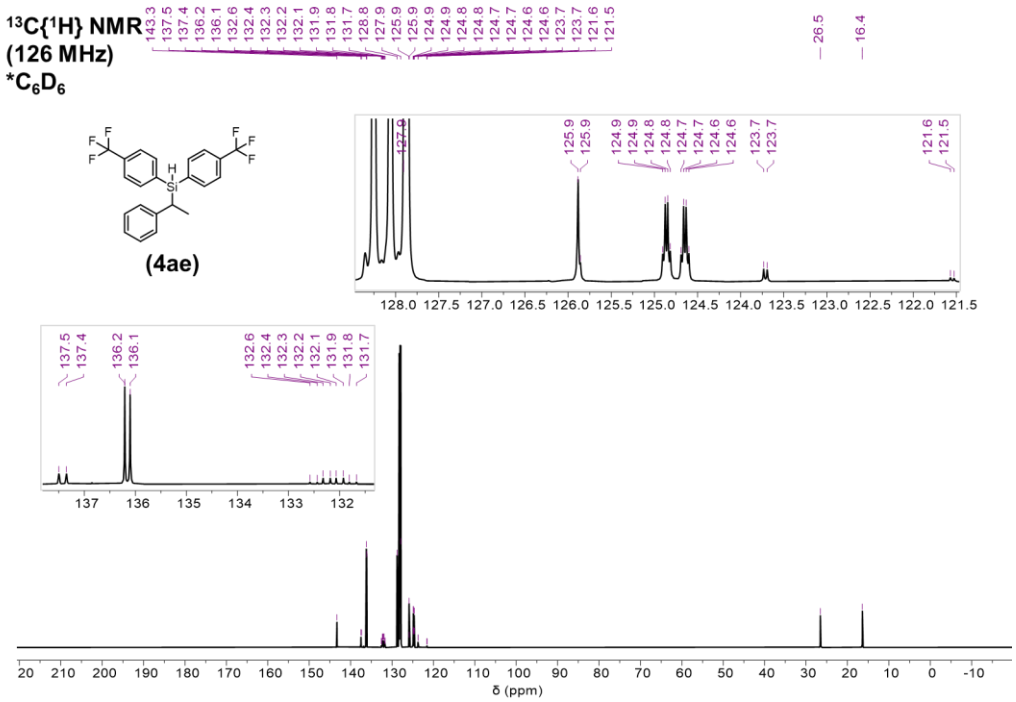

Figure A.127. $^{13}C\{^{1}H\}$ NMR spectrum of (1-phenylethyl)di[4-(trifluoromethyl)phenyl]silane (**4ae**) recorded in CD_3CN at 298 K.

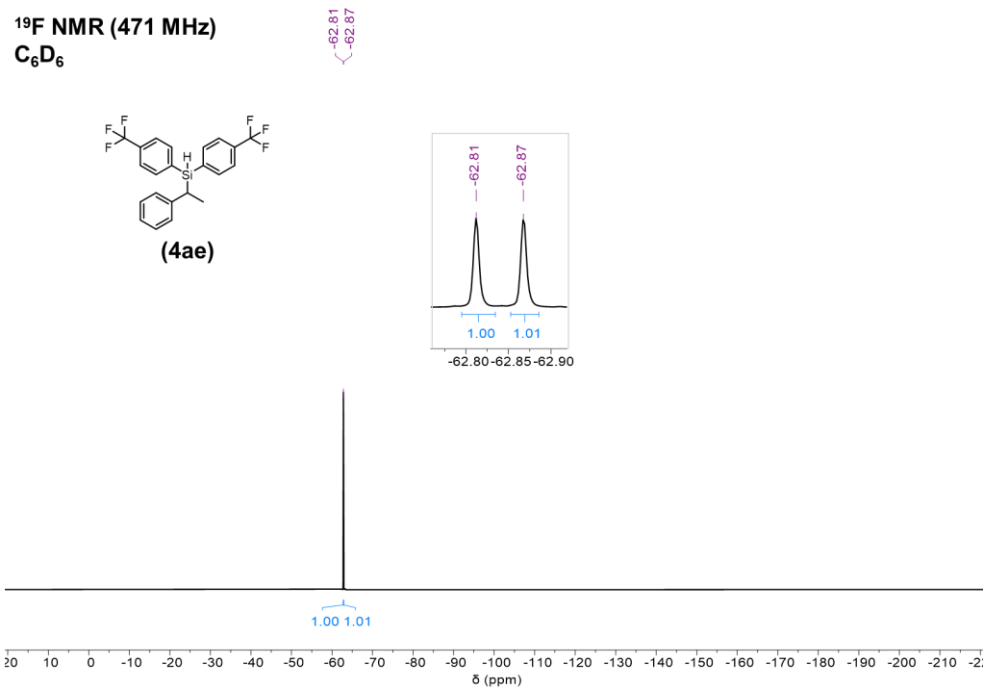

Figure A.128. ^{19}F NMR spectrum of (1-phenylethyl)di[4-(trifluoromethyl)phenyl]silane (**4ae**) recorded in CD_3CN at 298 K.

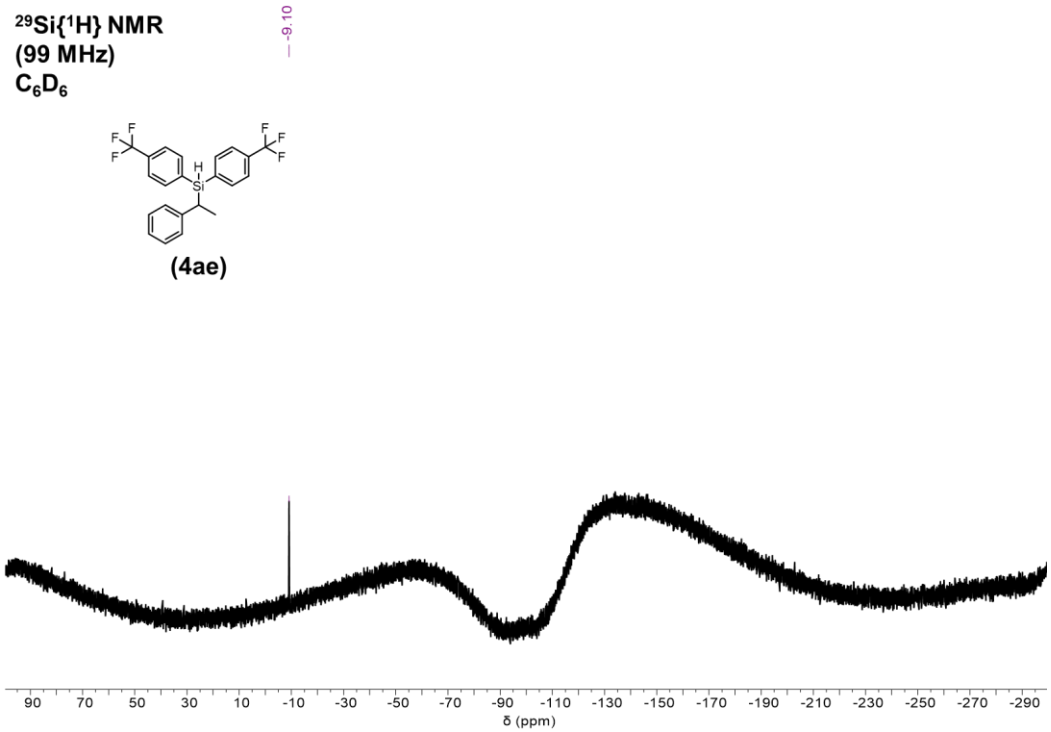

Figure A.129. $^{29}Si\{^1H\}$ NMR spectrum of (1-phenylethyl)di[4-(trifluoromethyl)phenyl]silane (**4ae**) recorded in CD_3CN at 298 K.

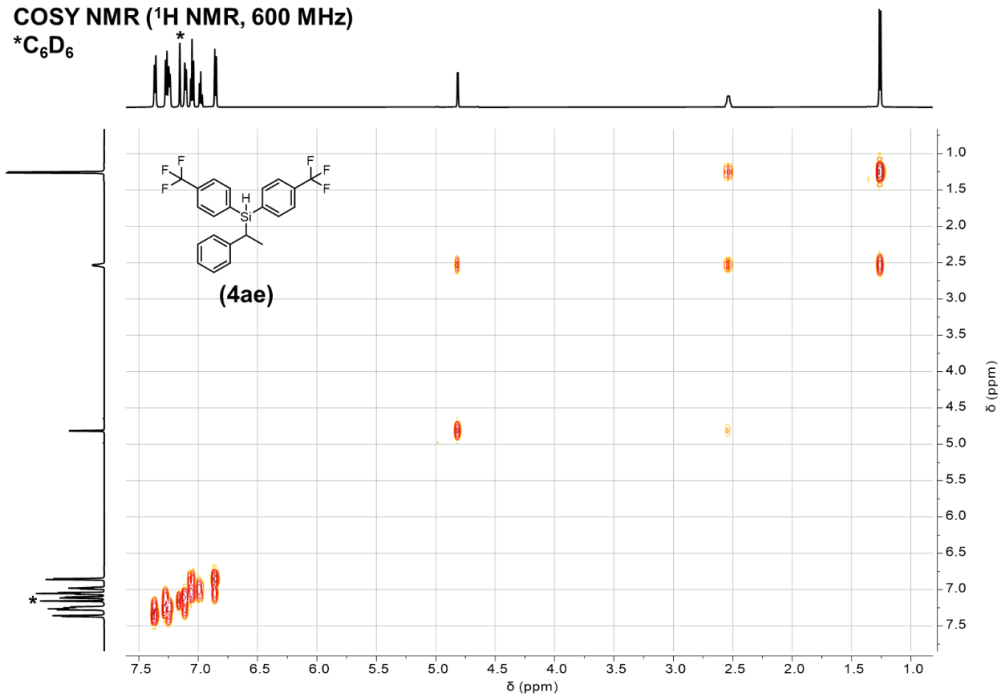

Figure A.130. COSY NMR spectrum of (1-phenylethyl)di[4-(trifluoromethyl)phenyl]silane (**4ae**) recorded in CD_3CN at 298 K.

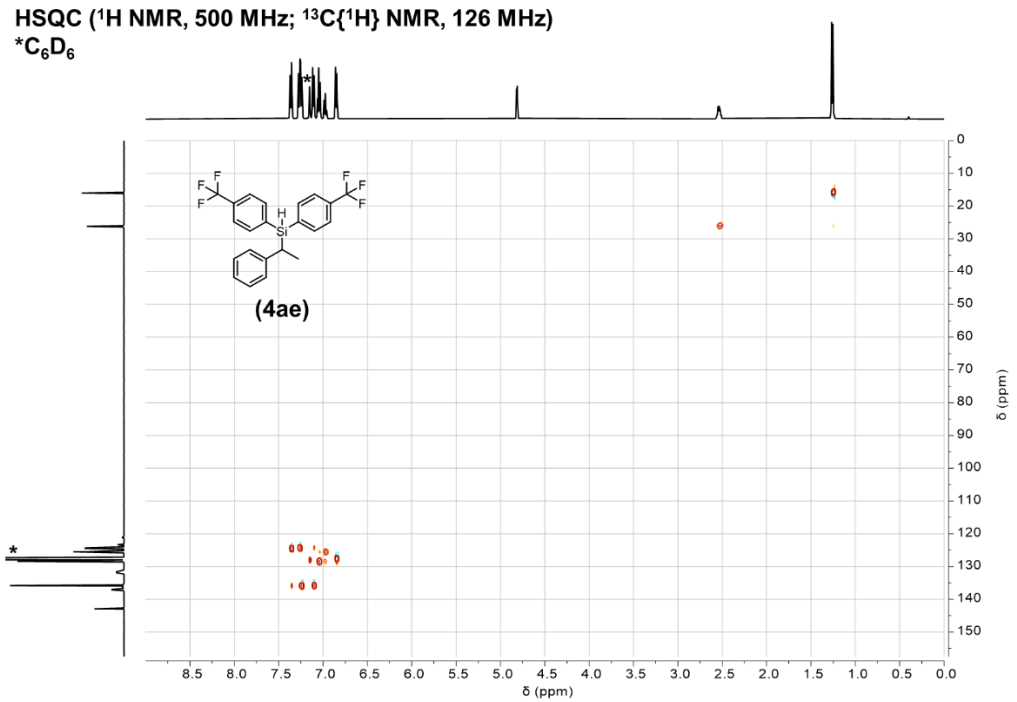

Figure A.131. HSQC NMR spectrum of (1-phenylethyl)di[4-(trifluoromethyl)phenyl]silane (**4ae**) recorded in CD_3CN at 298 K.

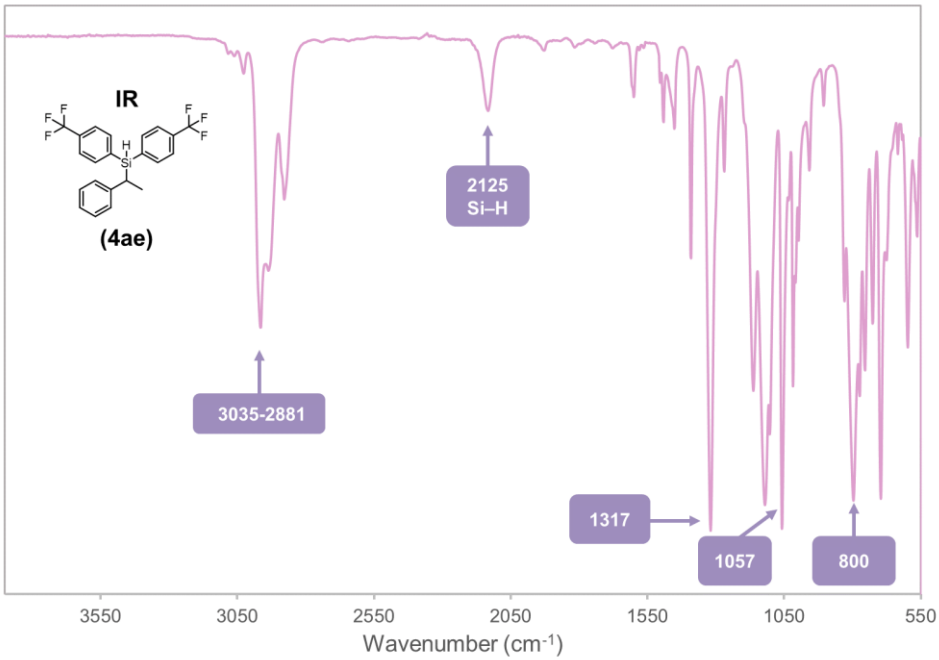

Figure A.132. IR spectrum of (1-phenylethyl)di[4-(trifluoromethyl)phenyl]silane (**4ae**) recorded neat at 298 K.

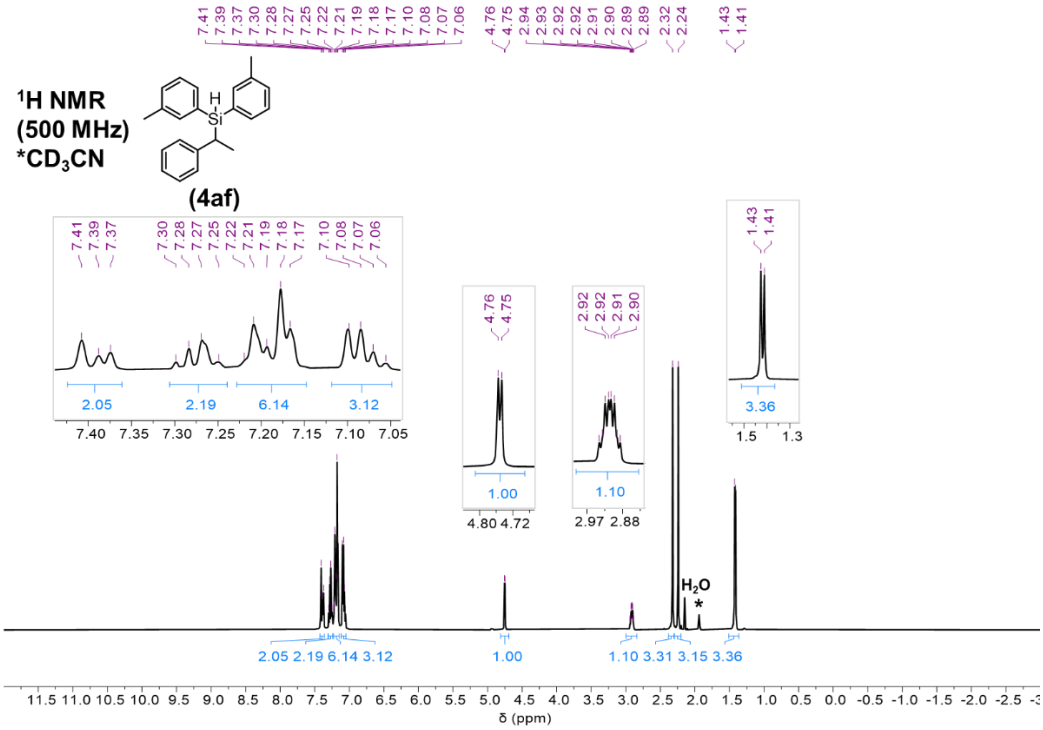

Figure A.133. ^{1}H NMR spectrum of (1-phenylethyl)di(3-methylphenyl)silane (**4af**) recorded in CD_3CN at 298 K.

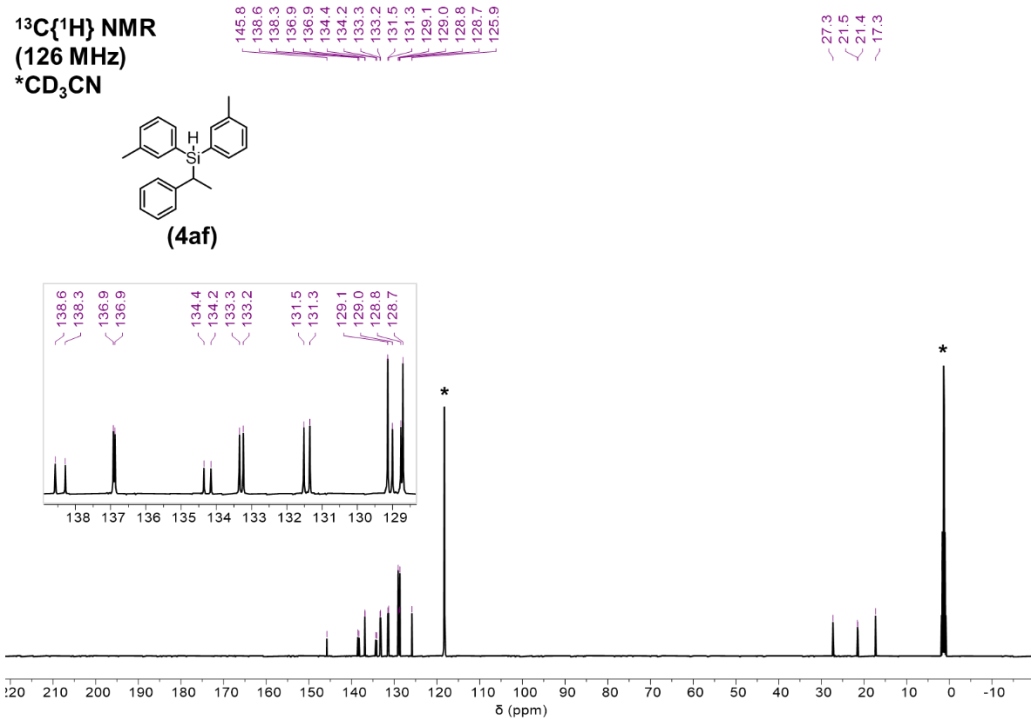

Figure A.134. $^{13}C\{^{1}H\}$ NMR spectrum of (1-phenylethyl)di(3-methylphenyl)silane (**4af**) recorded in CD_3CN at 298 K.

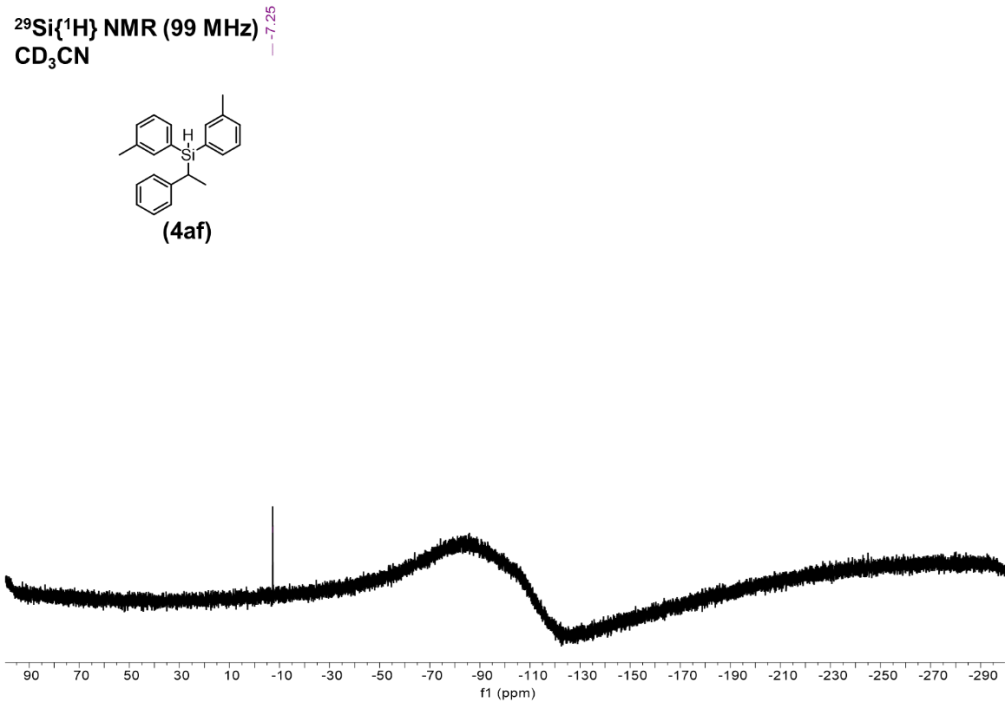

Figure A.135. $^{29}Si\{^{1}H\}$ NMR spectrum of (1-phenylethyl)di(3-methylphenyl)silane (**4af**) recorded in CD_3CN at 298 K.

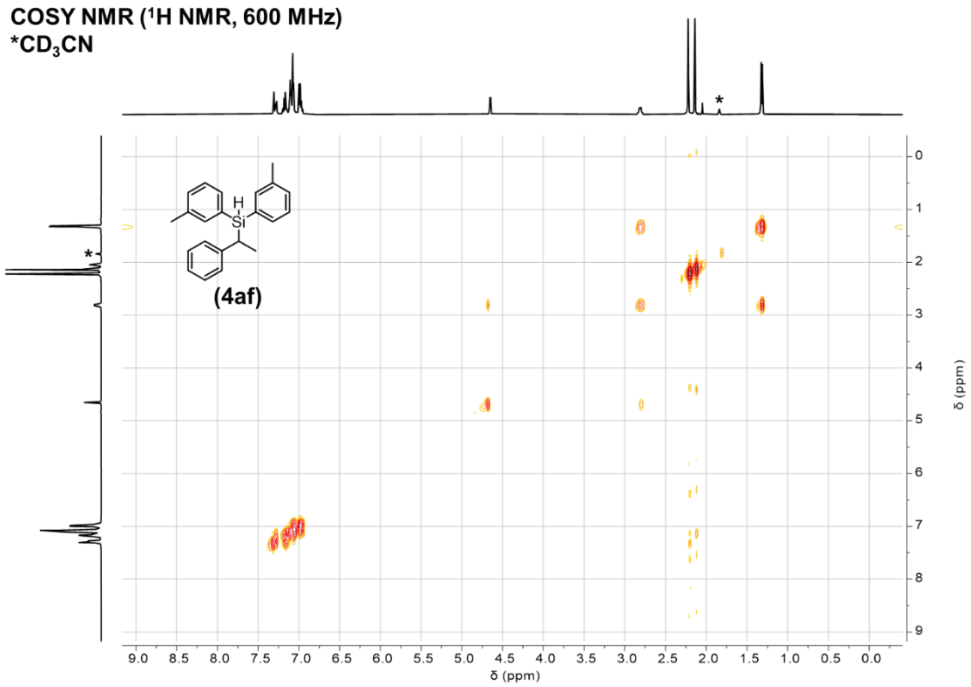

Figure A.136. COSY NMR spectrum of (1-phenylethyl)di(3-methylphenyl)silane (**4af**) recorded in CD_3CN at 298 K.

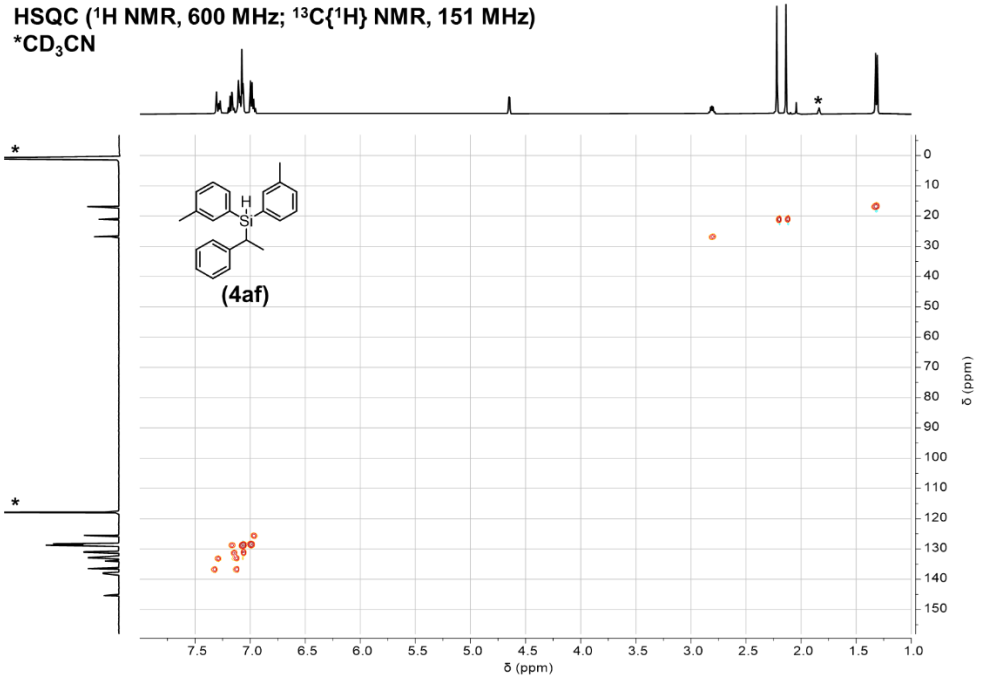

Figure A.137. HSQC NMR spectrum of (1-phenylethyl)di(3-methylphenyl)silane (**4af**) recorded in CD_3CN at 298 K.

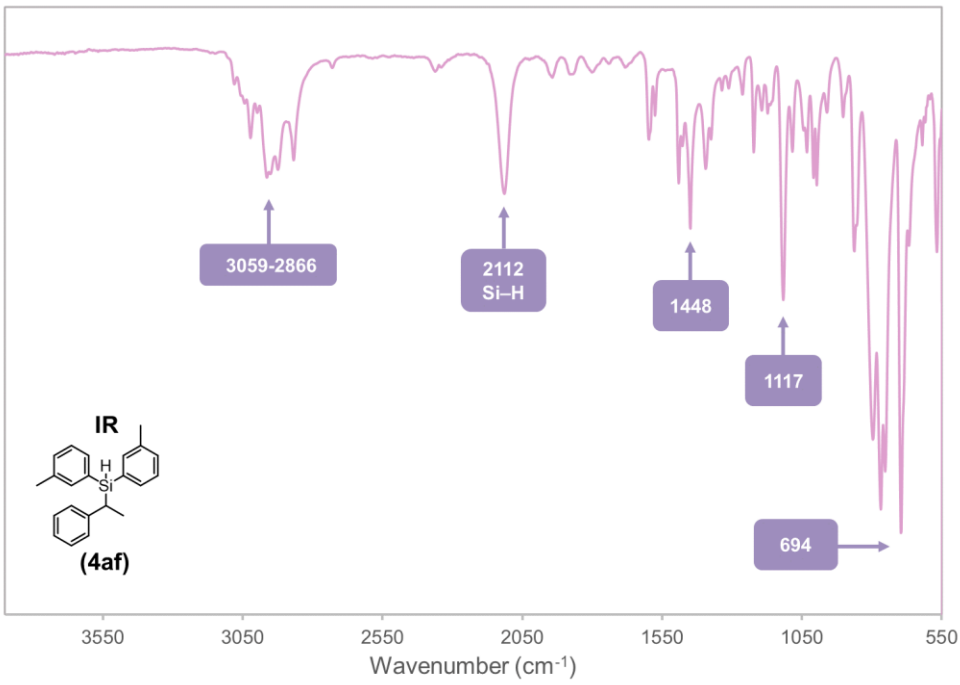

Figure A.138. IR spectrum of (1-phenylethyl)di(3-methylphenyl)silane (**4af**) recorded neat at 298 K.

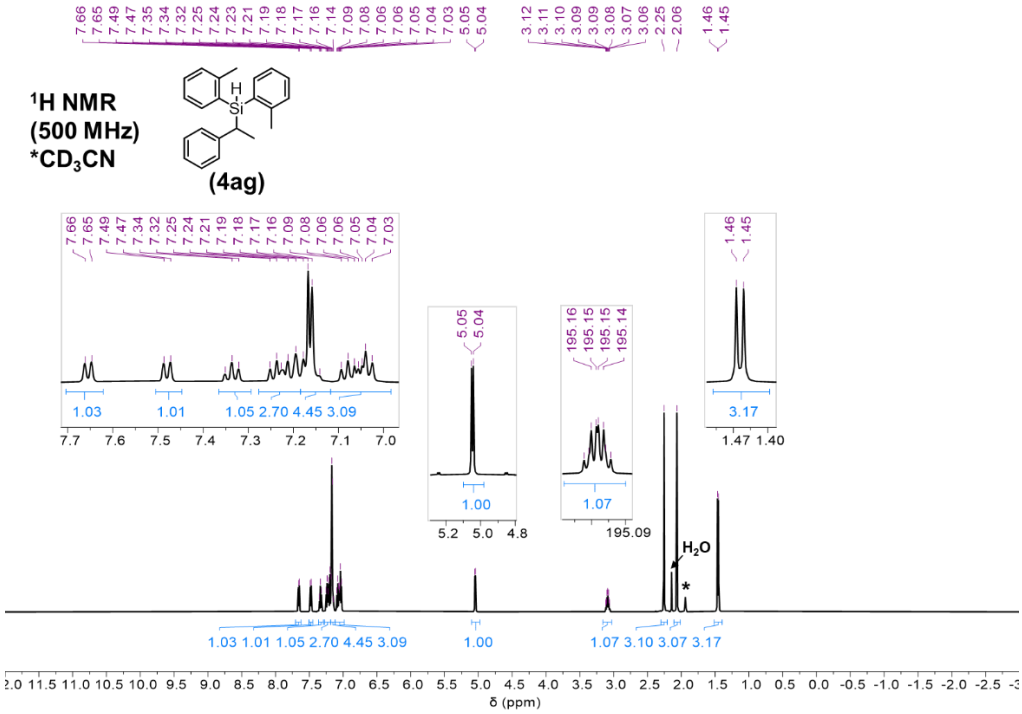

Figure A.139. ^{1}H NMR spectrum of (1-phenylethyl)di(2-methylphenyl)silane (**4ag**) recorded in CD_3CN at 298 K.

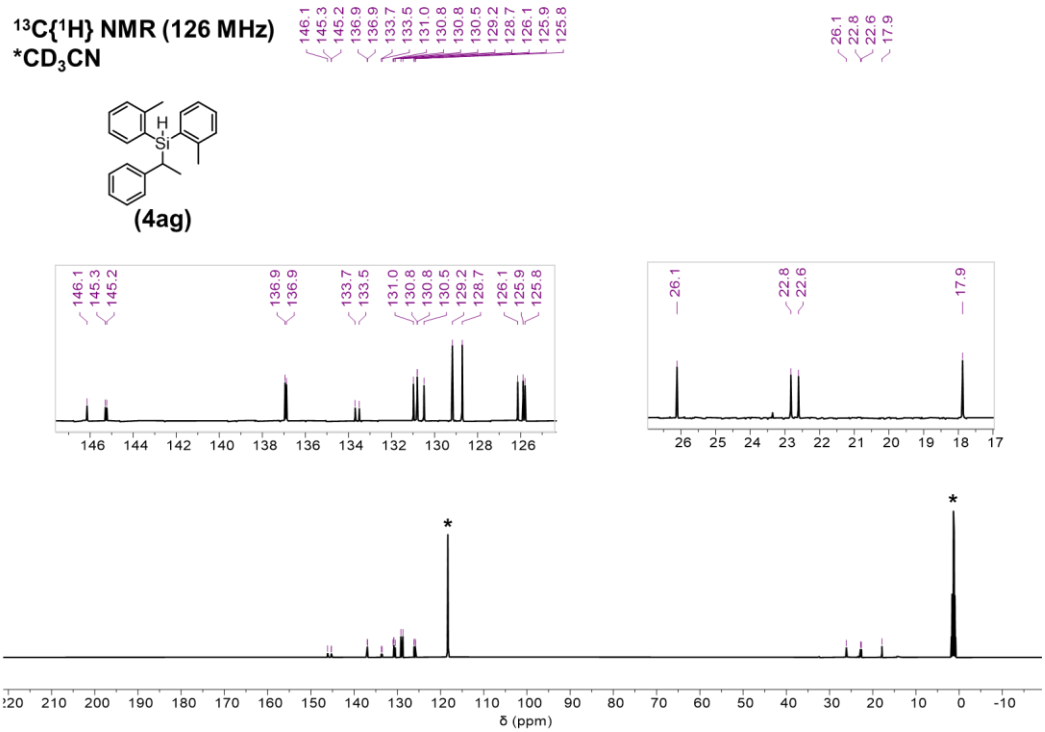

Figure A.140. $^{13}C\{^{1}H\}$ NMR spectrum of (1-phenylethyl)di(2-methylphenyl)silane (**4ag**) recorded in CD_3CN at 298 K.

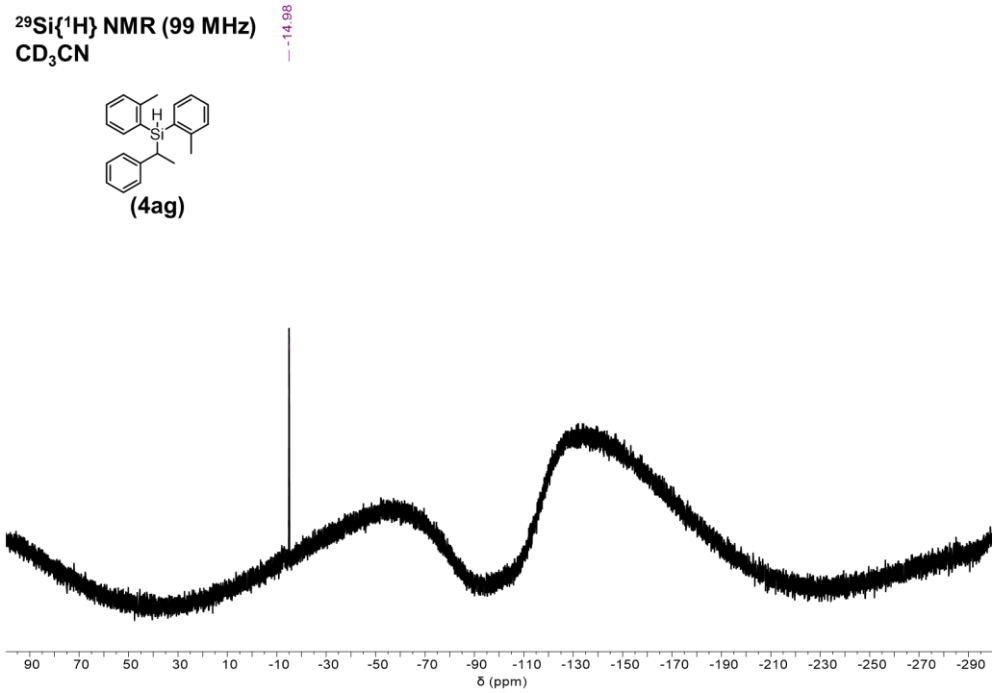

Figure A.141. $^{29}Si\{^{1}H\}$ NMR spectrum of (1-phenylethyl)di(2-methylphenyl)silane (**4ag**) recorded in CD_3CN at 298 K.

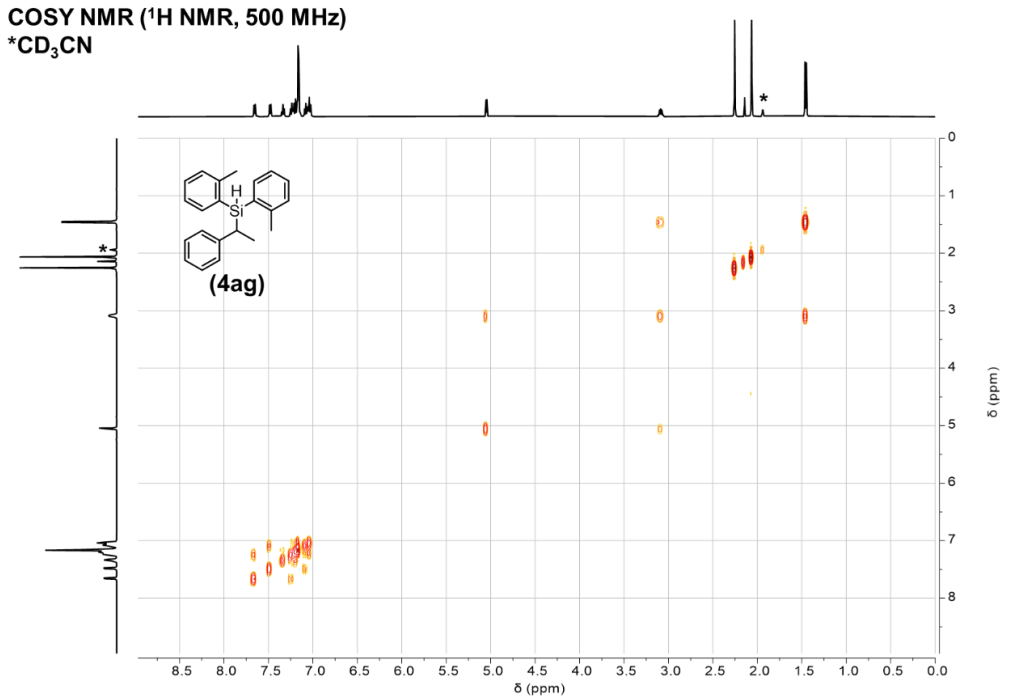

Figure A.142. COSY NMR spectrum of (1-phenylethyl)di(2-methylphenyl)silane (**4ag**) recorded in CD_3CN at 298 K.

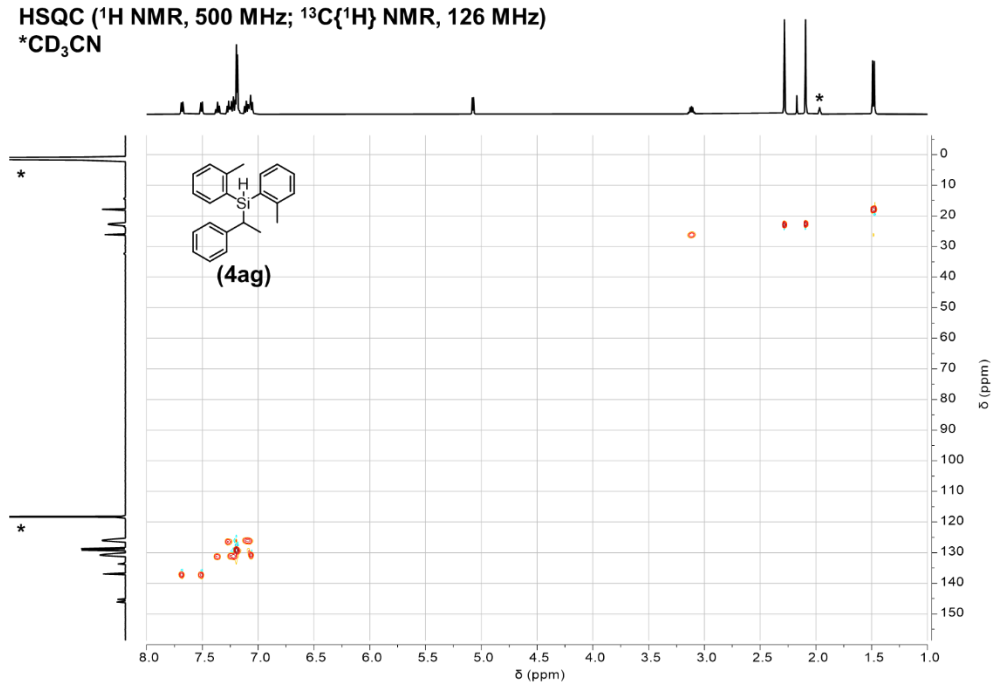

Figure A.143. HSQC NMR spectrum of (1-phenylethyl)di(2-methylphenyl)silane (**4ag**) recorded in CD_3CN at 298 K.

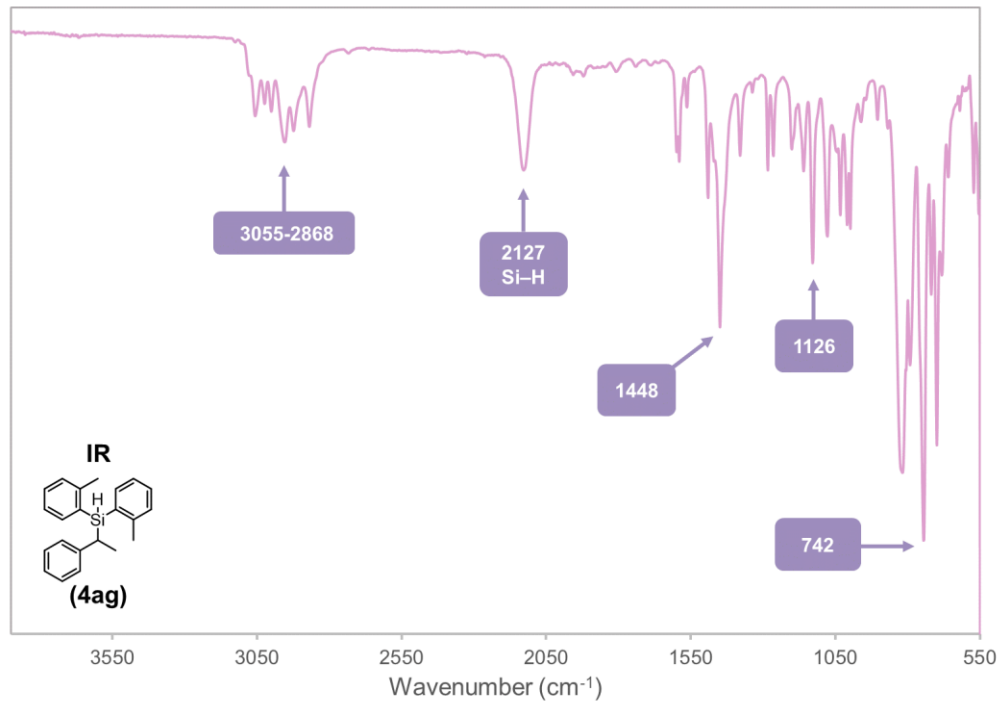

Figure A.144. IR spectrum of (1-phenylethyl)di(2-methylphenyl)silane (**4ag**) recorded neat at 298 K.

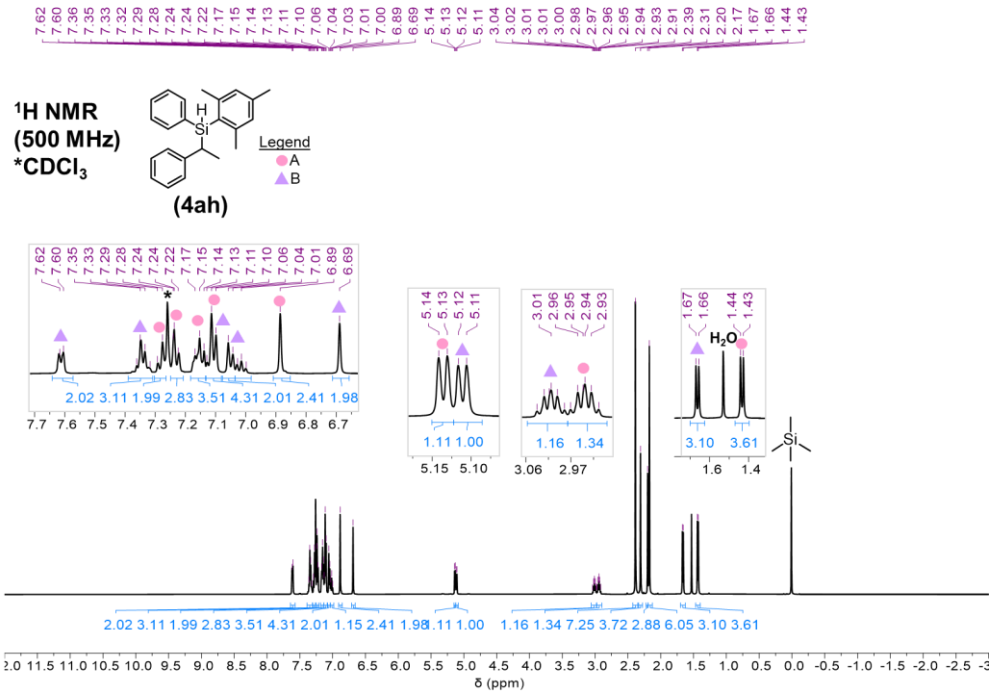

Figure A.145. ^{1}H NMR spectrum of (1-phenylethyl)phenylmesitylsilane (**4ah**) diastereomers **A** and **B** (**A**/**B** = 1.1:1) after the first column recorded in $CDCl_3$ at 298 K.

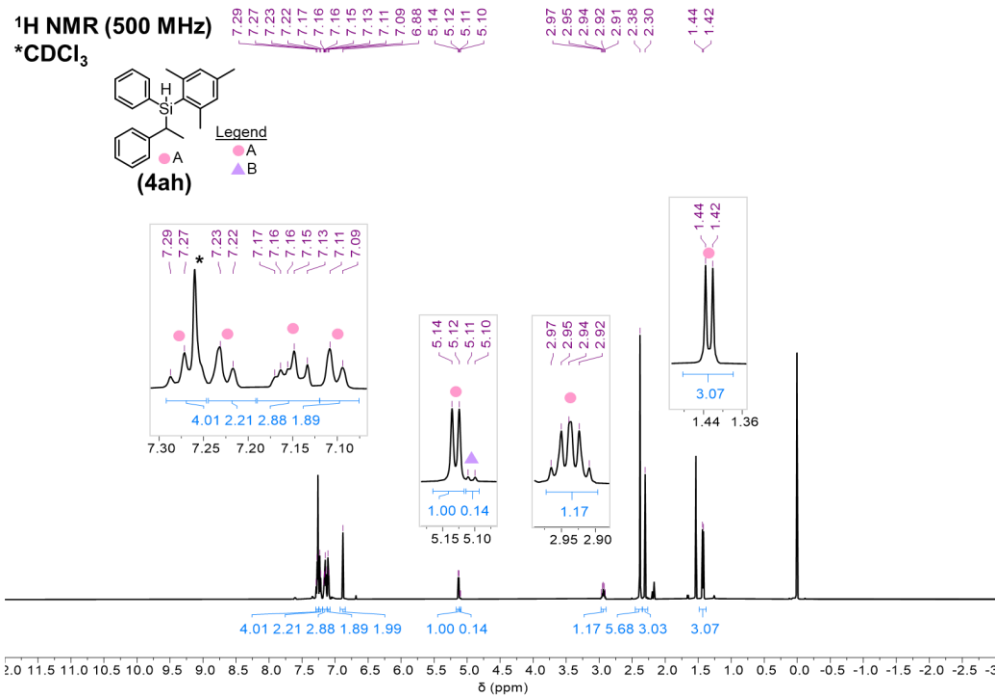

Figure A.146. ^{1}H NMR spectrum of (1-phenylethyl)phenylmesitylsilane (**4ah**) after the second column with diastereomer **A** as the major species (**A**/**B** = 7.1:1) recorded in $CDCl_3$ at 298 K.

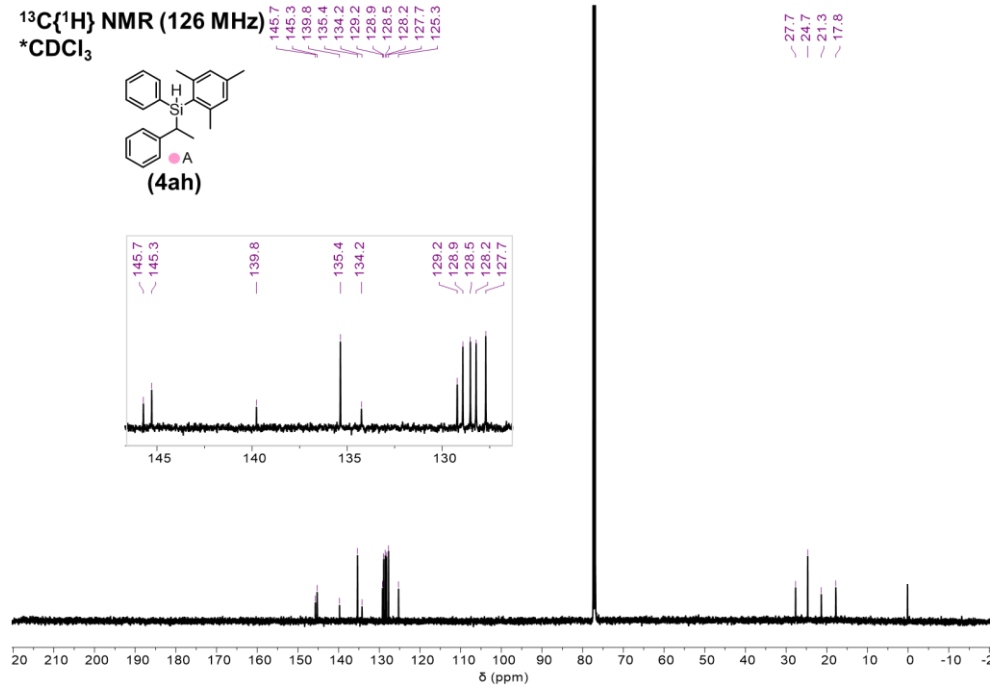

Figure A.147. ^{13}C{^{1}H} NMR spectrum of (1-phenylethyl)phenylmesitylsilane (**4ah**) after the second column with diastereomer **A** as the major species (**A**/**B** = 7.1:1) recorded in $CDCl_3$ at 298 K.

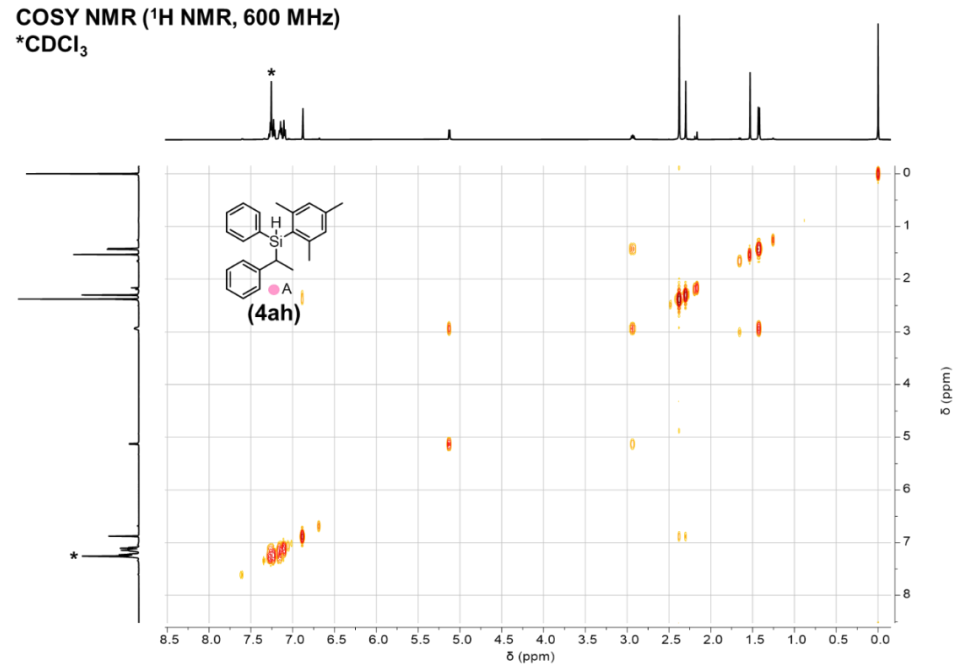

Figure A.148. COSY NMR spectrum of (1-phenylethyl)phenylmesitylsilane (**4ah**) after the second column with diastereomer **A** as the major species (**A**/**B** = 7.1:1) recorded in $CDCl_3$ at 298 K.

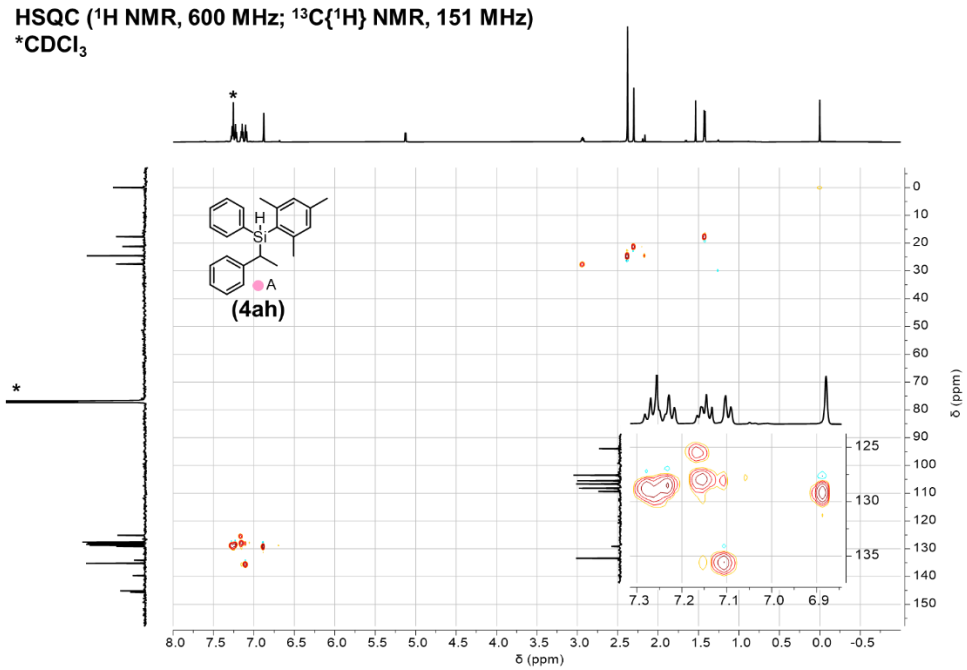

Figure A.149. HSQC NMR spectrum of (1-phenylethyl)phenylmesitylsilane (**4ah**) after the second column with diastereomer **A** as the major species (**A**/**B** = 7.1:1) recorded in $CDCl_3$ at 298 K.

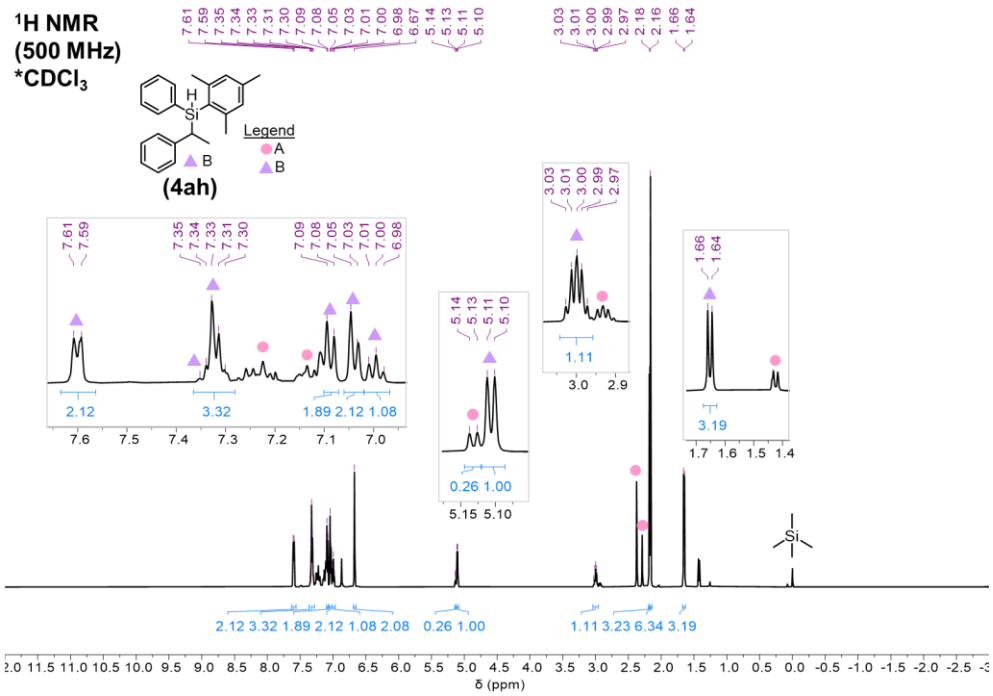

Figure A.150. ^{1}H NMR spectrum of (1-phenylethyl)phenylmesitylsilane (**4ah**) after the second column with diastereomer **B** as the major species (**A**/**B** = 1:3.8) recorded in $CDCl_3$ at 298 K.

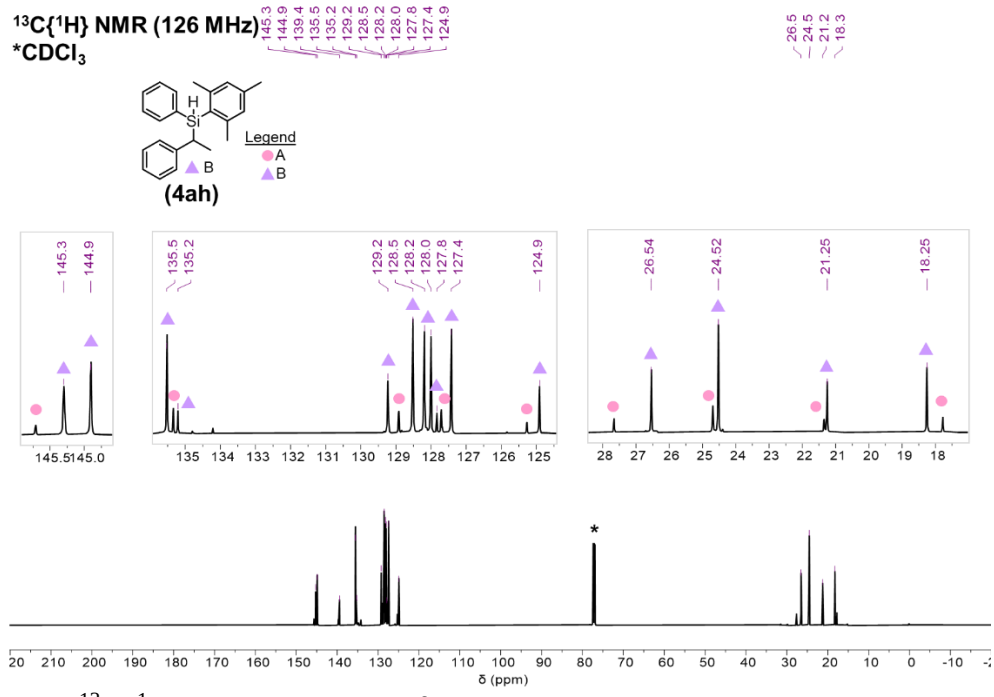

Figure A.151. ^{13}C{^{1}H} NMR spectrum of (1-phenylethyl)phenylmesitylsilane (**4ah**) after the second column with diastereomer **B** as the major species (**A**/**B** = 1:3.8) recorded in $CDCl_3$ at 298 K.

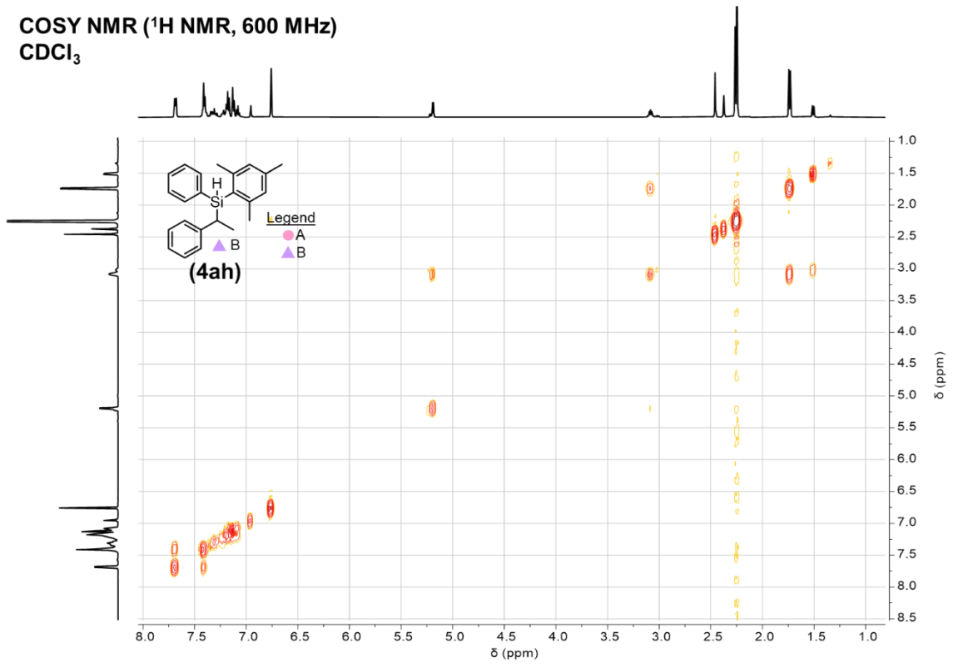

Figure A.152. COSY NMR spectrum of (1-phenylethyl)phenylmesitylsilane (**4ah**) after the second column with diastereomer **B** as the major species (**A**/**B** = 1:3.8) recorded in $CDCl_3$ at 298 K.

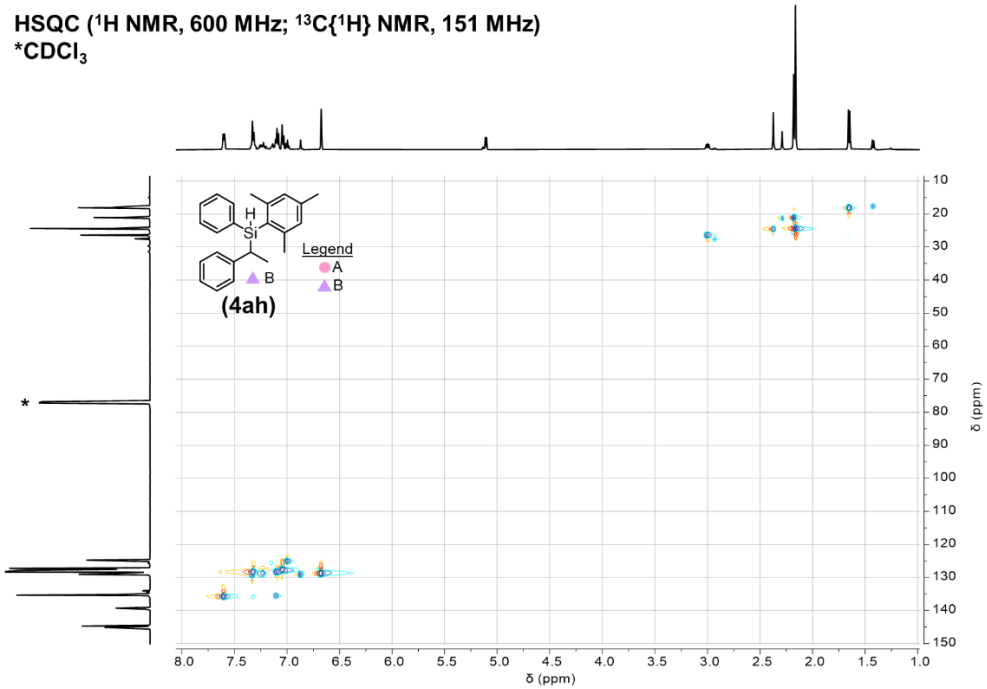

Figure A.153. HSQC NMR spectrum of (1-phenylethyl)phenylmesitylsilane (**4ah**) after the second column with diastereomer **B** as the major species (**A**/**B** = 1:3.8) recorded in $CDCl_3$ at 298 K.

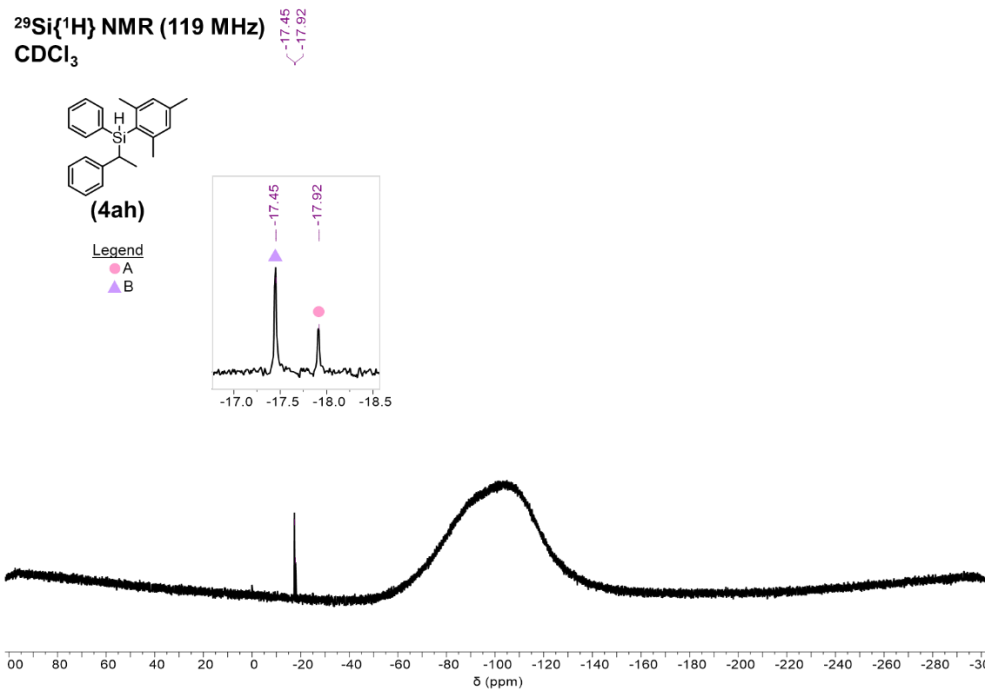

Figure A.154. ^{29}Si NMR spectrum of (1-phenylethyl)phenylmesitylsilane (**4ah**) diastereomers **A** and **B** (**A**/**B** = 1:3.8) after the first column recorded in $CDCl_3$ at 298 K.

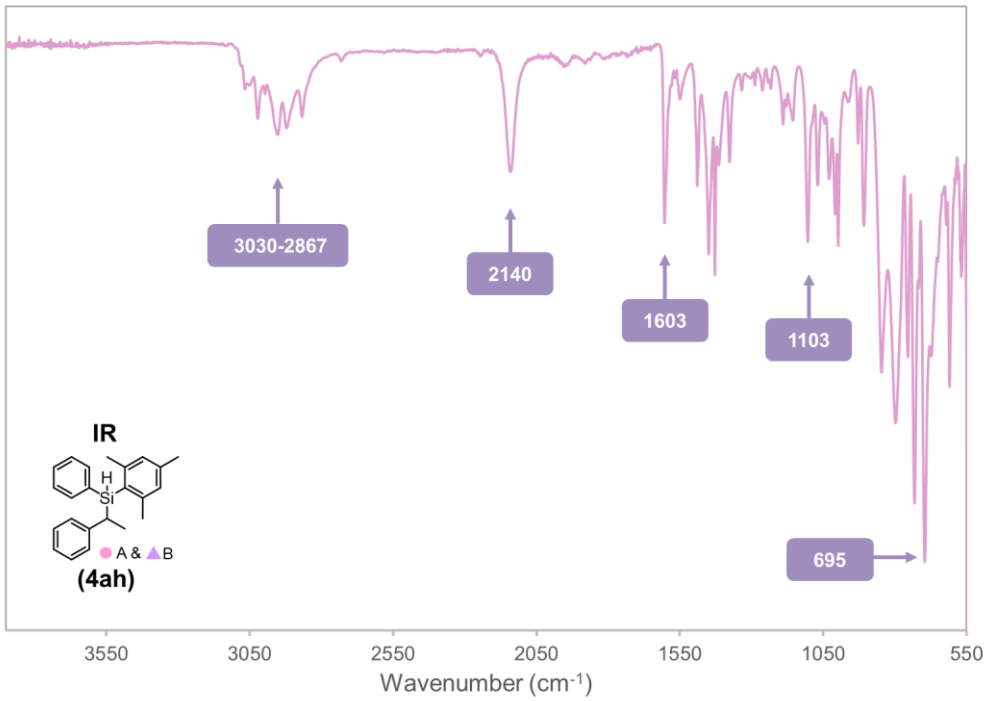

Figure A.155. IR spectrum of (1-phenylethyl)phenylmesitylsilane (**4ah**) diastereomers **A** and **B** (**A**/**B** = 1.1:1) after the first column recorded neat at 298 K.

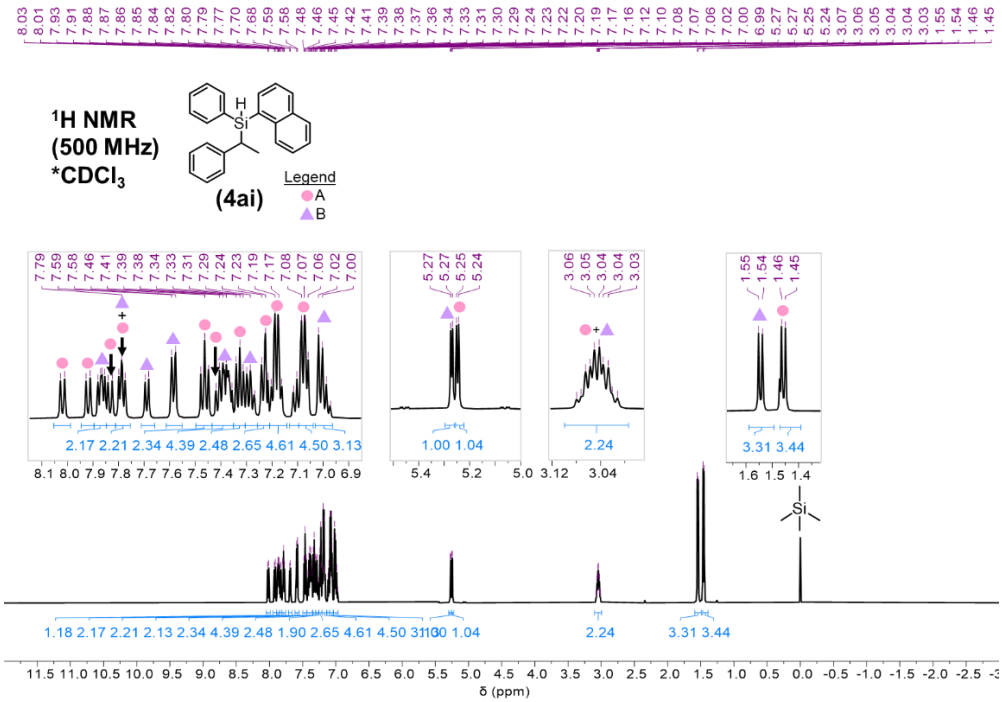

Figure A.156. ^{1}H NMR spectrum of (1-phenylethyl)(2-naphthyl)phenylsilane (**4ai**) diastereomers **A** and **B** (**A**/**B** = 1.04:1) after the first column recorded in $CDCl_3$ at 298 K.

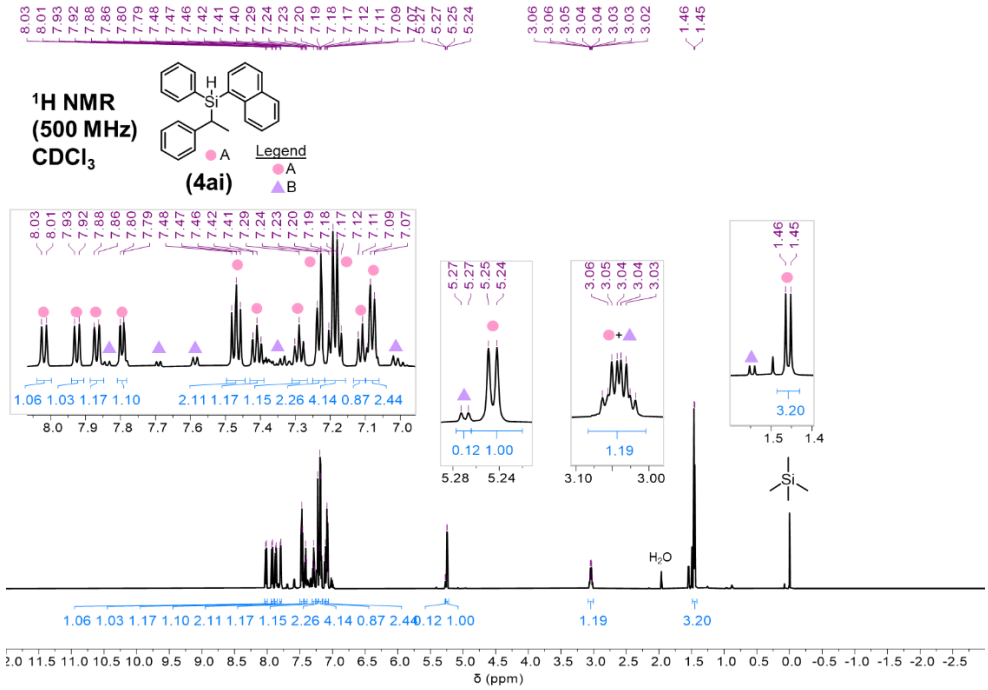

Figure A.157. ^{1}H NMR spectrum of (1-phenylethyl)(2-naphthyl)phenylsilane (**4ai**) after the second column with diastereomer **A** as the major species (**A**/**B** = 8.3:1) recorded in $CDCl_3$ at 298 K.

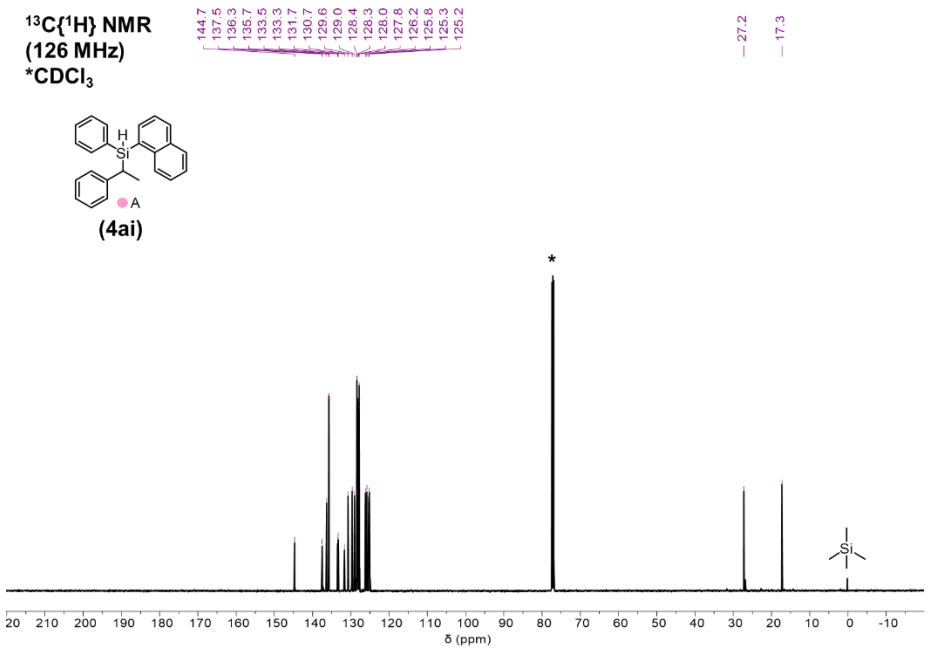

Figure A.158. $^{13}C\{^{1}H\}$ NMR spectrum of (1-phenylethyl)(2-naphthyl)phenylsilane (**4ai**) after the second column with diastereomer **A** as the major species (**A**/**B** = 8.3:1) recorded in $CDCl_3$ at 298 K.

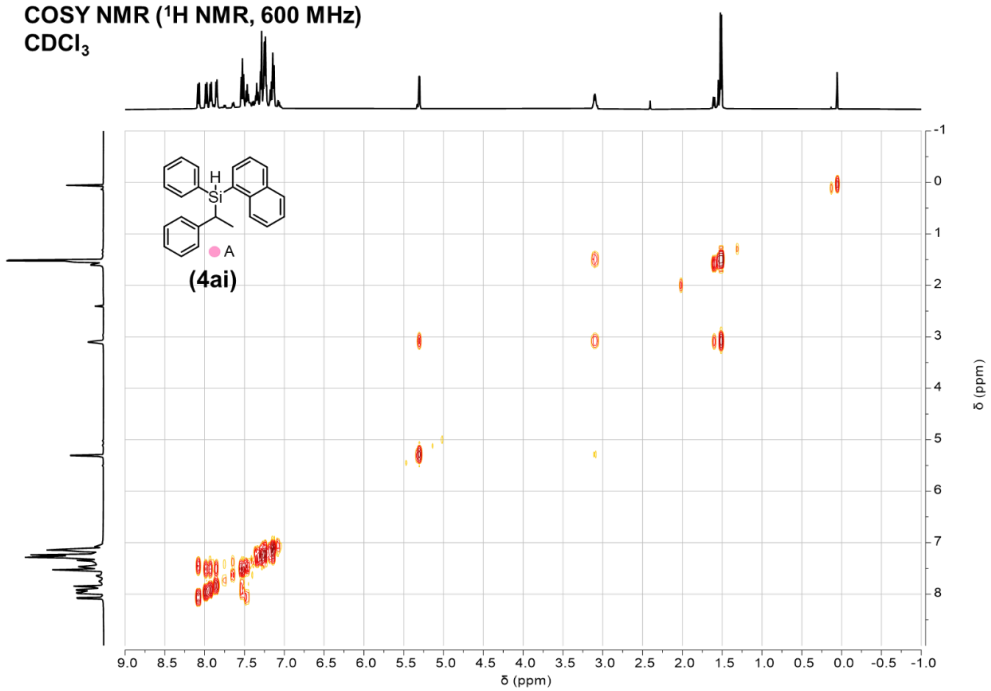

Figure A.159. COSY NMR spectrum of (1-phenylethyl)(2-naphthyl)phenylsilane (**4ai**) after the second column with diastereomer **A** as the major species (**A**/**B** = 8.3:1) recorded in $CDCl_3$ at 298 K.

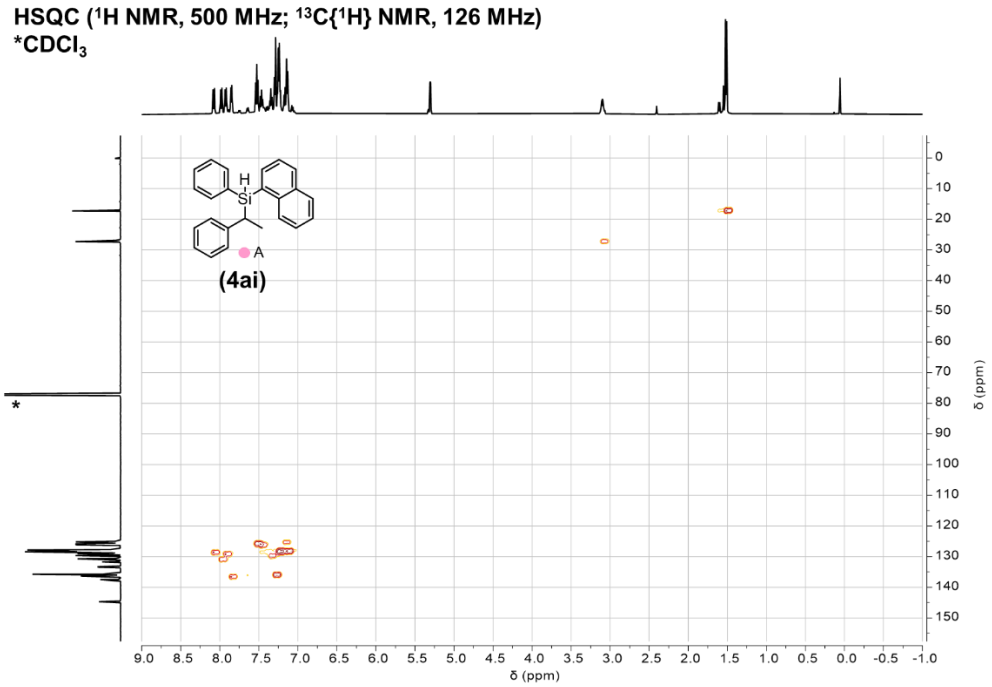

Figure A.160. HSQC NMR spectrum of (1-phenylethyl)(2-naphthyl)phenylsilane (**4ai**) after the second column with diastereomer **A** as the major species (**A**/**B** = 8.3:1) recorded in $CDCl_3$ at 298 K.

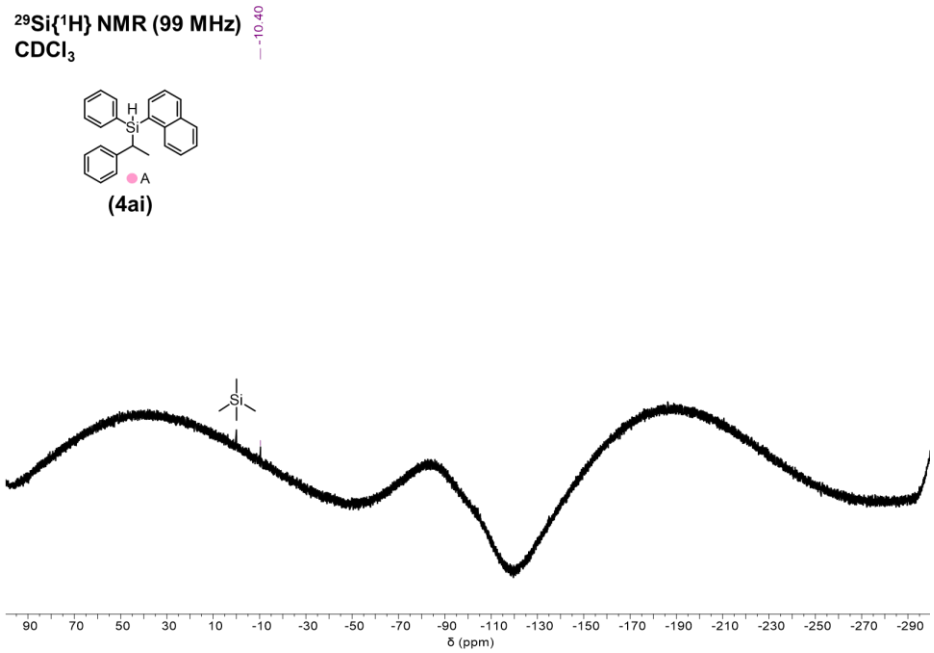

Figure A.161. ^{29}Si NMR spectrum of (1-phenylethyl)(2-naphthyl)phenylsilane (**4ai**) after the second column with diastereomer **A** as the major species (**A**/**B** = 8.3:1) recorded in $CDCl_3$ at 298 K.

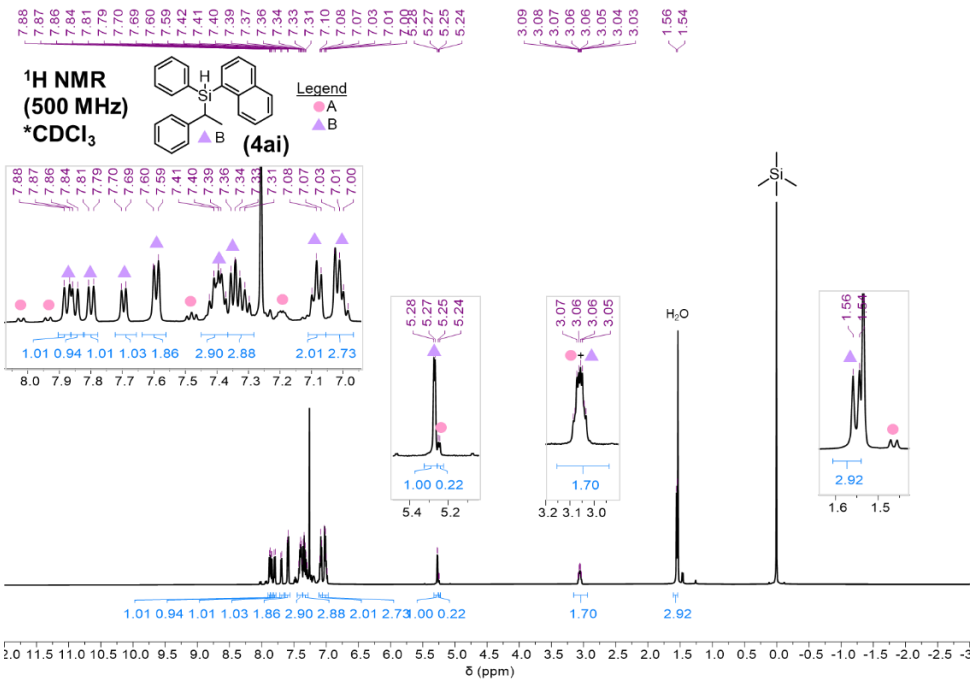

Figure A.162. ^{1}H NMR spectrum of (1-phenylethyl)(2-naphthyl)phenylsilane (**4ai**) after the second column with diastereomer **B** as the major species (**A**/**B** = 1:4.5) recorded in $CDCl_3$ at 298 K.

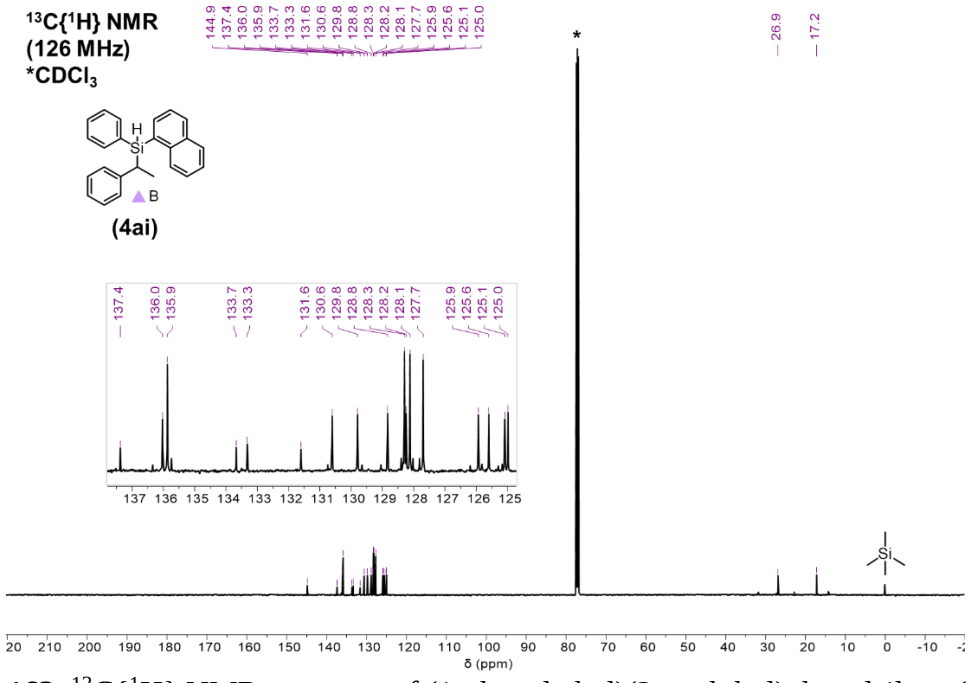

Figure A.163. ^{13}C{^{1}H} NMR spectrum of (1-phenylethyl)(2-naphthyl)phenylsilane (**4ai**) after the second column with diastereomer **B** as the major species (**A**/**B** = 1:4.5) recorded in $CDCl_3$ at 298 K.

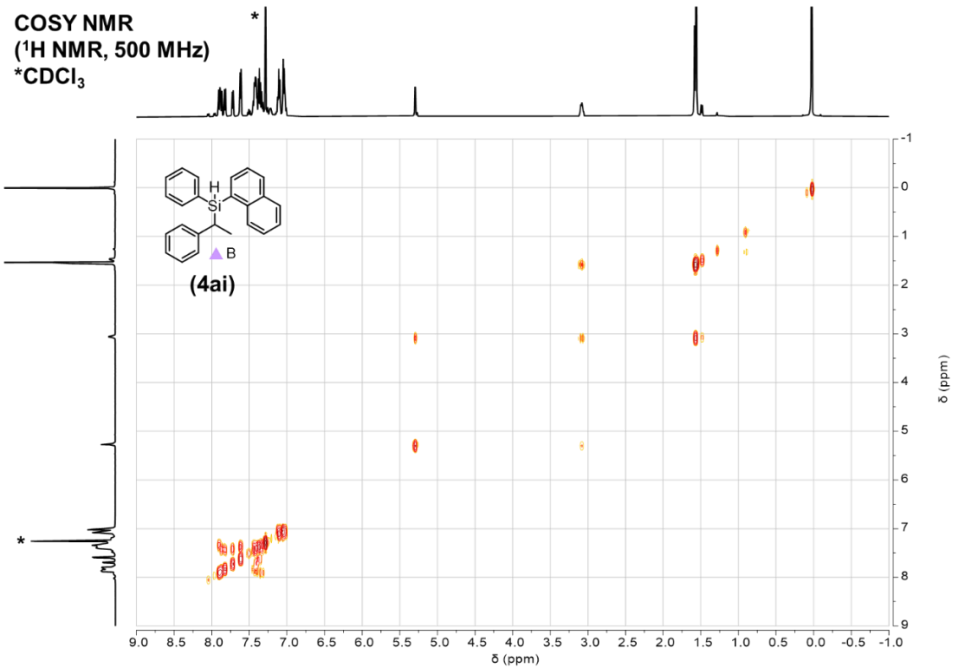

Figure A.164. COSY NMR spectrum of (1-phenylethyl)(2-naphthyl)phenylsilane (**4ai**) after the second column with diastereomer **B** as the major species (**A**/**B** = 1:4.5) recorded in $CDCl_3$ at 298 K.

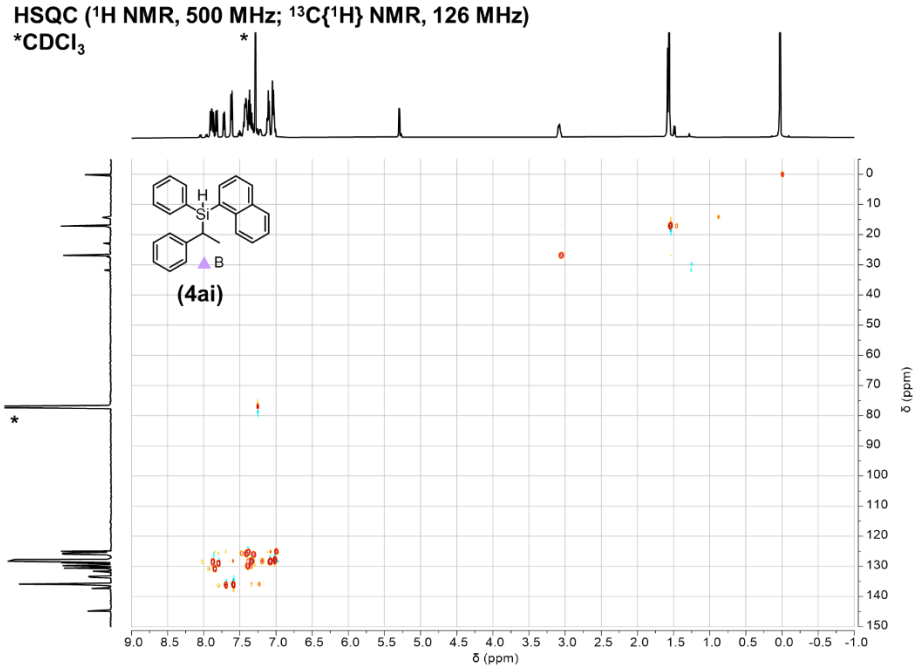

Figure A.165. HSQC NMR spectrum of (1-phenylethyl)(2-naphthyl)phenylsilane (**4ai**) after the second column with diastereomer **B** as the major species (**A**/**B** = 1:4.5) recorded in $CDCl_3$ at 298 K.

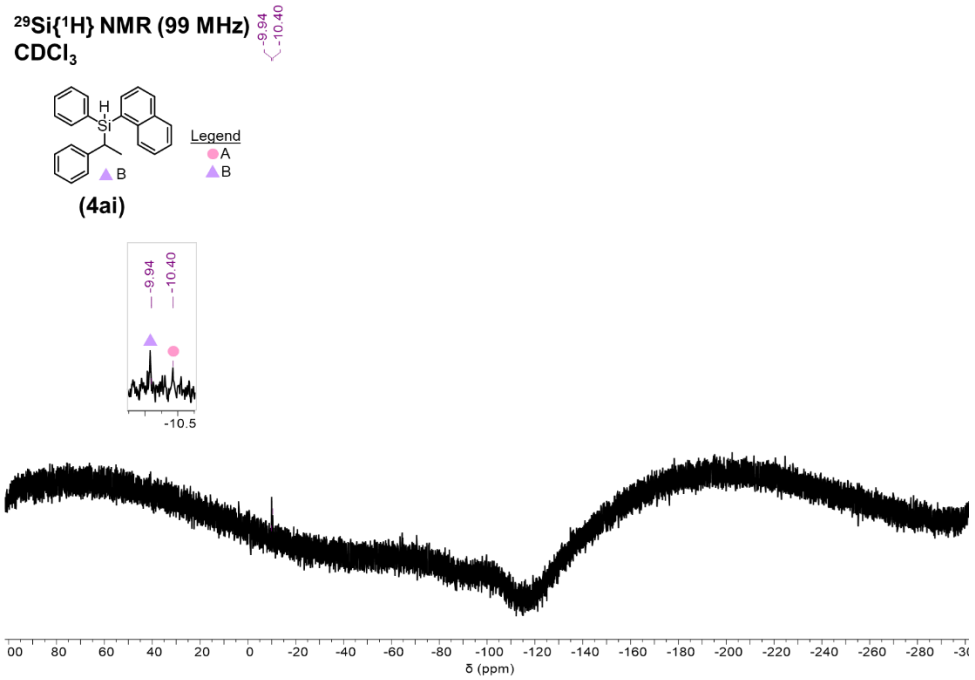

Figure A.166. ^{29}Si NMR spectrum of (1-phenylethyl)(2-naphthyl)phenylsilane (**4ai**) diastereomers **B** as the major species (**A**/**B** = 1:4.5) after the second column recorded in $CDCl_3$ at 298 K.

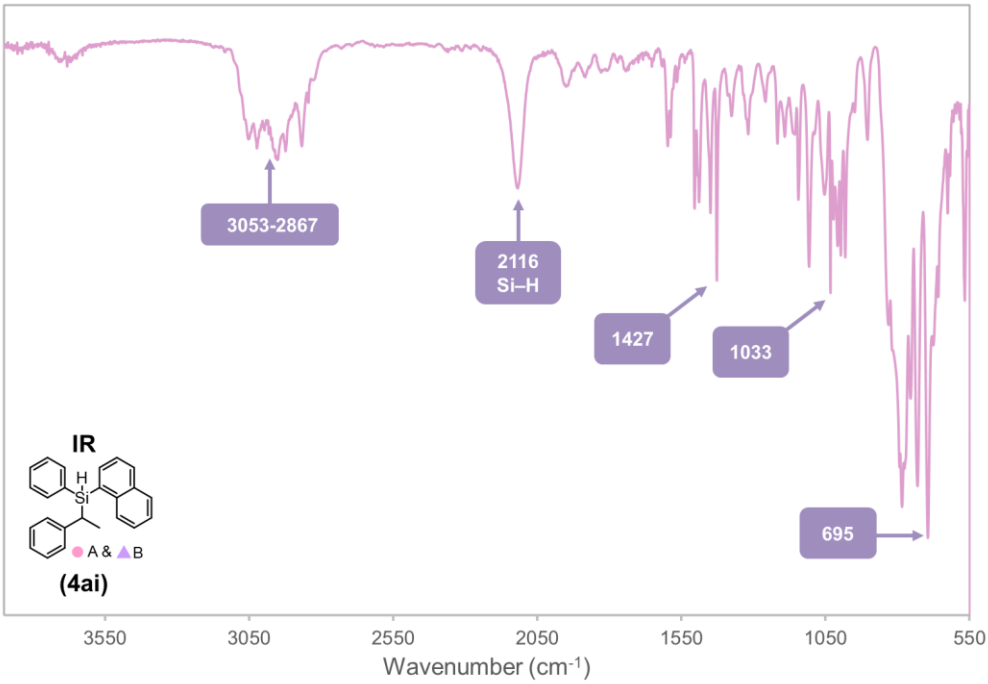

Figure A.167. IR spectrum of (1-phenylethyl)(2-naphthyl)phenylsilane (**4ai**) diastereomers **A** and **B** (**A**/**B** = 1.04:1) after the first column recorded neat at 298 K.

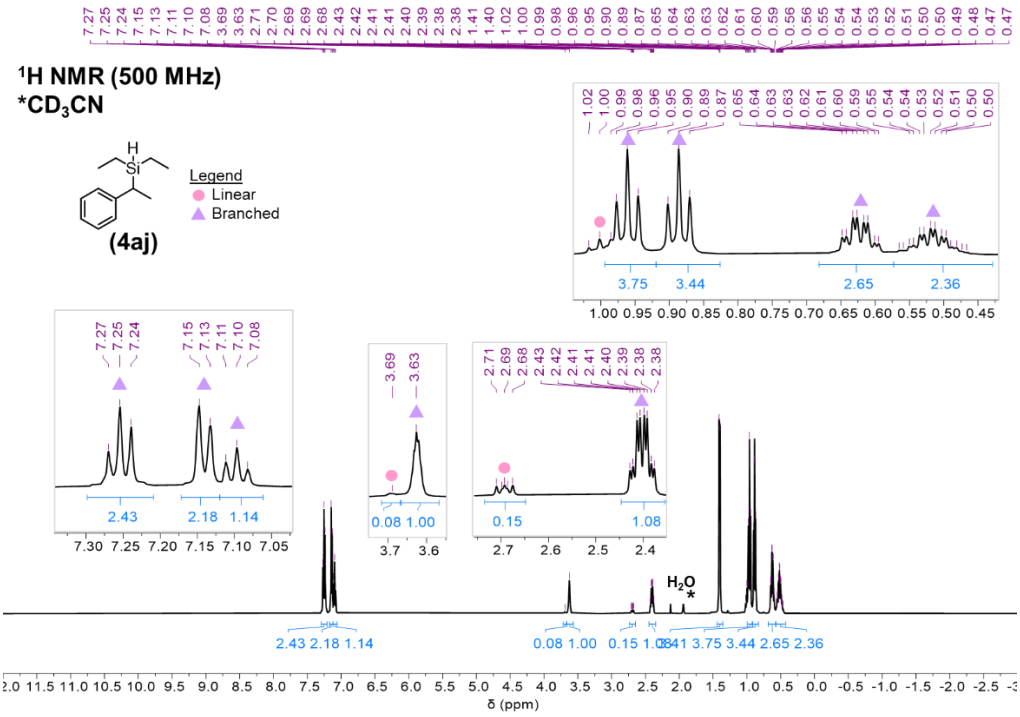

Figure A.168. ^{1}H NMR spectrum of (1-phenylethyl)diethylsilane (**4aj**) recorded in CD_3CN at 298 K.

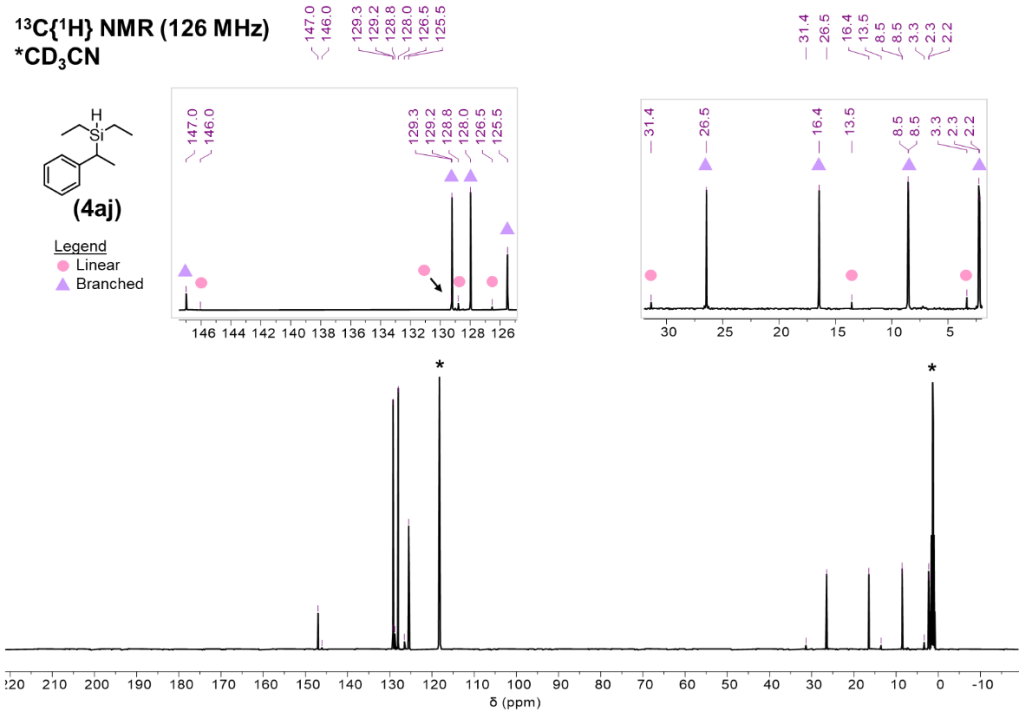

Figure A.169. ^{13}C{^{1}H} NMR spectrum of (1-phenylethyl)diethylsilane (**4aj**) recorded in CD_3CN at 298 K.

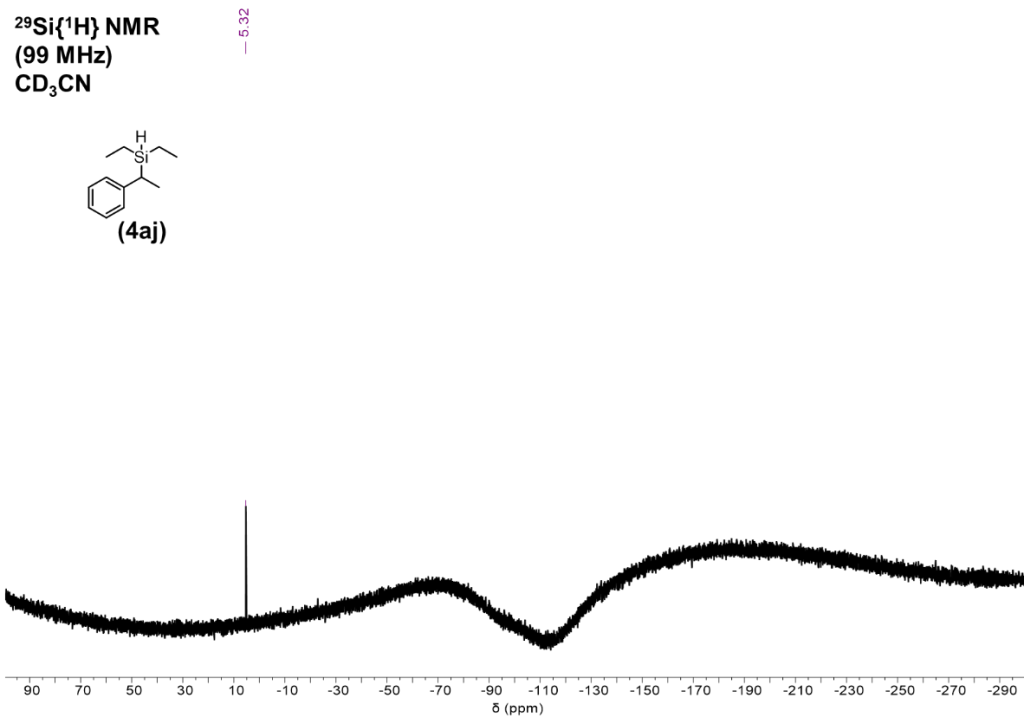

Figure A.170. ^{29}Si NMR spectrum of (1-phenylethyl)diethylsilane (**4aj**) recorded in CD_3CN at 298 K.

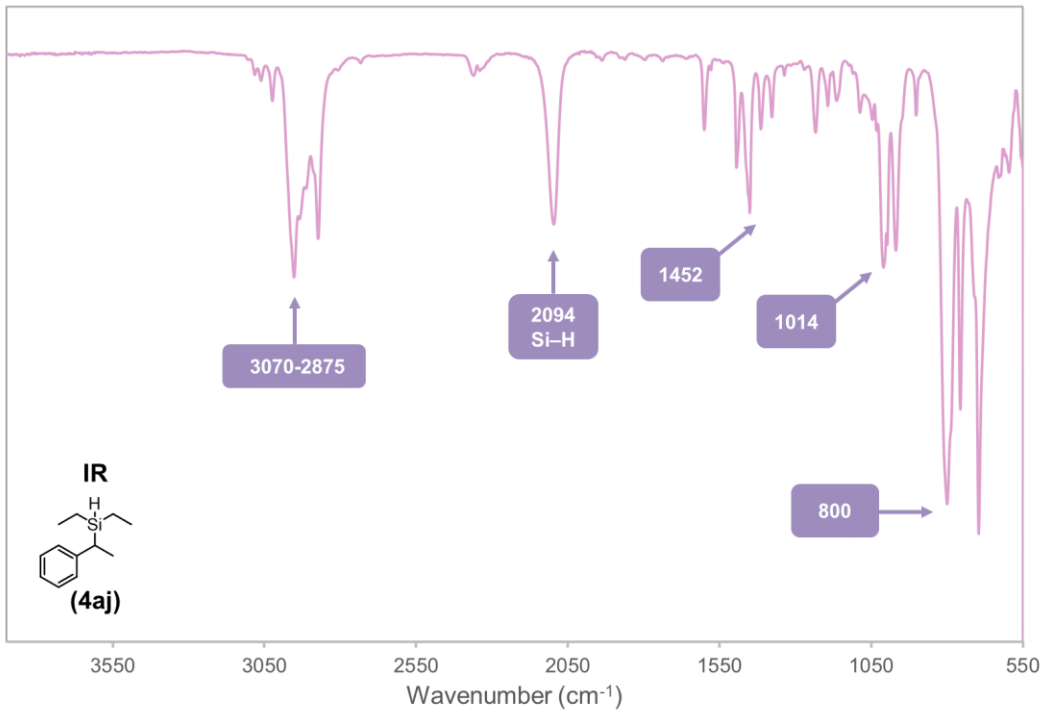

Figure A.171. IR spectrum of (1-phenylethyl)diethylsilane (**4aj**) recorded neat at 298 K.

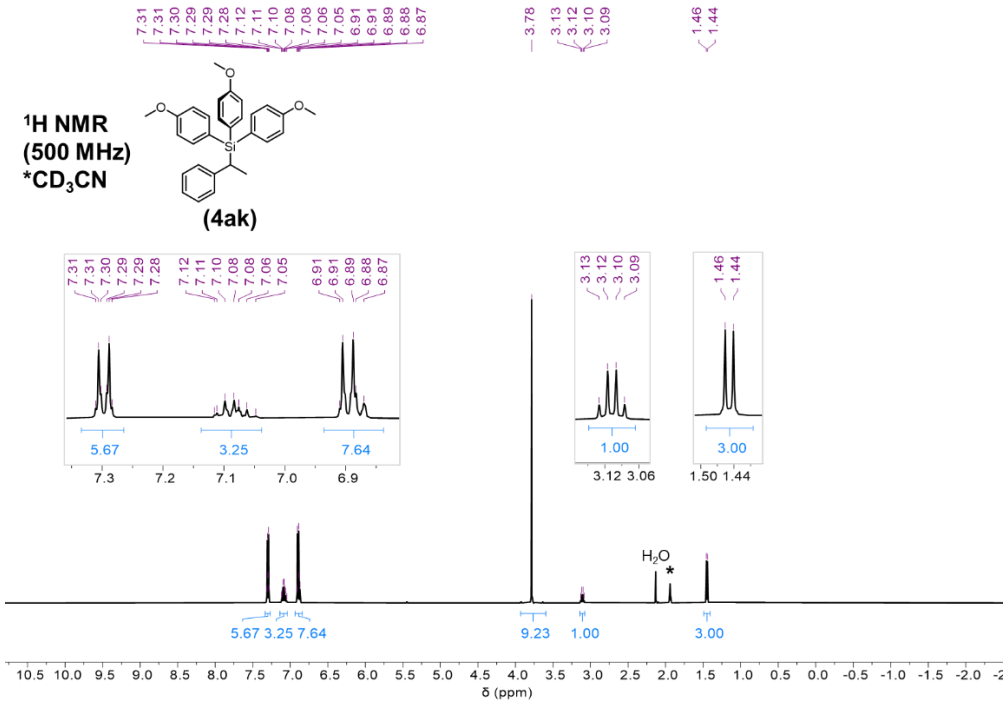

Figure A.172. ^{1}H NMR spectrum of (1-phenylethyl)tri(4-methoxyphenyl)silane (**4ak**) recorded in CD_3CN at 298 K.

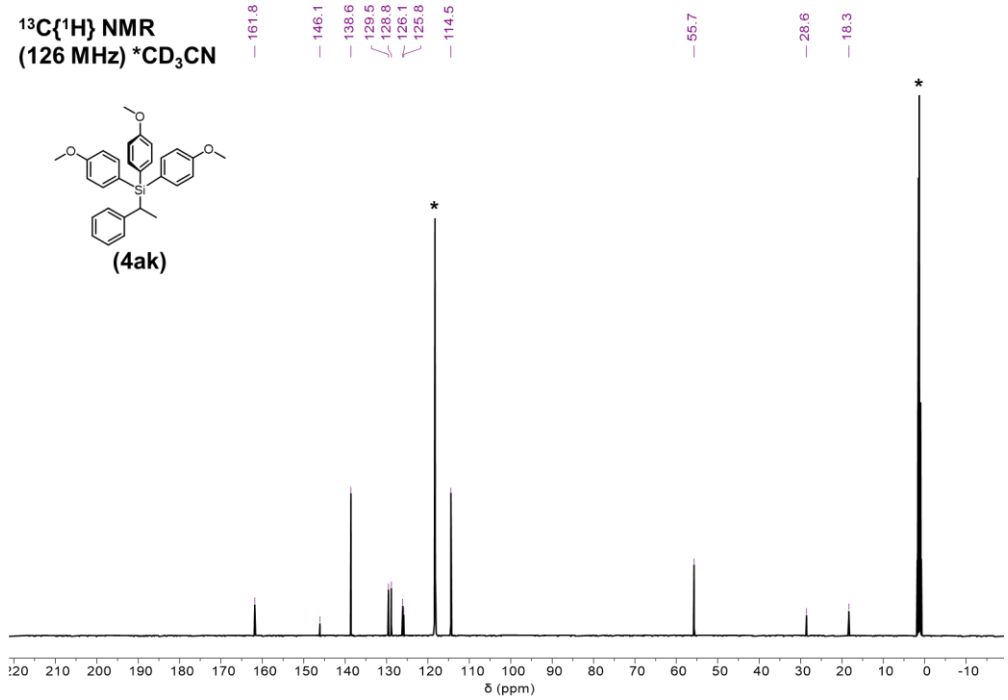

Figure A.173. $^{13}C\{^{1}H\}$ NMR spectrum of (1-phenylethyl)tri(4-methoxyphenyl)silane (**4ak**) recorded in CD_3CN at 298 K.

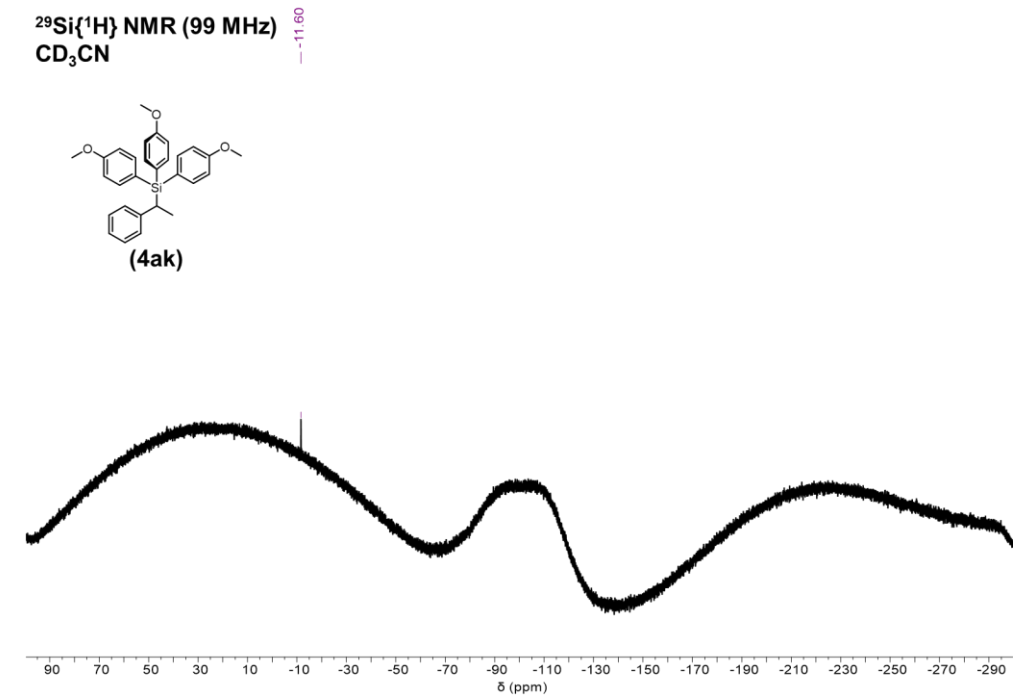

Figure A.174. ^{29}Si NMR spectrum of (1-phenylethyl)tri(4-methoxyphenyl)silane (**4ak**) recorded in CD_3CN at 298 K.

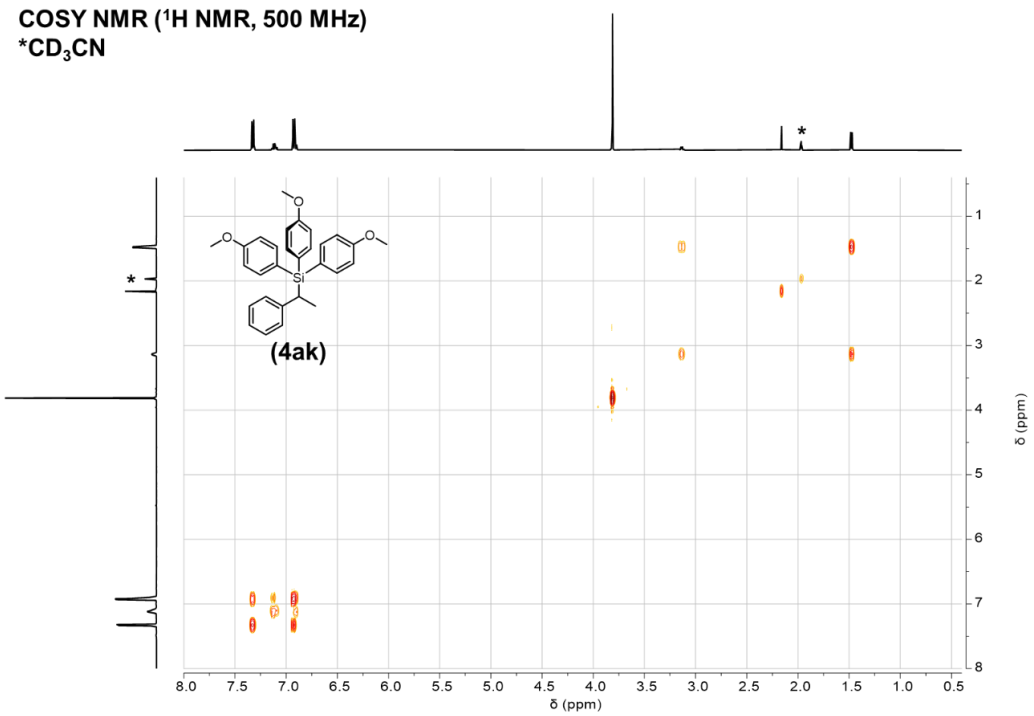

Figure A.175. COSY NMR spectrum of (1-phenylethyl)tri(4-methoxyphenyl)silane (**4ak**) recorded in CD_3CN at 298 K.

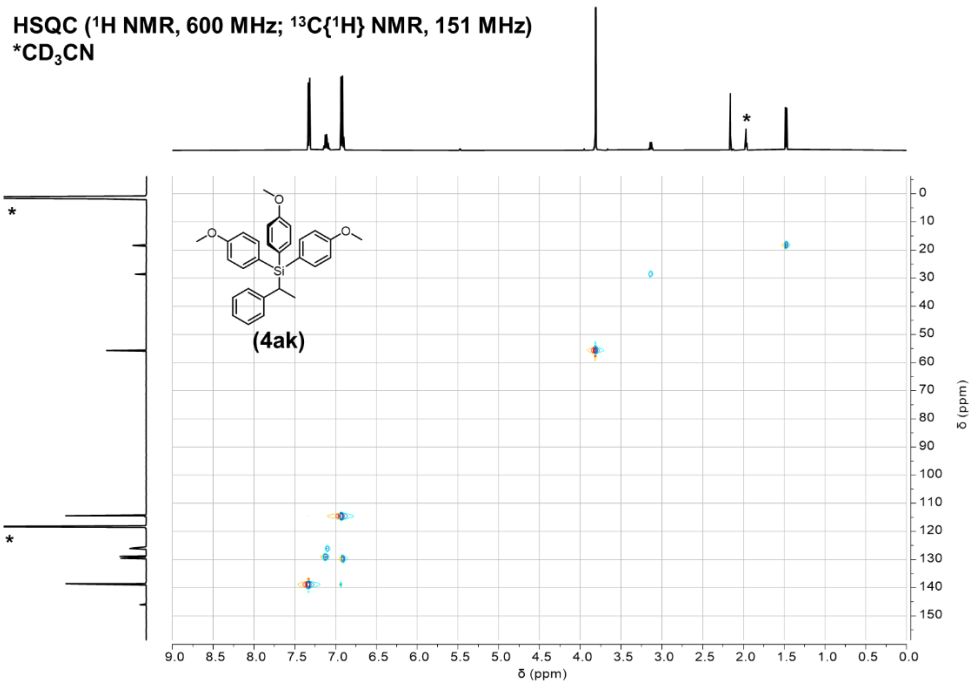

Figure A.176. HSQC NMR spectrum of (1-phenylethyl)tri(4-methoxyphenyl)silane (**4ak**) recorded in CD_3CN at 298 K.

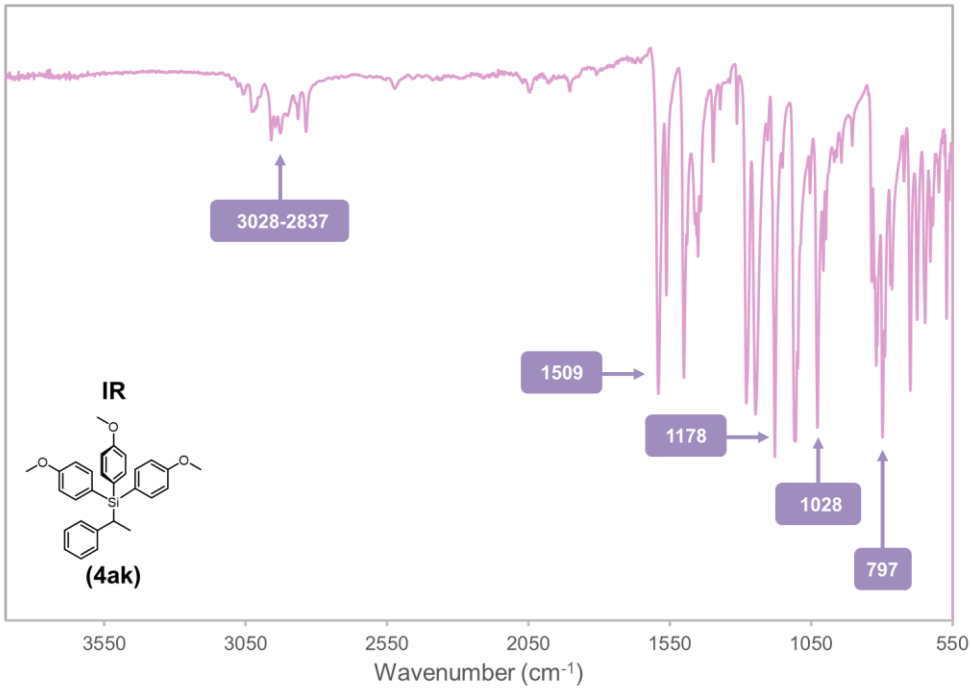

Figure A.177. IR spectrum of (1-phenylethyl)tri(4-methoxyphenyl)silane (**4ak**) recorded neat at 298 K.

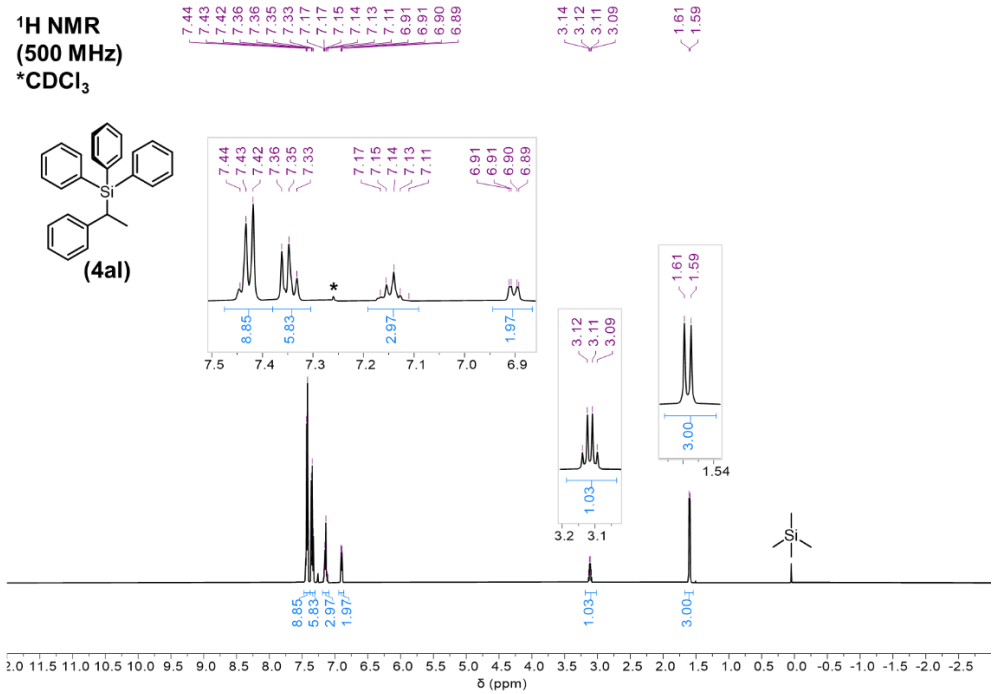

Figure A.178. ^{1}H NMR spectrum of (1-phenylethyl)triphenylsilane (**4al**) recorded in $CDCl_3$ at 298 K.

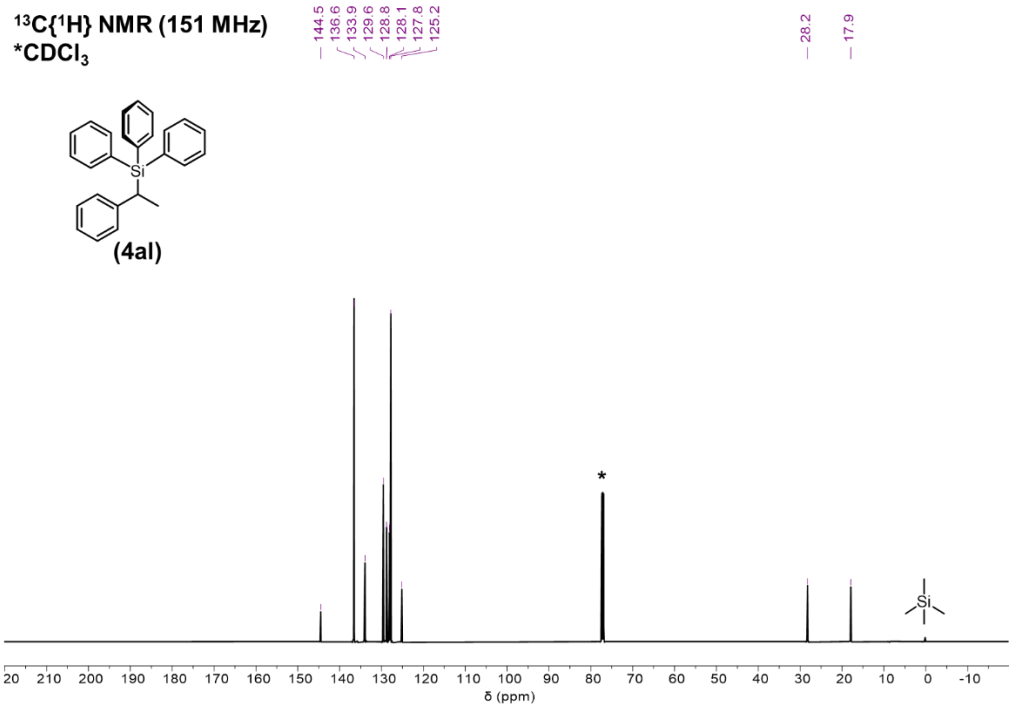

Figure A.179. $^{13}C\{^{1}H\}$ NMR spectrum of (1-phenylethyl)triphenylsilane (**4al**) recorded in $CDCl_3$ at 298 K.

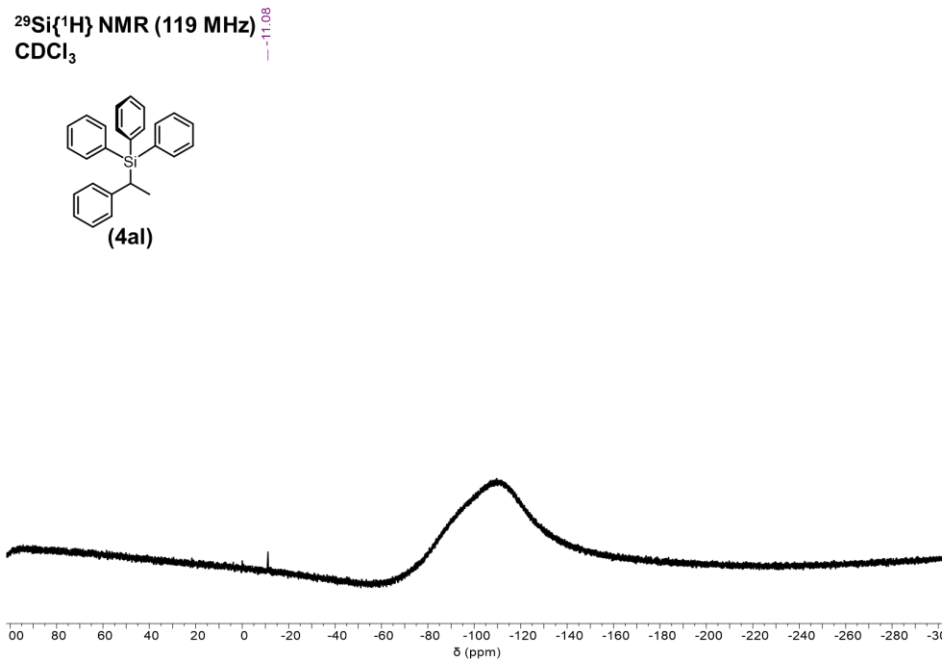

Figure A.180. ^{29}Si NMR spectrum of (1-phenylethyl)triphenylsilane (**4al**) recorded in $CDCl_3$ at 298 K.

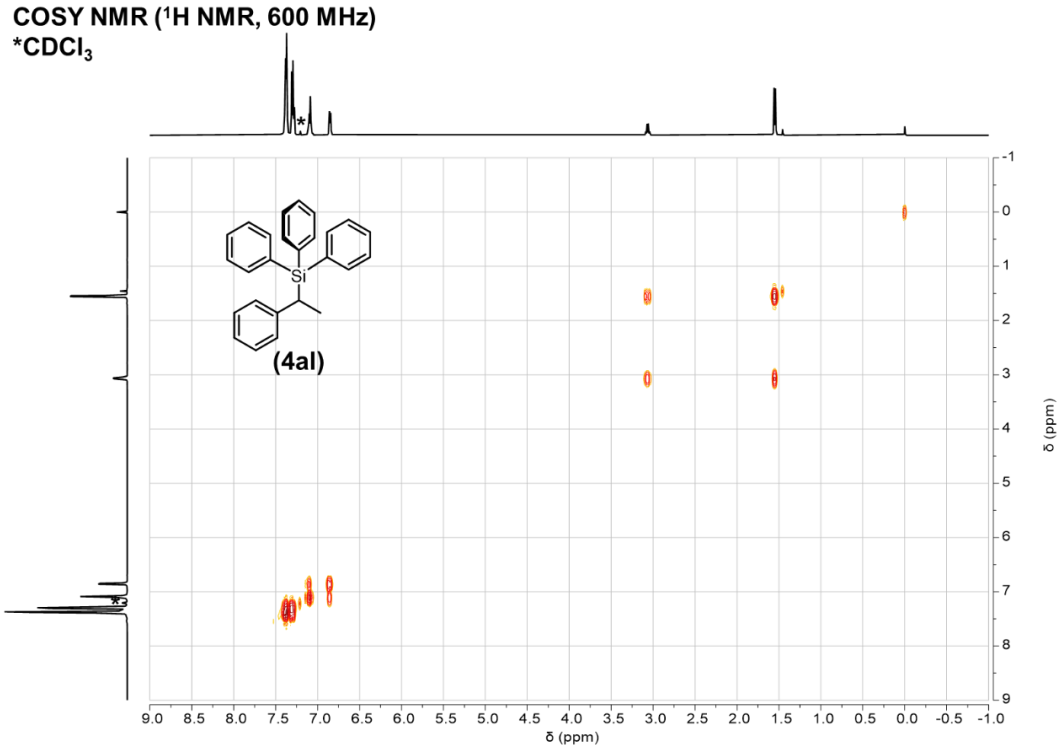

Figure A.181. COSY NMR spectrum of (1-phenylethyl)triphenylsilane (**4al**) recorded in $CDCl_3$ at 298 K.

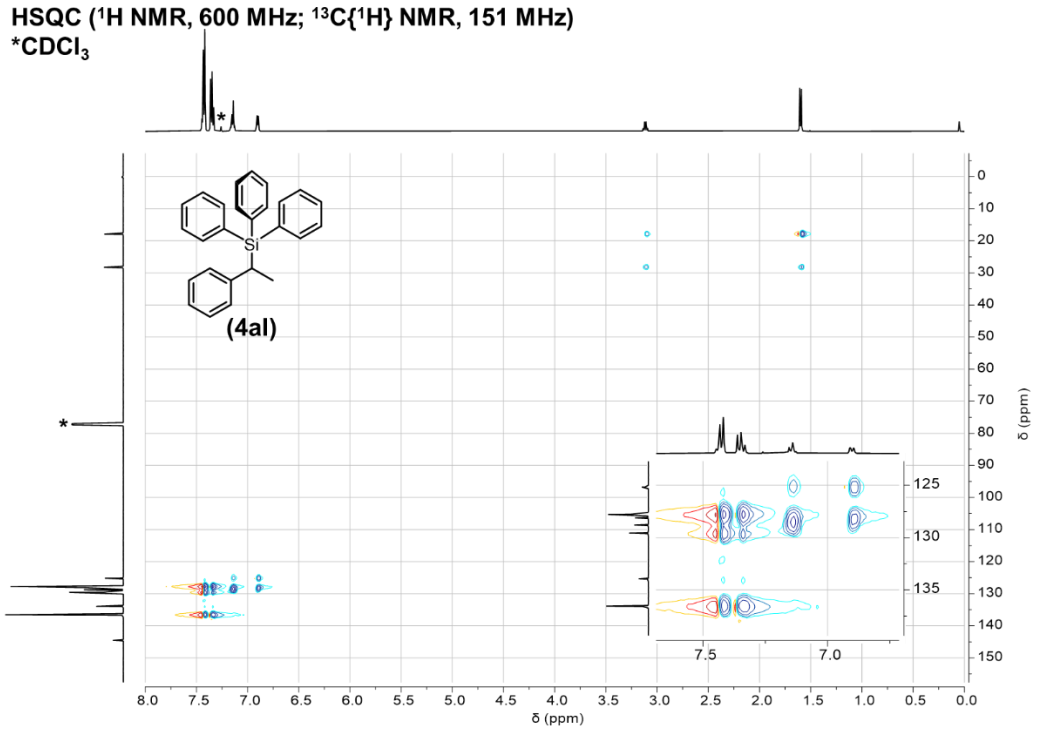

Figure A.182. HSQC NMR spectrum of (1-phenylethyl)triphenylsilane (**4al**) recorded in $CDCl_3$ at 298 K.

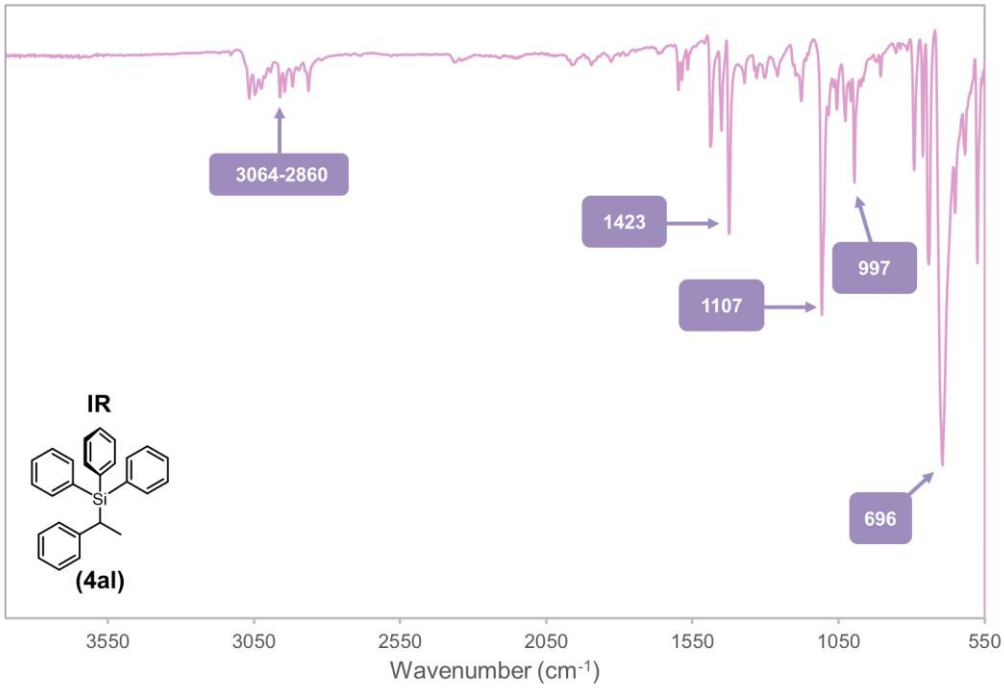

Figure A.183. IR spectrum of (1-phenylethyl)triphenylsilane (**4al**) recorded neat at 298 K.

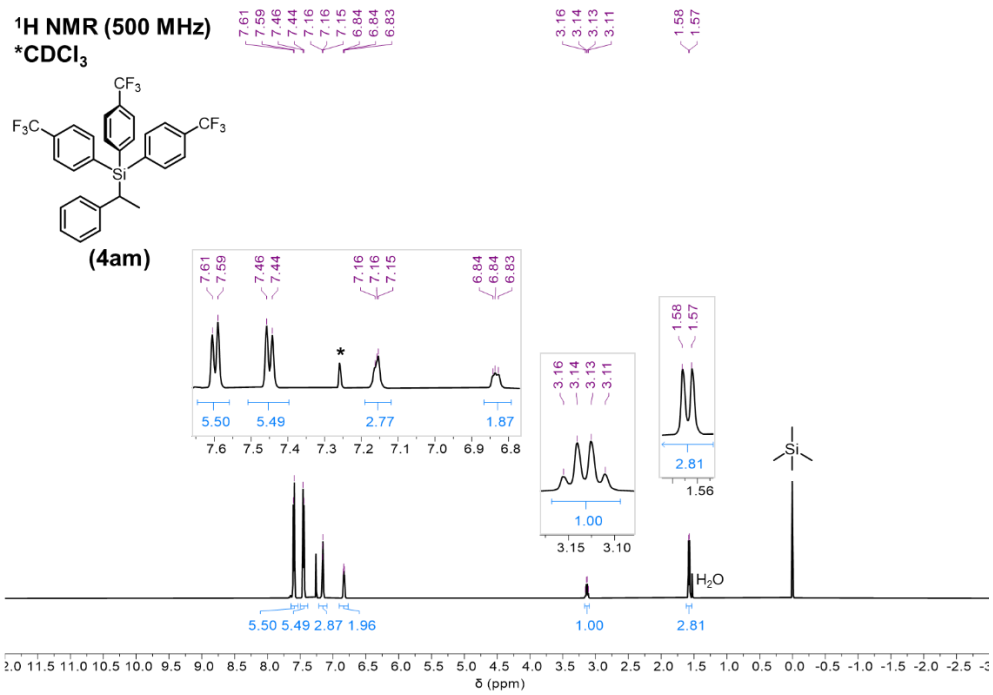

Figure A.184. ^{1}H NMR spectrum of (1-phenylethyl)tri[4-(trifluoromethyl)phenyl]silane (**4am**) recorded in $CDCl_3$ at 298 K.

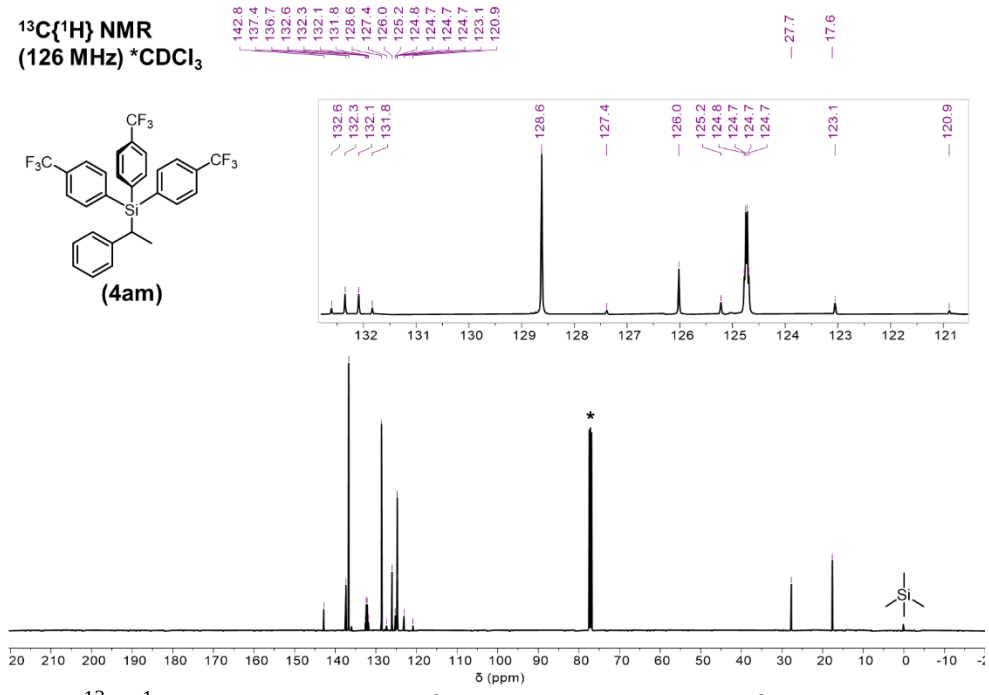

Figure A.185. $^{13}C\{^{1}H\}$ NMR spectrum of (1-phenylethyl)tri[4-(trifluoromethyl)phenyl]silane (**4am**) recorded in $CDCl_3$ at 298 K.

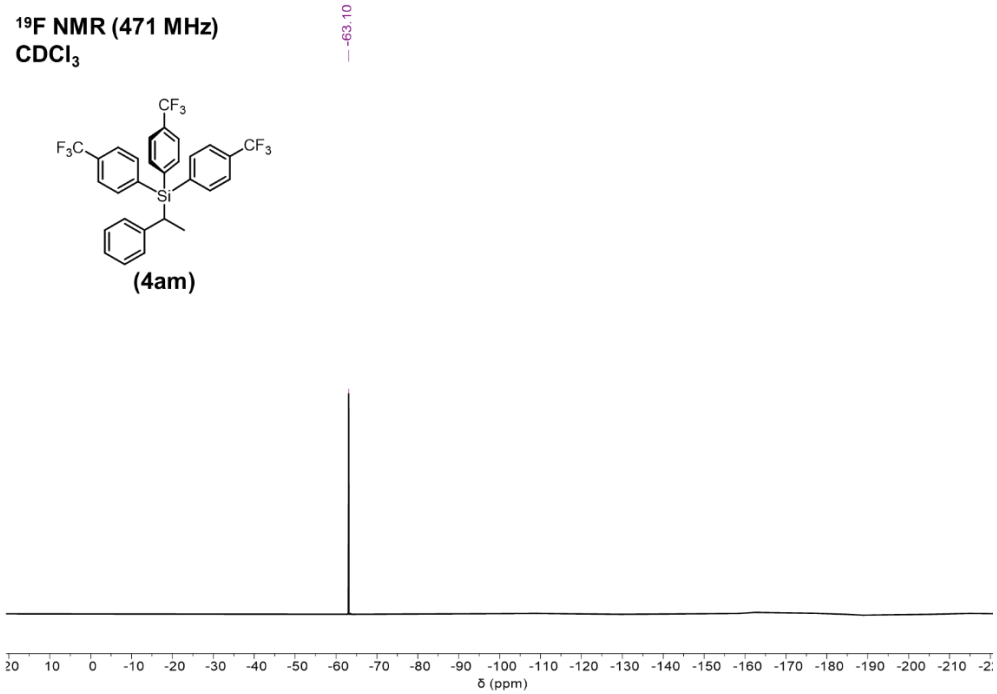

Figure A.186. ^{19}F NMR spectrum of (1-phenylethyl)tri[4-(trifluoromethyl)phenyl]silane (**4am**) recorded in $CDCl_3$ at 298 K.

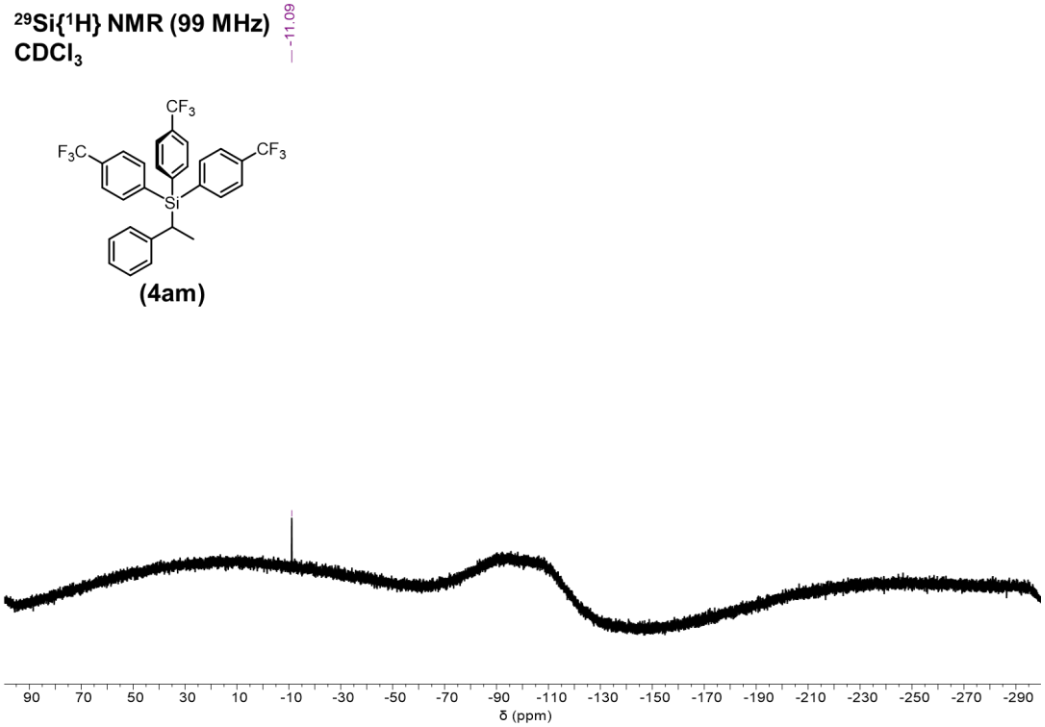

Figure A.187. ^{29}Si NMR spectrum of (1-phenylethyl)tri[4-(trifluoromethyl)phenyl]silane (**4am**) recorded in $CDCl_3$ at 298 K.

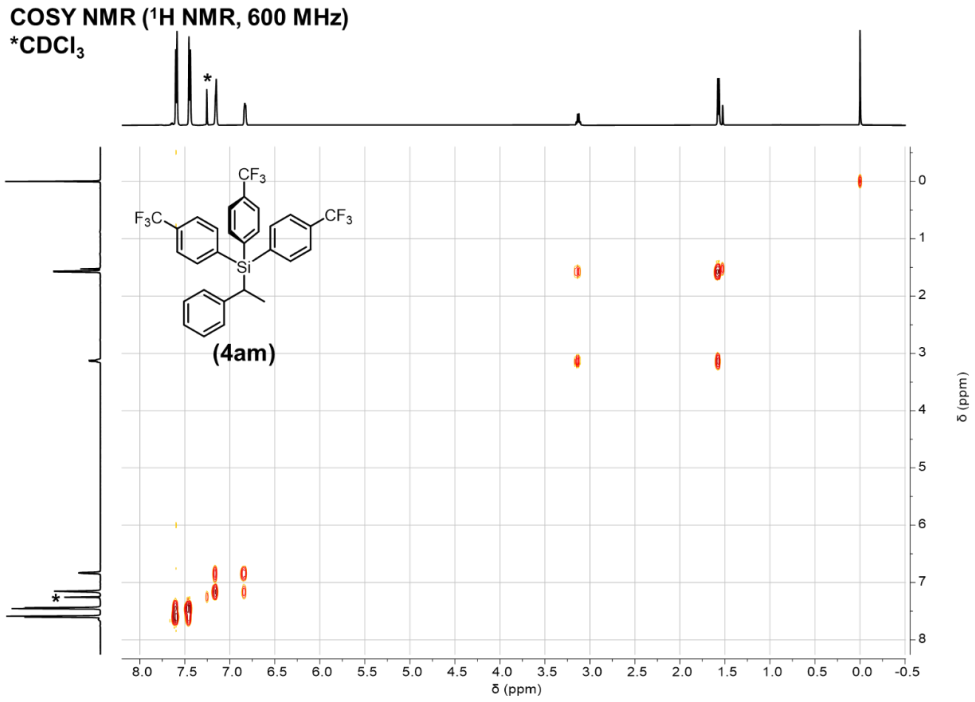

Figure A.188. COSY NMR spectrum of (1-phenylethyl)tri[4-(trifluoromethyl)phenyl]silane (**4am**) recorded in $CDCl_3$ at 298 K.

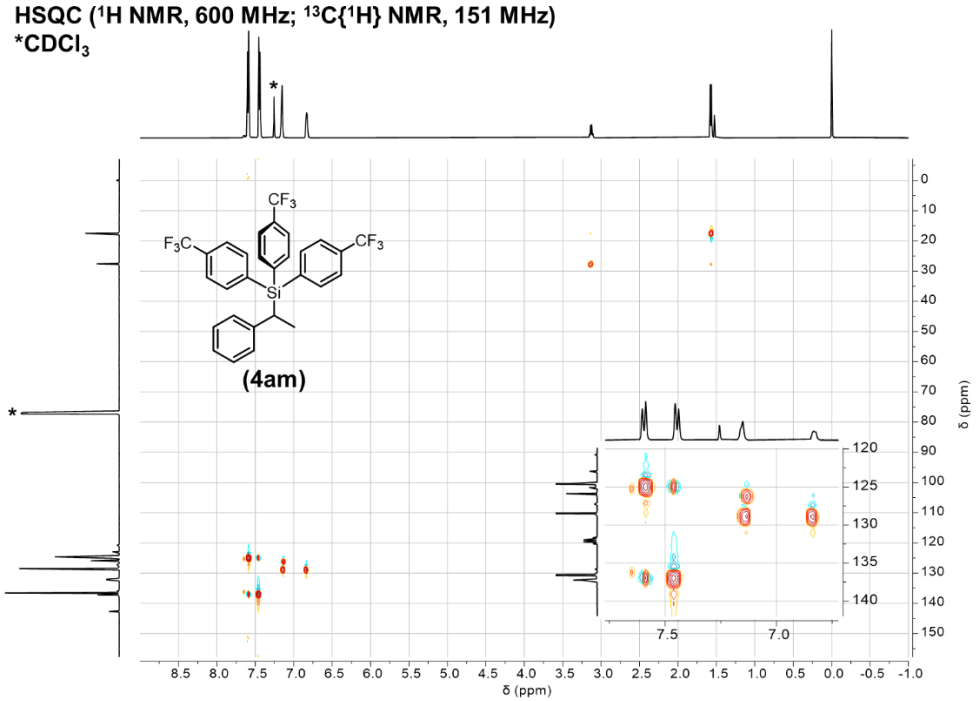

Figure A.189. HSQC NMR spectrum of (1-phenylethyl)tri[4-(trifluoromethyl)phenyl]silane (**4am**) recorded in $CDCl_3$ at 298 K.

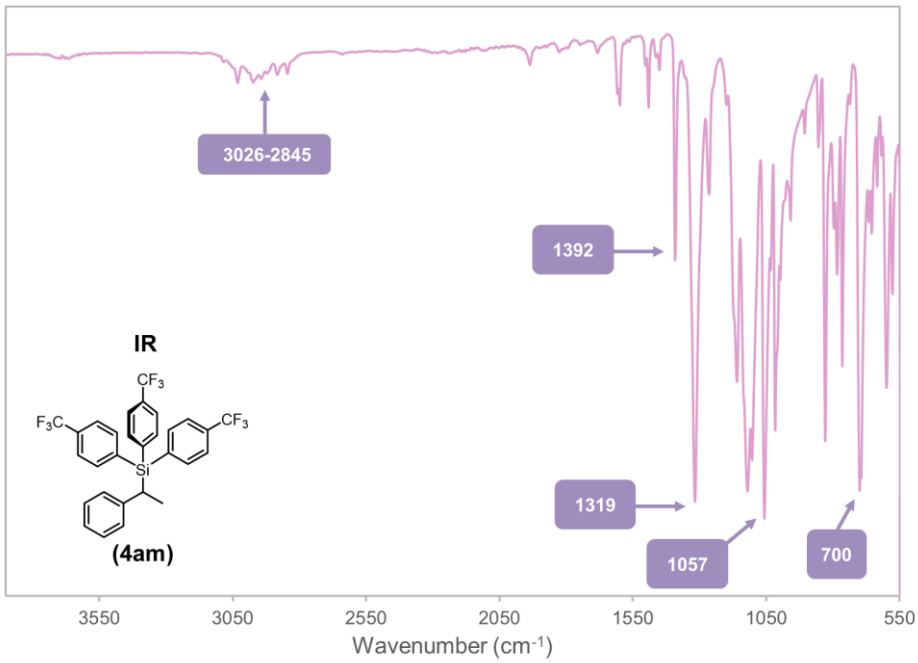

Figure A.190. IR spectrum of (1-phenylethyl)tri[4-(trifluoromethyl)phenyl]silane (**4am**) recorded neat at 298 K.

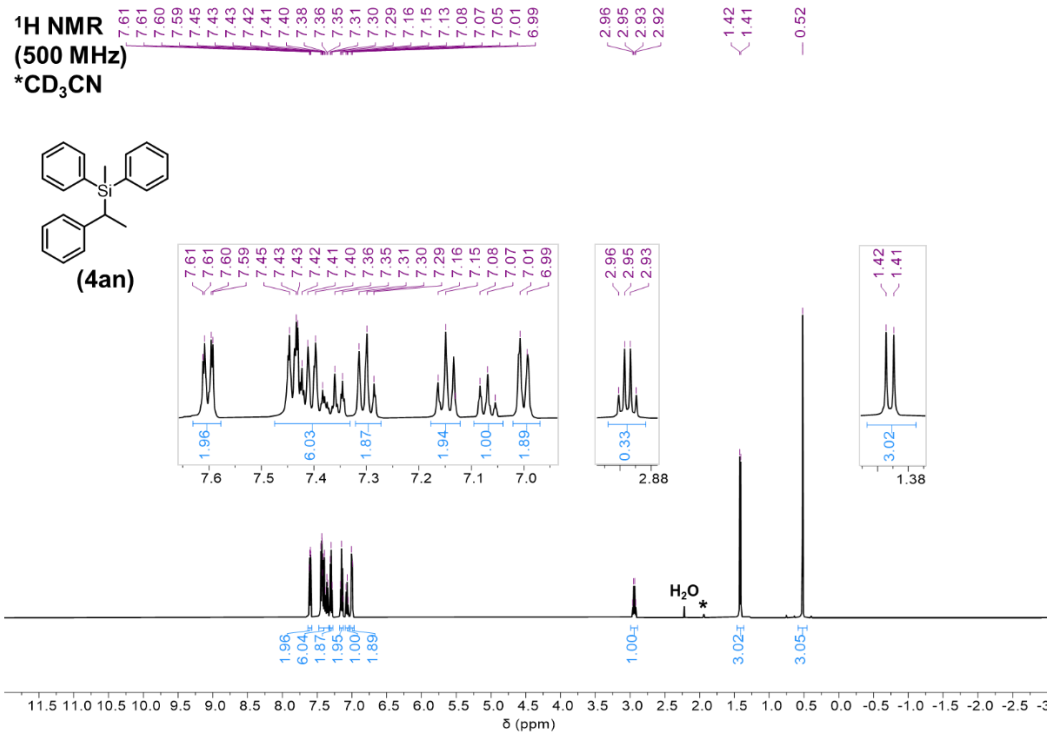

Figure A.191. ^{1}H NMR spectrum of (1-phenylethyl)diphenylmethylsilane (**4an**) recorded in CD_3CN at 298 K.

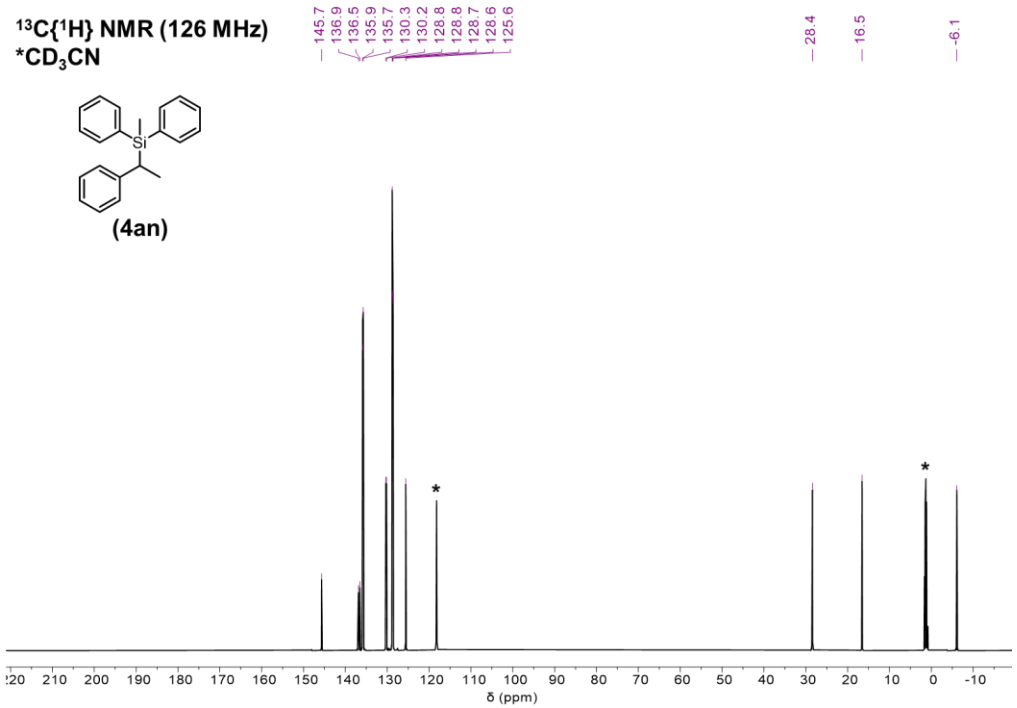

Figure A.192. $^{13}C\{^{1}H\}$ NMR spectrum of (1-phenylethyl)diphenylmethylsilane (**4an**) recorded in CD_3CN at 298 K.

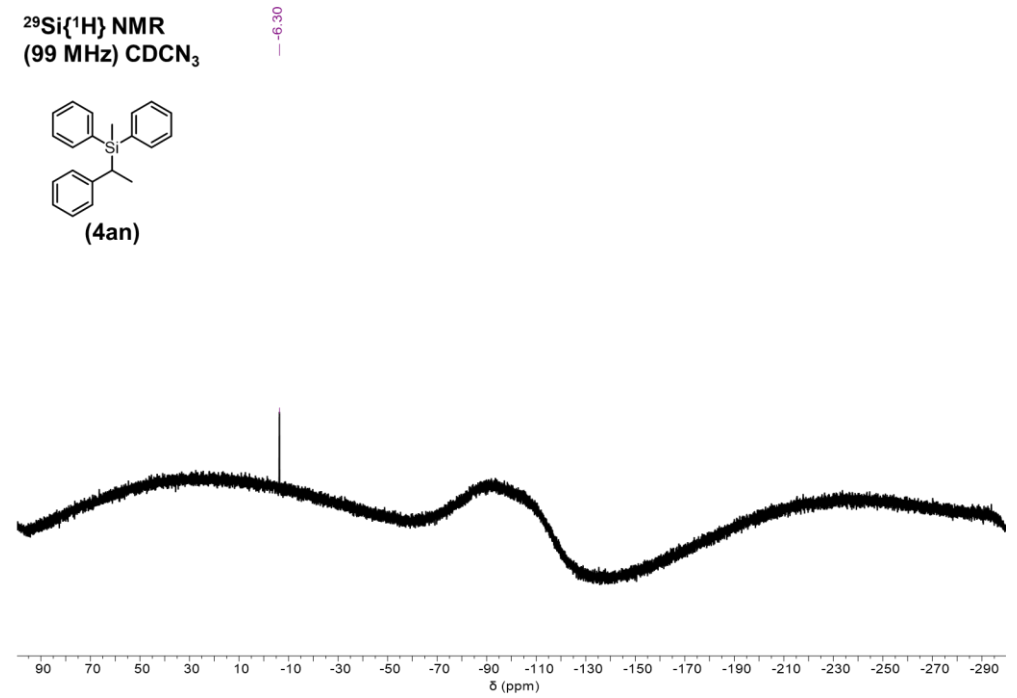

Figure A.193. ^{29}Si NMR spectrum of (1-phenylethyl)diphenylmethylsilane (**4an**) recorded in CD_3CN at 298 K.

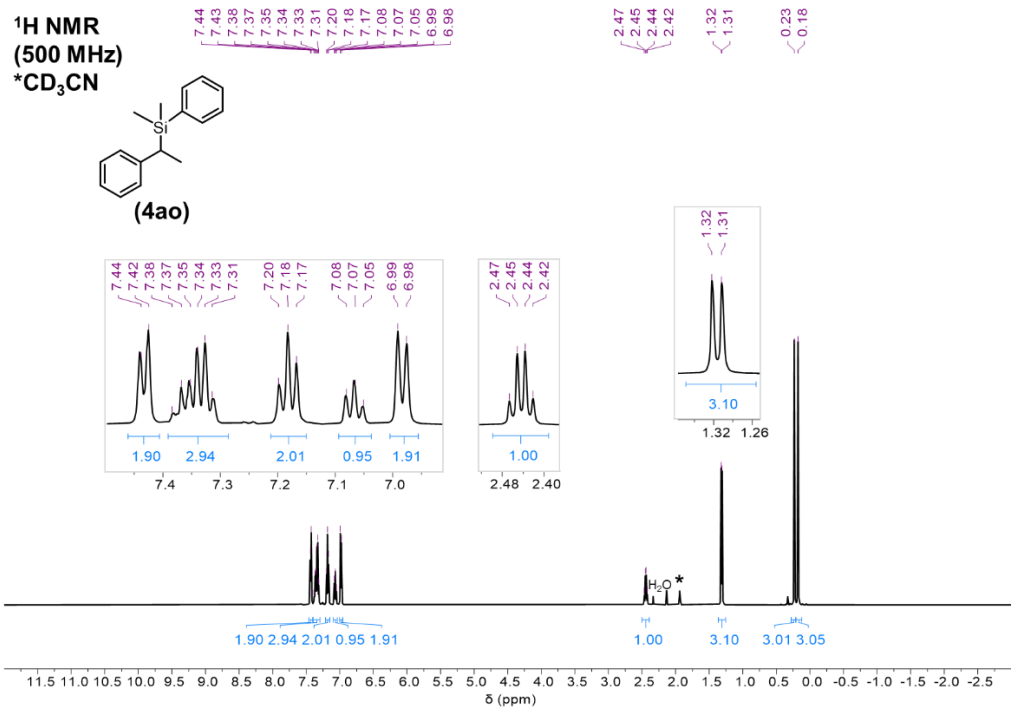

Figure A.194. ^{1}H NMR spectrum of (1-phenylethyl)phenyldimethylsilane (**4ao**) recorded in CD_3CN at 298 K.

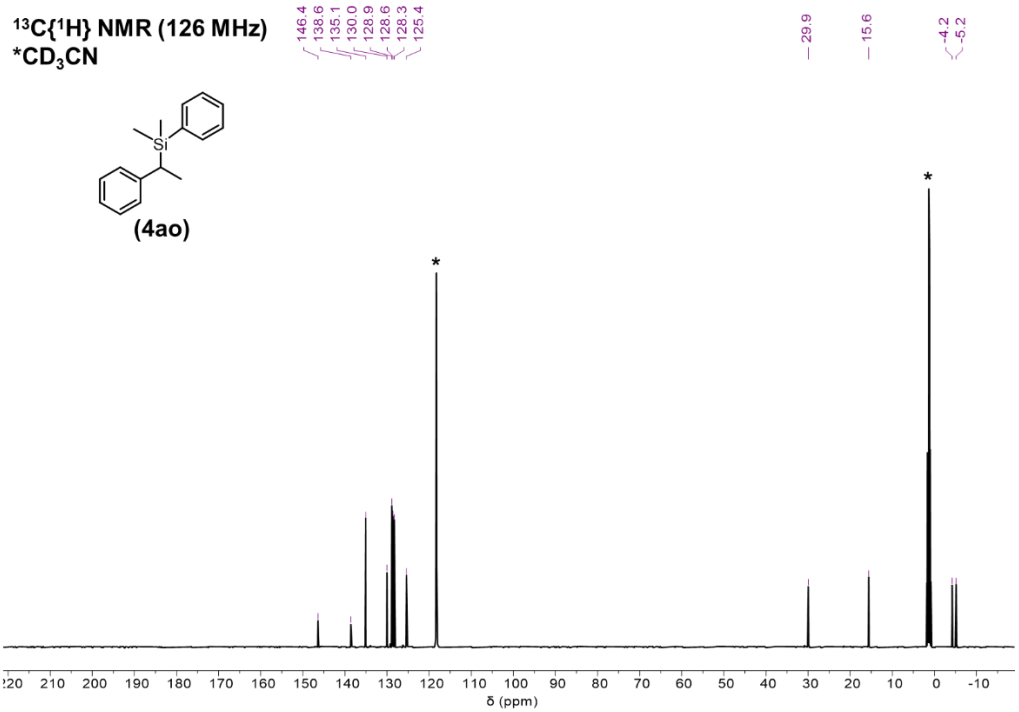

Figure A.195. $^{13}C\{^{1}H\}$ NMR spectrum of (1-phenylethyl)phenyldimethylsilane (**4ao**) recorded in CD_3CN at 298 K.

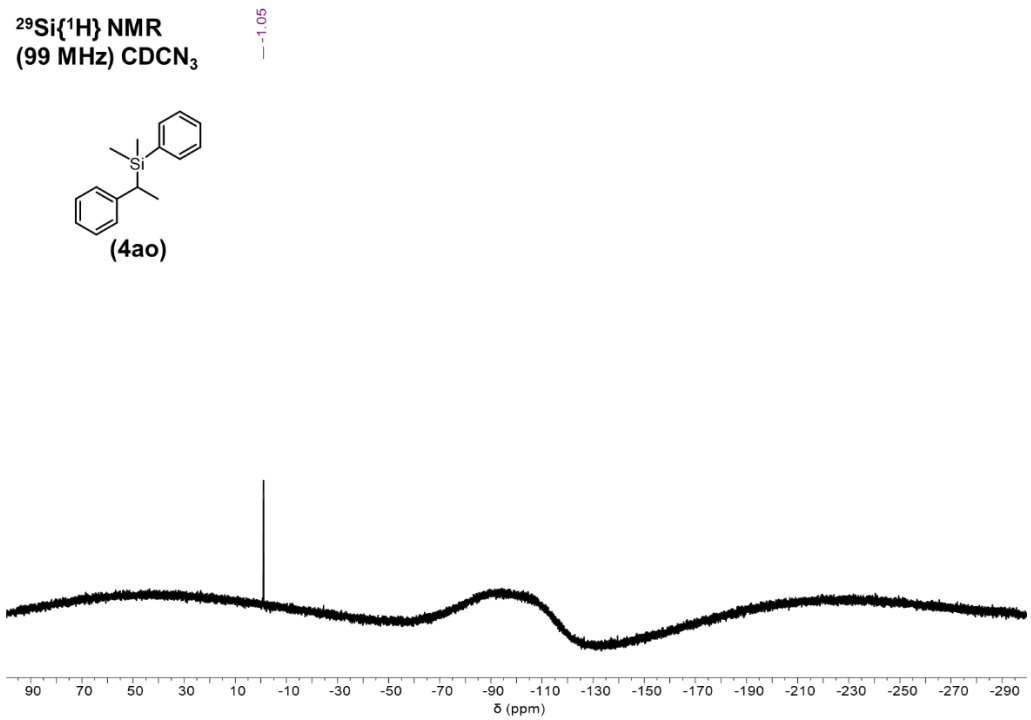

Figure A.196. ^{29}Si NMR spectrum of (1-phenylethyl)phenyldimethylsilane (**4ao**) recorded in CD_3CN at 298 K.

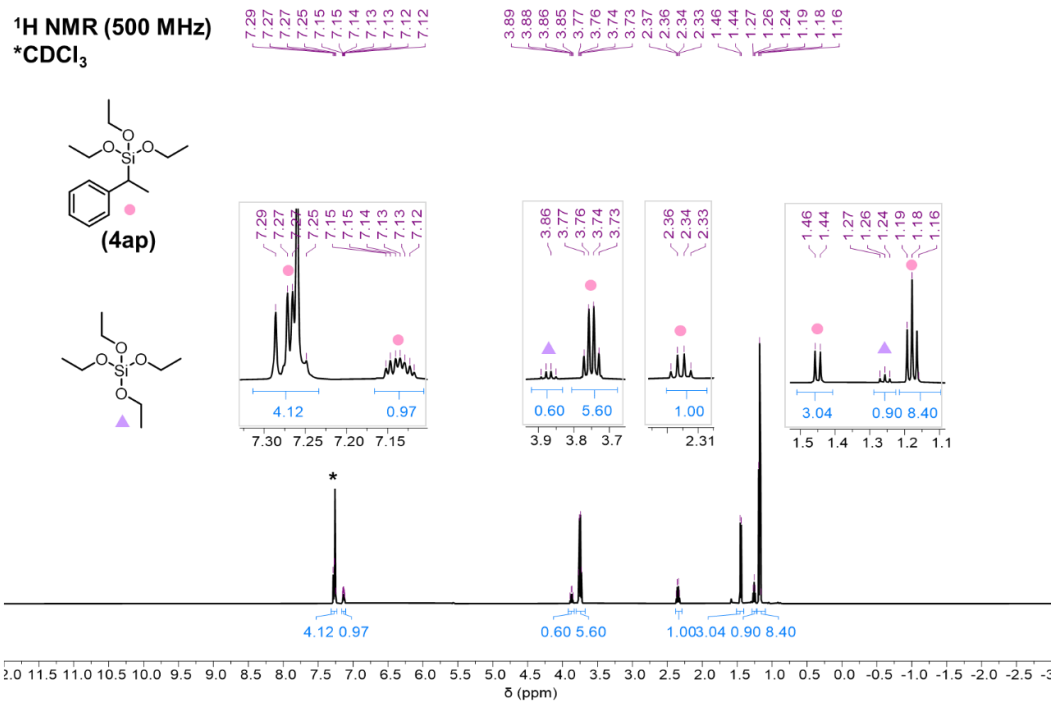

Figure A.197. ^{1}H NMR spectrum of (1-phenylethyl)triethoxysilane (**4ap**) recorded in $CDCl_3$ at 298 K.

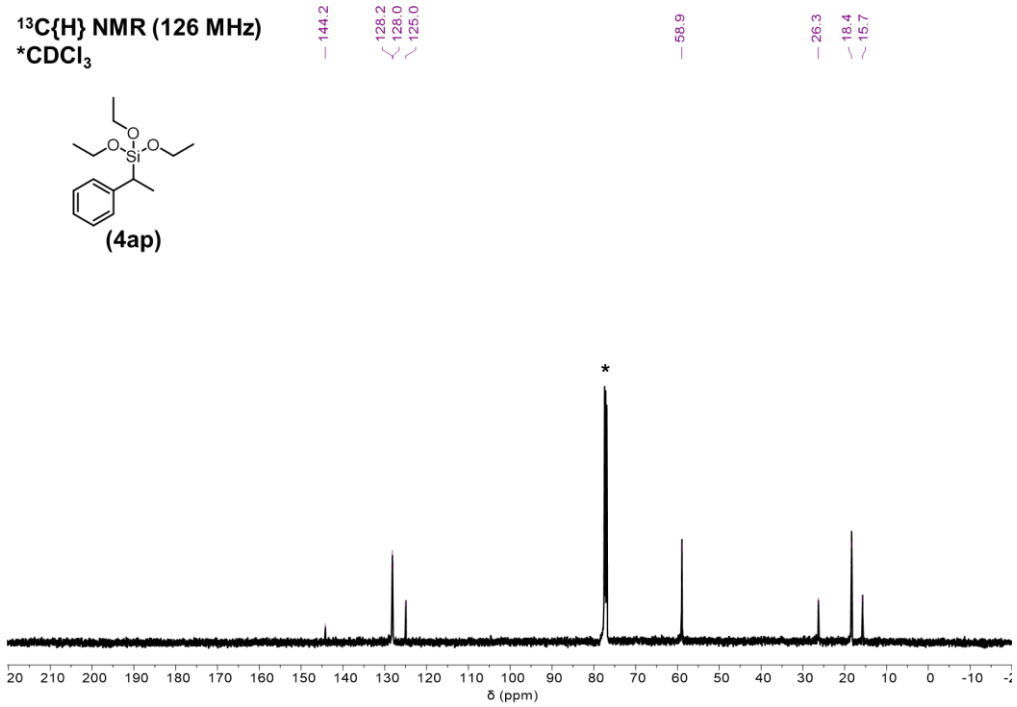

Figure A.198. $^{13}C\{^{1}H\}$ NMR spectrum of (1-phenylethyl)triethoxysilane (**4ap**) recorded in $CDCl_3$ at 298 K.

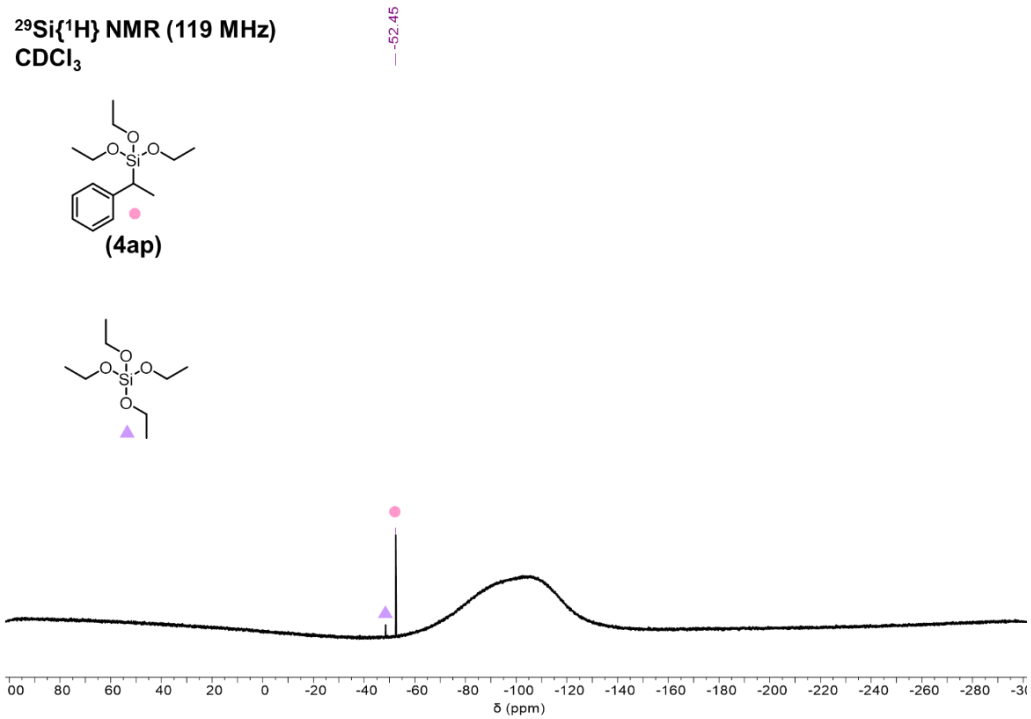

Figure A.199. ^{29}Si NMR spectrum of (1-phenylethyl)triethoxysilane (**4ap**) recorded in $CDCl_3$ at 298 K.

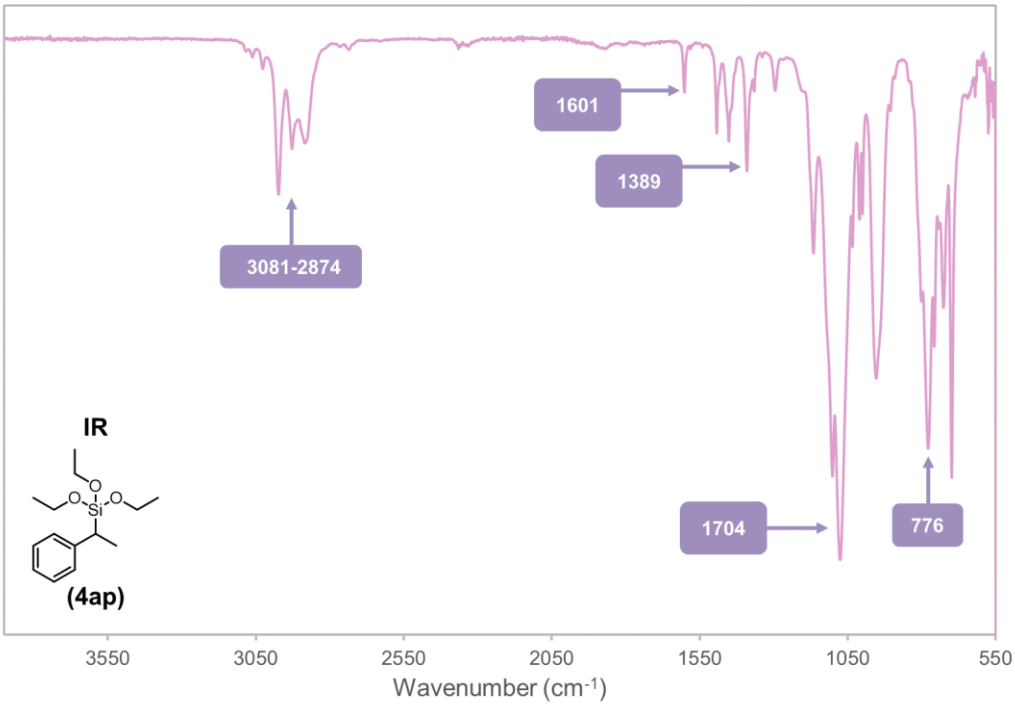

Figure A.200. IR NMR spectrum of (1-phenylethyl)triethoxysilane (**4ap**) recorded neat at 298 K.

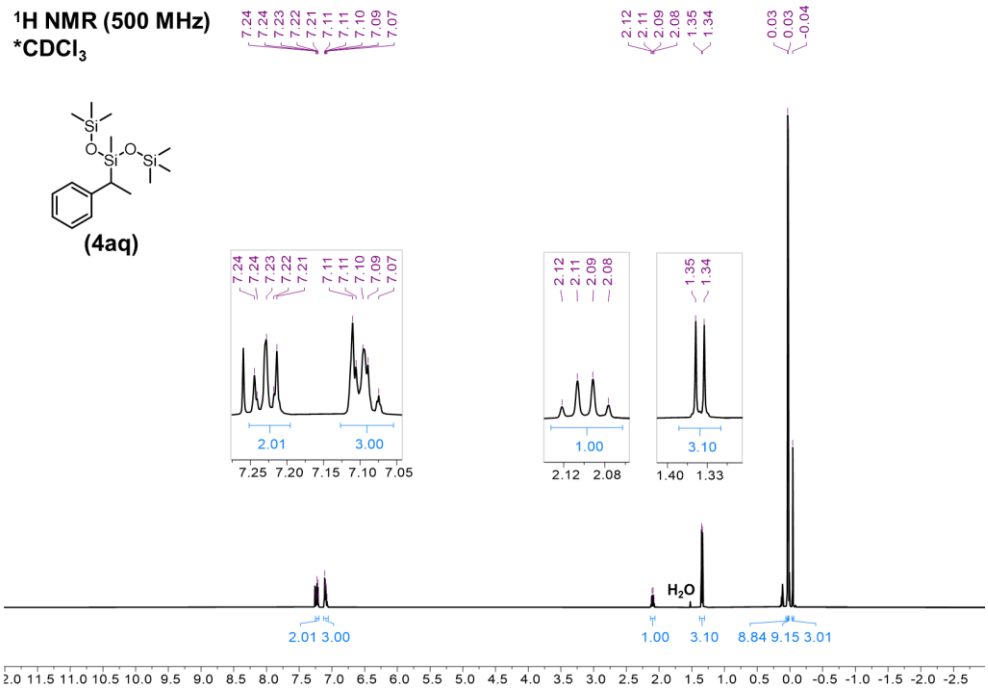

Figure A.201. ^{1}H NMR spectrum of 1,1,1,3,5,5,5-Heptamethyl-3-(1-phenylethyl)trisiloxane (**4aq**) recorded in $CDCl_3$ at 298 K.

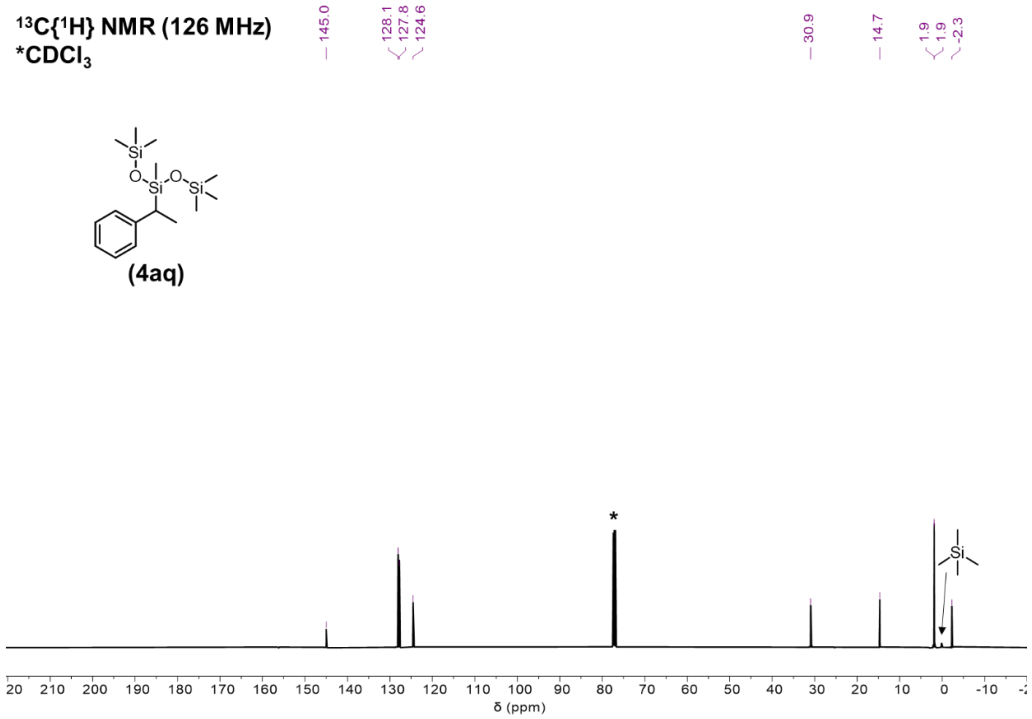

Figure A.202. $^{13}C\{^{1}H\}$ NMR spectrum of 1,1,1,3,5,5,5-Heptamethyl-3-(1-phenylethyl)trisiloxane (**4aq**) recorded in $CDCl_3$ at 298 K.

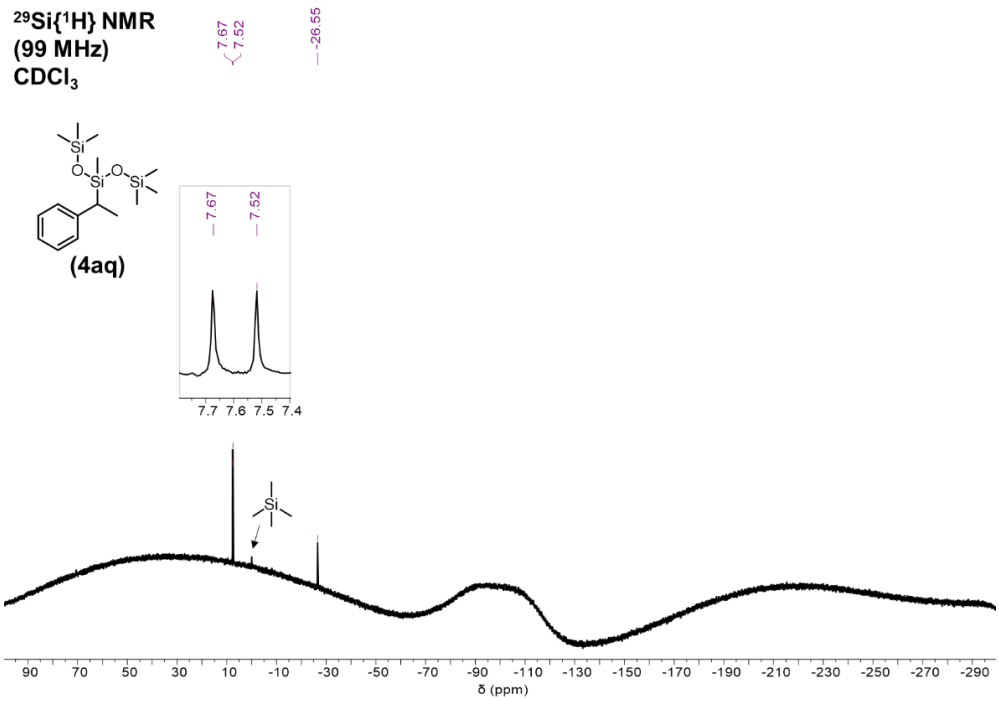

Figure A.203. ^{29}Si NMR spectrum of 1,1,1,3,5,5,5-Heptamethyl-3-(1-phenylethyl)trisiloxane (**4aq**) recorded in $CDCl_3$ at 298 K.

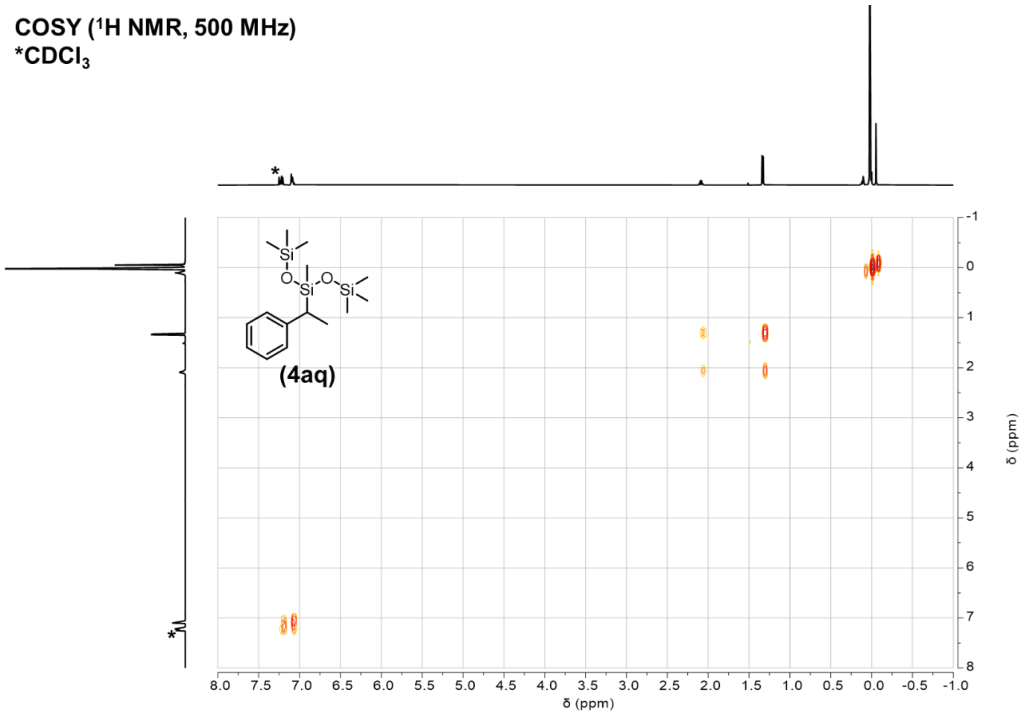

Figure A.204. COSY NMR spectrum of 1,1,1,3,5,5,5-Heptamethyl-3-(1-phenylethyl)trisiloxane (**4aq**) recorded in $CDCl_3$ at 298 K.

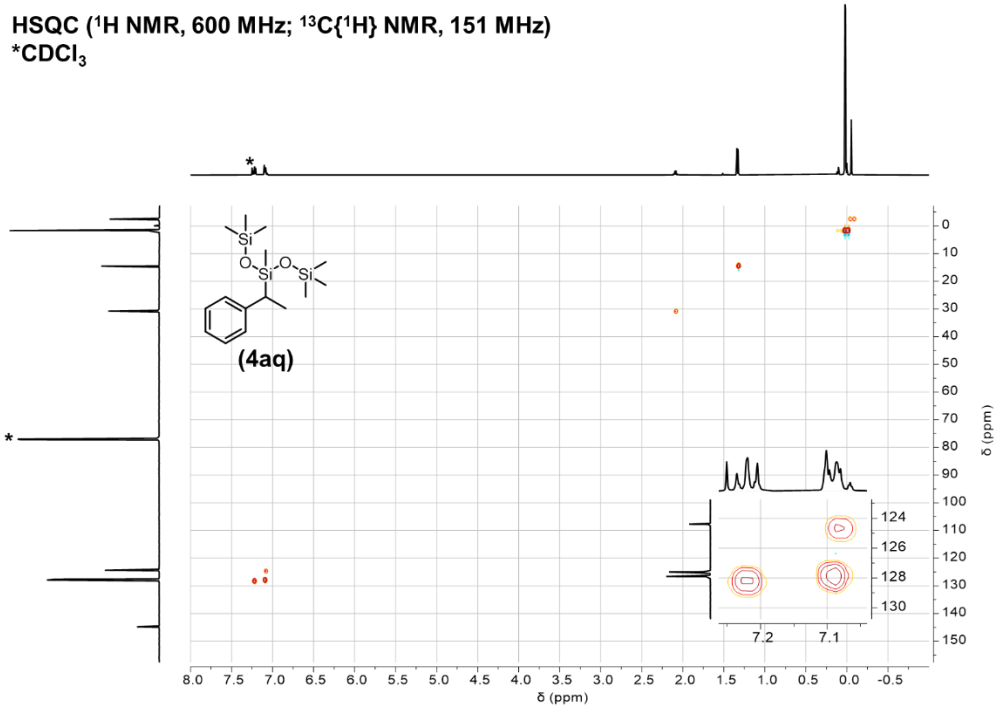

Figure A.205. HSQC NMR spectrum of 1,1,1,3,5,5,5-Heptamethyl-3-(1-phenylethyl)trisiloxane (**4aq**) recorded in $CDCl_3$ at 298 K.

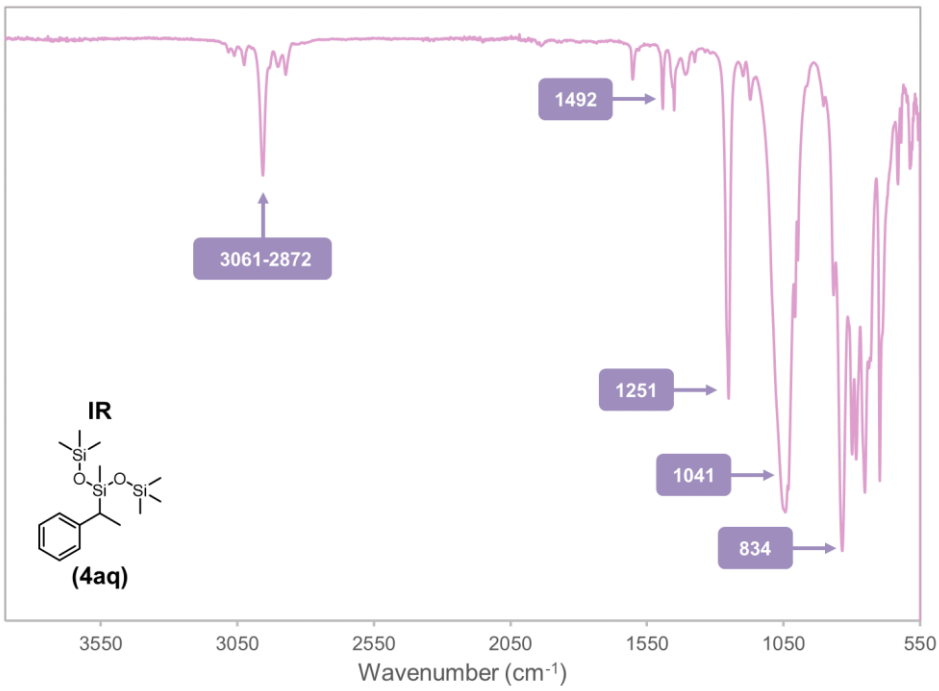

Figure A.206. IR NMR spectrum of 1,1,1,3,5,5,5-Heptamethyl-3-(1-phenylethyl)trisiloxane (**4aq**) recorded neat at 298 K.

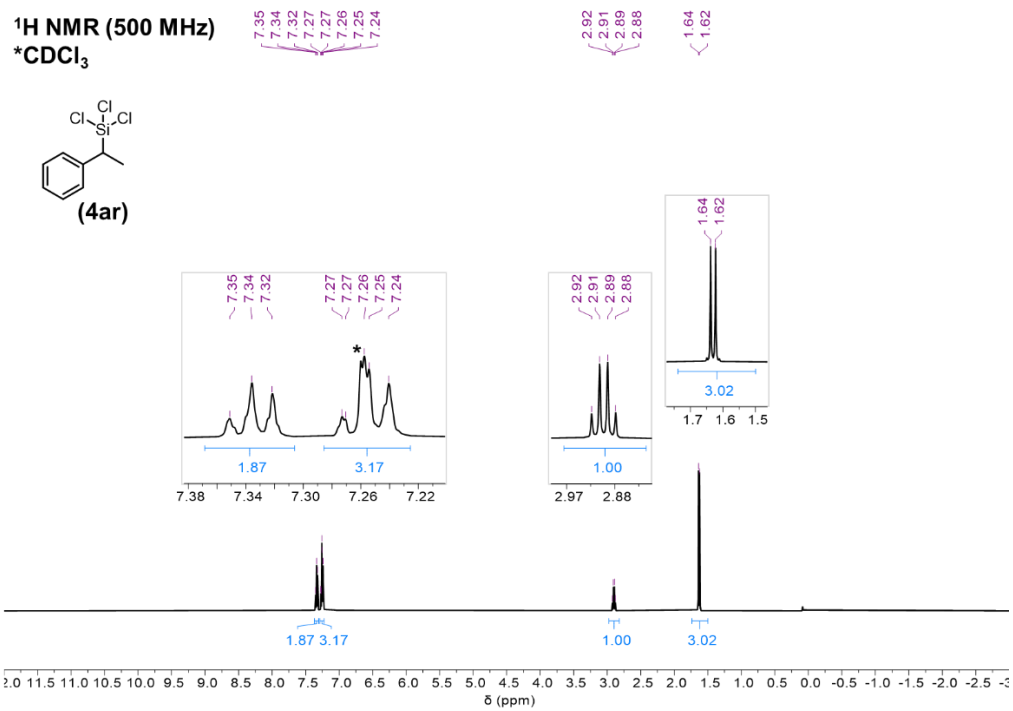

Figure A.207. ^{1}H NMR spectrum of (1-phenylethyl)trichlorosilane (**4ar**) recorded in $CDCl_3$ at 298 K.

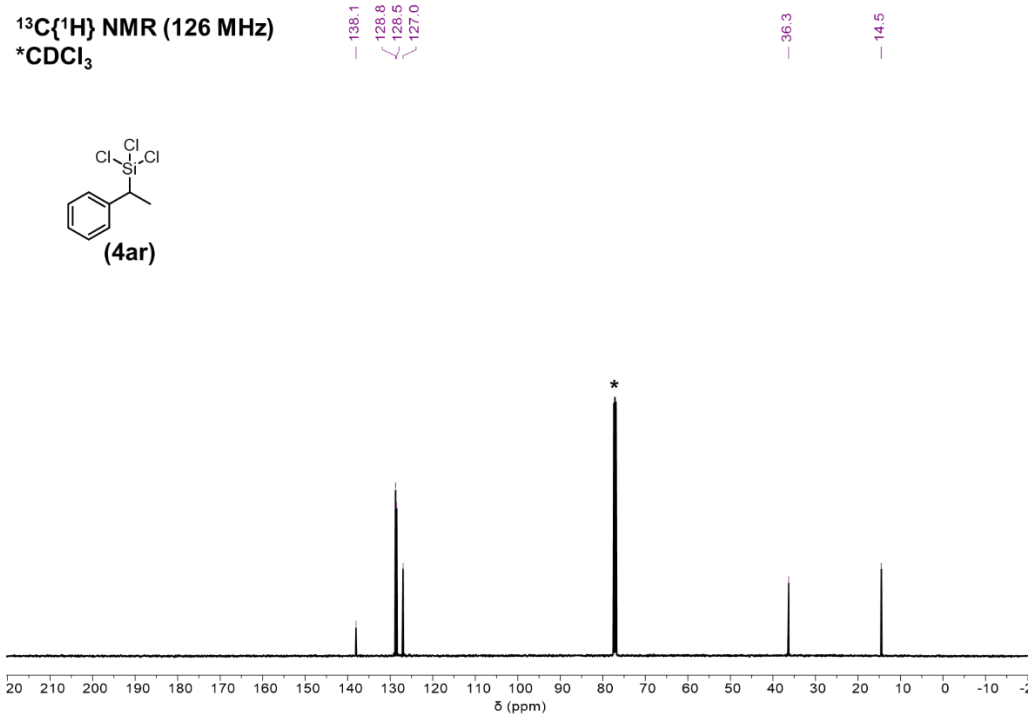

Figure A.208. $^{13}C\{^{1}H\}$ NMR spectrum of (1-phenylethyl)trichlorosilane (**4ar**) recorded in $CDCl_3$ at 298 K.

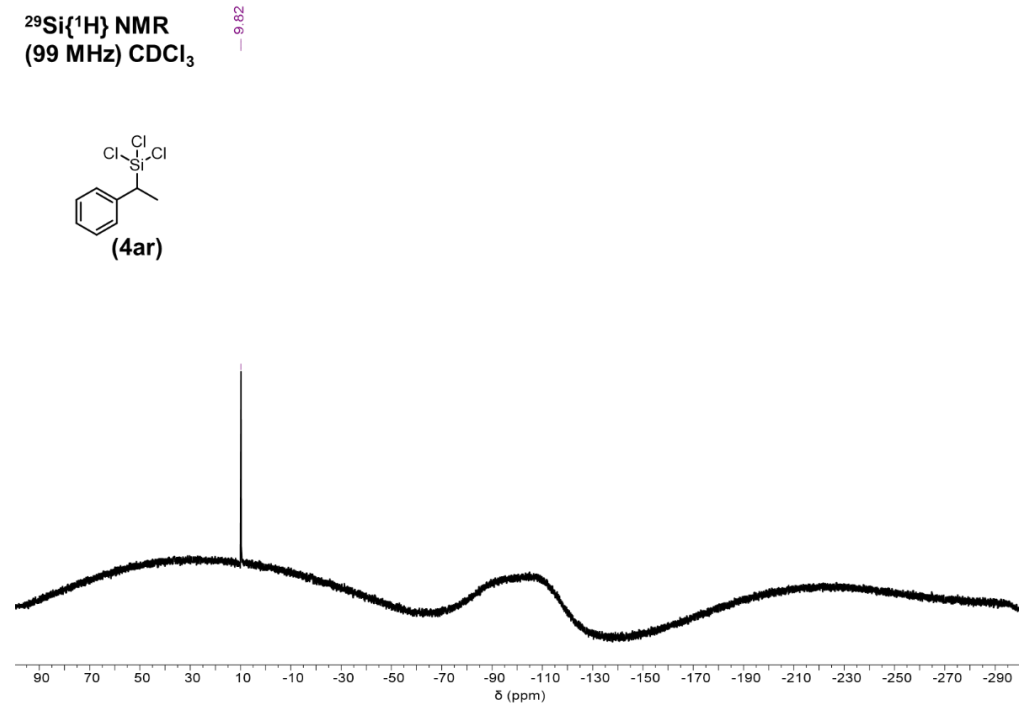

Figure A.209. ^{29}Si NMR spectrum of (1-phenylethyl)trichlorosilane (**4ar**) recorded in $CDCl_3$ at 298 K.

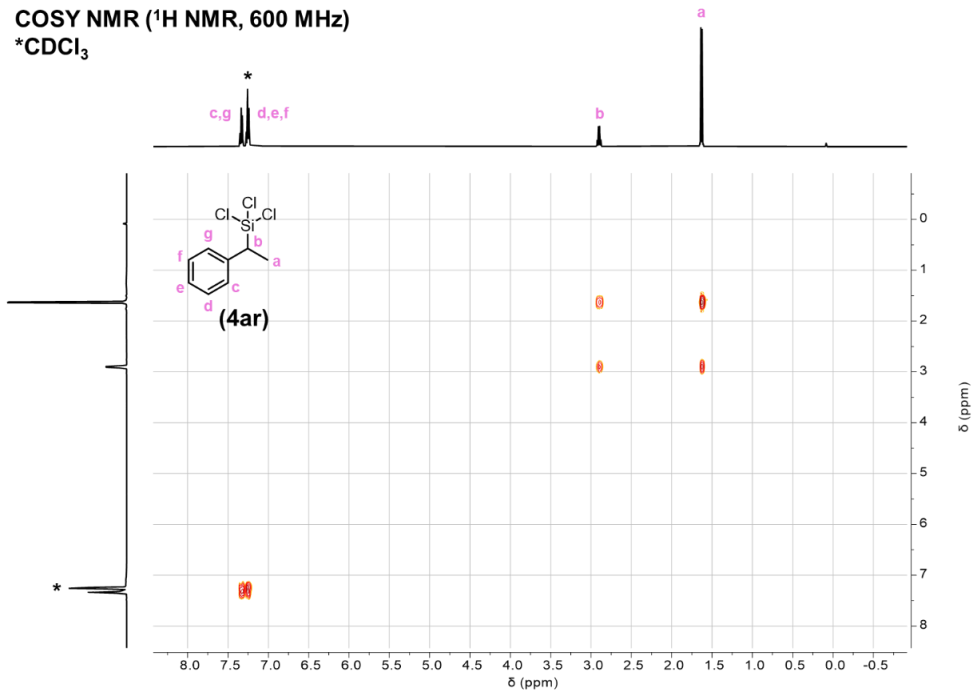

Figure A.210. COSY NMR spectrum of (1-phenylethyl)trichlorosilane (**4ar**) recorded in $CDCl_3$ at 298 K.

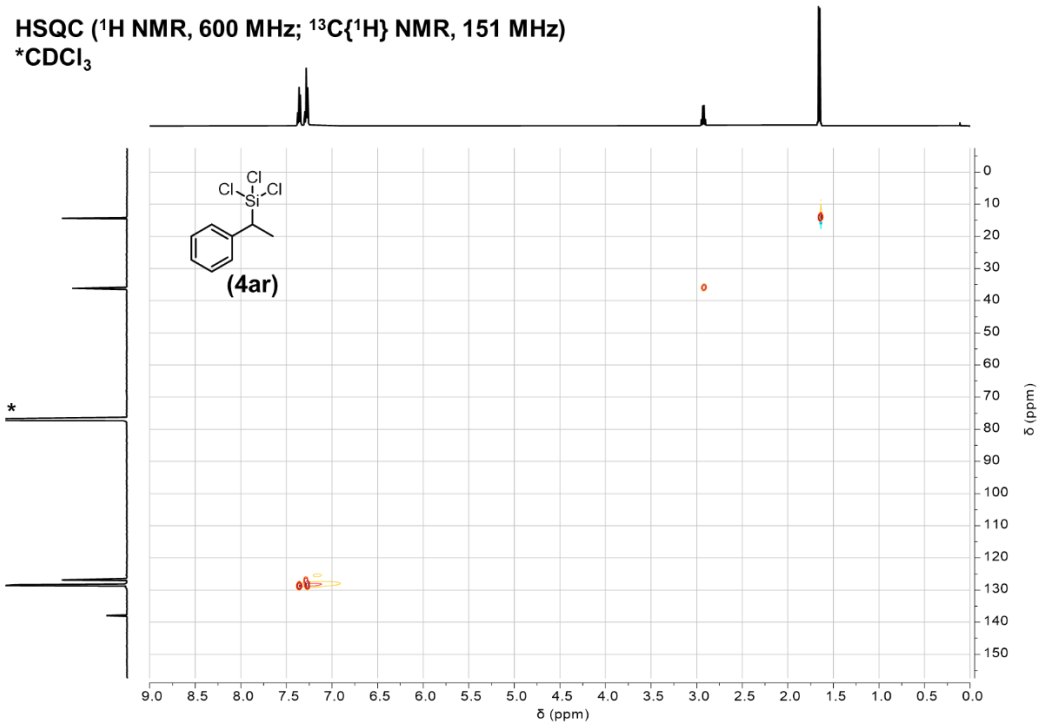

Figure A.211. HSQC NMR spectrum of (1-phenylethyl)trichlorosilane (**4ar**) recorded in $CDCl_3$ at 298 K.

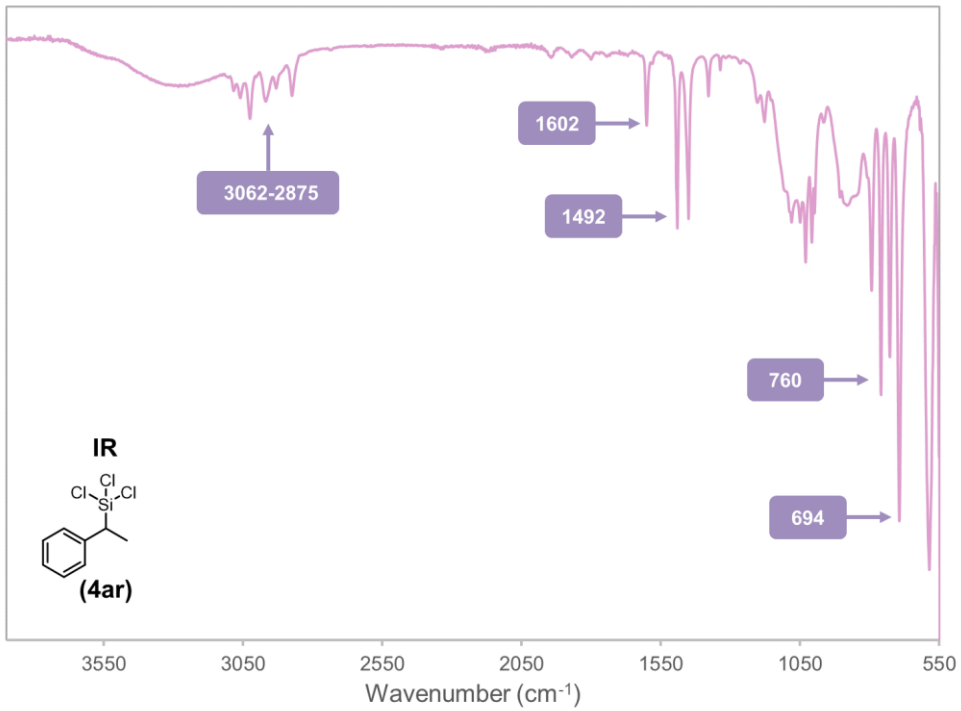

Figure A.112. IR spectrum of (1-phenylethyl)trichlorosilane (**4ar**) recorded neat at 298 K.

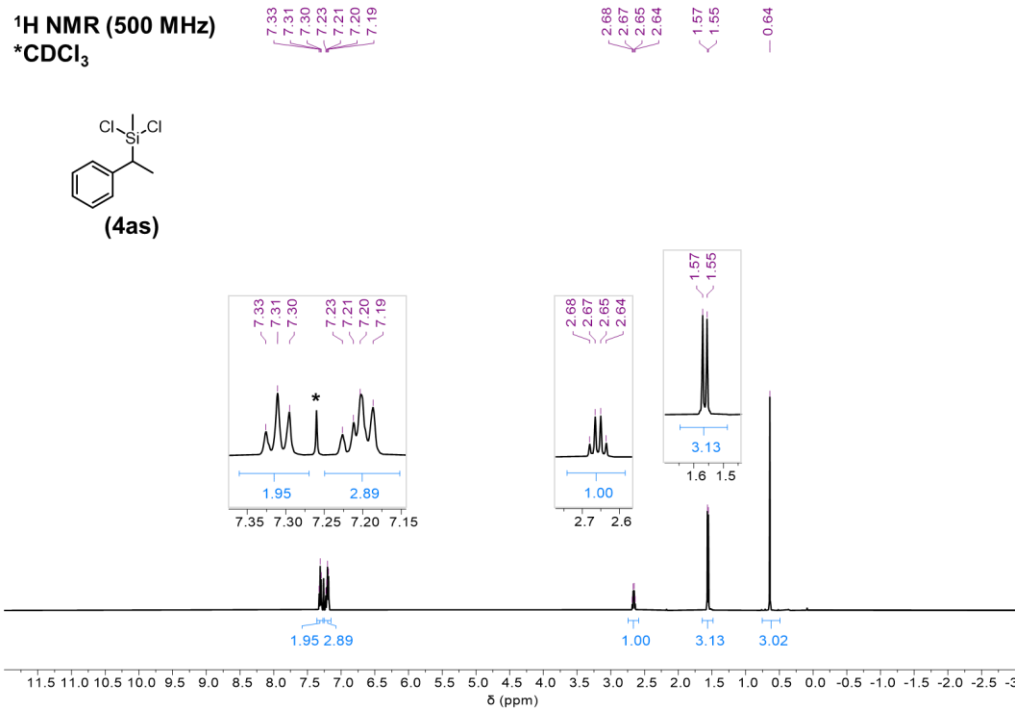

Figure A.113. ^{1}H NMR spectrum of (1-phenylethyl)dichloromethylsilane (**4as**) recorded in $CDCl_3$ at 298 K.

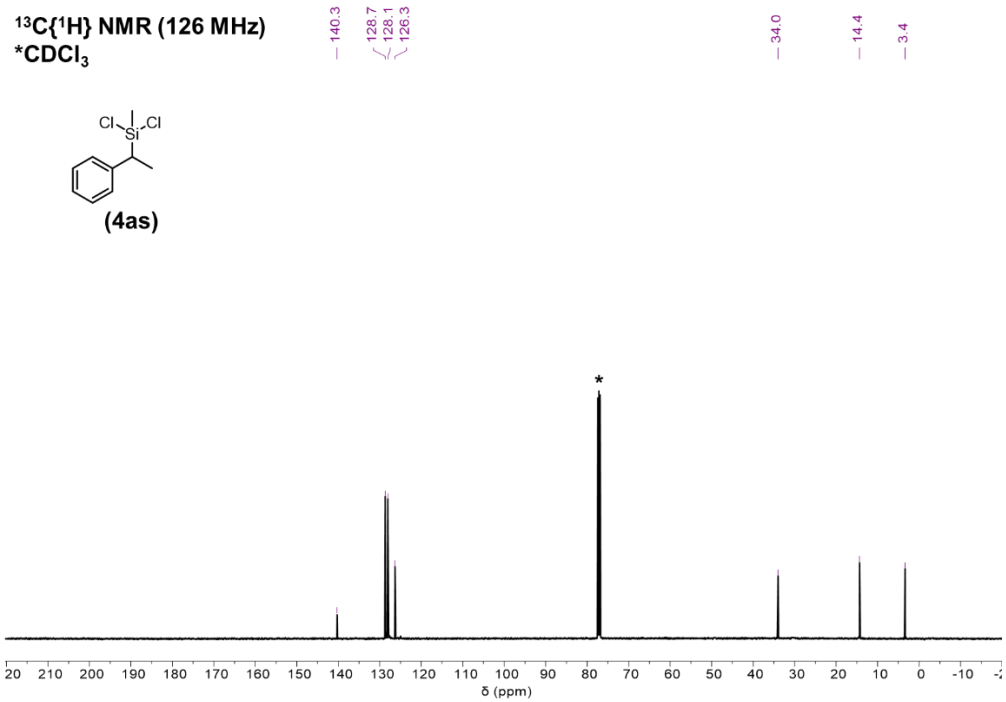

Figure A.114. $^{13}C\{^{1}H\}$ NMR spectrum of (1-phenylethyl)dichloromethylsilane (**4as**) recorded in $CDCl_3$ at 298 K.

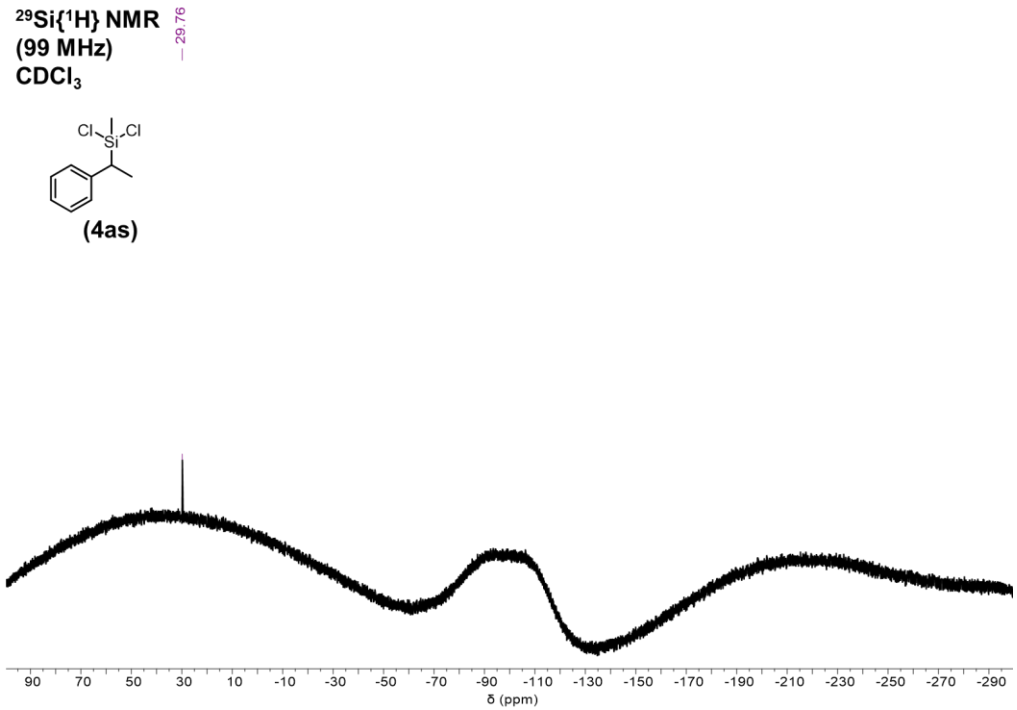

Figure A.115. ^{29}Si NMR spectrum of (1-phenylethyl)dichloromethylsilane (**4as**) recorded in $CDCl_3$ at 298 K.

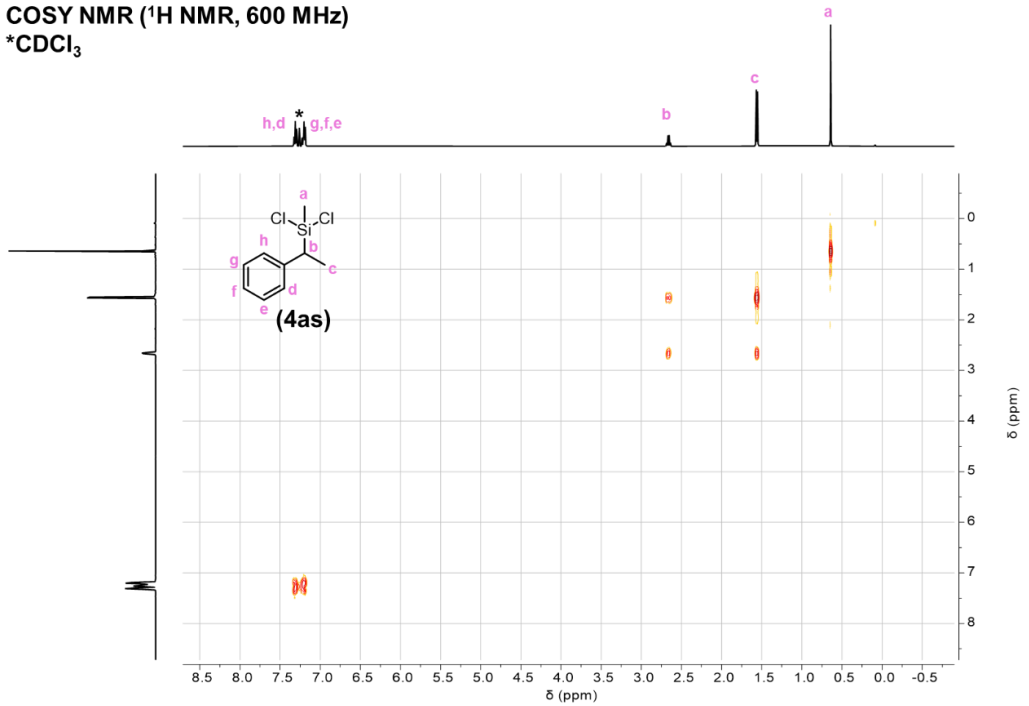

Figure A.116. COSY NMR spectrum of (1-phenylethyl)dichloromethylsilane (**4as**) recorded in $CDCl_3$ at 298 K.

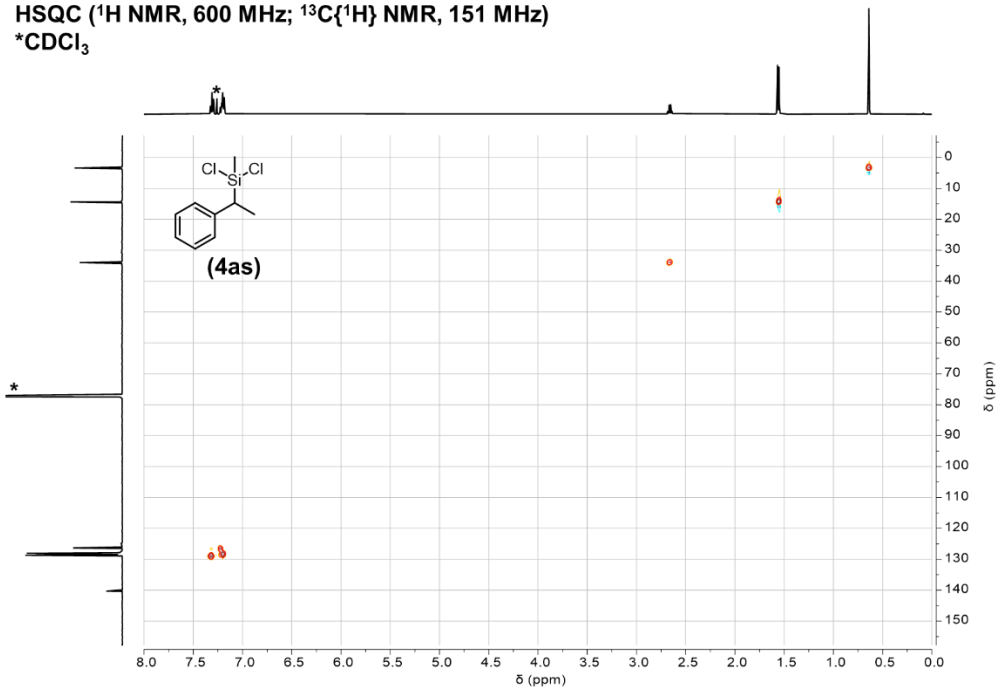

Figure A.117. HSQC NMR spectrum of (1-phenylethyl)dichloromethylsilane (**4as**) recorded in $CDCl_3$ at 298 K.

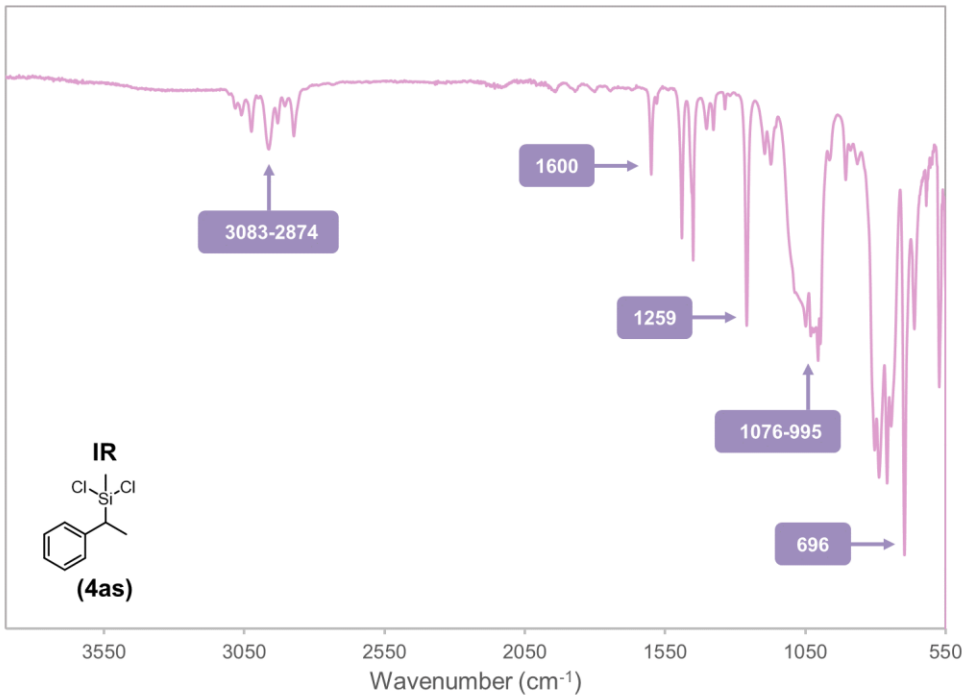

Figure A.118. IR NMR spectrum of (1-phenylethyl)dichloromethylsilane (**4as**) recorded neat at 298 K.

APPENDIX B

SUPPLEMENTARY CONTENT FOR CHAPTER III

Experimental details

B.1.1. Materials and Methods

All syntheses and manipulations were carried out under nitrogen using standard Schlenk (vacuum 10^{-2} mbar) techniques or in a nitrogen-filled glovebox unless otherwise indicated. All reagents and solvents were used after drying and stored under nitrogen, unless otherwise indicated. Tetrahydrofuran (THF; Fisher Chemical; HPLC grade, unstabilized), hexanes (Fisher Chemical; HPLC grade), diethyl ether (B&J Brand; HPLC grade, unstabilized) and acetonitrile (Fisher Chemical; HPLC grade) were dispensed under nitrogen from an LC Technology SP-1 solvent system. Benzene (ACS grade) and pentane (HPLC grade) were refluxed overnight with CaH_2 and distilled under nitrogen before use. The dried solvents were thereafter stored on activated 4Å molecular sieves under nitrogen. CD_3CN, C_6D_6 and $CDCl_3$ were purchased from Cambridge Isotope Laboratories, degassed by freeze-pump-thaw, and thereafter stored on activated 4Å molecular sieves under nitrogen. All stock solutions were prepared by mass and were dispensed into the reaction vessel by difference from syringe, as detailed in the procedure for each experiment.

The following reagents were used from commercial sources without further purification: lithium aluminum deuteride (Aldrich Chemical), styrene-d_8 (**2a-*d*$_8$**; Fisher Scientific), 4-methoxystyrene (**2c**; Alfa Aesar), 4-methylstyrene (**2e**; TCI), 4-fluorostyrene (**2f**; Matrix), 2-methylstyrene (**2h**; TCI), durene (Eastman Chemical Company), and 1,3,5-trimethoxybenzene (TCI).

2s and **DPE** were synthesized via reported procedures.[6,125]

B.1.2. General Experimental

Nuclear magnetic resonance (NMR) spectra were collected at room temperature (298 K) unless otherwise stated on a Bruker AV-III HD 600 NMR (600.13 MHz for ^{1}H; 150.90 MHz for 13C; 564.69 MHz for ^{19}F; 119.23 MHz for ^{29}Si; 92.12 MHz for ^{2}H), Bruker Avance-III HD 500 NMR (499.90 MHz for ^{1}H; 126 MHz for ^{13}C; 471 MHz for ^{19}F; 99 MHz for ^{29}Si), or Varian Inova 500 NMR (499.90 MHz for ^{1}H; 126 MHz for ^{13}C; 471 MHz for ^{19}F; 99 MHz for ^{29}Si). ^{1}H and ^{13}C

spectra were referenced to the residual solvent peak ($CDCl_3$: ^1H δ = 7.26 ppm, ^{13}C δ = 77.16 ppm; C_6D_6: ^1H δ = 7.16 ppm, ^{13}C δ = 128.06 ppm, CD_3CN: ^1H δ = 1.94 ppm, ^{13}C δ = 1.32 ppm ($NCCD_3$)). Chemical shifts for ^1H, ^{13}C, and ^{29}Si NMR spectra are reported in parts per million (ppm, δ) relative to tetramethylsilane at 0.00 ppm. Peaks are characterized as follows: s (singlet), d (doublet), t (triplet), q (quartet), pent (pentet), hept (heptet), m (multiplet), qd (quartet of doublets), br (broad), app (apparent), and/or ms (multiple signals). Coupling constants, *J*, are reported in Hz. $^1J_{H-Si}$ coupling constants were determined, when possible, using the ^{29}Si satellites in the ^1H NMR spectrum.

Infrared (IR) spectroscopy for air-stable organic compounds was performed on an Agilent Nicolet 6700 FT-IR using the ATR sampling technique. IR spectra for air-sensitive nickel complexes were recorded as self-supported pellets diluted with KBr using a Bruker Alpha II FT-IR spectrometer that is housed in a nitrogen-filled glovebox. All bands are reported in wavenumbers (cm^{-1}) and are described as broad (br), strong (s), medium (m), and weak (w).

B.1.3. Synthesis of 3a-d_2

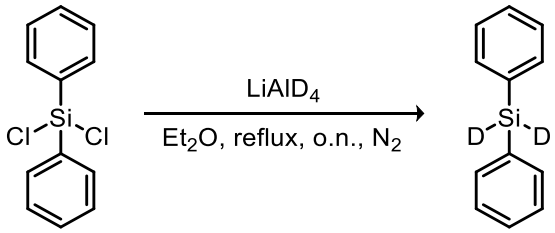

d. (1.3 equiv) **3a-*d*$_2$**

Diphenylsilane-*d*$_2$ (3a-*d*$_2$) was synthesized via a modified literature procedure:[276] An oven-dried Schlenk flask equipped with a magnetic stir bar was charged with Cl_2SiPh_2 (2.0 mL, 9.5 mmol, 1.3 equiv) and Et_2O (18 mL). $LiAlD_4$ (0.30 g, 7.2 mmol, 1.0 equiv) was added to the stirring reaction, and the reaction was heated to reflux for 24 h. The reaction was then cooled to room temperature and quenched with the slow addition of water until all fizzing ceased. The remaining solution was filtered through Celite and washed with Et_2O (5 mL). The aqueous layer was separated and extracted with Et_2O (3 x 20 mL). The organic layers were combined and dried over $MgSO_4$. The solids were filtered off and the filtrate was concentrated under reduced pressure to yield a pale-yellow oil. The crude product was purified by filtering through silica and eluting with hexanes. The filtrate was concentrated under reduced pressure to yield **3a-*d*$_2$** as a clear, colorless oil (0.758 g, 4.07 mmol, 57% yield). NMR spectra match values previously reported.[276] The

density of **3a-*d*$_2$** was determined by measuring 10 µL of sample using a 25-µL syringe and measuring the weight of the sample; this was repeated three times, and the average of the three trials was found to be 1.0 ± 0.1 g/mL.

B.1.4. Monitoring Hydrosilylation of styrene (2a) and d_2-diphenylsilane by ^{2}H NMR

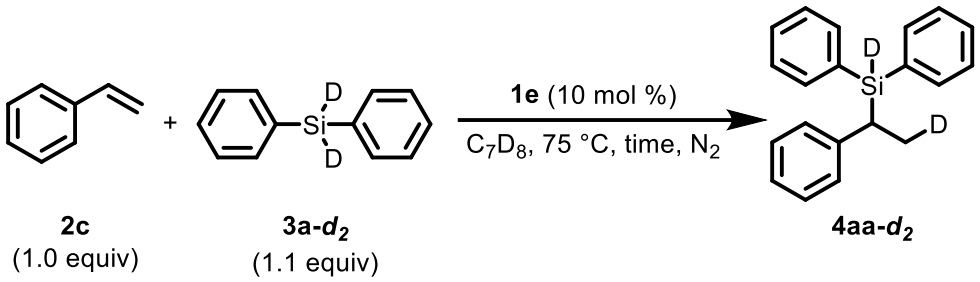

In a nitrogen-filled glovebox, **1e** (7.5 mg, 0.013 mmol, 0.10 equiv) was added to a J-Young NMR tube and solvated in 9:1 C_7H_8/C_7D_8 (0.60 mL, 0.22 M), which was added using disposable 1-mL syringes. To this solution was added **2a** (17 µL, 0.14 mmol, 1.0 equiv) and **3a-*d*$_2$** (28 µL, 0.15 mmol, 1.1 equiv) using a 50-µL syringe. The NMR tube was sealed, brought out of the glovebox, and placed into the NMR (Bruker AV-III HD 600), which had been preheated to 75 °C. Reaction progress was monitored by ^{2}H NMR over time. Qualitative analysis of the formation of **4aa-d$_2$** was determined by the appearance of peaks that correspond to **2c** (doublet of doublet at 5.57 ppm), **3a-*d*$_2$** (singlet at 5.03 ppm), **4aa-d$_2$** (broad singlet at 5.01 ppm, broad multiplet at 2.66, and broad doublet at 1.37 ppm), and **1e** (broad multiplet at 2.60 ppm).

B.1.5. Deuterium Incorporation and Crossover Experiments

a. Deuterium Labelling Study using D_2SiPh_2

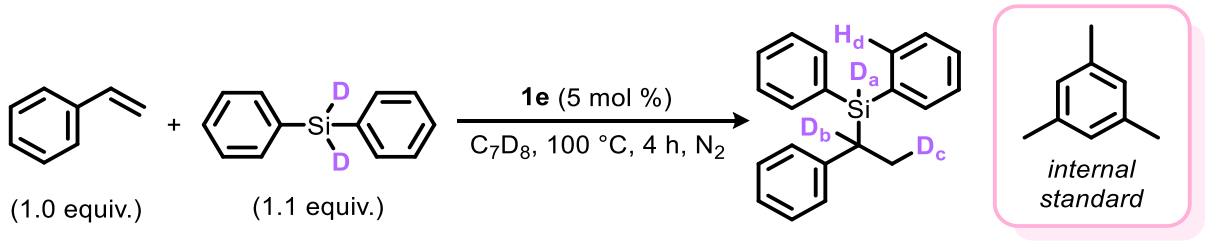

In a nitrogen-glovebox, **1e** (3.7 mg, 0.0065 mmol, 0.050 equiv) was weighed out into a J-Young NMR tube and solvated in C_7D_8 (0.60 mL, 0.22 M), which was added using a disposable 1-mL syringe. To this solution was added **2a** (15 µL, 0.13 mmol, 1.0 equiv), **3a-*d*$_2$** (27 µL, 0.14 mmol, 1.1 equiv) and mesitylene (4.5 µL, 0.032 mmol). The NMR tube was sealed, brought out of the glovebox, and placed onto a preheated oil bath at 100 °C. After 4 h, the reaction was

quenched in a liquid N_2 bath, thawed, and analyzed by ^1H NMR. For ^2H NMR, the sample was concentrated under vacuum and redissolved in 1:5 C_7D_8:C_7H_8. ^2H NMR shows deuterium incorporation in three positions with calculated amounts: **D_a** = 44%, **D_b** = 3%, **D_c** = 45%. Calculations for D_a and D_c are based on the relative integration of the respective peaks against the C(aryl)–H_d (7.33 ppm, d, 2H) in the ^1H NMR. This calculation assumes that no D incorporation occurs at the C(aryl)–H_d position, which is confirmed in the ^2H NMR spectrum (Figure S16). Because of overlapping peaks, integration of the benzylic position (H/D_b) are not reliable. To determine the D incorporation at this site, relative integrations of the D_a and D_b position in the ^2H NMR were used.

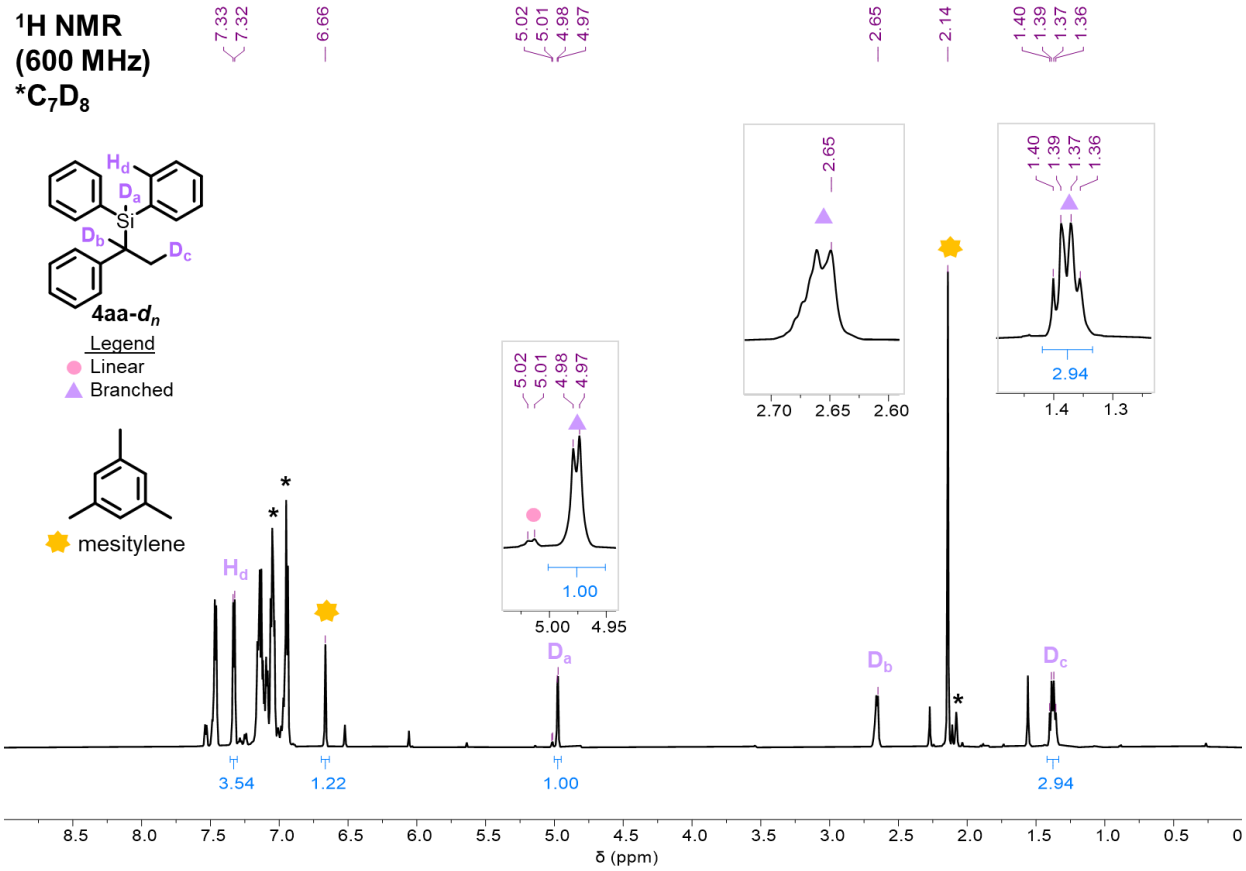

Figure B.1. ^1H NMR spectrum of **4aa-*d_n*** after the hydrosilylation of **2a** and **3a-*d_2*** recorded in C_7D_8 at 25 °C.

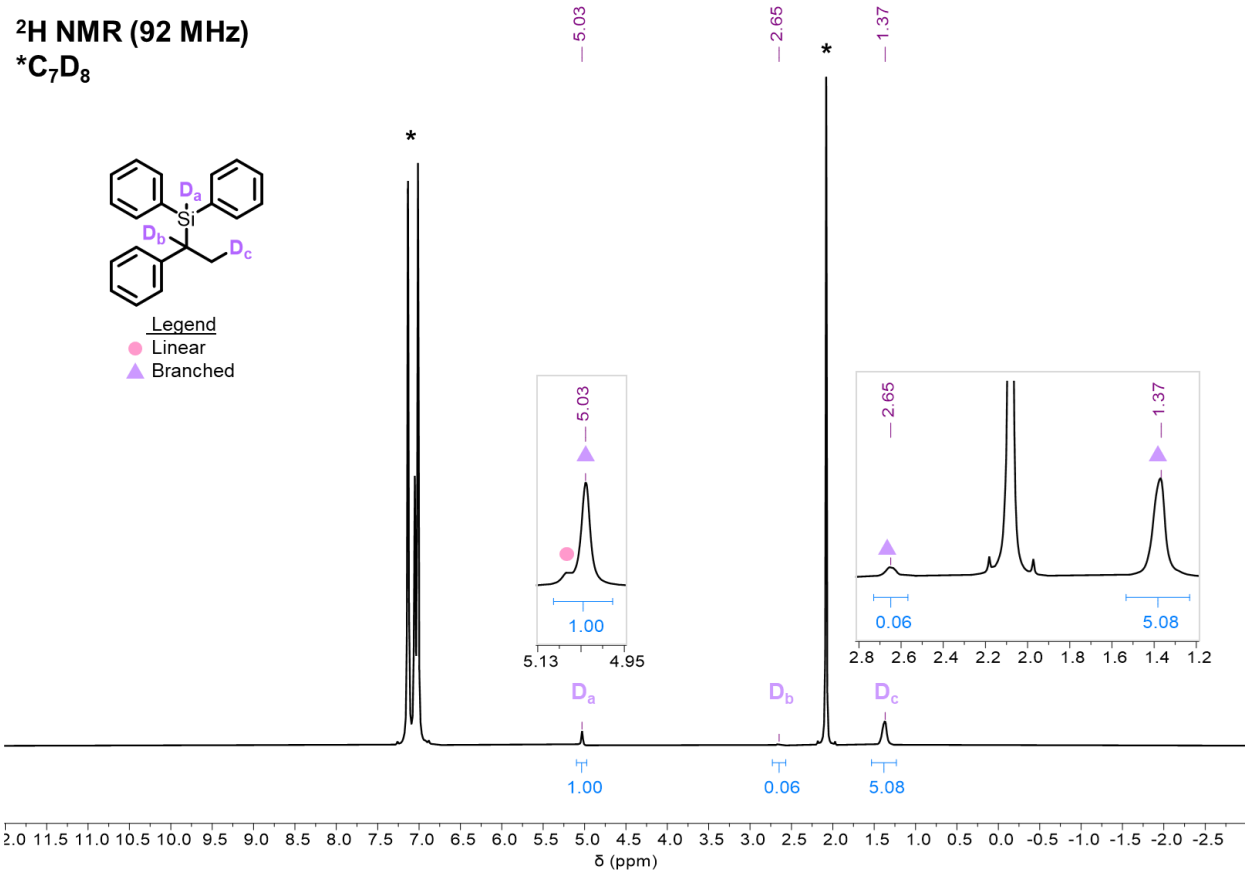

Figure B.2. ^{2}H NMR spectrum of **4aa-*d*$_n$** after hydrosilylation of **2a** with **3a-*d*$_2$** recorded in 1:5 C_7D_8:C_7H_8 at 25 °C.

b. Deuterium Labelling Study Using Styrene-d$_8$ (2a-d$_8$)

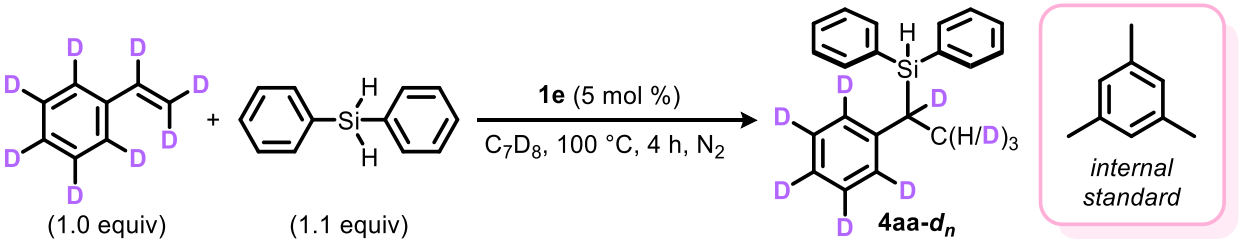

In a nitrogen-glovebox, **1e** (3.7 mg, 0.0065 mmol, 0.050 equiv) was weighed out into a J-Young NMR tube and solvated in C_7D_8 (0.60 mL, 0.22 M), which was added using a disposable 1-mL syringe. To this solution was added **styrene-*d*$_8$** (15 L, 0.13 mmol, 20. equiv.), **3a** (27 µL, 0.14 mmol, 1.1 equiv) and mesitylene (5.0 µL, 0.036 mmol). The NMR tube was sealed and placed onto a preheated oil bath at 100 °C. After 4 h, the reaction was quenched in a liquid N_2 bath, thawed, and analyzed by ^{1}H NMR. For ^{2}H NMR, the sample was concentrated under reduced pressure and redissolved in 1:9 C_7D_8:C_7H_8. ^{2}H NMR shows deuterium incorporation in three

positions with calculated amounts: **D_a** = 34%, **D_b** = 70%, **D_c** = 46%. Calculations for D_a, D_b, and D_c are based on the relative integration of the respective peaks against the C(aryl)–H_d (7.33 ppm, d, 2H) in the ^{1}H NMR. This calculation assumes that no D incorporation occurs at the C(aryl)–H_d position, which is confirmed in the ^{2}H NMR spectrum (Figure S18).

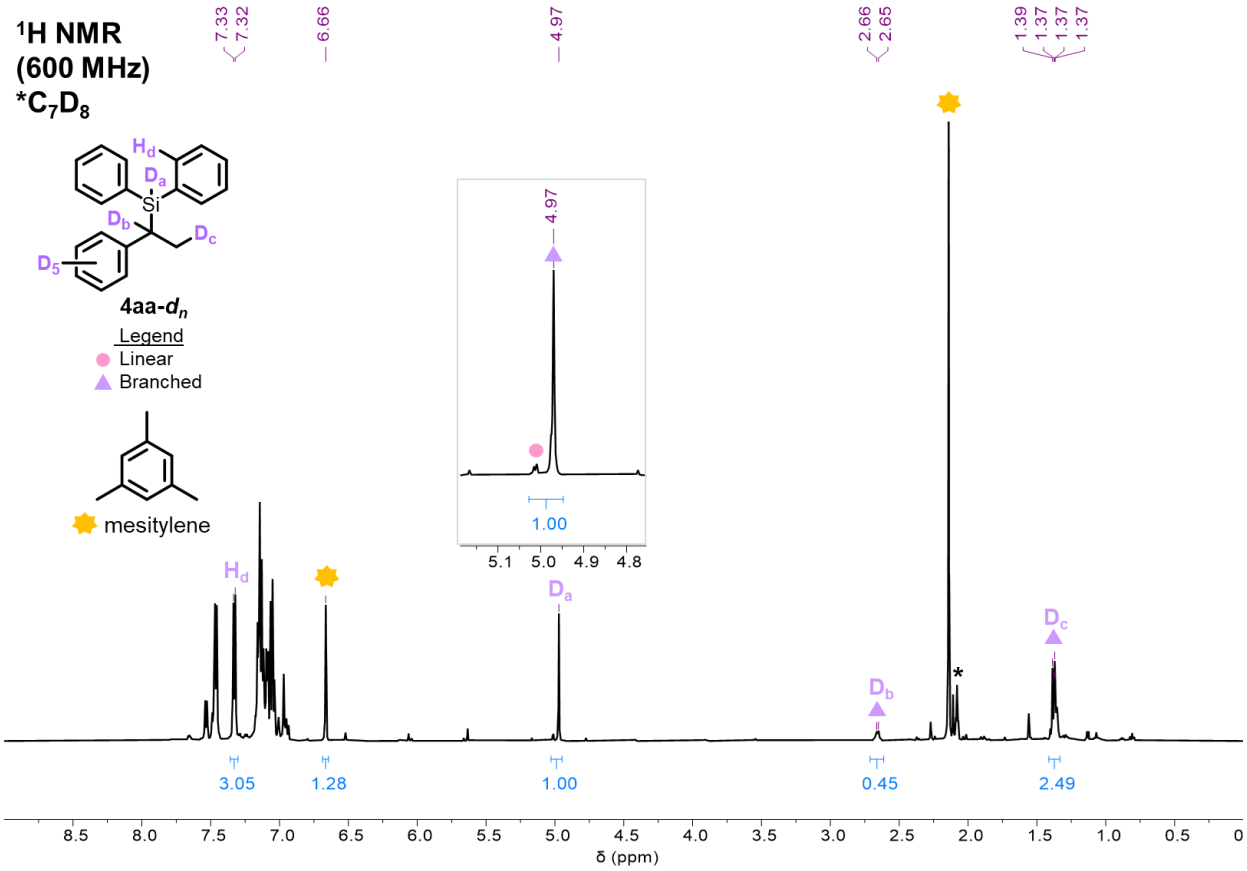

Figure B.3. ^{1}H NMR spectrum of crude reaction after heating the hydrosilylation reaction of **styrene-*d_8*** and **3a** at 100 °C for 4 h. Recorded in C_7D_8 at 25 °C.

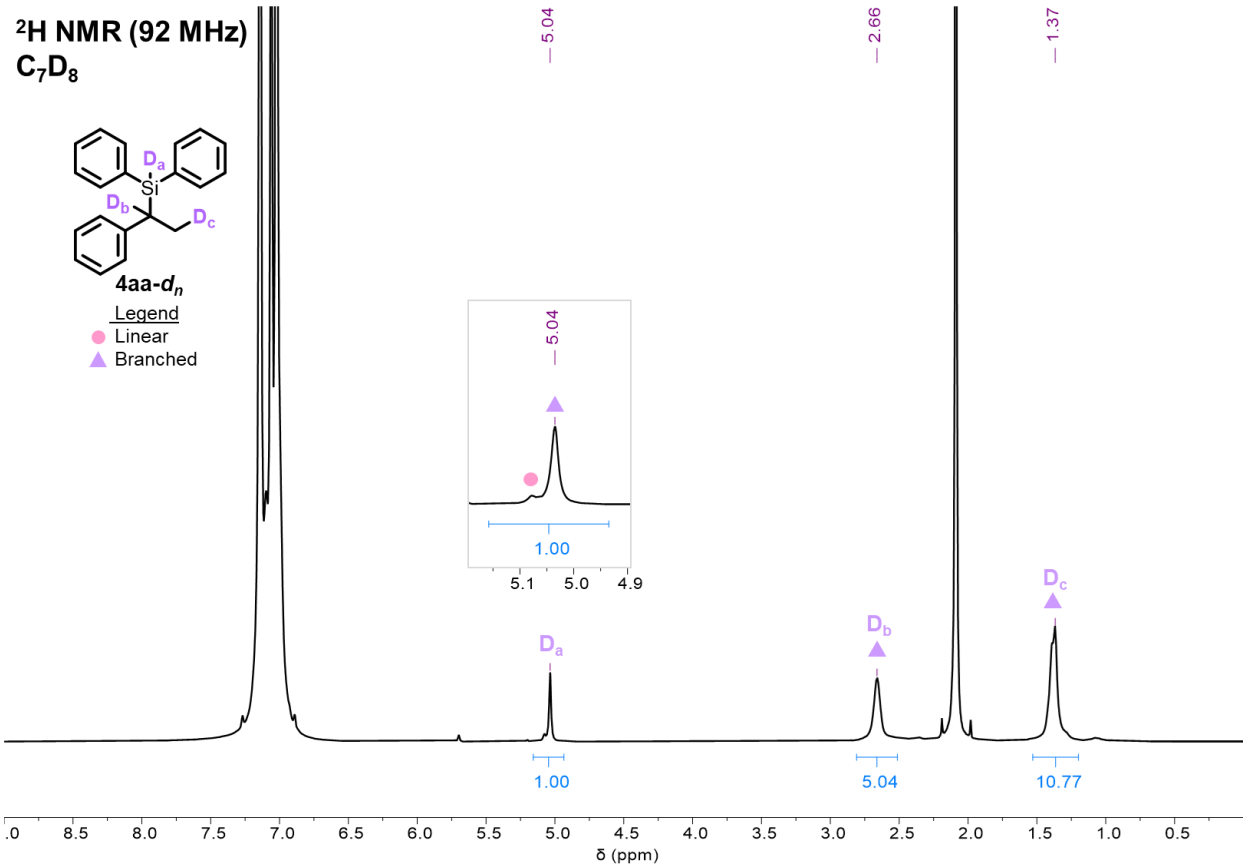

Figure B.4. ^{2}H NMR spectrum of **4aa-*d*$_n$** after hydrosilylation of ***d*$_8$-styrene** with **3a** recorded in 1:9 C_7D_8:C_7H_8 at 25 °C.

c. Crossover Experiment

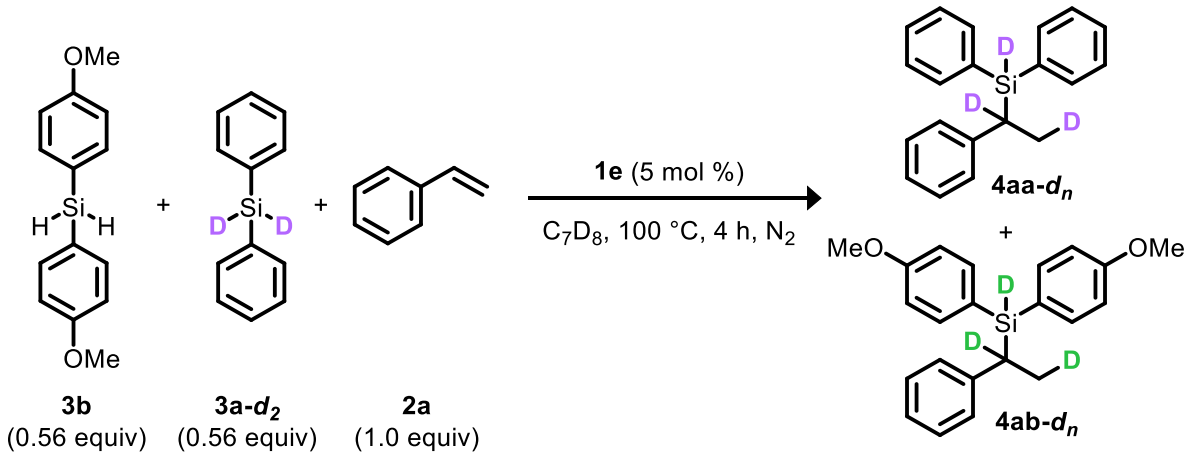

In a nitrogen-filled glovebox, **1e** (3.9 mg, 0.0068 mmol, 0.050 equiv) was weighed out into a J-Young NMR tube and solvated in C_7D_8 (0.60 mL, 0.22 M), which was added using a disposable 1-mL syringe. To this solution was added **2a** (15 µL, 0.13 mmol, 1.0 equiv), **3a-*d*$_2$** (14 µL, 0.072

mmol, 0.56 equiv), **3b** (18 mg, 0.072 mmol, 0.56 equiv) and mesitylene (5.0 µL, 0.036 mmol). The NMR tube was sealed, brought out of the glovebox, and placed onto a preheated oil bath at 100 °C. After 4 h, the reaction was quenched in a liquid N_2 bath, thawed, and analyzed by ^{1}H NMR. For ^{2}H NMR, the sample was concentrated under reduced pressure and redissolved in 1:5 C_7D_8:C_7H_8. Complete scrambling between **4aa** and **4ac** was observed for all three **H**/**D** positions labelled below.

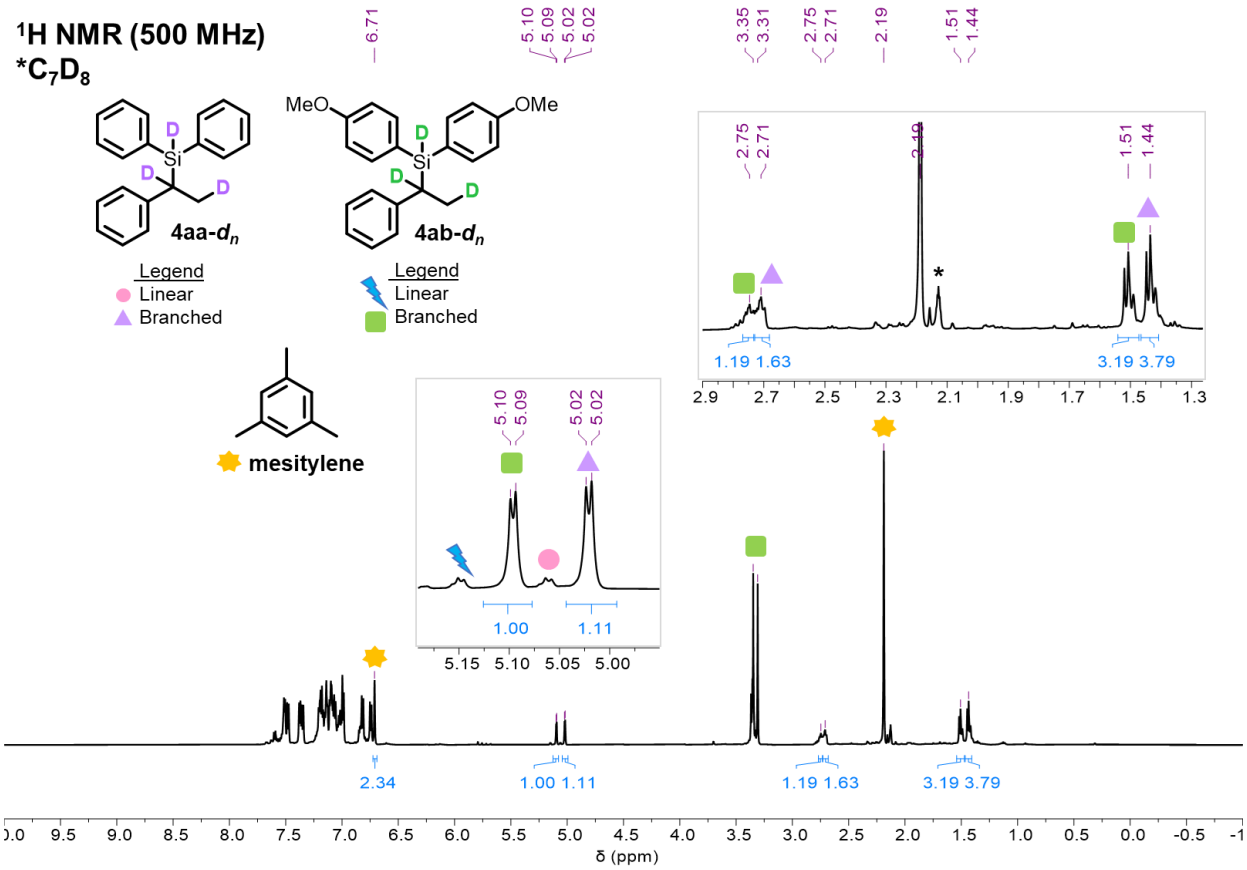

Figure B.5. ^{1}H NMR spectrum of the crossover between **3a-*d*$_2$** and **3b** with **2a** to form **4aa-*d*$_n$** and **4ab-*d*$_n$** recorded in C_7D_8 at 25 °C.

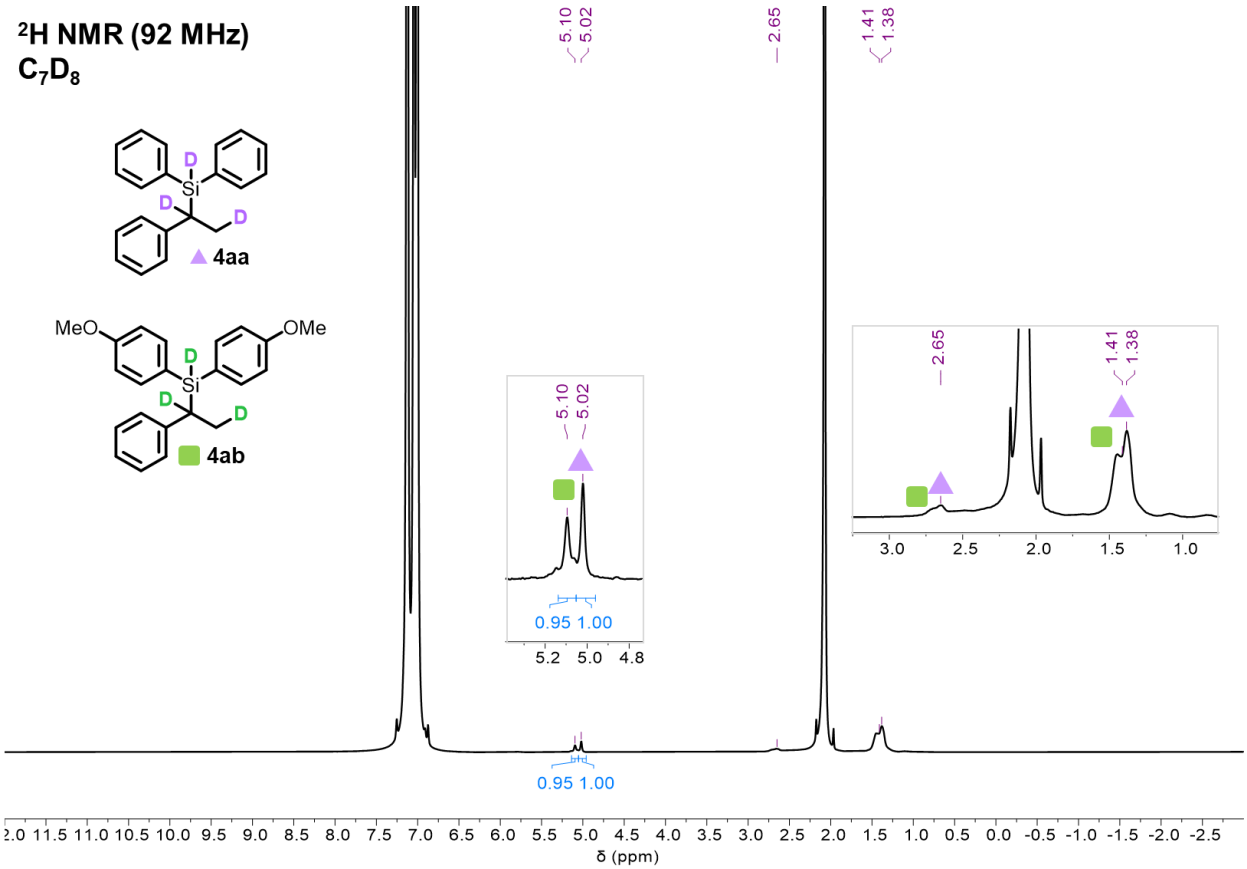

Figure B.6. ^{2}H NMR spectrum of the crossover of **3a-*d*$_2$** and **3b** with **2a** to afford **4aa-*d*$_n$** and **4ab-*d*$_n$** recorded in 1:5 C_7D_8:C_7H_8 at 25 °C.

B.1.6. Kinetics Experiments

a. Kinetic Isotope Effects

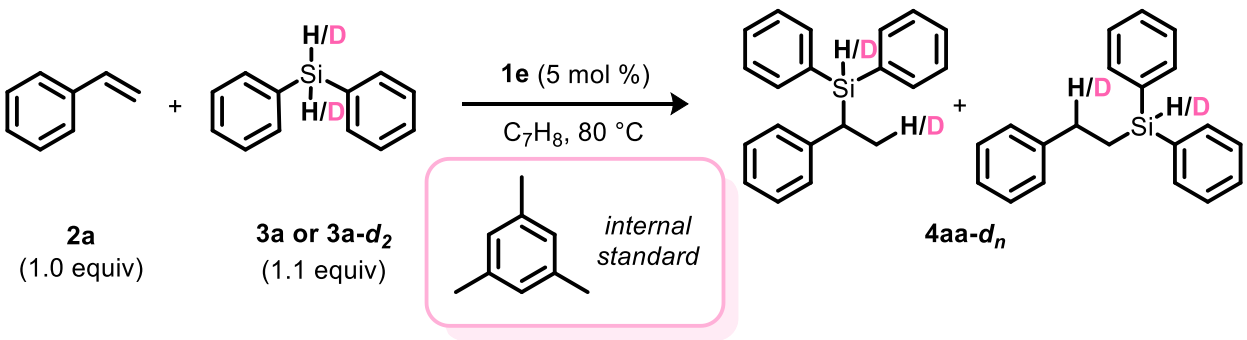

In a nitrogen-filled glovebox, a stock solution of **1e** (37 mg, 0.65 mmol) was prepared in toluene (2.0 mL) using volumetric glassware and distributed (0.40 mL) using a disposable 1-mL syringe to four 1-dram vials equipped with stir bars. To each vial was added **2a** (30 µL, 0.26 mmol, 1.0 equiv), and mesitylene (20 µL, 0.14 mmol) using a 50-µL syringe. Additional toluene (0.80

mL) was added to each vial using a disposable 1-mL syringe to obtain a final reaction concentration of 0.22 M. The vial was sealed with a septum cap, brought out of the glovebox, injected with **3a** (54 µL, 0.29 mmol, 1.1 equiv) or **3a-*d*$_2$** (54 µL, 0.29 mmol, 1.1 equiv), and placed on an aluminum vial block preheated to 80 °C. Throughout the course of the reaction, 20 µL aliquots were removed with a 25-µL syringe, filtered into a GC vial through Celite, and diluted with hexanes. The filtrate from the Celite plug was analyzed by GC to assess the reaction progress and selectivity. The product concentration was determined by relative integration (by GC) of the product peaks against mesitylene, in accordance with a calibration curve.

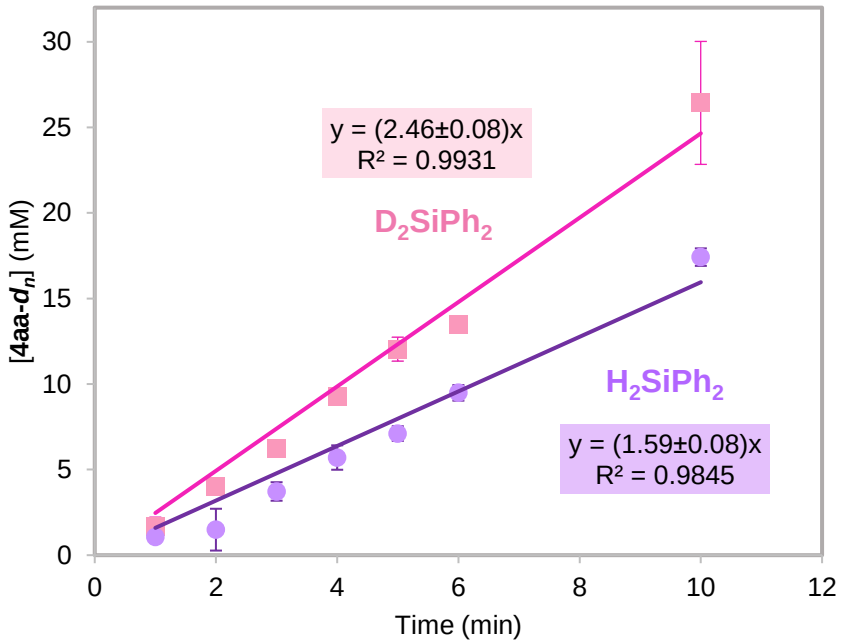

Figure B.7. Initial rates of the formation of **4aa-*d*$_n$** versus time (min).

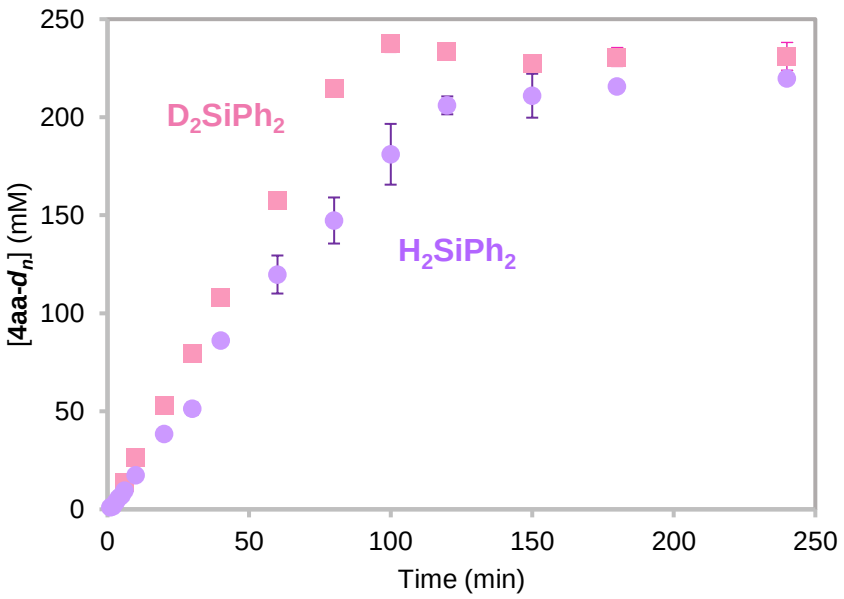

Figure B.8. Full kinetic profile of the formation of **4aa-*d*$_n$** versus time (min).

Table B.1. Formation of **4aa-*d*$_n$** over time with **3a** or **3a-*d*$_2$**.

Time (min)	Reaction with **3a**		Reaction with **3a-*d*$_2$**	
	[**4aa**] (mM)	Selectivity (*l*/*b*)	[**4aa-*d*$_2$**] (mM)	Selectivity (*l*/*b*)
1	1.1 ± 0.3	1:1.9	1.7 ± 0.5	1:1.5
2	2 ± 1	1:3.2	4.0 ± 0.1	1:6.4
3	3.7 ± 0.5	1:6.2	6.3 ± 0.4	1:37
4	5.7 ± 0.7	1:7.4	9.26 ± 0.08	1:17
5	7.1 ± 0.4	1:7.3	12.0 ± 0.7	1:34
6	9.5 ± 0.5	1:8.8	13.46 ± 0.07	1:30
10	17.4 ± 0.5	1:9.5	26 ± 4	1:28
20	38 ± 2	1:9.0	53 ± 4	1:19
30	51 ± 3	1:8.3	79.4 ± 0.2	1:22
40	86 ± 1	1:7.4	107.99 ± 0.02	1:22
60	120 ± 10	1:7.0	157 ± 5	1:20
80	150 ± 12	1:7.1	215 ± 7	1:22
100	180 ± 16	1:7.4	237.4 ± 0.4	1:21
120	206 ± 4	1:8.6	233 ± 2	1:23
150	210 ± 11	1:8.6	228 ± 7	1:25
180	216 ± 2	1:8.3	231 ± 4	1:20
240	220 ± 2	1:8.4	231 ± 6	1:22

b. Eyring Plot

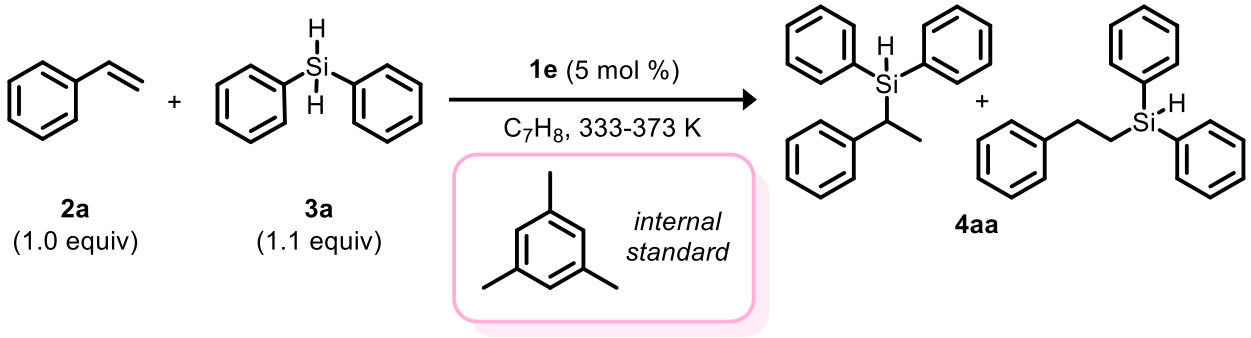

In a nitrogen-filled glovebox, **1e** (7.6 mg, 0.013 mmol, 0.050 equiv) was weighed out into a 1-dram scintillation vial equipped with a stir bar. Toluene (1.2 mL) was added to each vial using a disposable 1-mL syringe, followed by **2a** (30 µL, 0.26 mmol, 1.0 equiv) and mesitylene (20 µL, 0.14 mmol) using a 50-µL syringe. The vial was sealed with a septum cap, brought out of the glovebox, injected with **3a** (54 µL, 0.29 mmol, 1.1 equiv), and placed on an aluminum vial block preheated to 333 K, 343 K, 353 K, or 373 K. Throughout the course of the reaction, 20 µL aliquots were removed with a 25-µL syringe, diluted with hexanes, and filtered through Celite into a GC vial. The filtrate from the Celite plug was analyzed by GC to assess the reaction progress and selectivity. Product concentration was determined by relative integration (by GC) of the product peaks against the internal standard, mesitylene, in accordance with a calibration curve. Two trials were run for all temperatures except for the reaction run at 353 K, at which only one trial was run.

Table B.2. Formation of **4aa** over time at varying reaction temperatures.

Temperature	Time (min)	[**4aa**] (mM)	Selectivity (*l*/*b*)
333 K	5	2.42 ± 0.02	1:7.3
	10	3.3 ± 0.7	1:4.8
	15	4.7 ± 0.7	1:5.4
	20	5.21 ± 0.03	1:4.3
	30	7.7 ± 0.5	1:3.9
	44	11.2 ± 0.7	1:3.3
	61	17.9 ±0.4	1:3.1
	80	22 ± 2	1:2.8
	100	30 ± 5	1:2.6
	120	37 ± 3	1:2.3
	190	70 ± 1	1:2.0
	243	97 ± 8	1:1.8
	337	132 ± 5	1:1.5

343 K	1	0.67	0:1.0
	2	2.0 ± 0.8	1:13
	3	2.5 ± 0.4	1:11
	4	3.4 ± 0.7	1:17
	5	4.25 ± 0.05	1:7.8
	7	5.8 ± 0.5	1:7.2
	10	9 ± 2	1:11
	15	13.08 ± 0.09	1:7.0
	20	19 ± 2	1:7.0
	30	27 ± 4	1:5.1
	47	50 ± 9	1:4.1
	60	56 ± 3	1:3.7
	80	80 ± 11	1:3.1
	90	122 ± 17	1:2.7
	120	132 ± 3	1:2.7
	148	150 ± 4	1:2.5
	202	169 ± 4	1:2.7
353 K	1	1.8	1:7.6
	2	3.4	1:10
	3	4.8	1:11
	4	6.4	1:6.9
	5	9.2	1:11
	6	10	1:7.7
	8	14	1:8.8
	10	16	1:8.8
	15	30	1:7.5
	20	37	1:6.5
	33	64	1:5.7
	64	141	1:5.0
	90	189	1:6.0
	129	184	1:6.1
	170	175	1:6.1
	240	170	1:6.7
373 K	0.5	1 ± 1	1:1.7
	1.0	5 ± 1	1:3.0
	1.7	14 ± 3	1:12
	2.2	20 ± 1	1:11
	3.5	37 ± 3	1:13
	4.0	42 ± 6	1:12

5.0	57 ± 5	1:14
6.0	78 ± 14	1:14
7.0	100 ± 13	1:14
10	138 ± 2	1:15
15	218 ± 7	1:17
30	231 ± 13	1:19
60	234 ± 8	1:18
120	225 ± 3	1:18
180	227 ± 6	1:18
240	227 ± 8	1:18

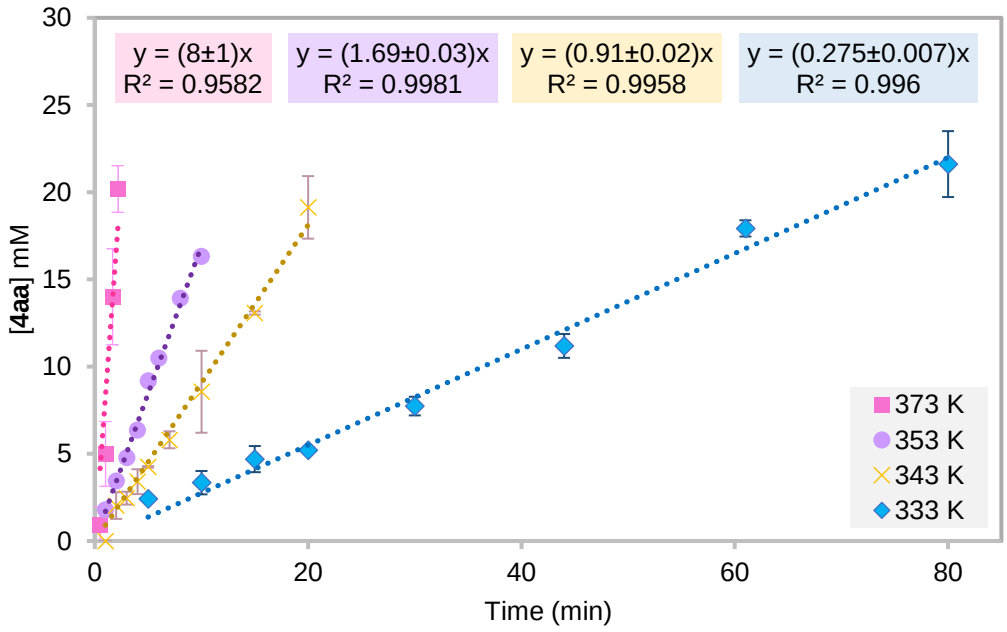

Figure B.9. Initial rates for the formation of **4aa** over time (min) at varying temperatures.

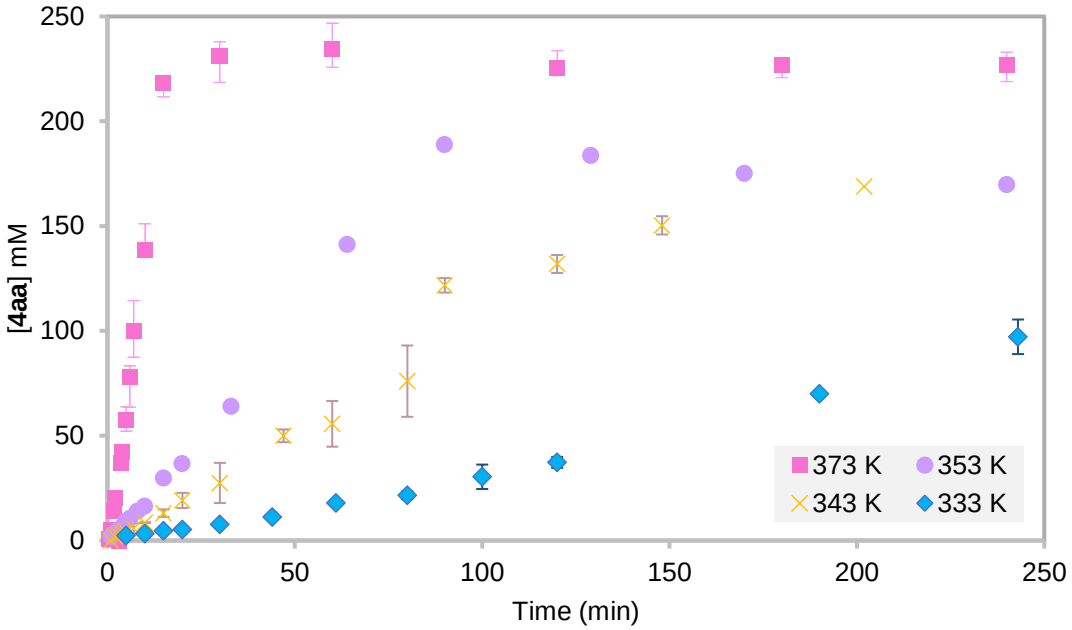

Figure B.10. Full kinetic profile for the formation of **4aa** over time (min) at varying temperatures.

Table B.3. Rates of formation of **4aa** at varying temperatures.

Temperature (K)	1/K (T^{-1})	Δ[**4aa**]/Δt (mM/min)	ln([(Δ[**4aa**]/Δt)·T^{-1}])
333	0.00268	0.275 ± 0.007	-7.10 ± 0.02
343	0.00283	0.91 ± 0.02	-5.94 ± 0.02
353	0.00292	1.69 ± 0.03	-4.34 ± 0.08
373	0.003003	8 ± 1	-3.8 ± 0.1

To construct the Eyring plot, ln([(Δ[**4aa**]/Δt)·T^{-1}]) was plotted as a function of 1/T. Using Microsoft Excel, the data were fit to a curve for the function y = mx + b, where y = ln[(Δ[**4aa**]/Δt)·T^{-1}] input, m = $-\Delta H \bullet R^{-1}$ output, x = T^{-1} input, and b = $\Delta S \bullet R^{-1} + \ln(k_B/h)$ output, as illustrated below.

$$\ln\left(\frac{\Delta[\mathbf{4aa}]/\Delta t}{T}\right) = \left(\frac{-\Delta H^{\ddagger}}{R}\right)\left(\frac{1}{T}\right) + \left(\frac{-\Delta S^{\ddagger}}{R}\right) + \ln\frac{k_B}{h}$$

Where…

R =	0.001987	$kcal \bullet mol^{-1} \bullet K^{-1}$	(Ideal gas constant)
k_B =	1.38×10^{-23}	$J \bullet K^{-1}$	(Boltzmann constant)
h =	6.63×10^{-34}	J•s	(Planck's constant)

Gibbs free energy of activation was determined using the following equation: $\Delta G^{\ddagger} = \Delta H^{\ddagger} - T\Delta S^{\ddagger}$

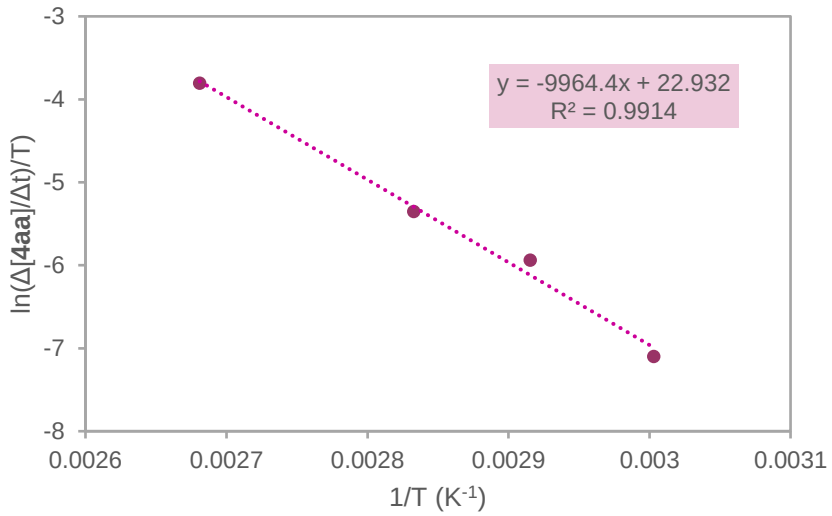

Figure B.11. Eyring plot.

$\Delta H^{\ddagger} =$ 20.4 ± 0.2 kcal•mol^{-1}
$\Delta S^{\ddagger} =$ -0.28 ± 0.2 cal•mol^{-1}•K^{-1}
$\Delta G^{\ddagger}_{373K} =$ 20.5 ± 0.2 kcal•mol^{-1}

c. Rate Law

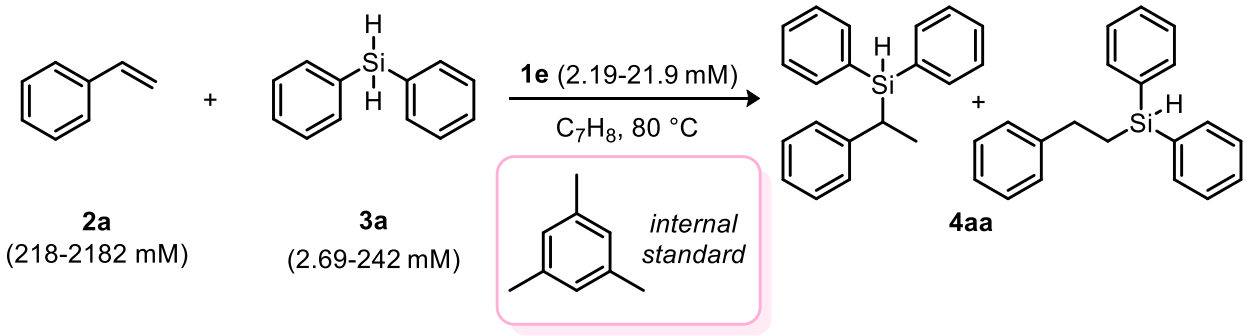

In a nitrogen-filled glovebox, a stock solution of **1e**, **2a**, and mesitylene was prepared and distributed into 1-dram vials equipped with stir bars using a disposable 1 mL-syringe. The vial was sealed with a septum cap, brought out of the glovebox, injected with the corresponding amount of **3a**, and placed on an aluminum vial block preheated to 80 °C. Throughout the course of the reaction, 20 µL aliquots were removed with a 25-µL syringe and filtered into a GC vial through Celite and diluted with hexanes. The filtrate was analyzed by GC to assess the reaction progress and selectivity. The product concentration was determined by relative integration (by GC) of the

product peaks against mesitylene, in accordance with calibration curves. Two trials were run for all experiments.

Table B.4. Amounts and concentrations of **1e**, **2a**, **3a** (mM) and observed rate determined by initial rates.

Entry	[**1e**] (mM)	[**2a**] (mM)	[**3a**] (mM)	Rate (mM/min)
1	2.19	218	242	0.79 ± 0.02
2	5.47	218	242	1.36 ± 0.06
3*	10.9	218	242	1.59 ± 0.08
4	21.9	218	242	3.37 ± 0.09
5	10.9	436	242	1.33 ± 0.04
6	10.9	1091	242	0.660 ± 0.007
7	10.9	2182	242	0.74 ± 0.03
8	10.9	218	26.9	0.18 ± 0.01
9	10.9	218	58.4	0.44 ± 0.04
10	10.9	218	121	1.13 ± 0.04

*These are the standard conditions. See data in "Kinetics to Measure KIE" section B.1.6.a for values (Figures B.7.-B.8., Table B.1.).

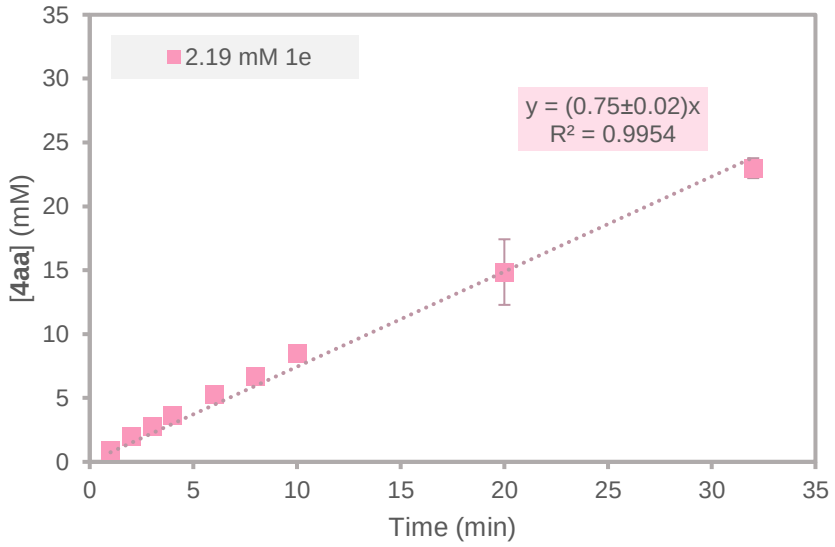

Figure B.12. Table B.4., Entry 1: Initial rate of formation of **4aa** with 2.19 mM **1e**, 218 mM **2a**, and 242 mM **3a**.

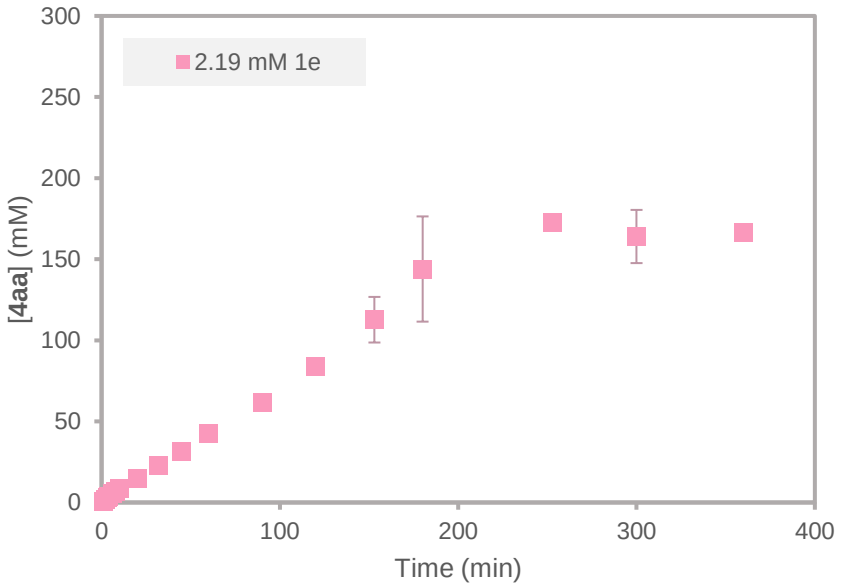

Figure B.13. Table B.4., Entry 1: Full reaction profile for the formation of **4aa** over time (min) with 2.19 mM **1e**, 218 mM **2a**, and 242 mM **3a**.

Table B.5. Table B.4., Entry 1: [**4aa**] (mM) and selectivity (*l*:*b*) of **4aa** formed with 2.19 mM **1e**, 218 mM **2a**, and 242 mM **3a**.

Time (min)	[**4aa**] (mM)	Selectivity (*l*:*b*)
1	0.94 ± 0.09	1:1.4
2	1.987 ± 0.006	1:1.1
3	2.8 ± 0.4	1:1.5
4	3.6 ± 0.1	1:1.5
6	5.3 ± 0.4	1:1.8
8	6.71 ± 0.08	1:1.9
10	8.5 ± 0.4	1:2.0
20	15 ± 3	1:2.2
32	22.9 ± 0.8	1:2.4
45	31.7 ± 0.7	1:2.7
60	43 ± 1	1:2.3
90	61.7 ± 0.5	1:2.2
120	84 ± 2	1:2.1
153	113 ± 14	1:1.9
180	140 ± 32	1:1.9
253	172.7 ± 0.9	1:1.9
300	160 ± 16	1:2.0
360	167 ± 5	1:2.0

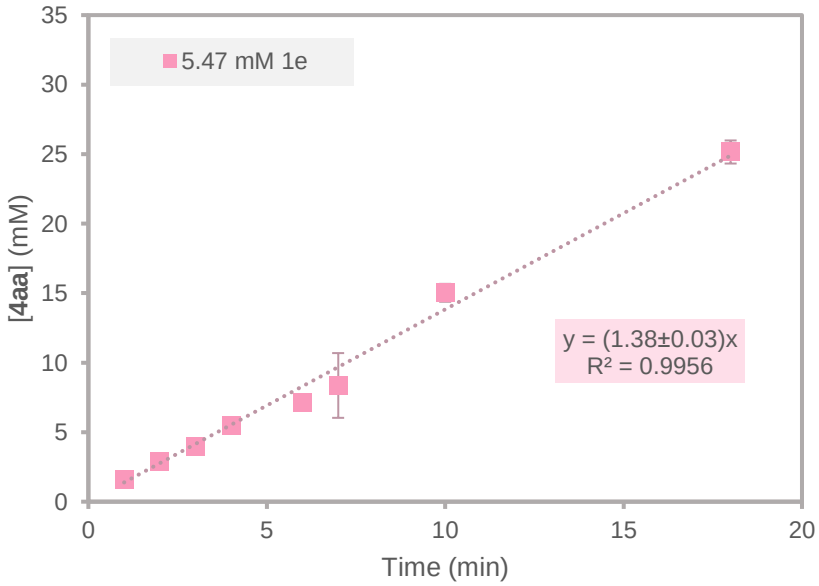

Figure B.14. Table B.4., Entry 2: Initial rate of formation of **4aa** with 5.47 mM **1e**, 218 mM **2a**, and 242 mM **3a**.

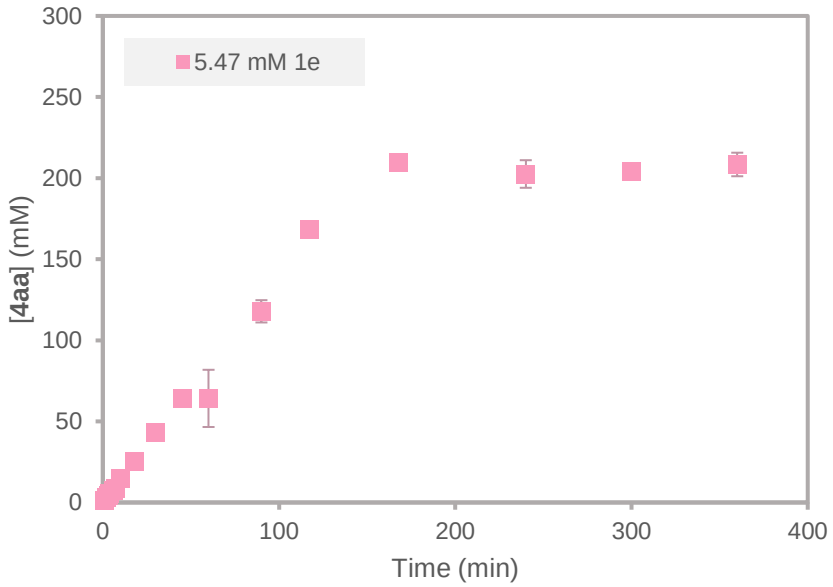

Figure B.15. Table B.4., Entry 2: Full reaction profile for the formation of **4aa** over time (min) with 5.47 mM **1e**, 218 mM **2a**, and 242 mM **3a**.

Table B.6. Table B.4., Entry 2: [**4aa**] (mM) and selectivity (*l*:*b*) of **4aa** formed with 5.47 mM **1e**, 218 mM **2a**, and 242 mM **3a**.

Time (min)	[**4aa**] (mM)	Selectivity (*l*/*b*)
1	1.6 ± 0.1	1:1.1
2	2.9 ± 0.2	1:1.5
3	3.9 ± 0.2	1:2.0
4	5.5 ± 0.3	1:2.2
6	7.2 ± 0.2	1:2.7
7	8 ± 2	1:4.4
10	15.0 ± 0.6	1:3.3
18	25.1 ± 0.8	1:3.7
30	42.9 ± 0.6	1:4.1
45	64.2 ± 0.2	1:4.2
60	60 ± 18	1:3.2
90	118 ± 7	1:4.1
117	168.51 ± 0.09	1:4.0
168	210 ± 4	1:4.6
240	203 ± 9	1:4.5
300	204.3 ± 0.9	1:4.7
360	208 ± 7	1:4.6

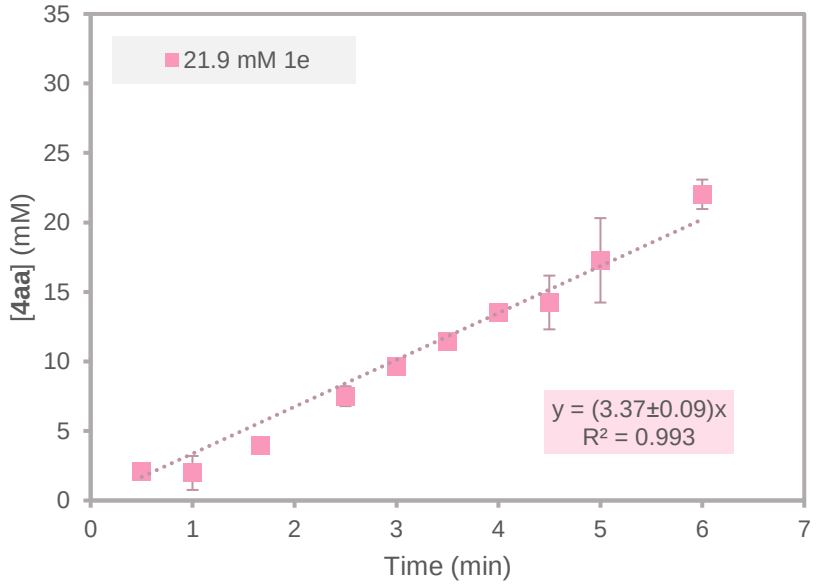

Figure B.16. Table B.4., Entry 4: Initial rate of the formation of **4aa** versus time (min) with 21.9 mM **1e**, 218 mM **2a**, and 242 mM **3a**.

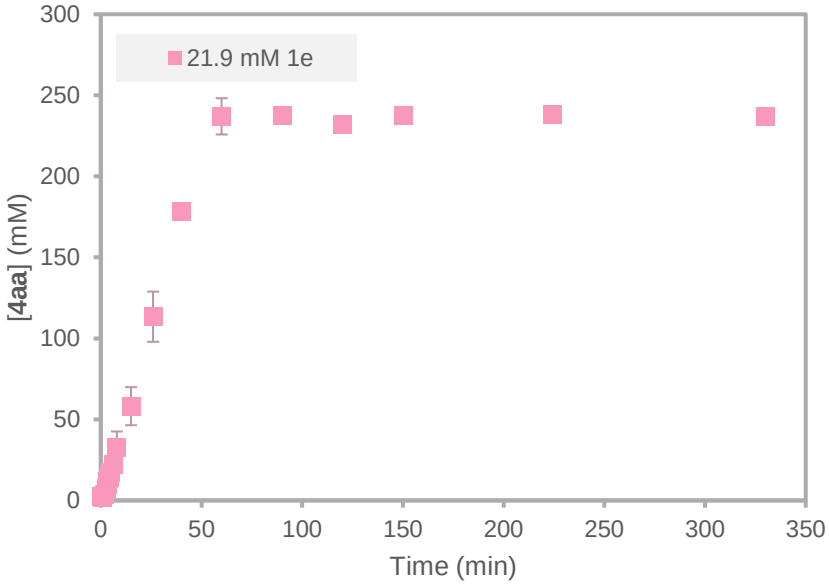

Figure B.17. Table B.4., Entry 4: Full reaction profile for the formation of **4aa** over time (min) with 21.9 mM **1e**, 218 mM **2a**, and 242 mM **3a**.

Table B.7. Table B.4., Entry 4: [**4aa**] (mM) and selectivity (*l*:*b*) of **4aa** formed with 21.9 mM **1e**, 218 mM **2a**, and 242 mM **3a**.

Time (min)	[**4aa**] (mM)	Selectivity (*l*:*b*)
0.5	2.1 ± 0.2	1:0.6
1	1.98 ± 0.09	1:2.3
1.7	3.975 ± 0.008	1:4.0
2.5	7.50 ± 0.01	1:3.7
3	10 ± 1	1:5.9
3.5	11.4 ± 0.1	1:6.8
4	13 ± 1	1:6.7
4.5	14.2 ± 0.3	1:9.0
5	17 ± 1	1:8.1
6	22.0 ± 0.4	1:9.9
8	32.9 ± 0.5	1:9.8
15	58.2 ± 0.9	1:14
26	113.4 ± 0.7	1:15
40	180 ± 12	1:18
60	237 ± 2	1:22
90	238 ± 1	1:23
120	232 ± 8	1:23
150	237 ± 3	1:24
224	238 ± 2	1:26
330	237 ± 1	1:27

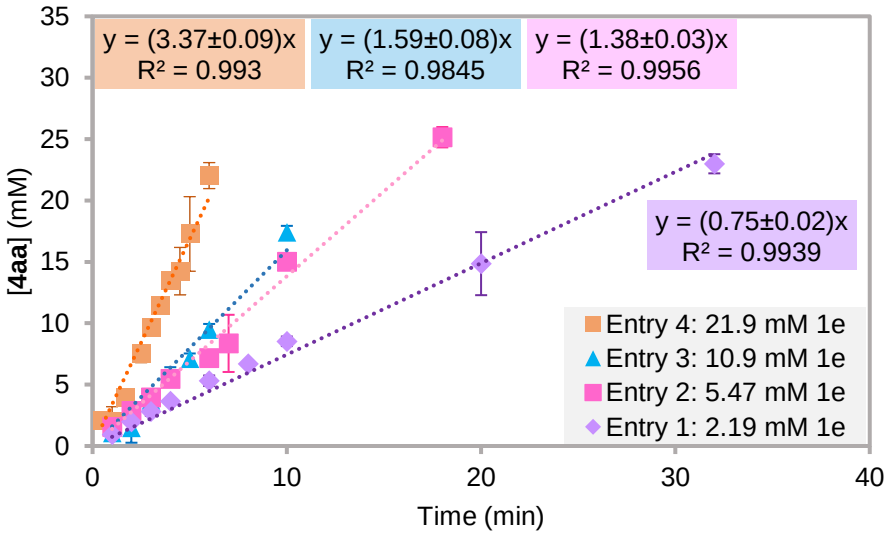

Figure B.18. Table B.4., Entry 1-4: Initial rates of the formation of **4aa** with 2.19, 5.47, 10.9, and 21.9 mM **1e** (all with 218 mM **2a**, 242 mM **3a**).

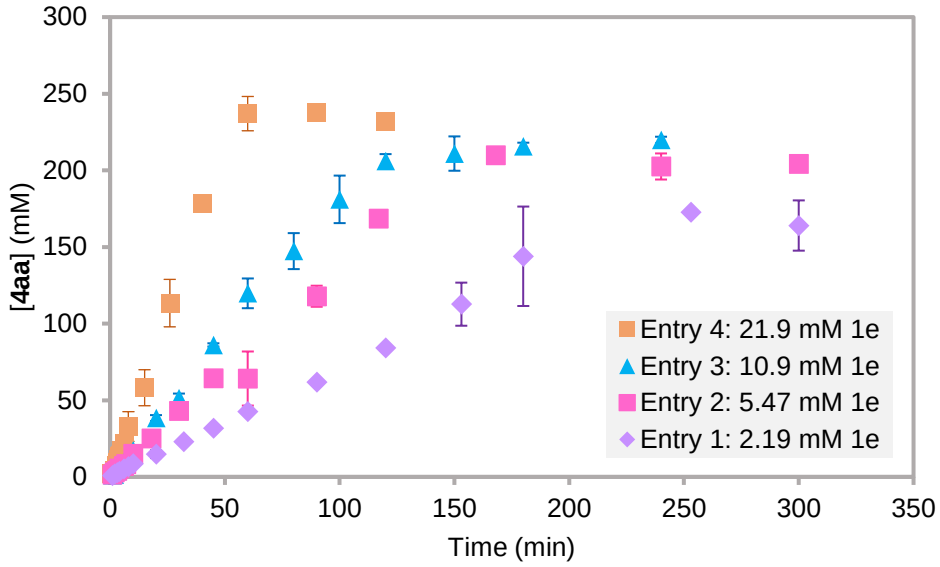

Figure B.19. Table B.4., Entry 1-4: Full reaction profile for the formation of **4aa** over time (min) with 2.19, 5.47, 10.9, and 21.9 mM **1e** (all with 218 mM **2a**, 242 mM **3a**).

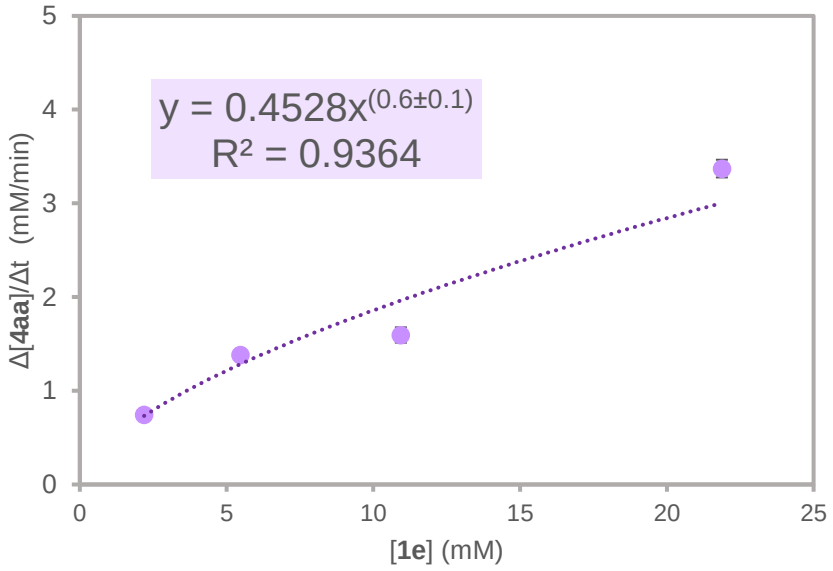

Figure B.20. Plot of Δ[**4aa**]/Δt (mM/min) versus [**1e**] (mM).

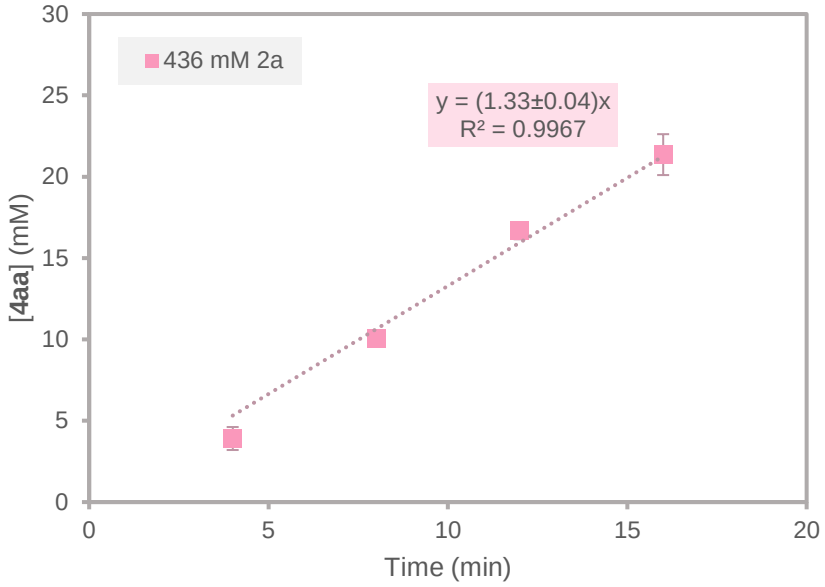

Figure B.21. Table B.4., Entry 5: Initial rate of the formation of **4aa** versus time (min) with 10.9 mM **1e**, 436 mM **2a**, and 242 mM **3a**.

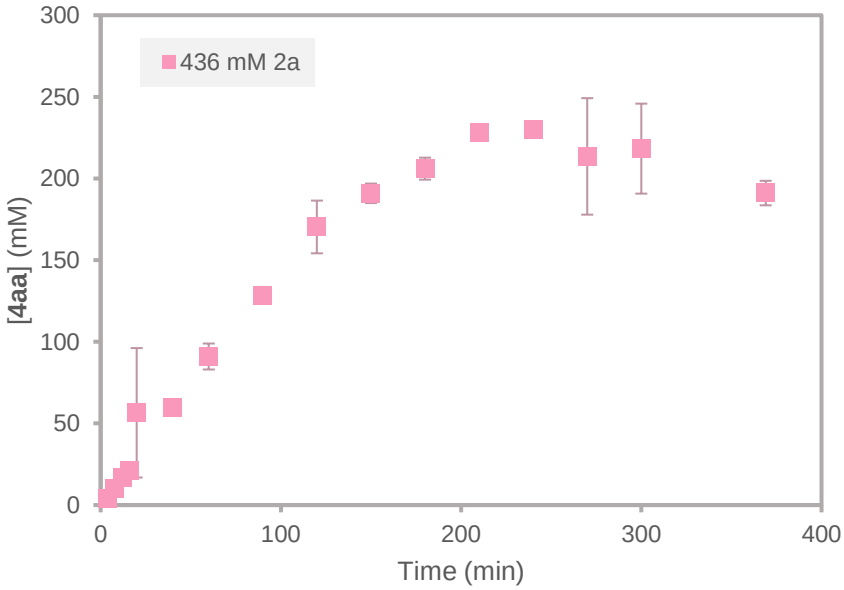

Figure B.22. Table B.4., Entry 5: Full reaction profile for the formation of **4aa** over time (min) with 10.9 mM **1e**, 436 mM **2a**, and 242 mM **3a**.

Table B.8. Table B.4., Entry 5: [**4aa**] (mM) and selectivity (*l*:*b*) of **4aa** formed with 10.9 mM **1e**, 436 mM **2a**, and 242 mM **3a**.

Time (min)	[**4aa**] (mM)	Selectivity (*l*:*b*)
4	3.9 ± 0.7	1:10.1
8	10.0 ± 0.5	1:6.2
12	16.7 ± 0.5	1:5.4
16	21 ± 1	1:5.2
20	56 ± 40	1:9.2
40	59 ± 2	1:4.3
60	90 ± 8	1:3.9
90	128 ± 5	1:3.4
120	170 ± 16	1:3.1
150	191 ± 6	1:2.9
180	206 ± 7	1:2.8
210	228 ± 3	1:2.7
240	230 ± 2	1:2.7
270	210 ± 36	1:2.7
300	220 ± 28	1:2.7
369	191 ± 8	1:2.6

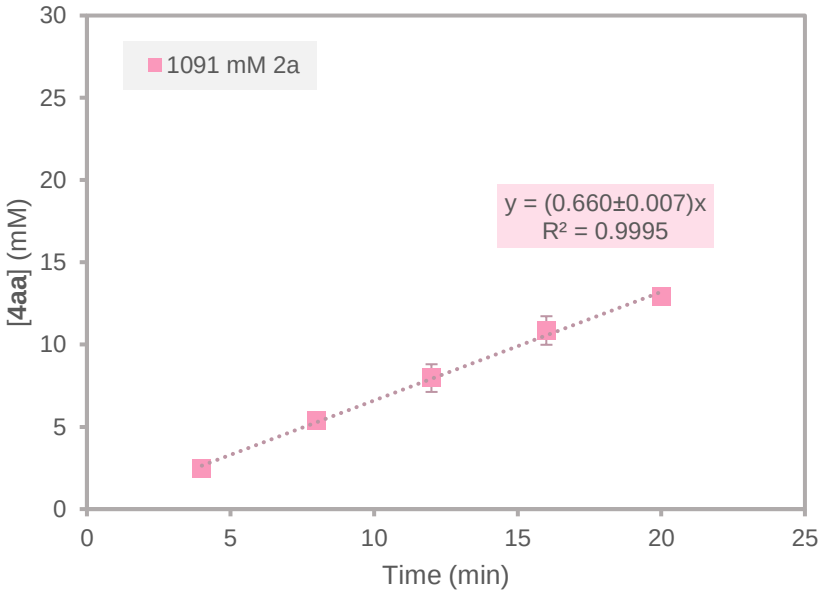

Figure B.23. Table B.4., Entry 6: Initial rate of the formation of **4aa** versus time (min) with 10.9 mM **1e**, 1091 mM **2a**, and 242 mM **3a**.

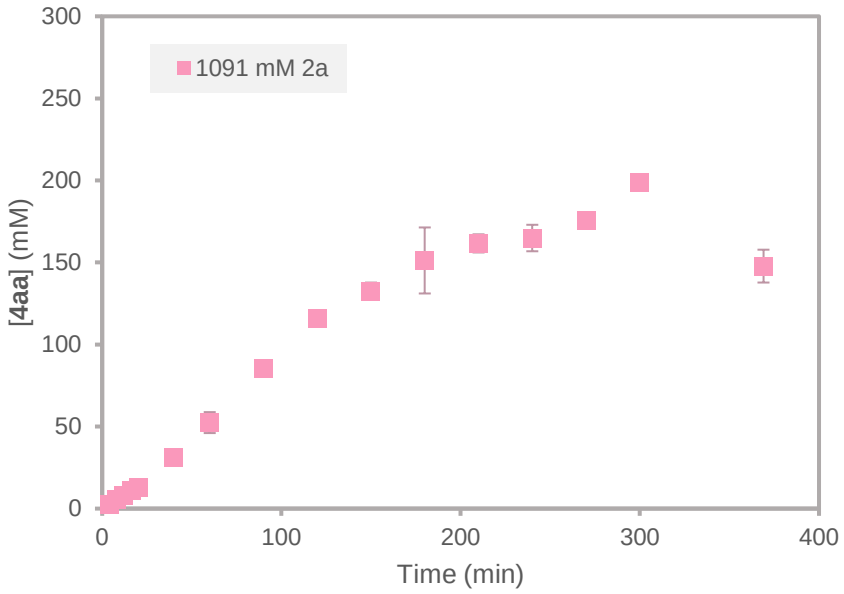

Figure B.24. Table B.4., Entry 6: Full reaction profile for the formation of **4aa** over time (min) with 10.9 mM **1e**, 1091 mM **2a**, and 242 mM **3a**.

Table B.9. Table B.4., Entry 6: [**4aa**] (mM) and selectivity (*l*:*b*) of **4aa** formed with 10.9 mM **1e**, 1091 mM **2a**, and 242 mM **3a**.

Time (min)	[**4aa**] (mM)	Selectivity (*l*:*b*)
4	2.5 ± 0.4	1:2.2
8	5.4 ± 0.3	1:2.4
12	8.0 ± 0.8	1:3.5
16	10.9 ± 0.9	1:3.1
20	13.0 ± 0.4	1:2.9
40	31 ± 1	1:2.2
60	52 ± 6	1:1.9
90	85.0 ± 0.8	1:1.6
120	116 ± 3	1:1.5
150	133 ± 5	1:1.4
180	150 ± 20	1:1.4
210	162 ± 5	1:1.3
240	165 ± 8	1:1.3
270	175 ± 3	1:1.3
300	198 ± 3	1:1.3
369	150 ± 10	1:1.3

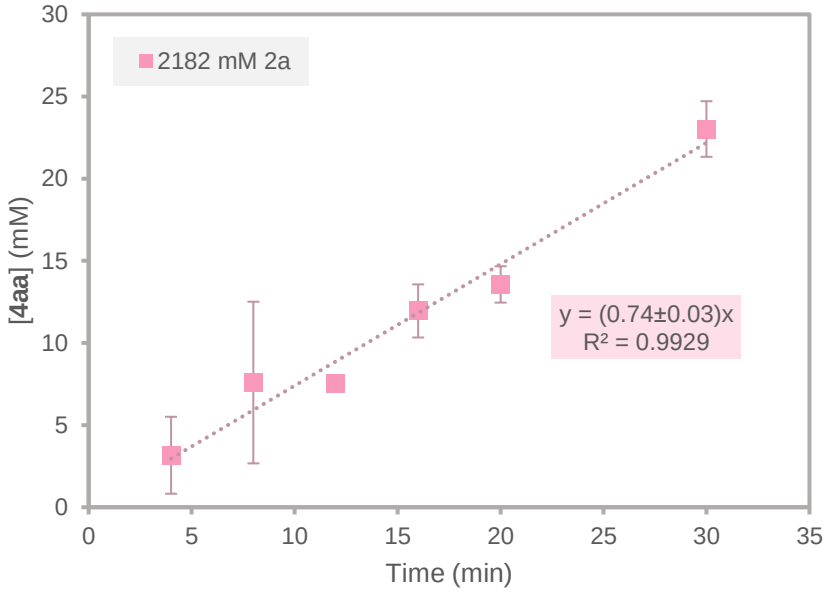

Figure B.25. Table B.4., Entry 7: Initial rate of the formation of **4aa** versus time (min) with 10.9 mM **1e**, 2182 mM **2a**, and 242 mM **3a**.

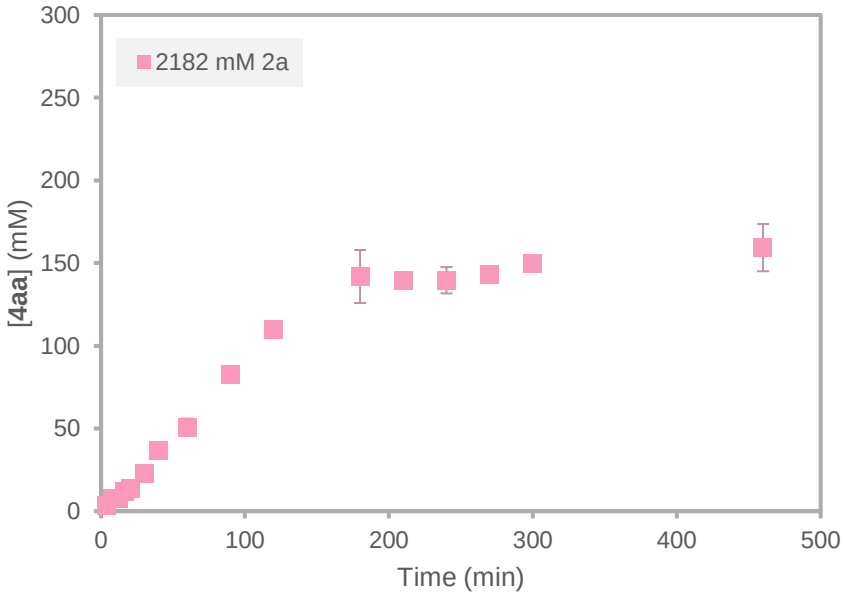

Figure B.26. Table B.4., Entry 7: Full reaction profile for the formation of **4aa** over time (min) with 10.9 mM **1e**, 2182 mM **2a**, and 242 mM **3a**.

Table B.10. Table B.4., Entry 7: [**4aa**] (mM) and selectivity (*l*:*b*) of **4aa** formed with 10.9 mM **1e**, 2182 mM **2a**, and 242 mM **3a**.

Time (min)	[**4aa**] (mM)	Selectivity (*l*:*b*)

4	3 ± 2	1:2.3
8	8 ± 5	1:2.1
12	7.5 ± 0.3	1:2.9
16	12 ± 2	1:3.0
20	14 ± 1	1:2.2
30	23 ± 1	1:2.0
40	37 ± 2	1:1.8
60	51 ± 5	1:1.6
90	82 ± 3	1:1.4
120	109.6 ± 0.4	1:1.4
180	140 ± 16	1:1.4
210	139 ± 2	1:1.4
240	140 ± 8	1:1.4
270	143 ± 2	1:1.4
300	149 ± 3	1:1.4
460	160 ± 14	1:1.5

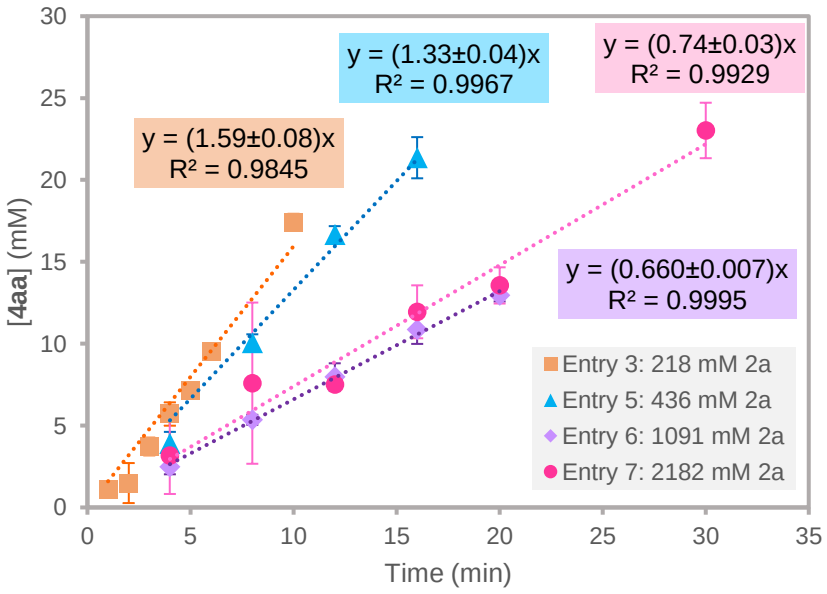

Figure B.27. Table B.4., Entry 3, 5-7: Initial rates of the formation of **4aa** versus time (min) with 218, 436, 1091, and 2182 mM **2a** (all with 10.9 mM **1e**, 242 mM **3a**).

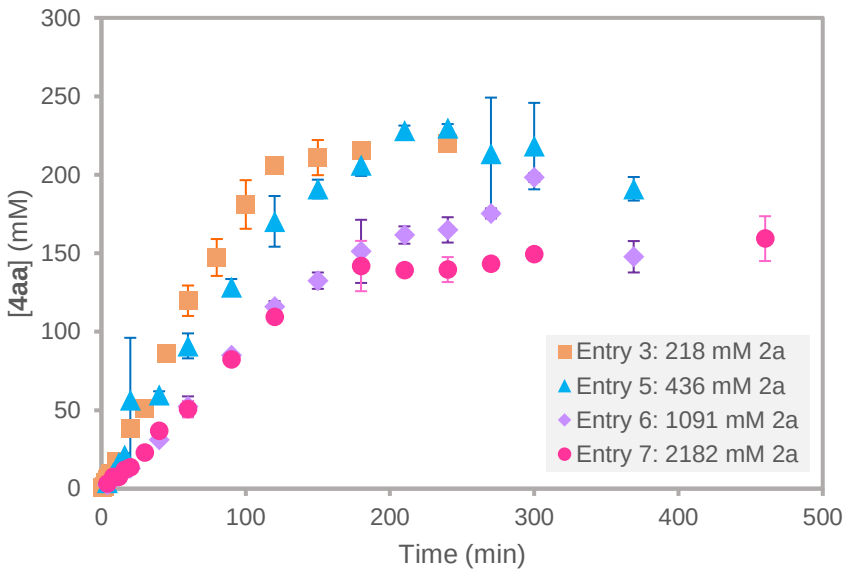

Figure B.28. Table B.4., Full reaction profile for the formation of **4aa** over time (min) 218, 436, 1091, and 2182 mM **2a** (all with 10.9 mM **1e**, 242 mM **3a**).

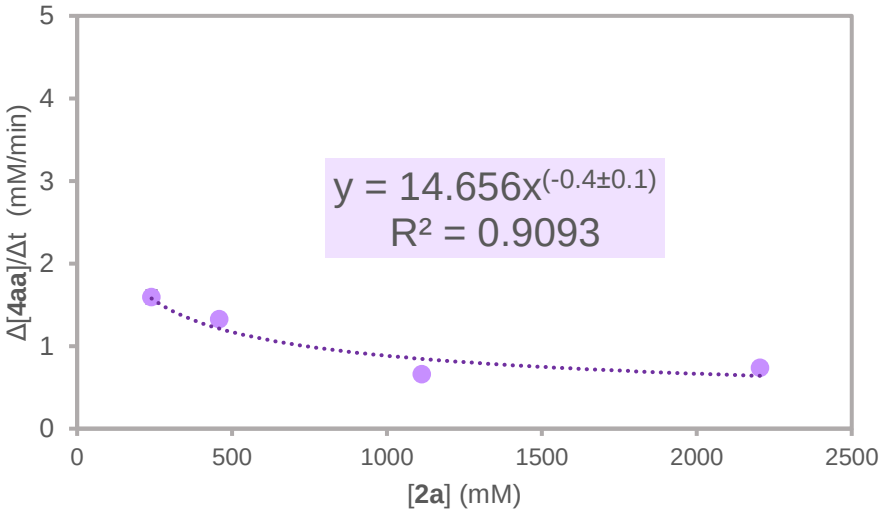

Figure B.29. Table B.4., Plot of Δ[**4aa**]/Δt (mM/min) versus [**2a**] (mM). Error bars are present but are not visible.

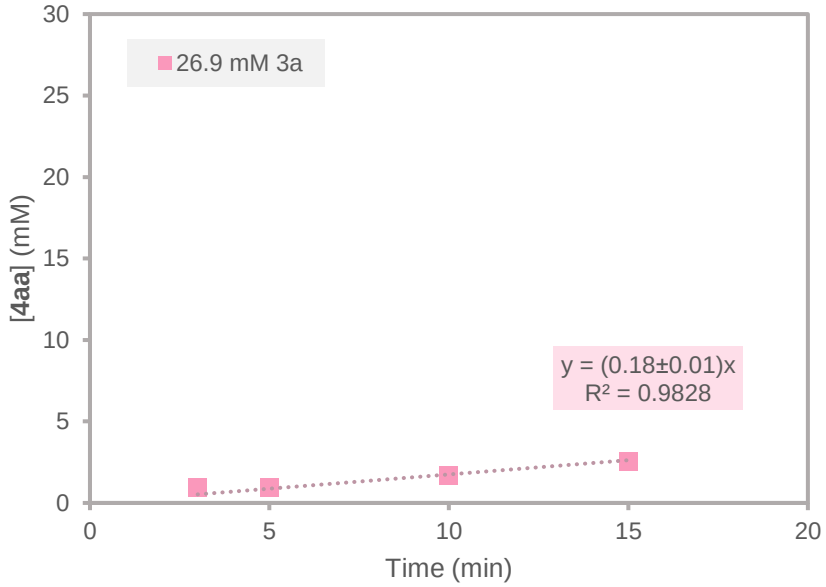

Figure B.30. Table B.4., Entry 8: Initial rate of the formation of **4aa** versus time (min) with 10.9 mM **1e**, 218 mM **2a**, and 26.9 mM **3a**. Error bars are present but are not visible.

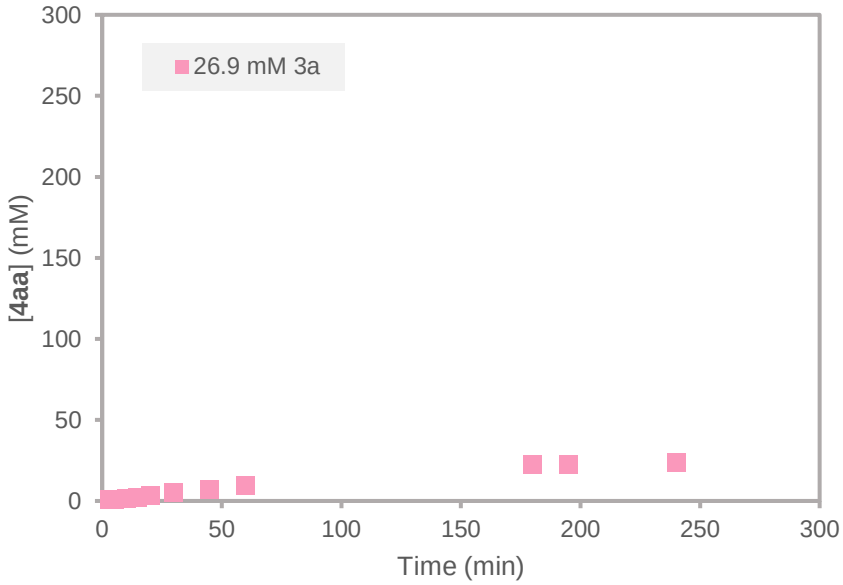

Figure B.31. Table B.4., Entry 8: Full reaction profile for the formation of **4aa** over time (min) with 10.9 mM **1e**, 218 mM **2a**, and 26.9 mM **3a**. Error bars are present but are not visible.

Table B.11. Table B.4., Entry 8: [**4aa**] (mM) and selectivity (*l*:*b*) of **4aa** formed with 10.9 mM **1e**, 218 mM **2a**, and 26.9 mM **3a**.

Time (min)	[**4aa**] (mM)	Selectivity (*l*:*b*)
3	0.9±0.4	1:7.2
5	0.9±0.4	1:6.1
10	1.7±0.3	1:12
15	2.5±0.2	1:19
20	3.3±0.4	1:18
30	5±1	1:19
45	7±1	1:19
60	9±2	1:12
180	23±4	1:6.2
195	23±3	1:6.2
240	24±3	1:6.0

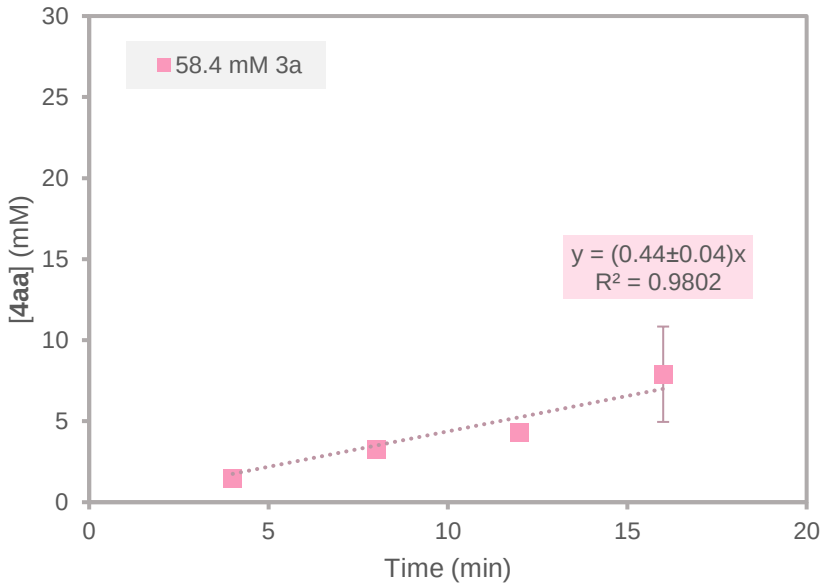

Figure B.32. Table B.4., Entry 9: Initial rate of the formation of **4aa** versus time (min) with 10.9 mM **1e**, 218 mM **2a**, and 58.4 mM **3a**.

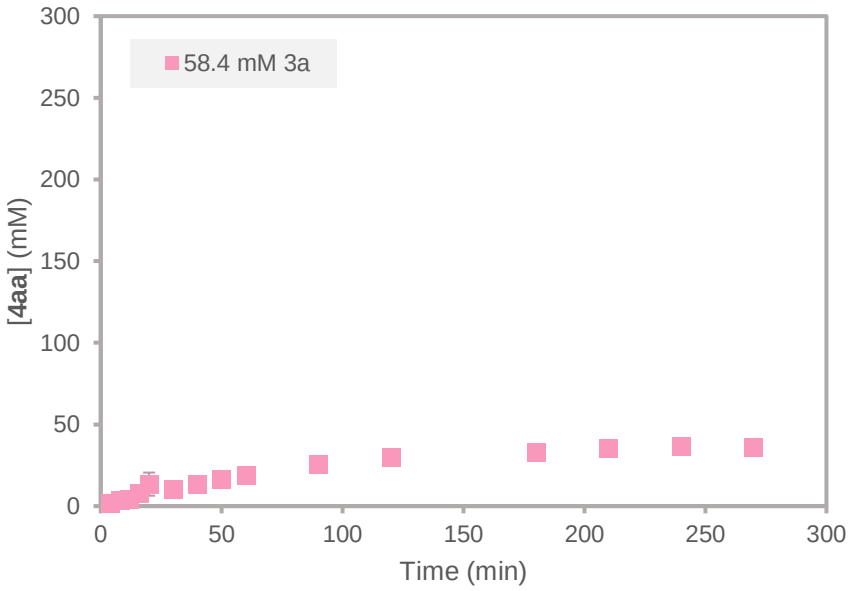

Figure B.33. Table B.4., Entry 9: Full reaction profile for the formation of **4aa** over time (min) with 10.9 mM **1e**, 218 mM **2a**, and 58.4 mM **3a**.

Table B.12. Table B.4., Entry 9: [**4aa**] (mM) and selectivity (*l*:*b*) of **4aa** formed with 10.9 mM **1e**, 218 mM **2a**, and 58.4 mM **3a**.

Time (min)	[**4aa**] (mM)	Selectivity (*l*:*b*)
4	1.5±0.2	1:2.0
8	3.25±0.03	1:2.1
12	4.3±0.3	1:3.8
16	8±3	1:3.9
20	13±7	1:5.2
30	9.9±0.3	1:4.5
40	13±2	1:4.4
50	16±2	1:4.4
60	18±2	1:4.3
90	25.6±0.4	1:4.1
120	29.7±0.1	1:4.1
180	33±3	1:4.0
210	35±4	1:4.0
240	36±4	1:4.0
270	36±5	1:4.2

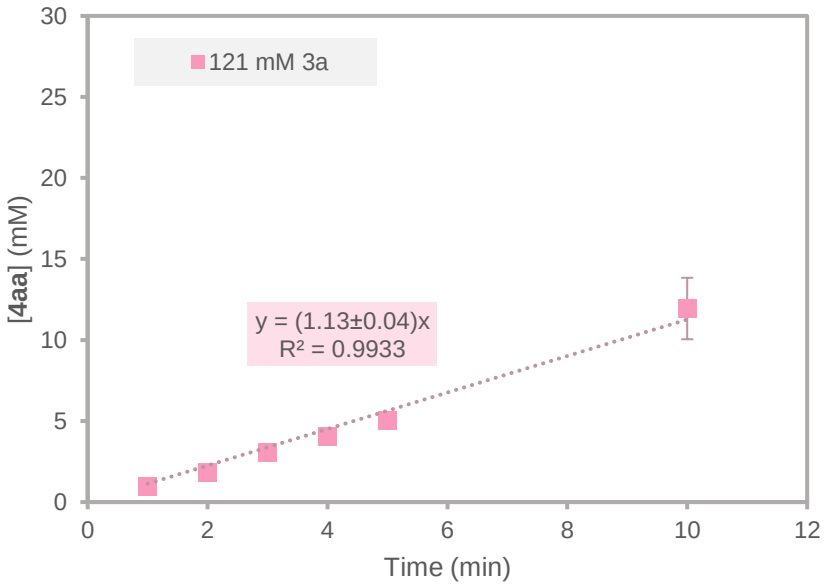

Figure B.34. Table B.4., Entry 10: Initial rate of the formation of **4aa** over time (min) with 10.9 mM **1e**, 218 mM **2a**, and 121 mM **3a**.

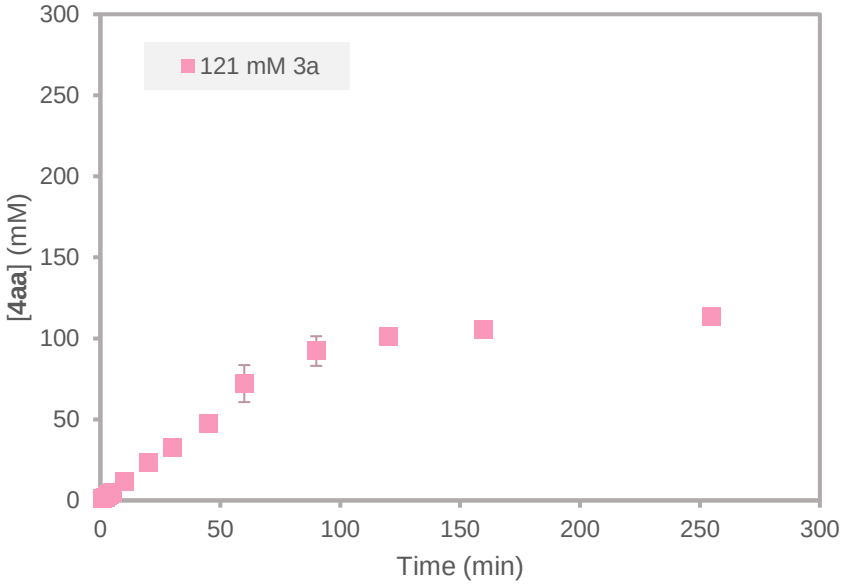

Figure B.35. Table B.4., Entry 10: Full reaction profile for the formation of **4aa** over time (min) with 10.9 mM **1e**, 218 mM **2a**, and 121 mM **3a**.

Table B.13. Table B.4., Entry 10: [**4aa**] (mM) and selectivity (*l*:*b*) of **4aa** formed with 10.9 mM **1e**, 218 mM **2a**, and 121 mM **3a**.

Time (min)	[**4aa**] (mM)	Selectivity (*l*:*b*)
1	1.0±0.3	1:2.7
2	1.8±0.1	1:3.5
3	3.1±0.3	1:5.3
4	4.0±0.07	1:6.4
5	5.0±0.3	1:7.2
10	12±2	1:7.9
20	23±1	1:8.1
30	32.8±0.8	1:7.8
45	47.1±0.8	1:7.3
60	72±11	1:6.8
90	92±9	1:6.0
120	101±5	1:5.7
160	105±4	1:5.5
255	114±1	1:5.3

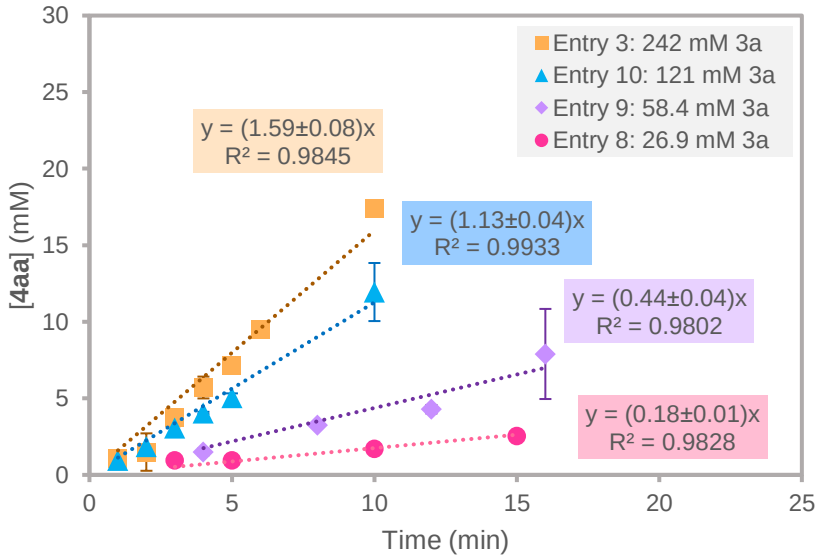

Figure B.36. Table B.13., Entry 3, 8-10: Initial rates of the formation of **4aa** versus time (min) with 26.9, 58.4, 121, and 242 mM **3a** (all with 10.9 mM **1e**, 218 mM **2a**).

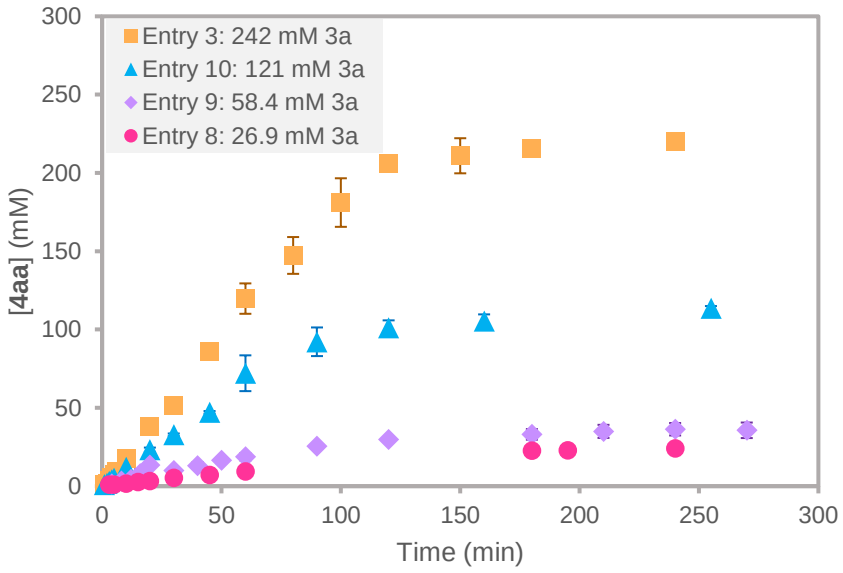

Figure B.37. Rates of formation of [**4aa**] (mM) with 26.9, 58.4, 121, and 242 mM **3a** (all with 10.9 mM **1e**, 218 mM **2a**).

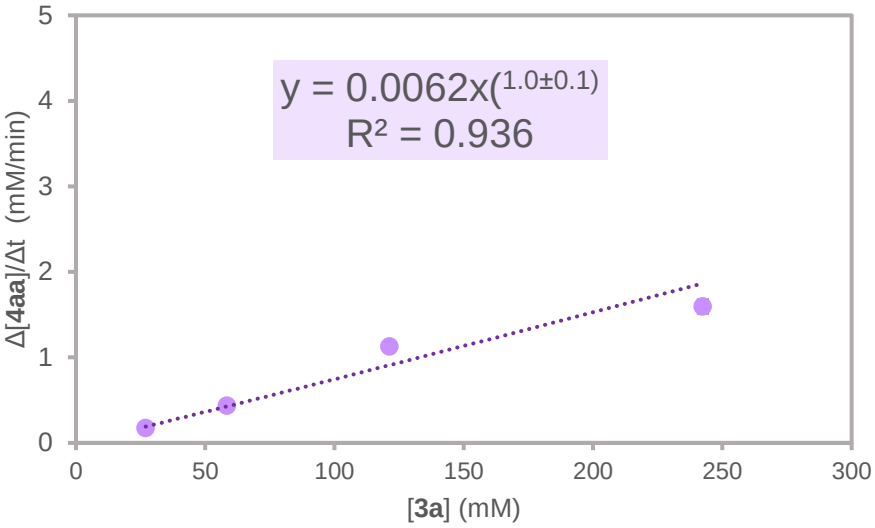

Figure B.38. Plot of Δ[**4aa**]/Δt (mM/min) versus [**3a**] (mM). Error bars are present but are not visible.

d. Hammett Plot

i. Silane Derivatives

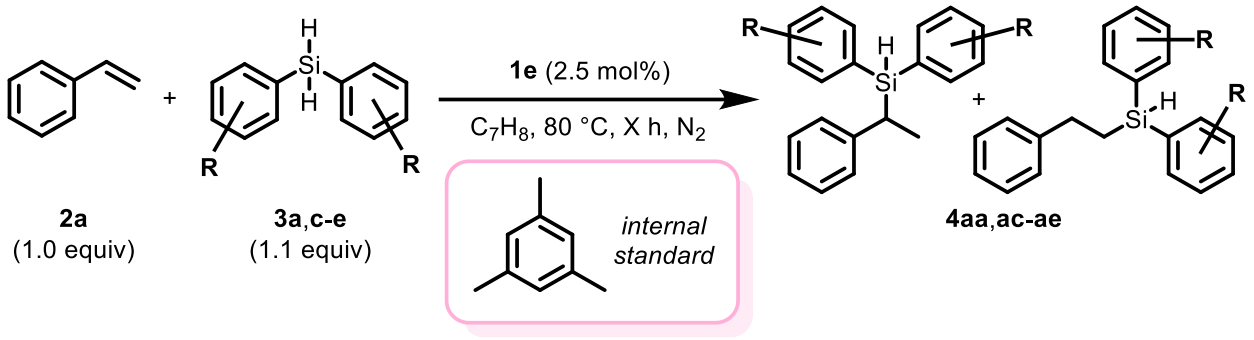

General Procedure: In a nitrogen-filled glovebox, a stock solution was prepared by weighing out **1e** (7.8 mg, 2.7x10^{-3} M) and dissolving in toluene (5.0 mL) using volumetric glassware. The stock solution of **1e** (1.9 mg, 3.3x10^{-3} mmol, 0.025 equiv, 1.2 mL of stock solution) was distributed into two 1-dram scintillation vials equipped with stir bars using a disposable 1-mL syringe. An additional amount of toluene (1.2 mL), **2a** (15 µL, 0.13 mmol, 1.0 equiv), and mesitylene (10 µL, 0.072 mmol) were added to each vial and then sealed with a septum cap. The reactions were brought out of the glovebox, injected with the corresponding amount of silane (**3a,c-e**, 0.14 mmol, 1.1 equiv), and placed on an aluminum vial block preheated to 80 °C. Throughout the course of the reaction, 20 µL aliquots were removed with a 25-µL syringe and filtered into a GC vial through Celite and diluted with hexanes. The filtrate was analyzed by GC to assess the reaction progress and selectivity. The product concentration was determined by relative integration (by GC) of the product peaks against mesitylene, in accordance with calibration curves. Two trials were run for all experiments.

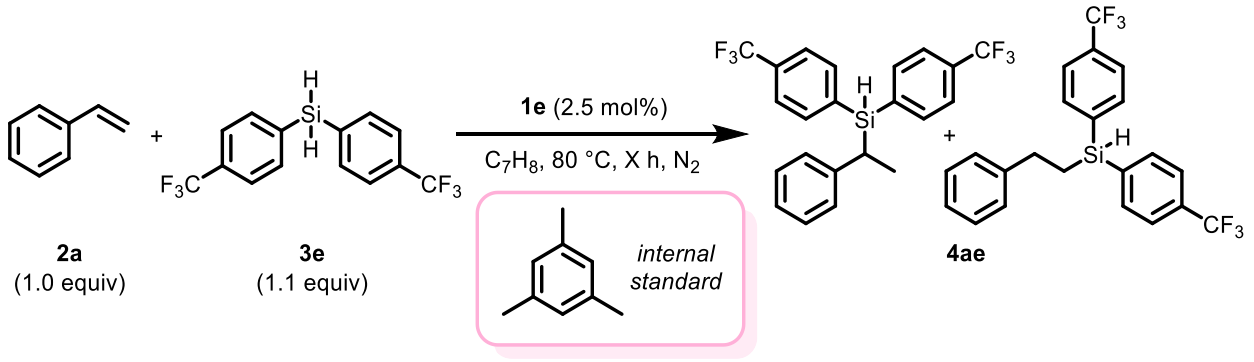

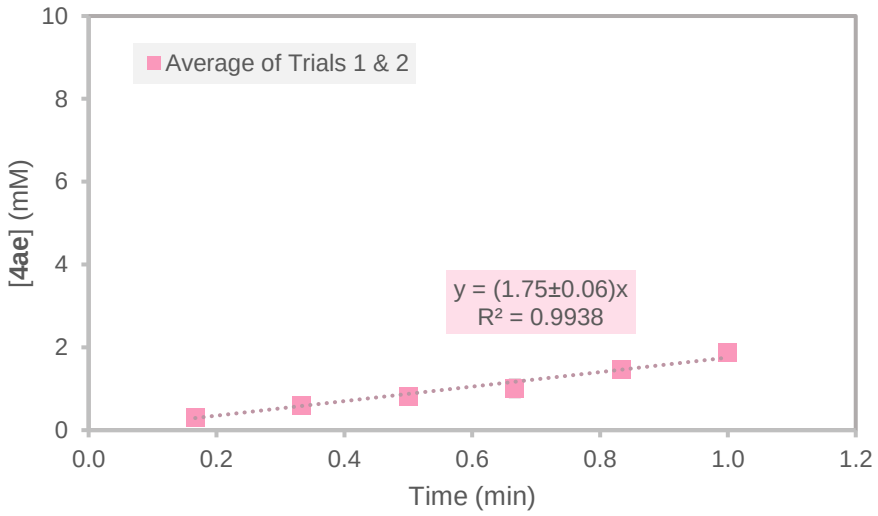

Figure B.39. Initial rate of the formation of **4ae** versus time (min).

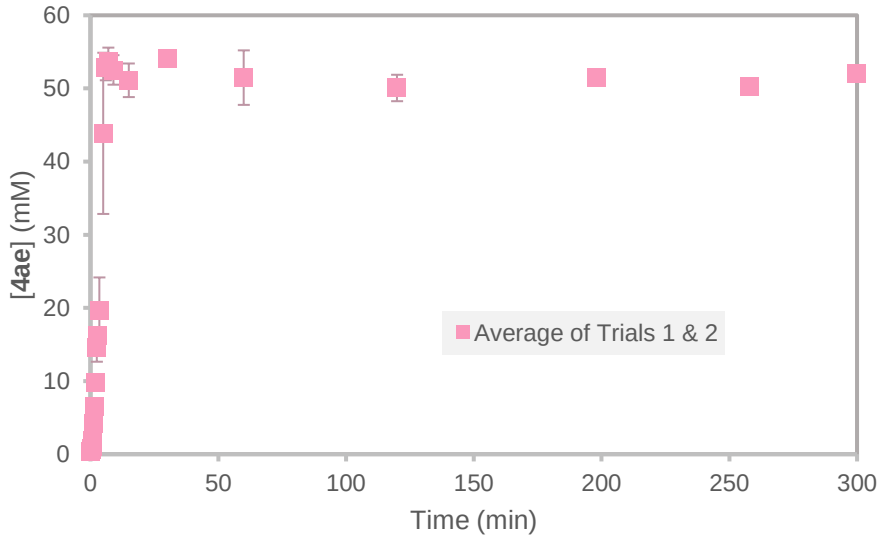

Figure B.40. Full reaction profile for the formation of **4ae** over time.

Table B.14. [**4ae**] (mM) and selectivity (*l*:*b*) of **4ae** formed.

Time (min)	[**4ae**] (mM)	Selectivity (*l*:*b*)
0.17	0.3 ± 0.1	1:0.2
0.33	0.6 ± 0.1	1:0.2
0.5	0.8 ± 0.2	1:0.3
0.67	1.0 ± 0.2	1:0.8
0.83	1.46 ± 0.05	1:1.4
1	1.9 ± 0.2	1:3.0
1.33	4.1 ± 0.5	1:8.4

1.66	6.6 ± 0.6	1:12
2	10 ± 1	1:13
2.5	15 ± 2	1:25
3	16.3 ± 0.4	1:27
3.5	20 ± 4	1:20
5	40 ± 11	1:52
6	53 ± 2	1:53
7	54 ± 2	1:56
9	53 ± 2	1:67
15	51 ± 2	1:62
30	54.1 ± 0.2	1:58
60	51 ± 4	1:58
120	50 ± 2	1:63
198	51.4 ± 0.5	1:67
258	50.3 ± 0.3	1:64
300	52 ± 3	1:69

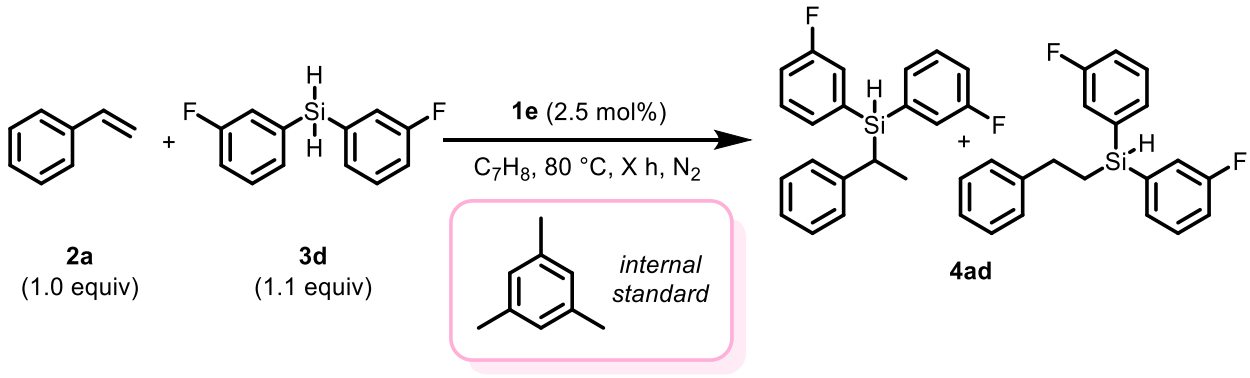

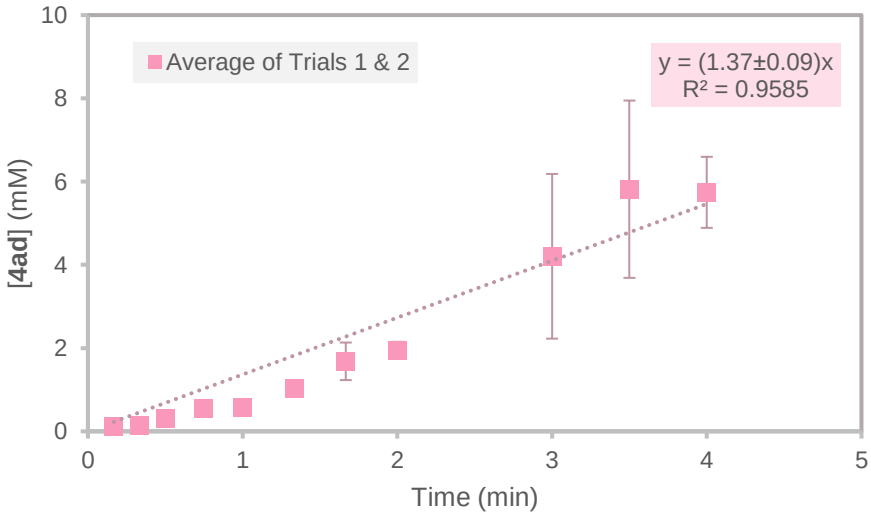

Figure B.41. Initial rate of the formation of **4ad** versus time (min).

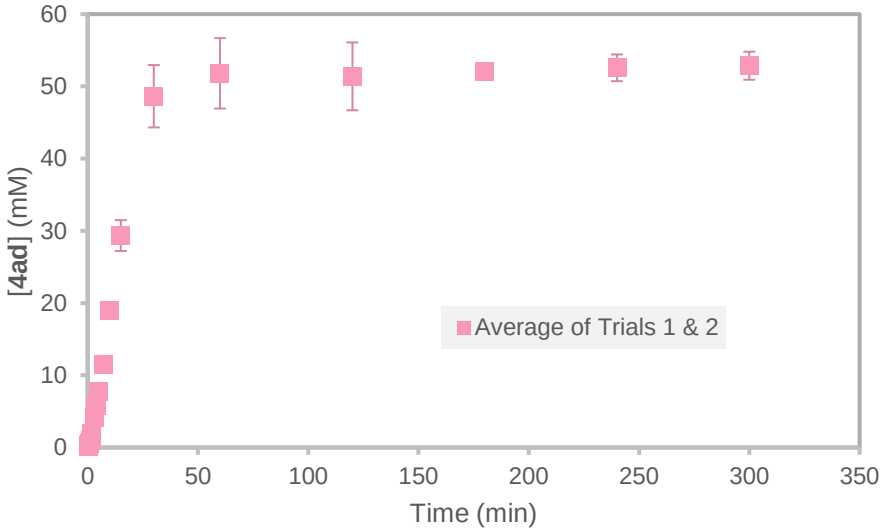

Figure B.42. Full reaction profile for the formation of **4ad** over time.

Table B.15. [**4ad**] (mM) and selectivity (*l*:*b*) of **4ad** formed.

Time (min)	[**4ad**] (mM)	Selectivity (*l*:*b*)
0.17	0.12 ± 0.08	1:0.3
0.33	015 ± 0.04	1:0.2
0.5	0.31 ± 0.07	1:0.4
0.75	0.55 ± 0.09	1:0.6
1	0.6 ± 0.1	1:0.8
1.33	1.0 ± 0.1	1:2.0
1.67	1.7 ± 0.4	1:2.9
2	1.9 ± 0.2	1:4.8
3	4 ± 2	1:4.7
3.5	6 ± 2	1:10.9
4	5.7 ± 0.9	1:12.7
5	7.73 ± 0.06	1:15.0
7	12 ± 1	1:17.8
10	18.955 ± 0.009	1:24.9
15	29 ± 2	1:27.6
30	49 ± 4	1:28.7
60	52 ± 5	1:27.7
120	51 ± 5	1:28.1
180	52.1 ± 0.2	1:27.8
240	53 ± 2	1:27.9
300	53 ± 2	1:28.3

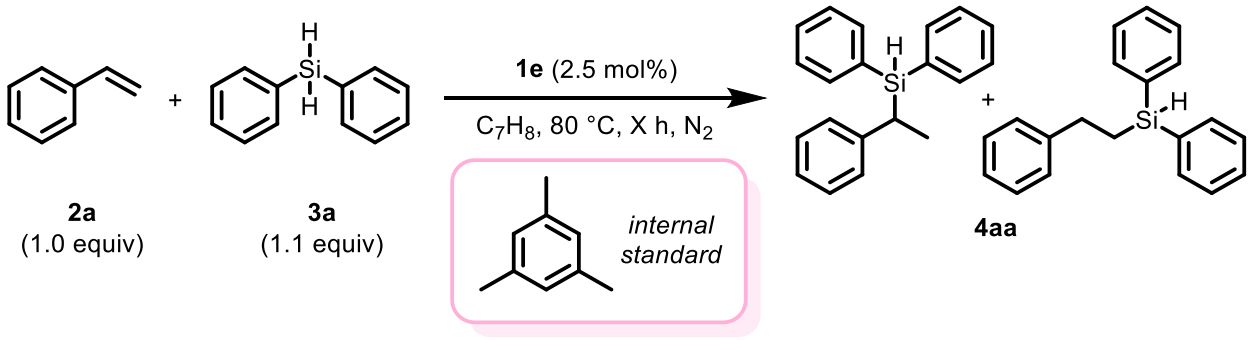

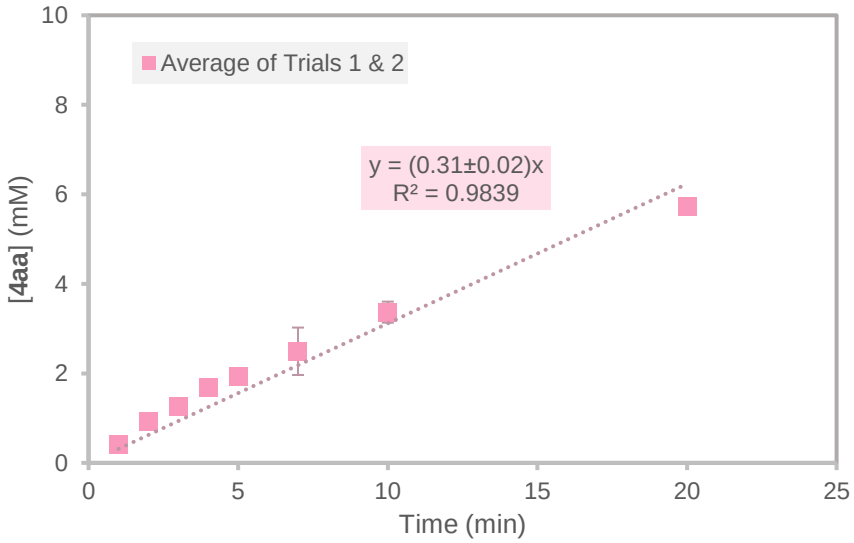

Figure B.43. Initial rate of the formation of **4aa** versus time (min).

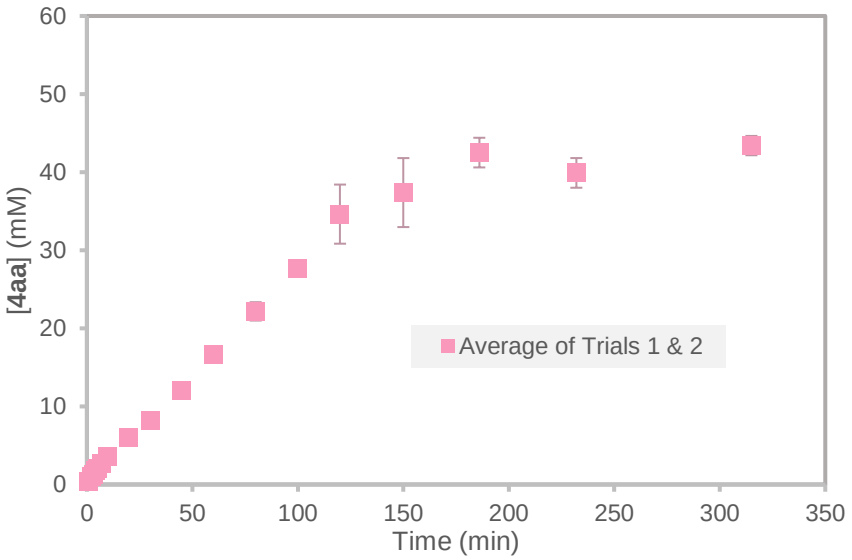

Figure B.44. Full reaction profile for the formation of **4aa** over time.

Table B.16. [**4aa**] (mM) yield and selectivity (*l*:*b*) of **4aa** formed.

Time (min)	[**4aa**] (mM)	Selectivity (*l*:*b*)

1	0.40 ± 0.04	1:1.3
2	0.93 ± 0.04	1:1.4
3	1.3 ± 0.1	1:1.4
4	1.7 ± 0.1	1:1.6
5	1.939 ± 0.004	1:1.6
7	2.5 ± 0.5	1:1.6
10	3.4 ± 0.2	1:1.8
20	5.73 ± 0.09	1:2.0
30	7.78 ± 0.06	1:2.1
45	11.4 ± 0.2	1:2.2
60	15.9 ± 0.3	1:2.3
80	21 ± 1	1:2.3
100	26.4 ± 0.4	1:2.3
120	33 ± 4	1:2.3
150	36 ± 4	1:2.6
186	40 ± 2	1:2.8
232	38 ± 2	1:2.7
315	41 ± 1	1:2.8

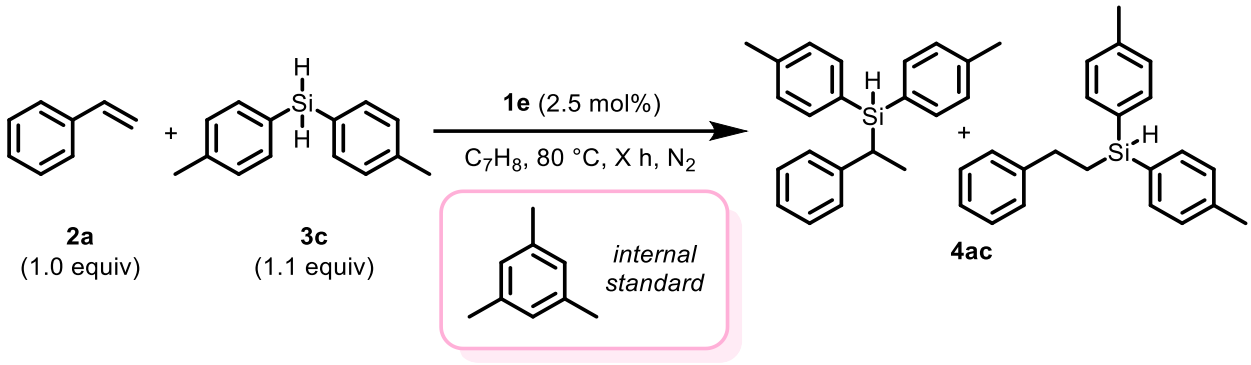

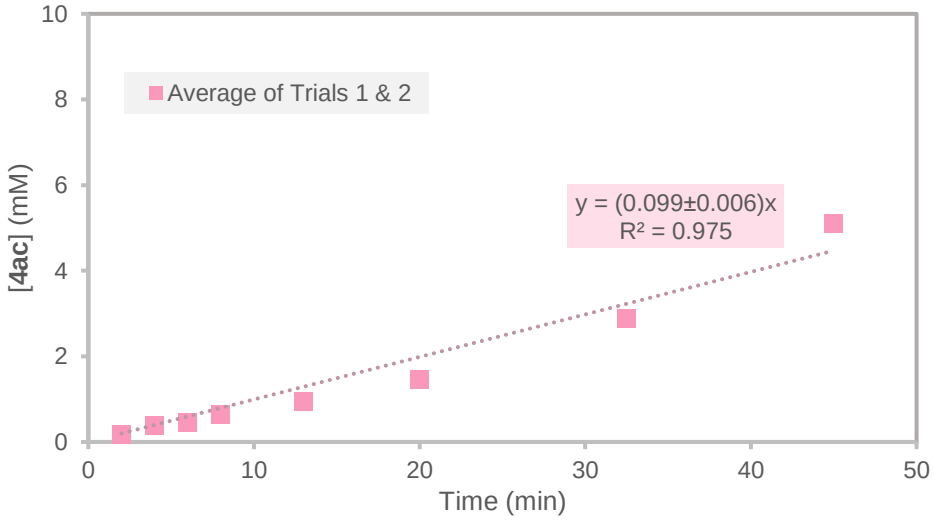

Figure B.45. Initial rate of the formation of **4ac** versus time (min).

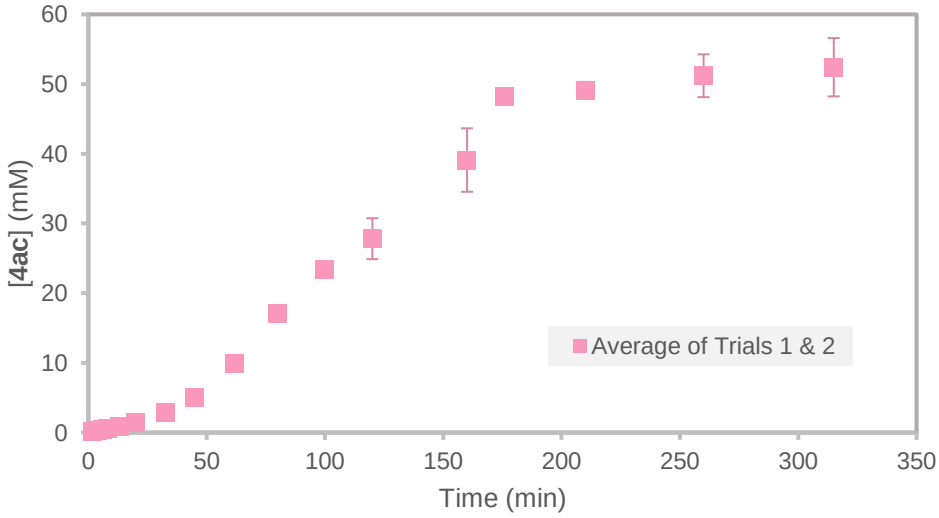

Figure B.46. Full reaction profile for the formation of **4ac** over time.

Table B.17. [**4ac**] (mM) and selectivity (*l*:*b*) of **4ac** formed.

Time (min)	[**4ac**] (mM)	Selectivity (*l*:*b*)
2	0.17 ± 0.04	1:2.5
4	0.380 ± 0.008	1:5.5
6	0.45 ± 0.06	1:8.2
8	0.643 ± 0.009	1:7.2
13	0.94 ± 0.05	1:19
20	1.47 ± 0.04	1:19
32.5	2.9 ± 0.1	1:9.6
45	5.09 ± 0.09	1:3.6
62	10 ± 1	1:2.2
80	17.0 ± 0.4	1:3.1
100	23.4 ± 0.9	1:1.8
120	28 ± 3	1:1.7
160	39 ± 5	1:1.6
176	48.2 ± 0.3	1:1.7
210	49 ± 1	1:1.8
260	51 ± 3	1:1.8
315	52 ± 4	1:1.8

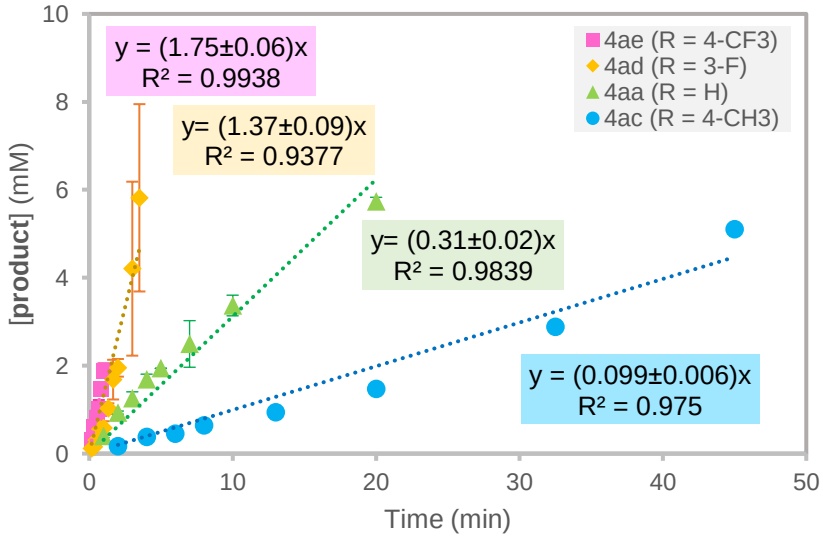

Figure B.47. Initial rates for the formation of the corresponding [**product**] (mM) versus time (min).

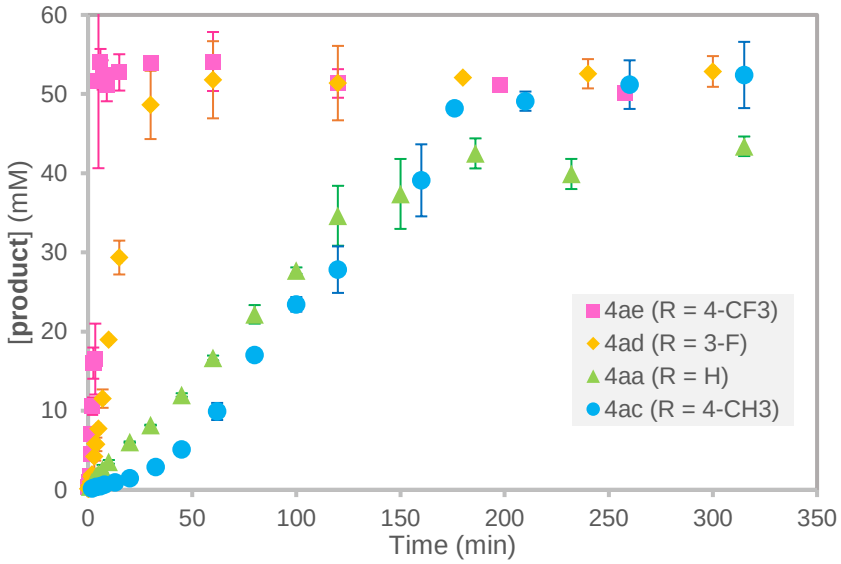

Figure B.48. Full reaction profile for the formation of product over time.

Table B.18. Corresponding functional group (**R**), σ value, k_{obs} (mM/min), k_X/k_H, and $\log(k_X/k_H)$ using **3a**,**c-e**.

R	σ	k_{obs} (mM/min)	k_X/k_H	$\log(k_X/k_H)$
4-CH_3 (**3c**)	-0.17	0.099 ± 0.006	0.32 ± 0.03	-0.50 ± 0.03
H (**3a**)	0	0.31 ± 0.02	1.00 ± 0.07	0.00 ± 0.03
3-F (**3d**)	0.337	1.37 ± 0.09	4.4 ± 0.4	0.64 ± 0.04
4-CF_3 (**3e**)	0.54	1.75 ± 0.06	7 ± 1	0.87 ± 0.08

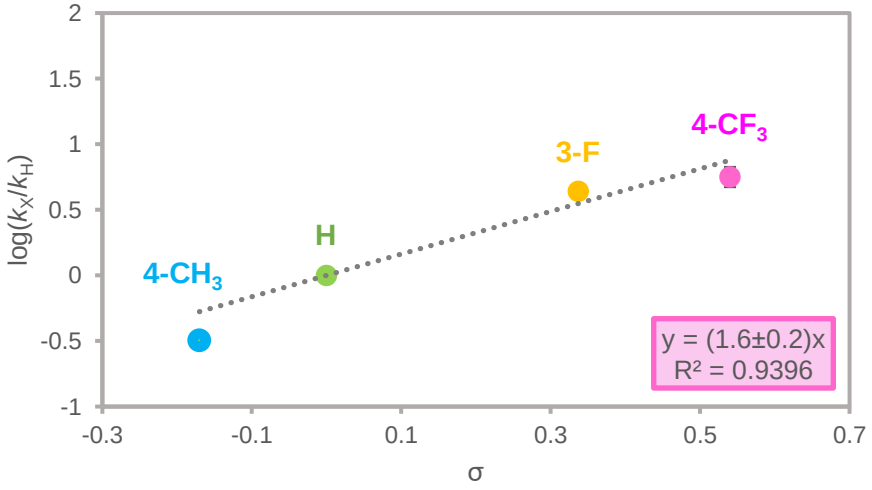

Figure B.49. Hammett Plot: $\log(k_X/k_H)$ versus σ of electronically varied silanes (**3a**,**c-e**). Error bars are present but are not visible.

ii. Styrene Derivatives

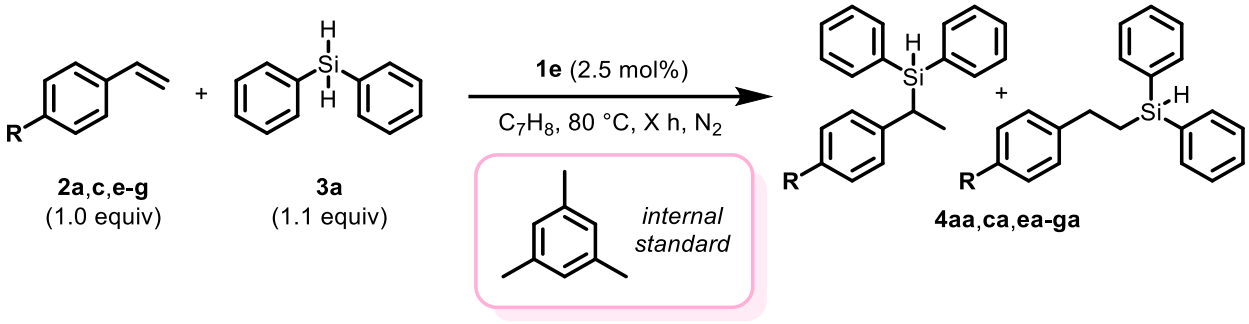

General Procedure: In a nitrogen-filled glovebox, a stock solution was prepared by weighing out **1e** (7.8 mg, 2.7×10^{-3} M) and dissolved in toluene (5.0 mL) using volumetric glassware. The stock solution of **1e** (1.9 mg, 3.3×10^{-3} mmol, 0.025 equiv, 1.2 mL of stock solution) was distributed into two 1-dram scintillation vials equipped with stir bars using a disposable 1 mL syringe. An additional amount of toluene (1.2 mL), the corresponding styrene (**2a**,**c**,**e-g**, 0.13 mmol, 1.0 equiv), and mesitylene (10 µL, 0.072 mmol) were added to each vial and then sealed with a septum cap. The reactions were brought out of the glovebox, injected with **3a** (0.14 mmol, 1.1 equiv), and placed on an aluminum vial block preheated to 80 °C. Throughout the course of the reaction, 20 µL aliquots were removed with a 25-µL microliter syringe and filtered into a GC vial through Celite and diluted with hexanes. The filtrate was analyzed by GC to assess the reaction progress and selectivity. The product concentration was determined by relative integration (by GC) of the product peaks against mesitylene, in accordance with calibration curves. Two trials were run for all experiments.

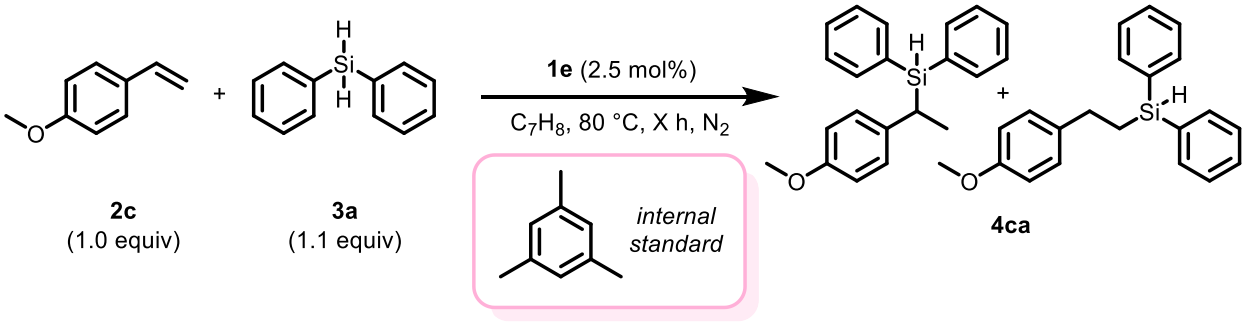

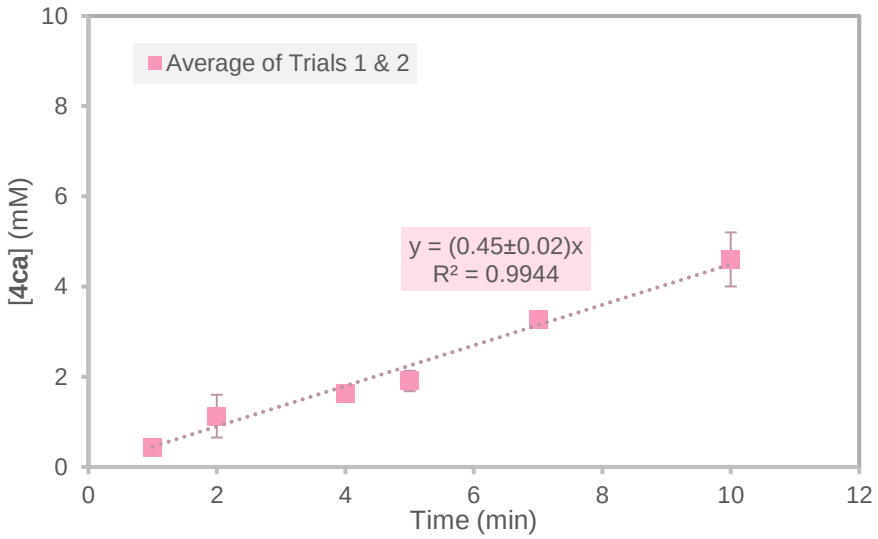

Figure B.50. Initial rate for the formation of **4ca** versus time (min).

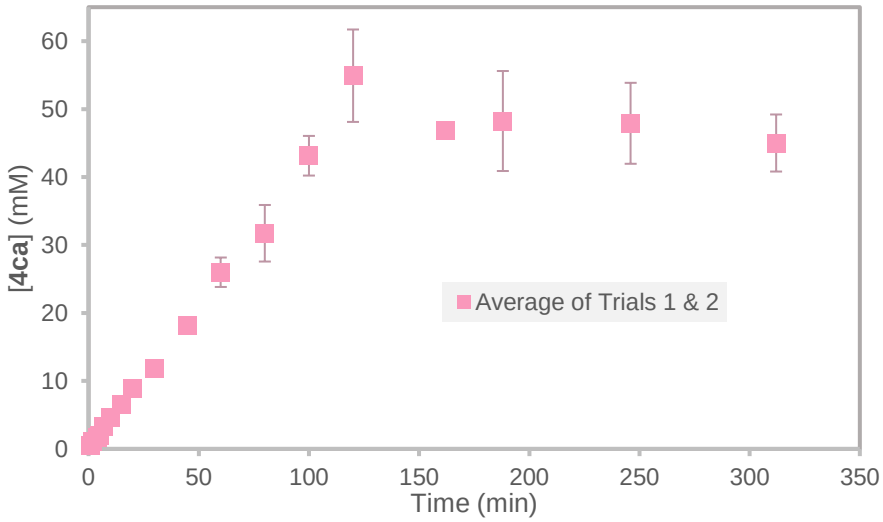

Figure B.51. Full reaction profile for the formation of **4ca** over time.

Table B.19. [**4ca**] (mM) and selectivity (*l*:*b*) of **4ca** formed.

Time (min)	[**4ca**] (mM)	Selectivity (*l*:*b*)
1	0.44 ± 0.08	1:0.4
2	1.1 ± 0.5	1:0.8
4	1.63 ± 0.01	1:2.5
5	1.9 ± 0.2	1:3.1
7	3.27 ± 0.09	1:3.2
10	4.6 ± 0.6	1:4.5
15	6.5 ± 0.6	1:5.0
20	8.8 ± 0.5	1:5.2

30	11.8 ± 0.6	1:5.2
45	18.15 ± 0.07	1:5.5
60	26 ± 2	1:5.6
80	32 ± 4	1:5.5
100	43 ± 3	1:5.7
120	55 ± 7	1:6.1
162	46.8 ± 0.6	1:6.1
188	48 ± 7	1:6.2
246	48 ± 6	1:6.1
312	45 ± 4	1:6.2

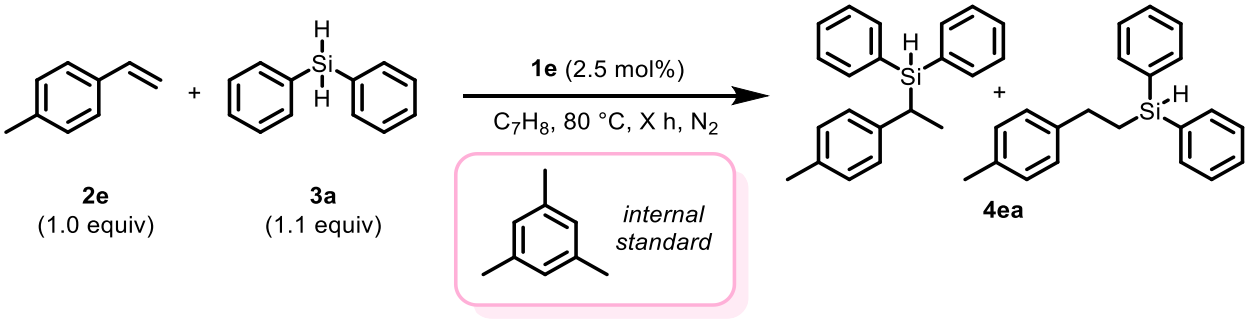

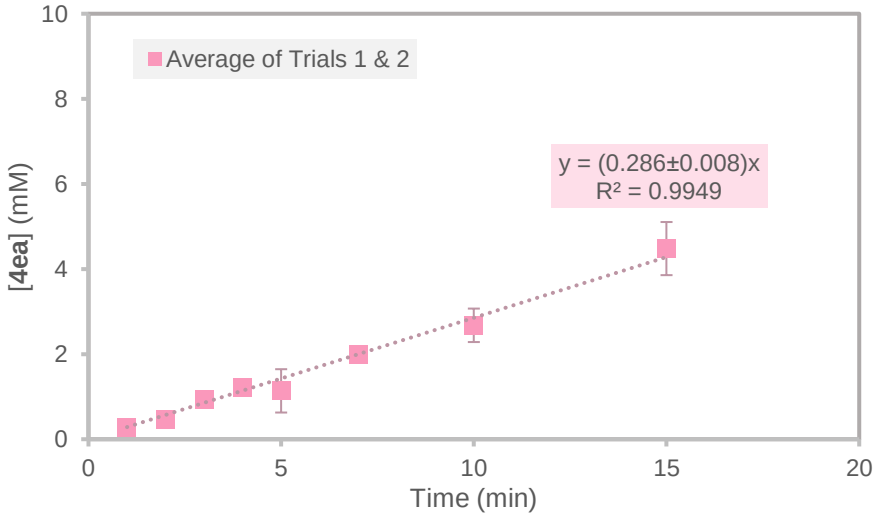

Figure B.52. Initial rate of the formation of **4ea** versus time (min).

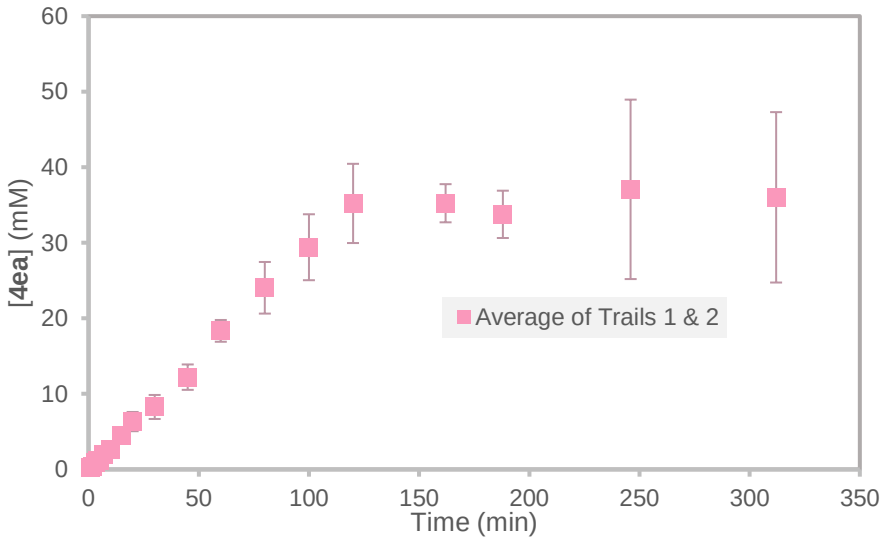

Figure B.53. Full reaction profile for the formation of **4ea** over time.

Table B.20. [**4ea**] (mM) and selectivity (*l*:*b*) of **4ea** formed.

Time (min)	[**4ea**] (mM)	Selectivity (*l*:*b*)
1	0.27 ± 0.02	1:0.4
2	0.46 ± 0.03	1:1.3
3	0.9 ± 0.3	1:1.3
4	1.2 ± 0.1	1:1.8
5	1.1 ± 0.5	1:1.7
7	1.999 ± 0.009	1:2.6
10	2.7 ± 0.4	1:3.0
15	4.5 ± 0.6	1:2.6
20	6 ± 1	1:3.2
30	8 ± 2	1:3.1
45	12 ± 2	1:3.2
60	18 ± 1	1:3.3
80	24 ± 3	1:3.3
100	29 ± 4	1:3.3
120	35 ± 5	1:3.6
162	35 ± 3	1:3.7
188	34 ± 3	1:3.5
246	40 ± 12	1:3.5
312	40 ± 11	1:3.5

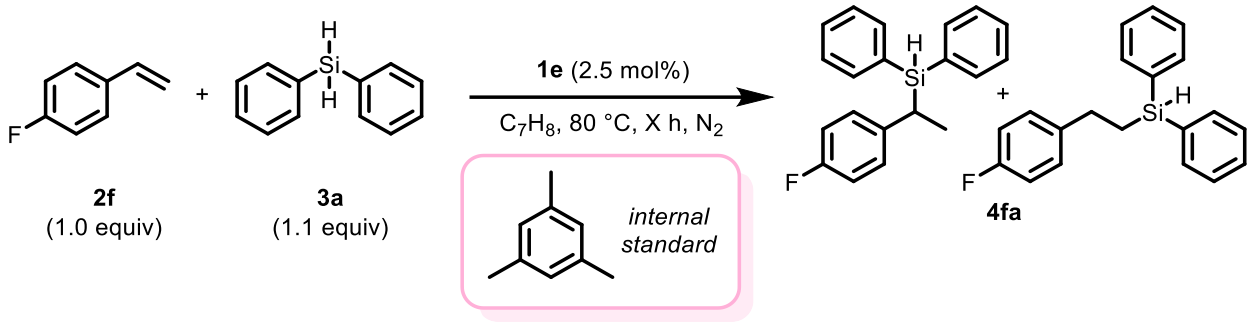

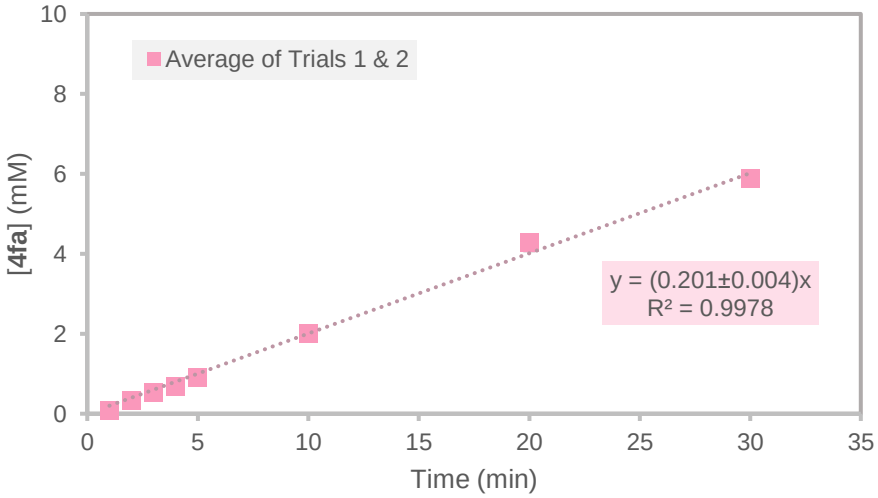

Figure B.54. Initial rate for the formation of **4fa** versus time (min).

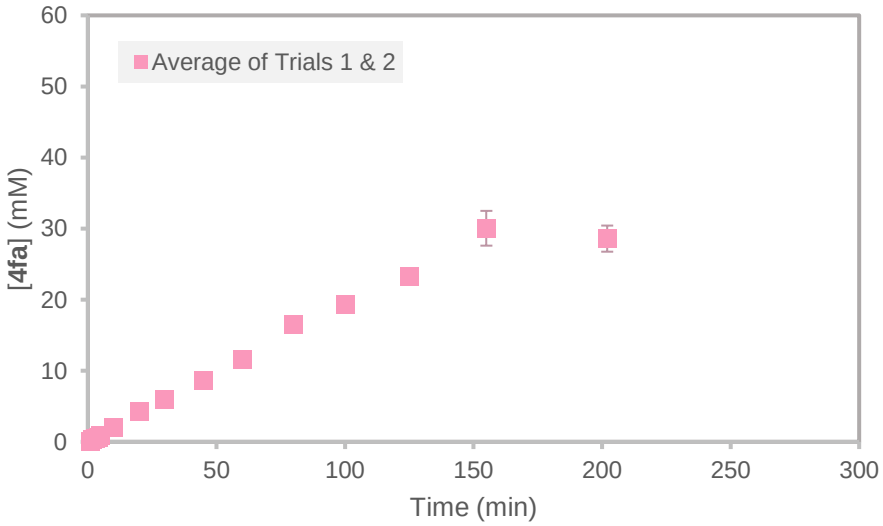

Figure B.55. Full reaction profile for the formation of **4fa** over time.

Table B.21. [**4fa**] (mM) and selectivity (*l*:*b*) of **4fa** formed.

Time (min)	[**4fa**] (mM)	Selectivity (*l*:*b*)
1	0.09 ± 0.01	1:0.5
300		

2	0.33 ± 0.07	1:1.2
3	0.54 ± 0.01	1:1.2
4	0.69 ± 0.01	1:1.5
5	0.90 ± 0.06	1:1.4
10	2.010 ± 0.005	1:1.6
20	4.3 ± 0.2	1:1.6
30	5.9 ± 0.1	1:1.5
45	8.7 ± 0.5	1:1.5
60	11.6 ± 0.4	1:1.4
80	16.5 ± 0.7	1:1.4
100	19.4 ± 0.2	1:1.4
125	23.3 ± 0.1	1:1.5
155	30 ± 2	1:1.6
202	29 ± 2	1:1.7
308	26 ± 2	1:1.7

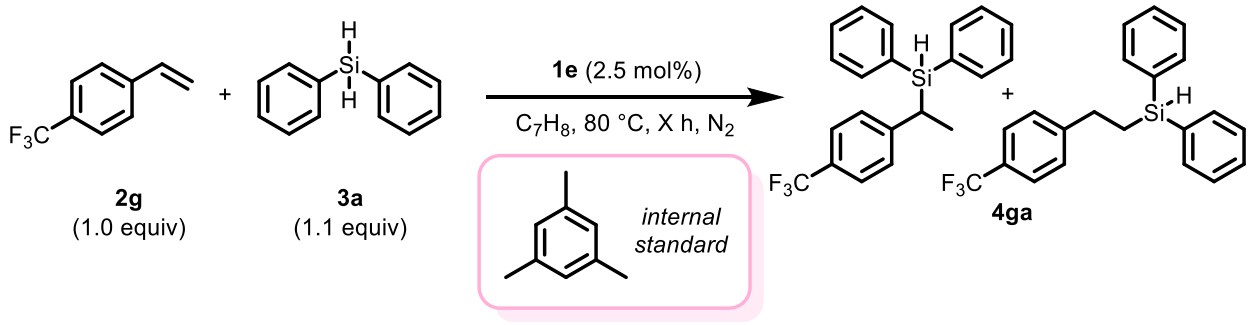

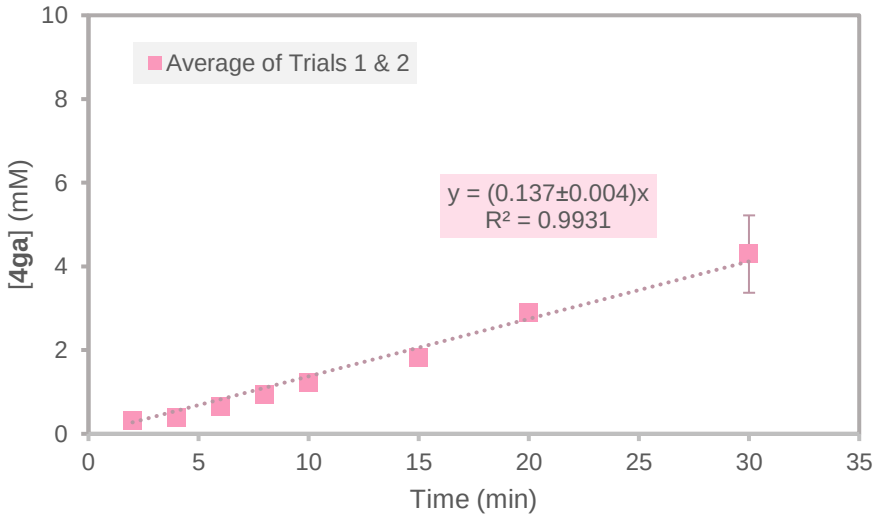

Figure B.56. Initial rate for the formation of **4ga** versus time (min).

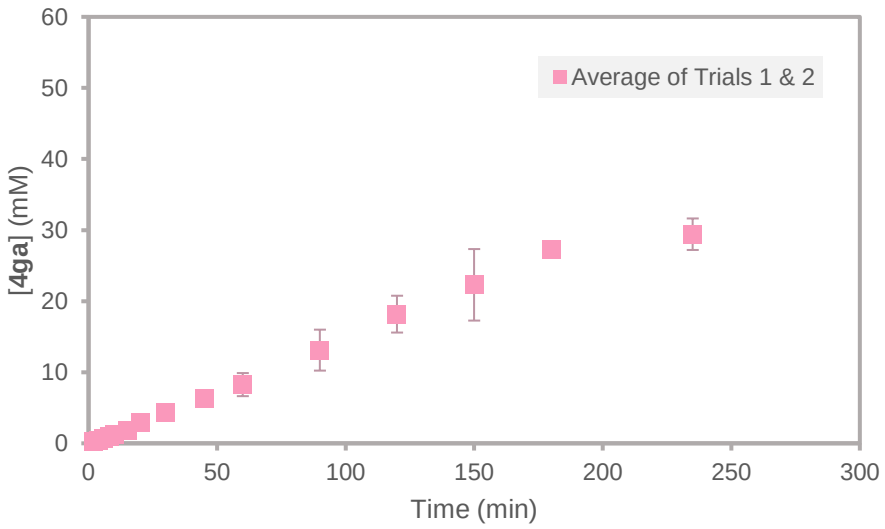

Figure B.57. Full reaction profile for the formation of **4ga** over time.

Table B.22. [**4ga**] (mM) and selectivity (*l*:*b*) of **4ga** formed.

Time (min)	[**4ga**] (mM)	Selectivity (*l*:*b*)
2	0.3 ± 0.2	1:1.0
4	0.3797 ± 0.0004	1:2.4
6	0.65 ± 0.01	1:3.5
8	0.93 ± 0.04	1:3.7
10	1.2 ± 0.1	1:4.0
15	1.8 ± 0.1	1:4.6
20	2.9 ± 0.2	1:4.8
30	4.3 ± 0.9	1:5.4
45	6.3 ± 0.9	1:5.7
60	8 ± 2	1:5.8
90	13 ± 3	1:5.6
120	18 ± 3	1:5.6
150	22 ± 5	1:5.5
180	27.2 ± 0.1	1:5.7
235	29 ± 2	1:6.1
320	33 ± 7	1:6.8

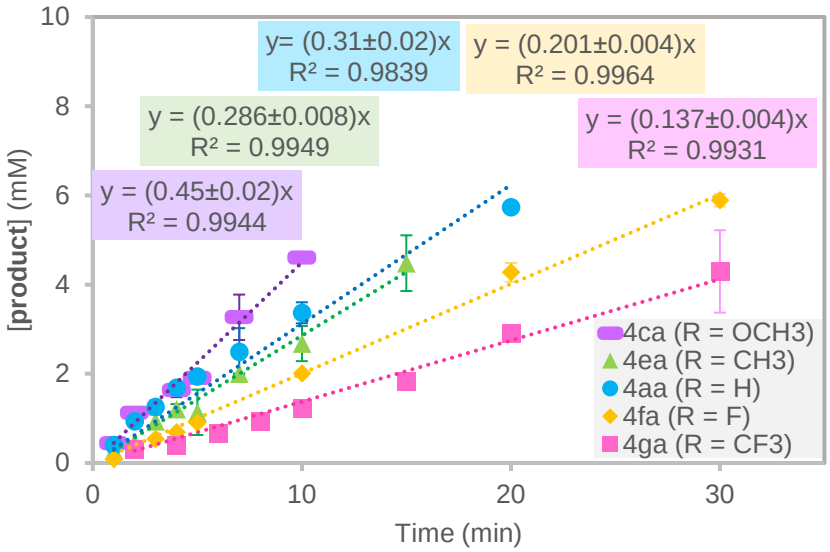

Figure B.58. Initial rate data for the formation of the corresponding [**product**] (mM) versus time (min).

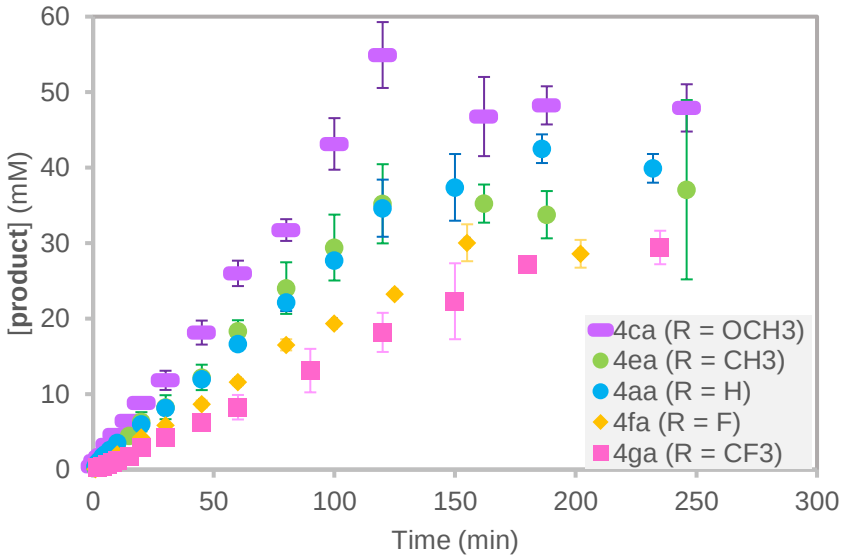

Figure B.59. Full reaction profile for the formation of product over time.

Table B.23. Functional group (**R**), σ value, k_{obs} (mM/min), k_X/k_H, and log(k_X/k_H) using **2a**,**c**-**g**.

R	ρ	k_{obs} (mM/min)	k_X/k_H	log(k_X/k_H)
4-OCH_3 (**2c**)	-0.268	0.45 ± 0.02	1.44 ± 0.04	0.16 ± 0.01
4-CH_3 (**2d**)	-0.17	0.285 ± 0.008	0.92 ± 0.02	-0.0382 ± 0.009
H (**2a**)	0	0.31 ± 0.02	1.00 ± 0.03	0.00 ± 0.01

4-F (**2e**)	0.062	0.208 ± 0.004	0.64 ± 0.01	-0.191 ± 0.009
4-CF_3 (**2f**)	0.54	0.137 ± 0.004	0.441 ± 0.009	-0.356 ± 0.009

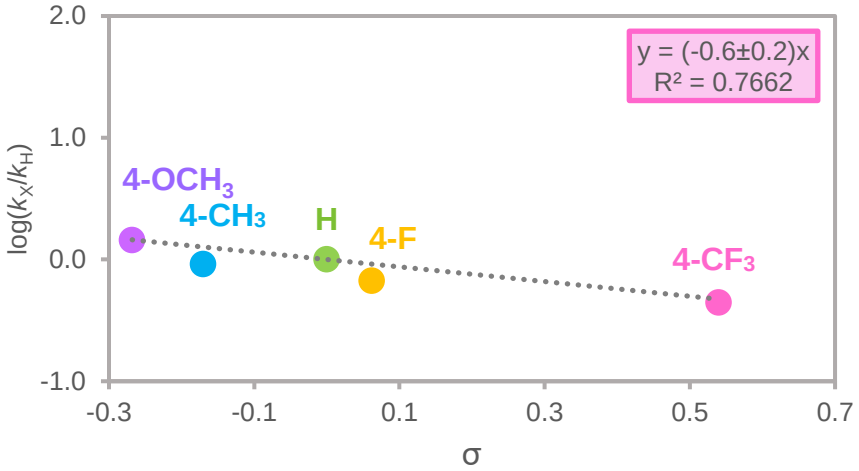

Figure B.60. Hammett Plot $\log(k_X/k_H)$ versus σ of electronically varied styrenes (**2a**,**c**-**g**). Error bars are present but are not visible.

B.1.7. Other Mechanistic Reactions

a. Hydrosilylation in the Presence of 1,1-Diphenylethylene (DPE)

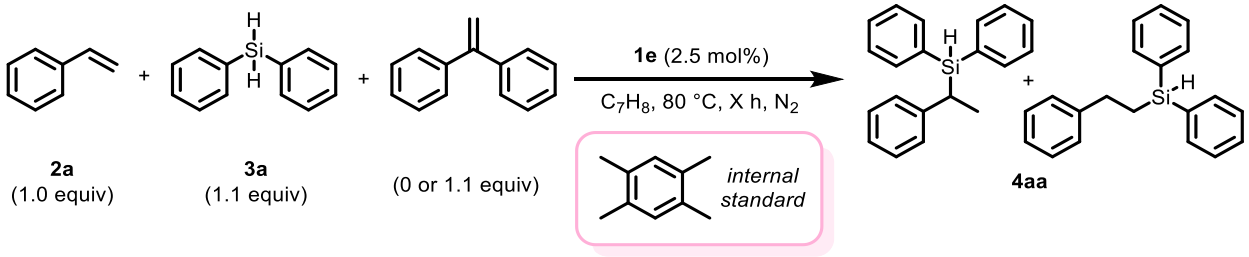

General Procedure: In a nitrogen-filled glovebox, a stock solution was prepared by weighing out **1e** (38 mg, 0.066 mmol, 0.033 M) and toluene (2.0 mL) was added. The stock solution of **1e** (7.6 mg, 0.013 mmol, 0.025 equiv, 0.40 mL of stock solution) was added to a 1-dram scintillation vial equipped with a stir bar using a disposable 1-mL syringe. An additional stock solution was prepared by weighing out durene (54 mg, 0.40 mmol, 0.13 M) and dissolved in toluene (3.0 mL). The stock solution of durene (11 mg, 0.082 mmol, 0.60 mL of stock solution) was added to the 1-dram scintillation vial containing **1e** using a disposable 1-mL syringe. An additional amount of toluene (0.20 mL) and **2a** (30 µL, 0.26 mmol, 1.0 equiv) were added to the vial, which was then sealed with a septum cap, and the vials were brought out of the glovebox. DPE was added via 100-µL syringe to the reactions (0 or 51 µL, 0 or 0.29 mmol, 0 or 1.1 equiv),

followed by **3a** (54 µL, 0.29 mmol, 1.1 equiv), which was added via a 100-µL syringe. The reaction was then placed on an aluminum vial block preheated to 80 °C. Throughout the course of the reaction, 20-µL aliquots were removed with a 25-µL syringe and filtered into a GC vial through Celite and diluted with hexanes. The filtrate was analyzed by GC to assess the reaction progress and selectivity. The product concentration was determined by relative integration (by GC) of the product peaks against mesitylene, in accordance with calibration curves. Two trials were run for both experiments and in parallel.

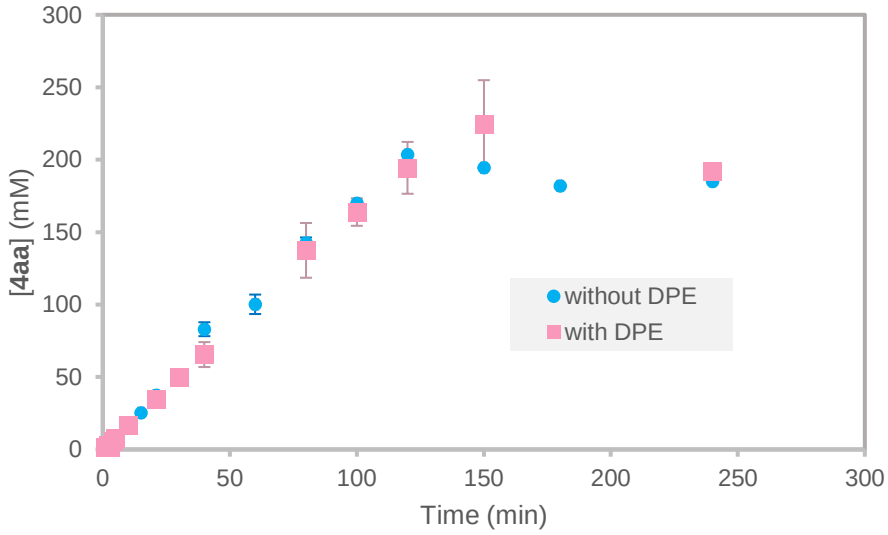

Figure B.61. Full reaction profile for the hydrosilylation of **2a** and **3a** catalyzed by **1e** with **DPE** (pink squares) and without **DPE** (blue circles) for the formation of **4aa** versus time (min).

Table B.24. Concentration of **4aa** (mM) and selectivity (*l*:*b*) over time for the hydrosilylation of **2a** and **3a** catalyzed by **1e** without and with DPE.

Time (min)	Without DPE		With DPE	
	[**4aa**] (mM)	Selectivity (*l*:*b*)	[**4aa**] (mM)	Selectivity (*l*:*b*)
1	0.7 ± 0.6	1:2.3	1.19 ± 0.02	1:2.0
2	2.518 ± 0.007	1:4.3	2.7 ± 0.1	1:4.0
3	4.2 ± 0.3	1:5.4	1 ± 2	1:4.3
4	5.7 ± 0.1	1:7.6	5.8 ± 0.5	1:6.4
5	7.0 ± 0.9	1:8.4	7.6 ± 0.1	1:6.7
10	15 ± 1	1:9.2	16.41 ± 0.05	1:8.0
15	25.3 ± 0.4	1:9.9	--	--
21	37.4 ± 0.7	1:9.1	35 ± 3	1:8.0
30	50 ± 3	1:8.4	49.8 ± 0.4	1:8.6

40	83 ± 5	1:7.6	65 ± 9	1:7.7
60	100 ± 7	1:7.1	--	--
80	143 ± 4	1:6.9	137 ± 19	1:7.2
100	169.97 ± 0.03	1:7.4	164 ± 9	1:7.5
120	203.46 ± 0.04	1:7.9	194 ± 18	1:8.1
150	194.46 ± 0.03	1:8.0	224 ± 30	1:9.2
180	181.956 ± 0.003	1:8.1	--	--
240	185.12 ± 0.04	1:8.9	192 ± 4	1:2.0

b. Reaction of 1e, Diphenylsilane (3a), and a 1,6-diene (2s)

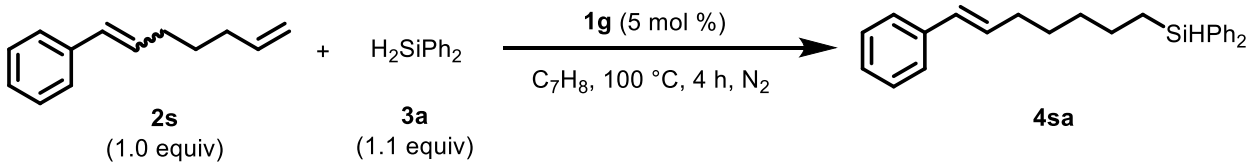

2s (1.0 equiv) **3a** (1.1 equiv) **4sa**

General Procedure: In a nitrogen-filled glovebox, **1e** (25 mg, 0.044 mmol, 0.05 equiv) was directly weighed out into a 4-dram scintillation vial equipped with a stir bar and toluene (4.0 mL, 0.22 M) was added using a disposable 5-mL syringe. The vial was capped with a septum cap, brought out of the glovebox, injected with **2s** (0.16 mL, 0.87 mmol, 1.0 equiv) and **3a** (0.18 mL, 0.96 mmol, 1.1 equiv), and placed in an oil bath pre-heated to 100 °C. After 4 h, the reaction was quenched by freezing it in liquid N_2, and then it was thawed and concentrated to obtain the crude product. The crude reaction was treated with hexanes (5.0 mL), filtered through silica (eluting with 5:95 benzene/hexanes) to remove remaining Ni catalyst, concentrated, and analyzed by ^{1}H NMR. The crude product was purified by column chromatography (gradient 0-5% benzene/hexanes) to isolate and identify each product formed in the reaction. ^{1}H NMR spectra match previously reported values.[6,287]

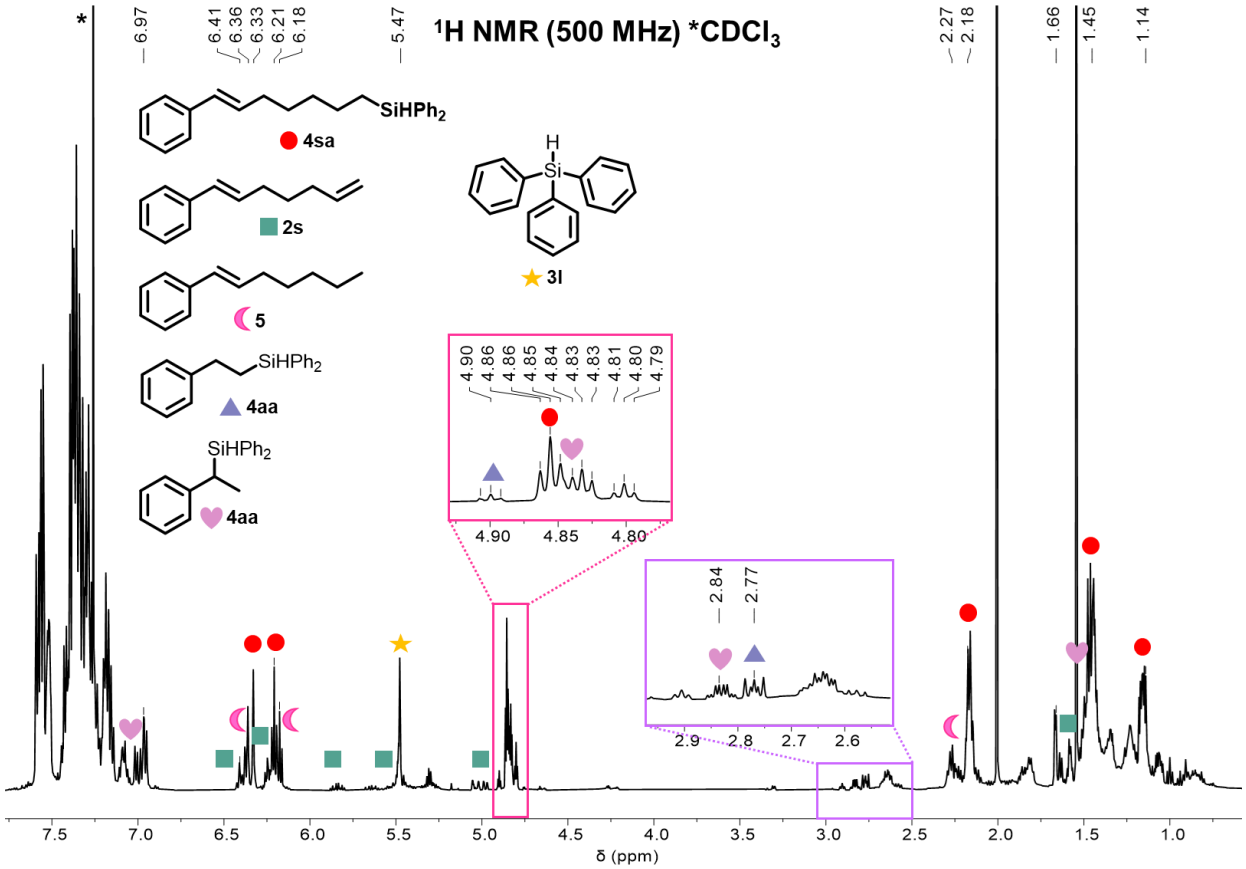

Figure B.62. ^{1}H NMR spectrum for the crude reaction mixture from **1e**-catalyzed hydrosilylation of **2s** and **3a** in $CDCl_3$ at 25 °C.

The major product of the reaction of **2s** and **3a** is the linear hydrosilylation product **4sa**. Unreacted **2s**, partially hydrogenated **2s** (**5**), and hydrosilylated styrene (**4aa**) were also found in the crude reaction mixture. No evidence of radical cyclization products **4sa'**, **6a**, or **7aa** were observed.

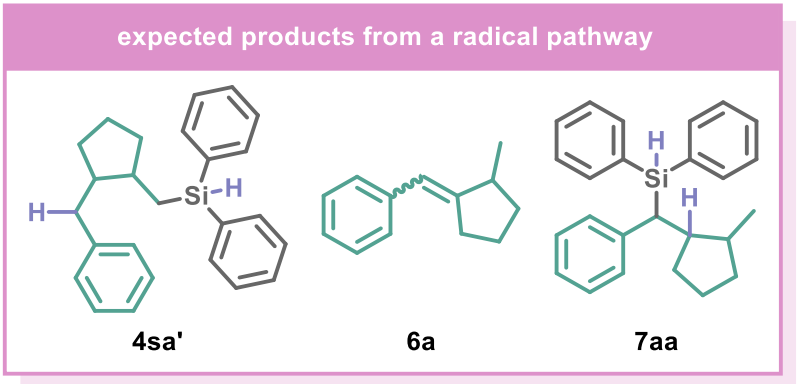

Further confirmation of the absence of the cyclized product (**6a**) in the hydrosilylation of **2s** with **3a** was obtained by independently synthesizing and isolating **6a** via a Wittig reaction according to a literature procedure[6] for comparison. It was difficult to discern the absence of **6a** by ^{1}H NMR due to possible overlapping peaks; therefore, GC analysis of both the crude reaction and independently synthesized **6a** confirmed the absence of **6a** in the crude, **1e**-catalyzed reaction between **2s** and **3a**.

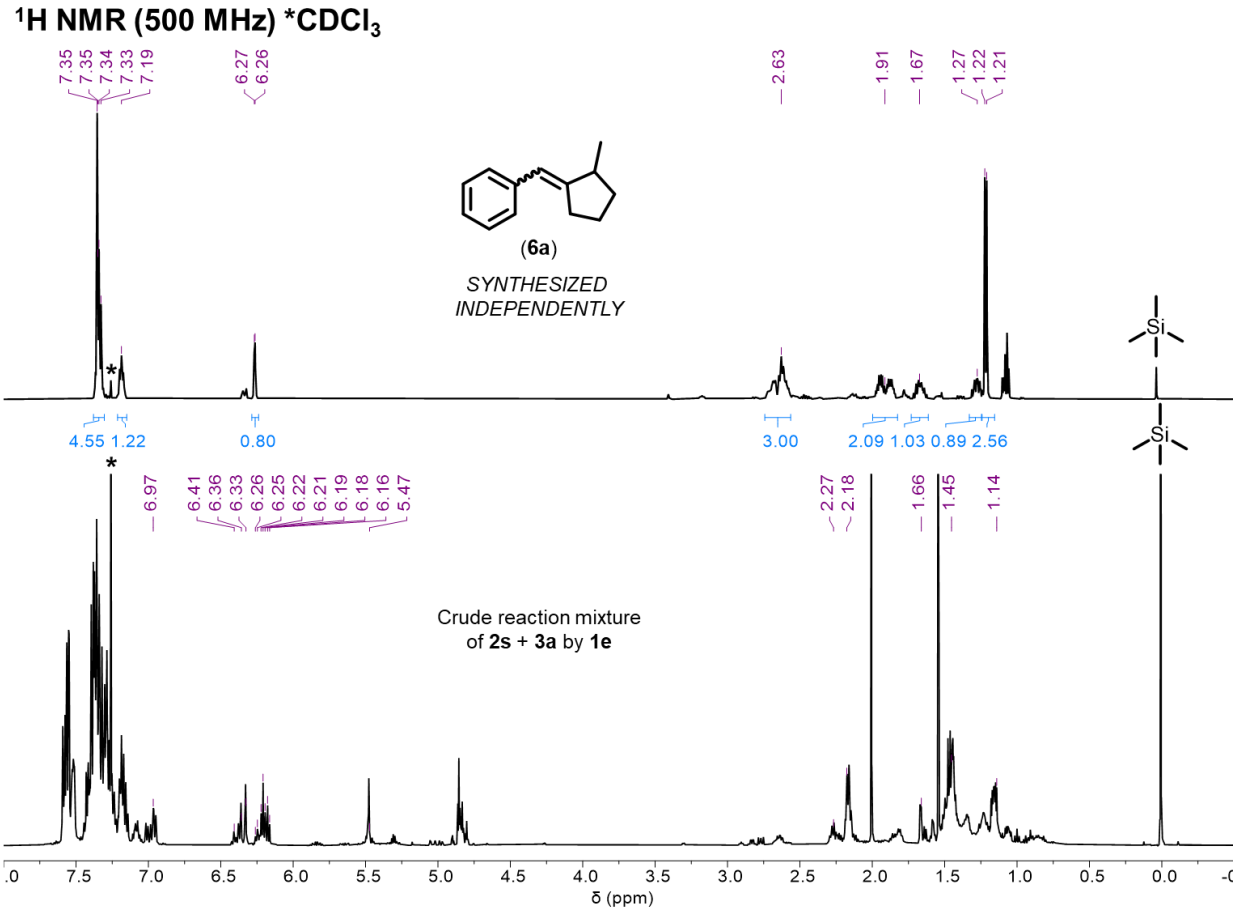

Figure B.63. ^{1}H NMR spectrum for the independently synthesized **6a** (top), and the crude reaction mixture from **1e**-catalyzed hydrosilylation of **2s** and **3a** (bottom) in $CDCl_3$ at 25 °C.

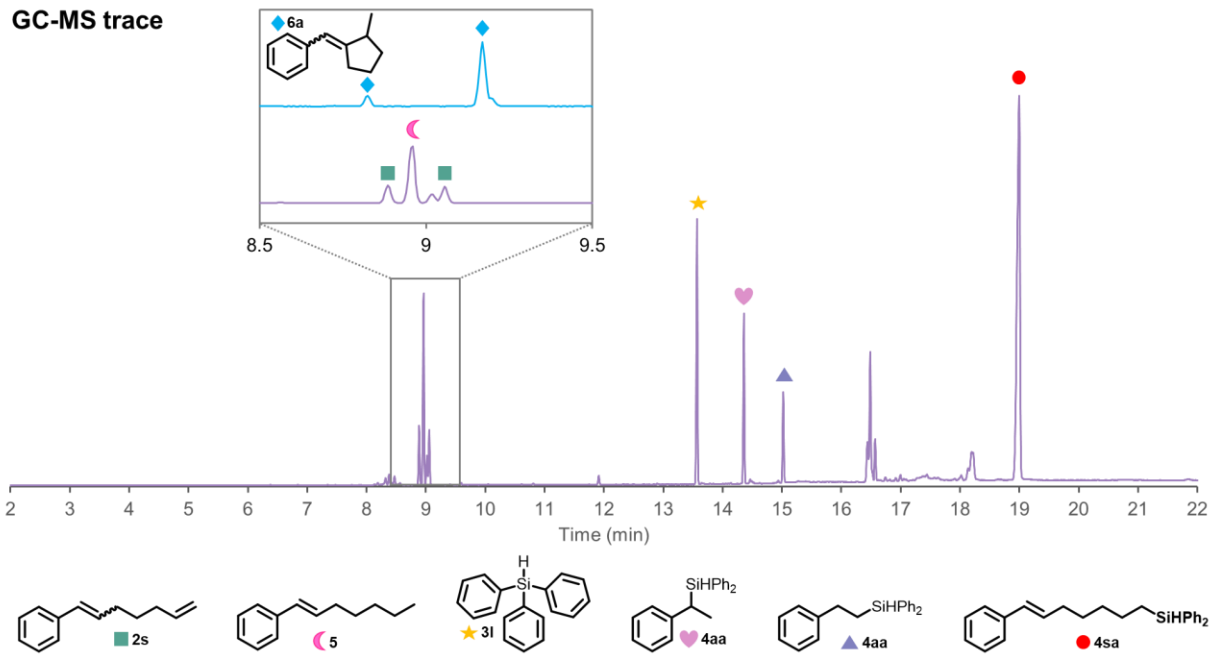

Figure B.64. GC-MS trace of the crude reaction mixture from **1e**-catalyzed hydrosilylation of **2s** and **3a** (purple trace) and of **6a** synthesized independently (blue trace).

c. Hydrosilylation of 3a with cyclized alkene (6a)

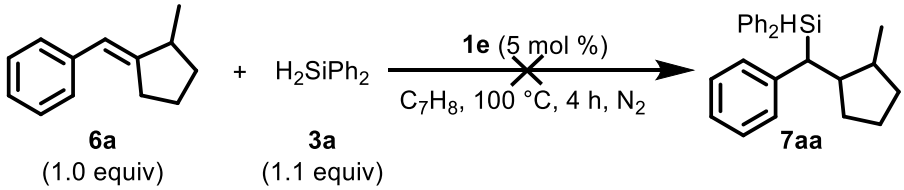

General Procedure: In a nitrogen-filled glovebox, **1e** (14 mg, 0.025 mmol, 0.050 equiv) was directly weighed out into a 1-dram scintillation vial equipped with a stir bar and toluene (2.3 mL, 0.22 M) was added using a disposable 5-mL syringe. The vial was capped with a septum cap, brought out of the glovebox, injected with **6a** (88 µL, 0.50 mmol, 1.0 equiv) and **3a** (100 µL, 0.55 mmol, 1.1 equiv), and placed in a pre-heated aluminum vial block to 100 °C. After 4 h, the reaction was quenched by freezing it in liquid N_2, and then it was thawed and concentrated to obtain the crude product. The crude reaction was treated with hexanes (1.0 mL), filtered through silica (eluting with 5:95 benzene/hexanes) to remove remaining Ni catalyst, concentrated, and analyzed by ^{1}H NMR and GC-MS. No evidence of the hydrosilylated product (**7aa**) of **6a** with **3a** was observed by ^{1}H NMR or GC-MS.

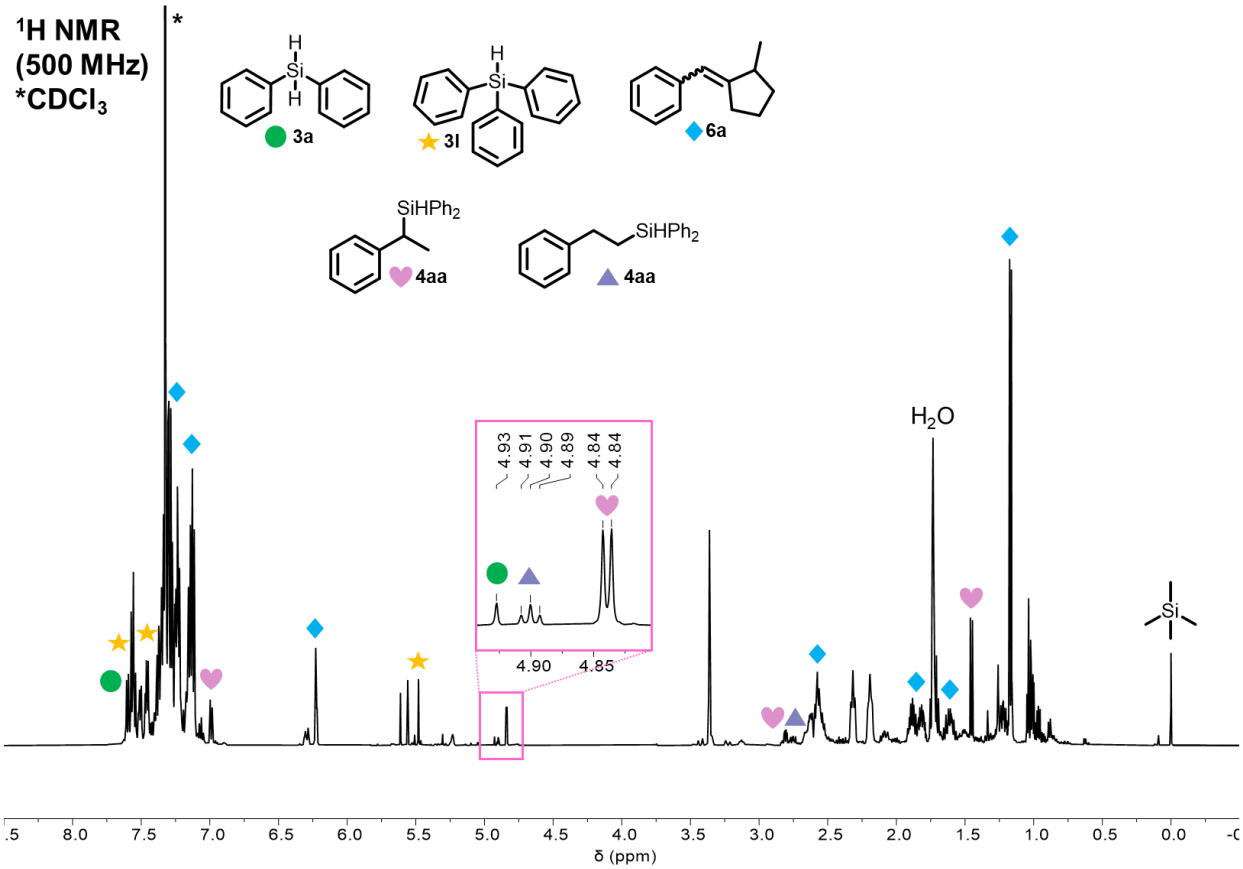

Figure B.65. ^{1}H NMR spectrum for the crude reaction mixture from **1e**-catalyzed hydrosilylation of **6a** and **3a** in $CDCl_3$ at 25 °C.

B.1.13. NMR and IR Spectra

a. Deuterated Diphenylsilane (3a-d_2)

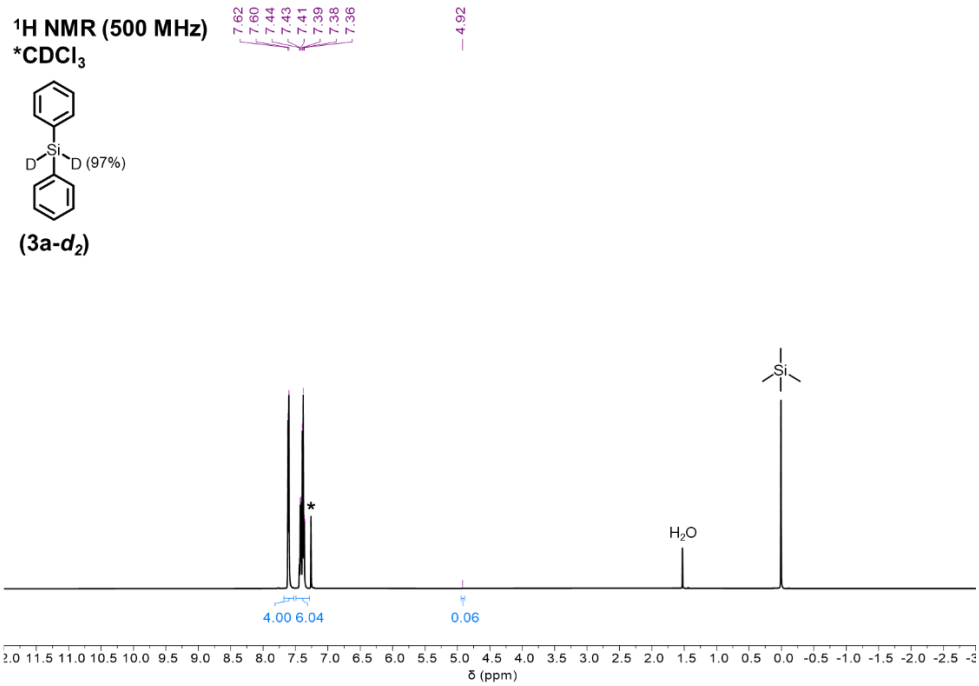

Figure B.66. ^{1}H NMR spectrum of diphenylsilane-d_2 (**3a-*d*$_2$**) recorded in $CDCl_3$ at 298 K.

APPENDIX C

SUPPLEMENTARY CONTENT FOR CHAPTER IV

Experimental Details

C.1.1. Materials and Methods

All syntheses and manipulations were carried out under nitrogen using standard Schlenk (vacuum 10^{-2} mbar) techniques or in a nitrogen-filled glovebox unless otherwise indicated. All reagents and solvents were used after drying and stored under nitrogen, unless otherwise indicated. Tetrahydrofuran (THF; Fisher Chemical; HPLC grade, unstabilized), hexanes (Fisher Chemical; HPLC grade), diethyl ether (B&J Brand; HPLC grade, unstabilized) and acetonitrile (Fisher Chemical; HPLC grade) were dispensed under nitrogen from an LC Technology SP-1 solvent system. Benzene (ACS grade) and pentane (HPLC grade) were refluxed overnight with CaH_2 and distilled under nitrogen before use. The dried solvents were thereafter stored on activated 4Å molecular sieves under nitrogen. CD_3CN, C_6D_6 and $CDCl_3$ were purchased from Cambridge Isotope Laboratories, degassed by freeze-pump-thaw, and thereafter stored on activated 4Å molecular sieves under nitrogen. All stock solutions were prepared by mass and were dispensed into the reaction vessel by difference from syringe, as detailed in the procedure for each experiment.

The following reagents were used from commercial sources without further purification: lithium aluminum deuteride (Aldrich Chemical), styrene-d_8 (**2a-*d*$_8$**; Fisher Scientific), 4-methoxystyrene (**2c**; Alfa Aesar), 4-methylstyrene (**2e**; TCI), 4-fluorostyrene (**2f**; Matrix), 2-methylstyrene (**2h**; TCI), durene (Eastman Chemical Company), and 1,3,5-trimethoxybenzene (TCI).

1l, **1m**, **1n** were synthesized via reported procedures.[126]

C.1.2. General Experimental

Nuclear magnetic resonance (NMR) spectra were collected at room temperature (298 K) unless otherwise stated on a Bruker AV-III HD 600 NMR (600.13 MHz for ^{1}H; 150.90 MHz for 13C; 564.69 MHz for ^{19}F; 119.23 MHz for ^{29}Si; 92.12 MHz for ^{2}H), Bruker Avance-III HD 500 NMR (499.90 MHz for ^{1}H; 126 MHz for ^{13}C; 471 MHz for ^{19}F; 99 MHz for ^{29}Si), or Varian Inova

500 NMR (499.90 MHz for ^{1}H; 126 MHz for ^{13}C; 471 MHz for ^{19}F; 99 MHz for ^{29}Si). ^{1}H and ^{13}C spectra were referenced to the residual solvent peak ($CDCl_3$: ^{1}H δ = 7.26 ppm, ^{13}C δ = 77.16 ppm; C_6D_6: ^{1}H δ = 7.16 ppm, ^{13}C δ = 128.06 ppm, CD_3CN: ^{1}H δ = 1.94 ppm, ^{13}C δ = 1.32 ppm ($NCCD_3$)). Chemical shifts for ^{1}H, ^{13}C, and ^{29}Si NMR spectra are reported in parts per million (ppm, δ) relative to tetramethylsilane at 0.00 ppm. Peaks are characterized as follows: s (singlet), d (doublet), t (triplet), q (quartet), pent (pentet), hept (heptet), m (multiplet), qd (quartet of doublets), br (broad), app (apparent), and/or ms (multiple signals). Coupling constants, *J*, are reported in Hz. $^{1}J_{H-Si}$ coupling constants were determined, when possible, using the ^{29}Si satellites in the ^{1}H NMR spectrum.

Infrared (IR) spectroscopy for air-stable organic compounds was performed on an Agilent Nicolet 6700 FT-IR using the ATR sampling technique. IR spectra for air-sensitive nickel complexes were recorded as self-supported pellets diluted with KBr using a Bruker Alpha II FT-IR spectrometer that is housed in a nitrogen-filled glovebox. All bands are reported in wavenumbers (cm^{-1}) and are described as broad (br), strong (s), medium (m), and weak (w).

C.1.3. Synthesis of Nickel Complexes

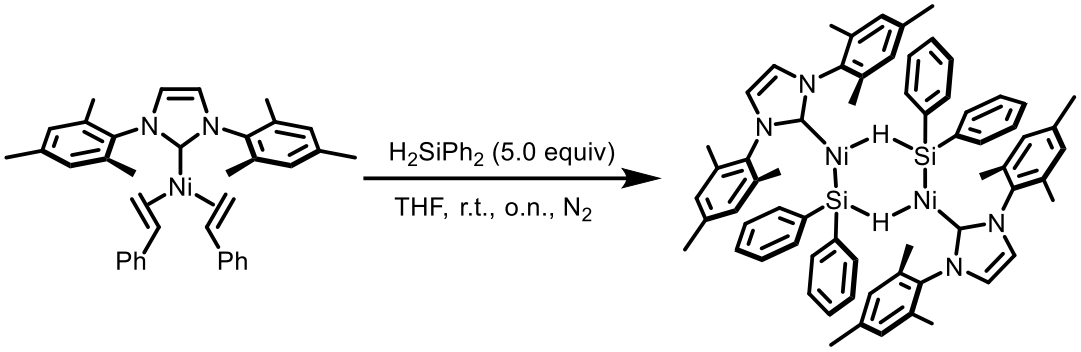

(IMes)Ni(μ-H–SiPh$_2$)$_2$Ni(IMes) (1g). To a 10-mL round bottom flask equipped with a magnetic stir bar was added **1e** (0.10 g, 0.18 mmol, 1.0 equiv) and H_2SiPh_2 (0.16 mL, 0.88 mmol, 5.0 equiv) in THF (5.0 mL). The reaction was stirred at room temperature overnight and then concentrated under reduced pressure to give a dark red solid. The product was purified by solvating the solid in minimal amounts of THF (2.0 mL) and precipitation with hexanes (5.0 mL). The product was collected by vacuum filtration to yield **1g** as an orange powder (0.064 g, 0.059 mmol, 67% yield). A single crystal for analysis was grown via hexanes/THF slow vapor diffusion (see section 12 below).

^{1}H NMR (500 MHz, C_6D_6, 298 K): 7.32 (d, *J* = 7.4 Hz, 12H), 7.19 (t, *J* = 7.4 Hz, 8H), 6.57 (s, 8H), 6.05 (s, 4H), 2.27 (s, 12H), 1.62 (s, 24H), -2.22 (s, 2H).

^{13}C{^{1}H} NMR (126 MHz, C_6D_6, 298 K): δ 195.9, 146.0, 137.0, 136.9, 136.9, 136.0, 129.3, 126.9, 126.4, 121.8, 21.3, 17.8.

^{29}Si NMR (119 MHz, C_6D_6, 298 K): δ 107.76 (s).

IR (ATR, neat) ν: 3133-2848 (w), 1588 (w), 1490 (w), 1220 (w), 688 (s).

ASAP/HRMS (m/z): [M^+] calculated for $C_{66}H_{70}N_4Ni_2Si_2$ 1090.3846, found 1090.3821.

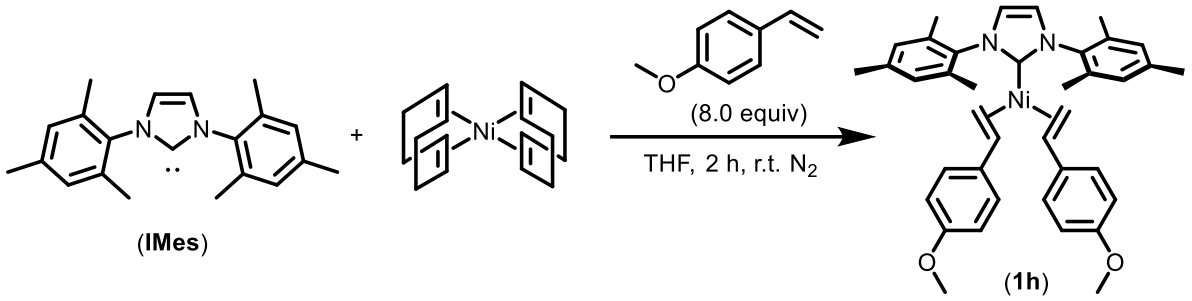

(4-methoxystyrene)$_2$Ni(IMes) (1h) To a 2-dram scintillation vial equipped with a magnetic stir bar was added Ni(cod)$_2$ (0.073 g, 0.26 mmol, 1.0 equiv), 4-methoxystyrene (0.28 mL, 2.1 mmol, 8.0 equiv), and THF (4.0 mL). This red solution was stirred for 15 min at room temperature. In a 2-dram scintillation vial was added **IMes** (0.080 g, 0.26 mmol, 1.0 equiv) and THF (4.0 mL). This solution was added dropwise to the Ni(cod)$_2$ and 4-methoxystyrene mixture to afford a red solution. This reaction was stirred for 2 h and then was concentrated under reduced pressure to give an orange solid. The crude product was dissolved in minimal amounts of THF (3.0 mL) and filtered through Celite. The filtrate was concentrated under reduced pressure, solvated in minimal THF (3.0 mL), and then hexanes (10 mL) was added to precipitate **1h** out of solution. The product was collected via vacuum filtration and dried under reduced pressure to yield **1h** as a yellow powder (0.069 g, 0.11 mmol, 42% yield).

^{1}H NMR (500 MHz, C_6D_6, 298 K): δ 6.80 (s, 2H), 6.75 (s, 2H), 6.68 (d, *J* = 8.4 Hz, 4H), 6.45 (d, *J* = 8.4 Hz, 4H), 6.28 (s, 2H), 3.43 (s, 6H), 3.37 (dd, *J* = 12.4, 9.6 Hz, 2H), 2.74-2.70 (ms, 4H), 2.20 (s, 6H), 2.11 (s, 6H), 2.02 (s, 6H).

^{13}C{^{1}H} NMR (126 MHz, C_6D_6, 298 K): δ 203.4, 156.8, 140.0, 138.5, 137.9, 136.3, 135.6, 129.6, 129.5, 125.1, 122.7, 113.6, 72.7, 54.8, 48.3, 21.1, 18.5, 18.3 .

IR (FT, KBr pellet) ν: 3163-2833 (w), 1508 (s), 1305 (s), 1039 (s), 831 (s).

ASAP/HRMS (m/z): [M^+] calculated for $C_{39}H_{44}N_2NiO_2$ 630.2756, found 630.2762.

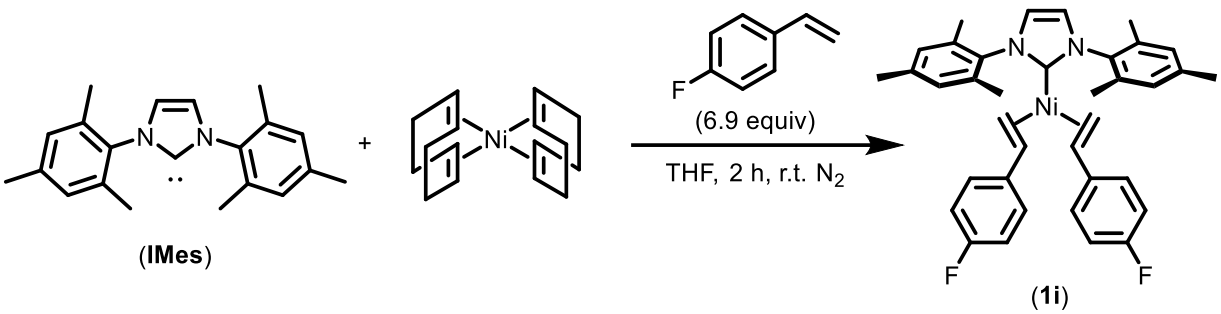

(4-fluorostyrene)$_2$Ni(IMes) (1i) To a 4-dram scintillation vial equipped with a magnetic stir bar was added Ni(cod)$_2$ (0.10 g, 0.36 mmol, 1.0 equiv), 4-fluorostyrene (0.30 mL, 2.7 mmol, 6.9 equiv), and THF (5.0 mL). This red solution was stirred for 30 s at room temperature. In a 2-dram scintillation vial was added **IMes** (0.11 g, 0.36 mmol, 1.0 equiv) and THF (5.0 mL). This solution was immediately added dropwise to the Ni(cod)$_2$ and 4-fluorostyrene mixture to afford a red solution. This reaction was stirred for 2 h and then was concentrated under reduced pressure to give an orange solid. The crude product was dissolved in a minimal amount of THF (3.0 mL) and filtered through Celite. The filtrate was concentrated under reduced pressure. The crude solid was solvated in minimal THF (1.0 mL), hexanes (3.0 mL) was added, and the reaction was placed in the freezer at -30 °C to crystallize overnight. The product was collected by decanting the liquid away from the solid, which was then dried under vacuum to yield **1i** as orange crystals (0.053 g, 0.087 mmol, 24% yield).

^{1}H NMR (500 MHz, C_6D_6, 298 K): δ 6.73-6.70 (ms, 8H), 6.27 (s, 2H), 6.22 (dd, *J* = 8.66 Hz, 5.68 Hz, 4H), 3.10 (dd, *J* = 12.5 Hz, 9.5 Hz, 2H), 2.67 (dd, *J* = 9.5 Hz, 2.2 Hz, 2H), 2.64 (dd, *J* = 12.5 Hz, 2.2 Hz, 2H) 2.12 (s, 6H), 2.06 (s, 6H), 1.96 (s, 6H)

^{13}C{^{1}H} NMR (126 MHz, C_6D_6, 298 K): δ 202.0, 161.5 (d, *J* = 240 Hz), 143.2 (d, *J* = 2.8 Hz), 138.7, 137.7, 136.2, 135.6, 129.5, 125.2 (d, *J* = 7.2 Hz), 122.9, 114.5 (d, *J* = 20.7 Hz), 71.5, 49.0, 21.0, 18.4, 18.2.

^{19}F NMR (471 MHz, C_6D_6, 298 K): δ -121.17 (m).

IR (FT, KBr pellet) ν: 3140-2857 (w), 1505 (s), 1321 (s), 831 (s), 694 (s).

ASAP/HRMS (m/z): [M^+] calculated for $C_{37}H_{38}F_2N_2Ni$ 606.2357, found 606.2361.

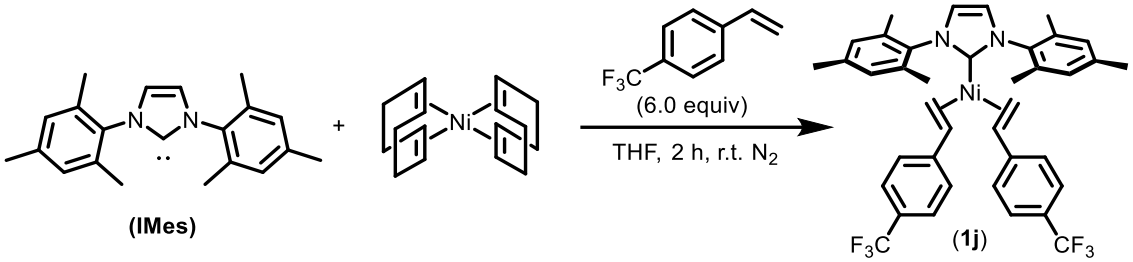

[4-(trifluoromethyl)styrene]$_2$Ni(IMes) (1j) To a 4-dram scintillation vial equipped with a magnetic stir bar was added Ni(cod)$_2$ (0.12 g, 0.45 mmol, 1.0 equiv), 4-(trifluoromethyl)styrene (0.40 mL, 2.7 mmol, 6.0 equiv), and THF (5.0 mL) to afford a red solution. A solution of **IMes** (0.14 g, 0.45 mmol, 1.0 equiv) and THF (5.0 mL) was immediately added to the Ni(cod)$_2$ and 4-(trifluoromethyl)styrene mixture to afford a red solution. This reaction was stirred for 2 h and then was concentrated under reduced pressure to give an orange solid. The crude product was dissolved in a minimal amount of THF (3.0 mL) and filtered through Celite. The filtrate was concentrated under reduced pressure. The crude solid was solvated in minimal THF (1.0 mL), hexanes (3.0 mL) was added, and the reaction was placed in the freezer at -30 °C to crystallize overnight. The product was collected by decanting the liquid away from the solid, which was dried under reduced pressure to yield **1j** as vibrant, orange crystals (0.12 g, 0.17 mmol, 37% yield).

^{1}H NMR (600 MHz, C_6D_6, 298 K): δ 7.27 (d, *J* = 8.1 Hz, 4H), 6.71 (s, 2H), 6.67 (s, 2H), 6.24 (d, *J* = 8.1 Hz, 4H), 6.22 (s, 2H), 2.98 (dd, *J* = 12.5, 9.4 Hz, 2H), 2.70 (dd, *J* = 9.4, 2.4 Hz, 2H), 2.68 (dd, *J* = 12.5, 2.4 Hz, 2H), 2.15 (s, 6H), 2.00 (s, 6H), 1.89 (s, 6H).

^{13}C{^{1}H} NMR (151 MHz, C_6D_6, 298 K): δ 200.2, 151.0, 139.0, 137.4, 136.0, 135.5, 129.6, 128.3, 126.0 (q, *J* = 271.0 Hz), 125.1 (q, *J* = 31.8 Hz), 124.8 (q, *J* = 3.8 Hz), 124.0, 123.2, 71.1, 50.3, 20.9, 18.3, 18.1.

^{19}F NMR (471 MHz, C_6D_6, 298 K): δ -61.38 (s).

IR (FT, KBr pellet) ν: 3142-2860 (w), 1608 (s), 1321 (s), 840 (s), 693 (s).
ASAP/HRMS (m/z): [M^+] calculated for $C_{39}H_{38}F_6N_2Ni$ 706.2293, found 706.2287.

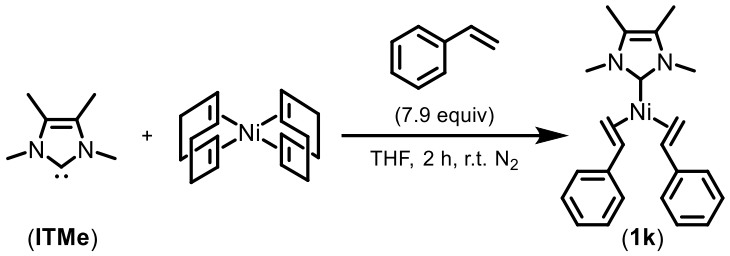

(styrene)$_2$Ni(ITMe) (1k) To a 100-mL round bottom flask equipped with a magnetic stir bar was added Ni(cod)$_2$ (1.2 g, 4.3 mmol, 1.0 equiv), styrene (3.9 mL, 34 mmol, 7.9 equiv), and THF (40 mL). This red solution was stirred for 15 min at room temperature. In a 4-dram scintillation vial was added **ITMe** (0.54 g, 4.3 mmol, 1.0 equiv) and THF (10 mL). This solution was added dropwise to the Ni(cod)$_2$ and styrene mixture to afford a red solution. This reaction was stirred for 2 h and then was concentrated under reduced pressure. The crude product was dissolved in a minimal amount of THF (5.0 mL) and filtered through Celite. The filtrate was concentrated under reduced pressure to give a dark orange solid. The crude solid was solvated in minimal THF (3.0 mL), hexanes (10 mL) was added, and the reaction was placed in the freezer at -30 °C to crystallize overnight. The product was collected by decanting the liquid away from the solid, which was then dried under vacuum to yield **1k** as orange crystals (0.70 g, 1.8 mmol, 42% yield). Two rotamers were isolated as **1k**, the major rotamer is labelled as **A** and the minor rotamer is labelled as **B**.

^{1}H NMR (600 MHz, C_6D_6, 298 K): δ 7.02 (t, *J* = 7.4 Hz, 11H, **A** and **B**), 6.96-6.87 (ms, 18H, **A** and **B**), 4.21 (m, 6H, **A** and **B**), 3.37 (dd, *J* = 12.8, 2.9 Hz, 3H, **B**), 3.11 (dd, *J* = 12.5, 2.6 Hz, 4H, **A**), 3.03 (dd, J = 9.0, 2.4 Hz, 4H, **A**), 2.98 (s, 3H, **B**), 2.73 (dd, J = 9.2, 2.9 Hz, 3H, **B**), 2.51 (s, 12H, **A**), 1.92 (s, 3H, **B**), 1.46 (s, 3H, **B**), 1.41 (s, 12H, **A**), 1.36 (s, 3H, **B**)

^{13}C{^{1}H} NMR (151 MHz, C_6D_6, 298 K): δ 197.5, 197.4, 147.1, 146.9, 125.21, 125.15, 125.0, 124.3, 123.8, 122.93, 122.89, 64.6, 64.2, 46.0, 45.6, 34.1, 33.2, 31.8, 8.7, 8.65, 8.55

C.1.4. Monitoring Hydrosilylation by ^{1}H NMR

a. Hydrosilylation of Styrene (2a) and Diphenylsilane (3a)

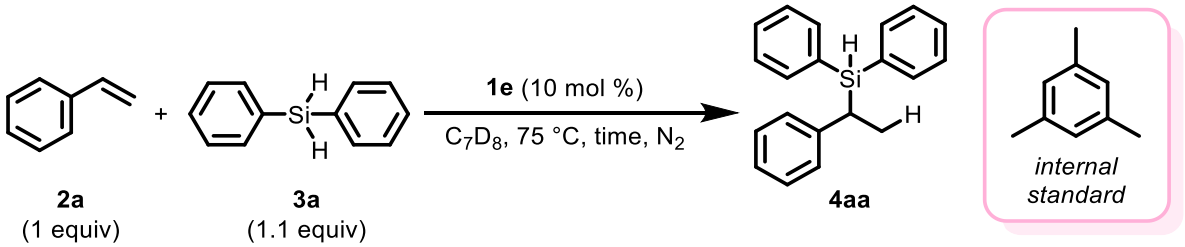

In a nitrogen-filled glovebox, **1e** (7.5 mg, 0.013 mmol, 0.10 equiv) was added to a J-Young NMR tube and solvated in C_7D_8 (0.60 mL, 0.22 M), which was added using a disposable 1-mL syringe. To this solution was added **2a** (17 µL, 0.14 mmol, 1.0 equiv) and **3a** (27 µL, 0.15 mmol, 1.1 equiv) using a 50-µL syringe and mesitylene (3.5 µL, 0.025 mmol) using a 10-µL syringe. The NMR tube was sealed, brought out of the glovebox, and placed into the NMR (Bruker AV-III HD 600), which had been preheated to 75 °C. Reaction progress was monitored by ^{1}H NMR over time. Quantitative analysis of the formation of **4aa** was determined by relative integrations between **4aa** (the doublet at 1.45 ppm, 3H) to the integration of the internal standard, mesitylene (singlet at 6.70 ppm, 3H).

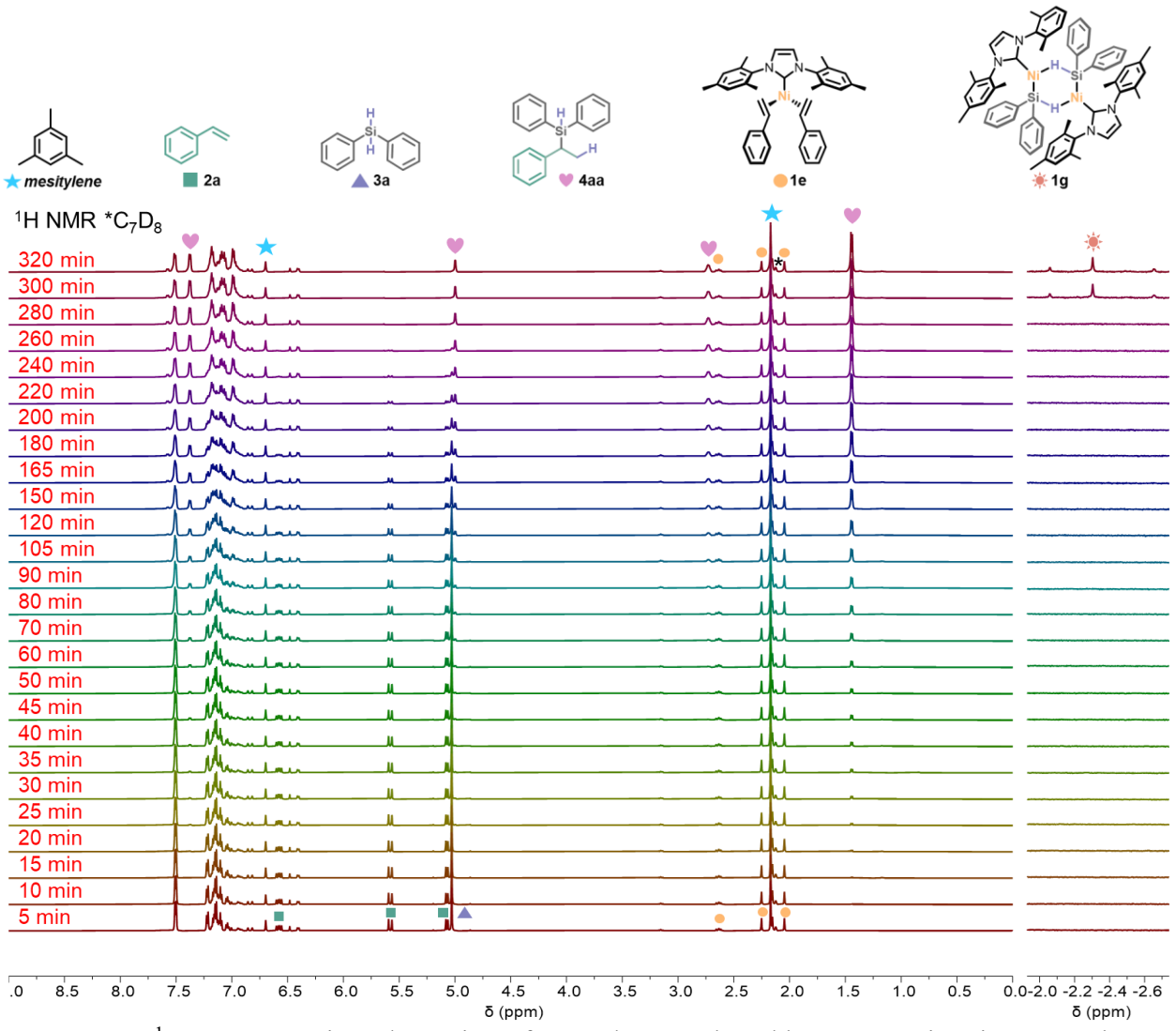

Figure C.1. ^{1}H NMR-monitored reaction of **2a** and **3a** catalyzed by **1e** over time in C_7D_8 taken at 75° C.

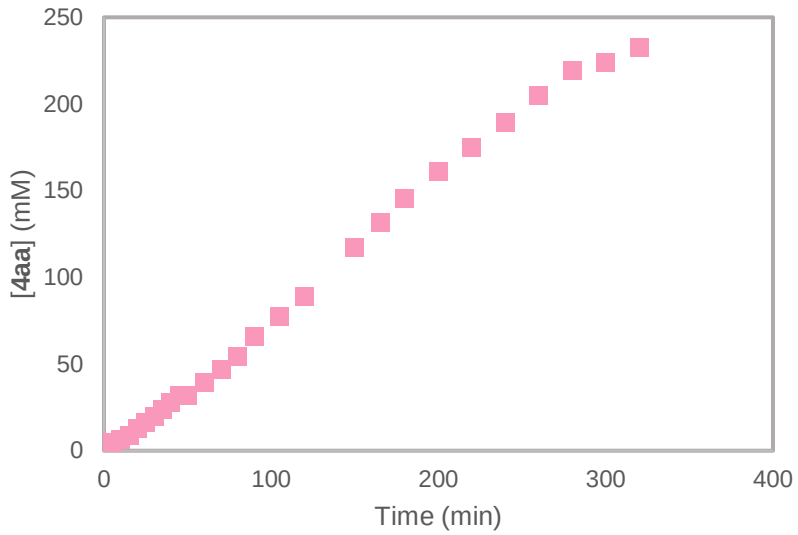

Figure C.2. Kinetic profile of [**4aa**] (mM) versus time (min).

Table C.1. Integrations of mesitylene and **4aa** and the calculated [**4aa**] (mM) over time.

Time (min)	∫mesitylene (6.70 ppm, 3H)	∫**4aa** (1.45 ppm, 3H)	[**4aa**] (mM)
5	1269.87	140.26	4.63
10	1175.73	174.36	6.22
15	1240.35	259.87	8.79
20	1240.26	373.87	12.64
25	1245.43	489.30	16.47
30	1270.37	605.01	19.97
35	1291.56	734.96	23.86
40	1339.31	887.73	27.79
45	1371.20	1033.00	31.59
50	1371.20	1033.00	31.59
60	1444.96	1359.04	39.44
70	1508.46	1688.50	46.94
80	1559.58	2025.13	54.45
90	1613.14	2540.56	66.04
105	1675.27	3093.50	77.43
120	1711.59	3624.94	88.81
150	1777.13	4970.51	117.29
165	1793.33	5637.69	131.83
180	1835.30	6373.91	145.63
200	1831.09	7033.36	161.07
220	1848.63	7718.53	175.08

240	1853.14	8371.87	189.44
260	1844.10	9002.50	204.71
280	1859.25	9717.16	219.16
300	1907.43	10173.60	223.66
320	1827.85	10149.70	232.85

b. Hydrosilylation of 4-Methoxystyrene (2c) and Diphenylsilane (3a)

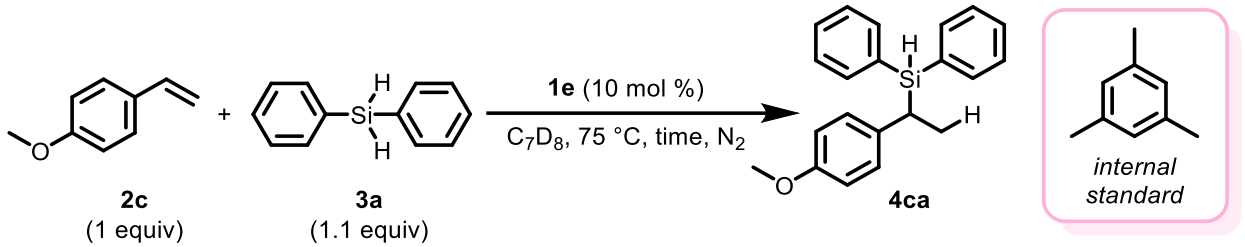

In a nitrogen-filled glovebox, **1e** (7.5 mg, 0.013 mmol, 0.10 equiv) was added to a J-Young NMR tube and solvated in C_7D_8 (0.60 mL, 0.22 M), which was added using a disposable 1-mL syringe. To this solution was added **2c** (18 µL, 0.13 mmol, 1.0 equiv) and **3a** (27 µL, 0.14 mmol, 11 equiv) using a 50-µL syringe and mesitylene (3.5 µL, 0.025 mmol) using a 10-µL syringe. The NMR tube was sealed, brought out of the glovebox, and placed into the NMR (Bruker AV-III HD 600), which had been preheated to 75 °C. Reaction progress was monitored by ^{1}H NMR over time. Quantitative analysis of the formation of **4ca** was not possible due to overlap of the product peaks with the hydrosilylated styrene (**4aa**), which formed from the pre-coordinated styrene on **1e** reacting with **3a**.

Peaks corresponding to (IMes)Ni(styrene)(4-methoxystyrene) (**1e/h**) were identified by reacting **1e** (1 equiv) with **2c** (1 equiv). See section B.1.7. for more information.

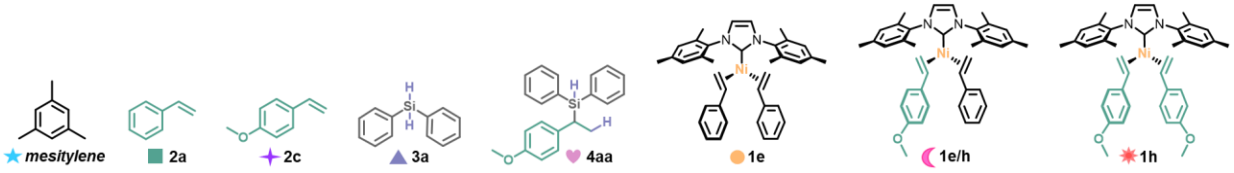

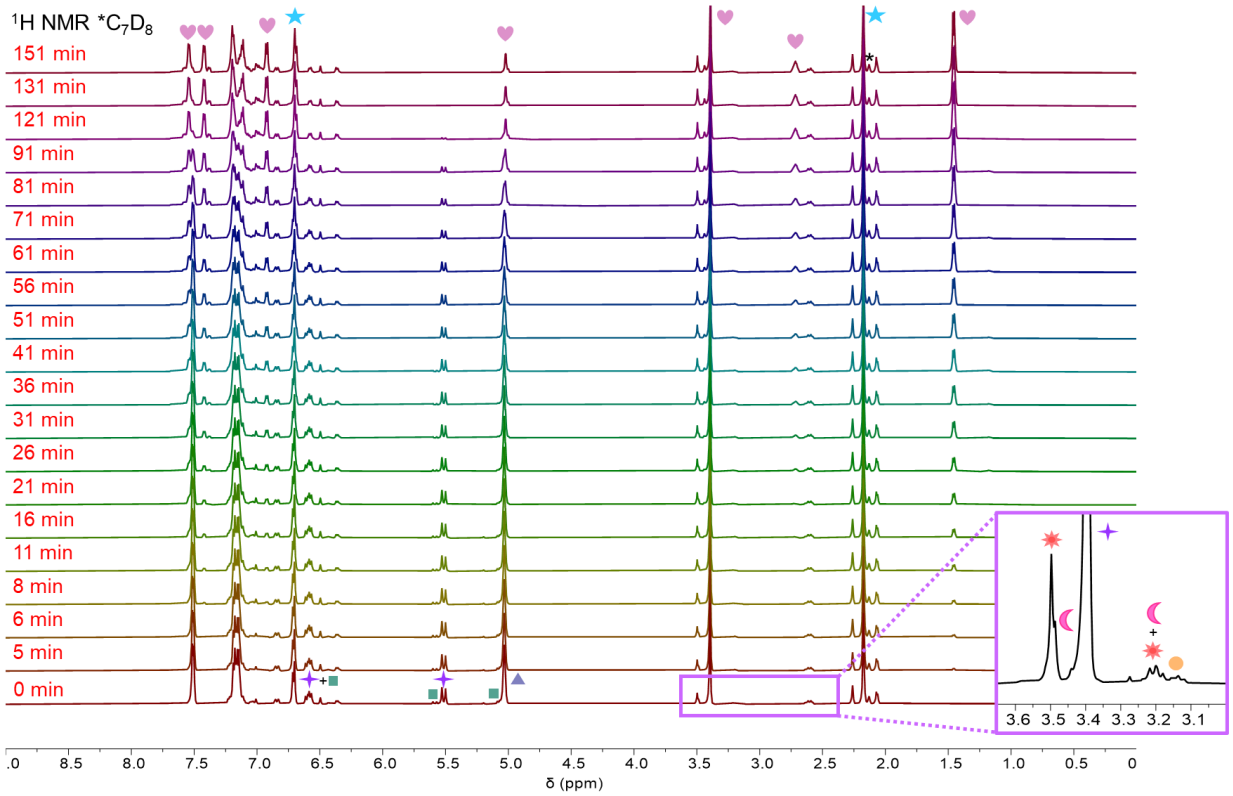

Figure C.3. ^{1}H NMR monitored reaction of **2c** and **3a** catalyzed by **1e** over time in C_7D_8 taken at 75 °C.

C.1.5. Styrene Ligand Exchange and Equilibrium Experiments

a. Reaction of 1e with Styrene Derivatives

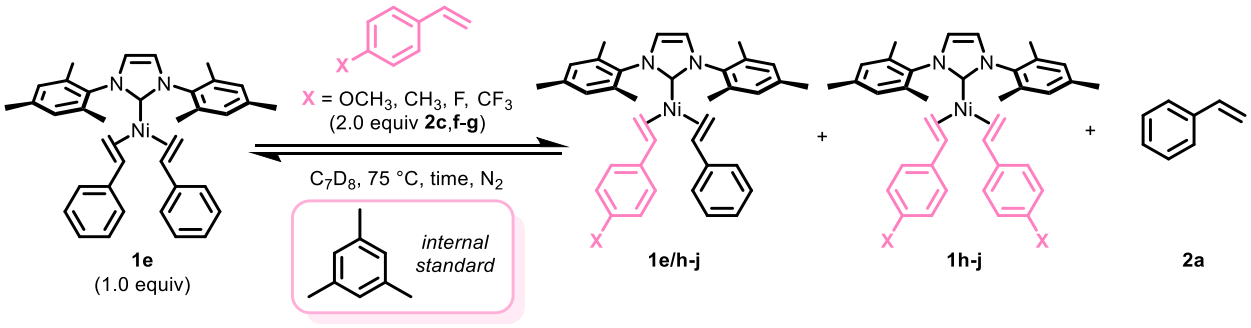

In a nitrogen-filled glovebox, **1e** (see Table 4) was weighed out directly into a J-Young NMR tube and solvated in C_7D_8 (0.60 mL, 0.22 M) using a disposable 1-mL syringe. To this solution was added the corresponding styrene derivative and mesitylene (3.0 µL, 0.022 mmol) using a 25-µL syringe. The NMR tube was sealed, removed from the glovebox, and placed in a pre-heated oil bath at 75 °C for 4 h. The reaction was removed from the heat and cooled to room temperature. The resulting reaction mixture was analyzed by ^{1}H and ^{19}F NMR. Quantitative

analysis by ^{1}H NMR was determined by the relative integrations of the newly formed products, starting materials, and the internal standard, mesitylene.

Peaks corresponding to (IMes)Ni(styrene)(4-X-styrene) (**1e/h**, **1e/i**, and **1e/j**) complexes were found by reacting **1e** (1.0 equiv) with **1h-j** (1.0 equiv) in a comproportionation reaction. See section 8b for more information.

Table C.2. Amount of **1e** and styrene derivatives (**2c**,**f**,**g**) added to the reaction.

Experiment #	Reagent	Equiv	mmol	Amount added
1	**1e**	1.0	0.013	7.5 mg
	4-OCH_3-styrene (**2c**)	2.0	0.026	3.50 µL
2	**1e**	1.0	0.015	7.5 mg
	4-F-styrene (**2f**)	1.8	0.027	3.25 µL
3	**1e**	1.0	0.013	7.5 mg
	4-CF_3-styrene (**2g**)	2.1	0.027	4.0 µL

Ligand Exchange Experiment #1:

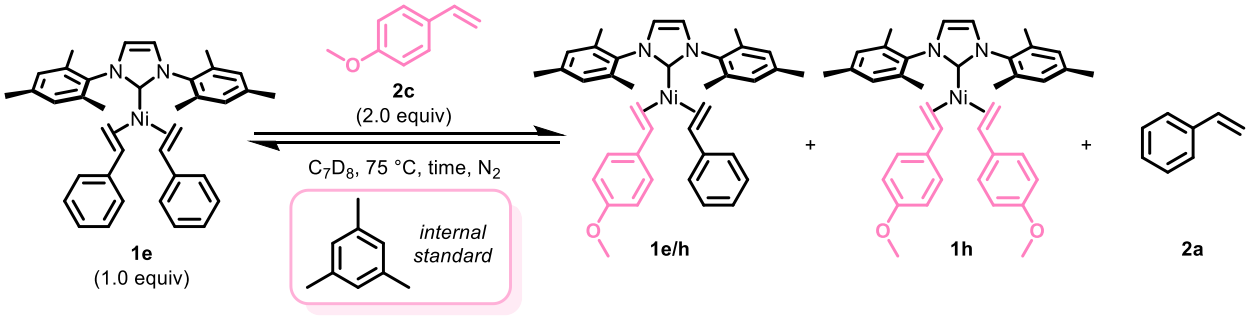

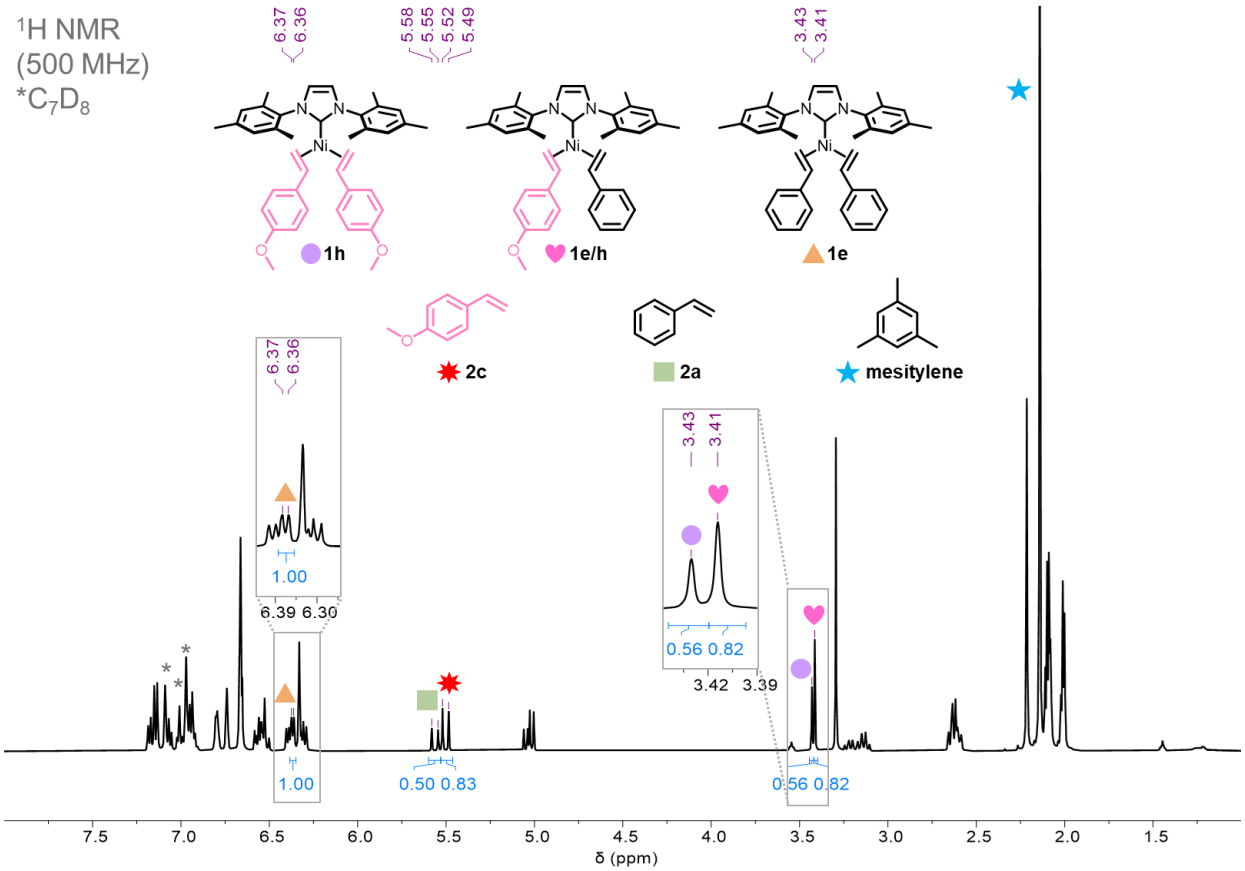

Figure C.5. ^{1}H NMR (500 MHz, 298 K) spectrum of the reaction of **1e** and 4-methoxystyrene (**2c**) after heating in C_7D_8 taken at 25 °C.

Table C.3. Integration of labeled peaks in the ^{1}H NMR spectrum and normalized integrations (integration/#H) of each species in solution.

Compound	Chemical Shift (ppm)	Integration	# of protons	Normalized integrations
1e	6.37	1.00	4	0.25
4-methoxystyrene (**2c**)	5.51	0.83	1	0.83
Styrene (**2a**)	5.57	0.50	1	0.50
1h	3.43	0.56	6	0.093
1e/h	3.41	0.82	3	0.27

Ligand Exchange Experiment #2:

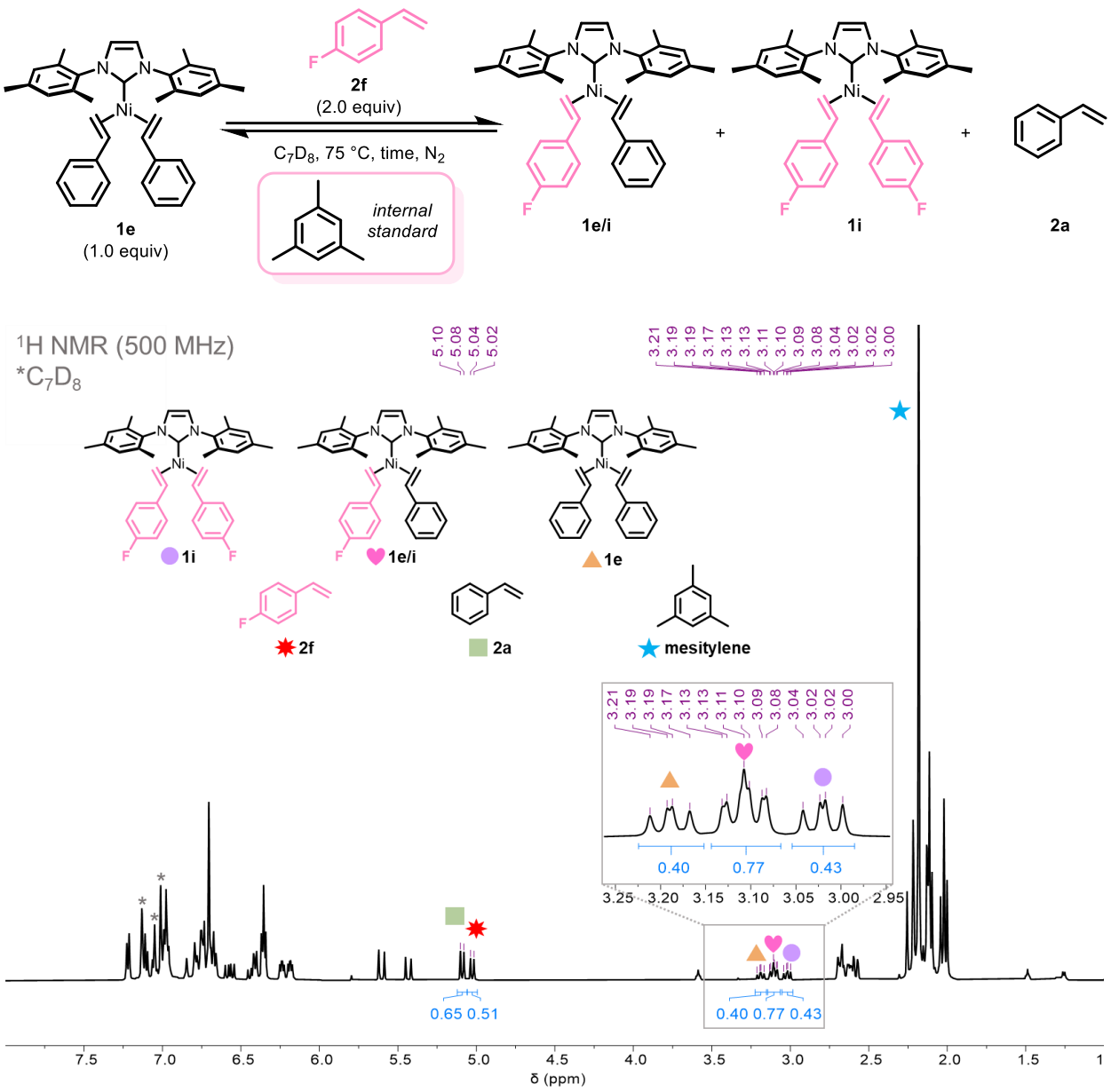

Figure C.6. ^{1}H NMR (500 MHz, 298 K) spectrum of the reaction of **1e** and 4-fluorostyrene (**2f**) after heating in C_7D_8 taken at 25 °C.

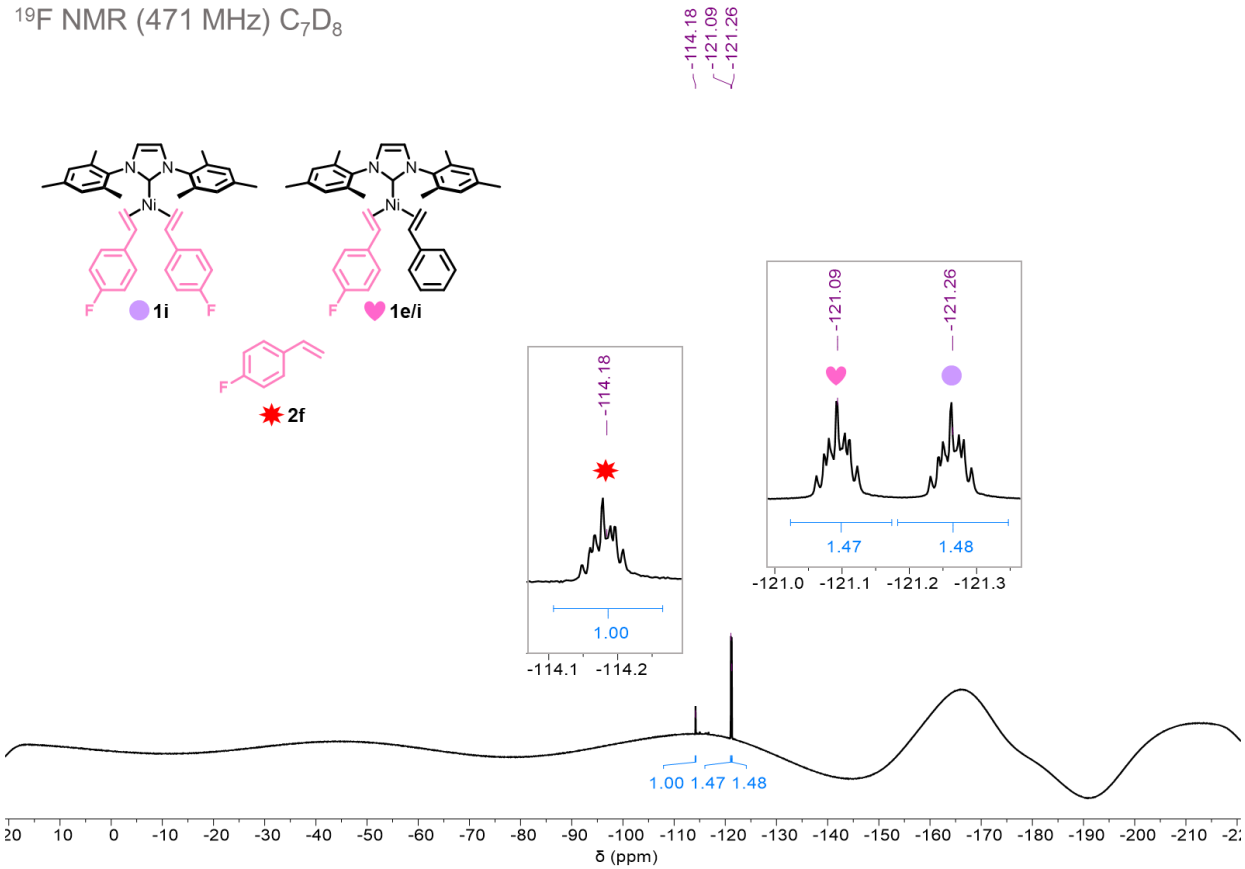

Figure C.7. ^{19}F NMR (471 MHz, 298 K) spectrum of the reaction of **1e** and 4-fluorostyrene (**2f**) after heating in C_7D_8 taken at 25 °C.

Table C.4. Integration of labeled peaks in the ^{1}H NMR spectrum and normalized integrations (integration/#H) of each species in solution.

Compound	Chemical Shift (ppm)	Integration	# of protons	Normalized integrations
1e	3.19	0.40	2	0.20
4-fluorostyrene (**2f**)	5.03	0.51	1	0.51
Styrene (**2a**)	5.09	0.65	1	0.65
1i	3.02	0.43	2	0.22
1e/i	3.11	0.77	2	0.39

Ligand Exchange Experiment #3:

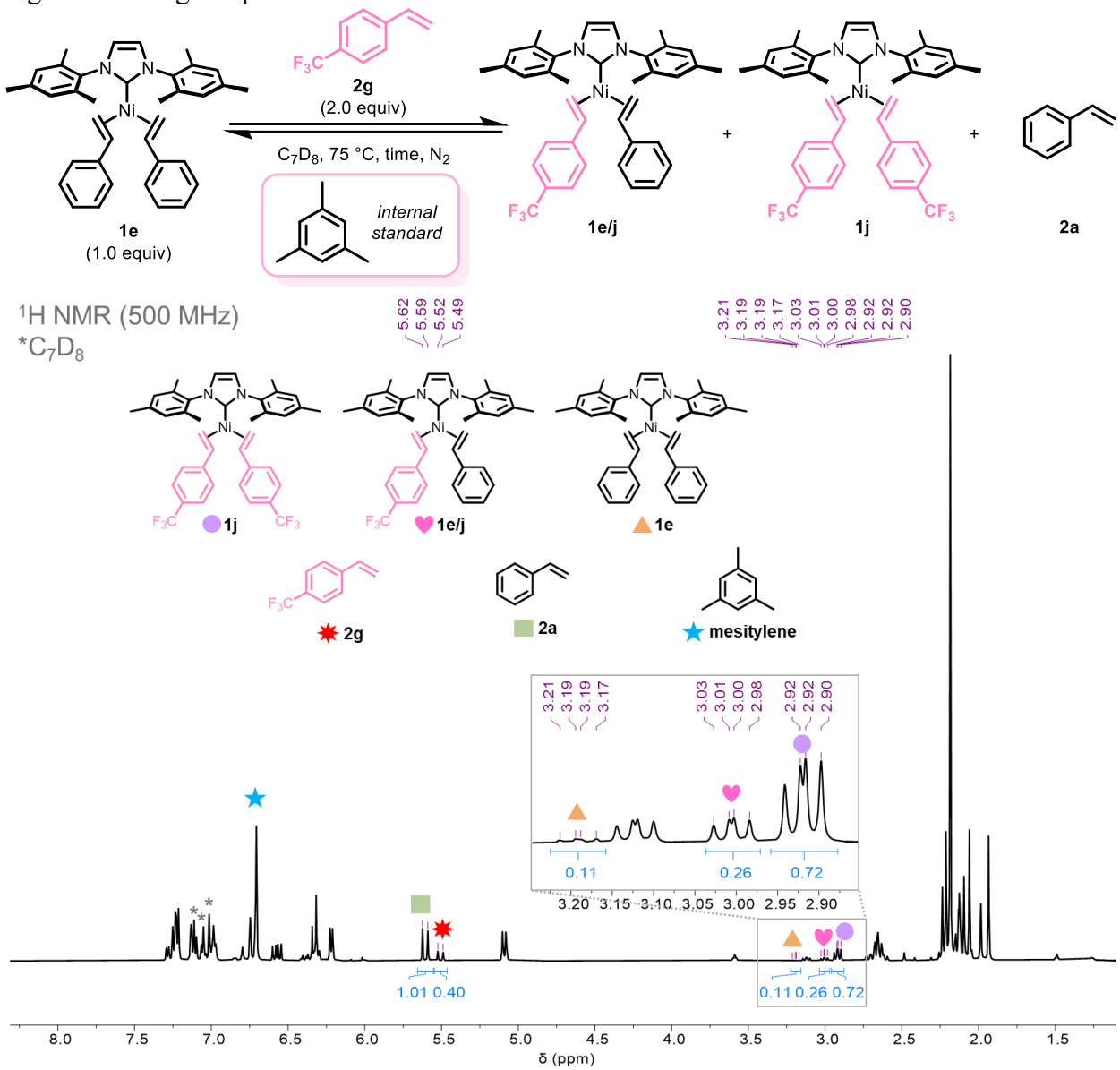

Figure C.8. ^{1}H NMR (500 MHz, 298 K) spectrum of the reaction of **1e** and 4-(trifluoromethyl)styrene (**2g**) after heating in C_7D_8 taken at 25 °C.

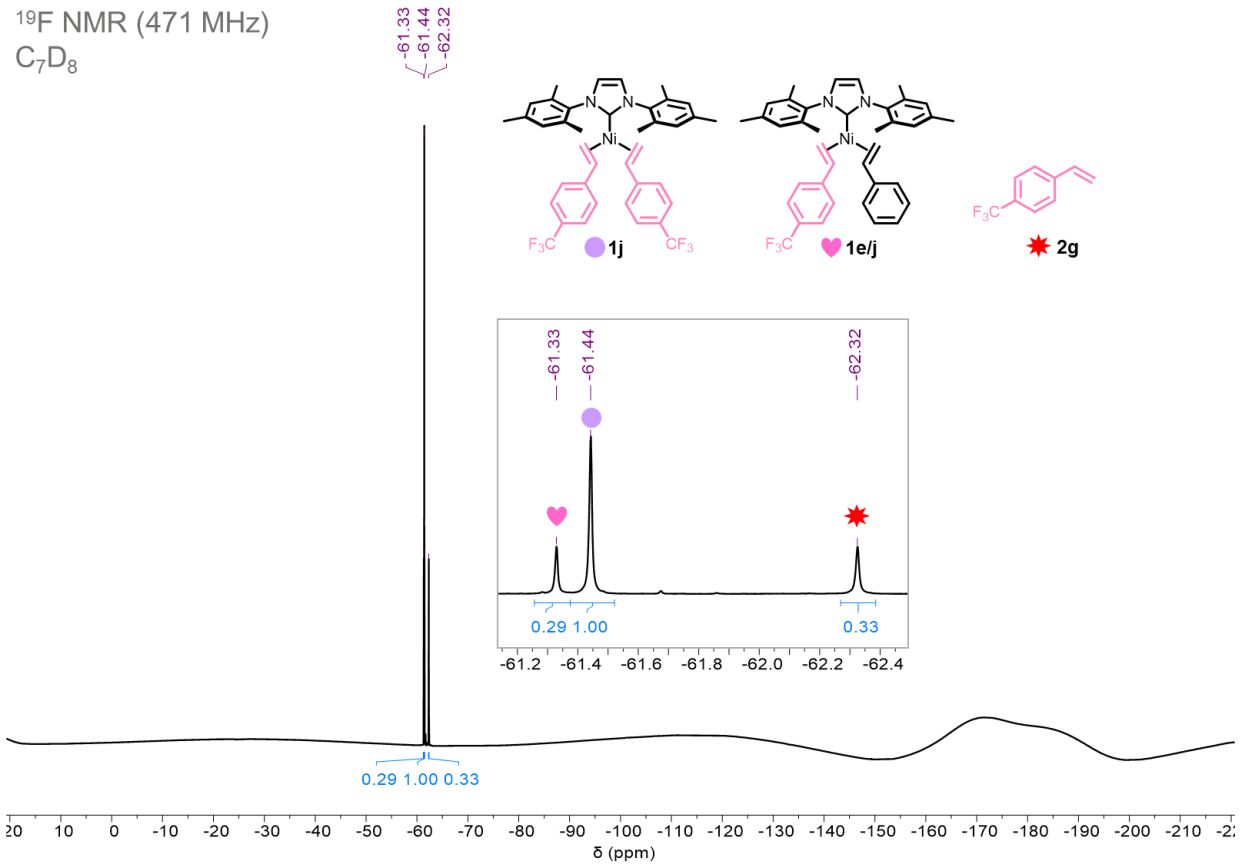

Figure C.9. ^{19}F NMR (471 MHz, 298 K) spectrum of the reaction of **1e** and 4-(trifluoromethyl)styrene (**2g**) after heating in C_7D_8 taken at 25 °C.

Table C.5. Integration of labeled peaks in the ^{1}H NMR spectrum and normalized integrations (integration/#H) of each species in solution.

Compound	Chemical Shift (ppm)	Integration	# of protons	Normalized integration
1e	3.19	0.11	2	0.055
4-(Trifluoromethyl)styrene (**2g**)	5.51	0.40	1	0.40
Styrene (**2a**)	5.61	1.01	1	1.0
1j	2.92	0.72	2	0.36
1e/j	3.03	0.26	1	0.26

Calculation of equilibrium constants:
Because we can observe the presence of complex **1e**, the intermediate complex **A**, the product complex **B**, 4-X-vinylarene, and styrene, the reaction was balanced in the following manner to include each component observed in solution:

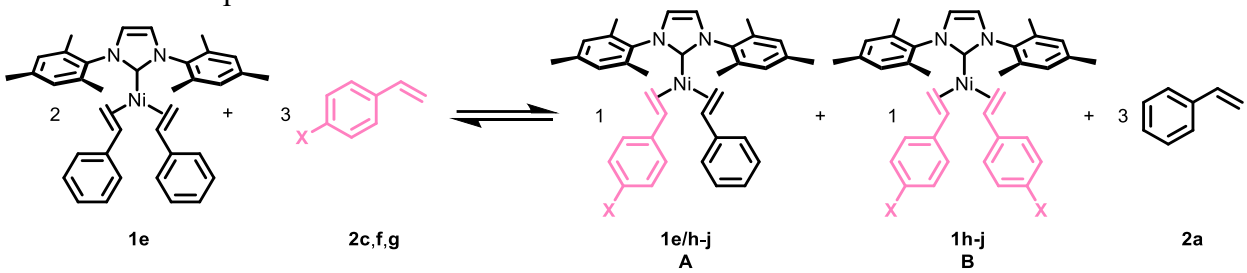

Therefore, we can use this balanced equation to write an equilibrium expression that describes this reaction:

$$K_{eq} = \frac{[\mathbf{A}][\mathbf{B}][\mathbf{2a}]^3}{[\mathbf{2\#}]^3[\mathbf{1e}]^2}$$

Using this equilibrium expression, we can calculate the K_{eq} for each reaction and further calculate the $\log(K_X/K_H)$ values (Table S8).

Table C.6. Corresponding Hammett parameters (σ), K_{eq}, K_X/K_H, and $\log(K_X/K_H)$ for the reactions of **2c**,**f**,**g** with **1e**.

X	σ	K_{eq}	$K_{eq(X)}/K_{eq(H)}$	$\log(K_{eq(X)}/K_{eq(H)})$
CF_3	0.54	498	498	2.70
F	0.062	4.28	4.28	0.632
H	0	-	1	0
OCH_3	-0.268	0.0892	0.0892	-1.05

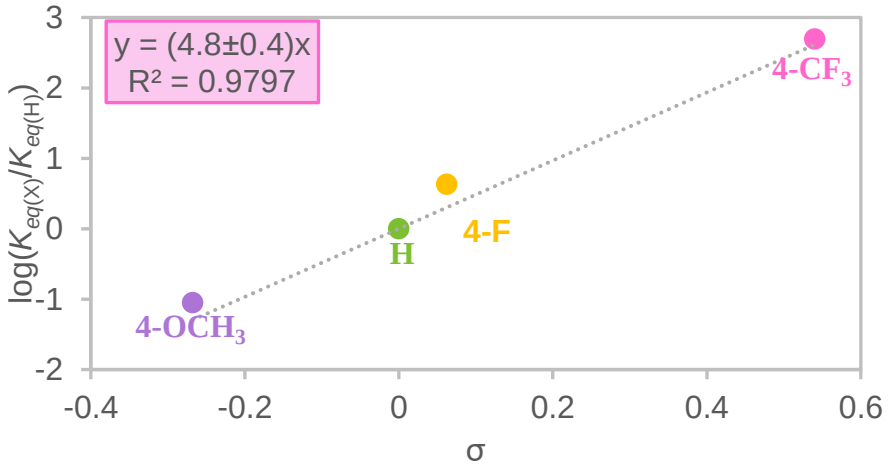

Figure C.10. Hammett Plot of the $\log(K_{eq(X)}/K_{eq(H)})$ versus σ for the ligand exchange experiments with **1e**.

b. Reaction of 1e with 1h-j

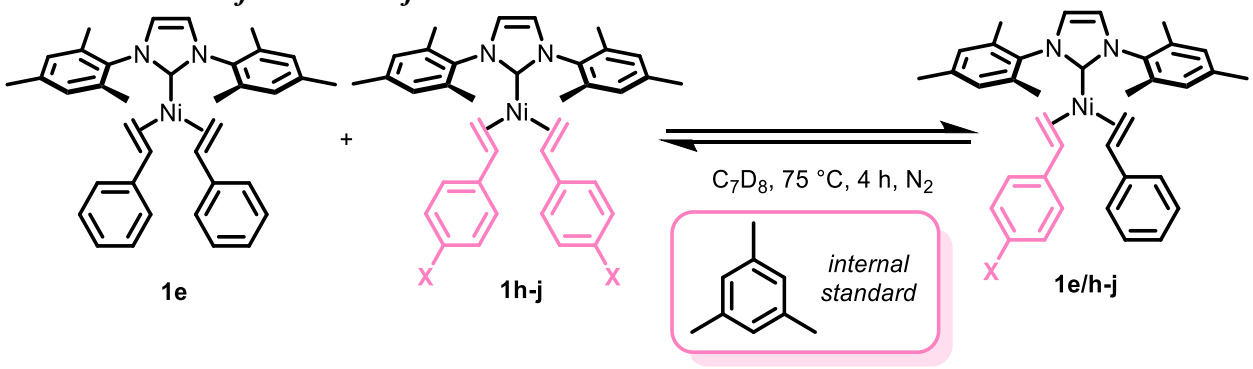

In a nitrogen-glovebox, the (IMes)Ni(4-X-vinylarene)$_2$ complex (**1h-j**, 0.0066 mmol, 1.0 equiv) was weighed out directly into a J-Young NMR tube and solvated in C_7D_8 (0.45 mL), which was added using a disposable 1-mL syringe. A stock solution of **1e** (25 mg, 0.044 mmol) in toluene (1.0 mL) was prepared in a volumetric flask. This stock solution (0.15 mL, 3.8 mg, 0.0066 mmol, 1.0 equiv) was distributed using a disposable 1-mL syringe into the NMR tube containing the (IMes)Ni(4-X-vinylarene)$_2$ complex. The internal standard, mesitylene (3.5 µL, 0.025 mmol), was added using a 10-µL syringe. The J-Young NMR tube was sealed, removed from the glovebox, and placed in a pre-heated oil bath at 75 °C for 4 h. The reaction was removed from the heat and cooled to room temperature. The resulting reaction mixture was analyzed by ^{1}H and ^{19}F NMR. The corresponding amounts of each Ni complex were used are seen in Table S9.

Table C.7. Corresponding amounts of **1h-1j** used for each experiment.

(IMes)Ni(4-X-vinylarene)$_2$	Amount (mg)	Amount (mmol)
(IMes)Ni(4-OCH$_3$-styrene)$_2$ (**1h**)	4.2	0.0066
(IMes)Ni(4-F-styrene)$_2$ (**1i**)	4.0	0.0066
(IMes)Ni(4-CF$_3$-styrene)$_2$ (**1j**)	4.7	0.0066

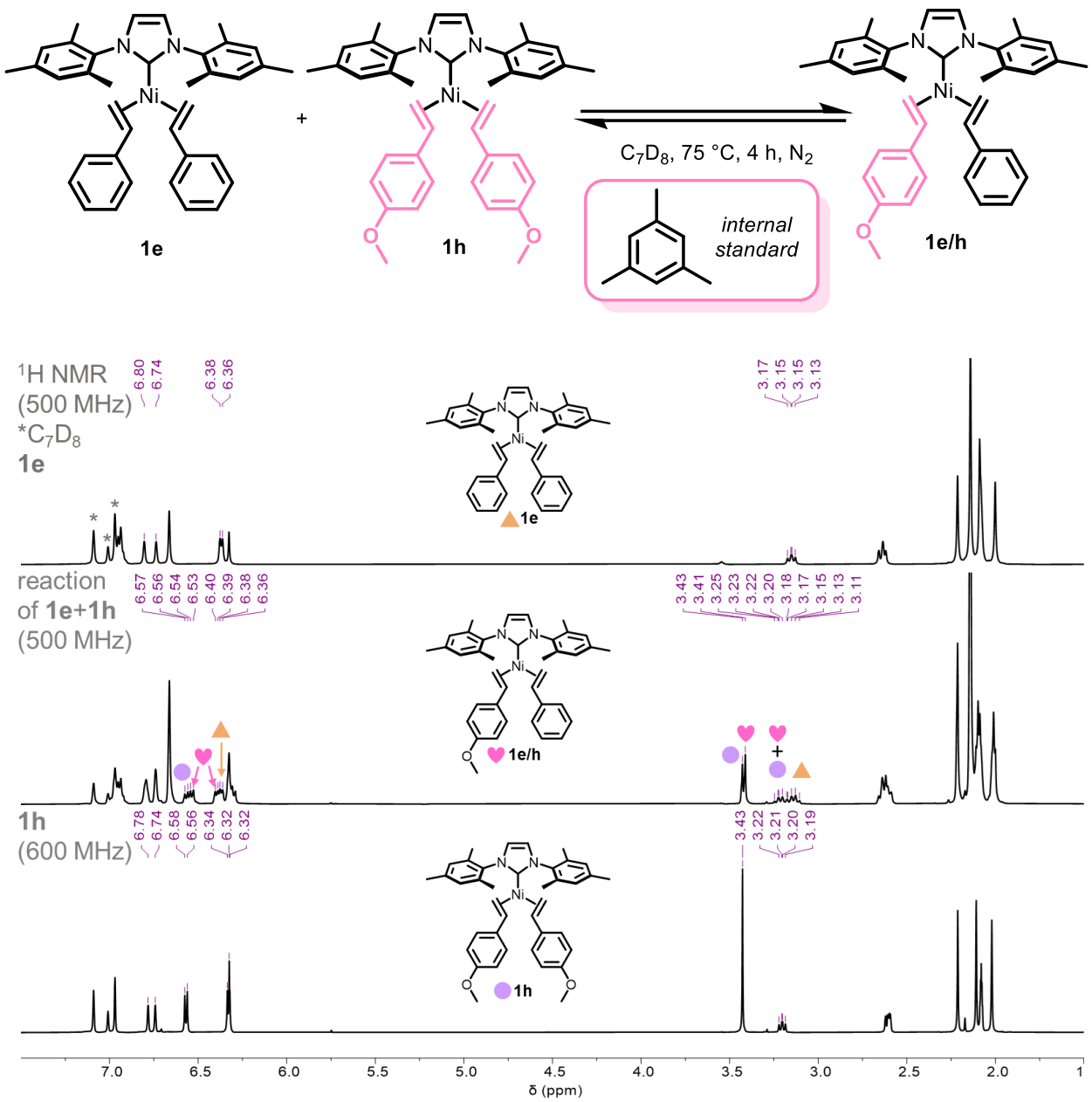

Figure C.11. From top to bottom are the ^{1}H NMR spectra of **1e**, the reaction of **1e** and **1h** to form **1e**/**h**, and **1h**, respectively, in C_7D_8 taken at 25 °C.

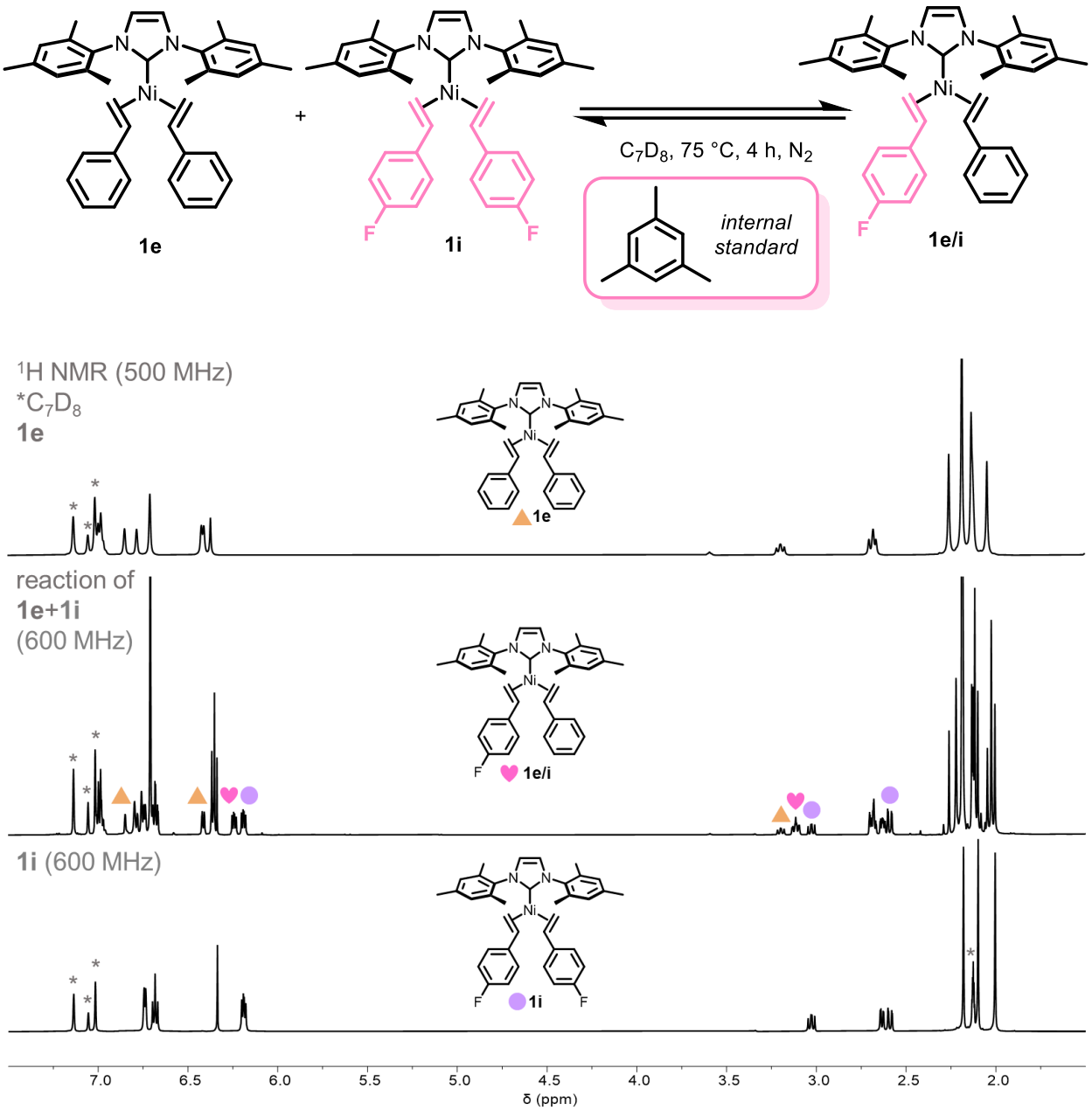

Figure C.12. From top to bottom are the ^{1}H NMR spectra of **1e**, the reaction of **1e** and **1i** to form **1e/i**, and **1i**, respectively, in C_7D_8 taken at 25 °C.

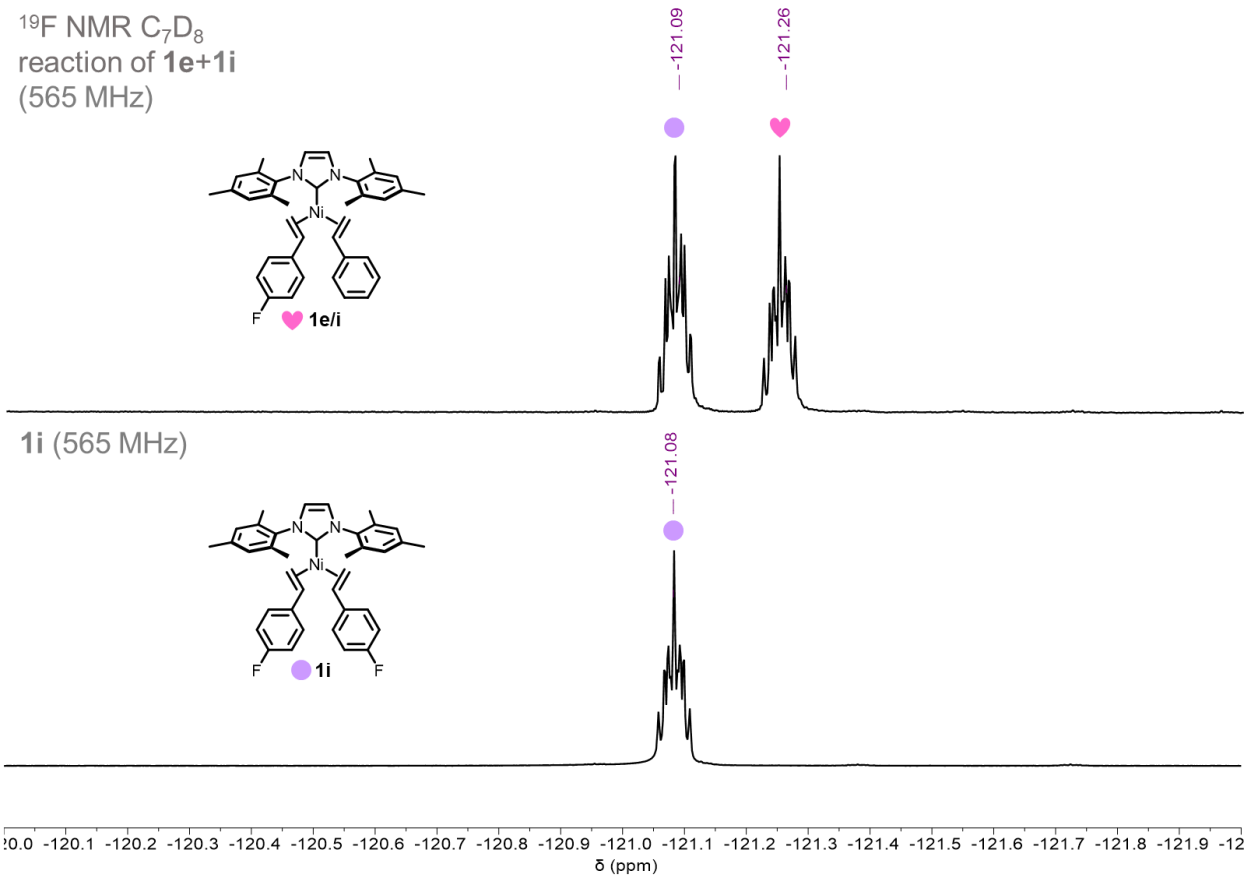

Figure C.13. From top to bottom are the ^{19}F NMR spectra of the reaction of **1e** and **1i** to form **1e/i**, and of **1i**, respectively, in C_7D_8 taken at 25 °C.

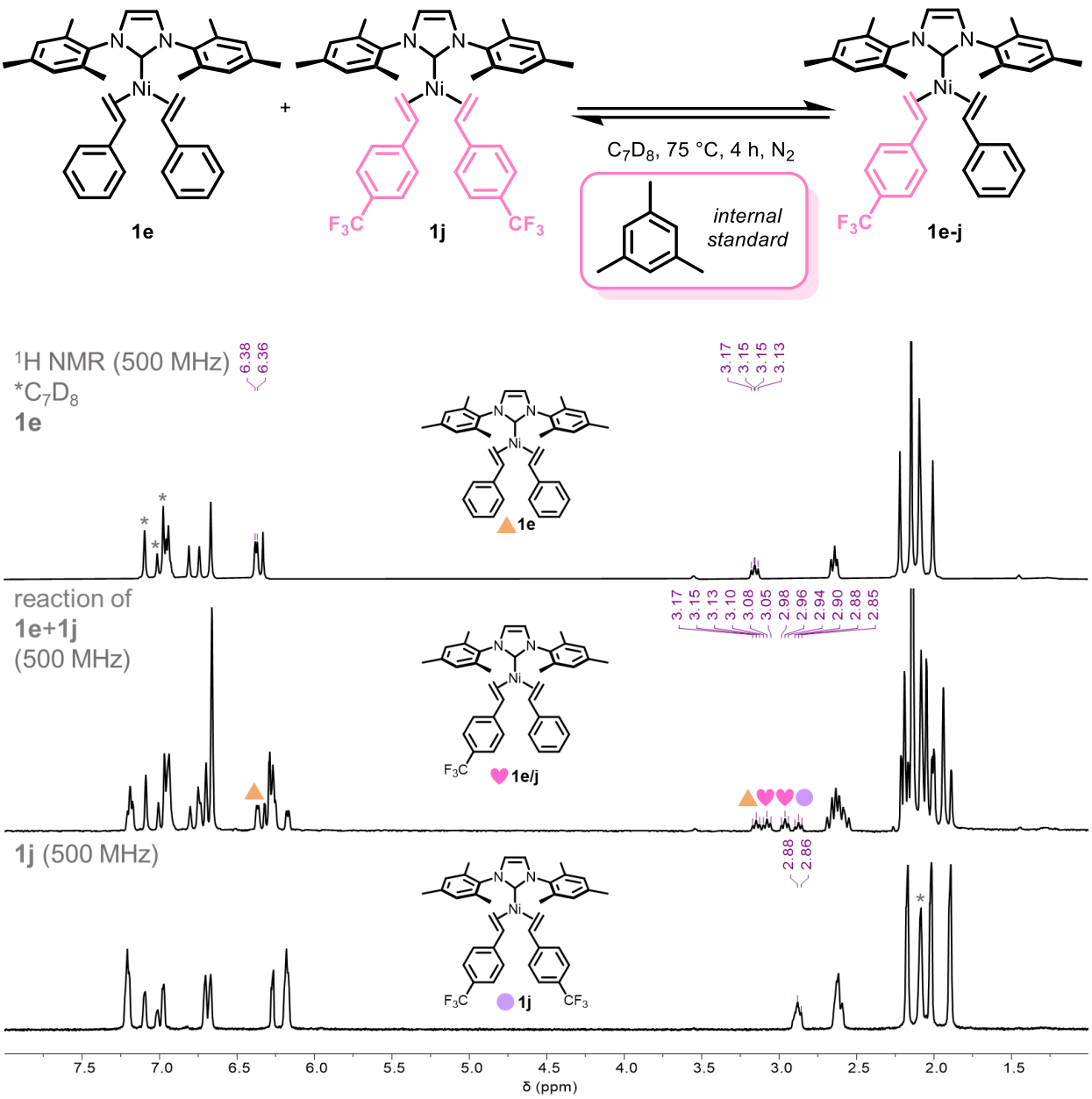

Figure C.14. From top to bottom are the ^{1}H NMR spectra of **1e**, the reaction of **1e** and **1j** to form **1e**/**j**, and or **1j**, respectively, in C_7D_8 taken at 25 °C.

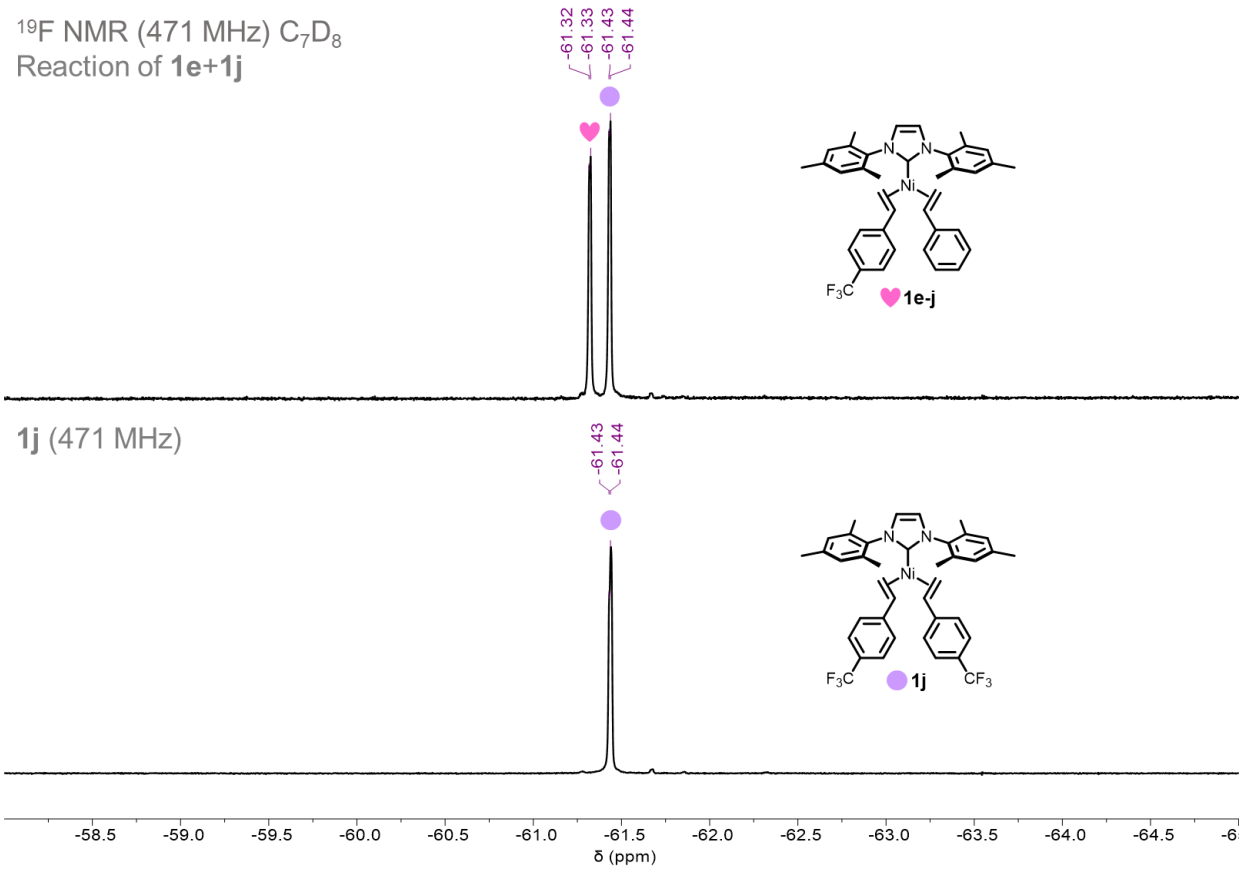

Figure C.15. From top to bottom are the ^{19}F NMR spectra of the reaction of **1e** and **1j** to form **1e**/**j**, and **1j** respectively, in C_7D_8 taken at 25 °C.

C.1.6. Kinetic Experiments

a. NHC Ligand Effects

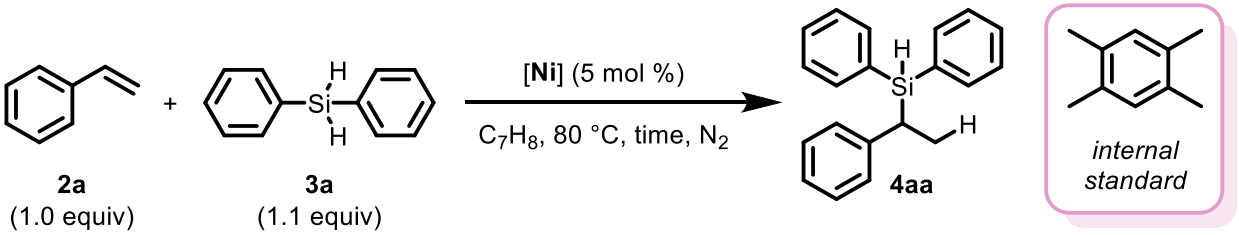

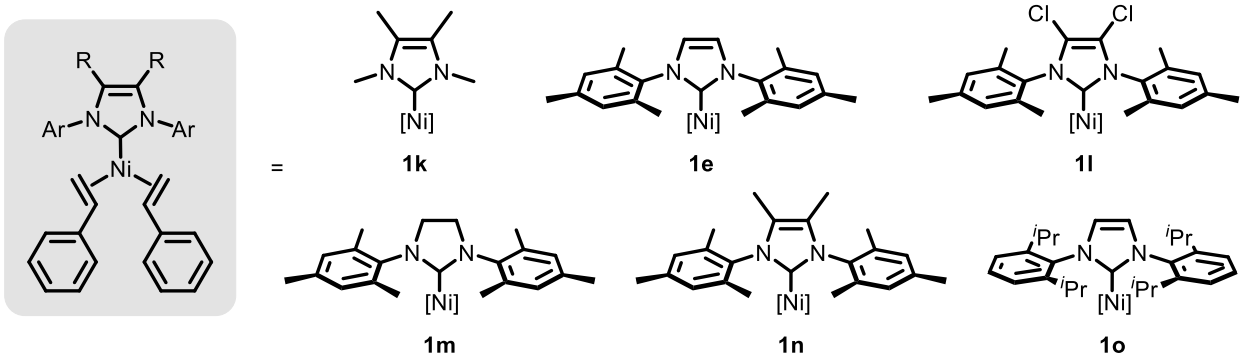

General Procedure: In a nitrogen-filled glovebox, a stock solution was prepared by weighing out the corresponding Ni catalyst (**1e**, **1k-1o**) and dissolving in toluene using volumetric glassware. The stock solution of the Ni catalyst (**1e**, **1k-1o**, $1.3x10^{-2}$ mmol, 0.005 equiv) was distributed into two 1-dram scintillation vials equipped with stir bars using a disposable 1-mL syringe. A separate stock solution of the internal standard, durene, and **2a** (30 µL, 0.26 mmol, 1.0 equiv) were prepared in toluene using volumetric glassware and distributed into each 1-dram scintillation vial to obtain a total volume of 1.2 mL. The vials were sealed with a septum cap and brought out of the glovebox, injected with **3a** (54 µL, 0.29 mmol, 1.1 equiv), and placed on an aluminum vial block preheated to 80 °C. Throughout the course of the reaction, 20 µL aliquots were removed with a 25-µL syringe and filtered into a GC vial through Celite and diluted with hexanes. The filtrate was analyzed by GC to assess the reaction progress and selectivity. The product concentration was determined by relative integration (by GC) of the product peaks against mesitylene, in accordance with calibration curves. Two trials were run for all experiments.

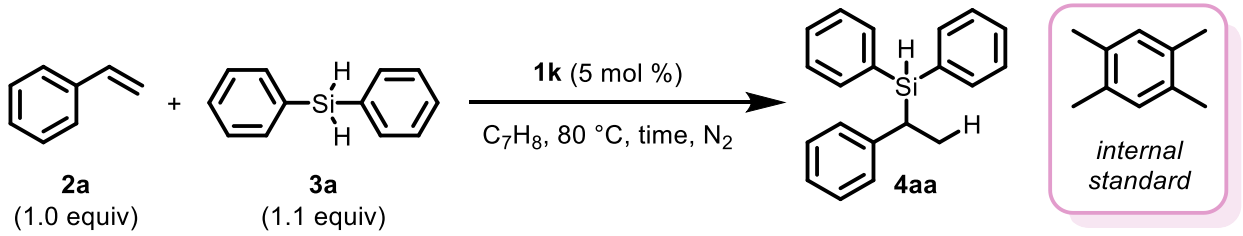

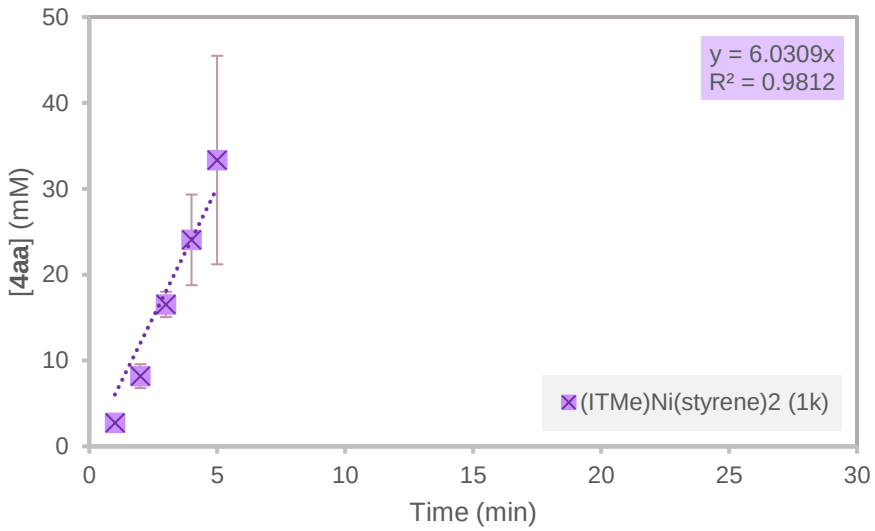

Figure C.16. Initial rate of the formation of **4aa** versus time (min).

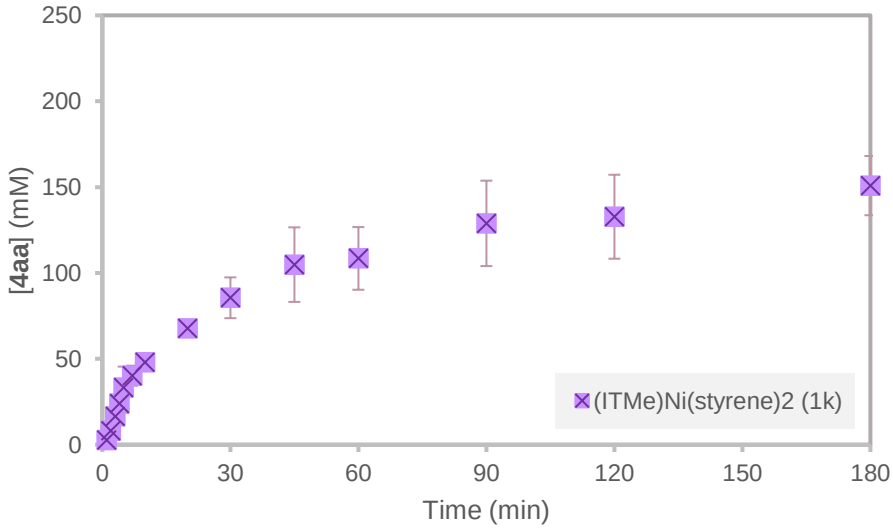

Figure C.17. Full reaction profile for the formation of **4aa** versus time (min).

Table C.8. [**4aa**] (mM) and selectivity (*l*:*b*) of **4aa** formed.

Time (min)	[**4aa**] (mM)	Selectivity (*l*:*b*)
1	2.8±0.9	1:6.7
2	8±1	1:12
3	16±1	1:16
4	24±5	1:17
5	33±12	1:19

7	40±6	1:20
10	48±2	1:23
20	67.69±0.04	1:23
30	86±12	1:20
45	105±22	1:15
60	108±18	1:12
90	129±25	1:8.1
120	133±24	1:6.2
180	151±17	1:4.1

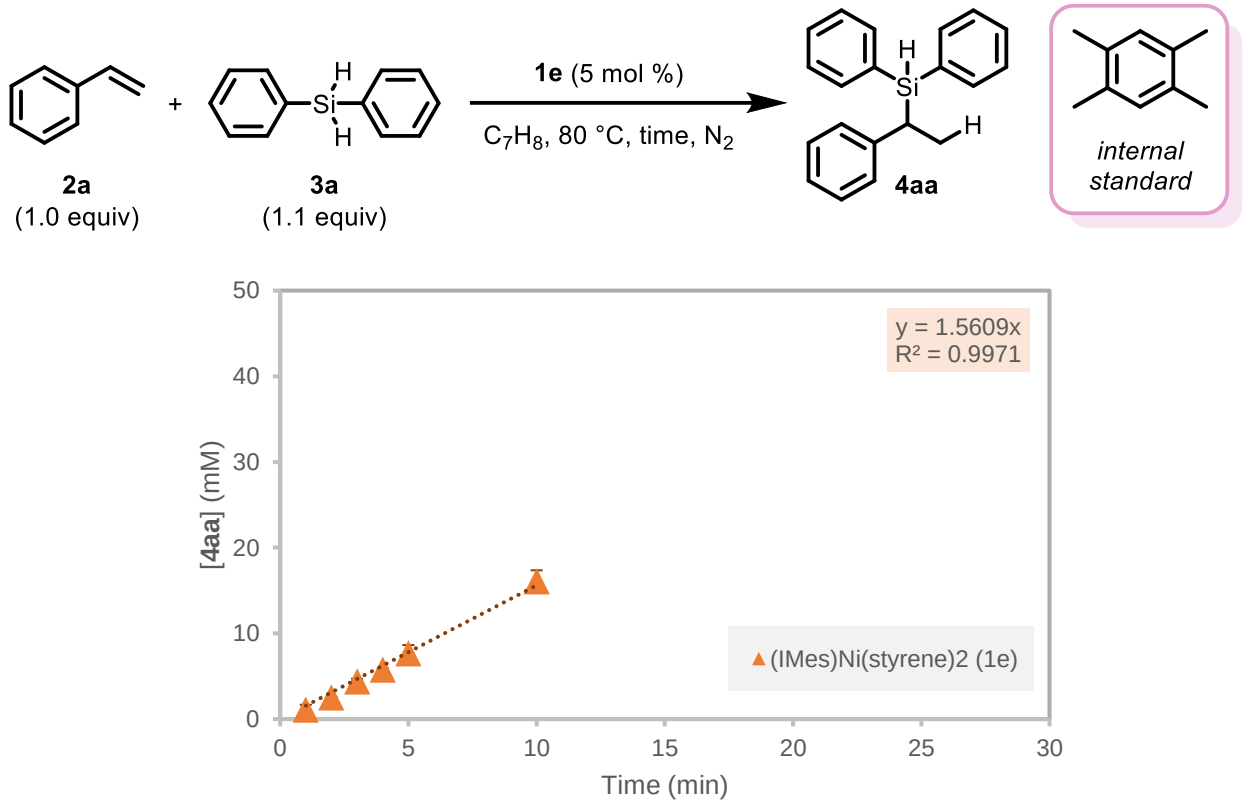

Figure C.18. Initial rate of the formation of **4aa** versus time (min).

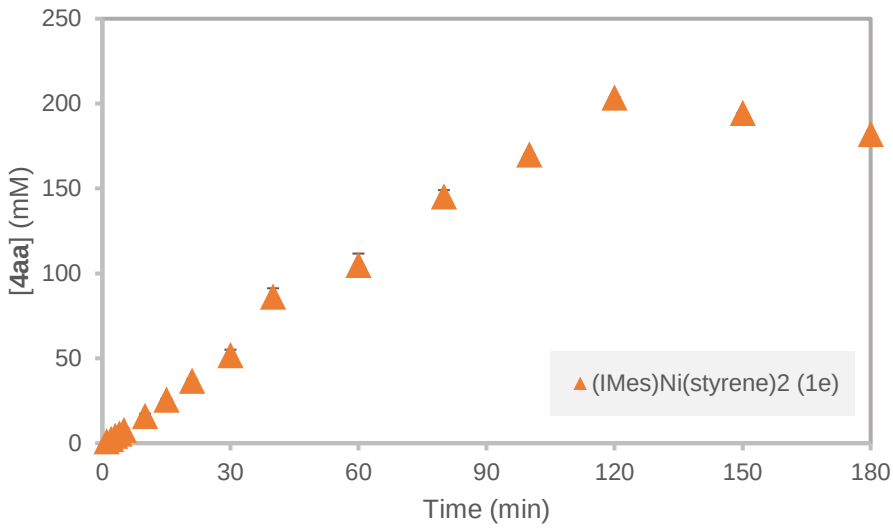

Figure C.19. Full reaction profile for the formation of **4aa** versus time (min).

Table C.9. [**4aa**] (mM) and selectivity (*l*:*b*) of **4aa** formed.

Time (min)	[**4aa**] (mM)	Selectivity (*l*:*b*)
1	1.1±0.6	1:2.1
2	2.524±0.007	1:4.0
3	4.4±0.3	1:5.9
4	5.8±0.1	1:7.7
5	7.7±0.9	1:8.0
10	16±1	1:9.7
15	25.6±0.4	1:10
21	36.9±0.7	1:9.4
30	52±3	1:8.7
40	86±5	1:8.0
60	105±7	1:7.5
80	145±4	1:7.2
100	170.01±0.03	1:7.4
120	203.56±0.04	1:7.9
150	194.51±0.03	1:8.0
180	182.02±0.03	1:8.1

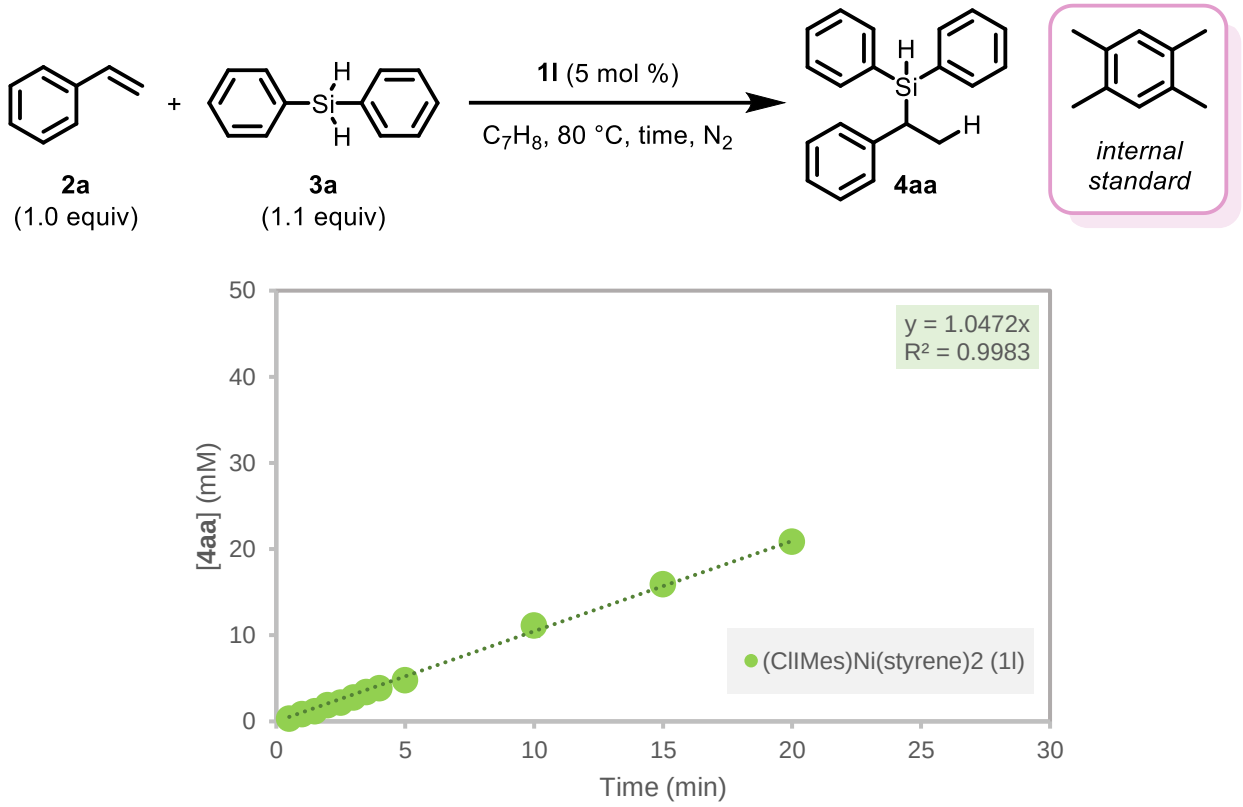

Figure C.20. Initial rate of the formation of **4aa** versus time (min).

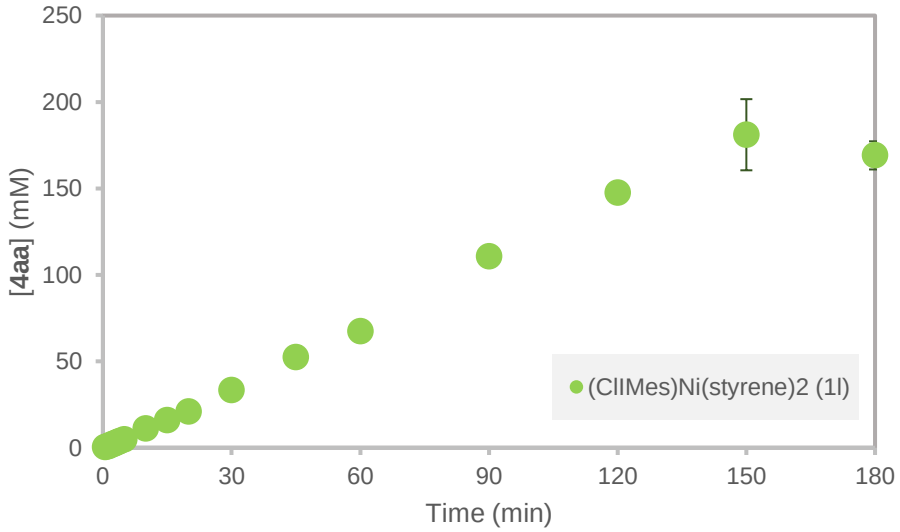

Figure C.21. Full reaction profile for the formation of **4aa** versus time (min).

Table C.10. [**4aa**] (mM) and selectivity (*l:b*) of **4aa** formed.

Time (min)	[**4aa**] (mM)	Selectivity (*l*:*b*)
0.5	0.314±0.002	1:0.7
1	0.8±0.1	1:0.9
1.5	1.2±0.1	1:1.2
2	1.9±0.1	1:1.6
2.5	2.19±0.02	1:1.7
3	2.8±0.2	1:2.0
3.5	3.39±0.06	1:2.3
4	3.86±0.01	1:2.5
5	4.77±0.06	1:2.9
10	11±1	1:4.3
15	15.9±0.9	1:5.1
20	20.9±0.9	1:5.4
30	33.3±0.5	1:6.1
45	52±6	1:6.0
60	67±2	1:5.6
90	111±2	1:5.5
120	148±5	1:5.4
150	181±21	1:5.9
180	169±8	1:6.0

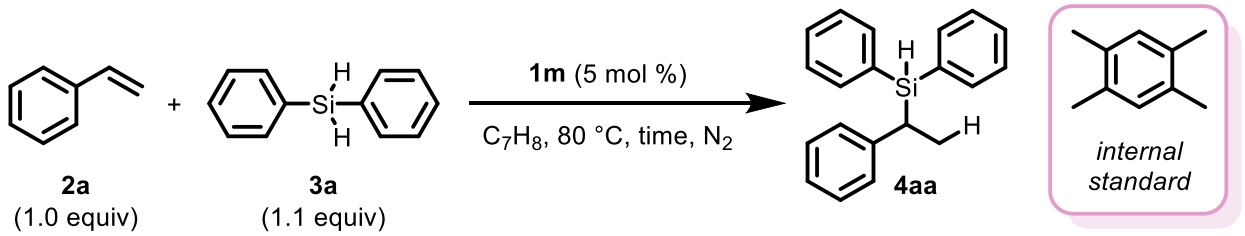

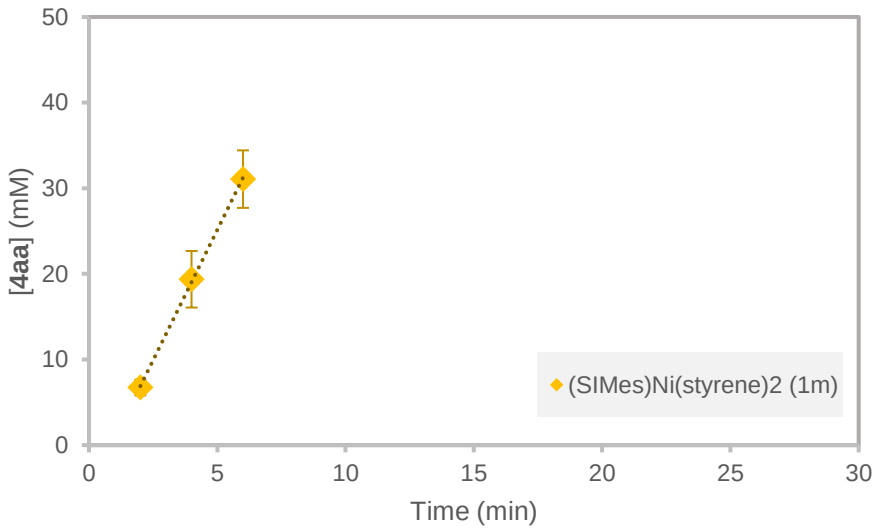

Figure C.22. Initial rate of the formation of **4aa** versus time (min).

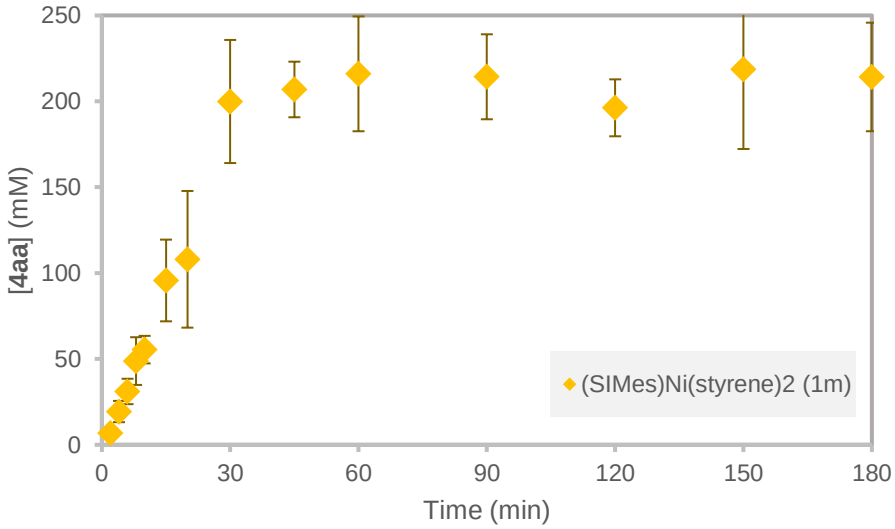

Figure C.23. Full reaction profile for the formation of **4aa** versus time (min).

Table C.11. [**4aa**] (mM) and selectivity (*l*:*b*) of **4aa** formed.

Time (min)	[**4aa**] (mM)	Selectivity (*l*:*b*)
2	7±2	27:1
4	19±6	48:1
6	31±7	70:1
8	49±13	76:1
10	55±8	78:1

15	96±24	78:1
20	108±40	71:1
30	200±36	82:1
45	207±16	86:1
60	216±33	78:1
90	214±24	79:1
120	196±17	81:1
150	219±46	78:1
180	214±31	75:1

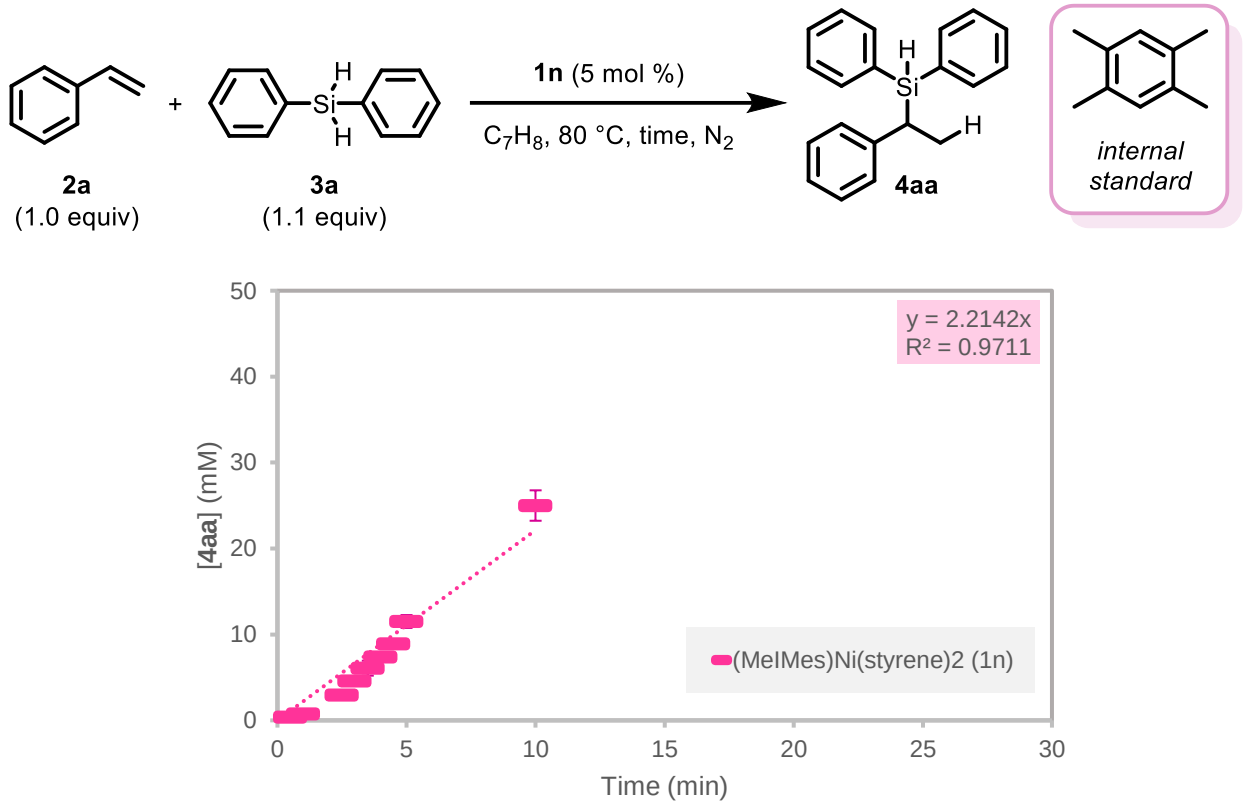

Figure C.24. Initial rate of the formation of **4aa** versus time (min).

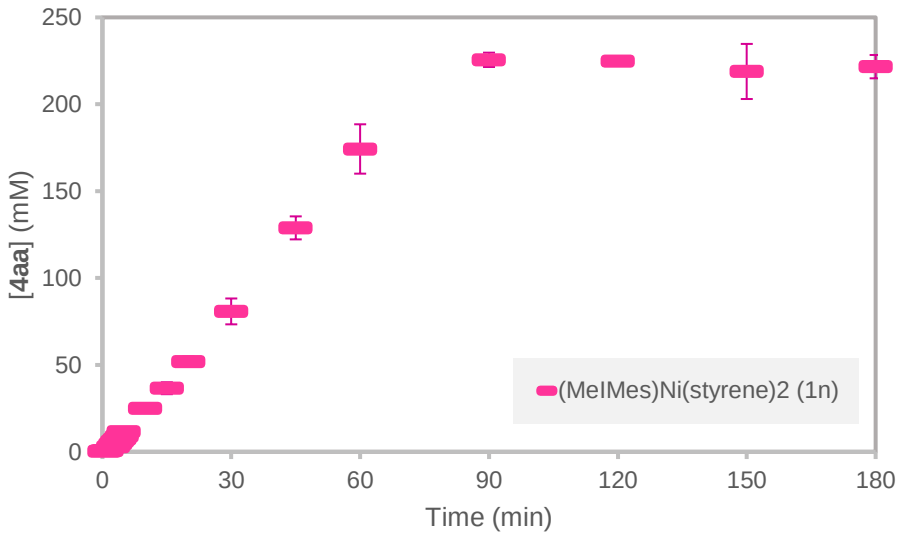

Figure C.25. Full reaction profile for the formation of **4aa** versus time (min).

Table C.12. [**4aa**] (mM) and selectivity (*l*:*b*) of **4aa** formed.

Time (min)	[**4aa**] (mM)	Selectivity (*l*:*b*)
0.5	0.4±0.2	0:1
1	0.8±0.2	1:2.1
2.5	2.9±0.3	1:10
3	4.6±0.4	1:6.4
3.5	6.1±0.9	1:6.7
4	7.4±0.4	1:17
4.5	8.9±0.5	1:20
5	11.5±0.7	1:26
10	25±1	1:42
15	36±3	1:53
20	52±3	1:56
30	81±7	1:59
45	129±7	1:49
60	174±14	1:49
90	225±4	1:48
120	225±1	1:47
150	219±16	1:47
180	222±6	1:49

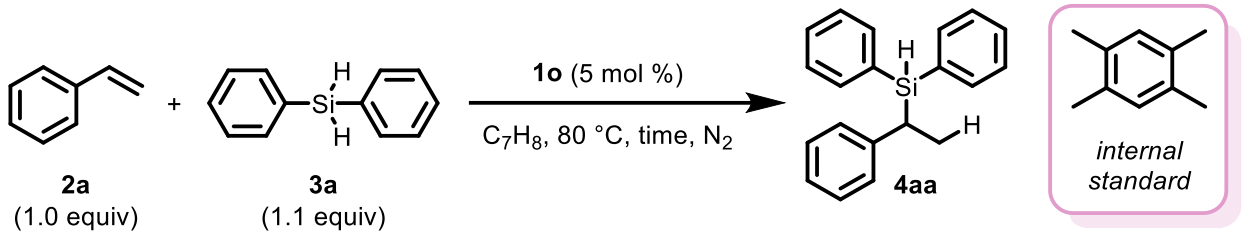

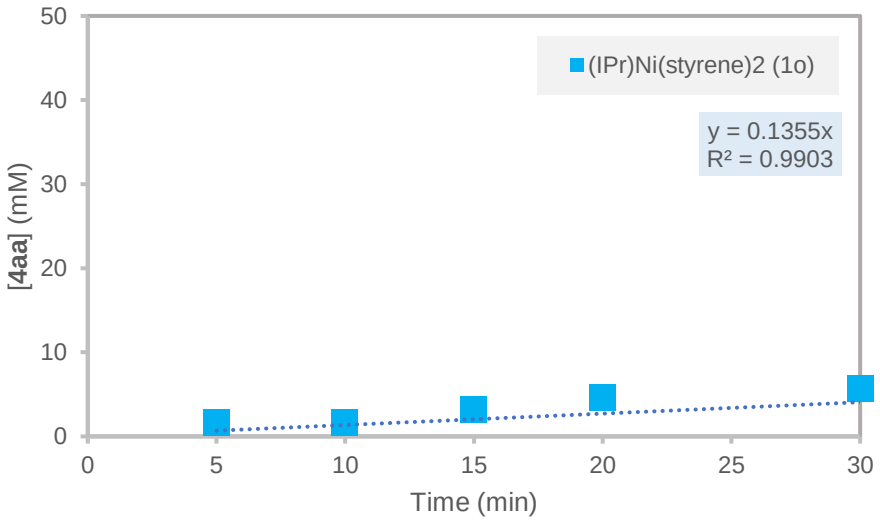

Figure C.26. Initial rate of the formation of **4aa** versus time (min).

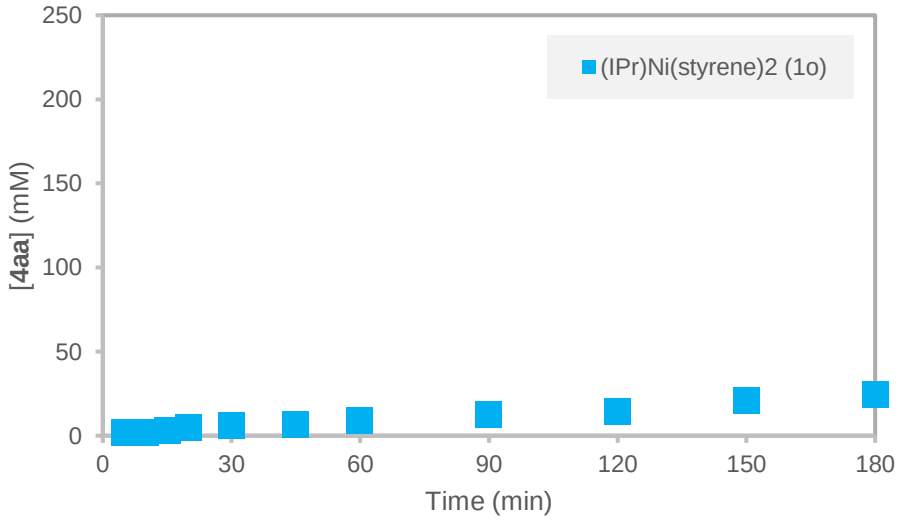

Figure C.27. Full reaction profile for the formation of **4aa** versus time (min).

Table C.13. [**4aa**] (mM) and selectivity (*l*:*b*) of **4aa** formed.

Time (min)	[**4aa**] (mM)	Selectivity (*l*:*b*)

5	1.66±1	0:1
10	1.59	1:4.5
15	3.2±0.7	1:10.8
20	4.6±0.4	1:10.0
30	5.7±0.1	1:11.5
45	6.5±0.4	1:10.0
60	8.7±0.4	1:9.6
90	12.6±0.1	1:8.4
120	14.0±0.1	1:6.6
150	21±4	1:5.2
180	24.1±0.9	1:4.3

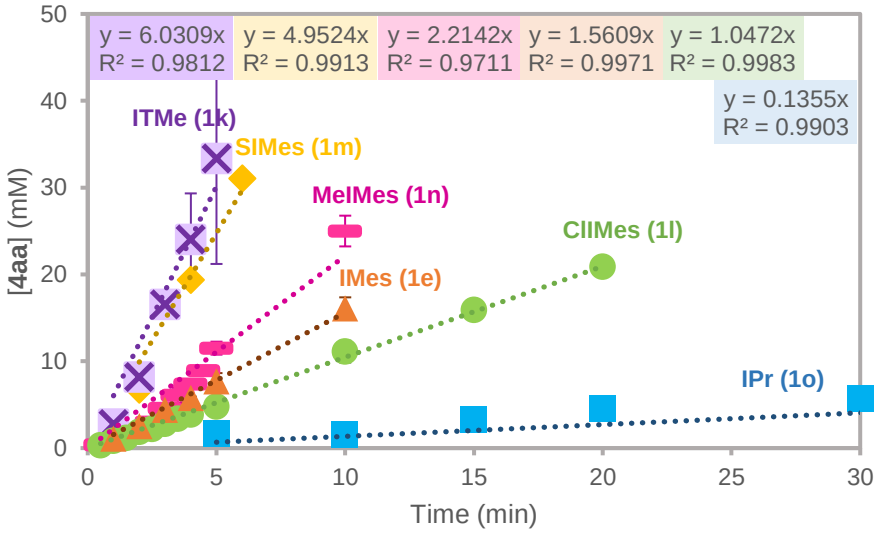

Figure C.28. Compiled initial rates data of the formation of **4aa** versus time (min) catalyzed by **1e**, **1k-1o**.

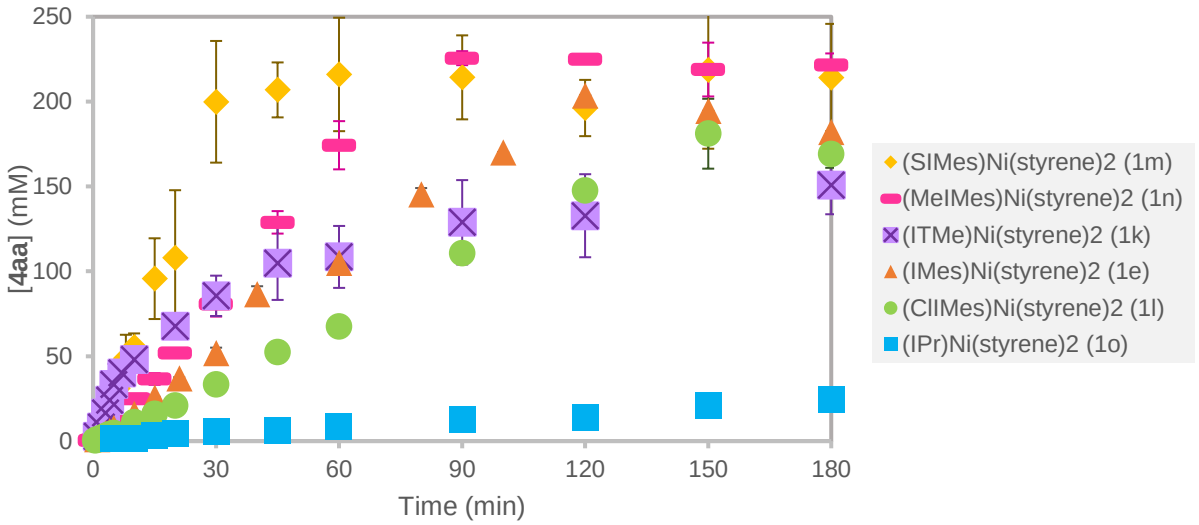

Figure C.29. Compiled full reaction profiles for the formation of **4aa** versus time (min) catalyzed by **1e**, **1k-1o**.

Table C.14. [**4aa**] (mM) and selectivity (*l:b*) of **4aa** formed.

Catalyst	%V_{Bur}	TEP	Initial rate (mM/min)	Relative Rate
(ITMe)Ni(styrene)$_2$ (**1k**)	26.1	2051.7	6.0309	45
(SIMes)Ni(styrene)$_2$ (**1m**)	34.3	2051.5	4.9524	37
(MeIMes)Ni(styrene)$_2$ (**1n**)	34.4	2052.0	2.2142	16
(IMes)Ni(styrene)$_2$ (**1e**)	33.7	2050.0	1.5609	12
(ClIMes)Ni(styrene)$_2$ (**1l**)	34.2	2055.1	1.0472	7.7
(IPr)Ni(styrene)$_2$ (**1o**)	36.9	2051.5	0.1355	1

TEP, Tolman electronic parameter

b. Variable Time Normalization Analysis Kinetics

Three separate experiments were conducted in duplicate to visualize whether or not the catalyst (**1e**) decomposed or experienced product inhibition throughout the course of the reaction using the method of variable time normalization analysis (VTNA).[157]

Experiments A and B:

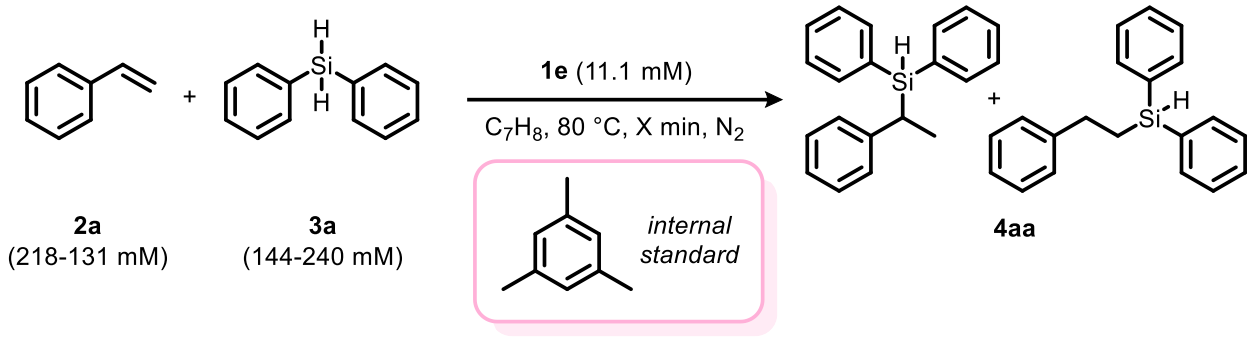

Experiment C:

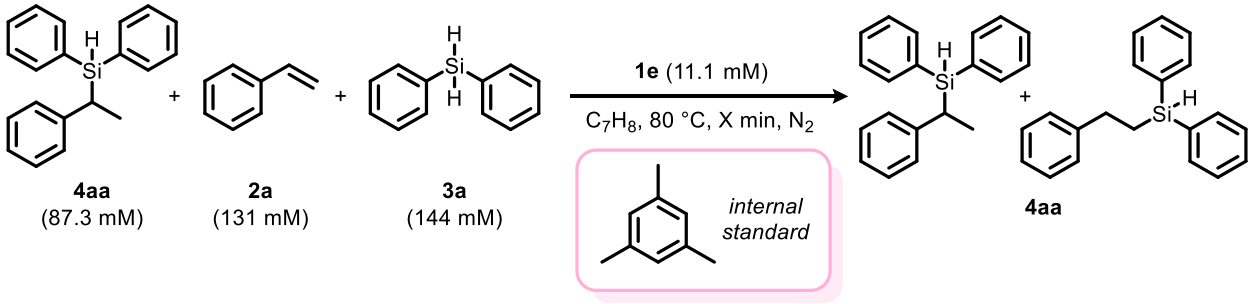

General Procedure: In a nitrogen-filled glovebox, **1e** (7.6 mg, 0.013 mmol, 1.0 equiv) was directly weighed into a 1-dram scintillation vial equipped with a stir bar and toluene (1.2 mL) was added using a disposable 1 mL syringe. **2a** (18 or 30 µL, 0.16 or 0.26 mmol, 12 or 20 equiv) and mesitylene (15 µL, 0.11 mmol) were added to the vial using a 50-µL syringe and then sealed with a septum cap. The reaction was brought out of the glovebox and **3a** (33 or 54 µL, 0.18 or 0.29 mmol, 14 or 22 equiv) and **4aa** (0 or 30 µL, 0 or 0.11 mmol, 0 or 8.5 equiv) were added via a 100-µL syringe, and the vial was placed on an aluminum vial block preheated to 80 °C. Throughout the course of the reaction, 20 µL aliquots were removed with a 25-µL syringe and filtered into a GC vial through Celite and diluted with hexanes. The filtrate was analyzed by GC to assess the reaction progress and selectivity. The product concentration was determined by relative integration (by GC) of the product peaks against mesitylene, in accordance with calibration curves. Two trials were run for all experiments. The initial concentrations of **2a**, **3a**, and **4aa** are listed in the table below for the corresponding experiment.

Table C.15. Corresponding amounts of **2a**, **3a**, **4aa**, and **1e** that were used for each experiment.

Experiment	[**2a**]$_0$ (mM)	[**3a**]$_0$ (mM)	[**4aa**]$_0$ (mM)	[**1e**] (mM)
A	218	240	0	11.1
B	131	144	0	11.1

C	131	144	87.3	11.1

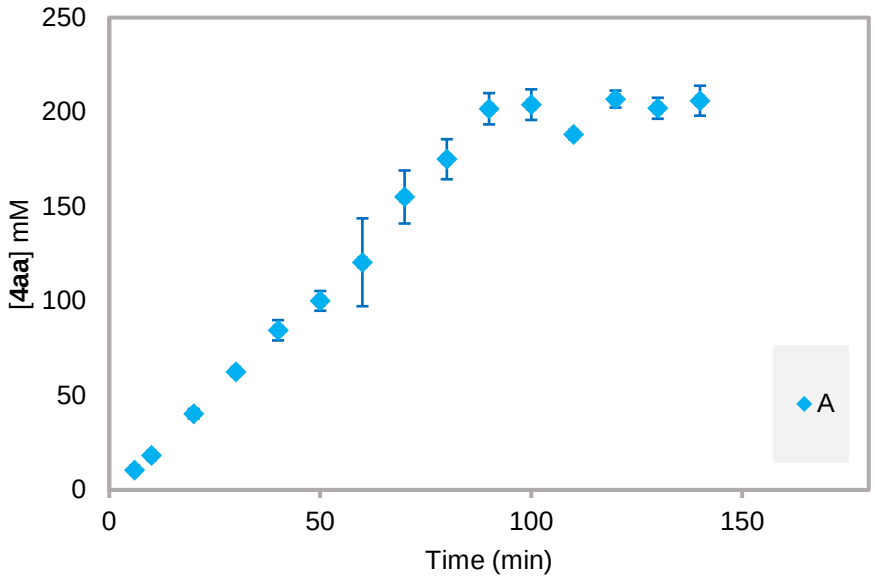

Figure C.30. Reaction profile of Experiment A monitoring the formation of **4aa** versus time (min).

Table C.16. Concentration of **4aa** (mM) and selectivity (*l*:*b*) over time for Experiment A.

Time (min)	[**4aa**] (mM)	Selectivity (*l*:*b*)
6	10.5 ± 0.9	1:81
10	18 ± 1	1:65
20	40 ± 2	1:68
30	62 ± 1	1:69
40	84 ± 5	1:67
50	100 ± 5	1:65
60	120 ± 23	1:59
70	155 ± 14	1:57
80	175 ± 10	1:57
90	202 ± 8	1:55
100	204 ± 8	1:55
110	188.1 ± 0.4	1:55
120	207 ± 4	1:60
130	202 ± 5	1:53
140	206 ± 8	1:54

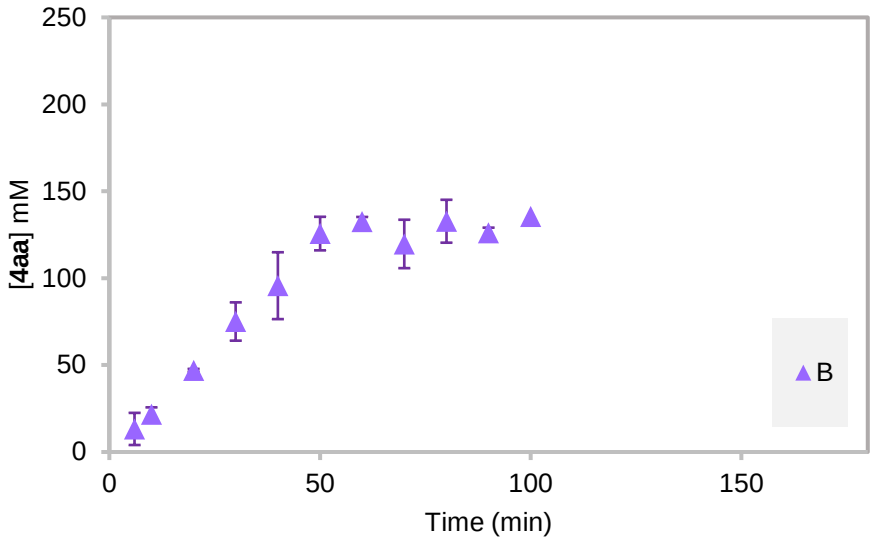

Figure C.31. Reaction profile of Experiment B monitoring the formation of **4aa** versus time (min).

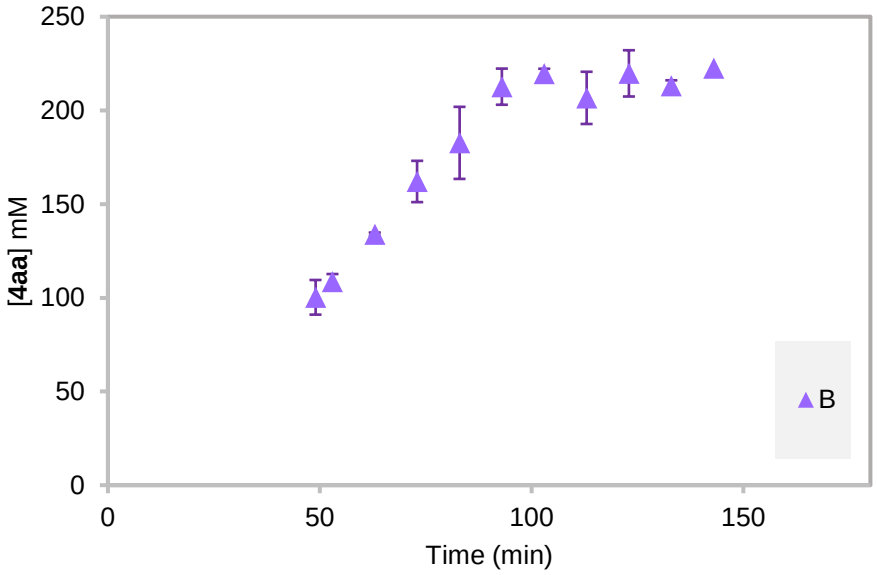

Figure C.32. Reaction profile of Experiment B post **4aa**-adjustment (+87 mM, assumes 40% product at time zero) and time-adjustment (+43 m) monitoring the formation of **4aa** versus time (min).

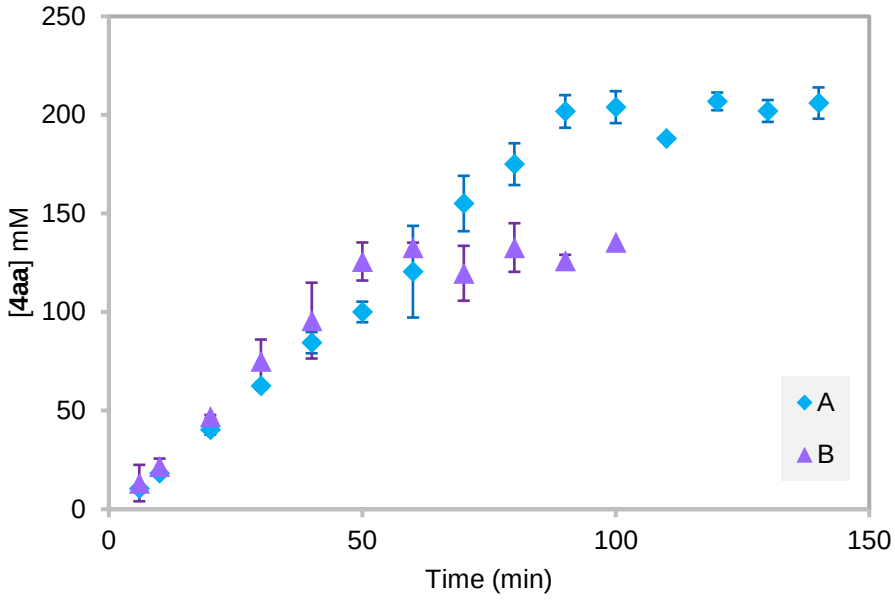

Figure C.33. Reaction profile overlay of Experiment A and Experiment B monitoring the formation of **4aa** versus time (min).

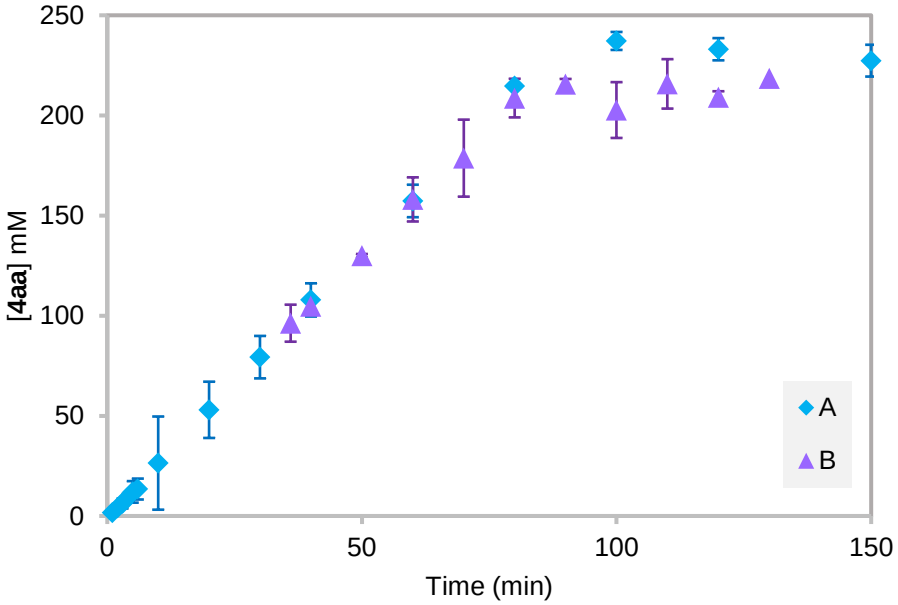

Figure C.34. Reaction profile of Experiment B post **4aa**-adjustment (+83 mM, this assumes 40% of **4aa** has already formed prior to the experiment) and time-adjustment (+43 min) monitoring the formation of [**4aa**] (mM) versus time (min).

Table C.17. Time-adjustment (min), concentration of **4aa** (mM), [**4aa**] adjustment (mM), and selectivity (*l:b*) over time for Experiment B.

Time (min)	Adjusted Time (min, +43 min)	[**4aa**] (mM)	Adjusted [**4aa**] (mM, +83 mM)	Selectivity (*l*:*b*)
6	49	13.3 ± 0.9	96.3	1:112
10	53	22 ± 2	105	1:150
20	63	47 ± 3	130	1:98
30	73	75 ± 1	158	1:114
40	83	96 ± 4	179	1:109
50	93	126 ± 19	209	1:98
60	103	133 ± 15	216	1:90
70	113	119.7 ± 0.4	202.6	1:87
80	123	133 ± 4	216	1:86
90	133	126 ± 12	209	1:83
100	143	135 ± 3	218	1:83

Overlaying Experiment A and B shows no deviation in kinetic profiles, indicating that neither catalyst decomposition nor product inhibition is occurring throughout the reaction.

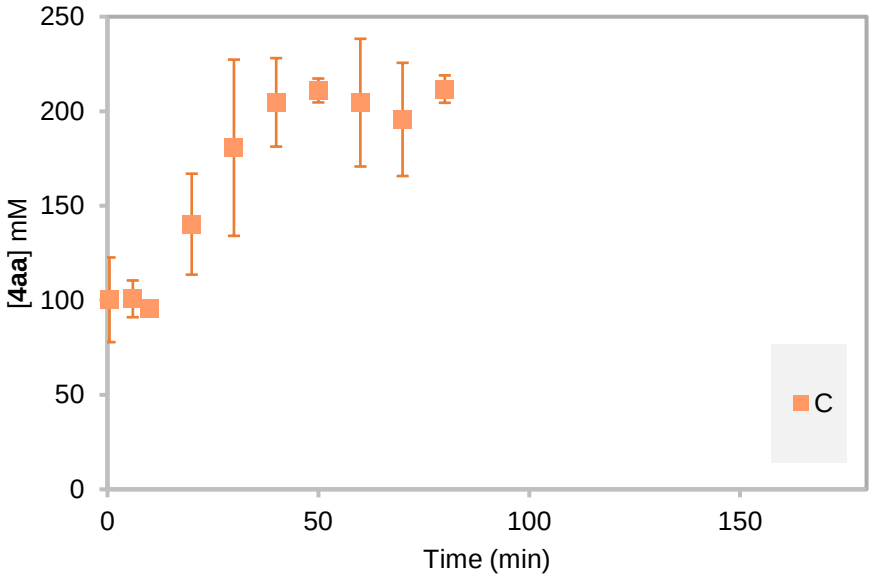

Figure C.35. Reaction profile of Experiment C monitoring the formation of **4aa** versus time (min).

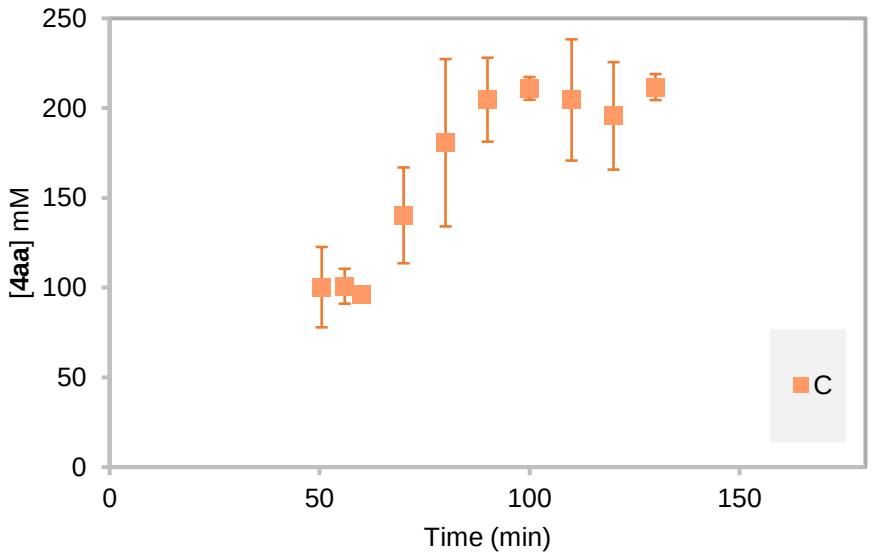

Figure C.36. Reaction profile of Experiment C post time-adjustment (+50 min) kinetic profile of Experiment C monitoring the formation of **4aa** versus time (min).

Table C.18. Time-adjustment (min), concentration of **4aa** (mM), and selectivity (*l*:*b*) over time for Experiment C.

Time (min)	Adjusted Time (min, +50 min)	[**4aa**] (mM)	Selectivity (*l*:*b*)
0.5	50.5	100 ± 22	1:52
6	56	101 ± 9	1:41
10	60	96 ± 2	1:35
20	70	140 ± 26	1:24
30	80	181 ± 46	1:17
40	90	205 ± 23	1:16
50	100	211 ± 6	1:16
60	110	205 ± 34	1:16
70	120	196 ± 30	1:28
80	130	212 ± 7	1:17

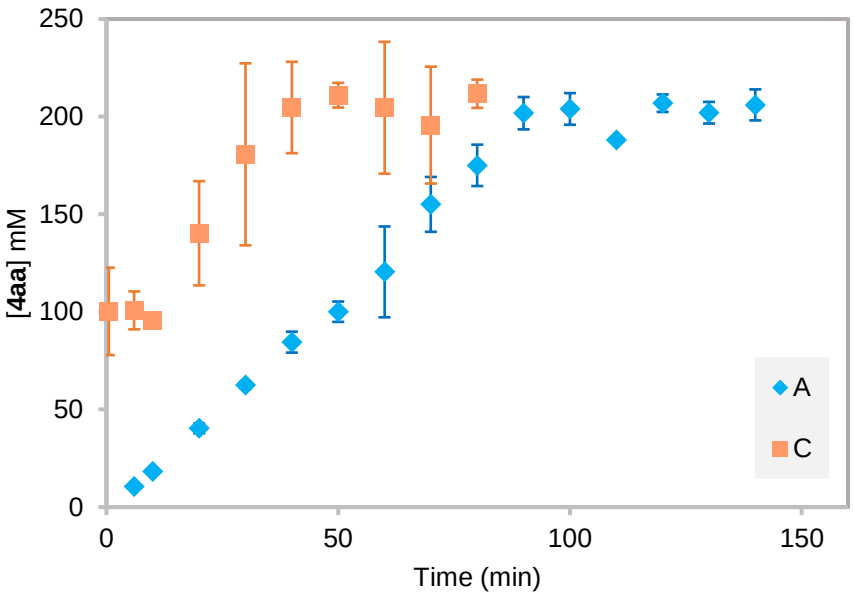

Figure C.37. Overlay of the reaction profiles of Experiment A and C for the formation of **4aa** versus time (min).

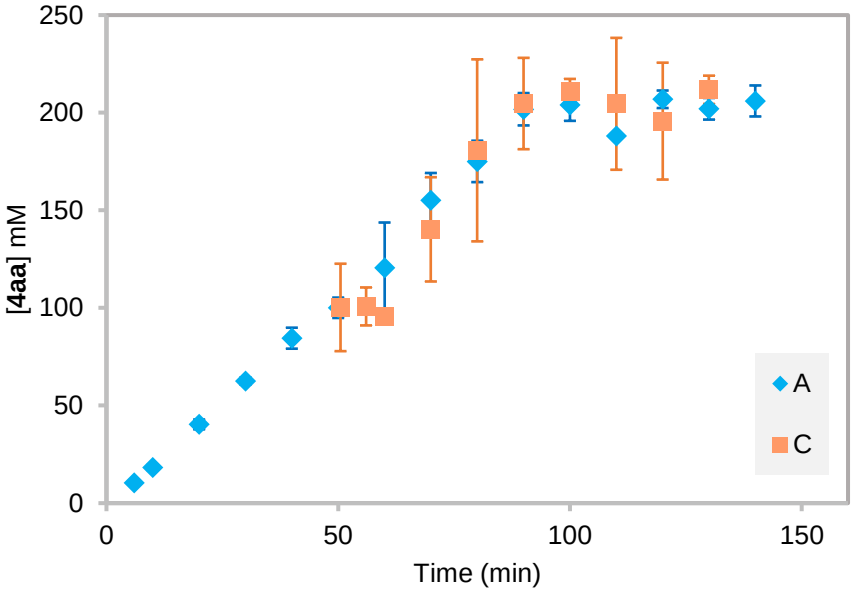

Figure C.38. Overlay of the reaction profiles of Experiment A and C (post time-adjustment +50 min) for the formation of **4aa** versus time (min).

Overlaying Experiment A and C shows no deviation in kinetic profiles, further indicating that product inhibition is not occurring throughout the reaction.

C.1.11. Cyclic Voltammetry of (NHC)Ni(styrene)$_2$ Complexes

In a nitrogen-filled glovebox, electrochemical measurements were made with potentiostat 561 (Bio-Logic SP300) using a typical three-electrode setup (glassy carbon working electrode, Ag/Ag^+ wire reference, and platinum wire counter electrode) in a 20 mL glass vial equipped with a magnetic stir bar. An electrolyte solution of $[NBu_4][ClO_4]$ was prepared in DMF (0.1 mM). The nickel complex of interest (~5 mg) was dissolved in the electrolyte solution (10 mL). Current was reported in mA, while all potentials were reported in volts (V) against Fc^+/Fc redox couple, at a scan rate of 100 mV/s. All scans reported are oxidative scans. Sweeping from left to right or right to left is specified for each complex.

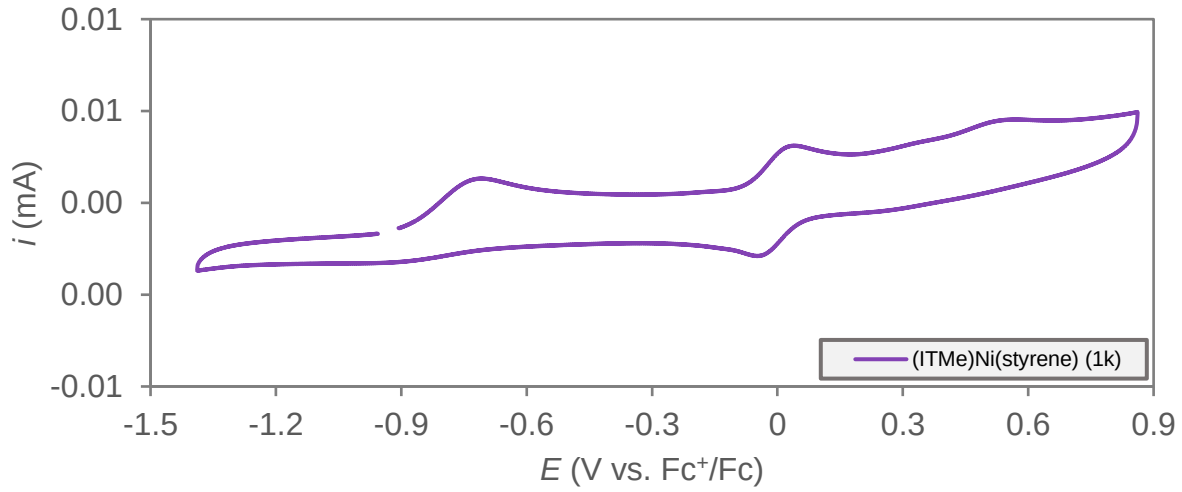

Figure C.39. Cyclic voltammogram of (ITMe)Ni(styrene)$_2$ (**1k**) in a 0.01 M $[NBu_4][ClO_4]$ solution in DMF at 100 mV•s$^-$ taken at 273 K. Oxidative scan sweeping from left to right.

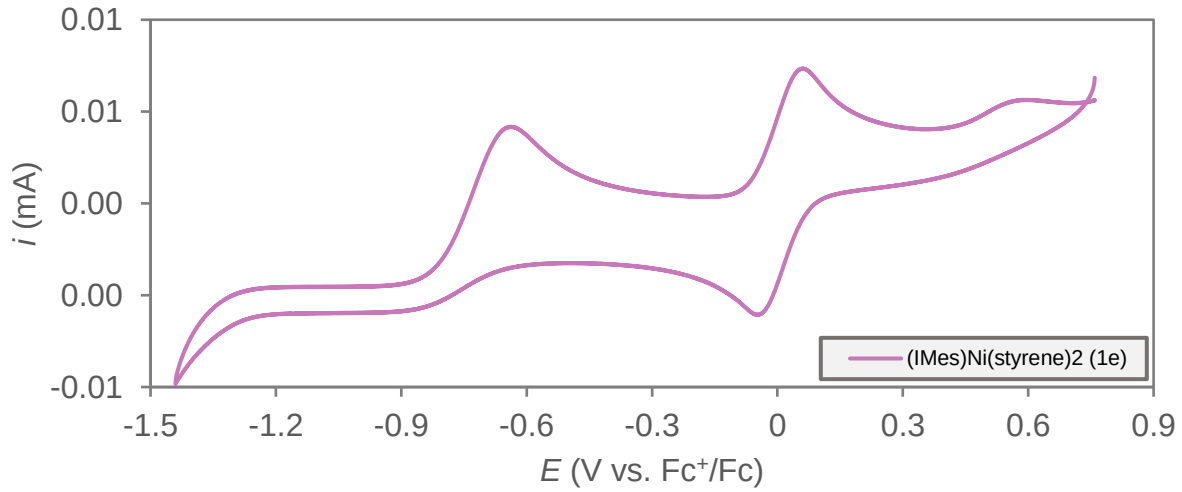

Figure C.40. Cyclic voltammogram of (IMes)Ni(styrene)$_2$ (**1e**) in a 0.01 M [NBu$_4$][ClO$_4$] solution in DMF at 100 mV•s$^-$ taken at 273 K. Oxidative scan sweeping from right to left.

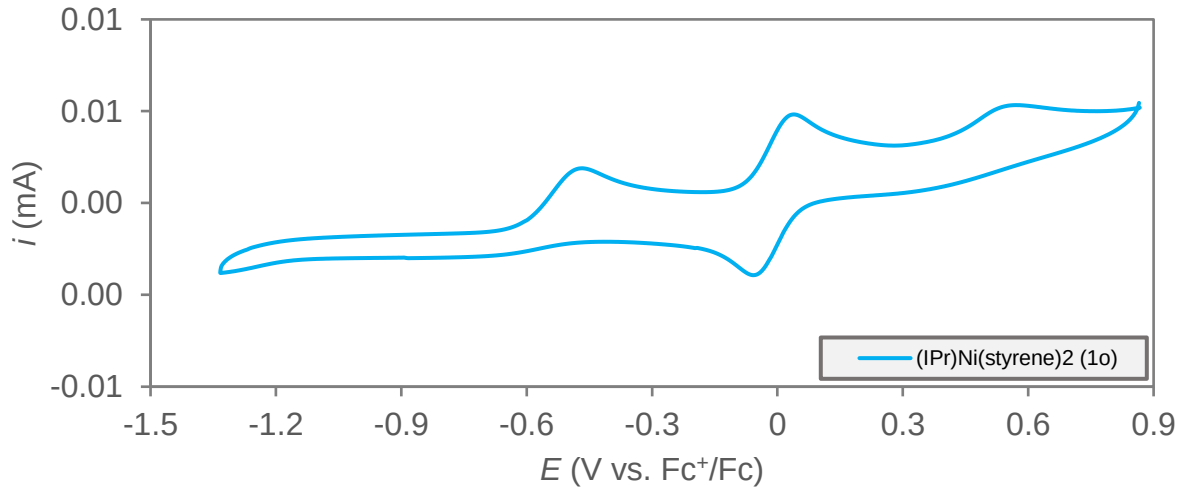

Figure C.41. Cyclic voltammogram of (IPr)Ni(styrene)$_2$ (**1o**) in a 0.01 M [NBu$_4$][ClO$_4$] solution in DMF at 100 mV•s$^-$ taken at 273 K. Oxidative scan sweeping from right to left.

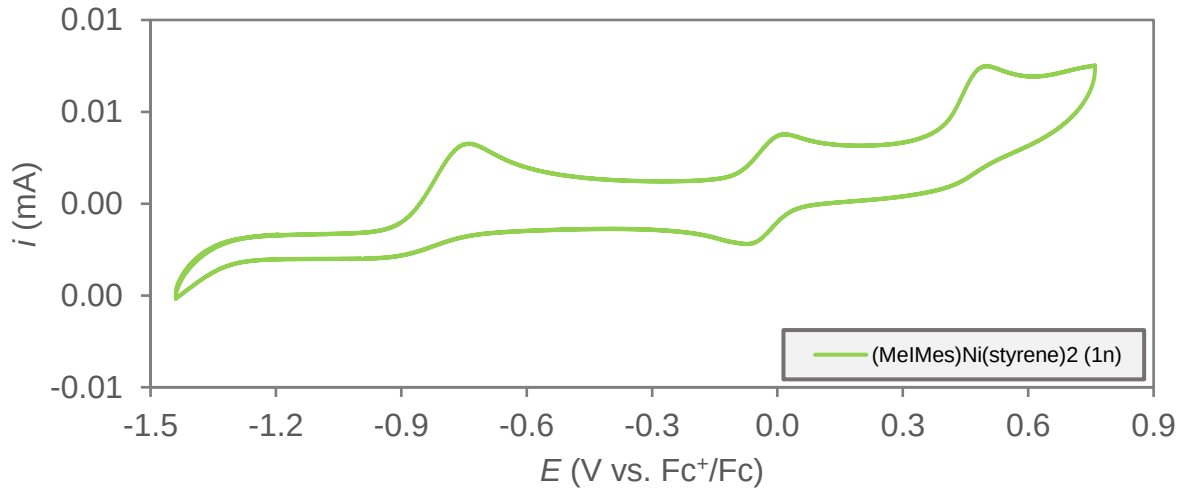

Figure C.42. Cyclic voltammogram of (MeIMes)Ni(styrene)$_2$ (**1n**) in a 0.01 M [NBu$_4$][ClO$_4$] solution in DMF at 100 mV•s$^-$ taken at 273 K. Oxidative scan sweeping from left to right.

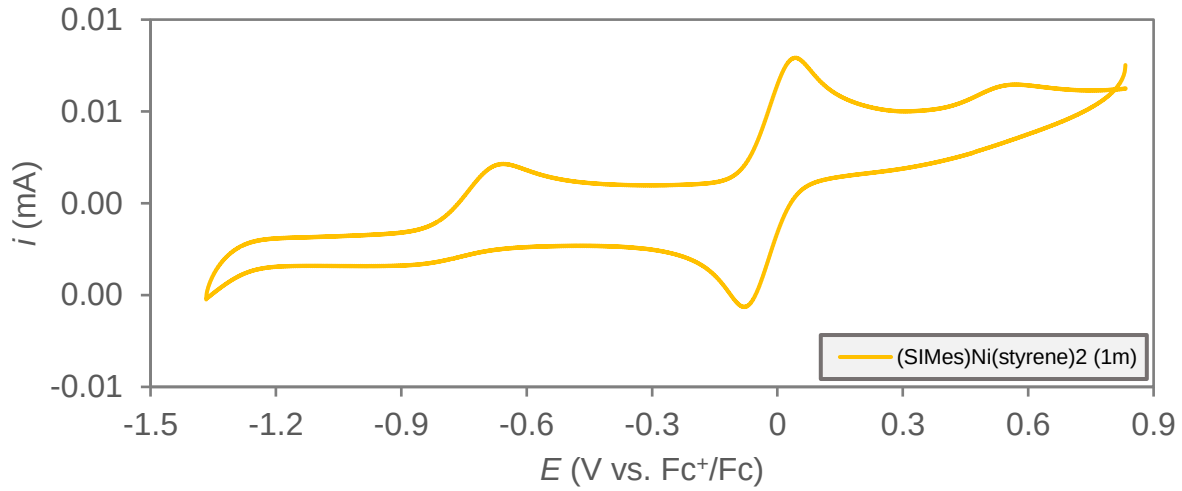

Figure C.43. Cyclic voltammogram of (SIMes)Ni(styrene)$_2$ (**1m**) in a 0.01 M [NBu$_4$][ClO$_4$] solution in DMF at 100 mV•s^{-} taken at 273 K. Oxidative scan sweeping from right to left.

C.1.12. Other Mechanistic Reactions

d. Stoichiometric Experiments Between 1e and 3a Monitored by ^{1}H NMR

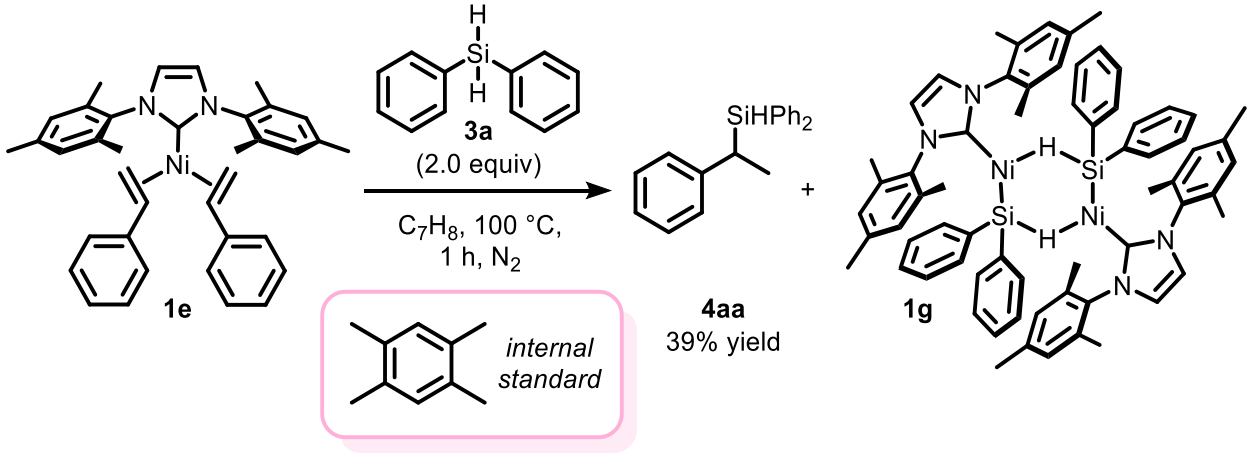

In a nitrogen-filled glovebox, **1e** (4.6 mg, 0.0080 mmol, 1.0 equiv) was weighed out directly into a J-Young NMR tube and solvated in C_7D_8 (0.75 mL, 0.010 M) using a disposable 1-mL syringe. To this solution was added **3a** (3.0 µL, 0.016 mmol, 2.0 equiv) and mesitylene (3.0 µL, 0.022 mmol) using a 10-µL syringe. The NMR tube was sealed, removed from the glovebox, and placed in a pre-heated NMR instrument at 100 °C. Reaction progress was monitored by ^{1}H NMR. Full conversion of **3a** was observed within 5 min. The reaction was further heated at 100 °C for a total 1 h, during which no further change in product distribution was observed. The

reaction was cooled to room temperature and opened to air. A 5-µL aliquot was removed with a 10-µL syringe and filtered into a GC vial through Celite and diluted with hexanes into a GC vial and analyzed by GC to assess the reaction progress and selectivity. The product concentration was determined by relative integration (by GC) of the product peaks against durene, in accordance with calibration curves.

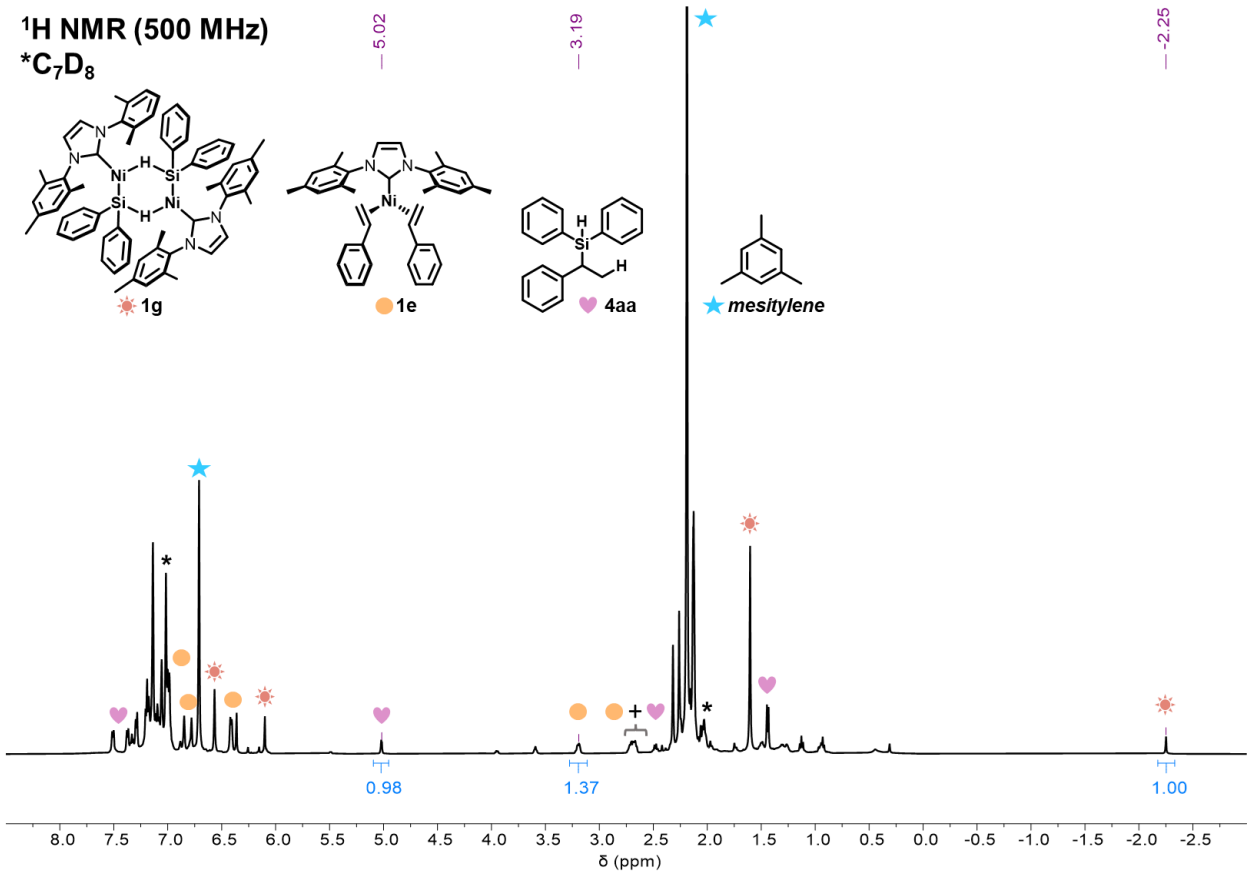

Figure C.44. ^{1}H NMR spectrum of the reaction between **1e** and **3a** after heating at 100 °C for 1 h recorded in C_7D_8 at 25 °C.

A distribution of **1e**, **1g**, and **4aa** were observed by ^{1}H NMR. Ethylbenzene was also observed by GC (which could be a product of hydrogenation and would account for the H mass balance); however, the peaks corresponding to ethylbenzene are not visible by ^{1}H NMR. 39% of the pre-coordinated styrene on **1e** reacted to form **4aa** determined by GC using mesitylene as an internal standard. Approximately a 2.0:1.4:1.0 (**4aa**:**1e**:**1g**) ratio was found by integrating the corresponding peaks at 5.02 ppm, 3.19 ppm, and -2.25 ppm, respectively.

C.1.12. Crystallographic data for 1g

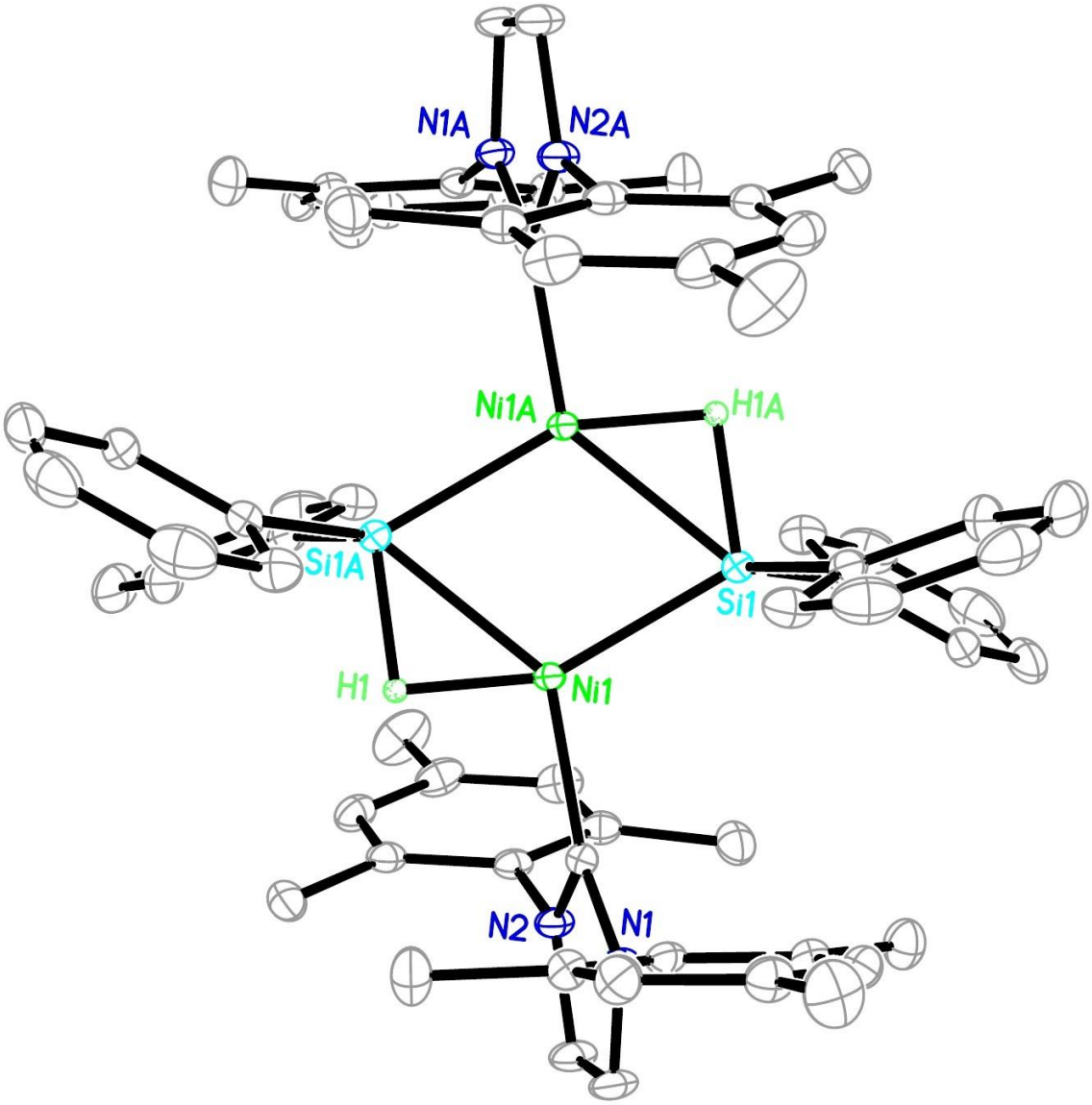

Figure C.45. Molecular structure of (IMes)Ni(μ-H–$SiPh_2$)$_2$Ni(IMes) (**1g**). Hydrogen atoms except for Ni–H–Si are omitted for clarity.

Diffraction intensities for **1g** were collected at 173 K on a Bruker Apex2 CCD DUO diffractometer using MoKα radiation, ƛ = 0.71073 Å. Space group was determined based on systematic absences. Absorption correction was applied by SADABS.[288] Structure was solved by direct methods and Fourier techniques and refined on F^2 using full matrix least-squares procedures. All non-H atoms were refined with anisotropic thermal parameters. All H atoms were found on the residual density maps and refined with isotropic thermal parameters except those in the terminal Me groups. The H atoms in these Me groups were treated in calculated positions in a rigid

group model but with ability for rotation of these–CH_3 groups around the corresponding C-C bonds (HFIX 138). All calculations were performed by the Bruker SHELXL-2014/7 package.[289]

Crystallographic Data for **1g**: $C_{66}H_{70}N_4Ni_2Si_2$, M = 1092.86, 0.16 x 0.14 x 0.14 mm, T = 173(2) K, Monolinic, space group $P2_1/c$, a = 13.1040(7) Å, b = 18.5796(10) Å, c = 13.4685(7) Å, β = 118.222(1)°, V = 2889.3(3) Å^3, Z = 2, Dc = 1.256 Mg/m^3, μ(Mo) = 0.737 mm^{-1}, F(000) = 1156, $2\theta_{max}$ = 56.58°, 24301 reflections, 7087 independent reflections [R_{int} = 0.0331], R1 = 0.0309, wR2 = 0.0772 and GOF = 1.029 for 7087 reflections (414 parameters) with I>2σ(I), R1 = 0.0420, wR2 = 0.0824 and GOF = 1.029 for all reflections, max/min residual electron density +0.381/-0.270 eÅ^{-3}.

C.1.13. NMR and IR Spectra

b. Nickel Complexes

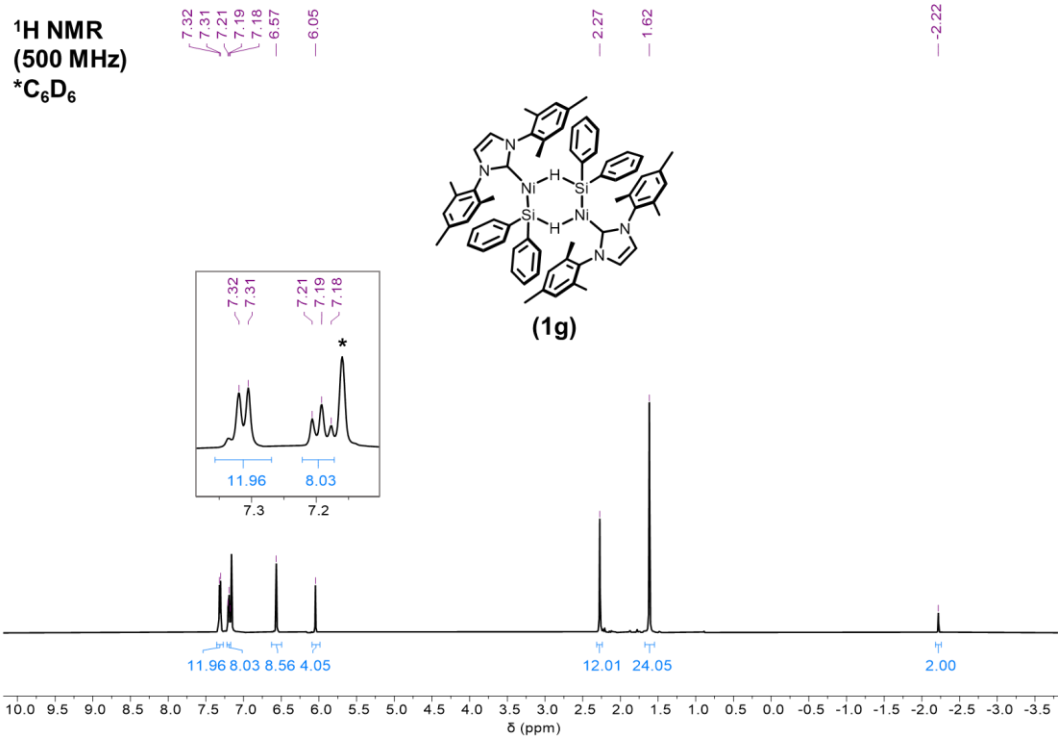

Figure C.46. ^{1}H NMR spectrum of (IMes)Ni(μ-H–$SiPh_2$)$_2$Ni(IMes) (**1g**) recorded in C_6D_6 at 298 K.

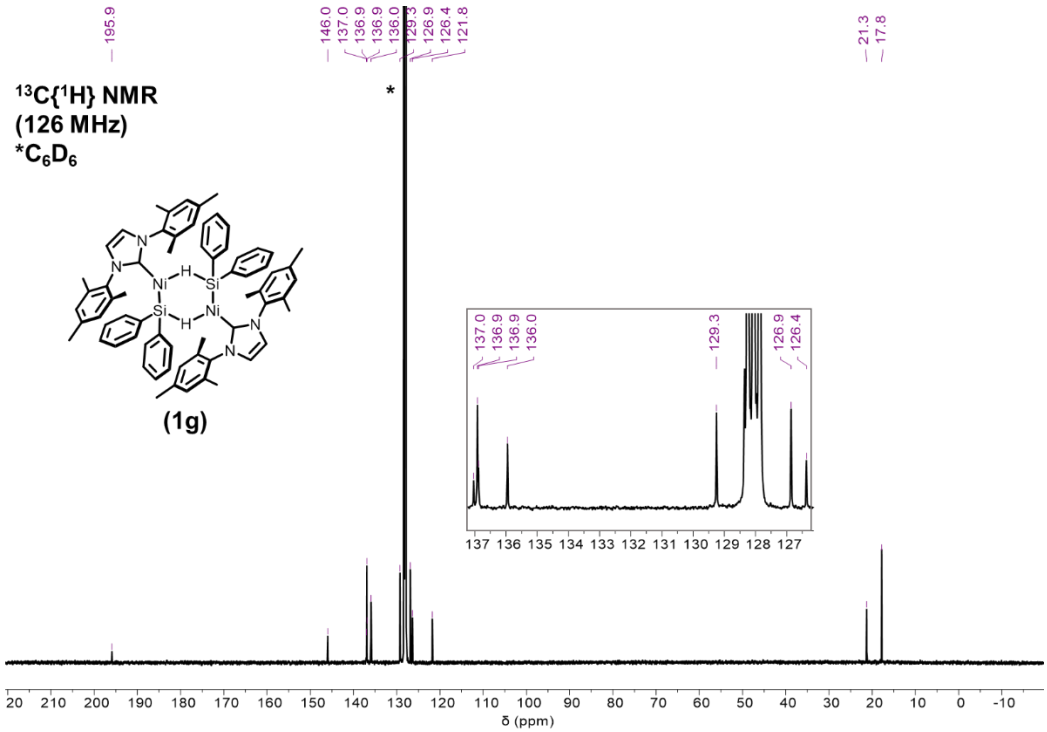

Figure C.47. $^{13}C\{^{1}H\}$ NMR spectrum of (IMes)Ni(μ-H–$SiPh_2$)$_2$Ni(IMes) (**1g**) recorded in C_6D_6 at 298 K.

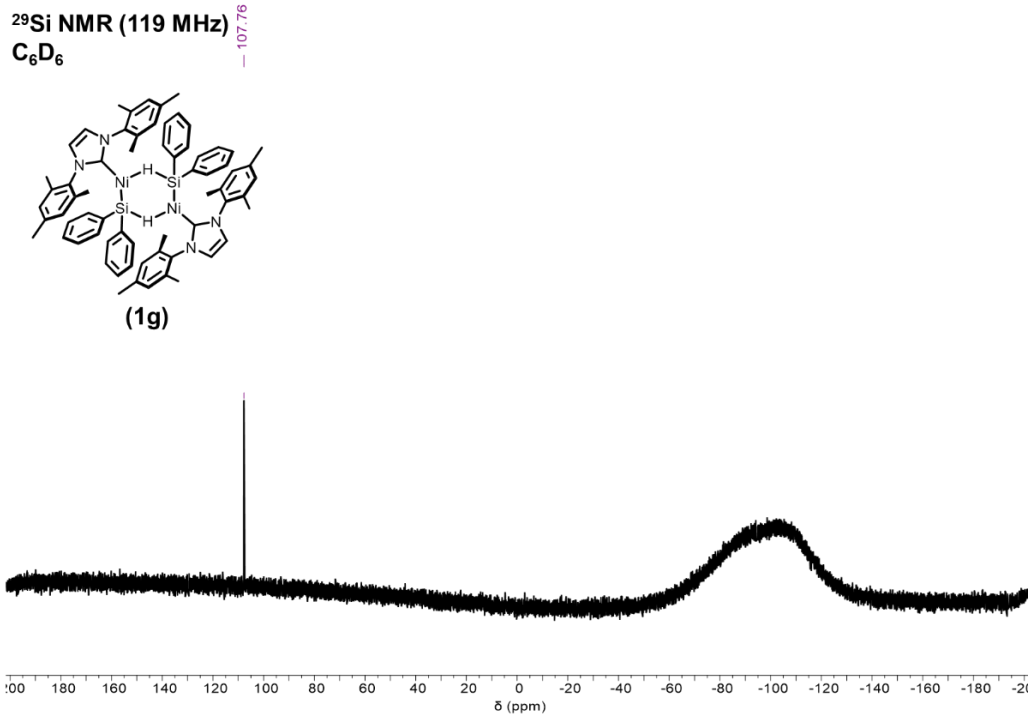

Figure C.48. ^{29}Si NMR spectrum of (IMes)Ni(μ-H–$SiPh_2$)$_2$Ni(IMes) (**1g**) recorded in C_6D_6 at 298 K.

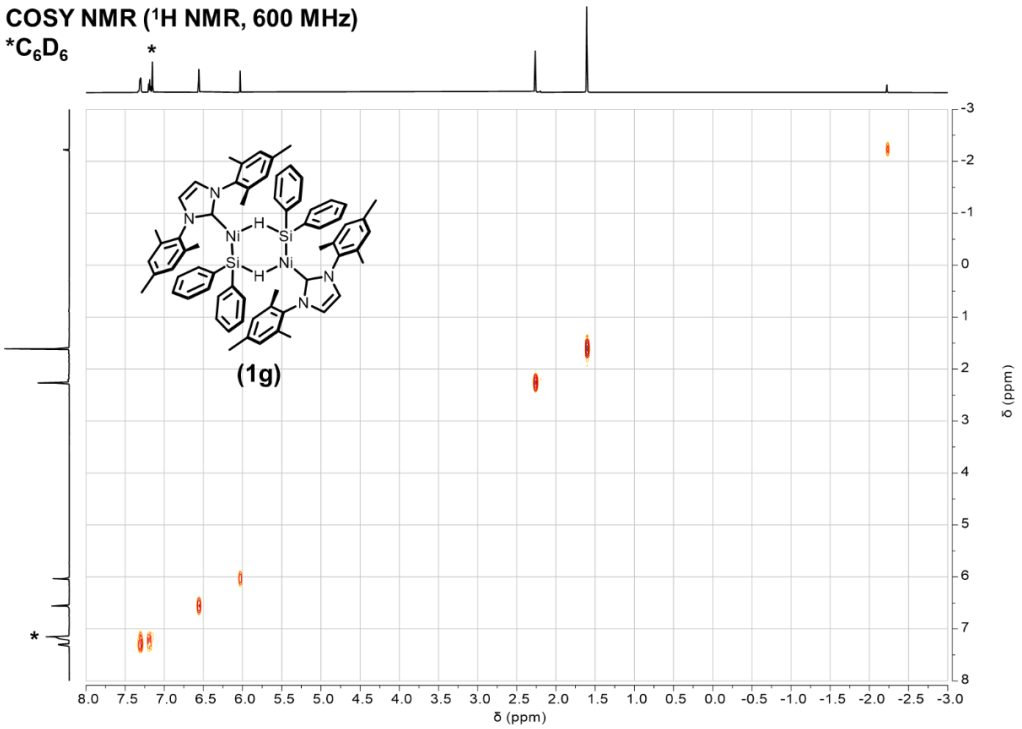

Figure C.49. COSY NMR spectrum of (IMes)Ni(μ-H–$SiPh_2$)$_2$Ni(IMes) (**1g**) recorded in C_6D_6 at 298 K.

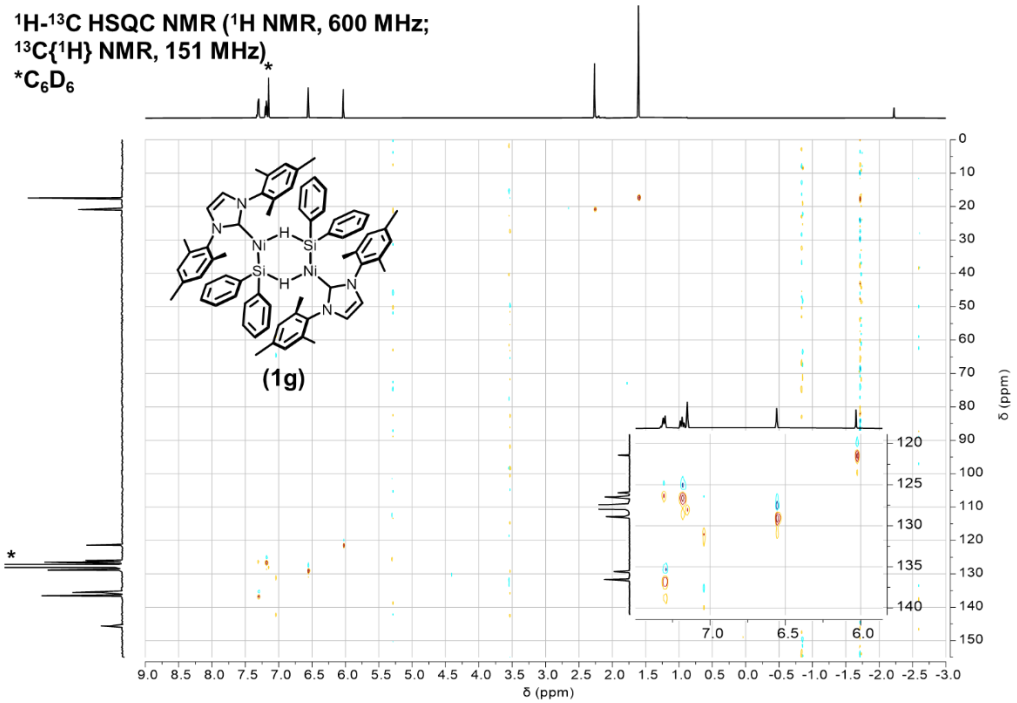

Figure C.50. HSQC NMR spectrum of (IMes)Ni(μ-H–$SiPh_2$)$_2$Ni(IMes) (**1g**) recorded in C_6D_6 at 298 K.

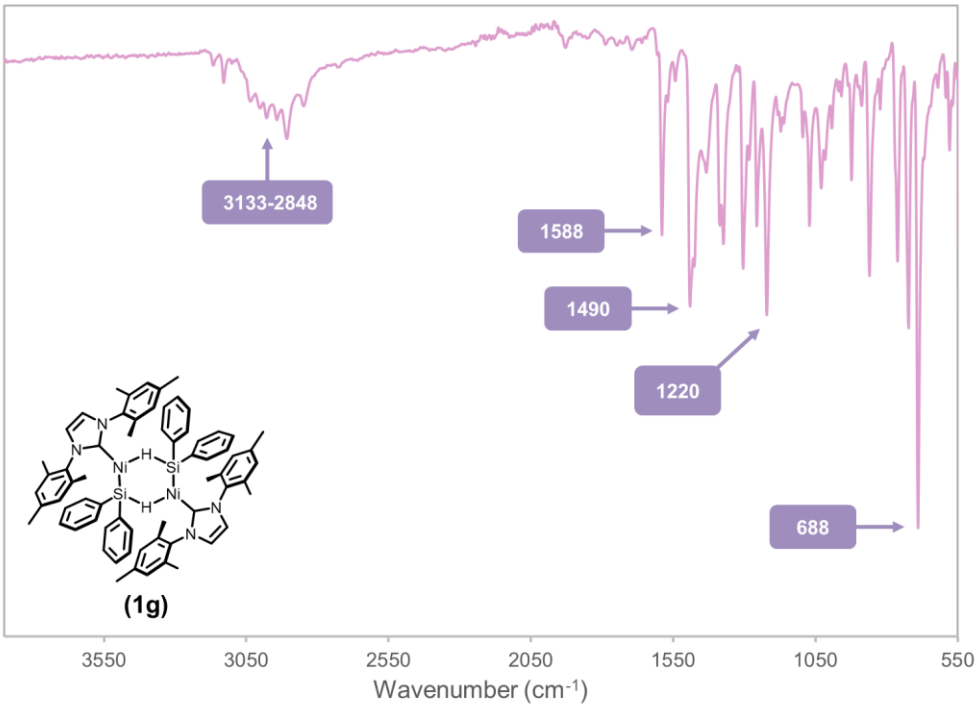

Figure C.51. IR spectrum of (IMes)Ni(μ-H–$SiPh_2$)$_2$Ni(IMes) (**1g**) recorded as a KBr pellet at 298 K.

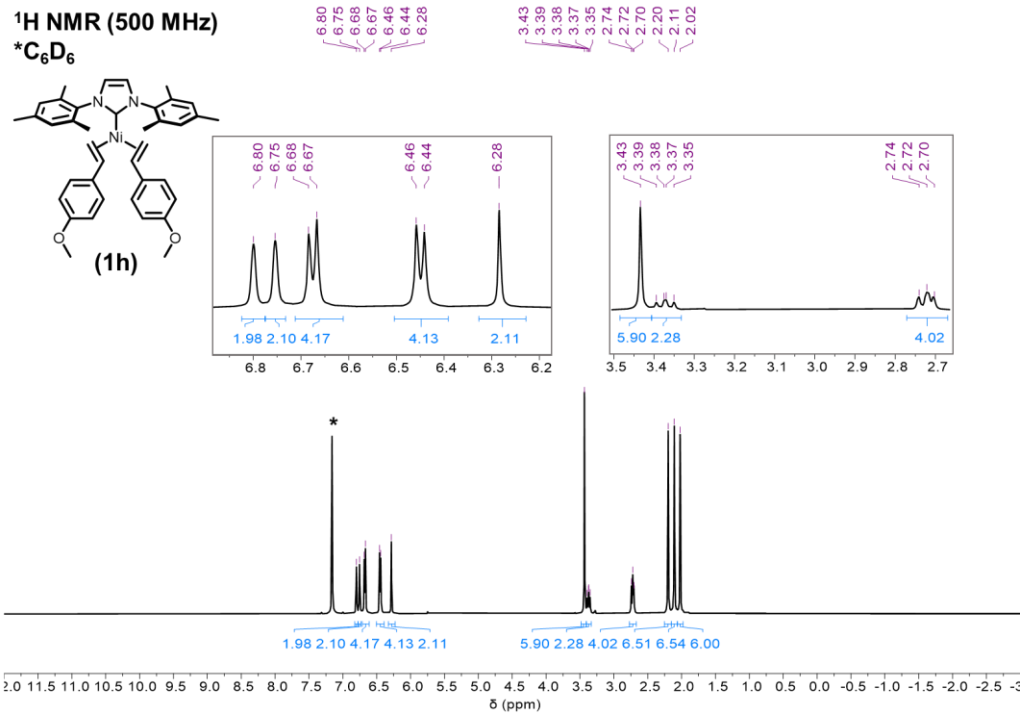

Figure C.52. ^{1}H NMR spectrum of (4-methoxystyrene)$_2$Ni(IMes) (**1h**) recorded in C_6D_6 at 298 K.

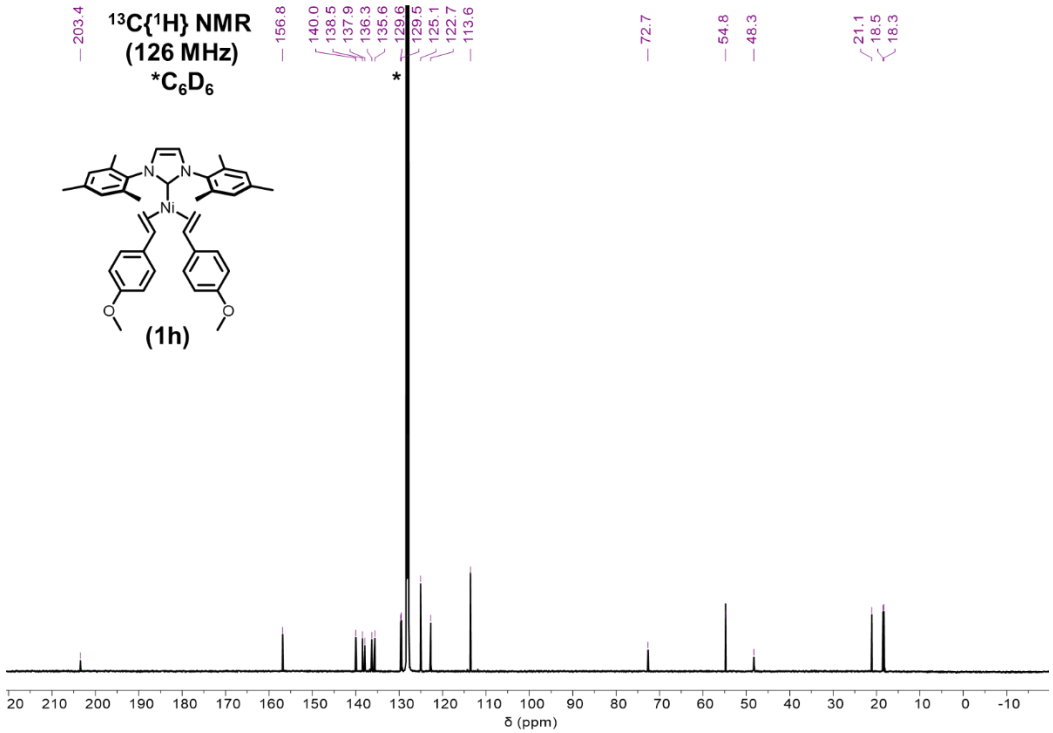

Figure C.53. $^{13}C\{^{1}H\}$ NMR spectrum of (4-methoxystyrene)$_2$Ni(IMes) (**1h**) recorded in C_6D_6 at 298 K.

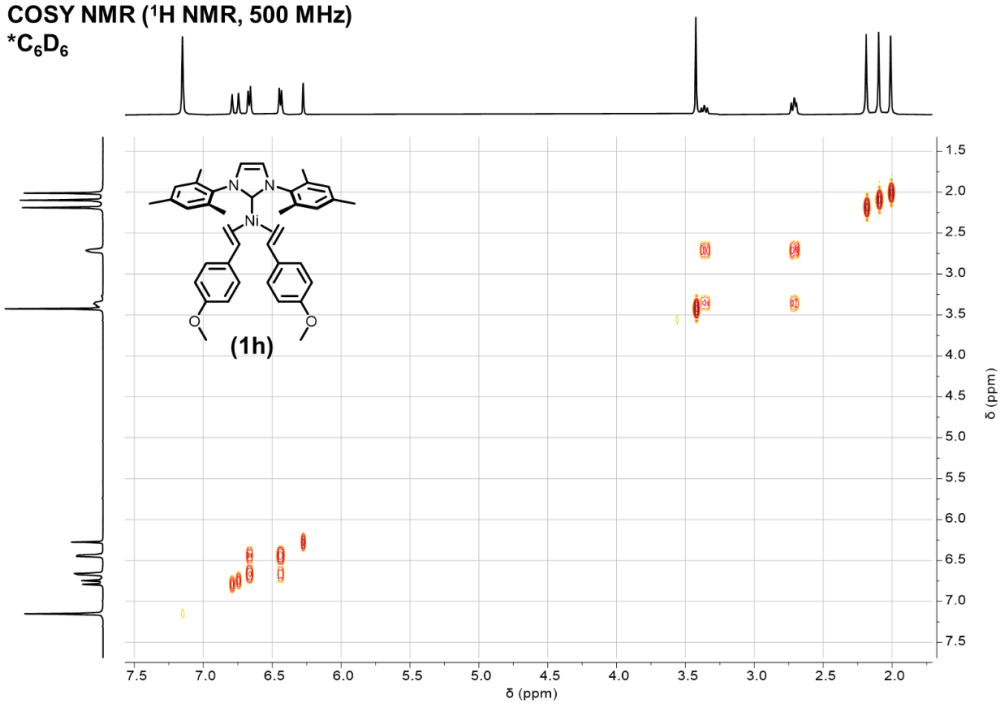

Figure C.54. COSY NMR spectrum of (4-methoxystyrene)$_2$Ni(IMes) (**1h**) recorded in C_6D_6 at 298 K.

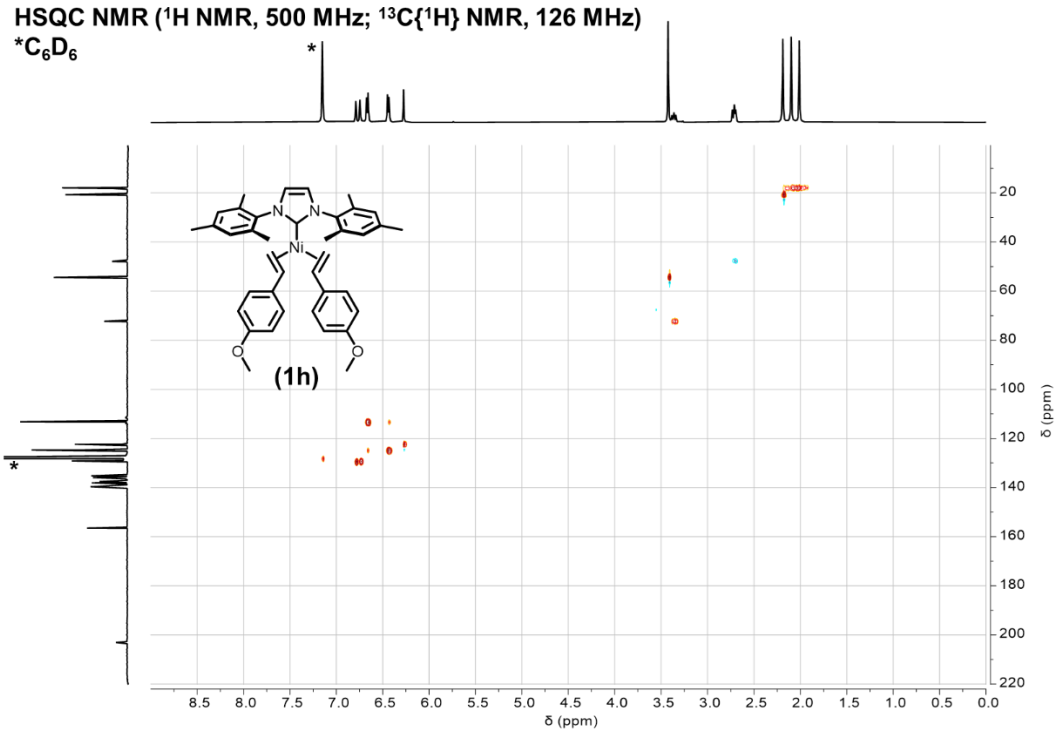

Figure C.55. HSQC NMR spectrum of (4-methoxystyrene)$_2$Ni(IMes) (**1h**) recorded in C_6D_6 at 298 K.

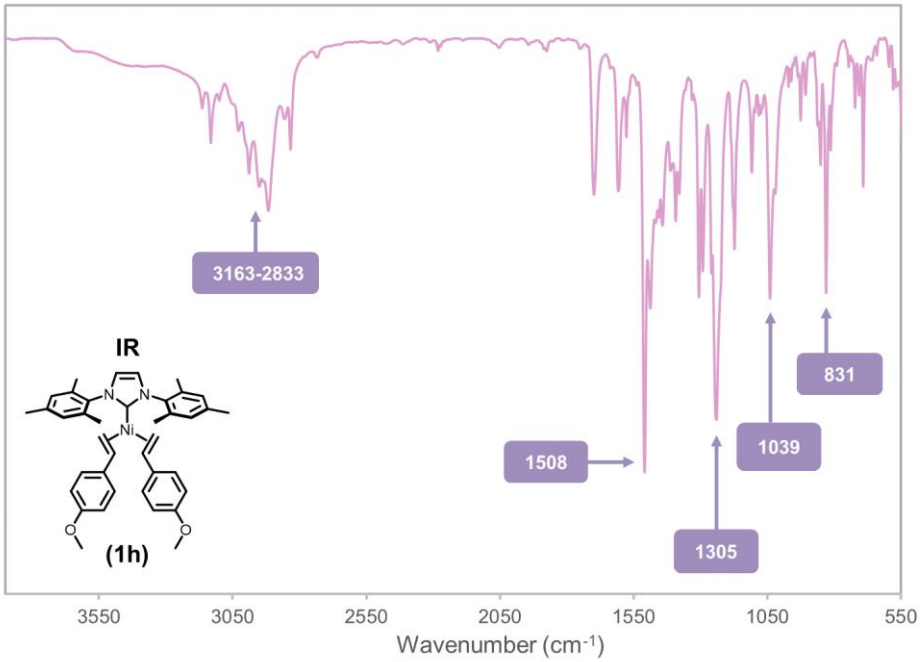

Figure C.56. IR spectrum of (4-methoxystyrene)$_2$Ni(IMes) (**1h**) recorded as a KBr pellet at 298 K.

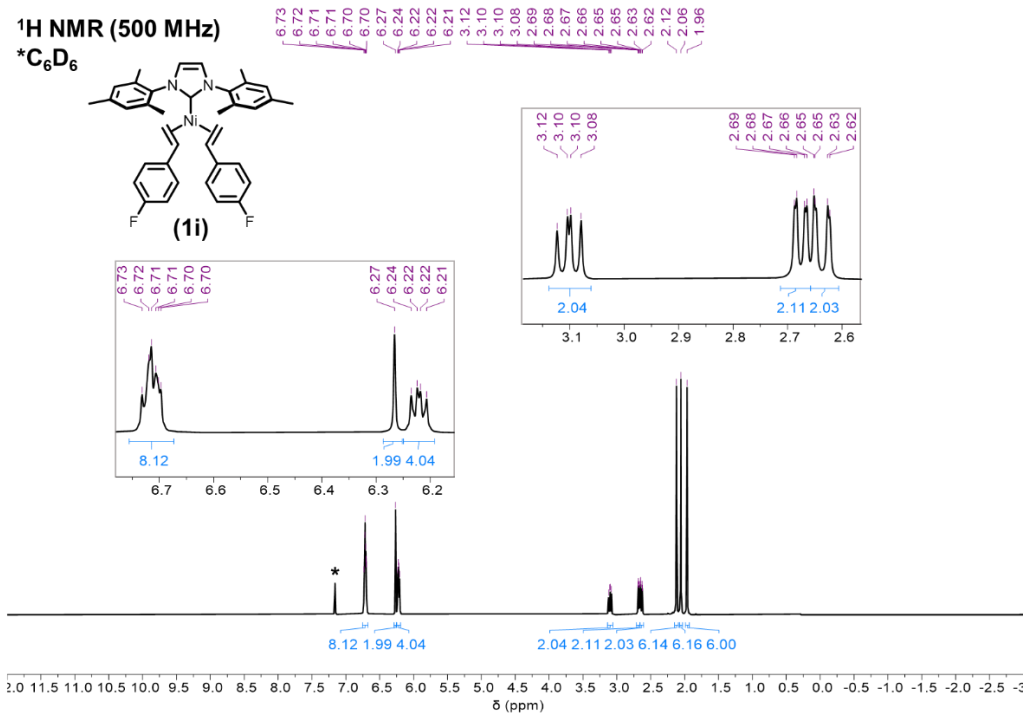

Figure C.57. ^{1}H NMR spectrum of (4-fluorostyrene)$_2$Ni(IMes) (**1i**) recorded in C_6D_6 at 298 K.

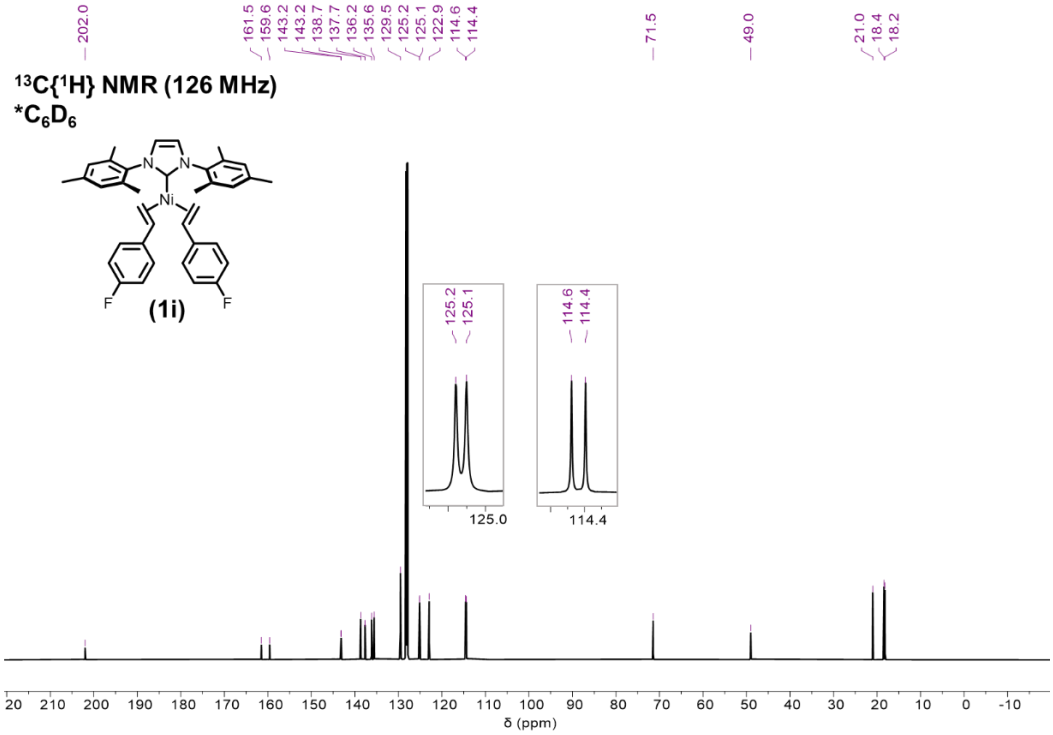

Figure C.58. $^{13}C\{^{1}H\}$ NMR spectrum of (4-fluorostyrene)$_2$Ni(IMes) (**1i**) recorded in C_6D_6 at 298 K.

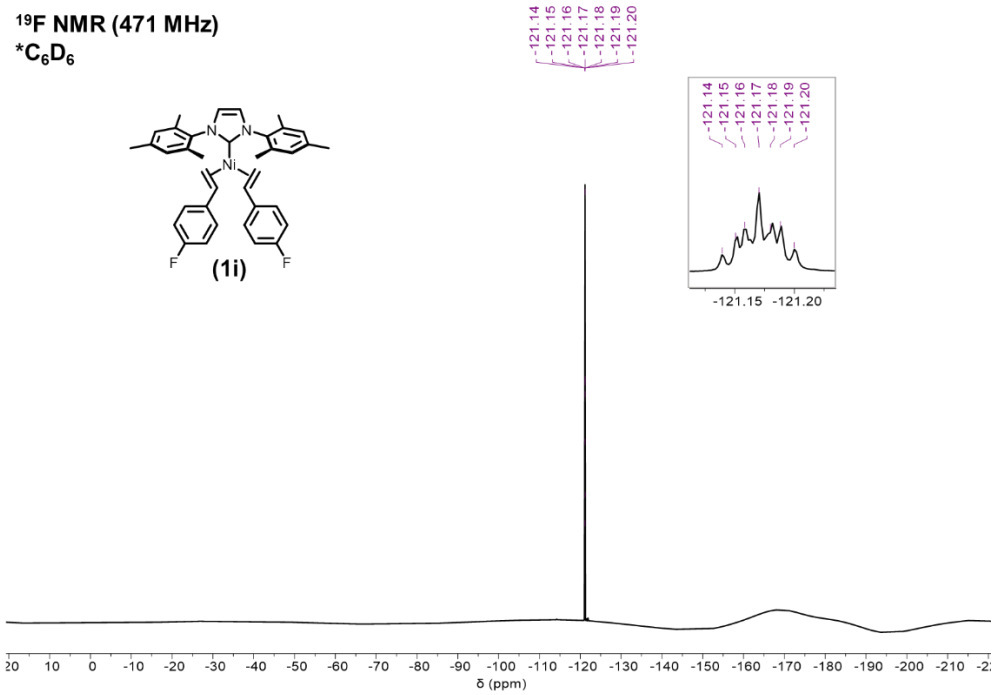

Figure C.59. ^{19}F NMR spectrum of (4-fluorostyrene)$_2$Ni(IMes) (**1i**) recorded in C_6D_6 at 298 K.

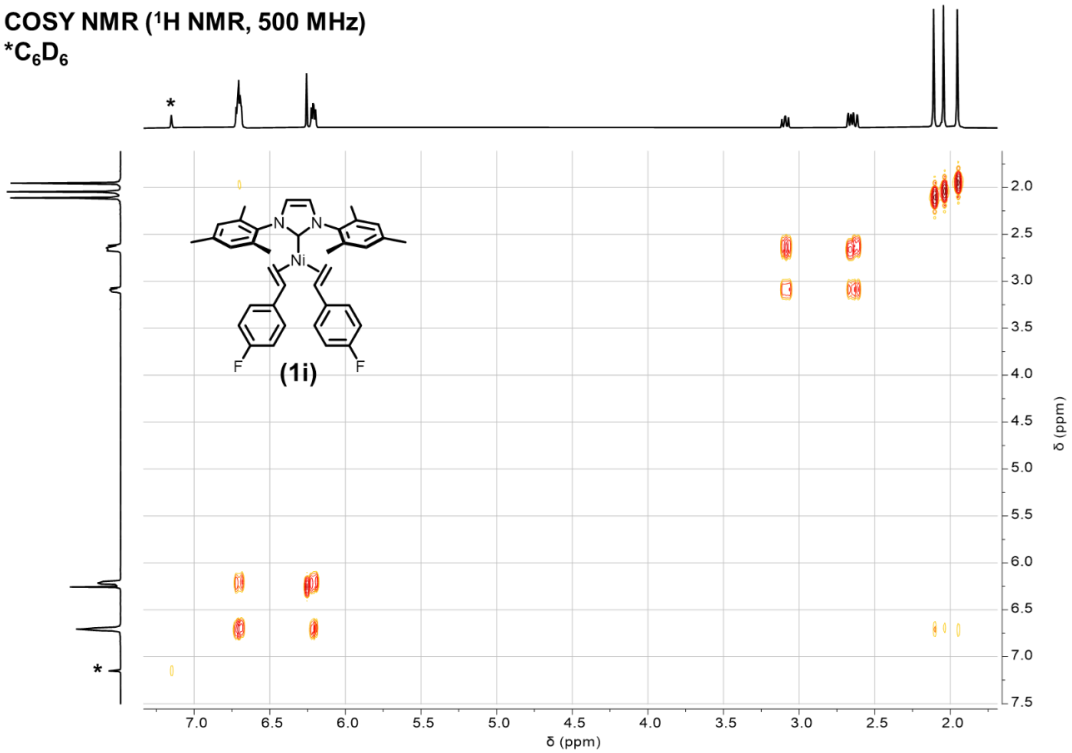

Figure C.60. COSY NMR spectrum of (4-fluorostyrene)$_2$Ni(IMes) (**1i**) recorded in C_6D_6 at 298 K.

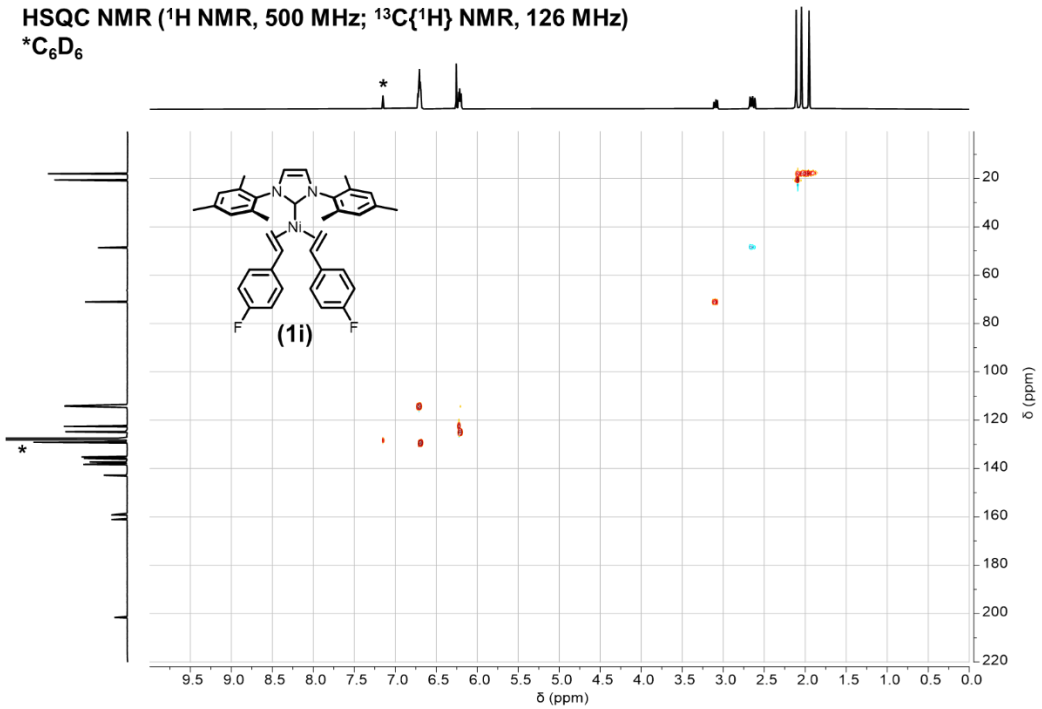

Figure C.61. HSQC NMR spectrum of (4-fluorostyrene)$_2$Ni(IMes) (**1i**) recorded in C_6D_6 at 298 K.

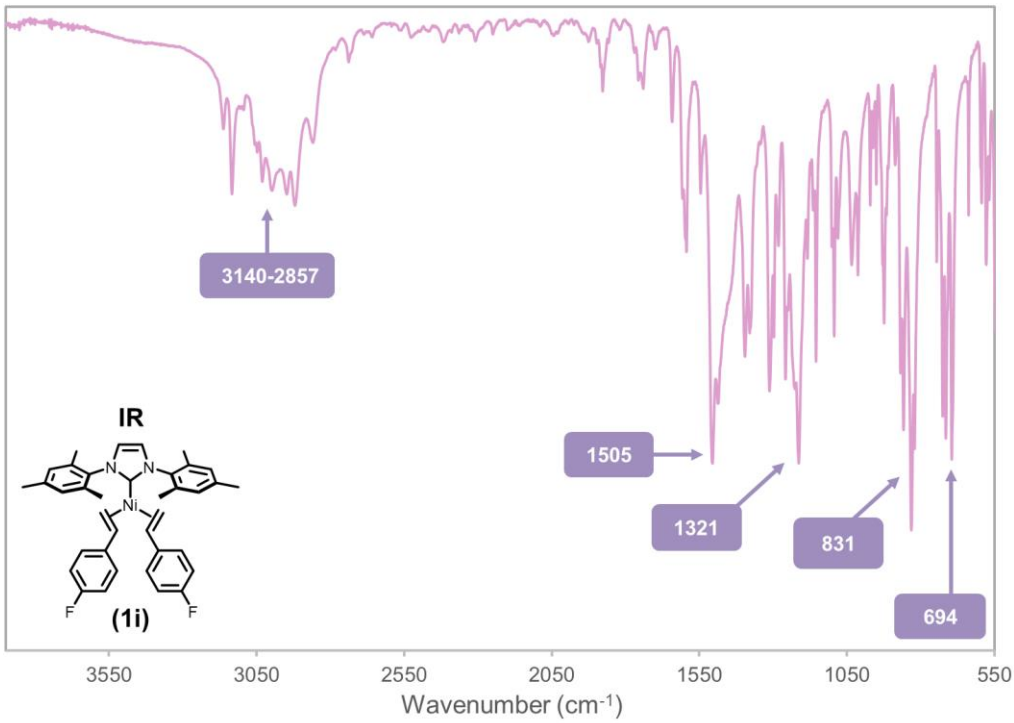

Figure C.62. IR spectrum of (4-fluorostyrene)$_2$Ni(IMes) (**1i**) recorded as a KBr pellet at 298 K.

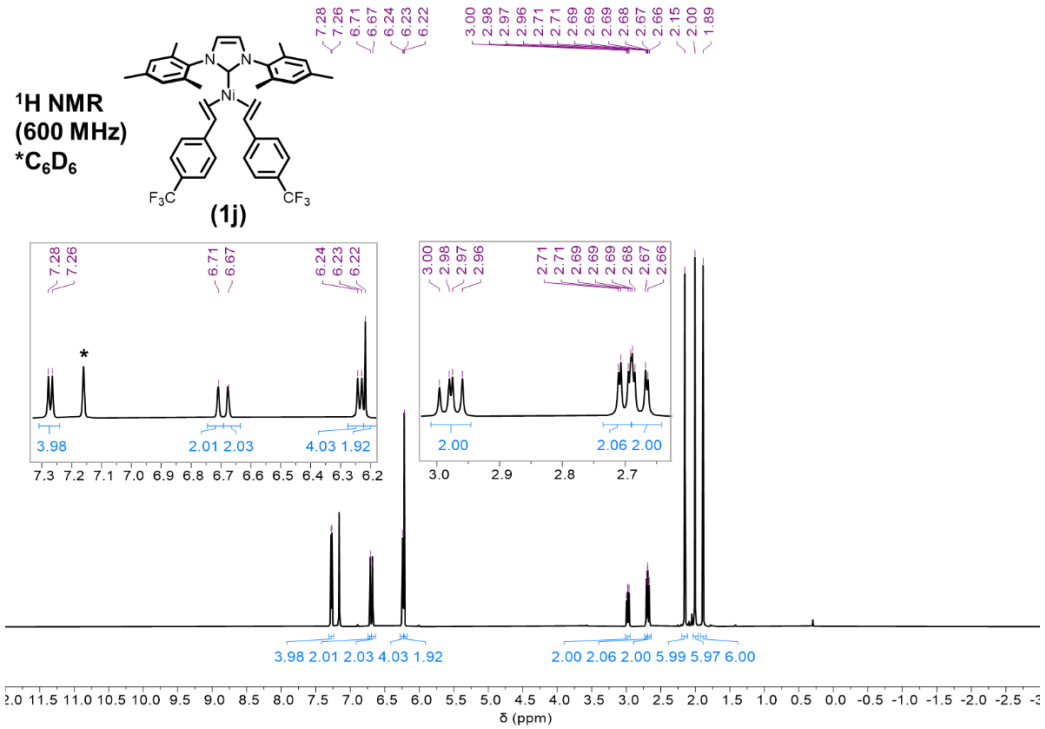

Figure C.63. ^{1}H NMR spectrum of (4-trifluoromethylstyrene)$_2$Ni(IMes) (**1j**) recorded in C_6D_6 at 298 K.

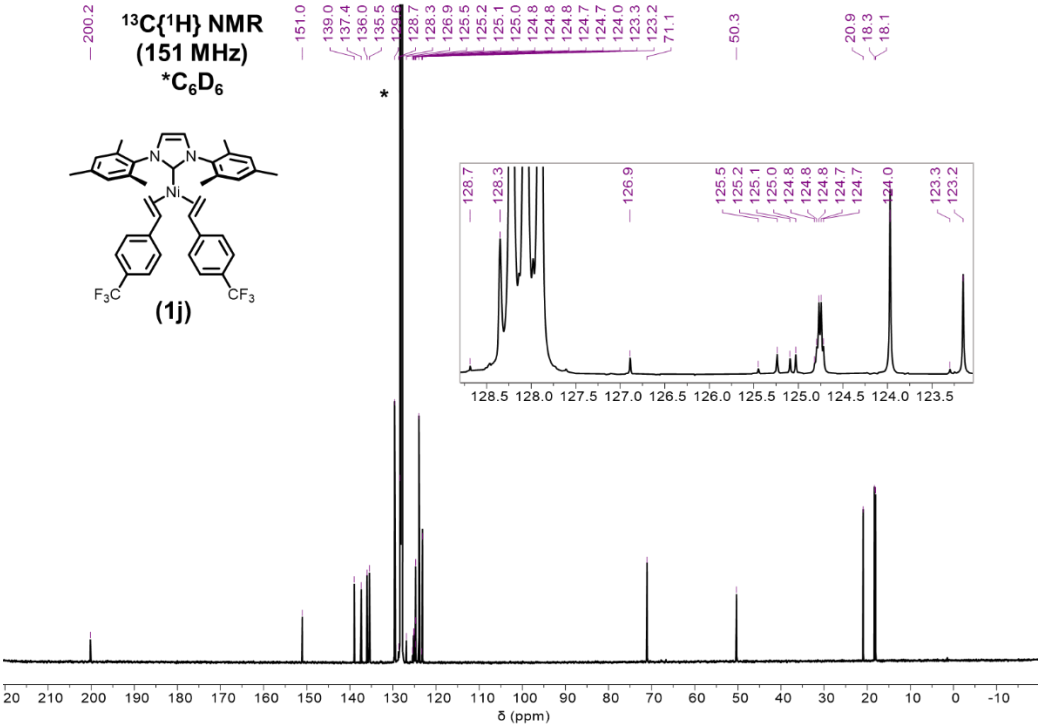

Figure C.64. ^{13}C{^{1}H} NMR spectrum of (4-trifluoromethylstyrene)$_2$Ni(IMes) (**1j**) recorded in C_6D_6 at 298 K.

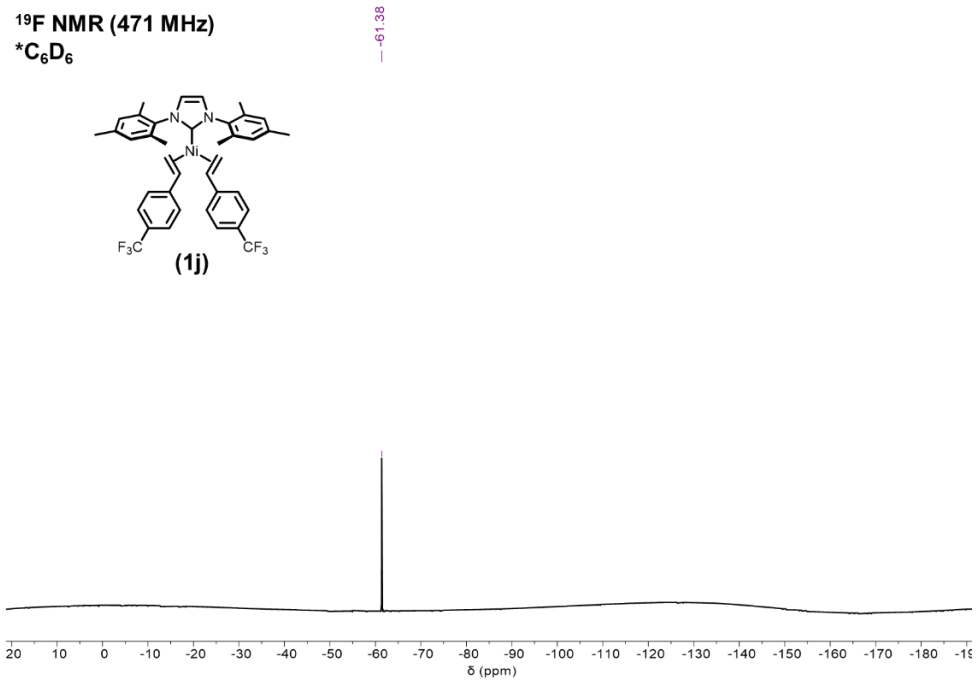

Figure C.65. ^{19}F NMR spectrum of (4-trifluoromethylstyrene)$_2$Ni(IMes) (**1j**) recorded in C_6D_6 at 298 K.

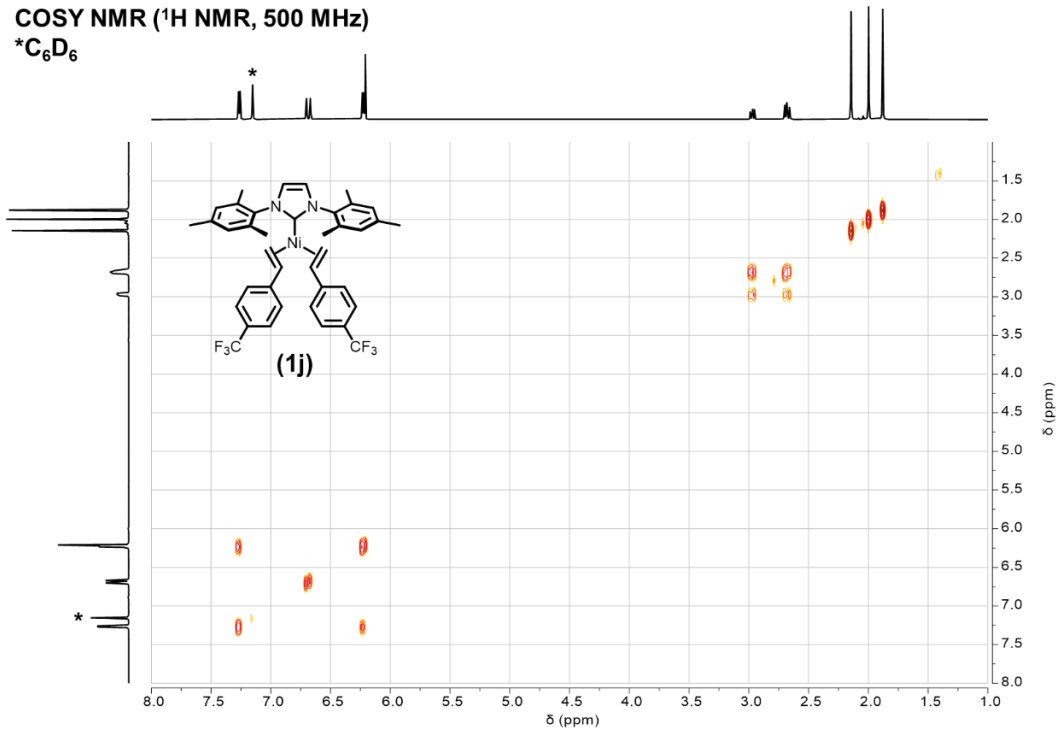

Figure C.66. COSY NMR spectrum of (4-trifluoromethylstyrene)$_2$Ni(IMes) (**1j**) recorded in C_6D_6 at 298 K.

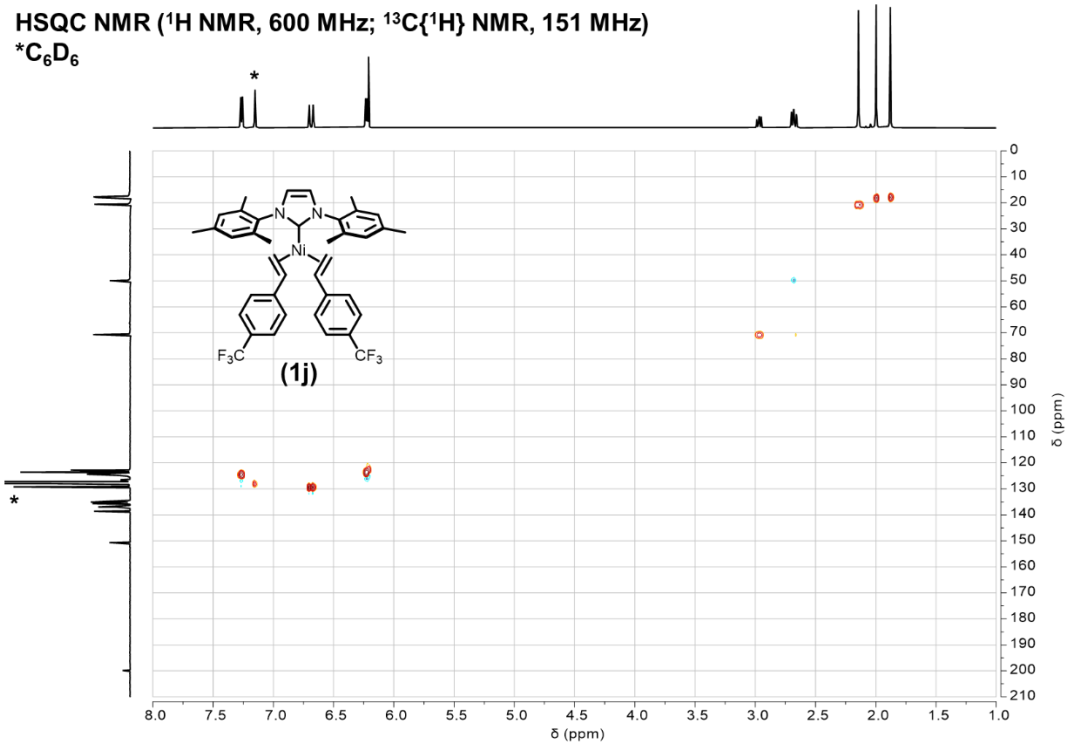

Figure C.67. HSQC NMR spectrum of (4-trifluoromethylstyrene)$_2$Ni(IMes) (**1j**) in C_6D_6 at 298 K.

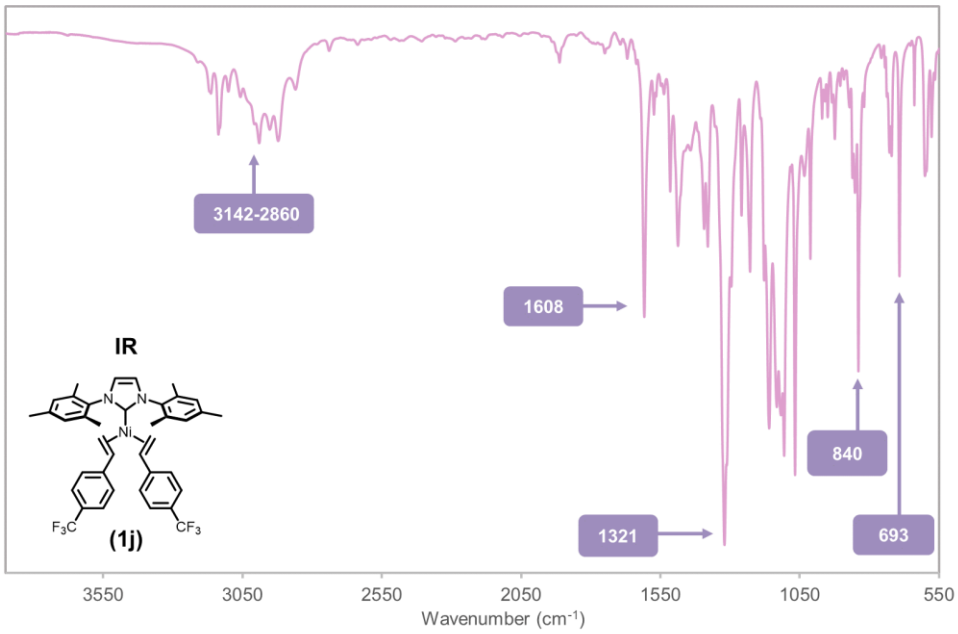

Figure C.68. IR spectrum of (4-trifluoromethylstyrene)$_2$Ni(IMes) (**1j**) recorded as a KBr pellet at 298 K.

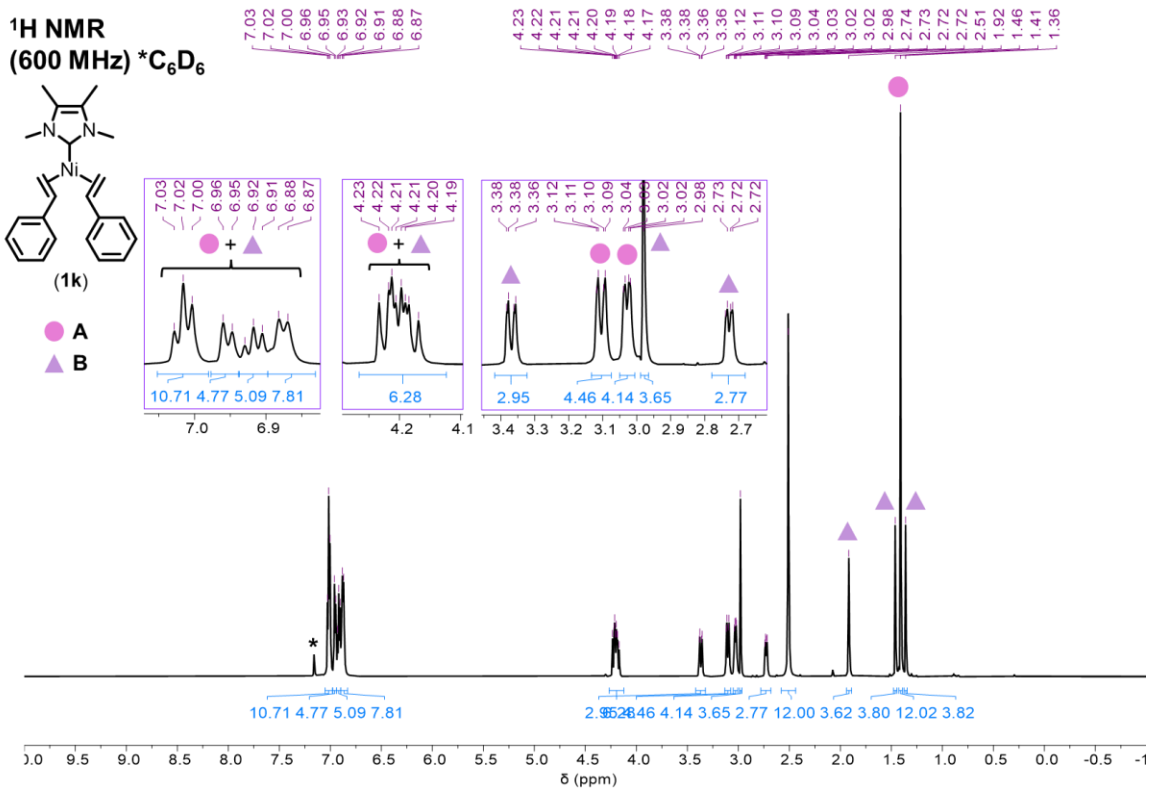

Figure C.69. ^{1}H NMR spectrum of (styrene)$_2$Ni(ITMe) (**1k**) recorded in C_6D_6 at 298.

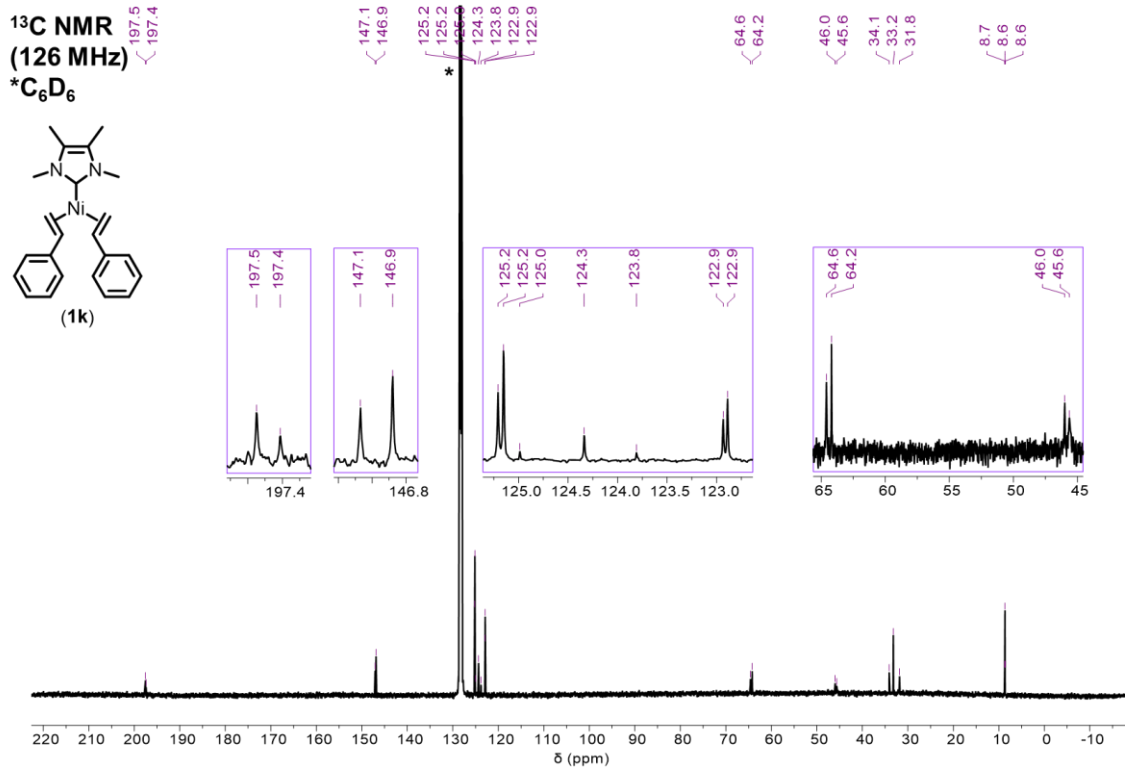

Figure C.70. ^{13}C{^{1}H} NMR spectrum of (styrene)$_2$Ni(ITMe) (**1k**) recorded in C_6D_6 at 298.

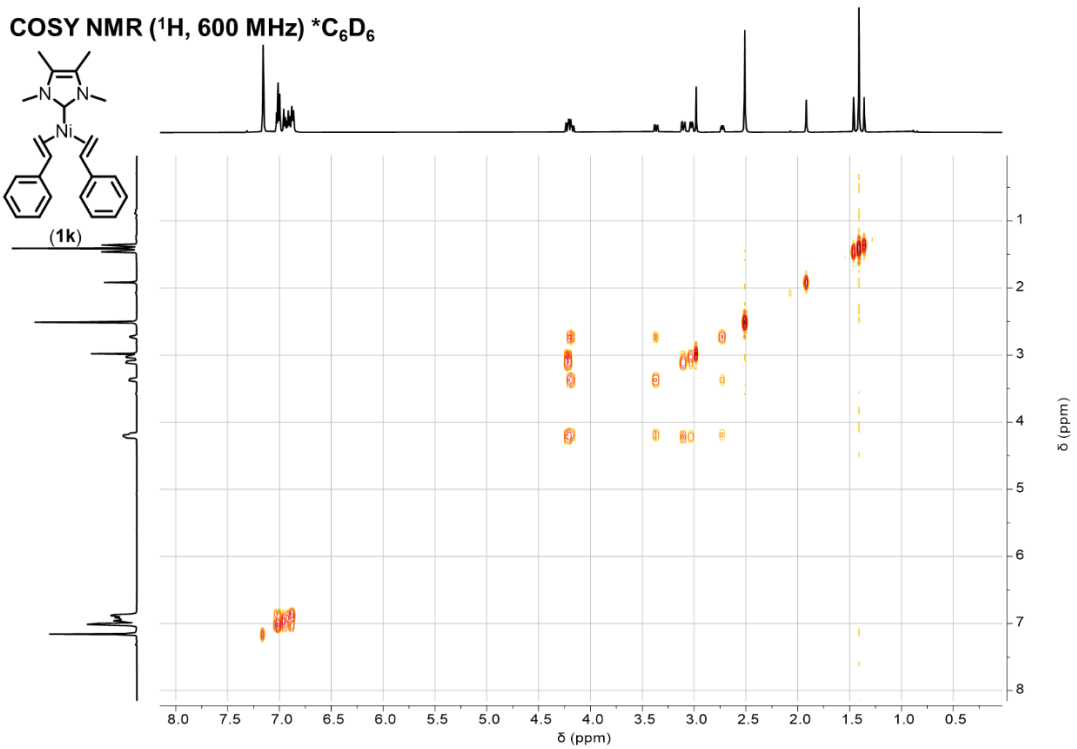

Figure C.71. COSY NMR spectrum of (styrene)$_2$Ni(ITMe) (**1k**) recorded in C_6D_6 at 298.

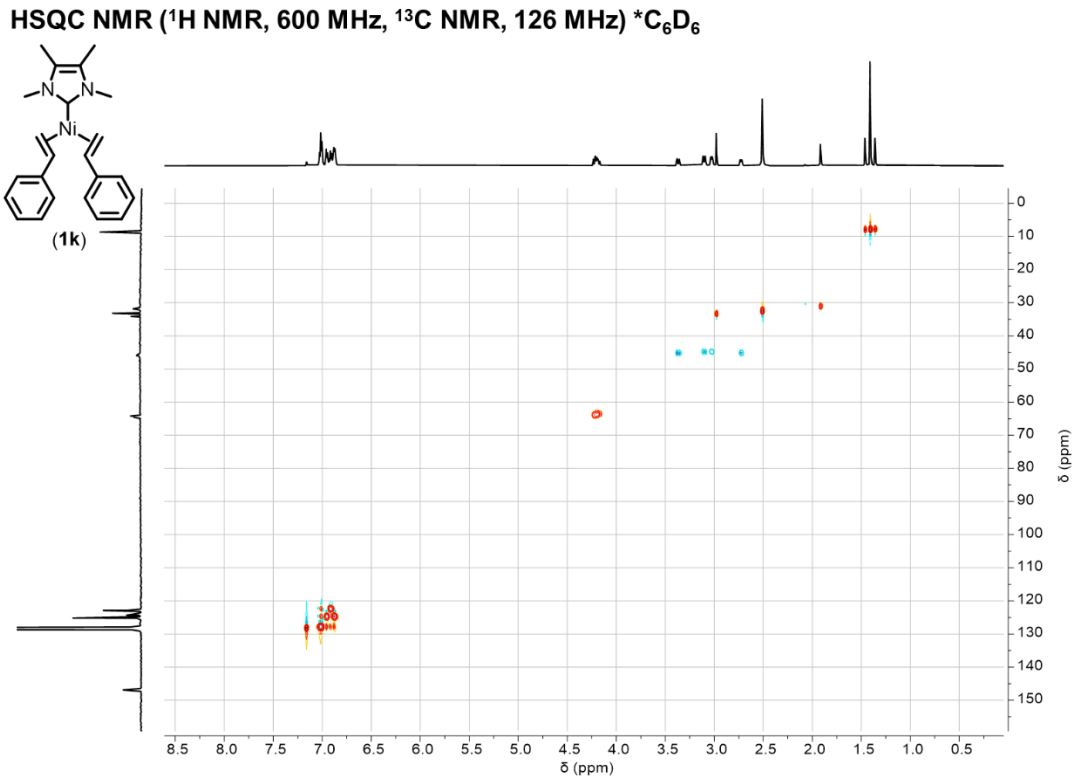

Figure C.72. HSQC NMR spectrum of (styrene)$_2$Ni(ITMe) (**1k**) recorded in C_6D_6 at 298.

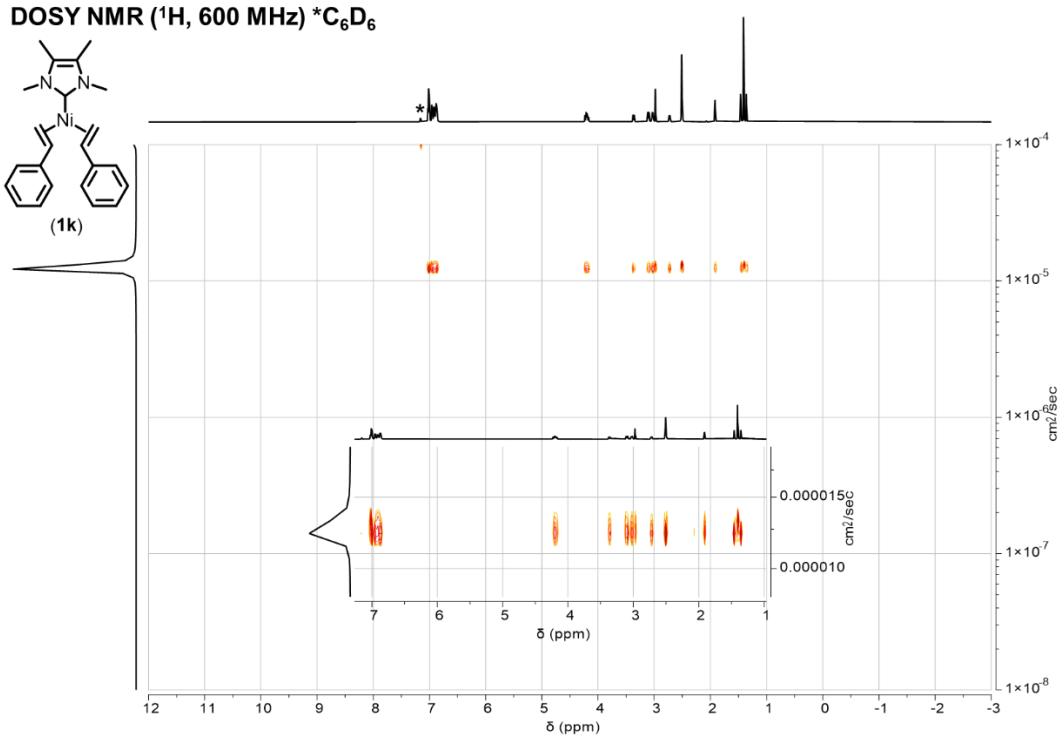

Figure C.73. DOSY NMR spectrum of (styrene)$_2$Ni(ITMe) (**1k**) recorded in C_6D_6 at 298.

APPENDIX D

SUPPLEMENTARY CONTENT FOR CHPATER V

Experimental details

D.1.1. Materials and Methods

All syntheses and manipulations were carried out under nitrogen using standard Schlenk (vacuum 10^{-2} mbar) techniques or in a nitrogen-filled glovebox unless otherwise indicated. All reagents and solvents were used after drying and stored under nitrogen, unless otherwise indicated. Tetrahydrofuran (THF; Fisher Chemical; HPLC grade, unstabilized), hexanes (Fisher Chemical; HPLC grade), and diethyl ether (B&J Brand; HPLC grade, unstabilized) were dispensed under nitrogen from an LC Technology SP-1 solvent system. Benzene (ACS grade) and pentane (HPLC grade) were refluxed overnight with CaH_2 and distilled under nitrogen before use. The dried solvents were thereafter stored on activated 4Å molecular sieves under nitrogen. C_6D_6 and $CDCl_3$ were purchased from Cambridge Isotope Laboratories, degassed by freeze-pump-thaw, and thereafter stored on activated 4Å molecular sieves under nitrogen. All stock solutions were prepared by mass and were dispensed into the reaction vessel by difference from syringe, as detailed in the procedure for each experiment.

ITMe[263], IMes[264], MeIMes[290], MeIPr[290], Ni(COD)(DQ)[291], **1a**[6], and **1b**[21] were synthesized via reported procedures.

D.1.2. General Experimental

Nuclear magnetic resonance (NMR) spectra were collected at room temperature (298 K) unless otherwise stated on a Bruker AV-III HD 600 NMR (600.13 MHz for ^{1}H; 150.90 MHz for 13C; 564.69 MHz for ^{19}F; 119.23 MHz for ^{29}Si; 92.12 MHz for ^{2}H), Bruker Avance-III HD 500 NMR (499.90 MHz for ^{1}H; 126 MHz for ^{13}C; 471 MHz for ^{19}F; 99 MHz for ^{29}Si), or Varian Inova 500 NMR (499.90 MHz for ^{1}H; 126 MHz for ^{13}C; 471 MHz for ^{19}F; 99 MHz for ^{29}Si). ^{1}H and ^{13}C spectra were referenced to the residual solvent peak ($CDCl_3$: ^{1}H δ = 7.26 ppm, ^{13}C δ = 77.16 ppm; C_6D_6: ^{1}H δ = 7.16 ppm, ^{13}C δ = 128.06 ppm, CD_3CN: ^{1}H δ = 1.94 ppm, ^{13}C δ = 1.32 ppm ($NC\mathit{C}D_3$)). Chemical shifts for ^{1}H and ^{13}C spectra are reported in parts per million (ppm, δ) relative to tetramethylsilane at 0.00 ppm. Peaks are characterized as follows: s (singlet), d (doublet), t (triplet),

q (quartet), pent (pentet), hept (heptet), m (multiplet), qd (quartet of doublets), br (broad), app (apparent), and/or ms (multiple signals). Coupling constants, *J*, are reported in Hz.

Infrared (IR) spectroscopy for air-stable organic compounds was performed on an Agilent Nicolet 6700 FT-IR using the ATR sampling technique. IR spectra for air-sensitive nickel complexes were recorded as self-supported pellets diluted with KBr using a Bruker Alpha II FT-IR spectrometer that is housed in a nitrogen-filled glovebox. All bands are reported in wavenumbers (cm^{-1}) and are described as broad (br), strong (s), medium (m), and weak (w).

D.1.3. Monitoring Isomerization by GC

a. Evaluation of NHCs

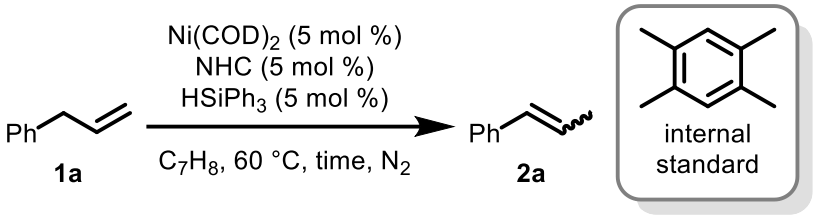

In a nitrogen-filled glovebox, a stock solution of $Ni(COD)_2$ (0.0025 g, 0.0091 mmol, 0.050 equiv added to each vial) and the corresponding NHC (0.0091 mmol, 0.050 equiv added to each vial) was prepared in toluene using volumetric glassware and distributed into a 1-dram vial using a disposable 1-mL syringe while stirring. To this stirring solution was added **1a** (24 µL, 0.18 mmol, 1.0 equiv) using a 50-µL syringe and separate stock solutions of $HSiPh_3$ (0.0024 g, 0.0091 mmol, 0.050 equiv added to each vial) and of durene (0.050 g, 0.037 mmol added to each vial) in toluene were also distributed to each vial using a disposable 1-mL syringe to obtain a total volume of 1.1 mL. The vial was sealed with a septum cap, brought out of the glovebox, and placed onto a preheated vial block at 60 °C. Throughout the course of the reaction, 20 µL aliquots were removed with a 25-µL syringe, filtered into a GC vial through Celite, and diluted with hexanes. The filtrate from the Celite plug was analyzed by GC to assess the reaction progress and selectivity. The product conversion was determined by relative integration (by GC) of the product peaks. All trials were run in duplicate.

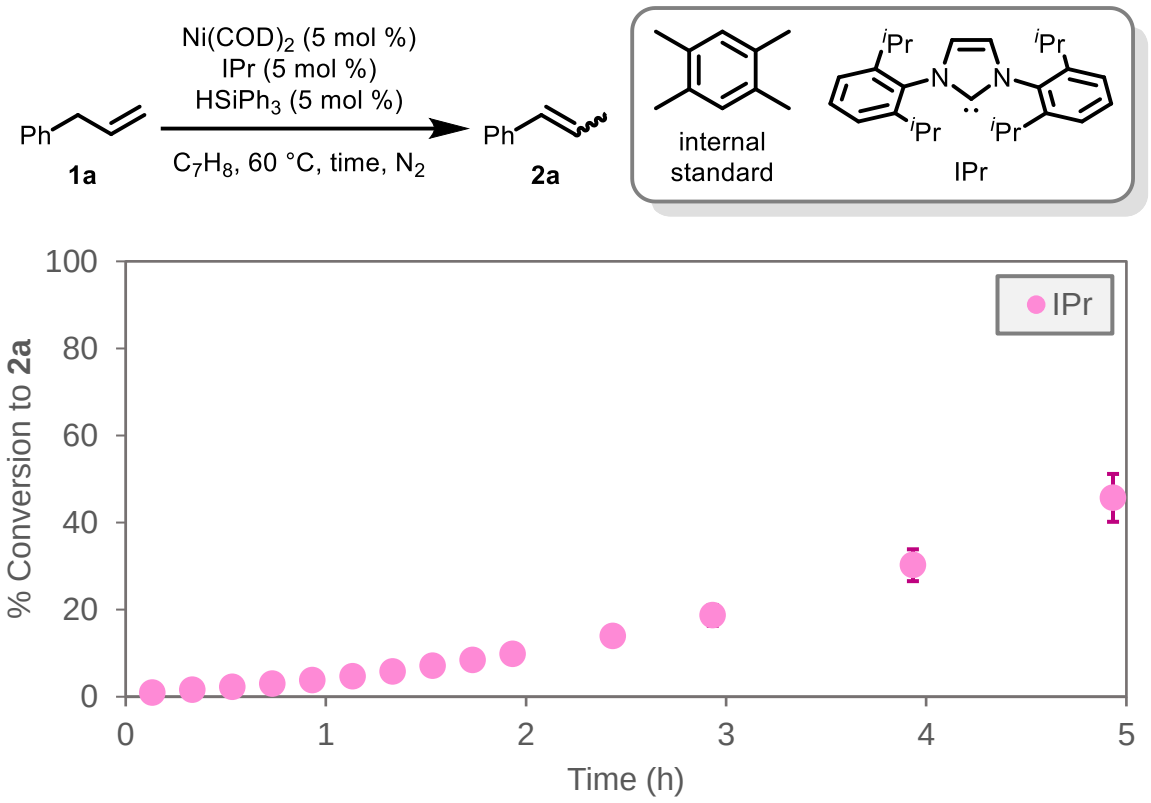

Figure D.1. Full kinetic profile of the formation of **2a** versus time (min) using IPr as the NHC.

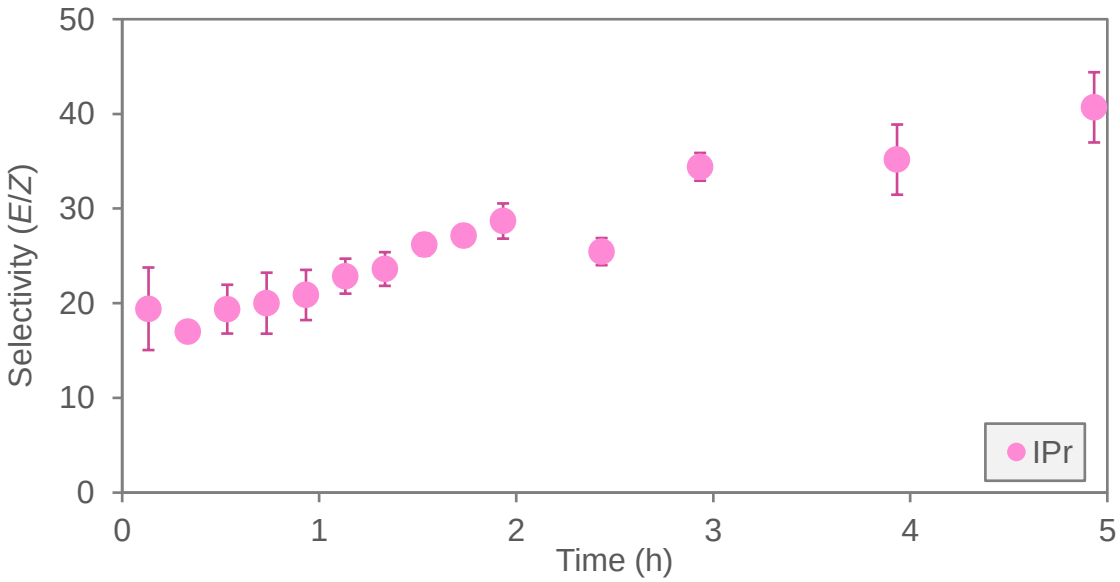

Figure D.2. Full selectivity (*E*/*Z*) profile of the formation of **2a** versus time (min) using IPr as the NHC.

Table D.1. % Conversion to **2a** and selectivity (*E:Z*) of **2a** formed using IPr as the NHC.

Time (h)	% Conversion to **2a**	Selectivity (*E*:*Z*) (std error)
0.13	0.88±0.08	19:1 (4)
0.33	1.59±0.07	17.0:1 (0.1)
0.53	2.2±0.2	19:1 (3)
0.73	3.0±0.3	20:1 (3)
0.93	3.8±0.5	21:1 (3)
1.13	4.7±0.7	23:1 (2)
1.33	5.8±0.9	24:1 (2)
1.53	7±1	26:1 (1)
1.73	8±1	27:1 (1)
1.93	10±1	29:1 (2)
2.43	14±2	25:1 (1)
2.93	19±2	34:1 (1)
3.93	30±4	35:1 (3)
4.93	46±6	41:1 (3)

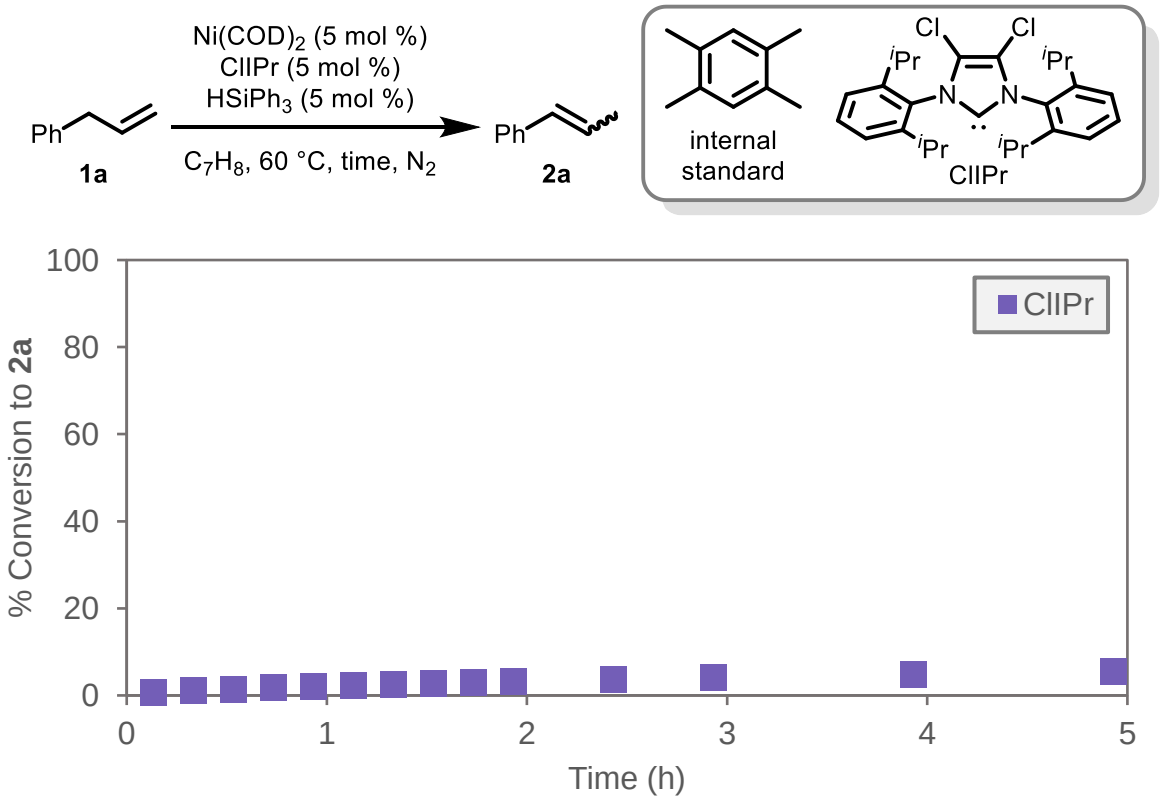

Figure D.3. Full kinetic profile of the formation of **2a** versus time (min) using ClIPr as the NHC.

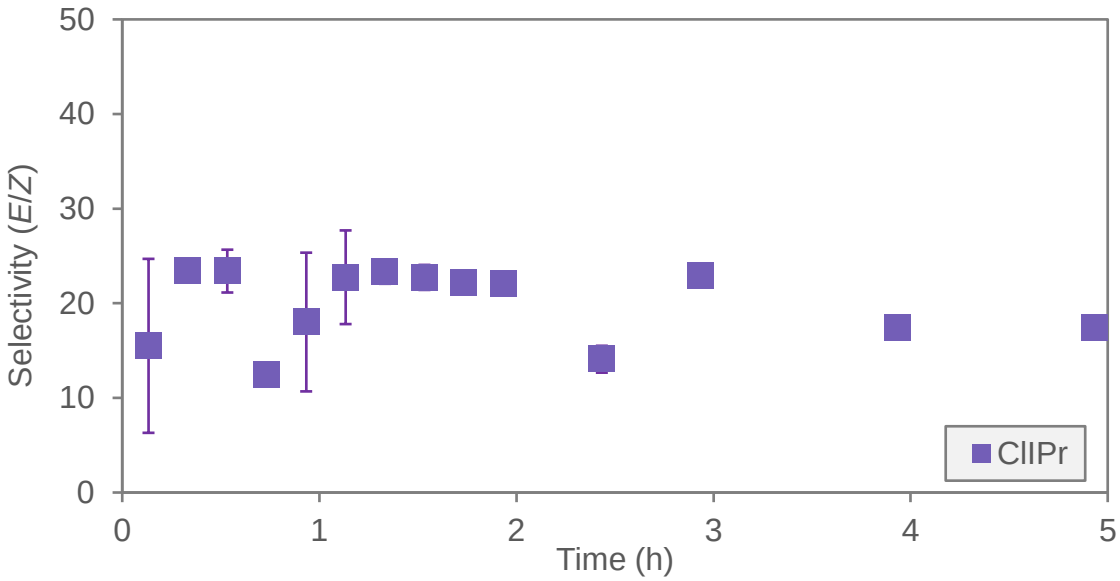

Figure D.4. Full selectivity (*E*/*Z*) profile of the formation of **2a** versus time (min) using ClIPr as the NHC.

Table D.2. % Conversion to **2a** and selectivity (*E:Z*) of **2a** formed using ClIPr as the NHC.

Time (h)	% Conversion to **2a**	Selectivity (*E*:*Z*) (std erorr)
0.13	0.7±0.1	16:1 (9)
0.33	1.0±0.1	23.5:1 (0.7)
0.53	1.3±0.1	23:1 (2)
0.73	1.8±0.2	12.5:1 (0.7)
0.93	2.11±0.01	18:1 (7)
1.13	2.2±0.2	23:1 (5)
1.33	2.4±0.3	23:1 (1)
1.53	2.7±0.3	23:1 (1)
1.73	2.9±0.2	22.2:1 (0.8)
1.93	3.1±0.4	22.0:1 (0.6)
2.43	3.7±0.5	14:1 (1)
2.93	4.1±0.4	22.9:1 (0.1)
3.93	4.8±0.5	17.4:1 (0.8)
4.93	5.6±0.4	17.4:1 (0.8)

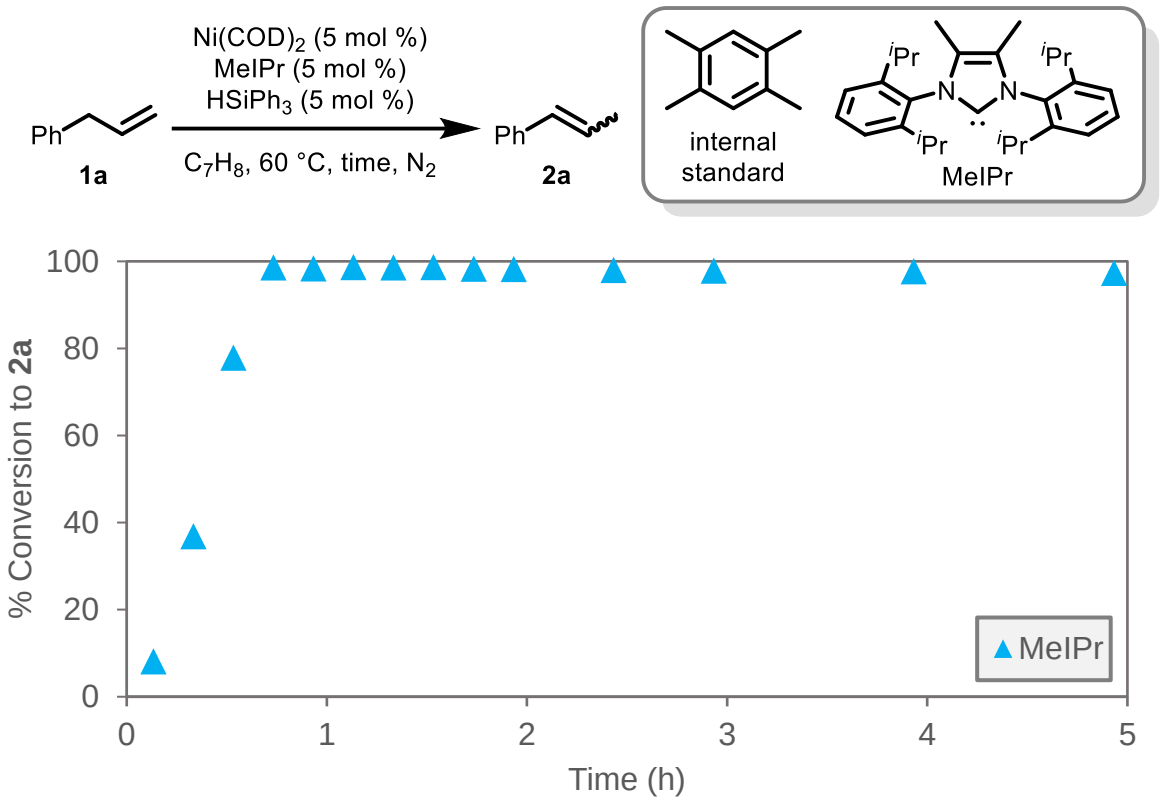

Figure D.5. Full kinetic profile of the formation of **2a** versus time (min) using MeIPr as the NHC.

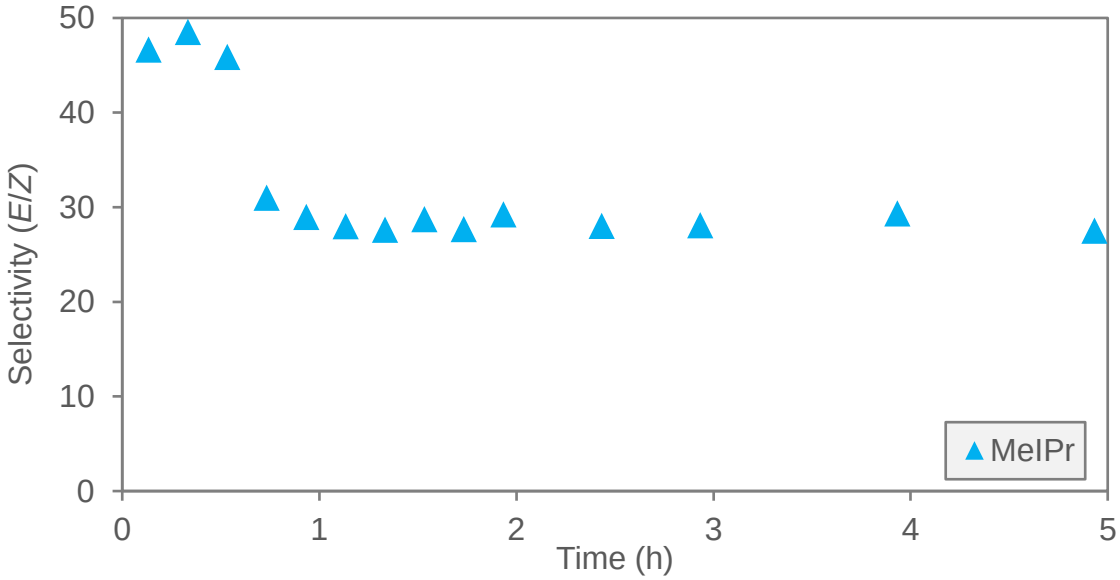

Figure D.6. Full selectivity (*E*/*Z*) profile of the formation of **2a** versus time (min) using MeIPr as the NHC.

Table D.3. % Conversion to **2a** and selectivity (*E*:*Z*) of **2a** formed using MeIPr as the NHC.

Time (h)	% Conversion to **2a**	Selectivity (*E*:*Z*)
0.13	8	47
0.33	37	49
0.53	78	46
0.73	99	31
0.93	98	29
1.13	99	28
1.33	99	28
1.53	99	29
1.73	98	28
1.93	98	29
2.43	98	28
2.93	98	28
3.93	98	29
4.93	97	28

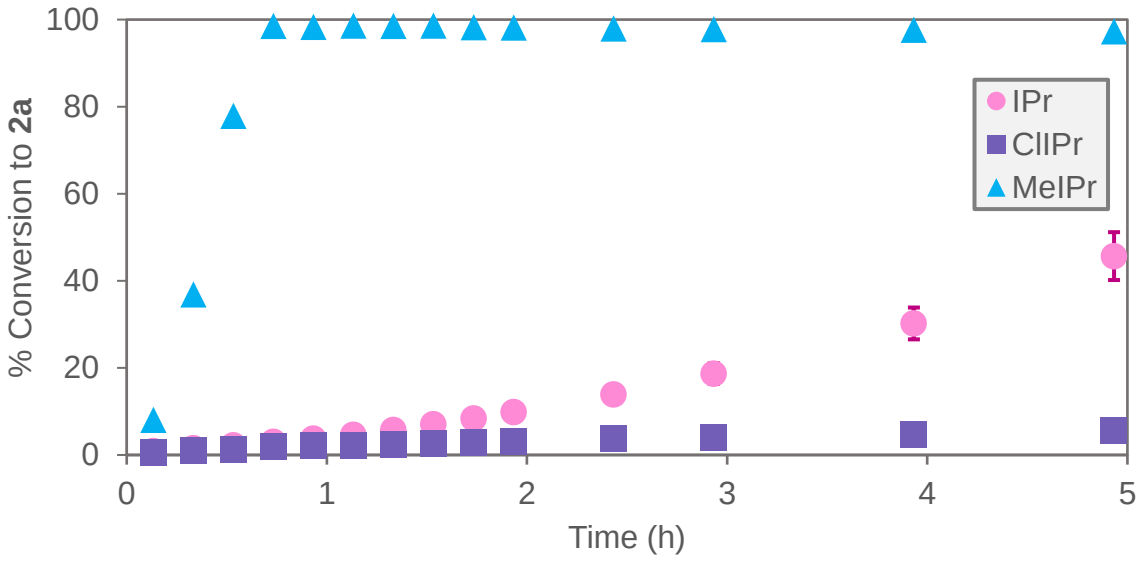

Figure D.7. Full kinetic profile of the formation of **2a** versus time (min).

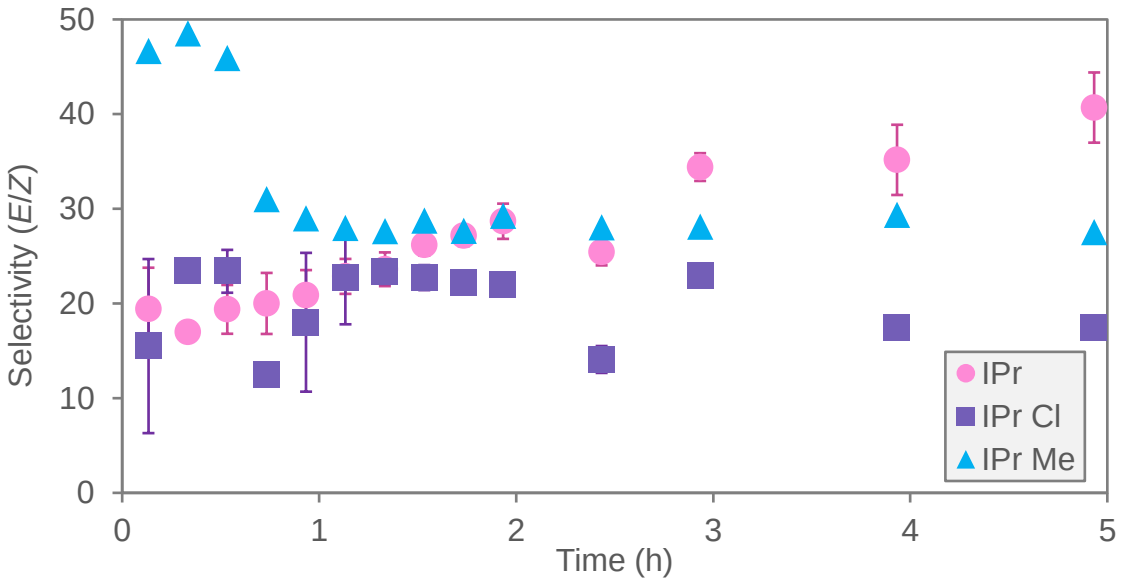

Figure D.8. Full selectivity (*E*/*Z*) profile of the formation of **2a** versus time (min).

b. Evaluation of Ni(0) Source

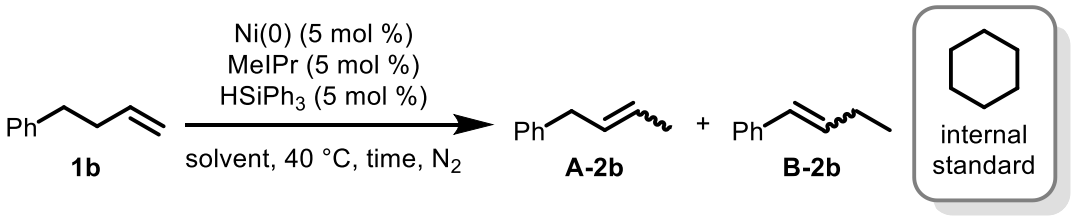

In a nitrogen-filled glovebox, $Ni(COD)_2$ (0.0016 g, 0.0060 mmol, 0.050 equiv) or Ni(COD)(DQ) (0.0020 g, 0.0060 mmol, 0.050 equiv) were weighed directly into a 1-dram vial equipped with a stir bar. A stock solution of MeIPr was prepared in the corresponding solvent and distributed into each vial with Ni using a disposable 1-mL syringe. A separate stock solution of $HSiPh_3$ (0.0016 g, 0.0.0062 mmol, 0.050 equiv added to each vial) and cyclooctane (2.5 µL, 0.019 mmol added to each vial) was prepared in toluene and distributed into each vial using a disposable 1-mL syringe. The vial was sealed with a septum cap, brought out of the glovebox, and placed onto a preheated vial block at 40 °C. Throughout the course of the reaction, 20 µL aliquots were removed with a 25-µL syringe, filtered into a GC-MS vial through Celite, and diluted with hexanes. The filtrate from the Celite plug was analyzed by GC-MS to assess the reaction progress and selectivity. The product concentration was determined by relative integration (by GC-MS) of the product peaks against cyclooctane, in accordance with calibration curves. Two trials were run for all experiments.

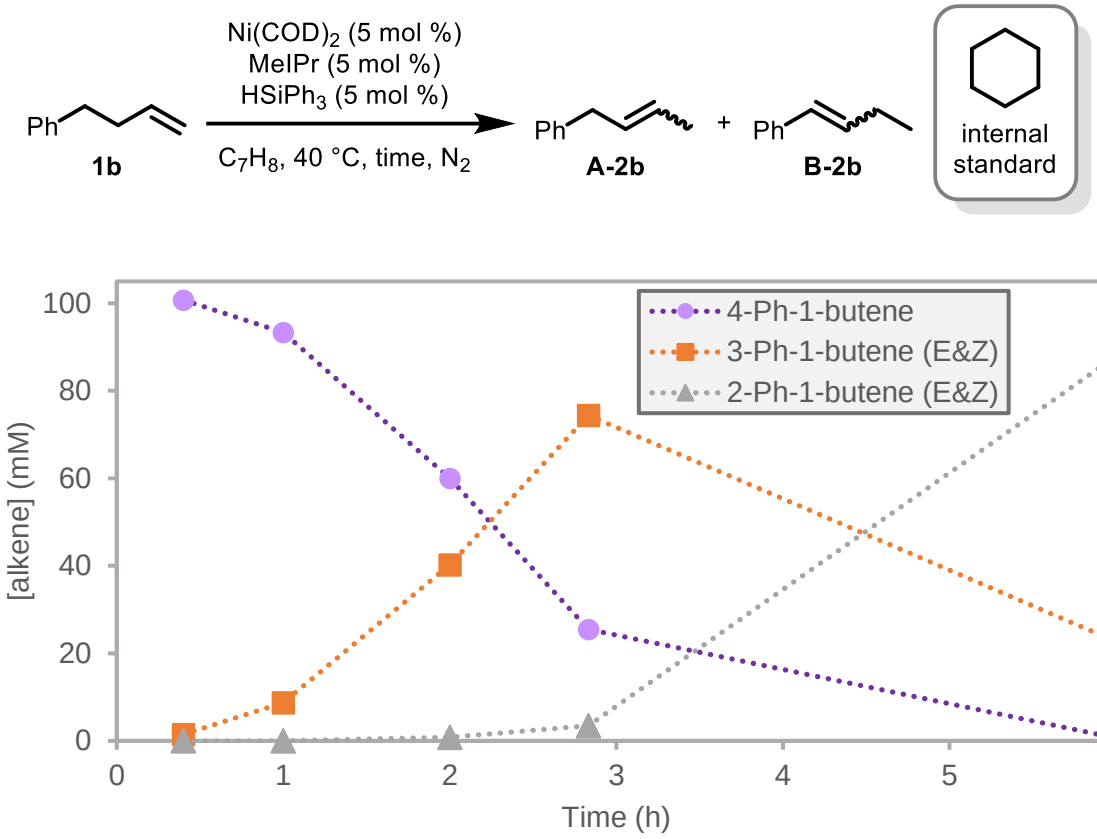

Figure D.8. Full kinetic profile of the isomerization of **1b** to **A-2b and B-2b** versus time (min) using $Ni(COD)_2$ in toluene.

Table D.5. Concentration of **1b**, **A-2b**, and **B-2b** formed using $Ni(COD)_2$ in toluene.

Time (h)	[1b] (mM)	[A-2b] (mM)	[B-2b] (mM)
0.4	100.7±0.2	1.5±0.2	0
1.0	93.4±0.6	8±3	0
2.0	60	40	0.8
2.8	25±6	74±4	3.5±0.9
6.0	0.6	23	88

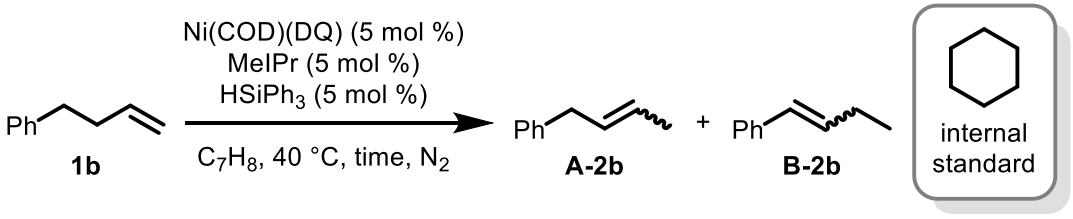

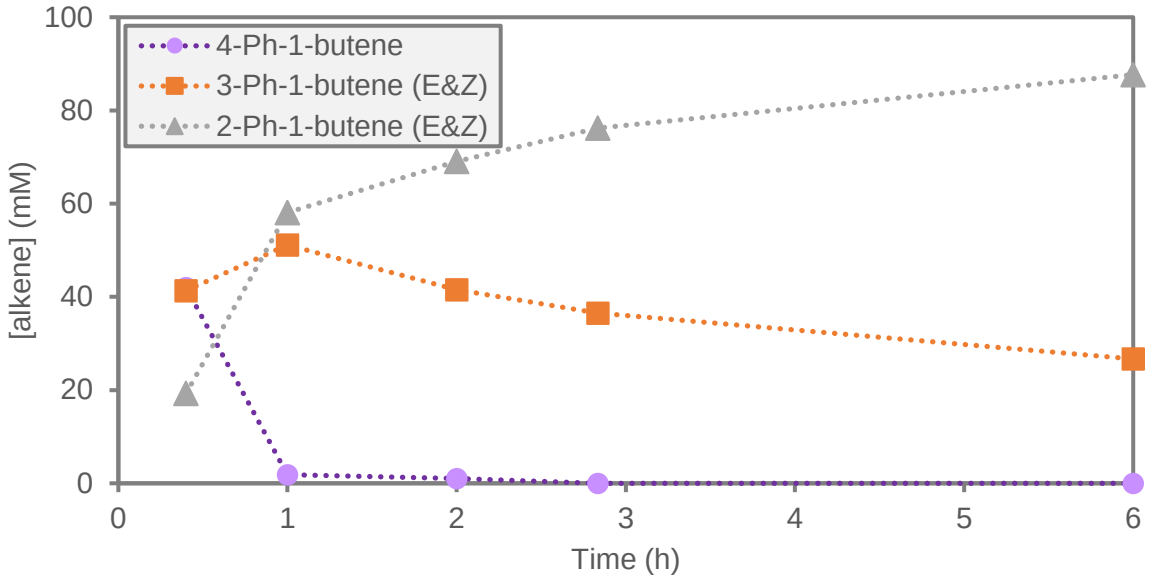

Figure D.9. Full kinetic profile of the isomerization of **1b** to **A-2b and B-2b** versus time (min) using Ni(COD)(DQ) in toluene.

Table D.6. Concentration of **1b**, **A-2b**, and **B-2b** formed using Ni(COD)(DQ) in toluene.

Time (h)	[1b] (mM)	[A-2b] (mM)	[B-2b] (mM)
0.4	42	41	19
1.0	1.0	51	58
2.0	1.0	42	69
2.8	0	37	76
6.0	0	27	88

No isomerization activity was observed using cyclohexane, *n*-octane, or hexane as the solvent medium due to catalyst insolubility at 40 °C.

D.1.4. Hydrosilylation

a. Authentic Hydrosilylation Product (4a-4d) Characterization and Isolation

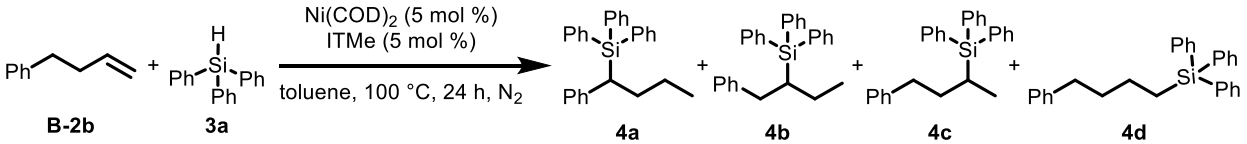

In a nitrogen-filled glovebox, $Ni(COD)_2$ (0.010 g, 0.036 mmol, 0.050 equiv), MeIMes (0.012 g, 0.036 mmol, 0.050 equiv), and $HSiPh_3$ (0.19 g, 0.73 mmol, 1.0 equiv) were weighed directly into a 1-dram vial equipped with a stir bar. To this vial was added toluene (3.0 mL) using

a disposable 6-mL syringe, the vial was sealed with a septum cap, brought out of the glovebox, and injected with **1b** (0.10 mL, 0.67 mmol, 1.0 equiv) using a 250-µL syringe, and placed onto a preheated vial block at 100 °C. After 24 h, an aliquot (10 µL) of the reaction was removed using a 25-µL syringe, filtered through Celite, and washed with hexanes directly into a GC vial to assess product selectivity. The reaction was quenched by cooling in a liquid N2 bath, thawing at room temperature, and the crude reaction was concentrated under reduced pressure. The resulting crude product was purified by column chromatography (silica, 0-5:95%, benzene/hexanes) and the product isomers were isolated separately to determine the product ^{1}H NMR peaks and GC/GC-MS peak retention times. Products **4a**, **4c** and **4d** were successfully isolated and characterized by ^{1}H NMR.

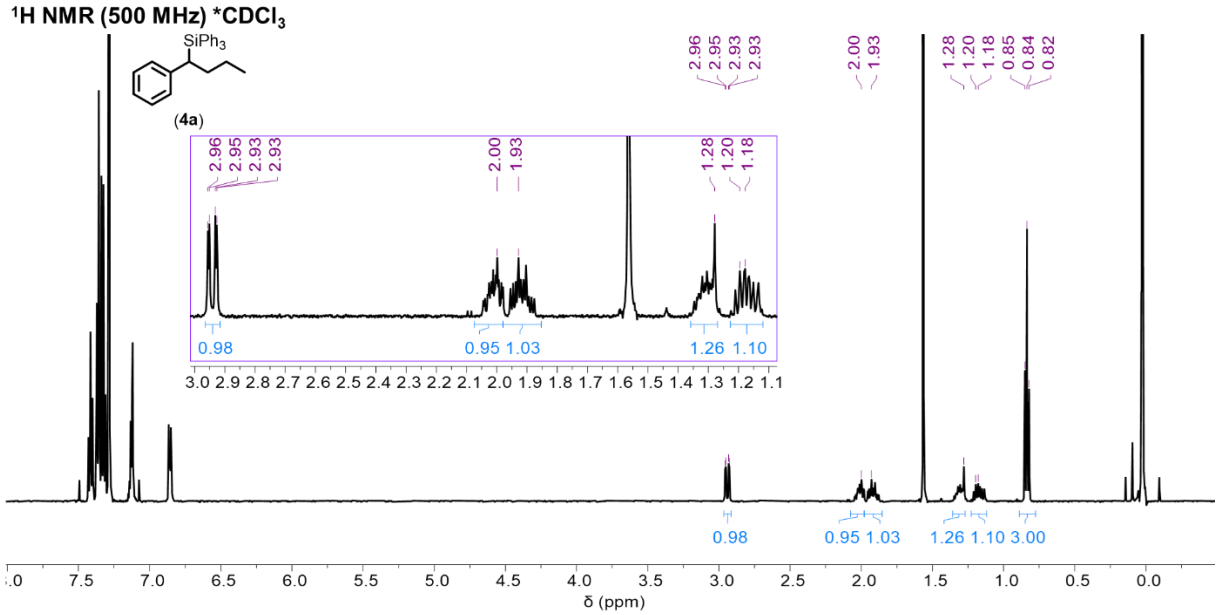

Figure D.10. ^{1}H NMR of **4a** recorded in $CDCl_3$ at 298 K.

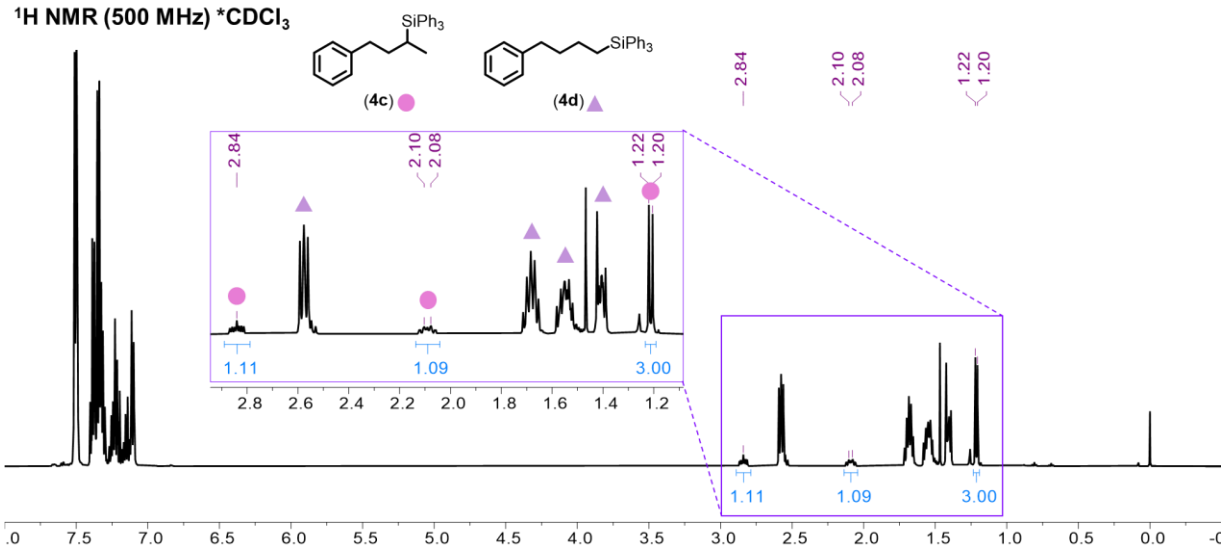

Figure D.11. ^{1}H NMR of **4c** (pink circles) and **4d** (purple triangles) recorded in $CDCl_3$ at 298 K.

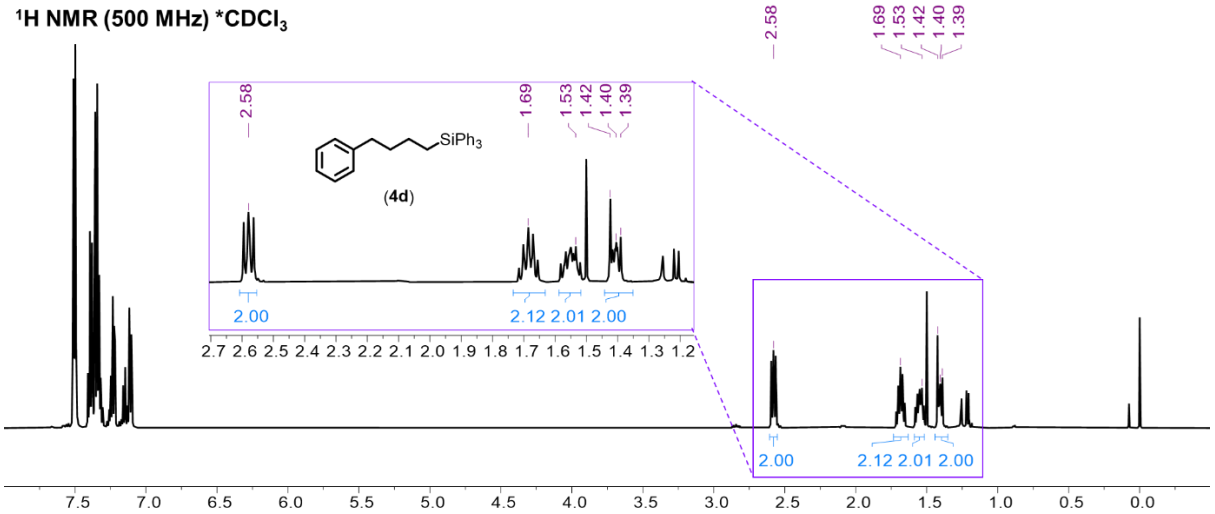

Figure D.12. ^{1}H NMR of **4d** recorded in $CDCl_3$ at 298 K.

b. Alkene Hydrosilylation Optimization

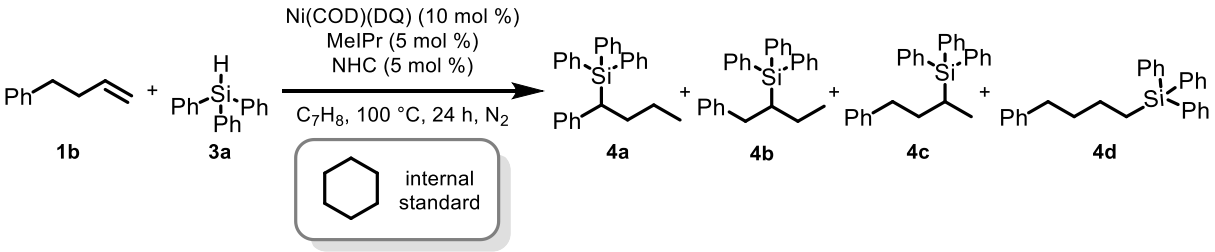

In a nitrogen-filled glovebox, Ni(COD)(DQ) (0.0040 g, 0.012 mmol, 0.10 equiv), MeIPr (0.0025 g, 0.0060 mmol, 0.050 equiv), and the corresponding NHC (MeIMes or IMes) were weighed directly into a 1-dram scintillation vial equipped with a stir bar. To this vial was added toluene (0.60 mL), and a previously prepared stock solution of **3a** (0.062 g, 0.24 mmol, 1.0 equiv) and cyclooctane (10 µL, 0.074 mmol) in toluene was distributed to obtain a total volume of 1.0 mL. The vial was sealed with a septum cap, removed from the glovebox, injected with **1b** (36 µL, 0.24 mmol, 1.0 equiv) and placed on a preheated vial block at 80 °C. After 24 h, an aliquot (~20 µL) was removed using a 25-µL syringe, filtered into a GC-MS vial through Celite, and diluted with hexanes. The filtrate from the Celite plug was analyzed by GC-MS to assess the reaction progress and selectivity. The product concentration was determined by relative integration (by GC-MS) of the alkene against cyclooctane, in accordance with calibration curves. Two trials were run for all experiments.

Table D.7. Reaction conditions of remote hydrosilylation reactions tested.

Entry	NHC	% conversion of 1b to HS products	Selectivity (4a/4b-4d)
1	MeIMes	75±1%	0.9:1
2	IMes	53±3%	1.9:1

c. Solvent Screen for the Hydrosilylation of B-2b and 3a

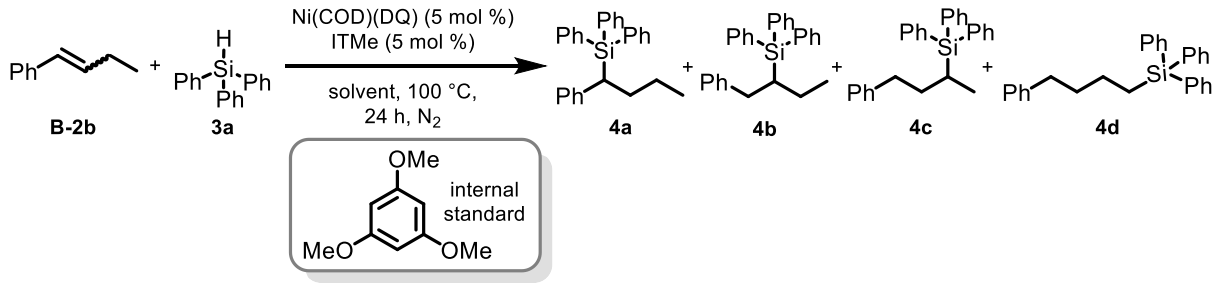

In a nitrogen-filled glovebox, Ni(COD)(DQ) (0.0020 g, 0.0060 mmol, 0.050 equiv) and ITMe (0.0076 g, 0.0060 mmol, 0.050 equiv) were weighed directly into a 1-dram vial equipped with a stir bar. A stock solution of $HSiPh_3$ (0.031 g, 0.12 mmol, 1.0 equiv added to each vial) was prepared in the corresponding solvent and distributed into each vial using a disposable 1-mL syringe. **B-2b** (17.5 µL, 0.12 mmol, 1.0 equiv) was added into the vial using a 25-µL syringe and the vial was sealed with a septum cap, brought out of the glovebox, and placed onto a preheated vial block at 100 °C. After 24 h, the reaction was quenched by cooling in a liquid N_2 bath, opening

to air, and trimethoxybenzene (0.00298 g, 0.0177 mmol added to each vial) was added to the reaction as a stock solution using volumetric glassware in toluene via a 250-µL syringe. After mixing, an aliquot (10 µL) of the reaction was removed using a 25-µL syringe, filtered through Celite, and washed with $CDCl_3$ directly into an NMR tube. The filtrate was analyzed by ^1H NMR and **4a** yield was determined by relative integration of the peak corresponding to **4a** (t, 0.81 ppm, 3H) and the internal standard, trimethoxybenzene (s, 6.09 ppm, 3H). Selectivity was determined by GC-MS. Two trials were run for all experiments.

Table D.8. Corresponding solvent and ^1H NMR integrations of trimethoxybenzene and **4a**, mmol of **4a**, and % yield of **4a**.

Solvent	∫ Trimethoxybenzene	∫4a	Mmol 4a	% Yield 4a
Toluene	3.00	6.38	0.0377	31.55±0.03%
	3.00	6.37	0.0377	
Cyclohexane	3.00	8.16	0.0483	40.9±0.8%
	3.00	8.38	0.0496	
n-octane	3.00	7.82	0.0463	43±6%
	3.00	9.61	0.0568	
Hexanes	3.00	4.07	0.0241	29±12%
	3.00	7.57	0.0448	

D.1.5. Remote Hydrosilylation

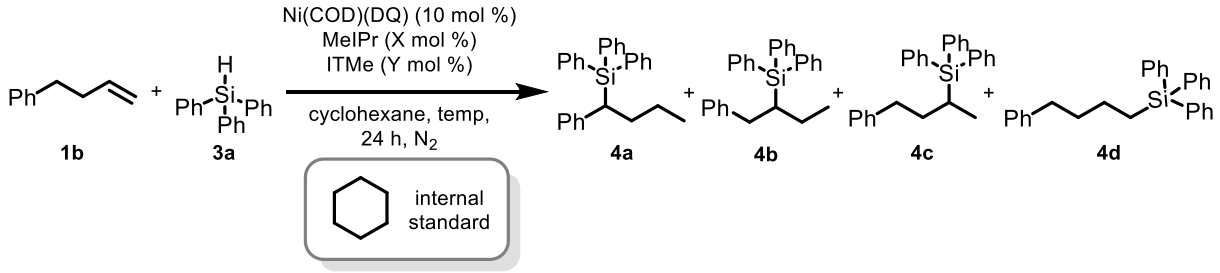

In a nitrogen-filled glovebox, Ni(COD)(DQ) (0.0040 g, 0.012 mmol, 0.10 equiv), MeIPr and ITMe were weighed directly into a 1-dram scintillation vial equipped with a stir bar. To this vial was added toluene (0.60 mL), and a previously prepared stock solution of **3a** (0.062 g, 0.24 mmol, 1.0 equiv) and cyclooctane (10 µL, 0.074 mmol) in toluene was distributed to obtain a total volume of 1.0 mL. The vial was sealed with a septum cap, removed from the glovebox, injected with **1b** (36 µL, 0.24 mmol, 1.0 equiv) and placed on a preheated vial block at 80 °C. After 24 h, an aliquot (~20 µL) was removed using a 25-µL syringe, filtered into a GC-MS vial through Celite, and diluted with hexanes. The filtrate from the Celite plug was analyzed by GC or GC-MS to

assess the reaction progress and selectivity. The product concentration was determined by relative integration (by GC-MS) of the alkene against cyclooctane, in accordance with calibration curves. Two trials were run for all experiments.

Table D.9. Reaction conditions of remote hydrosilylation reactions tested.

Entry	MeIPr/ITMe catalyst loading	Temperature (° C)	Time (h)	% conversion of 1b to A-2b and B-2b	% conversion of 1b to HS products	Selectivity (4a/4b-4d)
1*	5:5 mol %	50	8.5	86±11%	0%	n/a
	5:5 mol %	100	24	80.4±0.4%	64.49±0.02%	3.1:1
2*	5:5 mol %	60	7.0	86±15%	0%	n/a
	5:5 mol %	100	24	77.5±0.4%	67.7±0.3%	4.2:1
3	5:5 mol %	100	21	80±2%	n/a	5.0:1
4	2.5:7.5 mol %	100	24	75±3%	n/a	3.8:1
5	5:5 mol %	90	24	63±8%	69±6%	10:1

*reactions were run using 10 mol % $Ni(COD)_2$ in toluene.

APPENDIX E

SUPPLEMENTARY CONTENT FOR CHAPTER VI

Experimental details

E.1.1. Materials and Methods

All syntheses and manipulations were carried out under nitrogen using standard Schlenk (vacuum 10^{-2} mbar) techniques or in a nitrogen-filled glovebox unless otherwise indicated. All reagents and solvents were used after drying and stored under nitrogen, unless otherwise indicated. Tetrahydrofuran (THF; Fisher Chemical; HPLC grade, unstabilized), hexanes (Fisher Chemical; HPLC grade), diethyl ether (B&J Brand; HPLC grade, unstabilized), dimethylformamide (DMF; Fischer Chemical; ACS grade) were dispensed under nitrogen from an LC Technology SP-1 solvent system. C_6D_6 and $CDCl_3$ were purchased from Cambridge Isotope Laboratories, degassed by freeze-pump-thaw, and thereafter stored on activated 4Å molecular sieves under nitrogen. All stock solutions were prepared by mass and were dispensed into the reaction vessel by difference from syringe, as detailed in the procedure for each experiment.

The following reagents were used from commercial sources without further purification: Zirconium (IV) oxynitrate hydrate ($ZrO(NO_3)_2•nH_2O$, we used the molecular weight for the hexahydrate form in all calculations,[292] Sigma Aldrich), ammonium hydroxide (NH_4OH; Fisher Scientific), sulfuric acid (H_2SO_4; Fisher Scientific), ferrocene (Acros), 2-allylphenol (**1l**, TCI), pyridine (Aldrich), tosyl chloride (TCI), sodium bicarbonate ($NaHCO_3$; Fisher Scientific), 3-bromo-thiophene-2-carboxylic acid (Oakwood), allylbromide (TCI), methyl iodide (MeI, TCI), Potassium hexafluorophosphate (KPF_6, Oakwood), magnesium turnings (Acros), iodine (Mallinckrodt), 1,4-dibromobenzene (Aldrich), silver nitrate ($AgNO_3$; VWR), potassium *tert*-butoxide (KO*t*-Bu; Strem), phenylacetaldehyde (Alfa Aesar), nickel tetrakistriphenylphosphite ($Ni[P(OPh)_3]_4$, Sigma-Aldrich), Nickel tetrakistriphenylphosphine ($Ni(PPh_3)_4$, Acros), bis(1,5-cyclooctadiene)nickel(0) ($Ni(cod)_2$, Strem), benzenethiol (Aldrich), 1,4-dichlorobenzene (Aldrich), bromobenzene (TCI), furan (TCI), acetophenone (Aldrich), benzaldehyde (Sigma-Aldrich), iodobenzene (Aldrich), phenylacetylene (TCI), aniline (Fischer Scientific), vinylacetic acid (Fischer Scientific), 3-sulfolene (**1r**, Sigma), 1-decene (**1z**, TCI), *N*-allylaniline (Acros), limonene (TCI), Tricyclohexylphosphine tetrafluoroborate ($PCy_3•BF_4$; Ambeed),

Bis(dibenzylideneacetone)palladium(0) ($Pd(dba)_2$; Frontier Scientific), tri-*tert*-butylphosphine ($P(t\text{-}Bu)_3$; Alfa Aesar), isobutyryl chloride (*i*-PrClCO; Thermo Scientific), styrene (TCI), bis(pinacolato)diboron (B_2Pin_2, Frontier Scientific), lithium *tert*-butoxide (LiO*t*-Bu, Alfa Aesar), diphenylsilane (Acros Organics), Nafion™ and Amberlyst®-15 were used from commercial sources without further purification. The [H^+] value (0.919 mmol/g) used for Nafion was the charge carrier density,[293] which was determined according to a literature procedure. The [H^+] value used for Amberlyst®-15 was (4.73 mmol/g).[294]

Procedure abbreviations: overnight (o.n.), Milli-Q water (MQ), chloroform ($CHCl_3$), dichloromethane (DCM), magnesium sulfate ($MgSO_4$), dimethylformamide (DMF), potassium carbonate (K_2CO_3), ethylacetate (EtOAc), methanol (MeOH), diethylether (Et_2O), ethanol (EtOH), tetrahydrofuran (THF), sodium sulfite (Na_2SO_3), sodium sulfate (Na_2SO_4), 1,3-bis(2,6-diisopropylphenyl)imidazole-2-ylidene (IPr), 1,5-hexadiene (hex).

Yields quantified by GC were determined using a calibration curve of the product against an internal standard (cyclooctane or durene). Conversions quantified by GC were determined by relative ratio(s) of the integrations of the starting material and product(s). At least two trials were run for all reactions, except for isolated yields, and the averages of these two trials are reported. The errors reported are the standard deviations of the two trials.

The following compounds and materials were synthesized via reported procedures: $Bn_2Mg(THF)_2$,[295] 2-(3-buten-1-yl)pyridine,[296] CD_3PPh_3Br,[297] $Ni[P(OEt)_3]_4$,[298] (IPr)Ni(hex),[230] **1a**,[230] **1b**,[230] **1c**,[230] **1d**,[230] **1e**,[230] **1f** (in 3 steps),[299–301] **1h**,[230] **1i**,[230] **1j**,[230] **1k**,[230] **1m**,[230] **1o**,[302] **1p**,[303] **1s**,[304] **1t**,[230] **1u**,[305] **1v**,[306] **1w**,[230] **1x**,[307] **1aa**,[230] *N*-allyl-*N*-phenylaniline,[308] homoallylcarbonate (in two steps),[309,310] 4-penten-1-yn-1-ylbenzene,[311] (1-cyclopropylethenyl)benzene,[230] and $(IPr)_2Ni_2Cl_2$.[312]

$ZrO_{2\text{-}700}$ (0.072 mmol H^+/g),[313] $SiO_{2\text{-}700}$ (0.29 mmol H^+/g),[314] and $Al_2O_{3\text{-}700}$ (0.15 mmol H^+/g)[315] were synthesized as previously reported. The [H^+] for each of these solids was determined by titration with $Bn_2Mg(THF)_2$ (see section 3a below for analogous procedure with SZO_{300}).

E.1.2. General Experimental

Nuclear magnetic resonance (NMR) spectra were collected at room temperature (298 K) unless otherwise stated on a Bruker Avance-III HD 500 NMR (499.90 MHz for ^1H; 160.49 MHz for ^{11}B; 126 MHz for ^{13}C; 471 MHz for ^{19}F; 99 MHz for ^{29}Si). ^1H and ^{13}C spectra were referenced to the

residual solvent peak ($CDCl_3$: ^1H δ = 7.26 ppm, ^{13}C δ = 77.16 ppm; C_6D_6: ^1H δ = 7.16 ppm, 13C δ = 128.06 ppm. Chemical shifts for ^1H, ^{13}C, and ^{29}Si NMR spectra are reported in parts per million (ppm, δ) relative to tetramethylsilane at 0.00 ppm. Peaks are characterized as follows: singlet (s), doublet (d), triplet (t), quartet (q), quintet (quint), multiplet (m), multiple signals (ms), broad (b), doublet of quartets (dq). Coupling constants, *J*, are reported in Hz. Infrared (IR) spectroscopy for air-stable organic compounds was performed on an Agilent Nicolet 6700 FT-IR using the ATR sampling technique. IR spectra for air-sensitive SZO_{300} was recorded as a self-supported pellet using a Bruker Alpha II FTIR spectrometer that is housed in a nitrogen-filled glovebox. All bands are reported in wavenumbers (cm^{-1}) and are described as broad (br), strong (s), medium (m), and weak (w). For catalytic reactions, yields were determined using Gas Chromatography-Mass Spectrometry (GC-MS) or Gas Chromatography-Flame Ionization Detector (GC) against an internal standard. GC-MS was carried out on a Shimadzu GC-2010 Plus/GCMS-QP2010 SE using a Restek Rtx®- 5 (Crossbond 5% diphenyl – 95% dimethyl polysiloxane; 15 m, 0.25 mm ID, 0.25 μm df) column. GC was carried out on a Thermo Fisher Trace 1300 Gas Chromatograph using a Restek Rtx®-5 (Crossbond 5% diphenyl – 95% dimethyl polysiloxane; 15 m, 0.25 mm ID, 0.25 μm df) column. High-resolution mass spectrometry (HRMS) was carried out on a Waters XEVO G2-XS TOF mass spectrometer.

E.1.3. Synthesis of Non-Commercial Reagents

c. Preparation of SZO_{300}

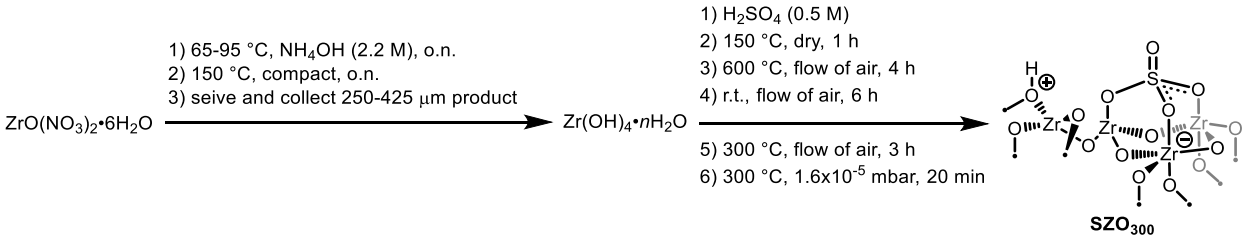

Sulfated zirconia (SZO_{300}) was synthesized via a modified literature procedure:[202] In a 1 L Erlenmeyer flask equipped with an overhead mechanical stirrer, $ZrO(NO_3)_2$•*n*H_2O (70 g, 210 mmol, 1.0 equiv) and MQ water (420 mL) were added and heated to 65 °C in a sand bath until all solids dissolved. To this stirring solution, aqueous NH_4OH (2.2 M, 280 mL, 620 mmol, 3.0 equiv) was added dropwise using an addition funnel over 2 h to form a white precipitate. Upon full addition of NH_4OH, the pH of the white slurry was ~10, as measured using pH paper. The stirring

slurry was then heated to 95 °C for 24 h. The reaction was filtered while hot via vacuum filtration using a medium fritted funnel. The white precipitate was transferred into a beaker with MQ water (700 mL) and stirred. After 30 minutes, the solid was collected via vacuum filtration using a medium fritted funnel, washed with MQ water (3000 mL), transferred into a beaker and pressed down to make the solid more compact, and placed in an oven set at 110 °C overnight. The resulting compacted $Zr(OH)_4•nH_2O$ was removed from the oven and allowed to cool to room temperature. The white solid was gently ground up using a motor and pestle and sieved to collected 250-425 µm-sized particles, yielding $Zr(OH)_4•nH_2O$ as a white solid (13 g).

$Zr(OH)_4•nH_2O$ (5.0 g) was added to an aqueous solution of H_2SO_4 (0.50 M, 100 mL, 50 mmol) at room temperature, in which gas evolution was observed. After 30 min, the gas evolution had ceased, and the solution was poured away from the white solid. The solid was suspended in MQ water (100 mL). After 30 min, the water was decanted and the solid was dried for 1 h in the oven set at 110 °C. The solid, SZO, was removed from the oven and allowed to cool to room temperature. In a quartz flow reactor, 1.6 g of SZO was heated to 600 °C (ramp rate of 5 °C/min) under a flow of dry air (flow rate = 90-100 mL/min) and held at 600 °C for 4 h. The material was allowed to cool to room temperature for 9 h under a flow of dry air. SZO was then dehydroxylated by heating to 300 °C (ramp rate = 5 °C/min) under a flow of air (flow rate = 90-100 mL/min) for 3 h, and then the reactor was evacuated to 10^{-8} bar for 20 min at 300 °C to yield SZO_{300}. The reactor was sealed while hot and under vacuum and was immediately transferred into a N_2 glovebox, and SZO_{300}, a white solid (1.5 g), was stored in the glovebox. The IR spectrum was recorded (**Figure E.1.**).

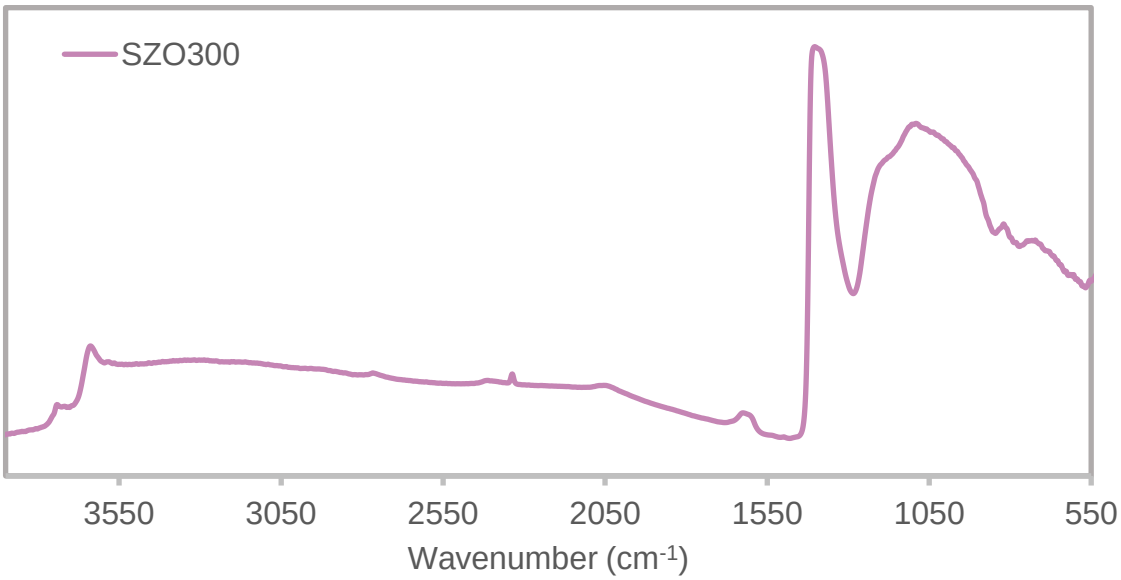

Figure E.1. IR of SZO_{300}.

SZO_{300} titration: The concentration of acidic sites, [H^+], was quantified by titration. SZO_{300} was weighed directly into an NMR tube. A stock solution of $Bn_2Mg(THF)_2$ and ferrocene (internal standard) in C_6D_6 was prepared using volumetric glassware and then distributed into the NMR tube with the acidic solid (amounts can be found in Table S1). A ^1H NMR spectrum (8 scans, 60 s relaxation delay, Figure S2) was recorded as quickly as possible, since that resulted in the most reproducible and reliable results. The concentration of acidic sites was quantified by relative integrations between toluene's methyl peak (singlet at 2.11 ppm, 3H) and ferrocene (singlet at 4.01 ppm, 10H). Titrations were run in duplicate, and the amounts and integrations of SZO_{300}, ferrocene, $Bn_2Mg(THF)_2$, and toluene are shown below. The average concentration of H^+ found on SZO_{300} was 0.219 mmol H^+/g for this batch. The concentration of H^+ of the different SZO_{300} batches varied between 0.190-0.219 mmol H^+/g, therefore an average of 0.200 mmol H^+/g was used to determine the mmol and equivalents of H^+ added to each reaction.

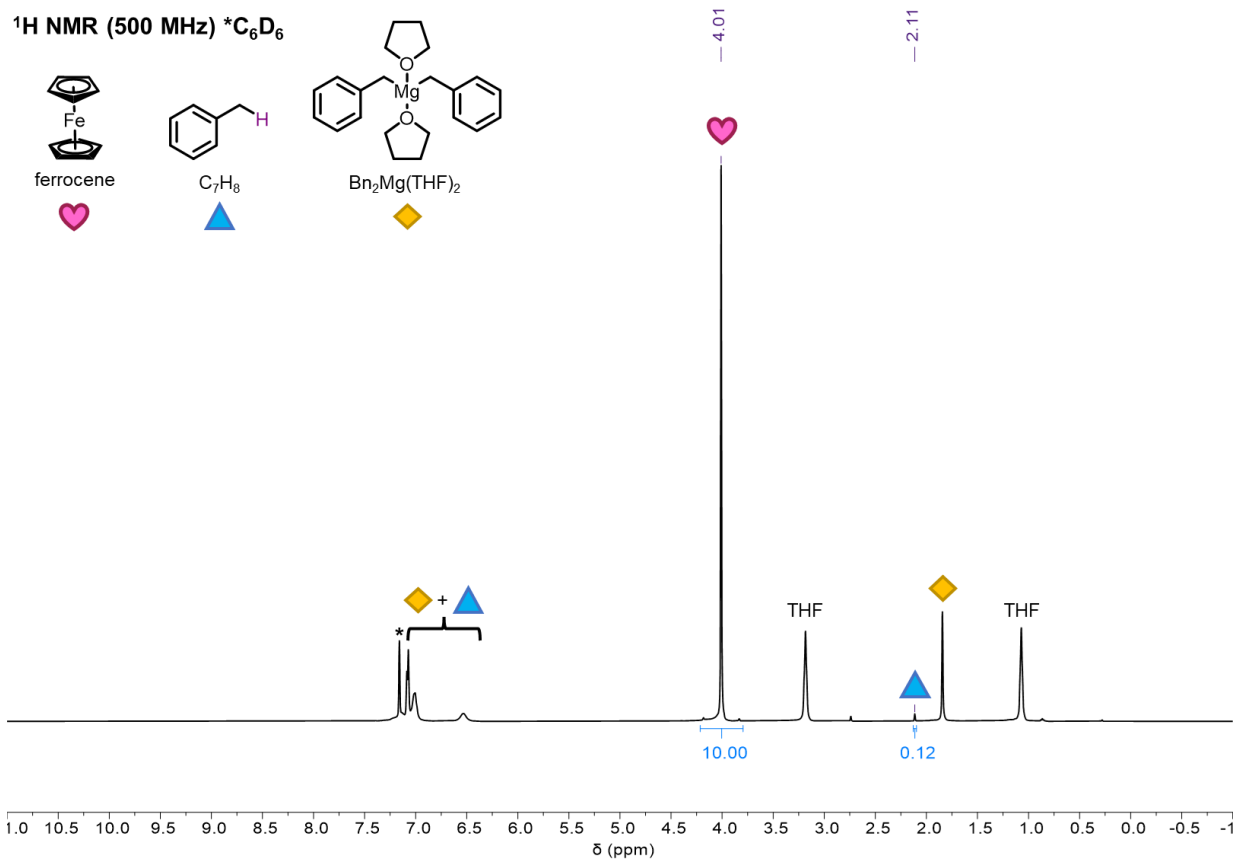

Figure E.2. ^{1}H NMR spectrum of the titration of SZO_{300} with $Bn_2Mg(THF)_2$ in C_6D_6.

Table E.1. Amounts added and integrations of peaks in the ^{1}H NMR used to titrate the acidic solid to determine [H^+].

Trial	SZO_{300} mass (mg)	Ferrocene mass (mg)	$Bn_2Mg(THF)_2$ mass (mg)	$\int C_7H_8$	$\int$ferrocene	mmol H^+/g SZO_{300}
1	10.1	10.0	15.8	0.13	10	0.225
2	10.4	10.0	15.8	0.12	10	0.213
Average						0.219

d. Synthesis of Starting Materials

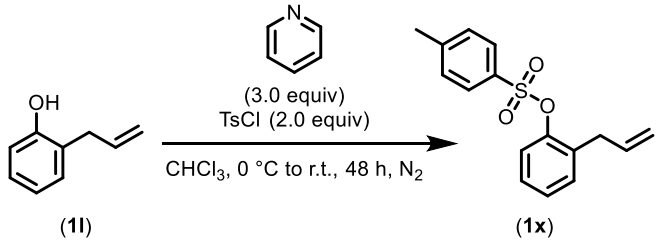

4-methylbenzenesulfonate-2-(2-propenyl)-phenol (1x): 1l (1.0 mL, 7.7 mmol, 1.0 equiv) and $CHCl_3$ (10 mL) were added to an oven-dried Schlenk flask equipped with a magnetic bar. The flask was cooled to 0 °C in an ice-water bath and pyridine (1.9 mL, 24 mmol, 3.1 equiv) was added followed by

tosyl chloride (small portions were added at a time, 2.9 g, 15 mmol, 2.0 equiv). The reaction warmed to room temperature and was left to stir for 48 h. The reaction was quenched with $NaHCO_3$ (20 mL) and extracted with DCM (3 x 50 mL). The combined organic layers were dried over $MgSO_4$, filtered, and the filtrate was concentrated under reduced pressure to obtain a yellow oil as the crude product. The crude product was purified by column chromatography (silica, 0:100 to 6:94 Et_2O/hexanes) to yield **1x** as a white, crystalline solid (0.886 g, 3.07 mmol, 40% yield). NMR spectra match values previously reported.[316]

IR (ATR, neat) v: 3081-2859 (w), 1485 (s), 1371 (s), 1177(s), 868 (s)

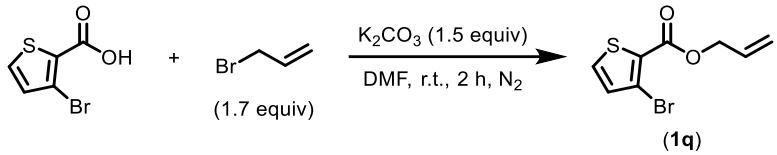

(**1q**)

2-propen-1-yl-3-bromo-2-thiophenecarboxylate (1q): 3-bromo-thiophene-2-carboxylic acid (0.50 g, 2.4 mmol, 1.0 equiv) and DMF (6.0 mL) were added to a nitrogen-flushed, two-neck round-bottom flask equipped with a stir bar. Anhydrous K_2CO_3 (0.50 g, 3.6 mmol, 1.5 equiv) was added, and the reaction was stirred for 10 min at room temperature. Allylbromide (0.35 mL, 4.0 mmol, 1.7 equiv) was then added to this stirring solution. After 2 h, the reaction was quenched with water (5.0 mL) and extracted with EtOAc (3 x 10 mL). The combined organic phases were washed with water (10 mL) and brine (10 mL), dried over $MgSO_4$, filtered, and the filtrate was concentrated under reduced pressure, giving a yellow oil as the crude product. The crude product was purified by column chromatography (silica, 0:100 to 10:90 EtOAc/hexanes) to yield **1q** as a colorless oil (0.168 g, 0.680 mmol, 28% yield).

^{1}H NMR (500 MHz, $CDCl_3$, 298 K): δ 7.47 (d, *J* = 5.2 Hz, 1H), 7.10 (d, *J* = 5.2 Hz, 1H), 6.01 (ddt, *J* = 17.2, 10.5, 5.6 Hz, 1H), 5.43 (dq, *J* = 17.2, 1.4 Hz, 1H), 5.29 (dq, *J* = 10.5, 1.4 Hz, 1H), 4.81 (dt, *J* = 5.6, 1.3 Hz, 2H)

^{13}C NMR (126 MHz, $CDCl_3$, 298 K): δ 160.5, 133.1, 131.8, 131.5, 127.5, 118.7, 117.3, 65.9

IR (ATR, neat) v: 3102-2887 (w), 1720 (s), 1414 (s), 1229 (s), 1066 (s)

ASAP/HRMS (m/z): [M^+] calculated for $C_8H_7BrO_2S$ 245.9350, found 245.9334

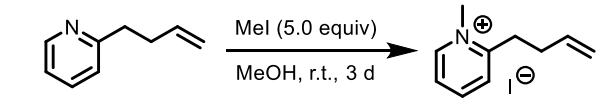

2-(3-buten-1-yl)pyridine (**S1**)

2-(3-buten-1-yl)-1-methylpyridinium iodide (S1): 2-(3-buten-1-yl)pyridine (0.60 mL, 4.2 mmol, 1.0 equiv) (the density predicted by SciFinder was used: 0.927 g/mL), methyl iodide (1.3 mL, 21 mmol, 5.0 equiv), and MeOH (6.0 mL) were combined in a round bottom flask equipped with a stir bar. The reaction was stirred at room temperature for three days. The solvent was removed under reduced pressure and an orange, highly viscous oil was obtained. This oil was washed with Et_2O (3 x 3 mL) and the crude product slowly turned into a pale-yellow solid. The crude product was purified by recrystallization in EtOH (4 mL) and Et_2O (100 mL), giving **S1** as pale-yellow crystals (0.257 g, 0.935 mmol, 22% yield).

^{1}H NMR (500 MHz, $CDCl_3$, 298 K): δ 9.43 (d, *J* = 6.1 Hz, 1H), 8.44 (td, *J* = 7.9, 0.9 Hz, 1H), 7.96 (t, *J* = 7.0 Hz, 1H), 7.90 (d, *J* = 8.2 Hz, 1H), 5.87 (ddt, *J* = 17.0, 10.3, 6.6 Hz, 1H), 5.16-5.09 (ms, 2H), 4.56 (s, 3H), 3.31 (t, *J* = 7.5 Hz, 2H), 2.61 (m, 2H)

^{13}C NMR (126 MHz, $CDCl_3$, 298 K): δ 158.1, 147.4, 145.4, 134.6, 128.6, 126.1, 118.2, 47.3, 32.8, 31.1

IR (ATR, neat) v: 3085-2845 (w), 1628 (s), 1509 (s), 1200 (s), 776 (s)

ASAP/HRMS (m/z): [M^+] calculated for $C_{10}H_{14}IN$ 275.0171, found 275.0316

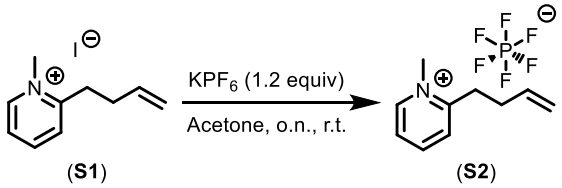

(**S1**) (**S2**)

2-(3-buten-1-yl)-1-methylpyridinium hexafluorophosphate (S2): S1(0.66 g, 2.3 mmol, 1.0 equiv) was dissolved in a minimal amount of acetone (~10 mL) in a 4-dram vial equipped with a stir bar. Potassium hexafluorophosphate (0.41 g, 2.2 mmol, 1.0 equiv) was also dissolved in minimal amounts of acetone (~8 mL) in a separate vial, and then this solution was added to the stirring solution of **S1**. A white precipitate formed, and the reaction was stirred for 30 min at room temperature. The reaction was concentrated, and a yellow solid formed. This crude product was recrystallized in EtOH (~20 mL) at 0 °C, and the solid was collected via vacuum filtration and washed with cold EtOH (~5 mL), yielding **S2** as a fluffy, white solid (0.306 g, 1.04 mmol, 45% yield).

^{1}H NMR (500 MHz, $(CD_3)_2CO$, 298 K): δ 9.01 (d, *J* = 6.1 Hz, 1H), 8.58 (t, *J*= 7.9 Hz, 1H), 8.12 (d, *J* = 8.0 Hz, 1H), 8.01 (t, *J* = 6.9 Hz, 1H), 5.98 (ddt, *J* = 17.1, 10.3, 6.6 Hz, 1H), 5.18 (dq, J = 17.1, 1.5 Hz, 1H), 5.08 (qd, J = 10.3, 1.5 Hz, 1H), 4.52 (s, 3H), 3.39 (t, J = 7.5 Hz, 2H), 2.68 (q, J = 7.5 Hz, 2H)

$^{13}C\{^{1}H\}$ NMR (126 MHz, $(CD_3)_2CO$, 298 K): δ 159.3, 147.6, 146.2, 136.6, 129.4, 126.4, 117.3, 46.4, 32.5, 31.5

$^{31}P\{^{1}H\}$ NMR (202 MHz, $(CD_3)_2CO$, 298 K): δ -144.35 (sept, J = 707.0 Hz)

^{19}F NMR (471 MHz, $(CD_3)_2CO$, 298 K): δ 72.23 (d, J = 707.5 Hz)

IR (ATR, neat) v: 3106-2914 (w), 1634 (m), 1442 (m), 1188 (m), 814 (s)

ASAP/HRMS (m/z): $[M^+]$ calculated for $C_{10}H_{14}F_6NP$ 293.0768, found 293.0672

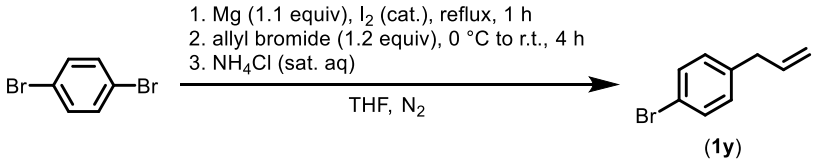

(**1y**)

1-Allyl-4-bromobenzene (1y): Magnesium turnings (0.36 g, 15 mmol, 1.8 equiv), iodine (single grain, catalytic amount), and THF (21 mL) were added to an oven-dried two-neck round bottom flask equipped with a stir bar. The mixture was stirred for 15 min, followed by gradual addition of 1,4-dibromobenzene (3.18 g, 13.5 mmol, 1.6 equiv) in several portions. The flask was equipped with a nitrogen-flushed condenser and heated to reflux in an oil bath. After 1 h the flask was removed from the oil bath and cooled to 0 °C in an ice-water bath. After stirring for 15 min, allyl bromide (1.4 mL, 8.3 mmol, 1.0 equiv) was added dropwise to the reaction mixture. The reaction was warmed to room temperature and left stirring for 4 h. The solution was then quenched with saturated NH_4Cl solution (20 mL) and extracted with Et_2O (3 x 30 mL). The combined organic layers were washed with saturated Na_2SO_3 solution (20 mL), dried over Na_2SO_4, and filtered. The filtrate was concentrated under reduced pressure to obtain a yellow oil as the crude product. The crude product was purified by column chromatography (10% $AgNO_3$ impregnated silica, 100% hexanes followed by an additional silica column 100% hexanes) to yield **1y** as a yellow oil (1.04 g, 5.3 mmol, 39% yield). NMR spectra match values previously reported.[317]

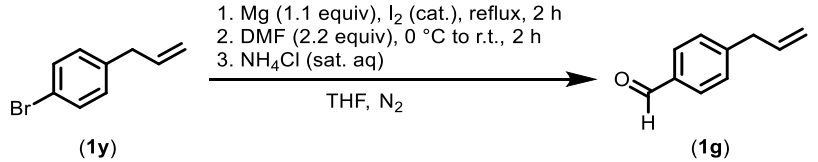

(**1y**) (**1g**)

4-Allyl-benzaldehyde (1g): Magnesium turnings (0.14 g, 5.8 mmol, 1.1 equiv), iodine (single grain, catalytic amount), and THF (10 mL) were added to an oven-dried Schlenk flask equipped with a stir bar. The mixture was stirred for 15 min, followed by gradual addition of **1y** (1.0 g, 5.1 mmol, 1.0 equiv)

in several portions. The flask was equipped with a nitrogen-flushed condenser and heated to reflux in an oil bath. After 2 h the flask was removed from the oil bath and cooled to 0 °C in an ice-water bath. After stirring for 15 min, DMF (0.85 mL, 11 mmol, 2.2 equiv) was added dropwise to the reaction mixture. The reaction was warmed to room temperature and left stirring for 2 h. The solution then was quenched with saturated NH_4Cl solution (10 mL) and extracted with Et_2O (3 x 15 mL). The combined organic layers were dried over Na_2SO_4 and filtered. The filtrate was concentrated under reduced pressure to obtain a yellow oil as the crude product. The crude product was purified by column chromatography (silica, 30:70 Et_2O/hexanes) to yield **1g** as a colorless oil (0.26 g, 1.8 mmol, 35% yield). NMR spectra match values previously reported.[317]

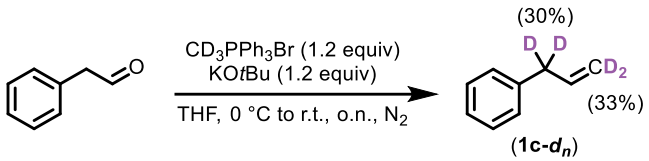

Allybenzene-*d*$_n$ (1c-*d*$_n$) was synthesized via modified literature procedure:[230] CD_3PPh_3Br (4.0 g, 11 mmol, 1.2 equiv) and THF (60 mL) were added to a nitrogen-flushed, oven-dried Schlenk flask equipped with a stir bar and cooled to 0 °C in an ice-water bath. To this stirring solution was added KO*t*-Bu (1.2 g, 11 mmol, 1.2 equiv) and the reaction turned a bright yellow color. The reaction was stirred for 1 h at 0 °C before phenylacetaldehyde (1.0 mL, 9.0 mmol, 1.0 equiv) was added dropwise with a disposable 3-mL syringe, turning the reaction a bright orange color. The reaction was stirred at 0 °C for 3 h before warming it to room temperature and allowing it to stir overnight. The following day, the reaction was opened to air and quenched with water (50 mL). The organic layer was separated, and the aqueous layer was extracted with Et_2O (3 x 50 mL). The combined organic layers were dried over $MgSO_4$, filtered, and the filtrate was concentrated under reduced pressure to obtain a crude yellow oil. The crude product was purified by column chromatography (silica, 100% pentane) to yield **1c-*d*$_n$** as a colorless oil (0.092 g, 0.77 mmol, 9% yield).

E.1.4. Evaluation of Reaction Conditions for Isomerization

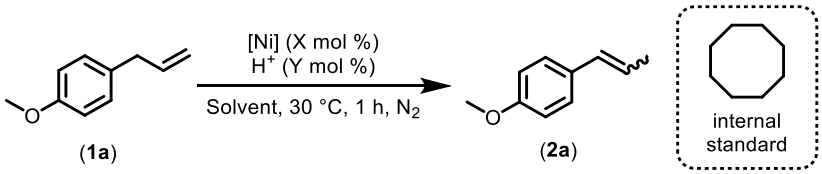

Homogeneous catalyst: In a nitrogen-filled glovebox, a stock solution of the Ni complex (0.0036 mmol, 0.030 equiv added to the vial) and cyclooctane (internal standard; 8.0 μL, 0.060 mmol added to the vial) in the reaction solvent was prepared; the appropriate amount was then added to a vial equipped with a stir bar using a 1-mL plastic syringe. The vial was sealed with a septum cap and brought out of the glovebox. A stock solution of H_2SO_4 (H^+) was prepared (0.0036 mmol, 0.030 equiv H_2SO_4) in the reaction solvent and the appropriate amount was injected into the vial using a 1-mL plastic syringe. The total volume of solvent used in the reaction was 2.0 mL. The vial was then injected with **1a** (18.5 μL, 0.120 mmol, 1 equiv) using a 25-μL syringe, heated to 30 °C on a preheated aluminum vial block, and stirred at a rate of 150 rpm. After one hour, an aliquot (~20 μL) was removed using a 25-μL syringe, diluted with hexane, and filtered through a Celite plug into a GC vial. The filtrate was analyzed by GC to assess the progress and selectivity of the reaction.

Heterogeneous catalyst: In a nitrogen-filled glovebox, the solid acid source (H^+; 0.00018-0.006 mmol H^+, 0.003-0.10 equiv H^+ added to the vial) was weighed directly into a 4-dram scintillation vial equipped with a stir bar. A stock solution of the Ni complex (0.0006-0.006 mmol, 0.01-0.10 equiv added to the vial) and cyclooctane (internal standard; 4.0 μL, 0.030 mmol added to the vial) in the reaction solvent was prepared; the appropriate amount was then added to the solid acid using a 1-mL plastic syringe. The total volume of solvent used in the reaction was 1.0 mL. The vial was sealed with a septum cap and brought out of the glovebox. The vial was then injected with **1a** (9.5 μL, 0.062 mmol, 1.0 equiv) using a 25-μL syringe, heated to 30 °C on a preheated aluminum vial block, and stirred at a rate of 150 rpm. After one hour, an aliquot (~20 μL) was removed using a 25-μL syringe, diluted with hexane, and filtered through a Celite plug into a GC vial. The filtrate was analyzed by GC to assess the progress and selectivity of the reaction.

Results from optimization screening reactions are summarized below in **Table E.2.**

Table E.2. Optimization of the isomerization of allylanisole **1a** to anethole **2a**.

Entry	Ni complex (mol %)	Acid source (mol % H^+)	solvent	Yield (%)	*E*/*Z*
1	$Ni[P(OEt)_3]_4$ (3)	H_2SO_4 (3)	MeOH	92 ± 8	34 : 1
2	$Ni[P(OEt)_3]_4$ (3)	H_2SO_4 (3)	Et_2O	86 ± 1	17 : 1
3	$Ni[P(OEt)_3]_4$ (3)	SZO_{300} (3)	Et_2O	78 ± 3	17 : 1
4	$Ni[P(OEt)_3]_4$ (3)	$ZrO_{2\text{-}700}$ (3)	Et_2O	0	— —
5	$Ni[P(OEt)_3]_4$ (3)	$Al_2O_{3\text{-}700}$ (3)	Et_2O	0	— —

6	$Ni[P(OEt)_3]_4$	(3)	$SiO_{2\text{-}700}$	(3)	Et_2O	0	— —
7[a]	$Ni[P(OEt)_3]_4$	(3)	Nafion™	(5)	Et_2O	10 ± 3	15 : 1
8[a]	$Ni[P(OEt)_3]_4$	(3)	Amberlyst®-15	(5)	Et_2O	20 ± 3	11 : 1
9	$Ni[P(OPh)_3]_4$	(3)	SZO_{300}	(3)	Et_2O	0.2046 ± 0.0007	1 : 0
10	$Ni(PPh_3)_4$	(3)	SZO_{300}	(3)	Et_2O	3.1 ± 0.3	5 : 1
11	$Ni(cod)_2$	(3)	SZO_{300}	(3)	Et_2O	0.5 ± 0.2	1 : 0
12	(IPr)Ni(hex)	(3)	SZO_{300}	(3)	Et_2O	0.5 ± 0.2	1 : 0
13	$Ni[P(OEt)_3]_4$	(3)	SZO_{300}	(3)	THF	46 ± 2	7 : 1
14	$Ni[P(OEt)_3]_4$	(3)	SZO_{300}	(3)	Toluene	19 ± 5	12 : 1
15	$Ni[P(OEt)_3]_4$	(3)	SZO_{300}	(3)	Hexanes	36.4 ± 0.2	11 : 1
16	None	---	SZO_{300}	(3)	Et_2O	0	— —
17	$Ni[P(OEt)_3]_4$	(3)	None	---	Et_2O	0.5 ± 0.1	1 —
18	$Ni[P(OEt)_3]_4$	(3)	SZO_{300}	(0.3)	Et_2O	37 ± 9	8 : 1
19	$Ni[P(OEt)_3]_4$	(3)	SZO_{300}	(1)	Et_2O	48 ± 5	10 : 1
20	$Ni[P(OEt)_3]_4$	(3)	SZO_{300}	(2)	Et_2O	68 ± 9	11 : 1
21	$Ni[P(OEt)_3]_4$	(3)	SZO_{300}	(5)	Et_2O	83 ± 1	22 : 1
22	$Ni[P(OEt)_3]_4$	(3)	SZO_{300}	(10)	Et_2O	72 ± 3	31 : 1
23	$Ni[P(OEt)_3]_4$	(1)	SZO_{300}	(1)	Et_2O	27 ± 4	13 : 1
24	$Ni[P(OEt)_3]_4$	(5)	SZO_{300}	(5)	Et_2O	79 ± 1	27 : 1
25	$Ni[P(OEt)_3]_4$	(10)	SZO_{300}	(10)	Et_2O	82 ± 2	28 : 1

[a]0.12 mmol **1a** scale

E.1.5. Additive Screening and Their Effect on Isomerization

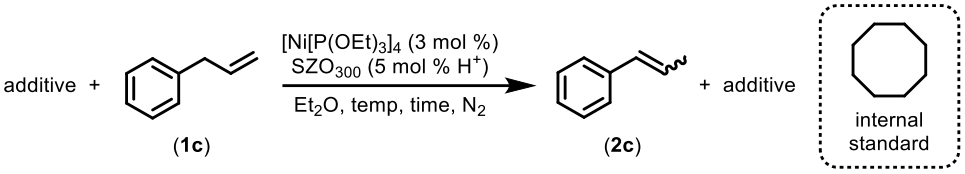

In a nitrogen-filled glovebox, SZO_{300} (15 mg, 0.0030 mmol H^+, 0.050 equiv H^+ per vial) was weighed directly into a 1-dram vial equipped with a stir bar. A stock solution of $Ni[P(OEt)_3]_4$ in Et_2O was prepared and the appropriate amount was distributed to the vial using a disposable 1-mL syringe (1.3 mg, 0.0018 mmol, 0.030 equiv was added to each vial). To each vial was added cyclooctane (internal standard; 5.0 µL, 0.037 mmol) using a 25-µL syringe. The total volume of Et_2O in the vial was 1.0 mL. The vial was sealed with a septum cap and brought out of the glovebox. The corresponding additive (0.060 mmol, 1.0 equiv) was added to the vial using a 10-µL syringe followed by **1c** (8.0 uL, 0.060 mmol, 1.0 equiv) using a 25-µL syringe. The reaction was then immediately heated to 30 °C using a preheated aluminum block and stirred at a rate of 150 rpm. The reaction progress was monitored by GC by taking aliquots (~20 µL) over time. The aliquots were diluted with hexanes (1 mL) and filtered through Celite into a GC vial. Two trials

were run for each experiment, and the yield averages and standard deviations are reported in Table S3 below.

Table E.3. Additive, reaction time, yield of **2c**, and *E*/*Z* selectivity for the additive screening experiments.

Entry	Additive	Time (h)	Yield 2c (%)	*E*/*Z* Selectivity (std error)
1	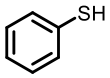	5	96±2	35.6:1 (0.7)
2	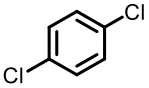	2	97.0±0.6	35:1 (1)
3	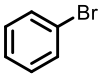	1	97±3	33.82:1 (0.05)
4		1	95±2	32.0:1 (0.7)
5	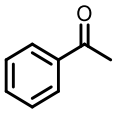	1	99±3	32.4:1 (0.9)
6	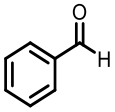	5	94±9	29:1 (3)
7		5	34±2	3.948:1 (0.008)
8	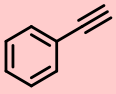	5	0.5±0.1	1:0
9	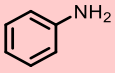	5	7±1	1.83:1 (0.02)

E.1.6. Evaluation of the Substrate Scope for Isomerization

a. General Procedure for the Isomerization and Isolation of Products

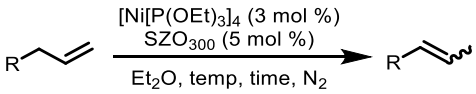

General Procedure: In a nitrogen-filled glovebox, $Ni[P(OEt)_3]_4$ (21.7 mg, 0.0300 mmol, 0.0300 equiv), SZO_{300} (250 mg, 0.0500 mmol H^+, 0.0500 equiv H^+), and Et_2O (17 mL) were added to a 4-dram scintillation vial equipped with a stir bar. The vial was sealed with a septum cap, brought out of the glovebox, injected with the alkene (1.00 mmol, 1.00 equiv) using a 250-µL syringe, and heated at 30 °C on a preheated aluminum vial block for an allotted amount of time specified below for each alkene. The reaction was stirred at a rate of 150 rpm. The reaction progress was monitored

by GC or GC-MS by taking aliquots (~5 µL) over time; the aliquots were diluted with hexanes (1 mL) and filtered through Celite into a GC vial. When the reaction was complete, it was removed from heat, opened to air, and the solution was filtered through Celite, washing Et_2O (2.0 mL). The filtrate was concentrated, and the product was purified as described below for each substrate.

b. General Procedure for the Isomerization and Isolation of Products

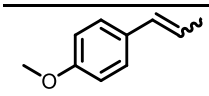

Anethole (**2a**)

Synthesis details: substrate **1a**, 30 °C, crude *E*/*Z* ratio determined by GC = 34:1 (*E*/*Z*)

Reaction time: 6 h

Purification details: column chromatography: silica, 0:100 to 5:95 Et_2O/hexanes gradient to give the product as a colorless oil (0.114 g, 0.769 mmol, 77% yield). NMR spectra match values previously reported.[228,318]

The major product isolated is the *E*-isomer, and the *Z*-isomer is seen in the NMR spectra as well. The ratio of these isomers determined by the integration of H in the β-position was found to be 32:1 (*E*/*Z*).

E-isomer:

^{1}H NMR (500 MHz, C_6D_6, 298 K): δ 7.20 (d, *J* = 8.7 Hz, 2H), 6.77 (d, *J* = 8.7 Hz, 2H), 6.32 (dq, *J* = 15.7, 1.8 Hz, 1H), 5.96 (dq, *J* = 15.7, 6.6 Hz, 1H), 3.31 (s, 3H), 1.70 (dd, *J* = 6.6, 1.7 Hz, 3H)

^{13}C{^{1}H} NMR (126 MHz, C_6D_6, 298 K): δ 159.3, 131.25, 131.21, 127.4, 123.1, 114.3, 54.8, 18.5

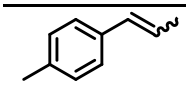

1-(4-methylphenyl)-1-propene (**2b**)

Synthesis details: substrate **1b**, 30 °C, crude *E*/*Z* ratio determined by GC-MS = 36:1 (*E*/*Z*)

Reaction Time: 3 h

Purification details: pipette plug: silica, 5:95; Et_2O/hexane to give the product as a colorless oil (0.123 g, 0.930 mmol, 93% yield). NMR spectra match values previously reported.[318,319]

The major product isolated is the *E*-isomer, and the *Z*-isomer is seen in the NMR spectra as well. The ratio of these isomers determined by integration of H in the β-position was found to be 34:1 (*E*/*Z*).

E-isomer:

^{1}H NMR (500 MHz, $CDCl_3$, 298 K): δ 7.20 (d, *J* = 8.1 Hz, 2H), 7.07 (d, *J* = 8.1 Hz, 2H), 6.35 (dd, *J* = 15.7, 1.3 Hz, 1H), 6.15 (dq, *J* = 15.7, 6.6 Hz, 1H), 2.29 (s, 3H), 1.84 (dd, *J* = 6.6, 1.6 Hz, 3H)

^{13}C{^{1}H} NMR (126 MHz, $CDCl_3$, 298 K): δ 136.5, 135.3, 131.0, 129.3, 125.8, 124.7, 21.2, 18.5

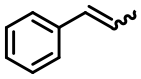

β-methylstyrene (**2c**)

Synthesis details: substrate **1c**, 30 °C, crude *E*/*Z* ratio determined by GC = 35:1(*E*/*Z*)

Reaction Time: 3 h

Purification details: pipette plug: silica, hexane to give the product as a colorless oil (0.111 g, 0.942 mmol, 94% yield). NMR spectra match values previously reported.[318]

The major product isolated is the *E*-isomer, and the *Z*-isomer is seen in the NMR spectra as well. The ratio of these isomers determined by the integration of H in the β-position was found to be 50:1 (*E*/*Z*).

E-isomer:

^{1}H NMR (500 MHz, C_6D_6, 298 K): δ 7.24 (d, *J* = 7.4 Hz, 2H), 7.14 (m, 2H), 7.05 (tt, *J* = 7.3, 1.4 Hz, 1H), 6.30 (dq, *J* = 15.7, 1.7 Hz, 1H), 6.03 (dq, *J* = 15.7, 6.6 Hz, 1H), 1.65 (dd, *J* = 6.6, 1.7 Hz, 3H)

^{13}C{^{1}H} NMR (126 MHz, C_6D_6, 298 K): δ 138.4, 131.7, 128.8, 127.1, 126.3, 125.5, 18.5

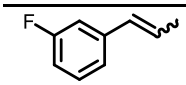

1-fluoro-3-(1-propen-1-yl)benzene (**2d**)

Synthesis details: substrate **1d**, 30 °C, crude *E*/*Z* ratio determined by GC-MS = 35:1 (*E*/*Z*)

Reaction time: 3 h

Purification details: pipette plug: silica, 100% hexane to give the product as a colorless oil (0.123 g, 0.903 mmol, 90% yield). NMR spectra match values previously reported.[230]

The major product isolated is the *E*-isomer, and the *Z*-isomer is seen in the NMR spectra as well. The ratio of these isomers determined by integration of H in the β-position was found to be 25:1 (*E*/*Z*).

E-isomer:

^{1}H NMR (500 MHz, C_6D_6, 298 K): δ 6.96 (m, 1H), 6.89 (td, *J* = 7.8, 5.8 Hz, 1H), 6.85-6.83 (m, 1H), 6.71 (m, 1H), 6.10 (d, *J* = 15.8 Hz, 1H), 5.88 (dq, *J* = 15.7, 6.6 Hz, 1H), 1.56 (dd, *J* = 6.7, 1.7 Hz, 3H)

^{13}C{^{1}H} NMR (126 MHz, C_6D_6, 298 K): δ 163.8 (d, *J* = 244.7 Hz), 140.9 (d, *J* = 7.8 Hz), 130.5 (d, *J* = 2.5 Hz), 130.2 (d, *J* = 8.3 Hz), 127.1, 122.1 (d, *J* = 2.8 Hz), 113.8 (d, *J* = 21.5 Hz), 112.7 (d, *J* = 21.7 Hz), 18.3

^{19}F NMR (471 MHz, C_6D_6, 298 zK): δ -113.72 (m)

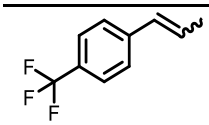

1-(4-trifluoromethylphenyl)-1-propene (**2e**)

Synthesis details: substrate **1e**, 30 °C, crude *E*/*Z* ratio determined by GC = 43:1 (*E*/*Z*)

Reaction Time: 2 h

Purification details: pipette plug: silica, 100% pentane to give the product as a white solid (0.154 g, 0.828 mmol, 83% yield). NMR spectra match values previously reported.[228]

The major product isolated is the *E*-isomer, and the *Z*-isomer is seen in the ^{19}F NMR spectrum as well. The ratio of these isomers determined by integration of F in the CF_3 group and was found to be 33:1 (*E*/*Z*).

E-isomer:

^{1}H NMR (500 MHz, $CDCl_3$, 298 K): δ 7.53 (d, *J* = 8.2 Hz, 2H), 7.41 (d, *J* = 8.2 Hz, 2H), 6.43 (d, *J* = 15.8 Hz, 1H), 6.34 (dq, *J* = 15.8, 6.4 Hz, 1H), 1.91 (d, *J* = 6.4 Hz, 3H)

$^{13}C\{^{1}H\}$ NMR (126 MHz, $CDCl_3$, 298 K): δ 141.5, 130.1, 128.8, 128.7 (q, *J* = 32 Hz), 125.6 (q, *J* = 3.8 Hz), 124.5 (q, *J* = 272 Hz), 18.7

^{19}F NMR (471 MHz, $CDCl_3$, 298 K): δ -62.39

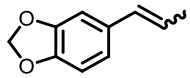

Isosafrole (**2f**)

Synthesis details: substrate **1f**, 30 °C, crude *E*/*Z* ratio determined by GC = 38:1 (*E*/*Z*)

Reaction time: 5 h

Purification details: pipette plug: silica, 100% pentane to give the product as a colorless oil (0.142 g, 0.874 mmol, 87% yield). NMR spectra match values previously reported.[228]

The major product isolated is the *E*-isomer, and the *Z*-isomer is seen in the NMR spectra as well. The ratio of these isomers determined by integration of H in the allyl-methyl position was found to be 31:1 (*E*/*Z*).

^{1}H NMR (500 MHz, C_6D_6, 298 K): δ 6.89 (s, 1H), 6.62 (s, 2H), 6.20 (dq, *J* = 15.7, 1.7 Hz, 1H), 5.83 (dq, *J* = 15.7, 6.7 Hz, 1H), 5.31 (s, 2H), 1.62 (dd, *J* = 6.7, 1.7 Hz, 3H)

$^{13}C\{^{1}H\}$ NMR (126 MHz, C_6D_6, 298 K): δ 148.6, 147.2, 133.0, 131.2, 123.7, 120.6, 108.5, 105.8, 100.9, 18.3

IR (ATR, neat) v: 3069-2774 (w), 1488 (s), 1245 (s), 1038 (s), 935 (w)

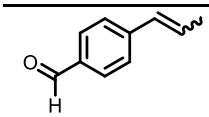

4-(1-propen-1-yl)benzaldehyde (**2g**)

Synthesis details: substrate **1g**, 30 °C, crude *E*/*Z* ratio determined by GC-MS = 57:1

Reaction time: 5 h

Purification details: column chromatography, silica, 0:100 to 5:95 Et_2O/pentane to give the product as a pale yellow oil (0.138 g, 0.941 mmol, 94% yield).

^{1}H NMR (500 MHz, C_6D_6, 298 K): δ 9.70 (s, 1H), 7.54 (d, *J* = 8.2 Hz, 2H), 7.05 (d, *J* = 8.2 Hz, 2H), 6.11 (dq, *J* = 15.8, 1.7 Hz, 1H), 5.96 (dq, *J* = 15.8, 6.6 Hz, 1H), 1.57 (dd, *J* = 6.6, 1.5 Hz, 3H)

$^{13}C\{^{1}H\}$ NMR (126 MHz, C_6D_6, 298 K): δ 190.7, 143.7, 135.7, 130.7, 130.1, 129.3, 126.4, 18.5

IR (ATR, neat) v: 3023-2725 (w), 1687 (s), 1600 (s), 1212 (s), 964 (m)

ASAP/HRMS (m/z): [M^+] calculated for $C_{10}H_{10}O$ 146.0732, found 146.0678

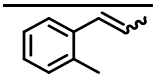

1-(2-methylphenyl)-1-propene (**2h**)

Synthesis details: substrate **1h**, 30 °C, crude *E*/*Z* ratio determined by GC = 12:1 (*E*/*Z*)

Purification details: pipette plug: silica, 100% pentane to give the product as a colorless oil (0.128 g, 0.968 mmol, 97% yield). NMR spectra match values previously reported.[318,319]

The major product isolated is the *E*-isomer, and the *Z*-isomer is seen in the NMR spectra as well. The ratio of these isomers determined by integration of H in the β-position was found to be 13:1 (*E*/*Z*). The *E*-product is fully characterized below, and the peaks visible and clearly assignable to the *Z*-isomer are given directly following the NMR characterization of the *E*-product.

Reaction time: 4 h

E-isomer

^{1}H NMR (500 MHz, C_6D_6, 298 K): δ 7.40 (dd, *J* = 7.4, 0.9 Hz, 1H), 7.06-7.10 (m, 1H), 7.05 (td, *J* = 7.3, 1.4 Hz, 1H), 7.01 (m, 1H), 6.56 (qd, *J* = 15.6, 1.7 Hz, 1H), 5.96 (dq, *J* = 15.6, 6.6 Hz, 1H), 2.15 (s, 3H), 1.69 (dd, *J* = 6.6, 1.7 Hz, 3H)

$^{13}C\{^{1}H\}$ NMR (126 MHz, C_6D_6, 298 K): δ 137.5, 134.9, 130.5, 129.6, 127.16, 126.83, 126.4, 126.0, 19.8, 18.8

Z-isomer:

^{1}H NMR (500 MHz, C_6D_6, 298 K): δ 7.22 (m, 0.09H), 6.43 (qd, *J* = 11.4, 6.0 Hz, 0.08H), 5.69 (dq, *J* = 11.4, 6.9 Hz, 0.08H), 2.12 (s, 0.25H), 1.61 (dd, *J* = 7.0, 1.8 Hz, 0.24H)

$^{13}C\{^{1}H\}$ NMR (126 MHz, C_6D_6, 298 K): δ 136.9, 136.4, 130.2, 129.52, 129.48 127.18, 126.81, 125.7, 19.9, 14.4

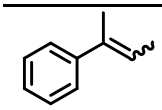

α,β-dimethylstyrene (**2i**)

Synthesis details: 0.895 mmol substrate **1i**, 3.4 mol % $Ni[P(OEt)_3]_4$, 5.6 mol % SZO_{300}, 50 °C, crude *E*/*Z* ratio determined by GC = 5.5:1 (*E*/*Z*)

Reaction time: 24 h

Purification details: pipette plug: silica, 100% pentane to give the product as a colorless oil. 0.118 g was isolated with 2.6% **1i**. The amount and yield of **2i** was adjusted to 0.115 g, 0.870 mmol, 97% yield. NMR spectra match previously reported values.[320]

The major product isolated is the *E*-isomer, and the *Z*-isomer is seen in the NMR spectra as well. The ratio of these isomers determined by integration of H in the β-position was found to be 7.7:1 (*E*/*Z*) and 2.6% **1i** Is seen. The *E*-isomer is fully characterized below, and the peaks visible and clearly assignable to the *Z*-isomer are given directly following the NMR characterization of the *E*-isomer.

E-isomer:

^{1}H NMR (500 MHz, $CDCl_3$, 298 K): δ 7.36 (d, *J* = 7.5 Hz, 2H), 7.29 (t, *J* = 7.5 Hz, 2H), 7.20 (t, *J* = 7.0, 1H), 5.86 (qq, *J* = 6.4, 1.2 Hz, 1H), 2.02 (s, 3H), 1.79 (dq, *J* = 6.9, 1.1 Hz, 3H)

$^{13}C\{^{1}H\}$ NMR (126 MHz, $CDCl_3$, 298 K): δ 144.2, 135.7, 128.3, 126.53, 125.7, 122.6, 15.6, 14.5

Z-isomer:

^{1}H NMR (500 MHz, $CDCl_3$, 298 K): δ 5.56 (qq, *J* = 6.9, 1.2 Hz, 0.13H), 1.59 (dq, *J* = 3.4 Hz, 1.3 Hz, 0.39 H)

$^{13}C\{^{1}H\}$ NMR (126 MHz, $CDCl_3$, 298 K): δ 142.0, 137.0, 128.21, 128.16, 126.51, 121.7, 25.5, 15.0

1-(methoxymethoxy)-2-(1*E*)-1-propen-1-ylbenzene (**2j**)

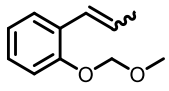

Synthesis details: substrate **1j**, 30 °C, crude *E*/*Z* ratio determined by GC = 19:1

Reaction time: 8 h

Purification details: column chromatography: silica, 100% pentane to give the product as a colorless oil (0.121 g, 0.681 mmol, 68% yield). NMR spectra match values previously reported.[321]

The major product isolated is the *E*-isomer, and the *Z*-isomer is seen in the NMR spectra as well. The ratio of these isomers determined by integration of H in the β-position was found to be 19:1 (*E*/*Z*). The *E*-isomer is fully characterized below, and the peaks visible and clearly assignable to the *Z*-isomer are given directly following the NMR characterization of the *E*-isomer.

E-isomer:

^{1}H NMR (500 MHz, C_6D_6, 298 K): δ 7.42 (dd, *J* = 7.7, 1.6 Hz, 1H), 7.11 (dd, *J* = 8.3, 1.0 Hz, 1H), 7.04-6.99 (ms, 2H), 6.15 (qd, *J* = 15.8, 6.6 Hz, 1H), 4.87 (s, 2H), 3.12 (s, 3H), 1.75 (dd, *J* = 6.6, 1.7 Hz, 3H)

^{13}C{^{1}H} NMR (126 MHz, C_6D_6, 298 K): δ 154.7, 128.1, 126.7, 126.5, 126.2, 122.2, 115.2, 94.8, 55.6, 18.9 (one signal overlaps with C_6D_6 signal)

^{13}C{^{1}H} NMR (126 MHz, $CDCl_3$, 298 K): δ 154.0, 128.0, 127.9, 126.7, 126.5, 125.7, 122.1, 115.0, 95.0, 56.2, 19.1

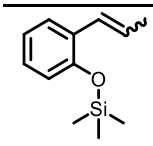

1-propen-1-yl-2-[(trimethylsilyl)oxy]benzene (**2k**)

Synthesis details: substrate **1k**, 30 °C, crude *E*/*Z* ratio determined by GC-MS = 28:1 (*E*/*Z*)

Reaction time: 5 h

Purification details: column chromatography: silica, 100% hexanes to give the product as a colorless oil (0.192 g, 0.930 mmol, 93% yield). NMR spectra match values previously reported.[322]

The major product isolated is the *E*-isomer, and the *Z*-isomer is seen in the NMR spectra as well. The ratio of these isomers determined by integration of H in the β-position was found to be 18:1 (*E*/*Z*). The *E*-product is fully characterized below, and the peaks visible and clearly assignable to the *Z*-isomer are given directly following the NMR characterization of the *E*-product.

<u>*E*-isomer:</u>

^{1}H NMR (500 MHz, C_6D_6, 298 K): δ 7.44 (dd, J = 7.7, 1.4 Hz, 1H), 7.00 (td, J = 7.7, 1.7 Hz, 1H), 6.92-6.86 (ms, 2H), 6.81 (dd, J = 8.0, 0.8 Hz, 1H), 6.13 (dq, J = 15.9, 6.6 Hz, 1H), 1.74 (dd, J = 6.6, 1.8 Hz, 3H), 0.17 (s, 9H)

^{13}C{^{1}H} NMR (126 MHz, C_6D_6, 298 K): δ 152.8 130.0, 128.0, 127.0, 126.9, 125.8, 122.1, 120.2, 18.9, 0.4

^{29}Si{^{1}H} NMR (99 MHz, C_6D_6, 298 K): 18.84

<u>*Z*-isomer</u>

^{1}H NMR (500 MHz, C_6D_6, 298 K): δ 7.32 (dd, J = 7.5, 1.3 Hz, 0.07H), 7.04 (m, 0.08H), 6.84 (m, 0.09), 5.73 (dq, J = 11.6, 7.1 Hz, 0.06H), 1.72 (d, J = 1.8 Hz, 0.10H), 0.15 (s, 0.48H)

^{13}C{^{1}H} NMR (126 MHz, C_6D_6, 298 K): δ 153.7, 130.9, 126.6, 121.4, 120.1, 14.7

IR (ATR, neat) v: 3065-2853 (w), 1483 (m), 1248 (s), 911 (s), 840 (s)

ASAP/HRMS (m/z): [M^+] calculated for $C_{12}H_{18}OSi$

206.1127, found 206.1101

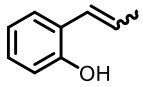

2-(1-propenyl)phenol (**2l**)

<u>Synthesis details:</u> substrate **1l**, 30 °C, crude *E*/*Z* ratio determined by GC-MS = 46:1 (*E*/*Z*)

<u>Reaction time:</u> 4 h

<u>Purification details:</u> column chromatography: silica, 0:100 to 5:95 gradient Et_2O/pentane to give the product as a white solid (0.132 g, 0.984 mmol, 98% yield). NMR spectra match values previously reported.[323]

^{1}H NMR (500 MHz, $CDCl_3$, 298 K): δ 7.32 (dd, *J* = 7.7, 1.4 Hz, 1H), 7.11 (td, *J* = 7.7, 1.6 Hz, 1H), 6.90 (td, *J* = 7.5, 0.9 Hz, 1H), 6.80 (dd, *J* = 8.1, 0.9 Hz, 1H), 6.60 (dq, *J* = 15.8, 1.8 Hz, 1H), 6.23 (dq, *J* = 15.8, 6.6 Hz, 1H), 5.06 (s, 1H), 1.93 (dd, *J* = 6.6, 1.7 Hz, 3H)

^{13}C{^{1}H} NMR (126 MHz, $CDCl_3$, 298 K): δ 152.4, 128.5, 128.1, 127.5, 125.4, 125.2, 121.0, 115.8, 19.0

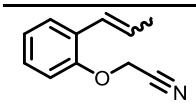

{2-[(1E)-1-propen-1-yl]phenoxy}acetonitrile (**2m**)

Synthesis details: 1.01 mmol of substrate **1m** was used, 30 °C, crude *E*/*Z* ratio determined by GC = 26:1 (*E*/*Z*)

Reaction time: 4 h

Purification details: column chromatography: silica, gradient 0:100 to 3:97 gradient EtOAc/hexanes to give the product as a colorless oil (0.173 g, 0.996 mmol, 98% yield). NMR spectra match values previously reported.[324]

The major product isolated is the *E*-isomer, and the *Z*-isomer is seen in the NMR spectra as well. The ratio of these isomers determined by integration of H in the β-position was found to be 25:1 (*E*/*Z*).

^{1}H NMR (500 MHz, C_6D_6, 298 K): δ 7.30 (dd, *J* = 7.7, 1.6 Hz, 1H), 6.90 (td, *J* = 7.8, 1.6 Hz, 1H), 6.82 (t, *J* = 7.5 Hz, 1H), 6.73 (dq, *J* = 15.9, 1.9 Hz, 1H), 6.41 (d, *J* = 8.2 Hz, 1H), 6.04 (dq, *J* = 15.9, 6.7 Hz, 1H), 3.57 (d, *J* = 1.0 Hz, 2H), 1.68 (dd, *J* = 6.7, 1.9 Hz, 3H)

^{13}C{^{1}H} NMR (126 MHz, C_6D_6, 298 K): δ 153.7, 128.5, 128.0, 127.6, 127.2, 125.3, 123.2, 115.4, 113.0, 53.4, 18.9

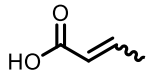

Crotonic acid (**2n**)

Synthesis details: substrate **1n**, 30 °C, only the *E*-isomer was observed by GC

Reaction time: 5 h

Purification details: column chromatography: silica, gradient 0:100 to 16:84 gradient Et_2O/hexanes to give the product as a crystalline white solid

(0.0639 g, 0.742 mmol, 74% yield). NMR spectra match previously reported values.[325]

^{1}H NMR (500 MHz, $CDCl_3$, 298 K): δ 11.37 (br s, 1H), 7.10 (dq, *J* = 15.5, 7.0 Hz, 1H), 5.86 (dq, *J* = 15.5, 1.7 Hz, 1H), 1.92 (dd, *J* = 7.0, 1.7 Hz, 3H).

^{13}C{^{1}H} NMR (126 MHz, $CDCl_3$, 298 K): δ 171.4, 147.6, 122.2, 18.3

IR (ATR, neat) v: 2976-2517 (br), 1683 (s), 1420 (m), 1222 (m), 965 (s)

ASAP/HRMS (m/z): [M^+] calculated for C_5H_8O
86.0368, found 86.0539

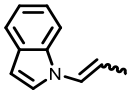

1-propen-1-yl-1*H*-indole (**2o**)

Synthesis details: substrate **1o**, 30 °C, crude *E*/*Z* ratio determined by GC = 8.5:1 (*E*/*Z*)

Reaction Time: 8 h

Purification details: column chromatography: silica, 0:100-3:97 EtOAc/hexanes to yield the product as a white solid (0.110 g, 0.700 mmol, 70% yield). NMR spectra match values previously reported.[326]

The major product isolated is the *E*-isomer, and the *Z*-isomer is seen in the NMR spectra as well. The ratio of these isomers determined by integration of H in the β-position was found to be 9.5:1 (*E*/*Z*). The *E*-isomer is fully characterized below, and the peaks visible and clearly assignable to the *Z*-isomer are given directly following the NMR characterization of the *E*-isomer.

E-isomer:

^{1}H NMR (500 MHz, C_6D_6, 298 K): δ 7.65-7.63 (m, 1H), 7.24-7.17 (ms, 3H), 7.01 (d, *J* = 3.3 Hz, 1H), 6.60 (dq, *J* = 14.0, 1.7 Hz, 1H), 6.52 (d, *J* = 3.3 Hz, 1H), 5.29 (dq, *J* = 14.0, 6.9 Hz, 1H), 1.49 (dd, *J* = 6.7, 1.7 Hz, 3H)

^{13}C{^{1}H} NMR (126 MHz, C_6D_6, 298 K): δ 135.9, 129.6, 125.1, 124.3, 122.7, 121.5, 120.8, 110.2, 109.9, 104.3, 15.1

Z-isomer:

---

^{1}H NMR (500 MHz, C_6D_6, 298 K): δ 7.68 (m, 0.11H), 6.95 (d, *J* = 3.3 Hz, 0.09H), 6.54 (d, *J* = 3.3 Hz, 0.11H), 6.42 (dq, *J* = 8.5, 1.7 Hz, 0.11H), 5.05 (dq, *J* = 8.4, 7.2 Hz, 0.11H), 1.42 (dd, *J* = 7.1, 1.8 Hz, 0.31H)

^{13}C{^{1}H} NMR (126 MHz, C_6D_6, 298 K): δ 127.4, 124.8, 122.6, 121.3, 117.7, 110.5, 103.5, 12.8

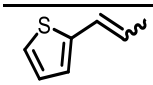

2-(1-propenyl)-thiophene (**2p**)

Synthesis details: 0.68 mmol substrate **1p**, 4.4 mol % $Ni[P(OEt)_3]_4$, 7.4 mol % SZO_{300}, 50 °C, crude *E*/*Z* ratio determined by ^{1}H NMR = 6.3:1 (*E*/*Z*)

Reaction time: 24 h

Purification details: pipette plug: silica, 100% pentane to give the product as a colorless oil (0.0739 g, 0.878 mmol, 88% yield). NMR spectra values match previously reported.[327,328]

The major product isolated is the *E*-isomer, and the *Z*-isomer is seen in the NMR spectra as well. The ratio of these isomers determined by integration of H in the β-position was found to be 7.4:1 (*E*/*Z*). The *E*-isomer is fully characterized below, and the peaks visible and clearly assignable to the *Z*-isomer are given directly following the NMR characterization of the *E*-isomer.

E-isomer

^{1}H NMR (500 MHz, C_6D_6, 298 K): δ 6.73 (d, *J* = 5.0 Hz, 1H), 6.70-6.67 (ms, 2H), 6.34 (dq, *J* = 15.6, 1.7 Hz, 1H), 5.94 (qd, *J* = 15.6, 6.7 Hz, 1H), 1.54 (dd, *J* = 6.7, 1.7 Hz, 3H)

^{13}C{^{1}H} NMR (126 MHz, C_6D_6, 298 K): δ 143.5, 127.4, 125.5, 124.9, 124.4, 123.2, 18.2

Z-isomer

^{1}H NMR (500 MHz, C_6D_6, 298 K): δ 6.88 (d, *J* = 5.0 Hz, 0.15H), 6.79 (d, *J* = 3.5 Hz, 0.14H), 6.75 (m, 0.14H), 6.49 (dq, *J* = 11.5, 1.8 Hz, 0.15H), 5.48 (qd, *J* = 11.4, 7.3 Hz, 0.14H), 1.82 (dd, *J* = 7.2, 1.7 Hz, 0.41H)

$^{13}C\{^{1}H\}$ NMR (126 MHz, C_6D_6, 298 K): δ 141.2, 126.9, 125.2, 124.6, 123.6, 15.1

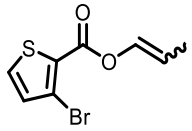

1-propen-1-yl-3-bromo-2-thiophenecarboxylate (**2q**)

Synthesis details: substrate **1q**, 30 °C, crude *E*/*Z* ratio determined by GC = 1:1.9 (*E*/*Z*)

Reaction time: 24 h

Purification details: column chromatography: silica, gradient 0:100 to 8:92 gradient EtOAc/hexanes to give the product as a white, waxy solid (0.242 g, 0.979 mmol, 98% yield).

The major product isolated is the *Z*-isomer, and the *E*-isomer is seen in the NMR spectra as well. The ratio of these isomers determined by integration of H in the β-position was found to be 1:1.7 (*E*/*Z*). Both products are fully characterized below.

E-isomer

^{1}H NMR (500 MHz, $CDCl_3$, 298 K): δ 7.51 (d, *J* = 5.2 Hz, 0.54H), 7.20 (m that overlaps with *Z*-isomer, 0.56H), 7.12 (d, *J* = 5.2 Hz, 0.58H), 5.61 (dq, *J* = 12.3, 7.1 Hz, 0.58H), 1.70 (dd, *J* = 7.0, 1.7 Hz, 1.82H)

$^{13}C\{^{1}H\}$ NMR (126 MHz, $CDCl_3$, 298 K): δ 158.1, 135.6, 133.36, 132.1, 126.6, 118.2, 111.2, 12.5

Z-isomer

^{1}H NMR (500 MHz, $CDCl_3$, 298 K): δ 7.53 (d, *J* = 5.2 Hz, 1H), 7.22 (m that overlaps with *E*-isomer, 1H), 7.14 (d, *J* = 5.2 Hz, 1H), 5.07 (dq, *J* = 6.9, 6.3 Hz, 1H), 1.80 (dd, *J* = 6.9, 1.8 Hz, 3H)

$^{13}C\{^{1}H\}$ NMR (126 MHz, $CDCl_3$, 298 K): δ 158.0, 134.6, 133.43, 132.3, 127.1, 118.0, 109.9, 10.4

IR (ATR, neat) v: 3105-2858 (w), 1726 (s), 1413 (s), 1224 (s), 1075 (s), 880 (m)

ASAP/HRMS (m/z): $[M^+]$ calculated for $C_8H_7BrO_2S$

245.9350, found 245.9334

2-sulfolene (**2r**)

Synthesis details: substrate **1r**, 30 °C.

Reaction time: 24 h

Reaction workup details: The filtered product was analyzed by NMR to yield a mixture of **2r** and **1r** (0.118 g, 0.99 mmol, >99% **1r** and **2r** recovered). The ratio of **1r** and **2r** was determined by integration of H in the alkene positions for **1r** (6.02 ppm, 2H) and for **2r** (6.72 ppm, 1H) and the conversion of **1r** to **2r** was found to 37%. **2r** is characterized below by ^{1}H and $^{13}C\{^{1}H\}$. NMR spectra match previously reported values.[329]

^{1}H NMR (500 MHz, $CDCl_3$, 298 K): δ 6.72 (m, 1H), 6.60 (dt, J = 6.7, 2.2 Hz, 1H), 3.17 (m, 2H), 2.90 (m, 2H)

$^{13}C\{^{1}H\}$ NMR (126 MHz, $CDCl_3$, 298 K): δ 139.3, 131.8, 47.4, 26.5

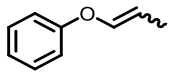

(1-propen-1-yloxy)benzene (**2s**)

Synthesis details: substrate **1s**, 30 °C, crude *E*/*Z* ratio determined by GC-MS = 1:2.3

Reaction time: 1 h

Purification details: pipette plug: silica, 5:95 Et_2O/hexanes to give the product as a colorless oil (0.0976 g, 0.727 mmol, 73% yield). NMR spectra match values previously reported.[330–332]

The major product isolated is the *Z*-isomer, and the *E*-isomer is seen in the NMR spectra as well. The ratio of these isomers determined by integration of H in the β-position was found to be 1:2.8 (*E*/*Z*). Because of significant overlap in the aryl region, both isomers are characterized together below.

^{1}H NMR (500 MHz, $CDCl_3$, 298 K): δ 7.35-7.31 (m, 7.1H, *E*- and *Z*-isomers), 7.07-6.99 (ms, 10.6H, *E*- and *Z*-isomers), 6.45 (m, 1H, *E*-isomer), 6.41 (m, 2.6H, *Z*-product), 5.41 (m, 1H, *E*-isomer), 4.90 (m, 2.6H, *Z*-isomer), 1.75 (m, 7.7H, *Z*-isomer), 1.70 (m, 3H, *E*-isomer)

$^{13}C\{^{1}H\}$ NMR (126 MHz, $CDCl_3$, 298 K): δ 157.7 (*Z*-isomer), 157.6 (*E*-isomer), 142.1 (*E*-isomer), 141.0 (*Z*-isomer), 129.7 (*E*- and *Z*-isomer),

122.50 (*E*-isomer), 122.47 (*Z*-isomer), 116.4 (*E*-isomer), 116.3 (*Z*-isomer), 108.4 (*E*-isomer), 107.6 (*Z*-isomer), 12.4 (*E*-isomer), 9.5 (*Z*-isomer)

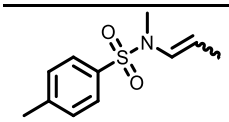

N-methyl-*N*-(prop-1-enyl)-p-toluenesulfonamide (**2t**)

Synthesis details: substrate **1t**, 30 °C, crude *E*/*Z* ratio determined by GC = 26:1 (*E*/*Z*)

Reaction time: 24 h

Purification details: pipette plug: silica, 0:100 to 20:80 EtOAc/hexane to give the product as a white solid (0.219 g, 0.972 mmol, 97% yield). NMR spectra match values previously reported.[333]

The major product isolated is the *E*-isomer, and the *Z*-isomer is seen in the NMR spectra as well. The ratio of these isomers determined by integration of H in the allyl-methyl position was found to be 24:1 (*E*/*Z*).

^{1}H NMR (500 MHz, $CDCl_3$, 298 K): δ 7.62 (d, *J* = 8.3 Hz, 2H), 7.30 (d, *J* = 8.0 Hz, 2H), 6.71 (dq, *J* = 14.0, 1.5 Hz, 1H), 4.71 (dq, *J* = 13.3, 6.8 Hz, 1H), 2.82 (s, 3H), 2.42 (s, 3H), 1.68 (dd, *J* = 6.6, 1.5 Hz, 3H)

^{13}C{^{1}H} NMR (126 MHz, $CDCl_3$, 298 K): δ 143.7, 134.8, 129.8, 128.4, 127.2, 106.5, 32.4, 21.7, 15.3

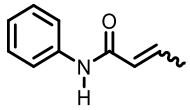

N-phenyl-2-butenamide (**2u**)

Synthesis details: substrate **1u**, 30 °C, crude *E*/*Z* ratio determined by GC = 33:1

Reaction time: 3 h

Purification details: column chromatography: silica, gradient 0:100 to 10:90 gradient EtOAc/DCM to give the product as a crystalline white solid (0.147 g, 0.912 mmol, 91% yield). NMR spectra match previously reported values.[334]

^{1}H NMR (500 MHz, $CDCl_3$, 298 K): δ 7.56 (d, *J* = 7.0 Hz, 2H), 7.32 (t, *J* = 8.0 Hz, 2H), 7.15 (br s, 1H), 7.11 (t, *J* = 7.4 Hz, 1H), 6.99 (dq, *J* = 15.0, 6.9 Hz, 1H), 5.95 (dq, *J* = 15.0, 1.7 Hz, 1H), 1.92 (dd, *J* = 6.9, 1.7 Hz, 3H)

$^{13}C\{^{1}H\}$ NMR (126 MHz, $CDCl_3$, 298 K): δ 164.3, 141.6, 138.2, 129.1, 125.6, 124.4, 120.2, 17.9

IR (ATR, neat) v: 3292-2742 (w), 1639 (m), 1443 (m), 1248 (m), 960 (m)

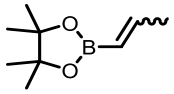

4,4,5,5-tetramethyl-2-1-propen-1-yl-1,3,2-dioxaborolane (**2v**)

Synthesis details: substrate **1v**, 30 °C, crude *E*/*Z* ratio determined by GC = 8.6:1 (*E*/*Z*)

Reaction time: 4 h

Purification details: Distillation (approximately 0.05 Torr, 25 °C) to give the product as a colorless oil (0.103 g, 0.613 mmol, 61% yield). NMR spectra match values previously reported.[228,335,336]

The major product isolated is the *E*-isomer, and the *Z*-isomer is seen in the NMR spectra as well. The ratio of these isomers determined by integration of H in the allylic methyl position was found to be 8.8:1 (*E*/*Z*). The *E*-product is fully characterized below, and the peaks visible and clearly assignable to the *Z*-isomer are given directly following the NMR characterization of the *E*-product.

E-isomer:

^{1}H NMR (500 MHz, C_6D_6, 298 K): δ 6.90 (dq, *J* = 17.8, 6.4 Hz, 1H), 5.77 (dq, *J* = 17.8, 1.7 Hz, 1H), 1.63 (dd, *J* = 6.4, 1.7 Hz, 3H), 1.09 (s, 12H)

$^{13}C\{^{1}H\}$ NMR (126 MHz, C_6D_6, 298 K): δ 149.6, 121.7 (br), 82.9, 24.96, 21.6

^{11}B NMR (160 MHz, C_6D_6, 298 K): δ 30.02

Z-isomer:

^{1}H NMR (500 MHz, C_6D_6, 298 K): δ 5.72 (m, 0.07H), 2.08 (dd, J = 6.9, 1.6 Hz, 0.35H), 1.07 (s, 1.62H)

$^{13}C\{^{1}H\}$ NMR (126 MHz, C_6D_6, 298 K): δ 149.8, 82.7, 24.97

^{11}B NMR (160 MHz, C_6D_6, 298 K): δ 22.89

IR (ATR, neat) v: 2979-2854 (w), 1642 (m), 1354 (s), 1143 (s), 849 (m)

2-(1-propen-1-yl)phenyl acetate (**2w**)

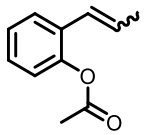

Synthesis details: substrate **1w**, 30 °C, crude *E*/*Z* ratio determined by GC-MS = 26:1 (*E*/*Z*)

Reaction time: 6 h

Purification details: pipette plug: silica, 100% pentane to give the product as a colorless oil (0.170 g, 0.965 mmol, 97% yield). NMR spectra values match values previously reported.[228]

The major product isolated is the *E*-isomer, and the *Z*-isomer is seen in the NMR spectra as well. The ratio of these isomers determined by integration of H in the β-position was found to be 16:1 (*E*/*Z*). The *E*-product is fully characterized below, and the peaks visible and clearly assignable to the *Z*-isomer are given directly following the NMR characterization of the *E*-product.

E-isomer:

^{1}H NMR (500 MHz, $CDCl_3$, 298 K): δ 7.51 (dd, *J* = 7.6, 1.7 Hz, 1H), 7.24-7.17 (ms, 2H), 7.01 (dd, *J* = 7.8, 1.4 Hz, 1H), 6.41 (dq, *J* = 15.8, 1.8 Hz, 1H), 6.25 (dq, *J* = 15.8, 6.6 Hz, 1H), 2.34 (s, 3H), 1.90 (dd, *J* = 6.6, 1.6 Hz, 3H)

^{13}C{^{1}H} NMR (126 MHz, $CDCl_3$, 298 K): δ 169.5, 147.6, 130.6, 128.6, 127.8, 126.6, 126.3, 124.41, 122.6, 21.06, 19.0

Z-isomer:

^{1}H NMR (500 MHz, $CDCl_3$, 298 K): δ 7.33 (m, 0.05H), 7.29 (m, 0.03H), 7.07 (dd, *J* = 7.9, 1.1 Hz, 0.05H), 6.31 (m, 0.05H), 5.87 (dq, *J* = 11.5, 7.0 Hz, 0.06H), 2.28 (s, 0.11H), 1.78 (dd, *J* = 7.0, 1.8 Hz, 0.13H)

IR (ATR, neat) v: 3053-2848 (w), 1765 (s), 1368 (m), 1201 (s), 962 (w)

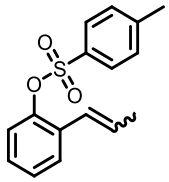

1-(4-methylbenzenesulfonate)-2-(2-propen-1-yl)phenol (**2x**)

Synthesis details: substrate **1x**, 30 °C, crude *E*/*Z* ratio determined by GC-MS = 29:1

Reaction time: 2 h

Purification details: column chromatography: silica, 0:100 to 4:96 Et_2O/hexanes to give the product as a viscous, colorless oil (0.287 g, 0.997 mmol, >99% yield).

The major product isolated is the *E*-isomer, and the *Z*-isomer is seen in the NMR spectra as well. The ratio of these isomers determined by integration of H in the β-position was found to be 29:1 (*E*/*Z*).

^{1}H NMR (500 MHz, $CDCl_3$, 298 K): δ 7.69 (d, *J* = 8.3 Hz, 2H), 7.39 (dd, *J* = 7.4, 2.3 Hz, 1H), 7.28 (d, *J* = 8.2 Hz, 2H), 7.19-7.13 (ms, 2H), 7.10 (m, 1H), 6.27 (dq, *J* = 15.9, 1.9 Hz, 1H), 6.00 (dq, *J* =15.8, 6.6 Hz, 1H), 2.43 (s, 3H), 1.71 (dd, *J* = 6.6, 1.7 Hz, 3H)

^{13}C{^{1}H} NMR (126 MHz, $CDCl_3$, 298 K): δ 146.5, 145.4, 132.9, 131.8, 129.7, 128.7, 128.3, 127.7, 127.2, 126.6, 124.1, 123.2, 21.8, 18.7

IR (ATR, neat) v: 3086-2849 (w), 1597 (m), 1363 (s), 1167 (s), 962 (m)

ASAP/HRMS (m/z): [M^+] calculated for $C_{16}H_{16}O_3S$
288.0820, found 288.0794

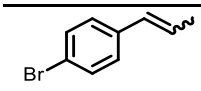

1-bromo-4-(1-propen-1-yl)benzene (**2y**)

Synthesis details: substrate **1y**, 30 °C, crude *E*/*Z* ratio determined by GC-MS = 42:1

Reaction time: 5 h

Purification details: column chromatography, silica, 0:100 to 5:95 Et_2O/pentane to give the product as a pale-yellow oil (0.181 g, 0.919 mmol, 92% yield).

The major product isolated is the *E*-isomer, and the *Z*-isomer is not seen in the NMR spectra.

E-isomer

^{1}H NMR (500 MHz, $CDCl_3$, 298 K) δ 7.36 (d, *J* = 8.4 Hz, 2H), 7.13 (d, *J* = 8.4 Hz, 2H), 6.29 (d, *J* = 16.1, 1H), 6.18 (dq, *J* = 15.7, 6.5 Hz, 1H), 1.84 (dd, *J* = 6.5, 1.2 Hz, 3H).

$^{13}C\{^{1}H\}$ NMR (126 MHz, $CDCl_3$, 298 K): δ 136.9, 131.6, 130.0, 127.5, 126.7, 120.4, 18.6

IR (ATR, neat) v: 3062-2727 (w), 1486 (m), 1070 (m), 966 (s), 840 (s)

ASAP/HRMS (m/z): [M^+] calculated for C_9H_9Br 195.9888, found 195.9955

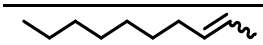

2-decene (**2z**)

Synthesis details: substrate **1z**, 30 °C, crude *E*/*Z* ratio determined by GC = 3.9:1

Reaction time: 8 h

Purification details: pipette plug: silica, 100% pentanes to give the product as a colorless oil (0.124 g, 0.881 mmol, 88% yield). NMR spectra match values previously reported.[337–339]

The major product isolated is *E*-2-decene (*E*-**2z**), and *Z*-2-decene (*Z*-**2z**) and other decene isomers (3-, 4-, and 5-decene) are seen in the NMR spectra as well (~87% 2-decene isomers and 13% internal isomers in the crude reaction determined by GC). The ratio of the 2-decene isomers determined by integration of H in the terminal methyl group was found to be 8.9:1 (*E*/*Z*). *E*-**2z** is fully characterized below, and the peaks visible and clearly assignable to *Z*-**2z** are given directly following the NMR characterization of the *E*-product.

E-isomer

^{1}H NMR (500 MHz, $CDCl_3$, 298 K): δ 5.43-5.40 (ms, 2H), 1.65 (d, J = 4.1 Hz, 2H), 1.38-1.27 (ms, 12H), 0.89 (t, J = 6.7 Hz, 3H)

$^{13}C\{^{1}H\}$ NMR (126 MHz, $CDCl_3$, 298 K): δ 131.9, 124.7, 32.8, 32.0, 29.8, 29.4, 29.3, 22.8, 18.1, 14.2

Z-isomer

^{1}H NMR (500 MHz, $CDCl_3$, 298 K): δ 1.61 (d, J = 5.9 Hz, 0.56H), 0.97 (t, J = 7.4 Hz, 0.39H)

1-Phenyl-2-butene (**2aa**)

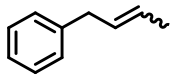

Synthesis details: substrate **1aa**, 0 °C, crude *E*/*Z* ratio determined by GC = 5.0:1 (*E*/*Z*)

Reaction time: 2.5 h

Purification details: pipette plug: silica, 100% hexanes to give the product as a colorless oil. 0.126 g was isolated with 7.3% **2ab**. The amount and yield of **2aa** was adjusted to 0.116 g, 0.881 mmol, 88% yield. NMR spectra match values previously reported.[230,340]

The major product isolated is the *E*-isomer, and the *Z*-isomer is seen in the NMR spectra as well. The ratio of these isomers determined by integration of H in the benzylic methylene position was found to be 5.0:1 (*E*/*Z*). Also, 7.3% of **2ab** is seen. The *E*-isomer is fully characterized below, and the peaks visible and clearly assignable to the *Z*-isomer are given directly following the NMR characterization of the *E*-isomer.

E-isomer:

^{1}H NMR (500 MHz, $CDCl_3$, 298 K): δ 7.31 (m, 2H), 7.24-7.18 (ms, 3H), 5.65-5.51 (ms, 2H), 3.35 (d, J = 6.1 Hz, 2H), 1.72 (m, 3H)

^{13}C{^{1}H} NMR (126 MHz, $CDCl_3$, 298 K): δ 141.2, 130.2, 128.6, 128.49, 126.5, 126.01, 39.2, 18.0

Z-isomer:

^{1}H NMR (500 MHz, $CDCl_3$, 298 K): δ 3.44 (d, J = 4.0 Hz, 0.41H), 1.76 (d, J =4.1 Hz, 0.57H)

^{13}C{^{1}H} NMR (126 MHz, $CDCl_3$, 298 K): δ 141.3, 129.2, 128.55, 126.1, 125.96, 125.0, 33.3, 13.0

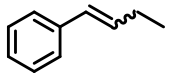

1-Phenyl-1-butene (**2ab**)

Synthesis details: substrate **1aa**, 70 °C, crude *E*/*Z* ratio determined by GC = 36:1 (*E*/*Z*)

Reaction time: 8 h

Purification details: pipette plug: silica, 100% hexanes to give the product as a colorless oil. 0.129 g was isolated with 6.3% **2aa** and 3.6% hydrogenated product. The amount and yield of **2ab** was adjusted to 0.115

g, 0.870 mmol, 87% yield. NMR spectra match values previously reported.[341,342]

The *Z*-isomer of **2ab** is not observed by NMR. *E*-**2ab** and the hydrogenated alkene are also observed, and the ratio of these products are determined by integration of H in the methyl-position was found to be 25:1.6:1 (*E*-**2ab**/*E*-**2aa**/hydrogenated product). The *E*-isomer of **2ab** is fully characterized below.

^{1}H NMR (500 MHz, $CDCl_3$, 298 K): δ 7.36 (d, m, 2H), 7.30 (t, *J* = 7.7 Hz, 2H), 7.19 (tt, *J* = 7.0, 1.3 Hz, 1H), 6.39 (dt, *J* = 15.9, 1.5 Hz, 1H), 6.28 (dt, 15.9, 6.5 Hz, 1H), 2.26 (quint, *J* = 7.2 Hz, 2H), 1.11 (t, *J* = 7.5 Hz, 3H)

^{13}C{^{1}H} NMR (126 MHz, $CDCl_3$, 298 K): δ 138.1, 132.8, 129.0, 128.6, 126.9, 126.1, 26.2, 13.8

---

e. Incompatible Substrates

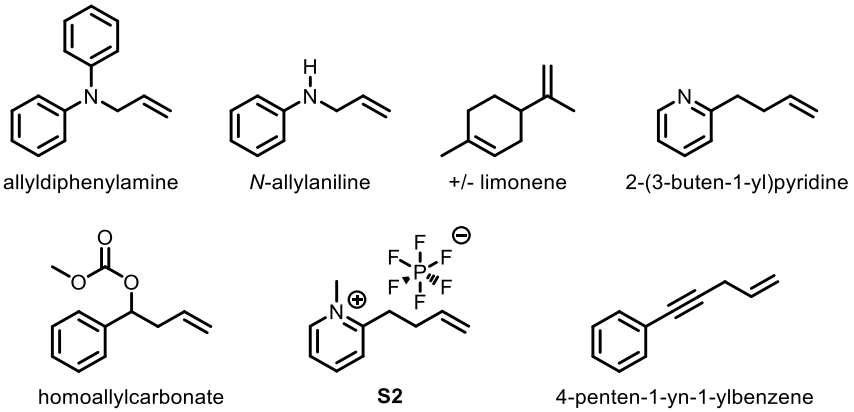

D.1.7. Isomerization Scale-Up Reaction

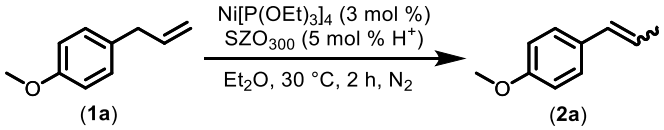

In a nitrogen-filled glovebox, SZO_{300} (2.03 g, 0.425 mmol H^+, 0.0500 equiv H^+), $Ni[P(OEt)_3]_4$ (0.185 g, 0.256 mmol, 0.0300 equiv) and Et_2O (3.0 mL) were added to a 4-dram vial equipped with a stir bar. The solid immediately turned from white to bright orange. The reaction was capped and gently stirred. After 30 min, the solution was decanted, and the remaining orange solid was washed with Et_2O (3 x 3.0 mL). After the third wash, the solid was dried under a flow of nitrogen

and transferred into a 250-mL Schlenk flask equipped with a stir bar. Et_2O (145 mL) was then added to the flask. The reaction flask was sealed and removed from the glovebox. Allylanisole (**1a**, 1.31 mL, 8.53 mmol, 1.00 equiv) was added to the flask, placed in a water bath preheated to 30 °C, and the reaction was stirred at 150 rpm. Aliquots (~20 µL) were taken over time to assess reaction progress. The reaction was complete after 2 h, and the selectivity of the reaction prior to workup was determined by GC to be 32:1 (*E*/*Z*). The reaction was exposed to air and filtered through Celite. The filtrate was concentrated to obtain **2a** as a white solid (1.24 g, 8.37 mmol, 98% yield). The selectivity of **2a** was found to be 33:1 (*E*/*Z*) by ^{1}H NMR.

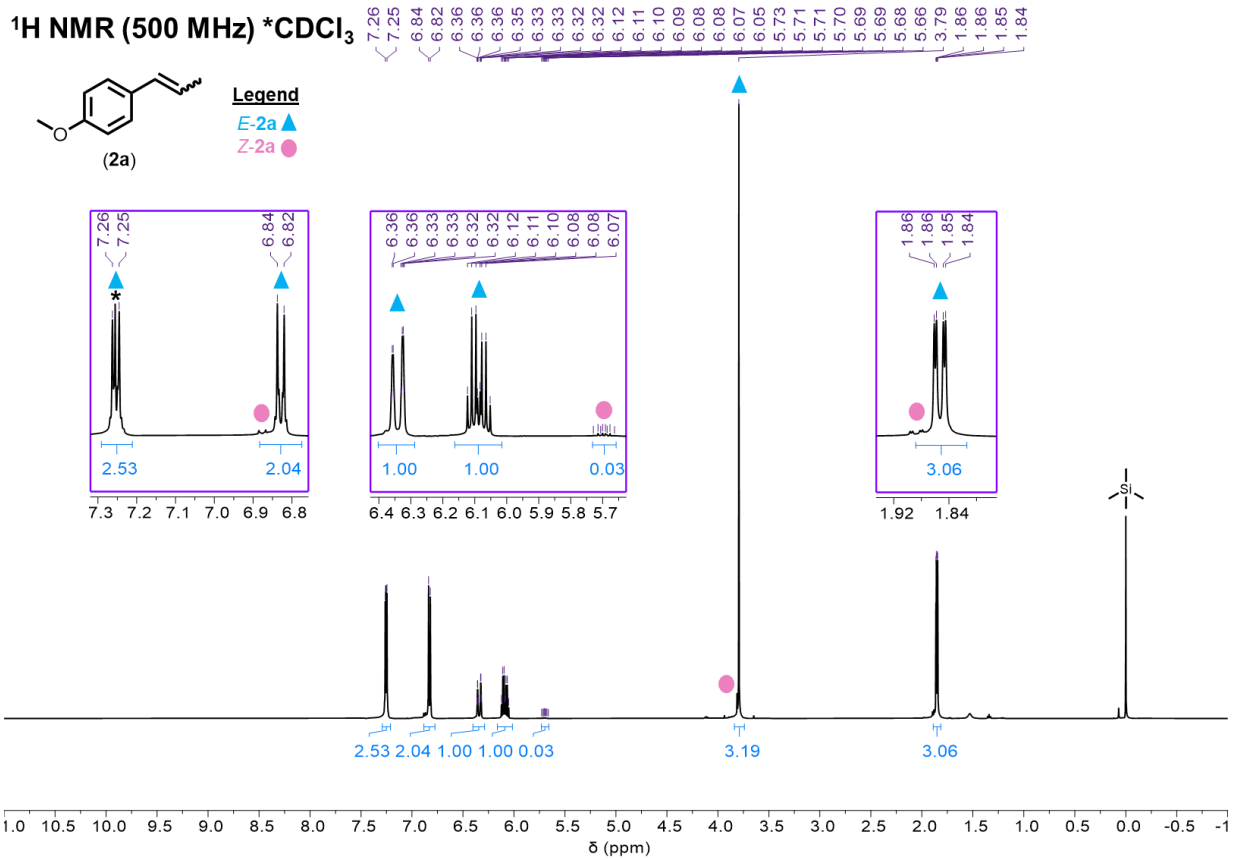

Figure E.2. ^{1}H NMR spectrum of the scaled-up isomerization of **1a** to form **2a** taken in $CDCl_3$ at 25 °C.

E.1.8. Comparison of Isomerization Rates between 1aa to 2aa and 2aa to 2ab

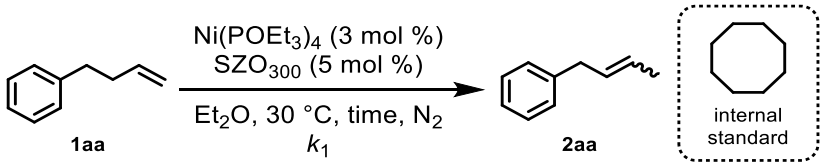

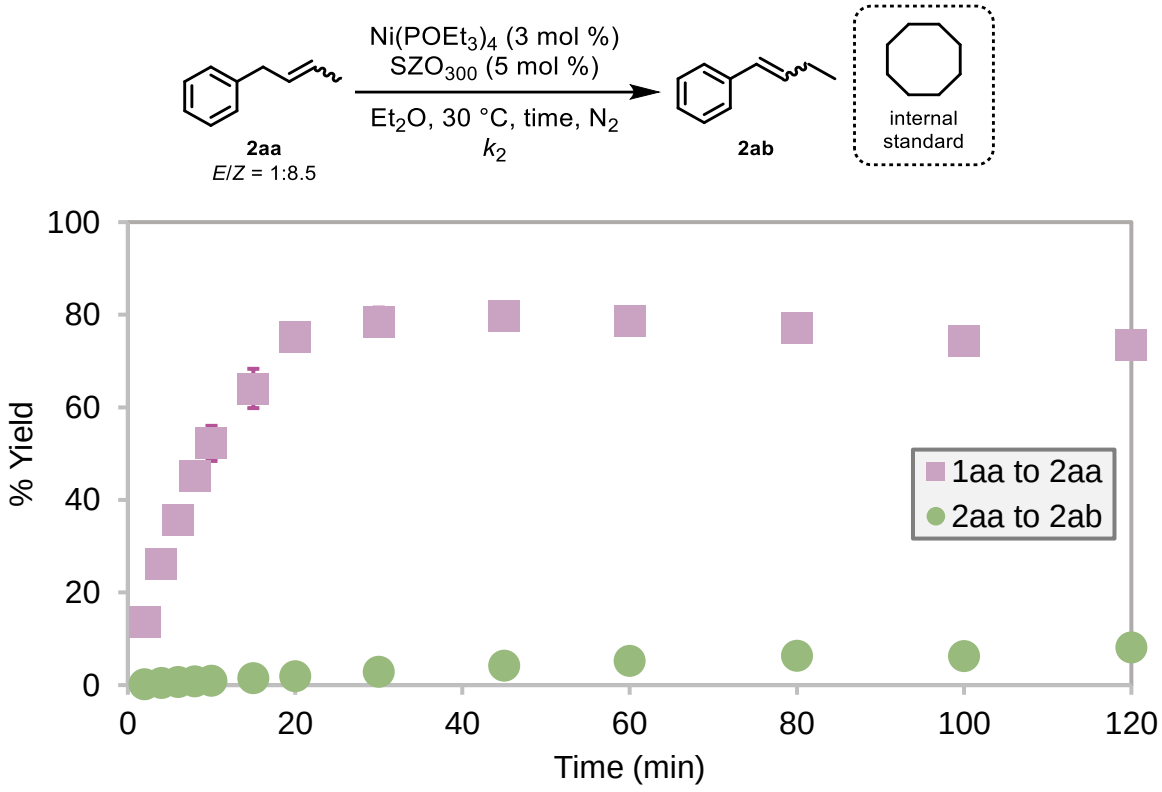

Figure E.3. Plot of the % yield versus reaction time of the formation of **2aa** (pink squares) or **2ab** (green circles).

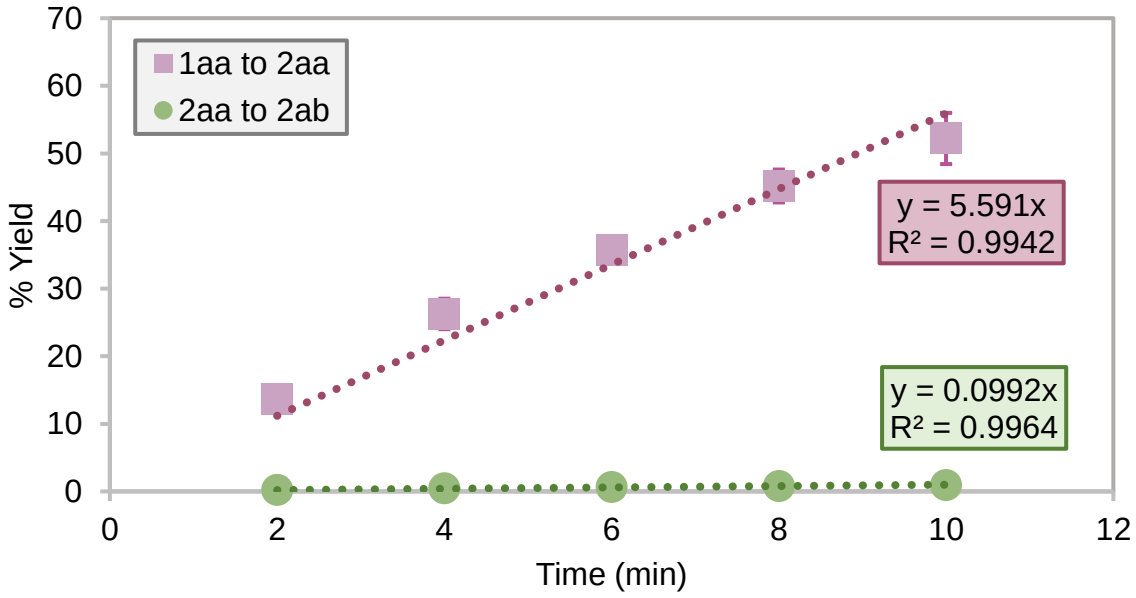

Figure E.4. Plot of the % yield versus reaction time of the formation of **2aa** (pink squares) or **2ab** (green circles) and corresponding slopes for the first 10 min.

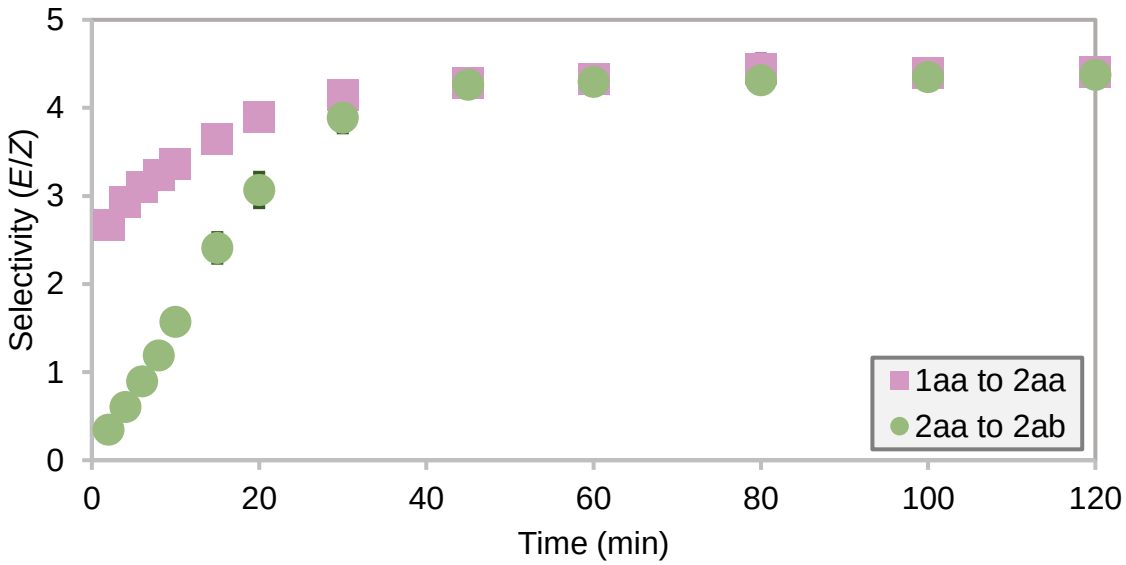

Figure E.5. Plot of the selectivity versus reaction time of the formation of **2aa** (pink squares) or **2ab** (green circles).

Table E.4. Yield and selectivity (*E*/*Z*) of **2aa** or **2ab** over time for the reaction of **1aa** to **2aa** (pink squares) and for the reaction of **2aa** to **2ab** (green circles).

Time (min)	1aa to 2aa Reaction		2aa to 2ab Reaction	
	% Yield	*E*/*Z* Selectivity (std error)	% Yield	*E*/*Z* Selectivity (std error)
2	13.712±0.002	2.67:1 (0.02)	0.21±0.06	0.347:1 (0.004)
4	26±2	2.93:1 (0.08)	0.45±0.04	0.603:1 (0.001)
6	36±2	3.096:1 (0.003)	0.65±0.06	0.90:1 (0.02)
8	45±2	3.2371:1 (0.0003)	0.8±0.1	1.19:1 (0.02)
10	52±4	3.36:1 (0.01)	0.9±0.2	1.57:1 (0.07)
15	64±4	3.64:1 (0.04)	1.5±0.3	2.4:1 (0.2)
20	75.3±0.2	3.90:1 (0.02)	2.0±0.4	3.1:1 (0.2)
30	78±3	4.14:1 (0.05)	2.9±0.6	3.9:1 (0.2)
45	80±2	4.28:1 (0.05)	4.2±0.9	4.26:1 (0.04)
60	79±2	4.33:1 (0.04)	5±1	4.30:1 (0.02)
80	77.0±0.9	4.4:1 (0.2)	6±2	4.315:1 (0.008)
100	74±1	4.39:1 (0.01)	6.3	4.349:1
120	73±2	4.41:1 (0.01)	8±1	4.374:1 (0.008)

Comparing the linear portion of the rates of reaction from the first 10 min of **1aa** to **2aa** and **2aa** to **2ab**, the rate of reaction of **1aa** to **2aa** is 55x faster than that of the reaction of **2aa** to **2ab**.

E.1.9. Comparison of the Substrate Scope of the Homogeneous and Heterogeneous Catalysts

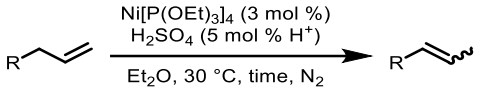

Homogeneous catalyst: In a nitrogen-filled glovebox, a stock solution of $Ni[P(OEt)_3]_4$ in Et_2O was prepared and distributed into a 1-dram vial equipped with a stir bar using a disposable 1-mL syringe (1.3 mg, 0.0018 mmol, 0.030 equiv was added to each vial). The vial was sealed with a septum cap and brought out of the glovebox. A separate stock solution of H_2SO_4 (0.16 µL, 0.0030 mmol, 0.050 equiv added to each vial) in Et_2O was prepared and then added to the vial using a 25-µL syringe. This addition resulted in an immediate color change to light orange. The total volume of Et_2O was 1.0 mL. The alkene (0.060 mmol, 1.0 equiv) was added to the vial using a 25-µL syringe. The reaction was then immediately heated to 30 °C using a preheated aluminum block and stirred at a rate of 150 rpm. The reaction progress was monitored by GC by taking aliquots (~20 µL) over time. The aliquots were diluted with hexanes (1 mL) and filtered through Celite into a GC vial. The reaction time, percent conversion of starting material, and selectivity (*E*/*Z*) are shown in Table S4 below and are compared to the analogous results using the heterogeneous catalyst.

Heterogeneous catalyst: In a nitrogen-filled glovebox, SZO_{300} (15 mg, 0.0030 mmol H^+, 0.050 equiv H^+ per vial) was weighed directly into a 1-dram vial equipped with a stir bar. A stock solution of $Ni[P(OEt)_3]_4$ in Et_2O was prepared and distributed to the vial using a disposable 1-mL syringe (1.3 mg, 0.0018 mmol, 0.030 equiv was added to each vial). This addition resulted in an immediate color change of the SZO_{300} from white to bright orange. The total volume of Et_2O in the vial was 1.0 mL. The vial was sealed with a septum cap and brought out of the glovebox. The alkene (0.060 mmol, 1.0 equiv) was added to the vial using a 25-µL syringe. The reaction was then immediately heated to 30 °C using a preheated aluminum block and stirred at a rate of 150 rpm. The reaction progress was monitored by GC by taking aliquots (~20 µL) over time. The aliquots were diluted with hexanes (1 mL) and filtered through Celite into a GC vial. The reaction time, percent conversion of starting material, and selectivity (*E*/*Z*) are shown in Table S4 below and are compared to the analogous results using the homogeneous catalyst.

Table E.5. Comparison of the reaction time, conversion to product, and selectivity of alkene isomerization using $Ni[P(OEt)_3]_4$ and H_2SO_4 or SZO_{300} with a variety of substrates

Product	H^+ source	Reaction time (h)	Conversion to product	Selectivity (*E*/*Z*)
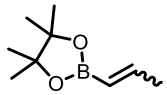 (**2v**)	H_2SO_4	24	0%	n.d.
	SZO_{300}	2	99.17±0.03%	8.17±0.09:1
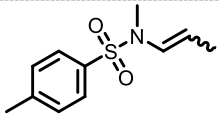 (**2t**)	H_2SO_4	24	1.00±0.05%	>99:1
	SZO_{300}	7	97.6±0.7%	>99:1
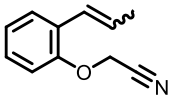 (**2m**)	H_2SO_4	0.5	3.0±0.3%[e]	>99:1
	SZO_{300}	4	100%[a]	25:1
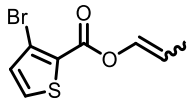 (**2q**)	H_2SO_4	7	13.192±0.002%[e]	1:1.690±0.006
	SZO_{300}	7	99.0±0.1%	1:1.9±0.3
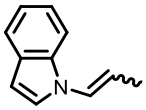 (**2o**)	H_2SO_4	1	65.45±0.06%[f]	>99:1
	SZO_{300}	7	96.22±0.02%	13.2±0.9:1
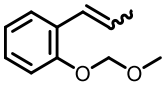 (**2j**)	H_2SO_4	0.5	99.20±0.04%	5.4±0.1:1
	H_2SO_4	24	98.9±0.2%[b]	6.1±0.3:1
	SZO_{300}	8	98%[a]	19:1
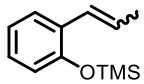 (**2k**)	H_2SO_4	0.5	100±0%[c]	4.4±0.4:1
	H_2SO_4	24	100±0%[d]	5.3±0.6:1
	SZO_{300}	5	100%[a]	28:1
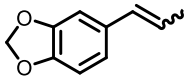 (**2f**)	H_2SO_4	TBD	TBD	TBD
	SZO_{300}	5	99%[a]	38:1
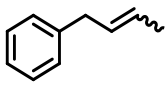 (**2aa**)	H_2SO_4	1 (0 °C)	90±3%[e]	2.9±0.4:1 **2aa**/**2ab** = 66±13:1
	SZO_{300}	2.5 (0 °C)	98%[a]	5.1:1 **2aa**/**2ab** = 34:1
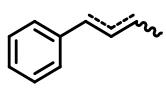 (**2aa** + **2ab**)	H_2SO_4	1 (30 °C)	98.8±0.2%	**2aa** *E*/*Z* = 5.58±0.08:1 **2ab** *E*/*Z* = 20±1:1 **2aa**/**2ab** = 1.47±0.05:1
	SZO_{300}	1 (30 °C)	84%[a]	**2aa** *E*/*Z* = 3.9:1 **2ab** *E*/*Z* = 1:0

				2aa/**2ab** = 8:1
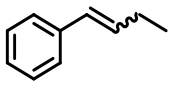 (**2ab**)	H_2SO_4	1 (70 °C)	4.9±0.7%[e]	>99:1 **2aa**/**2ab** = 1:1.50±0.02
	SZO_{300}	8 (70 °C)	90%[a]	36:1 **2aa**/**2ab** = 1:9.3
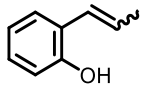 (**2l**)	H_2SO_4	0.5	100±0%	>99:1
	SZO_{300}	4	97±2%	>99:1

p.r. = positional ratio of major product to other phenyl butene positional isomers
n.d. = not determined
[a]Only one trial was performed and was run on a 1 mmol scale of alkene.
[b]2% of the deprotected product (2-hydroxy-β-methylstyrene **2l**) was formed.
[c]1% of the deprotected product (2-hydroxy-β-methylstyrene **2l**) was formed.
[d]20% of the deprotected product (2-hydroxy-β-methylstyrene **2l**) was formed.
[e]Conversion and selectivity remain the same after the reported time point.
[f]Conversion remain the same after the reported time point.

E.1.10. Comparison of Acid Sources (H_2SO_4, SZO_{300}, Nafion™, and Amberlyst®-15)

a. Comparison of H_2SO_4 and SZO_{300} as the Acid Sources

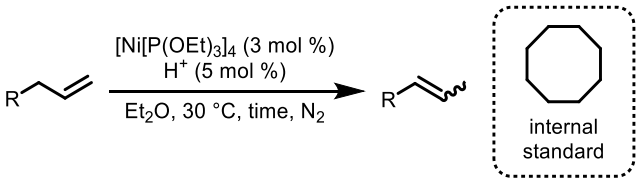

General Procedure A.

Homogeneous catalyst: In a nitrogen-filled glovebox, a stock solution of $Ni[P(OEt)_3]_4$ (2.6 mg, 0.0036 mmol, 0.030 equiv per vial) and cyclooctane (8 µL, 0.06 mmol per vial) was prepared in Et_2O and distributed into a 1-dram vial using a disposable 1-mL syringe. The vial was sealed with a septum cap and brought out of the glovebox. A separate stock solution of H_2SO_4 in Et_2O was prepared and the appropriate amount of solution (0.50 M, 12 µL, 0.0060 mmol, 0.050 equiv per vial) was added to the vial using a 25-µL syringe. This addition resulted in an immediate color change to light orange. The total volume of Et_2O in the vial was 2.0 mL. The alkene (0.120 mmol, 1.00 equiv) was added to the vial using a 25-µL syringe. The reaction was then immediately heated to 30 °C using a preheated aluminum block and stirred at a rate of 150 rpm. The reaction progress was monitored by GC by taking aliquots (~20 µL) over time. The aliquots were diluted with hexanes (1 mL) and filtered through Celite into a GC vial and analyzing by GC.

General Procedure B.

Heterogeneous catalyst: In a nitrogen-filled glovebox, SZO_{300} (30.0 mg, 0.00600 mmol H^+, 0.0500 equiv H^+ per vial) was weighed into a 1-dram vial equipped with a stir bar. A stock solution of $Ni[P(OEt)_3]_4$ (2.60 mg, 0.00360 mmol, 0.0300 equiv per vial) and cyclooctane (8-9 μL per vial) was prepared in Et_2O and distributed into a 1-dram vial using a disposable 1-mL syringe. This addition resulted in an immediate color change of the SZO_{300} from white to bright orange. The total volume of Et_2O in the vial was 2.0 mL. The vial was sealed with a septum cap and brought out of the glovebox. The alkene (0.120 mmol, 1.00 equiv) was added to the vial using a 25-μL syringe. The reaction was then immediately heated to 30 °C using a preheated aluminum block and stirred at a rate of 150 rpm. The reaction progress was monitored by GC by taking aliquots (~20 μL) over time. The aliquots were diluted with hexanes (1 mL) and filtered through Celite into a GC vial and analyzed by GC.

i. Allylbenzene (1c)

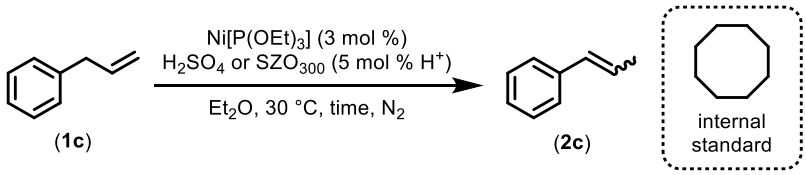

Using General Procedure A and B, the yield and *E*/*Z* selectivity of the isomerization of **1c** (16 uL, 0.12 mmol, 1.0 equiv) was measured over time. The data are seen in Figures S4-S5 and Table S5 below.

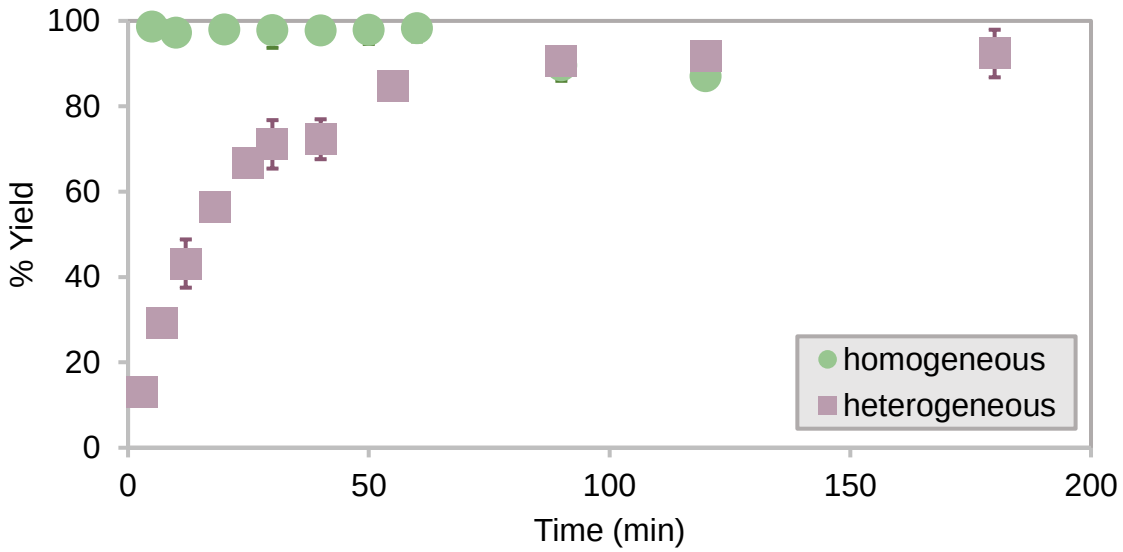

Figure E.6. Plot of the yields versus reaction time of the formation of **2c** using the homogeneous catalyst $Ni[P(OEt)_3]_4/H_2SO_4$ (green circles) and the heterogeneous catalyst $Ni[P(OEt)_3]_4/SZO_{300}$ (pink squares).

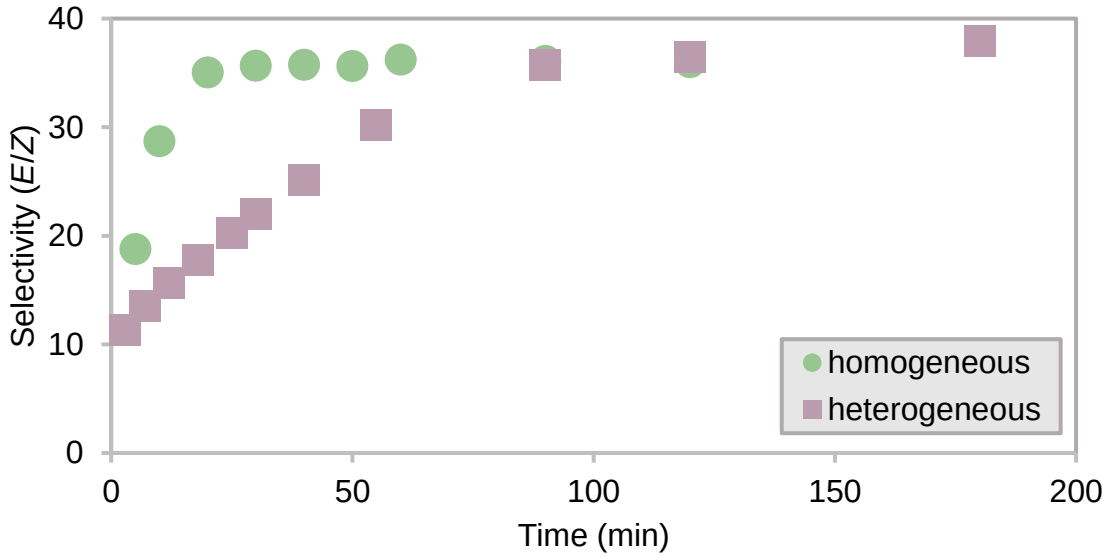

Figure E.7. Plot of the selectivity versus reaction time of the formation of **2c** using the homogeneous catalyst $Ni[P(OEt)_3]_4/H_2SO_4$ (green circles) and the heterogeneous catalyst $Ni[P(OEt)_3]_4/SZO_{300}$ (pink squares).

Table E.6. Yield and *E*/*Z* selectivity of **2c** as a function of time using the homogeneous catalyst $Ni[P(OEt)_3]_4/H_2SO_4$ and the heterogeneous catalyst $Ni[P(OEt)_3]_4/SZO_{300}$.

Homogeneous catalyst			Heterogeneous catalyst		
Time (min)	**% Yield**	***E*/*Z* Selectivity (std error)**	**Time (min)**	**% Yield**	***E*/*Z* Selectivity (std error)**
5	99±1	18.8:1 (0.2)	3	13±3	11.3:1 (0.6)
10	97±3	28.7:1 (0.2)	7	29±2	13.5:1 (0.1)
20	98±3	35.0:1 (0.2)	12	43±6	15.6:1 (0.5)
30	97±4	35.7:1 (0.3)	18	56.4±0.3	17.74:1 (0.09)
40	97±3	35.8:1 (0.6)	25	66.8±0.3	20.262:1 (0.005)
50	98±3	35.6:1 (0.5)	30	71±6	22.04:1 (0.08)
60	98±3	36.2:1 (0.2)	40	72±5	25.1:1 (0.6)
90	90±4	36.09:1 (0.06)	55	84.7±0.2	30.2:1 (0.3)
120	87±1	36.03:1 (0.3)	90	91±2	35.70:1 (0.08)
--	--	--	120	91.8±0.2	36:1 (1)
--	--	--	180	92±6	37.9:1 (0.6)

ii. Allylanisole (1a)

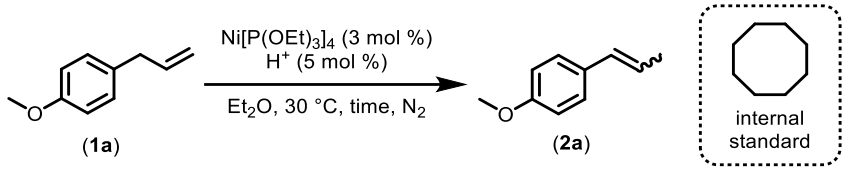

Using General Procedure A and B, the yield and *E*/*Z* selectivity of the isomerization of **1a** (19 uL, 0.12 mmol, 1.0 equiv) was measured over time. The data are seen in Figures S6-S7 and Table S6 below.

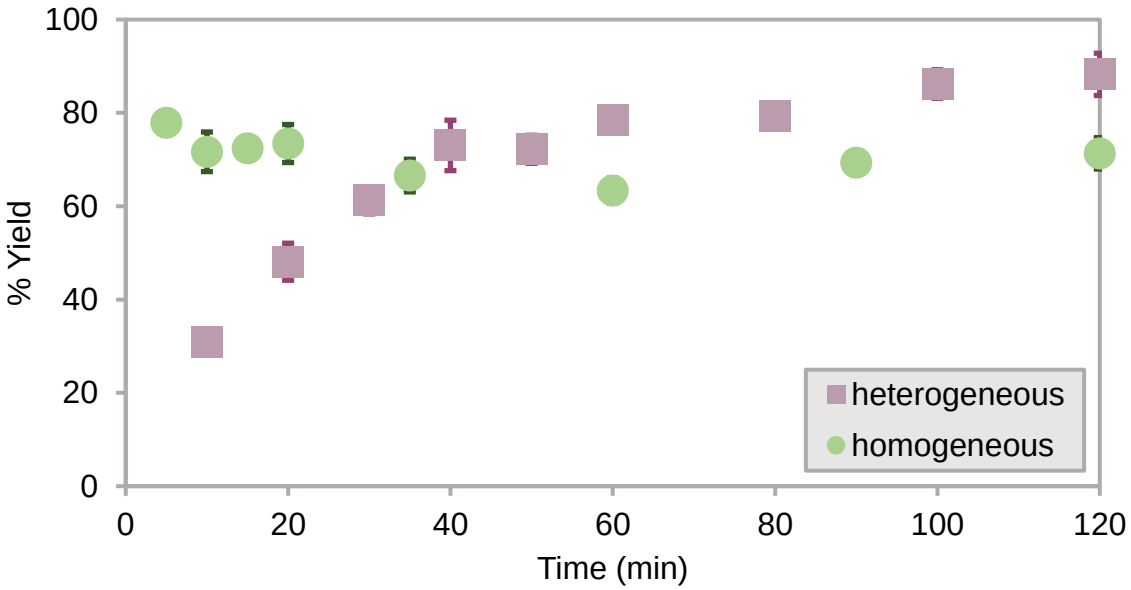

Figure E.8. Plot of the yields versus reaction time of the formation of **2a** using the homogeneous catalyst $Ni[P(OEt)_3]_4/H_2SO_4$ (green circles) and the heterogeneous catalyst $Ni[P(OEt)_3]_4/SZO_{300}$ (pink squares).

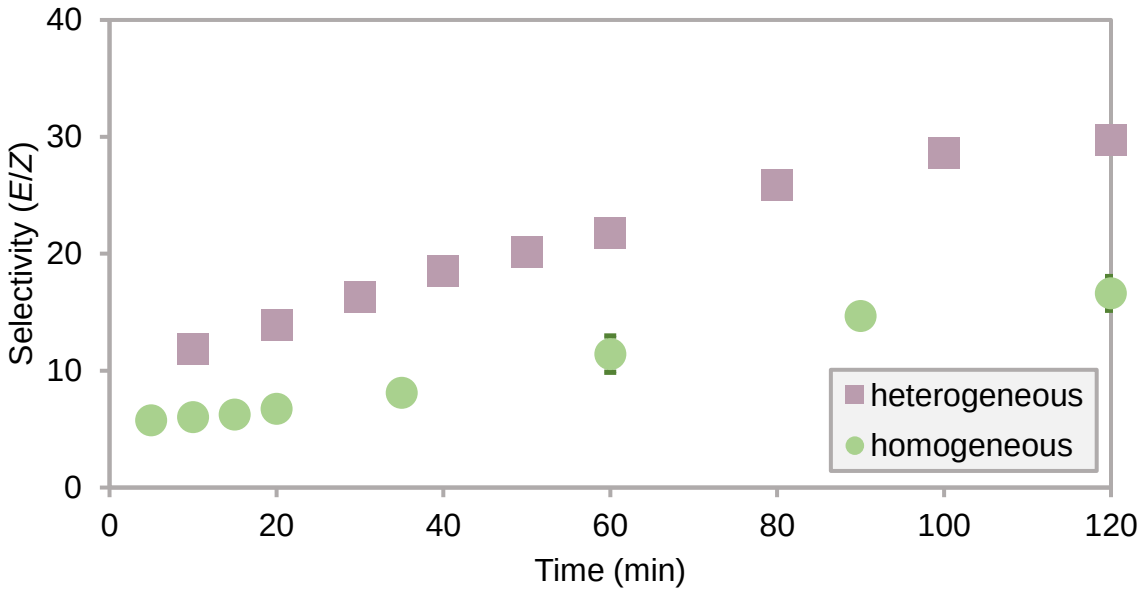

Figure E.9. Plot of the selectivity versus reaction time of the formation of **2a** using the homogeneous catalyst $Ni[P(OEt)_3]_4/H_2SO_4$ (green circles) and the heterogeneous catalyst $Ni[P(OEt)_3]_4/SZO_{300}$ (pink squares).

Table E.7. Yield and *E*/*Z* selectivity of **2a** as a function of time using the homogeneous catalyst $Ni[P(OEt)_3]_4/H_2SO_4$ and the heterogeneous catalyst $Ni[P(OEt)_3]_4/SZO_{300}$.

Homogeneous catalyst			Heterogeneous catalyst		
Time (min)	**% Yield**	***E*/*Z* Selectivity (std error)**	**Time (min)**	**% Yield**	***E*/*Z* Selectivity (std error)**
5	78±3	5.8:1 (0.3)	10	32±3	11.9:1 (0.2)
10	72±4	6.0:1 (0.4)	20	49±4	13.9:1 (0.1)
15	72±1	6.2:1 (0.6)	30	62±3	16.3:1 (0.1)
20	73±4	6.7:1 (0.6)	40	75±6	18.55:1 (0.06)
35	67±4	8.1:1 (0.8)	50	74±3	20.11:1 (0.06)
60	63±3	11:1 (2)	60	80.217±0.006	21.8:1 (0.2)
90	69	14.7:1	80	81±2	25.9:1 (0.2)
120	71±3	17:1 (1)	100	88±3	28.6:1 (0.3)
--	--	--	120	90±5	29.8:1 (0.9)
--	--	--	160	94±4	31.9:1 (0.3)
--	--	--	180	88±2	31.7:1 (0.4)

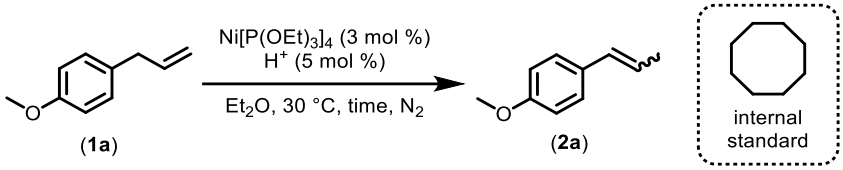

Procedure using Nafion™ and Amberlyst®-15: In a nitrogen-filled glovebox, a stock solution was prepared by dissolving $Ni[P(OEt)_3]_4$ in Et_2O. This stock solution was then transferred into a 2-dram scintillation vial, which was then sealed with a septum cap and removed from the glovebox. Outside the glovebox, Nafion™ (7.0 mg, 0.0063 mmol H^+, 0.048 equiv H^+) or Amberlyst®-15 (1.3 mg, 0.0061 mmol H^+, 0.047 equiv H^+) was added to a 1-dram scintillation vial equipped with stir bar. The vial was sealed with a septum cap and flushed with N_2 for 30 min. The stock solution of $Ni[P(OEt)_3]_4$ (2.6 mg, 0.0036 mmol, 0.030 equiv) was added to the vial containing the solid acid using a disposable Luer-Lock 3-mL syringe. The total volume of Et_2O added to the vial was 2.0 mL. Then, **1a** (19 µL, 0.12 mmol, 1.0 equiv) was added, and the reaction was heated to 30 °C on a pre-heated aluminum block and stirred at a rate of 150 rpm. Throughout the course of the reaction, 20-µL aliquots were removed with a 25-µL syringe, diluted with hexanes, and filtered into a GC vial through Celite. The filtrate was analyzed by GC to assess the reaction progress and product selectivity. Two trials were run and the averages and standard deviations of the two trials are reported below. The data are seen in **Figures E.10.-E.12.** and **Table E.8.-E.9.** below.

The data for SZO_{300} used in **Figures E.10.-E.11** below is the same as was used above in section **E.1.10.a.ii.**

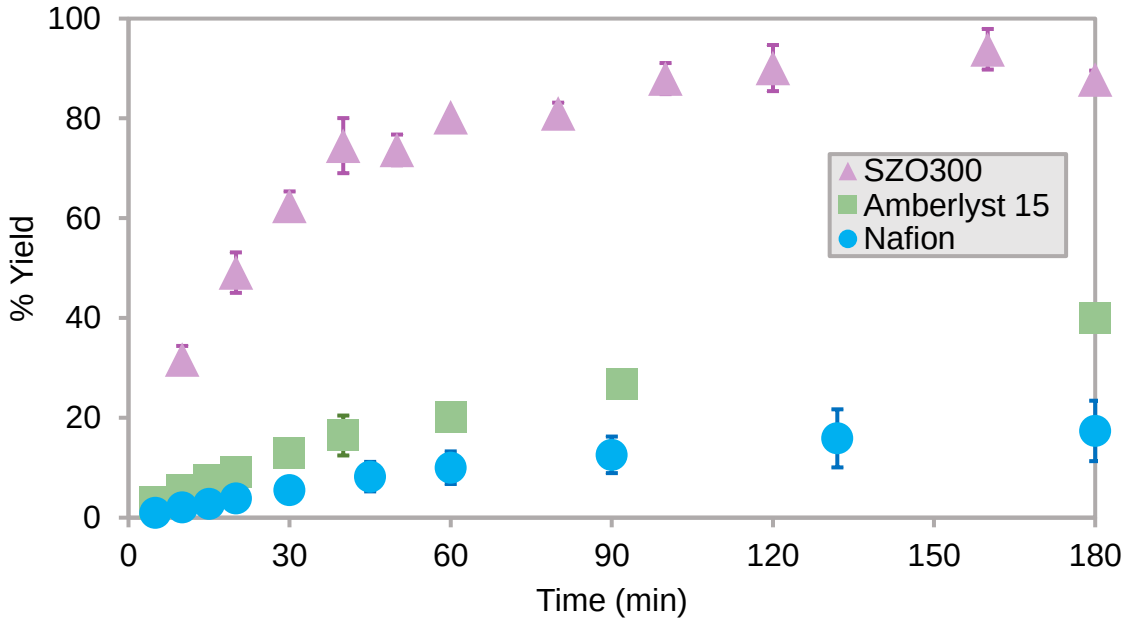

Figure E.10. Plot of the yields versus reaction time of the formation of **2a** using the heterogeneous catalysts $Ni[P(OEt)_3]_4/SZO_{300}$ (pink triangles), $Ni[P(OEt)_3]_4$/Amberlyst®-15 (green squares), and $Ni[P(OEt)_3]_4$/Nafion™ (blue circles).

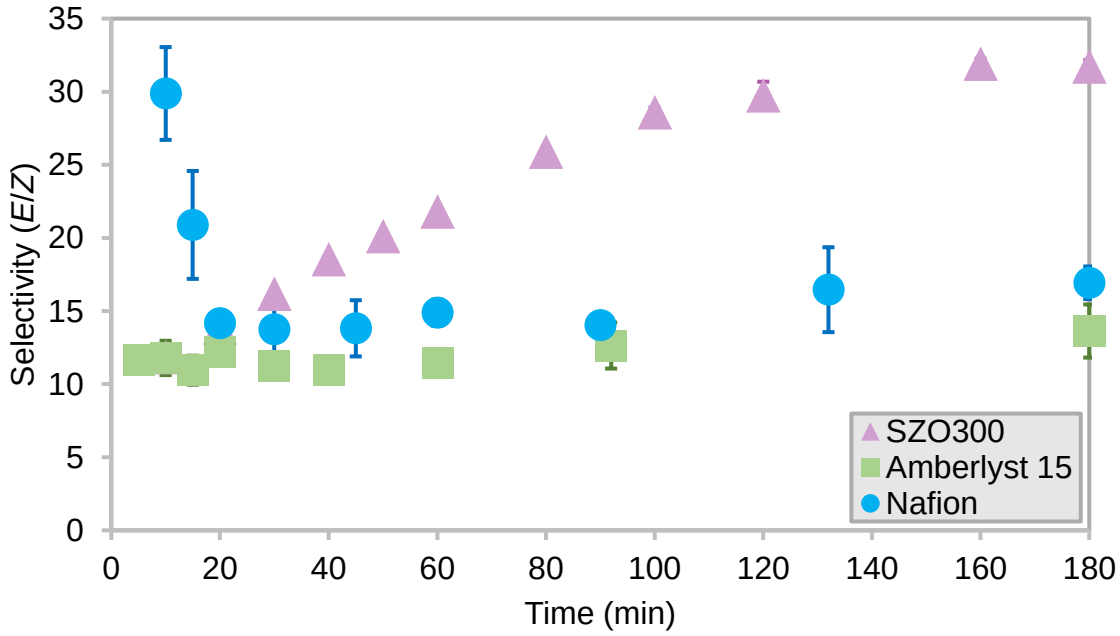

Figure E.11. Plot of the selectivity versus reaction time of the formation of **2a** using the heterogeneous catalysts $Ni[P(OEt)_3]_4/SZO_{300}$ (pink triangles), $Ni[P(OEt)_3]_4$/Amberlyst®-15 (green squares), and $Ni[P(OEt)_3]_4$/Nafion™ (blue circles).

Table E.8. Yield and *E*/*Z* selectivity of **2a** as a function of time using the heterogeneous catalysts Ni[P(OEt)$_3$]$_4$/Amberlyst®-15 and Ni[P(OEt)$_3$]$_4$/Nafion™.

Amberlyst®-15			Nafion™		
Time (min)	**% Yield**	***E*/*Z* Selectivity (std error)**	**Time (min)**	**% Yield**	***E*/*Z* Selectivity (std error)**
5	3.1±0.5	11.7:1 (0.3)	5	1.0±0.2	1:0
10	6±1	12:1 (1)	10	2.1±0.2	30:1 (3)
15	7±1	11:1 (1)	15	2.7±0.3	21:1 (4)
20	9±1	12.2:1 (0.3)	20	3.8±0.4	14.2:1 (0.7)
30	13±3	11.3:1 (0.1)	30	6±3	14:1 (2)
40	17±4	11.0:1 (0.4)	45	8±3	14:1 (2)
60	20±3	11.48:1 (0.03)	60	10±4	14.9:1 (0.9)
92	26±3	13:1 (2)	90	13±6	14.0:1 (0.8)
180	40±1	14:1 (2)	132	16±6	16:1 (3)

The relative rates of each system were calculated by calculating the slope of the linear portion (the first ~45 min) (Figure S10).

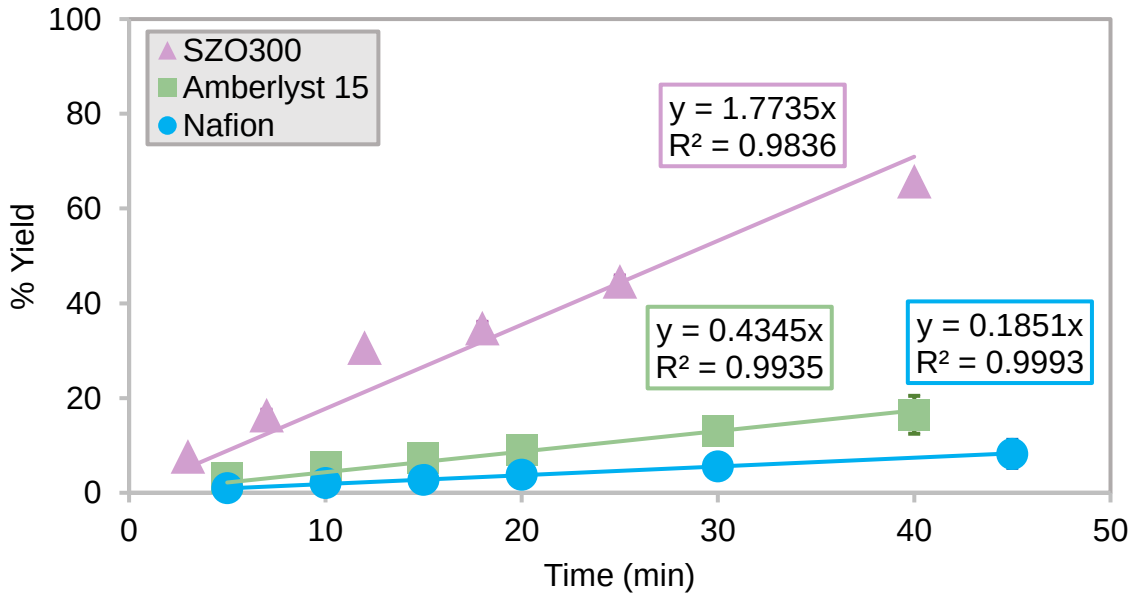

Figure E.12. Plot of the linear portion of the data from Figure S8.

Table E.9. Acid source, rate, and relative rates of the formation of **2a** using the heterogeneous catalysts Ni[P(OEt)$_3$]$_4$/Amberlyst®-15 and Ni[P(OEt)$_3$]$_4$/Nafion™.

Acid source (H^+)	Rate (% yield/min)	Rate of SZO_{300}/Rate of H^+
SZO_{300}	1.7735	--
Amberlyst®-15	0.4345	4
Nafion™	0.1851	10

b. Isomerization with Ni[P(OEt)$_3$]$_4$/Zr(OH)$_4$•H$_2$SO$_4$

i. Allylanisole (1a)

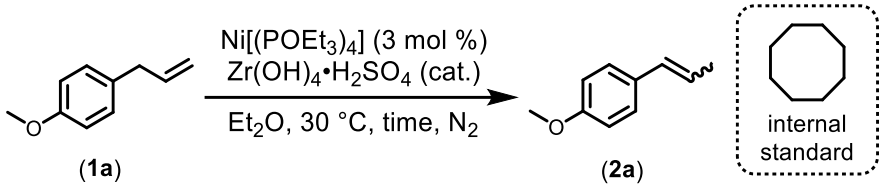

In a nitrogen-filled glovebox, $Zr(OH)_4•H_2SO_4$ (15.0 mg) was weighed into a 1-dram vial equipped with a stir bar. A stock solution of $Ni[P(OEt)_3]_4$ (1.30 mg, 0.00180 mmol, 0.0300 equiv per vial) and cyclooctane (5 µL per vial) was prepared in Et_2O and distributed into a 1-dram vial using a disposable 1-mL syringe. The total volume of Et_2O in the vial was 1.0 mL. The vial was sealed with a septum cap and brought out of the glovebox. **1a** (9.5 µL, 0.030 mmol, 1.0 equiv) was added to the vial using a 25-µL syringe. The reaction was then immediately heated to 30 °C using a preheated aluminum block and stirred at a rate of 150 rpm. The reaction progress was monitored by GC by taking aliquots (~20 µL) over time. The aliquots were diluted with hexanes (1 mL) and filtered through Celite into a GC vial and analyzed by GC.

The data for SZO_{300} used in **Table E.10.** is the same as was used above in section **E.1.10.a.ii.**

Table E.10. Yield and selectivity (*E*/*Z*) of **2a** at 80 and 120 min.

Time (min)	$Ni[P(OEt)_3]_4/Zr(OH)_4•H_2SO_4$		$Ni[P(OEt)_3]_4/SZO_{300}$	
	% Yield	Selectivity (*E*/*Z*) (std error)	% Yield	Selectivity (*E*/*Z*)
80	88±2	20.1±0.6:1	81±2	25.9±0.2:1
120	90±2	27.2±0.1:1	90±5	30±1:1

ii. N-methyl-N-(prop-1-enyl)-p-toluenesulfonamide

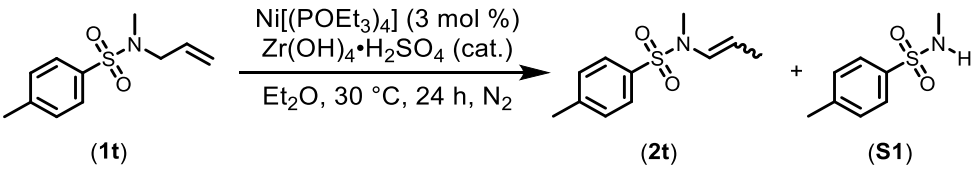

In a nitrogen-filled glovebox, $Ni[P(OEt)_3]_4$ (21.7 mg, 0.0300 mmol, 0.0300 equiv), $Zr(OH)_4•H_2SO_4$ (250 mg), and Et_2O (17 mL) were added to a 4-dram scintillation vial equipped with a stir bar. The vial was sealed with a septum cap, brought out of the glovebox, injected with **1t** (0.221 mL, 1.00 mmol, 1.00 equiv) using a 250-µL syringe, and heated at 30 °C on a preheated aluminum vial block for 24 h. The reaction was stirred at a rate of 150 rpm. After 24 h, the reaction was removed from heat, opened to air, and the solution was filtered through Celite, washing Et_2O (2.0 mL). The filtrate was concentrated and analyzed by ^1H NMR.

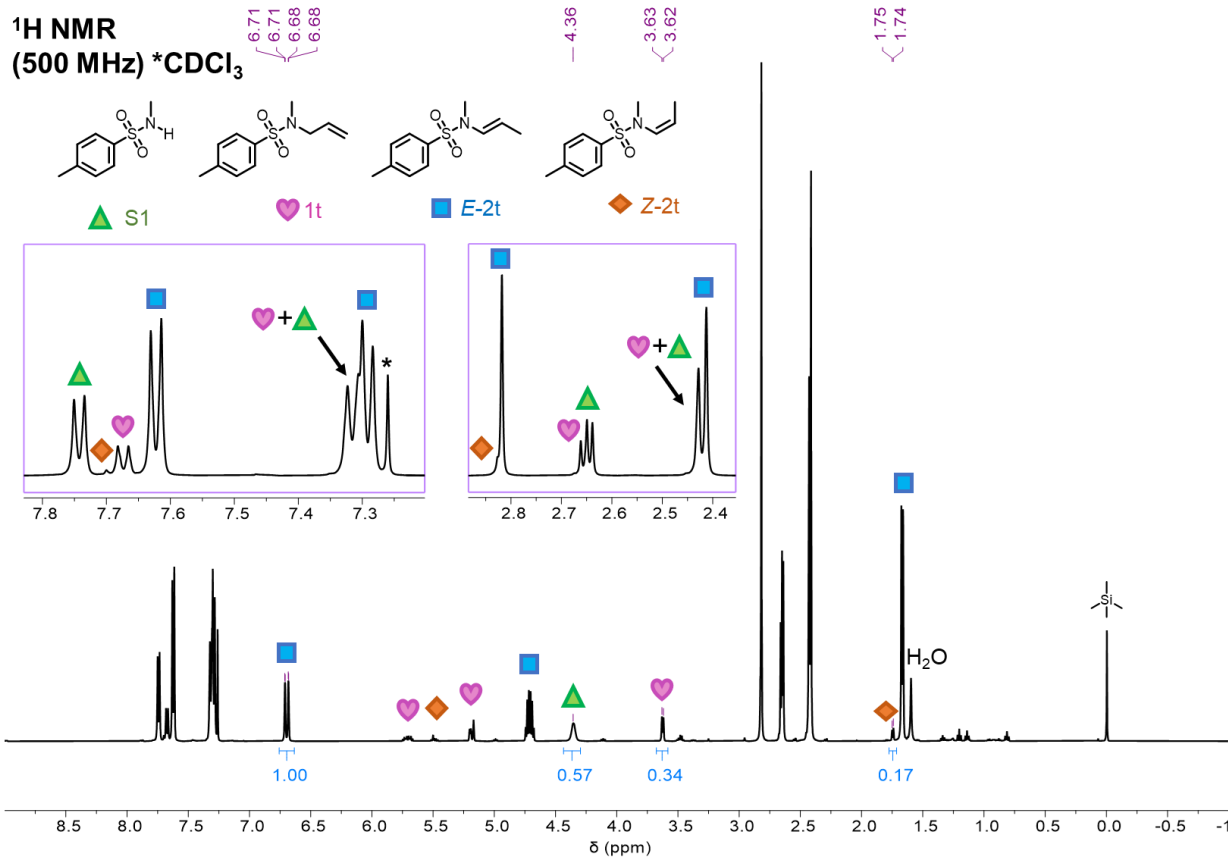

Figure E.12. ^{1}H NMR spectrum of the crude reaction for the isomerization of **1t** by $Ni[P(OEt)_3]_4/Zr(OH)_4•H_2SO_4$ recorded in $CDCl_3$ at 25 °C.

Table E.11. Corresponding compound in crude reaction, ^{1}H NMR integration, # of protons, normalized protons, and relative amounts of each compound in the ^{1}H NMR.

Compound	Chemical shift (ppm)	Integration	#H	Normalized H	Relative amount (%)
S1	4.36	0.57	1	0.56	32
1t	3.63	0.34	2	0.17	9
***E*-2t**	6.70	1.00	1	1.0	56
***Z*-2t**	1.75	0.17	3	0.057	3

E.1.11. Grafted Catalyst ([Ni]-SZO) in Catalysis

a. Preparation of Grafted Catalyst

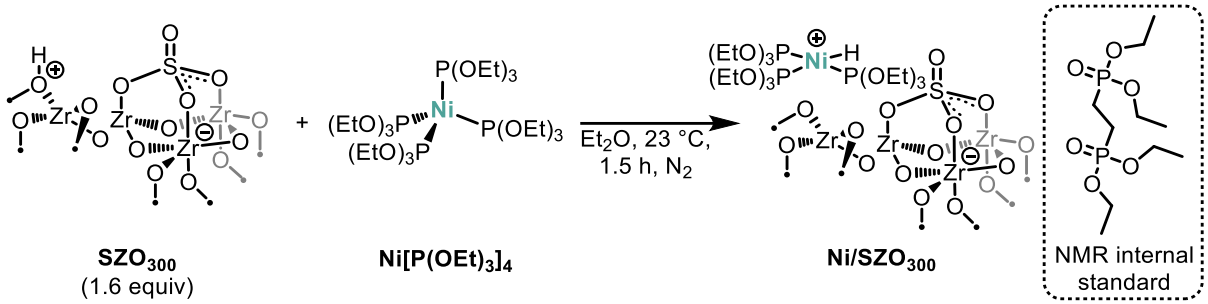

In a nitrogen-filled glovebox, SZO_{300} (150 mg, 0.0300 mmol H^+, 1.60 equiv H^+), $Ni[P(OEt)_3]_4$ (13.5 mg, 0.0187 mmol, 1.00 equiv), and Et_2O (1.0 mL) were added into a 4-dram vial equipped with a stir bar. The white SZO_{300} solid immediately turns into a bright orange color. The vial was sealed with a Teflon-lined thermoset cap and was gently stirred at room temperature for 1.5 h. The liquid was decanted from the orange solid, and the solid was washed three times with Et_2O (3 x 1.0 mL). The Et_2O reaction solution and washes were combined, and an aliquot of the washings (0.30 mL) was added to an NMR tube with C_6D_6 (0.3 mL) and analyzed by ^{31}P NMR using tetraethyl-ethylenediphosphonate (3.0 µL, 0.0113 mmol) as an internal standard to quantify the amount of $Ni[P(OEt)_3]_4$ remaining in solution. The solid was dried under vacuum (10^{-5} mbar) overnight to yield $Ni[P(OEt)_3]_4/SZO_{300}$ as a free-flowing orange powder. The IR spectrum and ^1H MAS NMR were recorded (**Figures E.13.-E.16.** and **Table E.12.**). Digestion of $Ni[P(OEt)_3]_4/SZO_{300}$ in 70% aqueous trace metal HNO_3 at 25 °C for one week, and quantification of Ni by ICP-MS gives $8.41x10^{-8}$ mmol Ni•g^{-1}.

^1H MAS (500 MHz, 298 K): δ 4.09 (C*H*$_2$), 1.28 (C*H*$_3$), -12.10 (Ni–*H*), -14.21 (Ni–*H*)

^{13}C MAS (126 MHz, 298 K): δ 61.8, 15.5

^{31}P MAS (202 Hz, 298 K): δ 134.28

IR (FT, neat pellet) v: 1933 (Ni–H)

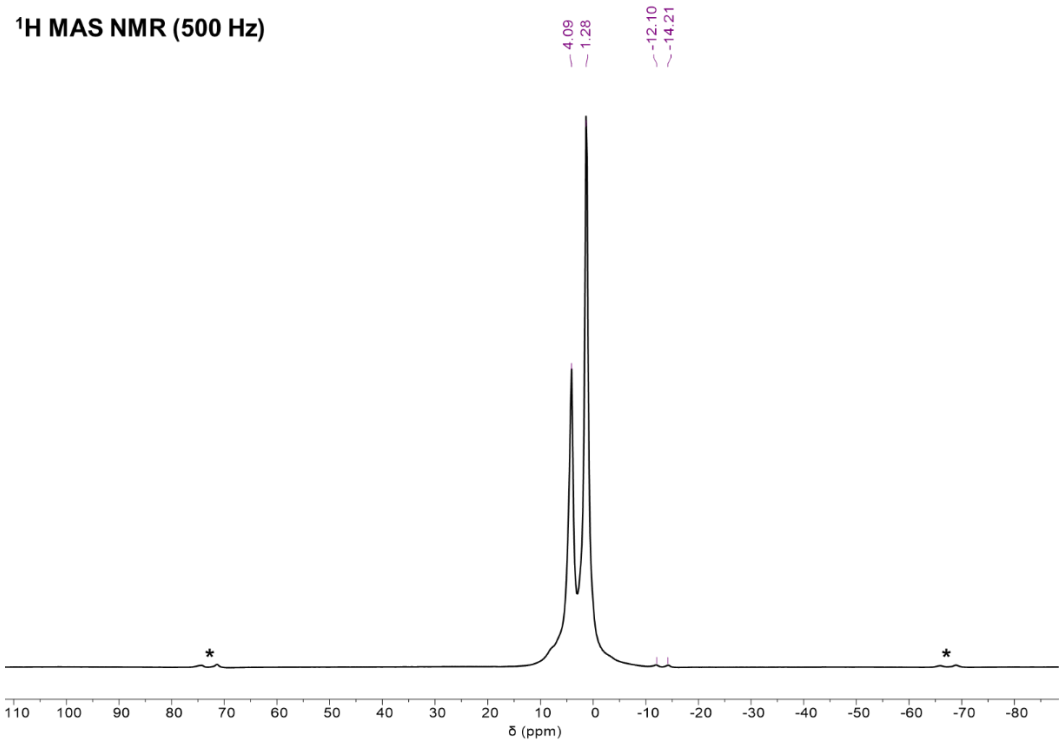

Figure E.13. ^{1}H solid-state NMR of the grafted catalyst [Ni]-SZO_{300} recorded under spinning rate of 35 kHz. Acquisition with 96 scans and a recycle delay of 3 s recorded at 25 °C. Asterisks denote spinning side bands.

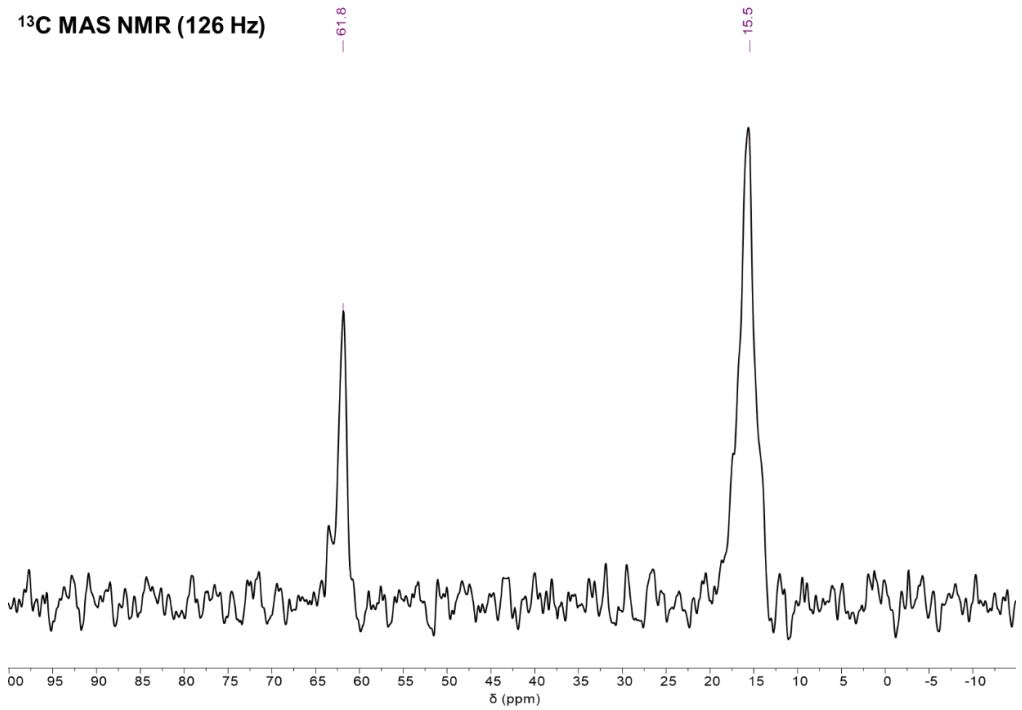

Figure E.14. ^{13}C solid-state NMR of the grafted catalyst [Ni]-SZO_{300} recorded under spinning rate of 25 kHz. Acquisition with 39089 scans recorded at 25 °C.

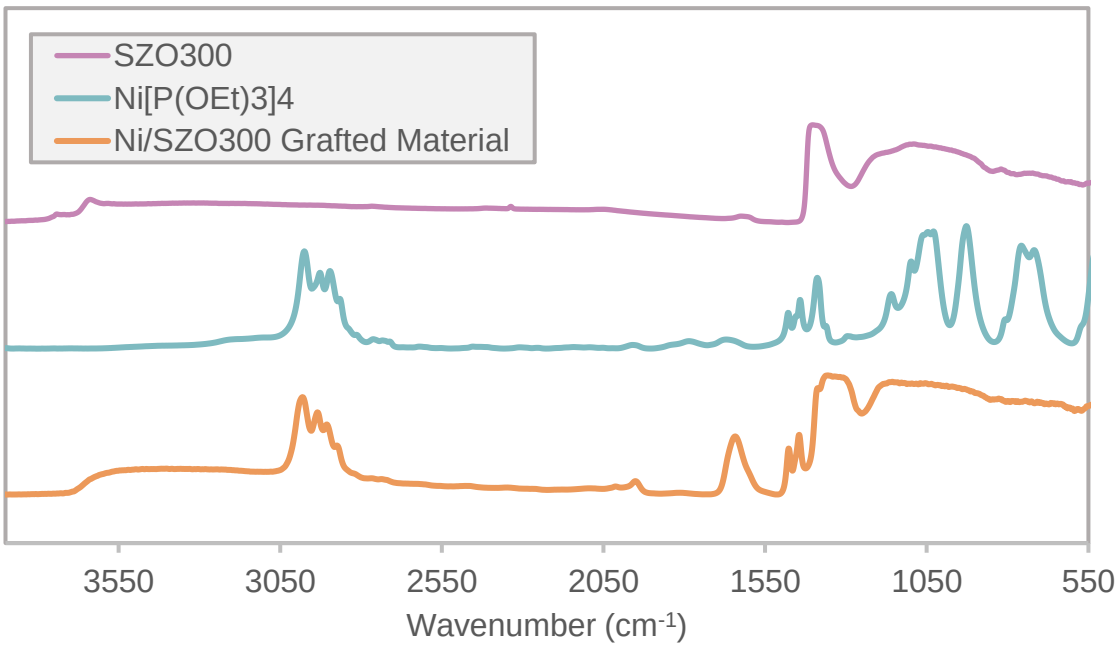

Figure E.15. IR of SZO_{300} (top, pink), $Ni[P(OEt)_3]_4$ (middle, teal), and [Ni]-SZO_{300} (bottom, orange).

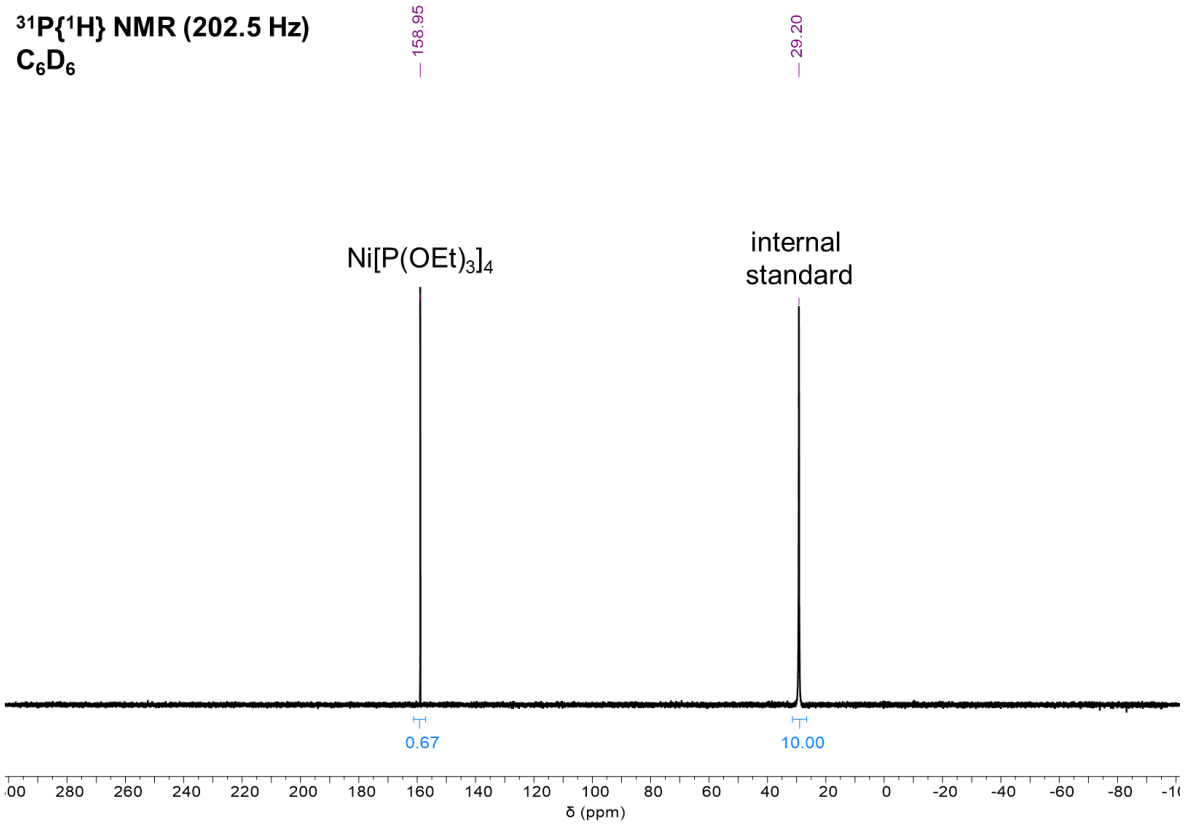

Figure E.16. $^{31}P\{^{1}H\}$ NMR spectrum of the Et_2O washings from the grafting study recorded in C_6D_6 at 25 °C.

Table E.12. Integration of labelled peaks in the $^{31}P\{^{1}H\}$ NMR spectrum, normalized integrations (integration/#H) of each species in solution, and calculated concentration of $Ni[P(OEt)_3]_4$.

Compound	Chemical shift (ppm)	Integration	# of P	Normalized integration	Amount of $Ni[P(OEt)_3]_4$ (mM)
Internal standard	29.20	10.00	2	5.00	N/A
$Ni[P(OEt)_3]_4$	158.95	0.67	4	0.168	0.635

The amount of $Ni[P(OEt)_3]_4$ grafted onto SZO_{300} is calculated to be 9.82 mg $Ni[P(OEt)_3]_4$. Therefore, a total of 73% $Ni[P(OEt)_3]_4$ was grafted onto SZO_{300}, and $Ni[P(OEt)_3]_4$ constitutes 6.15 wt. % of the overall grafted catalyst using a 3:5 $Ni[P(OEt)_3]_4/SZO_{300}$ ratio. This wt. % Ni value is used to determine the amount of grafted catalyst added to each reaction.

b. Isomerization of 1c by the Grafted Catalyst ([Ni]-SZO)

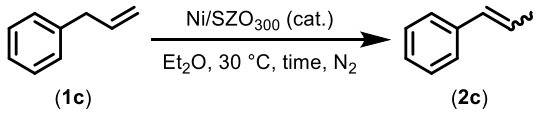

Procedure using in situ catalyst: General Procedure B was followed, and the % conversion to **2c** and selectivity (*E*/*Z*) of the isomerization of **1c** (16 µL, 0.12 mmol, 1.0 equiv) was monitored by GC over time. % Conversion of **1c** to **2c** and selectivity (*E*/*Z*) is reported, and the data is seen in **Figure E.17.** and **Table E.13.** below.

Procedure using grafted catalyst: In a nitrogen-filled glovebox, [Ni]-SZO grafted catalyst (30.0 mg, 0.00255 mmol Ni, 0.0213 equiv) was weighed into a 1-dram vial equipped with a stir bar. To this was added Et_2O (2.0 mL) using a disposable 3-mL syringe and sealed with a septum cap. The reaction was immediately injected with **1c** (16 µL, 0.12 mmol, 1.0 equiv) using a 25-µL syringe and gently stirred. The reaction progress was monitored by GC by taking aliquots (~20 µL) over time. The aliquots were diluted with hexanes (1 mL) and filtered through Celite into a GC vial and analyzed by GC. % Conversion of **1c** to **2c** and selectivity (*E*/*Z*) is reported, and the data is seen in **Figure E.17.** and **Table E.13.** below.

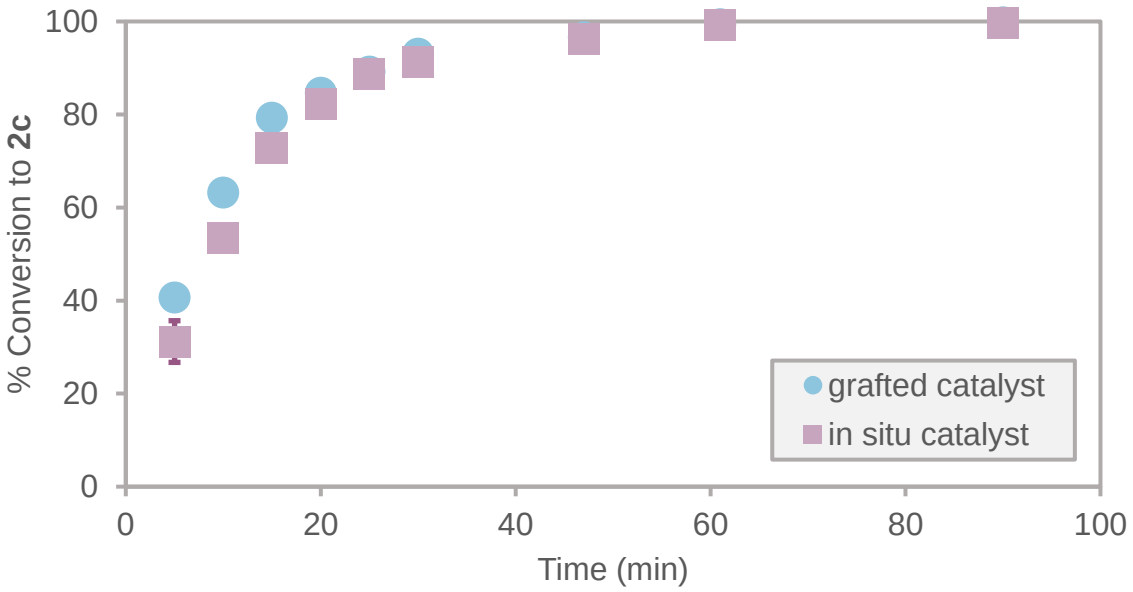

Figure E.17. Plot of the % conversion to **2c** versus reaction time using the in situ generated catalyst Ni[P(OEt)$_3$]$_4$/SZO$_{300}$ (pink squares) and the grafted catalyst [Ni]-SZO$_{300}$ (blue circles).

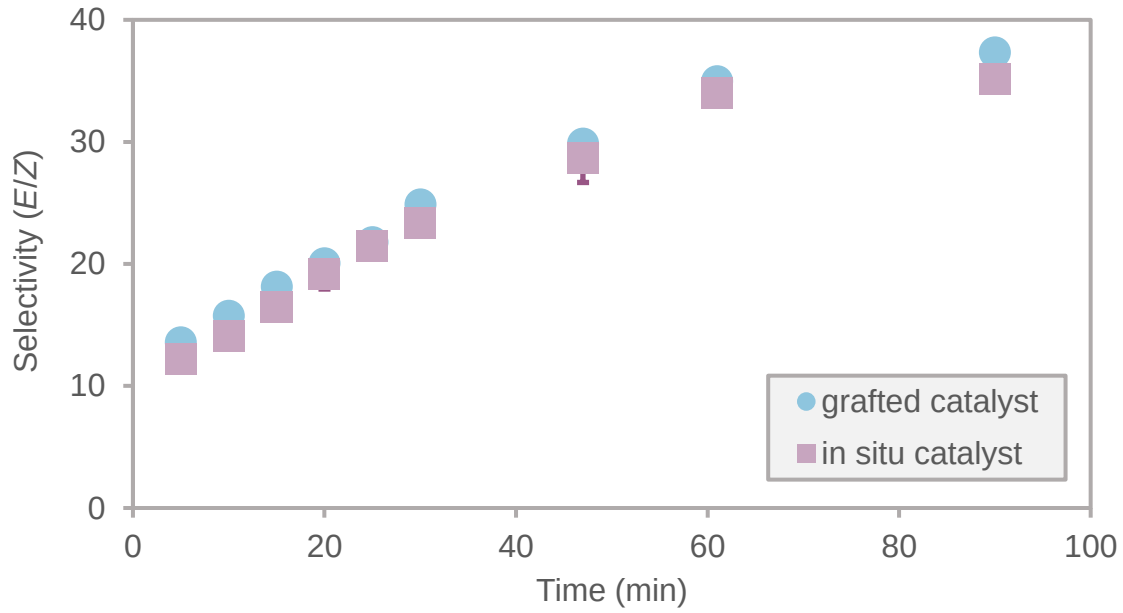

Figure E.18. Plot of the selectivity (*E*/*Z*) of **2c** versus reaction time using the in situ generated catalyst Ni[P(OEt)$_3$]$_4$/SZO$_{300}$ (pink squares) and the grafted catalyst [Ni]-SZO (blue circles).

Table E.13. % Conversion to **2c** and *E*/*Z* selectivity of **2c** as a function of time using the in situ generated and the grafted Ni[P(OEt)$_3$]$_4$/SZO$_{300}$ catalysts.

Time (min)	in situ catalyst		Grafted catalyst	
	% 2c	*E*/*Z* Selectivity (std error)	% 2c	*E*/*Z* Selectivity (std error)
5	31±5	12.2:1 (0.9)	40.69±3	13.6:1 (0.8)
10	53±3	14.1:1 (0.3)	63	16:1
15	73±1	16.50:1 (0.07)	79.3±0.5	18.1:1 (0.2)
20	82.2±0.8	19:1 (1)	84.72±0.05	20.06:1 (0.09)
25	88.8±0.3	21.4:1 (0.5)	89±1	21.8:1 (0.4)
30	91±1	23.4:1 (0.8)	93±1	24.9:1 (0.4)
47	96±2	29:1 (2)	96.6±0.2	29.9:1 (0.7)
61	99.3±0.4	34.0:1 (0.9)	99.44±0.05	35.0:1 (0.8)
90	99.7±0.4	35.1:1 (0.7)	99.8±0.3	37.33:1 (0.01)

c. [Ni]-SZO Air Stability Test

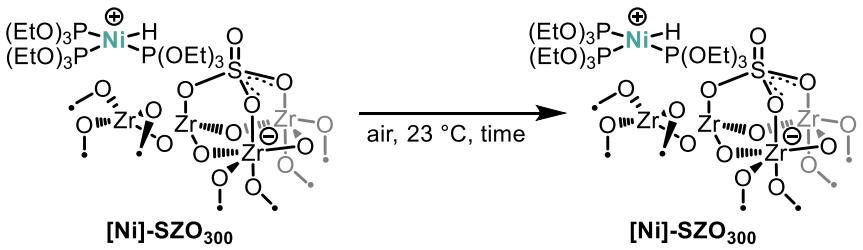

The [Ni]-SZO grafted catalyst (60.1 mg) was weighed directly into an 8 mL vial, sealed with a Teflon-lined thermoset cap, and removed from the glovebox. The vial of catalyst was placed in the fumehood, the Teflon-lined thermoset cap was removed, and the progression of catalyst exposure to ambient atmosphere was documented through photographs over time (**Figure E.19.**).

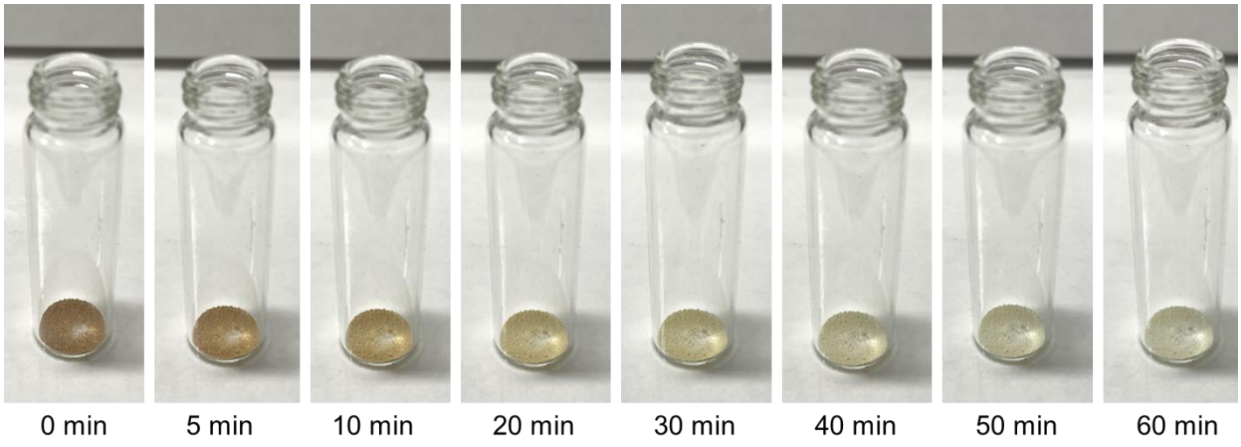

Figure E.19. Visual representation of exposing the grafted Ni/SZO$_{300}$ material to atmosphere over time.

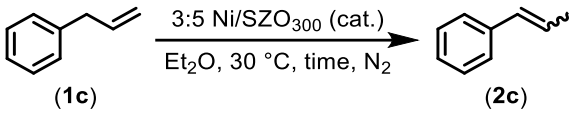

After exposing the vial of [Ni]-SZO grafted catalyst to ambient atmospheric conditions for 1 h, a stir bar was added, the vial was sealed with a septum cap, and the vial was flushed with nitrogen for 10 min. To this was added Et_2O (3.7 mL) using a disposable 3-mL syringe and **1c** (30 µL, 0.23 mmol, 1.0 equiv) using a 50 µL-syringe. The reaction was immediately heated to 30 °C using a preheated aluminum vial block and stirred at a rate of 150 rpm. Reaction progress was monitored by GC by taking aliquots (~20 µL) over time. The aliquots were diluted with hexanes (1 mL) and filtered through Celite into a GC vial and analyzed by GC.

No isomerization activity was observed after 1.5 h, indicating that the catalyst fully decomposes after exposure to air for 1 h.

E.1.12. Catalyst Stability and Heterogeneity Experiments

a. Catalyst Aging Tests

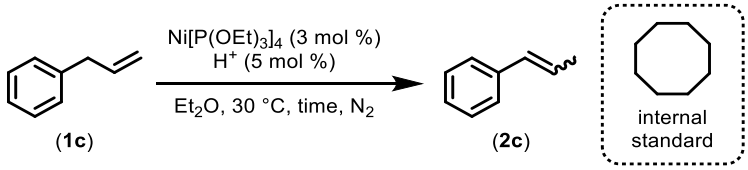

The **General Procedures A and B** was followed with the following exceptions:

- For the homogeneous catalyst using H_2SO_4:
  - The cyclooctane was excluded from the stock solution of $Ni[P(OEt)_3]_4$
  - The vial was set aside to age for 24 h after addition of the H_2SO_4 stock solution
  - Cyclooctane (8.0 µL, 0.059 mmol) was added to the vial just before the addition of **1c**
- For the heterogeneous catalyst using SZO_{300}:
  - The cyclooctane was excluded from the stock solution of $Ni[P(OEt)_3]_4$
  - The vial was sealed with a Teflon-lined cap and set aside in the glovebox to age for 24 h after addition of the $Ni[P(OEt)_3]_4$ stock solution to the SZO_{300}
  - Cyclooctane (8.0 µL, 0.59 mmol) was added to the vial just before the addition of **1c**

The data are seen in **Figures E.20.-E.21.** and **Table E.14.-E.15.** below.

The data in **Figures E.20.-E.21.** for the fresh homogeneous and heterogeneous catalysts are duplicated from section **E.1.10.a.i.**

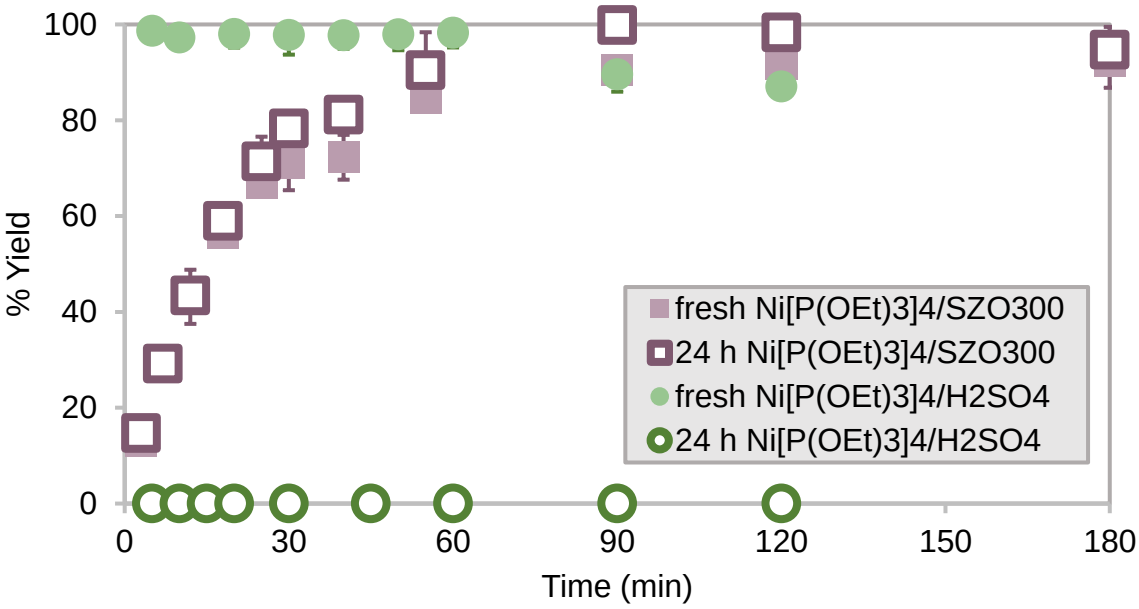

Figure E.20. Plot of yield versus time of the formation of **2c** using freshly prepared $Ni[P(OEt)_3]_4/SZO_{300}$ (pink filled squares), aged $Ni[P(OEt)_3]_4/SZO_{300}$ (pink hollow squares), freshly prepared $Ni[P(OEt)_3]_4/H_2SO_4$ (green filled circles), and aged $Ni[P(OEt)_3]_4/H_2SO_4$ (green hollow circles).

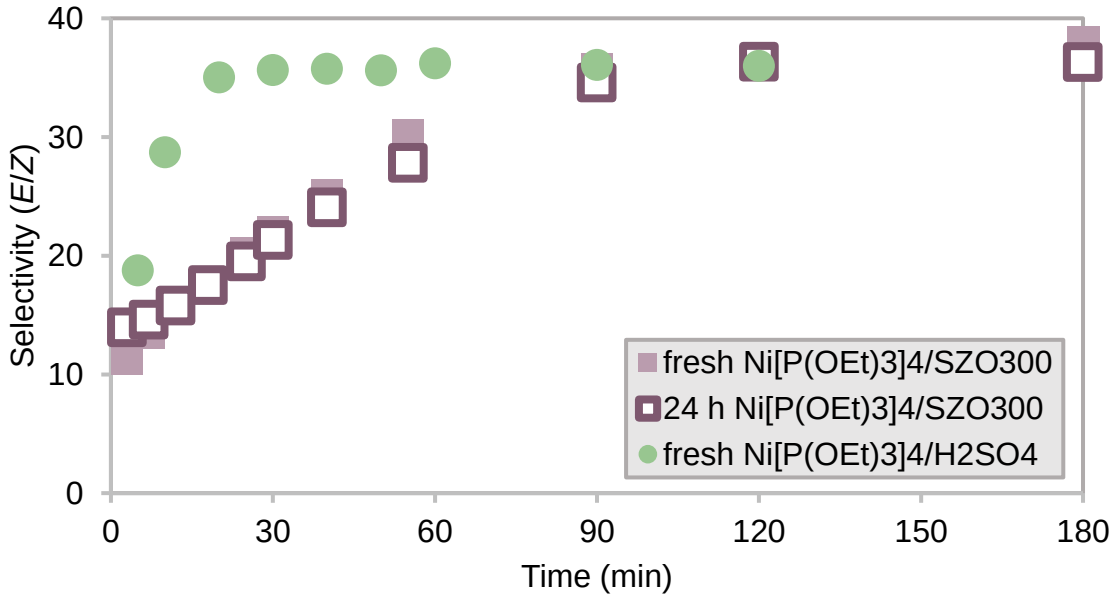

Figure E.21. Plot of selectivity versus time of the formation of **2c** using freshly prepared $Ni[P(OEt)_3]_4/SZO_{300}$ (pink filled squares), aged $Ni[P(OEt)_3]_4/SZO_{300}$ (pink hollow squares), and freshly prepared $Ni[P(OEt)_3]_4/H_2SO_4$ (green filled circles). Error bars are present but are not visible.

Table E.14. Yield and *E*/*Z* selectivity of **2c** over time using freshly prepared and aged $Ni[P(OEt)_3]_4$/ SZO_{300}.

Time (min)	Fresh catalyst		Aged catalyst	
	% Yield	*E*/*Z* Selectivity (std error)	% Yield	*E*/*Z* Selectivity (std error)
3	13±3	11.3:1 (0.6)	15±2	13.98:1 (0.02)
7	29±2	13.5:1 (0.1)	29±1	14.61:1 (0.02)
12	43±6	15.6:1 (0.5)	43±1	15.8:1 (0.2)
18	56.4±0.3	17.74:1 (0.09)	59±1	17.5:1 (0.5)
25	66.8±0.3	20.262:1 (0.005)	71±5	19.5:1 (0.5)
30	71±6	22.04:1 (0.08)	78±4	21.3:1 (0.6)
40	72±5	25.1:1 (0.6)	81±3	24.1:1 (0.4)
55	84.7±0.2	30.2:1 (0.3)	91±8	27.8:1 (0.2)
90	91±2	35.70:1 (0.08)	99±1	34.6:1 (0.3)
120	91.8±0.2	36:1 (1)	98.3±0.5	36.4:1 (0.5)
180	92±6	37.9:1 (0.6)	95±5	36.3:1 (0.3)

Table E.15. Yield and *E*/*Z* selectivity of **2c** over time using freshly prepared and aged $Ni[P(OEt)_3]_4/H_2SO_4$.

Time (min)	Fresh catalyst		Aged catalyst	
	% Yield	*E*/*Z* Selectivity (std error)	% Yield	*E*/*Z* Selectivity (std error)
5	99±1	18.7:1 (0.2)	0	--
10	97±3	28.7:1 (0.2)	0	--
20	98±3	35.0:1 (0.2)	0	--
30	97±4	35.7:1 (0.3)	0	--
40	97±3	35.8:1 (0.6)	0	--
50	98±3	35.6:1 (0.5)	0	--
60	98±3	36.2:1 (0.2)	0	--
90	90±4	36.09:1 (0.06)	0	--
120	87±1	36.0:1 (0.3)	0	--

b. Hot-Filtration Test

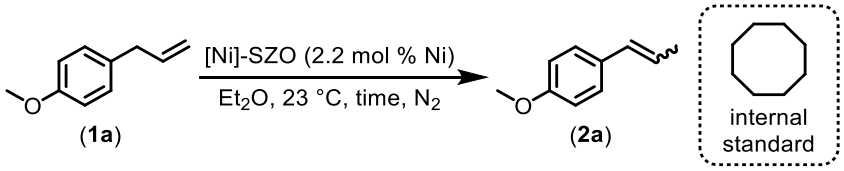

In a nitrogen-filled glovebox, [Ni]-SZO (31.5 mg, 0.00268 mmol Ni, 0.0222 equiv) was weighed into a 1-dram vial equipped with a stir bar. To this was added cyclooctane (10 µL per vial) using a 25-µL syringe and Et_2O (2.0 mL) using a disposable 3-mL syringe. The vial was sealed with a septum cap and **1a** (18.0 µL, 0.120 mmol, 1.00 equiv) was added to the vial using a 25-µL syringe.

After 20 min of reaction time, the reaction was filtered through a 0.1 µm PTFE syringe filter directly into a 1-dram vial equipped with a stir bar. This process separated the solid catalyst from the solution. The reaction progress of the filtrate was monitored by GC by taking aliquots (~20 µL) over time. The GC aliquots were diluted with hexanes (1 mL) and filtered through Celite into a GC vial and analyzed by GC. Another set of reactions was prepared in the same fashion except was not filtered throughout the reaction. All reactions were run in duplicate. Quantification of Ni by ICP-MS of the reaction filtrates gives 0.00014±0.00001 mmol Ni leached into solution, therefore 5.1±0.5% of [Ni] on the heterogeneous catalyst leached into solution.

The data in **Figures E.22.-E.23.** for non-filtered reaction were obtained as described in General Procedure B. The data are seen in **Figures E.22.-E.23.** and **Table E.16.** below.

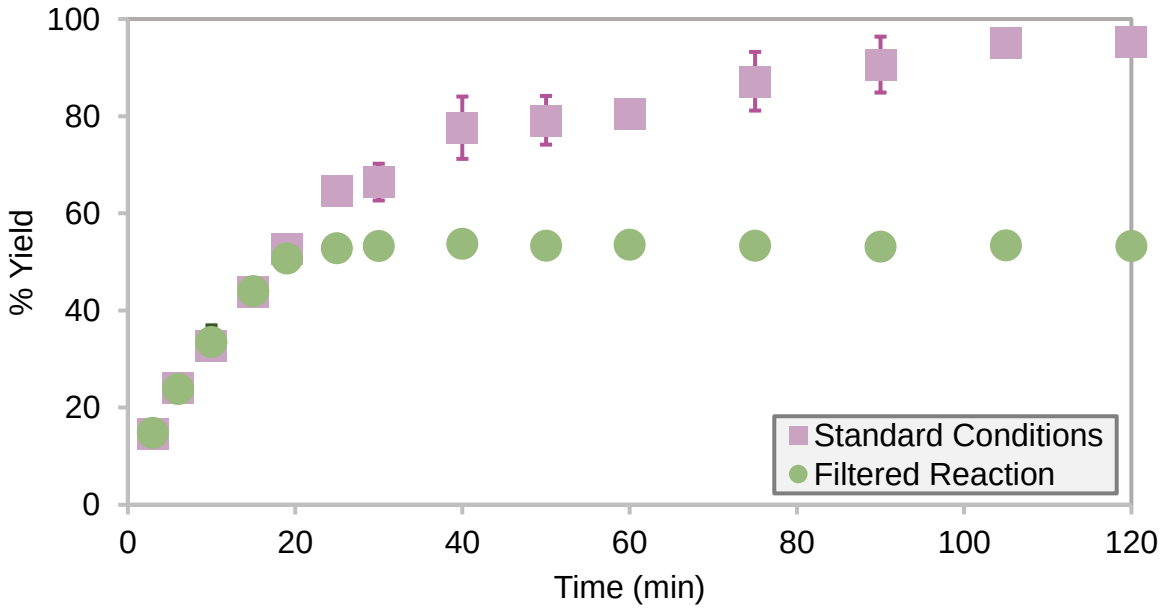

Figure E.22. Plot of yield versus time of the formation of **2a** of the non-filtered reaction (pink squares) and filtered reaction (green circles).

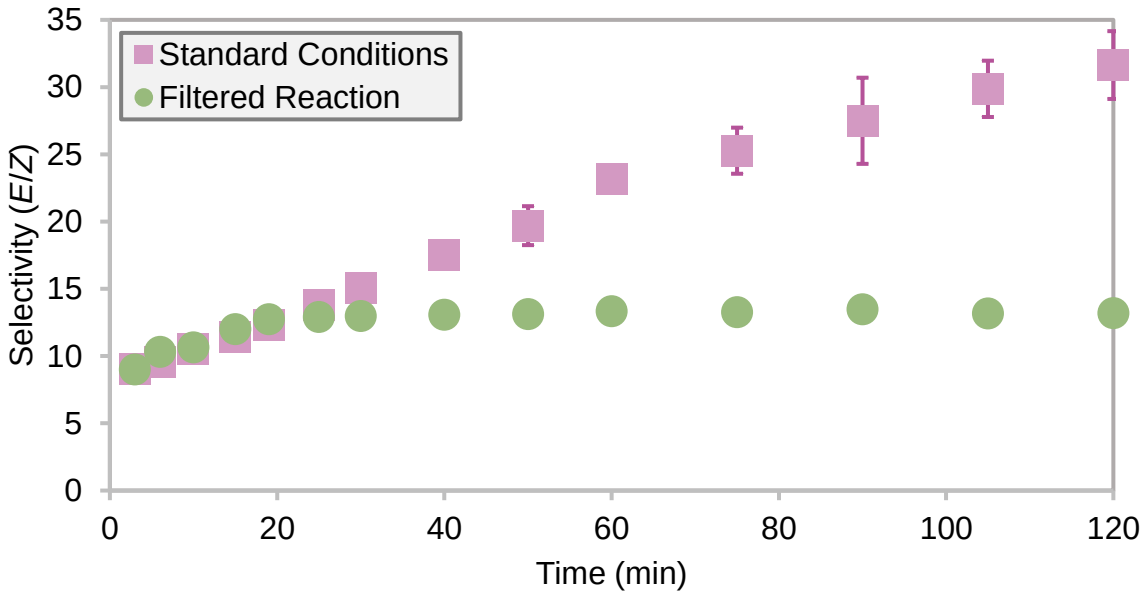

Figure E.23. Plot of the selectivity versus reaction time of the formation of **2a** of the non-filtered reaction (pink squares) and filtered reaction (green circles).

Table E.16. Yield and selectivity (*E*/*Z*) of **2a** over time for the non-filtered reaction (pink squares) and the filtered reaction (green circles).

Time (min)	Non-Filtered Reaction		Filtered Reaction	
	% Yield	*E*/*Z* Selectivity (std error)	% Yield	*E*/*Z* Selectivity (std error)
3	14.6±0.8	9.027:1 (0.002)	14.82±0.04	9.0:1 (0.2)
6	24±1	9.5:1 (0.2)	24±2	10.3:1 (0.7)
10	33±3	10.5:1 (0.1)	34±3	10.6:1 (0.4)
15	43.9±0.5	11.4:1 (0.2)	44±2	12.010:1 (0.002)
19	52.7±0.1	12.3:1 (0.1)	51±2	12.7:1 (0.1)
25	65±1	13.8:1 (0.2)	53±2	12.9:1 (0.2)
30	66±4	15.1:1 (0.5)	53.3±0.8	13.0:1 (0.3)
40	78±6	17.5:1 (0.8)	54±1	13.072:1 (0.002)
50	79±5	20:1 (1)	53±1	13.13:1 (0.05)
60	80.6±0.2	23.2:1 (0.3)	54±1	13.3:1 (0.3)
75	87±6	25:1 (2)	53±1	13.3:1 (0.4)
90	91±6	28:1 (3)	53±1	13.5:1 (0.6)
105	95±2	30:1 (2)	53±1	13.2:1 (0.1)
120	95.33±0.07	32:1 (3)	53±1	13.2:1 (0.2)

As timed aliquots were filtered through Celite, a control experiment was performed to rule out the possibility of Celite quenching the homogeneous [Ni] catalyst that leaches into solution was performed. This was tested by monitoring **1a** isomerization by GC in the presence of Celite.

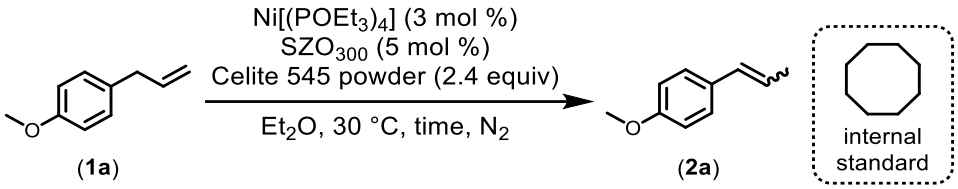

The General Procedure B was followed with the addition of Celite 545 powder (0.0150 g, 0.142 mmol, 2.40 equiv) to the reaction mixture after combining $Ni[(POEt_3)_4$ and SZO_{300}.

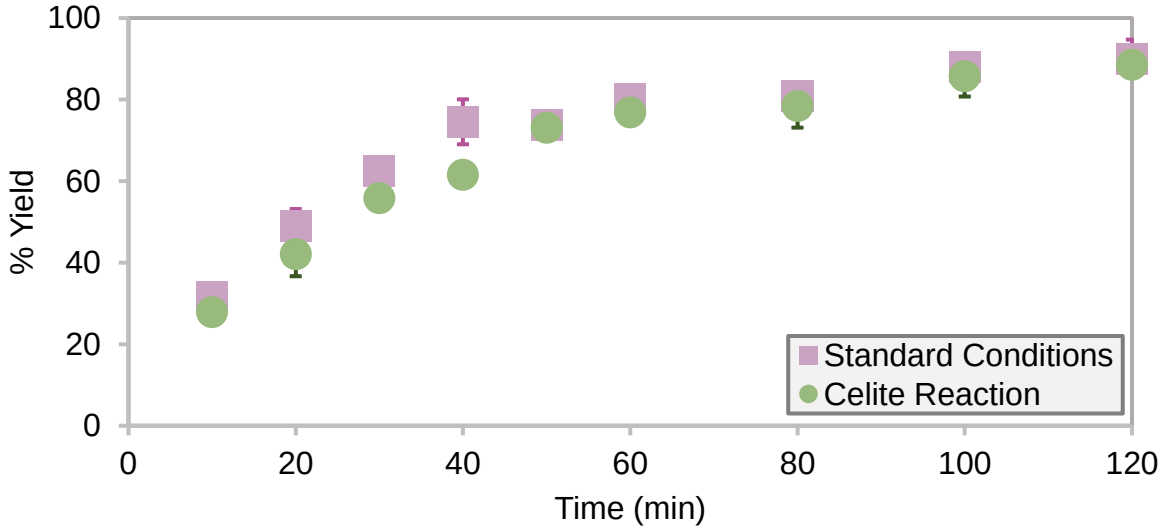

Figure E.24. Plot of yield versus time of the formation of **2a** for the reaction at standard conditions (pink squares) and the reaction in the presence of Celite (green circles).

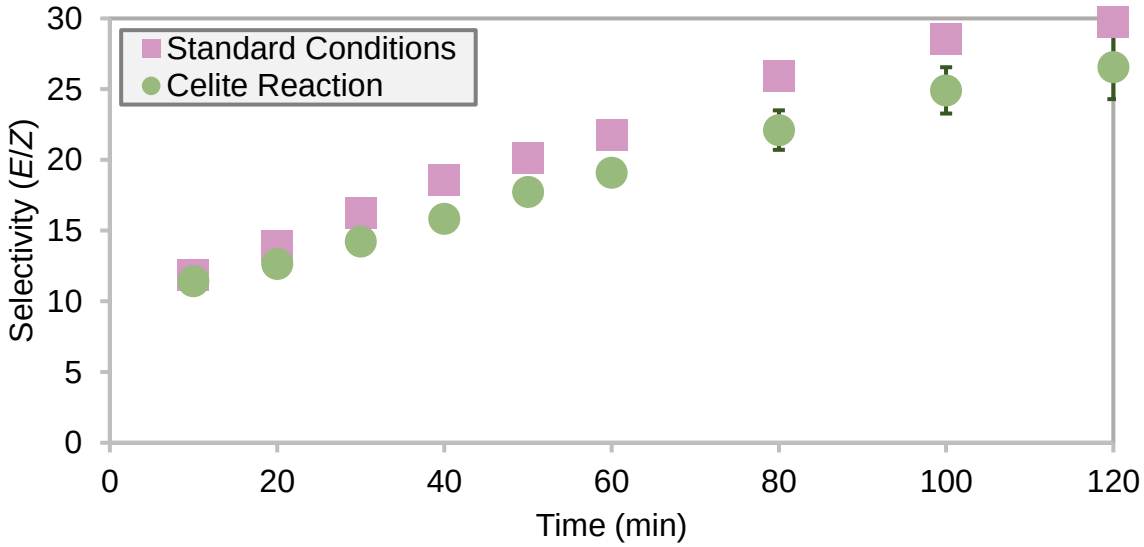

Figure E.25. Plot of the selectivity versus reaction time of the formation of **2a** for the reaction at standard conditions (pink squares) and the reaction in the presence of Celite (green circles).

Table E.17. Yield and selectivity (*E*/*Z*) of **2a** over time for the reaction run at standard conditions (pink squares) and for the reaction in the presence of Celite (green circles).

Time (min)	Standard Conditions		Celite Reaction	
	% Yield	*E*/*Z* Selectivity (std error)	% Yield	*E*/*Z* Selectivity (std error)
10	32±3	11.9:1 (0.2)	28	11.4:1 (0.7)
20	49±4	13.9:1 (0.1)	42	12.64:1 (0.02)
30	62±3	16.3:1 (0.1)	55.84	14.24:1 (0.04)
40	75±6	18.55:1 (0.06)	62	15.9:1 (0.1)
50	74±3	20.11:1 (0.06)	73	17.73:1 (0.06)
60	80.217±0.007	21.8:1 (0.2)	77	19.1:1 (0.6)
80	81±2	25.9:1 (0.2)	78	22:1 (1)
100	88±3	28.6:1 (0.3)	86	25:1 (2)
120	90±5	29.8:1 (0.9)	89	27:1 (2)
160	94±4	31.9:1 (0.3)	--	--
180	88±2	31.7:1 (0.4)	--	--

c. Recyclability Study

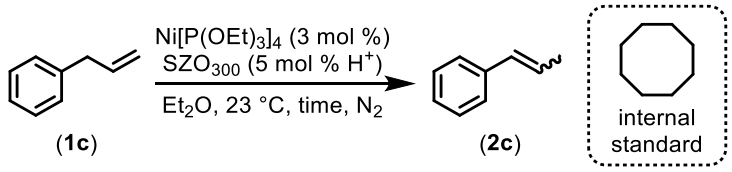

In a nitrogen-filled glovebox, SZO_{300} (15 mg, 0.0030 mmol H^+, 0.050 equiv H^+) was added to a 1-dram vial equipped with a stir bar. $Ni[P(OEt)_3]_4$ (1.3 mg, 0.0018 mmol, 0.030 equiv added to the vial), cyclooctane (5 µL, 0.04 mmol added to the vial), and **1c** (8.0 µL, 0.060 mmol, 1.0 equiv added to the vial) were added to the vial using a disposable 1-mL syringe as a stock solution in Et_2O. The total volume of Et_2O added to each vial was 1.0 mL. The solid immediately turned bright orange upon addition of the stock solution. The vial was sealed with a septum cap and stirred for 1 h 10 min. Stirring was ceased, and the solids were allowed to settle to the bottom. The reaction vial was opened, and the solution was decanted and filtered through Celite. An aliquot (~20 µL) of the filtrate was removed from this solution, placed in a GC vial, diluted with hexanes (1 mL), and analyzed by GC. A separate stock solution of cyclooctane and allylbenzene was prepared in Et_2O using volumetric glassware, transferred into a 5-dram scintillation vial, and sealed with a Teflon-lined thermoset cap when not in use. *** The solid, which remained in the reaction vial, was dried by flowing nitrogen over it for 5 min. A portion of the cyclooctane/allylbenzene (8.0 µL, 0.060 mmol, 1.0 equiv allylbenzene and 5 µL, 0.04 mmol cyclooctane added to each vial)

stock solution was added to the dried solid using a 1-mL syringe. The reaction was sealed and stirred for the allotted amount of time detailed below in Table SX. The reaction vial was opened, and the solution was decanted and filtered through Celite. An aliquot (~20 µL) of the filtrate was removed from this solution, placed in a GC vial, diluted with hexanes (1 mL), and analyzed by GC. This process starting from *** above was repeated 3 times using the cyclooctane and allylbenzene stock solution for a total of 5 cycles. After the 5th cycle, the reaction solution was decanted, the catalyst was dried using a flow of N_2, and the reaction vial was capped and placed in the freezer to store overnight along with the stock solution. The next day, the reaction vial and stock solution were removed, allowed to warm room temperature, and the recyclability studies were continued, starting the process again at *** for a total of 10 cycles. The data are seen in **Figures E.26.** and **Table E.18.** below.

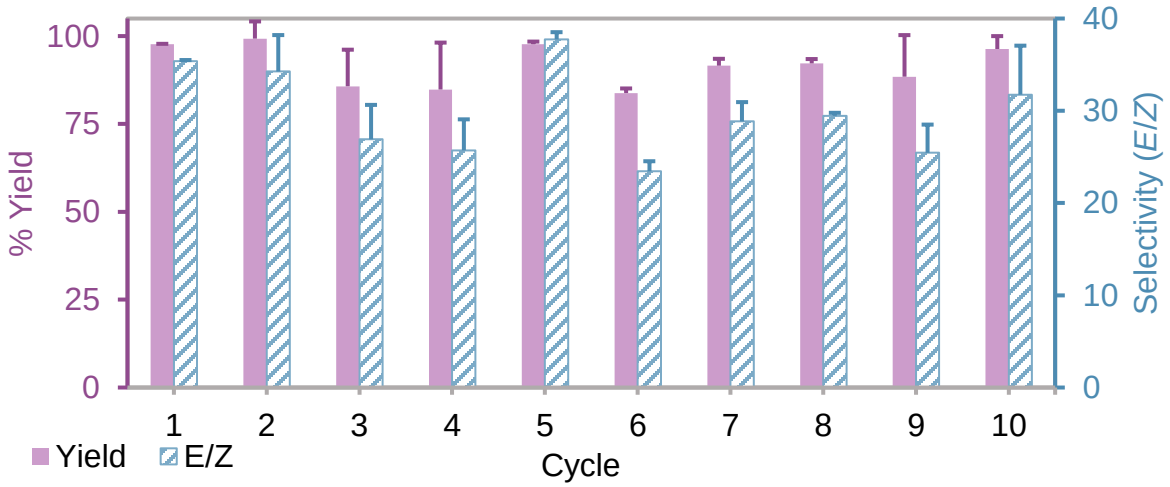

Figure E.26. Bar graph of the yield (left axis, solid pink bars) and *E*/*Z* selectivity (right axis, striped blue bars) of **2c** versus cycle number.

Table E.18. The yield and *E*/*Z* selectivity of the isomerization of **1c** per cycle.

Cycle	Reaction time (h)	% Yield	*E*/*Z* Selectivity (std error)
1	1.17	97.7±0.1	35.4:1 (0.1)
2	1	99±5	34:1 (4)
3	1	86±10	27:1 (4)
4	1	85±13	26:1 (3)
5	2.5	97.7±0.8	37.7:1 (0.8)
Decanted solution, dried catalyst, sealed vial, and placed in freezer overnight.			
6	1	84±1	23:1 (1)
7	1.17	92±2	29:1 (2)
8	2	92±1	29.5:1 (0.3)

9	1	88±12	25:1 (3)
10	1	96±4	32:1 (5)

No significant catalyst decomposition was observed after 10 cycles.

E.1.13. Mechanistic Investigation

a. Reactivity with Vinylcyclopropane

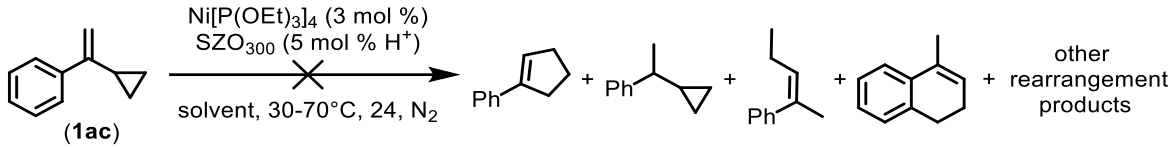

Using **General Procedure B, 1ac** (9.0 µL, 0.060 mmol, 1.0 equiv) was employed as the alkene, and the reaction was performed at 30, 50, and 70 °C, separately. The crude reaction was analyzed by GC. Two trials were performed for both experiments. **Table S13** displays the data for the trails run for 24 h at 30, 50, and 70 °C. No conversion of **1ac** was observed.[239] The data are seen in **Table E.19.** below.

Table E.19. Temperature, solvent, % **1ac** remaining, and % conversion to **2ac**.

Temperature (°C)	solvent	% 1ac remaining	% conversion to other rearrangement products
30	Et_2O	100	0
50	Et_2O	100	0
70[a]	hexanes	100	0

[a]6 h

b. Reactivity with a 1,6-diene

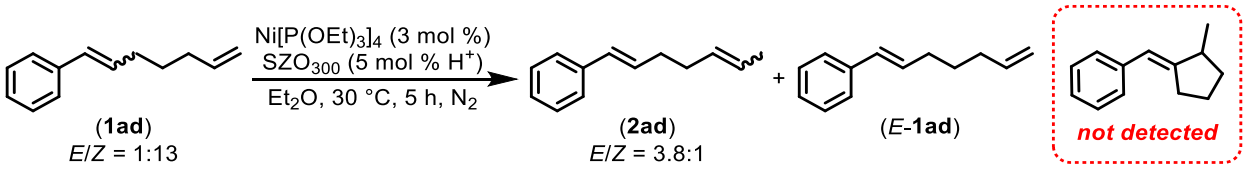

Using **General Procedure 6a**, **1ad** was employed as the alkene. After 5 h of stirring at 30 °C, the reaction was opened to air, filtered through Celite, washed with hexanes (1 mL), and concentrated to obtain a crude oil. The crude product was purified via a pipette plug (silica; 100% pentane). ^{1}H NMR spectrum matches previously reported values.[216] The data are seen in Figure S16 below.

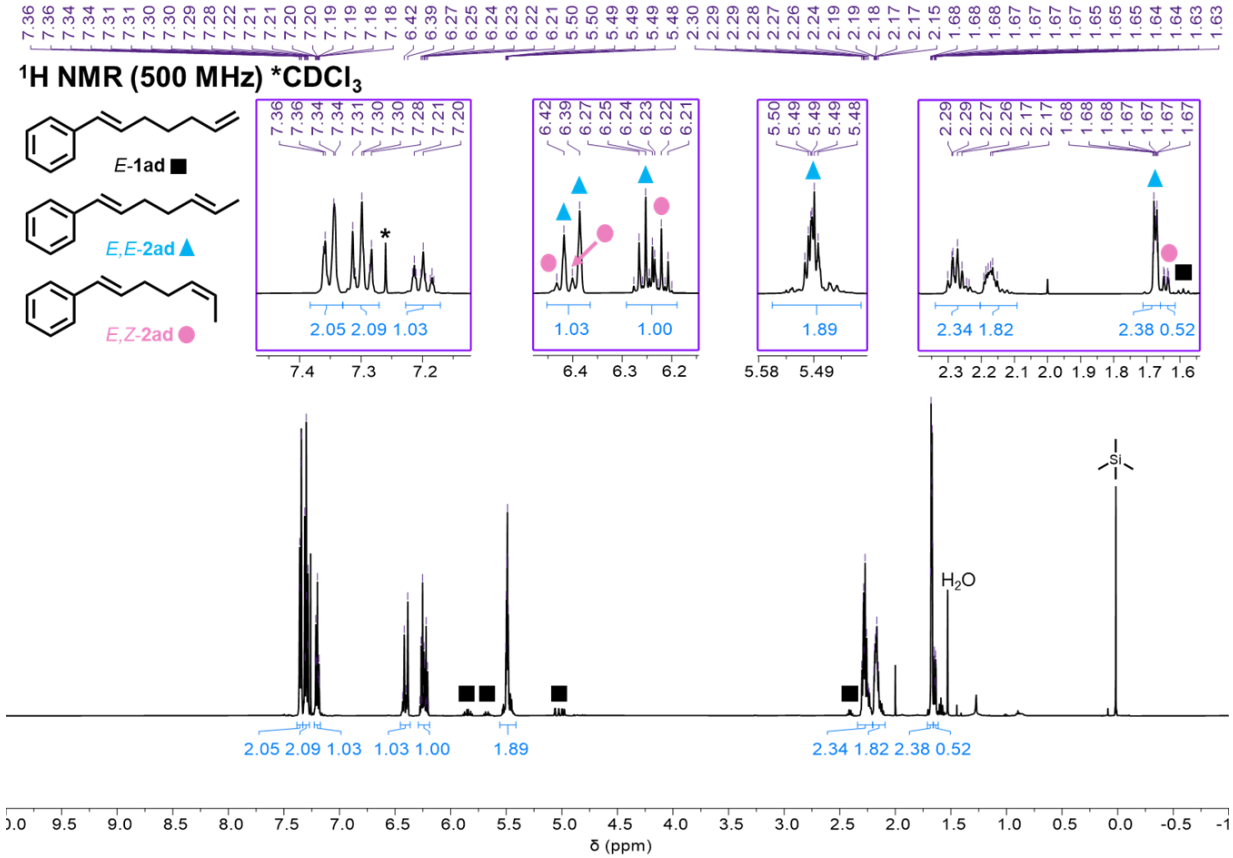

Figure E.27. ^{1}H NMR spectrum for the crude reaction mixture from Ni[P(OEt)$_3$]$_4$/SZO$_{300}$-catalyzed isomerization of **1ad** in $CDCl_3$ at 25 °C.

The major product of the reaction was found to be *E*,*E*-**2ad** (77%), *E*,*Z*-**2ad** (20%), and *E*-**1ad** (3%) as determined by GC analysis. No formation of the radical cyclization product was observed.

c. Deuterium Crossover Experiment

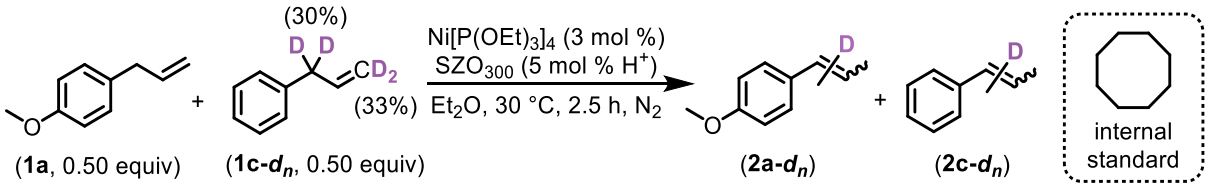

In a nitrogen-filled glovebox, SZO$_{300}$ (141 mg, 0.0281 mmol H$^+$, 0.0500 equiv H$^+$), Ni[P(OEt)$_3$]$_4$ (12.2 mg, 0.0169 mmol, 0.0300 equiv), and Et$_2$O (9.60 mL) were added to a 1-dram scintillation vial equipped with a stir bar. The vial was sealed with a septum cap and brought out of the glovebox. **1a** (44 µL, 0.28 mmol, 0.50 equiv) and **1c-*d*$_n$** (40 µL, 0.28 mmol, 0.50 equiv) were added to the vial using a 50-µL syringe. The reaction was then immediately heated to 30 °C using a preheated aluminum block and stirred at a rate of 150 rpm. After 2.5 h (reaction completion

determined by GC-MS), the reaction was opened to air and the solution was filtered through Celite, washing Et2O (1.0 mL). The filtrate was concentrated, and the product was purified by column chromatography (silica, 0:100 to 8:92 Et_2O/hexanes) to separate **2a-*d*$_n$** from **2c-*d*$_n$**. The products of the reaction were analyzed by ^1H (in $CDCl_3$) and ^2H NMR (in $CHCl_3/CDCl_3$, 5:1). ^2H NMR shows deuterium incorporation into all positions along the allyl group in both products **2a-*d*$_n$** and **2c-*d*$_n$**. The density of **1c-*d*$_n$** was determined by measuring 10 µL of sample using a 25-µL syringe and measuring the weight of the sample; this was repeated three times, and the average of the three trials was found to be 0.85 ± 0.06 g/mL. The data are seen in **Figures E.28.-E.31.** below.

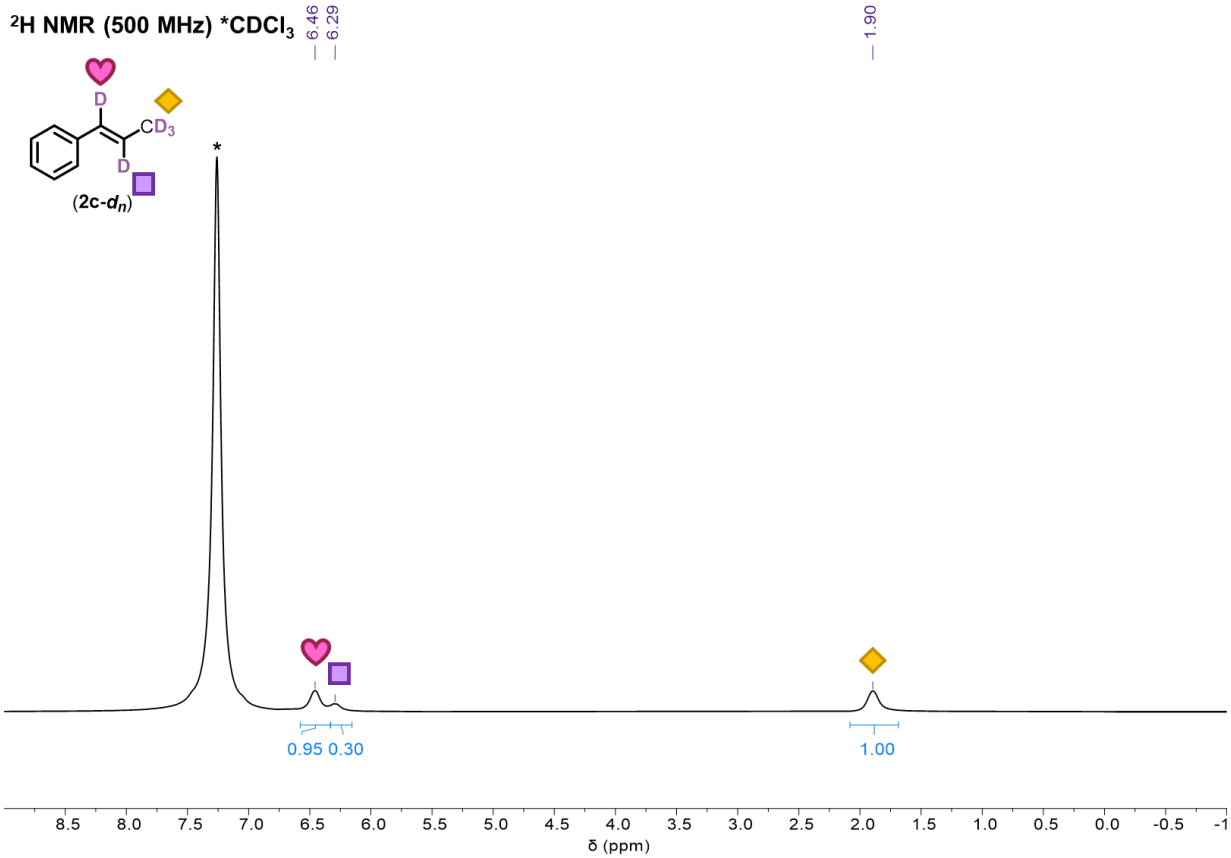

Figure E.28. ^2H NMR spectrum of **2c-*d*$_n$** after isomerization of **1c-*d*$_n$** in the presence of **1a** recorded in $CHCl_3/CDCl_3$ (5:1) at 25 °C.

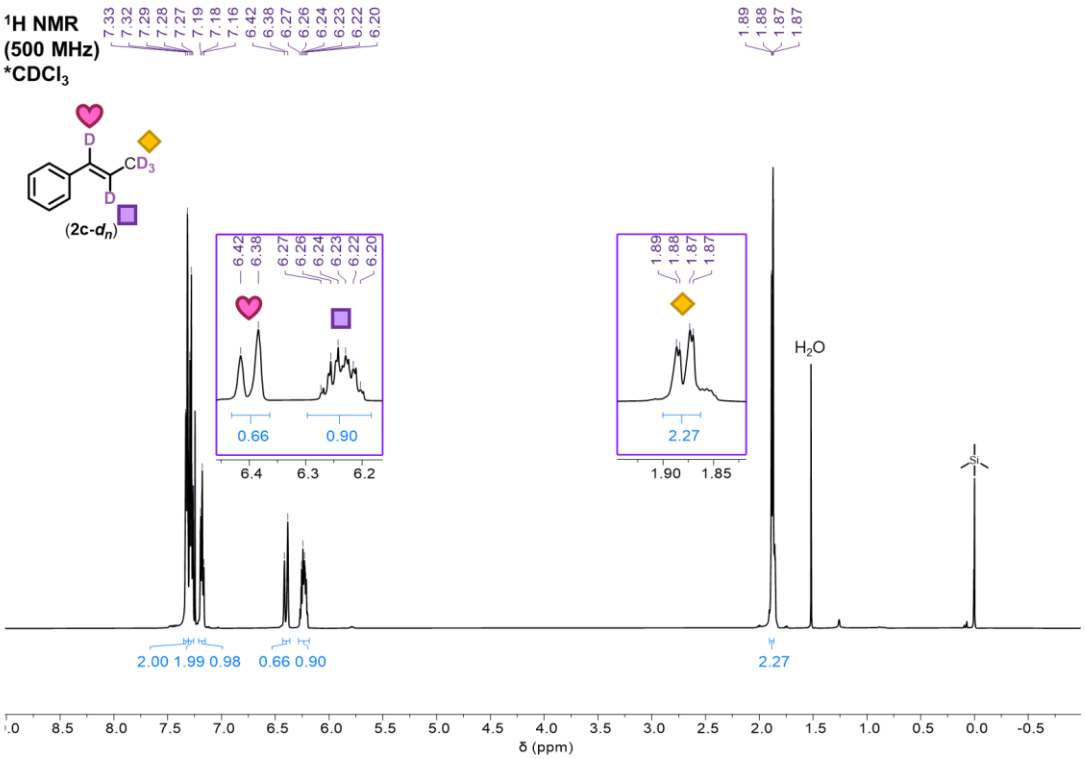

Figure E.29. ^{1}H NMR spectrum of **2c-*d*$_n$** after isomerization of **1c-*d*$_n$** in the presence of **1a** recorded in $CDCl_3$ at 25 °C.

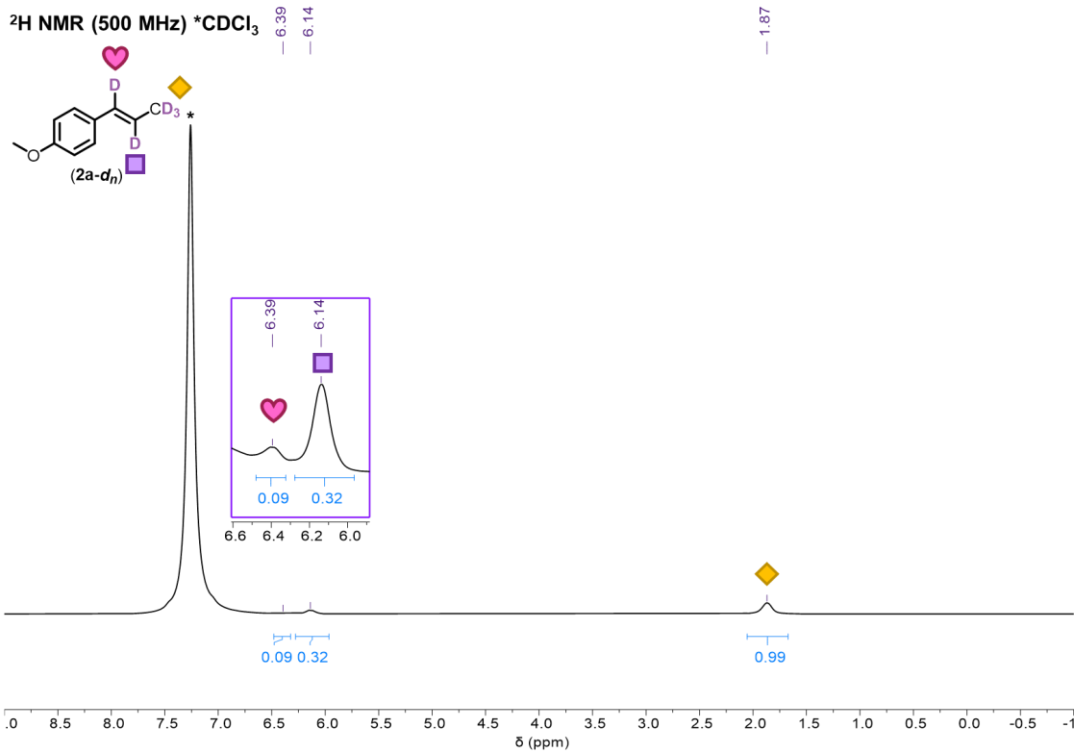

Figure E.30. ^{2}H NMR spectrum of **2a-*d*$_n$** after isomerization of **1a** in the presence of **1c-*d*$_n$** recorded in $CHCl_3/CDCl_3$ (5:1) at 25 °C.

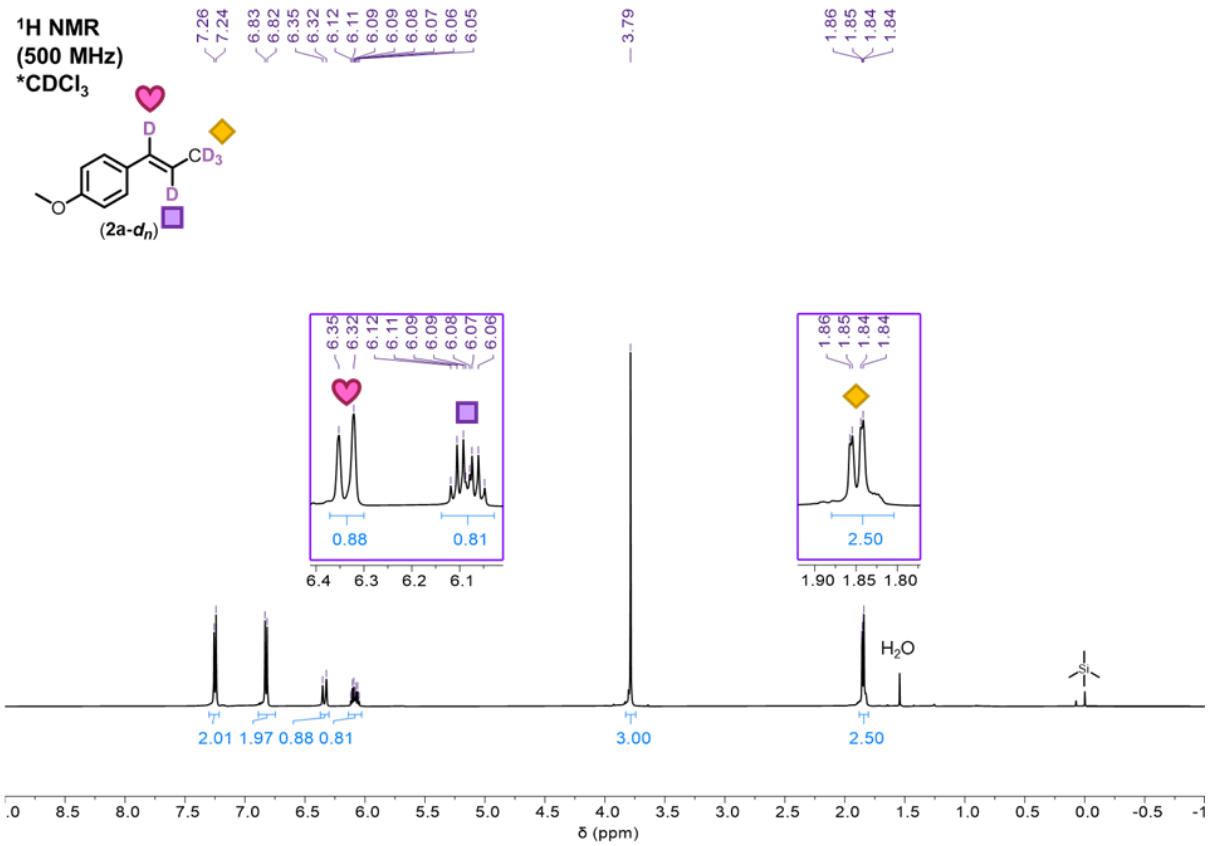

Figure E.31. ^{1}H NMR spectrum of **2a-*d*$_n$** after isomerization of **1a** in the presence of **1c-*d*$_n$** recorded in $CDCl_3$ at 25 °C.

E.1.14. Comparison to Other Homogeneous Isomerization Catalysts

a. (IPr)$_2$Ni$_2$Cl$_2$

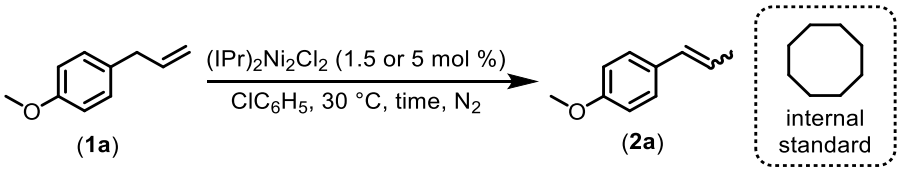

Reaction conditions and procedure were taken from literature.[228] In a nitrogen-filled glovebox, $(IPr)_2NiCl_2$ (see Table S14 for amounts) was directly weighed into a 2-dram vial equipped with a stir bar. To this vial was then added cyclooctane (internal standard; 8 or 12 µL, 0.059 or 0.089 mmol) using a 25-µL syringe and ClC_6H_5 (0.3 or 0.6 mL, 0.4 M) using a disposable 6-mL syringe. The vial was sealed with a septum cap, removed from the glovebox, injected with **1a** (1.0 equiv, either nitrogen-sparged or not see Table S14 for amounts) using a 25-µL syringe, and placed on a

pre-heated aluminum vial block set to 30 °C. The reaction was stirred at a rate of 150 rpm. Reaction progress was monitored by GC analysis by taking aliquots (~5 µL) of the solution over time; the aliquots were diluted with 1 mL hexanes and filtered through Celite into a GC vial. Two trials were run, and the averages and standard deviations are reported below. Table S14 below shows the corresponding amount of $(IPr)_2NiCl_2$ and **1a** used for each experiment. The data are seen in Table S15 and Figures S21-S22 below.

Table E.20. The amounts and equivalents of $(IPr)_2Ni_2Cl_2$ and ClC_6H_5 and indication if the alkene was nitrogen-sparged for the experiments.

$(IPr)_2NiCl_2$				1a				$Cl\text{-}C_6H_5$
mol %	**mg**	**mmol**	**equiv**	**µL**	**mmol**	**equiv**	**Nitrogen-sparged**	**Volume (mL)**
1.5	1.6	0.0018	0.015	19	0.12	1.0	no	0.3
1.5	3.3	0.0036	0.015	39	0.25	1.0	yes	0.6
5	5.7	0.0060	0.050	19	0.12	1.0	yes	0.3

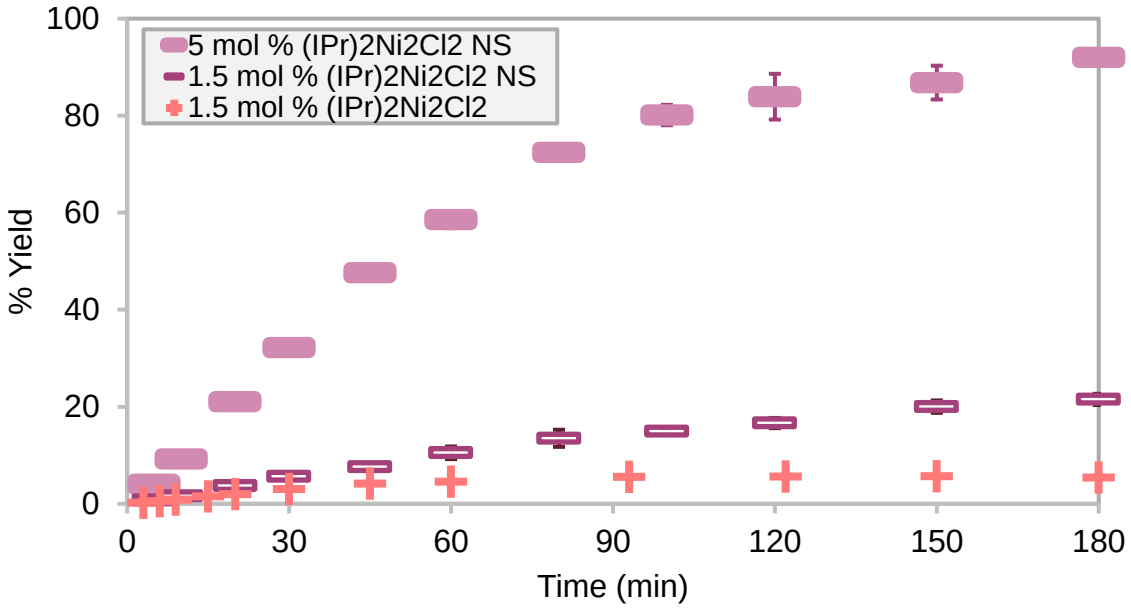

Figure E.32. Plot of the yield of **2a** versus time using 5 mol % $(IPr)_2Ni_2Cl_2$ with degassed alkene (light pink filled rectangles), 1.5 mol % $(IPr)_2Ni_2Cl_2$ with degassed alkene (dark pink hollow rectangles), and 1.5 mol % $(IPr)_2Ni_2Cl_2$ without degassing alkene prior to isomerization (red crosses) at 30 °C. NS, nitrogen-sparged.

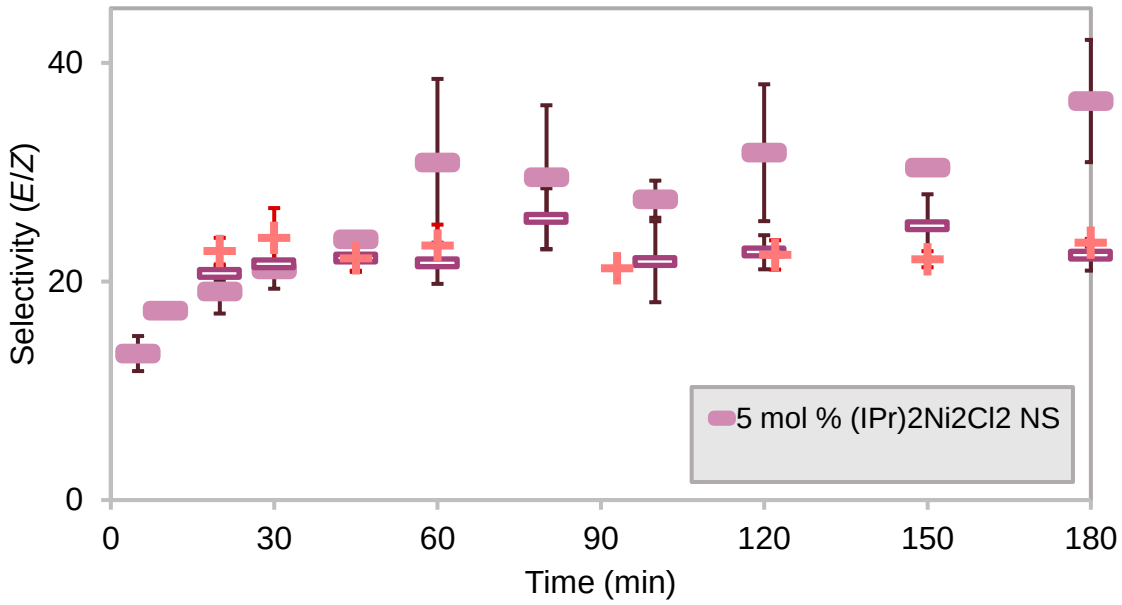

Figure E.33. Plot of the selectivity of **2a** versus time using 5 mol % $(IPr)_2Ni_2Cl_2$ with degassed alkene (light pink filled rectangles), 1.5 mol % $(IPr)_2Ni_2Cl_2$ with degassed alkene (dark pink hollow rectangles), and 1.5 mol % $(IPr)_2Ni_2Cl_2$ without degassing alkene prior to isomerization (red crosses) at 30 °C. NS, nitrogen-sparged.

Table E.21. Yield and *E*/*Z* selectivity of **2a** over time catalyzed by 1.5 mol % and 5 mol % $(IPr)_2Ni_2Cl_2$ with and without degassed alkene at 30 °C. NS, nitrogen-sparged.

Time (min)	1.5 mol % $(IPr)_2Ni_2Cl_2$ Not NS alkene		1.5 mol % $(IPr)_2Ni_2Cl_2$ NS alkene		5 mol % $(IPr)_2Ni_2Cl_2$ NS alkene	
	% Yield	*E*/*Z* Selectivity (std error)	% Yield	*E*/*Z* Selectivity (std error)	% Yield	*E*/*Z* Selectivity (std error)
3	0.241±0.002	1:0	--	--	--	--
5	--	--	0.7±0.1	1:0	4.0±0.2	13:1 (2)
6	0.56±0.07	1:0	--	--	--	--
9	0.89±0.08	1:0	--	--	--	--
10	--	--	1.6±0.1	1:0	9.2±0.7	17.3:1 (0.4)
15	1.6±0.1	1:0	--	--	--	--
20	2.0±0.1	23:1 (1)	3.654±0.001	20.7:1 (0.7)	21±2	19:1 (2)
30	3.1±0.3	24:1 (3)	5.5±0.3	22:1 (2)	32.2±0.7	21.1:1 (0.7)
45	4.2±0.3	22:1 (1)	7.4±0.6	22:1 (1)	48±2	23.9:1 (0.4)
60	4.6±0.3	23:1 (2)	10±1	22:1 (2)	59±2	32:1 (7)
80	--	--	13±2	26:1 (3)	72±1	30.43:1 (0.04)
93	5.6±0.6	21.211:1 (0.0006)	--	--	--	--
100	6±1	--	14.5±0.5	22:1 (4)	80±2	28:1 (2)
120	5.7±0.9	22:1 (1)	16±1	23:1 (2)	84±5	32:1 (6)
150	5±1	22.0:1 (0.7)	20±1	25:1 (3)	87±4	30.43:1 (0.04)
180	5±1	23.6:1 (0.3)	21±1	22:1 (1)	92±1	37:1 (6)

b. Ni(cod)$_2$ + PCy$_3$•HBF$_4$ + NBu$_4$Br

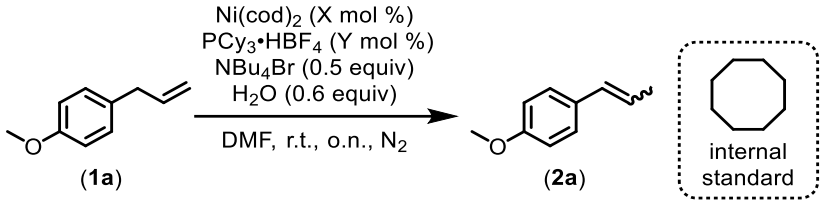

Reaction conditions and procedure were taken from literature with slight modifications.[229] In a nitrogen-filled glovebox, Ni(cod)$_2$ (see Table S16 below for amounts), PCy$_3$•HBF$_4$ (see Table S16 below for amounts), and tetrabutylammonium bromide (40 mg, 0.12 mmol, 0.50 equiv) were directly weighed into a 1-dram scintillation vial equipped with a stir bar. To this vial was added DMF (5.0 mL) using a disposable 6 mL-syringe and cyclooctane (internal standard; 8.0-10 µL,0.059-0.074 mmol added to the vial) using a 25-µL syringe. The vial was sealed with a septum cap, brought out of the glovebox, injected with nitrogen-sparged H_2O (2.5 µL, 0.14 mmol, 0.56 equiv) using a 10-µL syringe followed by **1a** (39 µL, 0.25 mmol, 1.0 equiv) using a 50-µL syringe, and heated at 30 °C on a preheated aluminum vial block. The reaction was stirred at a rate of 150 rpm. Throughout the course of the reaction, 40-µL aliquots were removed with a 50-µL syringe, diluted with hexanes, and filtered into a GC vial through Celite. The filtrate was analyzed by GC to assess the reaction progress and product selectivity. Two trials were run for all experiments and the averages and standard deviations for the two trials are reported below in **Table E.23.** and the data is seen in **Figure E.34.-E.35.**

Table E.22. The catalyst loading, amount, and mmol of Ni(cod)$_2$ and PCy$_3$•HBF$_4$ for each experiment.

Reaction conditions	Ni(cod)$_2$			PCy$_3$•HBF$_4$		
	mol %	mg	mmol	mol %	mg	mmol
Standard (30 °C)	10	7.0	0.025	11	10	0.027
Ours (30 °C)	3	2.1	0.0076	3	2.8	0.0076

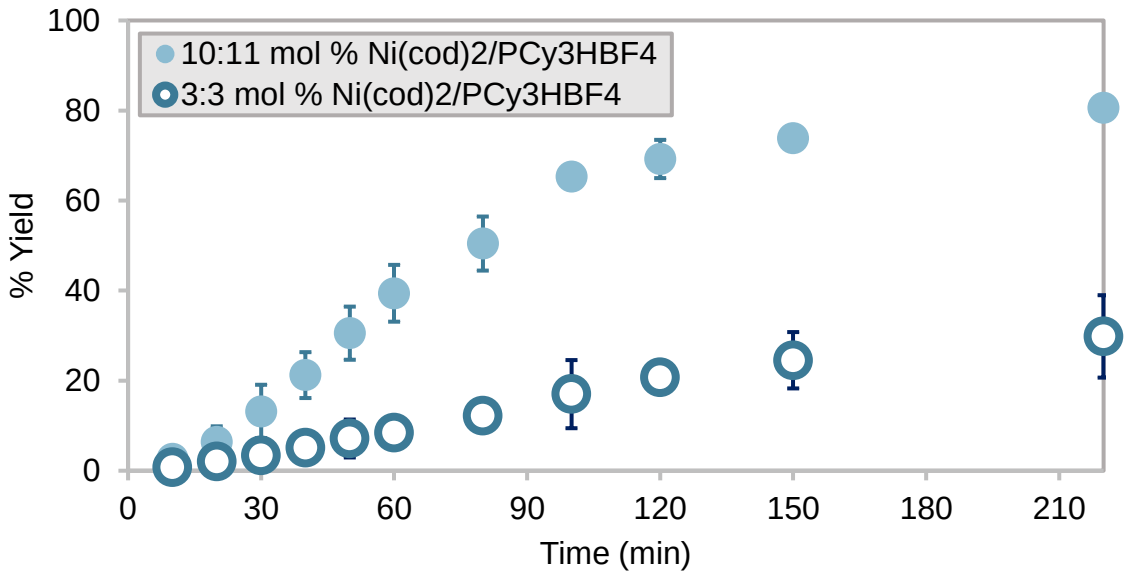

Figure E.35. Plot of the yield of **2a** versus reaction time using 10 mol % $Ni(cod)_2$ and 11 mol % PCy_3•HBF_4 (blue filled circles) and 3 mol % $Ni(cod)_2$ and mol % PCy_3•HBF_4 (blue hollow circles) at 30 °C.

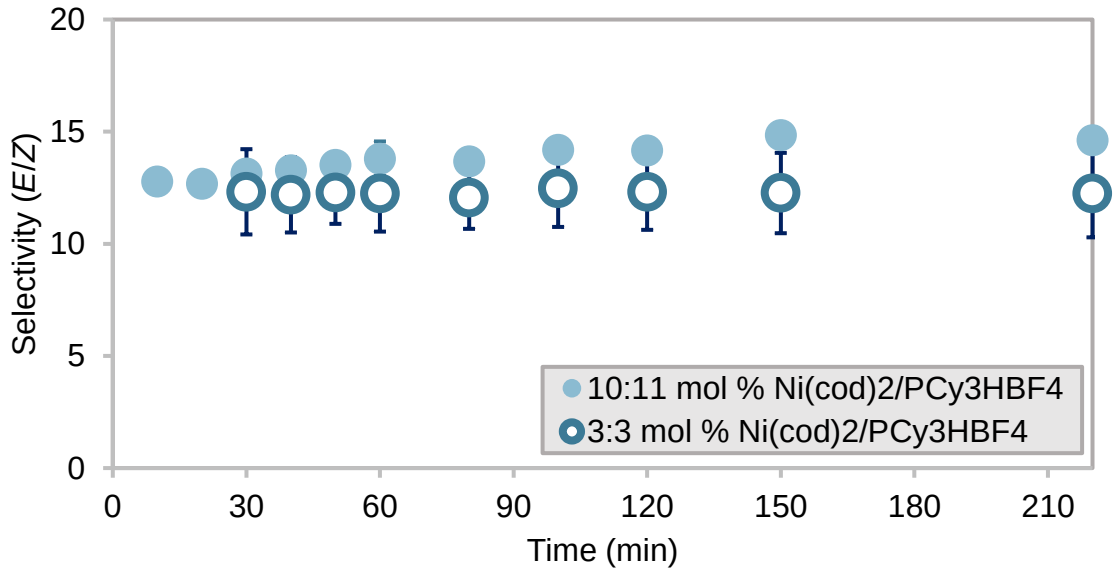

Figure E.36. Plot of the selectivity of **2a** versus reaction time using 10 mol % $Ni(cod)_2$ and 11 mol % PCy_3•HBF_4 (blue filled circles) and 3 mol % $Ni(cod)_2$ and mol % PCy_3•HBF_4 (blue hollow circles) at 30 °C.

Table E.23. Yield and *E*/*Z* selectivity of **2a** over time using 10 mol % $Ni(cod)_2$ and 11 mol % PCy_3•HBF_4 and 3 mol % $Ni(cod)_2$ and mol % PCy_3•HBF_4 at 30 °C.

Time (min)	10 mol % $Ni(cod)_2$ & 11 mol % PCy_3•HBF_4		3 mol % $Ni(cod)_2$ & 3 mol % PCy_3•HBF_4	
	% Yield	*E*/*Z* Selectivity (std error)	% Yield	*E*/*Z* Selectivity (std error)
10	2.7±1	12.8:1 (0.2)	0.7±0.1	1:0
20	6.4±4	12.7:1 (0.1)	2±1	1:0
30	13.2±6	13.1:1 (0.4)	3±2	12:1 (2)
40	19.6±5	13.3:1 (0.5)	5±3	12:1 (2)
50	29.3±6	13.5:1 (0.2)	7±4	12:1 (1)
60	37.9±6	13.8:1 (0.8)	8±3	12:1 (2)
80	50.5±6	13.68:1 (0.02)	12±4	12:1 (1)
100	65.4±0.4	14.19:1 (0.03)	17±8	12:1 (2)
120	69.2±4	14.16:1 (0.03)	20.7±0.4	12:1 (2)
150	73.8±0.8	14.8:1 (0.5)	25±6	12:1 (2)
220	80.6	15:1	30±9	12:1 (1)

c. (IPr)Ni(1,5-hexadiene)

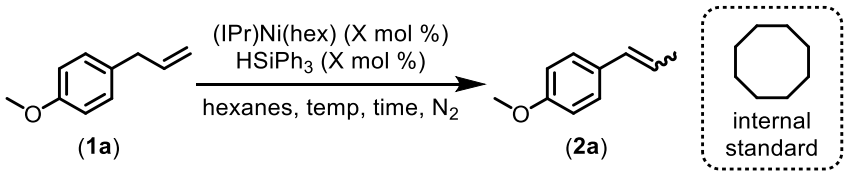

Reaction conditions and procedure were taken from literature.[230] In a nitrogen-filled glovebox, (IPr)Ni(hex) (see **Table E.24.** below for amounts) was directly weighed into a 1-dram scintillation vial equipped with a stir bar. A stock solution of $HSiPh_3$ in hexanes (see **Table E.24.** below for amounts) was prepared and distributed to the vials using a disposable 1-mL syringe. To this vial was added cyclooctane (internal standard; 8.0 µL, 0.059 mmol added to the vial) using a 25-µL syringe and additional hexanes to obtain a total reaction volume of 0.38 mL using a disposable 1-mL syringe. The vial was sealed with a septum cap, brought out of the glovebox, and the following details were performed for the corresponding experiments:

- Standard reaction conditions (80 °C): the vials were heated at 80 °C on a preheated aluminum vial block for 30 min and then injected with **1a** (19 µL, 0.12 mmol, 1.0 equiv) using a 25-µL syringe.
- Our reaction conditions (30 °C): **1a** (19 µL, 0.12 mmol, 1.0 equiv) was injected using a 25-µL syringe and the vials were heated at 30 °C on a preheated aluminum vial block.

The reactions were stirred at a rate of 150 rpm. Throughout the course of the reaction, 5-µL aliquots were removed with a 25-µL syringe, diluted with hexanes, and filtered into a GC vial through Celite. The filtrate was analyzed by GC to assess the reaction progress and product selectivity. Two trials were run for all experiments and the averages and standard deviations for the two trials are reported below in **Table E.25.** and the data is seen in Figure S25-S26.

Table E.24. Amounts of (IPr)Ni(hex) and $HSiPh_3$ for each experiment.

Reaction conditions	(IPr)Nihex)			$HSiPh_3$		
	mol %	mg	mmol	mol %	mg	mmol
Standard (80 °C)	5	3.2	0.0060	3	1.6	0.0061
Ours (30 °C)	3	1.9	0.0036	5	0.95	0.0036

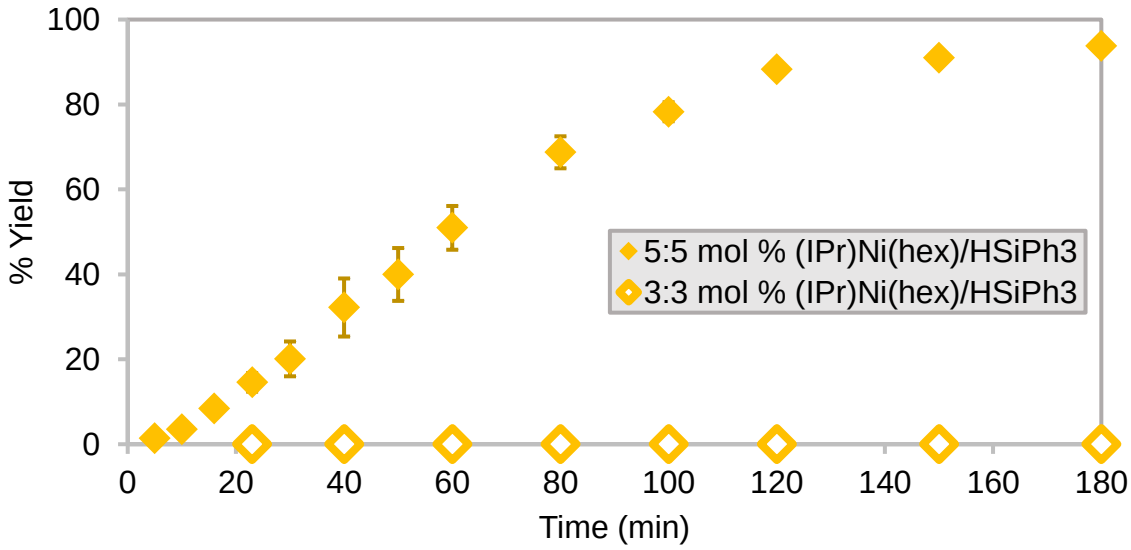

Figure E.37. Plot of the yield of **2a** versus reaction time using 5 mol % (IPr)Ni(hex) and 5 mol % $HSiPh_3$ at 80 °C (yellow filled diamonds) and 3 mol % (IPr)Ni(hex) and 3 mol % $HSiPh_3$ at 30 °C (yellow hollow diamonds).

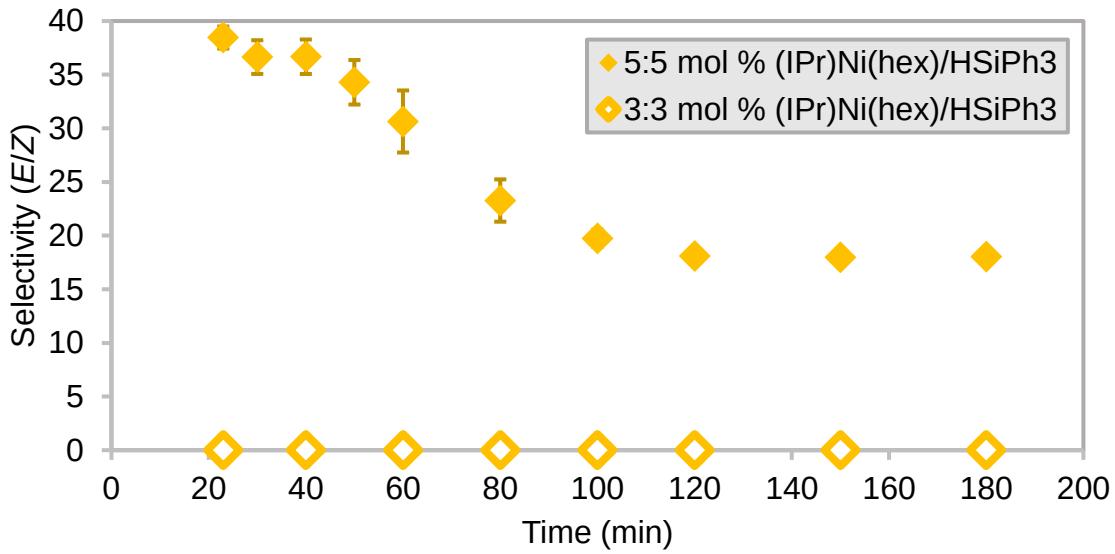

Figure E.38. Plot of the selectivity of **2a** versus reaction time using 5 mol % (IPr)Ni(hex) and 5 mol % $HSiPh_3$ at 80 °C (yellow filled diamonds) and 3 mol % (IPr)Ni(hex) 3 mol % and $HSiPh_3$ at 30 °C (yellow hollow diamonds).

Table E.25. Yield of **2a** and selectivity (*E*/*Z*) over time using 5 mol % (IPr)Ni(hex) and 5 mol % $HSiPh_3$ at 80 °C and 3 mol % (IPr)Ni(hex) and 3 mol % $HSiPh_3$ at 30 °C.

Time (min)	5 mol % (IPr)Ni(hex) & 5 mol % $HSiPh_3$		3 mol % (IPr)Ni(hex) & 3 mol % $HSiPh_3$	
	% Yield	*E*/*Z* Selectivity (std error)	% Yield	*E*/*Z* Selectivity (std error)
5	1.4±0.2	1:0	--	--
10	3.5	1:0	--	--
16	8±2	1:0	--	--
23	15±4	38:1 (1)	0	n.d.
30	20±7	37:1 (2)	--	--
40	32±6	37:1 (2)	0	n.d.
50	40±5	34:1 (2)	--	--
60	51±4	31:1 (2)	0	n.d.
80	69±2	23:1 (2)	0	n.d.
100	78.3±0.8	19.7:1 (0.8)	0	n.d.
120	88±2	18.1:1 (0.2)	0	n.d.
150	91.0±0.2	18.0:1 (0.4)	0	n.d.
180	94±2	18.05:1 (0.09)	0	n.d.

n.d. = not determined

d. Pd(dba)$_2$ +P(t-Bu)$_3$ + i-PrC(O)Cl

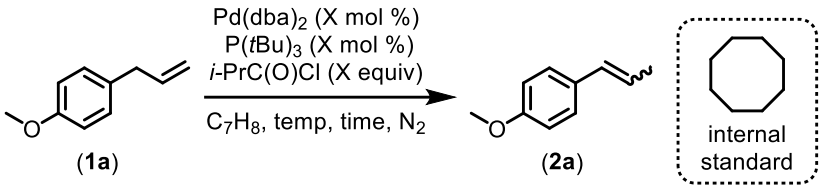

Reaction conditions and procedure were taken from literature with slight modifications.[237] In a nitrogen-filled glovebox, stock solutions of Pd(dba)$_2$, P(*t*-Bu)$_3$, and isobutyryl chloride (*i*-PrC(O)Cl) (see **Table E.26.** below for amounts) were prepared in toluene and distributed into 1-dram scintillation vials equipped with stir bars using disposable 1-mL syringes or a 100-µL syringe. To these vials were added cyclooctane (internal standard; 10 µL, 0.074 mmol) using a 25-µL syringe and additional toluene to obtain a total volume of 2.9 mL using a disposable 3-mL syringe. The vials were sealed with septum caps, brought out of the glovebox, injected with **1a** (19 µL, 0.12 mmol, 1.0 equiv) using a 25-µL syringe, and heated at 30 or 80 °C on a preheated aluminum vial block. The reaction was stirred at a rate of 150 rpm. Throughout the course of the reaction, 40-µL aliquots were removed with a 50-µL syringe, diluted with hexanes, and filtered into a GC vial through Celite. The filtrate was analyzed by GC to assess the reaction progress and product selectivity. Two trials were run for all experiments and the averages and standard deviations for the two trials are reported below in **Table E.27.** and the data is seen in **Figure E.39.-E.40.**

Table E.26. The catalyst loading, amount, mmol, and equiv of Pd(dba)$_2$, P(*t*-Bu)$_3$, and *i*-PrC(O)Cl for each catalytic trial.

Reaction conditions	Pd(dba)$_2$			P(*t*-Bu)$_3$			*i*-PrC(O)Cl		
	mol %	mg	mmol	mol %	mg	mmol	mol %	µL	mmol
Standard (80 °C)	0.5	0.35	6.1×10^{-4}	0.5	0.12	5.9×10^{-4}	0.5	0.065	6.2×10^{-4}
Ours (30 °C)	3	2.1	3.7×10^{-3}	3	0.74	3.7×10^{-3}	3	0.39	3.7×10^{-3}

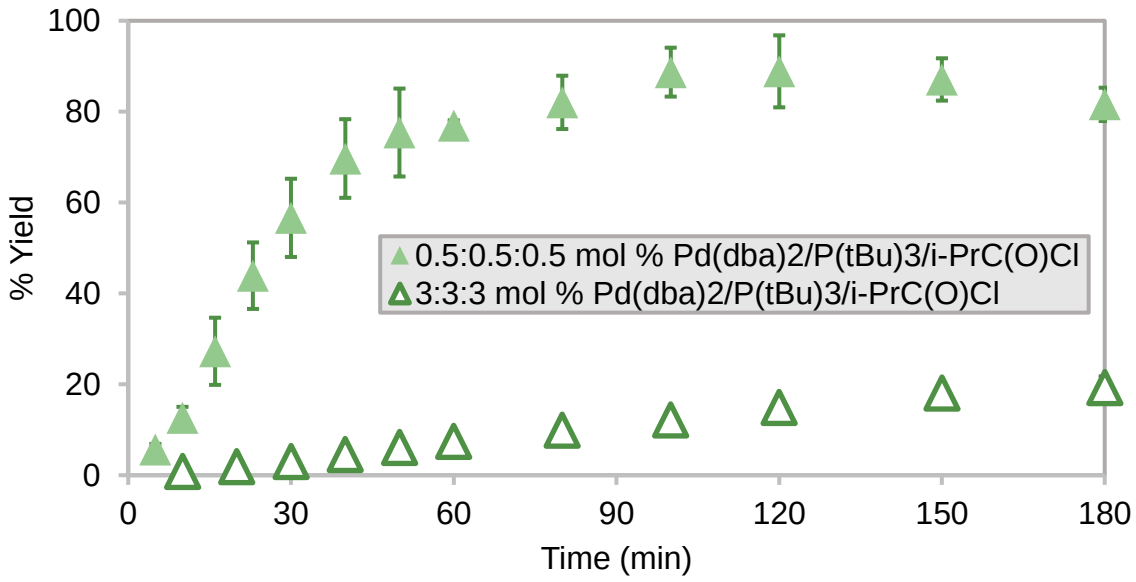

Figure E.39. Plot of the yield of **2a** versus reaction time of the formation of **2a** using 0.5 mol % $Pd(dba)_2$, 0.5 mol % P(*t*-Bu)$_3$, and 0.5 mol % *i*-PrC(O)Cl at 80 °C (green filled triangles) and 3 mol % $Pd(dba)_2$, 3 mol % P(*t*-Bu)$_3$, and 3 mol % *i*-PrC(O)Cl at 30 °C (green hollow triangles).

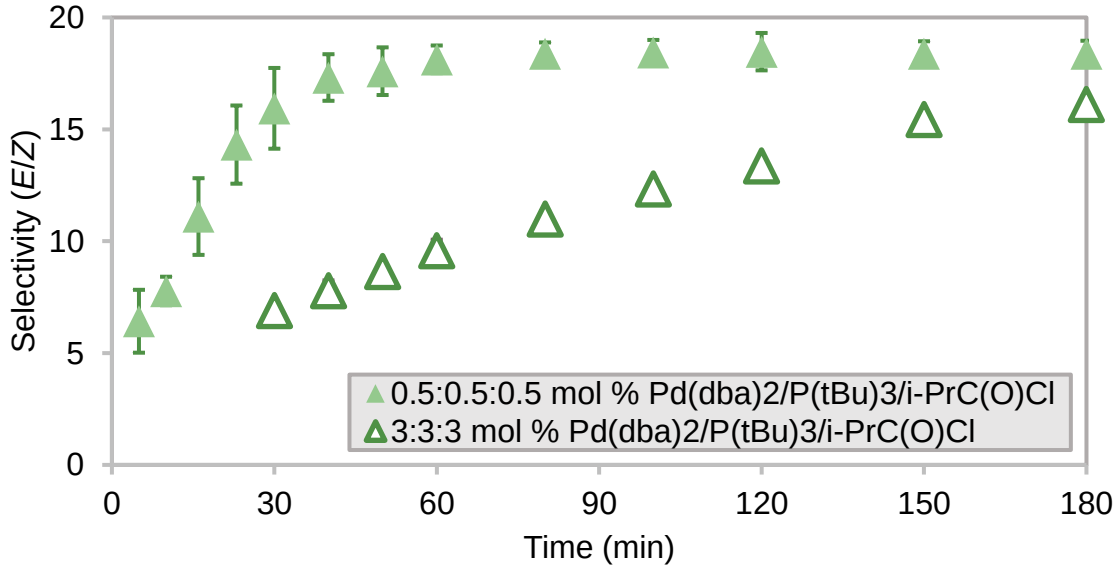

Figure E.40. Plot of the selectivity of **2a** versus reaction time of the formation of **2a** using 0.5 mol % $Pd(dba)_2$, 0.5 mol % P(*t*-Bu)$_3$, and 0.5 mol % *i*-PrC(O)Cl at 80 °C (green filled triangles) and 3 mol % $Pd(dba)_2$, 3 mol % P(*t*-Bu)$_3$, and 3 mol % *i*-PrC(O)Cl at 30 °C (green hollow triangles).

Table E.27. Yield and selectivity (*E*/*Z*) of **2a** over time using 0.5 mol % $Pd(dba)_2$, 0.5 mol % P(*t*-Bu)$_3$, and 0.5 mol % *i*-PrC(O)Cl at 80 °C and 3 mol % $Pd(dba)_2$, 3 mol % P(*t*-Bu)$_3$, and 3 mol % *i*-PrC(O)Cl at 30 °C.

0.5 mol % $Pd(dba)_2$, 0.5 mol % P(t-Bu)$_3$, and 0.5 mol % i-PrC(O)Cl at 80 °C			***3 mol % $Pd(dba)_2$, 3 mol % P(t-Bu)$_3$, and 3 mol % i-PrC(O)Cl at 30 °C***		
Time (min)	**% Yield**	***E*/*Z* Selectivity (std error)**	**Time (min)**	**% Yield**	***E*/*Z* Selectivity (std error)**
5	6±1	6.4:1 (1)	10	0.836±0.009	1:0
10	13±2	7.8:1 (0.6)	20	1.9±0.1	1:0
16	27±7	11.1:1 (2)	30	3.0±0.3	6.91:1 (0.04)
23	44±7	14.3:1 (2)	40	5±1	7.8:1 (0.5)
30	57±9	15.9:1 (2)	50	6.1±0.5	8.6:1 (0.2)
40	70±9	17.3:1 (1)	60	7±1	9.6:1 (0.5)
50	80±10	17.6:1 (1)	80	10±1	10.9:1 (0.4)
60	77±1	18.1:1 (0.6)	100	12±1	12.341:1 (0.003)
80	82±6	18.4:1 (0.5)	120	14.9±0.1	13.4:1 (0.2)
100	89±5	18.4:1 (0.6)	150	18±1	15.5:1 (0.2)
120	89±8	18.5:1 (0.8)	180	19±3	16.1:1 (0.3)
150	87±5	18.4:1 (0.6)	--	--	--
180	82±4	18.4:1 (0.6)	--	--	--

e. Comparison of the Isomerization Catalysts Under Their Respective Reaction Conditions

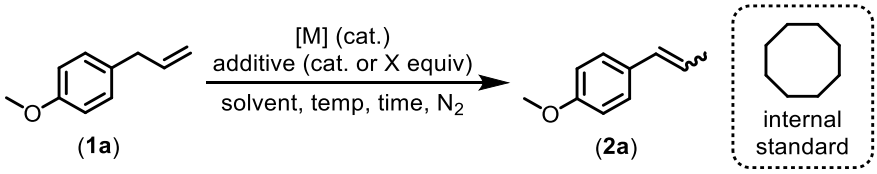

The data from sections **E.1.12.a-d.** are replicated below and combined into four plots to compare the catalysts.

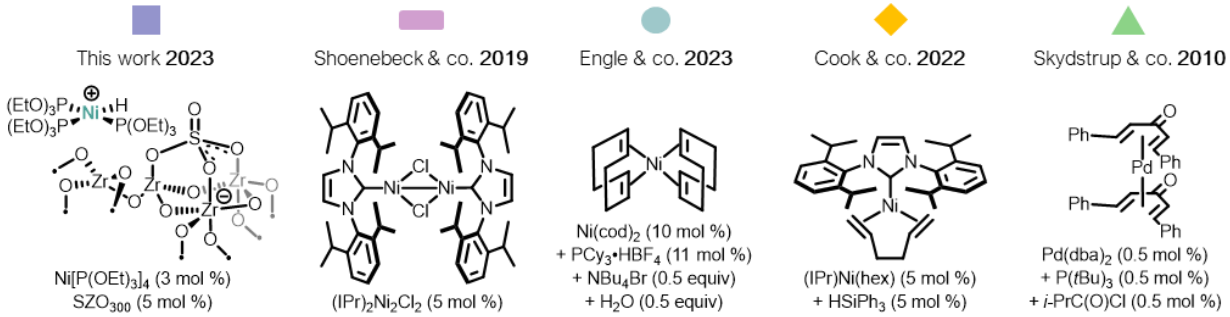

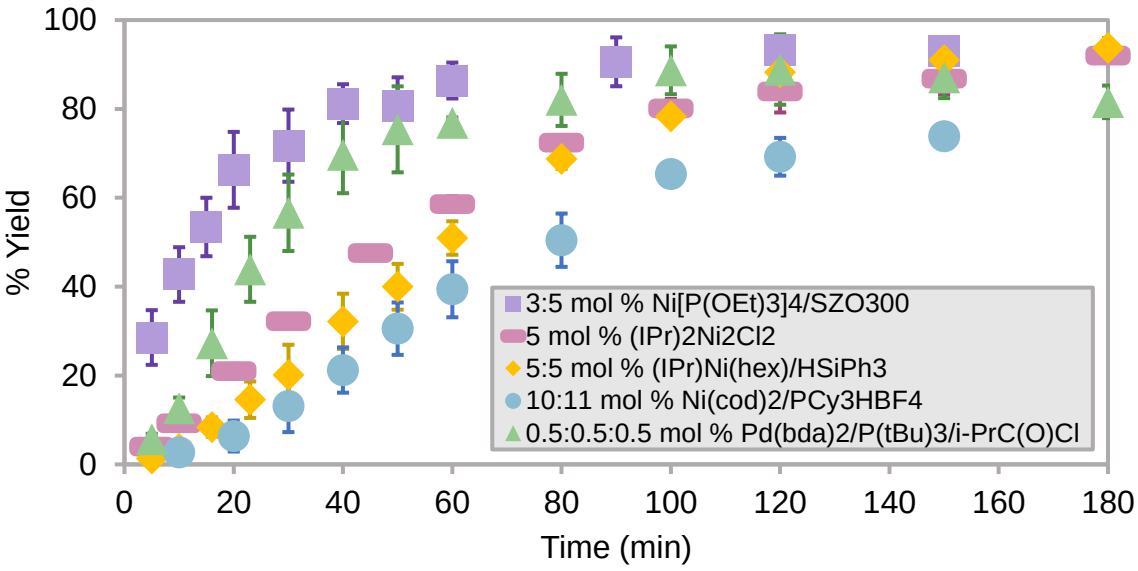

Figure E.41. Plot of the yield of **2a** versus reaction time comparing the following catalytic conditions: 3 mol % $Ni[P(OEt)_3]_4$ + 5 mol % SZO_{300} at 30 °C (purple squares), 5 mol % $(IPr)_2Ni_2Cl_2$ at 30 °C (pink rectangles), 10 mol % $Ni(cod)_2$ + 11 mol % PCy_3•HBF_4 at 30 °C (blue circles), 5 mol % (IPr)Ni(hex) + 5 mol % $HSiPh_3$ at 80 °C (yellow diamonds), and 0.5 mol % $Pd(dba)_2$ + 0.5 mol % P(*t*-Bu)$_3$ + 0.5 mol % *i*-PrC(O)Cl at 80 °C (green triangles).

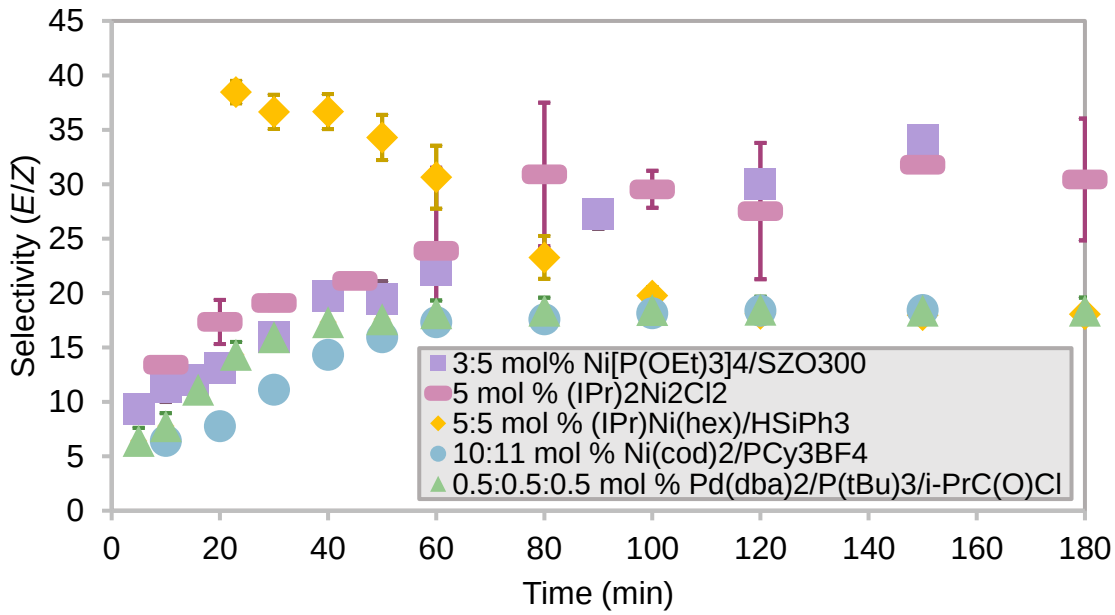

Figure E.42. Plot of the selectivity of **2a** versus reaction time comparing the following catalytic conditions: 3 mol % $Ni[P(OEt)_3]_4$ + 5 mol % SZO_{300} at 30 °C (purple squares), 5 mol % $(IPr)_2Ni_2Cl_2$ at 30 °C (pink rectangles), 10 mol % $Ni(cod)_2$ + 11 mol % PCy_3•HBF_4 at 30 °C (blue circles), 5 mol % (IPr)Ni(hex) + 5 mol % $HSiPh_3$ at 80 °C (yellow diamonds), and 0.5 mol % $Pd(dba)_2$ + 0.5 mol % P(*t*-Bu)$_3$ + 0.5 mol % *i*-PrC(O)Cl at 80 °C (green triangles).

f. Comparison of the Isomerization Catalysts Under our Optimized Reaction Conditions

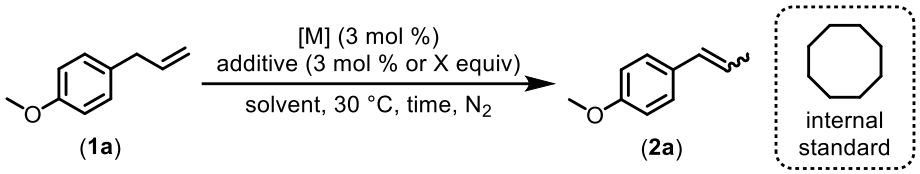

We performed time studies using 3 mol % total Ni or Pd and 3 mol % total additive/ligand at 30 °C, but we kept the respective reaction's optimized solvent. The data from sections **E.1.12.a.-d.** are replicated below and combined into four plots to compare the catalysts.

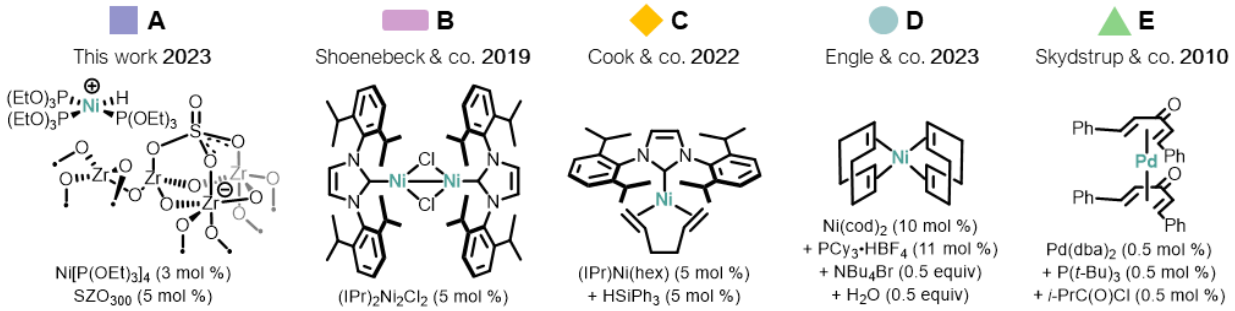

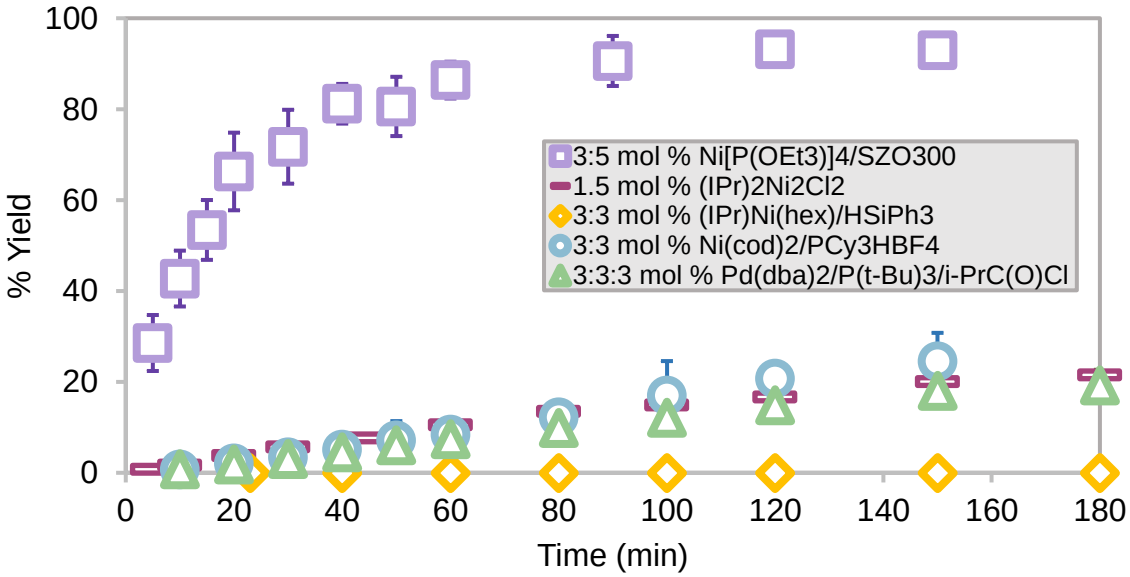

Figure E.43. Plot of the yields of **2a** versus reaction time using 3 mol % $Ni[P(OEt)_3]_4$ + 5 mol % SZO_{300} (purple squares), 1.5 mol % $(IPr)_2Ni_2Cl_2$ (dark pink rectangles), 3 mol % $Ni(cod)_2$ + 3 mol % PCy_3•HBF_4 (blue circles), 3 mol % (IPr)Ni(hex) + 3 mol % $HSiPh_3$ (yellow diamonds), and 3 mol % $Pd(dba)_2$ + 3 mol % P(*t*-Bu)$_3$ + 3 mol % *i*-PrC(O)Cl (green triangles) all at 30 °C.

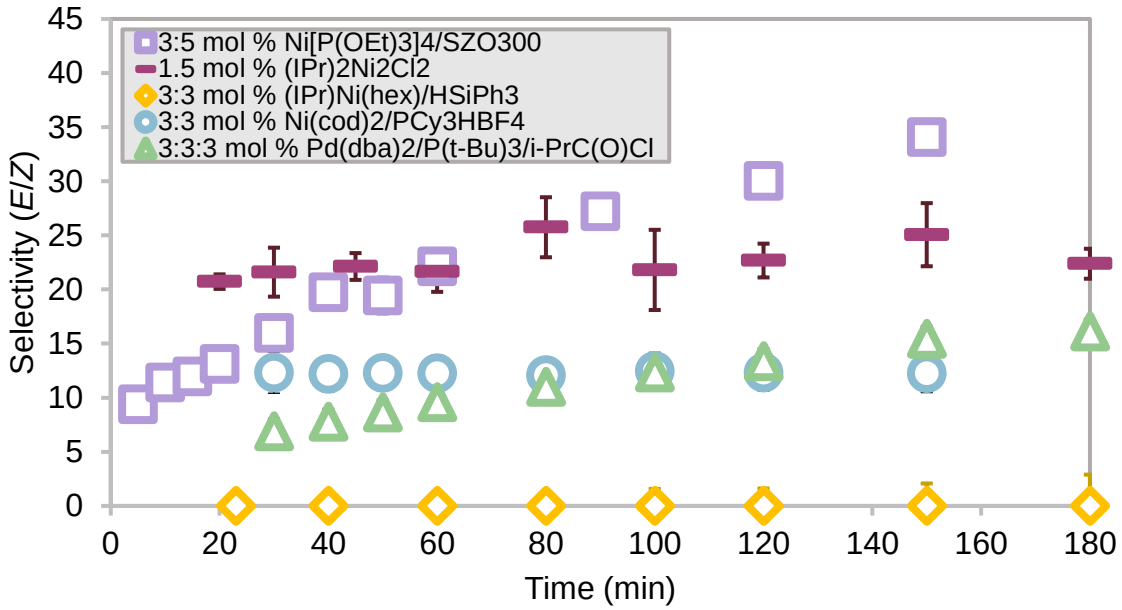

Figure E.44. Plot of the yields of **2a** versus reaction time using 3 mol % $Ni[P(OEt)_3]_4$ + 5 mol % SZO_{300} (purple squares), 1.5 mol % $(IPr)_2Ni_2Cl_2$ (dark pink rectangles), 3 mol % $Ni(cod)_2$ + 3 mol % PCy_3•HBF_4 (blue circles), 3 mol % (IPr)Ni(hex) + 3 mol % $HSiPh_3$ (yellow diamonds), and 3 mol % $Pd(dba)_2$ + 3 mol % P(*t*-Bu)$_3$ + 3 mol % *i*-PrC(O)Cl (green triangles) all at 30 °C.

E.1.15. Evaluation of Other Catalytic Reactions

a. Hydrovinylation

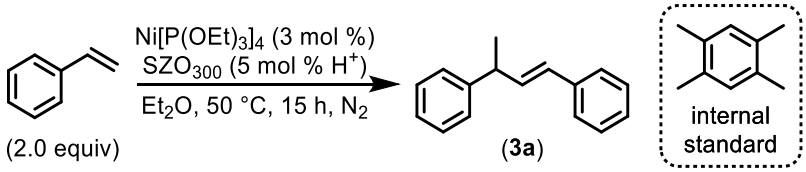

In a nitrogen-filled glovebox, a 1-dram vial equipped with a stir bar was charged with SZO_{300} (15 mg, 0.0030 mmol H^+, 0.0050 equiv H^+). To this vial was added a stock solution of $Ni[P(OEt)_3]_4$ (1.3 mg, 0.0018 mmol, 0.030 equiv added to each vial) and durene (internal standard; 4.1 mg, 0.031 mmol) in Et_2O to obtain a total volume of 1.0 mL. The reactions were sealed with a septum cap, removed from the glovebox, injected with styrene (14.0 µL, 0.122 mmol, 2.00 equiv) using a 25-µL syringe, and placed on a pre-heated aluminum block set to 50 °C. After 15 h, the reaction was removed from the heat and opened to air, and an aliquot (~20 µL) was removed using a 25 µL syringe and filtered through a Celite plug and washed with $CDCl_3$ (0.6 mL) directly into an NMR tube. Quantification the hydrovinylation product was determined by relative integrations between the hydrovinylation product (the doublet at 1.46 ppm, 3H) to the integration of the internal

standard, durene (singlet at 2.18 ppm, 12H). Two trials were run for the experiment and the average and standard deviation of the yield are seen below in Table S22. Confirmation of the hydrovinylation product was obtained by scaling up this reaction (x3), filtering the reaction through a Celite plug, and concentrating to isolate the crude product (**3a**) to determine product selectivity by ^{1}H NMR, which match literature values.[343] The data is seen in **Figure E.45.** and **Table E.28.**

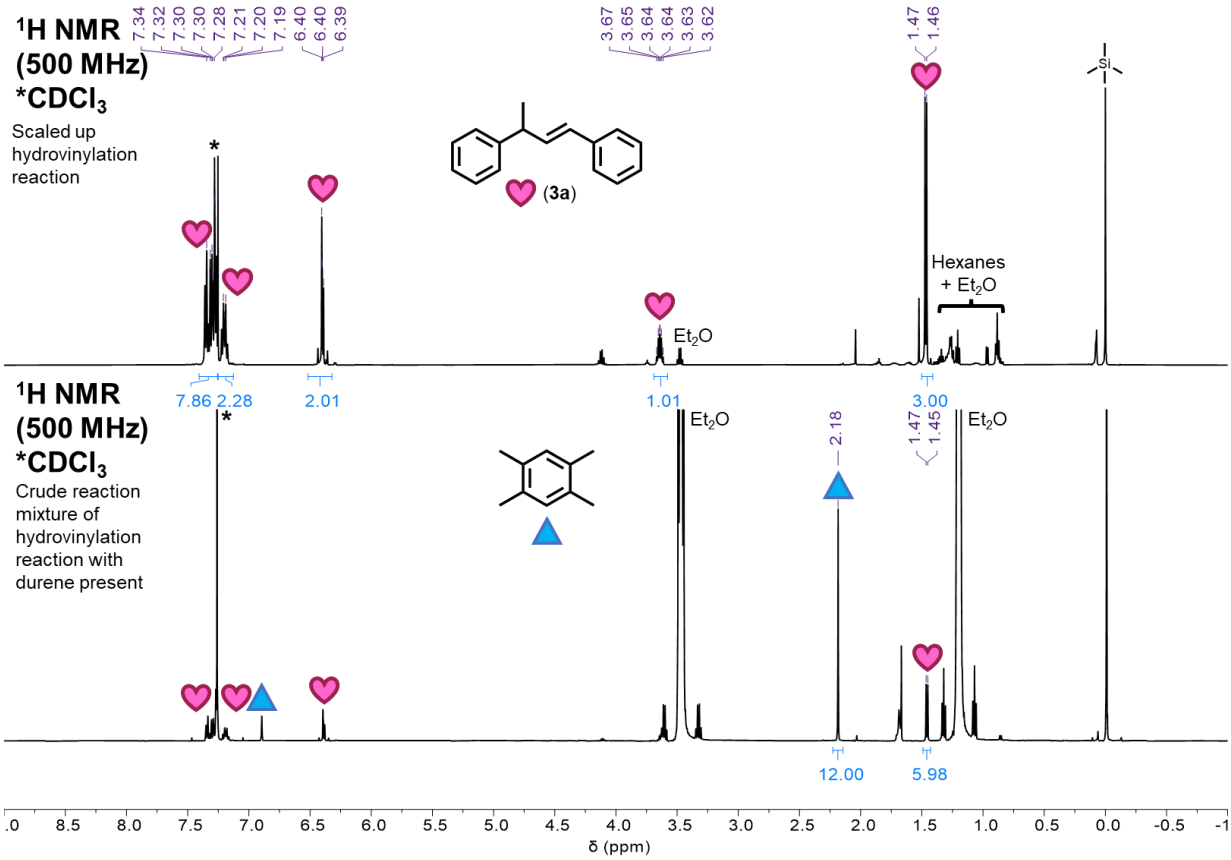

Figure E.45. ^{1}H NMR spectrum of the scaled-up hydrovinylation product **3a** (top), and of the crude reaction mixture from the Ni[P(OEt)$_3$]$_4$/SZO$_{300}$-catalyezd hydrovinylation of styrene (bottom). Both spectra recorded in $CDCl_3$ at 25 °C.

Table E.28. Integrations of durene and **3a**, mmol of **3a**, and the % yield of **3a**.

Trial	∫Durene	∫3a	3a mmol	% Yield 3a
1	12	5.98	0.061	99%
2	12	5.46	0.055	91%
Average				94±6%

b. Hydroboration

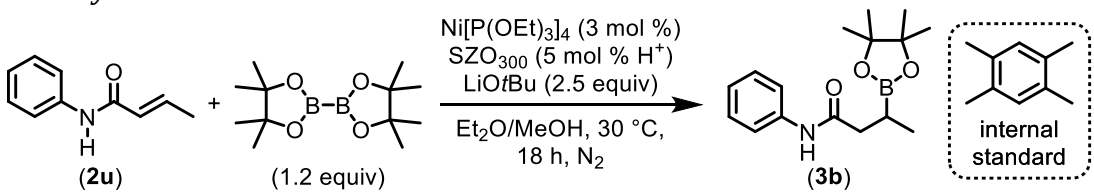

In a nitrogen-filled glovebox, a 1-dram vial equipped with a stir bar was charged with SZO_{300} (15 mg, 0.0030 mmol H^+, 0.0050 equiv H^+). To this vial was added a stock solution of $Ni[P(OEt)_3]_4$ (1.3 mg, 0.0018 mmol, 0.030 equiv added to each vial) and durene (internal standard; 5.0 mg, 0.037 mmol) in Et_2O to obtain a volume of 0.50 mL. LiO*t*-Bu (12 mg, 0.15 mmol, 2.5 equiv) was added to the vials and the reactions were sealed with a septum cap and removed from the glovebox. On the bench, a stock solution of B_2Pin_2 (18 mg, 0.071 mmol, 1.2 equiv added to each vial) and *N*-Phenylbut-2-enamide (**2u**, 9.6 mg, 0.060 mmol, 1.0 equiv added to each vial) was prepared in nitrogen-sparged and dry MeOH. This stock solution was distributed to each reaction vial using a disposable 1-mL syringe to obtain a total reaction volume of 1.0 mL and the reaction was immediately placed on a pre-heated aluminum block set to 30 °C. After 18 h, an aliquot (~20 uL) was removed using a 25-µL syringe, filtered through Celite, and washed with hexanes (~1 mL) directly into a GC vial. Quantitative analysis of the formation of the hydroboration product was determined by relative integration (by GC-MS) of the product peaks against durene, in accordance with a calibration curve. Two trials were run, and the average and standard deviation of the yield are seen below in **Table E.29.** A control reaction was performed under identical reaction conditions in the absence of $Ni[P(OEt)_3]_4$ and SZO_{300}. Two trials were run, and the average and standard deviation of the yield are seen below in **Table E.29.**

Table E.29. Corresponding mmol and the % yield of **3b** in the presence and absence (control) of $Ni[P(OEt)_3]_4/SZO_{300}$.

Reaction	Product mmol	% Yield 3b
$Ni[P(OEt)_3]_4/SZO_{300}$	0.033±0.004	55±7
control	0.0006±0.0002	0.9±0.3

After analyzing the reactions by GC-MS, the crude hydroboration reactions were combined, filtered through a Celite plug, concentrated, and purified by column chromatography (0:100 to 5:95 MeCN/DCM) to obtain the product as a white solid. This product was fully characterized, and the product selectivity was confirmed by ^1H NMR. The data is seen in **Figure E.46.-E.51.**

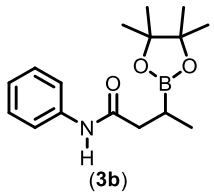

^{1}H NMR (500 MHz, $CDCl_3$, 298 K): δ 7.54 (bs, 1H), 7.50 (d, *J* = 7.9 Hz, 2H), 7.30 (t, *J* = 7.9 Hz, 2H), 7.07 (t, *J* = 7.3 Hz, 1H), 2.49 (dd, *J* = 14.7, 8.4 Hz, 1H), 2.41 (dd, *J* = 14.7, 5.7 Hz, 1H), 1.49 (m, 1H), 1.26 (d, *J* = 2.4, 12H), 1.08 (d, J = 7.6 Hz, 3H).

^{13}C{^{1}H} NMR (126 MHz, $CDCl_3$, 298 K): δ 171.5, 138.4, 129.1, 124.0, 119.7, 83.6, 41.5, 24.96, 24.87, 15.6

^{11}B NMR (160 MHz, $CDCl_3$, 298 K): δ 34.29 (s)

IR (ATR, neat) v: 3239-2848 (w), 1657 (s), 1313 (s), 1141 (s), 867 (s)

ASAP/HRMS (m/z): [M^+] calculated for $C_{16}H_{24}BNO_3$ 289.1849, found 289.1868

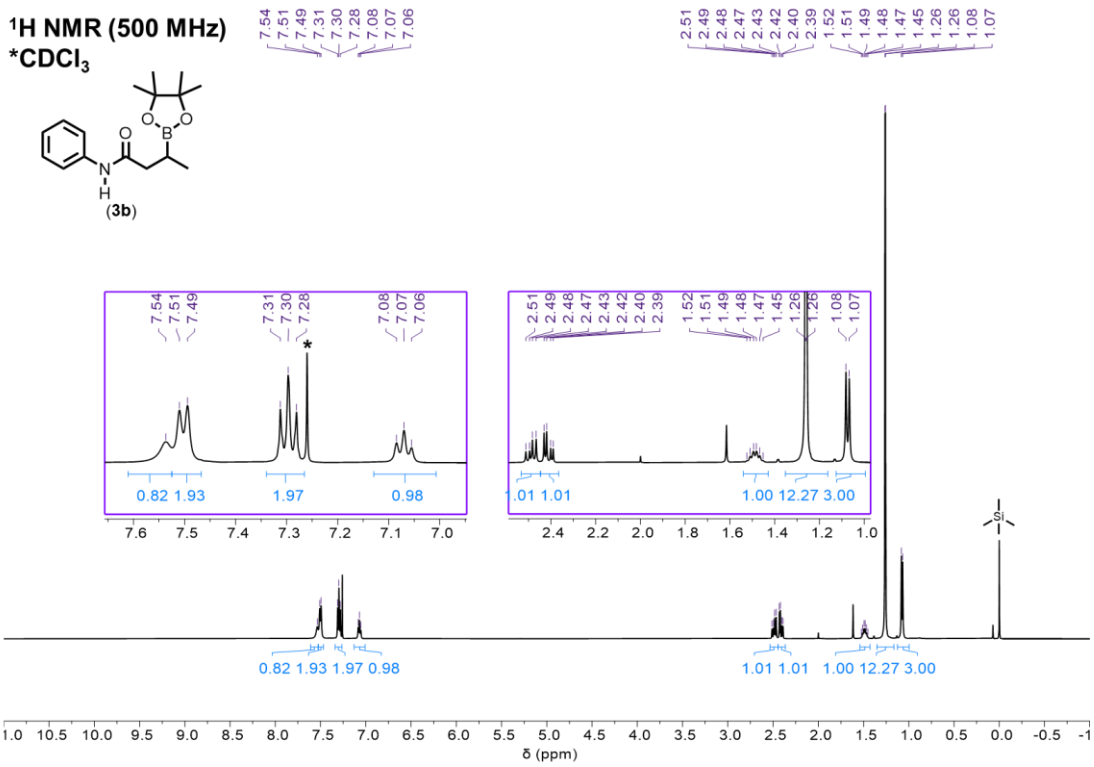

Figure E.46. ^{1}H NMR spectrum of *N*-Phenyl-3-(4,4,5,5-tetramethyl-1,3,2-dioxaborolan-2-yl)pentanamide (**3b**) recorded in $CDCl_3$ at 25 °C.

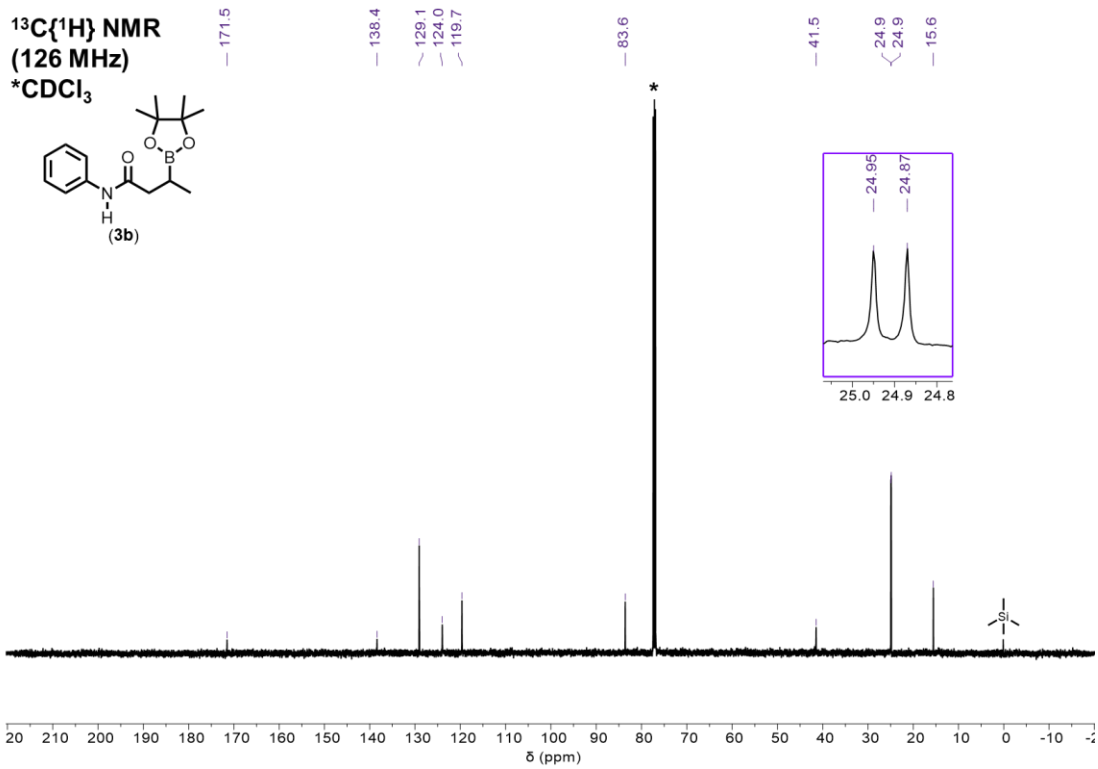

Figure E.47. $^{13}C\{^{1}H\}$ NMR spectrum of *N*-Phenyl-3-(4,4,5,5-tetramethyl-1,3,2-dioxaborolan-2-yl)pentanamide (**3b**) recorded in $CDCl_3$ at 25 °C.

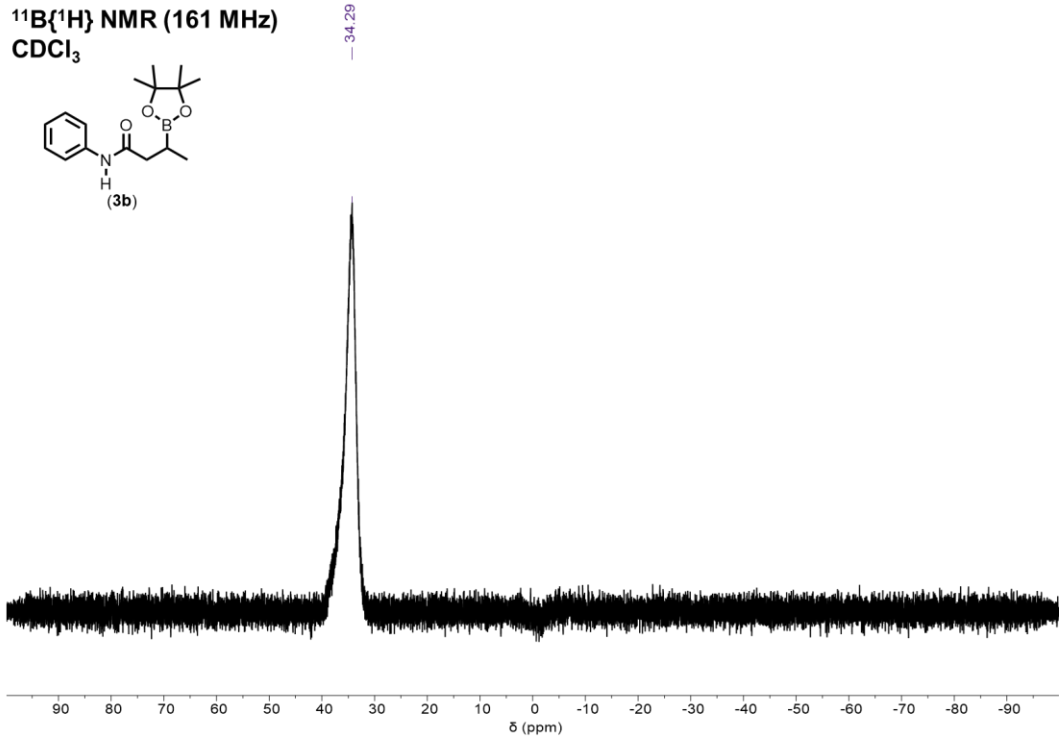

Figure E.48. ^{11}B NMR NMR spectrum of *N*-Phenyl-3-(4,4,5,5-tetramethyl-1,3,2-dioxaborolan-2-yl)pentanamide (**3b**) recorded in $CDCl_3$ at 25 °C.

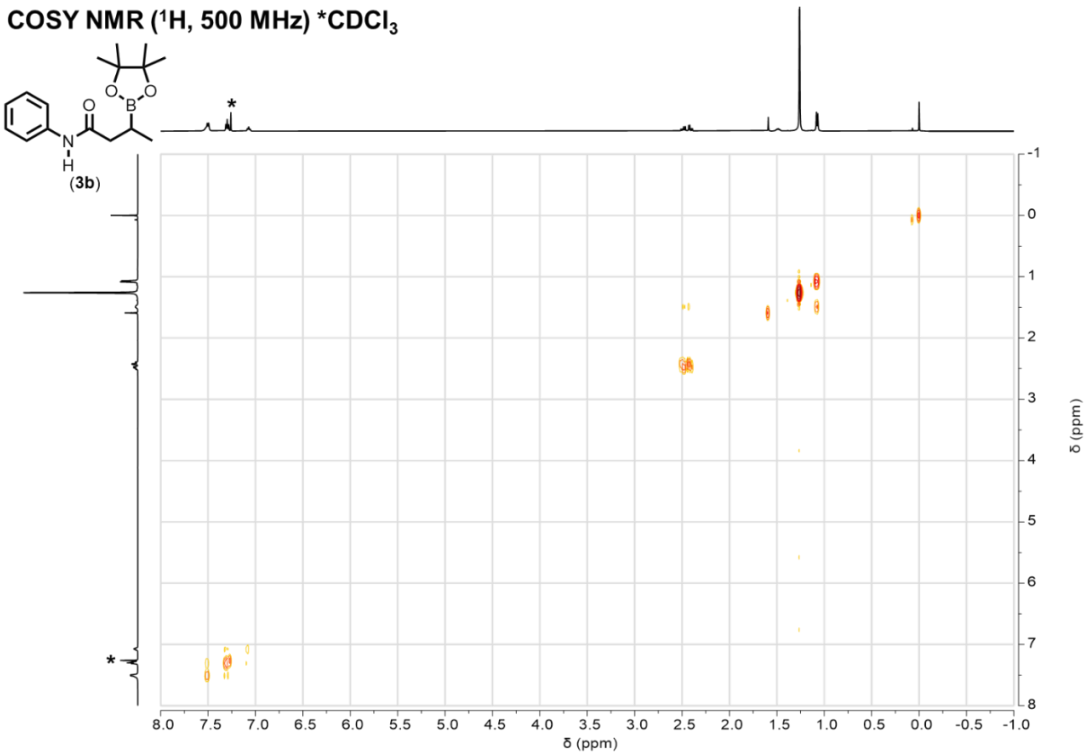

Figure E.49. COSY NMR spectrum of *N*-Phenyl-3-(4,4,5,5-tetramethyl-1,3,2-dioxaborolan-2-yl)pentanamide (**3b**) recorded in $CDCl_3$ at 25 °C.

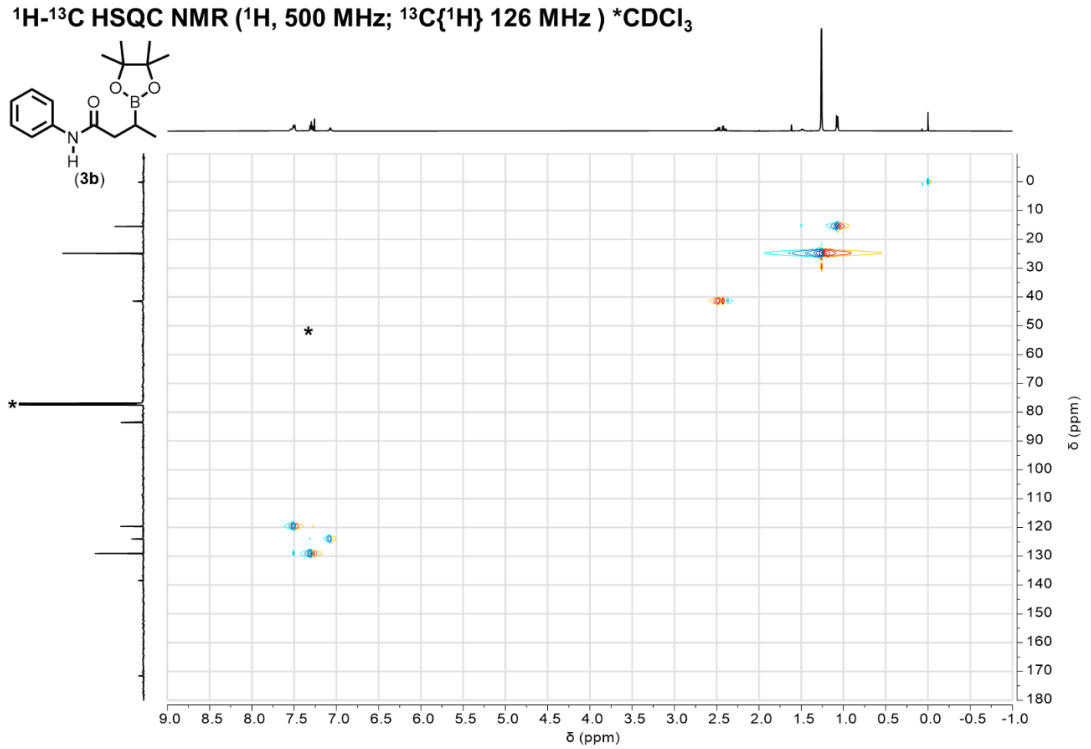

Figure E.50. HSQC NMR spectrum of *N*-Phenyl-3-(4,4,5,5-tetramethyl-1,3,2-dioxaborolan-2-yl)pentanamide (**3b**) recorded in $CDCl_3$ at 25 °C.

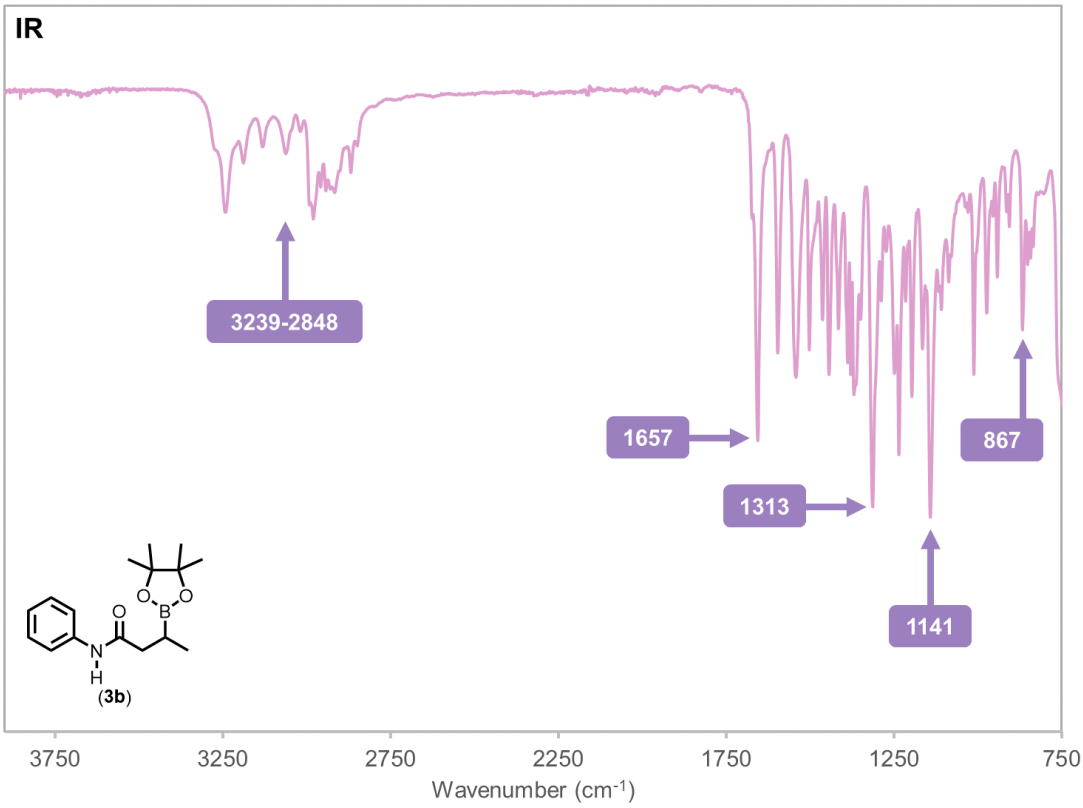

Figure E.51. IR spectrum of *N*-Phenyl-3-(4,4,5,5-tetramethyl-1,3,2-dioxaborolan-2-yl)pentanamide (**3b**) recorded in $CDCl_3$ at 25 °C.

c. Hydrosilylation

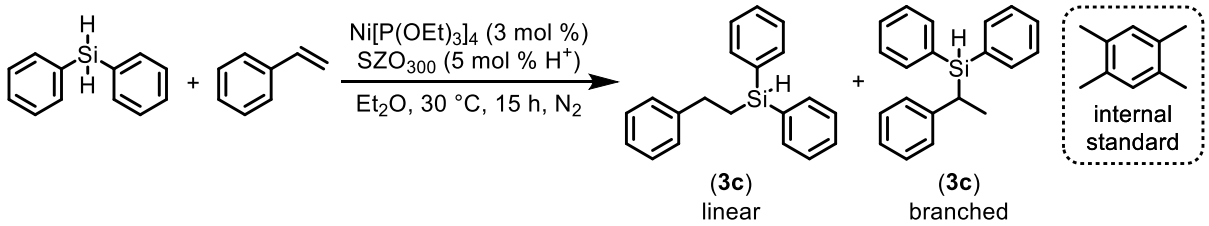

In a nitrogen-filled glovebox, a 1-dram vial equipped with a stir bar was charged with SZO_{300} (15 mg, 0.0030 mmol H^+, 0.0050 equiv H^+). To this was added a stock solution of $Ni[P(OEt)_3]_4$ (1.3 mg, 0.0018 mmol, 0.030 equiv added to each vial) and durene (internal standard; 4.1 mg, 0.031 mmol) in Et_2O to obtain a total volume of 1.0 mL. The reactions were sealed with a septum cap, removed from the glovebox, injected with styrene (7.0 µL, 0.061 mmol, 1.0 equiv) and diphenylsilane (11 µL, 0.059 mmol, 1.0 equiv) using a 25-µL syringe, and placed on a pre-heated aluminum block set to 30 °C. After 15 h, an aliquot (~20 µL) was removed using a 25-µL syringe and filtered through a Celite plug, washed with hexanes (~1 mL) directly into a GC vial. Quantitative analysis of the formation of the hydrosilylation product was determined by relative

integration (by GC) of the product peaks against durene, in accordance with a calibration curve. Two trials were run, and the average and standard deviation of the yield are seen below in Table S24. Confirmation of the hydrosilylation products was obtained by concentrating the crude reaction, dissolving in $CDCl_3$, filtering through a Celite plug directly into an NMR tube, and analyzed by ^1H NMR, which match literature values.[344]

Table E.30. mmol, % yield, and the selectivity (*l*/*b*) of **3c** from the hydrosilylation reactions.

Trial	Product mmol	% Yield	Selectivity (*l*/*b*)
1	0.014	23	1:9
2	0.011	19	1:6
average		21±3	1:7±2

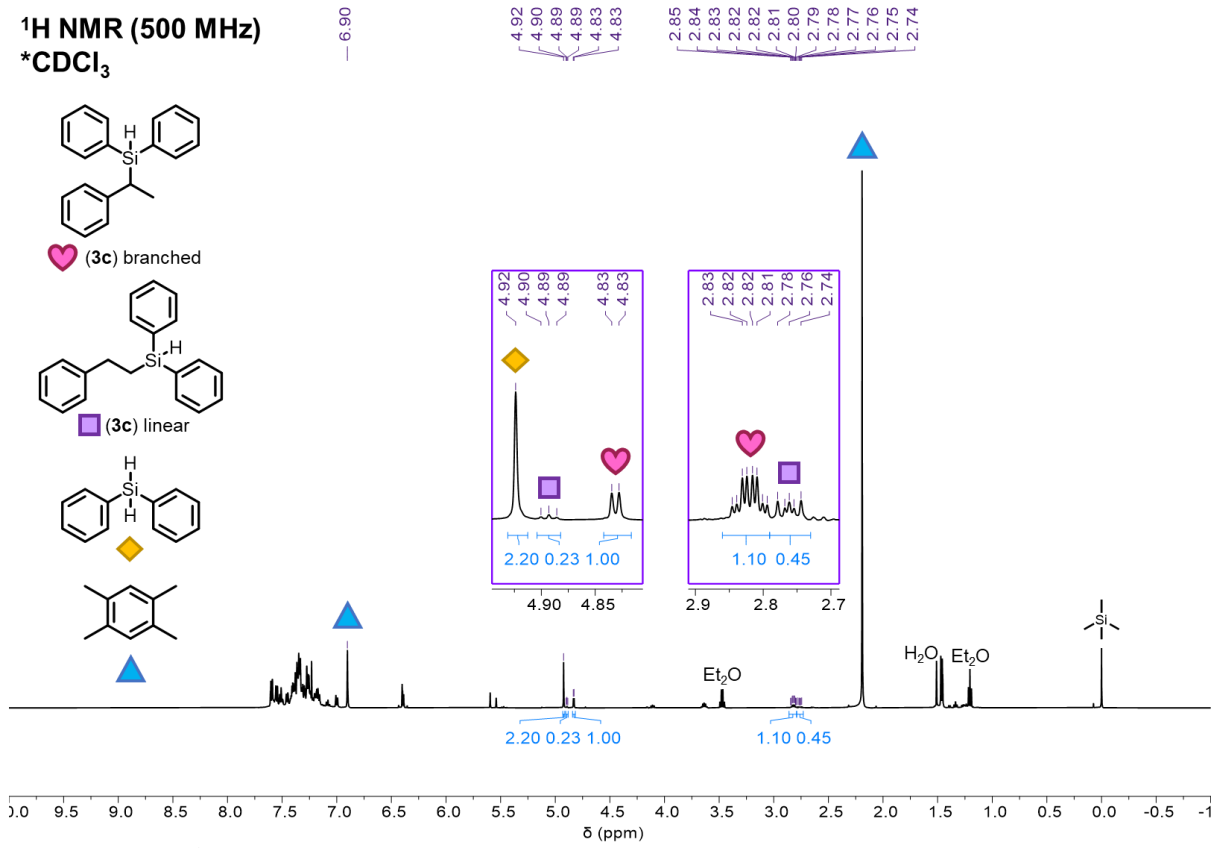

Figure E.51. ^1H NMR spectrum of the crude reaction of $Ni[P(OEt)_3]_4/SZO_{300}$-catalyzed hydrosilylation reaction of diphenylsilane and styrene recorded in $CDCl_3$ at 25 °C.

E.1.16. NMR and IR Spectra

a. Alkene and Starting Materials

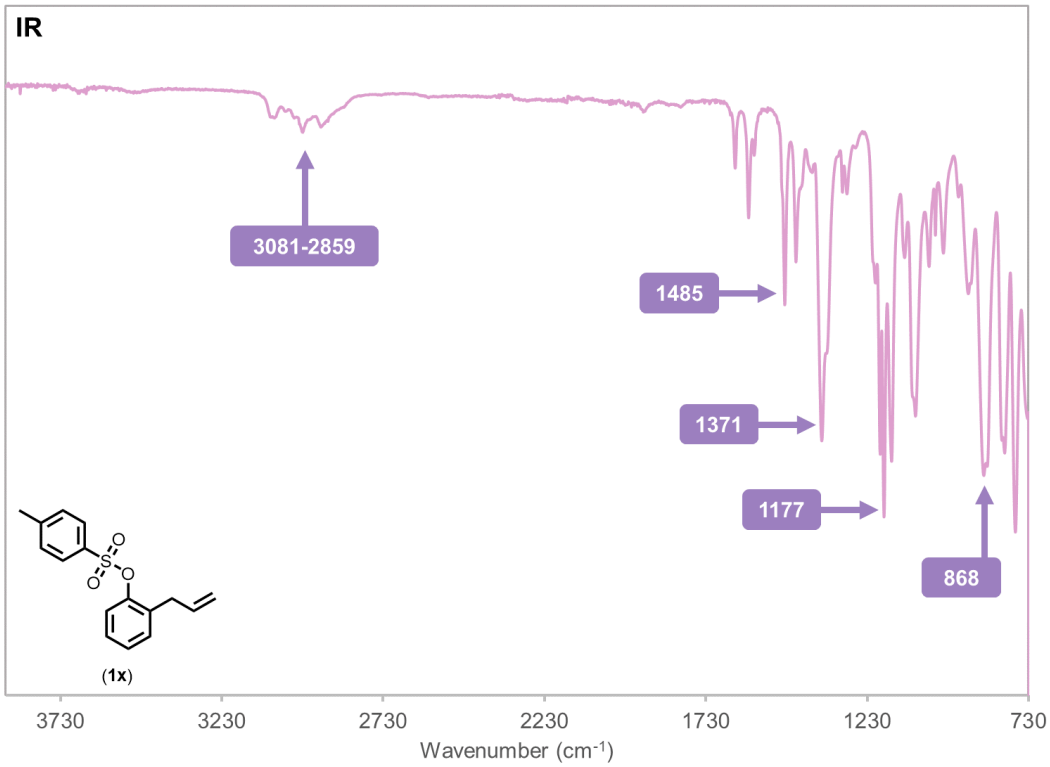

Figure E.52. IR spectrum of 4-methylbenzenesulfonate-2-(2-propenyl)-phenol (**1x**) recorded neat at 25 °C.

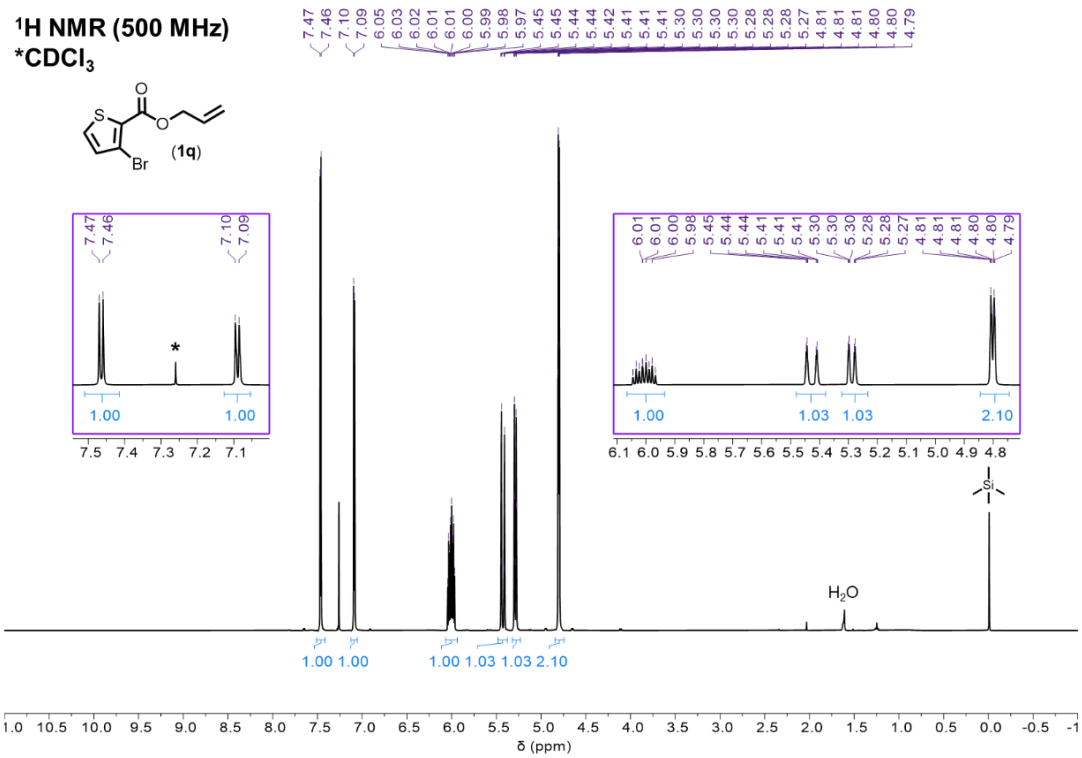

Figure E.53. ^{1}H NMR spectrum of 2-propen-1-yl-3-bromo-2-thiophenecarboxylate (**1q**) recorded in $CDCl_3$ at 25 °C.

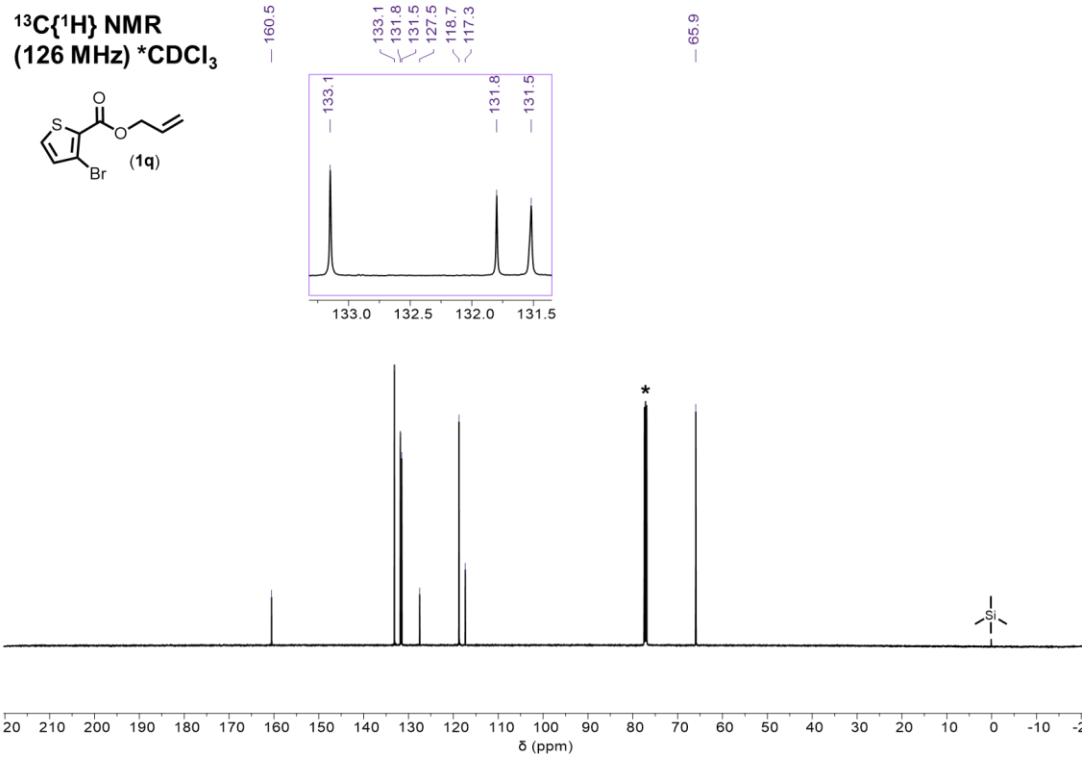

Figure E.54. ^{13}C{^{1}H} NMR spectrum of 2-propen-1-yl-3-bromo-2-thiophenecarboxylate (**1q**) recorded in $CDCl_3$ at 25 °C.

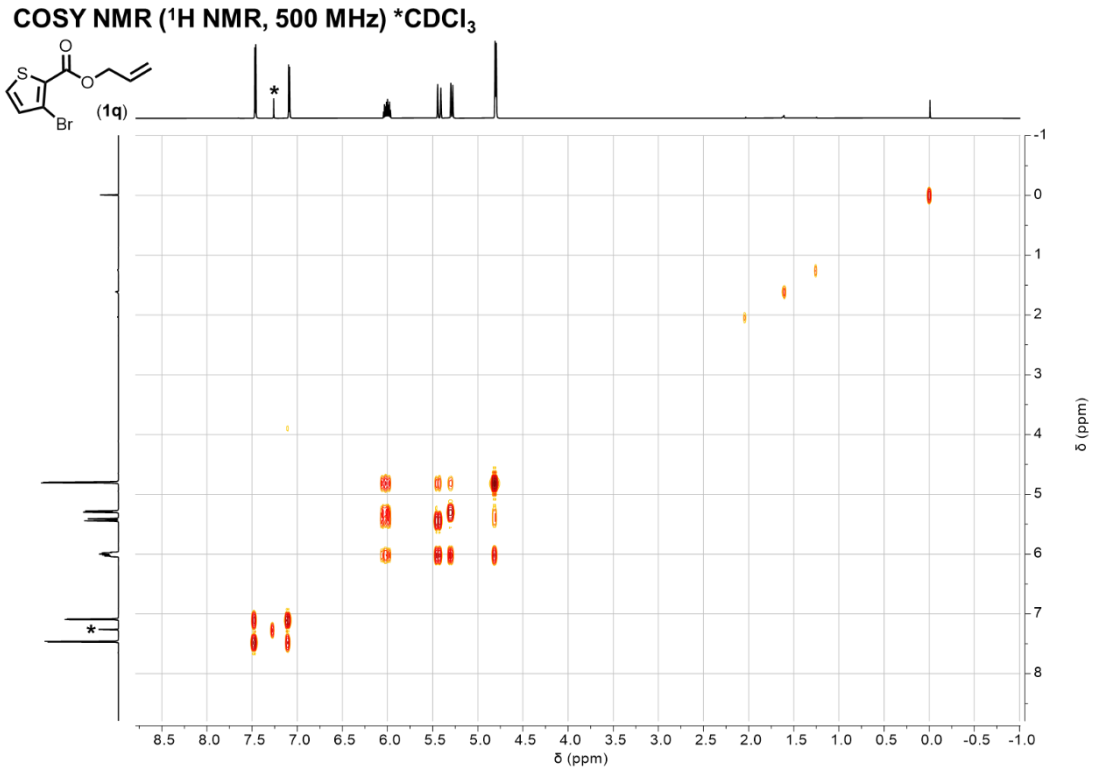

Figure E.55. COSY NMR spectrum of 2-propen-1-yl-3-bromo-2-thiophenecarboxylate (**1q**) recorded in $CDCl_3$ at 25 °C.

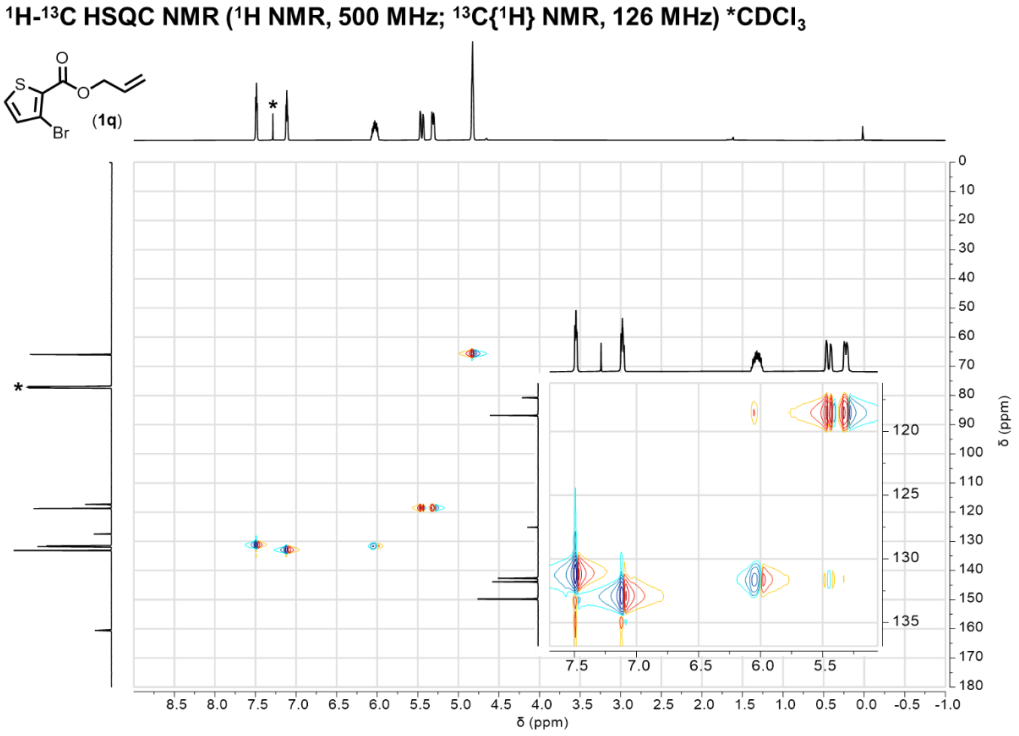

Figure E.56. ^{1}H-^{13}C HSQC NMR spectrum of 2-propen-1-yl-3-bromo-2-thiophenecarboxylate (**1q**) recorded in $CDCl_3$ at 25 °C.

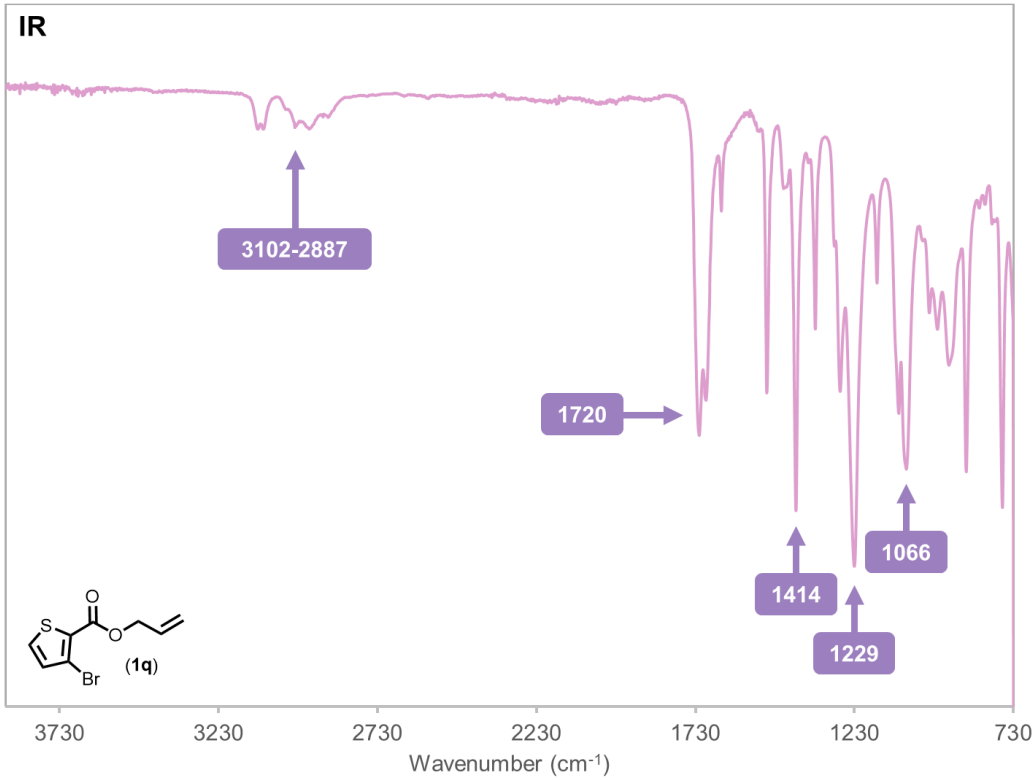

Figure E.57. IR spectrum of 2-propen-1-yl-3-bromo-2-thiophenecarboxylate (**1q**) recorded neat at 25 °C.

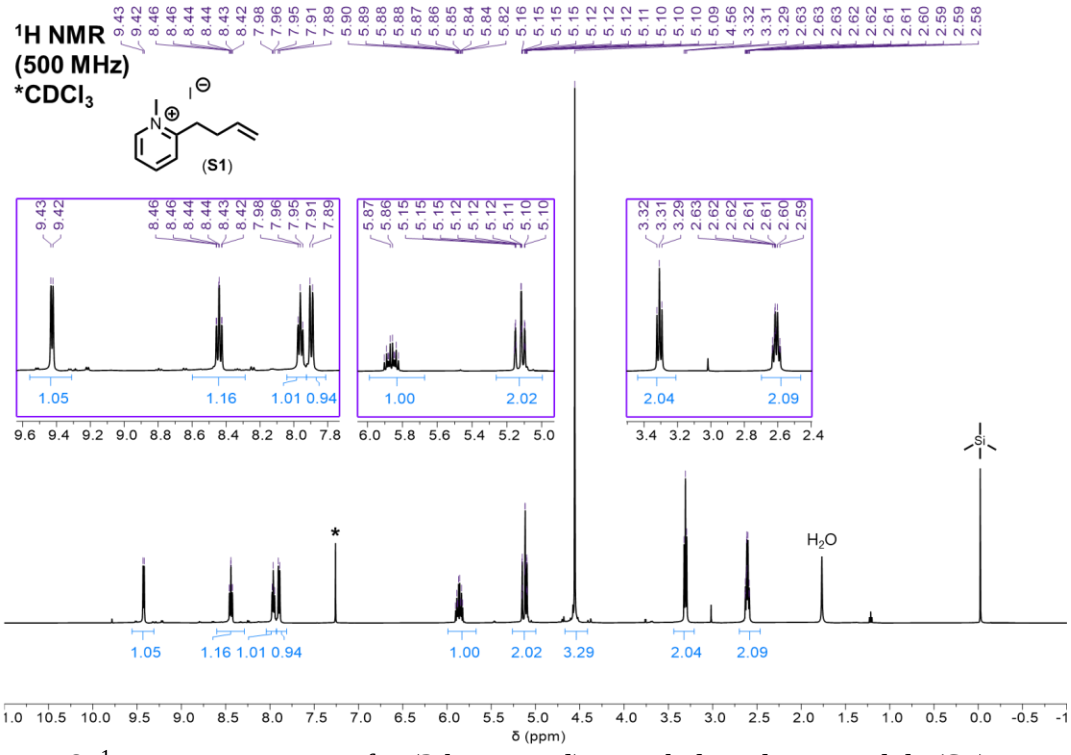

Figure E.58. ^{1}H NMR spectrum of 2-(3-buten-1-yl)-1-methylpyridinium iodide (**S1**) recorded in $CDCl_3$ at 25 °C.

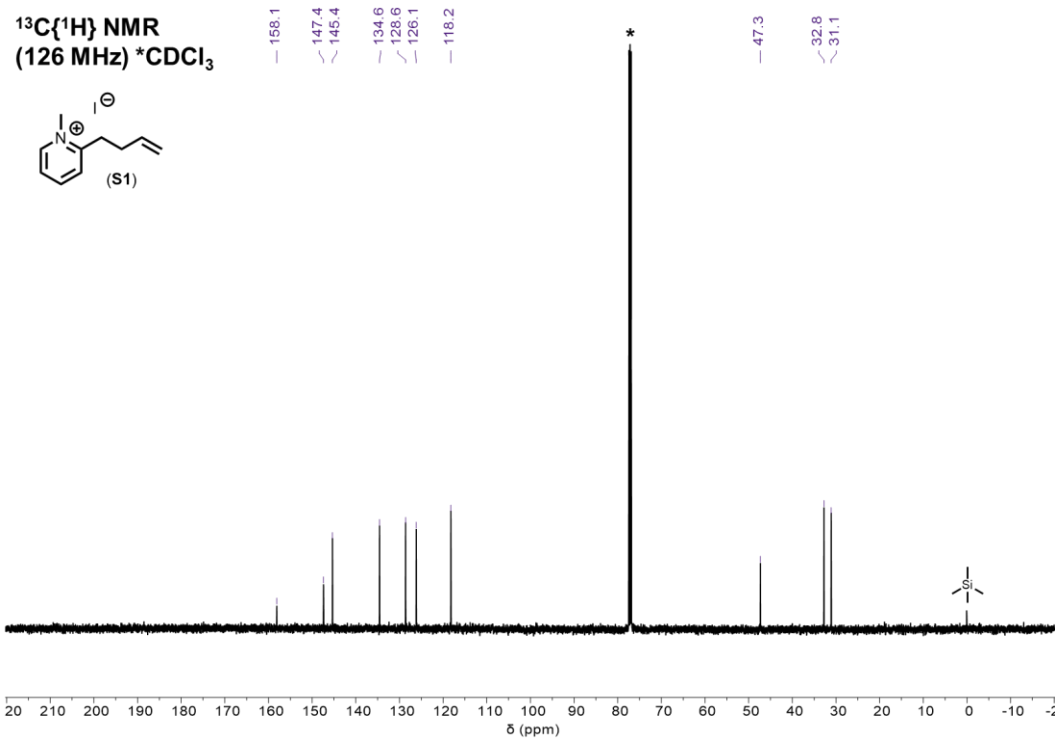

Figure E.59. $^{13}C\{^{1}H\}$ NMR spectrum of 2-(3-buten-1-yl)-1-methylpyridinium iodide (**S1**) recorded in $CDCl_3$ at 25 °C.

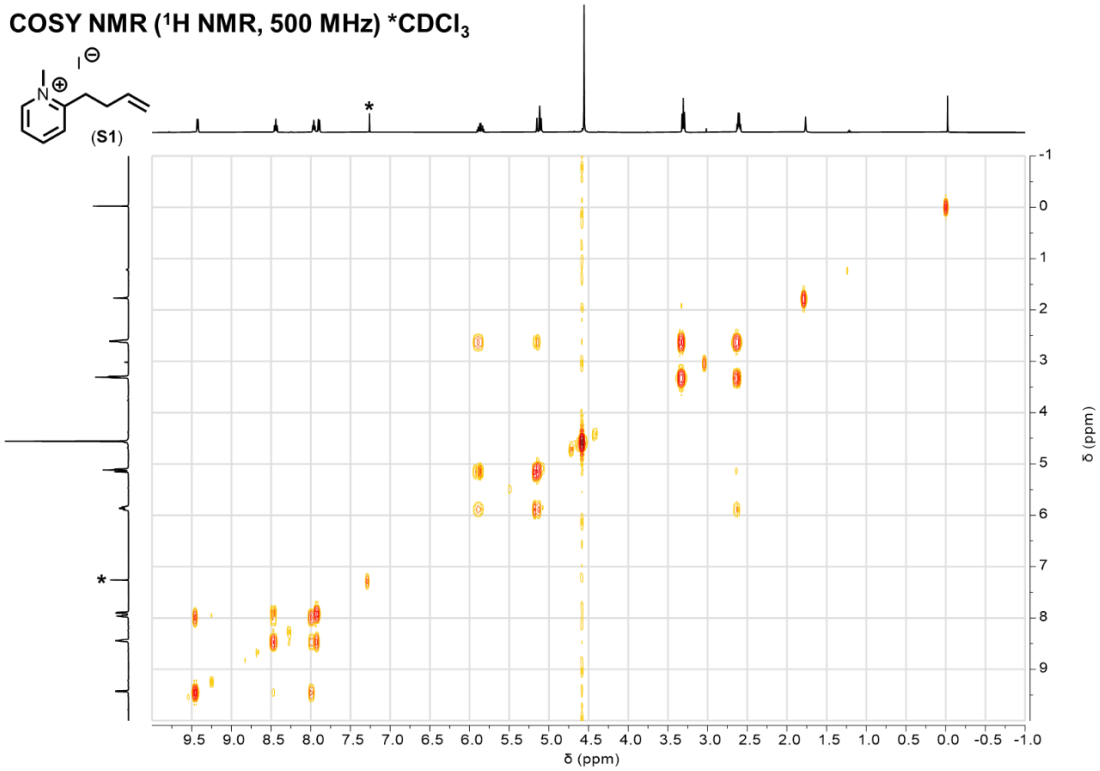

Figure E.60. COSY NMR spectrum of 2-(3-buten-1-yl)-1-methylpyridinium iodide (**S1**) recorded in $CDCl_3$ at 25 °C.

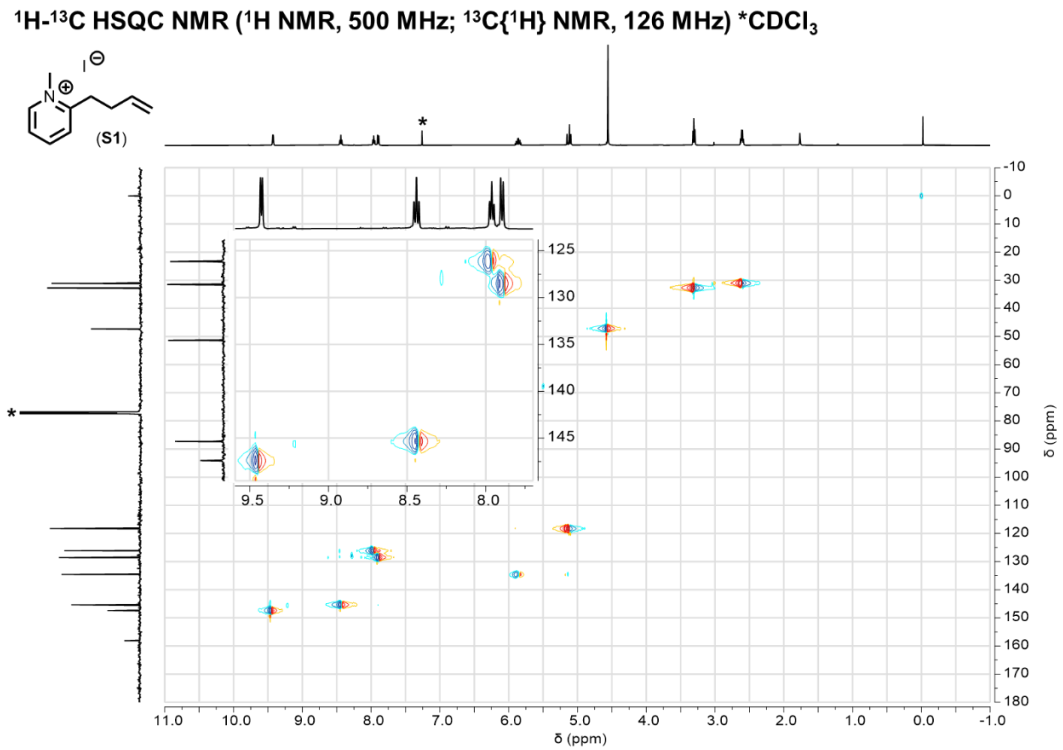

Figure E.61. ^{1}H-^{13}C HSQC NMR spectrum of 2-(3-buten-1-yl)-1-methylpyridinium iodide (**S1**) recorded in $CDCl_3$ at 25 °C.

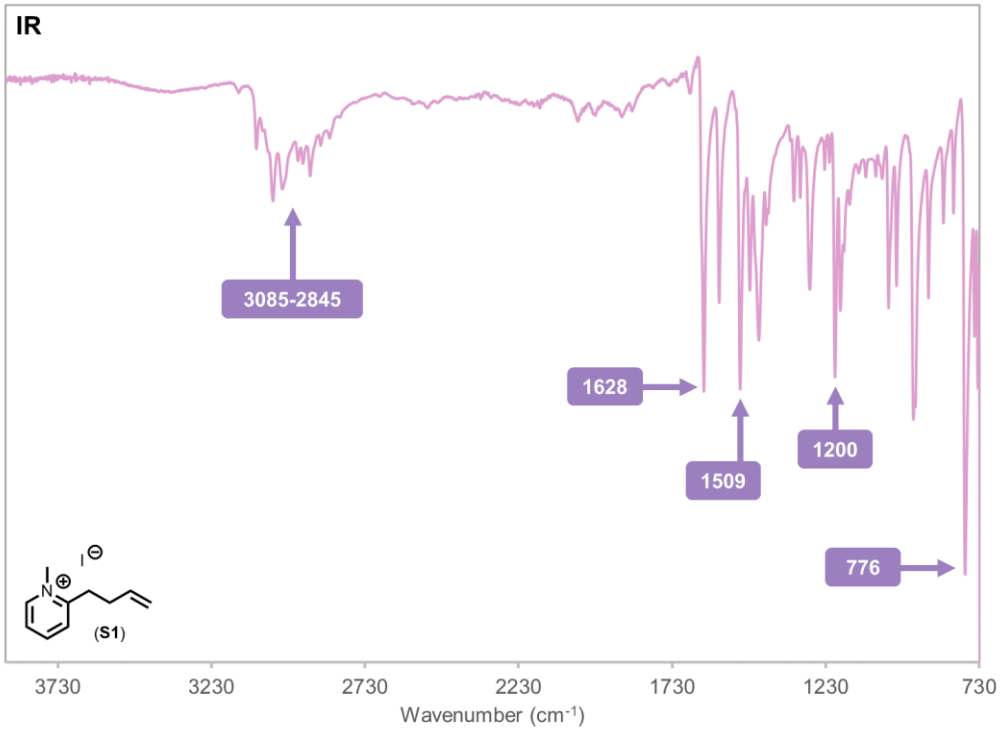

Figure E.62. IR spectrum of 2-(3-buten-1-yl)-1-methylpyridinium iodide (**S1**) recorded neat at 25 °C.

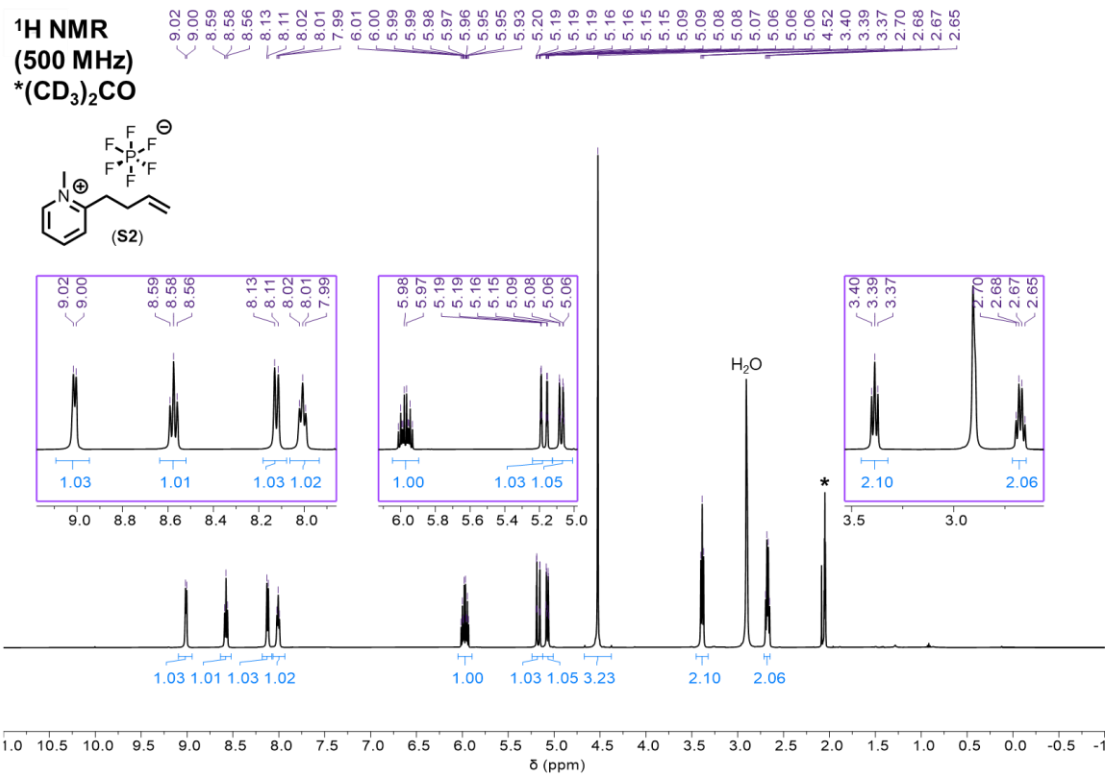

Figure E.63. ^{1}H NMR spectrum of 2-(3-buten-1-yl)-1-methylpyridinium hexafluorophosphate (**S2**) recorded in $(CD_3)_2CO$ at 25 °C.

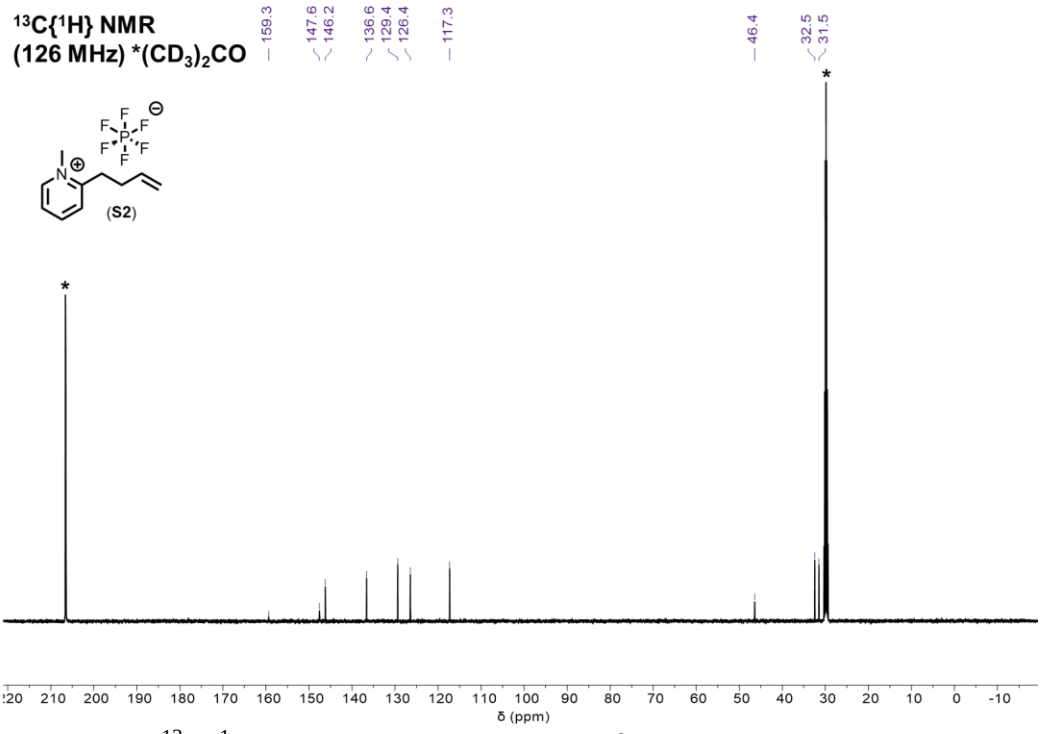

Figure E.64. $^{13}C\{^{1}H\}$ NMR spectrum of 2-(3-buten-1-yl)-1-methylpyridinium hexafluorophosphate (**S2**) recorded in $(CD_3)_2CO$ at 25 °C.

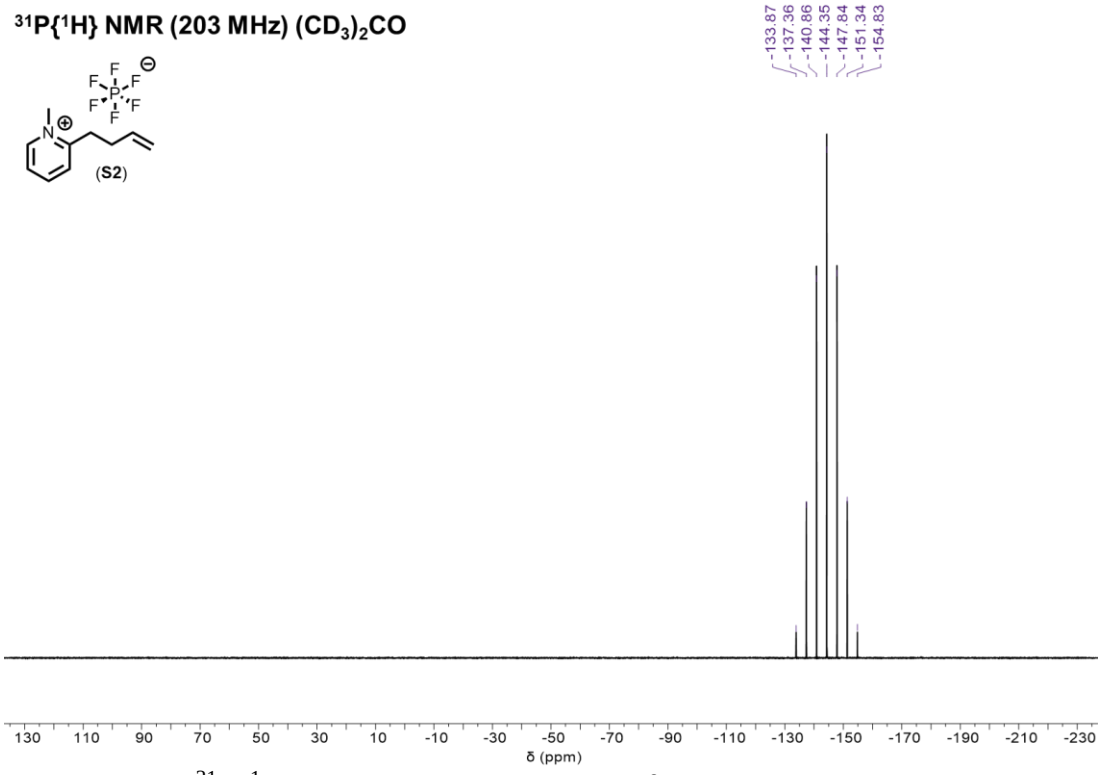

Figure E.65. $^{31}P\{^{1}H\}$ NMR spectrum of 2-(3-buten-1-yl)-1-methylpyridinium hexafluorophosphate (**S2**) recorded in $(CD_3)_2CO$ at 25 °C.

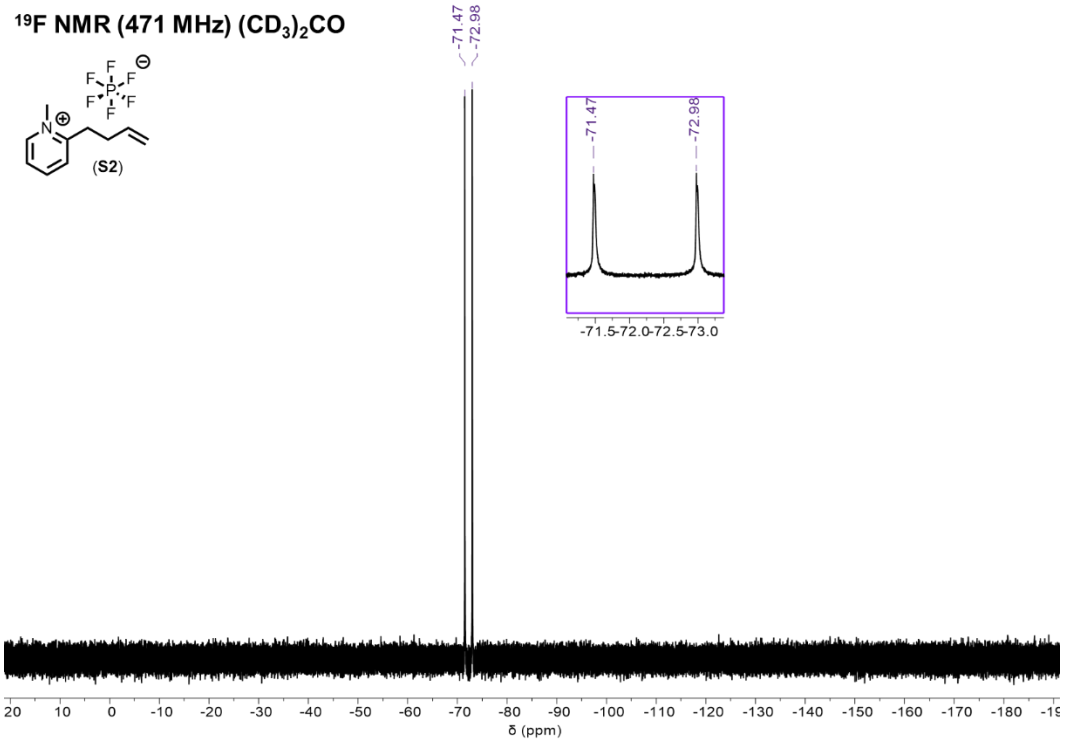

Figure E.66. ^{19}F NMR spectrum of 2-(3-buten-1-yl)-1-methylpyridinium hexafluorophosphate (**S2**) recorded in $(CD_3)_2CO$ at 25 °C.

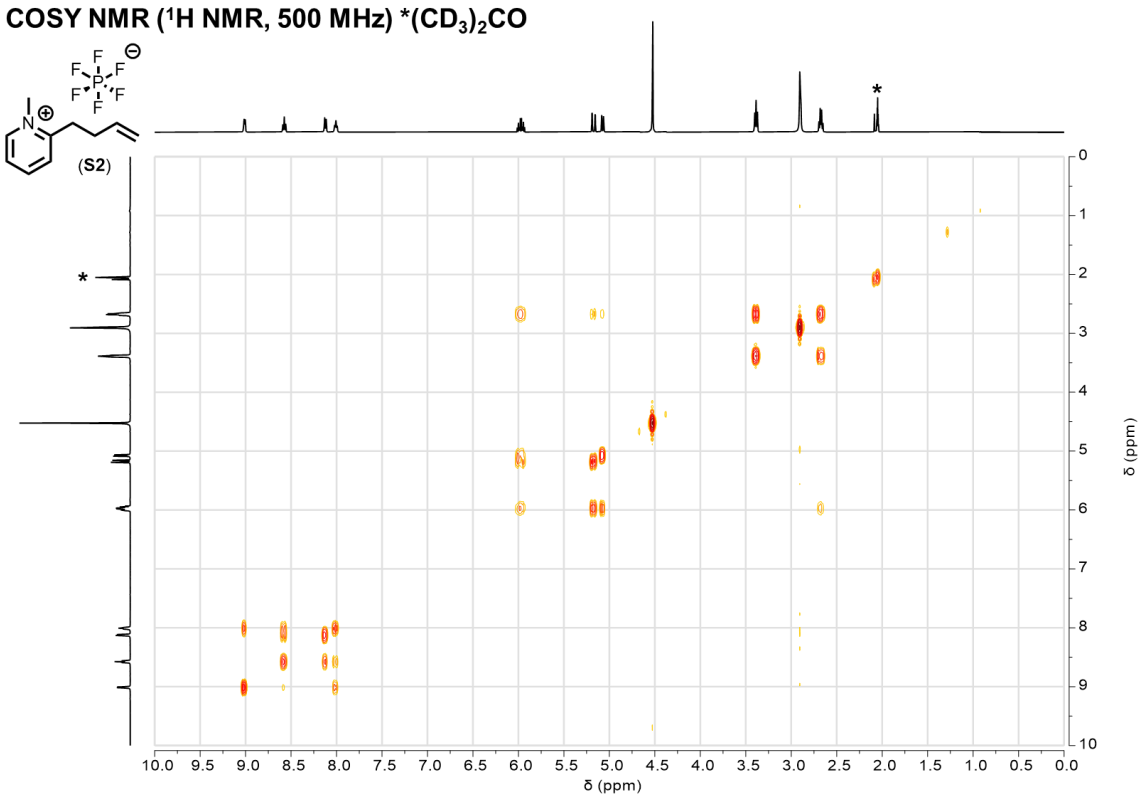

Figure E.67. COSY NMR spectrum of 2-(3-buten-1-yl)-1-methylpyridinium hexafluorophosphate (**S2**) recorded in $(CD_3)_2CO$ at 25 °C.

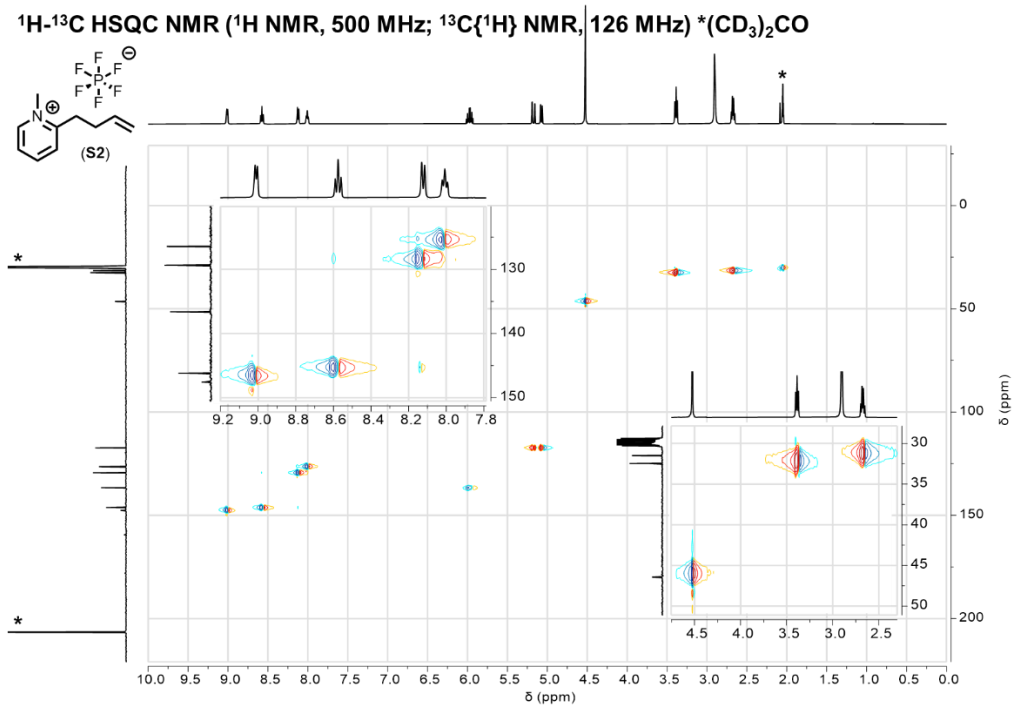

Figure E.68. ^{1}H-^{13}C HSQC NMR spectrum of 2-(3-buten-1-yl)-1-methylpyridinium hexafluorophosphate (**S2**) recorded in $(CD_3)_2CO$ at 25 °C.

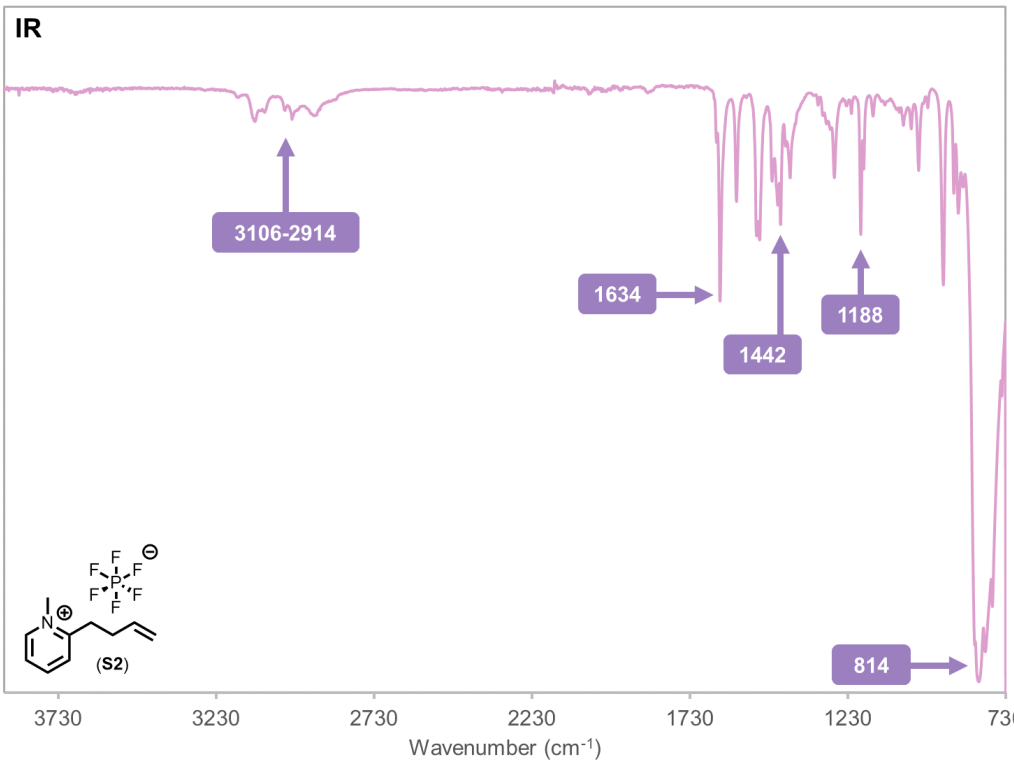

Figure E.69. IR spectrum of 2-(3-buten-1-yl)-1-methylpyridinium hexafluorophosphate (**S2**) recorded neat at 25 °C.

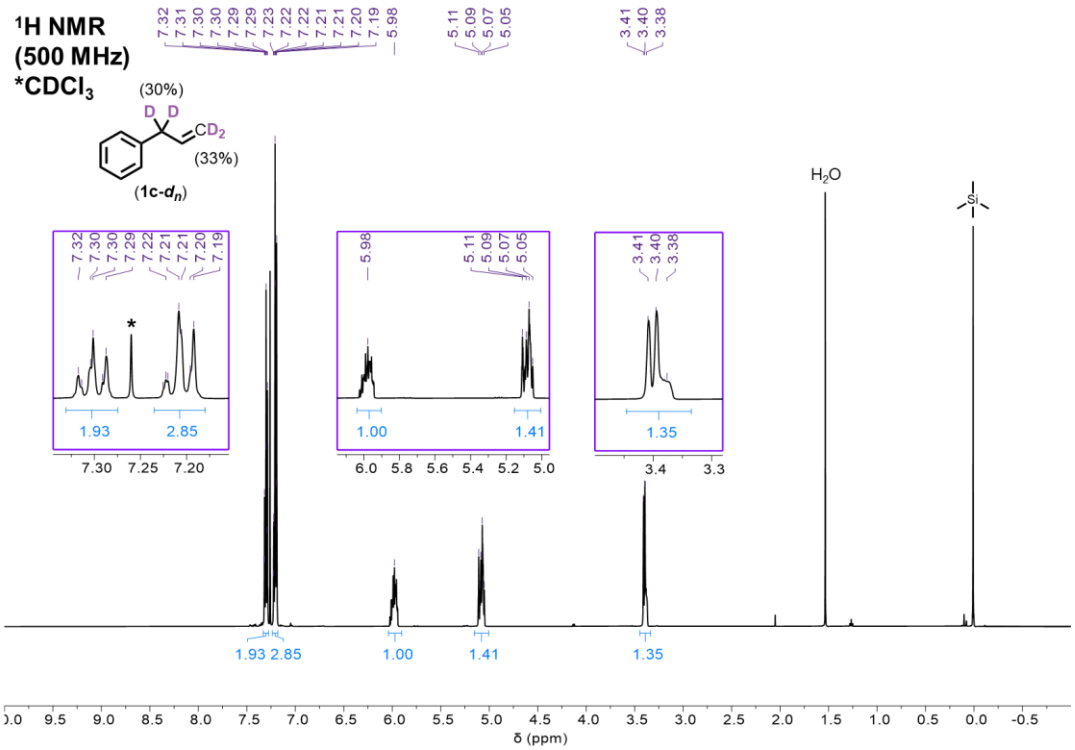

Figure E.70. ^{1}H NMR spectrum of allybenzene-d_n (**1c-d_n**) recorded in $CDCl_3$ at 25 °C.

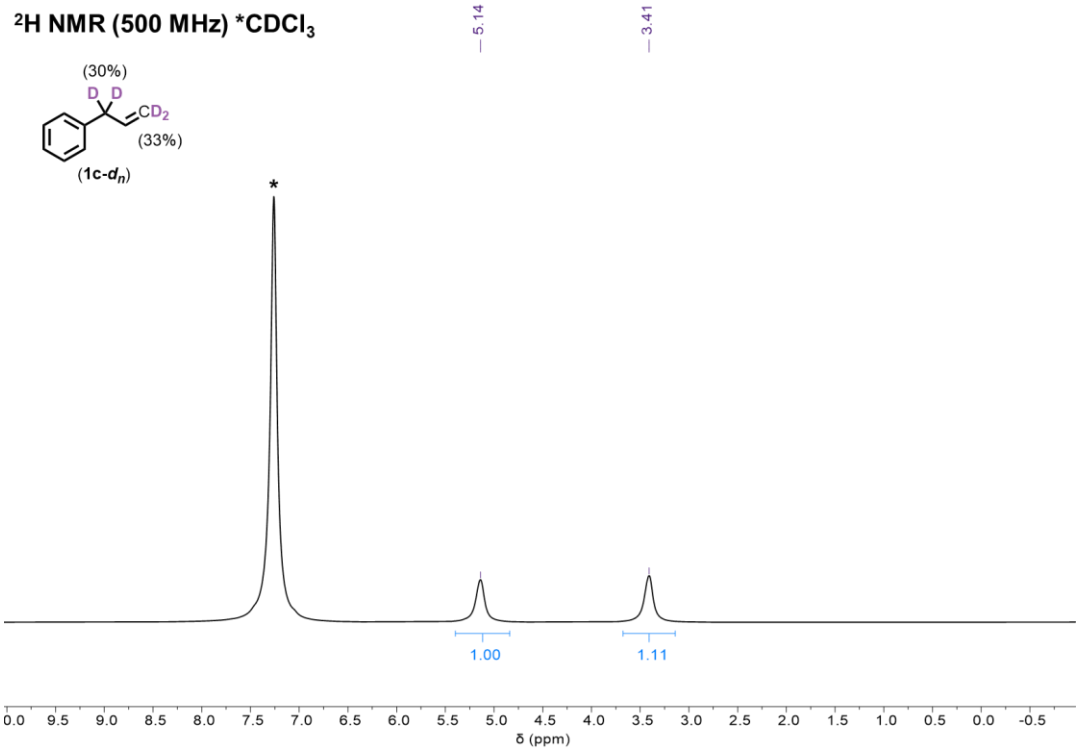

Figure E.71. ^{2}H NMR spectrum of allybenzene-d_n (**1c-*d*$_n$**) recorded in 1:5 $CDCl_3/CHCl_3$ at 25 °C.

a. **Isomerization Products**

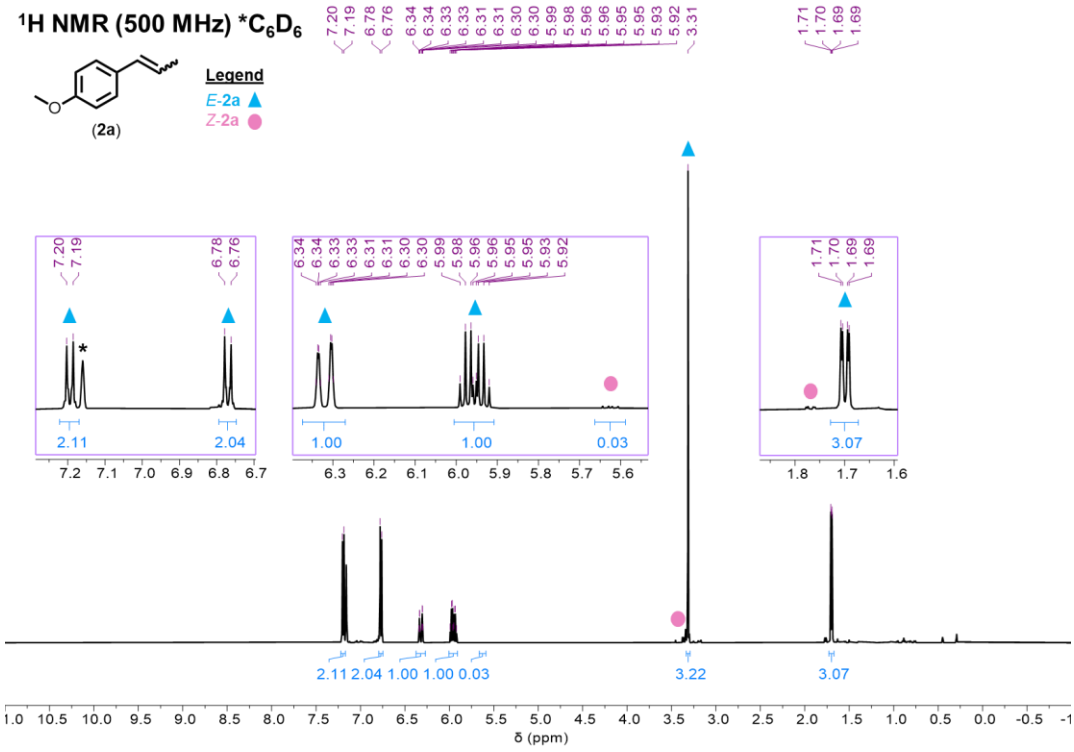

Figure E.72. ^{1}H NMR spectrum of anethole (**2a**) recorded in C_6D_6 at 25 °C.

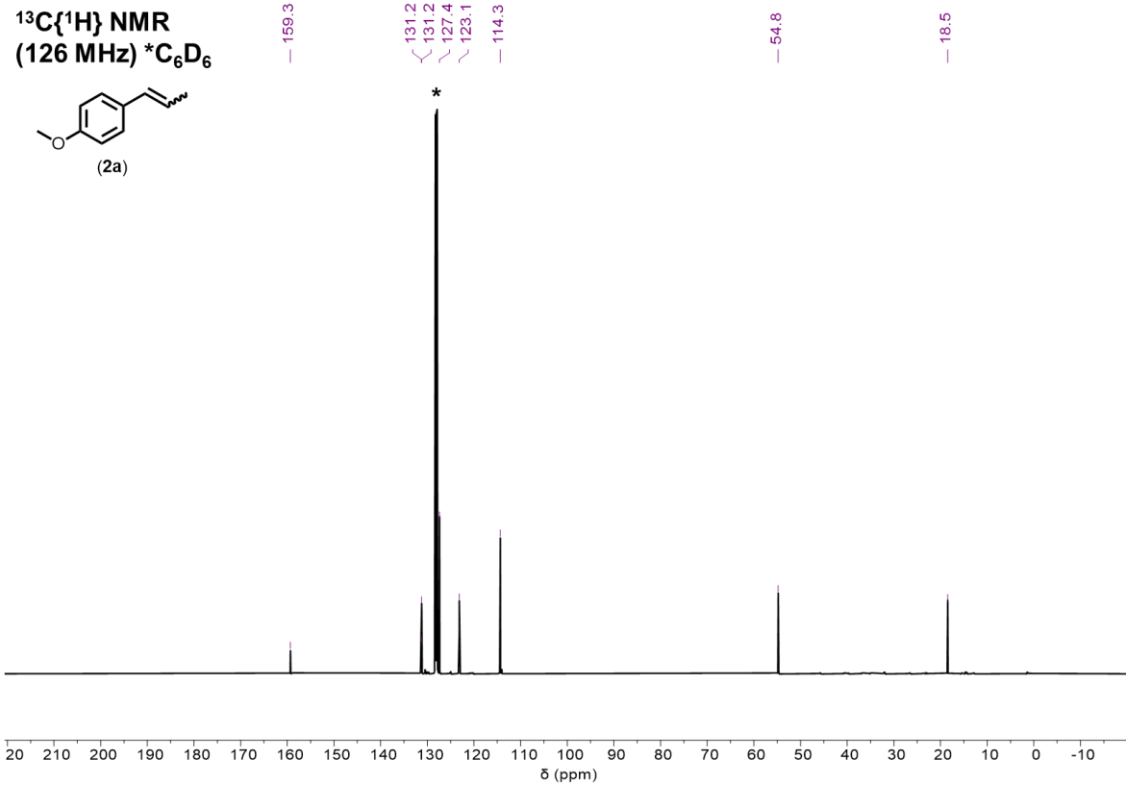

Figure E.73. ^{13}C{^{1}H} NMR spectrum of anethole (**2a**) recorded in C_6D_6 at 25 °C.

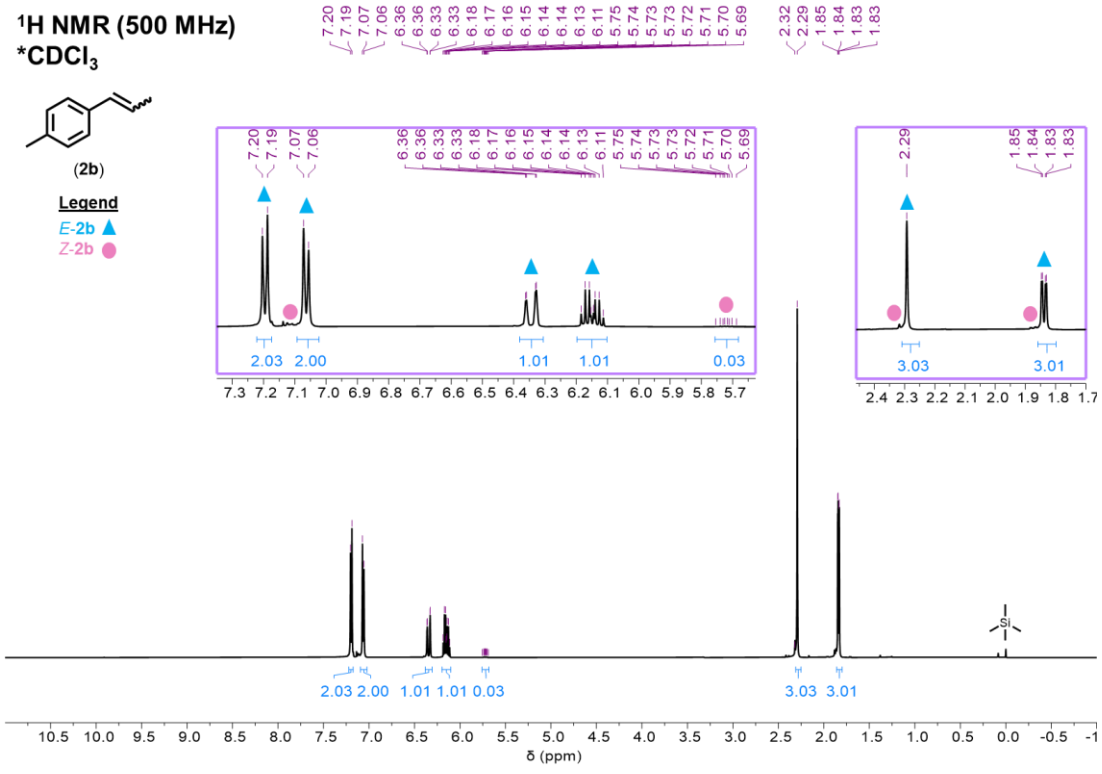

Figure E.74. ^{1}H NMR spectrum of 1-(4-methylphenyl)-1-propene (**2b**) recorded in $CDCl_3$ at 25 °C.

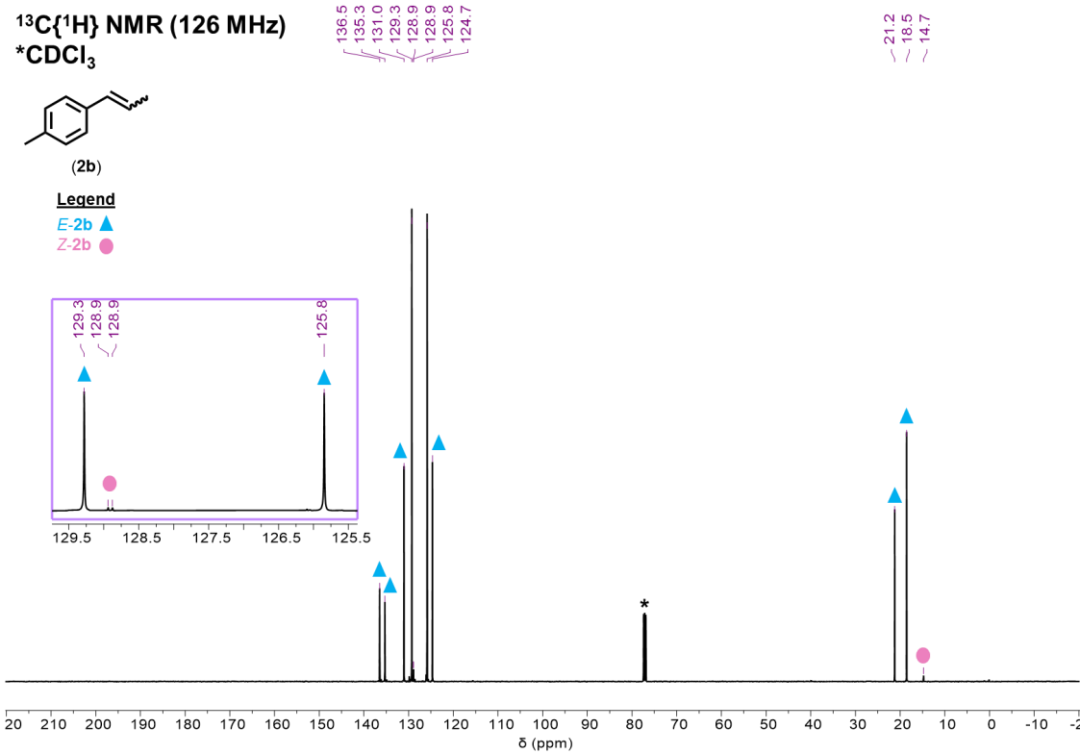

Figure E.75. ^{13}C{^{1}H} NMR spectrum of 1-(4-methylphenyl)-1-propene (**2b**) recorded in $CDCl_3$ at 25 °C.

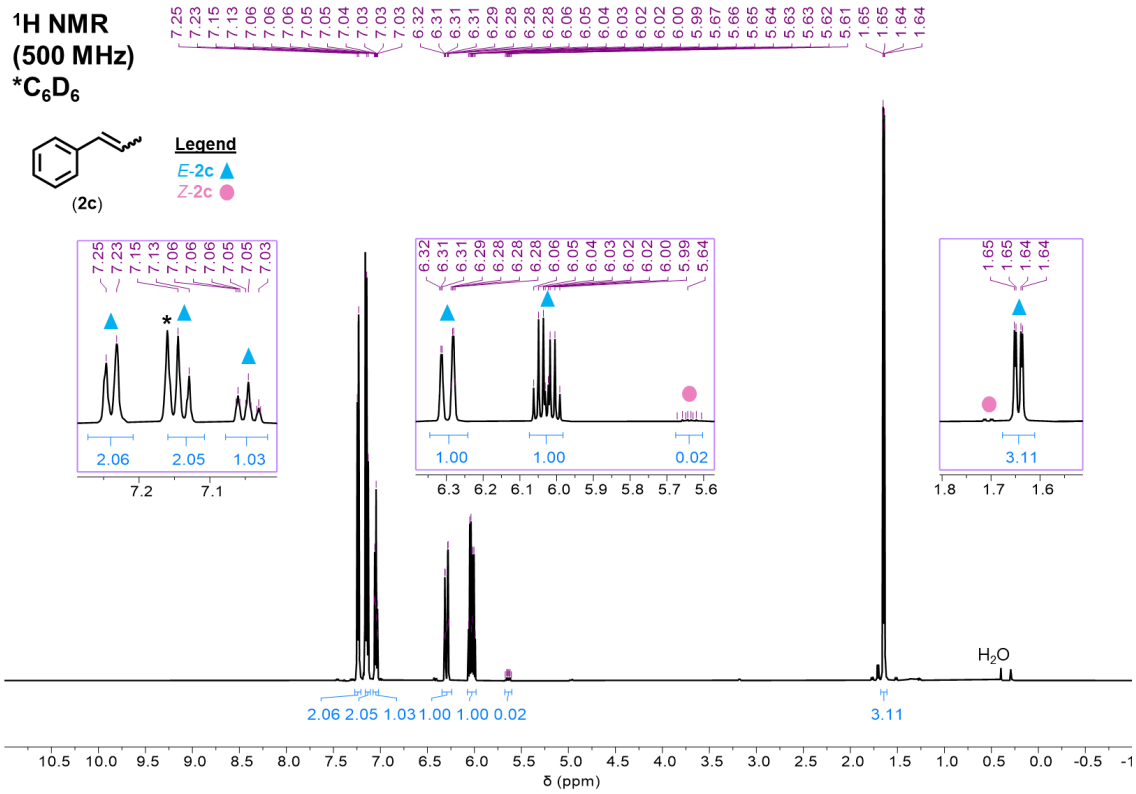

Figure E.76. ^{1}H NMR spectrum of β-methylstyrene (**2c**) recorded in C_6D_6 at 25 °C.

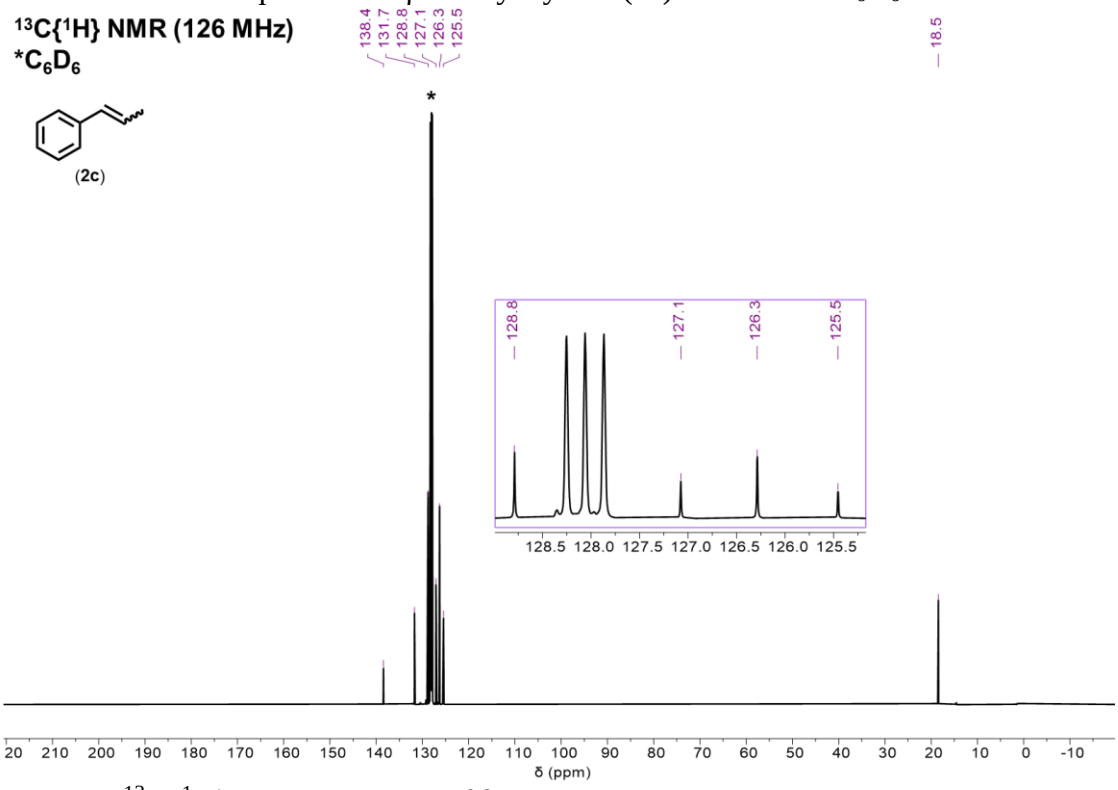

Figure E.77. ^{13}C{^{1}H} NMR spectrum of β-methylstyrene (**2c**) recorded in C_6D_6 at 25 °C.

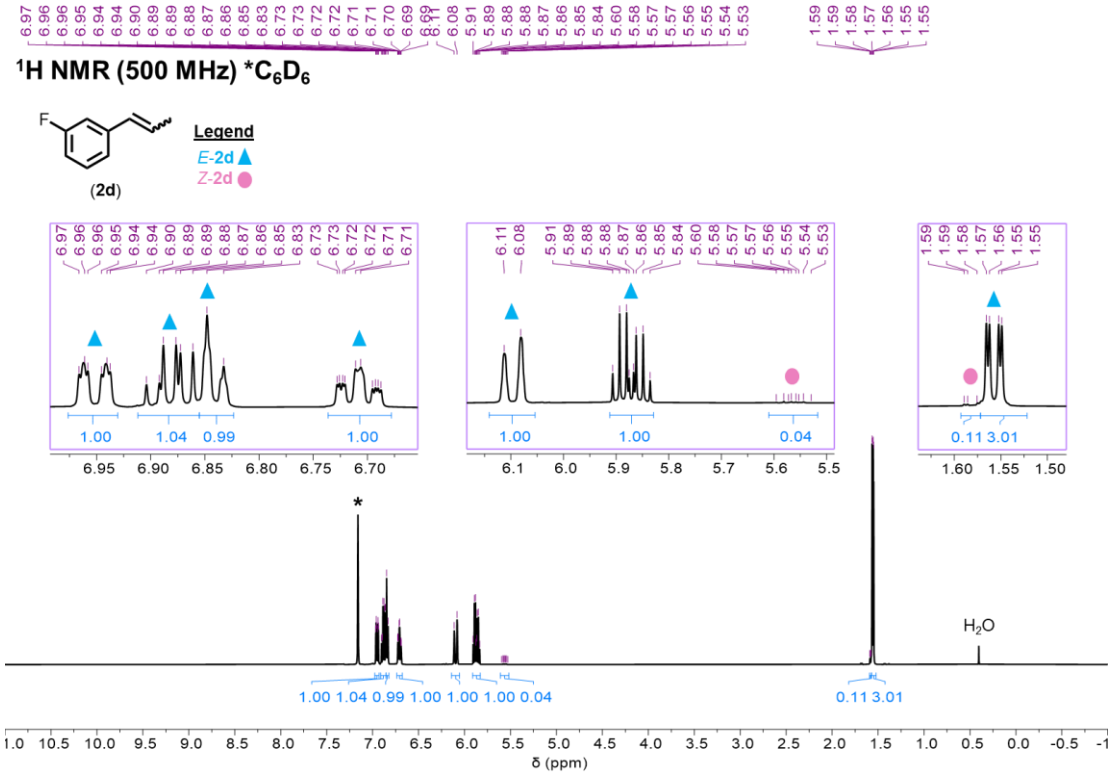

Figure E.78. ^{1}H NMR spectrum of 1-fluoro-3-(1-propen-1-yl)benzene (**2d**) recorded in C_6D_6 at 25 °C.

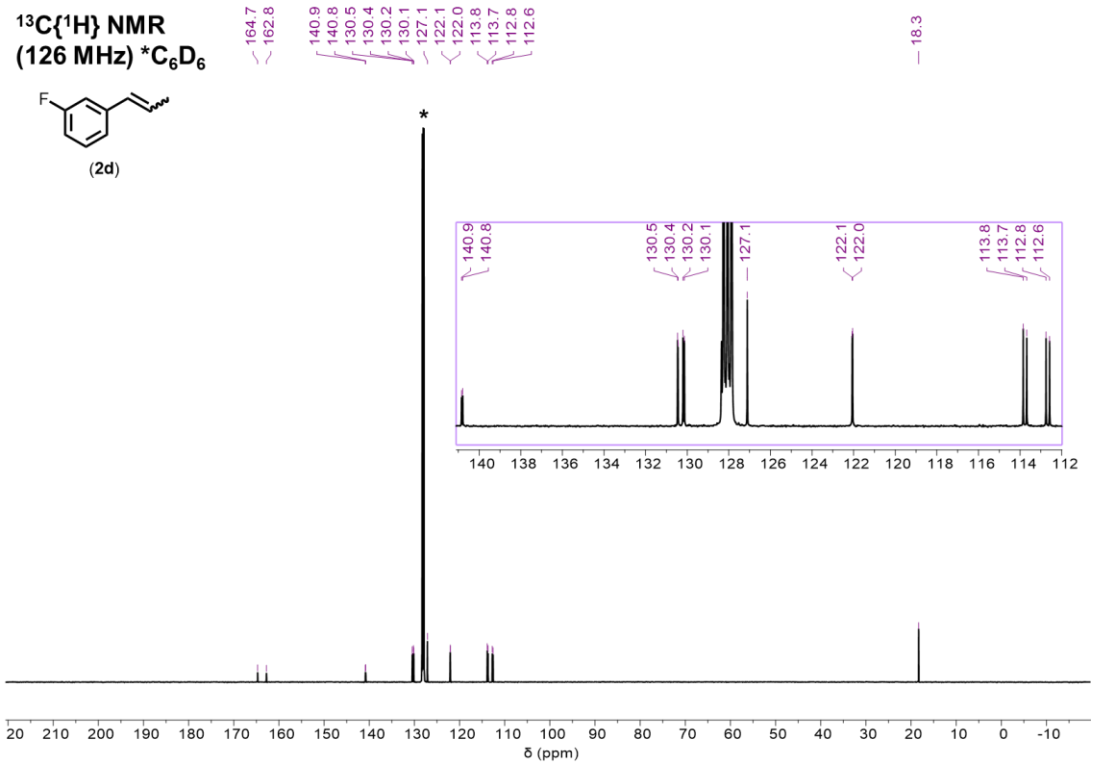

Figure E.79. ^{13}C{^{1}H} NMR spectrum of 1-fluoro-3-(1-propen-1-yl)benzene (**2d**) recorded in C_6D_6 at 25 °C.

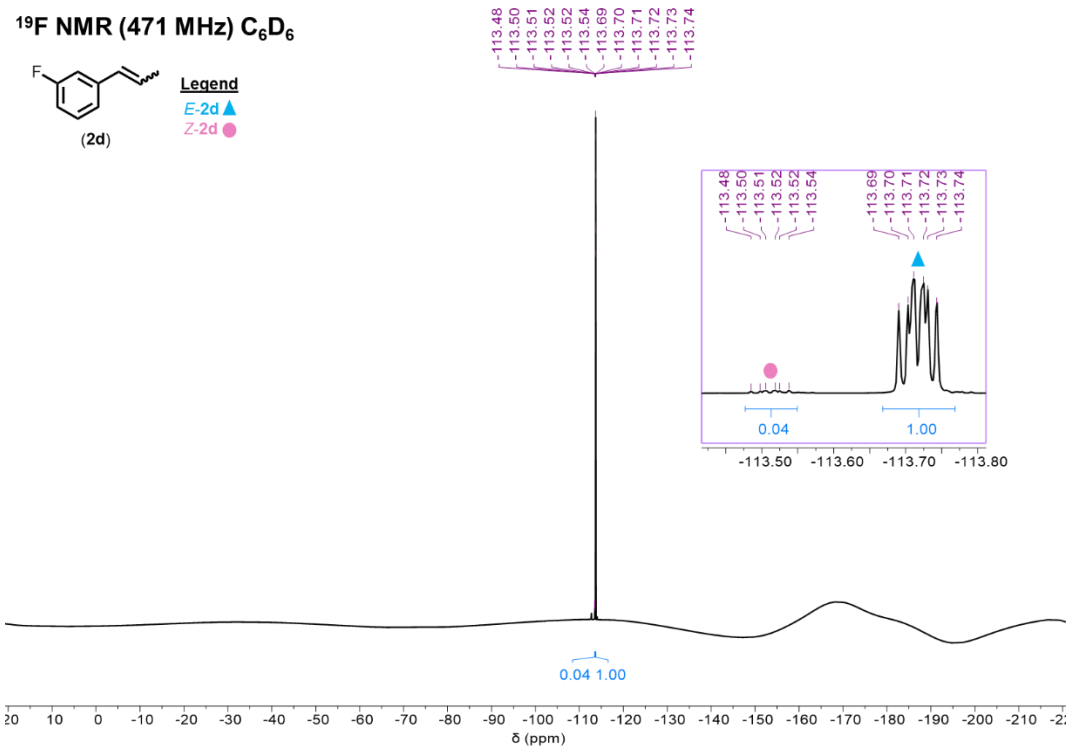

Figure E.80. ^{19}F NMR spectrum of 1-fluoro-3-(1-propen-1-yl)benzene (**2d**) recorded in C_6D_6 at 25 °C.

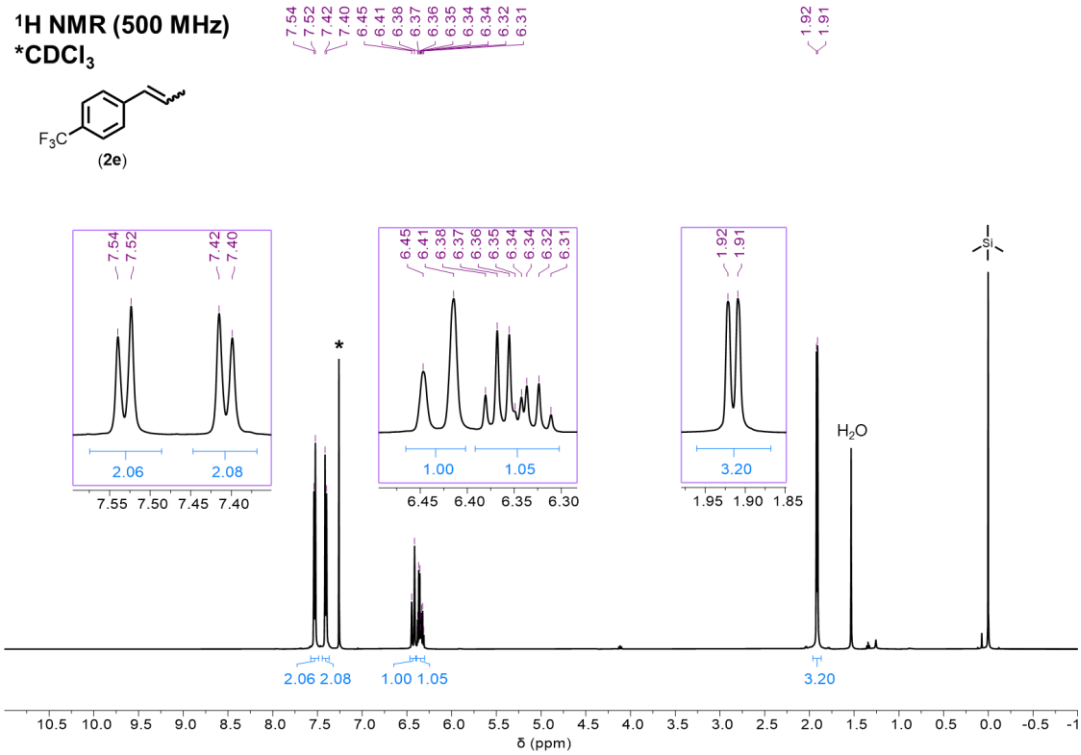

Figure E.81. ^{1}H NMR spectrum of 1-(4-trifluoromethylphenyl)-1-propene (**2e**) recorded in $CDCl_3$ at 25 °C.

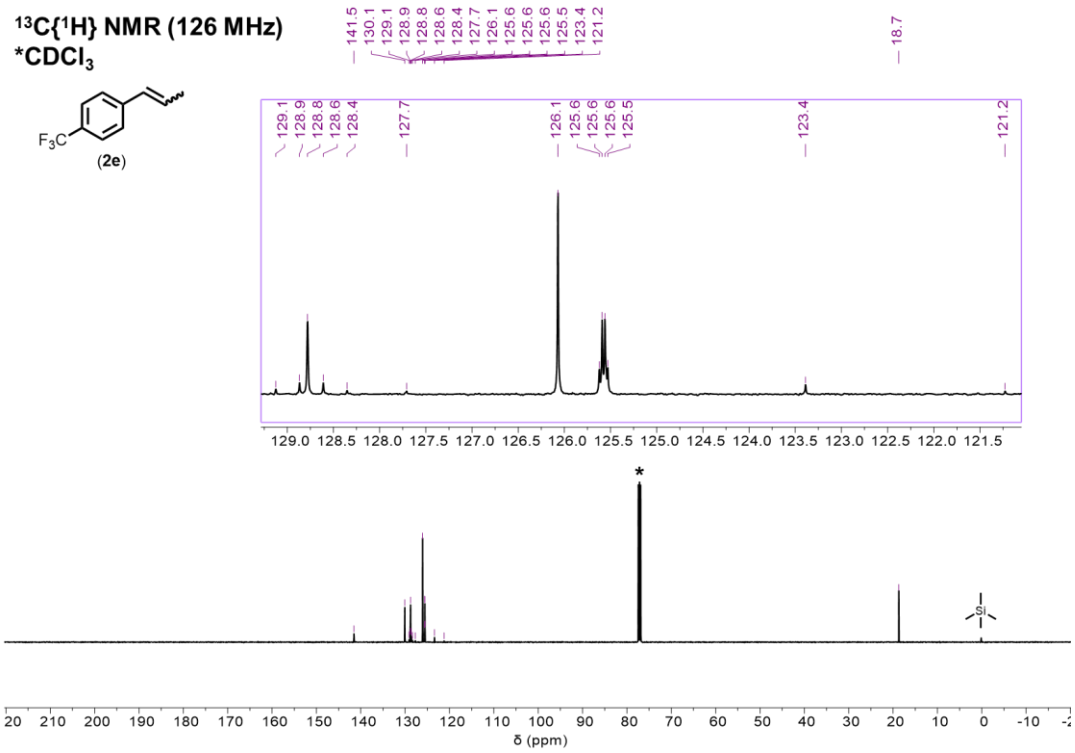

Figure E.82. $^{13}C\{^{1}H\}$ NMR spectrum of 1-(4-trifluoromethylphenyl)-1-propene (**2e**) recorded in $CDCl_3$ at 25 °C.

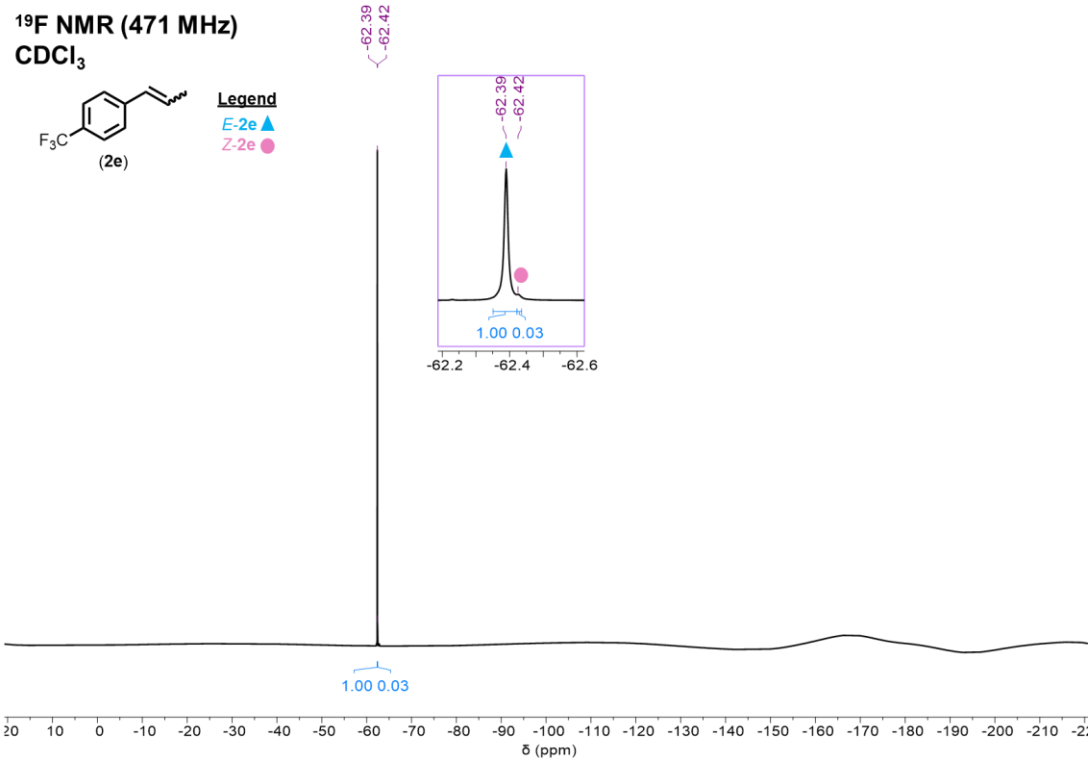

Figure E.83. ^{19}F NMR spectrum of 1-(4-trifluoromethylphenyl)-1-propene (**2e**) recorded in $CDCl_3$ at 25 °C.

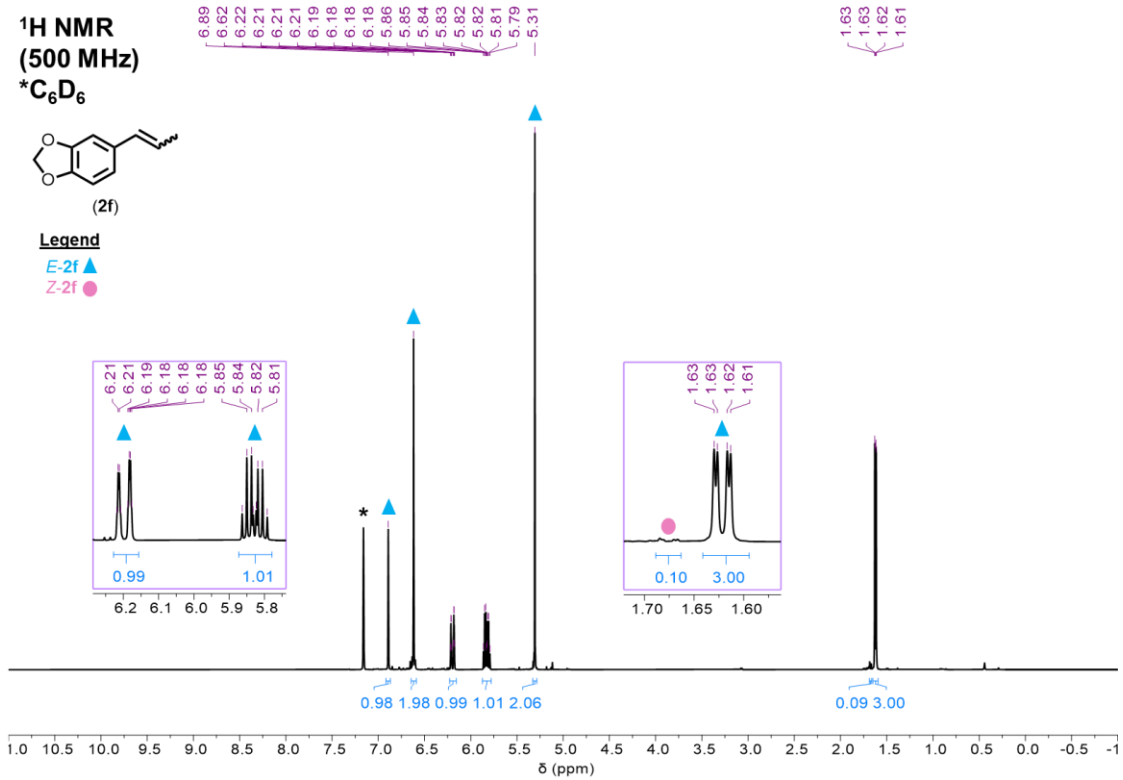

Figure E.84. ^{1}H NMR spectrum of isosafrole (**2f**) recorded in C_6D_6 at 25 °C.

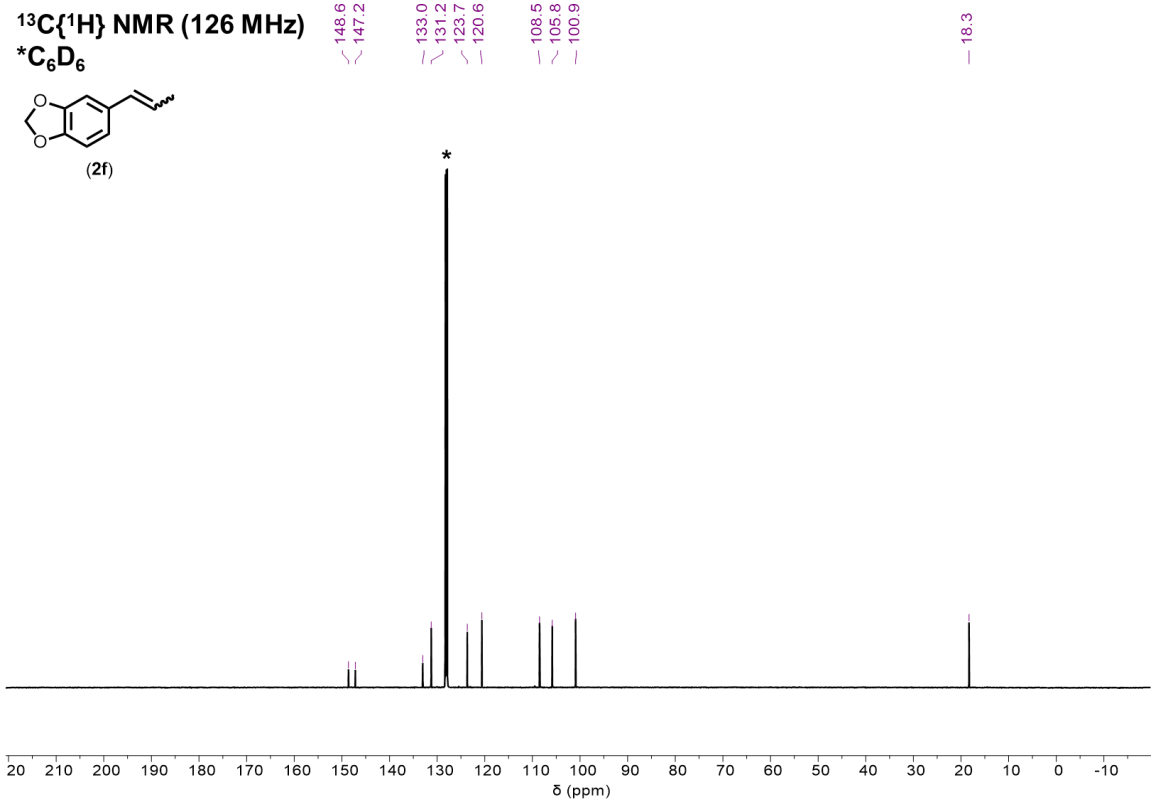

Figure E.85. ^{13}C{^{1}H} NMR spectrum of isosafrole (**2f**) recorded in C_6D_6 at 25 °C.

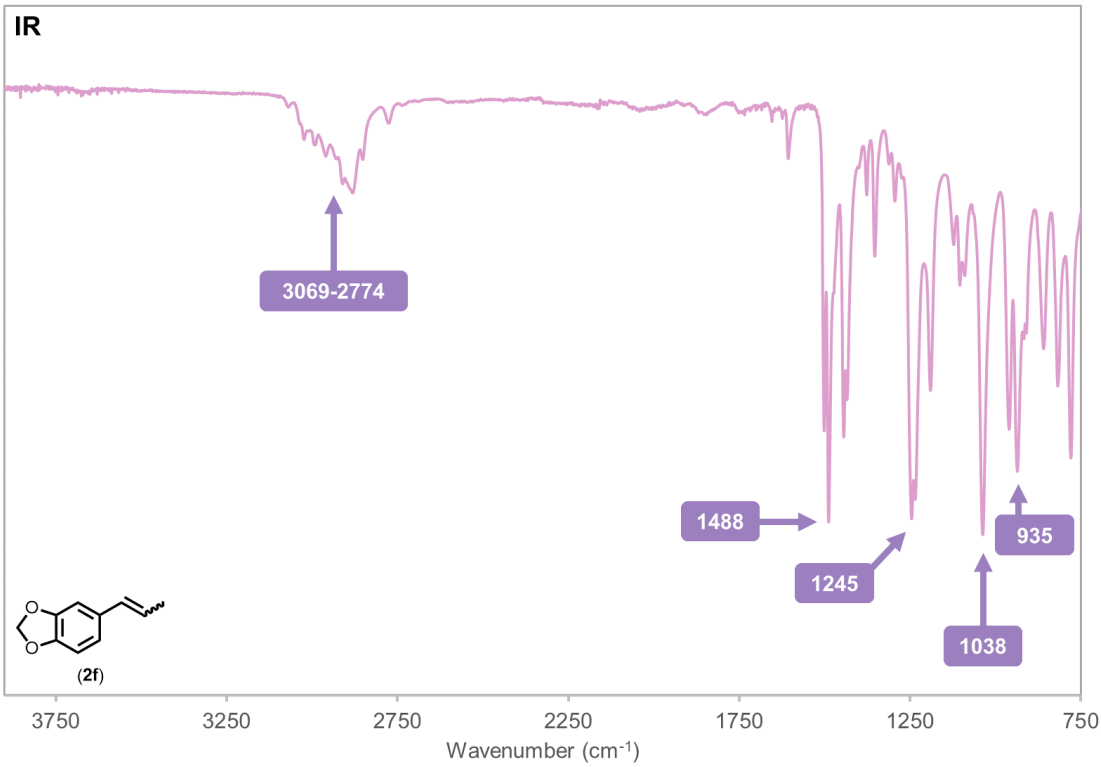

Figure E.86. IR spectrum of isosafrole (**2f**) recorded neat at 25 °C.

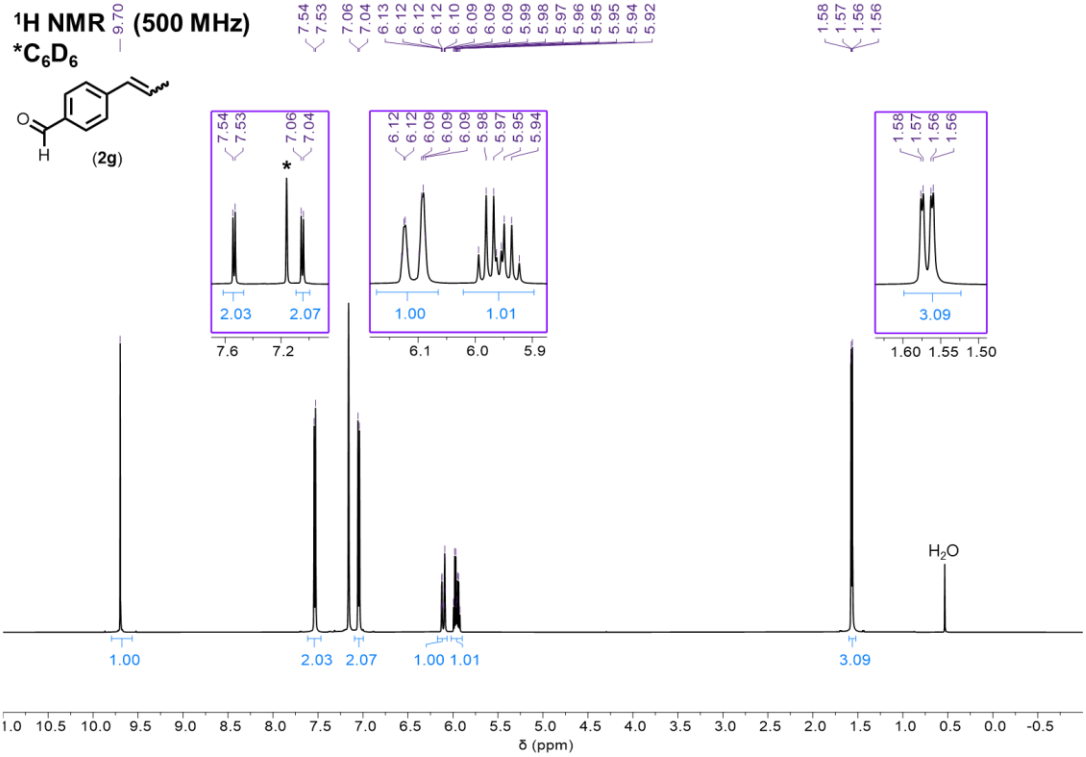

Figure E.87. ^{1}H NMR spectrum of 4-(1-propen-1-yl)benzaldehyde (**2g**) recorded in C_6D_6 at 25 °C.

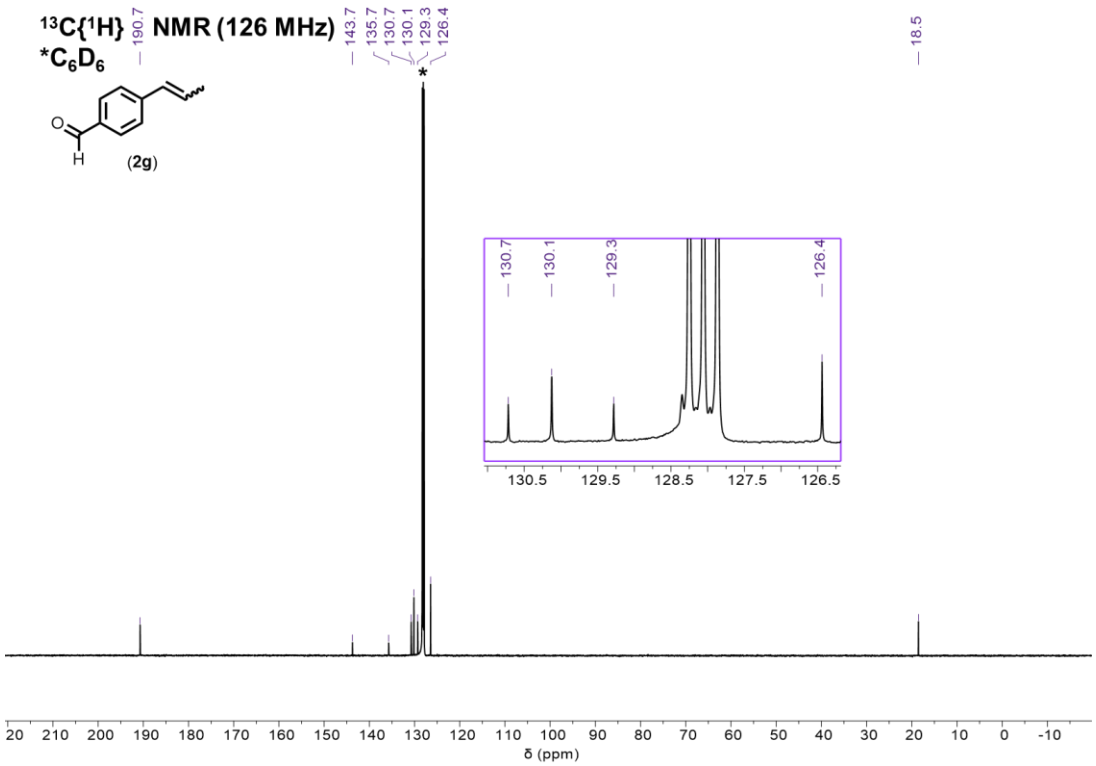

Figure E.88. $^{13}C\{^{1}H\}$ NMR spectrum of 4-(1-propen-1-yl)benzaldehyde (**2g**) recorded in C_6D_6 at 25 °C.

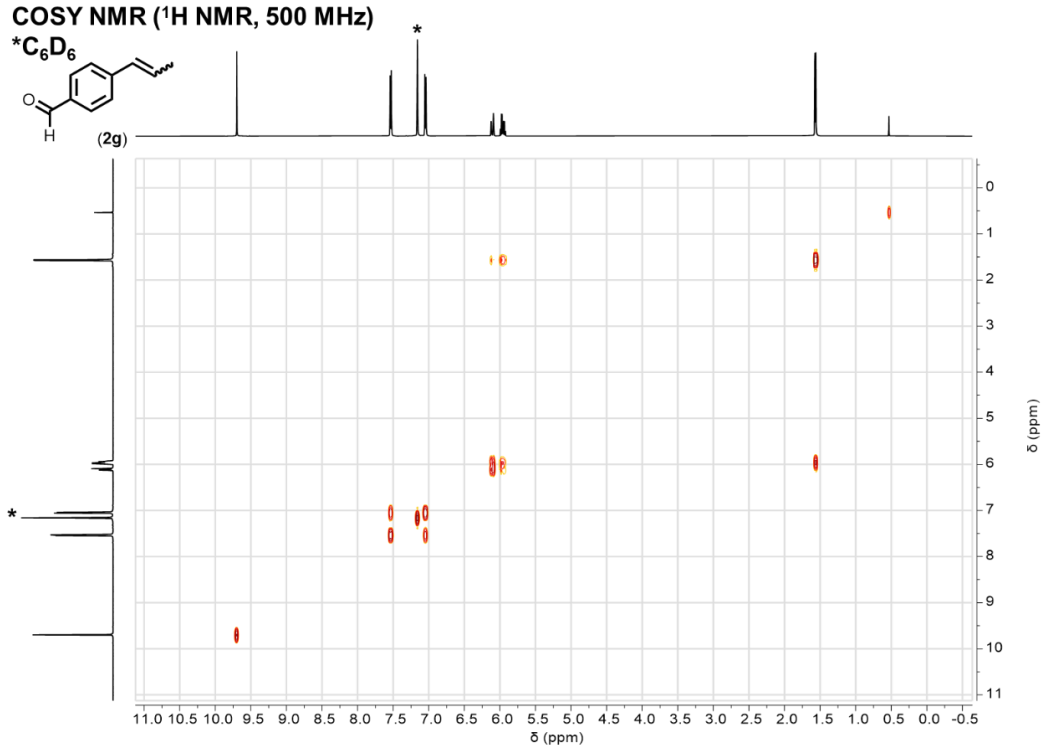

Figure E.89. COSY NMR spectrum of 4-(1-propen-1-yl)benzaldehyde (**2g**) recorded in C_6D_6 at 25 °C.

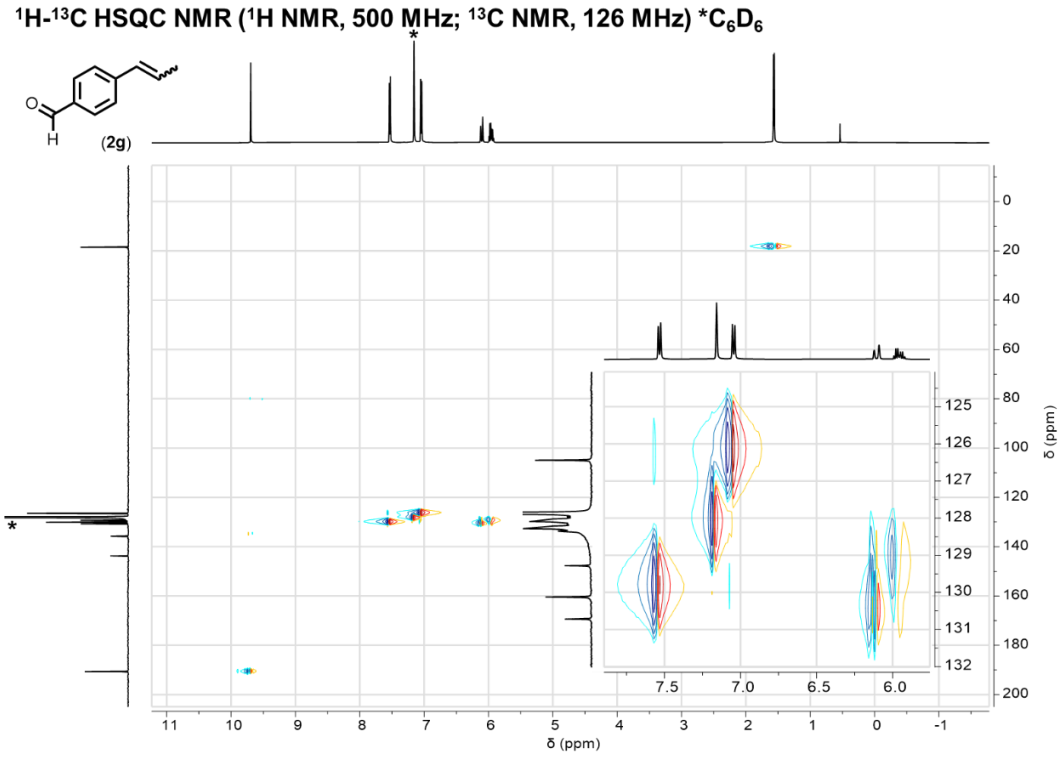

Figure E.90. ^{1}H-^{13}C HSQC NMR spectrum of 4-(1-propen-1-yl)benzaldehyde (**2g**) recorded in C_6D_6 at 25 °C.

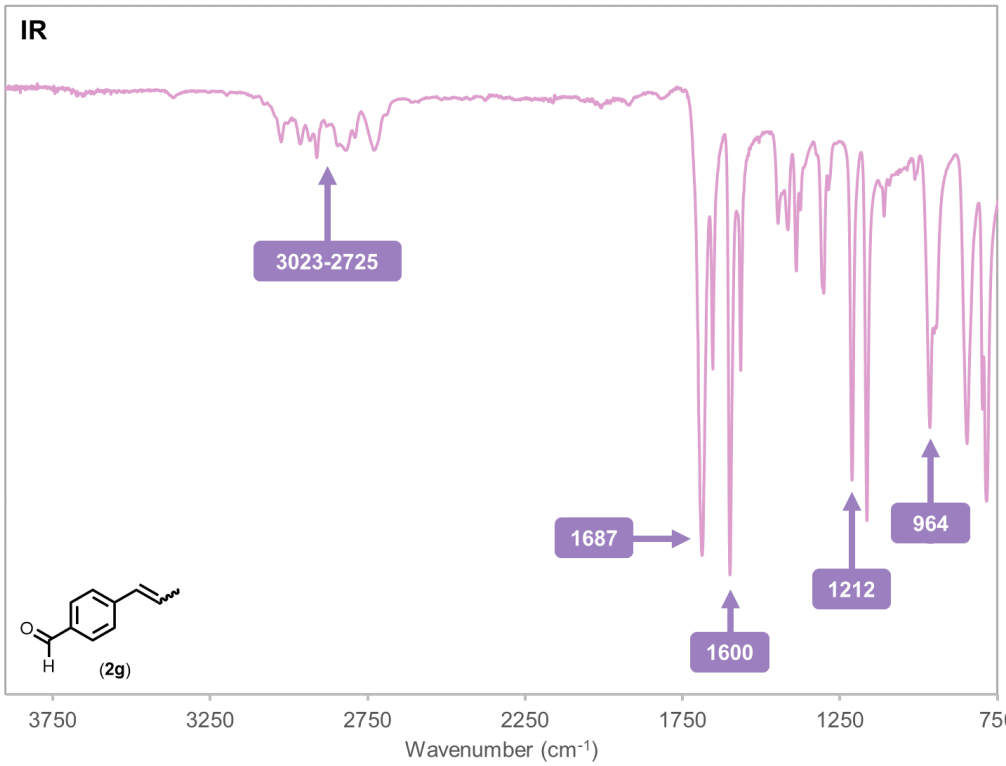

Figure E.91. IR spectrum of 4-(1-propen-1-yl)benzaldehyde (**2g**) recorded neat at 25 °C.

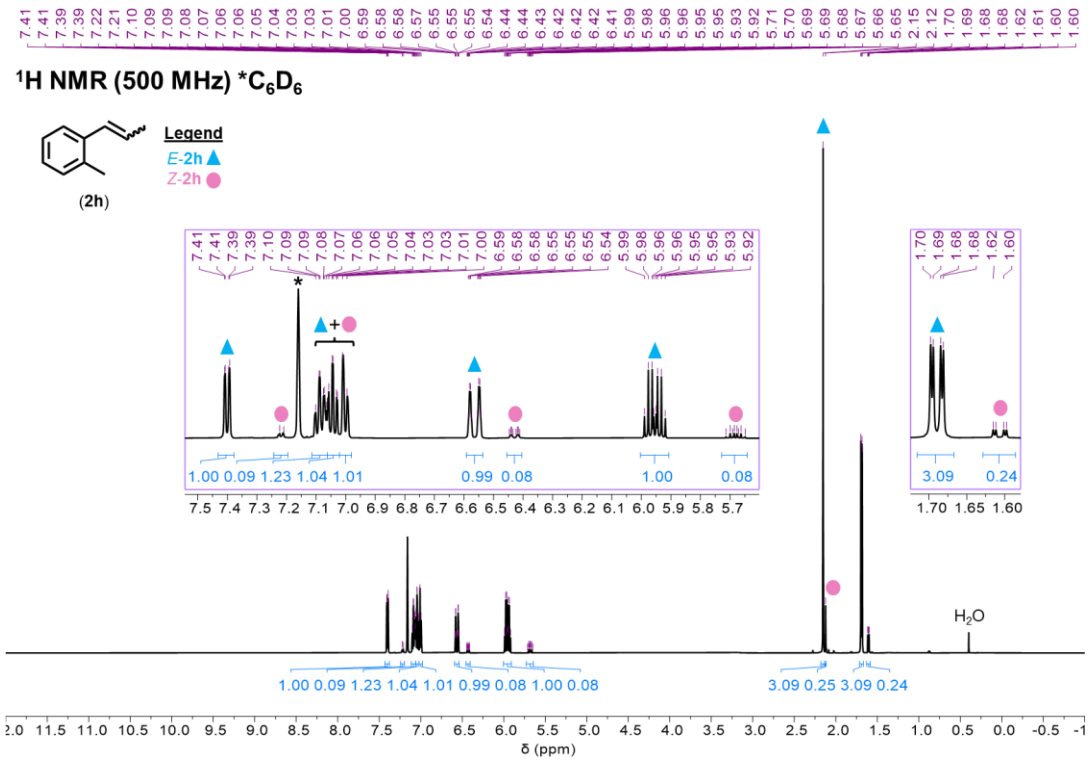

Figure E.92. ^{1}H NMR spectrum of 1-(2-methylphenyl)-1-propene (**2h**) recorded in C_6D_6 at 25 °C.

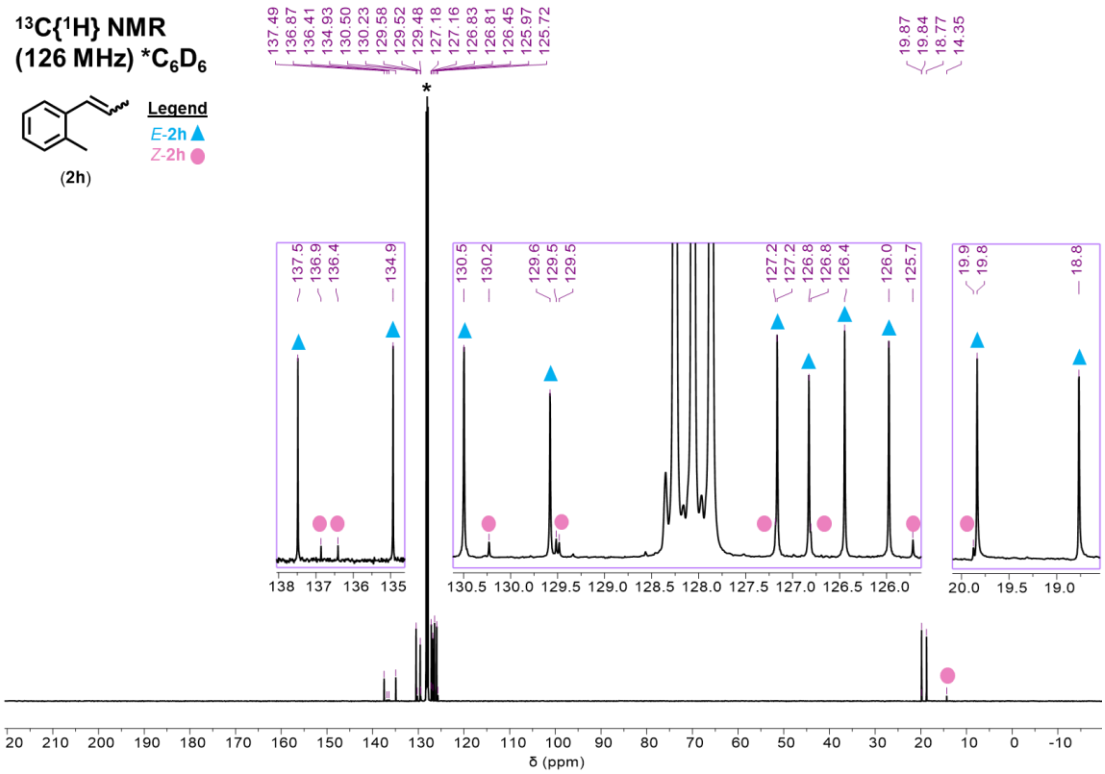

Figure E.93. $^{13}C\{^{1}H\}$ NMR spectrum of 1-(2-methylphenyl)-1-propene (**2h**) recorded in C_6D_6 at 25 °C.

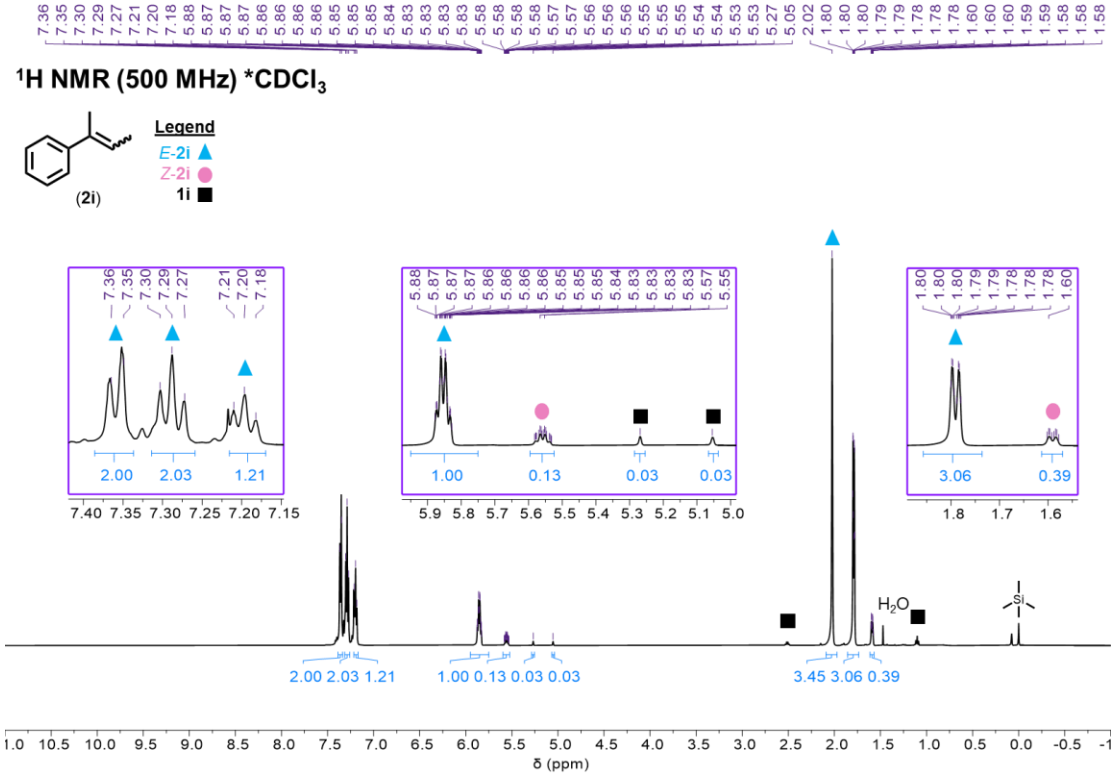

Figure E.94. ^{1}H NMR spectrum of α,β-dimethylstyrene (**2i**) recorded in $CDCl_3$ at 25 °C.

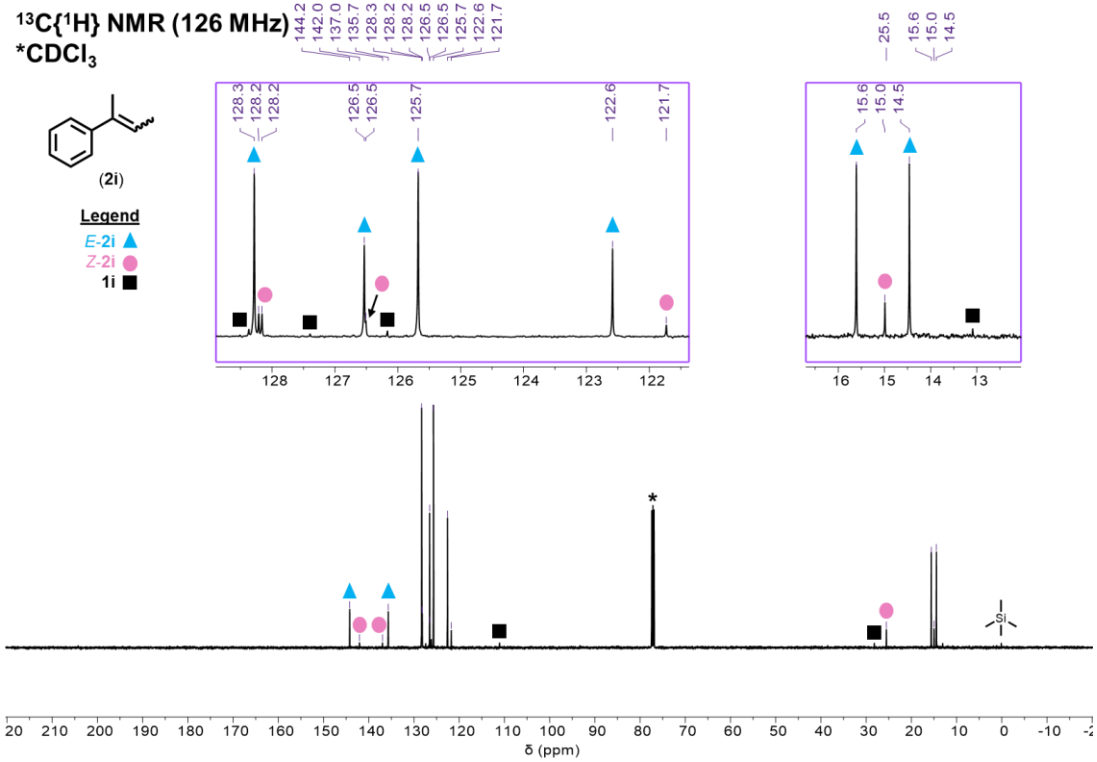

Figure E.95. $^{13}C\{^{1}H\}$ NMR spectrum of α,β-dimethylstyrene (**2i**) recorded in $CDCl_3$ at 25 °C.

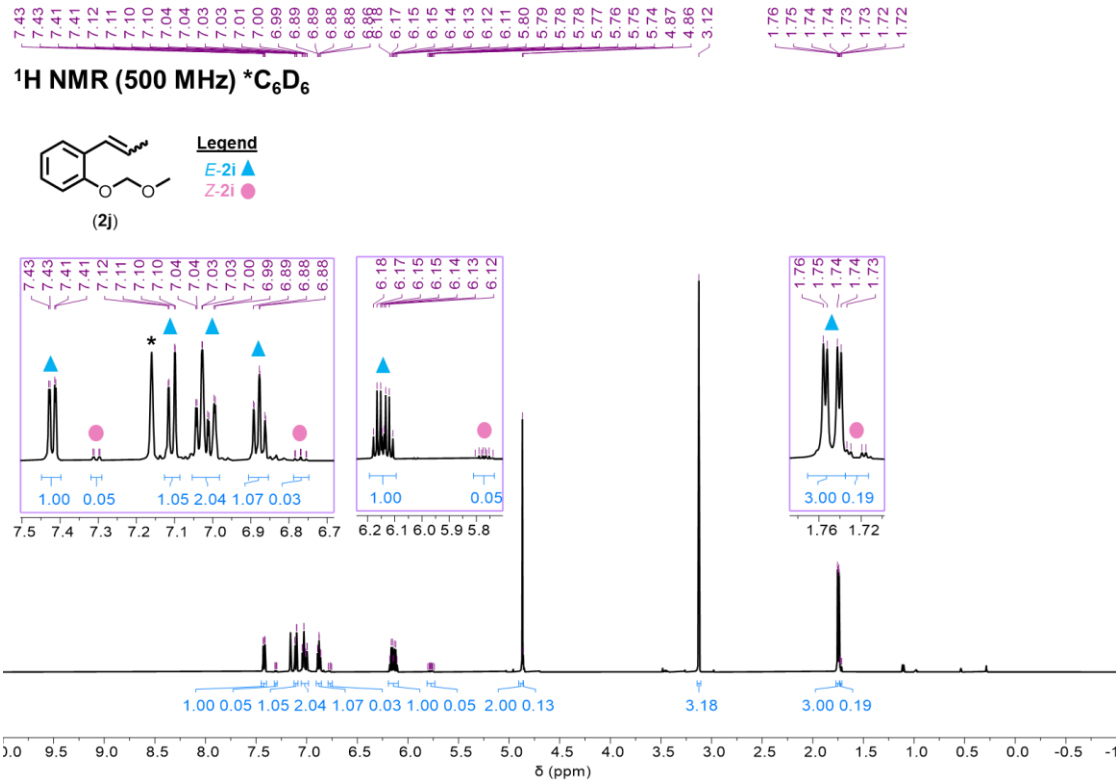

Figure E.96. ^{1}H NMR spectrum of 1-(methoxymethoxy)-2-(1*E*)-1-propen-1-ylbenzene (**2j**) recorded in C_6D_6 at 25 °C.

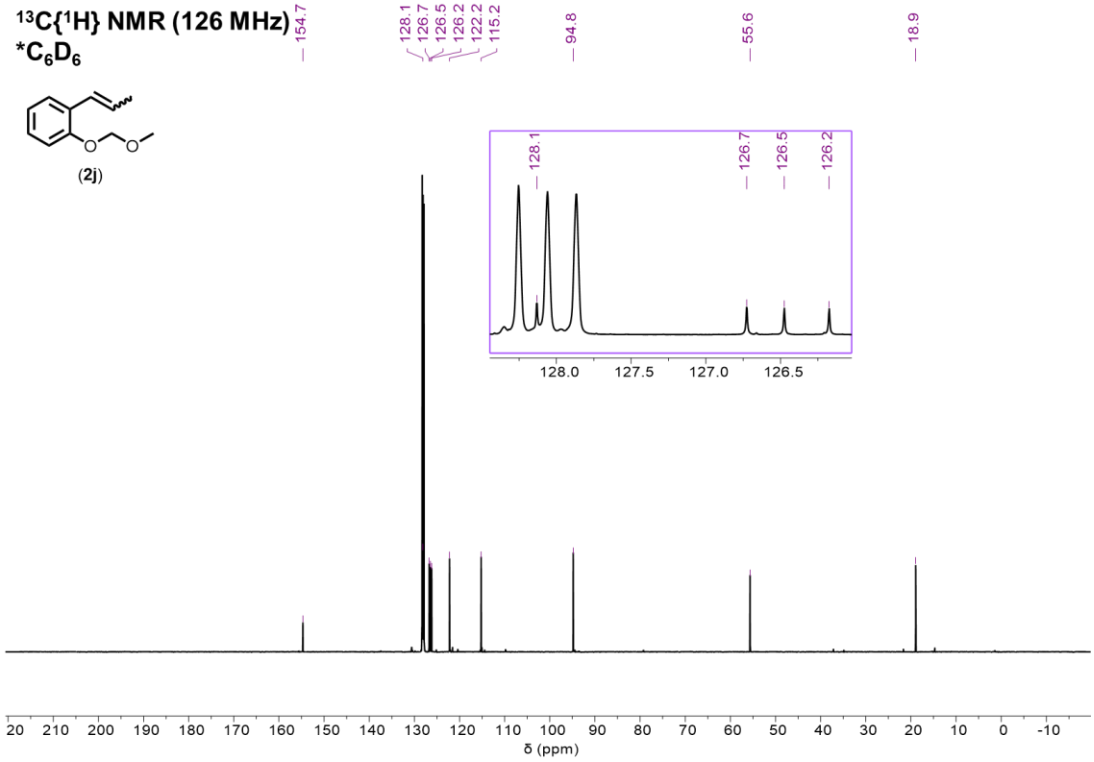

Figure E.97. $^{13}C\{^{1}H\}$ NMR spectrum of 1-(methoxymethoxy)-2-(1*E*)-1-propen-1-ylbenzene (**2j**) recorded in C_6D_6 at 25 °C.

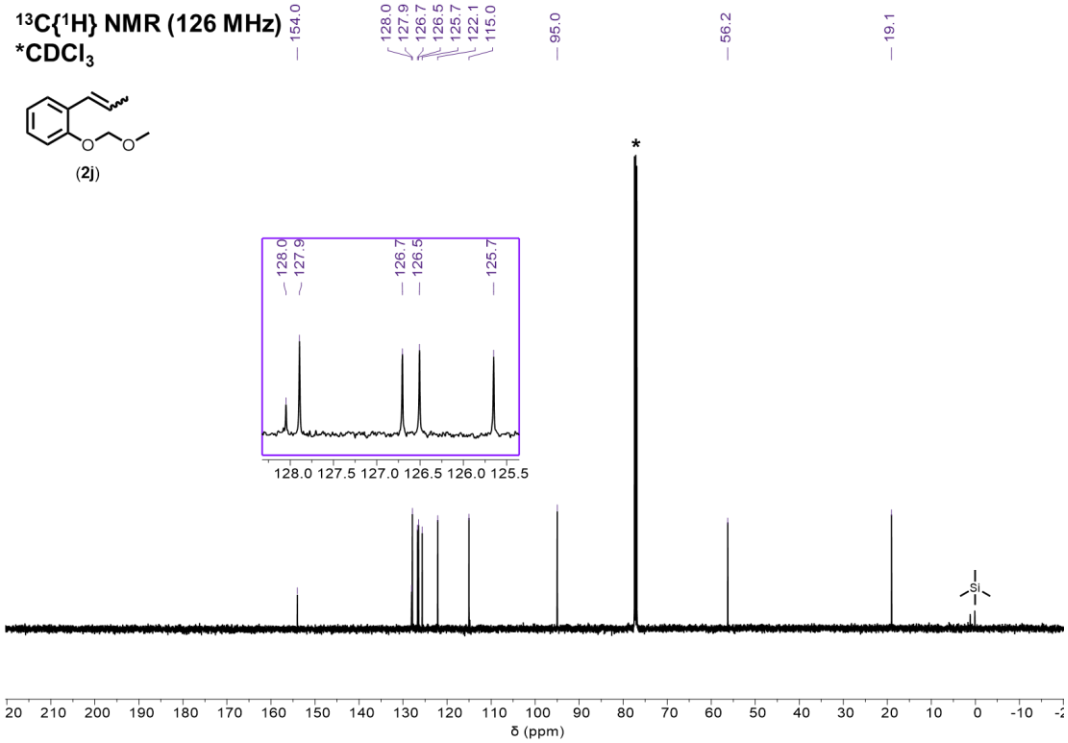

Figure E.98. $^{13}C\{^{1}H\}$ NMR spectrum of 1-(methoxymethoxy)-2-(1*E*)-1-propen-1-ylbenzene (**2j**) recorded in $CDCl_3$ at 25 °C.

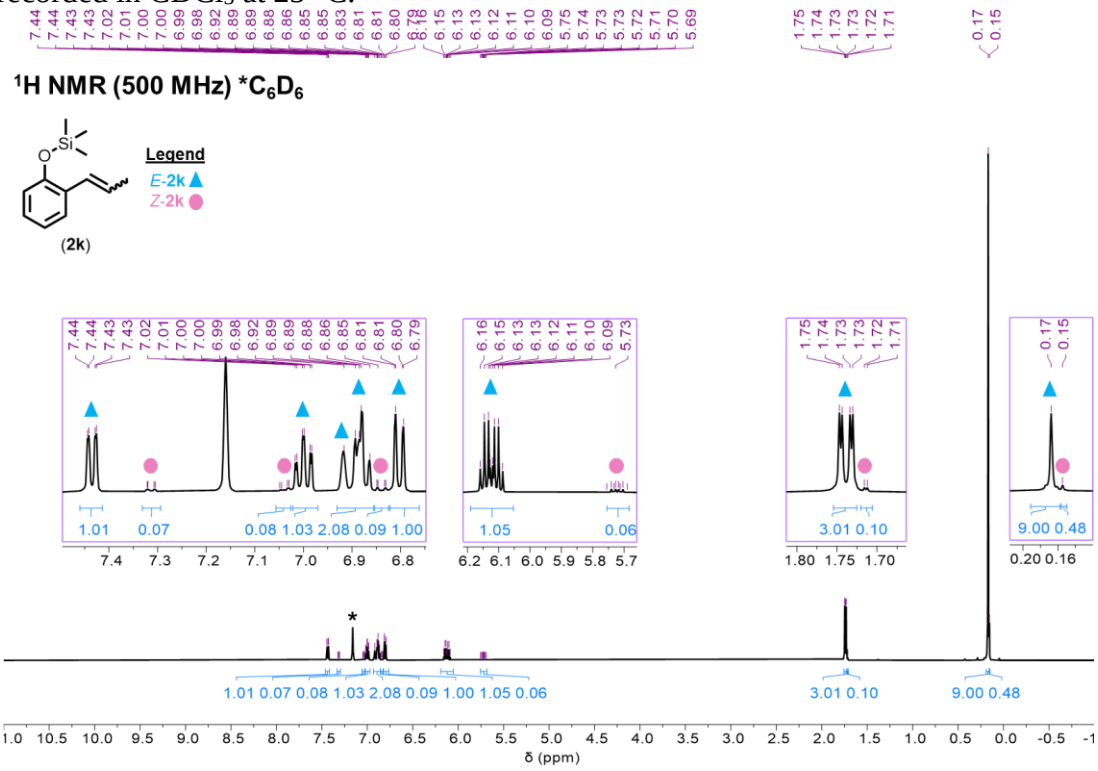

Figure E.99. ^{1}H NMR spectrum of 1-propen-1-yl-2-[(trimethylsilyl)oxy]benzene (**2k**) recorded in C_6D_6 at 25 °C.

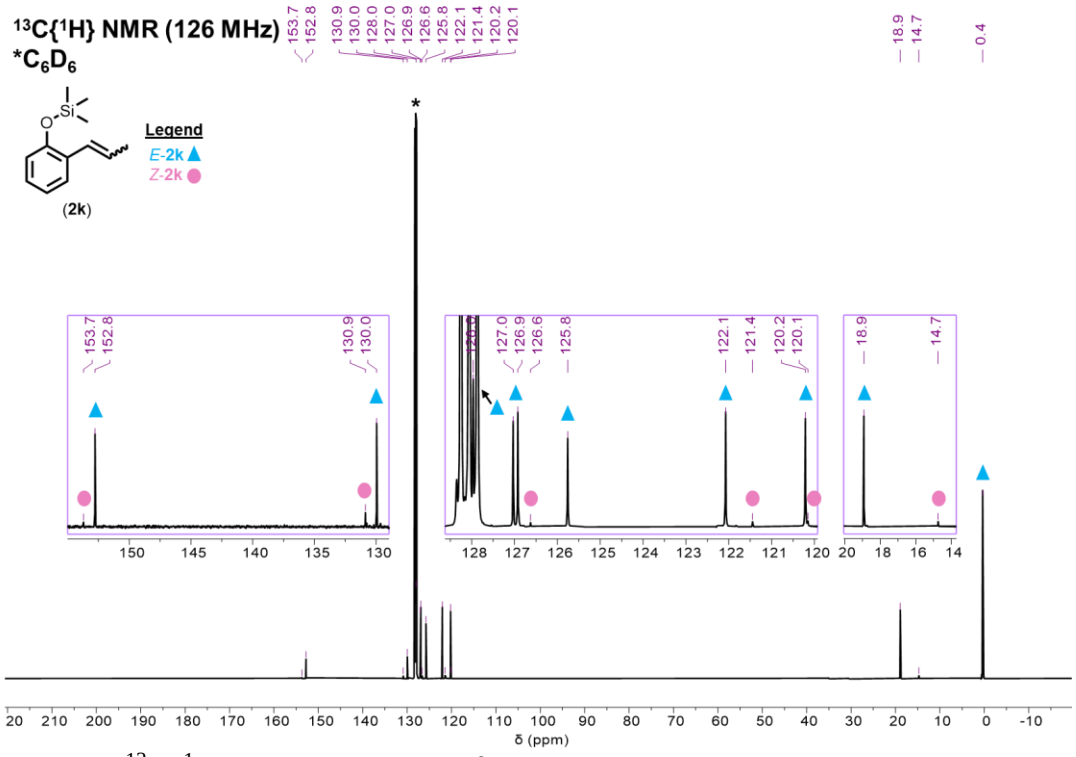

Figure E.100. ^{13}C{^{1}H} NMR spectrum of 1-propen-1-yl-2-[(trimethylsilyl)oxy]benzene (**2k**) recorded in C_6D_6 at 25 °C.

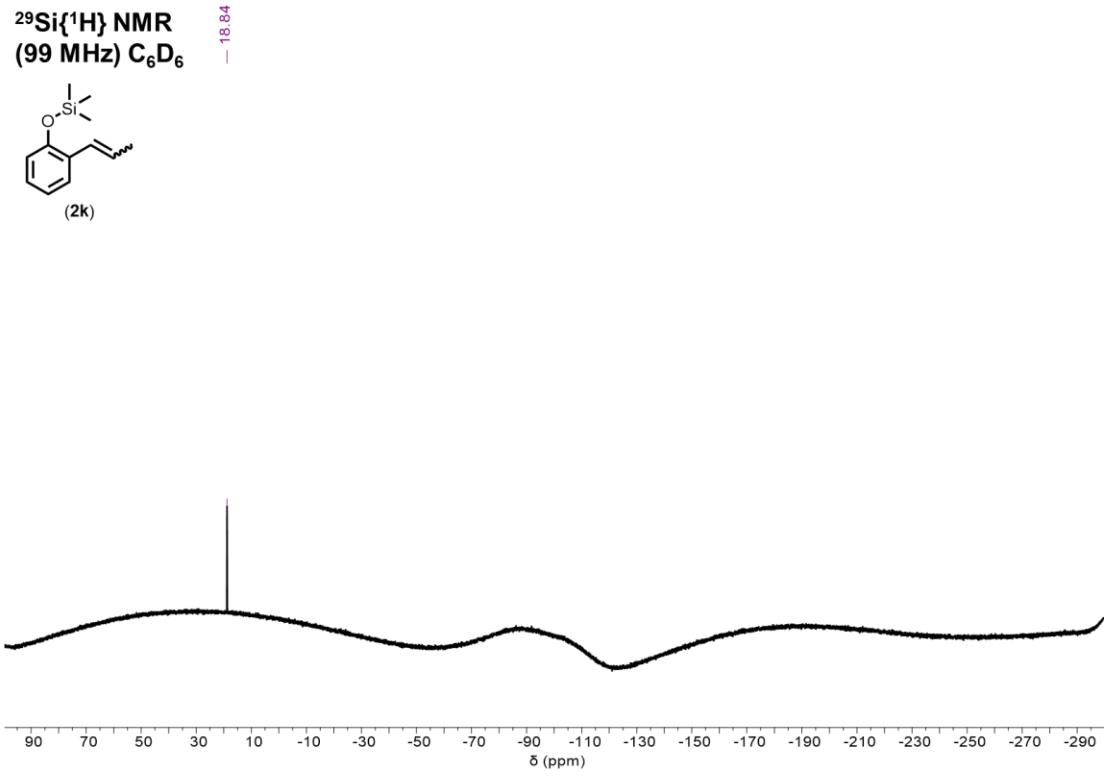

Figure E.101. $^{29}Si\{^{1}H\}$ NMR spectrum of 1-propen-1-yl-2-[(trimethylsilyl)oxy]benzene (**2k**) recorded in C_6D_6 at 25 °C.

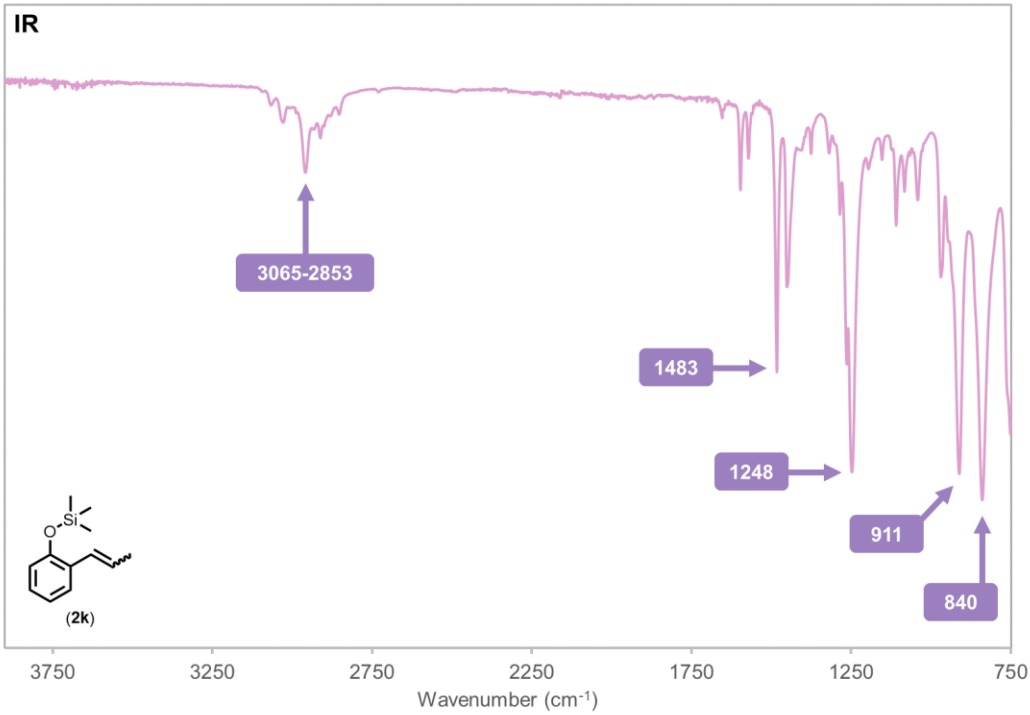

Figure E.102. IR spectrum of 1-propen-1-yl-2-[(trimethylsilyl)oxy]benzene (**2k**) recorded neat at 25 °C.

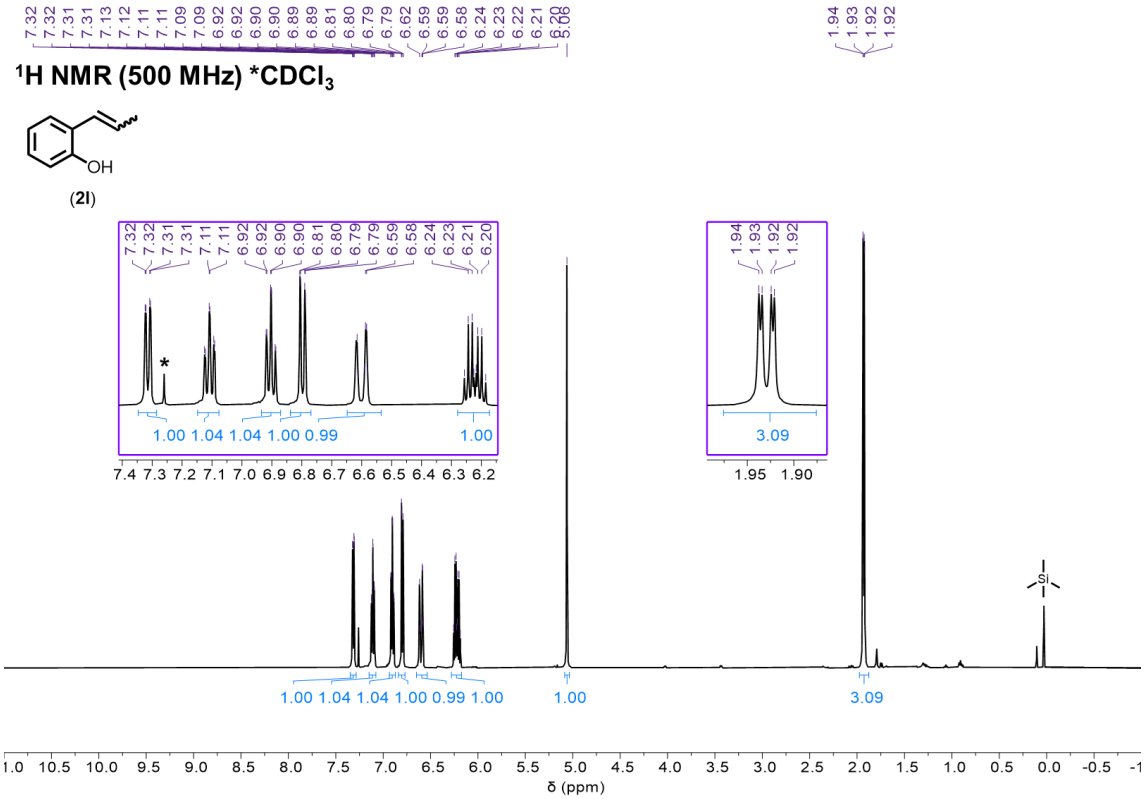

Figure E.103. ^{1}H NMR spectrum of 2-(1-propenyl)phenol (**2l**) recorded in $CDCl_3$ at 25 °C.

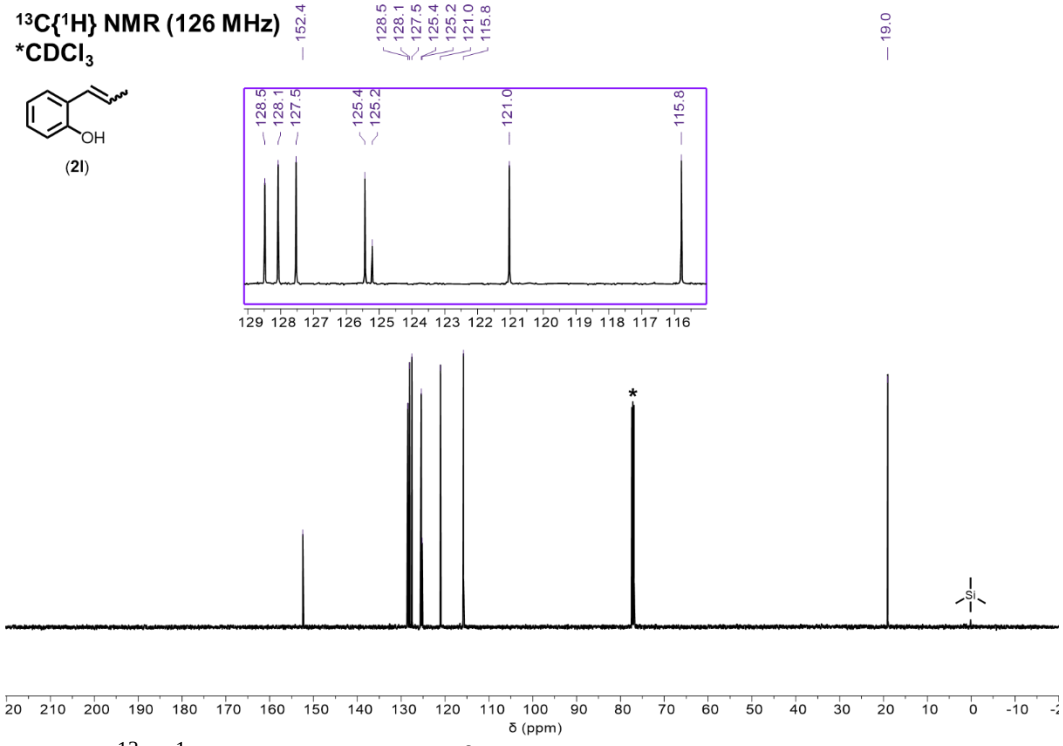

Figure E.104. ^{13}C{^{1}H} NMR spectrum of 2-(1-propenyl)phenol (**2l**) recorded in $CDCl_3$ at 25 °C.

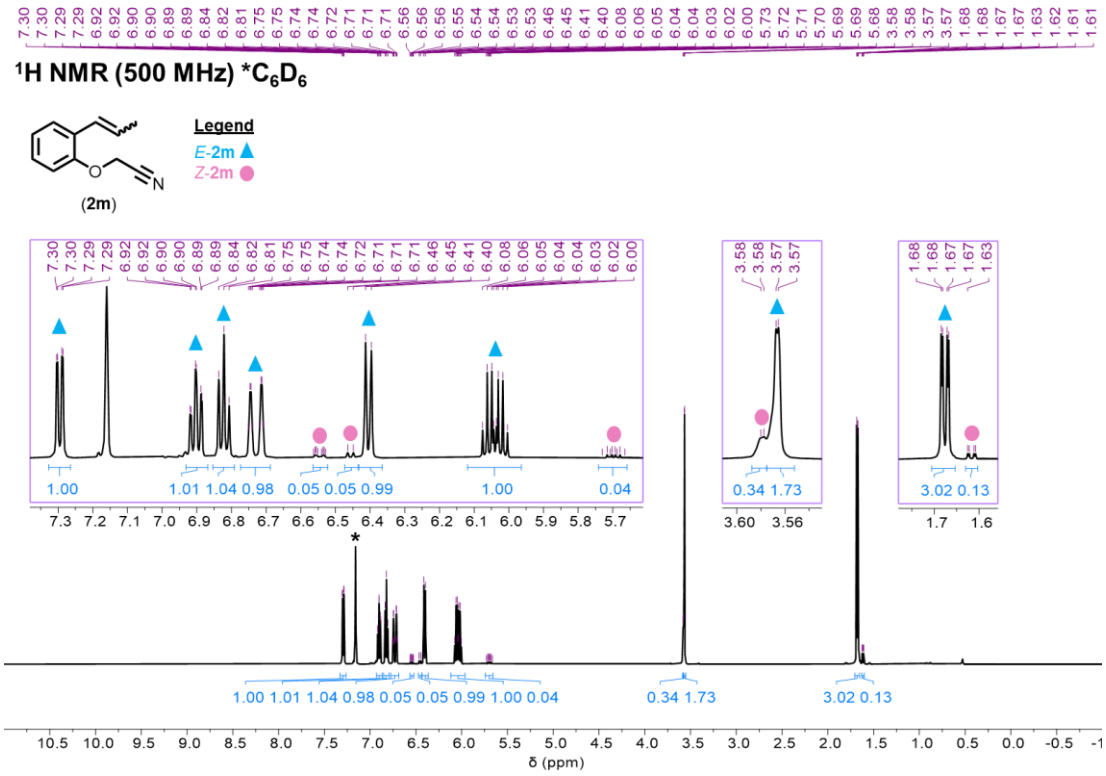

Figure E.105. ^{1}H NMR spectrum of {2-[(1E)-1-propen-1-yl]phenoxy}acetonitrile (**2m**) recorded in C_6D_6 at 25 °C.

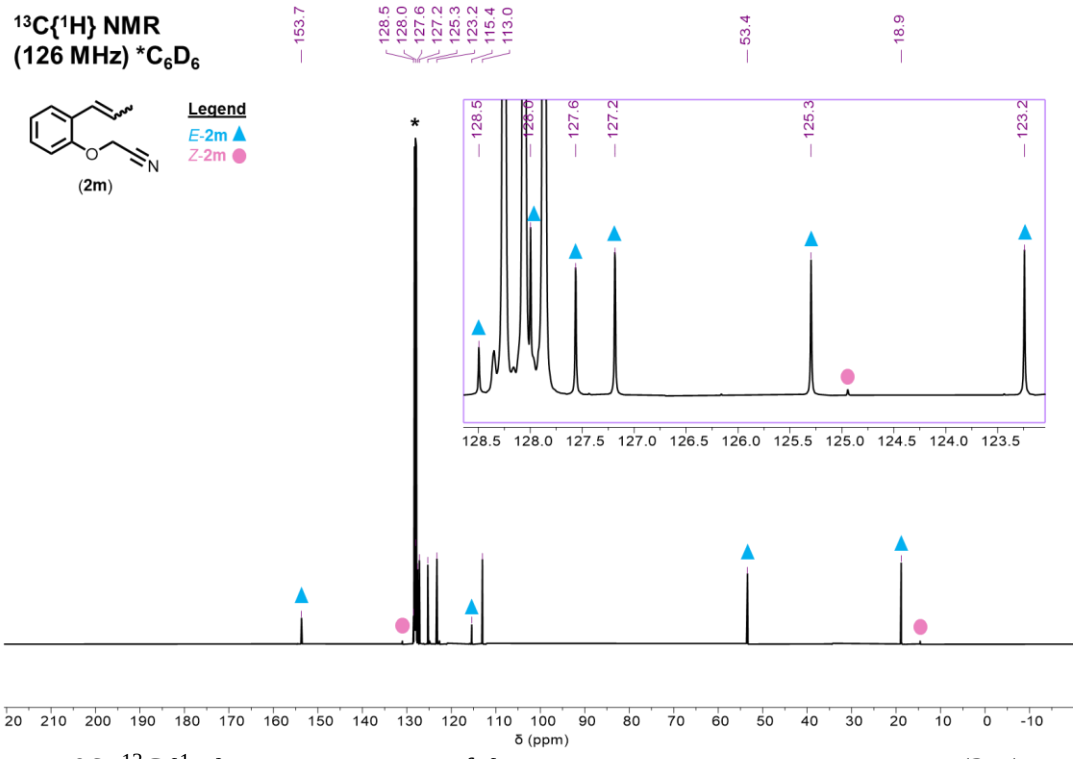

Figure E.106. ^{13}C{^{1}H} NMR spectrum of {2-[(1E)-1-propen-1-yl]phenoxy}acetonitrile (**2m**) recorded in C_6D_6 at 25 °C.

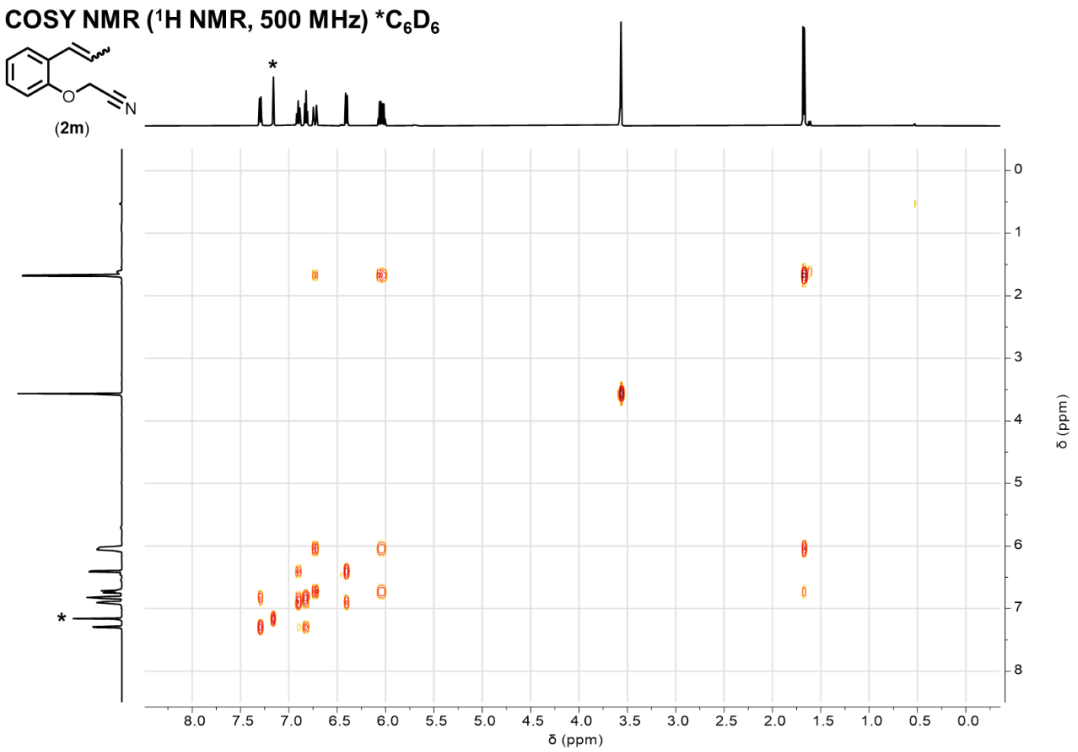

Figure E.107. COSY NMR spectrum of {2-[(1E)-1-propen-1-yl]phenoxy}acetonitrile (**2m**) recorded in C_6D_6 at 25 °C.

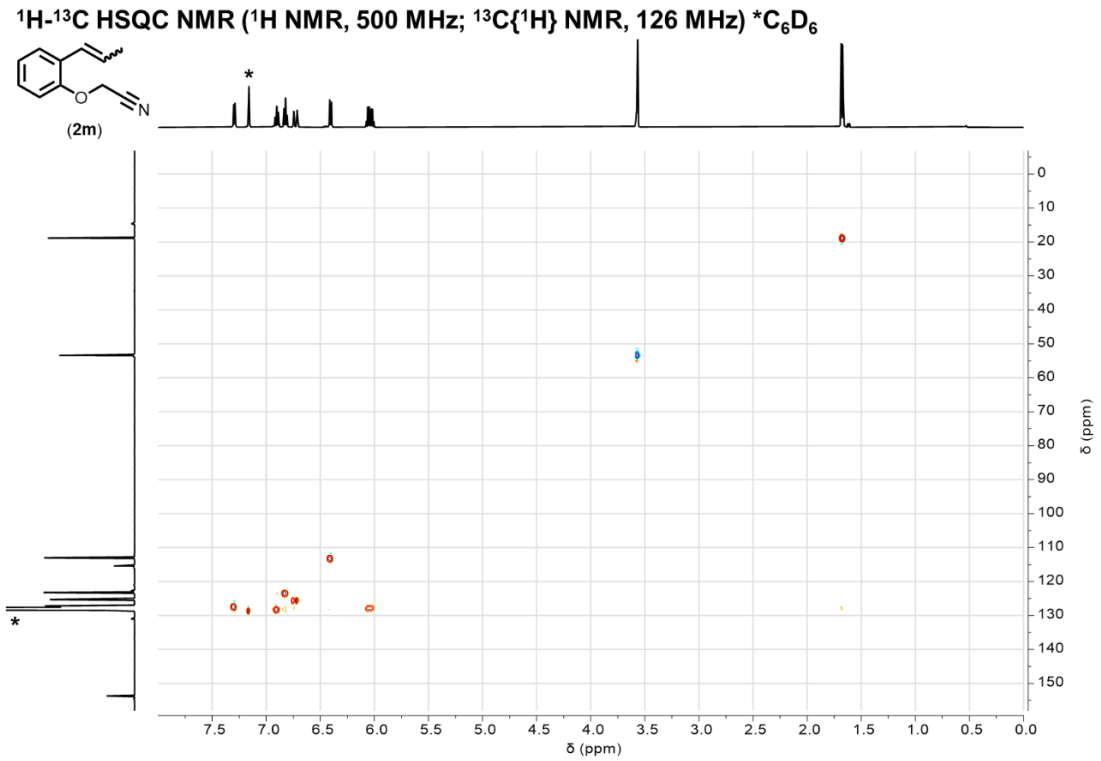

Figure E.108. ^{1}H-^{13}C HSQC NMR spectrum of {2-[(1E)-1-propen-1-yl]phenoxy}acetonitrile (**2m**) recorded in C_6D_6 at 25 °C.

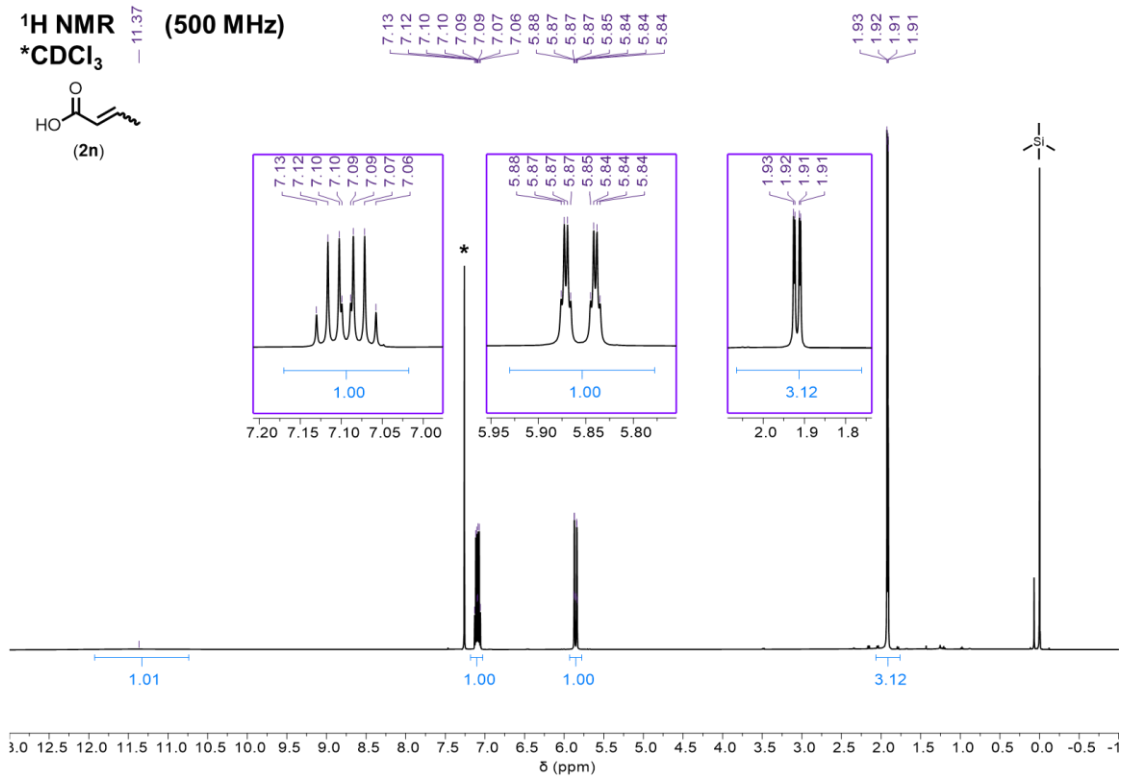

Figure E.109. ^{1}H NMR spectrum of crotonic acid (**2n**) recorded in $CDCl_3$ at 25 °C.

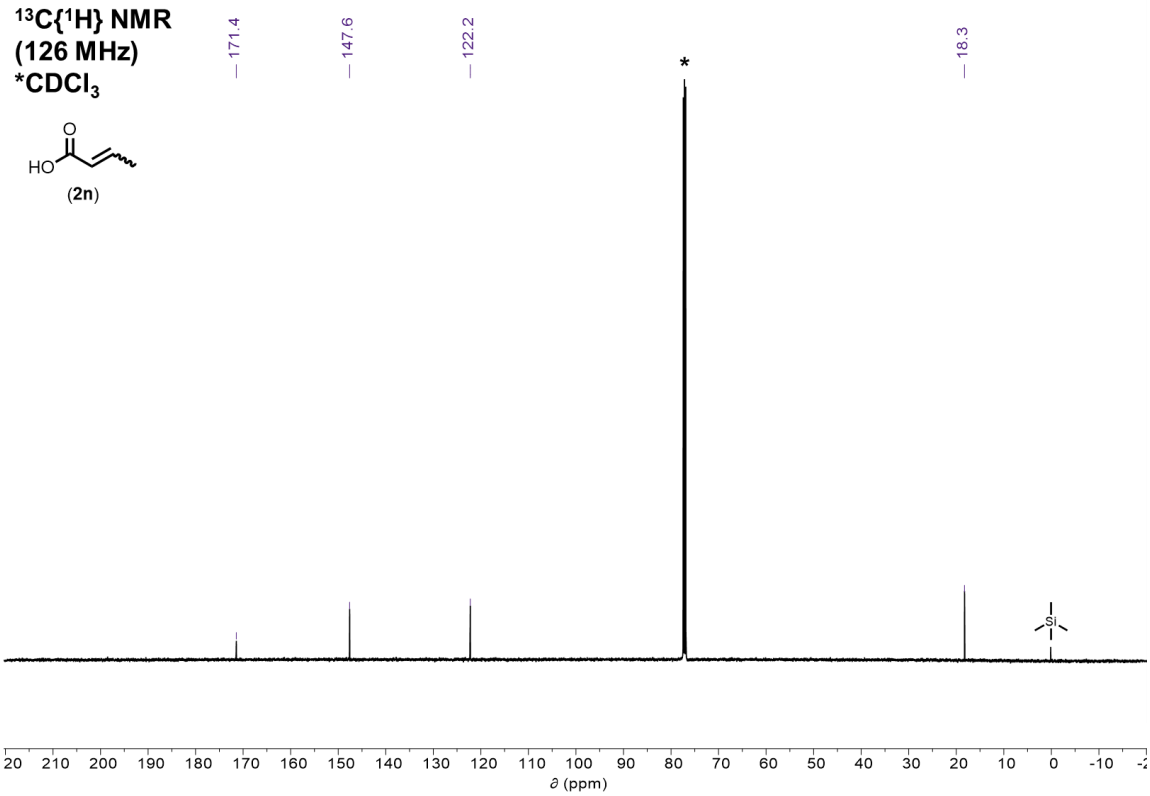

Figure E.110. $^{13}C\{^{1}H\}$ NMR spectrum of crotonic acid (**2n**) recorded in $CDCl_3$ at 25 °C.

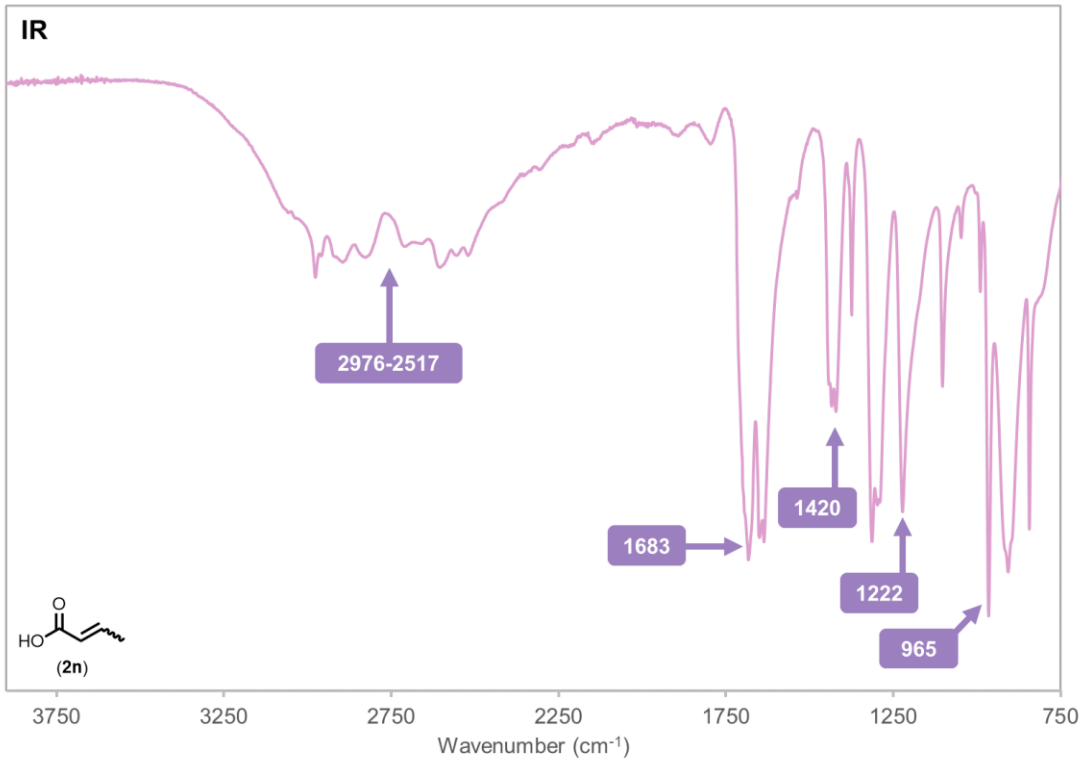

Figure E.111. IR spectrum of crotonic acid (**2n**) recorded neat at 25 °C.

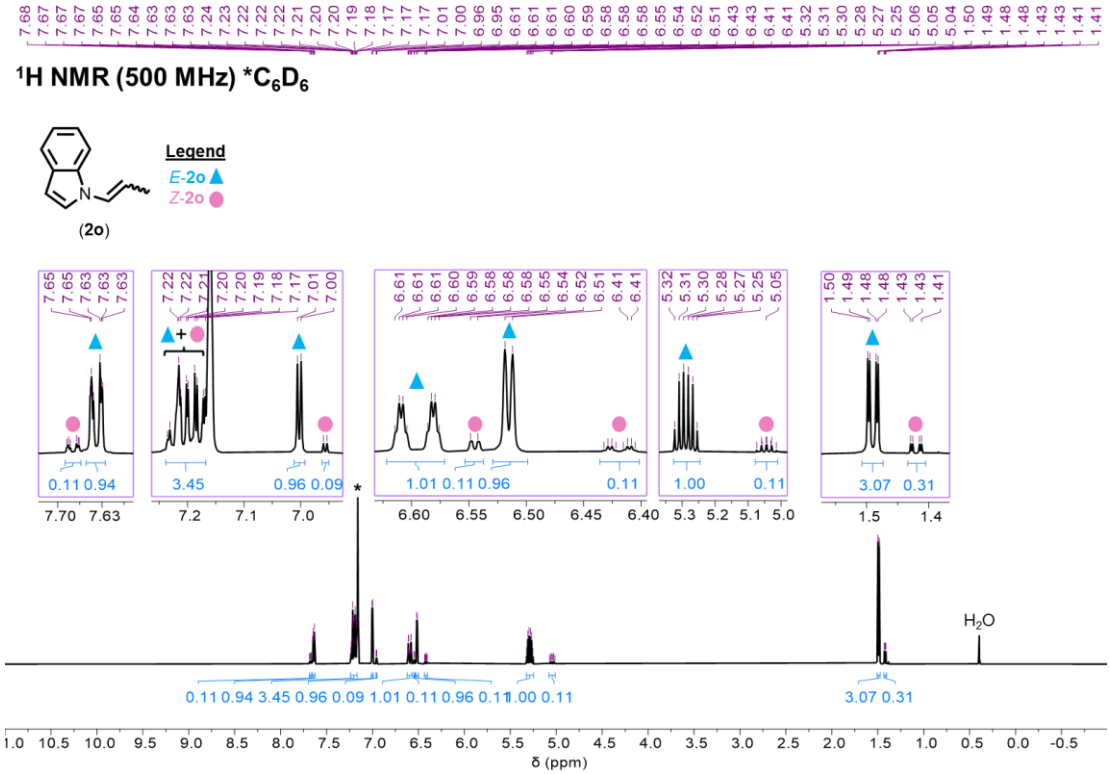

Figure E.112. ^{1}H NMR spectrum of 1-propen-1-yl-1*H*-indole (**2o**) recorded in C_6D_6 at 25 °C.

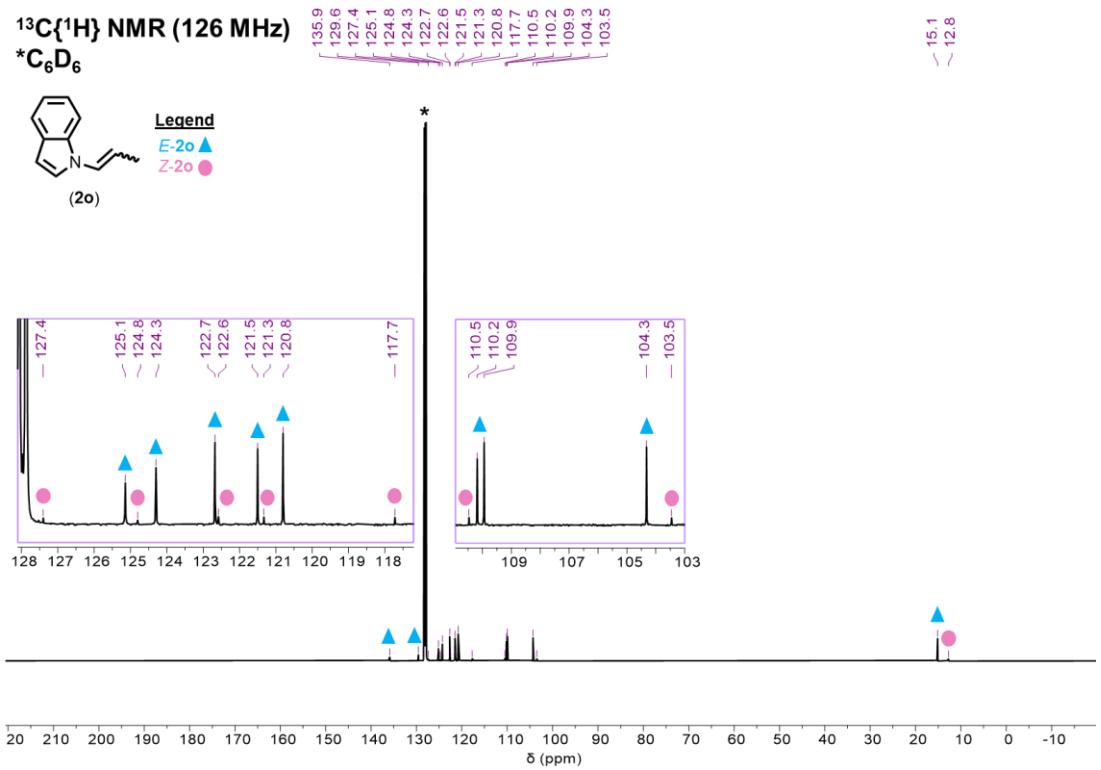

Figure E.113. $^{13}C\{^{1}H\}$ NMR spectrum of 1-propen-1-yl-1*H*-indole (**2o**) recorded in C_6D_6 at 25 °C.

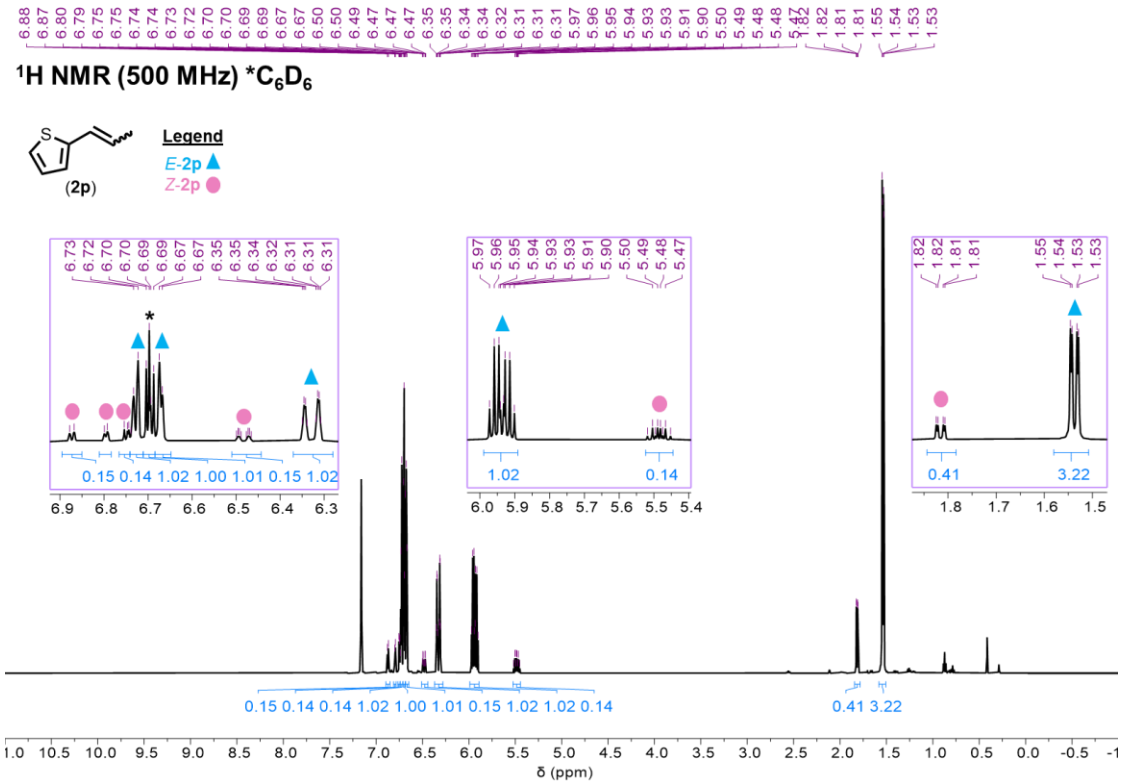

Figure E.114. ^{1}H NMR spectrum of 2-(1-propenyl)-thiophene (**2p**) recorded in C_6D_6 at 25 °C.

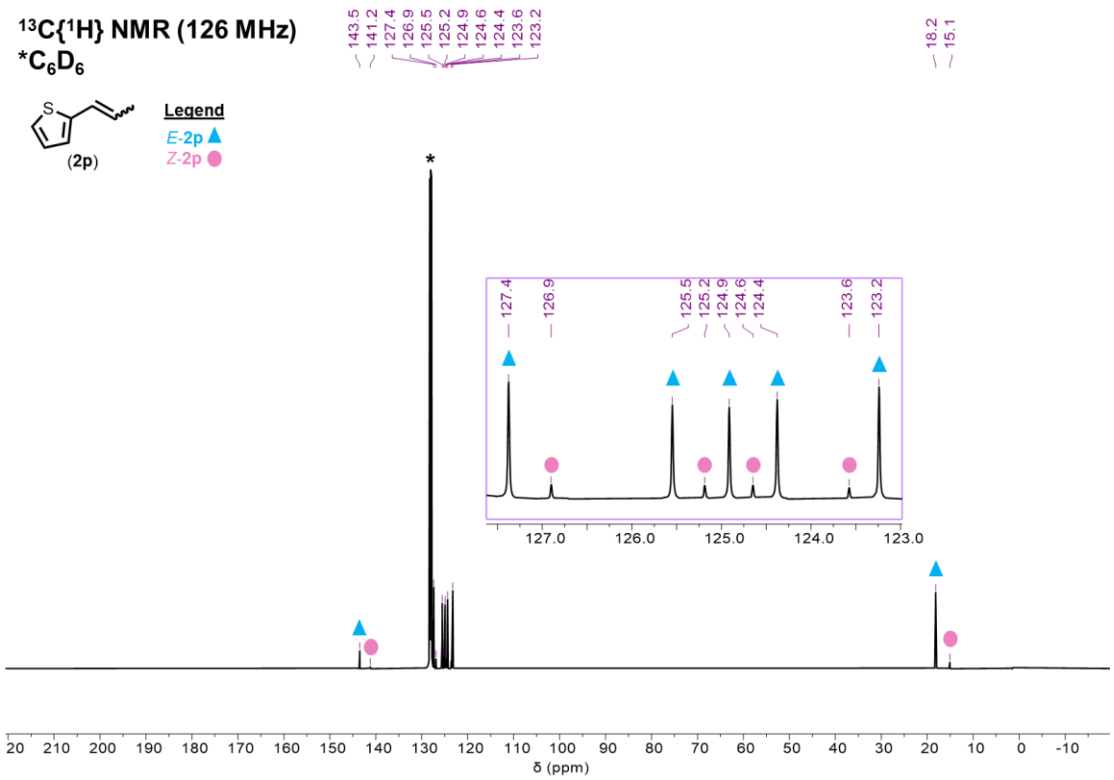

Figure E.115. $^{13}C\{^{1}H\}$ NMR spectrum of 2-(1-propenyl)-thiophene (**2p**) recorded in C_6D_6 at 25 °C.

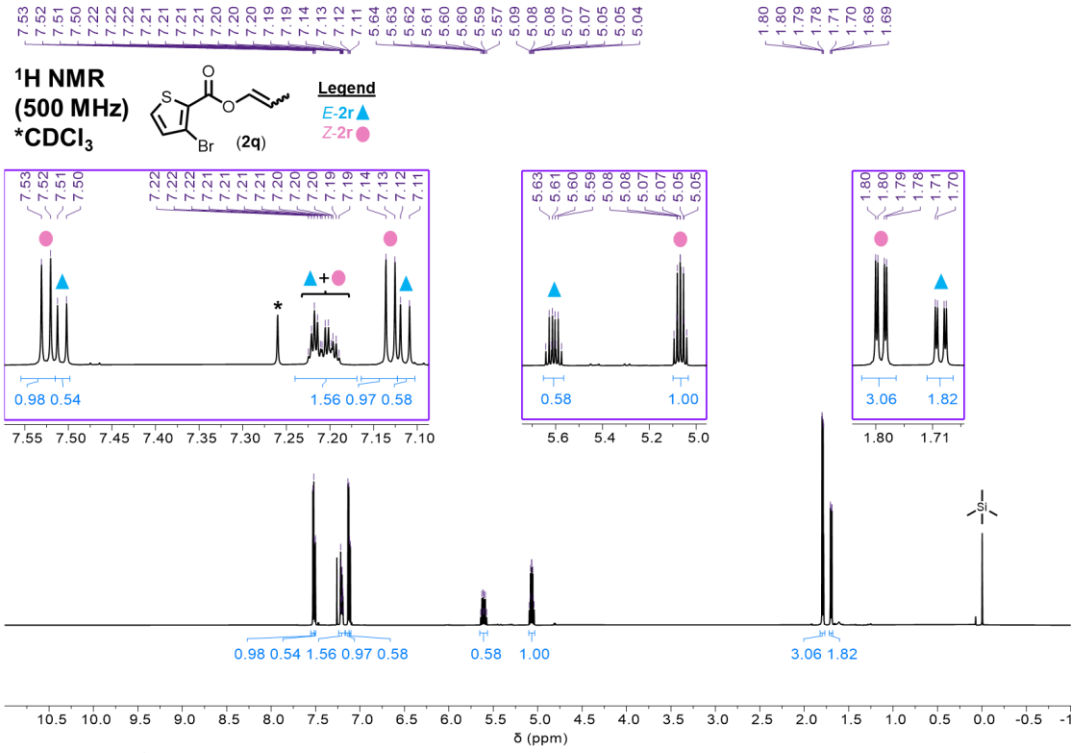

Figure E.116. ^{1}H NMR spectrum of 1-propen-1-yl-3-bromo-2-thiophenecarboxylate (**2q**) recorded in $CDCl_3$ at 25 °C.

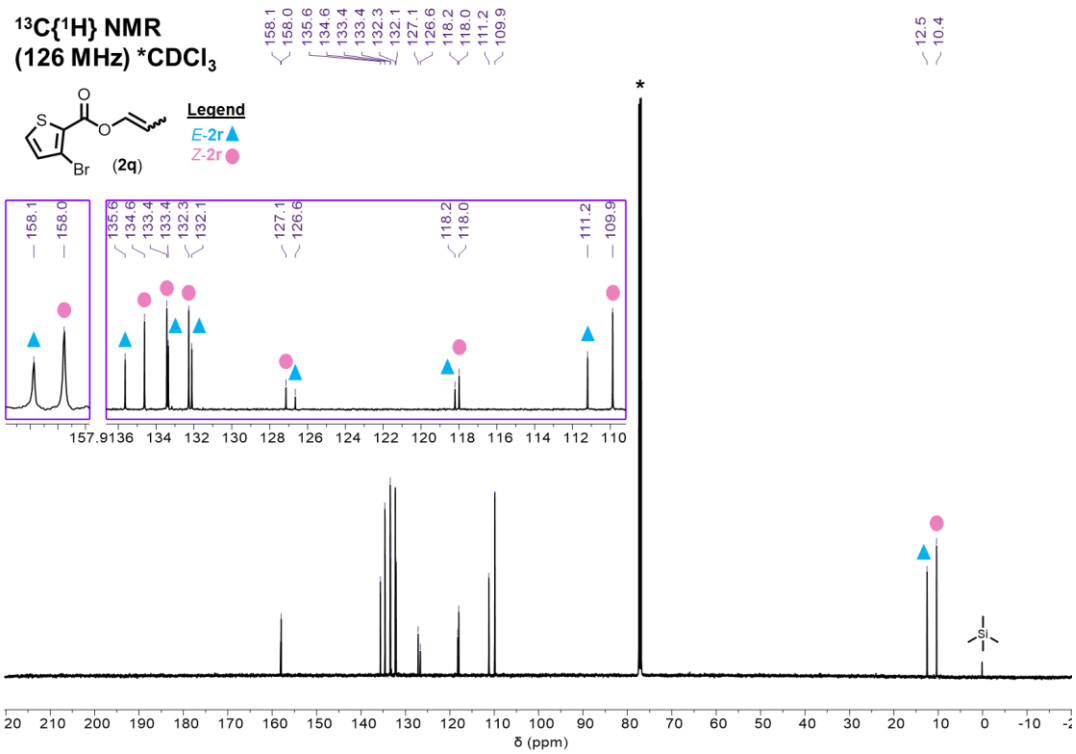

Figure E.117. $^{13}C\{^{1}H\}$ NMR spectrum of 1-propen-1-yl-3-bromo-2-thiophenecarboxylate (**2q**) recorded in $CDCl_3$ at 25 °C.

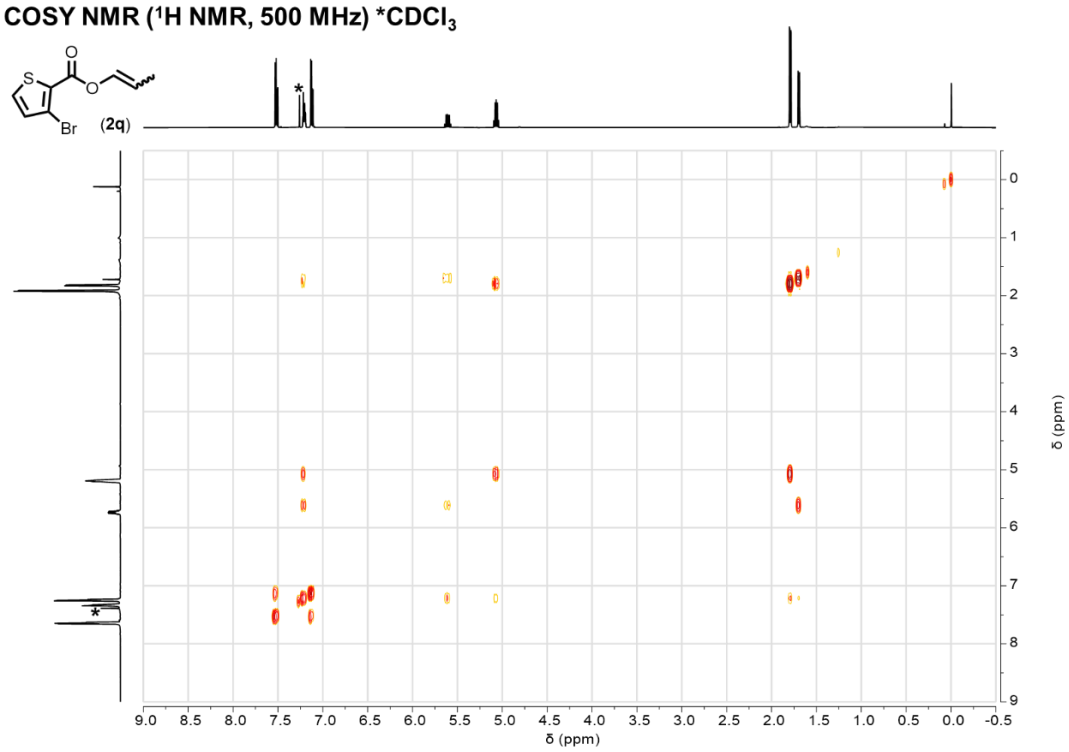

Figure E.118. COSY NMR spectrum of 1-propen-1-yl-3-bromo-2-thiophenecarboxylate (**2q**) recorded in $CDCl_3$ at 25 °C.

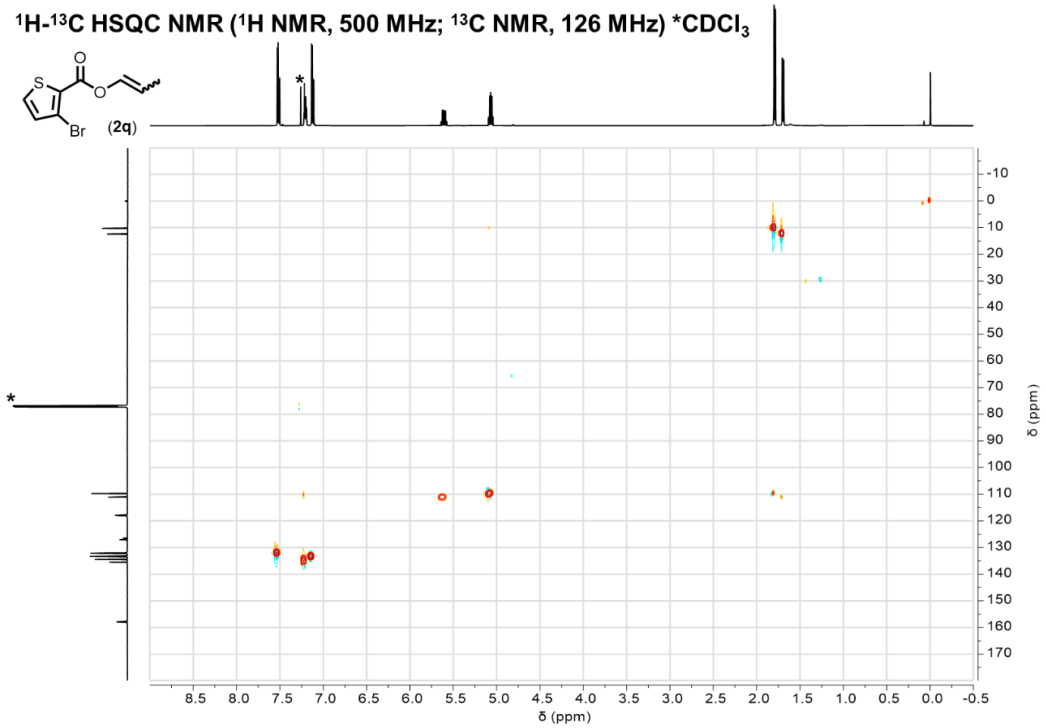

Figure E.119. ^{1}H-^{13}C HSQC NMR spectrum of 1-propen-1-yl-3-bromo-2-thiophenecarboxylate (**2q**) recorded in $CDCl_3$ at 25 °C.

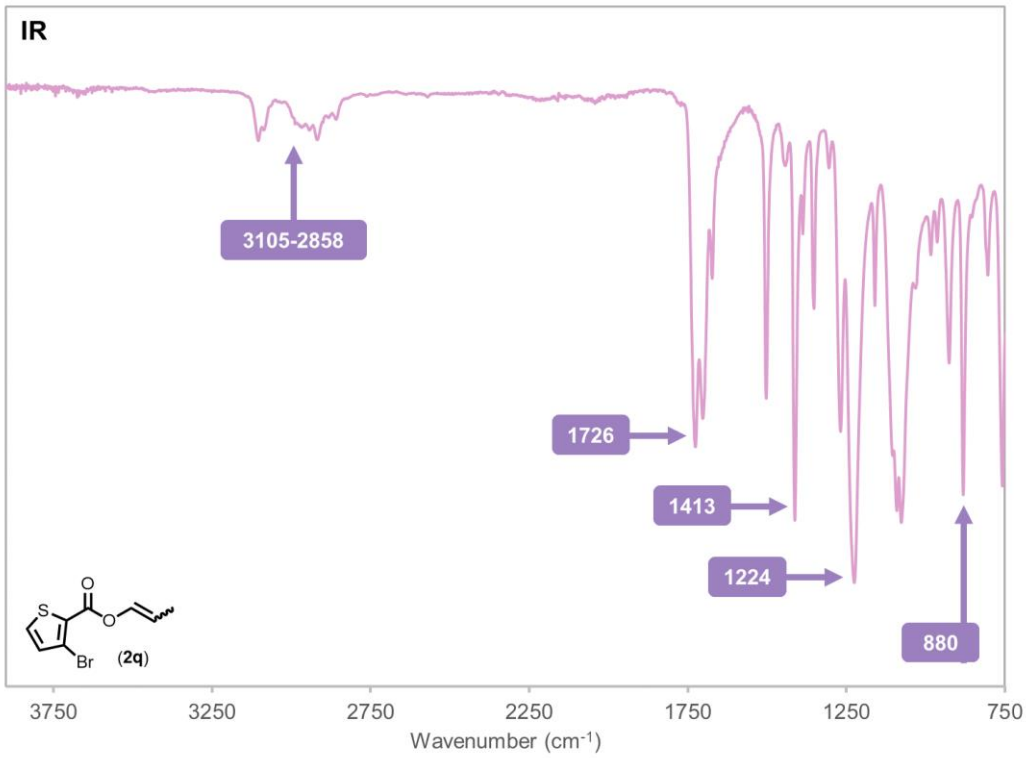

Figure E.120. IR spectrum of 1-propen-1-yl-3-bromo-2-thiophenecarboxylate (**2q**) recorded neat at 25 °C.

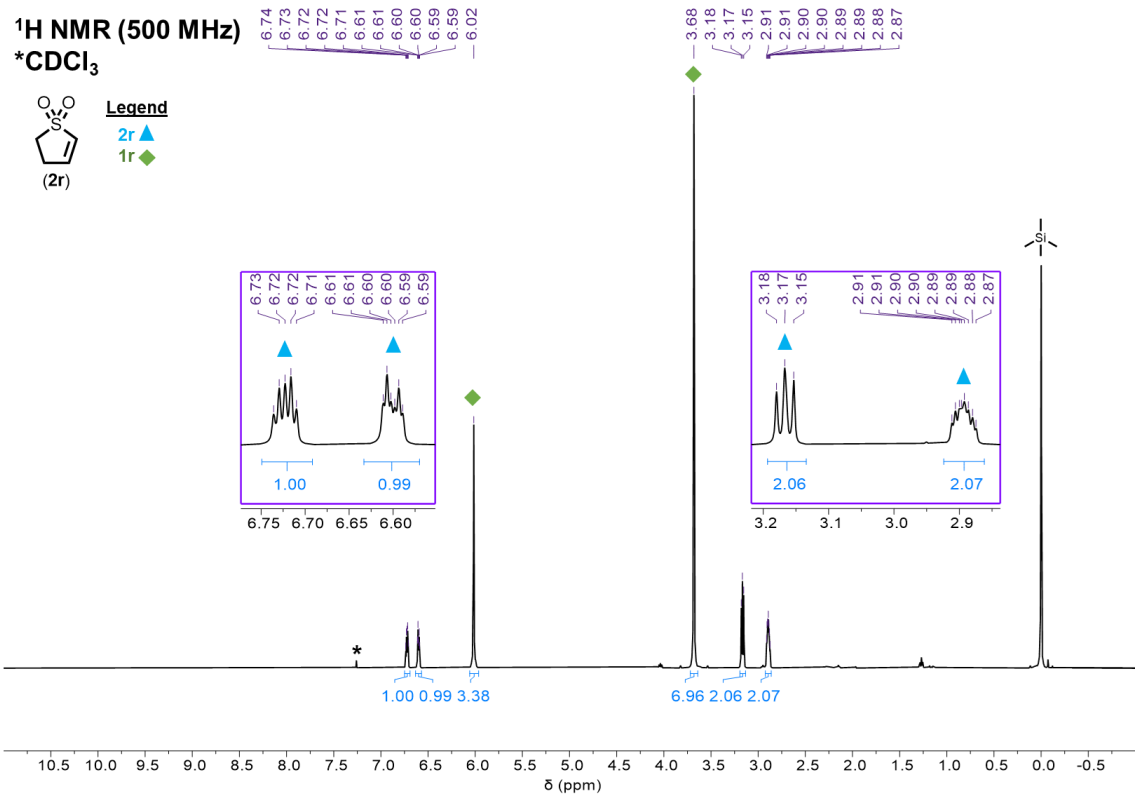

Figure E.121. ^{1}H NMR spectrum of 2-sulfolene (**2r**) recorded in $CDCl_3$ at 25 °C.

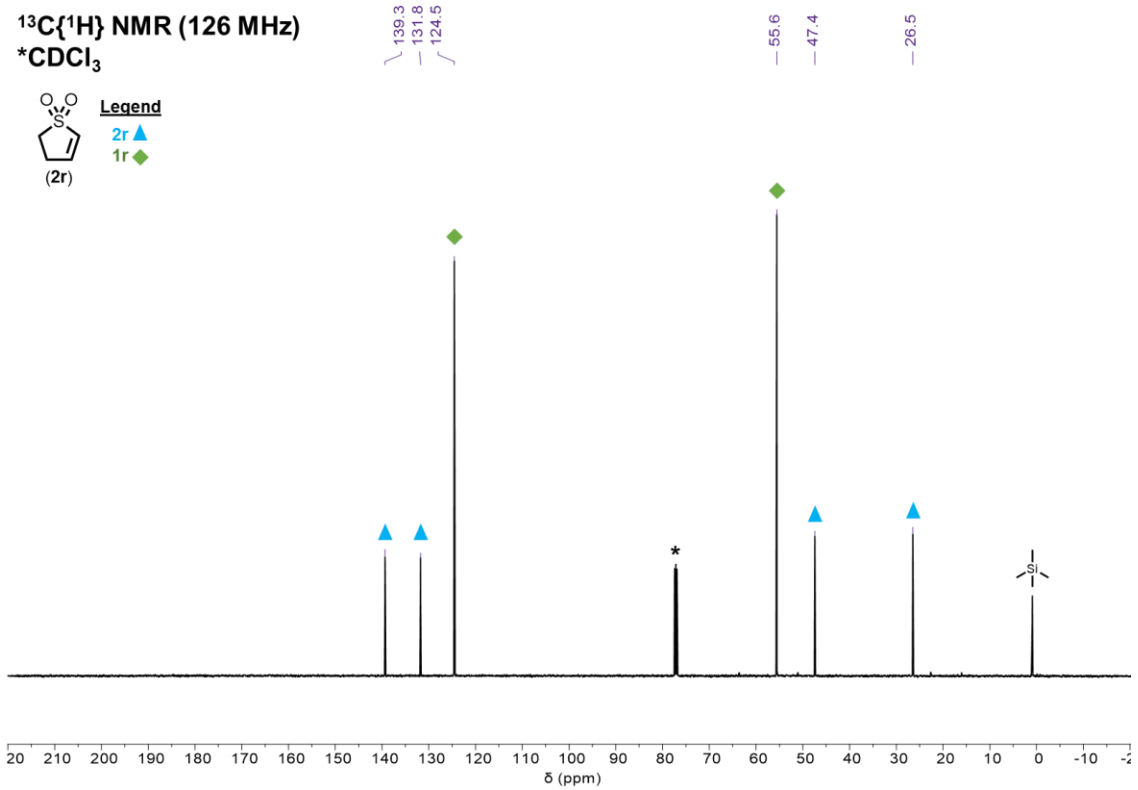

Figure E.122. $^{13}C\{^{1}H\}$ NMR spectrum of 2-sulfolene (**2r**) recorded in $CDCl_3$ at 25 °C.

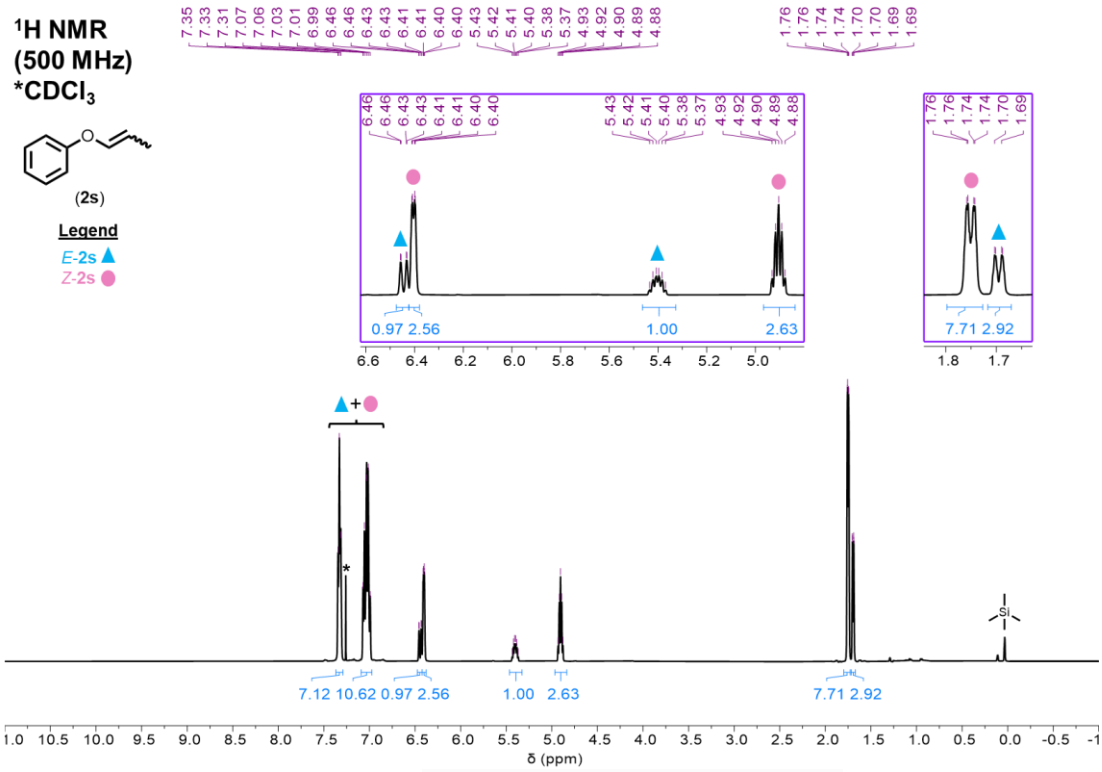

Figure E.123. ^{1}H NMR spectrum of (1-propen-1-yloxy)benzene (**2s**) recorded in $CDCl_3$ at 25 °C.

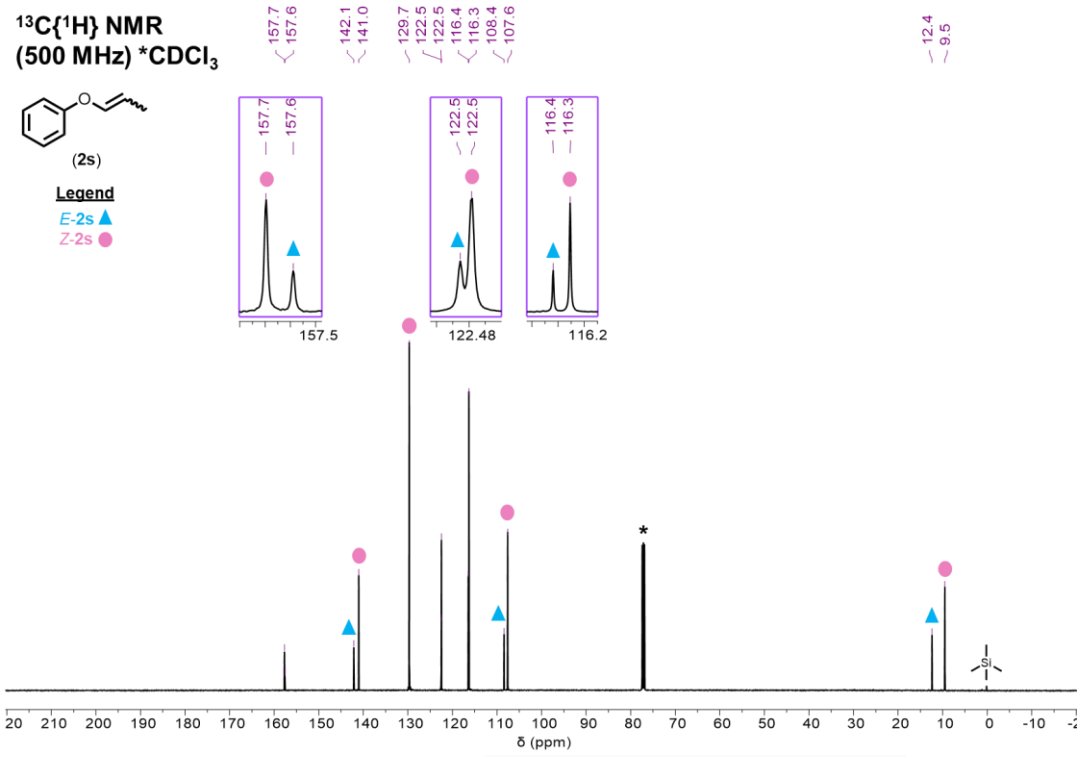

Figure E.124. ^{13}C{^{1}H} NMR spectrum of (1-propen-1-yloxy)benzene (**2s**) recorded in $CDCl_3$ at 25 °C.

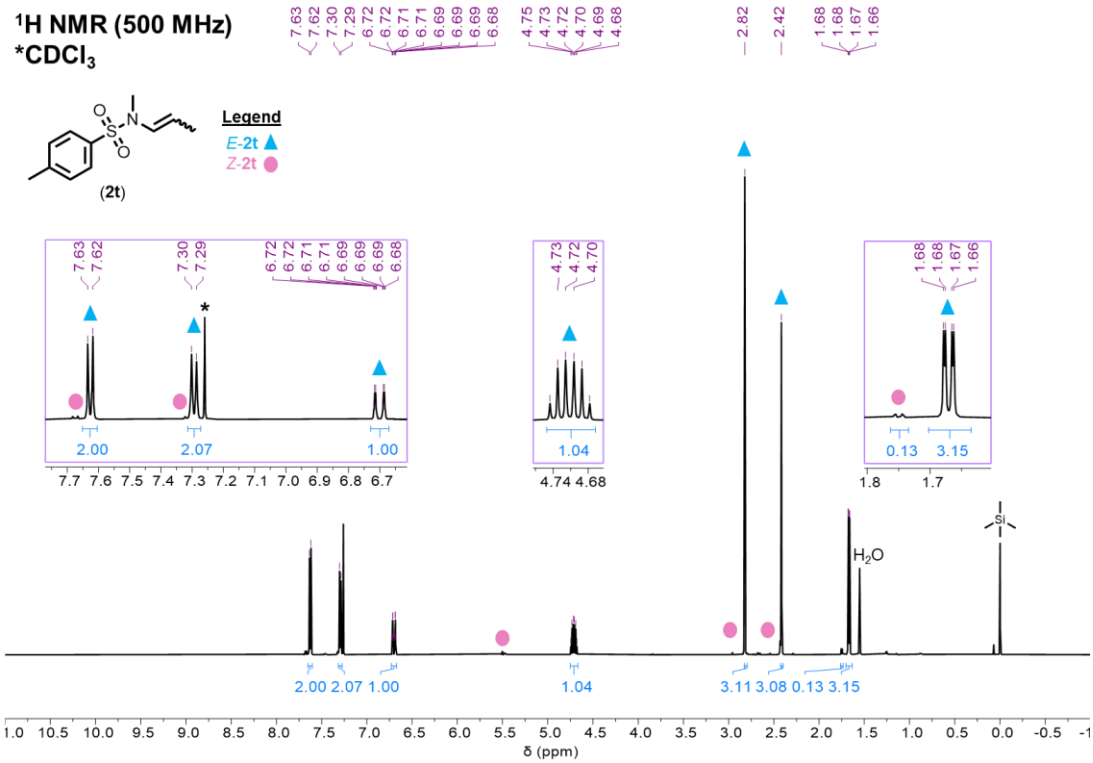

Figure E.125. ^{1}H NMR spectrum of *N*-methyl-*N*-(prop-1-enyl)-p-toluenesulfonamide (**2t**) recorded in $CDCl_3$ at 25 °C.

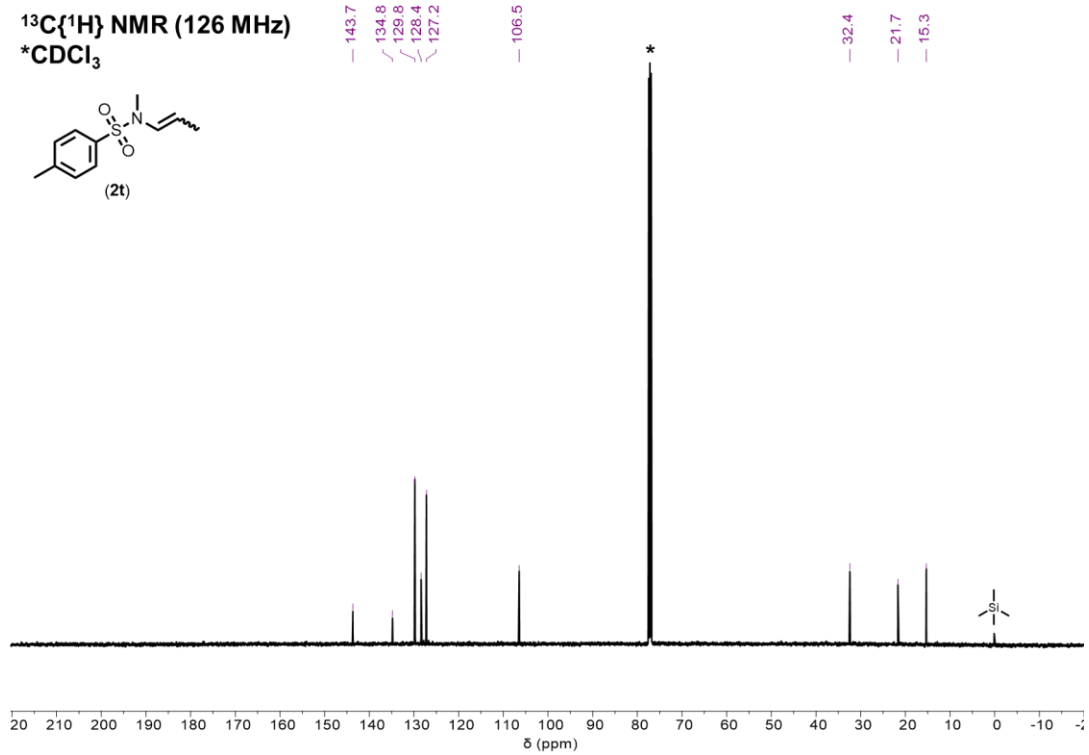

Figure E.126. ^{13}C{^{1}H} NMR spectrum of *N*-methyl-*N*-(prop-1-enyl)-p-toluenesulfonamide (**2t**) recorded in $CDCl_3$ at 25 °C.

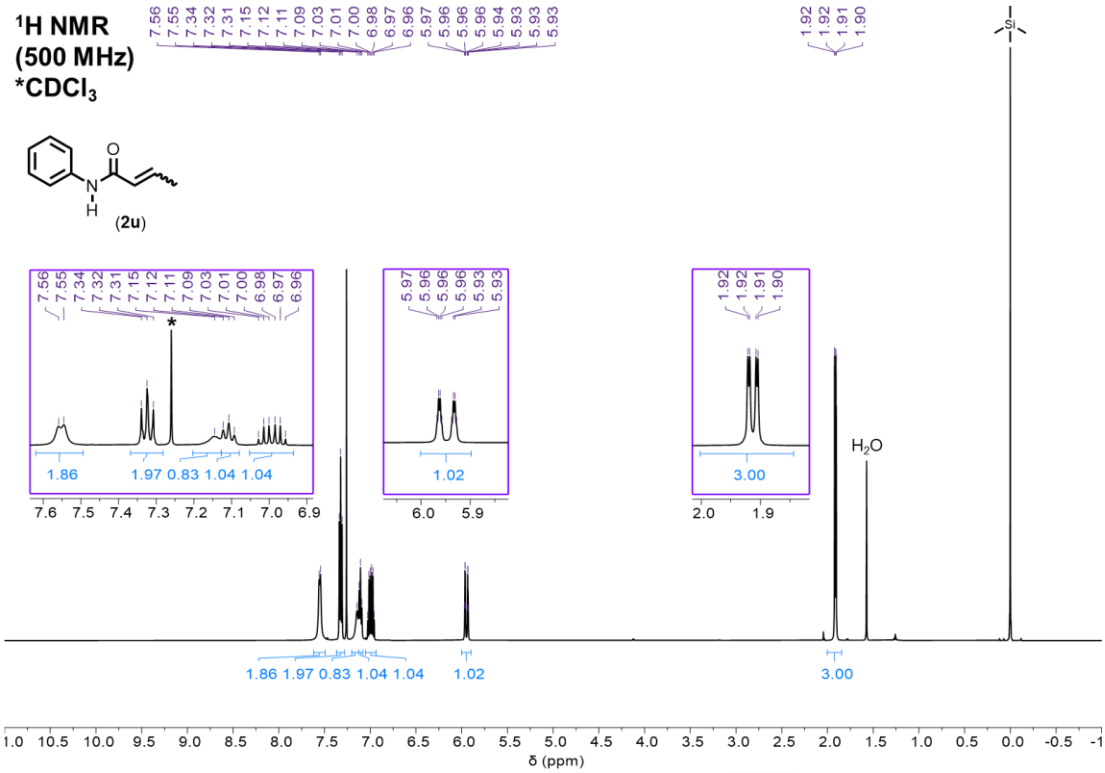

Figure E.127. ^{1}H NMR spectrum of *N*-phenyl-2-butenamide (**2u**) recorded in $CDCl_3$ at 25 °C.

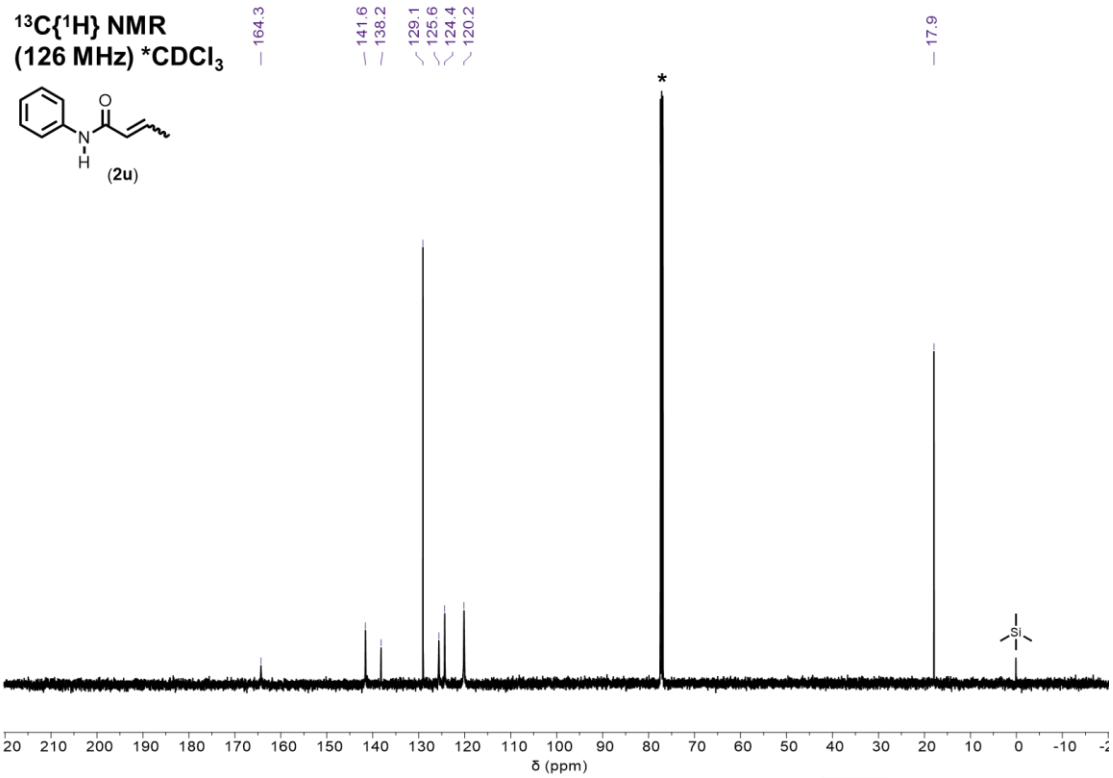

Figure E.128. $^{13}C\{^{1}H\}$ NMR spectrum of *N*-phenyl-2-butenamide (**2u**) recorded in $CDCl_3$ at 25 °C.

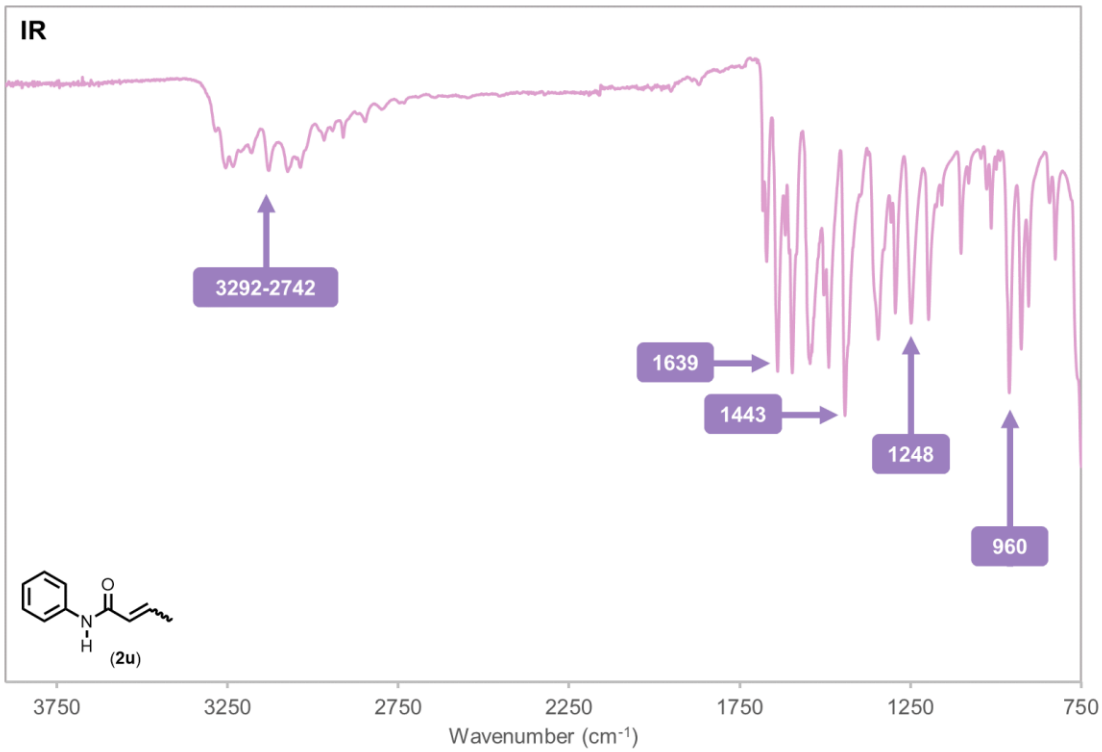

Figure E.129. IR spectrum of *N*-phenyl-2-butenamide (**2u**) recorded neat at 25 °C.

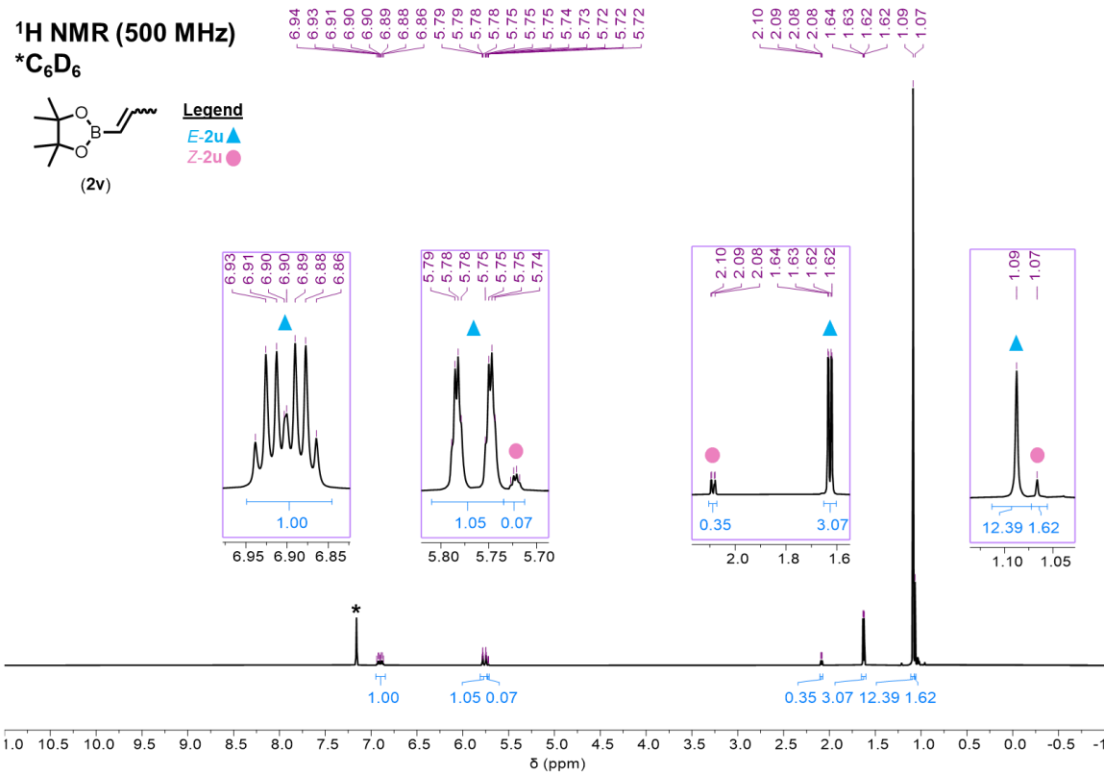

Figure E.130. ^{1}H NMR spectrum of 4,4,5,5-tetramethyl-2-1-propen-1-yl-1,3,2-dioxaborolane (**2v**) recorded in C_6D_6 at 25 °C.

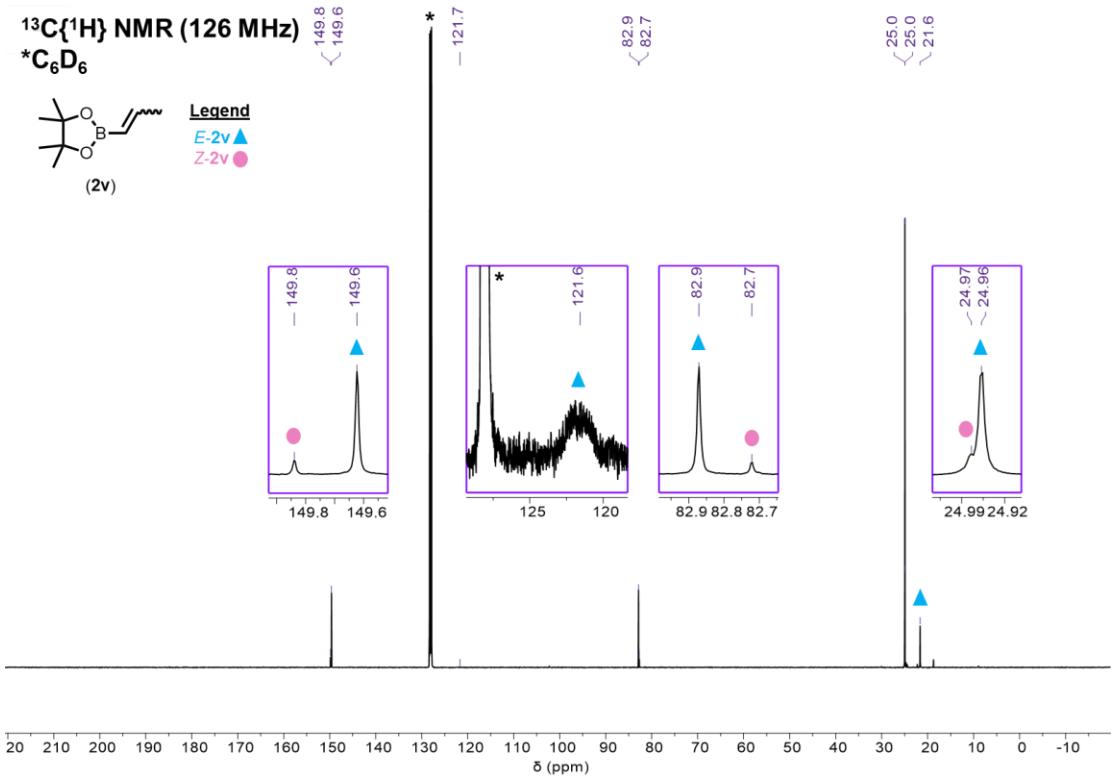

Figure E.131. $^{13}C\{^{1}H\}$ NMR spectrum of 4,4,5,5-tetramethyl-2-1-propen-1-yl-1,3,2-dioxaborolane (**2v**) recorded in C_6D_6 at 25 °C.

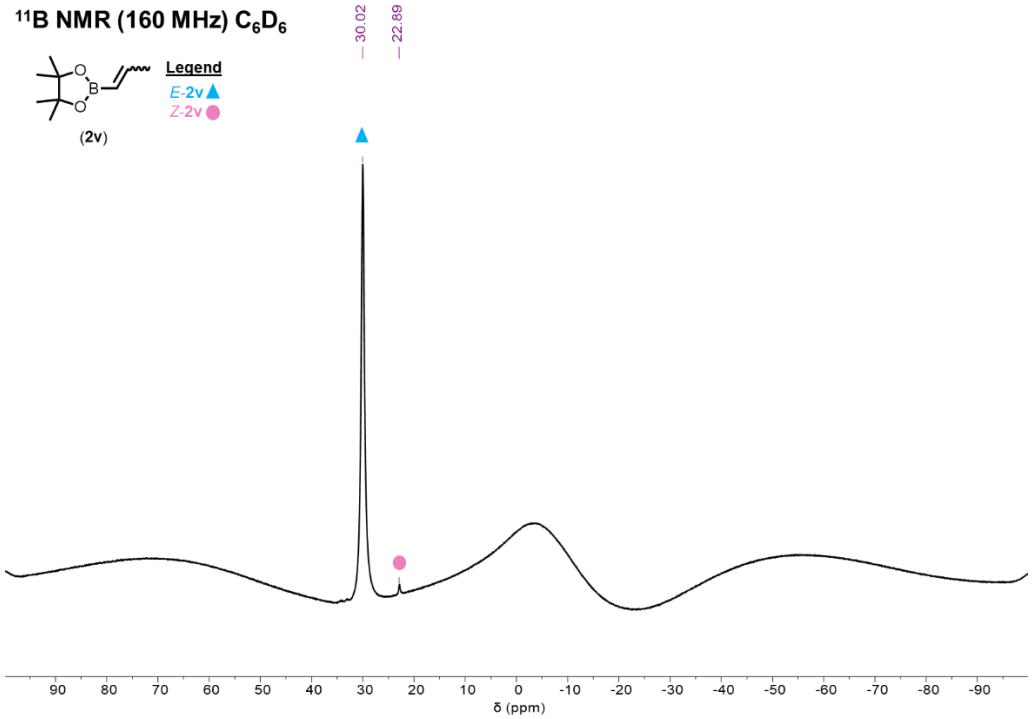

Figure E.132. ^{11}B NMR spectrum of 4,4,5,5-tetramethyl-2-1-propen-1-yl-1,3,2-dioxaborolane (**2v**) recorded in C_6D_6 at 25 °C.

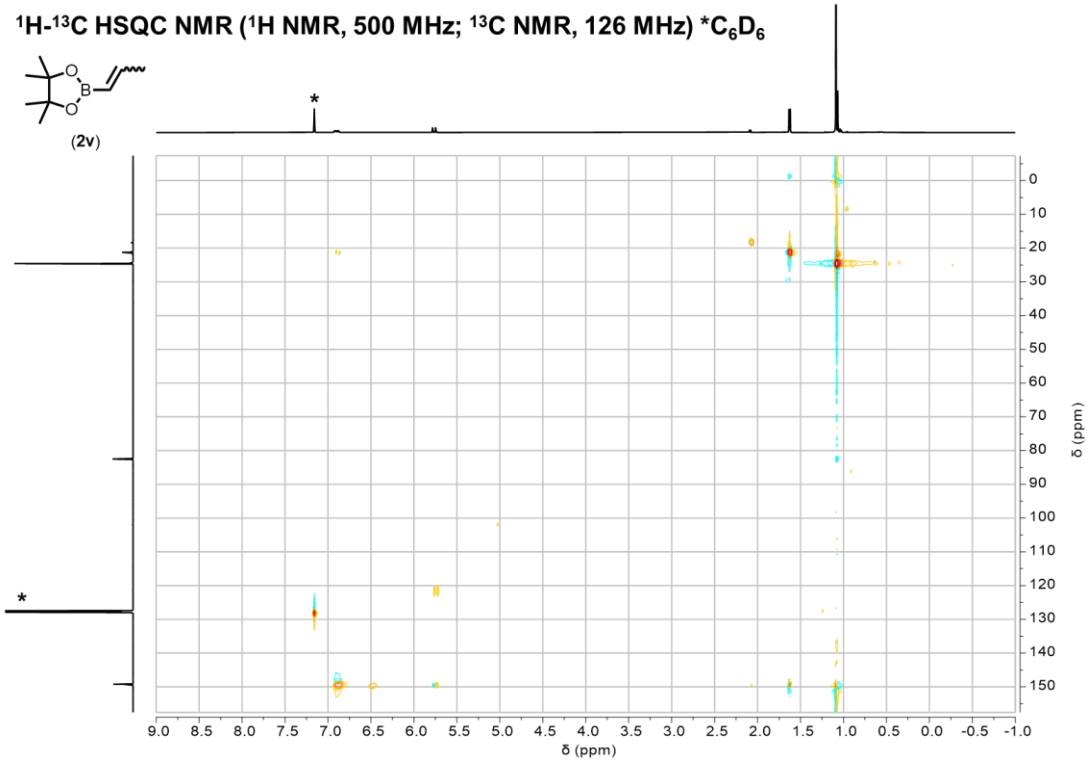

Figure E.133. ^{1}H-^{13}C NMR spectrum of 4,4,5,5-tetramethyl-2-1-propen-1-yl-1,3,2-dioxaborolane (**2v**) recorded in C_6D_6 at 25 °C.

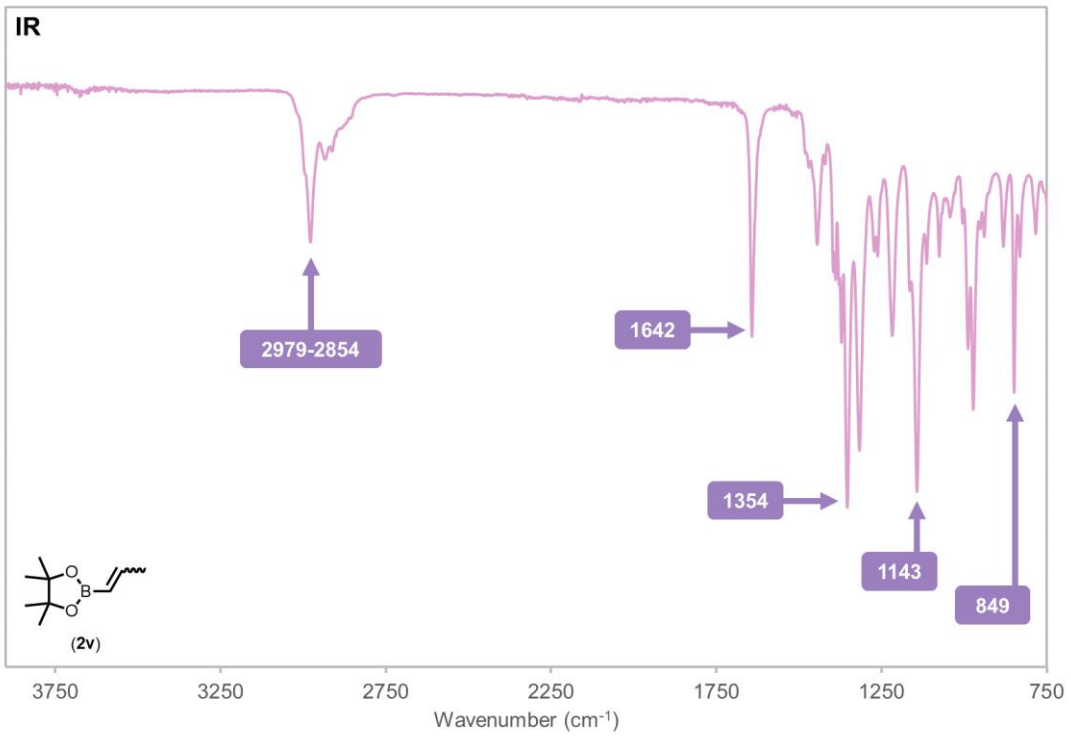

Figure E.134. IR spectrum of 4,4,5,5-tetramethyl-2-1-propen-1-yl-1,3,2-dioxaborolane (**2v**) recorded neat at 25 °C.

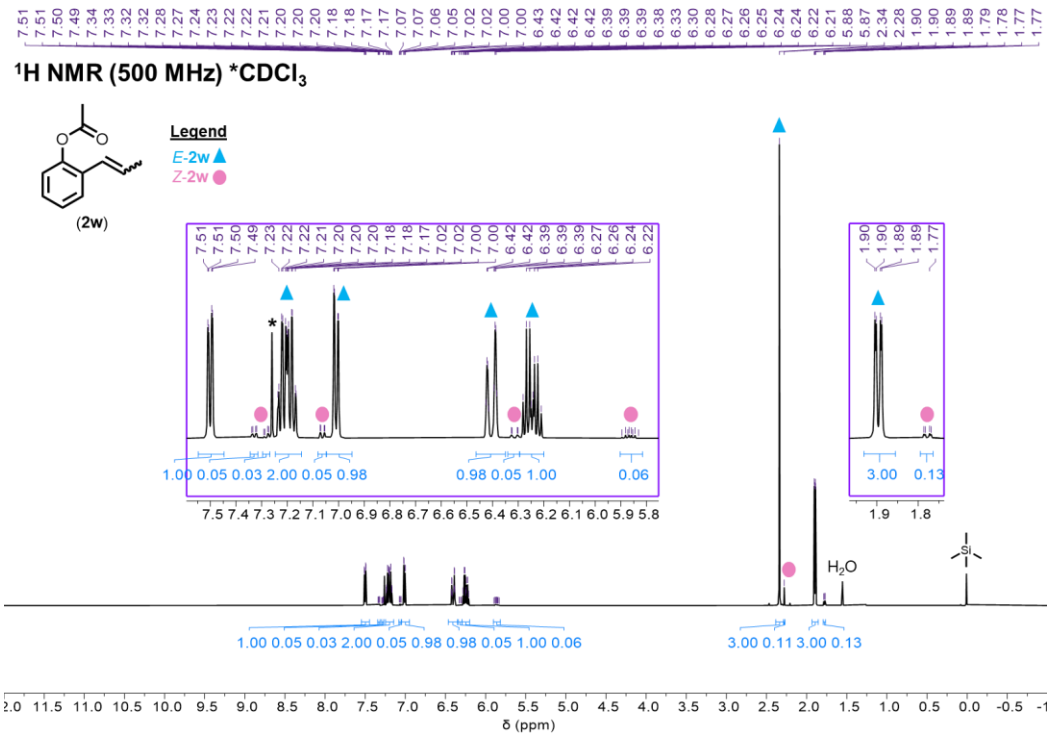

Figure E.135. ^{1}H NMR spectrum of 2-(1-propen-1-yl)phenyl acetate (**2w**) recorded in $CDCl_3$ at 25 °C.

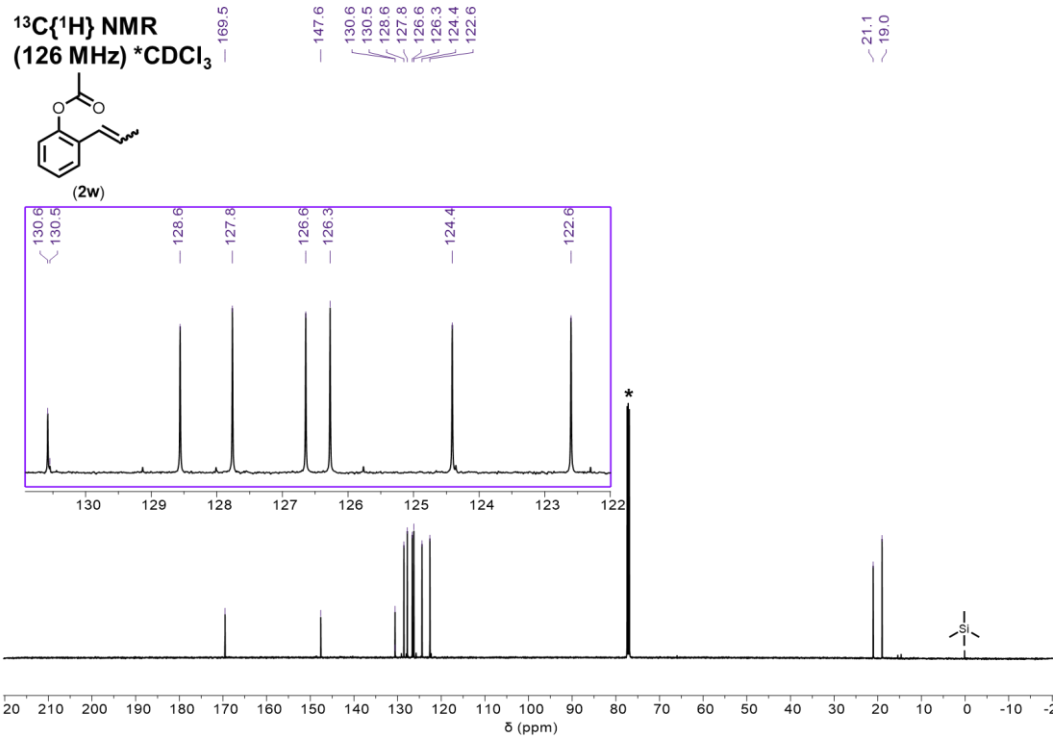

Figure E.136. ^{13}C{^{1}H} NMR spectrum of 2-(1-propen-1-yl)phenyl acetate (**2w**) recorded in $CDCl_3$ at 25 °C.

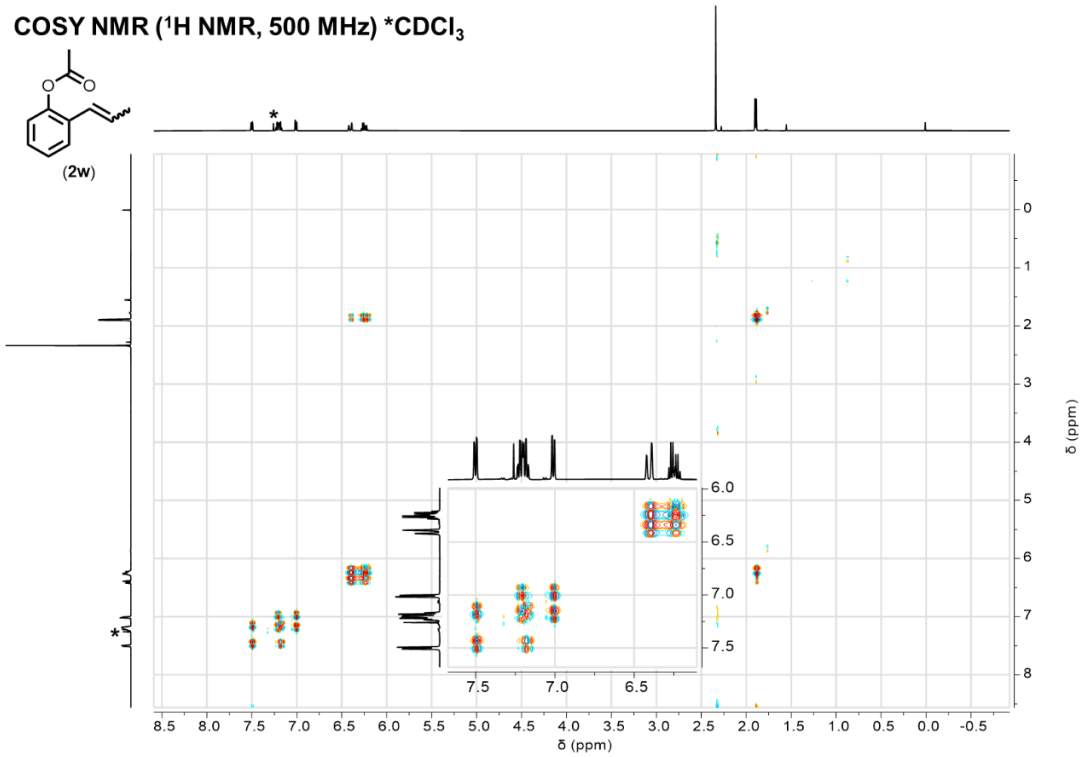

Figure E.137. COSY NMR spectrum of 2-(1-propen-1-yl)phenyl acetate (**2w**) recorded in $CDCl_3$ at 25 °C.

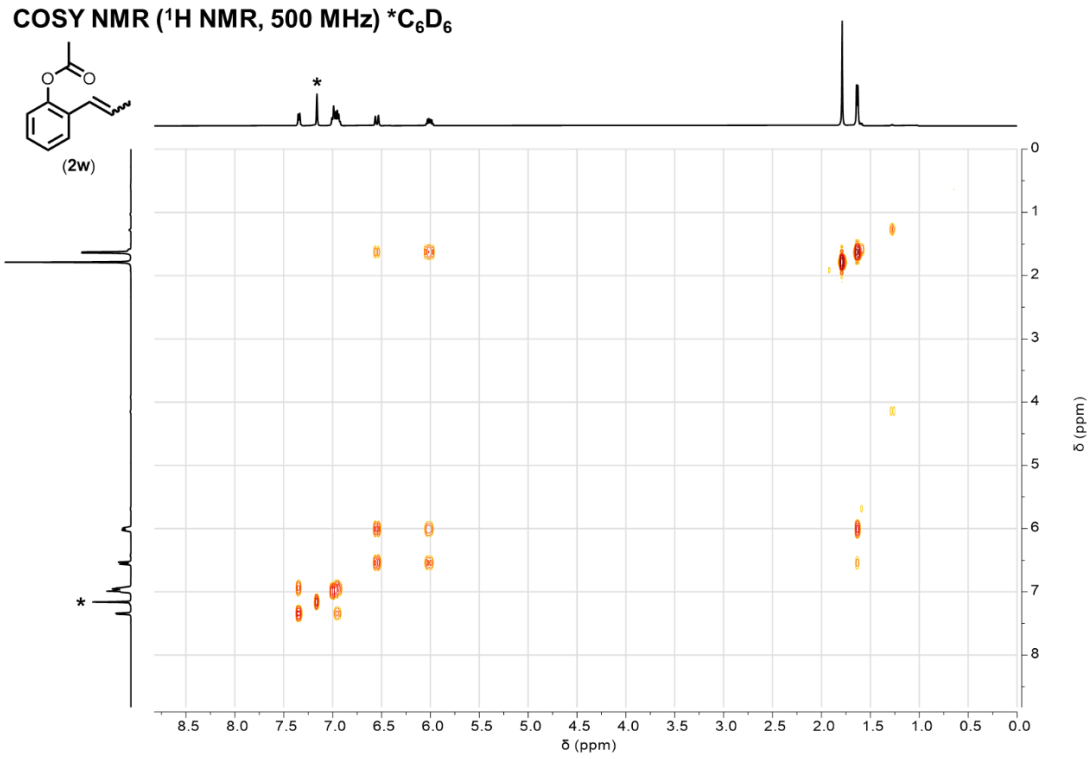

Figure E.138. COSY NMR spectrum of 2-(1-propen-1-yl)phenyl acetate (**2w**) recorded in C_6D_6 at 25 °C.

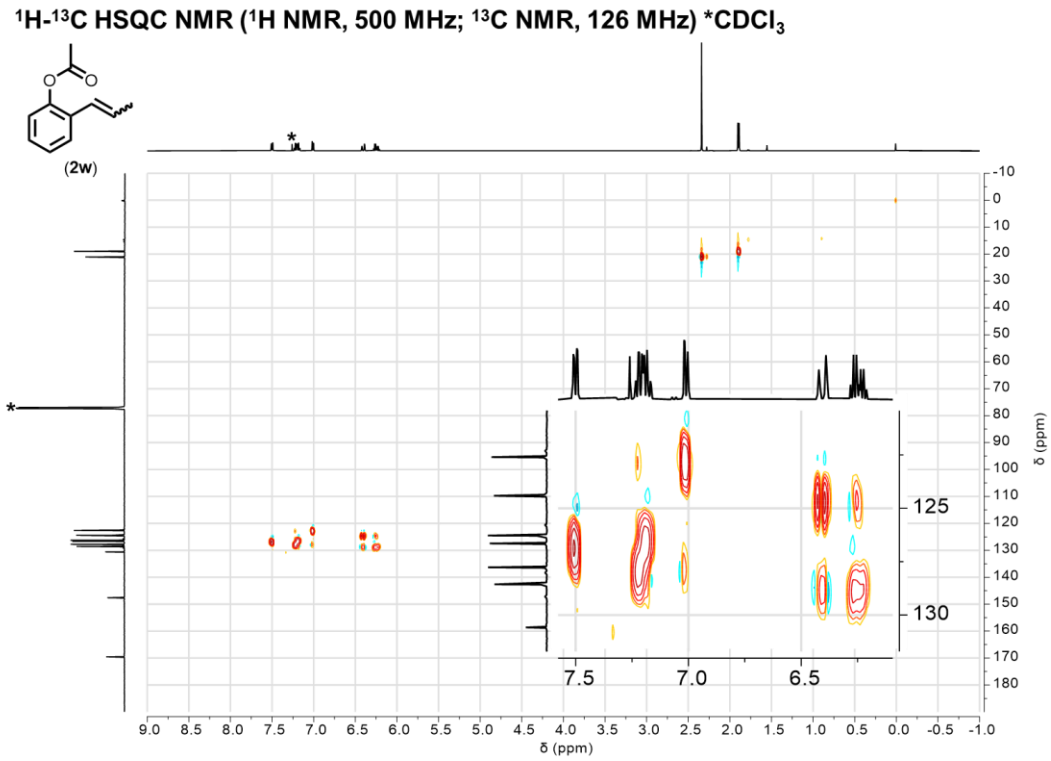

Figure E.139. ^{1}H-^{13}C HSQC NMR spectrum of 2-(1-propen-1-yl)phenyl acetate (**2w**) recorded in $CDCl_3$ at 25 °C.

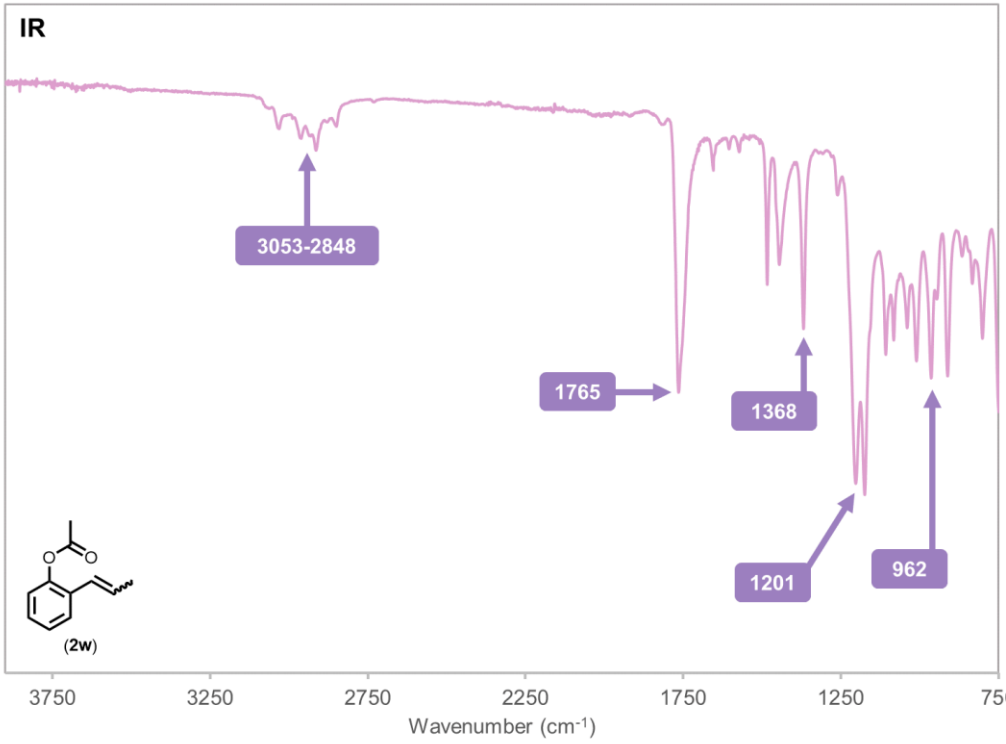

Figure E.140. IR spectrum of 2-(1-propen-1-yl)phenyl acetate (**2w**) recorded neat at 25 °C.

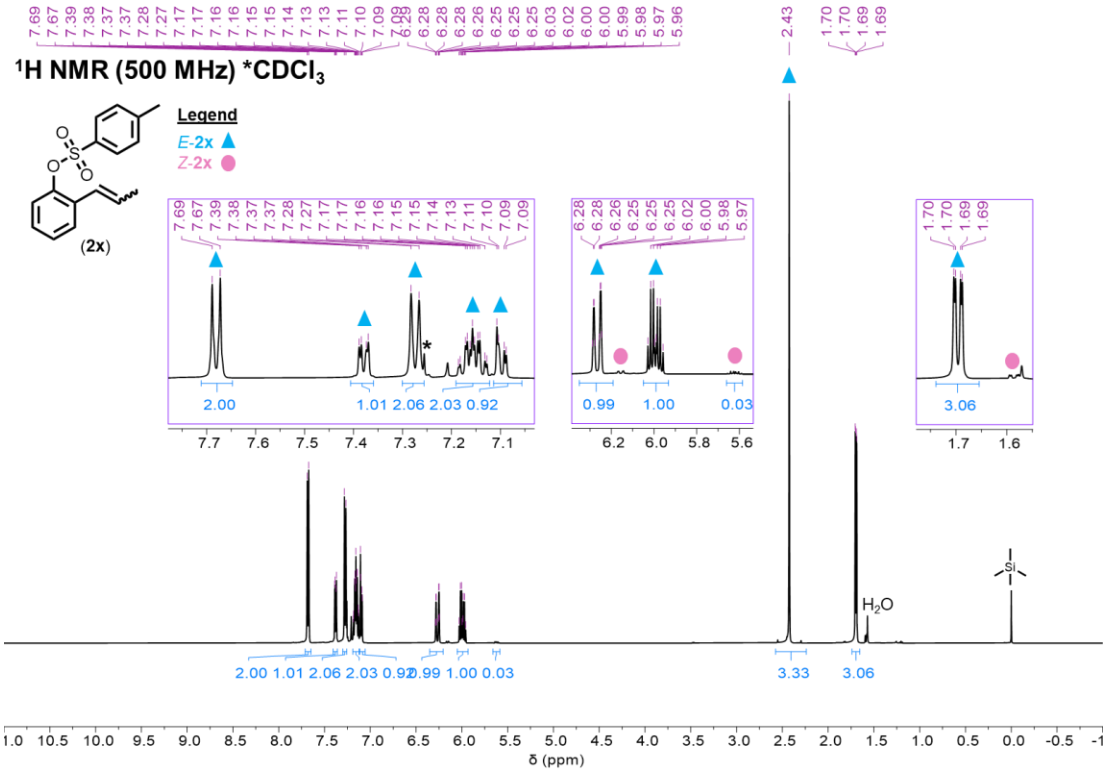

Figure E.141. ^{1}H NMR spectrum of 1-(4-methylbenzenesulfonate)-2-(2-propen-1-yl)phenol (**2x**) recorded in $CDCl_3$ at 25 °C.

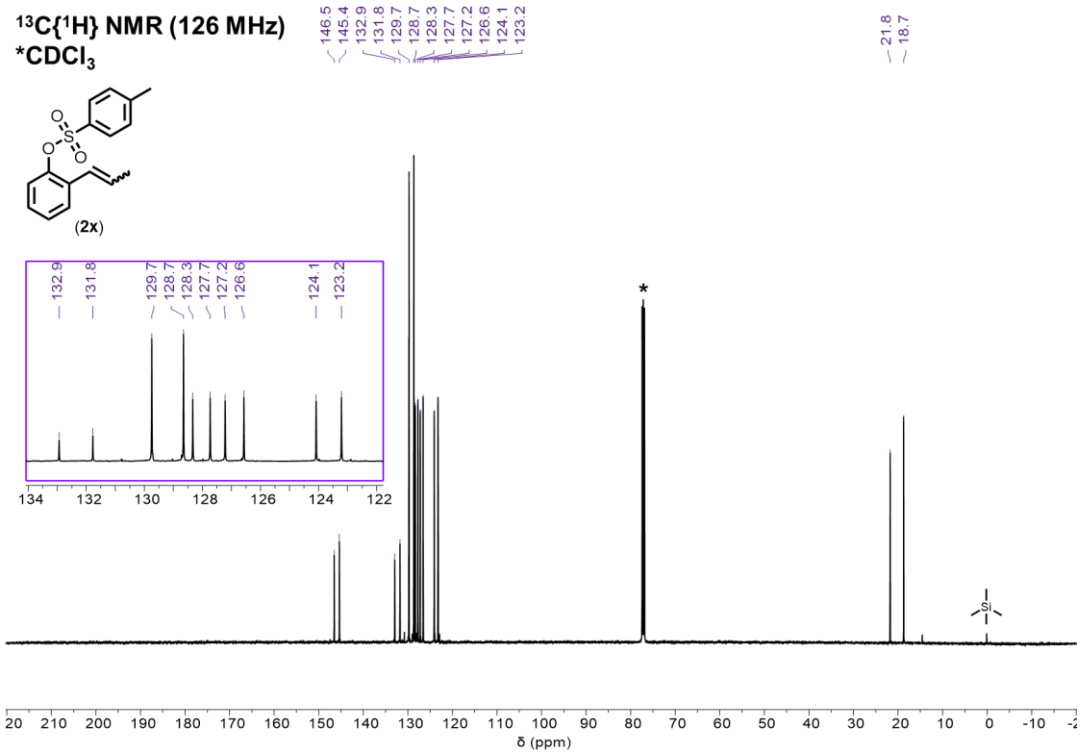

Figure E.142. ^{13}C{^{1}H} NMR spectrum of 1-(4-methylbenzenesulfonate)-2-(2-propen-1-yl)phenol (**2x**) recorded in $CDCl_3$ at 25 °C.

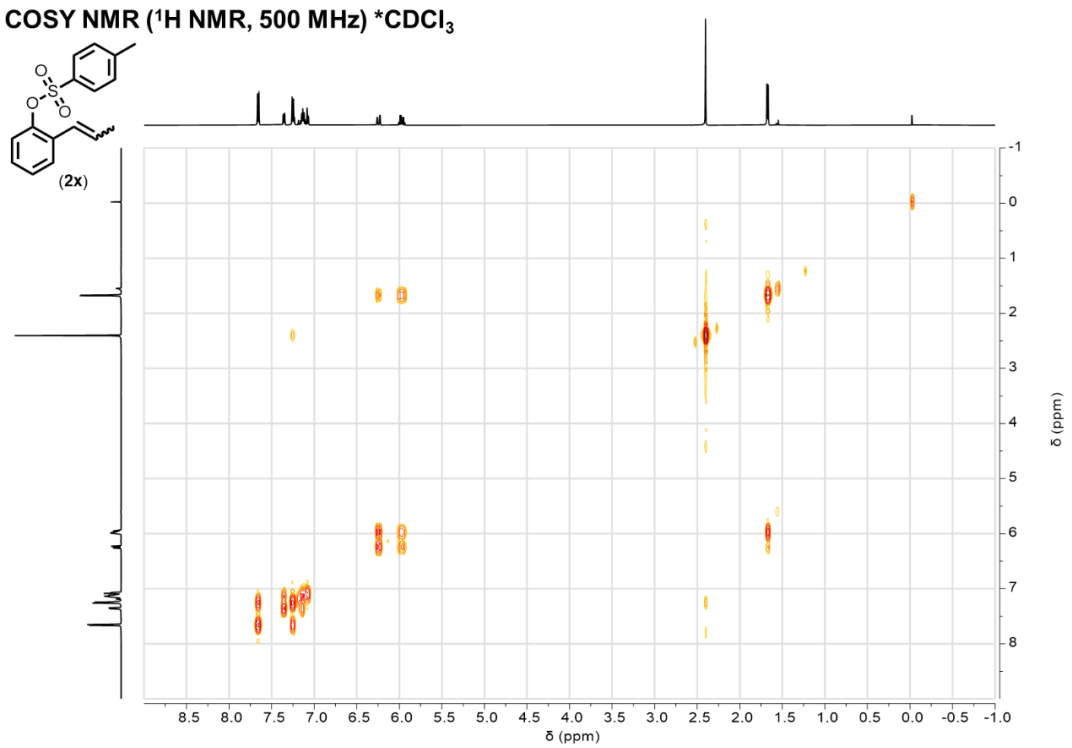

Figure E.143. COSY NMR spectrum of 1-(4-methylbenzenesulfonate)-2-(2-propen-1-yl)phenol (**2x**) recorded in $CDCl_3$ at 25 °C.

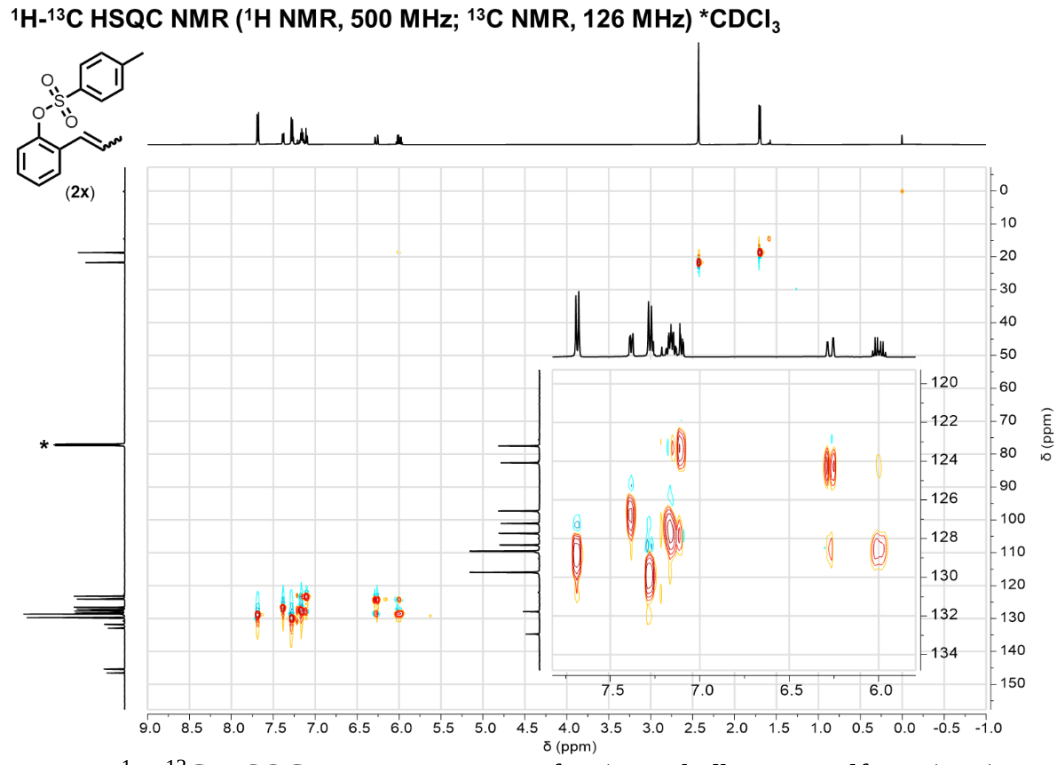

Figure E.144. ^{1}H-^{13}C HSQC NMR spectrum of 1-(4-methylbenzenesulfonate)-2-(2-propen-1-yl)phenol (**2x**) recorded in $CDCl_3$ at 25 °C.

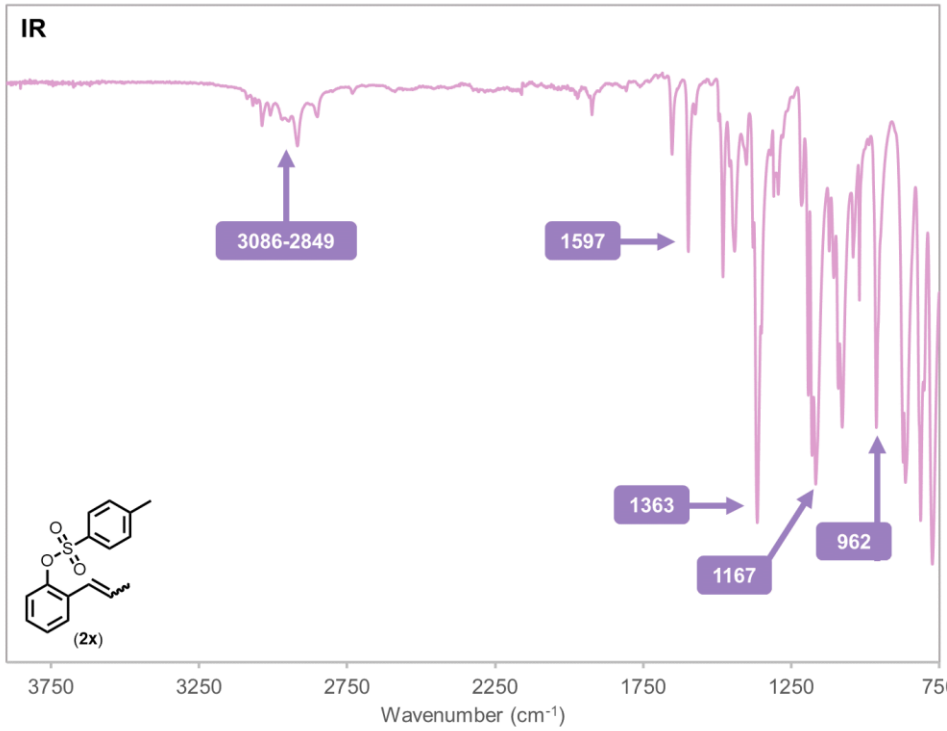

Figure E.145. IR spectrum of 1-(4-methylbenzenesulfonate)-2-(2-propen-1-yl)phenol (**2x**) recorded neat at 25 °C.

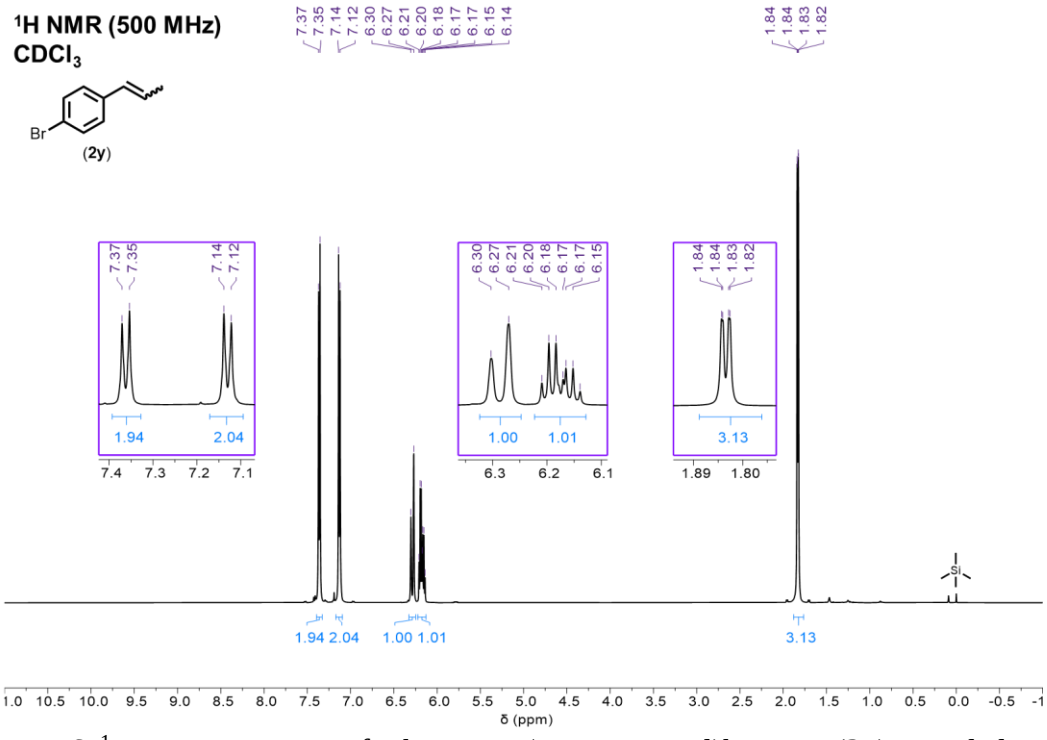

Figure E.146. ^{1}H NMR spectrum of 1-bromo-4-(1-propen-1-yl)benzene (**2y**) recorded in $CDCl_3$ at 25 °C.

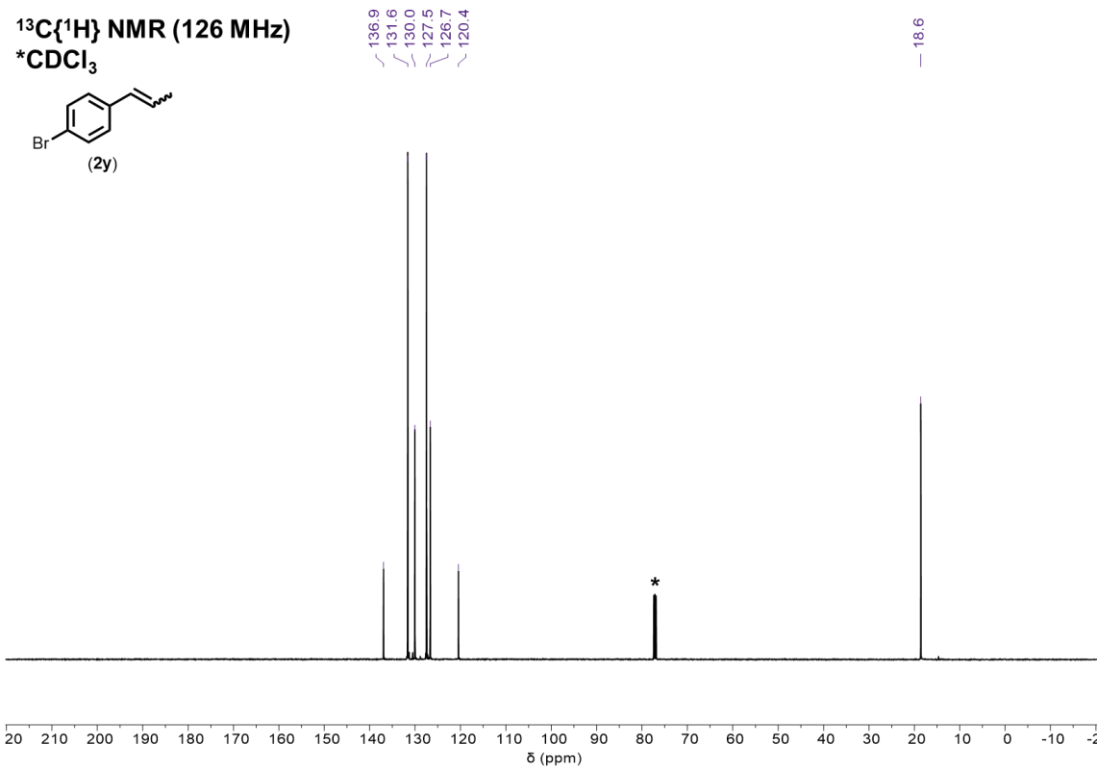

Figure E.147. $^{13}C\{^{1}H\}$ NMR spectrum of 1-bromo-4-(1-propen-1-yl)benzene (**2y**) recorded in $CDCl_3$ at 25 °C.

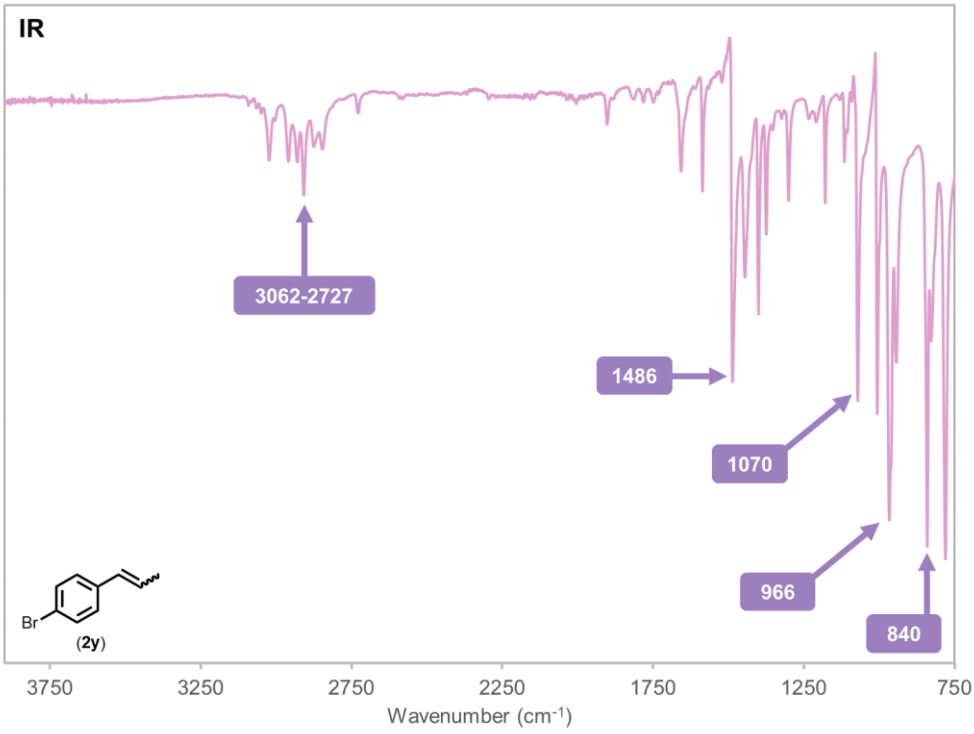

Figure E.148. IR NMR spectrum of 1-bromo-4-(1-propen-1-yl)benzene (**2y**) recorded neat at 25 °C.

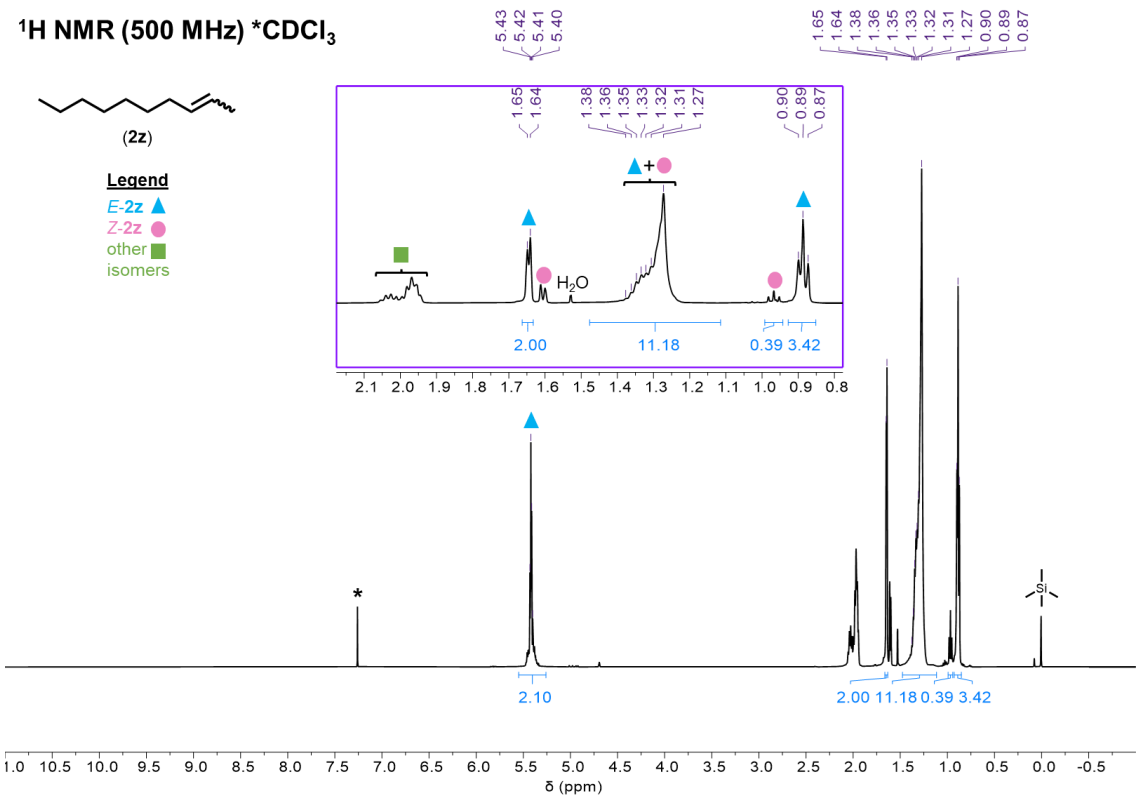

Figure E.149. ^{1}H NMR spectrum of 2-decene (**2z**) recorded in $CDCl_3$ at 25 °C.

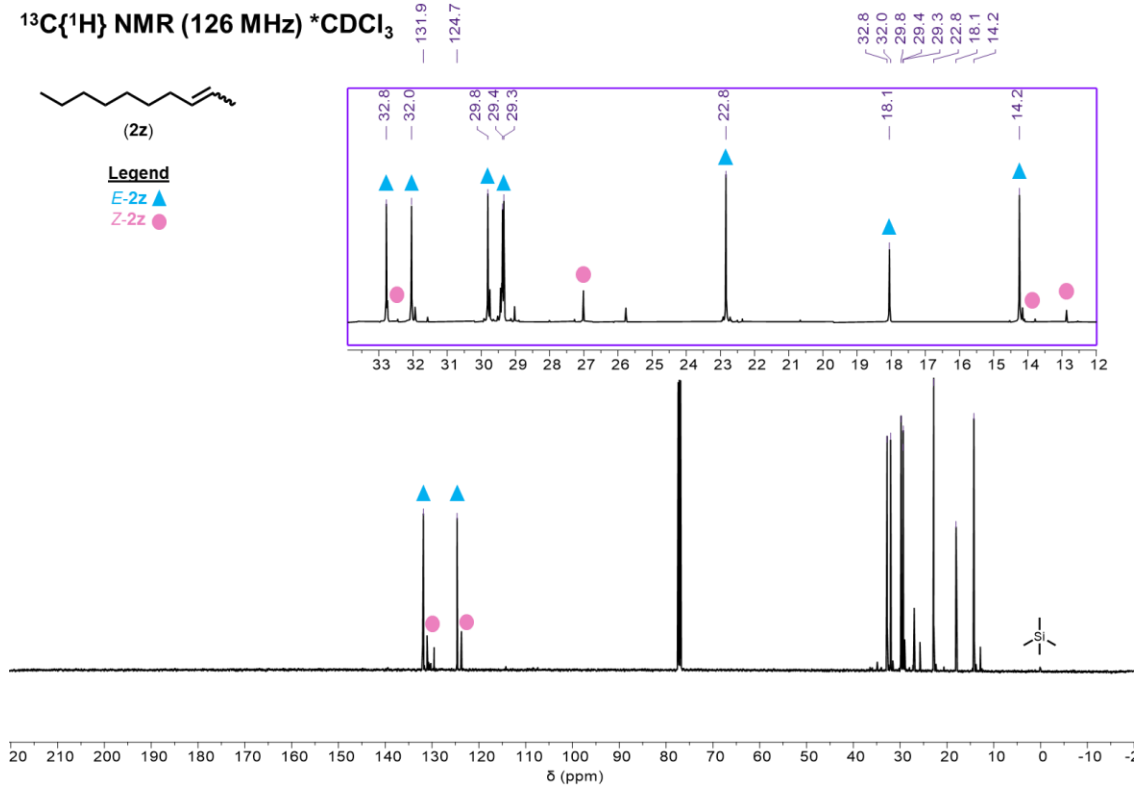

Figure E.150. $^{13}C\{^{1}H\}$ NMR spectrum of 2-decene (**2z**) recorded in $CDCl_3$ at 25 °C.

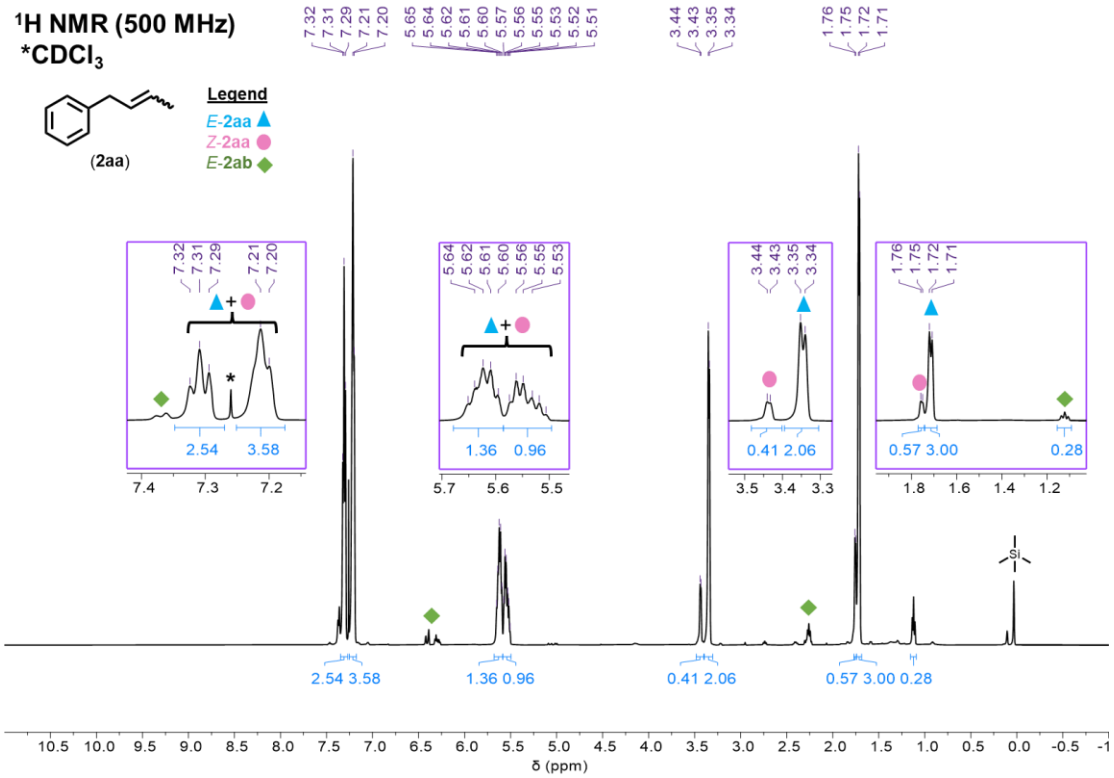

Figure E.151. ^{1}H NMR spectrum of 1-phenyl-2-butene (**2aa**) recorded in $CDCl_3$ at 25 °C.

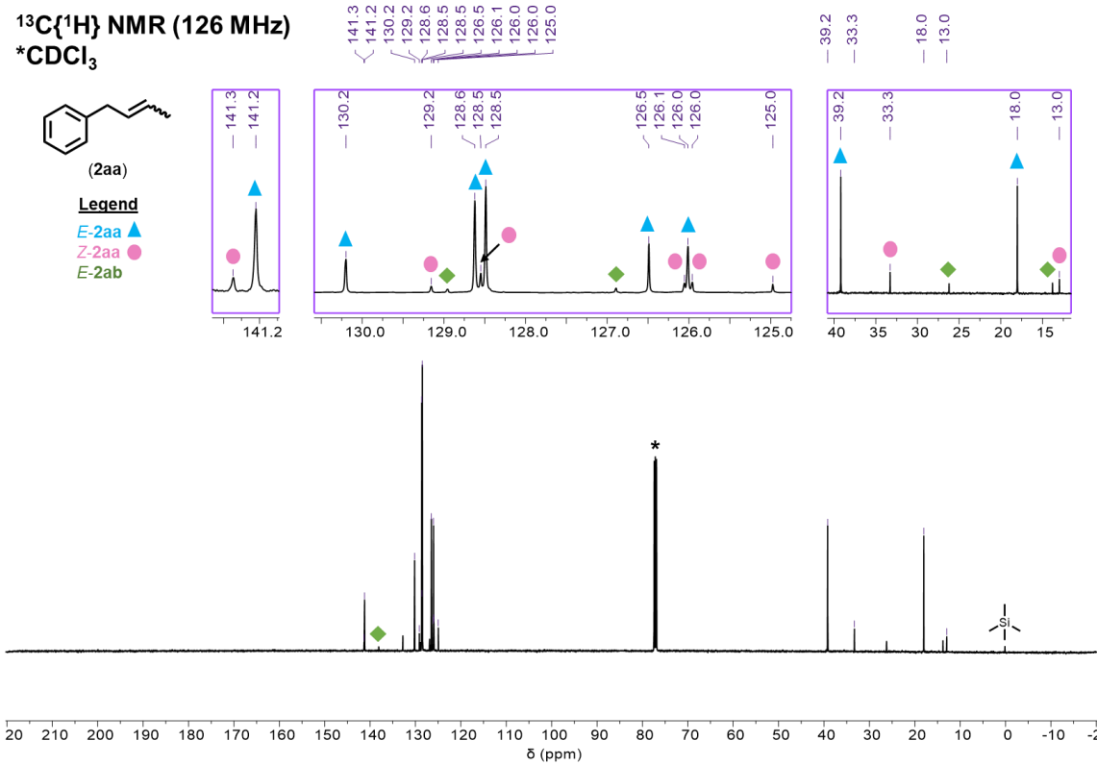

Figure E.152. ^{13}C{^{1}H} NMR spectrum of 1-phenyl-2-butene (**2aa**) recorded in $CDCl_3$ at 25 °C.

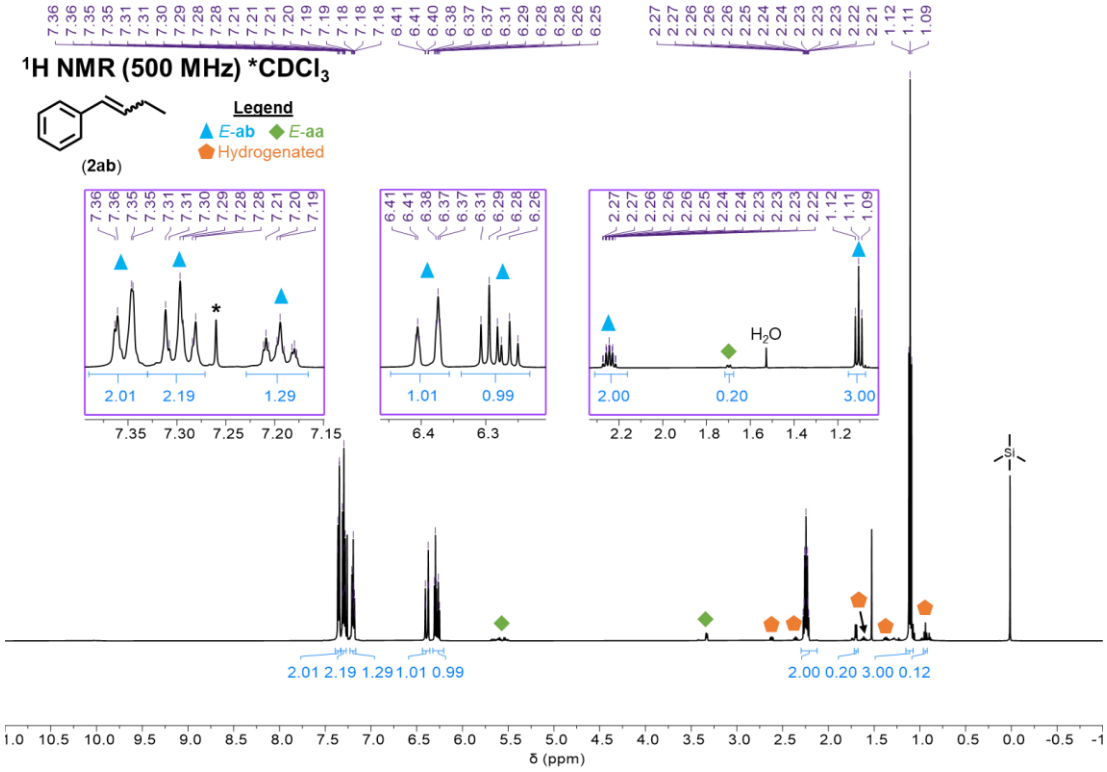

Figure E.153. ^{1}H NMR spectrum of 1-phenyl-1-butene (**2ab**) recorded in $CDCl_3$ at 25 °C.

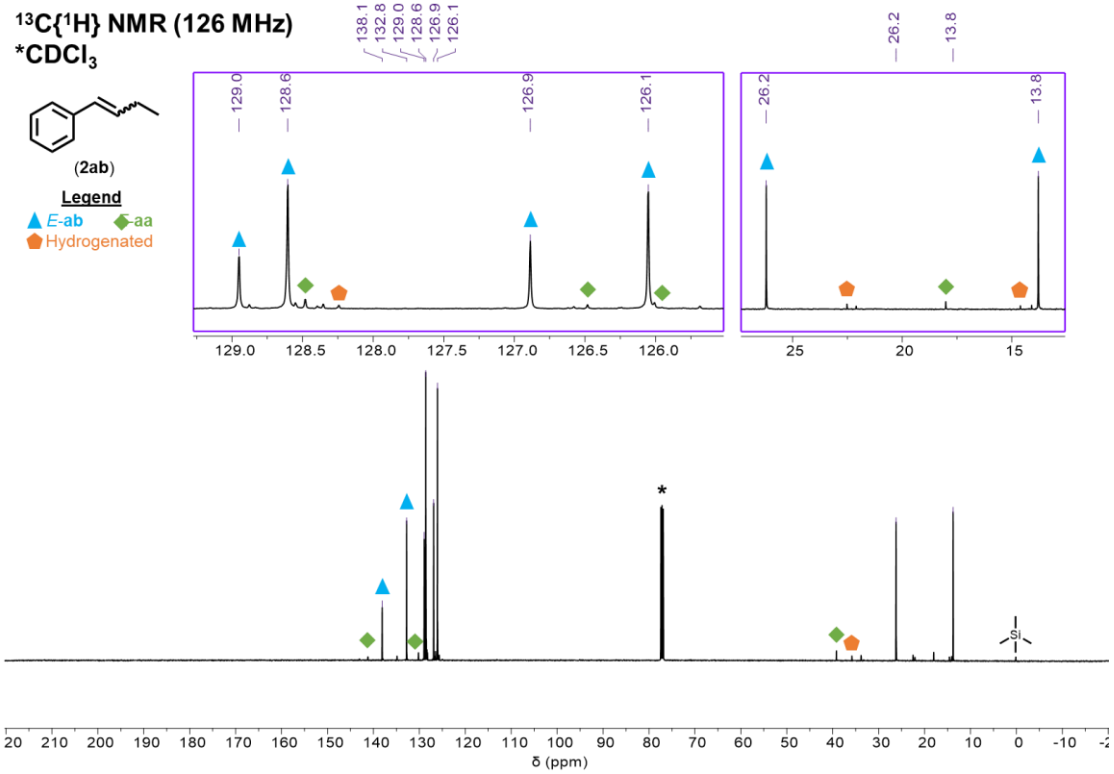

Figure E.154. ^{13}C{^{1}H} NMR spectrum of 1-phenyl-1-butene (**2ab**) recorded in $CDCl_3$ at 25 °C.

REFERENCES CITED

(1) Keim, W. Oligomerization of Ethylene to α-Olefins: Discovery and Development of the Shell Higher Olefin Process (SHOP). *Angew. Chem. Int. Ed.* **2013**, *52*, 12492–12496.

(2) Maier, C.; Calafut, T. 1 - Chemistry. In *Polypropylene*; Maier, C., Calafut, T., Eds.; William Andrew Publishing: Norwich, NY, **1998**; pp 3–9.

(3) Evans, D.; Osborn, J. A.; Wilkinson, G. Hydroformylation of Alkenes by Use of Rhodium Complex Catalysts. *J. Chem. Soc. Inorg. Phys. Theor.* **1968**, No. 0, 3133–3142.

(4) Franke, R.; Selent, D.; Börner, A. Applied Hydroformylation. *Chem. Rev.* **2012**, *112*, 5675–5732.

(5) Bernales, V.; Froese, R. D. Rhodium Catalyzed Hydroformylation of Olefins. *J. Comput. Chem.* **2019**, *40*, 342–348.

(6) Kawamura, K. E.; Chang, A. S.; Martin, D. J.; Smith, H. M.; Morris, P. T.; Cook, A. K. Modular Ni(0)/Silane Catalytic System for the Isomerization of Alkenes. *Organometallics* **2022**, *41*, 486–496.

(7) Dong, K.; Fang, X.; Gülak, S.; Franke, R.; Spannenberg, A.; Neumann, H.; Jackstell, R.; Beller, M. Highly Active and Efficient Catalysts for Alkoxycarbonylation of Alkenes. *Nat. Commun.* **2017**, *8*, 14117.

(8) Miller, Z. D.; Li, W.; Belderrain, T. R.; Montgomery, J. Regioselective Allene Hydrosilylation Catalyzed by N-Heterocyclic Carbene Complexes of Nickel and Palladium. *J. Am. Chem. Soc.* **2013**, *135*, 15282–15285.

(9) Bini, L.; Müller, C.; Vogt, D. Ligand Development in the Ni-Catalyzed Hydrocyanation of Alkenes. *Chem. Commun.* **2010**, *46*, 8325–8334.

(10) Obligacion, J. V.; Chirik, P. J. Earth-Abundant Transition Metal Catalysts for Alkene Hydrosilylation and Hydroboration. *Nat. Rev. Chem.* **2018**, *2*, 15–34.

(11) Speier, J. L. Homogeneous Catalysis of Hydrosilation by Transition Metals. In *Advances in Organometallic Chemistry*; Stone, F. G. A., West, R., Eds.; Academic Press, **1979**; Vol. 17, pp 407–447.

(12) Markó István E.; Stérin Sébastien; Buisine Olivier; Mignani Gérard; Branlard Paul; Tinant Bernard; Declercq Jean-Paul. Selective and Efficient Platinum(0)-Carbene Complexes As Hydrosilylation Catalysts. *Science* **2002**, *298*, 204–206.

(13) Meister, T. K.; Riener, K.; Gigler, P.; Stohrer, J.; Herrmann, W. A.; Kühn, F. E. Platinum Catalysis Revisited—Unraveling Principles of Catalytic Olefin Hydrosilylation. *ACS Catal.* **2016**, *6*, 1274–1284.

(14) Pappas, I.; Treacy, S.; Chirik, P. J. Alkene Hydrosilylation Using Tertiary Silanes with α-Diimine Nickel Catalysts. Redox-Active Ligands Promote a Distinct Mechanistic Pathway from Platinum Catalysts. *ACS Catal.* **2016**, *6*, 4105–4109.

(15) Hossain, I.; Schmidt, J. A. R. Cationic Nickel(II)-Catalyzed Hydrosilylation of Alkenes: Role of P, N-Type Ligand Scaffold on Selectivity and Reactivity. *Organometallics* **2020**, *39*, 3441–3451.

(16) Fontaine, F.-G.; Nguyen, R.-V.; Zargarian, D. Hydrosilylation of Alkenes and Ketones Catalyzed by Nickel(II) Indenyl Complexes. *Can. J. Chem.* **2003**, *81*, 1299–1306.

(17) Chen, Y.; Sui-Seng, C.; Boucher, S.; Zargarian, D. Influence of SiMe3 Substituents on Structures and Hydrosilylation Activities of ((SiMe$_3$)1 or 2-Indenyl)Ni(PPh$_3$)Cl. *Organometallics* **2005**, *24*, 149–155.

(18) Benítez Junquera, L.; Puerta, M. C.; Valerga, P. R-Allyl Nickel(II) Complexes with Chelating N-Heterocyclic Carbenes: Synthesis, Structural Characterization, and Catalytic Activity. *Organometallics* **2012**, *31*, 2175–2183.

(19) Cramer, R.; Lindsey, R. V. Jr. The Mechanism of Isomerization of Olefins with Transition Metal Catalysts. *J. Am. Chem. Soc.* **1966**, *88*, 3534–3544.

(20) Tolman, C. A. Chemistry of Tetrakis(Triethyl Phosphite)Nickel Hydride, HNi[P(OEt)$_3$]$_4^+$. IV. Mechanism of Olefin Isomerization. *J. Am. Chem. Soc.* **1972**, *94*, 2994–2999.

(21) Kapat, A.; Sperger, T.; Guven, S.; Schoenebeck, F. E-Olefins through Intramolecular Radical Relocation. *Science* **2019**, *363*, 391–396.

(22) Kramer, S.; Mielby, J.; Buss, K.; Kasama, T.; Kegnæs, S. Nitrogen-Doped Carbon-Encapsulated Nickel/Cobalt Nanoparticle Catalysts for Olefin Migration in Allylarenes. *ChemCatChem* **2017**, *9*, 2930–2934.

(23) Shin, M.; Suh, Y.-W. Ethylene Oligomerization over SiO2−Al2O3 Supported Ni$_2$P Catalyst. *ChemCatChem* **2020**, *12*, 135–140.

(24) Hartmann, M.; Pöppl, A.; Kevan, L. Ethylene Dimerization and Butene Isomerization in Nickel-Containing MCM-41 and AlMCM-41 Mesoporous Molecular Sieves: An Electron Spin Resonance and Gas Chromatography Study. *J. Phys. Chem.* **1996**, *100*, 9906–9910.

(25) Cvetanović, R. J.; Foster, N. F. Isomerization of Butenes on Some ZnO-, NiO- and Cr_2O_3-Containing Catalysts and the Effect of Controlled Impurities and of Potash Additions. *Discuss. Faraday Soc.* **1959**, *28*, 201–206.

(26) Ng, F. T. T.; Creaser, D. C. Ethylene Dimerization over Modified Nickel Exchanged Y-Zeolite. *Appl. Catal. Gen.* **1994**, *119*, 327–339.

(27) Marciniec, B. Catalysis by Transition Metal Complexes of Alkene Silylation–Recent Progress and Mechanistic Implications. *Coord. Chem. Pol.* **2005**, *249*, 2374–2390.

(28) Roy, A. K. A Review of Recent Progress in Catalyzed Homogeneous Hydrosilation (Hydrosilylation). In *Advances in Organometallic Chemistry*; West, R., Hill, A. F., Fink, M. J., Eds.; Academic Press, **2007**; Vol. 55, pp 1–59.

(29) Bogdan Marciniec. *Hydrosilylation*; Springer, 2009.

(30) Troegel, D.; Stohrer, J. Recent Advances and Actual Challenges in Late Transition Metal Catalyzed Hydrosilylation of Olefins from an Industrial Point of View. *Ind. Chem.* **2011**, *255*, 1440–1459.

(31) Nakajima, Y.; Shimada, S. Hydrosilylation Reaction of Olefins: Recent Advances and Perspectives. *RSC Adv.* **2015**, *5*, 20603–20616.

(32) Komiyama, T.; Minami, Y.; Hiyama, T. Recent Advances in Transition-Metal-Catalyzed Synthetic Transformations of Organosilicon Reagents. *ACS Catal.* **2017**, *7*, 631–651.

(33) Nakao, Y.; Hiyama, T. Silicon-Based Cross-Coupling Reaction: An Environmentally Benign Version. *Chem. Soc. Rev.* **2011**, *40*, 4893–4901.

(34) Sore, H. F.; Galloway, W. R. J. D.; Spring, D. R. Palladium-Catalysed Cross-Coupling of Organosilicon Reagents. *Chem. Soc. Rev.* **2012**, *41*, 1845–1866.

(35) Denmark, S. E.; Ambrosi, A. Why You Really Should Consider Using Palladium-Catalyzed Cross-Coupling of Silanols and Silanolates. *Org. Process Res. Dev.* **2015**, *19*, 982–994.

(36) Jones, G. R.; Landais, Y. The Oxidation of the Carbon-Silicon Bond. *Tetrahedron* **1996**, *52*, 7599–7662.

(37) Matsuoka, K.; Komami, N.; Kojima, M.; Mita, T.; Suzuki, K.; Maeda, S.; Yoshino, T.; Matsunaga, S. Chemoselective Cleavage of Si–C(Sp^3) Bonds in Unactivated Tetraalkylsilanes Using Iodine Tris(Trifluoroacetate). *J. Am. Chem. Soc.* **2021**, *143*, 103–108.

(38) Roy, A.; Oestreich, M. At Long Last: The Me_3Si Group as a Masked Alcohol. *Angew. Chem. Int. Ed.* **2021**, *60*, 4408–4410.

(39) Franz, A. K.; Wilson, S. O. Organosilicon Molecules with Medicinal Applications. *J. Med. Chem.* **2013**, *56*, 388–405.

(40) Rémond, E.; Martin, C.; Martinez, J.; Cavelier, F. Silicon-Containing Amino Acids: Synthetic Aspects, Conformational Studies, and Applications to Bioactive Peptides. *Chem. Rev.* **2016**, *116*, 11654–11684.

(41) Showell, G. A.; Mills, J. S. Chemistry Challenges in Lead Optimization: Silicon Isosteres in Drug Discovery. *Drug Discov. Today* **2003**, *8*, 551–556.

(42) Lewis, L. N.; Stein, J.; Gao, Y.; Colborn, R. E. Platinum Catalysts Used in the Silicones Industry. *Platin. Met. Rev.* **1997**, *41*, 66–75.

(43) Du, X.; Huang, Z. Advances in Base-Metal-Catalyzed Alkene Hydrosilylation. *ACS Catal.* **2017**, *7*, 1227–1243.

(44) Obligacion, J. V.; Chirik, P. J. Earth-Abundant Transition Metal Catalysts for Alkene Hydrosilylation and Hydroboration. *Nat. Rev. Chem.* **2018**, *2*, 15–34.

(45) de Almeida, L. D.; Wang, H.; Junge, K.; Cui, X.; Beller, M. Recent Advances in Catalytic Hydrosilylations: Developments beyond Traditional Platinum Catalysts. *Angew. Chem. Int. Ed.* **2021**, *60*, 550–565.

(46) Maciejewski, H.; Marciniec, B.; Kownacki, I. Catalysis of Hydrosilylation: Part XXXIV. High Catalytic Efficiency of the Nickel Equivalent of Karstedt Catalyst [{Ni(η-CH_2 $CHSiMe_2)_2O\}_2$ {μ-(η-CH_2 $CHSiMe_2)_2O\}$]. *J. Organomet. Chem.* **2000**, *597*, 175–181.

(47) Lipschutz, M. I.; Tilley, T. D. Synthesis and Reactivity of a Conveniently Prepared Two-Coordinate Bis(Amido) Nickel(II) Complex. *Chem. Commun.* **2012**, *48*, 7146–7148.

(48) Srinivas, V.; Nakajima, Y.; Ando, W.; Sato, K.; Shimada, S. (Salicylaldiminato)Ni(II)-Catalysts for Hydrosilylation of Olefins. *Catal. Sci. Technol.* **2015**, *5*, 2081–2084.

(49) Buslov, I.; Becouse, J.; Mazza, S.; Montandon-Clerc, M.; Hu, X. Chemoselective Alkene Hydrosilylation Catalyzed by Nickel Pincer Complexes. *Angew. Chem. Int. Ed.* **2015**, *54*, 14523–14526.

(50) Mathew, J.; Nakajima, Y.; Choe, Y.-K.; Urabe, Y.; Ando, W.; Sato, K.; Shimada, S. Olefin Hydrosilylation Catalyzed by Cationic Nickel(II) Allyl Complexes: A Non-Innocent Allyl Ligand-Assisted Mechanism. *Chem. Commun.* **2016**, *52*, 6723–6726.

(51) Buslov, I.; Keller, S. C.; Hu, X. Alkoxy Hydrosilanes As Surrogates of Gaseous Silanes for Hydrosilylation of Alkenes. *Org. Lett.* **2016**, *18*, 1928–1931.

(52) Srinivas, V.; Nakajima, Y.; Ando, W.; Sato, K.; Shimada, S. Bis(Acetylacetonato)Ni(II)/$NaBHEt_3$-Catalyzed Hydrosilylation of 1,3-Dienes, Alkenes and Alkynes. *J. Organomet. Chem.* **2016**, *809*, 57–62.

(53) Nakajima, Y.; Sato, K.; Shimada, S. Development of Nickel Hydrosilylation Catalysts. *Chem. Rec.* **2016**, *16*, 2379–2387.

(54) Vijaykumar, G.; Pariyar, A.; Ahmed, J.; Shaw, B. K.; Adhikari, D.; Mandal, S. K. Tuning the Redox Non-Innocence of a Phenalenyl Ligand toward Efficient Nickel-Assisted Catalytic Hydrosilylation. *Chem. Sci.* **2018**, *9*, 2817–2825.

(55) Yang, J.; Postils, V.; Lipschutz, M. I.; Fasulo, M.; Raynaud, C.; Clot, E.; Eisenstein, O.; Tilley, T. D. Efficient Alkene Hydrosilation with Bis(8-Quinolyl)Phosphine (NPN) Nickel Catalysts. The Dominant Role of Silyl-over Hydrido-Nickel Catalytic Intermediates. *Chem. Sci.* **2020**, *11*, 5043–5051.

(56) Wu, X.; Ding, G.; Lu, W.; Yang, L.; Wang, J.; Zhang, Y.; Xie, X.; Zhang, Z. Nickel-Catalyzed Hydrosilylation of Terminal Alkenes with Primary Silanes via Electrophilic Silicon–Hydrogen Bond Activation. *Org. Lett.* **2021**, *23*, 1434–1439.

(57) Hashimoto, T.; Shiota, K.; Ishimaru, T.; Yamaguchi, Y. Hydrosilylation of Alkenes Using a Hydrosiloxane as a Surrogate for Me_2SiH_2 and Catalyzed by a Nickel-Pincer Complex. *Eur. J. Org. Chem.* **2021**, *2021*, 5449–5452.

(58) Pratt, S. L.; Faltynek, R. A. Hydrosilation Catalysis via Silylmanganese Carbonyl Complexes: Thermal vs. Photochemical Activation. *J. Organomet. Chem.* **1983**, *258*, C5–C8.

(59) Hilal, H. S.; Abu-Eid, M.; Al-Subu, M.; Khalaf, S. Hydrosilylation Reactions Catalysed by Decacarbonyldimanganese(O). *J. Mol. Catal.* **1987**, *39*, 1–11.

(60) Carney, J. R.; Dillon, B. R.; Campbell, L.; Thomas, S. P. Manganese-Catalyzed Hydrofunctionalization of Alkenes. *Angew. Chem. Int. Ed.* **2018**, *57*, 10620–10624.

(61) Mukhopadhyay, T. K.; Flores, M.; Groy, T. L.; Trovitch, R. J. A β-Diketiminate Manganese Catalyst for Alkene Hydrosilylation: Substrate Scope, Silicone Preparation, and Mechanistic Insight. *Chem. Sci.* **2018**, *9*, 7673–7680.

(62) Yang, X.; Wang, C. Manganese-Catalyzed Hydrosilylation Reactions. *Chem. – Asian J.* **2018**, *13*, 2307–2315.

(63) Yang, X.; Wang, C. Diverse Fates of β-Silyl Radical under Manganese Catalysis: Hydrosilylation and Dehydrogenative Silylation of Alkenes. *Chin. J. Chem.* **2018**, *36*, 1047–1051.

(64) Dong, J.; Yuan, X.-A.; Yan, Z.; Mu, L.; Ma, J.; Zhu, C.; Xie, J. Manganese-Catalysed Divergent Silylation of Alkenes. *Nat. Chem.* **2021**, *13*, 182–190.

(65) Chalk, A. J.; Harrod, J. F. Homogeneous Catalysis. IV. Some Reactions of Silicon Hydrides in the Presence of Cobalt Carbonyls. *J. Am. Chem. Soc.* **1967**, *89*, 1640–1647.

(66) Chen, C.; Hecht, M. B.; Kavara, A.; Brennessel, W. W.; Mercado, B. Q.; Weix, D. J.; Holland, P. L. Rapid, Regioconvergent, Solvent-Free Alkene Hydrosilylation with a Cobalt Catalyst. *J. Am. Chem. Soc.* **2015**, *137*, 13244–13247.

(67) Sun, J.; Deng, L. Cobalt Complex-Catalyzed Hydrosilylation of Alkenes and Alkynes. *ACS Catal.* **2016**, *6*, 290–300.

(68) Noda, D.; Tahara, A.; Sunada, Y.; Nagashima, H. Non-Precious-Metal Catalytic Systems Involving Iron or Cobalt Carboxylates and Alkyl Isocyanides for Hydrosilylation of Alkenes with Hydrosiloxanes. *J. Am. Chem. Soc.* **2016**, *138*, 2480–2483.

(69) Gorczyński, A.; Zaranek, M.; Witomska, S.; Bocian, A.; Stefankiewicz, A. R.; Kubicki, M.; Patroniak, V.; Pawluć, P. The Cobalt(II) Complex of a New Tridentate Schiff-Base Ligand as a Catalyst for Hydrosilylation of Olefins. *Catal. Commun.* **2016**, *78*, 71–74.

(70) Schuster, C. H.; Diao, T.; Pappas, I.; Chirik, P. J. Bench-Stable, Substrate-Activated Cobalt Carboxylate Pre-Catalysts for Alkene Hydrosilylation with Tertiary Silanes. *ACS Catal.* **2016**, *6*, 2632–2636.

(71) Ibrahim, A. D.; Entsminger, S. W.; Zhu, L.; Fout, A. R. A Highly Chemoselective Cobalt Catalyst for the Hydrosilylation of Alkenes Using Tertiary Silanes and Hydrosiloxanes. *ACS Catal.* **2016**, *6*, 3589–3593.

(72) Wang, C.; Teo, W. J.; Ge, S. Cobalt-Catalyzed Regiodivergent Hydrosilylation of Vinylarenes and Aliphatic Alkenes: Ligand- and Silane-Dependent Regioselectivities. *ACS Catal.* **2017**, *7*, 855–863.

(73) Liu, Y.; Deng, L. Mode of Activation of Cobalt(II) Amides for Catalytic Hydrosilylation of Alkenes with Tertiary Silanes. *J. Am. Chem. Soc.* **2017**, *139*, 1798–1801.

(74) Lee, K. L. (Aminomethyl)Pyridine Complexes for the Cobalt-Catalyzed Anti-Markovnikov Hydrosilylation of Alkoxy- or Siloxy(Vinyl)Silanes with Alkoxy- or Siloxyhydrosilanes. *Angew. Chem. Int. Ed.* **2017**, *56*, 3665–3669.

(75) Raya, B.; Jing, S.; RajanBabu, T. Control of Selectivity through Synergy between Catalysts, Silanes and Reaction Conditions in Cobalt-Catalyzed Hydrosilylation of Dienes and Terminal Alkenes. *ACS Catal* **2017**, *7*, 2275–2283.

(76) Sanagawa, A.; Nagashima, H. Cobalt(0) and Iron(0) Isocyanides as Catalysts for Alkene Hydrosilylation with Hydrosiloxanes. *Organometallics* **2018**, *37*, 2859–2871.

(77) Gao, Y.; Wang, L.; Deng, L. Distinct Catalytic Performance of Cobalt(I)–*N*-Heterocyclic Carbene Complexes in Promoting the Reaction of Alkene with Diphenylsilane: Selective 2,1-Hydrosilylation, 1,2-Hydrosilylation, and Hydrogenation of Alkene. *ACS Catal.* **2018**, *8*, 9637–9646.

(78) Gutiérrez-Tarriño, S.; Concepción, P.; Oña-Burgos, P. Cobalt Catalysts for Alkene Hydrosilylation under Aerobic Conditions without Dry Solvents or Additives. *Eur. J. Inorg. Chem.* **2018**, *2018*, 4867–4874.

(79) Verhoeven, D. G. A.; Kwakernaak, J.; van Wiggen, M. A. C.; Lutz, M.; Moret, M.-E. Cobalt(II) and (I) Complexes of Diphosphine-Ketone Ligands: Catalytic Activity in Hydrosilylation Reactions. *Eur. J. Inorg. Chem.* **2019**, *2019*, 660–667.

(80) Kim, D.; Chen, C.; Mercado, B. Q.; Weix, D. J.; Holland, P. L. Mechanistic Study of Alkene Hydrosilylation Catalyzed by a β-Dialdiminate Cobalt(I) Complex. *Organometallics* **2020**, *39*, 2415–2424.

(81) Dai, Z.; Yu, Z.; Bai, Y.; Li, J.; Peng, J. Cobalt Bis(2-Ethylhexanoate) and Terpyridine Derivatives as Catalysts for the Hydrosilylation of Olefins. *Appl. Organomet. Chem.* **2021**, *35*, e6027.

(82) Dong, Y.; Xie, S.; Zhang, P.; Fan, Q.; Du, X.; Sun, H.; Li, X.; Fuhr, O.; Fenske, D. Selectivity Reverse of Hydrosilylation of Aryl Alkenes Realized by Pyridine N-Oxide with [PSiP] Pincer Cobalt(III) Hydride as Catalyst. *Inorg. Chem.* **2021**, *60*, 4551–4562.

(83) Yang, W.; Fan, Q.; Du, X.; Xie, S.; Huang, W.; Li, X.; Sun, H.; Fuhr, O.; Fenske, D. [P,C]-Chelate Cobalt(III) Hydride Catalyzed Hydrosilylation of Alkenes. *Organometallics* **2021**, *40*, 2836–2843.

(84) Docherty, J. H.; Dominey, A. P.; Thomas, S. P. Cobalt-Catalysed, Ligand-Controlled Regiodivergent Alkene Hydrosilylation. *Asian J. Org. Chem.* **2021**, *10*, 2379–2384.

(85) Huang, W.; Lu, J.; Fan, Q.; Li, X.; Hinz, A.; Sun, H. Synthesis of Aryl Cobalt and Iron Complexes and Their Catalytic Activity on Hydrosilylation of Alkenes. *New J. Chem.* **2022**, *46*, 7512–7521.

(86) Nesmeyanov, A. N.; Freidlina, R. Kh.; Chukovskaya, E. C.; Petrova, R. G.; Belyavsky, A. B. Addition, Substitution, and Telomerization Reactions of Olefins in the Presence of Metal Carbonyls or Colloidal Iron. *Tetrahedron* **1962**, *17*, 61–68.

(87) A. Schroeder, M.; S. Wrighton, M. Pentacarbonyliron(0) Photocatalyzed Reactions of Trialkylsilanes with Alkenes. *J. Organomet. Chem.* **1977**, *128*, 345–358.

(88) Bart, S. C.; Lobkovsky, E.; Chirik, P. J. Preparation and Molecular and Electronic Structures of Iron(0) Dinitrogen and Silane Complexes and Their Application to Catalytic Hydrogenation and Hydrosilation. *J. Am. Chem. Soc.* **2004**, *126*, 13794–13807.

(89) Tondreau Aaron M.; Atienza Crisita Carmen Hojilla; Weller Keith J.; Nye Susan A.; Lewis Kenrick M.; Delis Johannes G. P.; Chirik Paul J. Iron Catalysts for Selective Anti-Markovnikov Alkene Hydrosilylation Using Tertiary Silanes. *Science* **2012**, *335*, 567–570.

(90) Kamata, K.; Suzuki, A.; Nakai, Y.; Nakazawa, H. Catalytic Hydrosilylation of Alkenes by Iron Complexes Containing Terpyridine Derivatives as Ancillary Ligands. *Organometallics* **2012**, *31*, 3825–3828

(91) Hojilla Atienza, C. C.; Tondreau, A. M.; Weller, K. J.; Lewis, K. M.; Cruse, R. W.; Nye, S. A.; Boyer, J. L.; Delis, J. G. P.; Chirik, P. J. High-Selectivity Bis(Imino)Pyridine Iron Catalysts for the Hydrosilylation of 1,2,4-Trivinylcyclohexane. *ACS Catal.* **2012**, *2*, 2169–2172.

(92) Peng, D.; Zhang, Y.; Du, X.; Zhang, L.; Leng, X.; Walter, M. D.; Huang, Z. Phosphinite-Iminopyridine Iron Catalysts for Chemoselective Alkene Hydrosilylation. *J. Am. Chem. Soc.* **2013**, *135*, 19154–19166.

(93) Greenhalgh, M. D.; Frank, D. J.; Thomas, S. P. Iron-Catalysed Chemo-, Regio-, and Stereoselective Hydrosilylation of Alkenes and Alkynes Using a Bench-Stable Iron(II) Pre-Catalyst. *Adv. Synth. Catal.* **2014**, *356*, 584–590.

(94) Greenhalgh, M. D.; Jones, A. S.; Thomas, S. P. Iron-Catalysed Hydrofunctionalisation of Alkenes and Alkynes. *ChemCatChem* **2015**, *7*, 190–222.

(95) Chen, J.; Cheng, B.; Cao, M.; Lu, Z. Iron-Catalyzed Asymmetric Hydrosilylation of 1,1-Disubstituted Alkenes. *Angew. Chem. Int. Ed.* **2015**, *54*, 4661–4664.

(96) Sunada, Y.; Noda, D.; Soejima, H.; Tsutsumi, H.; Nagashima, H. Combinatorial Approach to the Catalytic Hydrosilylation of Styrene Derivatives: Catalyst Systems Composed of Organoiron(0) or (II) Precursors and Isocyanides. *Organometallics* **2015**, *34*, 2896–2906.

(97) Hayasaka, K.; Kamata, K.; Nakazawa, H. Highly Efficient Olefin Hydrosilylation Catalyzed by Iron Complexes with Iminobipyridine Ligand. *Bull. Chem. Soc. Jpn.* **2016**, *89*, 394–404.

(98) Du, X.; Zhang, Y.; Peng, D.; Huang, Z. Base–Metal-Catalyzed Regiodivergent Alkene Hydrosilylations. *Angew. Chem. Int. Ed.* **2016**, *55*, 6671–6675.

(99) Challinor, A. J.; Calin, M.; Nichol, G. S.; Carter, N. B.; Thomas, S. P. Amine-Activated Iron Catalysis: Air- and Moisture-Stable Alkene and Alkyne Hydrofunctionalization. *Adv. Synth. Catal.* **2016**, *358*, 2404–2409.

(100) Toya, Y.; Hayasaka, K.; Nakazawa, H. Hydrosilylation of Olefins Catalyzed by Iron Complexes Bearing Ketimine-Type Iminobipyridine Ligands. *Organometallics* **2017**, *36*, 1727–1735.

(101) Docherty, J. H.; Peng, J.; Dominey, A. P.; Thomas, S. P. Activation and Discovery of Earth-Abundant Metal Catalysts Using Sodium Tert-Butoxide. *Nat. Chem.* **2017**, *9*, 595–600.

(102) Hu, M.-Y.; He, Q.; Fan, S.-J.; Wang, Z.-C.; Liu, L.-Y.; Mu, Y.-J.; Peng, Q.; Zhu, S.-F. Ligands with 1,10-Phenanthroline Scaffold for Highly Regioselective Iron-Catalyzed Alkene Hydrosilylation. *Nat. Commun.* **2018**, *9*, 221.

(103) Agahi, R.; Challinor, A. J.; Dunne, J.; Docherty, J. H.; Carter, N. B.; Thomas, S. P. Regiodivergent Hydrosilylation, Hydrogenation, [2π + 2π]-Cycloaddition and C–H Borylation Using Counterion Activated Earth-Abundant Metal Catalysis. *Chem. Sci.* **2019**, *10*, 5079–5084.

(104) Kamitani, M.; Kusaka, H.; Yuge, H. Development of Activator-Free Iron Pincer Complexes for Alkene Hydrosilylation and Elucidation of Its Activation Mechanism. *Chem. Lett.* **2019**, *48*, 1196–1198.

(105) Smith, P. W.; Dong, Y.; Tilley, T. D. Efficient and Selective Alkene Hydrosilation Promoted by Weak, Double Si–H Activation at an Iron Center. *Chem. Sci.* **2020**, *11*, 7070–7075.

(106) Sun, W.; Li, M.-P.; Li, L.-J.; Huang, Q.; Hu, M.-Y.; Zhu, S.-F. Phenanthroline-Imine Ligands for Iron-Catalyzed Alkene Hydrosilylation. *Chem. Sci.* **2022**, *13*, 2721–2728.

(107) Nozakura, S.; Konotsune, S. Cyanoethylation of Trichlorosilane. I. β-Addition. *Bull. Chem. Soc. Jpn.* **1956**, *29*, 322–326.

(108) Kumada, M.; Kiso, Y.; Umeno, M. Nickel(II) Complexes as Catalysts in the Hydrosilylation of Olefins. *J. Chem. Soc. Chem. Commun.* **1970**, No. 10, 611–611.

(109) Bennett, E. W.; Orenski, P. J. Nickel Complexes As Hydrosilation Catalysts. *J. Organomet. Chem.* **1971**, *28*, 137–144.

(110) Lewis, L. N. On the Mechanism of Metal Colloid Catalyzed Hydrosilylation: Proposed Explanations for Electronic Effects and Oxygen Cocatalysis. *J. Am. Chem. Soc.* **1990**, *112*, 5998–6004

(111) Stein, J.; Lewis, L. N.; Smith, K. A.; Lettko, K. X. Mechanistic Studies of Platinum-Catalyzed Hydrosilylation. *J. Inorg. Organomet. Polym.* **1991**, *1*.

(112) Hurst, M. R.; Zakharov, L. N.; Cook, A. K. The Mechanism of Oxidative Addition of Pd(0) to Si–H Bonds: Electronic Effects, Reaction Mechanism, and Hydrosilylation. *Chem. Sci.* **2021**, *12*, 13045–13060.

(113) Cartledge, F. K. Steric Effects on Reactivity in Silicon Chemistry. *Organometallics* **1983**, *2*, 425–430.

(114) Ploom, A.; Tuulmets, A.; Järv, J. Structure-Reactivity Relationships in Organosilicon Chemistry Revisited. *Cent. Eur. J. Chem.* **2011**, *9*, 910–916.

(115) Hurst, M. R.; Davis, A. G.; Cook, A. K. The Influence of Silane Steric Bulk on the Formation and Dynamic Behavior of Silyl Palladium Hydrides. *Organometallics* **2022**, *41*, 997–1005.

(116) Chen, J.; Lu, Z. Asymmetric Hydrofunctionalization of Minimally Functionalized Alkenes via Earth Abundant Transition Metal Catalysis. *Org. Chem. Front.* **2018**, *5*, 260–272.

(117) Zaranek, M.; Pawluc, P. Markovnikov Hydrosilylation of Alkenes: How an Oddity Becomes the Goal. *ACS Catal.* **2018**, *8*, 9865–9876.

(118) Cheng, B.; Lu, P.; Zhang, H.; Cheng, X.; Lu, Z. Highly Enantioselective Cobalt-Catalyzed Hydrosilylation of Alkenes. *J. Am. Chem. Soc.* **2017**, *139*, 9439–9442.

(119) Cheng, B.; Liu, W.; Lu, Z. Iron-Catalyzed Highly Enantioselective Hydrosilylation of Unactivated Terminal Alkenes. *J. Am. Chem. Soc.* **2018**, *140*, 5014–5017.

(120) Gribble, M. W.; Pirnot, M. T.; Bandar, J. S.; Liu, R. Y.; Buchwald, S. L. Asymmetric Copper Hydride-Catalyzed Markovnikov Hydrosilylation of Vinylarenes and Vinyl Heterocycles. *J. Am. Chem. Soc.* **2017**, *139*, 2192–2195.

(121) Lewis, L. N.; Uriarte, R. J. Hydrosilylation Catalyzed by Metal Colloids: A Relative Activity Study. *Organometallics* **1990**, *9*, 621–625.

(122) Stein, J.; Lewis, L. N.; Gao, Y.; Scott, R. A. In Situ Determination of the Active Catalyst in Hydrosilylation Reactions Using Highly Reactive Pt(0) Catalyst Precursors. *J. Am. Chem. Soc.* **1999**, *121*, 3693–3703.

(123) Miller, Z. D.; Dorel, R.; Montgomery, J. Regiodivergent and Stereoselective Hydrosilylation of 1,3-Disubstituted Allenes. *Angew. Chem. Int. Ed.* **2015**, *54*, 9088–9091.

(124) Chaulagain, M. R.; Mahandru, G. M.; Montgomery, J. Alkyne Hydrosilylation Catalyzed by Nickel Complexes of N-Heterocyclic Carbenes. *Recent Adv. Organonickel Chem.* **2006**, *62*, 7560–7566.

(125) Wu, J.; Faller, J. W.; Hazari, N.; Schmeier, T. J. Stoichiometric and Catalytic Reactions of Thermally Stable Nickel(0) NHC Complexes. *Organometallics* **2012**, *31*, 806–809.

(126) Felten, S.; Marshall, S. F.; Groom, A. J.; Vanderlinden, R. T.; Stolley, R. M.; Louie, J. Synthesis and Characterization of [(NHC)Ni(Styrene)$_2$] Complexes: Isolation of Monocarbene Nickel Complexes and Benchmarking of $\%V_{Bur}$ in (NHC)Ni-π Systems. *Organometallics* **2018**, *37*, 3687–3697.

(127) Kelly III, R. A.; Clavier, H.; Giudice, S.; Scott, N. M.; Stevens, E. D.; Bordner, J.; Samardjiev, I.; Hoff, C. D.; Cavallo, L.; Nolan, S. P. Determination of *N*-Heterocyclic Carbene (NHC) Steric and Electronic Parameters Using the [(NHC)Ir(CO)$_2$Cl] System. *Organometallics* **2008**, *27*, 202–210.

(128) Gusev, D. G. Electronic and Steric Parameters of 76 *N*-Heterocyclic Carbenes in $Ni(CO)_3(NHC)$. *Organometallics* **2009**, *28*, 6458–6461.

(129) Clavier, H.; Nolan, S. P. Percent Buried Volume for Phosphine and *N*-Heterocyclic Carbene Ligands: Steric Properties in Organometallic Chemistry. *Chem. Commun.* **2010**, *46*, 841–861.

(130) Beller, M.; Andreo, M. G.; Zapf, A.; Karch, R.; Kleinwächter, I.; Briel, O. Carbene-Diene Complexes of Nickel, Palladium and Platinum. DE10062577B4.

(131) Chalk, A. J.; Harrod, J. F. Homogeneous Catalysis. II. The Mechanism of the Hydrosilation of Olefins Catalyzed by Group VIII Metal Complexes1. *J. Am. Chem. Soc.* **1965**, *87*, 16–21.

(132) Brookhart, M.; Grant, B. E. Mechanism of a Cobalt(III)-Catalyzed Olefin Hydrosilation Reaction: Direct Evidence for a Silyl Migration Pathway. *J. Am. Chem. Soc.* **1993**, *115*, 2151–2156.

(133) Xie, H.; Kuang, J.; Wang, L.; Li, Y.; Huang, L.; Fan, T.; Lei, Q.; Fang, W. A DFT Study on Palladium and Nickel-Catalyzed Regioselective and Stereoselective Hydrosilylation of 1,3-Disubstituted Allenes. *Organometallics* **2017**, *36*, 3371–3381.

(134) Miller, Z. D.; Dorel, R.; Montgomery, J. Regiodivergent and Stereoselective Hydrosilylation of 1,3-Disubstituted Allenes. *Angew. Chem.* **2015**, *127*, 9216–9219.

(135) Halpern, J.; Okamoto, T. Kinetics of the Migratory Insertion of Olefin into Rhodium-Hydrogen Bonds. Influence of Electronic Factors. *Inorganica Chim. Acta* **1984**, *89*, L53–L54.

(136) Doherty, N. M.; Bercaw, J. E. Kinetics and Mechanism of the Insertion of Olefins into Transition Metal-Hydride Bonds. *J. Am. Chem. Soc.* **1985**, *107*, 2670–2682.

(137) Hanley, P. S.; Hartwig, J. F. Intermolecular Migratory Insertion of Unactivated Olefins into Palladium–Nitrogen Bonds. Steric and Electronic Effects on the Rate of Migratory Insertion. *J. Am. Chem. Soc.* **2011**, *133*, 15661–15673.

(138) Rix, F. C.; Brookhart, M.; White, P. S. Electronic Effects on the β-Alkyl Migratory Insertion Reaction of Para-Substituted Styrene Methyl Palladium Complexes. *J. Am. Chem. Soc.* **1996**, *118*, 2436–2448.

(139) Parkin, G.; Bercaw, J. E. Elimination Processes for Alkyl, Hydride, and Hydroxy Derivatives of Permethyltungstenocene. *Organometallics* **1989**, *8*, 1172–1179.

(140) Watson, W. H.; Wu, G.; Richmond, M. G. Diphosphine Isomerization and C−H and P−C Bond Cleavage Reactivity in the Triosmium Cluster $Os_3(CO)_{10}(bpcd)$: Kinetic and Isotope Data for Reversible Ortho Metalation and X-Ray Structures of the Bridging and Chelating

Isomers of $Os_3(CO)_{10}$(bpcd) and the Benzyne-Substituted Cluster $HOs_3(CO)_8(\mu_3\text{-}C_6H_4)[\mu_2,\eta^1\text{-}PPhC{=}C(PPh_2)C(O)CH_2C(O)]$. *Organometallics* **2006**, *25*, 930–945.

(141) Jones, W. D. Isotope Effects in C−H Bond Activation Reactions by Transition Metals. *Acc. Chem. Res.* **2003**, *36*, 140–146.

(142) Morlok, M. M.; Janak, K. E.; Zhu, G.; Quarless, D. A.; Parkin, G. Intramolecular NH···S Hydrogen Bonding in the Zinc Thiolate Complex $[TmPh]ZnSCH_2C(O)NHPh$: A Mechanistic Investigation of Thiolate Alkylation as Probed by Kinetics Studies and by Kinetic Isotope Effects. *J. Am. Chem. Soc.* **2005**, *127*, 14039–14050.

(143) Churchill, D. G.; Janak, K. E.; Wittenberg, J. S.; Parkin, G. Normal and Inverse Primary Kinetic Deuterium Isotope Effects for C−H Bond Reductive Elimination and Oxidative Addition Reactions of Molybdenocene and Tungstenocene Complexes: Evidence for Benzene σ-Complex Intermediates. *J. Am. Chem. Soc.* **2003**, *125*, 1403–1420.

(144) Boller, T. M.; Murphy, J. M.; Hapke, M.; Ishiyama, T.; Miyaura, N.; Hartwig, J. F. Mechanism of the Mild Functionalization of Arenes by Diboron Reagents Catalyzed by Iridium Complexes. Intermediacy and Chemistry of Bipyridine-Ligated Iridium Trisboryl Complexes. *J. Am. Chem. Soc.* **2005**, *127*, 14263–14278.

(145) King, A. E.; Ryland, B. L.; Brunold, T. C.; Stahl, S. S. Kinetic and Spectroscopic Studies of Aerobic Copper(II)-Catalyzed Methoxylation of Arylboronic Esters and Insights into Aryl Transmetalation to Copper(II). *Organometallics* **2012**, *31*, 7948–7957.

(146) Cook, A. K.; Sanford, M. S. Mechanism of the Palladium-Catalyzed Arene C–H Acetoxylation: A Comparison of Catalysts and Ligand Effects. *J. Am. Chem. Soc.* **2015**, *137*, 3109–3118.

(147) Zell, T.; Schaub, T.; Radacki, K.; Radius, U. Si–H Activation of Hydrosilanes Leading to Hydrido Silyl and Bis(Silyl) Nickel Complexes. *Dalton Trans.* **2011**, *40*, 1852–1854.

(148) Schmidt, D.; Zell, T.; Schaub, T.; Radius, U. Si–H Bond Activation at {(NHC)2Ni0} Leading to Hydrido Silyl and Bis(Silyl) Complexes: A Versatile Tool for Catalytic Si–H/D Exchange, Acceptorless Dehydrogenative Coupling of Hydrosilanes, and Hydrogenation of Disilanes to Hydrosilanes. *Dalton Trans.* **2014**, *43*, 10816–10827.

(149) Arduengo, A. J. I.; Gamper, S. F.; Calabrese, J. C.; Davidson, F. Low-Coordinate Carbene Complexes of Nickel(0) and Platinum(0). *J. Am. Chem. Soc.* **1994**, *116*, 4391–4394.

(150) Díez-González, S.; Marion, N.; Nolan, S. P. N-Heterocyclic Carbenes in Late Transition Metal Catalysis. *Chem. Rev.* **2009**, *109*, 3612–3676.

(151) Hopkinson, M. N.; Richter, C.; Schedler, M.; Glorius, F. An Overview of *N*-Heterocyclic Carbenes. *Nature* **2014**, *510*, 485–496.

(152) Fortman, G. C.; Nolan, S. P. *N*-Heterocyclic Carbene (NHC) Ligands and Palladium in Homogeneous Cross-Coupling Catalysis: A Perfect Union. *Chem. Soc. Rev.* **2011**, *40* (10), 5151–5169.

(153) Thakur, A.; Louie, J. Advances in Nickel-Catalyzed Cycloaddition Reactions To Construct Carbocycles and Heterocycles. *Acc. Chem. Res.* **2015**, *48* (8), 2354–2365.

(154) Marín, M.; Rama, R. J.; Nicasio, M. C. Ni-Catalyzed Amination Reactions: An Overview. *Chem. Rec.* **2016**, *16*, 1819–1832.

(155) Poater, A.; Cosenza, B.; Correa, A.; Giudice, S.; Ragone, F.; Scarano, V.; Cavallo, L. SambVca: A Web Application for the Calculation of the Buried Volume of *N*-Heterocyclic Carbene Ligands. *Eur. J. Inorg. Chem.* **2009**, *2009*, 1759–1766.

(156) Tolman, C. A. Electron Donor-Acceptor Properties of Phosphorus Ligands. Substituent Additivity. *J. Am. Chem. Soc.* **1970**, *92*, 2953–2956.

(157) Nielsen, C. D.-T.; Burés, J. Visual Kinetic Analysis. *Chem. Sci.* **2019**, *10*, 348–353.

(158) Albinati, Alberto.; Caseri, W. R.; Pregosin, P. S. Hydrosilylation with platinum complexes. Preparation, low-temperature NMR spectra, and x-ray crystal structure of the novel bis-olefin catalyst cis-$PtCl_2(PhCH{:}CH_2)_2$. *Organometallics* **1987**, *6*, 788–793.

(159) Dorta, R.; Stevens, E. D.; Scott, N. M.; Costabile, C.; Cavallo, L.; Hoff, C. D.; Nolan, S. P. Steric and Electronic Properties of *N*-Heterocyclic Carbenes (NHC): A Detailed Study on Their Interaction with $Ni(CO)_4$. *J. Am. Chem. Soc.* **2005**, *127*, 2485–2495.

(160) Azpeitia, S.; Garralda, M. A.; Huertos, M. A. Rhodium(III) Catalyzed Solvent-Free Tandem Isomerization–Hydrosilylation From Internal Alkenes to Linear Silanes. *ChemCatChem* **2017**, *9*, 1901–1905.

(161) Kochi, T.; Ichinose, K.; Shigekane, M.; Hamasaki, T.; Kakiuchi, F. Metal-Catalyzed Sequential Formation of Distant Bonds in Organic Molecules: Palladium-Catalyzed Hydrosilylation/Cyclization of 1,n-Dienes by Chain Walking. *Angew. Chem. Int. Ed.* **2019**, *58*, 5261–5265.

(162) Sarma, B. B.; Kim, J.; Amsler, J.; Agostini, G.; Weidenthaler, C.; Pfänder, N.; Arenal, R.; Concepción, P.; Plessow, P.; Studt, F.; Prieto, G. One-Pot Cooperation of Single-Atom Rh and Ru Solid Catalysts for a Selective Tandem Olefin Isomerization-Hydrosilylation Process. *Angew. Chem. Int. Ed.* **2020**, *59*, 5806–5815.

(163) Abeynayake, N. S.; Zamora-Moreno, J.; Gorla, S.; Donnadieu, B.; Muñoz-Hernández, M. A.; Montiel-Palma, V. 14-Electron Rh and Ir Silylphosphine Complexes and Their Catalytic Activity in Alkene Functionalization with Hydrosilanes. *Dalton Trans.* **2021**, *50*, 11783–11792.

(164) Prieto, U.; Azpeitia, S.; Sebastian, E. S.; Freixa, Z.; Garralda, M. A.; Huertos, M. A. Steric Effects in the Catalytic Tandem Isomerization-Hydrosilylation Reaction. *ChemCatChem* **2021**, *13*, 1403–1409.

(165) Srivastava, R.; Jakoobi, M.; Thieuleux, C.; Quadrelli, E. A.; Camp, C. A Family of Rhodium(I) NHC Chelates Featuring O-Containing Tethers for Catalytic Tandem Alkene Isomerization–Hydrosilylation. *Dalton Trans.* **2021**, *50*, 869–879.

(166) Takahashi, T.; Hasegawa, M.; Suzuki, N.; Saburi, M.; Rousset, C. J.; Fanwick, P. E.; Negishi, E. Zirconium-Catalyzed Highly Regioselective Hydrosilation Reaction of Alkenes and X-Ray Structures of Silyl(Hydrido)Zirconocene Derivatives. *J. Am. Chem. Soc.* **1991**, *113*, 8564–8566.

(167) Buslov, I.; Song, F.; Hu, X. An Easily Accessed Nickel Nanoparticle Catalyst for Alkene Hydrosilylation with Tertiary Silanes. *Angew. Chem. Int. Ed.* **2016**, *55*, 12295–12299.

(168) Jakoobi, M.; Dardun, V.; Veyre, L.; Meille, V.; Camp, C.; Thieuleux, C. Developing a Highly Active Catalytic System Based on Cobalt Nanoparticles for Terminal and Internal Alkene Hydrosilylation. *J. Org. Chem.* **2020**, *85*, 11732–11740.

(169) Das, A.; Schleinitz, J.; Karmazin, L.; Vincent, B.; Le Breton, N.; Rogez, G.; Guenet, A.; Choua, S.; Grimaud, L.; Desage-El Murr, M. A Single Bioinspired Hexameric Nickel Catechol–Alloxazine Catalyst Combines Metal and Radical Mechanisms for Alkene Hydrosilylation. *Chem. – Eur. J.* **2022**, *28*, e202200596.

(170) Chang, A. S.; Kawamura, K. E.; Henness, H. S.; Salpino, V. M.; Greene, J. C.; Zakharov, L. N.; Cook, A. K. (NHC)Ni(0)-Catalyzed Branched-Selective Alkene Hydrosilylation with Secondary and Tertiary Silanes. *ACS Catal.* **2022**, *12*, 11002–11014.

(171) Zi-Qi Li; Turki Alturaifi; Matthew Joannou; Peng Liu; Keary Engle. Hemilabile Quinone Ligands Enable Nickel-Catalyzed C−S(Alkyl) Bond Formation in the Carbosulfenylation of Unactivated Alkenes **2023**, *ChemRxiv*.

(172) Kochi, T.; Kanno, S.; Kakiuchi, F. Nondissociative Chain Walking as a Strategy in Catalytic Organic Synthesis. *Tetrahedron Lett.* **2019**, *60*, 150938.

(173) Massad, I.; Marek, I. Alkene Isomerization through Allylmetals as a Strategic Tool in Stereoselective Synthesis. *ACS Catal.* **2020**, *10*, 5793–5804.

(174) Larionov, E.; Li, H.; Mazet, C. Well-Defined Transition Metal Hydrides in Catalytic Isomerizations. *Chem. Commun.* **2014**, *50*, 9816–9826.

(175) Liu, X. L., Bin; Liu, Qiang. Base-Metal-Catalyzed Olefin Isomerization Reactions. *Synthesis* **2019**, *51*, 1293–1310.

(176) Molloy, J. J.; Morack, T.; Gilmour, R. Positional and Geometrical Isomerisation of Alkenes: The Pinnacle of Atom Economy. *Angew. Chem. Int. Ed.* **2019**, *58*, 13654–13664.

(177) Dumesic, J. A.; Huber, G. W.; Boudart, M. Principles of Heterogeneous Catalysis. In *Handbook of Heterogeneous Catalysis*; **2008**.

(178) Cui, X.; Li, W.; Ryabchuk, P.; Junge, K.; Beller, M. Bridging Homogeneous and Heterogeneous Catalysis by Heterogeneous Single-Metal-Site Catalysts. *Nat. Catal.* **2018**, *1*, 385–397.

(179) Baxendale, I. R.; Lee, A.-L.; Ley, S. V. A Concise Synthesis of Carpanone Using Solid-Supported Reagents and Scavengers. *J. Chem. Soc. Perkin 1* **2002**, No. 16, 1850–1857.

(180) Larsen, C. R.; Paulson, E. R.; Erdogan, G.; Grotjahn, D. B. A Facile, Convenient, and Green Route to (*E*)-Propenylbenzene Flavors and Fragrances by Alkene Isomerization. *Synlett* **2015**, *26*, 2462–2466.

(181) Liu, Z.; Song, J.; Zhang, Y.; Sun, S.; Kun, Z.; Chen, J.; Xie, C.; Jia, X. A Rh-Catalyzed Isomerization of 1-Alkenes to (*E*)-2-Alkenes: From a Homogeneous Rh/PPh_3 Catalyst to a Heterogeneous $Rh/POP\text{-}PPh_3\text{-}SO_3Na$ Catalyst. *Catal. Sci. Technol.* **2023**, *13*, 963–967.

(182) Dunning, H. N. Review of Olefin Isomerization. *Ind. Eng. Chem.* **1953**, *45*, 551–564.

(183) Chuc, L. T. N.; Chen, C.-S.; Lo, W.-S.; Shen, P.-C.; Hsuan, Y.-C.; Tsai, H.-H. G.; Shieh, F.-K.; Hou, D.-R. Long-Range Olefin Isomerization Catalyzed by Palladium(0) Nanoparticles. *ACS Omega* **2017**, *2*, 698–711.

(184) Copéret, C.; Chabanas, M.; Petroff Saint-Arroman, R.; Basset, J.-M. Homogeneous and Heterogeneous Catalysis: Bridging the Gap through Surface Organometallic Chemistry. *Angew. Chem. Int. Ed.* **2003**, *42*, 156–181.

(185) Copéret, C.; Comas-Vives, A.; Conley, M. P.; Estes, D. P.; Fedorov, A.; Mougel, V.; Nagae, H.; Núñez-Zarur, F.; Zhizhko, P. A. Surface Organometallic and Coordination Chemistry toward Single-Site Heterogeneous Catalysts: Strategies, Methods, Structures, and Activities. *Chem. Rev.* **2016**, *116*, 323–421.

(186) Maier, S.; Cronin, S. P.; Vu Dinh, M.-A.; Li, Z.; Dyballa, M.; Nowakowski, M.; Bauer, M.; Estes, D. P. Immobilized Platinum Hydride Species as Catalysts for Olefin Isomerizations and Enyne Cycloisomerizations. *Organometallics* **2021**, *40*, 1751–1757.

(187) Desai, S. P.; Ye, J.; Zheng, J.; Ferrandon, M. S.; Webber, T. E.; Platero-Prats, A. E.; Duan, J.; Garcia-Holley, P.; Camaioni, D. M.; Chapman, K. W.; Delferro, M.; Farha, O. K.; Fulton, J. L.; Gagliardi, L.; Lercher, J. A.; Penn, R. L.; Stein, A.; Lu, C. C. Well-Defined Rhodium–Gallium Catalytic Sites in a Metal–Organic Framework: Promoter-Controlled Selectivity in Alkyne Semihydrogenation to E-Alkenes. *J. Am. Chem. Soc.* **2018**, *140*, 15309–15318.

(188) Sheng, D.; Zhang, Y.; Song, Q.; Xu, G.; Peng, D.; Hou, H.; Xie, R.; Shan, D.; Liu, P. Isomerization of 1-Butene to 2-Butene Catalyzed by Metal–Organic Frameworks. *Organometallics* **2020**, *39*, 51–57.

(189) Hicks, K. E.; Wolek, A. T. Y.; Farha, O. K.; Notestein, J. M. The Dependence of Olefin Hydrogenation and Isomerization Rates on Zirconium Metal–Organic Framework Structure. *ACS Catal.* **2022**, *12*, 13671–13680.

(190) Conley, M. P.; Mougel, V.; Peryshkov, D. V.; Forrest, W. P. Jr.; Gajan, D.; Lesage, A.; Emsley, L.; Copéret, C.; Schrock, R. R. A Well-Defined Silica-Supported Tungsten Oxo Alkylidene Is a Highly Active Alkene Metathesis Catalyst. *J. Am. Chem. Soc.* **2013**, *135*, 19068–19070.

(191) Staples, O.; Ferrandon, M. S.; Laurent, G. P.; Kanbur, U.; Kropf, A. J.; Gau, M. R.; Carroll, P. J.; McCullough, K.; Sorsche, D.; Perras, F. A.; Delferro, M.; Kaphan, D. M.; Mindiola, D. J. Silica Supported Organometallic IrI Complexes Enable Efficient Catalytic Methane Borylation. *J. Am. Chem. Soc.* **2023**, *145*, 7992–8000.

(192) Zhang, J.; Mason, A. H.; Motta, A.; Cesar, L. G.; Kratish, Y.; Lohr, T. L.; Miller, J. T.; Gao, Y.; Marks, T. J. Surface vs Homogeneous Organo-Hafnium Catalyst Ion-Pairing and Ligand Effects on Ethylene Homo- and Copolymerizations. *ACS Catal.* **2021**, *11*, 3239–3250.

(193) Cramer, R.; Lindsey, R. V. Jr. The Mechanism of Isomerization of Olefins with Transition Metal Catalysts. *J. Am. Chem. Soc.* **1966**, *88*, 3534–3544.

(194) Tolman, C. A. Chemistry of Tetrakis(Triethyl Phosphite) Nickel Hydride, $HNi[P(OEt)_3]_4^+$. I. Nickel Hydride Formation and Decay. *J. Am. Chem. Soc.* **1970**, *92*, 4217–4222.

(195) Tolman, C. A. Chemistry of Tetrakis(Triethyl Phosphite)Nickel Hydride, $HNi[P(OEt)_3]_4^+$. IV. Mechanism of Olefin Isomerization. *J. Am. Chem. Soc.* **1972**, *94*, 2994–2999.

(196) Hodges, A. M.; Linton, M.; Mau, A. W.-H.; Cavell, K. J.; Hey, J. A.; Seen, A. J. Perfluorinated Membranes as Catalyst Supports. *Appl. Organomet. Chem.* **1990**, *4*, 465–473.

(197) Raje, A. P.; Datta, R. Activity and Stability of Ion-Exchange Resin-Supported Tetrakis(Triethyl Phosphite)Nickel Hydride Catalyst: Vapor Phase Isomerization of n-Butene. *J. Mol. Catal.* **1992**, *72*, 97–116.

(198) Witzke, R. J.; Chapovetsky, A.; Conley, M. P.; Kaphan, D. M.; Delferro, M. Nontraditional Catalyst Supports in Surface Organometallic Chemistry. *ACS Catal.* **2020**, *10*, 11822–11840.

(199) Samudrala, K. K.; Conley, M. P. Effects of Surface Acidity on the Structure of Organometallics Supported on Oxide Surfaces. *Chem. Commun.* **2023**, *59*, 4115–4127.

(200) Stalzer, M. M.; Nicholas, C. P.; Bhattacharyya, A.; Motta, A.; Delferro, M.; Marks, T. J. Single-Face/All-Cis Arene Hydrogenation by a Supported Single-Site D0 Organozirconium Catalyst. *Angew. Chem. Int. Ed.* **2016**, *55*, 5263–5267.

(201) Syed, Z. H.; Kaphan, D. M.; Perras, F. A.; Pruski, M.; Ferrandon, M. S.; Wegener, E. C.; Celik, G.; Wen, J.; Liu, C.; Dogan, F.; Goldberg, K. I.; Delferro, M. Electrophilic Organoiridium(III) Pincer Complexes on Sulfated Zirconia for Hydrocarbon Activation and Functionalization. *J. Am. Chem. Soc.* **2019**, *141*, 6325–6337.

(202) Tafazolian, H.; Culver, D. B.; Conley, M. P. A Well-Defined Ni(II) α-Diimine Catalyst Supported on Sulfated Zirconia for Polymerization Catalysis. *Organometallics* **2017**, *36*, 2385–2388.

(203) Culver, D. B.; Tafazolian, H.; Conley, M. P. A Bulky Pd(II) α-Diimine Catalyst Supported on Sulfated Zirconia for the Polymerization of Ethylene and Copolymerization of Ethylene and Methyl Acrylate. *Organometallics* **2018**, *37*, 1001–1006.

(204) Klet, R. C.; Kaphan, D. M.; Liu, C.; Yang, C.; Kropf, A. J.; Perras, F. A.; Pruski, M.; Hock, A. S.; Delferro, M. Evidence for Redox Mechanisms in Organometallic Chemisorption and Reactivity on Sulfated Metal Oxides. *J. Am. Chem. Soc.* **2018**, *140*, 6308–6316.

(205) Kaphan, D. M.; Klet, R. C.; Perras, F. A.; Pruski, M.; Yang, C.; Kropf, A. J.; Delferro, M. Surface Organometallic Chemistry of Supported Iridium(III) as a Probe for Organotransition Metal–Support Interactions in C–H Activation. *ACS Catal.* **2018**, *8*, 5363–5373.

(206) Gao, J.; Zhu, L.; Conley, M. P. Cationic Tantalum Hydrides Catalyze Hydrogenolysis and Alkane Metathesis Reactions of Paraffins and Polyethylene. *J. Am. Chem. Soc.* **2023**, *145*, 4964–4968.

(207) Hino, M.; Arata, K. Synthesis of Solid Superacid Catalyst with Acid Strength of H0⩽–16.04. *J. Chem. Soc. Chem. Commun.* **1980**, No. 18, 851–852.

(208) Seen, A. J. Nafion: An Excellent Support for Metal-Complex Catalysts. *Catal. Funct. Synth. Resins Issue Catal. Access. Stab.* **2001**, *177*, 105–112.

(209) Rimoldi, M.; Fodor, D.; van Bokhoven, J. A.; Mezzetti, A. A Stable 16-Electron Iridium(Iii) Hydride Complex Grafted on SBA-15: A Single-Site Catalyst for Alkene Hydrogenation. *Chem. Commun.* **2013**, *49*, 11314–11316.

(210) Imoto, H.; Moriyama, H.; Saito, T.; Sasaki, Y. Synthesis of Cationic Hydride and Related Complexes of Palladium and Nickel with Tricyclohexylphosphine or Triisopropylphosphine. *J. Organomet. Chem.* **1976**, *120*, 453–460.

(211) Hitchcock, P. B.; Lappert, M. F.; MacBeath, C.; Scott, F. P. E.; Warhurst, N. J. W. The Synthesis and Characterisation of Some Divinyldisiloxane—(Tertiary Phosphine) Complexes of Platinum(0) and Nickel(0). *J. Organomet. Chem.* **1997**, *528*, 185–190.

(212) Panigrahi, D.; Mondal, M.; Gupta, R.; Mani, G. Four- and Five-Coordinate Nickel(Ii) Complexes Bearing New Diphosphine–Phosphonite and Triphosphine–Phosphite Ligands: Catalysts for N-Alkylation of Amines. *RSC Adv.* **2022**, *12*, 4510–4520.

(213) Collins, K. D.; Glorius, F. Intermolecular Reaction Screening as a Tool for Reaction Evaluation. *Acc. Chem. Res.* **2015**, *48*, 619–627.

(214) Crossley, S. W. M.; Barabé, F.; Shenvi, R. A. Simple, Chemoselective, Catalytic Olefin Isomerization. *J. Am. Chem. Soc.* **2014**, *136*, 16788–16791.

(215) Li, G.; Kuo, J. L.; Han, A.; Abuyuan, J. M.; Young, L. C.; Norton, J. R.; Palmer, J. H. Radical Isomerization and Cycloisomerization Initiated by H• Transfer. *J. Am. Chem. Soc.* **2016**, *138*, 7698–7704.

(216) Liu, X.; Zhang, W.; Wang, Y.; Zhang, Z.-X.; Jiao, L.; Liu, Q. Cobalt-Catalyzed Regioselective Olefin Isomerization Under Kinetic Control. *J. Am. Chem. Soc.* **2018**, *140*, 6873–6882.

(217) Zhang, S.; Bedi, D.; Cheng, L.; Unruh, D. K.; Li, G.; Findlater, M. Cobalt(II)-Catalyzed Stereoselective Olefin Isomerization: Facile Access to Acyclic Trisubstituted Alkenes. *J. Am. Chem. Soc.* **2020**, *142*, 8910–8917.

(218) Liu, H.; Cai, C.; Ding, Y.; Chen, J.; Liu, B.; Xia, Y. Cobalt-Catalyzed E-Selective Isomerization of Alkenes with a Phosphine-Amido-Oxazoline Ligand. *ACS Omega* **2020**, *5*, 11655–11670.

(219) Yu, X.; Zhao, H.; Li, P.; Koh, M. J. Iron-Catalyzed Tunable and Site-Selective Olefin Transposition. *J. Am. Chem. Soc.* **2020**, *142*, 18223–18230.

(220) Xu, S.; Geng, P.; Li, Y.; Liu, G.; Zhang, L.; Guo, Y.; Huang, Z. Pincer Iron Hydride Complexes for Alkene Isomerization: Catalytic Approach to Trisubstituted (*Z*)-Alkenyl Boronates. *ACS Catal.* **2021**, *11*, 10138–10147.

(221) Xu, S.; Liu, G.; Huang, Z. Iron Catalyzed Isomerization of α-Alkyl Styrenes to Access Trisubstituted Alkenes. *Chin. J. Chem.* **2021**, *39*, 585–589.

(222) Larsen, C. R.; Grotjahn, D. B. Stereoselective Alkene Isomerization over One Position. *J. Am. Chem. Soc.* **2012**, *134*, 10357–10360.

(223) Kinetic Control via Chelation through the Oxygen Is Also a Possibility. See Ref 224.

(224) Clark, H. C.; Kurosawa, H. Chemistry of Hydrides. XV. Mechanism of Double-Bond Migration Induced by Platinum(II) Hydrides. *Inorg. Chem.* **1973**, *12*, 1566–1569.

(225) Yu, Y.; Smith, J. M.; Flaschenriem, C. J.; Holland, P. L. Binding Affinity of Alkynes and Alkenes to Low-Coordinate Iron. *Inorg. Chem.* **2006**, *45*, 5742–5751.

(226) Lemaire-Audoire, S.; Savignac, M.; Genêt, J. P.; Bernard, J.-M. Selective Deprotection of Allyl Amines Using Palladium. *Tetrahedron Lett.* **1995**, *36*, 1267–1270.

(227) Bao, L.; Liang, H.; Zhang, H.; Yan, Z.; Sun, C.; Pang, S. Polystyrene-Supported Nickel Complex Catalysed Deprotection of Allylic Tertiary Amine with Sodium Borohydride. *IOP Conf. Ser. Mater. Sci. Eng.* **2020**, *772*, 012101.

(228) Kapat, A.; Sperger, T.; Guven, S.; Schoenebeck, F. *E*-Olefins through Intramolecular Radical Relocation. *Science* **2019**, *363*, 391–396.

(229) Rubel, C.; Ravn, A.; Yang, S.; Li, Z.-Q.; Engle, K.; Vantourout, J. Stereodivergent, Kinetically Controlled Isomerization of Terminal Alkenes via Nickel Catalysis. **2022**, *ChemRxiv*.

(230) Kawamura, K. E.; Chang, A. S.; Martin, D. J.; Smith, H. M.; Morris, P. T.; Cook, A. K. Modular Ni(0)/Silane Catalytic System for the Isomerization of Alkenes. *Organometallics* **2022**, *41*, 486–496.

(231) Saputra, L.; Arifin; Gustini, N.; Sinambela, N.; Indriyani, N. P.; Sakti, A. W.; Arrozi, U. S. F.; Martoprawiro, M. A.; Patah, A.; Permana, Y. Nitrile Modulated-Ni(0) Phosphines in Trans-Selective Phenylpropenoids Isomerization: An Allylic Route by a Regular η^1-N(*end-on*) or an Alkyl Route via a Flipped-Nitrile? *Mol. Catal.* **2022**, *533*, 112768.

(232) Huang, L.; Lim, E. Q.; Koh, M. J. Secondary Phosphine Oxide-Activated Nickel Catalysts for Site-Selective Alkene Isomerization and Remote Hydrophosphination. *Chem Catal.* **2022**, *2*, 508–518.

(233) Tricoire, M.; Wang, D.; Rajeshkumar, T.; Maron, L.; Danoun, G.; Nocton, G. Electron Shuttle in *N*-Heteroaromatic Ni Catalysts for Alkene Isomerization. *JACS Au* **2022**, *2*, 1881–1888.

(234) Cruz, T. F. C.; Lopes, P. S.; Gomes, P. T. Allylnickel(II) Complexes of Bulky 5-Substituted-2-Iminopyrrolyl Ligands. *Polyhedron* **2021**, *207*, 115357.

(235) Iwamoto, H.; Tsuruta, T.; Ogoshi, S. Development and Mechanistic Studies of (E)-Selective Isomerization/Tandem Hydroarylation Reactions of Alkenes with a Nickel(0)/Phosphine Catalyst. *ACS Catal.* **2021**, *11*, 6741–6749.

(236) Kathe, P. M.; Caciuleanu, A.; Berkefeld, A.; Fleischer, I. Tandem Olefin Isomerization/Cyclization Catalyzed by Complex Nickel Hydride and Brønsted Acid. *J. Org. Chem.* **2020**, *85*, 15183–15196.

(237) Gauthier, D.; Lindhardt, A. T.; Olsen, E. P. K.; Overgaard, J.; Skrydstrup, T. In Situ Generated Bulky Palladium Hydride Complexes as Catalysts for the Efficient Isomerization of Olefins. Selective Transformation of Terminal Alkenes to 2-Alkenes. *J. Am. Chem. Soc.* **2010**, *132*, 7998–8009.

(238) Bullock, R. M.; Samsel, E. G. Hydrogen Atom Transfer Reactions of Transition-Metal Hydrides. Utilization of a Radical Rearrangement in the Determination of Hydrogen Atom Transfer Rates. *J. Am. Chem. Soc.* **1987**, *109*, 6542–6544.

(239) Liu, Y.; Wang, Q.-L.; Chen, Z.; Zhou, C.-S.; Xiong, B.-Q.; Zhang, P.-L.; Yang, C.-A.; Zhou, Q. Oxidative Radical Ring-Opening/Cyclization of Cyclopropane Derivatives. *Beilstein J. Org. Chem.* **2019**, *15*, 256–278.

(240) Zuo, G.; Louie, J. Highly Active Nickel Catalysts for the Isomerization of Unactivated Vinyl Cyclopropanes to Cyclopentenes. *Angew. Chem. Int. Ed.* **2004**, *43*, 2277–2279.

(241) RajanBabu, T. V. Asymmetric Hydrovinylation Reaction. *Chem. Rev.* **2003**, *103*, 2845–2860.

(242) RajanBabu, T. V. In Pursuit of an Ideal Carbon-Carbon Bond-Forming Reaction: Development and Applications of the Hydrovinylation of Olefins. *Synlett* **2009**, *2009*, 853–885.

(243) Hilt, G. Hydrovinylation Reactions – Atom-Economic Transformations with Steadily Increasing Synthetic Potential. *Eur. J. Org. Chem.* **2012**, *2012*, 4441–4451.

(244) Suginome, M.; Ohmura, T. Transition Metal-Catalyzed Element-Boryl Additions to Unsaturated Organic Compounds. In *Boronic Acids*; 2011; pp 171–212.

(245) Marciniec, B. Hydrosilylation of Alkenes and Their Derivatives. In *Hydrosilylation: A Comprehensive Review on Recent Advances*; Marciniec, B., Ed.; Springer Netherlands: Dordrecht, **2009**; pp 3–51.

(246) Keim, W. Oligomerization of Ethylene to α-Olefins: Discovery and Development of the Shell Higher Olefin Process (SHOP). *Angew. Chem. Int. Ed.* **2013**, *52*, 12492–12496.

(247) Obligacion, J. V.; Chirik, P. J. Earth-Abundant Transition Metal Catalysts for Alkene Hydrosilylation and Hydroboration. *Nat. Rev. Chem.* **2018**, *2*, 15–34.

(248) Geier, S. J.; Vogels, C. M.; Melanson, J. A.; Westcott, S. A. The Transition Metal-Catalysed Hydroboration Reaction. *Chem. Soc. Rev.* **2022**, *51*, 8877–8922.

(249) Miyaura, Norio.; Suzuki, Akira. Palladium-Catalyzed Cross-Coupling Reactions of Organoboron Compounds. *Chem. Rev.* **1995**, *95*, 2457–2483.

(250) Valente, C.; Organ, M. G. The Contemporary Suzuki–Miyaura Reaction. In *Boronic Acids*; **2011**; pp 213–262.

(251) Farhang, M.; Akbarzadeh, A. R.; Rabbani, M.; Ghadiri, A. M. A Retrospective-Prospective Review of Suzuki–Miyaura Reaction: From Cross-Coupling Reaction to Pharmaceutical Industry Applications. *Polyhedron* **2022**, *227*, 116124.

(252) Nakao, Y.; Hiyama, T. Silicon-Based Cross-Coupling Reaction: An Environmentally Benign Version. *Chem. Soc. Rev.* **2011**, *40*, 4893–4901.

(253) Jones, G. R.; Landais, Y. The Oxidation of the Carbon-Silicon Bond. *Tetrahedron* **1996**, *52*, 7599–7662.

(254) Roy, A.; Oestreich, M. At Long Last: The Me3Si Group as a Masked Alcohol. *Angew. Chem. Int. Ed.* **2021**, *60*, 4408–4410.

(255) Tamao, K.; Ishida, N.; Tanaka, T.; Kumada, M. Silafunctional Compounds in Organic Synthesis. Part 20. Hydrogen Peroxide Oxidation of the Silicon-Carbon Bond in Organoalkoxysilanes. *Organometallics* **1983**, *2*, 1694–1696.

(256) Fleming, I.; Henning, R.; Plaut, H. The Phenyldimethylsilyl Group as a Masked Form of the Hydroxy Group. *J. Chem. Soc. Chem. Commun.* **1984**, No. 1, 29–31.

(257) Marciniec, B. Functionalisation and Cross-Linking of Organosilicon Polymers. In *Hydrosilylation: A Comprehensive Review on Recent Advances*; Marciniec, B., Ed.; Springer Netherlands: Dordrecht, **2009**; pp 159–189.

(258) Marciniec, B. Hydrosilylation Polymerisation. In *Hydrosilylation: A Comprehensive Review on Recent Advances*; Marciniec, B., Ed.; Springer Netherlands: Dordrecht, **2009**; pp 191–214.

(259) Marciniec, B. Organosilicon – Organic Hybrid Polymers and Materials. In *Hydrosilylation: A Comprehensive Review on Recent Advances*; Marciniec, B., Ed.; Springer Netherlands: Dordrecht, **2009**; pp 241–286.

(260) Hirano, K.; Yorimitsu, H.; Oshima, K. Nickel-Catalyzed β-Boration of α,β-Unsaturated Esters and Amides with Bis(Pinacolato)Diboron. *Org. Lett.* **2007**, *9*, 5031–5033.

(261) Yu, X.; Zhao, H.; Xi, S.; Chen, Z.; Wang, X.; Wang, L.; Lin, L. Q. H.; Loh, K. P.; Koh, M. J. Site-Selective Alkene Borylation Enabled by Synergistic Hydrometallation and Borometallation. *Nat. Catal.* **2020**, *3*, 585–592.

(262) Chang, A. S.; Kawamura, K. E.; Henness, H. S.; Salpino, V. M.; Greene, J. C.; Zakharov, L. N.; Cook, A. K. (NHC)Ni(0)-Catalyzed Branched-Selective Alkene Hydrosilylation with Secondary and Tertiary Silanes. *ACS Catal.* **2022**, *12*, 11002–11014.

(263) Kuhn, N.; Kratz, T. Synthesis of Imidazol-2-Ylidenes by Reduction of Imidazole-2(3H)-Thiones. *Synthesis* **2002**, *1993*, 561–562.

(264) Bantreil, X.; Nolan, S. P. Synthesis of N-Heterocyclic Carbene Ligands and Derived Ruthenium Olefin Metathesis Catalysts. *Nat. Protoc.* **2011**, *6*, 69–77.

(265) Hintermann, L. Expedient Syntheses of the N-Heterocyclic Carbene Precursor Imidazolium Salts IPr·HCl, IMes·HCl and IXy·HCl. *Beilstein J. Org. Chem.* **2007**, *3*, 22.

(266) You, S.; Zhang, R.; Cai, M. A Magnetically Recyclable Palladium-Catalyzed Formylation of Aryl Iodides with Formic Acid as CO Source: A Practical Access to Aromatic Aldehydes. *Synthesis* **2021**, *53*, 1962–1970.

(267) Kathe, P. M.; Berkefeld, A.; Fleischer, I. Nickel Hydride Catalyzed Cleavage of Allyl Ethers Induced by Isomerization. *Synlett* **2021**, *32*, 1629–1632.

(268) Ren, T.; Chen, Q.; Zhao, C.; Zheng, Q.; Xie, H.; North, M. Introducing the Tishchenko Reaction into Sustainable Polymer Chemistry. *Green Chem.* **2020**, *22*, 1542–1547.

(269) Zhang, S.; Bedi, D.; Cheng, L.; Unruh, D. K.; Li, G.; Findlater, M. Cobalt(II)-Catalyzed Stereoselective Olefin Isomerization: Facile Access to Acyclic Trisubstituted Alkenes. *J. Am. Chem. Soc.* **2020**, *142*, 8910–8917.

(270) Denmark, S. E.; Butler, C. R. Vinylation of Aromatic Halides Using Inexpensive Organosilicon Reagents. Illustration of Design of Experiment Protocols. *J. Am. Chem. Soc.* **2008**, *130*, 3690–3704.

(271) Chu, L.; Qing, F.-L. Copper-Mediated Oxidative Trifluoromethylation of Boronic Acids. *Org. Lett.* **2010**, *12*, 5060–5063.

(272) Shin, J. H.; Seong, E. Y.; Mun, H. J.; Jang, Y. J.; Kang, E. J. Electronically Mismatched Cycloaddition Reactions via First-Row Transition Metal, Iron(III)–Polypyridyl Complex. *Org. Lett.* **2018**, *20*, 5872–5876.

(273) Fauvel, A.; Deleuze, H.; Landais, Y. New Polymer-Supported Organosilicon Reagents. *Eur. J. Org. Chem.* **2005**, *2005*, 3900–3910.

(274) Wu, Y.; Liu, C.; Wang, C.; Lu, S.; Zhang, B. Selective Transfer Semihydrogenation of Alkynes with H_2O (D_2O) as the H (D) Source over a Pd-P Cathode. *Angew. Chem. Int. Ed.* **2020**, *59*, 21170–21175.

(275) Paul, C. E.; Rajagopalan, A.; Lavandera, I.; Gotor-Fernández, V.; Kroutil, W.; Gotor, V. Expanding the Regioselective Enzymatic Repertoire: Oxidative Mono-Cleavage of Dialkenes Catalyzed by Trametes Hirsuta. *Chem. Commun.* **2012**, *48*, 3303–3305.

(276) Prince, P. D.; Bearpark, M. J.; McGrady, G. S.; Steed, J. W. Hypervalent Hydridosilicates: Synthesis, Structure and Hydride Bridging. *Dalton Trans.* **2008**, No. 2, 271–282.

(277) Binder, J.; Fischer, R. C.; Flock, M.; Stammler, H.-G.; Torvisco, A.; Uhlig, F. Novel Aryl-Substituted Silanes Part II: Synthesis and Characterization of Diaryl Silicon Dihydrides. *Phosphorus Sulfur Silicon Relat. Elem.* **2016**, *191*, 478–487.

(278) Hirone, N.; Sanjiki, H.; Tanaka, R.; Hata, T.; Urabe, H. Acceleration of the Substitution of Silanes with Grignard Reagents by Using Either LiCl or YCl_3/MeLi. *Angew. Chem. Int. Ed.* **2010**, *49*, 7762–7764.

(279) Guo, J.; Shen, X.; Lu, Z. Regio- and Enantioselective Cobalt-Catalyzed Sequential Hydrosilylation/Hydrogenation of Terminal Alkynes. *Angew. Chem. Int. Ed.* **2017**, *56*, 615–618.

(280) Zuo, Z.; Xu, S.; Zhang, L.; Gan, L.; Fang, H.; Liu, G.; Huang, Z. Cobalt-Catalyzed Asymmetric Hydrogenation of Vinylsilanes with a Phosphine–Pyridine–Oxazoline Ligand: Synthesis of Optically Active Organosilanes and Silacycles. *Organometallics* **2019**, *38*, 3906–3911.

(281) Yang, X.; Bai, Y.; Li, J.; Dai, Z.; Peng, J. Hydrosilylation of Alkenes Catalyzed by Fe Powder. *Phosphorus Sulfur Silicon Relat. Elem.* **2019**, *194*, 1–4.

(282) DeLucia, N. A.; Das, N.; Vannucci, A. K. Mild Synthesis of Silyl Ethers via Potassium Carbonate Catalyzed Reactions between Alcohols and Hydrosilanes. *Org. Biomol. Chem.* **2018**, *16*, 3415–3418.

(283) Marin-Luna, M.; Pölloth, B.; Zott, F.; Zipse, H. Size-Dependent Rate Acceleration in the Silylation of Secondary Alcohols: The Bigger the Faster. *Chem. Sci.* **2018**, *9*, 6509–6515.

(284) Tang, Z.-L. A New Route to Preparations of Silyl Ethers by Reactions of Silyl Triflimides with Alcohol or Ether. *Chin. J. Chem.* **2008**, *26*, 525–530.

(285) Scharfbier, J.; Gross, B. M.; Oestreich, M. Stereospecific and Chemoselective Copper-Catalyzed Deaminative Silylation of Benzylic Ammonium Triflates. *Angew. Chem. Int. Ed.* **2020**, *59*, 1577–1580.

(286) Li, J.; Peng, J.; Bai, Y.; Zhang, G.; Lai, G.; Li, X. Phosphines with 2-Imidazolium Ligands Enhance the Catalytic Activity and Selectivity of Rhodium Complexes for Hydrosilylation Reactions. *J. Organomet. Chem.* **2010**, *695*, 431–436.

(287) Yu, X.; Zhao, H.; Li, P.; Koh, M. J. Iron-Catalyzed Tunable and Site-Selective Olefin Transposition. *J. Am. Chem. Soc.* **2020**, *142*, 18223–18230.

(288) G. M. Sheldrick, Bruker/Siemens Area Detector Absorption Correction Program, Bruker AXS, Madison, WI, **1998**.

(289) Sheldrick, G. M. Crystal Structure Refinement with SHELXL. *Acta Cryst* **2015**, *C71*, 3–8.

(290) Beillard, A.; Métro, T.-X.; Bantreil, X.; Martinez, J.; Lamaty, F. Cu(0), O_2 and Mechanical Forces: A Saving Combination for Efficient Production of Cu–NHC Complexes. *Chem. Sci.* **2017**, *8*, 1086–1089.

(291) Tran, V. T.; Li, Z.-Q.; Apolinar, O.; Derosa, J.; Joannou, M. V.; Wisniewski, S. R.; Eastgate, M. D.; Engle, K. M. Ni(COD)(DQ): An Air-Stable 18-Electron Nickel(0)–Olefin Precatalyst. *Angew. Chem. Int. Ed.* **2020**, *59*, 7409–7413.

(292) Https://Www.Sigmaaldrich.Com/US/En/Product/Aldrich/346462.

(293) Peron, J.; Mani, A.; Zhao, X.; Edwards, D.; Adachi, M.; Soboleva, T.; Shi, Z.; Xie, Z.; Navessin, T.; Holdcroft, S. Properties of Nafion® NR-211 Membranes for PEMFCs. *J. Membr. Sci.* **2010**, *356*, 44–51.

(294) Siril, P. F.; Cross, H. E.; Brown, D. R. New Polystyrene Sulfonic Acid Resin Catalysts with Enhanced Acidic and Catalytic Properties. *J. Mol. Catal. Chem.* **2008**, *279*, 63–68.

(295) Bailey, P. J.; Coxall, R. A.; Dick, C. M.; Fabre, S.; Henderson, L. C.; Herber, C.; Liddle, S. T.; Loroño-González, D.; Parkin, A.; Parsons, S. The First Structural Characterisation of a Group 2 Metal Alkylperoxide Complex: Comments on the Cleavage of Dioxygen by Magnesium Alkyl Complexes. *Chem. – Eur. J.* **2003**, *9*, 4820–4828.

(296) Gladfelder, J. J.; Ghosh, S.; Podunavac, M.; Cook, A. W.; Ma, Y.; Woltornist, R. A.; Keresztes, I.; Hayton, T. W.; Collum, D. B.; Zakarian, A. Enantioselective Alkylation of 2-Alkylpyridines Controlled by Organolithium Aggregation. *J. Am. Chem. Soc.* **2019**, *141*, 15024–15028.

(297) Fortier, S.; Walensky, J. R.; Wu, G.; Hayton, T. W. Synthesis of a Phosphorano-Stabilized U(IV)-Carbene via One-Electron Oxidation of a U(III)-Ylide Adduct. *J. Am. Chem. Soc.* **2011**, *133*, 6894–6897.

(298) Bartlett, S. A.; Badiola, K. A.; Arandiyan, H.; Masters, A. F.; Maschmeyer, T. The Autocatalytic Isomerization of Allylbenzene by Nickel(0) Tetrakis(Triethylphosphite). *Eur. J. Inorg. Chem.* **2018**, *2018*, 3384–3387.

(299) Chen, C.; Luo, Z.; Yang, H.; Feng, Y. A Novel Synthetic Route for Berberine Chloride. *Chin. J. Org. Chem.* **2016**, *36*, 1426–1430.

(300) Gensler, W.; Stouffer, J. Notes - Compounds Related to Podophyllotoxin. IX. 3,4-Methylenedioxyphenylithium. *J. Org. Chem.* **1958**, *23*, 908–910.

(301) Davies, J.; Janssen-Müller, D.; Zimin, D. P.; Day, C. S.; Yanagi, T.; Elfert, J.; Martin, R. Ni-Catalyzed Carboxylation of Aziridines En Route to β-Amino Acids. *J. Am. Chem. Soc.* **2021**, *143*, 4949–4954.

(302) Hong, X.; Tan, Q.; Liu, B.; Xu, B. Isocyanide-Induced Activation of Copper Sulfate: Direct Access to Functionalized Heteroarene Sulfonic Esters. *Angew. Chem. Int. Ed.* **2017**, *56* (14), 3961–3965.

(303) Albarrán-Velo, J.; Gotor-Fernández, V.; Lavandera, I. Markovnikov Wacker-Tsuji Oxidation of Allyl(Hetero)Arenes and Application in a One-Pot Photo-Metal-Biocatalytic Approach to Enantioenriched Amines and Alcohols. *Adv. Synth. Catal.* **2021**, *363*, 4096–4108.

(304) Huo, X.; Quan, M.; Yang, G.; Zhao, X.; Liu, D.; Liu, Y.; Zhang, W. Hydrogen-Bond-Activated Palladium-Catalyzed Allylic Alkylation via Allylic Alkyl Ethers: Challenging Leaving Groups. *Org. Lett.* **2014**, *16*, 1570–1573.

(305) Zhou, S.; Zhang, G.; Fu, L.; Chen, P.; Li, Y.; Liu, G. Copper-Catalyzed Asymmetric Cyanation of Alkenes via Carbonyl-Assisted Coupling of Alkyl-Substituted Carbon-Centered Radicals. *Org. Lett.* **2020**, *22*, 6299–6303.

(306) Clary, J. W.; Rettenmaier, T. J.; Snelling, R.; Bryks, W.; Banwell, J.; Wipke, W. T.; Singaram, B. Hydride as a Leaving Group in the Reaction of Pinacolborane with Halides under Ambient Grignard and Barbier Conditions. One-Pot Synthesis of Alkyl, Aryl, Heteroaryl, Vinyl, and Allyl Pinacolboronic Esters. *J. Org. Chem.* **2011**, *76*, 9602–9610.

(307) Qi, X.; Chen, P.; Liu, G. Catalytic Oxidative Trifluoromethoxylation of Allylic C−H Bonds Using a Palladium Catalyst. *Angew. Chem. Int. Ed.* **2017**, *56*, 9517–9521.

(308) Wipf, P.; Maciejewski, J. P. Titanocene(III)-Catalyzed Formation of Indolines and Azaindolines. *Org. Lett.* **2008**, *10*, 4383–4386.

(309) Hamaguchi, T.; Takahashi, Y.; Tsuji, H.; Kawatsura, M. Nickel-Catalyzed Hydroarylation of in Situ Generated 1,3-Dienes with Arylboronic Acids Using a Secondary Homoallyl Carbonate as a Surrogate for the 1,3-Diene and Hydride Source. *Org. Lett.* **2020**, *22*, 1124–1129.

(310) Blaisdell, T. P.; Caya, T. C.; Zhang, L.; Sanz-Marco, A.; Morken, J. P. Hydroxyl-Directed Stereoselective Diboration of Alkenes. *J. Am. Chem. Soc.* **2014**, *136*, 9264–9267.

(311) Bieber, L. W.; da Silva, M. F. Copper Catalyzed Regioselective Coupling of Allylic Halides and Alkynes Promoted by Weak Inorganic Bases. *Tetrahedron Lett.* **2007**, *48*, 7088–7090.

(312) Dible, B. R.; Sigman, M. S.; Arif, A. M. Oxygen-Induced Ligand Dehydrogenation of a Planar Bis-μ-Chloronickel(I) Dimer Featuring an NHC Ligand. *Inorg. Chem.* **2005**, *44*, 3774–3776.

(313) Pokrovski, K.; Jung, K. T.; Bell, A. T. Investigation of CO and CO2 Adsorption on Tetragonal and Monoclinic Zirconia. *Langmuir* **2001**, *17* (14), 4297–4303.

(314) Cook, A. K.; Copéret, C. Alkyne Hydroamination Catalyzed by Silica-Supported Isolated Zn(II) Sites. *Organometallics* **2018**, *37*, 1342–1345.

(315) Meyet, J.; Searles, K.; Newton, M. A.; Wörle, M.; van Bavel, A. P.; Horton, A. D.; van Bokhoven, J. A.; Copéret, C. Monomeric Copper(II) Sites Supported on Alumina Selectively Convert Methane to Methanol. *Angew. Chem. Int. Ed.* **2019**, *58*, 9841–9845.

(316) Oliverio, M.; Costanzo, P.; Paonessa, R.; Nardi, M.; Procopio, A. Catalyst-Free Tosylation of Lipophilic Alcohols in Water. *RSC Adv.* **2013**, *3*, 2548–2552.

(317) Hu, Y.; Zhang, S.; Yu, X.; Feng, X.; Yamaguchi, M.; Bao, M. Spirocarbocycle Synthesis from Chloromethylarenes via Transition-Metal-Catalyzed Allylative Dearomatization and Ring Closure Metathesis. *J. Org. Chem.* **2022**, *87*, 8229–8236.

(318) Mayer, M.; Welther, A.; Jacobi von Wangelin, A. Iron-Catalyzed Isomerizations of Olefins. *ChemCatChem* **2011**, *3*, 1567–1571.

(319) Nakayama, K.; Maeta, N.; Horiguchi, G.; Kamiya, H.; Okada, Y. Radical Cation Diels–Alder Reactions by TiO2 Photocatalysis. *Org. Lett.* **2019**, *21*, 2246–2250.

(320) Nave, S.; Sonawane, R. P.; Elford, T. G.; Aggarwal, V. K. Protodeboronation of Tertiary Boronic Esters: Asymmetric Synthesis of Tertiary Alkyl Stereogenic Centers. *J. Am. Chem. Soc.* **2010**, *132*, 17096–17098.

(321) Hogan, A.-M. L.; Tricotet, T.; Meek, A.; Khokhar, S. S.; O'Shea, D. F. Applications of Enantioselective Carbolithiation of Ortho-Substituted β-Methylstyrenes. *J. Org. Chem.* **2008**, *73*, 6041–6044.

(322) Wu, Q.; Wang, L.; Jin, R.; Kang, C.; Bian, Z.; Du, Z.; Ma, X.; Guo, H.; Gao, L. Nickel-Catalyzed Allylic C(Sp^2)–H Activation: Stereoselective Allyl Isomerization and Regiospecific Allyl Arylation of Allylarenes. *Eur. J. Org. Chem.* **2016**, *2016*, 5415–5422.

(323) Jolly, P. I.; Fleary-Roberts, N.; O'Sullivan, S.; Doni, E.; Zhou, S.; Murphy, J. A. Reactions of Triflate Esters and Triflamides with an Organic Neutral Super-Electron-Donor. *Org. Biomol. Chem.* **2012**, *10*, 5807–5810.

(324) Bieniek, M.; Samojłowicz, C.; Sashuk, V.; Bujok, R.; Śledź, P.; Lugan, N.; Lavigne, G.; Arlt, D.; Grela, K. Rational Design and Evaluation of Upgraded Grubbs/Hoveyda Olefin Metathesis Catalysts: Polyfunctional Benzylidene Ethers on the Test Bench. *Organometallics* **2011**, *30*, 4144–4158.

(325) Flanagan, J. C. A.; Myung, J.; Criddle, C. S.; Waymouth, R. M. Poly(Hydroxyalkanoate)s from Waste Biomass: A Combined Chemical–Biological Approach. *ChemistrySelect* **2016**, *1*, 2327–2331.

(326) Tasic, G.; Simic, M.; Popovic, S.; Husinec, S.; Maslak, V.; Savic, V. Indirect N-Vinylation of Indoles via Isomerisation of N-Allyl Derivatives: Synthesis of (±)-Debromoarborescidine B. *Tetrahedron Lett.* **2013**, *54*, 4536–4539.

(327) Brown, H. C.; Basavaiah, D.; Kulkarni, S. U.; Bhat, N. G.; Prasad, J. V. N. V. Vinylic Organoboranes. 9. A General Stereospecific Synthesis of (*Z*)- and (*E*)-Disubstituted Alkenes via Organoboranes. *J. Org. Chem.* **1988**, *53*, 239–246.

(328) Liu, H.; Xu, M.; Cai, C.; Chen, J.; Gu, Y.; Xia, Y. Cobalt-Catalyzed Z to E Isomerization of Alkenes: An Approach to (E)-β-Substituted Styrenes. *Org. Lett.* **2020**, *22*, 1193–1198.

(329) Lim, K. M.-H.; Hayashi, T. Rhodium-Catalyzed Asymmetric Arylation of Allyl Sulfones under the Conditions of Isomerization into Alkenyl Sulfones. *J. Am. Chem. Soc.* **2015**, *137*, 3201–3204.

(330) Arata, M.; Miura, T.; Chiba, K. Electrocatalytic Formal [2+2] Cycloaddition Reactions between Anodically Activated Enyloxy Benzene and Alkenes. *Org. Lett.* **2007**, *9*, 4347–4350.

(331) Crivello, J. V.; Kong, S. Efficient Isomerization of Allyl Ethers and Related Compounds Using Pentacarbonyliron. *J. Org. Chem.* **1998**, *63*, 6745–6748.

(332) Brett Runge, M.; Mwangi, M. T.; Bowden, N. B. New Selectivities from Old Catalysts. Occlusion of Grubbs' Catalysts in PDMS to Change Their Reactions. *Transit. Met. Mediat. Metathesis* **2006**, *691*, 5278–5288.

(333) Sarkar, N.; Banerjee, A.; Nelson, S. G. [4 + 2] Cycloadditions of N-Alkenyl Iminium Ions: Structurally Complex Heterocycles from a Three-Component Diels−Alder Reaction Sequence. *J. Am. Chem. Soc.* **2008**, *130*, 9222–9223.

(334) Formentín, P.; Gimeno, N.; Steinke, J. H. G.; Vilar, R. Reactivity of Grubbs' Catalysts with Urea- and Amide-Substituted Olefins. Metathesis and Isomerization. *J. Org. Chem.* **2005**, *70*, 8235–8238.

(335) Matteson, D. S.; Majumdar, D...Alpha.-Trimethylsilyl Boronic Esters. Pinacol Lithio(Trimethylsilyl)Methaneboronate, Homologation of Boronic Esters with [Chloro(Trimethylsilyl)Methyl]Lithium, and Comparisons with Some Phosphorus and Sulfur Analogs. *Organometallics* **1983**, *2*, 230–236.

(336) Coombs, J. R.; Zhang, L.; Morken, J. P. Synthesis of Vinyl Boronates from Aldehydes by a Practical Boron–Wittig Reaction. *Org. Lett.* **2015**, *17*, 1708–1711.

(337) Belger, C.; Neisius, N. M.; Plietker, B. A Selective Ru-Catalyzed Semireduction of Alkynes to Z Olefins under Transfer-Hydrogenation Conditions. *Chem. – Eur. J.* **2010**, *16*, 12214–12220.

(338) de Haan, J. W.; Van de Ven, L. J. M. Configurations and Conformations in Acyclic, Unsaturated Hydrocarbons. A 13C NMR Study. *Org. Magn. Reson.* **1973**, *5*, 147–153.

(339) Ma, E.; Jiang, Y.; Chen, Y.; Qi, L.; Yan, X.; Li, Z. Salicylate-Directed C−O Bond Cleavage: Iron-Catalyzed Allylic Substitution with Grignard Reagents. *Asian J. Org. Chem.* **2018**, *7*, 914–917.

(340) Meng, Q.-Y.; Schirmer, T. E.; Katou, K.; König, B. Controllable Isomerization of Alkenes by Dual Visible-Light-Cobalt Catalysis. *Angew. Chem. Int. Ed.* **2019**, *58*, 5723–5728.

(341) Ikeda, S.; Miyashita, H.; Sato, Y. Tandem Coupling of Allyl Electrophiles, Alkynes, and Me3Al or Me2Zn in the Presence of a Nickel Catalyst. *Organometallics* **1998**, *17*, 4316–4318.

(342) Dilauro, G.; Francesca Quivelli, A.; Vitale, P.; Capriati, V.; Perna, F. M. Water and Sodium Chloride: Essential Ingredients for Robust and Fast Pd-Catalysed Cross-Coupling Reactions between Organolithium Reagents and (Hetero)Aryl Halides. *Angew. Chem. Int. Ed.* **2019**, *58*, 1799–1802.

(343) Wang, Y.; Shao, Z.; Zhang, K.; Liu, Q. Manganese-Catalyzed Dual-Deoxygenative Coupling of Primary Alcohols with 2-Arylethanols. *Angew. Chem. Int. Ed.* **2018**, *57*, 15143–15147.

(344) Guo, J.; Shen, X.; Lu, Z. Regio- and Enantioselective Cobalt-Catalyzed Sequential Hydrosilylation/Hydrogenation of Terminal Alkynes. *Angew. Chem. Int. Ed.* **2017**, *56*, 615–618.